JOURNAL OF BIOLOGICAL REGULATORS & HOMEOSTATIC AGENTS
Volume 33, No. 3, May - June, 2020

CONTENTS

Editorials

S. Adina, G. Dipalma, I.R. Bordea, O. Lucaciu, C. Feurdean, A.D. Inchingolo, R. Septimiu, G. Malcangi, S. Cantore, D. Martin and F. Inchingolo. Orthopedic joint stability influences growth and maxillary development: clinical aspects 747

S. Marini, M. Maggiorotti, N. Dardes, M. Bonetti, M. Martinelli, L. Re, F. Carinci and C. Tavera. Oxygen-ozone therapy as adjuvant in the current emergency in SARS-COV-2 infection: a clinical study 757

G. Ronconi, G. Tetè, S.K. Kritas, C.E. Gallenga, Al. Caraffa, R. Ross and P. Conti. COVID-19 induced by SARS-CoV-2 causes Kawasaki-like disease in children: role of pro-inflammatory and anti-inflammatory cytokines 767

Original articles

W.-T. Cai, P. Guan, M.-X. Lin, B. Fu, B. Wu and J. Wu. MiRNA-206 suppresses the metastasis of osteosarcoma via targeting Notch3 775

Y.-R. Yang, X.-F. Yang, H.-C. Duan and J.-Q. Qiao. Cyclooxygenase-2 inhibitor Rofecoxib prevents chondrocytes against hypertrophy via Wnt/β-catenin pathway 785

Q.-H. Pan, Y.-H. Fan, Y.-Z. Wang, D.-M. Li, C.-E. Hu and R.-X. Li. Long noncoding RNA NNT-AS1 functions as an oncogene in breast cancer via repressing ZFP36 expression 795

X.-H. Hu, J.-P. Chen and R.-H. Yu. Lipoxin A4 alleviates lung injury in sepsis rats through P38/MAPK signaling pathway 807

L. Cai, W-T. Li, L-L. Zhang, X-Q. Lu, M. Chen and Y. Liu. Long noncoding RNA GAS5 enhanced by curcumin relieves post-stroke depression by targeting miR-10b/BDNF in rats 815

H-X. Wang, X-Y. Wang, J-W. Fei, F-H. Li, J. Han and X. Qin. MicroRNA-23B inhibits non-small cell lung cancer proliferation, invasion and migration via downregulation of RUNX2 and inhibition of WNT/B-catenin signaling pathway 825

L. Fang, X.-F. Xu, Y. Lu, Y.-Y. Wu and J.-J. Li. MicroRNA-495 attenuates proliferation and inflammatory response in rheumatoid arthritis fibroblast-like synoviocytes through attenuating β-catenin pathway 837

J. Li, R-J. Li, X. Zhao and H-Q. Liu. Role of Sigma-1 receptor agonist in hepatic ischemia-reperfusion injury 845

M-Q. Zhuang, J. Li, Xhan, K-L. Su, G-J. Hao and J-Q. Han. G protein regulated inducer of neurite outgrowth 1 is a potential marker for lung cancer prognosis 853

D. Liu, S. Jia, D. Sun, S.-Y. Wang, F.-C. Meng and W.-C. Guo. Rapamycin repairs damaged nerve cells and neurological function in rats with spinal cord injury through ERK signaling pathway 865

K. Liu and Q. Xu. LncRNA PVT1 regulates gallbladder cancer progression through miR-30d-5p 875

S.-C. Ma, R. Chen, T.-N. Yang, F. Zhang and D. Zhao. Baicalein inhibits the proliferative activity of human prostate cancer cell line PC3 by downregulating Ezrin 885

J-D. Gao, R-J. Li, P-L. Ma, L-L. Yu, J-T. Li and H-T. Tian Knockdown of lncRNA HCP5 protects against cerebral ischemia/reperfusion injury by regulating miR-652-3p 893

T.-N. Zhao, L.-D. Yuan, L.-X. Chen, Y. Yuan and D.-L. Cai. PI3K/Akt and ERK1/2 pathways are responsible for sodium butyrate-induced inhibition of neuronal apoptosis in rats with cerebral infarction 901

Z.-D. Zhu, Y.-F. Chen and H.-M. Shi. MiR-93 inhibits myocardial apoptosis in rats with myocardial ischemia-reperfusion injury through regulating Mfn2 expression 909

Q. Xu and K. Liu. MiR-369-3p inhibits tumorigenesis of hepatocellular carcinoma by binding to PAX6 917

X. Fei, HY. Jin, Y. Gao, LM. Kong and XD. Tan. Hsa-miR-10a-5p Promotes pancreatic cancer growth by BDNF/SEMA4C pathway 927

C. Wang, N. Liu and H.-T. Yang. Desflurane pretreatment can reduce sepsis-evoked lung injury in rats via inhibiting STAT3 pathway 935

N. Zhang, X-S. Li, Y. Zhang, S-F. Cheng, J-X. Du and J-P. Liu. Long Noncoding RNA KCNQ1OT1 promotes cell motility in hepatocellular carcinoma by regulating miR-506-3p/FOXQ1 943

W.-L. Wang and Y.-J. Zhao. Effects of fine particulate $PM_{2.5}$ on emphysema of mice via regulating FOXO3A/BIM axis 953

J-X. Fu, G-Q. Sun, H-L. Wang and H-X. Jiang. LncRNA OIP5-AS1 induces epithelial-to-mesenchymal transition and renal fibrosis in diabetic nephropathy via binding to miR-30c-5p 961

L. Guo, HL. Situ, ZY. Wang, Y. Lin and QJ. Chen. Mechanism of Jinrong granule in inhibiting the invasion of breast cancer cells by the CXCL-1-CXCR2/CCL20 pathway 969

M. Di Pietro, S. Filardo, V. Alfano, M. Pelloni, E. Spendiani, A. Po, D. Paoli, E. Ferretti and R. Sessa. *Chlamydia trachomatis* elicits TLR3 expression but disrupts the inflammatory signaling down-modulating NFκB and IRF3 transcription factors in human Sertoli cells 977

L-X. Li, Y-T. Xia, X-Y. Sun, L-R. Li, L. Yao, M-I. Ali, W. Gu, J-P. Zhang, J. Liu, S-G. Huang, H-C. Dai and G-Q. Liu. CXCL-10/CXCR3 in macrophages regulates tissue repair by controlling the expression of Arg1, VEGFa and TNFα 987

Letters to the Editor

C.L. Pătru, N. Cernea, R.G. Căpitănescu, O. Sîrbu, M.C. Marinaș, L.C. Zorilă and D.G. Iliescu. 3D and 2D ultrasound evaluation of the uterine corpus: normal appearances and common pitfalls 1001

CS. Gao, JJ. Dong, XF. Yang, L. Yan, J. Liang and HF. Sun. Effects of angiotensinogen and insulin-like growth factor 1 on the pathogenesis of diabetic nephropathy 1007

D.-L. Wang, C. Han, L.-D. Zhao, G.-Y. Hu, Y. Jiang, C.-G. Li, L.-L. Shi and M.-J. Zhou. Role of miRNA-499-5p in patients with atrial fibrillation and heart failure 1015

B. Kozlowska, B. Sochanowicz, H. Polkowska-Motrenko, M. Kruszewski, A. Cicha-Mikołajczyk, L. Kraj, M. Kusmierczyk and P. Leszek. Failing heart and importance in myocardial trace element: preliminary report 1021

M. Duan, Y. Yang and XH. Zheng Meta-analysis of the treatment for neonatal respiratory distress syndrome by INSURE strategy 1027

LJ. Tao, JY. Gu, YL. Jiang, M. Rui, XY. Du and Y. Zhu. Influence of nutritional status on the short-term rehabilitation outcomes of elderly hip fracture patients 1033

A. Derakhshani, M.R. Mofateh, S. Masieri, H. Ghadri, C. Cavaliere, E. Fakron and M. Fereidouni. Role of invariant natural killer T cells in patients with tonsillar hypertrophy: the tonsil as an immunological organ 1039

M-D. Li, Qiong Yu, J-L. Fu, Y. Shi, Y-R. Lind G. Shi. Tuberous sclerosis complex with multisystem manifestations 1045

F-P. Meng and L-N. Zhou. Positive role of cognitive-behavioral therapy on sexual dysfunction and behavioral problems in prostate cancer-treated patients 1049

P.P. Poli, A. Mascellaro, S. Campolo, F. Signorino, G. Allocca and C. Maiorana. Efficacy of a diagnostic real-time polymerase chain reaction test in the detection and quantification of periodontal and peri-implant pathogens: a pilot study 1053

A.I. Linjawi, M.A. Alsadat, M.A. Othman, L.M. Fakhry, A.S. Basalaim, R.A. Alansari, H.A. Baeshen and A.M. Abushal. Awareness, perception and readiness regarding clear aligner therapy among orthodontists and other dental specialists 1061

A. Alnazeh, M.A. Kamran, I. Alshahrani, A.H. Ali, O.M Saad and A. Fahad. Effect of fixed orthodontic appliance therapy on periodontal health status of patients evaluated through community periodontal index 1067

F. Lu, S-Z. Li, X. Gao, Y-N. Gong, P-X. Shi and C. Zhang. Diagnostic value of circulating miR-208b and miR-499 in peripheral blood of patients with acute myocardial infarction 1071

Rl. Gong, Rr. Jin, Xp. Yu and Wl. Wang. LncRNA SNHG1 acts as an oncogene through regulating miR-145-5p in ovarian cancer 1077

C. Liao, L. Hu and C. Lan. Hashimoto's thyroiditis associated with an extra-thyroidal triad of pretibial myxedema, ophthalmopathy, and acropachy 1085

J-E. Yang. N. Jia, D. Wang, Y. He, L. Dong and A-G. Yang. Ginsenoside Rb1 regulates neuronal injury and Keap1-Nrf2/ARE signaling pathway in cerebral infarction rats 1091

HC. Feng, CM. Wang, MZ. Tang, XJ. Wu, ZC. Zhou, MD. Wei, W. He, SJ. Li, ZK. Zeng and BH. He. Antidepressant effect of total saponins of radix Bupleuri and the underlying mechanism on a mouse model of depression 1097

W. Yang, X. Wu, X-Y. Xu, H-Y. Wang, Y. Li, S-N. Jian and Y-W. Liu. Mechanisms of effect of early inhalation of budesonide on pulmonary function, osteopontin and α-SMA in asthmatic rats 1105

C. Huang, L. Xiao, HL. Luo and ZM. Zhu. Preoperative neutrophil-to-lymphocyte ratio combined with serum CEA, CA19-9, CA125 and CA72-4 levels in the clinical pathological staging of gastric cancer-based on propensity score matching 1111

J.H. Park, D.Y. Choi, H. Park, K.W. Lee and J.A. Cho. Oxytocin modulates immunostatus, metabolic state and gut microbiome 1117

L. Englmeier. A theory on SARS-COV-2 susceptibility: reduced TLR7-activity as a mechanistic link between men, obese and elderly 1125

G. Imataka, Y. Fujita, Y. Kano and S. Yoshihara. Abnormal predominantly frontal high voltage and slow EEG findings with acute encephalopathy associated with acute focal bacterial nephritis 1131

H.A. Baeshen. Comparison of bone metabolism markers and cellular profile between conventional lingual and labial fixed orthodontic appliances 1135

YF. Wang, LL. Ju, X. Luo, H. Zhang and ZL. Bian. Decreased expression of centrosomal protein 350 is associated with poor prognosis in hepatocellular carcinoma 1141

TT. Zhang, ZK. Yu, CF. Xiu, YT. Bai, M. Peng and ZH. Guo. Changes of plasma von Willebrand factor and von Willebrand factor-cleaving protease levels in pregnancy-induced hypertension 1147

M. Śnietura, A. Brewczynski, D. Waniczek, A. Kopec, A. Stanek-Widera, M. Muc-Wierzgoń and T. Rutkowski. Is p16 expression still a surrogate marker for human **papillomavirus** infection in oral squamous cell carcinomas? 1153

R-X. Liang, H. Zheng and Y-L. Yang. Novel compound heterozygous mutations in ganglioside GM3 synthase deficiency 1157

C. Loreto, C. Ledda, R. Tumino, C. Lombardo, E. Vitale, V. Filetti, R. Caltabiano and V. Rapisarda. Activation of Caspase-3 in malignant mesothelioma induced by asbestiform fiber: an *in vivo* study 1163

L. Cannavò, U. Cucinotta, G. Zirilli, M. Lima, G.B. Pajno, M. Wasniewska and M. Valenzise. Malignant insulinoma, a very rare case of pediatric hypoglycaemia 1167

A. Foletti, P. Baron, P. Berchialla, D. Francone, F. Malandrone, L. Ostacoli and S. Carletto. Use of biophysical treatment for the management of mild anxiety, depression and stress: a randomized controlled trial 1171

S. Tartaglione, E. Berardelli, C. De Vito, A. Nardi, G. Gennarini, G. Girelli, A. Angeloni and E. Anastasi. Is there an association between biochemical parameters and prostate-specific antigen "grey zone"? An Italian pilot study 1179

E. Cantone, M. Cavaliere, E. Begvarfaj, S. Motta and M. Iengo. New therapeutic strategies for the treatment of recurrent respiratory tract infections in children 1185

G. Barassi, A. Younes, A. Di Iulio, S. Guerri, V. Guglielmi, F. Della Rovere, M. Supplizi and A. Di Iorio. Fibromyalgia and therapeutic integration: role of quantum medicine 1193

S. Dragonieri, V.N. Quaranta, P. Carratu, F. Orsini, T. Ranieri and O. Resta. Six consecutive days reproducibility of exhaled volatile organic compounds analysis by e-nose 1999

S. Cocuzza, A. Maniaci, M. Di Luca, I. La Mantia, C. Grillo, G. Spinato, G. Motta, D. Testa and S. Ferlito. Long-term results of nasal surgery: comparison of mini-invasive turbinoplasty 1203

P.C. Passarelli, E. Rella, G.B. Piccirillo, V. Desantis, V. Giovannini, A. Speranza, M. De Leonardis, P. Papi, G. Pompa, P.F. Manicone and A. D'Addona. How frequent are postoperative complications after an impacted mandibular third molar extraction? 1209

A. Moffa, M. Casale, V. Fiore, V. Rinaldi, R. Giancaspro, M.A. Lopez, P. Baptista, M. Gelardi and M. Cassano. Impact of intranasal nebulized ectoine on morbidity and short-term quality of life after pediatric adenoidectomy 1213

R. Apponi, S. Presti, E. Spinas and L. Giannetti. Biological, genetic and aetiology aspects in molar incisor hypomineralization 1219

S. Dal Fior, C. Gaido, I. Carnino, F. Gamna, C. Busso, G. Massazza and M.A. Minetto. Clinical predictors of response to ozone therapy for treatment of discogenic and non-discogenic low back pain 1223

S. Ghafoor, T. Akhtar, M.B. Khawar and N. Sheikh. Alterations in hepatic trace elements and ferritin expression in high energy diet fed rat model 1229

LC. Wang, AQ. Gu, CL. Sun, Xu. Hong, XS. NI, RJ. Wang, XY. Zhao and QC. Wang. Cross-sectional study of factors correlated to quality of life in patients with coronary artery disease and diabetic retinopathy 1235

JOURNAL OF BIOLOGICAL REGULATORS & HOMEOSTATIC AGENTS Vol. 34, no. 3, 747-756 (2020)

EDITORIAL

ORTHOPEDIC JOINT STABILITY INFLUENCES GROWTH AND MAXILLARY DEVELOPMENT: CLINICAL ASPECTS

S. ADINA[1*], G. DIPALMA[2*], I.R. BORDEA[1], O. LUCACIU[1], C. FEURDEAN[1], A.D. INCHINGOLO[2], R. SEPTIMIU[1], G. MALCANGI[2], S. CANTORE[2,3], D. MARTIN[4§] and F. INCHINGOLO[2§]

[1]"Iuliu Hatieganu" University of Medicine and Pharmacy, Department of Oral Health, Cluj-Napoca, Romania; [2]Department of Interdisciplinary Medicine, University of Bari "Aldo Moro", Bari, Italy; [3]Sorriso & Benessere Ricerca e Clinica S.r.l., Bari, Italy; [4]Private Practice, San Sebastian, Spain

Received April 7, 2020 - Accepted May18, 2020

[*]These authors contributed equally to this work as co-first Authors
[§]These authors contributed equally to this work as co-last Authors

Orthopedic temporomandibular joint (TMJ) instability is very common among children and adults. It is often associated with pain in the cervicofacial region, and muscle contraction. To investigate whether muscle contraction can cause permanent posterior rotation of the head and whether treatment with splint and kinetotherapy is efficient, a literature review was carried out of patients with pain in the cervicofacial area. Additionally, the case of a 15-year old patient presenting with permanent posterior rotation of cranium, with no movement between the first two vertebra and pain in the cervicofacial area was reported. Kinetotherapy followed by rapid maxillary expansion improved the function of cervical vertebrae and reduced the cervicofacial pain within the first two weeks. Kinetotherapy, rapid maxillary expansion, and orthodontic treatment with a stable joint position could be a good therapy to control occipital-atlas function.

The cranio-cervico-mandibular (CCM) system has been defined as a functionally based system; any dysfunction of the CCM system is a site for disease. Pain in the facial region is associated with temporomandibular disorder (TMD) in 70% of the cases (1). Although only one in four people are aware of TMD, 60-70% of the general population suffers from this disease (1).

TMD is a disease that affects the temporomandibular joint (TMJ), myofascial muscle, and cervical spine. Pain is the most common symptom of TMD but determining the etiology of pain can be challenging. Pain can be described by patients in multiple ways: shooting, burning, throbbing, aching, stinging, cramping, and tingling. Different types of pain can provide clues for appropriate diagnosis. Sharp pain can be caused by primary neuralgia, whereas burning pain can be caused by mechanical nerve irritation. Muscle spasm can result in cramping pain. Aching pain is associated with inflammation. A complete clinical evaluation must differentiate the pain caused by a joint pathology from the pain caused by muscular disorders (2). The specific treatment plan is determined by the diagnosis; therefore, an accurate diagnosis is crucial.

TMD disorders are most commonly classified using the research diagnostic criteria (RDC) for

Key words: orthopedic TMJ instability; occipital-atlas fusion; cervicofacial pain

Corresponding Author:
Ioana Roxana Bordea,
"Iuliu Hatieganu" University of Medicine and Pharmacy,
Oral Health, Victor Babeș Street No. 15,
400000 Cluj-Napoca, Romania
e-mail: roxana.bordea@ymail.com

0393-974X (2020)
Copyright © by BIOLIFE, s.a.s.
This publication and/or article is for individual use only and may not be further reproduced without written permission from the copyright holder.
Unauthorized reproduction may result in financial and other penalties
DISCLOSURE: ALL AUTHORS REPORT NO CONFLICTS OF INTEREST RELEVANT TO THIS ARTICLE.

temporo-mandibular disorders (RDC/TMD). TMJ pain and clicking, myofascial pain, reduced range of motion, and mandibular deviation during function are the principle signs and symptoms of TMJ disorders. These symptoms could be associated with ear-related problems, headache, cervical spine-dysfunction, and altered cervical posture (3). In case of facial pain due to TMD, patients often describe an increase in pain intensity during mastication. Schiffman et al. classified orofacial pain as physical (Axis 1) and psychological (Axis 2) (3).

Orthopedic joint problems are very common among pediatric and elderly patients. Patients with joint problems complain about pain in the joint and ear regions, whereas patients with muscular pain usually describe pain in a more generalized area (2).

For good health, the patient must have a stable orthopedic joint with the condyles in the uppermost position in the temporal fossa and the disc in a concave-convex relation and the teeth in maximum intercuspation. In this position, all muscles will be relaxed so that the masticatory system can function correctly. Some authors reported that disc displacement (DD) is very frequent in children aged between 6 and 15 years, and that it progresses with age (4). Disturbance of mandibular growth can occur because of mandibular dysfunction. When DD is present in one joint, growth will be impeded; growth can also be affected by nonfunctional masticatory muscles. TMD could be associated with cervical anomalies that could impediment growth. If posterior rotation of the cranium is diagnosed at an early age, could this influence mandibular growth? Could Atlas-occipital fusion (AOA) and permanent posterior rotation of the cranium present the same radiologic characteristic?

MATERIALS AND METHODS

This systematic review was performed in accordance with the guidelines of the Cochrane Collaboration (5) and the Centre for Reviews and Dissemination (6). The review was processed in accordance with the Preferred Reporting items from the Systematic Reviews and Meta-Analyses Statement (7).

The authors identified 8,023 publications in electronic databases, using PubMed, Scopus, and Web of Science to search all the articles. Inclusion criteria for this review consisted of clinical trials, case reports, and free full text articles published in the last 5 years that studied TMJ pain and myofascial pain. Literature reviews, meta-analyses, and research on treatment with laser therapy, alternative medicine treatment, medication therapy, general disease, ozone therapy, and platelet reach plasma (PRP) were all excluded. The included articles are summarized in Table I. Eight eligible studies were included in this review. The full-text articles were assessed by two independent reviewers for eligibility. The quality assessment (risk of bias) of the selected studies was evaluated by the same reviewers according to the Cochrane risk of bias tool.

A 15-year-old girl was referred to the orthodontic department for treatment. She demonstrated a posterior cross bite with 9-mm maxillary transverse deficiency resulting in bilateral ectopic canine, a severe Class II malocclusion, crowding in the upper and lower arch, and oral breathing. The lower midline was shifted to the right due to crowding, and the upper midline was in the correct position. Clinical examination revealed a convex profile with retrognathic and small mandible, obtuse naso-labial angle, labial incompetence, and facial asymmetry with menton deviated to the right. We used Rocabado's map of pain to palpate the TMJ. Both left and right TMJ were sensitive to palpation. In addition, the masticatory muscle was tender and sensitive to palpation. The upper and lower incisors were protruded, and the molar relationship was Class II on both sides. The patient had an anterior open bite of 6 mm and an overjet of 5 mm. She was complaining of cervicofacial pain. When the muscles were palpated, the patient experienced pain in the upper trapezius and temporalis. When we examined the Lateral Cephalometric radiograph, we found that the C1 vertebra was in contact with the occipital bone and suspected an atlanto-occipital fusion with a posterior rotation of the cranium. We took another X-ray with the head in flexion and saw no movement between the occipital bone and atlas (Fig. 1).

There are few existing studies on occipito-atlas fusion. We were unable to find one involving differential diagnoses between osseous fusion and muscle contraction on its own. Atlanto-occipital assimilation (AOA) of atlas, and assimilation of atlas are abnormalities that are rarely recorded in anatomical, morphological, and radiological studies. It is usually associated with reduction in dimensions of foramen magnum, leading to acute or chronic

neurovascular compression and clinical manifestations of varying severity. Although atlanto-occipital fusion is rare, it is important for the diagnostic and therapeutic approaches of physicians and surgeons (8-10). Research by Sonnesen et al. showed a correlation between craniofacial and upper cervical spine morphology (11). Neurological disorders in patients with AOA often occur in the 3rd and 4th decades of life and require surgical treatment. AOA diagnosis is of vital importance for radiologists, neurologists, orthopedists, and neurosurgeons.

The treatment plan included muscle relaxation with physiotherapy, correction of transverse discrepancy, resolving the upper crowding, aligning and leveling the upper canines while avoiding protrusion of the upper incisors, leveling and aligning the lower arch while avoiding protrusion of the lower incisors, leveling and aligning both arches, Spee and Wilson curve, and establishing a Class I canine relationship with normal and stable overbite and overjet. Extraction of the first upper premolar was necessary in order to align the upper canine. In the lower arch, we corrected crowding by removing the right second impacted premolars and the first left premolar. We explained to the patient that, because of bimaxillary retrusion and the significance of her open bite, she would need surgical intervention later, after her growth has finished. The risks and benefits of the treatment plan were discussed with the patient and her parents.

For correction of the transverse discrepancy, we decided to use a hybrid hyrax anchored at the level of the first premolars and first molars. Expansion began immediately with one turn per day and continued for one month. At the same time, the patient was instructed to start physiotherapy during her first week in the office and then continue at home. The patient continued to be treated with hybrid hyrax for five months. After this period, we removed the upper first premolars. We continued the premolar extraction and fixed appliance with upper and lower brackets. The treatment time for the fixed appliances was 20 months.

After treatment, the patient had a stable occlusion and acceptable overbite and overjet. Moreover, the examination of lateral cephalogram revealed correction of the atlanto-occipital fusion (Fig. 2). The correlation between upper spine and cranio-facial morphology was observed. The overbite was correlated with upper spine morphological deviations. In earlier studies, a correlation was shown between upper spine morphological deviations and mandibular retrognathia, large inclination of the jaws and of the cranial base angle (12).

Cervical column morphology in adult patients with OSA was compared to the cervical morphology of adult patients with neutral occlusion and no history of sleep apnea. The results show that morphological deviation of upper cervical vertebrae was correlated with obstructive sleep apnea (13). The cephalometric analyses is shown in Table II.

Cephalometric analysis after the treatment showed a correction of the atlanto-occipital relation, which suggests that the original position was due to muscle contraction. Looking at the growth prediction (14), C2 was concave trapezoid, C3 was concave trapezoid, C4 was concave trapezoid. This indicates that the patient was in stage 4 according to Bacetti and her growth peak was 1 to 2 years prior to treatment. During the treatment period, she grew 5.4 mm at her anterior cranial base and her mandible grew 1.2 mm (13).

RESULTS

In their study, Schiffman et al. compared four treatment strategies for TMD with and without disc displacement and limited mouth opening (15). The treatment options proposed in this study were: medical management, non-surgical rehabilitation, arthroscopic surgery, and arthroplasty. A further Schiffman's study followed his report from 2007, (16) in which the success of the treatment was evaluated using two measures. These included the Symptom Severity Index (SSI) to evaluate TMJ pain and the Craniomandibular Index (CMI) to evaluate jaw dysfunction. The International Association of Oral and Maxillofacial Surgery recommendations and treatment strategies were used for a closed lock disorder to evaluate the TMJ disc status at 24 months and the TMJ hard tissue status at 60 months post-treatment. The patients included in the study were divided into two groups and then randomly assigned into groups for four treatment strategies. The study group that demonstrated limited mouth opening for less than 6 months was defined as non-chronic and patients with limited mouth opening more than 6 months were defined as chronic (15).

The medical treatment strategy consisted of counseling and a treatment strategy: a 6-day regimen of oral methylprednisolone followed by prescription of

Table I. *Articles included in the review*

Author	Sample size	Primary outcome	Pain management	Clinical assessment	Follow-up
Schiffman et al. (2014)	106 patients	TMJ pain, limited mouth opening, disc displacement without reduction	Pharmaceutical administration, nonsurgical rehabilitation, arthroscopy surgery and arthroplasty	Mandibular range of motion, TMJ sounds, impairment of chewing	3,6,12,18,24, 60 months
Walczynska et al. (2014)	60 patients	TMJ pain, cervical spine pain, neck pain	Occlusal splint, self control parafunctional habits	Medical history and physical examination based on a survey card according to RDC/TMD	3 weeks, 3 months
Silveira et al. (2015)	40 patients	Neck pain, TMJ pain, jaw dysfunction, muscle tenderness	-	Neck disability index and the limitations of daily High level of muscle tenderness in upper trapezius and temporalis	-
Costa et al. (2015)	60 patients	Masticatory myofascial pain according to RDC/TMD, mild anxiety(25%), mild depression	Group 1 counseling(verbal and written information Group 2 counseling+ occlusal splints (only at night whilst sleeping)	Symptoms of anxiety and depression and pain catastrophizing Self reported questionnaire consisting of 9 statements related to pain	2 and 5 months
Conti et al. (2015)	60 patients	TMJ pain and disc displacement with reduction and arthralgia	Group 1-anterior reposition and occlusal splint, group 2 nociceptive Trigeminal Inhibition Clenching Suppression system devices, manufacturer is not specified, group 3 counseling for behavioral changes and self-care	Evaluated by means of visual analogue scale, pressure pain threshold of the TMJ, maximum range of motion and TMJ sounds Possible adverse effects were recorded (discomfort while using the device and occlusal changes)	2 and 6 weeks, 3 months 21
Calixtre et al. (2016)	12 patients	TMJ disorder, myofascial pain	Cervical mobilization and exercise on clinical signs and mandibular function	Self reported pain, jaw function according to Mandibular functional impairment Questionnaire (MFIQ), pain free maximum mouth opening and pressure pain thresholds of masseter and temporalis	3 times-twice before (baseline phase), once after intervention
Grootel et al. (2017)	72 patients	TMJ disorders, pain and restricted jaw movement, myofascial pain	Splint therapy and physiotherapy	Scoring of the intensity of predominant pain by Visual analogue scale The progress and ultimate effect of treatment –evaluated by index treatment duration control(TDC)	10-21 weeks or 12-30 weeks, 1 year follow-up
Ishiyama et al. (2017)	25 patients	Prevention of TMD pain in patients with OSA treated with oral appliance	jaw opening exercise	Two weeks before insertion of the appliance OA and two weeks after using VAS in the morning and daytime	2 weeks, 1, 3 month

non-steroidal anti-inflammatory drugs for up to 6 weeks (ibuprofen 800 mg, 3 per day) and a muscle relaxant, typically cyclobenzaprine 10 mg, at bedtime. The rehabilitation strategy included medical management, cognitive behavioral therapy, physical therapy with mobilization of the joint, and a flat splint for 6 months. Arthroscopy was performed using Moses and Poker method (17) of an injection in the superior joint space of bupivacaine and Ringer's lactate solution. A blunt trocar was used to remove all adhesions in the intracapsular space. Arthroplasty was performed using open joint surgery to remove the disc. All patients were followed-up once a month for 6 months.

The success rate was considered as corresponding to patient concerns, and was as follows: 87% had an improvement in their ability to eat most foods, 77% had an improvement in their ability to open their mouth more than 35 mm, and 54% had pain decreased. Joint noises changed little over time.

All the patients were investigated by MRI; in each case, disc displacement without reduction was confirmed. Changes in disc displacement were measured only at the 24-month follow-up visit. The results were:

out of 25 patients in medical management, only 3 showed disc changes. One patient's disc had normal positioning and two patients were diagnosed with disc displacement with reduction;

out of 20 patients in rehabilitation, only 3 showed disc displacement with reduction;

out of 32 patients who underwent joint arthroscopy, two patients had non-reducing disc which were reported to have normal positioning and five patients had disc displacement with reduction.

In Walczynska-Dragon's study, they suggested a correlation between TMD, cervical spine pain, and mobility (18). The study included 30 patients with TMD, cervical spine pain, and limited cervical range of movements. Patients were included in the study if they had pain in the area between occiput and C7 for at least 12 months (18).

The examination protocol included:

- medical history and physical examination based on RDC/TMD;
- VAS scale for pain diagnosis;
- TMJ evaluation;
- Cervical spine motion and muscle palpation.

The treatment was performed with an anterior splint SVED (Sagittal Vertical Extrusion Device) to decrease muscle activity. The splint was worn for 8 to 10 hours a day during sleep. After 3 months of therapy, TMJ function improved considerably. Cervical pain

Table II. *Cephalometric analysis*

	Initial	Final
Anterior cranial base SN	58.6mm	64 mm
Mandibular length Go-Me	57.8mm	59 mm
SNA	76	76
SNB	68.5	70
ANB	7.6	5.9
IMPA	89.6	90.4
Upper incisors-SN	112	112
Ramus Height Ar-Go	36.1 mm	43
Posterior cranial base S-AR	27.5 mm	32



A **B**

Fig. 1. *Lateral cephalometric in normal position (**A**); Lateral cephalometric in flexion position with C1 in contact with occipital bone (**B**).*

diminished after 3 weeks and only 8% of patients reported pain at 3 months.

Silveira's study revealed that TMD pathologies are often associated with neck disability in patients with and without chronic TMD (19). High levels of muscle tenderness were found in the upper trapeziums and temporalis. Patients also presented with high levels of jaw and neck dysfunction. This study showed that higher the tenderness in the muscle, the higher the level of jaw and neck disability.

Costa et al. demonstrated that an occlusal splint could provide an improvement in temporomandibular disorder subjects (20). Sixty patients with masticatory myofascial pain were divided into two groups; one received counseling while the other group received occlusal splints and counseling. The occlusal surface of the splint was flat, 2.5-mm thick in the posterior region, and was worn with anterior guidance for a 5-month period. The patients were instructed to wear their splint only at night, whilst sleeping. The patients were evaluated for symptoms of anxiety, depression and pain catastrophizing using nine statements related to pain perception. The inclusion criteria were myofascial pain according to RDC/TMD with pain duration of at least 3 months. Exclusion criteria were occlusal risk factors for TMD, vascular disorders, trauma, and medication (anticonvulsants, muscle relaxant, antidepressants). The conclusions suggested that minimally invasive strategies could provide improvement and occlusal splint could add a plus value.

Conti et al. assessed the benefit of using intraoral devices in patients with disc displacement with reduction (DDWR) and arthralgia (21). Sixty patients with arthralgia were divided randomly into 3 groups. Inclusion criteria were patients with pain in the preauricular region for at least 30 days which increased during mastication and talking, and who also had disc displacement with reduction (II a) and arthralgia (IIIa.) Exclusion criteria were trauma, systemic diseases, disc displacement without reduction, dental pain, patients with full or partial dentures, and a history of TMJ surgery. They found that anterior repositioning appliances provided a significant effect in ameliorating pain at the TMJ

level and that joint sound decreased in frequency. The exact position of the disc was not recorded because no MRI imaging was used. The degree of protrusion was when joint clicking was eliminated, and splint was worn only at nighttime. The Nociceptive Trigeminal Inhibition Clenching Suppression System (NTI-tss) was also used. In this group, pain was reduced, but the TMJ sound increased.

According to the results of Calixtre et al., treatment of temporomandibular disorders with cervical spine joint mobilization and segmental stabilization decreased muscular pain and improved TMJ function (22). The interrelation between TMJ and cervical spine can be better understood by the neuroanatomical convergence of nociceptive neurons that received trigeminal and neck sensory inputs. There is a strong association between neck disability and TMD. The same study showed that sternocleidomastoid and anterior scalene muscles were increased. This study continued over 9 weeks. Patients had a primary diagnosis of myofascial pain with or without limited mouth opening. The distance between upper-lower central incisors was measured at the limit of pain-free mouth opening. The patients were also assessed for joint clicking. Exclusion criteria included arthritis without myofascial pain, trauma, systemic disease, and a history of any form of treatment. Patients had moderate or severe symptoms of TMD, according to Fonseca Anamnestic Index. Physiotherapy techniques involving manual therapy, active and passive stretching, strengthening of the involved muscles, and postural exercises were used for treatment (22). The protocol reported by La Touche was used, including 10 sessions of approximately 35 min each: 20 minof manual therapy, 10 min of muscle conditioning exercises, and 5 min of stretching (23).



Fig. 2. *Final lateral cephalometric in normal position with correction of C1 fusion.*

Van Grootel compared the outcome of physiotherapy *versus* splint therapy using Treatment Duration Control (TDC) index for enabling a randomize clinical trial (RCT) (24). This study evaluated the number of visits and length of treatment needed to determine whether treatment was successful. A total of 72 patients were selected. They had solely myogenous TMD and were randomly divided into two groups, physiotherapy and splint therapy. Exclusion criteria were disc displacement, arthralgia, arthritis, arthrosis, or those who had undergone previous treatment with occlusal splint or occlusal adjustment.

Clinical and experimental studies of Solow showed that there was a possible role of occlusal interference in myogenous TMD (24). Patients with occlusal interference on the nonactive side which did not have contact with the active side and patients with forward sliding of at least 2 mm and lateral shift of at least 1 mm from centric occlusion were excluded from this study to reduce the influence of confounding factors. The patients were randomly assigned to two different therapy groups: the experimental group received physiotherapy of the masticatory system and occlusal therapy while the control group treatment was splint wear. The splint used in this study was the Michigan type and was used on the upper jaw, only at nighttime, with small adjustments. The patients were examined every 6 weeks. When the symptoms decreased, the splint was gradually withdrawn; during the first week, patients wore the splint for six nights, and only five nights in the second week (24). Physiotherapy used in this study involved learning techniques to avoid stress related to pain from the masticatory system, and relieving this pain with self-massage and relaxation. Recommended exercises included neck, head, shoulders, and tongue postures, controlling rotation and translation while opening the jaw, the

Jacobson method of relaxation, stretching the muscles that close the jaw, and resisting the urge to open the jaw. Techniques to reduce habits such as lip biting, clenching or grinding, and unilateral chewing were introduced. For 3 weeks, every 2 to 3 days, patients who were in the physiotherapy group participated in a program with a personal instructor and were then instructed to continue exercises at home for 6 weeks. Physiotherapy and occlusal therapy registered the same success rate and overall success rate of stepped care. There was no relationship of dependence between therapy sequences.

In their study, Ishiyama and coll. included how jaw-opening exercises affected prevention of TMD in patients with sleep apnea who wore an oral appliance (25). A number of 25 OSA (obstructive sleep apnea) patients were consecutively enrolled into a two-arm, randomized, double-blinded, placebo-controlled trial. They concluded that this exercise prior to OSA therapy reduced the risk of TMD pain in patients who were prescribed oral appliances.

DISCUSSION

Although growth modification has been considered important from the beginning of orthodontics, the concepts underlying its use and the views of its clinical usefulness have varied greatly over time. To orthodontists in the late 19th and early 20th centuries, growth modification was easy because it was assumed that growth was largely controlled by environmental factors and was judged as successful because the dental occlusion improved. By midcentury, cephalometrics had shown that most of the changes produced by the treatment methods of that time were tooth movement, not modified growth.

Splint and physical therapy proved to be effective in treatment of TMD associated with pain. Permanent posterior rotation of the cranium or atlas occipital fusion could impede mandibular growth and a correct position of the maxilla. A more accurate diagnosis should be performed when AOA is suspected as it could just be a muscular problem that needs to be treated with physiotherapy and occlusal splint. An adaptive head position can be a factor in altering the direction of facial growth. Determination of head position and mandible growth direction can be important indicators in patients with TMD treatment (26). The results may prove valuable for planning the treatment of children with Class II, during their growth period. The morphology of the upper spine was correlated with craniofacial morphology, maxillary transverse deficit, open bite, and cervical neck dysfunction.

Maxillary deficit and oral breathing can cause muscle contraction, TMJ instability, and cervical spine dysfunction. Treatment of maxillary transverse deficit should be started as early as possible together with kinetotherapy of the neck and TMJ which will have more significant improvement on growth. From a clinical point of view, orthodontists should recognize that the expected effects of joint stability on maxillary growth might differ between patients with short- and long-face. The greater counter-clockwise rotation of the maxilla would induce mandibular clockwise rotation and a subsequent increment of anterior facial height. There is no doubt that within certain limits, at least in the short term, some modification of growth of the different components of the midface can be obtained with intermaxillary traction. Furthermore, it is necessary to understand the crosslink with other oral or metabolic alterations before providing orthodontic treatment (27-34), according to the evidence based dentistry (35-43). In some cases, this may be sufficient to avoid orthognathic surgery, or at least reduce the severity of the surgical correction needed after completion of growth. Individual variations in treatment outcomes, however, are high. For all types of growth modification, and to prevent TMD/TMJ, specific clinical frameworks are needed to predict the outcome and to define guidelines and indications for an orthopedic approach.

REFERENCES

1. Dohan Ehrenfest DM, Del Corso M, Inchingolo F, Charrier JB. Selecting a relevant in vitro cell model for testing and comparing the effects of a Choukroun's platelet-rich fibrin (PRF) membrane and a platelet-rich plasma (PRP) gel: tricks and traps. Oral Surg Oral Med Oral Pathol Oral Radiol Endod 2010; 110(4):409-11; author reply 411-3. doi: 10.1016/j.tripleo.2010.05.056.
2. Dohan Ehrenfest DM, Del Corso M, Inchingolo F,

Sammartino G, Charrier JB. Platelet-rich plasma (PRP) and platelet-rich fibrin (PRF) in human cell cultures: growth factor release and contradictory results. Oral Surg Oral Med Oral Pathol Oral Radiol Endod.2010; 110(4):418-21; author reply 421-2. doi: 10.1016/j.tripleo.2010.05.059.

3. Schiffman E, Ohrbach R, Truelove E, et al. Diagnostic Criteria for Temporomandibular Disorders (DC/TMD) for Clinical and Research Applications: recommendations of the International RDC/TMD Consortium Network and Orofacial Pain Special Interest Group. J Oral Facial Pain Headache 2014; 28: 6-27.
4. Ikeda K, Kawamura A, Ikeda R. Prevalence of disc displacement of various severities among young pre-orthodontic population: A magnetic resonance imaging study. J Prosthodont 2014; 35:397-401.
5. Akers J, Aguiar-Ibáñez R, Sari AB, et al. Systematic reviews: CRD's guidance for undertaking reviews in healthcare. 3rd ed. York, UK: York Publishing Services Ltd; 2009.
6. Higgins JPT, Green S, editors. Cochrane Handbook for Systematic Reviews of Interventions Version 5.1.0: updated March 2011.
7. Moher D, Shamseer L, Clarke M, et al. Preferred reporting items for systematic review and meta-analysis protocols (PRISMA-P) 2015 statement. Syst Rev 2015; 4:1.
8. Koç A, Karabıyık Ö, Tursem T, et al. Demonstration of craniocervical junction abnormalities for diagnosis of atlanto-occipital assimilation using MRI. Anatomy 2012; 7:76-82.
9. Iizuka H, Sorimachi Y, Ara T, et al. Relationship between the morphology of the atlanto-occipital joint and the radiographic results in patients with atlanto-axial subluxation due to rheumatoid arthritis. Eur Spine J 2008; 17:826-30.
10. Eunhye O, Sug-Joon A, Sonnesen L. Ethnic differences in craniofacial and upper spine morphology in children with skeletal Class II malocclusion. Angle Orthod 2018; 88:283-91.
11. Sonnesen L, Petri N, Kjaer I, et al. Cervical column morphology in adult patients with obstructive sleep apnoea. Eur J Orthod 2018; 30:521-36.
12. Arntsen T, Sonnesen L. Cervical vertebral column morphology related to craniofacial morphology and head posture in preorthodontic children with Class II malocclusion and horizontal maxillary overjet. Am J Orthod Dentofacial Orthop 2011; 140:e1-7.
13. Cantore S, Ballini A, Farronato D, et al. Evaluation of an oral appliance in patients with mild to moderate obstructive sleep apnea syndrome intolerant to continuous positive airway pressure use: Preliminary results. Int J Immunopathol Pharmacol 2016; 29:267-73.
14. Ballini A, Santacroce L, Cantore S, Saini R, Mastrangelo F, Desiate A, Scacco S. Orthodontic forces modulate insulin-like growth factor binding protein-5 changes in gingival crevicular fluid. J Biol Regul Homeost Agents 2016; 30:1235-40
15. Schiffman EL, Velly AM, Look JO, et al. Effects of four treatment strategies for temporomandibular joint closed lock. Int J Oral Maxillofac Surg 2014; 43:217226.
16. Schiffman EL, Look JO, Hodges JS, et al. Randomized effectiveness study of four therapeutic strategies for TMJ closed lock. J Dent Res 2007; 86:58-63.
17. Moses JJ. Poker ID. Temporomandibular joint arthroscopy: the endaural approach. Int J Oral Maxillofac Surg 1989; 18:347-51.
18. Walczyńska-Dragon K, Baron S, Nitecka-Buchta A et al. Correlation between TMD and cervical spine pain and mobility: is the whole body balance TMJ related? Biomed Res Int 2014:582414.
19. Silveira A, Gadotti IC, Armijo-Olivo S, et al. Jaw dysfunction is associated with neck disability and muscle tenderness in subjects with and without chronic temporomandibular disorders. Biomed Res Int 2015; 512792. doi: 10.1155/2015/512792
20. Costa YM, Porporatti AL, Stuginski-Barbosa J, et al. Additional effect of occlusal splints on the improvement of psychological aspects in temporomandibular disorder subjects: A randomized controlled trial. Arch Oral Biol 2015; 60:738-44.
21. Conti PC, Corrêa ASDM, Lauris JRP, et al. Management of painful temporomandibular joint clicking with different intraoral devices and counseling: a controlled study. J Appl Oral Sci 2015; 23:529-35.
22. Calixtre LB, Grüninger BLDS, Haik MN, et al. Effects of cervical mobilization and exercise on pain, movement and function in subjects with temporomandibular disorders: a single group pre-post test. J Appl Oral Sci 2016; 24:188-97.
23. Van Grootel, RJ, Buchner R, Wismeijer D, et al.

Towards an optimal therapy strategy for myogenous TMD, physiotherapy compared with occlusal splint therapy in an RCT with therapy-and-patient-specific treatment durations. BMC Musculoskelet Disord 2017; 18:76.
24. Solow RA. The dental literature on occlusion and myogenous orofacial pain: Application of critical thinking. Cranio 2016; 34:323-31.
25. Ishiyama H, Inukai S, Nishiyama A, et al. Effect of jaw-opening exercise on prevention of temporomandibular disorders pain associated with oral appliance therapy in obstructive sleep apnea patients: A randomized, double-blind, placebo-controlled trial. J Prosthodont Res 2017; 61:259-67.
26. Dubojska A, Smiech-Slomkowska G. Natural head position and growth of the facial part of the skull. Cranio 2013; 31:109-17.
27. Ballini A, Cantore S, Farronato D, et al. Periodontal disease and bone pathogenesis: the crosstalk between cytokines and porphyromonas gingivalis. J Biol Regul Homeost Agents 2015; 29:273-81.
28. Grassi FR, Ciccolella F, D'Apolito G, et al. Effect of low-level laser irradiation on osteoblast proliferation and bone formation. J Biol Regul Homeost Agents 2011; 25:603-14.
29. Ballini A, Tetè S, Scattarella A, et al. The role of anti-cyclic citrullinated peptide antibody in periodontal disease. Int J Immunopathol Pharmacol 2010; 23: 677-81.
30. Scattarella A, Ballini A, Grassi FR, et al. Treatment of oroantral fistula with autologous bone graft and application of a non-reabsorbable membrane. Int J Med Sci 2010; 7:267-71.
31. Foti C, Romita P, Rigano L, et al. Isobornyl acrylate: an impurity in alkyl glucosides. Cutan Ocul Toxicol 2016; 35:115-19
32. Grassi FR, Pappalettere C, Di Comite M, et al. Effect of different irrigating solutions and endodontic sealers on bond strength of the dentin-post interface with and without defects. Int J Med Sci 2012; 9:642-54.
33. Cicinelli E, Ballini A, Marinaccio M, Poliseno A, Coscia MF, Monno R, De Vito D. Microbiological findings in endometrial specimen: our experience. Arch Gynecol Obstet 2012; 285:1325-29.
34. Scattarella A, Ballini A, Grassi FR, et al. Treatment of oroantral fistula with autologous bone graft and application of a non-reabsorbable membrane. Int J Med Sci 2010; 7:267-71.
35. Ballini A, Capodiferro S, Toia M, Cantore S, Favia G, De Frenza G, Grassi FR. Evidence-based dentistry: what's new? Int J Med Sci 2007 6; 4:174-8.
36. Ballini A, Santacroce L, Cantore S, et al. Probiotics efficacy on oxidative stress values in inflammatory bowel disease: a randomized double-blinded placebo-controlled pilot study. Endocr Metab Immune Disord Drug Targets 2019; 19:373-81.
37. Inchingolo F, Dipalma G, Cirulli N, et al. Microbiological results of improvement in periodontal condition by administration of oral probiotics. J Biol Regul Homeost Agents 2018; 32:1323-28.
38. Cantore S, Ballini A, Mori G, et al. Anti-plaque and antimicrobial efficiency of different oral rinses in a 3-day plaque accumulation model. J Biol Regul Homeost Agents 2016; 30:1173-78.
39. Di Comite M, Crincoli V, Fatone L, et al. Quantitative analysis of defects at the dentin-post space in endodontically treated teeth. Materials 2015; 8: 3268-3283.
40. Ballini A, Scacco S, Coletti D, Pluchino S, Tatullo M. Mesenchymal stem cells as promoters, enhancers, and playmakers of the translational regenerative medicine. Stem Cells Int 2017; 2017: 3292810. doi: 10.1155/2018/6927401
41. Inchingolo F, Martelli FS, Gargiulo Isacco C, et al. Chronic periodontitis and immunity, towards the implementation of a personalized medicine: a translational research on gene single nucleotide polymorphisms (SNPs) linked to chronic oral dysbiosis in 96 Caucasian patients. Biomedicines 2020; 8: E115.
42. Pettini F, Savino M, Corsalini M, Cantore S, Ballini A. Cytogenetic genotoxic investigation in peripheral blood lymphocytes of subjects with dental composite restorative filling materials. J Biol Regul Homeost Agents 2015; 29: 229-33.
43. Ballini A, Cantore S, Altini C, et al. 99mTc-diphosphonates bone scintigraphy for vitality evaluation in cleft palate.Eur Rev Med Pharmacol Sci 2018; 22:8497-501.

JOURNAL OF BIOLOGICAL REGULATORS & HOMEOSTATIC AGENTS Vol. 34, no. 3, 757-766 (2020)

EDITORIAL

OXYGEN-OZONE THERAPY AS ADJUVANT IN THE CURRENT EMERGENCY IN SARS-COV-2 INFECTION: A CLINICAL STUDY

S. MARINI[1], M. MAGGIOROTTI[2], N. DARDES[3], M. BONETTI[4], M. MARTINELLI[5], L. RE[6], F. CARINCI[7] and C. TAVERA[8]

[1]Dati & Ricerca S.r.l., Rome, Italy; [2]New FIO National Secretary, Rome, Italy; [3]Paideia Clinic, Rome, Italy; [4]New FIO Neuroradiology Department, Brescia City Clinical Institute, Brescia, Italy; [5]Villa S. Pietro Hospital, Rome, Italy; [6]Medinat, Camerano, Ancona, Italy; [7]Dental Faculty, University of Ferrara, Ferrara, Italy; [8]Potenziativa Medical Center, Como, Italy

Received April 29, 2020 – Accepted May 5, 2020

Protocol issue date: May 23, 2020
Version No .: 13.0
Promoter of the study: NUOVA F.I.O. (Italian Oxygen-Ozone Federation)
Via G. Antonelli, 47 - 00197 Rome
List of participating Centers in Appendix II

The aim of the multicentre study promoted by Nuova FIO is to evaluate the beneficial effects of the systemic Oxygen-Ozone (O2O3) therapy in patients suffering from SARS COV–2 disease in the early phases of the disease, before worsening, up to the need of tracheal intubation. The study is based on the rationale on that the systemic oxygen-ozone treatment could be effective, positively influencing the disease evolution and/or being able to mitigate the onset of the cytokine storm syndrome at least partially.

GENERAL INFORMATION

In these times of emergency for the pandemic of SARS-CoV-2 many treatment solutions are under investigation (1). Within this scenario, the oxygen-ozone mixture, which has shown to improve oxygen delivery, but above all, has revealed a powerful anti-oedema, anti-inflammatory, and immune-regulatory activity, could represent a useful integration to other treatment strategies (2). The immune-regulatory effect can be ascribed to the anti-inflammatory activity, which is expressed through the release of cytokines with immune-stimulating and immunosuppressant power in an equal balanced equilibrium (2-5). Currently, in some cases of SARS-CoV-2 infection, an excessive release of cytokines (cytokine storm) seems to occur, especially IL-6 (5, 6). This may determine an exaggerated immune response, with detrimental effects on various organs and systems and possible onset an Acute Respiratory Distress Syndrome (ARDS) and Multi-Organ Failure (MOF). Systemic oxygen-ozone therapy could usefully interfere with this pathological mechanism (2- 5).

The therapeutic use of ozone (6-8) involves various possible methods of administration: local, intravenous, and rectal systemic, infiltrative (9-11). For patients hospitalized for CoViD-19, only the intravenous systemic pathway will be examined (12-15) (Table I). This approach will be implemented through the ozonization of a predetermined quantity of blood, in plastic bags and glass bottles (disposable certified medical devices) suitable for use in this procedure, and subsequent re-entry of the ozonized blood into the

Key words: oxygen-ozone; SARS-COV-2; COVID-19; clinical study; protocol

Corresponding Author:
Dr Stefano Marini,
Scientific Director, Dati & Ricerca S.r.l.,
Via di S. Valentino 7, 00197, Rome, Italy
Tel.: +39 335377929
e-mail: sfm.marini@gmail.com

0393-974X (2020)
Copyright © by BIOLIFE, s.a.s.
This publication and/or article is for individual use only and may not be further reproduced without written permission from the copyright holder.
Unauthorized reproduction may result in financial and other penalties
DISCLOSURE: ALL AUTHORS REPORT NO CONFLICTS OF INTEREST RELEVANT TO THIS ARTICLE.

patient's venous circulation. This procedure is not part of the transfusion procedures because the sampling and the re-introduction into the circulation takes place always using the same venous access, without detachment of the bag either during the sampling or during the re-infusion phase. In addition, the quantity collected does not exceed 200 ml and no blood storage takes place (Good clinical practices of the NuovaFIO scientific society www.lineeguidaozono.it).

RATIONALE IN THE USE OF OZONE FOR THE CURRENT HEALTH SITUATION

The oxygen-ozone systemic intravenous administration improves the oxygen delivery capacity in the body, exerts an anti-oedema action (which is expected to counteract oedema lesions) useful to improve respiratory function. The typical anti-inflammatory and immune-modulating action of the mixture could prove invaluable in improving the body's response to the virus, especially in light of the most recent evidence which relates the worsening of the clinical picture to the host's response.

In association with this therapy, the administration of antioxidants will be allowed in order to reconstitute the substrate for the therapeutic action of ozone. The administration of antioxidants (16, 17) and the dosage should be recorded in detail for each single case treated.

In consideration of the negligible risks and the potential benefit, it seems possibly useful to propose this treatment for a structured verification.

STUDY DESIGN

The study is controlled, international, multicentre, conducted in open, with a control group represented by patients with equivalent initial characteristics, but treated only with the drug therapy deemed appropriate, without oxygen-ozone. Control group data will be collected retrospectively or prospectively. The controls will be grouped in homogeneous clusters matching with the cases treated, based on the parameters of severity, age, gender, and co-morbidity.

The treatment is proposed as compassionate (adjuvant treatment) and always in association with the therapies which in any case will be identified as the most suitable for the patient's benefit. It is believed that a week of continuous treatment may be a useful period to verify the effects, as emerged from the pilot study carried out at the Misericordia hospital in Udine (March 2020, unpublished data). The study will be conducted in compliance with the regulatory rules in force in Italy, the Good Clinical Practices ICH and the Good Clinical Practices established by the "Nuova FIO" Scientific Society.

MATERIALS AND METHODS FOR OXYGEN-OZONE THERAPY TRIAL

1. Systemic intravenous treatment with oxygen-ozone therapy takes place through the collection of venous blood.
2. The volume of blood drawn will be equal to 1.5g/Kg body weight.
3. The blood is collected in a bag or in a bottle containing citrate, CE marked and having the characteristics that are intended exclusively for use for oxygen-ozone therapy.
4. The volume of blood collected is immediately mixed with a gaseous volume of oxygen/ozone at a concentration of 30 mcg/ml.
5. The blood/gas mixture ratio must be 1/1 (for example: 100 ml blood/100 ml oxygen-ozone).
6. The reinfusion of the blood added with the oxygen ozone gas mixture must be immediate.
7. Posology of Treatment: once every 24 hours.
8. Duration of treatment: seven days.
9. For further technical details, please refer to the New FIO 2019 document "Guidelines and Good Clinical Practices" (available on the web at www.lineeguidaozono.it).

MONITORING OF THE EFFECTIVENESS AND OBJECTIVES OF THE STUDY

Objective: To compare the clinical progression of patients treated with O2-O3 to that of the control group.

Monitoring parameters

NEWS Score (National Early Warning Score) (18)
G.R .; G.B .; Platelets; LDH, D-Dimer; PCR; IL6;

AST; ALT; PT Ratio.

FiO 2; PaO 2; Paco 2; Ph; VES; lactate; procalcitonin; Troponin-1; Ferritin.

PRIMARY ENDPOINTS:

Clinical progression:

a) Variation of the NEWS Score
b) Recourse to NIV
c) need for assisted ventilation by tracheal intubation
d) Onset of MOF
e) Mortality
f) Variation of the P-F RATIO (the minimum variation of 30% is considered positive outcome)
g) Variation of PaO2 in ambient air

SECONDARY ENDPOINTS:

a) Duration of subcritical conditions expressed by NEWS Score
b) Variation of IL-6
c) Variation of the ancillary laboratory data indicated above

SELECTION OF PATIENTS

Not less than 200 cases will be recruited with sequential continuous access criteria. Patients with the following characteristics will be enrolled:

1. Moderate non-hypercapnic hypoxic respiratory failure not ventilated
2. Positive confirmed buffer for COVID 19
3. Disease severity: NEWS Score Medium.

INCLUSION CRITERIA:

1. Rhino-pharyngeal swab positive for Covid-19
2. Hospitalized Patients
3. Males or females aged between 18 and 80
4. Informed Consent Signed
5. Chest CT scan with third stage changes (25% infiltrates)
6. PAO2 ≥ of 65 mmHg
7. Women of childbearing age with a negative test result prior to enrolment or in menopause or sterilized for at least one year
8. Disease severity level corresponding to the AVERAGE NEWS (National Early Warning Score) (18).

The NEWS score (18) provides 3 clinical alert levels:

- LOW: score 0: check every 12h; score from 1 to 4: check between 4-6h;
- MEDIUM: score from 5 to 6; score of 3 for a single parameter: check every hour
- HIGH: score ≥7: continuous monitoring and resuscitation advice.

Appendix I - NEWS 2 Score (National Early Warning Score) (18)

A rapid alert score (EWS) is a standardized guide for quickly determining a patient's degree of clinical severity and the timeliness and appropriateness of intervention. NEWS2 is the latest version of the National Early Warning Score (NEWS), which supports a system for standardizing the assessment and response to acute diseases. It is based on six measurements of physiological parameters: respiratory rate, oxygen saturation, body temperature; systolic pressure; heart rate; state of consciousness. Each parameter is graduated in levels, each of which is assigned a numerical value. The sum of the numerical values provides the measure of the deviation from normal physiology. The score is increased in cases where oxygen therapy is necessary (2 point increase). NEWS must not be used in children and adolescents ≤16 and in pregnant women: in these subjects the physiological response to acute states may, in fact, be different from that of the remaining patient population. Even the altered physiology of COPD patients can influence NEWS which must be corrected by clinical interpretation.

- The NEWS score provides 3 clinical alert levels:
- LOW: score 0: check every 12h; score from 1 to 4: check between 4-6h;
- MEDIUM: score from 5 to 6; score equal to 3 for a single parameter: check every hour
- HIGH: score ≥7: continuous monitoring and resuscitation advice.
- https://www.rcplondon.ac.uk/projects/outputs/national-early-warning-score-news-2

Physiological parameter	Score 3	2	1	0	1	2	3
Respiration rate (per minute)	≤8		9–11	12–20		21–24	≥25
SpO_2 Scale 1 (%)	≤91	92–93	94–95	≥96			
SpO_2 Scale 2 (%)	≤83	84–85	86–87	88–92 ≥93 on air	93–94 on oxygen	95–96 on oxygen	≥97 on oxygen
Air or oxygen?		Oxygen		Air			
Systolic blood pressure (mmHg)	≤90	91–100	101–110	111–219			≥220
Pulse (per minute)	≤40		41–50	51–90	91–110	111–130	≥131
Consciousness				Alert			CVPU
Temperature (°C)	≤35.0		35.1–36.0	36.1–38.0	38.1–39.0	≥39.1	

NEW score	Clinical risk	Response
Aggregate score 0–4	Low	Ward-based response
Red score Score of 3 in any individual parameter	Low–medium	Urgent ward-based response*
Aggregate score 5–6	Medium	Key threshold for urgent response*
Aggregate score 7 or more	High	Urgent or emergency response**

Fig. 1. *Summary table for NEWS scoring (18)*
** Response by a clinician or team with competence in the assessment and treatment of acutely ill patients and in recognising when the escalation of care to a critical care team is appropriate.*
*** The response team must also include staff with critical care skills, including airway management*

EXCLUSION CRITERIA:

1. Full presence of MOF
2. Presence of known neoplasm in treatment or follow-up for less than 5 years
3. Platelets count <50,000 mm
4. Age <18 years or> 80 years
5. G6PDH deficiency (favism) or ongoing thyroiditis
6. Women with proven pregnancy or who do not use effective contraception methods
7. Patients with coagulopathies
8. Patients with angina or myocardial infarction in the 12 months prior to potential recruitment
9. HIGH NEWS Score
10. History of drug abuse or use of illegal drugs: use of soft drugs, e.g. marijuana within 6 months from screening or hard drugs, e.g. cocaine, amphetamine, phencyclidine within 1 year of screening
11. Alcohol abuse, i.e. regular use of more than 2 units of alcohol per day or 10 units per week or medical history of alcoholism (one unit of alcohol is equal to 250 ml of beer, 125 ml of wine or 25 ml of alcohol) or alcoholics recovered
12. Patient with a history of serious psychiatric disorders
13. Expected poor patient compliance
14. Previous participation in this clinical study
15. Participation in another clinical trial at the same time or in the previous 180 days (calculated from the date of the final exam of the previous study).

EVALUATION CRITERIA

The duration of the treatment will be equal to 7 (±1) days. The systemic Oxygen-Ozone treatment in the study can be stopped at any time by the end of the 7-day treatment period, in the event of symptom resolution or for safety reasons. Patients will be

followed for a total study duration of 14 (±2) days, with a period of 7 (±1) days treatment.

Each patient will be evaluated at the following time intervals:

T0, T + 24 hours, T + 48 hours, T + 72 hours, T + 96 hours, T + 120 hours, T + 144 hours, T + 168 hours, T + 14 days

Clinical data will be collected daily for 7 days of treatment and, 7 (± 2) days after the end of therapy, when a clinical check will be carried out in the hospitalization department or by remote telephone to establish the disease evolution during follow up.

At the above time intervals and in particular at T 0 (baseline) and T + 168 hours, the following items will be evaluated:

CBC with formula, Blood gas analysis, Ferritin, LDH, D-Dimer, Creatinine, AST, ALT, IL-6, PCR, GT range, VES, Albumin, Cholesterol, PT Ratio, Troponin, Pro-calcitonin, Lactate, Serum electrolytes, T lymphocyte subpopulations, NEWS Score.

Expected duration of treatment and daily observation of the patients enrolled in the study: 7 days (the administration of O2-O3 every 24 h starting from time T + 24) plus follow-up visit after 14 days. The patient's clinical evaluation will last until the systemic oxygen and ozone treatment is discontinued and a follow-up visit will be performed on day +14, 7 days after the last O2-O3 therapy.

SAFETY ASSESSMENT

The safety assessment will be based on the results of the blood chemistry tests already foreseen and mentioned among the rating criteria. Any adverse events will be recorded and reported, with a cause-and-effect assessment by the medical investigator. All concomitant disease and concomitant medication will be recorded.

STATISTICAL EVALUATION

Being a pilot study, never previously carried out on

Table I. *Clinical study procedures summary flow-chart*

Visit	TO	T+24H	T+48H	T+72H	7+96H	T+120H	T+144H	T+168		T+14days Telephone follow-up
Day	Day 1 Screening Start of therapy							Day 8(± 1) End of treatment, 7 (± 1) days after start of therapy		Day 14 (±2) Final visit 7 (±2) days after start of therapy
Informed consent	X									
Demographics	X									
Medical history and concomitant diseases	X	X(1)	X(1)	X(1)	X(1)	X(1)	X(1)	X(1)		X(1)
Concomitant treatments	X	X(2)	X(2)	X(2)	X(2)	X(2)	X(2)	X(2)		X(2)
Lifestyle / Habits	X									
Physical exam	X	X								
Vital signs measurement	X	X								
Pregnancy test and contraception control (if woman potentially fertile)	X									
Protocol blood test	X	X	X	X	X	X	X	X		X
Inclusion / Exclusion criteria	X									
02-03 Administration to the patient	X	X	X	X	X	X	X			
Efficacy assessment by the investigator		X	X	X	X	X	X	X		
Total evaluation of efficacy by the patient		X								X(9)
Evaluation of tolerability by the investigator		X	X	X	X	X	X	X		
Adverse events reporting		X	X	X	X	X	X	X		X

(1) From Visit 2 to Visit T + 14 days, concomitant diseases changes will be reported

(2) From Visit 2 and Visit T + 14 days, concomitant treatments changes will be reported

(3) At Visit 1, information on consumption of alcohol, nicotine (including all nicotine-containing products), the history of drug abuse or use of illegal drugs will be collected

this type of pathology, the sample size (no ≥ 200) was calculated arbitrarily, in the hypothesis of collecting a sufficient number of patients representative to be able to draw reliable conclusions on the possible benefit the investigational treatment could bring to patients with COVID-19 infection.

Each participating centre will provide a series of at least 10 patients treated with Ozone according to the protocol and an equivalent number of patients treated with standard therapy, matching the 10 patients treated with ozone in terms of severity, range of age, gender, concomitant diseases and concomitant treatments.

Primary Endpoints:

1. Variation of the NEWS Score
2. Recourse to NIV
3. need for assisted ventilation by tracheal intubation
4. Onset of MOF
5. Mortality
6. Variation of the P-F RATIO (the minimum variation of 30% is considered positive outcome)
7. Variation of PaO2 in ambient air.
8. Secondary endpoints:
9. Duration of subcritical conditions expressed by NEWS Score
10. Variation of IL-6
11. Variation of ancillary laboratory data

ETHICAL CONSIDERATIONS: INFORMED CONSENT FORM

A dedicated informed consent form will be used and approved by the Ethics Committee.

Each patient will be described in detail and explained the rationale of the study, the advantages and the risks that this entails and each patient, after declaring full understanding and clearing up any doubts, will put his signature accompanied by date and time on the consent form, together with that of the proposer healthcare professional (Appendix III-IV).

Each patient will also receive a consent form for the processing of sensitive data, which however, will be anonymized during the collection and statistical processing. In compliance with the rules in force regarding sensitive personal data and rules governing clinical studies, the staff dedicated to monitoring and verification of the data collected, regulatory authorities and representatives of the Ethics Committee will have right of access to original data (Appendix V-VI). To this end, each participating clinical center will be assigned a 2-digit progressive number (01, 02, 03 ...) and after a dash, each patient recruited in the study will be attributed a progressive number, starting from 001, 002, 003. So, for example, the first patient enrolled from center 01 will be marked with the number 01-001.

CONCLUSIONS

The study will be carried out in different qualified centres treating COVID–19. The effect of the systemic administration of Oxygen Ozone will be evaluated in terms of both survival and progression of the disease compared with a control group. The outcome of this trial will enable to ascertain if oxygen-ozone therapy may effectively contribute to the fight against SARS-CoVID-19.

REFERENCES

1. https://www.aifa.gov.it/aggiornamento-sui-farmaci-utilizzabili-per-il-trattamento-della-malattia-covid19.
2. Taslipinar MY, Alp BF, Aydin I, et al. The effects of N-acetylcysteine and ozone therapy on oxidative stress and inflammation in acetaminophen-induced nephrotoxicity model. Ren Fail 2013; 35(5):640-47.
3. Chang JD, Lu HS, Chang YF, Wang D. Ameliorative effect of ozone on cytokine production in mice injected with human rheumatoid arthritis synovial fibroblast cells. Rheumatol Int 2005; 26(2):142-51.
4. 13. Bocci CA, Valacchi G, Corradeschi F, Fanetti G. Studies on the biological effects of ozone: Effect on the total antioxidant status and on interleukin-8 production. Mediators Inflamm 1998; 7(5):313-17.
5. Chang JD, Lu HS, Chang YF, Wang D. Ameliorative effect of ozone on cytokine production in mice injected with human rheumatoid arthritis synovial fibroblast cells. Rheumatol Int 2005; 26(2):142-51.
6. Zamora ZB, Borrego A, Lopez OY, et al. Effects of ozone oxidative preconditioning on TNF-α release and antioxidant-prooxidant intracellular balance in

mice during endotoxic shock. Mediators Inflamm 2005; 2005(1):16-22.
7. Bocci V, Valacchi G, Corradeschi F, et al. Studies on the biological effects of ozone: Generation of reactive oxygen species (ROS) after exposure of human blood to ozone. Biol Regul Homeost Agents 1998; 12(3):67-75.
8. Bocci V. OZONE: A new medical drug. 2nd ed. Springer 2011.
9. Viebahn-Hänsler R, León Fernández OS, Fahmy Z. ozone in medicine: the low dose ozone concept—guidelines and treatment strategies. Ozone Sci 2012; 34:408-24.
10. Zanardi I, Borrelli E, Valacchi G, Travagli V, Bocci V. Ozone. A Multifaceted Molecule with Unexpected Therapeutic Activity. Curr Med Chem 2016; 23(4):304-14.
11. Elvis, Etka A: Ozone therapy. A clinical review. J Nat Sci Biol Med 2011; 2(1):66-70.
12. Sunnen GV. SARS and Ozone therapy theoretical Considerations. (May 2003) https://www.ziondaily.com/2.0/web/health_10e/view.php?id=9389
13. Rowen RJ. Ozone and oxidation therapies as a solution to the emerging crisis in infectious disease management: a review of current knowledge and experience. Med Gas Res 2019; 9(4):232-37.
14. Rowen RJ, Robins H. A Plausible "penny" costing effective treatment for corona virus - ozone therapy. J Infect Dis Epidemiol 2020; 6:113.
15. Turrent J, Menéndez S. Ozone Therapy. Experiences in Critically ill Patients. Published on line in: Library of Medical Research 2013: https://lomr.org/ozone-therapy-experiences-in-critically-ill-patients/
16. Borrelli E, Alexandre A, Iliakis E, Alexandre A, Bocci V. Disc herniation and knee arthritis as chronic oxidative stress diseases: the therapeutic role of oxygen ozone therapy. J Arthritis 2015; 4:161.
17. Shore SA. The metabolic response to ozone. Front Immunol 2019; 10:2890.
18. Royal College of Physicians. National Early Warning Score (NEWS) 2: Standardising the assessment of acute-illness severity in the NHS. Updated report of a working party. London: RCP, 2017.

Appendix II - LIST OF CENTERS ADHERING TO THE NUOVA FIO PROTOCOL

1. Ospedale di Piacenza, Dr. Micheli
2. Ospedale Bassini Milano, Dr. Gentile
3. Ospedale Fatebenefratelli Erba (CO), Dr. Donato
4. Ospedale SS. Trinità Hospital - ASSL Cagliari, Dr. Marcia
5. Azienda Ospedaliera Universitaria Careggi (FI), Dr. Pellicanò
6. ASL Salerno Presidio Ospedaliera Vallo della Lucania (SA), Dr. Giuliani
7. ASP 7 Ragusa, Dr. Bentivegna
8. ICS Maugeri Pavia, Dr. Miotti
9. Ospedale di Rovereto, Dr. Pedrotti
10. Policlinico Universitario degli Studi di Bari, Dr. Campobasso
11. Ospedale Riuniti di Ancona, Dr. Bernardini
12. Ospedale San Luca di Lucca, Dr. Cellai
13. Ospedale San Giuseppe Empoli, Dr. Vanni
14. Ospedale Cotugno Napoli, Dr Parrella
15. Asst Valle Olona Busto Arsizio Varese, Dr Gottardello
16. Ministero della Salute Slovacchia, Dr. Vjlitelka
17. Saudi German Hospital Dubai, Dr. Piracci
18. Victor Babes Hospital, Timisoara, Romania, Dr. Tiron
19. Victor Babes Hospital, Bucarest, Romania, Dr. Tiron
20. Ospedale San Pietro Fatebenefratelli, Roma, Dr. Martinelli

Appendix III - Informed consent to health treatment with OXYGEN-OZONE
(it consists of two pages)

LAW 22 December 2017, n. 219 - Art.1 - Paragraph 3. Each person has the right to know their own health conditions and to be informed in a complete, updated and comprehensible way regarding the diagnosis, prognosis, benefits and risks of diagnostic tests and the proposed health treatments, as well as regarding the possible alternatives and the consequences of any refusal of the health treatment and diagnostic assessment or of the renunciation of the same. Patient can refuse in whole or in part to receive the information or indicate the family members or a trusted person in charge of receiving it and to express consent in his place if the patient so wishes. The refusal or renunciation of information by a person in charge is recorded in the medical

record and in the electronic health record.

Paragraph 4. The informed consent, acquired in the ways and with the tools most appropriate to the patient's condition, is documented in writing or through video recordings or, for the person with disabilities, through devices that allow them to communicate. Informed consent, in any form expressed, is included in the medical record and in the electronic health record.

Paragraph 5. Every person capable of acting has the right to refuse, in whole or in part, with the same forms as in paragraph 4, any diagnostic assessment or health treatment proposed by the doctor for his pathology or individual acts of the treatment itself. It also has the right to withdraw at any time, with the same forms as in paragraph 4, the consent given, including any indication when the withdrawal involves the interruption of the treatment.

I subscribed ……..……
Born in …….....…
on…….....…….....….

INFORMATION

I have been informed by Dr. .... to be affected by: COVID-19 I agree to be subjected to SYSTEMIC OZONE OXYGEN therapy and I declare that the signature on this form confirms the information path I had with the health professionals who will treat me, in a longer and more complete explanation than what is summarized here for brevity. I therefore declare that I have been informed verbally on the diagnosis of the disease from which I am affected, on its therapeutic indications, on the treatment to which I will be subjected. I am aware that the volumetric doses and the oxygen-ozone concentrations and the sequence of operations established by the Oxygen-Ozone Therapy Guidelines will be used (published and updated on the website ww.lineeguidaozono.it) considered the safest possible at the current state of knowledge. I am aware that systemic ozone administration is contraindicated in glucose-6-phosphate dehydrogenase (G6PD) deficiency "Favismo". Although there are no scientific studies that contraindicate their use (on the contrary, positive experiences of oxygen ozone therapy for the treatment of some pathologies related to pregnancy are reported).

I'm are aware of the possible adverse or side effects, i.e. TRANSITORY TACHYCARDIA, TRANSITIONAL LOCAL PAIN, PHLEBOPATHIES, INFECTIONS, ECCHYMOSIS AND HAEMATOMAS IN INOCULATION, VAGAL REACTIONS and what are the currently known percentages of each reported effect.

Appendix IV – CONSENT

In conclusion, after receiving the requested clarifications, I sign this document and, knowing that with the signing of the parties, the deed acquires the value of the acceptance of my informed consent and of attestation of the facts reported therein, I specifically declare:

A) to be aware that I can withdraw my consent at any time;
B) to have understood what the healthcare professional has explained and clarified, as summarized above;
C) to have discussed the details of the treatment with Dr. ..... solving all my doubts;
D) to accept the risks of therapy that have been explained to me;
E) I ask to proceed with the treatment itself;
F) consent to the execution of the oxygen-ozone therapy treatment;
G) any additional notes to be crossed where not necessary.

I authorize the physician, where necessary, to vary the planned intervention, this in order to achieve the best therapeutic effect, or in order to deal with any pathological states that are presently not yet evident.

I am aware that I can withdraw my consent at any time during the therapeutic process.

I have been informed of the potential and operational limits of the health facility in which I am hosted, as well as of the possibility of performing this therapy in other structures. I have clear that any further doubt or curiosity that could arise later, will be satisfied by the same physicians.

Place…….....…….
Date …….....……
Signature of the doctor who informed the patient
…….....

Place .....…….
Date …….....……
Patient signature …….....
(signature and date must both be signed by the patient)

Appendix V - INFORMATION ON PERSONAL DATA pursuant to art.13 of the European Regulation 2016/679 (GDPR ")

HOLDERS and PURPOSE OF THE PROCESSING

The Data Controllers of the personal data referred to or referable to it processed during the clinical study by the Title "Use of ozone as an adjuvant in the current emergency from SARS VOC 2 infection", (the "Study") are:

The promoter _____

The Center_____

Each of the Data Controllers will independently process their data and, in particular, the data related to your health (the "Data") as necessary in relation to the objective of the Study and in accordance with the provisions of GDPR, by Legislative Decree 30 June 2003 n. 196 (Italy), by the rules of good clinical practice (Legislative Decree June 24, 2003 n. 211) and as described below. The acquisition, processing, use and storage of data are indispensable for carrying out the Study; any refusal will not allow your participation in the Study.

CODING

After obtaining your personal data, the doctors who will follow you during the Study, and their collaborators, will identify you with a code (the "Code"). With the exception of your name, all the Data that will be collected or used during the Study (including date of birth, gender, weight, stature and clinical data inherent to your state of health) will be recorded, processed and stored by marking them with the Code (of below, these data will be referred to as the "Coded Data"). No personal identification (name, initials, date of birth or other data) will be included in the Coded Data. For the entire duration of the Study, your personal data may be consulted from time to time only by specifically appointed persons and for checking that the encoded data have been correctly reported from the paper files and databases of your study doctor.

PROCESSING METHODS AND COMMUNICATION OF DATA TO THIRD PARTIES

The Data will be collected, used, processed and stored both in paper and electronic format. During of the Study or after its conclusion will have access to your personal data:

• the owner's staff and the members of the Ethics Committee;

• health and control authorities;

• the investigating doctors, the person in charge of monitoring and verifying the study management methods.

Your data will not be disclosed or made available to the public. The Coded Data will be published only keeping its strictly in anonymous form at congresses and scientific conferences or through scientific or statistical publications.

HOW THE CODED DATA WILL BE USED?

The Coded Data will be used for the purposes of the Study as well as during or for the purpose of communications with competent authorities in the health sector or in other sectors;

• to support the planning of future studies;

• research compatible with the outcome of this study, including statistical purposes.

Occasionally, the Coded Data may be exported to countries that may have less standards data protection laws in force in Italy or in the European Union. Any transfer will be carried out in the manner provided for in articles 44 and following of the GDPR.

HOW LONG WILL YOUR DATA BE STORED?

The documents and records containing the Data will be kept for the maximum retention period required or permitted by local regulations.

WHAT RIGHTS DO YOU HAVE ON YOUR PERSONAL DATA?

Access rights, cancellation, limitation and portability. The interested parties are recognized the rights referred to in art. from 15 to 20 of the GDPR.

By way of example, each interested party may therefore:

• obtain confirmation that personal data processing is being processed;

• if a treatment is in progress, obtain access to personal data and information relating to processing and requesting a copy of personal data;

• obtain the correction of inaccurate personal data and the integration of incomplete personal data;

• obtain, if one of the conditions provided for by art. 17 of the GDPR, the cancellation of personal data concerning him;

• obtain, in the cases provided for by art. 18 of the GDPR, the limitation of the treatment;

• receive personal data concerning him in a structured format, commonly used and readable by automatic device and request their transmission to another holder, if

technically feasible. Right to opposition. Each interested party has the right to object at any time to the processing of his data personal data carried out for the pursuit of a legitimate interest of the Owners. In case of opposition, your personal data will no longer be processed, provided that there are no legitimate reasons for proceeding with the treatment that prevail over the interests, rights and freedoms of the interested party or for the assessment, exercise or defense of a right in court.

• Right to propose a complaint with the Guarantor. Each interested party may propose a complaint with the Guarantor for the Protection of Personal Data in the event that you believe that the rights you hold pursuant to GDPR, in the manner indicated on the Guarantor's website accessible at the address: www.garanteprivacy.it have been violated.

• For further information and communications during the study, you can contact the following staff:

Dr./Prof._____ Tel ._____

Appendix VI - CONSENT TO THE PROCESSING OF PERSONAL DATA

Having read the information above and having understood its contents, by signing this letter, I agree:

- to the processing of my personal data with the methods and purposes indicated above;
- to the possible transfer of my personal data outside the European Economic Area.

To be filled in manually by the patient

_____

_____

Name and surname of the patient in capital letters

_____

_____

Patient's signature and date

(signature and date must both be signed by the patient)

To be filled in manually by the doctor

I conducted the explanation of the protocol and the processing of personal data and I personally obtained the consent of the patient

Name and Surname of the Doctor in capital letters

_____

_____

Doctor's signature _____

Date _____

EDITORIAL

COVID-19 INDUCED BY SARS-CoV-2 CAUSES KAWASAKI-LIKE DISEASE IN CHILDREN: ROLE OF PRO-INFLAMMATORY AND ANTI-INFLAMMATORY CYTOKINES

G. RONCONI[1], G. TETÉ[2], S.K. KRITAS[3], C.E. GALLENGA[4], Al. CARAFFA[5], R. ROSS[6] and P. CONTI[7]

[1]Clinica dei Pazienti del Territorio, Fondazione Policlinico Gemelli, Rome, Italy; [2]Specialization School in Oral Surgery, Vita-Salute San Raffaele University, Milan, Italy; [3]Department of Microbiology and Infectious Diseases, School of Veterinary Medicine, Aristotle University of Thessaloniki, Macedonia, Greece; [4]PhD course Molecular Medicine, Department of Morphology, Surgery, Experimental Medicine, University of Ferrara and UOC Ophthalmology, S.M. Croci Hospital Ravenna, Italy; [5]School of Pharmacy, University of Camerino, Camerino, Italy; [6]University of Pennsylvania School of Veterinary Medicine, Philadelphia, PA, USA; [7]Postgraduate Medical School, University of Chieti, Chieti, Italy

Received May 20, 2020– Accepted June 1, 2020

Acute severe respiratory syndrome coronavirus-2 (SARS-CoV-2) caused a global pandemic coronavirus disease 2019 (COVID-19). In humans, SARS-CoV-2 infection leads to acute respiratory distress syndrome which presents edema, hemorrhage, intra-alveolar fibrin deposition, and vascular changes characterized by thrombus formation, micro-angiopathy and thrombosis. These clinical signs are mediated by pro-inflammatory cytokines. In recent studies it has been noted that COVID-19 pandemic can affect patients of all ages, including children (even if less severely) who were initially thought to be immune. Kawasaki disease is an autoimmune acute febrile inflammatory condition, which primarily affects young children. The disease can present immunodeficiency with the inability of the immune system to fight inflammatory pathogens and leads to fever, rash, alterations of the mucous membranes, conjunctiva infection, pharyngeal erythema, adenopathy, and inflammation. In the COVID-19 period, virus infection aggravates the condition of Kawasaki disease, but it has also been noted that children affected by SARS-V-2 may develop a disease similar to Kawasaki's illness.However, it is uncertain whether the virus alone can give Kawasaki disease-like forms. As in COVID-19, Kawasaki disease and its similar forms are mediated by pro-inflammatory cytokines produced by innate immunity cells such as macrophages and mast cells (MCs). In light of the above, it is therefore pertinent to think that by blocking pro-inflammatory cytokines with new anti-inflammatory cytokines, such as IL-37 and IL-38, it is possible to alleviate the symptoms of the disease and have a new available therapeutic tool. However, since Kawasaki and Kawasaki-like diseases present immunodeficiency, treatment with anti-inflammatory/immunosuppressant molecules must be applied very carefully.

Key words: cytokine; inflammation; mast cells; COVID-19; SARS-CoV-2; children; Kawasaki; immunity

Corresponding Author:
Prof. Pio Conti,
Postgraduate Medical School,
University of Chieti,
Viale Unità d'Italia 73, Chieti, Italy
Tel./Fax: +39 0871 574136
e-mail: pconti@unich.it

0393-974X (2020)
Copyright © by BIOLIFE, s.a.s.
This publication and/or article is for individual use only and may not be further reproduced without written permission from the copyright holder.
Unauthorized reproduction may result in financial and other penalties
DISCLOSURE: ALL AUTHORS REPORT NO CONFLICTS OF INTEREST RELEVANT TO THIS ARTICLE.

Acute severe respiratory syndrome coronavirus-2 (SARS-CoV-2), emerged in Wuhan City, Hubei Province, China, and caused a global pandemic coronavirus disease 2019 (COVID-19), officially declared early in 2020 by the World Health Organization (WHO). In humans, SARS-CoV-2 infection leads to respiratory syndrome ranging from light to severe to fatal pneumonia (1). Histologically, acute respiratory distress syndrome presents edema, hemorrhage and intra-alveolar fibrin deposition. In addition, COVID-19 causes vascular changes characterized by alveolar damage with fibrin thrombus formation, micro-angiopathy and thrombosis (2). All these clinical signs are mediated by the pro-inflammatory cytokines that provoke the so-called "cytokine storm". Protective measures against the novel SARS-CoV-2 have not been sufficient to guarantee the lack of infection in many patients and healthcare professionals (for example, approximately one doctor's death occurred in every 5,000) who died after being affected by COVID-19 (3). Most of the deaths were older men with previous illnesses, while women were less affected (4). The current, diagnostic gold standard of COVID-19 is carried out mostly through the transcription-polymerase chain reaction (RT-PCR) laboratory method, a molecular diagnostic research of SARS-CoV-2 RNA, although these methods are not totally error-free (5). The analysis is carried out through sputum or collection of the nasopharynx samples.

In recent studies it has been noted that the coronavirus pandemic (COVID-19) can affect patients of all ages, including children, who were initially thought to be immune, even if they have fewer symptoms and the disease is less severe. Furthermore, pregnant women affected by COVID-19 can have a preterm birth. The incubation time of the virus varies widely between individuals and can range from a minimum of 2 days to a maximum of 25 days. Veena G. Jones, et al. in an interesting article (in press), describes the case of a 6-month-old infant diagnosed with Kawasaki disease (KD), who was suffering from COVID-19 (6). This is the first case where it is shown that even children are not immune from this terrible and deadly infection. The young patient presented the classic clinical symptoms of COVID-19, including fever and systemic inflammation. Moreover, children affected by COVID-19 can present other signs including flu, mycoplasma, cough, nasopharyngeal secretions, pharyngitis, nasal congestion, runny nose, tachypnea, wheezing, diarrhea, fatigue, vomiting, and headache; but they can also be positive for the SARS-CoV-2 and be asymptomatic (7).

In addition, laboratory results may display an increase of inflammatory markers in the blood, such as creatine kinase, lactate dehydrogenase and C reactive protein (CRP), and a slight decrease in lymphocytes, showing that SARS-CoV-2 can also induce a small immunodeficiency even in children (8). In most cases, children are affected mildly by COVID-19 and are therefore almost never hospitalized in intensive care units.

The COVID-19 treatment guidelines include the intravenous use of immunoglobulin, plasma containing anti-SARS-CoV-2 antibodies, from people who had been coronavirus positive, high-doses of anti-inflammatory compounds and many other commercially available drugs (9). Fever and systemic inflammation that can involve several internal organs including the lung, kidneys, liver and glands are mediated by pro-inflammatory cytokines including IL-1 family members. Therefore, pro-inflammatory cytokine inhibitors should be added to conventional therapies. Unfortunately, these cytokines are only in the experimental stage and currently are not commercially available (10).

A large number of children and adolescents affected by COVID-19 present a mysterious disease similar to the inflammatory Kawasaki disease (KD). Although in these cases the death toll is very low, and children affected by the virus often show signs of non-serious disease; this new event worries the scientific community (6).

Kawasaki disease

There is good evidence to think that KD**,** discovered by Tomisaku Kawasaki about 50 years ago, is an autoimmune acute febrile inflammatory disease, probably infectious, which primarily affects children under 5 years of age. SARS-CoV-2 infection is thought to lead to an immunodeficiency,

with "childhood exanthem" (6). The infectious immunodeficiency theory is supported by the inability of the immune system to fight inflammatory and infective pathogens, although the pathogenesis of the disease is still unknown. This condition can present persistent high fever, rash, alterations of the mucous membranes, conjunctiva infection, pharyngeal erythema, adenopathy, inflammation of small and large arteries with persistent aneurysm dilations. In the COVID-19 period, an increase in the frequency of children with Kawasaki-like illness was noted (11). Coronavirus-19 infection aggravates the condition of Kawasaki disease, an event still unclear. Although children are less frequently affected by SARS-CoV-2, and they have less severe forms, only a small percentage are affected, many of them are carriers of the virus. At present, it is uncertain whether the virus alone can give KD-like forms. However, SARS-CoV-2 serum-positive children diagnosed by PCR swab may exhibit characteristics similar to Kawasaki disease. In these children, intravenous immunoglobulin therapy appears to be effective in curbing the disease. These observations, if investigated, could shed light on KD (12). Therefore, KD is a complication of viral immunodeficiency that affects above all the vascular system with the various attached immune cells which, once activated, produce pro-inflammatory cytokines generated by innate immune cells.

Mast cells

Mast Cells (MCs) reside in the mucosal tissues and are implicated in the pathophysiology of inflammation of various organs, including lung (13). They can be found near epithelial cells, glands, smooth muscle cells, and nerves. Since the nerves are ubiquitous and MCs are located nearby, we can deduce that these cells circulate everywhere throughout the body, including the vascular endothelium. In the perivascular space, MCs participate in the reactions of the vascularized tissue in defense of external insults, but after activation they can cause severe inflammation (14). MCs are immune cells derived from $CD34^+$ precursor cells of the hematopoietic bone marrow; they mature in the tissues and, after activation by appropriate antigens and cytokines, they participate in the inflammatory network that arises in the vascular damage that occurs in KD. Therefore, they are deeply implicated in the vascular inflammatory system of many diseases. Activated MCs can release pro-inflammatory cytokines such as interleukin (IL)-1, IL-6, IL-33, and tumor necrosis factor (TNF), fueling the severity of vasculitis in several inflammatory diseases including KD and other similar diseases. Various factors can modulate the growth, survival and function of MCs. For example, IL-1 has been reported to activate MCs to produce IL-6 without degranulation, fueling the inflammatory process (15). In fact, MCs activated by SARS-CoV-2 produce IL-1 causing the secretion of IL-6, an inflammatory process that can lead to death of the patient. Therefore, MCs are regulatory cells aid in microbial and parasitic infections, but also participate in the inflammatory state and hypersensitivity reactions mediated by pro-inflammatory cytokines, such as IL-1, IL-6, IL-33 and TNF. SARS-CoV-2 activates the innate immune system including MCs and macrophages that try to suppress viral replication, but in doing this, these cells produce pro-inflammatory cytokines that aggravate the pathological state (10). Coronavirus-19 activates MCs to release stored enzymes such as histamine, tryptase and chimase as well as cytokines, including IL-1, IL-6, IL-33 and TNF, all mediators that contribute to lung inflammation and can lead to death. This inflammatory network can be amplified in the vascular system of KD. The virus SARS-CoV-2 activates immune cells, mainly macrophages, lymphocytes and MCs that produce IL-1, an event that can lead to death in children affected by COVID-19. Excessive production of cytokines by MCs in children affected by KD can aggravate the inflammatory state with clinical consequences. In viral infections and other conditions, pro-inflammatory cytokines, in particular IL-1 and TNF, indiscriminately affect almost all cells, tissues and organs, including blood vessels (16). The inhibition of these powerful inflammatory proteins with natural antagonizing proteins could represent a new anti-inflammatory strategy that could save many human lives. Therapies based on anti-IL-1 and anti-TNF represent a new opportunity against inflammation and therefore a growing area of research for the treatment of many diseases (17). Microbial infection can lead to

septic shock and acute respiratory distress syndrome mediated by pro-inflammatory cytokines (IL-1, IL-6 and TNF) which often leads to organ dysfunction and death, events that encourage the development of new therapies aimed at blocking cytokines (18). This is the first time to our knowledge that pro-inflammatory cytokines are reported to mediate Kawasaki-like disease caused by SARS-CoV-2.

Alveolar macrophages

Macrophages, are fixed tissue cells which polarize with multiple signals, including those from viruses (19). They are born in the marrow from committed progenitor cells and through the CCR2 signal they pass through the blood and become mature monocytes which can reach the tissues where they transform into macrophages. Macrophages are cells of the innate immune system with phagocytic capacity on micro-organisms, but also capable of producing powerful inflammatory substances such as cytokines. Alveolar macrophages represent the most abundant immune cell type in airspaces and, when activated by SARS-CoV-2, they cause inflammatory reaction in the lung, provoking COVID-19 in patients. Coronavirus-19-infected subjects have mainly severe lung problems and therefore severe breathing difficulties mediated by innate immune cells. The infected pulmonary macrophages mainly release pro-inflammatory cytokines IL-1, IL-6, IL-33 and TNF and also chemokines which worsen the clinical picture in the lung. Furthermore, macrophages can express PD-1 during pathogen infection which can be associated with the severity of the disease (20). PD-1 is an immune molecule closely associated with dysfunction of $CD4^+$ and $CD8^+$ T cells and is expressed by macrophages, albeit with an unclear role. By blocking PD-1, an improvement of the innate lung activity can be obtained. In SARS-CoV-2 infection, in addition to the stimulation of pro-inflammatory cytokines, up-regulation of pro-inflammatory chemokines can also be obtained, such as CCL3, CCL5, CCL2 and CXCL10, contributing to aggravate the symptoms of COVID-19 and KD. By blocking PD-1 and/or inflammatory cytokines, an improvement in lung activity affected by viral infection can be obtained.

IL-1

IL-1 is a pro-inflammatory and immune cytokine that plays an important role both in the pathophysiological responses to infections and in inflammatory processes (21). IL-1 includes two distinct cytokines IL-1α and IL-1β ligands which bind the IL-1R1 receptor, leading to the generation of other inflammatory mediators. IL-1β is induced with the activation of caspase-1and almost all pathological virus induce IL-1 through TLR ligands (21). IL-1, and in particular IL-1α, since is constitutively present in the endothelium, plays a key role in vasculitis including Kawasaki's disease. In this disease, endothelial cell stresses occur with an increase and release of IL-1 (22). Microorganisms such as SARS-Cov-2 can activate human vascular endothelial cells to produce pro-inflammatory cytokines such as IL-1, IL-6, IL-33 and TNF. These local and systemic effects are obtained both at mRNA and protein levels. Endothelial cells can produce pro-inflammatory cytokines which, in turn, with an autocrine mechanism, can stimulate endothelial cells and mediate vasculitis. In a recent article, it was reported that by preventing signaling and blocking IL-1 with the IL-1-receptor antagonist (IL-1Ra), rapid clinical improvement and a reduction in dilation of the coronary arteries is achieved (23). Furthermore, the concentrations of some inflammatory parameters, such as reactive protein C (CRP), are also improved. However, when IL-1Ra is used to treat inflammatory diseases it is quickly destroyed by the body, and daily administration is necessary to achieve a satisfactory effect (24). These interesting results demonstrate the importance of IL-1 in Kawasaki-like disease, although further studies are needed to confirm them. Therefore, it is pertinent to think that, by using the new IL-37 and IL-38 cytokines that suppress inflammation, therapeutic improvement can be achieved in both Kawasaki-like disease and COVID-19.

IL-6

The IL-6 family is a group of cytokines consisting of IL-6, IL-11, IL-27 and other cytokines that use the same receptor (glycoprotein 130 kDa) (24). IL-6 is a four-strand cytokine that exerts its

inflammatory function by binding to its IL-6R receptor. Many immune cells can produce IL-6, including macrophages and mast cells, in response to appropriate antigen. IL-6 has a physiological defense function against viral infections, but when it is produced in excess it causes a powerful pro-inflammatory reaction. Human activated airway-MCs secrete IL-6, suggesting this might contribute to the pathogenesis of the respiratory tract including lung. In fact, inflammatory IL-6 is significantly elevated in COVID-19, and can also be induced by IL-1 (10). SARS-CoV-2 has been shown to be a very aggressive human pathogen that causes upper and lower respiratory tract infection with lethal outcome. Therefore, IL-6 secretion is associated with the pathogenesis of the virus. High levels of IL-6 produced by activated endothelial cells can participate in the "cytokine storm" phenomenon and in the coagulation system with the formation of micro-thrombi, as occurs in COVID-19. Since IL-6 has pleiotropic activity and is produced during inflammation, including that caused by SARS-CoV-2, it represents an important therapeutic target. In addition, suppression of IL-1 and IL-33 with anti-inflammatory anti-cytokines (IL-37 and IL-38) may aid in COVID-19.

IL-33

IL-33 is secreted after cellular damage by the vascular endothelium, epithelial cells and the formation of necrotic cells, and for this reason it is also called "alarmin" (21). IL-33 is produced by macrophages and MCs after viral infection, causing inflammation. This cytokine carries out its biological effect after binding to the natural ST2 receptor (25). Acute severe respiratory syndrome caused by SARS-CoV-2 is an inflammatory disease which has recently been identified, but the exact mechanism of how the virus causes disease is still largely unknown. We recently reported that MC cell Toll-like receptor (TLR4) is involved. Intra-tracheal and lung exposure to SARS-CoV-2 leads to receptor activation ST2 and IL-33 secretion. Here, we hypothesize that by blocking the IL-33 or ST2 receptor, there may be a significant decrease in the number of inflammatory cells and cytokines involved in COVID-19 inflammation. The participation of cytokines produced by MCs in COVID-19 disease could be independent of cellular activation with IgE.

TNF

TNF is a cytokine also released from many activated cells including macrophages and mast cells after proper stimulation. MCs are the only immune cells that contain preformed TNF, stored in the granules, and can be quickly released (within 10 minutes), after activation. In addition, stimulated MCs may increase TNF mRNA gene expression levels, late *de novo* synthesis, as demonstrated by Northern blot analysis (26). TNF production is attributed to the sentinel cells such as macrophages, dendritic cells and MCs. SARS-CoV-2, after the first days of infection can cause bronchial and alveolar inflammation with the involvement of epithelial and endothelial cells, a phenomenon that can also lead to cell apoptosis with the contribution of TNF. The main pathological role of TNF is to participate in the inflammatory network where other important cytokines are involved, including those of IL-1family members. TNF is an important cytokine in the pathogenesis of immune-mediated responses to infections against virus. High levels of TNF-related apoptosis-inducing ligand (TRAIL) can occur in COVID-19 disease with serious damage to the respiratory system related to the increase in infiltrations of pro-inflammatory cells in the lungs, but TRAIL can have different and contradictive roles in SARS-CoV-2 infection (27).

Recent studies show a particular interest in TNF inhibitors with anti-inflammatory therapeutic perspectives, although the use of these therapies may lead to an increased susceptibility or reactivation of concomitant infections, due to their immunosuppressive action.

IL-37

The most important property of members of the IL-1 family is pro-inflammatory, but in the past decade this family has been shown to include important anti-inflammatory cytokines (21). Of the latter, two are specific anti-receptors IL-1Ra and IL-36Ra, while another two, IL-37 and IL-38, have non-specific

broad anti-inflammatory effects. IL-37 is one of the most recently characterized cytokines and has an anti-inflammatory power (28). Various studies have described this cytokine as an immunosuppressant of both innate and acquired response. IL-37 acts in a non-specific way by suppressing several pro-inflammatory molecules, including IL-1, IL-6, IL-18, IL-33, and TNF, and also several chemokines, all mediators of COVID-19 (29). The synthesis of IL-37 occurs through the activation of TLR (and/or IL-1R), first with the generation of IL-37 mRNA and pro-IL-37 of which, through caspase-1, one part matures in the nucleus and the other, through a known protease, matures outside the cell.

Here, we assume that in Kawasaki-like illness, where the vascular system is affected by IL-1 pro-inflammatory cytokine family members, IL-37 could alleviate the symptoms of SARS-CoV-2-induced disease. However, since IL-37 is an immunosuppressant, it should be used carefully in pathological states such as Kawasaki and Kawasaki-like diseases where immunodeficiency already exists.

IL-38

IL-38 is the newest cytokine of the IL-1 family members which, by binding to IL-1R6 receptor with the cofactor IL-1R9 and IL-1RAPL1 (IL-1 receptor accessory protein-like 1), causes inhibition of inflammation (21). IL-38 has an inhibitory effect on several pro-inflammatory cytokines and on the C reactive protein (CRP) that is elevated in SARS-CoV-2 infected patients. IL-38 is mainly produced by macrophages and B cells and is present in inflamed tissues where it appears to be responsible for physically counteracting inflammation. We recently reported that IL-38 inhibits IL-1 and CXCL8 in microglia activated by neurotensin (NT). Again, this IL-37-like cytokine is likely to have inhibitory effects on COVID-19 and Kawasaki-like disease, where pro-inflammatory IL-1 family members play a key role.

Preventing the secretion of IL-1, IL-6, IL-33, and TNF from immune cells such as macrophages and MCs and their ability to cause severe inflammation, may constitute a potential new treatment approach for Kawasaki and Kavasaki-like diseases.

However, since Kawasaki and Kawasaki-like diseases present immunodeficiency, treatment with anti-inflammatory/immunosuppressant cytokines must be considered seriously and applied very carefully.

REFERENCES

1. Bhatraju PK, Ghassemieh BJ, Nichols M, et al. Covid-19 in Critically Ill Patients in the Seattle Region - Case Series. N Engl J Med 2020; 382(21):2012-22.
2. Ackermann M, Verleden SE, Kuehnel M, et al. Pulmonary vascular endothelialitis, thrombosis, and angiogenesis in Covid-19. N Engl J Med 2020; doi: 10.1056/NEJMoa2015432.
3. Yoshida I, Tanimoto T, Schiever N, Patelli F, Kami M. Characteristics of doctors' fatality due to COVID-19 in Western Europe and Asia-Pacific countries. QJM. 2020. pii: hcaa159. doi: 10.1093/qjmed/hcaa159.
4. Conti P, Younes A. Coronavirus COV-19/SARS-CoV-2 affects women less than men: clinical response to viral infection. J Biol Regul Homeost Agents 2020; 34(2). doi: 10.23812/Editorial-Conti-3. [Epub ahead of print]
5. Harahsheh AS, Dahdah N, Newburger JW. Missed or delayed diagnosis of Kawasaki disease during the 2019 novel coronavirus disease (COVID-19) Pandemic. J Pediatr 2020; doi: 10.1016/j.jpeds.2020.04.052).
6. Jones VG, Mills M, Suarez D, et al. COVID-19 and Kawasaki disease: novel virus and novel case. Hospital Pediatrics 2020; hpeds.2020-0123; doi: https://doi.org/10.1542/hpeds.2020-0123.
7. Zimmermann P. COVID-19 in children, pregnancy and neonates: a review of epidemiologic and clinical features. Pediatri Infect Dis 2020; J39(6):469-77.
8. Michael Henry B, Benoit SW, et al. Laboratory abnormalities in children with mild and severe coronavirus disease 2019 (COVID-19): a pooled analysis and review. Clin Biochem 2020; pii: S0009-9120(20)30331-3. doi: 10.1016/j.clinbiochem.2020.05.012.
9. Clemente V, D'Arcy P, Bazzaro M. Deubiquitinating enzymes in coronaviruses and possible therapeutic opportunities for COVID-19. Int J Mol Sci. 2020;21(10). pii: E3492. doi: 10.3390/ijms21103492.

10. Conti P, Ronconi G, Caraffa A, et al. Induction of pro-inflammatory cytokines (IL-1 and IL-6) and lung inflammation by Coronavirus-19 (COVI-19 or SARS-CoV-2): anti-inflammatory strategies. J Biol Regul Homeost Agents 2020; 34(2). pii: 1. doi: 10.23812/CONTI-E. [Epub ahead of print]
11. Licciardi F, Pruccoli G, Denina M, et al. SARS-CoV-2-induced Kawasaki-like hyperinflammatory syndrome: A Novel COVID phenotype in children. Pediatrics 2020; pii: e20201711. doi: 10.1542/peds.2020-1711.
12. Viner RM, Whittaker E. Kawasaki-like disease: emerging complication during the COVID-19 pandemicLancet. 2020. doi: 10.1016/S0140-6736(20)31129-6 [Epub ahead of print].
13. Casale TB, Costa JJ, Galli SJ. TNF alpha is important in human lung allergic reactions. Am J Respir Cell Mol Biol 1996; 15(1):35-44.
14. Sismanopoulos N, Delivanis DA, Mavrommati D, Hatziagelaki E, Conti P, Theoharides TC. Do mast cells link obesity and asthma? Allergy 2013; 68(1):8-15.
15. Kandere-Grzybowska K, Leterneau R, Kempuraj D, et al. IL-1 induces vesicular secretion of IL-6 without degranulation from human mast cells. J Immunol 2003;171(9):4830-6. doi: 10.4049/jimmunol.171.9.4830.
16. Conti P, Lauritano D, Caraffa A, et al. Microglia and mast cells generate proinflammatory cytokines in the brain and worsen inflammatory state: Suppressor effect of IL-37. Eur J Pharmacol 2020; 875:173035. doi: 10.1016/j.ejphar.2020.173035. Epub 2020 Feb 22.
17. Conti P, Lauritano D, Caraffa A, et al. Mast Cells Mediate Rheumatoid Arthritis-Inhibitory Role of IL-37. Crit Rev Immunol 2019;3 9(4):267-274.
18. Lauritano D, Ronconi G, Caraffa A, et al. New aspect of allergic contact dermatitis, an inflammatory skin disorder mediated by mast cells: Can IL-38 help? Med Hypotheses 2020; 139:109687. doi: 10.1016/j.mehy.2020.109687.
19. Mantovani A. Redundancy and robustness versus division of labour and specialization in innate immunity. Semin Immunol 2018; 36:28-30.
20. Ma CJ, Ni L, Zhang Y, et al. PD-1 negatively regulates interleukin-12 expression by limiting STAT-1 phosphorylation in monocytes/macrophages during chronic hepatitis C virus infection. Immunology 2011; 132(3):421-31.
21. Dinarello CA. The IL-1 family of cytokines and receptors in rheumatic diseases. Nat Rev Rheumatol 2019; 15(10):612-32.
22. Dusser P, Koné-Paut I. IL-1 Inhibition May Have an Important Role in Treating Refractory Kawasaki Disease. Front Pharmacol 2017; 8:163.
23. Cavalli G, Dinarello CA. Anakinra therapy for non-cancer inflammatory diseases. Front Pharmacol 2018; 9:1157).
24. Dinarello CA. Blocking interleukin-1β in acute and chronic autoinflammatory diseases. J Intern Med 2011;2 69(1):16-28.
25. Conti P, Lauritano D, Caraffa A, et al. New insight into systemic mastocytosis mediated by cytokines IL-1β and IL-33: Potential inhibitory effect of IL-37. Eur J Pharmacol 2019; 858:172473.
26. Conti P, Gallenga CE, Caraffa A, Ronconi G, Kritas SK. Impact of mast cells in fibromyalgia and low-grade chronic inflammation: Can IL-37 play a role? Dermatol Ther 2020; 33(1):e13191.
27. Peteranderl C, Herold S. The impact of the interferon/TNF-related apoptosis-inducing ligand signaling axis on disease progression in respiratory viral infection and beyond. Front Immunol 2017; 8:313).
28. Tsilioni I, Patel AB, Pantazopoulos H, et al. IL-37 is increased in brains of children with autism spectrum disorder and inhibits human microglia stimulated by neurotensin. Proc Natl Acad Sci U S A 2019; 116(43):21659-65.
29. Conti P, Gallenga CE, Tetè G, et al. How to reduce the likelihood of coronavirus-19 (CoV-19 or SARS-CoV-2) infection and lung inflammation mediated by IL-1. J Biol Regul Homeost Agents 2020; 34(2). doi: 10.23812/Editorial-Conti-2.

MiRNA-206 SUPPRESSES THE METASTASIS OF OSTEOSARCOMA VIA TARGETING Notch3

W.-T. CAI[1*], P. GUAN[1*], M.-X. LIN[1], B. FU[1], B. WU[1] and J. WU[1]

[1]Department of Spinal surgery, Hainan General Hospital, Hainan Affiliated Hospital of Hainan Medical University, Haikou, China; [2]Departments of Geriatrics, Hainan General Hospital, Hainan Affiliated Hospital of Hainan Medical University, Haikou, China

Received February 2, 2020 – Accepted April 16, 2020

*These Authors contributed equally to this work

To investigate the role of microRNA-206 (miRNA-206) in the malignant progression of osteosarcoma and the underlying mechanism, expression pattern of miRNA-206 in osteosarcoma tissues and cell lines was determined by quantitative real-time polymerase chain reaction (qRT-PCR). Correlation between miRNA-206 level and prognosis of osteosarcoma patients was analyzed. Regulatory effects of miRNA-206 on the proliferation and metastasis of U2OS and MG63 cells were evaluated by cell counting kit-8 (CCK-8), Transwell and wound healing assay. Through dual-luciferase reporter gene assay, the target gene of miRNA-206 was verified. A series of rescue experiments were conducted to explore the role of miRNA-206/Notch3 in regulating the malignant progression of osteosarcoma. MiRNA-206 was downregulated in osteosarcoma tissues and cell lines, and its level was correlated to poor prognosis and distant metastasis of osteosarcoma patients. Overexpression of miRNA-206 attenuated the proliferative and metastatic abilities of osteosarcoma cells, and miRNA-206 knockdown obtained the opposite trends. Notch3 was verified to be the target gene of miRNA-206, which was upregulated in osteosarcoma and accelerated osteosarcoma cells to proliferate and metastasize. Finally, rescue experiments showed that Notch3 overexpression partially reversed the regulatory effects of miRNA-206 on cellular behaviors of osteosarcoma cells. MiRNA-206 is downregulated in osteosarcoma. Overexpression of miRNA-206 accelerates osteosarcoma cells to proliferate and metastasize by targeting Notch3, thus accelerating the malignant progression of osteosarcoma.

Osteosarcoma is one of the most common primary malignancies that originates in mesenchymal tissue, and affects patients of all ages, especially children and adolescents. Over 60% of osteosarcoma patients are under 25 years of age (1). Osteosarcoma mainly involves distal femur, proximal tibia and proximal humerus. As a highly malignant tumor, lung metastasis of osteosarcoma severely influences the prognosis (2). With the advances in tumor treatment, the 5-year survival of osteosarcoma reaches 70% (3), nevertheless, lung metastasis and drug-resistance are the two difficulties in clinical treatment of osteosarcoma. Nearly 50% of osteosarcoma patients experience lung metastasis after comprehensive treatment, and 80% die of metastatic osteosarcoma within 5 years (4, 5). Prevention and control of metastatic osteosarcoma urgently need to be solved (6). Hallmarks that predict the metastasis and drug-

Key words: miRNA-206; Notch3; osteosarcoma; metastasis

Corresponding Author:
Wentao Cai, MD
Department of Spinal Surgery,
Hainan General Hospital, Hainan Affiliated Hospital of Hainan Medical University, No.19, Xiuhua Road, Xiuying District, Haikou, Hainan, 570311 China
Tel.: +86 013519882516
e-mail: cwt7724@126.com

0393-974X (2020)
Copyright © by BIOLIFE, s.a.s.
This publication and/or article is for individual use only and may not be further reproduced without written permission from the copyright holder.
Unauthorized reproduction may result in financial and other penalties
DISCLOSURE: ALL AUTHORS REPORT NO CONFLICTS OF INTEREST RELEVANT TO THIS ARTICLE.

resistance of osteosarcoma are extensively studied, in order to improve the clinical outcome of patients.

Since the discovery of miRNAs in 1993, gene therapy based on miRNAs has been well studied. MicroRNA (miRNA) is a class of single-stranded, small RNA that mediates gene expressions at post-transcriptional level (7, 8). A complex regulatory network formed by miRNA and its upstream and downstream genes participates in a series of biological processes, especially in tumor diseases (9). MiRNA is expected to serve as a therapeutic target and prognostic hallmark for tumors. Previous data analysis showed that expression of miRNA-206 was abnormal in osteosarcoma. Therefore, this study firstly investigated the expression pattern of miRNA-206 in osteosarcoma tissues and cell lines. The potential function of miRNA-206 in regulating cellular behaviors of osteosarcoma and the underling mechanism were subsequently explored.

MATERIALS AND METHODS

Sample collection

Forty-two paired osteosarcoma tissues and adjacent normal tissues were surgically resected and pathologically diagnosed. None of patients had undergone preoperative anti-tumor therapy. This study was approved by the Ethics Committee of Hainan General Hospital, Hainan Affiliated Hospital of Hainan Medical University. All subjects gave informed, signed consent to participate in the study.

Cell culture

Osteosarcoma cell lines (HOS, SOSP-9607, 143B, SaoS-2, U2OS and MG63) and osteoblasts hFOB were provided by American Type Culture Collection (ATCC) (Manassas, VA, USA). Cells were cultured in Roswell Park Memorial Institute 1640 (RPMI 1640) (HyClone, South Logan, UT, USA) containing 10% fetal bovine serum (FBS) (Life Technologies, Gaithersburg, MD, USA) and maintained in a 37°C, 5% CO_2 incubator. Medium was replaced every 2-3 days. Cell passage was conducted at 90% of confluence.

Transfection plasmids were provided by GenePharma (Shanghai, China). Cells seeded in the 6-well plates with 70% of confluence were subjected to transfection using Lipofactamine 3000 (Invitrogen, Carlsbad, CA, USA). At 48 h, cells were harvested for subsequent experiments.

Cells were seeded in the 96-well plate with 2×10^3 cells per well. Absorbance (A) at 450 nm was recorded at the appointed time points using the cell counting kit-8 (CCK-8) kit (Dojindo Laboratories, Kumamoto, Japan) for depicting the viability curve.

Transfected cells for 48 h were digested and adjusted to 5.0×10^5/mL. 200 μL/well suspension was applied in the upper side of Transwell chamber (Millipore, MA, USA). In the bottom, 700 μL of medium containing 10% FBS was applied. After 48 h of incubation, cells that migrated to the bottom were subjected to fixation in methanol for 15 min, crystal violet staining for 20 min and cell counting using a microscope. Penetrating cells were counted in 5 randomly selected fields per sample.

Cells were seeded in a 6-well plate with 5.0×10^5/well. Until 90% of confluence, a 1 mL pipette tip was used for creating an artificial wound in the confluent cell monolayer. Percentage of wound closure was calculated at 6 and 24 h, respectively.

Quantitative real-time polymerase chain reaction (qRT-PCR)

Total RNA was extracted from cells using TRIzol reagent (Invitrogen, Carlsbad, CA, USA), and purified by DNase I treatment. Extracted RNA was reversely transcribed into complementary deoxyribose nucleic acid (cDNA) using Primescript RT Reagent (TaKaRa, Otsu, Japan). The obtained cDNA was subjected to qRT-PCR using SYBR®Premix Ex Taq™ (TaKaRa, Otsu, Japan). β-actin and U6 were used as internal references. Each sample was performed in triplicate, and relative level calculated by $2^{-\Delta\Delta Ct}$ was analyzed by iQ5 2.0. Primer sequences were as follows: MiRNA-206: forward: 5'-ATCCAGTGCGTGTCGTG-3'; reverse: 5'-TGCTTGGAATGTAAGGAAG-3'; U6: forward: 5'-CTCGCTTCGGCAGCACA-3', reverse: 5'-AACGCTTCACGAATTTGCGT-3'; Notch3: forward: 5'-CGTGGCTTCTTTCTACTGTGC-3', reverse: 5'-CGTTCACCGGATTTGTGTCAC-3'; β-actin: forward: 5'-CCTGGCACCCAGCACAAT-3', reverse: 5'-GCTGATCCACATCTGCTGGAA-3'.

Dual-luciferase reporter gene assay

Cells were co-transfected with Notch3 3'UTR WT/Notch3 3'UTR MUT and NC/miRNA-206 mimics/miRNA-206 inhibitor using Lipofectamine 2000. After 24

hours, co-transfected cells were harvested for determining luciferase activity using a dual-luciferase reporter assay system (Promega, Madison, WI, USA).

Statistical analysis

Statistical Product and Service Solutions (SPSS) 22.0 software (IBM, Armonk, NY, USA) was used for data analyses. Data were expressed as mean ± standard deviation. Intergroup differences were analyzed by the *t*-test. Comparison between multiple groups was made using One-way ANOVA test followed by Post Hoc Test (Least Significant Difference). Kaplan-Meier was introduced for survival analysis, and Log-rank test was conducted to compare differences between the two curves. $P<0.05$ was considered as statistically significant.

RESULTS

MiRNA-206 was upregulated in osteosarcoma tissues and correlated to poor prognosis

Compared with adjacent normal tissues, miRNA-206 was upregulated in osteosarcoma tissues (Fig. 1 A, B). Identically, miRNA-206 level remained lower in osteosarcoma cell lines relative to osteoblasts (Fig. 1C). In the 6 selected osteosarcoma cell lines, U2OS and MG63 cells expressed the lowest levels of miRNA-206, and were selected for the following experiments.

Kaplan-Meier curves revealed worse survival in osteosarcoma patients with low-level miRNA-206 than those with high-level miRNA-206 (Fig. 1D). Moreover, follow-up data of enrolled osteosarcoma patients were analyzed. It is suggested that miRNA-206 level was negatively correlated to distant metastasis, rather than age, gender, tumor stage and lymph node metastasis (Table I). The above data illustrated that miRNA-206 may be a hallmark for predicting the malignant progression of osteosarcoma.

Overexpression of miRNA-206 suppressed proliferation and metastasis of osteosarcoma cells

To explore the biological role of miRNA-206 in osteosarcoma, we first constructed miRNA-206 mimics and inhibitor. QRT-PCR verified their transfection efficacy in U2OS and MG63 cells (Fig. 2A). Transfection of miRNA-206 mimics in U2OS cells markedly decreased the viability at 72 h and 96 h. Meanwhile, transfection of miRNA-206 inhibitor elevated the viability in MG63 cells at 72 h and 96 h (Fig. 2B). Transwell assay demonstrated fewer migratory cells after overexpression of miRNA-206 in U2OS cells, and knockdown of miRNA-206 enhanced the migratory ability in MG63 cells (Fig. 2C). Wound healing assay identically revealed that miRNA-206 overexpression decreased the percentage of wound closure, and conversely, miRNA-206 knockdown enhanced the percentage of wound closure (Fig. 2D).

Notch3 was the target gene of miRNA-206

Bioinformatics predicted the binding sequences between miRNA-206 and Notch3 (Fig. 3A, upper panel). As dual-luciferase reporter gene assay confirmed, luciferase activity decreased in osteosarcoma cells co-transfected with Notch3 3'UTR WT and miRNA-206 mimics, which was elevated by co-transfection of Notch3 3'UTR WT and miRNA-206 inhibitor (Fig. 3A, bottom panel). It is confirmed that Notch3 could bind to miRNA-206. QRT-PCR data revealed that Notch3 was upregulated in osteosarcoma tissues relative to adjacent ones (Fig. 3B). A negative correlation between miRNA-206 level and Notch3 level was identified in 30 cases of selected osteosarcoma tissues (Fig. 3C).

MiRNA-206 mediated osteosarcoma progression by inhibiting Notch3

Transfection of Notch3 overexpression plasmid greatly upregulated Notch3 level in U2OS and MG63 cells (Fig. 4A). MiRNA-206 level was downregulated by Notch3 overexpression in osteosarcoma cells (Fig. 4B). Overexpression of Notch3 enhanced the number of migratory cells as Transwell assay revealed (Fig. 4C). Besides, Notch3 overexpression elevated the percentage of wound closure (Fig. 4D). A series of rescue experiments were conducted to explore the potential function of miRNA-206/Notch3 in osteosarcoma. Co-overexpression of Notch3 and miRNA-206 reversed the downregulated Notch3 in osteosarcoma cells overexpressing miRNA-206 (Fig. 4E). At 72 h and 96 h, the decreased viability

Table I. *Association of miR-206 expression with clinicopathologic characteristics of osteosarcoma.*

Parameters	Number of cases	miR-206 expression		P-value
		High	Low	
Age (years)				0.653
<60	16	10	6	
≥60	26	18	8	
T stage				0.261
T1-T2	26	19	7	
T3-T4	16	9	7	
Lymph node metastasis				0.817
No	28	19	9	
Yes	14	9	5	
Distance metastasis				0.040
No	32	24	8	
Yes	10	4	6	

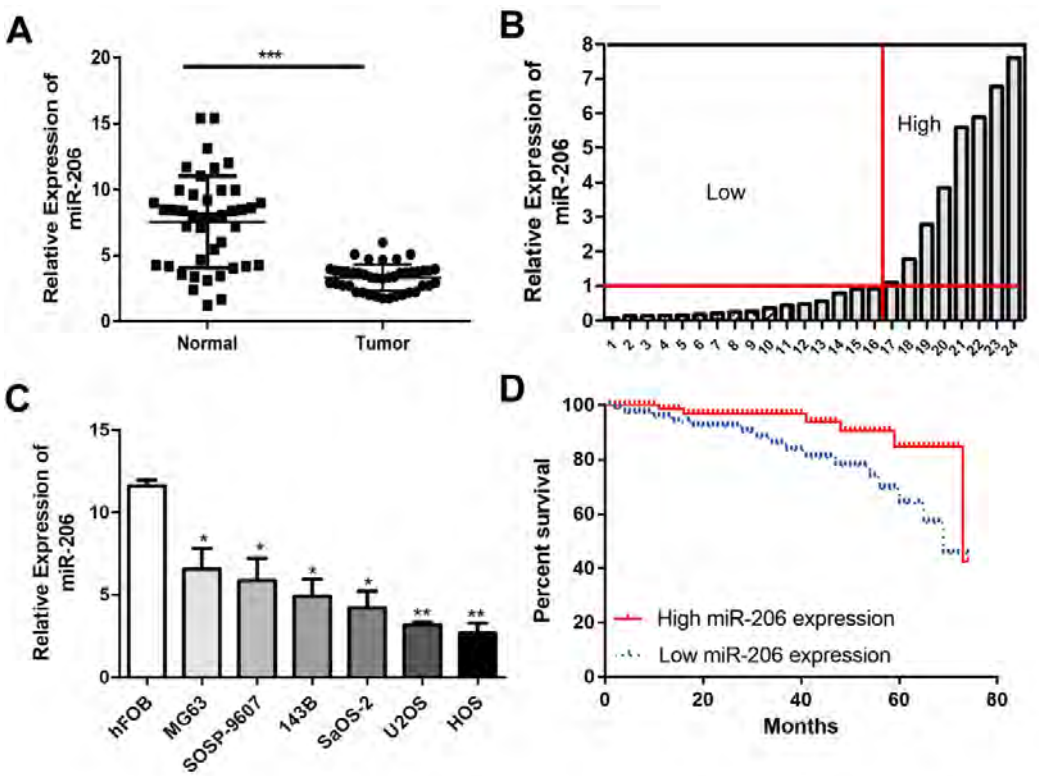


Fig. 1. *MiR-206 was upregulated in osteosarcoma tissues and correlated to poor prognosis. **A**) MiR-206 level in osteosarcoma tissues and adjacent normal tissues determined by qRT-PCR. **B**) Relative level of miR-206 in 24 cases of osteosarcoma tissues. **C**) MiR-206 level in osteosarcoma cell lines (HOS, SOSP-9607, 143B, SaoS-2, U2OS and MG63) and osteoblasts hFOB. **D**) Kaplan-Meier curves revealed the survival in osteosarcoma patients with high-level or low-level miR-206. *P<0.05, **P<0.01, ***P<0.001.*

due to miRNA-206 overexpression was reversed by co-overexpression of miRNA-206 and Notch3 (Fig. 4F). Similarly, the inhibitory effects of miRNA-206 on migration and wound closure were reversed by Notch3 overexpression (Fig. 4 G, H).

DISCUSSION

MiRNA is differentially expressed in tissues and organs. About 50% of osteosarcoma patients experience distant metastases, mainly of the lung, and they suffered a relatively poor prognosis. Prevention and inhibition of osteosarcoma metastasis are the key in osteosarcoma treatment (10-12). Potential function of miRNA-206 in osteosarcoma is rarely studied, therefore, this study firstly examined whether miRNA-206 was downregulated in osteosarcoma cell lines, suggesting a negative regulation in the metastasis of osteosarcoma.

Life quality and disease prognosis are extremely influenced by the metastasis of osteosarcoma. Gene therapy has been well studied in recent years (13-

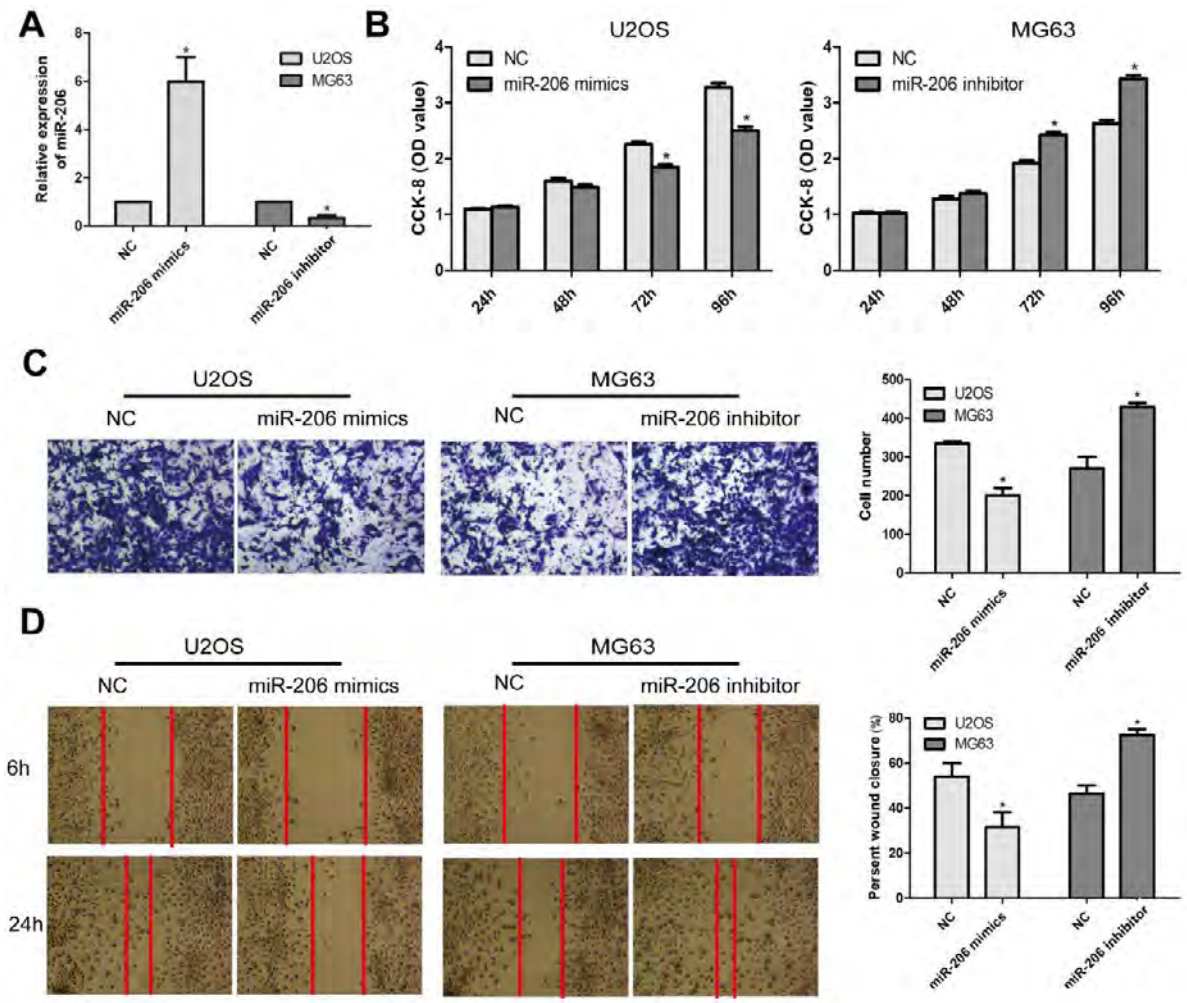


Fig. 2. *Overexpression of miR-206 suppressed proliferation and metastasis of osteosarcoma cells. **A)** Transfection efficacy of miR-206 mimics and inhibitor in U2OS and MG63 cells determined by qRT-PCR. **B)** CCK-8 assay revealed the viability in U2OS cells transfected with NC or miR-206 mimics at 24, 48, 72 and 96 h (left). Viability in MG63 cells transfected with NC or miR-206 inhibitor at 24, 48, 72 and 96 h (right). **C)** Transwell assay revealed the migration in U2OS cells transfected with NC or miR-206 mimics and that in MG63 cells transfected with NC or miR-206 inhibitor (magnification 20×). **D)** Wound healing assay revealed the percentage of wound closure in U2OS cells transfected with NC or miR-206 mimics and that in MG63 cells transfected with NC or miR-206 inhibitor (magnification 20×). *P<0.05.*

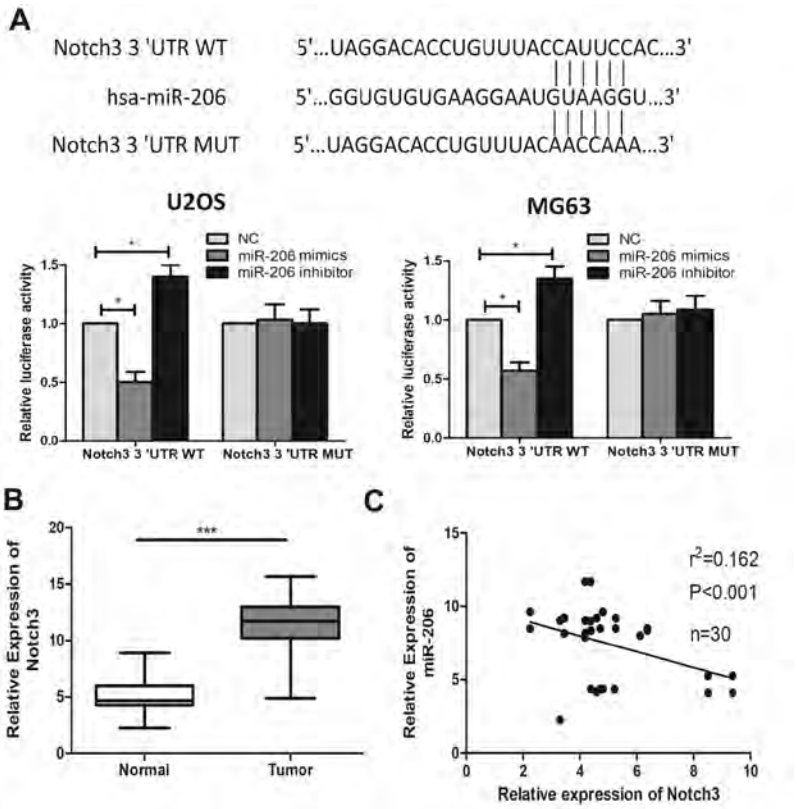


Fig. 3. *Notch3 was the target gene of miR-206.* ***A)*** *Potential binding sequences between Notch3 and miR-206 (upper panel). Relative luciferase activity in U2OS and MG63 cells co-transfected with Notch3 3'UTR WT/ Notch3 3'UTR MUT and NC/miR-206 mimics/miR-206 inhibitor (bottom panel).* ***B)*** *Notch3 level in osteosarcoma tissues and adjacent normal tissues determined by qRT-PCR.* ***C)*** *Correlation analysis on levels of miR-206 and Notch3 in 30 cases of osteosarcoma tissues. *P<0.05, ***P<0.001.*

15). MiRNAs are newly discovered non-coding, small RNAs with 22-28 nucleotides long, which are widely found in eukaryotes (16). MiRNAs degrade or inhibit translation of target miRNAs by complementary base pairing to mRNA 3'UTR, thereafter mediating gene expressions. A single miRNA has various target genes. As an endogenous RNA interference trigger, miRNA-induced cell regulation is closer to the physiological level than that of simple gene knockout (17, 18).

MiRNA-206 is a tumor-suppressor gene downregulated in many types of malignant tumors (19). This study identified the downregulation of miRNA-206 in osteosarcoma tissues, and its close correlation to pathological indexes and prognosis of osteosarcoma patients. *In vitro* effects of miRNA-206 on osteosarcoma cells were further explored. MiRNA-206 overexpression attenuated U2OS and MG63 cells to proliferate and metastasize. Knockdown of miRNA-206 obtained the opposite trends.

MiRNA regulation is a complex process involving multiple factors (19, 20). A single miRNA could be regulated by multiple upstream genes, and it also mediates multiple downstream genes, exerting diverse biological functions in tumors (20). Searching for the specific downstream genes of a miRNA contributes to clarify the underlying mechanism (20, 21). Bioinformatics is the preferred method for predicting the potential targets of a miRNA, followed by functional verification (21). The predictive principle of the bioinformatics method is to theoretically rank, sort and screen the possible targets according to the complementary strand (22, 23). A large number of potential targets could be quickly obtained through this method, however, the predicted targets require further verification (23). In this study, the regulatory mechanism of

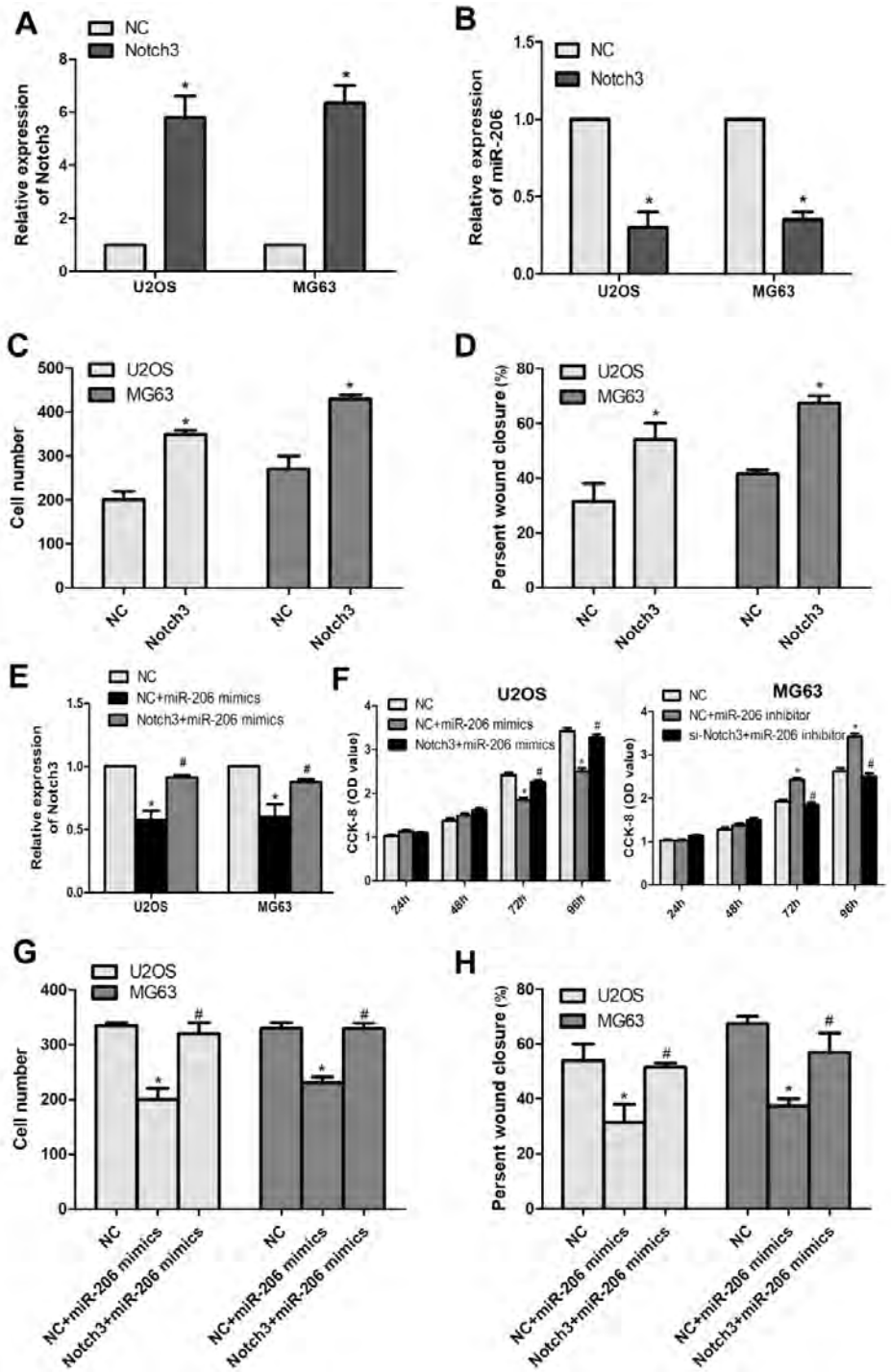


Fig. 4. *MiR-206 mediated osteosarcoma progression by inhibiting Notch3.* ***A)*** *Transfection efficacy of Notch3 overexpression plasmid in U2OS and MG63 cells determined by qRT-PCR.* ***B)*** *Relative level of miR-206 in U2OS and MG63 cells transfected with Notch3 overexpression plasmid or NC.* ***C)*** *Transwell assay revealed the migration in U2OS and MG63 cells transfected with Notch3 overexpression plasmid or NC.* ***D)*** *Wound healing assay revealed the percentage of wound closure in U2OS and MG63 cells transfected with Notch3 overexpression plasmid or NC. U2OS and MG63 cells were transfected with NC, NC+miR-206 mimics or Notch3 overexpression plasmid+miR-206 mimics.* ***E)*** *Relative level of Notch3 in each group.* ***F)*** *CCK-8 assay revealed the viability at 24, 48, 72 and 96 h.* ***G)*** *Transwell assay revealed the migration in each group.* ***H)*** *Wound healing assay revealed the percentage of wound closure in each group. *#P<0.05.*

miRNA-206 on the metastases of osteosarcoma was not clear, thus, we attempted to provide a novel basis for targeted therapy for osteosarcoma from the aspect of the miRNA-mRNA interaction. miRanda, TargetScan and PicTar were used to predicte the potential targets of miRNA-206. After online prediction and literature review, Notch3 was finally screened out and its functional role in osteosarcoma was further investigated. Notch3 was upregulated in osteosarcoma tissues. In 30 cases of selected osteosarcoma tissues, a negative correlation was identified between miRNA-206 level and Notch3 level. Identically, the mRNA level of Notch3 was negatively regulated by miRNA-206 in U2OS and MG63 cells. Overexpression of Notch3 markedly accelerated the proliferative and metastatic abilities of osteosarcoma cells. A series of rescue experiments demonstrated that Notch3 overexpression partially reversed the regulatory effects of miRNA-206 on cellular behaviors of osteosarcoma cells. It is concluded that miRNA-206/Notch3 axis exerted a vital role in the progression of osteosarcoma.

In conclusion, miRNA-206 is downregulated in osteosarcoma. Overexpression of miRNA-206 accelerates osteosarcoma cells to proliferate and metastasize by targeting Notch3, thus accelerating the malignant progression of osteosarcoma.

ACKNOWLEDGEMENTS

This study was funded by the General Scientific Research Project of Hainan Provincial Department of Health (Project No.: 14a210267); Project of Hainan Natural Science Foundation (Project No.: 20158345)

REFERENCES

1. Clark JC, Dass CR, Choong PF. A review of clinical and molecular prognostic factors in osteosarcoma. J Cancer Res Clin Oncol 2008; 134:281-97.
2. Berman SD, Calo E, Landman AS, et al. Metastatic osteosarcoma induced by inactivation of Rb and p53 in the osteoblast lineage. Proc Natl Acad Sci U S A 2008; 105:11851-56.
3. Janeway KA, Grier HE. Sequelae of osteosarcoma medical therapy: a review of rare acute toxicities and late effects. Lancet Oncol 2010; 11:670-78.
4. Niswander LM, Kim SY. Stratifying osteosarcoma: minimizing and maximizing therapy. Curr Oncol Rep 2010; 12:266-70.
5. Broadhead ML, Clark JC, Choong PF, Dass CR. Making gene therapy for osteosarcoma a reality. Expert Rev Anticancer Ther 2010; 10:477-80.
6. Osborne TS, Khanna C. A review of the association between osteosarcoma metastasis and protein translation. J Comp Pathol 2012; 146:132-42.
7. Ambros V. microRNAs: tiny regulators with great potential. Cell 2001; 107:823-26.
8. Inui M, Martello G, Piccolo S. MicroRNA control of signal transduction. Nat Rev Mol Cell Biol 2010; 11:252-63.
9. Baffa R, Fassan M, Volinia S, et al. MicroRNA expression profiling of human metastatic cancers identifies cancer gene targets. J Pathol 2009; 219:214-21.
10. Ren L, Hong SH, Cassavaugh J, et al. The actin-cytoskeleton linker protein ezrin is regulated during osteosarcoma metastasis by PKC. Oncogene 2009; 28:792-802.
11. Khanna C, Wan X, Bose S, et al. The membrane-cytoskeleton linker ezrin is necessary for osteosarcoma metastasis. Nat Med 2004; 10:182-86.
12. Khanna C, Khan J, Nguyen P, et al. Metastasis-associated differences in gene expression in a murine model of osteosarcoma. Cancer Res 2001; 61:3750-59.
13. Zhang P, Yang Y, Zweidler-McKay PA, Hughes DP. Critical role of notch signaling in osteosarcoma invasion and metastasis. Clin Cancer Res 2008; 14:2962-69.
14. Guo Y, Zi X, Koontz Z, et al. Blocking Wnt/LRP5 signaling by a soluble receptor modulates the epithelial to mesenchymal transition and suppresses met and metalloproteinases in osteosarcoma Saos-2 cells. J Orthop Res 2007; 25:964-71.
15. Lafleur EA, Koshkina NV, Stewart J, Jia SF, Worth LL, Duan X, Kleinerman ES. Increased Fas expression reduces the metastatic potential of human osteosarcoma cells. Clin Cancer Res 2004; 10:8114-19.
16. Zhang B, Pan X, Cobb GP, Anderson TA. microRNAs as oncogenes and tumor suppressors. Dev Biol 2007; 302:1-12.

17. Kong YW, Ferland-McCollough D, Jackson TJ, Bushell M. microRNAs in cancer management. Lancet Oncol 2012; 13:e249-e258.
18. Zhang W, Dahlberg JE, Tam W. MicroRNAs in tumorigenesis: a primer. Am J Pathol 2007; 171:728-38.
19. Meister G, Landthaler M, Patkaniowska A, Dorsett Y, Teng G, Tuschl T. Human Argonaute2 mediates RNA cleavage targeted by miRNAs and siRNAs. Mol Cell 2004; 15:185-97.
20. Reinhart BJ, Weinstein EG, Rhoades MW, Bartel B, Bartel DP. MicroRNAs in plants. Genes Dev 2002; 16:1616-26.
21. Hutvagner G, Zamore PD. A microRNA in a multiple-turnover RNAi enzyme complex. Science 2002; 297:2056060.
22. Lim LP, Lau NC, Garrett-Engele P, et al. Microarray analysis shows that some microRNAs downregulate large numbers of target mRNAs. Nature 2005; 433:769-73.
23. Doench JG, Sharp PA. Specificity of microRNA target selection in translational repression. Genes Dev 2004; 18:504-11.

CYCLOOXYGENASE-2 INHIBITOR ROFECOXIB PREVENTS CHONDROCYTES AGAINST HYPERTROPHY VIA Wnt/β-CATENIN PATHWAY

Y.-R. YANG[1*], X.-F. YANG[1*], H.-C. DUAN[1] and J.-Q. QIAO[2]

[1]Department of Gastroenterology, Gansu Gem Flower Hospital, Lanzhou, China;
[2]Department of Orthopaedic, Gansu Gem Flower Hospital, Lanzhou, China

Received February 6, 2020 – Accepted April 20, 2020

[*]These Authors contributed equally to this work

Previous reports indicated that specific cyclooxygenase-2 (COX-2) inhibitor suppresses osteoarthritis (OA). This study aimed to further explore the possible mechanism of Rofecoxib as a COX-2 inhibitor on the inhibition of chondrocyte (CH) hypertrophic development and tested the optimal treatment of Rofecoxib on CH. Basically, IL-1β was used as a stimulus to establish a degenerated CH model. Immunofluorescence, Western blot, and RT-PCR were performed to determine the gene expression of Axin2, β-catenin, GSK3β, collagen X, collagen II, COX-2, PGE-2, SOX-9, Runx-2, and MMP-13 expression. Cell Counting Kit (CCK-8) assay was used to analyze the viability of CHs. The data indicated that Rofecoxib significantly inhibited COX-2 expression and had less harmful effects on CH viability. Rofecoxib reversed the IL-1β-induced upregulation of collagen X, COX-2, PGE-2, Runx-2, and MMP-13 expression, and promoted the viability of collagen II, SOX-9 expression of CHs. Furthermore, Rofecoxib suppressed Axin2, β-catenin, and GSK3β expression of the Wnt pathway, which was activated by IL-1β or human recombinant Wnt-1 protein treatment. Therefore, Rofecoxib is an effective COX-2 inhibitor that protects CHs from hypertrophy by suppression of the Wnt/β-catenin pathway.

Osteoarthritis (OA) is a chronic degenerative disease with progressive articular cartilage damage among the elderly population. There is no specific drug for OA treatment. The primary purpose of the clinical therapeutic strategy is to reduce the load on the joints, delay the progression of the disease, and alleviate the symptoms. Non-steroidal anti-inflammatory drugs and analgesics are commonly used for patients in the acute phase (1). Joint replacement is mainly suitable for advanced patients, and is the best way to correct deformity and eliminate symptoms. Articular cartilage damage can be caused by advanced age, obesity, prolonged strain, and trauma (2). Compensatory hyperplasia of subchondral bone, metalloproteinases (MMPs), and various inflammatory factors have essential effects on the chronic degradation and development of OA. MMPs are involved in mediating collagen degradation processes of OA, while arachidonic acid metabolites are involved in mediating pain and inflammation (3). Cyclooxygenase (COX) metabolizes arachidonic acid to form prostaglandin H2 (PGH2), which is then metabolized by prostaglandin E (PGE) synthase to PGE2, an inflammatory mediator promoting the progression of OA (4).

Safe and effective specific COX-2 inhibitors have

Key words: cyclooxygenase-2 inhibitor; Rofecoxib; chondrocyte hypertrophy; Wnt/β-catenin

Corresponding Author:
Jingquan Qiao, BM
Department of Gastroenterology,
Gansu Gem Flower Hospital, No. 731, Fuli West Road,
Xigu District, Lanzhou, Gansu, 730060, China
Tel./Fax: +86015117102052
e-mail: jingqucan19740613@163.com

0393-974X (2020)
Copyright © by BIOLIFE, s.a.s.
This publication and/or article is for individual use only and may not be further reproduced without written permission from the copyright holder.
Unauthorized reproduction may result in financial and other penalties
DISCLOSURE: ALL AUTHORS REPORT NO CONFLICTS OF INTEREST RELEVANT TO THIS ARTICLE.

been widely used in the clinical treatment of OA. *In vitro* experiments have confirmed that specific COX-2 inhibitors do not affect the function of normal articular chondrocytes (CHs), but reverse the imbalance of proteoglycan (PG) metabolism caused by inflammatory cytokines, indicating its protective and repairing effects on the cartilage (5). Expression of COX-2 in OA explant CHs produces PGE2, reduces proteoglycan synthesis, and increases degradation of aggrecan and type II collagen, accompanied by MMP-13 and ADAMTS-5 upregulation (6). Articular cartilage in OA undergoes devastating changes with a hypertrophic CH phenotype and is associated with the activation of the Wnt/β-catenin pathway and increased MMP-13 production (7, 8). Aberrant activation of β-catenin could lead to a hypertrophic phenotype of CH (9). Evidence has verified that COX-2 activates Wnt/β-catenin and mediates cell metabolism in many aspects. He et al. facilitated COX-2 regulating VSMC calcification by activating Wnt/β-catenin pathway (10). Based on canonical Wnt signaling, COX-2 promotes osteoblast differentiation but inhibits CH differentiation in CD90+ mSSCs (11). In addition, suppressing COX-2 expression results in an inhibition of the Wnt/β-catenin signaling pathway, which contributes to chondroprotective activity (12-14). Therefore, specific COX-2 inhibitors are now widely used in the treatment of OA (15, 16). Previous research showed that selective COX-2 inhibitor decreases β-catenin protein levels in adenomatous polyposis coli (17). Golovchenko et al. reported that β-catenin deficiency impairs trabecular bone formation in hypertrophic CHs (18).

In this research, we tested Rofecoxib, an efficient and safe COX-2 inhibitor that has been approved in OA rheumatoid arthritis (RA) treatment, to elucidate its anti-hypertrophic effect via the suppression of Wnt/β-catenin signaling pathway. The results of our study supply a novel understanding of Rofecoxib and another COX-2 inhibitor in the therapy of OA.

MATERIALS AND METHODS

Patient tissue samples collection

We collected knee cartilages from 3 patients (1 male and 2 females, with an average age of 36 years) undergoing amputation for malignant bone neoplasms of femur proximal end, none of whom had a personal history of OA. Specimens were taken from the cartilage area at the

Table I. *Primer sequences of the genes for RT-PCR*

Gene name	Forward (5'>3')	Reverse (5'>3')
Collagen II	TGGACGATCAGGCGAAACC	GCTGCGGATGCTCTCAATCT
SOX-9	AGCGAACGCACATCAAGAC	CTGTAGGCGATCTGTTGGGG
Runx-2	TGGTTACTGTCATGGCGGGTA	TCTCAGATCGTTGAACCTTGCTA
COX-2	CTGGCGCTCAGCCATACAG	CGCACTTATACTGGTCAAATCCC
PEG-2	CGCCTCAACCACTCCTACAC	GACACCGATCCGCAATCCTC
MMP-13	AGGGCAGAATCATCACGAAGT	AGGGTCTCGATTGGATGGCA
Axin2	CAACACCAGGCGGAACGAA	GCCCAATAAGGAGTGTAAGGACT
β-catenin	CCTATGCAGGGGTGGTCAAC	CGACCTGGAAAACGCCATCA
GSK3β	GGCAGCATGAAAGTTAGCAGA	GGCGACCAGTTCTCCTGAATC
GAPDH	ACAACTTTGGTATCGTGGAAGG	GCCATCACGCCACAGTTTC

RT-PCR: quantitative reverse-transcription polymerase chain reaction

edge of the exposed area of the articular surface. The knee osteoarticular cartilage specimens were all obtained with the patients' consent: patients volunteered to participate in this project, and all information related to patient privacy was confidential.. The present study was approved by the Ethics Committee of Gansu Gem Flower Hospital.

CHs isolation and treatment

The separation of articular CHs was performed by one-step digestion with type II collagenase. The soft tissue attached around the joints was removed, and then the thin layer of cartilage on the surface was scraped. The cartilage was cut into pieces and mixed with 0.15% type II collagenase (DMEM/F-12 solution) in an oscillating box (37°C, 80 r/min) for 4-6 h. After the cartilage tissue disappeared and the digestive juice became cloudy, the medium was centrifuged at 1,000 r/min for 8 min and the supernatant was discarded to collect the CHs. CHs were seeded into 25 cm^2 flasks at a concentration of 1×10^8 L^{-1} and cultured in the medium (DMEM/F12 containing 10% fetal bovine serum, Gibco, Rockville, MD, USA). The passage 0 or 1 CHs were treated with a ranged concentration of Rofecoxib (0-4 nM), and cultured with 3 nM Rofecoxib for ranged time points (0-72 h). IL-1β (10 ng/ml) was used to degenerate CHs, and human recombinant wnt1 (19) (2.5 ng/ml, ab84080. Abcam, USA) protein was used to activate the Wnt signaling pathway.

Immunofluorescence

Cell coverslips were fixed with 4% paraformaldehyde for 20 min, permeabilized with 0.2% Triton-X-100 for 10 min, and PBS-BSA (5% bovine serum albumin (BSA) in phosphate buffered saline (PBS) incubated for 30 min. The type X collagen antibody (ab58632, Abcam, USA) was added and incubated overnight at 4°C. The next day, goat anti-rabbit Dylight 568 fluorescent secondary antibody (Invitrogen, Carlsbad, CA, USA) and 4',6-diamidino-2-phenylindole (DAPI) were added to incubate at room

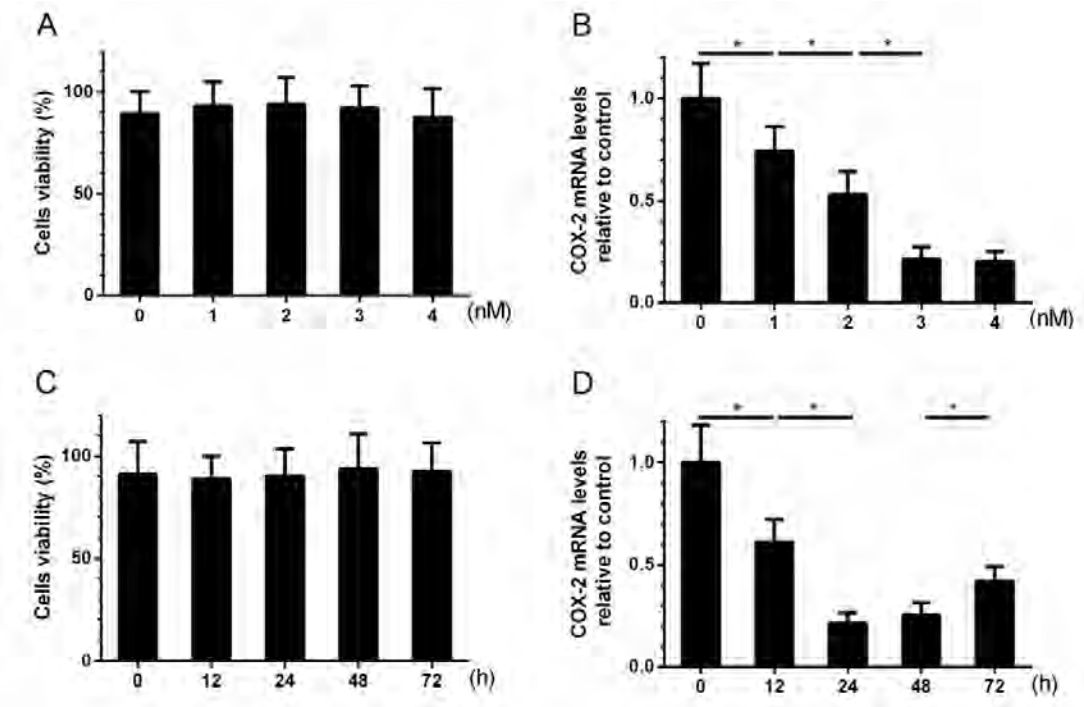


Fig. 1. *Rofecoxib made less deleterious effects on CHs viability. CHs was cultured with different concentration of Rofecoxib (0-4 nM) for 24 h, or cultured with 3 nM Rofecoxib for 0-72 h.* ***A, C****) Cell viability was measured by CCK8 assay.* ***B, D****) mRNA levels of COX-2 were determined by RT-PCR. The values are mean ± SD of three independent experiments. (*P < 0.05 compared to control)*

temperature for 1 h. The fluorescence intensity was observed under an inverted fluorescence microscope.

Reverse transcription-PCR (RT-PCR) analysis

After the intervention, the TRIzol kit (Invitrogen, Carlsbad, CA, USA) was used to extract the total RNA of CHs and identify their purity and integrity. The mRNA was reverse-transcribed into cDNA through 95°C denaturation for 15 s, annealing at 60°C for 30 s, extension at 72°C for 75 s for 40 times cycle. Primer probes against PEG-2, COX-2, collagen II, SOX-9, MMP-13, Runx-2, Axin2, β-catenin, and GSK3β were designed according to the sequence of Genbank shown as Table I. Gene expression was normalized to glyceraldehyde 3-phosphate dehydrogenase (GAPDH) and calculated according to the method of $2^{-\Delta\Delta Ct}$.

Western blot

CHs were lysed on ice with radioimmunoprecipitation assay (RIPA) lysate (Beyotime, Shanghai, China) for 30 min and transferred to a 1.5 mL centrifuge tube. After centrifugation at 4°C for 10 min, the supernatant was taken, and the protein concentration was determined by the bicinchoninic acid (BCA) method (Beyotime, Shanghai, China). 50 μg protein was subjected to electrophoresis at 100 V via sodium dodecyl sulfate-polyacrylamide gel electrophoresis (SDS-PAGE) and transferred onto the polyvinylidene fluoride (PVDF) membranes (Millipore, Billerica, MA, USA). The membrane was then blocked by 5%~10% skim milk for 1 h. After washing, Axin2 (ab32197, Abcam, USA), β-catenin (ab32572, Abcam, USA), and GSK3β (ab93926, Abcam, USA) primary antibody was added and incubated at 4°C overnight. The membrane was incubated with secondary antibody for 2 h at room temperature. Then the chemiluminescence electrochemiluminescence (ECL) substrate (Beyotime, Shanghai, China) was added to expose the bands. The image was subjected to data conversion processing using ImageJ software (Rawak Software, Inc., Hamburg, Germany) with the ratio of the gray value of the target bands to the control.

Cell viability assay

The viability of CHs was measured with the Cell Counting Kit (CCK-8) method. NP cells were seeded and incubated for cell attachment. The cells were then treated with specific drugs for indicated time points. CHs seeded at 1×10^4/well in 96-well plates were produced with CCK8 kit (Beyotime, Shanghai, China) according to the manufacturer's instructions. The intensity of the CCK8 product was detected by a microplate reader. Cell viability was shown as a percentage relative to non-treated value.

Statistical analysis

The experimental data were statistically analyzed by SPSS 19.0 statistical software (SPSS IBM, Armonk, NY USA). All the experimental data were expressed as mean ± standard deviation (SD). Differences between two groups were analyzed by using the Student's *t*-test. A comparison between multiple groups was made using One-way ANOVA test followed by Post Hoc Test (Least Significant Difference). $P< 0.05$ indicates that the difference was significant.

RESULTS

Rofecoxib exerts little toxic effects toward CHs viability

To determine the optimized concentration and stimuli time of Rofecoxib, we used the CCK8 assay to analyze the viability of CHs and RT-PCR to detect the suppressed efficiency of COX-2. As shown in Fig. 1 A and B, CHs were cultured with a concentration of Rofecoxib ranging from 0 to 4 nM for 24 h; there were no significant differences among the concentrations to the viability of CHs. Additionally, the mRNA expression of COX-2 was gradually decreased until 3 nM as well as 4 nM. Therefore, 3 nM Rofecoxib was used to test the appropriate stimuli time, which maintained from 0 to 72 h. The result indicated Rofecoxib was little toxic to CHs and forcefully suppressed the expression of COX-2 at the time point of 24 h (Fig. 1 C, D). Therefore, Rofecoxib is safe for culturing CHs *in vitro*. The results also showed that Rofecoxib can suppress COX-2 expression at an optimal concentration of 3 nM with 24 h culture.

Rofecoxib prevents CHs from IL-1β induced hypertrophy

To determine whether Rofecoxib plays a role in the hypertrophic progress of CHs, we used IL-1β to accelerate the degeneration of CH and tested the hypertrophic makers of CH. Under the treatment

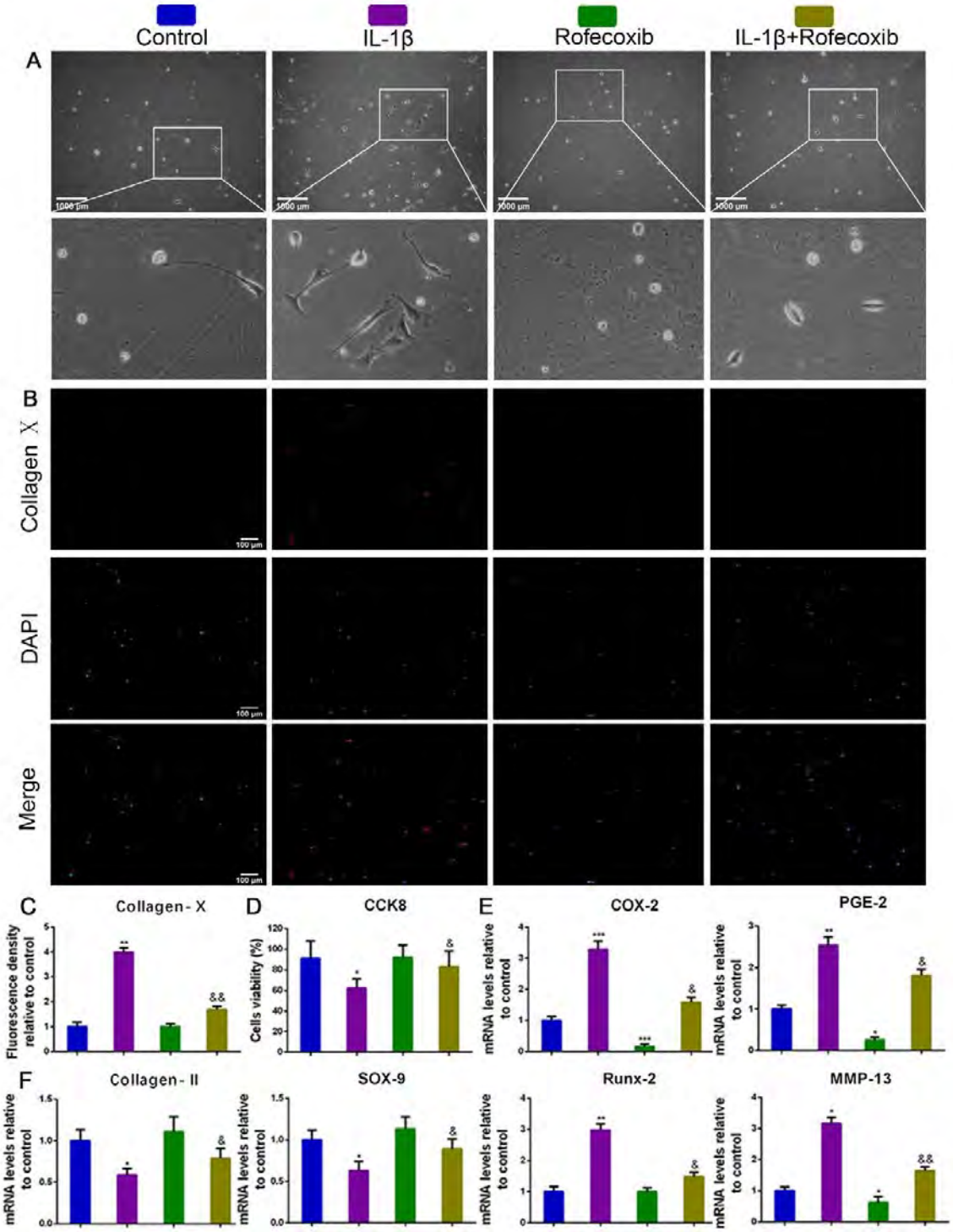


Fig. 2. *Rofecoxib prevents CHs from IL-1β induced hypertrophy. CHs were pre-cultured with IL-1β (10 ng/ml) or Rofecoxib (3 nM) for 24 h. For co-treated group, CHs were pre-cultured with IL-1β (10 ng/ml) 24 h, and then treated with Rofecoxib (3 nM) for further 24 h.* ***A****) CHs after stimulation (magnification:40×).* ***B***, ***C****) Protein expression level of collagen X was determined by (B) immunofluorescence (magnification: 200×) and (C) quantification analysis.* ***D****) Cell viability was measured by CCK8 assay.* ***E, F****) The mRNA expression levels of (E) COX-2, PGE-2, and (F) collagen II, SOX-9, Runx-2, and MMP-13 were assayed by RT-PCR. The values are mean ± SD of three independent experiments. (*P < 0.05, **P < 0.01, ***P < 0.001 compared to control; &P < 0.05, &&P < 0.01 compared to IL-1β)*

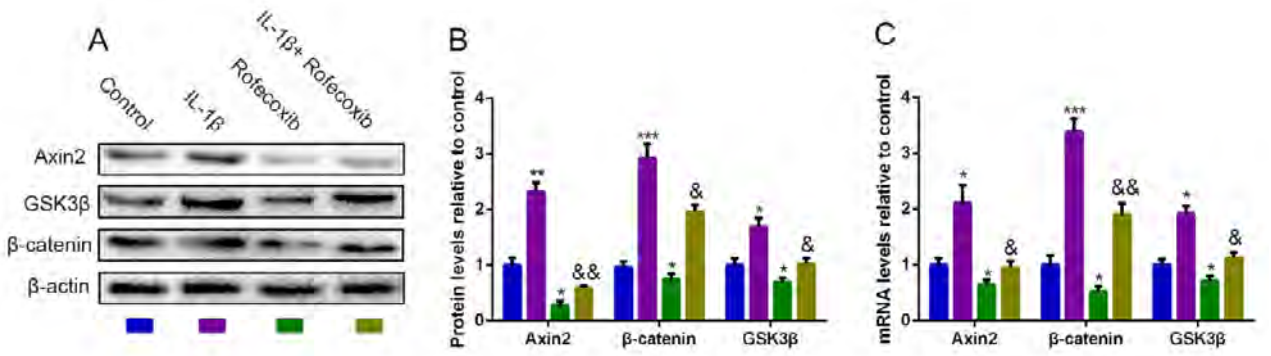


Fig. 3. *Rofecoxib suppresses IL-1β induced Wnt/β-catenin pathway in CHs. CHs were pre-cultured with IL-1β (10 ng/ml) or Rofecoxib (3 nM) for 24 h. For co-treated group, CHs were pre-cultured with IL-1β (10 ng/ml) 24 h, and then treated with Rofecoxib (3 nM) for another 24 h.* ***A***, ***B****)The protein expression level of Axin2, GSK3β, and β-catenin were determined by (A)WB and (B) quantification analysis.* ***C****) Axin2, GSK3β, and β-catenin mRNA expression were assayed by RT-PCR. The values are mean ± SD of three independent experiments. (*P < 0.05, **P < 0.01, ***P < 0.001 compared to control; &P< 0.05, &&P < 0.01 compared to IL-1β).*

of IL-1β, the morphology of CHs changed from elliptical, round to long, hypertrophic with many tentacles. However, Rofecoxib partly reversed the side effect of IL-1β, which kept the basic shape of CHs (Fig. 2A). Collagen X was markedly overexpressed in hypertrophic CHs compared with the CHs. In our study, IL-1β significantly increased the level of Collagen X which was while Rofecoxib had the opposite effects (Fig. 2 B, C). After treatment with IL-1β, Rofecoxib not only obviously suppressed the mRNA expression of COX-2, resulting in a reduction of PGE-2 but also contributed to the viability of CHs (Fig. 2 D, E). In addition, compared with the control group, IL-1β treatment led to a significant hypertrophic phenotype by the upregulation of MMP-13 and Runx-2 mRNA levels but downregulation of collagen II and SOX-9. However, Rofecoxib powerfully resisted the upregulation of MMP-13 and Runx-2 and resulted as a protective role in collagen II and SOX-9 (Fig. 2F). These results suggested Rofecoxib efficiently inhibits COX-2 expression and prevents CHs from IL-1β-induced hypertrophy.

Rofecoxib suppresses IL-1β induced Wnt/β-catenin pathway in CHs

To determine whether IL-1β induces CH hypertrophy by the activation of Wnt/β-catenin pathway and whether Rofecoxib plays a role in suppression of Wnt/β-catenin pathway, we measured the Axin2, GSK3β, and β-catenin protein and mRNA expression under the stimulation of IL-1β with or without Rofecoxib. As shown in Fig. 3 A and B, Axin2, GSK3β, and β-catenin were significantly suppressed by Rofecoxib but upregulated by IL-1β. Rofecoxib also obviously resisted the IL-β-induced Axin2, GSK3β, and β-catenin upregulation. The result of RT-PCR was also parallel to the protein levels (Fig. 3C). The data indicated that IL-1β could activate the Wnt/β-catenin pathway in CHs, which could be inhibited by Rofecoxib.

Rofecoxib prevents CHs from hypertrophy via the suppression of Wnt/β-catenin pathway

To determine whether the activation of the Wnt/β-catenin pathway is related to the hypertrophic progress of CH, we used the active human recombinant Wnt-1 to upregulate the gene expression in the Wnt pathway. We observed that Wnt-1 protein made the CHs go into hypertrophic morphology, and Rofecoxib could alleviate this progression (Fig. 4A). Moreover, Rofecoxib also suppressed the collagen X expression, which was activated by Wnt-1 protein, and the effect was more significant with a higher concentration treatment (Fig. 4 B, C). As

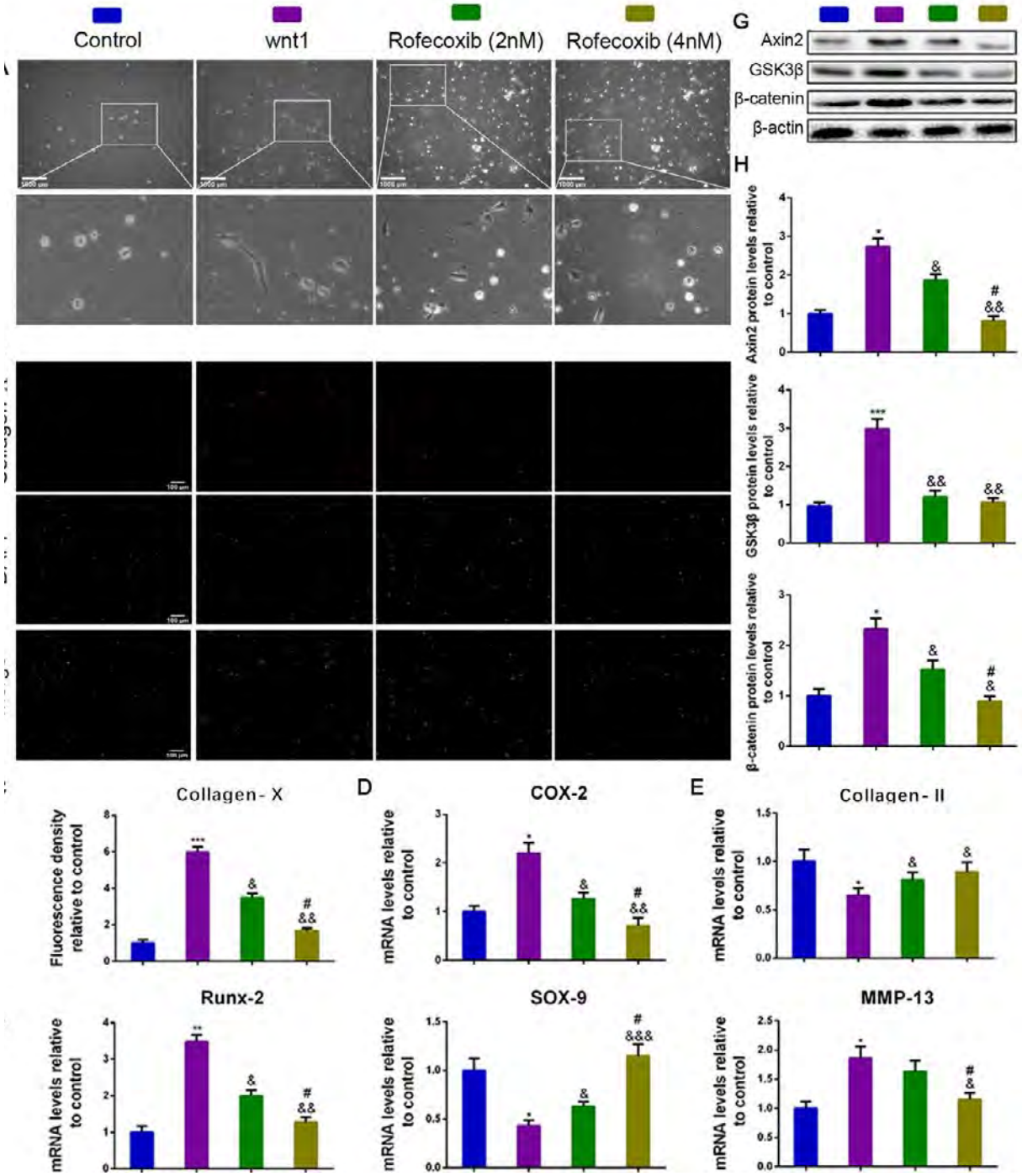


Fig. 4. *Rofecoxib protects CHs hypertrophy via Wnt/β-catenin pathway. CHs were pre-cultured with wnt1 (2.5 ng/ml) for 24 h. For co-treated group, CHs were pre-cultured with wnt1 (2.5 ng/ml) for 24 h and then treated with Rofecoxib (2 nM or 4 nM) for another 24 h.* ***A)*** *CHs after stimulation (magnification:40×).* ***B, C)*** *The protein expression level of collagen X was determined by (B) immunofluorescence (magnification:200×) and (C) quantification analysis.* ***D-F)*** *The mRNA expression levels of (D) COX-2, (E) collagen II, and (F) Runx-2, SOX-9, MMP-13 were assayed by RT-PCR.* ***G, H)*** *The protein expression level of Axin2, GSK3β, and β-catenin were determined by (G) WB and (H) quantification analysis. The values are mean ± SD of three independent experiments. (*P < 0.05, **P < 0.01, ***P < 0.001 compared to control; &P < 0.05, &&P < 0.01, &&&P < 0.001 compared to IL-1β; #P < 0.05 compared to 2nM Rofecoxib)*

shown in Fig. 4 D-F, Wnt-1 protein accelerated the mRNA expression of COX-2, Runx-2, and MMP-13, which are generally overexpressed in hypertrophic CHs, whereas Rofecoxib could alleviate that effect, especially in a 4 nM dose. Finally, we tested Axin2, GSK3β, and β-catenin protein expression with Western blot. Compared to the control, Wnt-1 protein played a decisive role in the activation of the Wnt/β-catenin pathway in CHs, in contrast, Rofecoxib led to a considerable inhibition of Axin2, GSK3β and β-catenin protein expression in a dose-dependent manner (Fig. 4 G, H). From these data, it can be observed that the high Wnt pathway is involved in the CHs hypertrophic development and Rofecoxib could protect CH hypertrophy by suppressing the Wnt/β-catenin pathway.

DISCUSSION

Cyclooxygenase has two isoenzymes, which are COX-1 and COX-2. The former is related to the normal physiological functions of the body, such as protecting the gastric mucosa and controlling platelet aggregation, while the other one is associated with inflammation or tumor progression. In normal conditions, COX-1 can be secreted by most cells, but COX-2 can only be expressed under pathological conditions (20, 21). In our study, IL-1β, used as an inducer of CH degenerated progress, significantly upregulated PGE-2, collagen X, Runx-2, and MMP-13 expression, and led to an evident decrease of collagen II, SOX-9, which proved a practical way to stimulate CHs to hypertrophy. The release of pro-inflammatory cytokines during arthritis plays a vital role in the destruction of the cartilage matrix, the most important of which are IL-1 and TNF. IL-1 activates transcriptional regulators by activating multiple kinase systems, promoting COX-2 mRNA transcription and protein synthesis (22). COX-2 contributes to the conversion of arachidonic acid to PGE2, resulting in the increased secretion of PGE2 and collagenase by CHs, which accelerates the degradation of proteoglycan and collagen II in cartilage matrix and inhibits their synthesis (23).

Hypertrophy is a typical phenotype of CH degeneration with a marked expression of MMP-13, collagen X, and Runx-2, which is closely related to the overexpression of COX-2 (24). It has been reported that NS398 (25), and Celecoxib (26) acted as COX-2 inhibitors to impact CH hypertrophic differentiation. In addition to this, Wnt/β-catenin is elucidated to play a vital role in hypertrophic differentiation of CH. Takegami et al. found Rspo2 promotes proliferating CHs into hypertrophy by Wnt/β-catenin signaling (27). Furthermore, the inhibition of Wnt/β-catenin signaling has also been proved to alleviate the progress of CHs hypertrophy. Okura et al. reported that Mianserin suppresses Wnt/β-catenin signaling and protects cartilage degradation from endochondral ossification (28). Kim et al. elucidated that SLIT3 delays the hypertrophic progression of CH regulates by β-catenin inhibition (29). However, whether the inhibition of COX-2 could interrupt Wnt/β-catenin is little referred. Celecoxib, another selective COX-2 inhibitor, is mentioned to suppress human colon cancer growth by inhibiting the Wnt/β-catenin pathway (30). Combination of the COX-2 inhibitors, celecoxib and R-Etodolac, is an effective therapeutic strategy in hepatocellular cancer by suppressing β-catenin (31). In this study, we tested Rofecoxib in the mediation of the degeneration of CH and found it efficiently decreased COX-2 and PGE-2 levels; importantly, it also suppressed the Axin2, β-catenin, and GSK3β expression in a dose-dependent manner. Rofecoxib is a COX-2 selective anti-inflammatory drug, which is reported to affect MMP-1 (32), IL-6, and PGE2 production, and increase aggrecan synthesis in cartilage (33). Bahrami (34) and Zagani (35) et al. claimed the usage of Rofecoxib targeting the Wnt/β-catenin pathway in the treatment of colorectal cancer.

Non-steroidal anti-inflammatory drug (NSAID) treatment can effectively relieve pain and temporarily improve joint function, and has been widely used in clinical practice. Rofecoxib and other COX-2 inhibitors selectively bind to the COX-2 binding site, reducing the possibility of digestive ulcers and impaired renal function (36). Moreover, COX-2 selective NSAIDs have less deleterious effects on the proliferation and death of CHs. Rofecoxib is an effective COX-2 inhibitor, which has little effects on CH viability as reported in previous study (37).

Summarily, our previous study shows a mechanism by which Rofecoxib inhibits COX-2 and delays the development of CH hypertrophy via the suppression of Wnt/β-catenin pathway.

In conclusion, Rofecoxib is an effective COX-2 inhibitor that protects CHs from hypertrophy by suppression of the Wnt/β-catenin pathway.

REFERENCES

1. Hunter DJ, Bierma-Zeinstra S. Osteoarthritis. Lancet 2019; 393:1745-59.
2. Guilak F, Nims RJ, Dicks A, Wu CL, Meulenbelt I. Osteoarthritis as a disease of the cartilage pericellular matrix. Matrix Biol 2018; 71-72:40-50.
3. Courties A, Gualillo O, Berenbaum F, Sellam J. Metabolic stress-induced joint inflammation and osteoarthritis. Osteoarthritis Cartilage 2015; 23:1955-65.
4. Huang CY, Hung LF, Liang CC, Ho LJ. COX-2 and iNOS are critical in advanced glycation end product-activated chondrocytes in vitro. Eur J Clin Invest 2009; 39:417-28.
5. Katagiri M, Ogasawara T, Hoshi K, et al. Suppression of adjuvant-induced arthritic bone destruction by cyclooxygenase-2 selective agents with and without inhibitory potency against carbonic anhydrase II. J Bone Miner Res 2006; 21:219-27.
6. Attur M, Al-Mussawir HE, Patel J, et al. Prostaglandin E2 exerts catabolic effects in osteoarthritis cartilage: evidence for signaling via the EP4 receptor. J Immunol 2008; 181:5082-88.
7. Guo X, Mak KK, Taketo MM, Yang Y. The Wnt/beta-catenin pathway interacts differentially with PTHrP signaling to control chondrocyte hypertrophy and final maturation. Plos One 2009; 4:e6067.
8. Yuan X, Liu H, Huang H, et al. The key role of canonical Wnt/beta-catenin signaling in cartilage chondrocytes. Curr Drug Targets 2016; 17:475-84.
9. Las HF, Pritzker KP, So A, Tsui HW, Chiu B, Inman RD, Tsui FW. Aberrant chondrocyte hypertrophy and activation of beta-catenin signaling precede joint ankylosis in ank/ank mice. J Rheumatol 2012; 39:583-93.
10. He F, Wang H, Ren WY, et al. BMP9/COX-2 axial mediates high phosphate-induced calcification in vascular smooth muscle cells via Wnt/beta-catenin pathway. J Cell Biochem 2018; 119:2851-63.
11. Wasnik S, Lakhan R, Baylink DJ, et al. Cyclooxygenase 2 augments osteoblastic but suppresses chondrocytic differentiation of CD90(+) skeletal stem cells in fracture sites. Sci Adv 2019; 5:w2108.
12. Wu L, Liu H, Zhang R, Li L, Li J, Hu H, Huang H. Chondroprotective activity of Murraya exotica through Inhibiting beta -catenin signaling pathway. Evid Based Complement Alternat Med 2013; 2013:752150.
13. Xu K, Ma C, Xu L, et al. Polygalacic acid inhibits MMPs expression and osteoarthritis via Wnt/beta-catenin and MAPK signal pathways suppression. Int Immunopharmacol 2018; 63:246-52.
14. Zhang Y, Wang J, Wheat J, et al. AML1-ETO mediates hematopoietic self-renewal and leukemogenesis through a COX/beta-catenin signaling pathway. Blood 2013; 121:4906-16.
15. Curtis E, Fuggle N, Shaw S, et al. Safety of Cyclooxygenase-2 inhibitors in osteoarthritis: outcomes of a systematic review and meta-analysis. Drugs Aging 2019; 36:25-44.
16. Bingham CR, Smugar SS, Wang H, Tershakovec AM. Early response to COX-2 inhibitors as a predictor of overall response in osteoarthritis: pooled results from two identical trials comparing etoricoxib, celecoxib and placebo. Rheumatology (Oxford) 2009; 48:1122-27.
17. Eisinger AL, Nadauld LD, Shelton DN, Prescott SM, Stafforini DM, Jones DA. Retinoic acid inhibits beta-catenin through suppression of Cox-2: a role for truncated adenomatous polyposis coli. J Biol Chem 2007; 282:29394-400.
18. Golovchenko S, Hattori T, Hartmann C, et al. Deletion of beta catenin in hypertrophic growth plate chondrocytes impairs trabecular bone formation. Bone 2013; 55:102-12.
19. Cai WY, Wei TZ, Luo QC, et al. The Wnt-beta-catenin pathway represses let-7 microRNA expression through transactivation of Lin28 to augment breast cancer stem cell expansion. J Cell Sci 2013; 126:2877-89.
20. Liggett JL, Zhang X, Eling TE, Baek SJ. Anti-tumor activity of non-steroidal anti-inflammatory drugs: cyclooxygenase-independent targets. Cancer Lett 2014; 346:217-24.
21. Fitzpatrick FA. Cyclooxygenase enzymes: regulation

and function. Curr Pharm Des 2004; 10:577-88.
22. Huang ZF, Massey JB, Via DP. Differential regulation of cyclooxygenase-2 (COX-2) mRNA stability by interleukin-1 beta (IL-1 beta) and tumor necrosis factor-alpha (TNF-alpha) in human in vitro differentiated macrophages. Biochem Pharmacol 2000; 59:187-94.
23. Ansari MY, Haqqi TM. Interleukin-1beta induced stress granules sequester COX-2 mRNA and regulates its stability and translation in human OA chondrocytes. Sci Rep 2016; 6:27611.
24. Cottrell JA, O'Connor JP. Pharmacological inhibition of 5-lipoxygenase accelerates and enhances fracture-healing. J Bone Joint Surg Am 2009; 91:2653-65.
25. Li N, Wang Q, Zhu T, et al. In vitro functional characterization of prostaglandin-endoperoxide synthase 2 during chondrocyte hypertrophic differentiation. Oncotarget 2016; 7:36280-92.
26. Welting TJ, Caron MM, Emans PJ, et al. Inhibition of cyclooxygenase-2 impacts chondrocyte hypertrophic differentiation during endochondral ossification. Eur Cell Mater 2011; 22:420-37.
27. Takegami Y, Ohkawara B, Ito M, et al. R-spondin 2 facilitates differentiation of proliferating chondrocytes into hypertrophic chondrocytes by enhancing Wnt/beta-catenin signaling in endochondral ossification. Biochem Biophys Res Commun 2016; 473:255-64.
28. Okura T, Ohkawara B, Takegami Y, et al. Mianserin suppresses R-spondin 2-induced activation of Wnt/beta-catenin signaling in chondrocytes and prevents cartilage degradation in a rat model of osteoarthritis. Sci Rep 2019; 9:2808.
29. Kim H, Choi YJ, Lee YS, et al. SLIT3 regulates endochondral ossification by beta-catenin suppression in chondrocytes. Biochem Biophys Res Commun 2018; 506:847-53.
30. Egashira I, Takahashi-Yanaga F, Nishida R, et al T. Celecoxib and 2,5-dimethylcelecoxib inhibit intestinal cancer growth by suppressing the Wnt/beta-catenin signaling pathway. Cancer Sci 2017; 108:108-115.
31. Behari J, Zeng G, Otruba W, et al. R-Etodolac decreases beta-catenin levels along with survival and proliferation of hepatoma cells. J Hepatol 2007; 46 849-57.
32. Guan PP, Guo JW, Yu X, et al. The role of cyclooxygenase-2, interleukin-1beta and fibroblast growth factor-2 in the activation of matrix metalloproteinase-1 in sheared-chondrocytes and articular cartilage. Sci Rep 2015; 5:10412.
33. Sanchez C, Mateus MM, Defresne MP, Crielaard JM, Reginster JY, Henrotin YE. Metabolism of human articular chondrocytes cultured in alginate beads. Longterm effects of interleukin 1beta and nonsteroidal antiinflammatory drugs. J Rheumatol 2002; 29:772-82.
34. Bahrami A, Amerizadeh F, ShahidSales S, et al. Therapeutic potential of targeting Wnt/beta-catenin pathway in treatment of colorectal cancer: rational and progress. J Cell Biochem 2017; 118:1979-83.
35. Zagani R, Hamzaoui N, Cacheux W, et al. Cyclooxygenase-2 inhibitors down-regulate osteopontin and Nr4A2-new therapeutic targets for colorectal cancers. Gastroenterology 2009; 137:1358-66.
36. de Boer TN, Huisman AM, Polak AA, et al. The chondroprotective effect of selective COX-2 inhibition in osteoarthritis: ex vivo evaluation of human cartilage tissue after in vivo treatment. Osteoarthritis Cartilage 2009; 17:482-88.
37. Chang JK, Wu SC, Wang GJ, Cho MH, Ho ML. Effects of non-steroidal anti-inflammatory drugs on cell proliferation and death in cultured epiphyseal-articular chondrocytes of fetal rats. Toxicology 2006; 228:111-23.

LONG NONCODING RNA NNT-AS1 FUNCTIONS AS AN ONCOGENE IN BREAST CANCER VIA REPRESSING ZFP36 EXPRESSION

Q.-H. PAN[1], Y.-H. FAN[1], Y.-Z. WANG[1], D.-M. LI[1], C.-E. HU[1] and R.-X. LI[2]

[1]Department of Supply Room, Shandong Binzhou Central Hospital, Binzhou, China;
[2]Department of Medical Section, People's Hospital of Huimin County, Binzhou, China

Received February 2, 2020 – Accepted April 20, 2020

Breast cancer is one of the most common cancers in women. This study focuses on the effects of Long non-coding RNAs (lncRNAs) NNT-AS1 on breast cancer cell growth and metastasis. Fifty-six pairs of breast cancer (BC) tissues and matched paracarcinoma tissues were obtained. The BC cell lines and normal human breast cell line were employed. NNT-AS1 in BC cells was knocked down by shRNA. Cell counting kit-8 assay (CCK-8), colony formation assay, cell cycle analysis, cell apoptosis analysis, cound healing assay, Transwell assay, cioinformatics analysis, Western blot analysis and Xenograft model were used. Quantitative real-time polymerase chain reaction (qRT-PCR) assay indicated that expression of NNT-AS1 was obviously upregulated in breast cancer tissues compared with adjacent tissues (n=56). Knockdown of NNT-AS1 could attenuate breast cancer cell viability, proliferation, invasion and migration, as well as promote cell apoptosis and induce cell cycle arrest at G0/G1 phase. ZFP36 was directly combined with NNT-AS1, and silencing of ZFP36 could rescue tumor suppression role by downregulating NNT-AS1 on cell proliferation and metastasis. Knockdown of NNT-AS1 could suppress cell growth and metastasis via interacting with ZFP36 *in vivo*. This study demonstrated that knockdown of NNT-AS1 had tumor-suppressive effect on breast cancer progression and metastasis via interacting with ZFP36 *in vitro* and *in vivo*, which provides a new insight into the treatment and prognosis evaluation of breast cancer.

Breast cancer (BC) is one of the most common cancers in women (1). Although the incidence of the disease in Euromerican developed countries tends to be stable and the mortality rate has declined, it is increasing yearly worldwide, especially in China (2). According to relative statistics, in the United States about 231,840 cases of BC were revealed, and the number of deaths due to BC was approximately 40,000 in 2015 (3). In China, according to the statistics of the Chinese Academy of Medical Sciences, the number of new cases of BC was about 200,000 in 2010 (4). The occurrence and development of BC is a complicated polygene-related process (5), the mechanism of which has not been fully recognized.

Studies have shown that the entire human genome contains 23,000 genes encoding Long non-coding RNAs (lncRNAs), while only about 20,000 genes encoding proteins (6). LncRNAs were thought to be garbage of gene transcription. Nevertheless, with the development of gene sequencing technology, it was found that lncRNAs play an important role in a series of cell activities (7). LncRNAs can interact

Key words: LncRNAs; breast cancer; ZEP36; tumor growth; metastasis

Corresponding Author:
Ruxin Li, BM.
Department of Medical Section,
People's Hospital of Huimin County, No. 396, Sunwu 5th Road,
Huimin County, Binzhou, Shandong, 251700 China.
Tel: 860543-5361267
e-mail: ruxing19710512@163.com

0393-974X (2020)
Copyright © by BIOLIFE, s.a.s.
This publication and/or article is for individual use only and may not be further reproduced without written permission from the copyright holder.
Unauthorized reproduction may result in financial and other penalties
DISCLOSURE: ALL AUTHORS REPORT NO CONFLICTS OF INTEREST RELEVANT TO THIS ARTICLE.

with proteins, mRNA and DNA, and have an effect on cell activity (8). Meanwhile, lncRNAs have been reported to play a biological role in a variety of cancers, including gastric (9), pancreatic (10), colorectal (11), lung (12), cervical (13) and prostate (14). NNT-AS1, a newly identified lncRNA has been documented to be upregulated and plays an oncogene role in colorectal cancer (15). However, the role and mechanism of NNT-AS1 in progression and development of BC remains unknown. In this present study, the expression of NNT-AS1 was detected in BC tissues and BC cell lines were employed to investigate the function of NNT-AS1 in BC.

MATERIALS AND METHODS

Clinical samples

Fifty-six pairs of BC tissues and matched paracarcinoma tissues were obtained from patients undergoing routine surgery in our hospital between June 2014 and July 2017. All surgical specimens were collected and then frozen immediately in liquid nitrogen until use. Tumor tissues were diagnosed and confirmed by pathological examination. This present research was approved by the ethics committee of Shandong Binzhou Central Hospital. Written informed consent was signed by all the participants before the study.

Cell culture

The BC cell lines MCF-7, SKBR3, LCC2, MDA-MB-453, T-47D, LCC9, MDA_MB-231 and normal human breast cell line (MCF-10A) were purchased from Shanghai Model Cell Bank (Shanghai, China). Cells were cultured in media Dulbecco's Modified Eagle Medium (DMEM) supplemented with 10% fetal bovine serum (FBS, Gibco, Rockville, MD, USA), 100 U/mL penicillin and 100 μg/mL streptomycin. All cells were cultured in an incubator at 37°C with 5% CO2.

Plasmid and transfection

For knockdown of NNT-AS1 in BC cells, shRNA sequence targeting for NNT-AS1 were designed as follows: lncRNA-shRNA: 5'-GCC AGT CCT TGT CAA TCA AAC -3' and the NC-shRNA was purchased from Genechem (Shanghai, China). MCF-7 and MDA_MB-231 cells were transfected with lncRNA-shRNA or NC-shRNA.

RNA extraction and quantitative real-time polymerase chain reaction (qRT-PCR)

Total RNA was extracted from collected frozen tissue samples and cell lines by using the TRIzol reagent (Invitrogen, Carlsbad, CA, USA) following the manufacturer's protocols. Reverse TranscriptionKit (TaKaRa, Dalian, China) was used to synthesize cDNAs. NNT-AS1 and ZFP36 mRNA levels were quantified by SYBR Green real-time PCR and normalized to GAPDH using the following primers: for NNT-AS1, forward, 5'- CCT CCA ACC CGG AAG AAC A -3' and reverse, 5'- TTC GTG AGG TCG CCT TTT GG -3'; for ZFP36, forward, 5'- TGC CAA ACC CCA CCC ATA AA -3' and reverse, 5'- TAC AAG GGA AGC AGA CGA CC -3'; and for GAPDH, forward, 5'-CGG AGT TGT TCG TAT TCG G-3' and reverse, 5'-TAC TAG CCG ATG ATG GCA TT-3'. QRT-PCR was performed by the ABI 7500 system (Applied Biosystems, Waltham, MA, USA). The relative expression of mRNA was measured using $2^{-\Delta\Delta CT}$.

Cell counting kit-8 assay

Cell viability was detected by cell counting kit-8 (CCK-8) assay (Promega, Madison, WI, USA) after the transfection according to the manufacturer's protocols. The transfected cells were grown in 96-well plates (2000 cells/well), added with10 μL CCK-8 solution into 90 μL DMEM medium and incubated for 3 h then the absorbance at 490 nm was measured at 12 h, 24 h, 48 h and 72 h, respectively, after the cells were transfection.

Colony formation assay

Cells were plated in 6-well plates at a density of 5×10^2 per well and cultured for 2 weeks. The colonies were fixed in ice-cold 70% methanol for 10 min and stained with 0.5% crystal violet for another 10 min, then each well was washed 3 times with phosphate buffered saline (PBS).

Cell cycle analysis

For cell cycle analysis, transfected MCF-7 and MDA_MB-231 cells were prepared and stained with propidium iodide using the BD Cycletest Plus DNA Reagent Kit (BD Biosciences, Franklin Lakes, NJ, USA). The relative ratio of cells in G0/G1, S, or G2/M phase was analyzed by Flowjo 7.6.

Cell apoptosis analysis

Transfected MCF-7 and MDA_MB-231 cell

suspensions were prepared and double stained with 5 μL Annexin V-FITC and 1 μL propidium iodide (PI, 50 μg/mL). After incubated in the dark for 15 min, cells were quantified by a flow cytometer equipped with CellQuest software (BD Bioscience, Franklin Lakes, NJ, USA). The percentage of apoptotic cells was analysed by Flowjo 7.6.

Wound healing assay

Transfected MCF-7 and MDA_MB-231 cells were cultured in the 6-well plates marked by a horizontal line on the back. The cell was scratched by a pipette tip across the confluent cell layer. Then the cells were washed gently and continued to culture with the serum-free medium for 24~48 h. Wound closure was captured using a light microscope (DFC500, Leica, Wetzlar, Germany).

Transwell assay

Cells were cultured in the upper invasion chamber (BD, Franklin Lakes, NJ, USA) coated with Matrigel. Serum-free medium was added into the upper chamber, whereas 10% FBS medium supplemented was then added into the lower. After 48 h, the cells cultured on the upside of the filter which had not invaded through the chamber were removed. Then the chamber was suspended by 100% precooling methanol, stained with 0.05% crystal violet and inspected with a microscope (Olympus, Tokyo, Japan). The values for the invasion cells were measured by counting five fields per membrane.

Bioinformatics analysis

Kaplan Meier-plotter (http://kmplot.com/analysis/index.php?p=service) and TANRIC (http://ibl.mdanderson.org/tanric/_design/basic/index.html) databases were utilized to forecast the prognosis of BC patients with ectopic expression of NNT-AS1 and ZFP36, respectively. RBPDB (http://rbpdb.ccbr.utoronto.ca/index.php) database was utilized to forecast RNA-binding proteins of NNT-AS1 to illustrate the potential downstream mechanism of action.

Western blot analysis

To investigate relative protein expression, cells were washed with ice-cold PBS and lysed using lysis buffer. Then we measured the concentration of collected protein using a protein assay kit purchased from Beyotime (Shanghai, China). The extracted protein (sum of 20 μg) was degenerated and chilled on ice. 10% sodium dodecyl sulphate-polyacrylamide gel electrophoresis (SDS-PAGE) was used to separate protein, and then it was shifted to polyvinylidene fluoride (PVDF) membranes purchased from Millipore (Billerica, MA, USA). 5% fat-free milk was used to block non-specific protein interactions in tris buffered saline-tween (TBST) buffer which contains Tris–HCl (50 mM), NaCl (150 mM) and Tween 20 (0.05%) at 4°C for 1 h. The membranes loaded with proteins were incubated at 4°C within the fat-free milk overnight with the following primary antibody against ZFP36 (1:500, cat. no AB43567, Absci, Nanjing, China) and GAPDH (1:500, cat.no AB41549, Absci, Nanjing, China). TBST buffer was used to wash the unbound antibody (10 min each time for three times). Then the membranes were incubated with secondary antibody conjugated with horseradish peroxide (1:1000, cat.no ABL3012-2, Absci, Nanjing, China) (1 h) at room temperature. After washing these membranes three times in TBST buffer, we developed the membranes using electrochemiluminescence (ECL) (Millipore, Billerica, MA, USA) following the instructions.

Xenograft model

The research was approved by the Animal Ethics Committee of Shandong Binzhou Central Hospital Animal Center. MCF-7 cells (6×10^5/mL) transfected with LncRNA-shRNA or NC-shRNA were implanted into both axillae of NOD/SCID mice (4-5 weeks old) subcutaneously. Tumor diameters were detected every 5 days. Tumor volume was calculated as the formula (volume= length × width^2 × 1/2). Mice were sacrificed and the grafts were removed after 4 weeks. Meanwhile, MCF-7 cells (1×10^7/mL) transfected with LncRNA-shRNA or NC-shRNA were also injected into mice from tail vein to induce pulmonary metastasis model. Lungs were taken to observed micro-metastasis after 4 weeks.

Statistical analysis

Statistical product and service solutions (SPSS) 19.0 software (IBM, Armonk, NY, USA) was used for statistical analysis, statistical data was presented with Graph PAD prism software, quantitative data was presented as mean ± SD (standard deviation). The independent samples *t*-test was used to perform statistical analysis. The regression and correlation analysis was analyzed using the Spearman *chi*-squared test. Results were taken as statistically significant at $P<0.05$.

RESULTS

NNT-AS1 expression was elevated in BC tissues and cell lines

Expression of NNT-AS1 was detected by qRT-PCR in 56 pairs of BC tissues and adjacent normal tissues. The result indicated that NNT-AS1 expression was remarkably increased in BC tissues compared with the paired normal tissues on mRNA level (Fig. 1A). Moreover, we further investigated that overexpression of NNT-AS1 led to a potential trend to reduce the long-term survival rate of BC patients according to the trend of the regression curve using TANRIC database analysis (Fig. 1B).

Then we investigated NNT-AS1 expression in several BC cell lines and normal breast cell line with qRT-RCR. It showed that, compared with MCF-10A cell line, all these BC cell lines expressed a relatively higher level of NNT-AS1, in which MCF-7 expressed the relatively highest (Fig. 1C). To identify the mode of action of NNT-AS1 in BC progression and development, we chose MCF-7 cell line for NNT-AS1 knockdown. The result showed that NNT-AS1 expression was effectively suppressed in MCF-7 cells by transfected with lncRNA-shRNA (Fig. 1D).

Knockdown of NNT-AS1 inhibited BC cell growth in vitro

To evaluate the biological role of NNT-AS1 in BC cell growth, we investigated NNT-AS1 on BC cell viability and proliferation. As shown in CCK8 assay, the viability of MCF-7 cells was significantly inhibited after being transfected with lncRNA-shRNA compared with NC-shRNA, in a time-

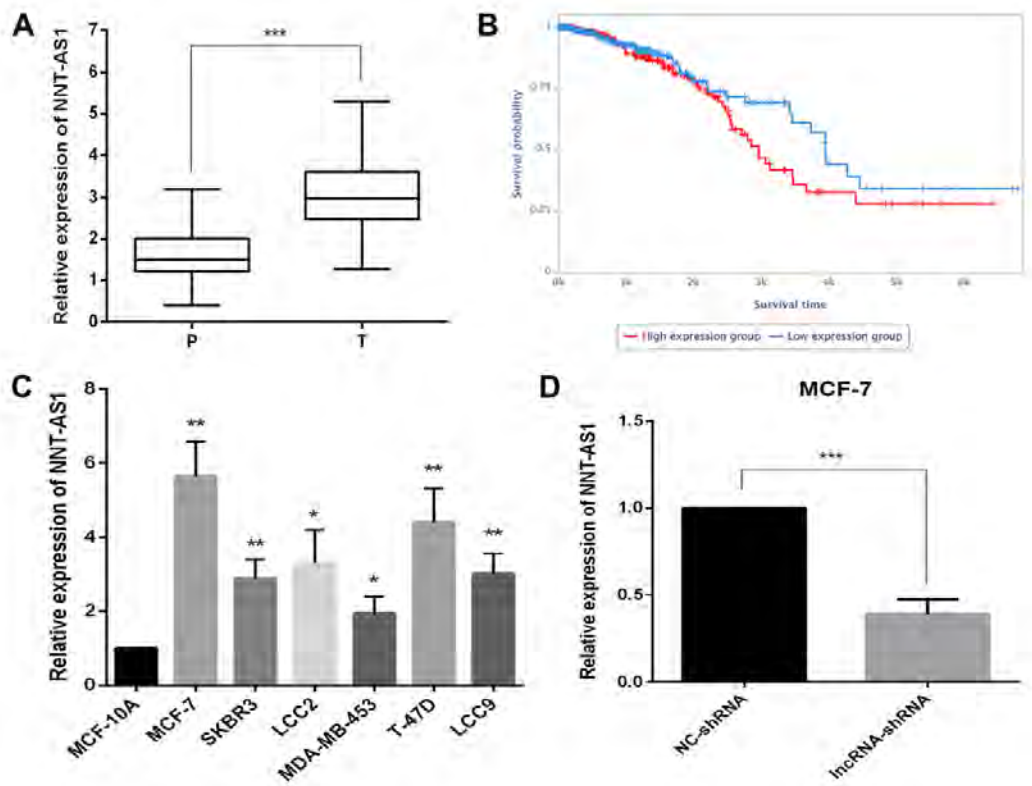


Fig. 1. *NNT-AS1 expression was elevated in BC tissues and cell lines.* ***A)*** *Analysis of NNT-AS1 expression in paracarcinoma tissues (P) and tumor tissues (T);* ***B)*** *Overexpression of NNT-AS1 led to a potential trend to reduce the long-term survival rate of BC patients;* ***C)*** *Analysis of NNT-AS1 expression in several BC cell lines and normal cell line;* ***D)*** *Analysis of transfection efficiency in MCF-7 cells. MCF-7 cells were transfected with NC-shRNA or lncRNA-shRNA. *P<0.05; **P<0.01; ***P<0.001.*

dependent manner, respectively (Fig. 2A).

Meanwhile, colony formation assay was also applied to further explore BC cell proliferation and demonstrated that there were fewer formed colonies in MCF-7 cells transfected with lncRNA-shRNA compared with NC-shRNA (Fig. 2B). Collectively, these results revealed that knockdown of NNT-AS1 could inhibit BC cell growth.

Knockdown of NNT-AS1 inhibited BC cell metastasis in vitro

We next evaluated the action role of NNT-AS1 in BC cell metastasis. As shown in wound-healing assay, decreased NNT-AS1 expression could suppress MCF-7 cell migration compared with the negative control (Fig. 2C). Meanwhile, effects of decreased NNT-AS1 expression on MCF-7 cell invasion measured by Transwell assay were the same (Fig. 2D) which demonstrated that there were fewer formed colonies in MDA_MB-231 cells transfected with lncRNA-shRNA compared with NC-shRNA (Fig. 3A and 3B). In addition, the same results were found in MDA_MB-231 cells (Fig. 3C and 3D). These results demonstrated that knockdown of NNT-AS1 could inhibit cell metastasis of BC.

Knockdown of NNT-AS1 promoted cell apoptosis and induced cell cycle arrest at G0/G1 phase

Since NNT-AS1 could regulate cell proliferation, we were considering whether cell apoptosis and cell cycle were also affected by ectopic NNT-AS1 expression. As shown in flow cytometric analysis,

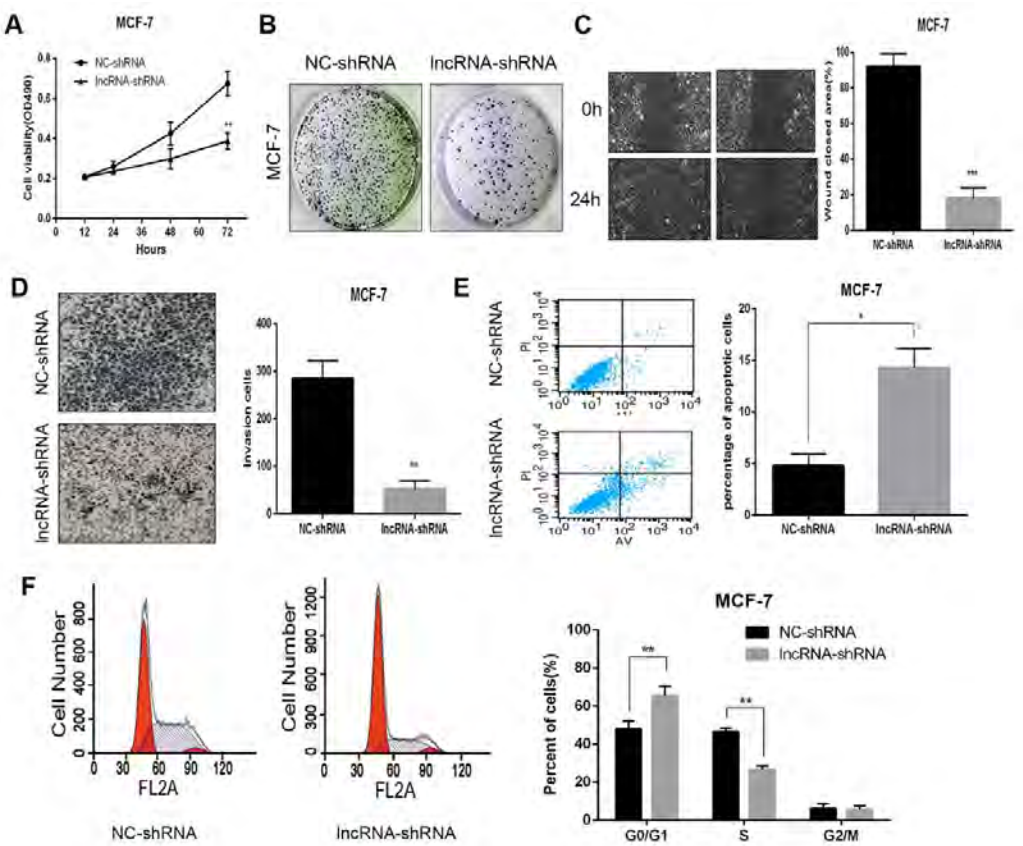


Fig. 2. *Knockdown of NNT-AS1 inhibited BC cell growth and metastasis in MCF-7 cells. **A**) CCK8 assay was performed to determine the viability of transfected MCF-7 cells; **B**) Colony formation assay was performed to determine the proliferation of transfected MCF-7 cells; **C**) Wound healing assay was performed to determine the migration of transfected MCF-7 cells; **D**) Transwell assay was performed to determine the invasion of transfected MCF-7 cells; **E**) Flow cytometric analysis was performed to detect the apoptotic rates of transfected MCF-7 cells; **F**) Flow cytometric analysis was performed to detect cell cycle progression of transfected MCF-7 cells. *P<0.05; **P<0.01; ***P<0.001.*

the apoptotic rate of MCF-7 cells transfected with lncRNA-shRNA increased remarkably compared with NC-shRNA (Fig. 2E). Moreover, the percentage of MCF-7 cells transfected with lncRNA-shRNA increased obviously in G0/G1 phase and decreased obviously in S phase compared withNC-shRNA (Fig. 2F). Furthermore, we found the same results in and MDA_MB-231cells (Fig. 3E). The results indicated that knockdown of NNT-AS1could impair BC cell proliferation by promoting cell apoptosis and inducing cell-cycle arrest in G0/G1 phase (Fig. 3F).

NNT-AS1 suppressed ZFP36 expression directly

To better understand the mechanism of how NNT-AS1 participated in BC tumorigenesis, we further forecasted the potential RNA-binding proteins of NNT-AS1 involved in the process using RBPDB database analysis. According to the analysis results, multiple proteins were predicted to be combined with sequence of NNT-AS1, in which ZFP36 seemed to be of great value after consulting the literature (Fig. 4A).

Meanwhile, to verify the actual binding relationship, ZFP36 expression was further detected of BC cells transfected with NNT-AS1 lncRNA-shRNA or NC-shRNA. The results indicated that ZFP36 was upregulated in MCF-7 cells transfected with lncRNA-shRNA on mRNA level and protein level compared with NC-shRNA (Fig. 4B and 4C). All these results indicated that ZFP36 was directly combined with NNT-AS1.

Silencing of ZFP36 rescued tumor suppression of downregulated NNT-AS1

Firstly, to identify the interactive relationship of NNT-AS1 and ZFP36, the expression of ZFP36 in BC tissues was measured. The results indicated that ZFP36 was obviously downregulated in BC tissues compared with the paraneoplastic tissues on the mRNA level (Fig. 4D), and the expression of ZFP36 was negatively correlated with the expression of NNT-

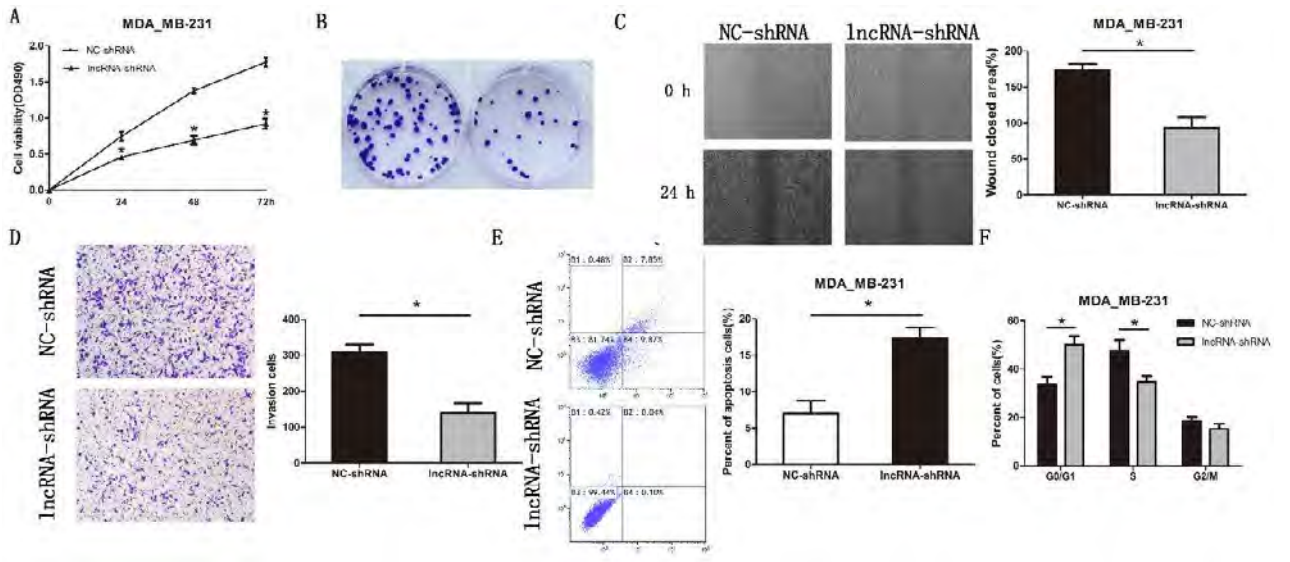


Fig. 3. *Knockdown of NNT-AS1 inhibited BC cell growth and metastasis inMDA_MB-231 cells.* ***A****) CCK8 assay was performed to determine the viability of transfected MDA_MB-231cells;* ***B****) Colony formation assay was performed to determine the proliferation of transfected MDA_MB-231 cells;* ***C****) Wound healing assay was performed to determine the migration of transfected MDA_MB-231 cells;* ***D****) Transwell assay was performed to determine the invasion of transfected MDA_MB-231 cells;* ***E****) Flow cytometric analysis was performed to detect the apoptotic rates of transfected MDA_MB-231 cells;* ***F****) Flow cytometric analysis was performed to detect cell cycle progression of transfected MDA_MB-231 cells. *P<0.05; **P<0.01; ***P<0.001.*

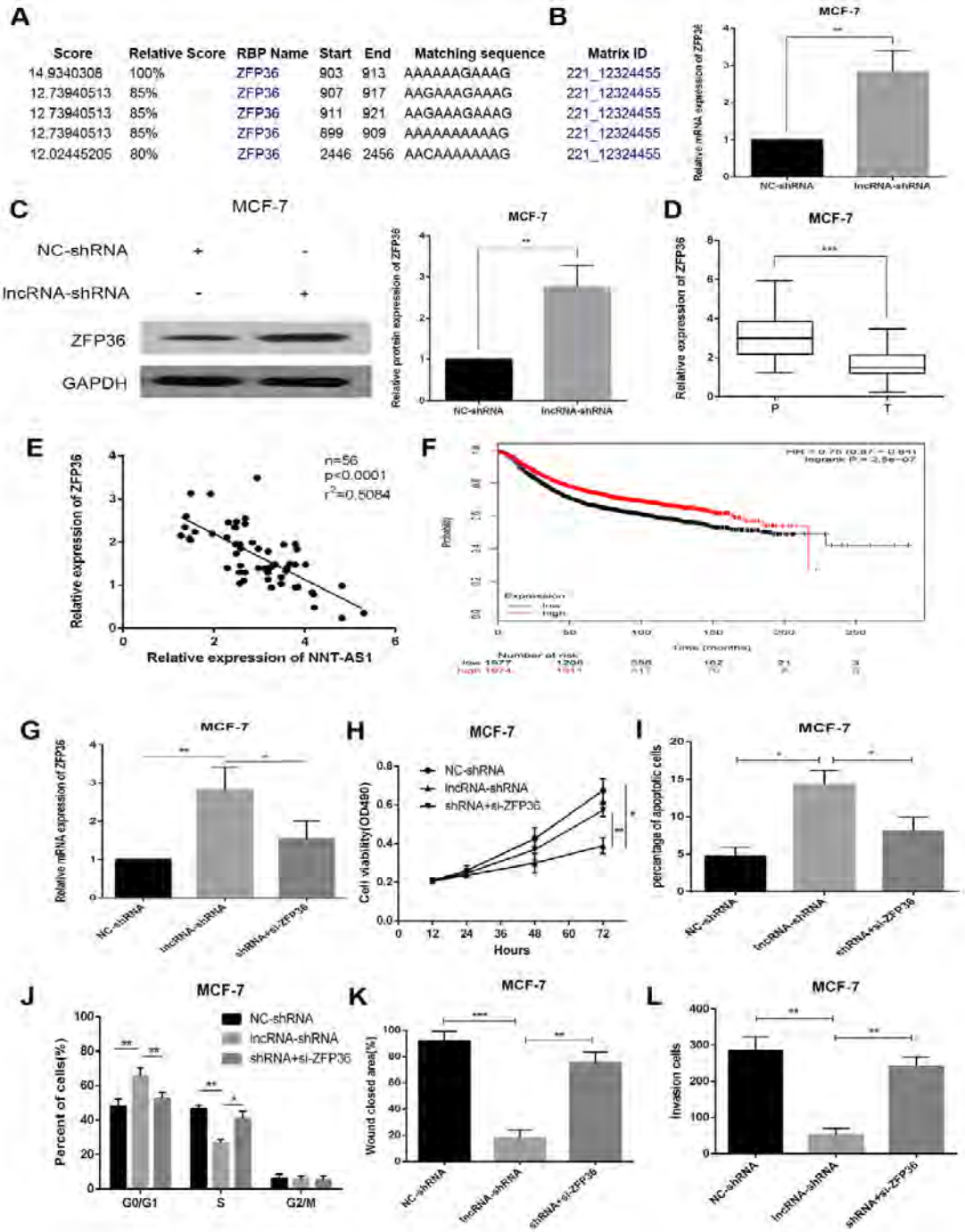


Fig. 4. *ZFP36 was directly combined with NNT-AS1.* ***A****) ZFP36 was selected as the potential RNA-binding protein of NNT-AS1 via using bioinformatics analysis;* ***B****) Analysis of ZFP36 expression in transfected MCF-7 cells on mRNA level;* ***C****) Analysis of ZFP36 expression in transfected MCF-7 cells on protein level;* ***D****) Analysis of ZFP36 expression in paracarcinoma tissues (P) and tumor tissues (T);* ***E****) Correlation between the expression of mRNA levels of NNT-AS1 and ZFP36 in BC tissues;* ***F****) ZFP36 was contributed to the improvement of prognosis of patients with BC;* ***G****) Analysis of transfection efficiency in MCF-7 cells transfected with NNT-AS1 NC-shRNA, lncRNA-shRNA and/or siRNA-ZFP36;* ***H****) ZFP36 silencing rescued suppressed cell proliferation by NNT-AS1 knockdown;* ***I****) ZFP36 silencing attenuated cell apoptosis by NNT-AS1 knockdown;* ***J****) ZFP36 silencing attenuated cell cycle distribution at G0/G1 phase;* ***K****) ZFP36 silencing increased cell migration of cells transfected with lncRNA-shRNA;* ***L****) ZFP36 silencing increased cell invasion of cells transfected with lncRNA-shRNA. *P<0.05; **P<0.01; ***P<0.001.*

AS1 in BC tissues (Fig. 4E). Moreover, using Kaplan Meier-plotter database analysis, we also identified that overexpression of ZFP36 led to a potential trend to prolong the survival rate of BC patients (Fig. 4F).

Secondly, we explored whether ZFP36 is responsible for the functional effects of NNT-AS1 in BC tumorigenesis. We silenced ZFP36 expression by transfecting with siRNA-ZFP36 in NNT-AS1-decreasedMCF-7 cells (Fig. 4G). ZFP36 silencing not only increased the proliferation of NNT-AS1-decreased cells (Fig. 4H), attenuated cell apoptosis and cell cycle distribution at G0/G1 phase (Fig. 4I and 4J), but also increased cell migration and invasion compared with NNT-AS1NC-shRNA (Fig. 4K and 4L). These results implied that NNT-AS1promoted BC tumorigenesis by partially repressing ZFP36 expression.

Knockdown of NNT-AS1 inhibited BC cell growth and metastasis in vivo

To finally validate whether NNT-AS1 could regulate BC tumorigenesis *in vivo*, we established a subcutaneous tumor mouse model and metastatic tumor mouse model to assess cell growth and metastasis. MCF-7 cells transfected with lncRNA-shRNA or NC-shRNA were injected into mice subcutaneously to induce subcutaneous tumor mouse model. NNT-AS1 expression in tumor grafts was detected by qRT-PCR and showed that NNT-AS1 expression in lncRNA-shRNA groups was decreased compared with NC-shRNA groups (Fig. 5A). Tumor weight obviously became less in lncRNA-shRNA groups compared with NC-shRNA groups (Fig. 5B). Tumor volume was significantly smaller in lncRNA-shRNA groups compared to NC-shRNA groups (Fig. 5C).

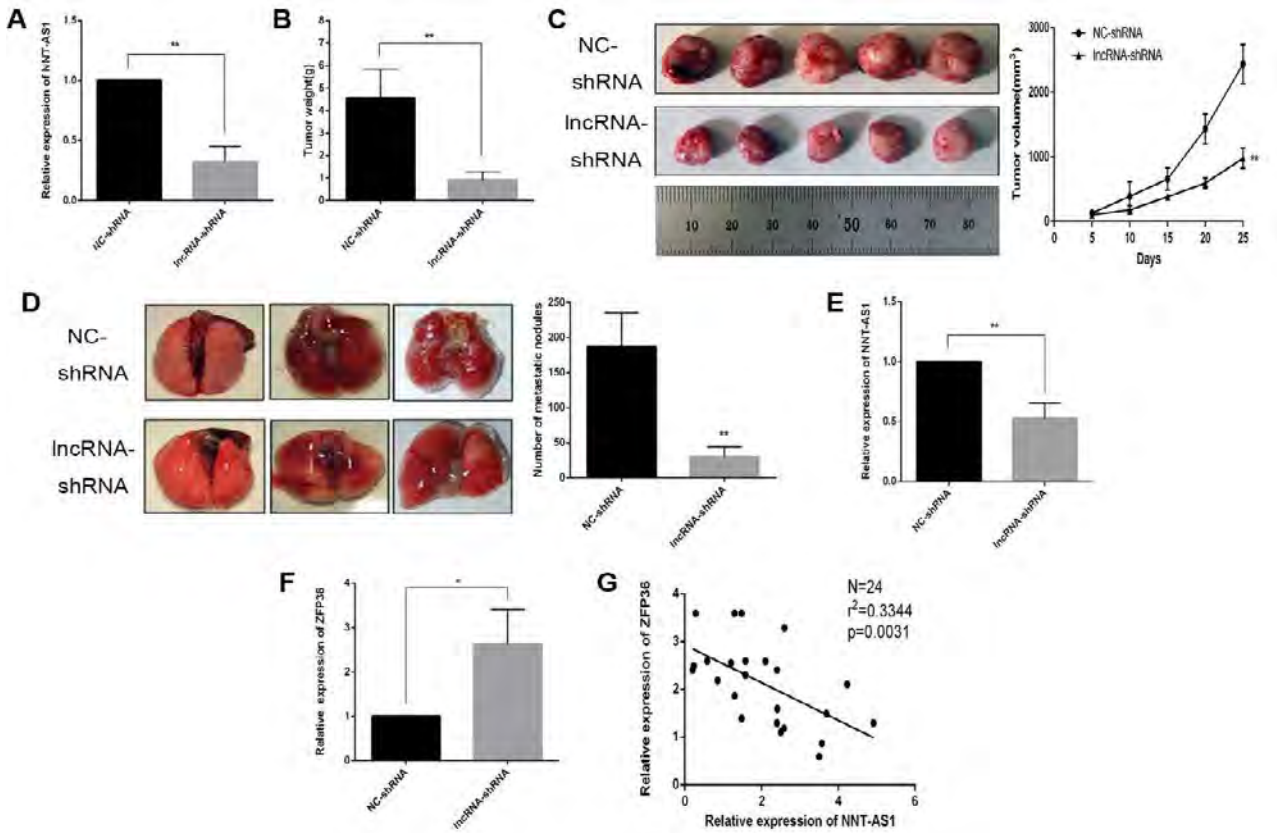


Fig. 5. *Knockdown of NNT-AS1 inhibited BC cell growth and metastasis in vivo.* ***A)*** *Analysis of NNT-AS1 expression in subcutaneous tumor tissues;* ***B)*** *Tumor weights are represented as means of tumor weights ±SD;* ***C)*** *Tumor volume was determined by using calipers;* ***D)*** *Analysis of the number of lung metastases in pulmonary metastasis model;* ***E)*** *Analysis of NNT-AS1 expression in pulmonary metastasis tumor tissues;* ***F)*** *Analysis of ZFP36 expression in tumor xenografts;* ***G)*** *Correlation between the expression of mRNA levels of NNT-AS1 and ZFP36 in tumor xenografts. *P<0.05; **P<0.01.*

Next, MCF-7 cells transfected with lncRNA-shRNA or NC-shRNA were injected into mice in the tail vein to induce metastatic tumor mouse model. Compared with the NC-shRNA groups, the number of lung metastases in lncRNA-shRNA groups was significantly decreased (Fig. 5D). Expression of NNT-AS1 in lung metastases tissues detected by qRT-PCR was also decreased in lncRNA-shRNA groups compared with NC-shRNA groups (Fig. 5E). To identify whether NNT-AS1 was interacted with ZFP36 *in vivo*, we also detected ZFP36 mRNA expression in tumor xenografts which demonstrated that ZFP36 expression was increased in lncRNA-shRNA groups compared with NC-shRNA groups (Fig. 5F), and ZFP36 expression was negatively correlated with NNT-AS1 expression (Fig. 5G). Collectively, these results implied that knockdown of NNT-AS1 could suppress BC cell growth and metastasis via interacting with ZFP36 *in vivo*.

DISCUSSION

Increasing evidence has suggested that lncRNAs play a vital role in carcinogenesis and cancer progression of various types of tumors. For example, Tong et al. (16) revealed that lncRNA RP11-190D6.2 could inhibit proliferation and invasion of epithelial ovarian cancer cells; Xu et al. (17) found that lncRNA CCAT2 is associated with poor prognosis in hepatocellular carcinoma and promotes tumor metastasis by regulating Snail2-mediated epithelial-mesenchymal transition. Su et al. (11) documented that lncRNA BLACAT1 indicates a poor prognosis of colorectal cancer and affects cell proliferation by epigenetically silencing of p15; Gao et al. (18) identified that lncRNA PVT1 facilitates cervical cancer progression via negative regulating of miR-424.

BC has always been a serious threat to women in the world. In recent years, increasing studies implied that lncRNAs played an important role in the occurrence and development of BC. For example, Wu et al. (19) revealed that lncRNA CCAT2 promotes BC growth and metastasis by regulating TGF-β signaling pathway; Liu et al. (20) demonstrated that lncRNA HIF1A-AS2, and UCA1 signature might serve as a diagnostic biomarker for differentiating between triple-negative and non-triple-negative BCs; Cai et al. (21) found that lncRNA SNHG16 contributes to BC cell migration by competitively binding miR-98 with E2F5. To date, there has been no study onf correlation between lncRNA NNT-AS1 and BC tumorigenesis. In the present study, we demonstrated that NNT-AS1 was obviously upregulated in BC tissues compared with adjacent normal tissues, and prognostic survival analysis also indicated that high expression of NNT-AS1 might prolong the long-term survival rate of patients with BC, implying that NNT-AS1 might play a crucial role in the progression and development of BC and become a novel and promising target for the treatment of BC. Moreover, knockdown of NNT-AS1could attenuate BC cell invasion and migration, as well as promote cell apoptosis and induce cell cycle arrest in G0/G1 phase to repress cell viability and proliferation. Furthermore, knockdown of NNT-AS1 could also suppress BC cell growth and metastasis *in vivo*. Taken together, these findings reveal that knockdown of NNT-AS1 exerts suppressive effect on cell growth and metastasis of BC.

To further identify the underlying mechanism of how NNT-AS1 affects BC cell tumorigenesis and metastasis, we predicted and chose ZFP36 as the potential binding protein of NNT-AS1 by using bioinformatic analysis and experimental verification. ZFP36, the abbreviation of zinc finger protein 36 homolog, also known as Tristetraprolin (TTP), is a protein that in humans, mice and rats is encoded by the ZFP36 gene (22). It is a member of the TIS11 (TPA-induced sequence) family, along with butyrate response factors 1 and 2 (23). ZFP36 binds to AU-rich elements (AREs) in the 3'-untranslated regions (UTRs) of the mRNAs of some cytokines and promotes their degradation (24). Abnormal regulation of ZFP36 is involved in various pathological processes including inflammatory and immune response (25). Importantly, dysregulation of ZFP36 also plays a vital role in cancers. ZFP36 is able to regulate several downstream transcripts which are closely connected to proliferation, apoptosis, chemotherapy efficiency and resistance and angiogenesis of tumors, and a deficiency of ZFP36 also contributes to invasion and metastasis of cancers (26). It is also

reported that ZFP36 could mediate anti-proliferation and induce cell cycle arrest in BC (27). However, the underlying upstream mechanism of ZFP36 in BC has not yet been well identified and reported. In our present study, we initially revealed that ZFP36 was directly combined with NNT-AS1, and ZFP36 expression was inversely correlated with NNT-AS1 in BC tissues and cell lines, whilst overexpression of ZFP36 led to a potential trend to prolong the survival rate of BC patients. Moreover, silencing of ZFP36 could rescue tumor suppression role by NNT-AS1 downregulation on BC cell growth and metastasis. The evidence indicated that NNT-AS1 might be the upstream of ZFP36 involved in BC tumorigenesis and metastasis.

In summary, our present study demonstrated that knockdown of NNT-AS1 suppressed BC progression and metastasis via interacting with ZFP36 *in vitro* and *in vivo*. Our findings may help to further elucidate the molecular mechanisms underlying BC progression and development and provide NNT-AS1 as an innovative and candidate target for treatment and prognosis evaluation on BC.

REFERENCES

1. McCaughan E, Parahoo K, Hueter I, Northouse L, Bradbury I. Online support groups for women with breast cancer. Cochrane Database Syst Rev 2017; 3:D11652.
2. Yu LY, Tang J, Zhang CM, et al. New immunotherapy strategies in breast cancer. Int J Environ Res Public Health 2017; 14.
3. DeSantis CE, Fedewa SA, Goding SA, Kramer JL, Smith RA, Jemal A. Breast cancer statistics, 2015: Convergence of incidence rates between black and white women. CA Cancer J Clin 2016; 66:31-42.
4. Linos E, Spanos D, Rosner BA, et al. Effects of reproductive and demographic changes on breast cancer incidence in China: a modeling analysis. J Natl Cancer Inst 2008; 100:1352-60.
5. Fan W, Chang J, Fu P. Endocrine therapy resistance in breast cancer: current status, possible mechanisms and overcoming strategies. Future Med Chem 2015; 7:1511-19.
6. Adams BD, Parsons C, Walker L, Zhang WC, Slack FJ. Targeting noncoding RNAs in disease. J Clin Invest 2017; 127:761-71.
7. Chaudhary R, Lal A. Long noncoding RNAs in the p53 network. Wiley Interdiscip Rev RNA 2017; 8.
8. Babaian A, Mager DL. Endogenous retroviral promoter exaptation in human cancer. Mob DNA 2016; 7:24.
9. Zhang L, Zhou Y, Huang T, Cheng AS, Yu J, Kang W, To KF. The interplay of LncRNA-H19 and its binding partners in physiological process and gastric carcinogenesis. Int J Mol Sci 2017; 18.
10. Yu Q, Zhou X, Xia Q, et al. Long non-coding RNA CCAT1 that can be activated by c-Myc promotes pancreatic cancer cell proliferation and migration. Am J Transl Res 2016; 8:5444-54.
11. Su J, Zhang E, Han L, et al. Long noncoding RNA BLACAT1 indicates a poor prognosis of colorectal cancer and affects cell proliferation by epigenetically silencing of p15. Cell Death Dis 2017; 8:e2665.
12. Ma P, Zhang M, Nie F, Huang Z, He J, Li W, Han L. Transcriptome analysis of EGFR tyrosine kinase inhibitors resistance associated long noncoding RNA in non-small cell lung cancer. Biomed Pharmacother 2017; 87:20-26.
13. Hu Y, Sun X, Mao C, et al. Upregulation of long noncoding RNA TUG1 promotes cervical cancer cell proliferation and migration. Cancer Med 2017; 6:471-82.
14. Jin Y, Cui Z, Li X, Jin X, Peng J. Upregulation of long non-coding RNA PlncRNA-1 promotes proliferation and induces epithelial-mesenchymal transition in prostate cancer. Oncotarget 2017; 8:26090-99.
15. Wang Q, Yang L, Hu X, et al. Upregulated NNT-AS1, a long noncoding RNA, contributes to proliferation and migration of colorectal cancer cells in vitro and in vivo. Oncotarget 2017; 8:3441-53.
16. Tong W, Yang L, Yu Q, Yao J, He A. A new tumor suppressor lncRNA RP11-190D6.2 inhibits the proliferation, migration, and invasion of epithelial ovarian cancer cells. Onco Targets Ther 2017; 10:1227-35.
17. Xu Y, Wang B, Zhang F, et al. Long non-coding RNA CCAT2 is associated with poor prognosis in hepatocellular carcinoma and promotes tumor metastasis by regulating Snail2-mediated epithelial-mesenchymal transition. Onco Targets Ther 2017;

10:1191-98.
18. Gao YL, Zhao ZS, Zhang MY, Han LJ, Dong YJ, Xu B. Long noncoding RNA PVT1 facilitates cervical cancer progression via negative regulating of miR-424. Oncol Res 2017; 25:1391-98.
19. Wu ZJ, Li Y, Wu YZ, et al. Long non-coding RNA CCAT2 promotes the breast cancer growth and metastasis by regulating TGF-beta signaling pathway. Eur Rev Med Pharmacol Sci 2017; 21:706-14.
20. Liu M, Xing LQ, Liu YJ. A three-long noncoding RNA signature as a diagnostic biomarker for differentiating between triple-negative and non-triple-negative breast cancers. Medicine (Baltimore) 2017; 96:e6222.
21. Cai C, Huo Q, Wang X, Chen B, Yang Q. SNHG16 contributes to breast cancer cell migration by competitively binding miR-98 with E2F5. Biochem Biophys Res Commun 2017; 485:272-78.
22. Sanduja S, Blanco FF, Young LE, Kaza V, Dixon DA. The role of tristetraprolin in cancer and inflammation. Front Biosci (Landmark Ed) 2012; 17:174-88.
23. Sanduja S, Blanco FF, Dixon DA. The roles of TTP and BRF proteins in regulated mRNA decay. Wiley Interdiscip Rev RNA 2011; 2:42-57.
24. Takeuchi O. [Regulation of immune responses by mRNA stability control]. Seikagaku 2010; 82:1124-28.
25. Beiter T, Hoene M, Prenzler F, et al. Exercise, skeletal muscle and inflammation: ARE-binding proteins as key regulators in inflammatory and adaptive networks. Exerc Immunol Rev 2015; 21:42-57.
26. Wang H, Ding N, Guo J, Xia J, Ruan Y. Dysregulation of TTP and HuR plays an important role in cancers. Tumour Biol 2016; 37:14451-61.
27. Pandiri I, Chen Y, Joe Y, Kim HJ, Park J, Chung HT, Park JW. Tristetraprolin mediates the anti-proliferative effects of metformin in breast cancer cells. Breast Cancer Res Treat 2016; 156:57-64.

LIPOXIN A4 ALLEVIATES LUNG INJURY IN SEPSIS RATS THROUGH P38/MAPK SIGNALING PATHWAY

X.-H. HU[1], J.-P. CHEN[2] and R.-H. YU[3]

[1]Department of ICU, Shanghai Xuhui District Central Hospital, Shanghai, China; [2]Health Care Center, Shanghai University of Medicine & Health Sciences, Shanghai, China; [3]Department of Respiratory Medicine, Shanghai Xuhui District Central Hospital, Shanghai, China

Received February 22, 2020 – Accepted April 22, 2020

The aim of the study was to explore the effect of lipoxin A4 (LXA4) on lung injury in sepsis rats through the p38/mitogen-activated protein kinase (MAPK) signaling pathway. Sprague-Dawley rats were used for the study. The rat model of sepsis-induced acute lung injury was established via cecal ligation (Sepsis group, n=20). LXA4 (0.1 mg/kg) was injected at 6 h after modeling (Treatment group, n=20), and a The Control group (n=20) was also set up. The 7-day survival rate was 100% in The Control group, and LXA4 raised the survival rate of rats in the Sepsis group from 40% to 60% (P<0.01). Alveolar fluid clearance (AFC) significantly declined and the wet/dry weight (W/D) ratio of lung tissues rose remarkably in the Sepsis group compared with those in the Control group, while LXA4 restored AFC and reduced the W/D ratio of lung tissues (P<0.05), suggesting that LXA4 treatment reduces lung fluids and partially enhances AFC, thus lowering the W/D ratio of lung. The total cell count, polymorphonuclear neutrophils (PMN) percentage and concentration of tumor necrosis factor-α (TNF-α) and interleukin (IL)-6 in bronchoalveolar lavage fluid (BALF) were obviously increased in the Sepsis group compared with those in the Control group, while they were markedly decreased in the Treatment group (P<0.05). The activity of myeloperoxidase (MPO) in lung tissue homogenate was evidently higher in the Sepsis group than that in The Control group, while it was notably lower in the Treatment group than that in the Sepsis group after LXA4 treatment (P<0.05). Moreover, it was observed microscopically that the morphology of lung tissues was intact in the Control group. Finally, the results of Western blotting manifested that the p-p38/MAPK protein expression was remarkably increased in the Sepsis group, indicating the activation of the p38/MAPK pathway, while it was remarkably decreased in the Treatment group, indicating the inhibited activity of the pathway (P<0.05). LXA4 has an anti-inflammatory effect on sepsis rats with lung injury, and such effect is related to the p38/MAPK signaling pathway.

Acute lung injury (ALI) and acute respiratory distress syndrome (ARDS) occur easily in critically ill patients, resulting in high mortality (1, 2). In the case of ALI, the protein permeability is increased and the alveolar fluid clearance (AFC) is changed, which are associated with the increased mortality (3-5). AFC refers to the capacity of the alveolar epithelial membrane to remove water from the air in the distal lungs (4, 6, 7). Studies have demonstrated that AFC is helpful for providing the appropriate and necessary

Key words: lipoxin A4; p38/MAPK signaling pathway; sepsis; lung injury in rats

Corresponding Author:
Ronghuan Yu, MM.
Department of Respiratory Medicine,
Shanghai Xuhui District Central Hospital,
966 Huaihai Middle Road, Shanghai 200031, China
Tel.: 86013671765665
e-mail: ronghuang19870116@163.com

0393-974X (2020)
Copyright © by BIOLIFE, s.a.s.
This publication and/or article is for individual use only and may not be further reproduced without written permission from the copyright holder. Unauthorized reproduction may result in financial and other penalties
DISCLOSURE: ALL AUTHORS REPORT NO CONFLICTS OF INTEREST RELEVANT TO THIS ARTICLE.

alveolar gas-liquid interface for adequate gas-blood exchange and resistance to exogenous pathogens (1, 4). In the acute phase of ALI/ARDS, inflammatory factors such as tumor necrosis factor-α (TNF-α) and IL-6 and IL-1β are released. With the progression of disease, there is neutrophil and macrophage infiltration in the alveoli, and even alveolar hemorrhage and erythrocyte infiltration, damaging the alveolar function. Progressively, the subacute phase is characterized by proliferation of type II alveolar cells and interstitial fibrosis. Finally, in the chronic phase, the acute edema/inflammation regresses with tissue repair, accompanied or not by exacerbated fibrosis, indicating incomplete or complete ablation, respectively (8). Therefore, alleviating inflammatory damage and promoting tissue repair are the keys to the treatment of ALI.

Lipoproteins are endogenous lipids involved in the regression of inflammation, including inhibiting the release of pro-inflammatory cytokines, reducing leukocyte-mediated damage and stimulating the increase of macrophages (9, 10). Lipoxin A4 (LXA4), a member of the lipoprotein family, serves as a "brake signal" in the inflammatory response, and promotes the inflammatory response into the regressive phase (10-12). It has been confirmed that LXA4 has unique resolution and anti-edema properties in the ALI model (13, 14). One study found that LXA4 exerts a potent protective effect against ALI, partly because the expression of E-cadherin and the airway epithelial permeability are retained (15). However, the correlation between the protective mechanism of LXA4 in sepsis-induced ALI and the p38/mitogen-activated protein kinase (MAPK) pathway is rarely studied.

MATERIALS AND METHODS

Establishment of rat model of sepsis-induced ALI

Male Sprague-Dawley (SD) rats aged 7 weeks were used as for this study. The rat model of sepsis-induced ALI was established via cecal ligation (Sepsis group), sham operation was performed without cecal ligation and puncture (The Control group), and LXA4 (0.1 mg/kg; cat. no sc-201060, Santa Cruz, CA, USA) was injected at 6 h after modeling (Treatment group). The rats were fed with standard food and water at 23-25°C under a 12/12 h light/dark cycle. Briefly, 6 h before the operation, the rats were deprived of food, but had access to water. After anesthesia via intraperitoneal injection of pentobarbital sodium at a dose of 40 mg/kg at the beginning of the operation for the modeling of sepsis-induced ALI, an abdominal median incision was made for laparotomy, and the cecum was externalized and ligated in the middle between the distal end and the bottom of the cecum. Then the cecum was punctured once with a 2.5 mm needle and gently pressed until excretion of feces. Next, the rectum was placed to the abdomen, and the abdominal incision was sutured. In The Control group, only sham operation was performed without cecal ligation and puncture, and the cecum was kept intact. This study was approved by the Animal Ethics Committee of Shanghai Xuhui District Central Hospital.

Detection of AFC

At 24 h after modeling or injection of LXA4, the rats were anesthetized and cannulated via tracheotomy. The left lung was resected to measure the wet/dry weight (W/D) ratio of lung tissues. Then the whole trachea, right lung and heart were removed to measure AFC, as follows: The solution (37°C) prepared by saline containing 5% albumin and 0.15 mg/mL Evans blue dye was slowly injected into the right lung. To ensure that all of the solution entered the alveolar space, 12 mL/kg oxygen was delivered after injection. Then the lung was inflated with 100% oxygen at an airway pressure of 5 cmH_2O in an incubator at 37°C. AFC was calculated using the following formula (16-18):

$AFC = [(Vi-Vf)/Vf] \times 100$, where $Vf = (Vi \times EBi)/EBf$ where Vi is the volume of solution prepared by saline and albumin, and Vf is the final volume of alveolar fluids, EB is the concentration of solution (i) and Evans blue dye in final alveolar fluids (f) (19-21).

Determination of total cell count, polymorphonuclear neutrophils (PMN) percentage and concentration of IL-6, TNF-α and MPO in bronchoalveolar lavage fluid (BALF)

The rats were anesthetized by intraperitoneal injection of 4% chloral hydrate. 4 ml 4°C saline was injected into the left lung lobe through the left trachea. The BALF was slowly sucked back after gently massaging the lung tissue for 30s, which was repeated for three times. Then the BALF was centrifuged at 1500r/min for 10 min. After centrifugation, the supernatant and cell precipitate were collected. The levels of TNF-α, IL-6 in BALF were measured according to the instructions of the ELISA kit.

Observation of pathological changes in lung injury via hematoxylin-eosin (HE) staining

After the rats were sacrificed and dissected, the lung tissues were isolated, and the blood was completely washed away with phosphate-buffered saline (PBS). Then the tissues were fixed in 4% paraformaldehyde for at least 24 h, embedded in paraffin and sliced into sections. The sections were preheated in an oven at 65°C overnight, deparaffinized with xylene, dehydrated with alcohol, stained with hematoxylin for the first time and counterstained with eosin, followed by dehydration with alcohol, transparentization with xylene and sealing. Finally, the morphological changes in lung tissues were observed under a microscope (Leica, Wetzlar, Germany), and the lung injury score was calculated.

Lung injury score

The degree of injury of HE-stained lung tissues was observed using the blind method, using four evaluation indexes: presence or absence of alveolar hemorrhage, alveolar congestion, thickness or formation of transparent membrane on the alveolar wall, and the number of infiltrating neutrophils or cells infiltrating the alveolar and vascular walls. As previously described (22), each item was evaluated using grades 0 to 4. The lung injury score (0-16 points) was given based on the summary of the four variables.

Western blotting

After the lung tissue homogenate was frozen, 60 μg of protein was separated via 12% sodium dodecyl sulphate-polyacrylamide gel electrophoresis (SDS-PAGE) in each group. When the protein sample ran to the bottom of the electrophoresis tank, it was transferred onto the NC membrane for 1 h, sealed with blocking buffer for 2 h, and incubated with p-p38 (cat.no 8632), p38 MAPK (cat.no 9129), p-JNK (cat.no 4668), JNK (cat.no 9252) primary antibodies and GAPDH primary antibodies (diluted at 1:1000 or 1:2000; cat.no 5174) and then with anti-rabbit and anti-rat secondary antibodies (diluted at 1:1000), followed by membrane scanning.

Detection of activity of myeloperoxidase

To measure the activity of myeloperoxidase (MPO), lung tissues were homogenized in 50 mmol/L PBS containing 0.5% cetyltrimethyl ammonium bromide and 5 mmol/L EDTA (pH 6.0), followed by centrifugation at 12,500 × g and 4°C for 20 min. After incubation with 50 mmol/L o-aminobenzoyl dichloride hydrochloride containing 30% H_2O_2, the supernatant was taken to detect the absorbance at 460 nm via spectrophotometry, indicating the activity of MPO.

Statistical analysis

The experimental data were expressed as mean ± standard deviation. The survival analysis was conducted by Kaplan-Meier, and Log-rank test was used to compare the survival curves. Differences between two groups were analyzed by using the Student's *t*-test. Comparison between multiple groups was made using One-way ANOVA test followed by Post Hoc Test (Least Significant Difference). $P<0.05$ suggested the statistically significant difference.

RESULTS

LXA4 treatment could improve the survival rate of rats with lung injury

It was found that the 7-day survival rate was 100% in the Control group, while it was increased from 40% to 60% in the Treatment group after LXA4 treatment compared with that in the Sepsis group, showing statistically significant differences ($P<0.01$). The above results suggest that LXA4 can reduce the mortality rate of rats with lung injury (Fig. 1).

LXA4 could restore AFC in sepsis rats with lung injury, and reduce W/D ratio of lung tissues through reducing lung fluids

AFC significantly declined in the Sepsis group compared with that in the Control group, while it was partially restored in the Treatment group compared with that in the Sepsis group, but still below the normal level ($P<0.05$). Consistent with the above results, the W/D ratio of lung tissues rose remarkably in the Sepsis group ($P<0.05$), while it distinctly declined in the Treatment group through reducing lung fluids and partially enhancing AFC ($P<0.05$) (Fig. 2).

LXA4 alleviated inflammatory response and lung injury

The total cell count, polymorphonuclear neutrophils (PMN) percentage and concentration of IL-6, TNF-α and MPO in bronchoalveolar lavage fluid (BALF) were evidently increased in the

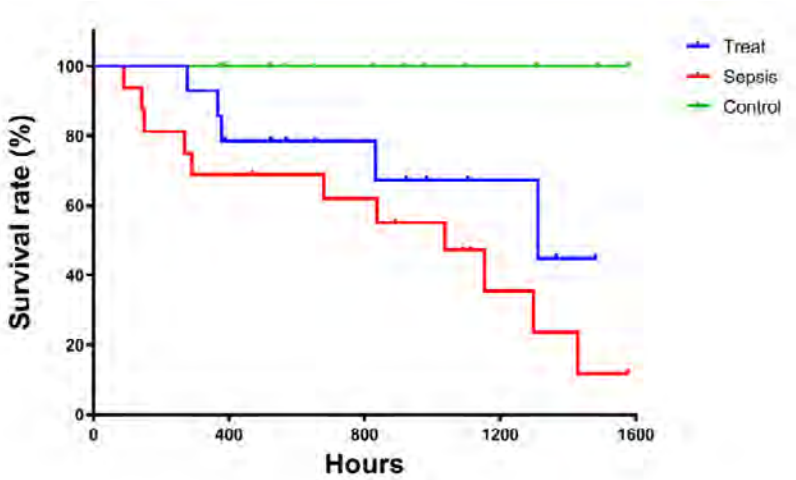


Fig. 1. *7-d survival rate of rats*

Sepsis group ($^{**}P<0.01$), while they were evidently decreased in the Treatment group ($^{\#}P<0.05$), demonstrating that LXA4 treatment alleviates lung injury through reducing the absolute cell count and PMN infiltration in BALF (Fig. 3).

Morphological changes in lung tissues and evaluation of injury degree

It was observed via HE staining that the lung structure was normal in the Control group. In the Sepsis group, there was severe lung injury, mainly manifested as inflammatory cell infiltration and hemorrhage visible under the microscope, and the hyaline membrane could even be seen. In the Treatment group, inflammatory cell infiltration and hemorrhage were markedly relieved, and the lung tissues had normal morphology. Moreover, the lung injury score evidently rose in the Sepsis group ($^{**}P<0.01$), while it clearly declined in the Treatment group ($^{\#}P<0.05$) (Fig. 4).

LXA4 relieved sepsis-induced lung injury through inhibiting p38/MAPK pathway

The proteins in the p38/MAPK pathway are markedly activated in severe lung injury tissues. In this study, the p-p38/MAPK and p-c-Jun N-terminal kinase (JNK) proteins were highly expressed in the Sepsis group ($^{**}P<0.05$), while they exhibited the opposite expressions in the Treatment group, indicating the inhibited activity of the pathway. The above results suggest that LXA4 relieves sepsis-induced lung injury through inhibiting the p38/MAPK pathway (Fig. 5).

DISCUSSION

After being delivered to the lung microenvironment, LXA4 can promote neutrophil apoptosis and enhance the ability of phagocytes to phagocytize apoptotic cells, thus exerting an anti-inflammatory effect in lung tissues (16, 17). Chronic inflammation and fibrosis will occur due to failure to completely scavenge neutrophils from lesions and restore tissue homeostasis. Therefore, lipoxins have been widely used as therapeutic agents for inflammation-related diseases, such as cancer (18-20), arthritis, asthma (20) and cardiovascular diseases (21). Endogenous LXA4 has a short life span, so understanding the mechanism of action of LXA4 in ALI will provide strong support for the development of stable lipoxin analogs or LXA4 receptor agonists.

To determine the effect of LXA4 on ALI, the rat model of ALI was established via cecal ligation in this study. It was proved via morphological evaluation that the W/D ratio of lung tissues rose

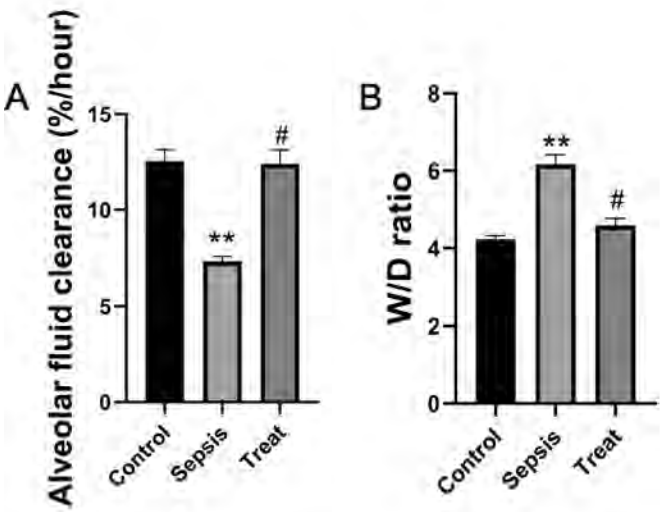


Fig. 2. *Changes in AFC and W/D ratio of lung tissues.* ***A)*** *AFC is obviously lower in the Sepsis group than that in the Control group (**P<0.01), while it is markedly increased in the Treatment group (#P<0.05).* ***B)*** *The W/D ratio is prominently higher in the Sepsis group than that in the Control group (**P<0.01), while it notably declines in the Treatment group (#P<0.05). (**P<0.01 vs Sepsis group, #P<0.05 vs Treatment group)*

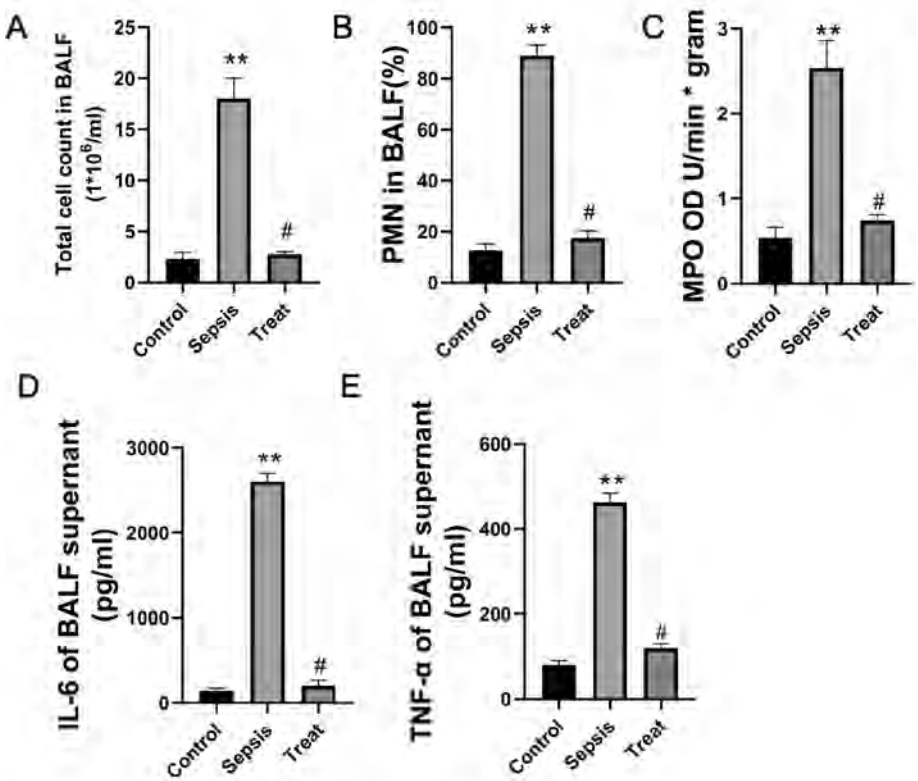


Fig. 3. *Changes in PMN percentage and inflammatory response in BALF in lung tissues.* ***A***, ***B)*** *The total cell count and PMN percentage in BALF are evidently increased in the Sepsis group compared with those in the Control group (**P<0.01), while they are clearly decreased in the Treatment group (#P<0.05).* ***C)*** *The concentration of MPO in lung tissues is markedly increased in the Sepsis group (**P<0.01), while it is distinctly decreased in the Treatment group (#P<0.05).* ***D***, ***E)*** *The concentration of IL-6 and TGF-α in BALF obviously rises in the Sepsis group in comparison with that in the Control group (**P<0.01), while it remarkably declines in the Treatment group compared with that in the Sepsis group (#P<0.05). (**P<0.01 vs Sepsis group, #P<0.05 vs Treatment group)*

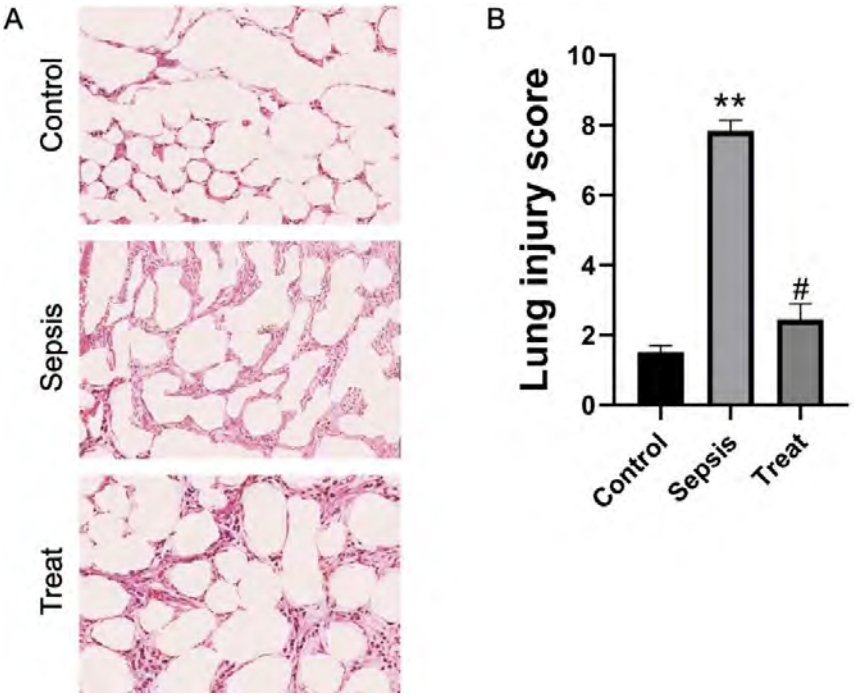


Fig. 4. *Morphological changes in lung tissues.* ***A****) According to the results of HE staining, The Control group has normal morphology of lung tissues, and there is severe lung injury in the Sepsis group, and mild lung injury in the Treatment group (magnification: 400×).* ***B****) The lung injury score is remarkably higher in the Sepsis group than that in the Control group (****P<0.01), while it is evidently lower in the Treatment group than that in the Sepsis group (*$^{\#}$*P<0.05). (****P<0.01 vs Sepsis group,* $^{\#}$*P<0.05 vs Treatment group)*

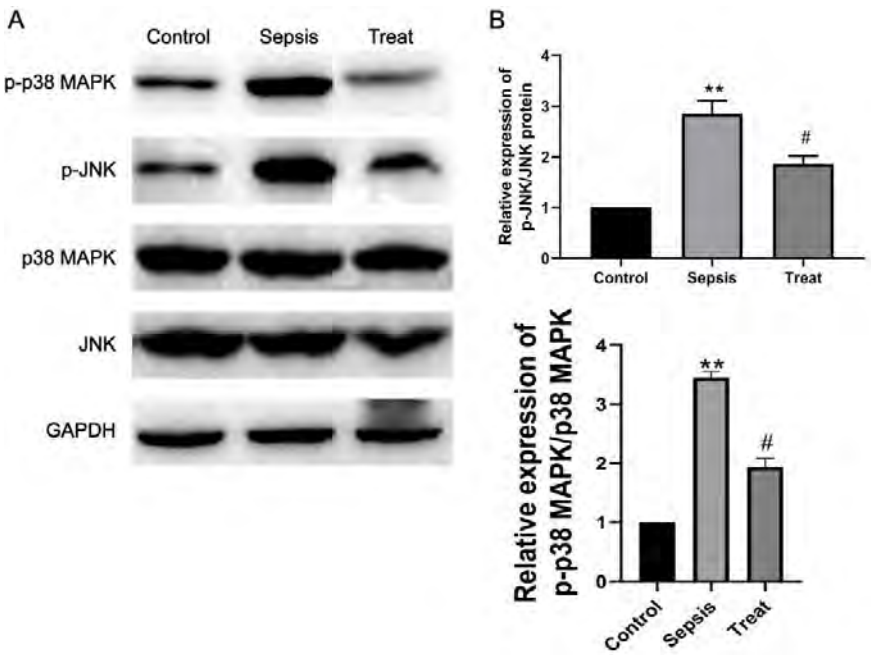


Fig. 5. *Changes in p38/MAPK and JNK protein expressions in injured lung tissues.* ***A****,* ***B****) The p-p38/MAPK and p-JNK proteins have significantly higher expressions in the Sepsis group than those in the Control group (****P<0.01), while they have prominently lower expressions in the Treatment group than those in the Sepsis group (*$^{\#}$*P<0.05). (****P<0.01 vs Sepsis group,* $^{\#}$*P<0.05 vs Treatment group)*

and AFC declined in the Sepsis group. According to the measurement results of concentration of pro-inflammatory cytokines in BALF and severity of lung injury, there was fluid accumulation after lung injury. After LXA4 treatment, the damage to fluid transport was partially restored, accompanied by decrease in inflammatory response and decline in lung morphological damage. The above phenomena were related to the increased survival rate of rats in the Treatment group. Based on previous research on the effect of LXA4 on acute pancreatitis-associated ALI (22), it was confirmed in this study that the effect of LXA4 on ALI is realized via inhibiting inflammation and restoring AFC. In the above two studies, the authors discovered the protective effect of LXA4 through the mechanism involving the cytoskeletal protein F-actin or AJ-labeled E-cadherin (23), both of which can maintain the integrity of barrier function. Similar to the authors' observations, it was found in this study that AFC could be partially restored by LXA4 treatment, which is also the result of maintaining the integrity of barrier function. In addition, the total cell count and PMN percentage in BALF are used as markers for acute pneumonia. MPO is a marker for PMN infiltration in the lung, so the concentration of MPO in lung tissue homogenate was evaluated. The results showed that the total cell count and PMN percentage in BALF in the Sepsis group were obviously higher than those in the Control group, and the Sepsis group also had evidently increased concentration of IL-6, TNF-α and MPO. After LXA4 treatment, both PMN percentage and MPO concentration declined, suggesting that LXA4 treats lung injury through reducing PMN infiltration in BALF. Moreover, the morphological damage of lung tissues was assessed using pathological examination. The results revealed that the Control group displayed normal structure of lung tissues, there was severe ALI in the Sepsis group, and lung injury was significantly improved by LXA4 in the Treatment group. To explore the mechanism of action of the p38/MAPK pathway in ALI, the changes in expressions of p-p38/MAPK and p-JNK proteins in lung tissues were determined. It was observed that the p-p38/MAPK and p-JNK proteins were highly expressed in the Sepsis group, while they had the opposite expressions in the Treatment group, indicating that LXA4 exerts an anti-inflammatory effect against lung injury via inhibiting the activity of the p38/MAPK pathway. However, there some limitations in the present study. The inhibitor of P38/MAPK signaling pathway was not included, the specific mechanisms need further investigation.

To sum up, these findings demonstrate that LXA4 is a potential new strategy for improving anti-inflammatory treatment to reduce damage to alveolar fluid transport in ALI.

ACKNOWLEDGEMENT

This study was funded by the Shanghai Medical Key Specialty Foundation (ZK2019C14).

REFERENCES

1. Vadasz I, Sznajder JI. Gas exchange disturbances regulate alveolar fluid clearance during acute lung injury. Front Immunol 2017; 8:757.
2. Chen LJ, Ding YB, Ma PL, et al. The protective effect of lidocaine on lipopolysaccharide-induced acute lung injury in rats through NF-kappaB and p38 MAPK signaling pathway and excessive inflammatory responses. Eur Rev Med Pharmacol Sci 2018; 22:2099-108.
3. Huppert LA, Matthay MA. Alveolar fluid clearance in pathologically relevant conditions: in vitro and in vivo models of acute respiratory distress syndrome. Front Immunol 2017; 8:371.
4. Matthay MA. Alveolar fluid clearance in patients with ARDS: does it make a difference? Chest 2002; 122:340S-343S.
5. Laffey JG, Matthay MA. Fifty years of research in ARDS. Cell-based therapy for acute respiratory distress syndrome. Biology and potential therapeutic value. Am J Respir Crit Care Med 2017; 196:266-73.
6. Planes C, Leyvraz C, Uchida T, et al. In vitro and in vivo regulation of transepithelial lung alveolar sodium transport by serine proteases. Am J Physiol Lung Cell Mol Physiol 2005; 288:L1099-L109.
7. Ware LB, Matthay MA. Clinical practice. Acute pulmonary edema. N Engl J Med 2005; 353:2788-96.

8. Matthay MA, Zemans RL. The acute respiratory distress syndrome: pathogenesis and treatment. Annu Rev Pathol 2011; 6:147-63.
9. Walker J, Dichter E, Lacorte G, Kerner D, Spur B, Rodriguez A, Yin K. Lipoxin a4 increases survival by decreasing systemic inflammation and bacterial load in sepsis. Shock 2011; 36:410-16.
10. Wu B, Walker J, Spur B, Rodriguez A, Yin K. Effects of Lipoxin A4 on antimicrobial actions of neutrophils in sepsis. Prostaglandins Leukot Essent Fatty Acids 2015; 94:55-64.
11. Cheng Q, Wang Z, Ma R, et al. Lipoxin A4 protects against lipopolysaccharide-induced sepsis by promoting innate response activator B cells generation. Int Immunopharmacol 2016; 39:229-35.
12. Wang YP, Wu Y, Li LY, et al. Aspirin-triggered lipoxin A4 attenuates LPS-induced pro-inflammatory responses by inhibiting activation of NF-kappaB and MAPKs in BV-2 microglial cells. J Neuroinflammation 2011; 8:95.
13. Wang Q, Lian QQ, Li R, et al. Lipoxin A(4) activates alveolar epithelial sodium channel, Na,K-ATPase, and increases alveolar fluid clearance. Am J Respir Cell Mol Biol 2013; 48:610-18.
14. Cheng X, He S, Yuan J, et al. Lipoxin A4 attenuates LPS-induced mouse acute lung injury via Nrf2-mediated E-cadherin expression in airway epithelial cells. Free Radic Biol Med 2016; 93:52-66.
15. Leger PL, Bonnin P, Renolleau S, Baud O, Charriaut-Marlangue C. Ischemic postconditioning in cerebral ischemia: Differences between the immature and mature brain? Int J Dev Neurosci 2015; 45:39-43.
16. Herold S, Mayer K, Lohmeyer J. Acute lung injury: how macrophages orchestrate resolution of inflammation and tissue repair. Front Immunol 2011; 2:65.
17. Serhan CN, Chiang N, Van Dyke TE. Resolving inflammation: dual anti-inflammatory and pro-resolution lipid mediators. Nat Rev Immunol 2008; 8:349-61.
18. Chen Y, Hao H, He S, et al. Lipoxin A4 and its analogue suppress the tumor growth of transplanted H22 in mice: the role of antiangiogenesis. Mol Cancer Ther 2010; 9:2164-74.
19. Janakiram NB, Rao CV. Role of lipoxins and resolvins as anti-inflammatory and proresolving mediators in colon cancer. Curr Mol Med 2009; 9:565-79.
20. Levy BD. Lipoxins and lipoxin analogs in asthma. Prostaglandins Leukot Essent Fatty Acids 2005; 73:231-37.
21. Vital SA, Becker F, Holloway PM, Russell J, Perretti M, Granger DN, Gavins FN. Formyl-peptide receptor 2/3/Lipoxin A4 receptor regulates neutrophil-platelet aggregation and attenuates cerebral inflammation: impact for therapy in cardiovascular disease. Circulation 2016; 133:2169-79.
22. Olkkola KT, Kontinen VK, Saari TI, Kalso EA. Does the pharmacology of oxycodone justify its increasing use as an analgesic? Trends Pharmacol Sci 2013; 34:206-14.
23. Raedschelders K, Ansley DM, Chen DD. The cellular and molecular origin of reactive oxygen species generation during myocardial ischemia and reperfusion. Pharmacol Ther 2012; 133:230-55.

LONG NONCODING RNA GAS5 ENHANCED BY CURCUMIN RELIEVES POST-STROKE DEPRESSION BY TARGETING miR-10b/BDNF IN RATS

L. CAI*, W-T. LI*, L-L. ZHANG, X-Q. LU, M. CHEN and Y. LIU

Department of Neurology, Shanghai Municipal Hospital of Traditional Chinese Medicine, Shanghai University of Traditional Chinese Medicine

Received February 23, 2020 -

*These Authors contributed equally to this work

The treatment for post-stroke depression (PSD) is mainly based on a therapeutic strategy combining anti-stroke and anti-depressant drugs. In the present study, the therapeutic effect of curcumin on rats with PSD was detected by open field tests and tail suspension tests, as well as the examination of corticosterone and corticotropin-releasing hormone (CRH) levels in the serum and neurotransmitter 5-hydroxytryptamine (5-HT), 5-hydroxyindoleacetic acid (5-HIAA) and dopamine (DA) levels in the hippocampus. Curcumin notably alleviated depression compared to the controls. Furthermore, long noncoding RNA growth arrest-specific transcript 5 (GAS5) enhanced by curcumin contributed to activation of the BDNF/Trkβ signaling pathway to promote the **expression of synaptic-related proteins. GAS5 was demonstrated to function as a sponge of miR-10b. GAS5 upregulation by curcumin could reduce miR-10b to compromise the BDNF mRNA levels. Taken together, these results revealed a novel mechanism of curcumin on PSD through the GAS5/miR-10b/BDNF regulatory axis.**

Post-stroke depression (PSD) is considered the most frequent and important neuropsychiatric consequence of stroke, and approximately one-third of stroke survivors experience major depression (1). Depression after stroke generally has a chronic course and is related to various adverse health outcomes, including increased disability, morbidity and mortality (2, 3). Antidepressant treatment initiated soon after stroke may prevent the emergence of PSD. The treatment of post-stroke depression is based on the treatment of stroke in combination with antidepressant drugs (4). *In vivo* and *in vitro* studies have shown that fluoxetine is one of the most commonly prescribed antidepressants and prevents degeneration of the nigrostriatal dopaminergic neurons; however, this phenomenon was accompanied by marked repression of microglial activation, neutrophil infiltration and expression of proinflammatory markers (5). Thus, treatment with antidepressants will likely minimize these side effects and the release of proinflammatory cytokines.

Brain-derived neurotrophic factor (BDNF) is a 119-amino acid non-glycosylated polypeptide (6). Initially synthesized as a 247-aa prepropeptide, the BDNF molecule is divided into an 18-aa signal sequence, a 110-aa prosequence (Pro BDNF), and a 119-aa mature segment. BDNF is a (7, 8) member of the neurotrophin family and has multiple functions,

Key words: curcumin; GAS5; miR-10b; PSD; BDNF/Trkβ

Correspondng Author:
Dr Yi Liu,
Department of Neurology,
Shanghai Municipal Hospital of Traditional Chinese Medicine,
Shanghai University of Traditional Chinese Medicine,
No. 274 Middle Zhi Jiang Road, Jing'an District, Shanghai,
200071, People's Republic of China
e-mail: liuyipub888@aliyun.com

0393-974X (2020)
Copyright © by BIOLIFE, s.a.s.
This publication and/or article is for individual use only and may not be further reproduced without written permission from the copyright holder. Unauthorized reproduction may result in financial and other penalties
DISCLOSURE: ALL AUTHORS REPORT NO CONFLICTS OF INTEREST RELEVANT TO THIS ARTICLE.

including neuronal survival, neuronal development and synaptic plasticity in the central nervous system (9). Activated BDNF acts through the high-affinity tropomysin-related kinase B (Trkβ) receptor (10).

In recent years, curcumin as a complementary and alternative therapy has been demonstrated to protect against neuropsychiatric disorders such as major depression, post-traumatic stress disorder, obsessive-compulsive disorder, bipolar disorder, psychotic disorders and autism (11, 12). Curcumin is acknowledged to have antioxidant, anti-inflammatory and even anticancer effects and to have a crucial role in the prevention and treatment of various illnesses. In studies on kidney injury, diabetes and cancer, curcumin was reported to be associated with the PI3K/AKT, WNT/β-catenin and mTOR signaling pathways (13-15). However, the molecular mechanism of curcumin underlying the prevention of depression in the nervous system is still obscure, and the connection between curcumin and BDNF/Trkβ also remains unclear. In this study, the therapeutic effect of curcumin on a rat model of PSD was examined, and the regulatory BDNF/Trkβ pathway in nerve cells was assessed.

MATERIALS AND METHODS

Animal study

Sprague Dawley rats (purchased from SLACCAS Co., Ltd., Shanghai, China) were housed in clean cages and maintained at 22±2°C with a constant 12-h light/dark schedule. The animals were allowed free access to food and water. This project was approved by the Medical Ethics Committee of Shanghai. The stroke model was established by unilateral internal carotid artery ligation in accordance with a previously published method (4). All rats were separately housed and randomly subjected to 11 types of different stimuli for 22 days: behavioral restriction for 2 h, ice water swimming for 5 min at 4°C, fasting for 24 h, loss of access to water for 24 h, tail clamping for 1 minute, light-dark reversal for 24 h, electric shock on a footplate for 10 min (1 mA electric current, 30 V voltage, once every 10 s, each for 1 second, total 60 times), inclination of the home cage at 45° for 24 h, moist padding for 24 h, an empty bottle for 2 h and shaking (50 Hz) at 45°C for 5 min. During the entire period, only one stimulus was administered per day, and all 11 types of stimuli were randomly ordered twice in 22 days, so the rats could not adapt to the stimulus. Curcumin was given at 200 mg/kg/day as previously described (16, 17), and fluoxetine (Eli Lilly, USA) was given at 10 mg/kg/day via intragastric administration for one month.

Establishment of a successful model was validated by behavioral examination, such as the open field test and tail suspension test, as well as biochemical indexes including the levels of corticosterone and corticotropin-releasing hormone (CRH) in serum and neurotransmitters such as 5-hydroxytryptamine (5-HT), 5-hydroxyindoleacetic acid (5-HIAA) and dopamine (DA) in the hippocampus. Behavioral examinations, such as the open field test (18) and tail suspension test (19), were performed to identify the effectiveness of the post-stroke depression model. In brief, a glass arena (40 cm L × 40 cm W × 30 cm H) was divided into the center and periphery by 16-beam animal activity monitors. First, each rat was released from the same corner of the arena, and the arena was explored freely for 10 min. The number of grids passed and the time of latency to the center were both recorded. In the tail suspension test, rats were hung by their tails 50 cm above the floor with adhesive tape for 6 min. The latency of the first episode of immobility and the duration of immobility in the entire 6-min period were recorded using criteria that were previously described (19). Immobility was defined as a motionless head and body. The latency of immobility was determined as the time between the onset of the test and the first episode of immobility. Peripheral blood was isolated from the caudal vein for the CORT and CRH tests using an ELISA kit (Thermo Fisher Scientific, Waltham, MA, USA) in accordance with the instructions provided. The cell lysates of the hippocampus treated with RIPA buffer were harvested for assays of neurotransmitters, including 5-HT, 5-HIAA and DA, using HPLC-ECD analysis (20). Twenty-microliter samples were added into the flow phase at 1 ml/min with 829 ml of 0.15 mol/L sodium citrate-hydrochloric acid buffer, 1 ml of 0.1 mol/L EDTA, 1.416 g of sodium heptanesulfonate and 150 ml of methanol and processed under 700 mV. The peaks at 3.5 min, 4.8 min and 8.5 min corresponded to 5-HIAA, DA and 5-HT, respectively.

RNAi oligos of GAS5 or miR-10b were inserted into the pLKO-EGFP vector (Addgene, #32684, Watertown, MA, USA). The full-length GAS5 sequence was inserted into the pLVX-EGFP vector (Addgene, #73331). Lentiviruses were packaged at 2×10^9 TU/ml (pLKO: VSVG: delta8.9 as

5:1:5 and pLVX: PSPAX: pMD as 4:3:1). The anesthetized rats were fixed in a stereotaxic apparatus, the hair on the head was removed, the skin was cut, and the bregma was exposed. Two microliters of lentivirus was gently injected into the bilateral hippocampus 3.0 mm behind the bregma, 2.0 mm to the right of the central line and 2.8 mm vertically. Rats were sacrificed, and the hippocampus was harvested seven days later for subsequent experiments.

Luciferase reporter assay

The 293T cells obtained from the American Type Culture Collection (ATCC, Manassas, VA, USA) were cultured in DMEM (Thermo Fisher Scientific) supplemented with 10% fetal bovine serum (Gibco, Carlsbad, CA, USA) with 5% CO_2 at 37°C. GAS5 and miR-10b were cloned into the pmirGLO vector (Promega, Madison, WI, USA). The plasmids were transfected into 293T cells using Lipofectamine 3000 (Thermo Fisher Scientific). Then, a dual-luciferase reporter assay system (Promega) was used to detect luciferase activity in the cell lysates 48 h post-transfection.

Western blot assay

The hippocampal tissue was harvested and placed in cold radioimmunoprecipitation assay buffer containing freshly prepared 2 mM PMSF (Beyotime Bio, Nantong, Jiangsu Province, China). Tissue blocks were ground on ice for 30 min and centrifuged at 13000 × g for 30 min at 4°C. Before loading onto a 12% sodium dodecyl sulfate-polyacrylamide gel, equal amounts of protein were boiled with 10× loading buffer for 5 min. Electrophoresis was performed at 80 V for 30 min and 120 V for 120 min. Separated proteins were transferred onto a polyvinylidene difluoride membrane at 120 V for 120 min. Membranes were blocked with 5% nonfat dry milk overnight at 4°C and then incubated with primary antibody, rabbit polyclonal anti-BDNF (1:1000; Sigma, Billerica, MA, USA), anti-Trkβ, anti-Trkβ (phospho Y515), anti-PI3K, anti-PI3K p85α (phospho Y607), anti-Akt, anti-Akt (phospho T308), anti-CREB, anti-CREB (phospho S133), and anti-SYN1 (1:1000; Abcam, Cambridge, MA, USA) overnight at 4°C. Equal loading of the proteins was confirmed by subsequent GAPDH immunoblots (1:5000; Sigma). Immunodetection was performed by electrochemiluminescence (Pierce, Rockford, IL, USA) after incubation with horseradish peroxidase-conjugated goat anti-rabbit or rabbit anti-mouse (1:5000; Jackson ImmunoResearch, USA) antibody for 1 hour at 37°C, and the X-ray films were finally photographed.

Immunofluorescence

Rats were anesthetized with 10% chloral hydrate and intracardially perfused with a saline solution followed by a 4% solution of paraformaldehyde in phosphate-buffered saline (PBS). Brains were postfixed for 24 h, transferred to 30% sucrose/PBS solution and sectioned on a sliding freezing microtome (Leica, Germany). Coronal sections (20 μm) were coated on the slides. Immunofluorescence (IF) staining was performed using anti-SYN1 (1:200; Abcam). After 4 washes with PBS (5 min per wash), the slices were incubated with goat anti-mouse secondary antibody (1:20000; Jackson ImmunoResearch, USA). Then, the cells were incubated with DAPI for 15 min and washed with PBS 4 times. After drying in air, the slices were coated with mounting medium and covered with cover glasses. The positive staining was statistically analyzed using *ImageJ*.

Real-time PCR

Total RNA of the hippocampus was extracted using TRIzol and quantified using a Nanodrop. One hundred nanograms of RNA was used to conduct reverse transcription with a High Capacity cDNA Reverse Transcription Kit. One microliter of product was used as the template for PCR preparation. Primers are listed in Table I. Analysis of the DNA templates from RNA reverse transcription and pull down samples of ChIP and 3C were conducted via qPCR using the QuantStudio 3 system (Thermo Fisher Scientific). In accordance with the given instructions, the PCR conditions were as follows: 95°C for 30 s for the initial denaturation, followed by 40 cycles at 95°C for 5 s, appropriate annealing temperatures (Table I) for 10 s and 72°C for 30 s. Ct values were collected and calculated by using the delta-delta method. The expression of GAPDH was used as a quality control.

Statistical analysis

The data are presented as the mean ± SEM. All statistical analyses were performed using SPSS 20.0 statistical software. Group comparisons were performed with one-way ANOVA. A p value less than 0.05 was considered significant.

RESULTS

Curcumin effectively alleviates the PSD phenotype in a rat model

Initially, rat models of PSD were prepared by unilateral internal carotid artery ligation and multiple stimuli and then treated with curcumin or fluoxetine (see the Materials and Methods for details). The fluoxetine-treated group was used as a positive control. The open field test and tail suspension test were employed to verify the mental states and the therapeutic effect of curcumin on the rats with PSD (Fig. 1 A-D). Moreover, the levels of CORT and CRH in the serum and the neurotransmitters 5-HT, 5-HIAA and DA in the hippocampus were investigated (Fig. 1 E-I). Our results determined that the rats with PSD displayed a pattern of weak behavioral changes and aberrant biochemical parameters in the serum and hippocampus compared to the normal control (NC) rats, but these parameters were alleviated upon curcumin or fluoxetine treatment. Then, the phenotype of SYN1 in the curcumin-treated neurons of the rats with PSD was investigated due to the important role of SYN1 in neuritogenesis and synaptogenesis (21) (Fig. 1 J , K and Fig. 2A, B). The expression of SYN1 was reduced in the dentate gyrus area of the hippocampus of the PSD group compared to the NC group but was significantly upregulated in the curcumin or fluoxetine groups compared to the PSD group. Taken together, these results determined that curcumin could effectively relieve PSD via enhancement of SYN1 expression.

*lncRNA GAS5 enhanced by curcumin contributes to BDNF/Trk*β *signaling pathway activation*

Previous studies revealed that fluoxetine and curcumin function in neurological disorders via the PI3K/Akt/CREB/BDNF-mediated signaling pathway (22-25). Therefore, this pathway was investigated, and the results showed that BDNF/

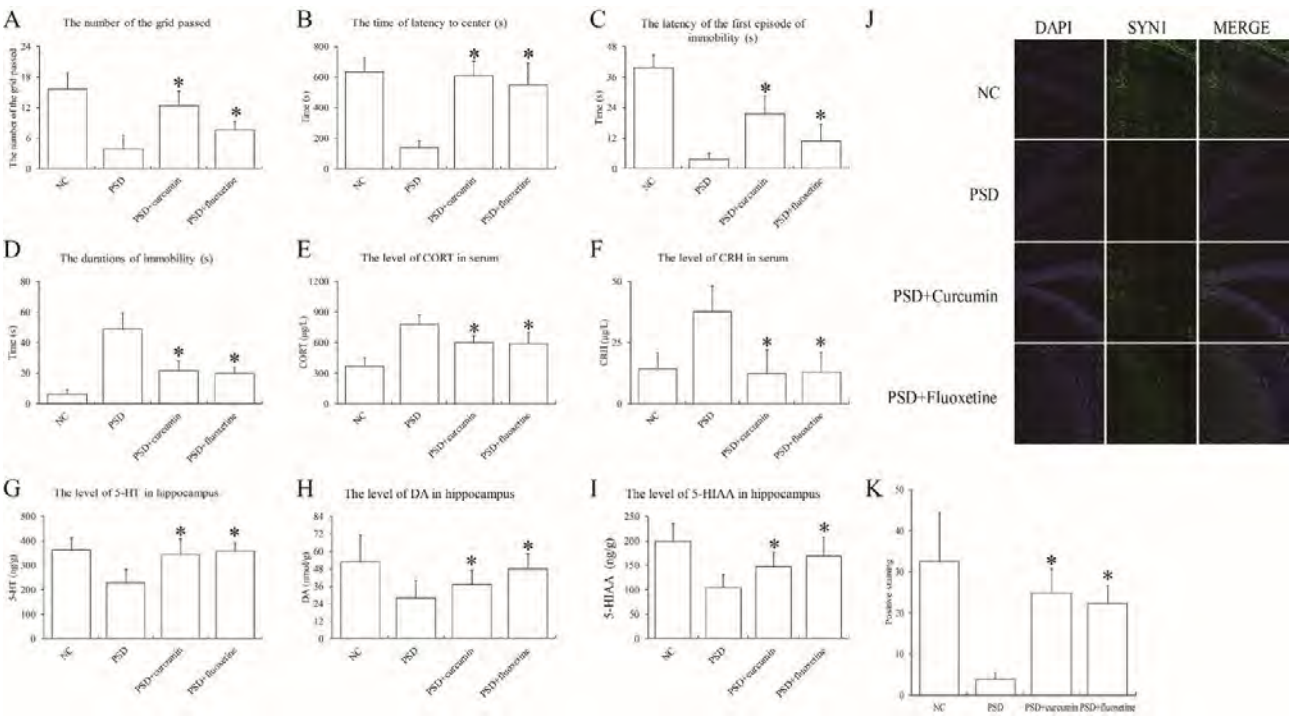


Fig. 1. *Analysis of the PSD model with curcumin treatment. The open field test was performed to determine the number of grids passed (**A**) and the latency to the center region (**B**). The tail suspension test was performed to determine the latency of the first episode of immobility (**C**) and the duration of immobility (**D**). The levels of CORT (**E**) and CRH (**F**) in the serum and the levels of 5-HT (**G**), DA (**H**), and 5-HIAA (**I**) in the hippocampal tissues were determined. The immunofluorescence results (**J**) and analysis (**K**) of SYN1 in the dentate gyrus of the hippocampus are shown. NC indicates negative control. PSD indicates post-stroke depression. Each group had five individuals. * represents a significant difference with a p value less than 0.05.*

Trkβ in the hippocampus declined in the PSD model compared to that in the NC group and increased after curcumin or fluoxetine treatment (Fig. 2 A, B), which was consistent with previous studies. For further analysis of the molecular mechanism of curcumin in the regulation of the BDNF/Trkβ pathway, the transcriptional levels of known long noncoding RNAs (lncRNAs), which are regulatory targets of curcumin in other diseases and include GAS5, HOTAIR, MEG3, PANDAR, PVT1, ROR, and UCA1, were investigated, and only GAS5 was obviously upregulated upon curcumin treatment in the hippocampal tissues among various lncRNAs (Fig. 2C). Thus, a potential link between GAS5 and the BDNF/Trkβ pathway was assumed. GAS5 was overexpressed or knocked down via intracerebroventricular injection of packaged lentivirus (Figure 2D-G). GAS5 could promote the BDNF transcriptional levels and activate the BDNF/Trkβ signaling pathway in the PSD model. However, GAS5 did not change either the Akt or CREB phosphorylation levels, which indicated that GAS5

Table I. *Primers used in this study*

Symbol names	Sequence	Annealing temperature
GAS5 full length	GTGAGGCGAAGCTGAGCAGGA GCTACAATAATGCACTTTT	56
GAS5 detection	GGTGGAGTTTGAATCAGGT GCTACAATAATGCACTTTT	58
GAS5 RNAi oligo	GGAAGCTGGATAACTGAACAA	
HOTAIR	ACGGGATTCACCGGGA GAGGAGGTTCCAGTTC	62
MEG3	ATTGGTACTACTACGG AGTGCAGTAGCTAGCC	54
PANDAR	AGATTATGCTGACCC GAGAGTTGGCAACTGG	60
PVT1	GGACCCTCTAGGCCC ACCGTCCTAGAGAC	58
ROR	AGCTAGTGGTCTCGACC GGTTTATTCCGTATAACT	55
UCA1	GATGCGAGGGCATAAT GAGCCGATCGGCCTC	56
miR-10b	GAATTACCGGTACCC TAGCCTTTGACCCGT	58
miR-26a	TTGAGGTTTCCCTGG AGCCGTTTTACGAAAT	60
miR-26b	AGAGTTAACCCTGAA AGACCCCATGGACCTA	58
BDNF	GCCGACCTGAGCC GACCGTTTAAGCCTGA	60
GAPDH	GGTGGACCTCATGGCCTACA CTCTCTTGCTCTCAGTATCCTTGCT	60

might function as a post-transcriptional regulator of BDNF. Taken together, these results showed that lncRNA GAS5 was another regulatory pathway enhanced by curcumin in BDNF/Trkβ signaling pathway activation for PSD treatment.

GAS5 competes to sponge miR-10b to prevent BDNF silencing

Previous studies revealed 17 potential miRNAs targeted to BDNF (26). Additionally, the RNA-RNA interaction database of humans and mice (http://starbase.sysu.edu.cn/) was employed to find the GAS5-associated miRNAs. Finally, miR-10b, miR-26a and miR-26b were identified as intersecting candidate miRNAs bridging BDNF and GAS5. Due to the differences among human, mouse and rat, the RNA interaction needs to be further authenticated. Hence, the transcriptional levels of these three miRNAs were detected, and miR-10b was shown to be upregulated upon GAS5 knockdown but downregulated upon GAS5 overexpression or curcumin treatment (Fig. 3A), and the changes in miR-26a and miR-26b were less significant than that in miR-10b. Moreover, a luciferase assay showed that

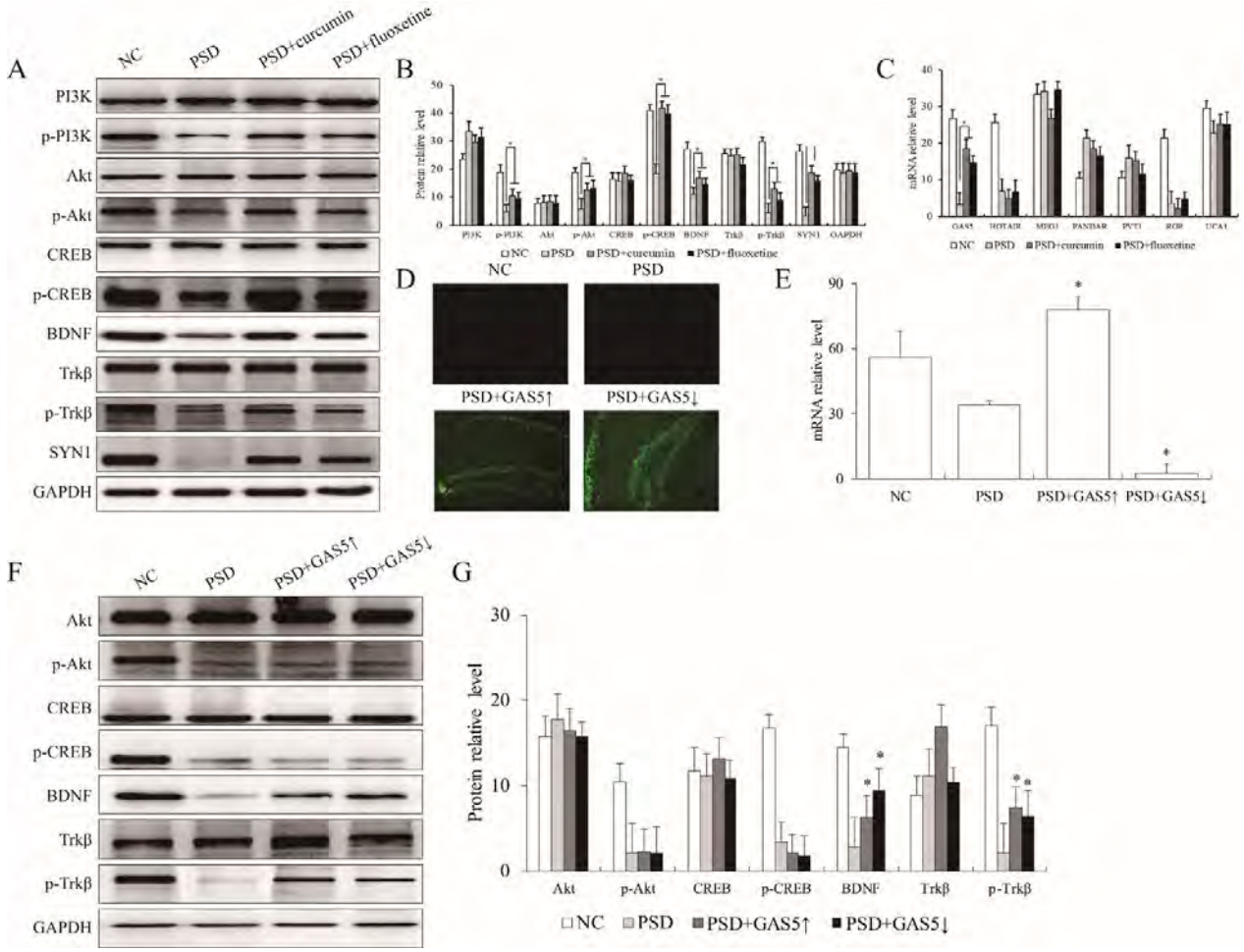


Fig. 2. *The response of the BDNF/Trk*β *pathway and GAS5 upon curcumin treatment. The BDNF/Trk*β signaling pathway activity (***A***) *and analysis (****B****) and analysis of the lncRNA level (****C****) in the hippocampus upon curcumin treatment in the PSD model. Identification of the lentivirus transfection for GAS5 overexpression or knockdown (****D****) and the GAS5 transcriptional levels (****E****) in the hippocampus. The BDNF/Trk*β signaling pathway activity (***F***) *and analysis (****G****) upon GAS5 overexpression or knockdown. NC indicates negative control. PSD indicates post-stroke depression. GAS5↑ and ↓ indicate overexpression or knockdown, respectively. Each group had five individuals. * represents a significant difference with a p value less than 0.05.*

miR-10b obviously reduced the luciferase activity of the GAS5 reporter compared to miR-26a and miR-26b in 293T cells (Fig. 3B). Likewise, both BDNF and GAS5 were increased in the hippocampus after miR-10b was knocked down via intracerebroventricular injection of packaged lentivirus (Fig. 3 C, D). Taken together, these data suggested that miR-10b targeted both BDNF and GAS5 and that GAS5 contributed to miR-10b consumption to prevent BDNF silencing.

DISCUSSION

PSD is a depressive symptom following ischemic stroke that has severe effects on the morbidity and mortality of patients (27). Therefore, psychiatric and psychopharmacologic treatments, including psychotherapy, surgical therapy, electroconvulsive therapy, drug therapy and natural products, have been developed for effective post-stroke therapy (28). The current drug therapy for post-stroke depression mainly includes antidepressants, which have some therapeutic effects in clinical applications; however, they also show toxic and side effects on the heart and brain, compliance is poor and the cost is high (3, 29) Stress has been shown to damage hippocampal neurogenesis, which is hypothesized to be a biological underpinning of depression (30). A In the present study, an aberrant behavioral and biochemical pattern and the declining SYN1 expression in the hippocampus of the PSD model were alleviated with an appropriate dosage of curcumin. BDNF is expressed in both the central and peripheral nervous systems of mammals, particularly in the cortex and hippocampus (31), and BDNF signaling perturbations are associated with some neurological diseases, including major depression in clinical studies (32). Moreover, the levels of BDNF in serum are substantially decreased in patients with

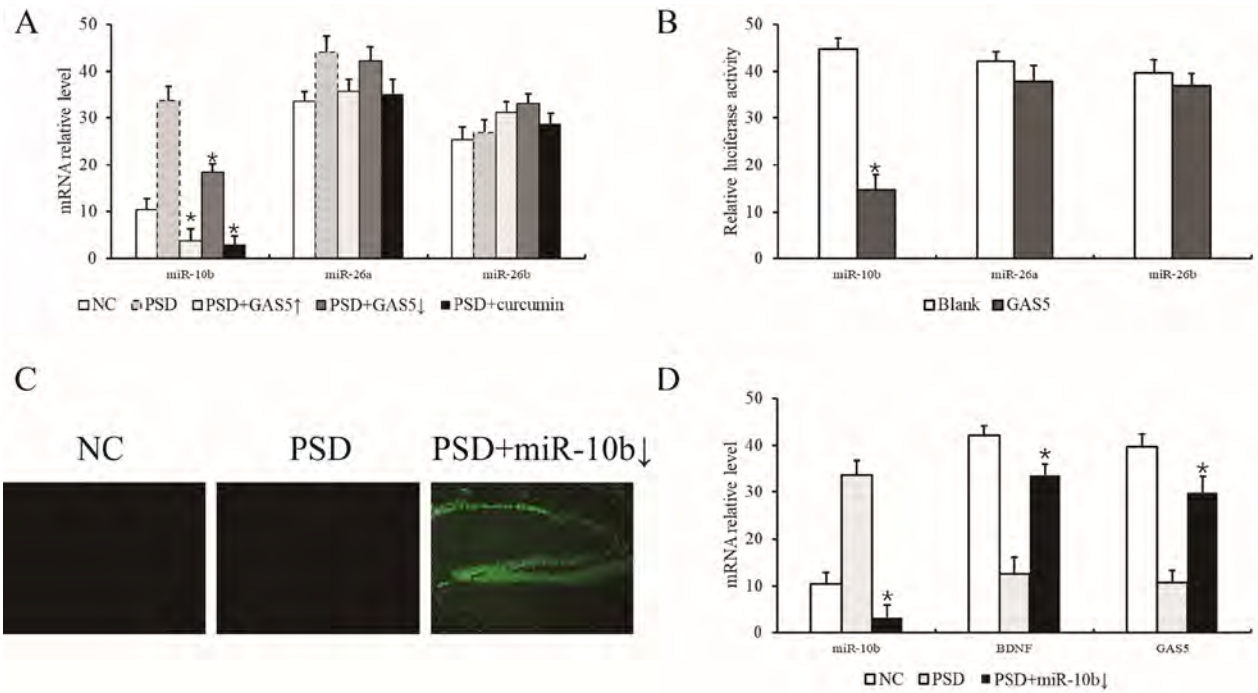


Fig. 3. *The relationship between miR-10b and GAS5 upon curcumin treatment in the PSD model. The transcriptional levels of miR-10b, miR-26a and miR-26b with GAS5 overexpression or knockdown and curcumin treatment in the PSD model (**A**). The luciferase reporter assays of GAS5 and miR-10b, miR-26a and miR-26b (**B**). Identification of the lentivirus transfection for miR-10b knockdown (**C**) and the effect on the transcriptional levels of BDNF and GAS5 (**D**). Each group had five individuals. * represents a significant difference with a p value less than 0.05.*

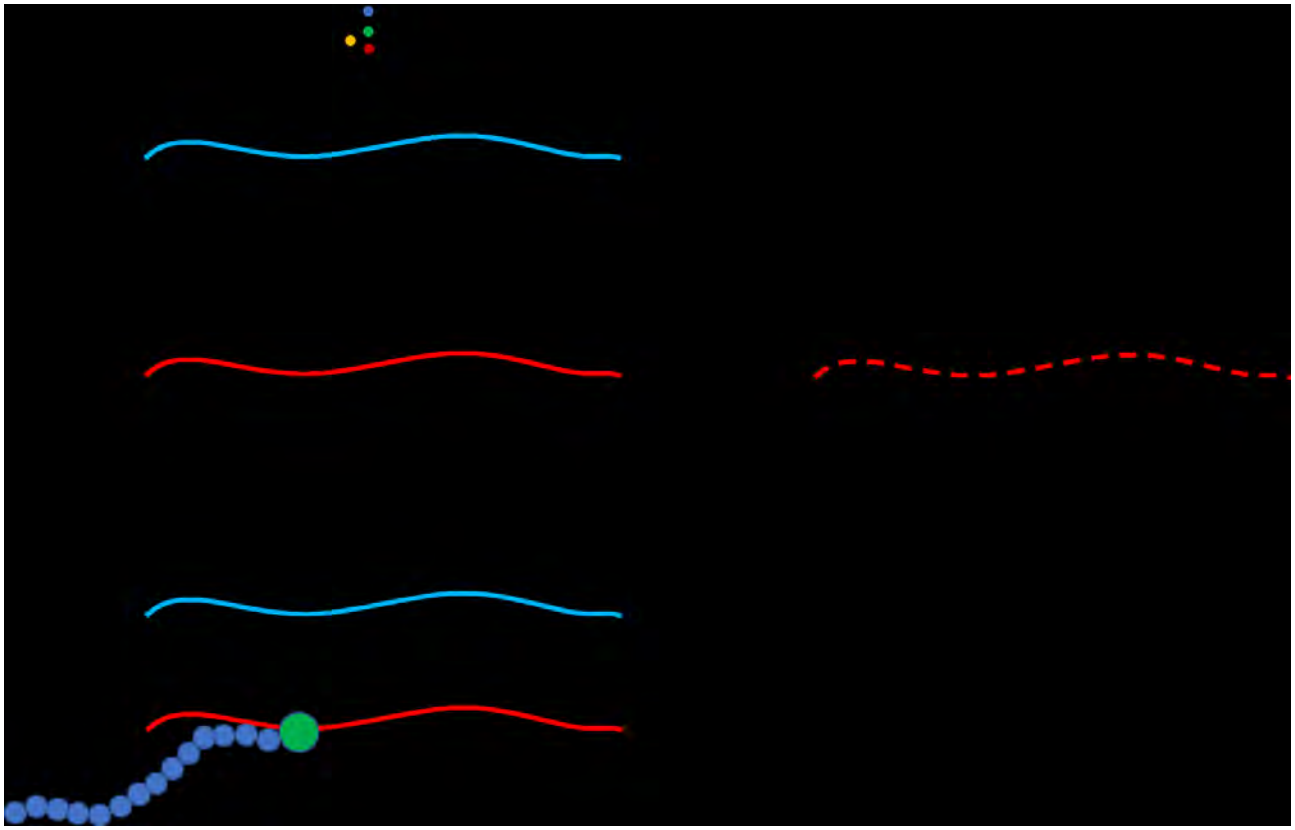


Fig. 4. *A graphic summary of the GAS5/miR-10b/BDNF regulatory axis response to curcumin in PSD.*

PSD (33). Animal models of depression indicate that BDNF deficiency is a major cause of depression and could be reversed by antidepressants (34, 35). Consistent with these previous studies, the BDNF/Trkβ signaling pathway was also activated by curcumin in the rats with PSD in this study.

Furthermore, current studies have revealed that multiple lncRNAs, such as GAS5, are closely associated with the therapeutic effect of curcumin in cancers (36, 37). However, the effective targeted lncRNAs of curcumin in PSD disease are unknown. Therefore, the levels of previously reported lncRNAs, including GAS5, HOTAIR, MEG3, PANDAR, PVT1, ROR and UCA1, were examined upon curcumin treatment, and GAS5 was shown to significantly respond to curcumin in the hippocampus of the rat model of PSD compared to other lncRNAs, which indicates that lncRNAs may play a tissue- or cell-specific role in gene regulation. Moreover, GAS5 can enhance the BDNF transcriptional levels. Multiple lines of evidence prove that CREB is activated by the PI3K/Akt pathway and further transcriptionally promotes BDNF. Interestingly, GAS5 does not change either Akt or CREB phosphorylation, although GAS5 can induce BDNF transcription, which implies that GAS5 may play a role in post-transcriptional regulation of BDNF. Thus, these data support the identification of a potential miRNA connecting GAS5 and BDNF. Similarly, published studies and known RNA interaction databases were employed to identify the targeted miRNAs of GAS5, and finally, miR-10b was shown to link GAS5 and BDNF in the PSD system (Figure 4).

Overall, these data reveal a novel regulatory pathway of GAS5/miR-10b/BDNF/Trkβ upon curcumin treatment in a rat model of PSD. These results describe the underlying molecular mechanism of curcumin in PSD therapy.

ACKNOWLEDGEMENTS

This research was supported by the Shanghai Municipal Commission of Health and Family Planning (ZY(2018-2020)-RCPY-3009). The study was approved by the Medical Ethics Committee of Shanghai, and all animal protocols were conducted following the guidelines accordingly.

REFERENCES

1. Alajbegovic A, Djelilovic-Vranic J, Nakicevic A, Todorovic L, Tiric-Campara M. Post stroke depression. Med Arch 2014; 68:47-50.
2. Stern-Nezer S, Eyngorn I, Mlynash M, W Snider R, Venkatsubramanian C, Wijman CAC, Buckwalter MS. Depression one year after hemorrhagic stroke is associated with late worsening of outcomes. NeuroRehabilitation 2017; 41:179-87.
3. Paolucci S. Advances in antidepressants for treating post-stroke depression. Expert Opin Pharmacother 2017; 18:1011-7.
4. Yan Y, Fan W, Liu L, Yang R, Yang W. The effects of Xingnao Jieyu capsules on post-stroke depression are similar to those of fluoxetine. Neural Regen Res 2013; 8:1765-72.
5. Loubinoux I, Kronenberg G, Endres M, et al. Post-stroke depression: mechanisms, translation and therapy. J Cell Mol Med 2012; 16:1961-9.
6. Khan H, Amin S, Patel S. Targeting BDNF modulation by plant glycosides as a novel therapeutic strategy in the treatment of depression. Life Sci 2018; 196:18-27.
7. Chen HG, Wan M, Jiao AH, et al. Research on changes in cognitive function, β-amyloid peptide and neurotrophic factor in stroke patients. Eur Rev Med Pharmacol Sci 2018; 22:6448-55.
8. Guo YC, Song XK, Xu YF, Ma JB, Zhang JJ, Han PJ. The expression and mechanism of BDNF and NGB in perihematomal tissue in rats with intracerebral hemorrhage. Eur Rev Med Pharmacol Sci 2017; 21:3452-58.
9. Guo W, Ji Y, Wang S, Sun Y, Lu B. Neuronal activity alters BDNF-TrkB signaling kinetics and downstream functions. J Cell Sci 2014; 127:2249-60.
10. Andero R, Choi DC, Ressler KJ. BDNF-TrkB receptor regulation of distributed adult neural plasticity, memory formation, and psychiatric disorders. Prog Mol Biol Transl Sci 2014; 122:169-92.
11. Lopresti AL. Curcumin for neuropsychiatric disorders: a review of in vitro, animal and human studies. J Psychopharmacol 2017; 31:287-302.
12. Kaufmann FN, Gazal M, Bastos CR, Kaster MP, Ghisleni G. Curcumin in depressive disorders: An overview of potential mechanisms, preclinical and clinical findings. Eur J Pharmacol 2016; 784:192-98.
13. Lin J, Huo X, Liu X. "mTOR Signaling Pathway": A Potential Target of Curcumin in the Treatment of Spinal Cord Injury. Biomed Res Int 2017; 2017:1634801.
14. Bahrami A, Amerizadeh F, ShahidSales S, et al. Therapeutic Potential of Targeting Wnt/beta-Catenin Pathway in Treatment of Colorectal Cancer: Rational and Progress. J Cell Biochem 2017; 118:1979-83.
15. Zhao J, Zhu J, Lv X, Xing J, Liu S, Chen C, Xu Y. Curcumin potentiates the potent antitumor activity of ACNU against glioblastoma by suppressing the PI3K/AKT and NF-kappaB/COX-2 signaling pathways. Onco Targets Ther 2017; 10:5471-82.
16. Zhang L, Fang Y, Xu Y, et al. Curcumin Improves Amyloid β-Peptide (1-42) Induced Spatial Memory Deficits through BDNF-ERK Signaling Pathway. PLoS One 2015; 10:e0131525.
17. Dai C, Xiao X, Zhang Y, et al. Curcumin Attenuates Colistin-Induced Peripheral Neurotoxicity in Mice. ACS Infect Dis 2020; 6:715-24.
18. Anchan D, Clark S, Pollard K, Vasudevan N. GPR30 activation decreases anxiety in the open field test but not in the elevated plus maze test in female mice. Brain Behav 2014; 4:51-9.
19. Malatynska E, Steinbusch HW, Redkozubova O, et al. Anhedonic-like traits and lack of affective deficits in 18-month-old C57BL/6 mice: Implications for modeling elderly depression. Exp Gerontol 2012; 47:552-64.
20. Wei LL, Chen H, Jiang Y, et al. Effects of echinacoside on histio-central levels of active mass in middle cerebral artery occlusion rats. Biomed Environ Sci 2012; 25:238-44.
21. Fornasiero EF, Bonanomi D, Benfenati F, Valtorta F. The role of synapsins in neuronal development. Cell Mol Life Sci 2010; 67:1383-96.
22. Srivastava P, Dhuriya YK, Kumar V, et al. PI3K/Akt/

MICRORNA-23B INHIBITS NON-SMALL CELL LUNG CANCER PROLIFERATION, INVASION AND MIGRATION VIA DOWNREGULATION OF RUNX2 AND INHIBITION OF WNT/B-CATENIN SIGNALING PATHWAY

H-X. WANG[1*], X-Y. WANG[2*], J-W. FEI[1], F-H. LI[1], J. HAN[1] and X. QIN[1]

[1]Department of Respiratory Medicine, Yantaishan Hospital, Yantai, China; [2]Department of Clinical Laboratory, Jinan Zhangqiu District Hospital of TCM, Jinan, China

Received January 10, 2020 – Accepted April 28, 2020

[*]These Authors contributed equally to this work

Non-small cell lung cancer (NSCLC) accounts for about 85% of all lung cancer cases. MicroRNAs (miRNAs/miRs) have been reported to play significant roles in the progression of human tumors, however, the expression and biological role of miR-23b in NSCLC remains elusive. Underexpression of miR-23b was detected in NSCLC tissues in comparison with the matched para-carcinoma tissues. The clinical value of miR-23b was analyzed, and the findings showed that miR-23b expression was negatively correlated with poor overall survival and malignant clinicopathologic characteristics of NSCLC patients. Furthermore, functional assays demonstrated that overexpression of miR-23b inhibited NSCLC cell viability, invasion and migration. Luciferase reporter assay and qRT-PCR revealed that RUNX2 was a functional target of miR-23b. The elevated expression of RUNX2 was positively correlated with overall survival of NSCLC patients. Additionally, Western blot analysis indicated that EMT and Wnt/β-catenin pathways were blocked by the upregulation of miR-23b. Taken together, these data demonstrated that dysregulation of miR-23b/RUNX2 signal may be a novel therapeutic target for the treatment of NSCLC.

Lung cancer has become a highly aggressive malignancy with a rapid rise in morbidities and mortalities. Non-small cell lung cancer (NSCLC) accounts for about 85% of all lung cancer cases, which also include adenocarcinoma, large cell carcinoma and squamous cell carcinoma (1). Patients with NSCLC are often diagnosed with metastatic or locally advanced disease at advanced stages (2). The development of NSCLC is multi-step processes including epigenetic and genetic changes (3). At present, surgical treatment remains the primary treatment as it is less sensitive to radiation therapy and antitumor drugs. Five-year survival rates can reach 20-30% in patients after surgery (4), however, not all patients can undergo surgical treatment. In addition, postoperative relapse remains a threat by reducing patient survival (5). In recent decades, despite the great effort that has been made in NSCLC research, the mechanism of its pathogenesis remains unclear. Therefore, understanding accurate molecular biology and elucidating potential target genes are essential to identify effective treatment for NSCLC prevention.

MicroRNAs (miRNAs) are a kind of regulatory RNAs, which are small endogenous non-coding RNAs, consisting 18-25 nucleotides, and negatively

Key words: NSCLC; miR-23b; RUNX2; Wnt/β-catenin

Corresponding Author:
Dr Xiao Qin,
Department of Respiratory Medicine,
Yantaishan Hospital,
91 Jiefang Road,
Yantai 264000, China
e-mail: dmy081031@163.com

0393-974X (2020)
Copyright © by BIOLIFE, s.a.s.
This publication and/or article is for individual use only and may not be further reproduced without written permission from the copyright holder.
Unauthorized reproduction may result in financial and other penalties
DISCLOSURE: ALL AUTHORS REPORT NO CONFLICTS OF INTEREST RELEVANT TO THIS ARTICLE.

regulate the target gene via binding to its 3'-UTR, resulting in transcript degradation or transcriptional suppression (6). Accumulating evidences has revealed that the majority of miRNAs are located in the tumor-associated genomic region, indicating that miRNA dysregulation may play a vital role in tumor development (7). Recently, studies have shown that miRNAs have aberrant expressions in different malignancies, such as breast cancer (8), cervical cancer (9) and prostate cancer (10). MiRNAs regulates a variety of biological processes, especially those participating in pivotal pathways which are implicated in tumor angiogenesis, metastasis, apoptosis and proliferation (11-13). As is well known, miRNAs can function as an oncogene or tumor suppressor by targeting their mRNAs in tumor development (14), however, the biological function and the underlying mechanisms of miR-23b in OS have not yet been investigated.

Runt-associated transcription factor 2 (RUNX2) is a member of the RUNX transcription factor family, and is known for its function in regulation of osteoblast differentiation and bone morphogenesis. Besides its roles in promoting bone formation, emerging evidence showed that RUNX2 was a key regulator of tumorigenesis. Overexpression of RUNX2 has been identified in diverse tumor tissues, and the abnormal activation of RUNX2 could promote the invasiveness and metastasis of tumor cells. In esophageal carcinoma, RUNX2 exerted positive roles via ERK and PI3K/AKT pathways (15). RUNX2 promoted migration and invasion in hepatocellular carcinoma via up-regulating of MMP9 expression (16). Additionally, overexpression of RUNX2 in melanoma can mediate the invasion and migration of cells (17). Therefore, the aim of the present study was to investigate the biological function and associated mechanism of miR-23b in NSCLC.

MATERIALS AND METHODS

Cell cultures and transfections

Human NSCLC cell lines (NCI-H460, NCI-H1299, A549 and SPC-A1) and normal bronchial epithelium cell line BEAS-2B were obtained from American Type Culture Collection (ATCC, USA). The cells were cultivated in Dulbecco's modified Eagle's medium (DMEM; Invitrogen, Carlsbad, CA, USA) which contained 10% FBS (Invitrogen, USA) in a humidified incubator with 5% CO_2 at 37°C. Lipofectamine 2000 (Invitrogen, USA) was applied to transfect miR-23b mimics, inhibitors or negative controls (Genepharma, Shanghai, China) into NSCLC cells.

Patients and samples

Fifty-nine pairs of NSCLC tissue samples and neighboring normal tissue specimens were obtained from the Yantaishan Hospital between April 2015 and March 2018. No patient had received anti-tumor treatments before tissue collection. All samples were snap-frozen in liquid nitrogen and stored at -80°C until further use. Written informed consent was obtained from all patients. The present study was approved by the Ethics Committee of the Yantaishan Hospital.

qRT-PCR

Total RNA was isolated from NSCLC cells or tissues by TRIzol reagent (Invitrogen). Reverse transcriptions for miR-23b or RUNX2 were carried out by TaqMan® MicroRNA Reverse Transcription kit (Promega, Madison, WI, USA) or M-MLV reverse transcriptase (Promega, USA). The ABI 7500 System (Applied Biosystems, Foster City, CA, USA) was utilized to perform qPCR with TaqMan MicroRNA Assay kit (Applied Biosystems) or SYBR Premix Ex Taq™ Kits (TaKaRa Bio, Tokyo, Japan) for miR-23b or RUNX2. U6 and GAPDH served as internal controls for miR-23b or RUNX2 mRNA. Data were analyzed by $2^{-\Delta\Delta Ct}$ method. The primers were shown in Table I. Statistical analysis was performed on the fold change.

MTT assay

3-(4, 5-dimethylthiazol-2-yl)-2, 5-diphenyltetrazolium bromide (MTT) assay was applied for monitoring cell viability. 24 h after transfections, NSCLC cells were collected and seeded into 96-well plate at a density of 2×10^3 cells/well for 1, 2, 3-days cultivation. Then, cells was added with 20 μl MTT solution and cultivated at 37°C for 4 h. Thereafter, DMSO was added to dissolve formazan crystals, and absorbance was recorded at 490 nm using a spectrophotometer (Bio Tek Instruments, USA).

Transwell assay

Transwell chambers (8 μm pore size, Corning, NY,

USA) were used to examine metastatic properties of NSCLC cells. For detection of migration, transfected NSCLC cells were suspended in serum-free medium and cultured in the top chamber. In the meantime, DMEM medium supplemented with 10% FBS was added to the lower chamber. After being incubated for 48 h at 37°C, non-traversed cells were carefully removed and traversed cells were fixed with 4% paraformaldehyde and stained with 0.5% crystal violet (Sigma-Aldrich; Merck KGaA) for 15 min. The cells in five randomly selected fields were counted microscopically (×200 Magnification, Olympus, Tokyo, Japan). For cell invasion, the chamber was coated with Matrigel (Franklin Lakes, NJ, USA). The subsequent steps were same as the migration assay described above.

Western blot assay

Total proteins were extracted using RIPA buffer (Beyotime, Jiangsu, China). Protein concentration was determined using a BCA kit (Beyotime). Then, 30 μg protein was separated by 10% SDS-PAGE, followed by transfection onto PVDF membranes (Millipore, Billerica, MA, USA). After blocking with 5% non-fat milk in TBST, the membrane was incubated with specific primary antibodies against cyclin D1 (1:1000, Abcam Cambridge, MA, USA), c-Myc (1:1000, Abcam), β-catenin(1:1000, Abcam), p-GSK3β (1:1000, Abcam), total GSK3β (1:1000, Abcam), E-cadherin (1:2000, Abcam), N-cadherin(1:2000, Abcam), Vimentin (1:1000, Abcam) and GAPDH (1:1000, Abcam) at 4°C overnight. After washing with TBST, the membrane was incubated with secondary antibody (1:4,000, ab7090; Abcam) at room temperature for 2 h. Finally, the membrane was visualized with the enhanced chemiluminescence reagent (ECL, Millipore). The expression level of HOXB5 was normalized to GAPDH.

Luciferase reporter assay

Two types of RUNX2 3'UTR fragments (wild-type or mutant) were inserted into the pGL3 vector (Promega, USA) to obtain the wild-type (WT) or mutant (MUT) reporter, RUNX2 3'UTR-WT or -MUT. NSCLC cells together with wild-type or mutant reporter of RUNX2 were cotransfected with miR-NC or miR-23b mimics by Lipofectamine 2000 (Invitrogen, USA). After 48 h of transfection, the Dual-Luciferase Reporter Assay System (Promega, USA) was applied to evaluate the luciferase activity. Firefly luciferase activity was normalized to renilla luciferase activity.

Statistical analysis

All data were from at least 3 independent experiments. SPSS software version 17.0 (SPSS Inc., Chicago, IL) was utilized to complete data analyses. Student's *t*-test or one-way analysis of variance (ANOVA) followed by

Table I. *Primer sequences for qRT-PCR*

Primer	Sequence
miR-23b forward	5'- GGTGCTCTGGCTGCTTGG -3'
miR-23b reverse	5'- GCCAAGGTCGTGGTTGCG -3'
U6 forward	5'-CTCGCTTCGGCAGCACA-3'
U6 reverse	5'- AACGCTTCACGAATTTGCGT-3'
RUNX2 forward	5'- GACGAGGCAAGAGTTTCACC-3'
RUNX2 reverse	5'- GGTTCCCGAGGTCCATCTAC-3'
GAPDH forward	5'-ACCTGACCTGCCGTCTAGAA-3'
GAPDH reverse	5'-TCCACCACCCTGTTGCTGTA-3'

U6: small nuclear RNA;snRNA; RUNX2: Runt-associated transcription factor 2; GAPDH: glyceraldehyde-3-phosphate dehydrogenase

Table II. *Correlation of miR-23b expression with the clinicopathological characteristics of the NSCLC patients.*

Clinicopathological features	Cases(n=59)	miR-23b# expression		P-value
		High(n=24)	Low(n=35)	
Age (years)				0.5531
>60	33	14	19	
≤60	26	10	16	
Gender				0.4783
Male	31	11	20	
Female	28	13	15	
Tumor size (cm)				0.3136
≥ 5.0	30	9	21	
<5.0	29	15	14	
Lymph node metastasis				0.0013*
Yes	25	18	7	
No	34	6	28	
Histology				0.3526
Squamous cell carcinoma	30	13	17	
Adenocarcinoma	29	11	18	
TNM stage				0.0022*
I +II	27	19	8	
III+IV	32	5	27	
Smoker				0.4987
Yes	31	14	17	
No	28	10	18	

*NSCLC: non-small cell lung cancer; TNM: tumor-node-metastasis. # The mean expression level of miR-23b was used as the cutoff; *Statistically significant.*

the Tukey's post hoc test was used to analyze difference between two or multiple groups. The survival rate was analyzed by Kaplan-Meier analysis and log-rank test. Significant difference was defined as $P < 0.05$.

RESULTS

MiR-23b was down-regulated in NSCLC with poor prognosis

qRT-PCR was used to detect the expression of miR-23b in NSCLC tissues and matched normal tissues, the result indicated that the expression of miR-23b in tumor samples were prominently downregulated when compared to the normal tissues (Fig. 1A). Next, we further analyzed the clinical value of miR-23b in NSCLC patients. All the enrolled subjects were divided into high- and low-miR-23b expression groups according to the mean value of miR-23b expression. NSCLC patients with lower miR-23b expression exhibited poorer overall survival (OS) than highly miR-23b-expressed patients (Fig. 1B). As demonstrated in Table II,

the decreased miR-23b in NSCLC patients was significantly correlated with lymph node metastasis and TNM stage ($P < 0.05$). However, there was no significant correlation between miR-23b expression and other clinicopathological features such as age and gender ($P > 0.05$).

High miR-23b expression inhibited NSCLC cell viability

Considering the decreased expression of miR-23b in NSCLC tissues, we speculated that miR-23b was also downregulated in NSCLC cells. As expected, miR-23b was downregulated in all NSCLC cells (NCI-H460, NCI-H1299, A549 and SPC-A1) in comparison with the normal bronchial epithelium cell line BEAS-2B (Fig. 2A). Thereafter, we selected A549 and NCI-H1299, the endogenous miR-23b expression of which was relatively low and high, to perform the subsequent gain- and loss-function assays by transfecting miR-23b mimics or inhibitor into them. As confirmed by qRT-PCR, expression levels of miR-23b were significantly upregulated by miR-125b-5p mimic but reduced by miR-23b inhibitor in A549 and NCI-H1299 cells (Fig. 2 B and C). MTT assays revealed that miR-23b overexpression inhibited, while the downregulation of miR-23b enhanced NSCLC cell proliferation (Fig. 2 D and E).

Upregulation of miR-23b suppressed NSCLC cell invasion and migration

As the anti-proliferation function of miR-23b in NSCLC cells had been verified, Transwell assays were performed to further determine its roles in NSCLC cell invasion and migration. The results implied that cells transfected with miR-23b mimic remarkably decreased the cell invasion and migration compared with those transfected with NC-miRNA in A549 cell (Fig. 3 A and B). On the other hand, miR-23b inhibitor significantly promoted NCI-H1299 cell invasion and migration (Fig. 3 C and D). Taken together, all these findings demonstrated that miR-23b could suppress NSCLC cell invasion and migration *in vitro*.

MiR-23b directly regulated RUNX2 in NSCLC cells

The potential mechanism underlying miR-23b-mediated regulation in biological process of NSCLC was explored, and Targetscan (http://www.targetscan.org/mmu_72/) analysis for miR-23b revealed that RUNX2 was a potential target of miR-23b. As shown

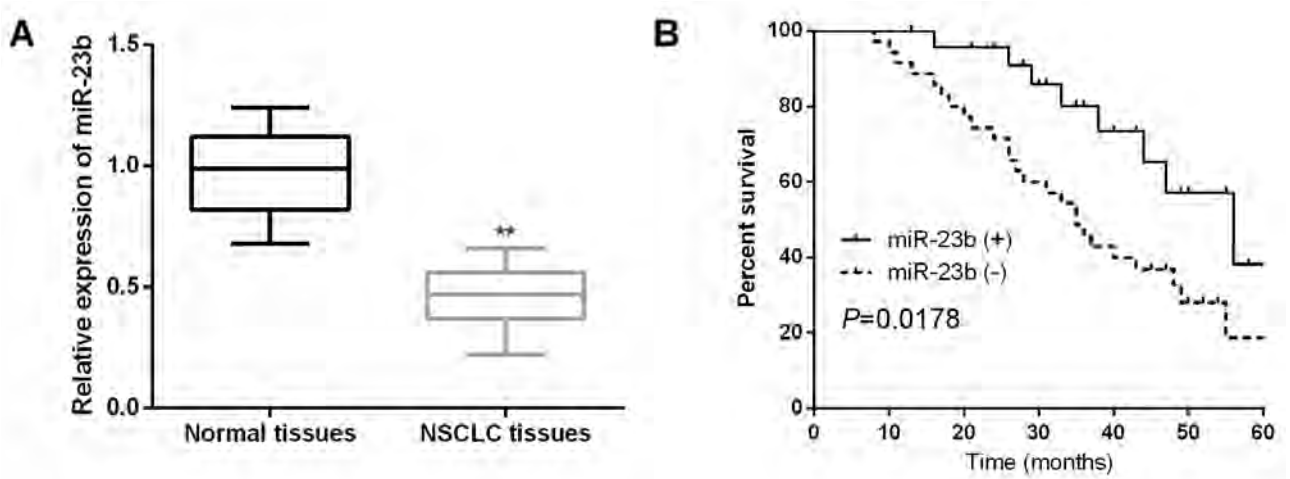


Fig. 1. *MiR-23b was underexpressed in NSCLC.* ***A)*** *Decreased miR-23b was verified by qRT-PCR.* ***B)*** *Kaplan–Meier analysis was used to determine the association between OS and miR-23b expressions in NSCLC patients. **P<0.01.*

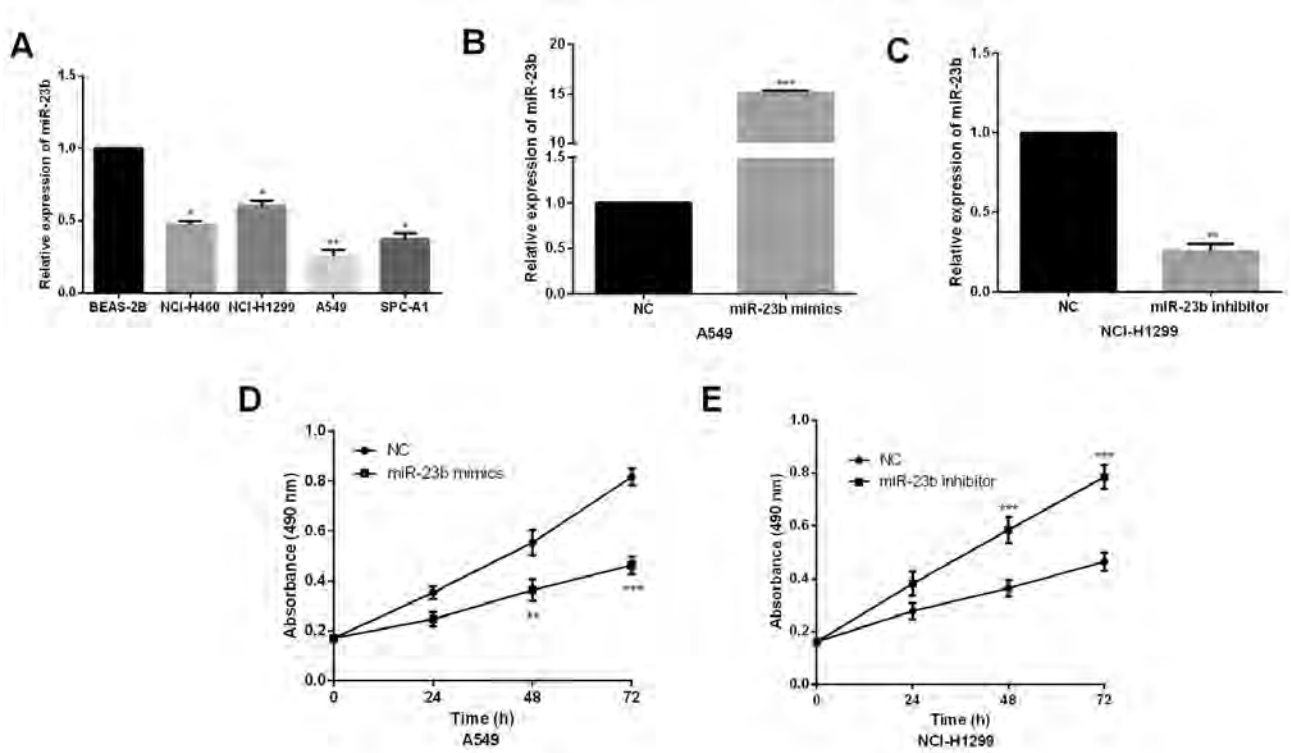


Fig. 2. *Effects of miR-23b on NSCLC cell viability.* ***A)*** *MiR-23b expressions in NSCLC cell lines were measured by qRT-PCR.* ***B, C)*** *Efficient overexpression or inhibition of miR-23b was confirmed by qRT-PCR.* ***D, E)*** *MTT assay was conducted to investigate the influence of miR-23b on NSCLC cell viability.*P<0.05, **P<0.01, ***P<0.001.*

in Fig. 4A, RUNX2 has a putative target sequence of miR-23b andwas identified as a direct target gene of miR-23b in NSCLC. The correlation was tested by luciferase reporter assays. As shown in Fig. 4B, the luciferase activity of RUNX2-3'UTR-WT was evidently decreased by miR-23b overexpression whereas the luciferase activity of RUNX2-3'UTR-MUT was not significantly influenced by miR-23b mimics. Moreover, qRT-PCR was also carried out to explore the effect of miR-23b on RUNX2 expression. Results showed that overexpression of miR-23b dramatically suppressed RUNX2 expression in A549 cells (Fig. 4C). In addition, the expression of RUNX2 in NCI-H1299 cells was evidently upregulated by miR-23b inhibitor (Fig. 4D). Therefore, all the above findings revealed that RUNX2 was a direct target of miR-23b in NSCLC cells.

RUNX2 was up-regulated in NSCLC with poor prognosis

As RUNX2 had been identified as a target of miR-23b, we next explored its prognostic significance in NSCLC patients. RUNX2 levels were markedly upregulated in NSCLC tissues and cell lines (NCI-H460, NCI-H1299, A549 and SPC-A1) as measured by qRT-PCR (Fig. 5 A and B). Moreover, Kaplan-Meier analysis demonstrated prominent shorter OS in patients with high RUNX2 levels than those with low RUNX2 levels (Fig. 5C).

MiR-23b inhibited Wnt/β-catenin signaling pathway via partially regulation of RUNX2

We then performed Western blot to investigate the roles of miR-23b in NSCLC cell EMT and Wnt/β-catenin signaling pathway. In miR-23b-

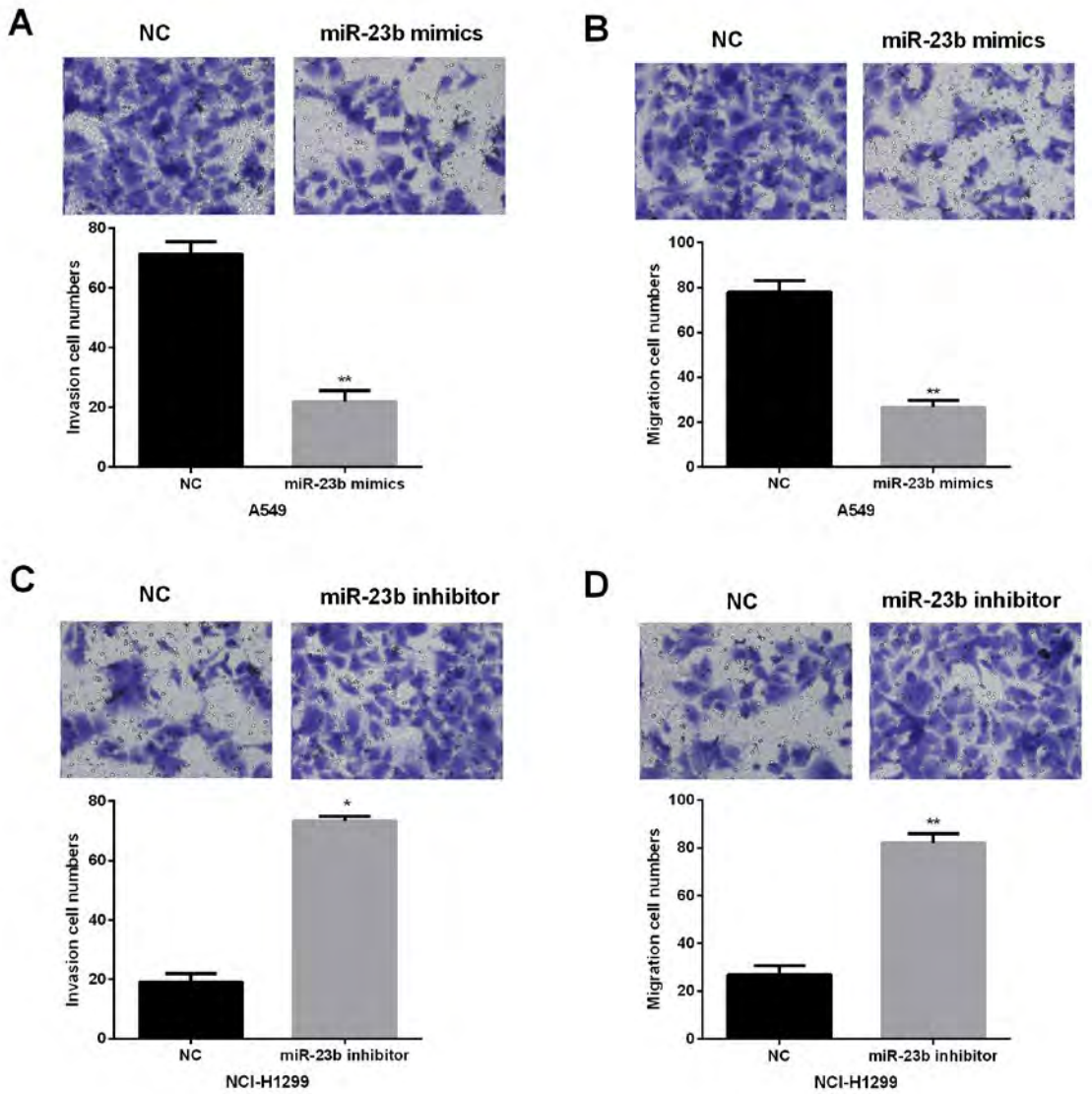


Fig. 3. *Influence of miR-23b on NSCLC cell invasion and migration.* ***A, B****) MiR-23b upregulation suppressed NSCLC cell invasion and migration as demonstrated by Transwell assay.* ***C, D****) The promoting role of miR-23b in NSCLC cell invasion and migration was confirmed by Transwell assay. *P<0.05, **P<0.01.*

overexpressed A549 cells, the expressions of EMT-related proteins were remarkably affected, including the up-regulated of E-cadherin, down-regulated of Vimentin and N-cadherin (Fig. 5D). As for expressions of proteins involved in Wnt/β-catenin pathway, such as activated β-catenin, c-Myc, cyclin D1, and p-GSK3β, overexpression of miR-23b significantly inhibited their levels **(**Fig. 5E). The functions were also verified by miR-23b inhibitor in NCI-H1299 cells. To sum up, miR-23b exerted anti-NSCLC functions via partially regulating of RUNX2 and modulating EMT and Wnt/β-catenin signaling pathway.

DISCUSSION

Due to the lack of understanding regarding NSCLC pathogenesis, it remains the leading factor

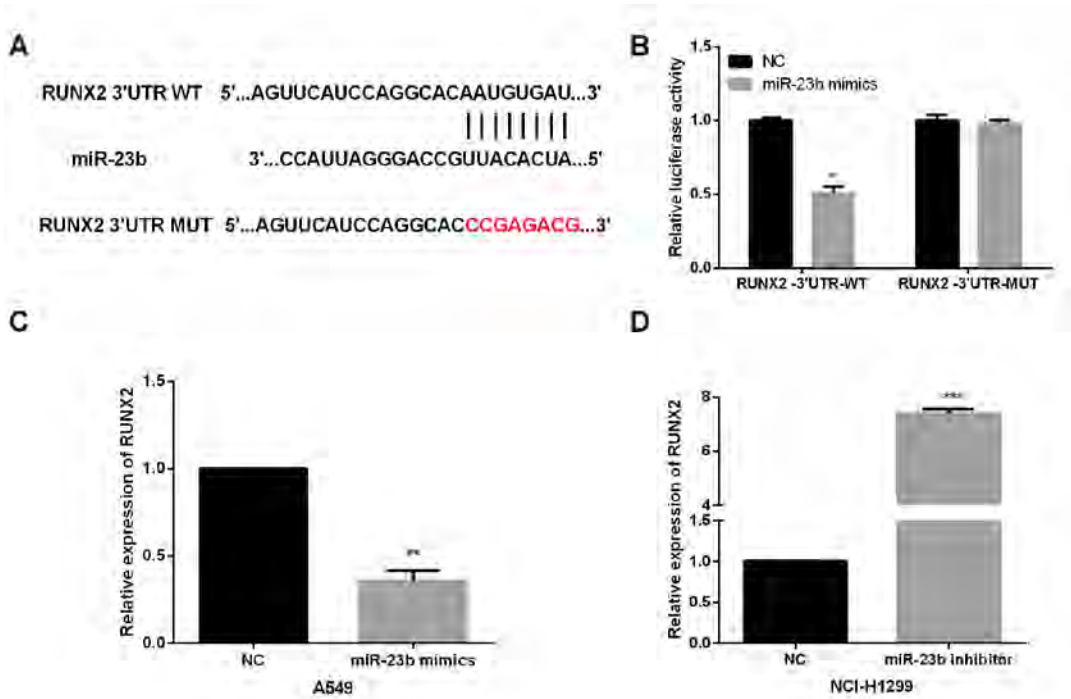


Fig. 4. *Target analysis of miR-23b in NSCLC cell lines.* ***A****) The putative binding sequences of miR-23b in RUNX2 3'UTR.* ***B****) Luciferase reporter assay was carried out in NSCLC cells cotransfected with miR-23b and RUNX2 3'UTR-WT or -MUT.* ***C, D****) The influence of miR-23b on RUNX2 expression was determined by qRT-PCR. *P<0.05, **P<0.01, ***P<0.001.*

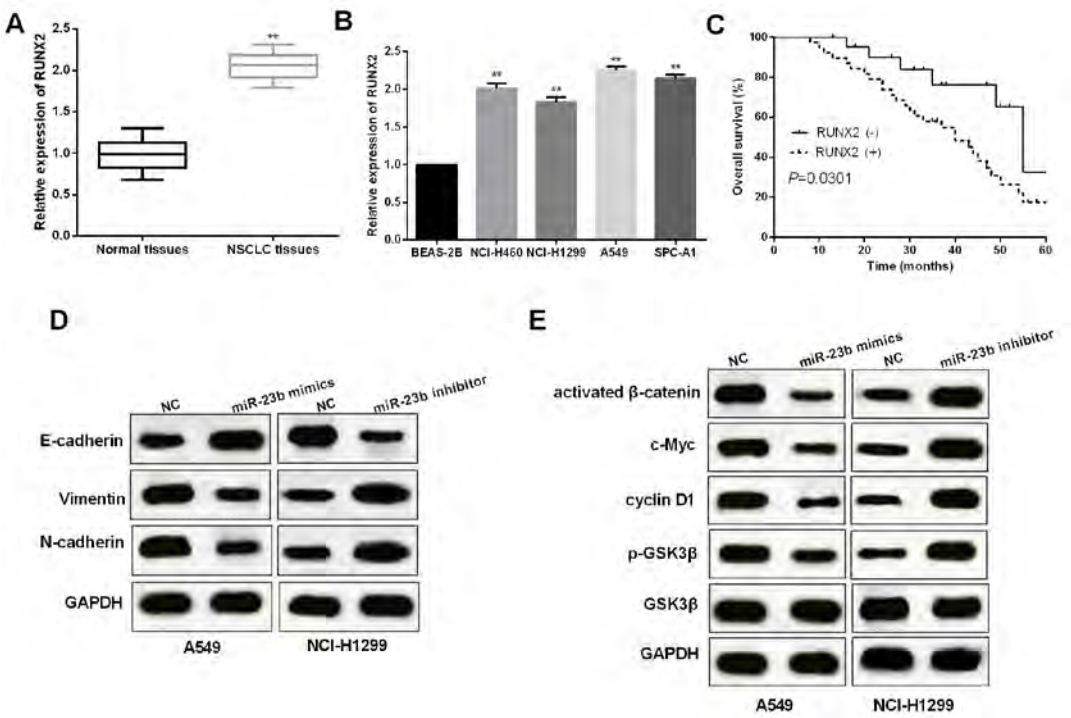


Fig. 5. *The underlying mechanisms of miR-23b in regulating NSCLC progression.* ***A, B****) RUNX2 expressions in NSCLC tissue samples and cell lines were detected.* ***C****) Comparison of OS between NSCLC patients with different RUNX2 expressions.* ***D, E****) MiR-23b regulated NSCLC cell EMT and Wnt/β-catenin. **P<0.01.*

of tumor death worldwide. Moreover, molecular targeted therapies have become a hot spot in tumor treatments (18). Therefore, identifying the mechanism of NSCLC tumorigenesis is important to develop effective therapeutic approach. In recent years, growing numbers of studies have shown that miR serves as a key prognostic and diagnostic biomarker in tumors with potential asa therapeutic target (19). Moreover, dysregulation of miRNAs has been widely identified in NSCLC. For instance, miR-195-5p inhibited NSCLC progression via direct regulation of CIAPIN1(20). Down-regulation of miR-148a in NSCLC indicated adverse clinical outcomes and functioned as an anti-tumor miRNA in NSCLC (21). Moreover, miR-24 promoted NSCLC cell migration and invasion through targeting ZNF367(22). In our study, we investigated the roles of miR-23b in NSCLC.

Emerging studies have demonstrated the dysregulation of miR-23b in tumor progression. miR-23b belongs to the miR-23b/27b/24–1 cluster, and it is well known that aberrant expression of miR-23b may inhibit or promote tumor genesis and development via regulation of oncogenes or tumor suppressors. For example, miR-23b suppressed ovarian cancer progression and functioned as an independent prognostic marker (23). In bladder cancer, miR-23b inhibited cell proliferation and impaired colony formation via regulation of Zeb1 (24). However, miR-23b was reported to be an oncogenic miR in hepatocellular carcinoma and activated AKT/GSK3β/β-catenin signaling pathway through regulating ST7L (25). In our study, down-regulation of miR-23b was verified in NSCLC, which indicated poor prognosis and aggressive clinicopathologic features of NSCLC patients. Moreover, functional assays also revealed that the upregulation of miR-23b dramatically inhibited NSCLC cell viability, invasion and migration. In addition, we also confirmed that RUNX2 was a direct target of miR-23b, partially participating in the inhibited roles of miR-23b in NSCLC.

miRNAs are involved in tumor development and progression by regulating specific targets or signaling pathways (26). Epithelial-to-mesenchymal transition (EMT) is a physiopathological or physiological process in which epithelial cells acquire motility features of mesenchymal cells (27). EMT is featured by destruction of tight junctions accompanied by upregulated expressions of mesenchymal marker (such as Vimentin and N-cadherin) and downregulated expressions of epithelial marker (such as E-cadherin) (28). Accumulating evidence has shown that EMT exerts pivotal roles in metastases of multiple tumors. In NSCLC, EMT was reported to play vital roles in invasion and metastases (29). Wnt/β-catenin signaling pathway is constitutively overactivated in several types of cancers, including, NSCLC (30), serving pivotal roles in tumor pathogenesis via promotion of tumor metastasis or growth (31). Therefore, the current study focused on the specific regulatory functions of miR-23b in NSCLC EMT and Wnt/β-catenin signaling, and the results showed that miR-23b exerted anti-NSCLC functions via modulating EMT and Wnt/β-catenin signaling pathway.

To conclude, miR-23b downregulation was frequently observed in NSCLC. MiR-23b overexpression could suppress NSCLC cell growth and metastasis via regulation of EMT and Wnt/β-catenin. Moreover, findings in this study also uncovered an anti-NSCLC role of miR-23b via directly downregulating oncogene RUNX2.

REFERENCES

1. Torre LA, Bray F, Siegel RL, Ferlay J, Lortet-Tieulent J, Jemal A. Global cancer statistics, 2012. CA Cancer J Clin 2015; 65:87-108.
2. Kastelijn EA, de Langen AJ, Peters BJM. Treatment of oncogene-driven non-small cell lung cancer. Curr Opin Pulm Med 2019; 25:300-307.
3. Chaffer CL, Weinberg RA. A perspective on cancer cell metastasis. Science 2011; 331:1559-64.
4. Wei R, DeVilbiss FT, Liu W Genetic polymorphism, telomere biology and non-small lung cancer risk. J Genet Genomics 2015; 42(10):549-61.
5. Alonso DF, Ripoll GV, Garona J, Iannucci NB, Gomez DE. Metastasis: recent discoveries and novel perioperative treatment strategies with particular interest in the hemostatic compound desmopressin. Curr Pharm Biotechnol 2011; 12:1974-80.

6. Shukla GC, Singh J, Barik S. MicroRNAs: Processing, maturation, target recognition and regulatory functions. Mol Cell Pharmacol 2011; 3:83-92.
7. Guo H, Ingolia NT, Weissman JS, Bartel DP. Mammalian microRNAs predominantly act to decrease target mRNA levels. Nature 2010; 466:835-40.
8. Gorbatenko A, Sokilde R, Sorensen EE, et al. HER2 and p95HER2 differentially regulate miRNA expression in MCF-7 breast cancer cells and downregulate MYB proteins through miR-221/222 and miR-503. Sci Rep 2019; 9:3352.
9. Granados-Lopez AJ, Ruiz-Carrillo JL, Servin-Gonzalez LS, et al. Use of mature miRNA strand selection in miRNAs families in cervical cancer development. Int J Mol Sci 2017; 18:
10. Osipov ID, Zaporozhchenko IA, Bondar AA, et al. Cell-Free miRNA-141 and miRNA-205 as prostate cancer biomarkers. Adv Exp Med Biol 2016; 924:9-12.
11. Yang XY, Li N, Deng WY, et al. [miRNA-96-5p inhibits the proliferation and migration of gastric cancer cells by targeting FoxQ1]. Zhonghua Zhong Liu Za Zhi 2019; 41:193-99.
12. Zhang J, Li S, Li Y, Liu H, Zhang Y, Zhang Q. miRNA-218 regulates the proliferation and apoptosis of cervical cancer cells via targeting Gli3. Exp Ther Med 2018; 16:2433-41.
13. Tiwari A, Mukherjee B, Dixit M. MicroRNA key to angiogenesis regulation: MiRNA biology and therapy. Curr Cancer Drug Targets 2018; 18:266-77.
14. Juzenas S, Salteniene V, Kupcinskas J, et al. Analysis of deregulated microRNAs and their target genes in gastric cancer. PLoS One 2015; 10:e0132327.
15. Lu H, Jiang T, Ren K, Li ZL, Ren J, Wu G, Han X. RUNX2 plays an oncogenic role in esophageal carcinoma by activating the PI3K/AKT and ERK signaling pathways. Cell Physiol Biochem 2018; 49:217-25.
16. Wang Q, Yu W, Huang T, Zhu Y, Huang C. RUNX2 promotes hepatocellular carcinoma cell migration and invasion by upregulating MMP9 expression. Oncol Rep 2016; 36:2777-84.
17. Boregowda RK, Olabisi OO, Abushahba W, et al. RUNX2 is overexpressed in melanoma cells and mediates their migration and invasion. Cancer Lett 2014; 348:61-70.
18. Moreira AL, Eng J. Personalized therapy for lung cancer. Chest 2014; 146:1649-57.
19. Levy B, Hu ZI, Cordova KN, Close S, Lee K, Becker D. Clinical utility of liquid diagnostic platforms in non-small cell lung cancer. Oncologist 2016; 21:1121-30.
20. Zheng J, Xu T, Chen F, Zhang Y. MiRNA-195-5p Functions as a tumor suppressor and a predictive of poor prognosis in non-small cell lung cancer by directly targeting CIAPIN1. Pathol Oncol Res 2019;
21. Chen Y, Min L, Zhang X, et al. Decreased miRNA-148a is associated with lymph node metastasis and poor clinical outcomes and functions as a suppressor of tumor metastasis in non-small cell lung cancer. Oncol Rep 2013; 30:1832-40.
22. Liu Z, Jiang L, Zhang G, Li S, Jiang X. MiR-24 promotes migration and invasion of non-small cell lung cancer by targeting ZNF367. J BUON 2018; 23:1413-19.
23. Li W, Liu Z, Chen L, Zhou L, Yao Y. MicroRNA-23b is an independent prognostic marker and suppresses ovarian cancer progression by targeting runt-related transcription factor-2. FEBS Lett 2014; 588:1608-15.
24. Majid S, Dar AA, Saini S, et al. MicroRNA-23b functions as a tumor suppressor by regulating Zeb1 in bladder cancer. PLoS One 2013; 8:e67686.
25. Zhuang L, Wang X, Wang Z, et al. MicroRNA-23b functions as an oncogene and activates AKT/GSK3beta/beta-catenin signaling by targeting ST7L in hepatocellular carcinoma. Cell Death Dis 2017; 8:e2804.
26. Zhang X. MiR-770 inhibits tumorigenesis and EMT by targeting JMJD6 and regulating WNT/β-catenin pathway in non-small cell lung cancer. Life Sciences S0024320517304319.
27. Nistico P, Bissell MJ, Radisky DC. Epithelial-mesenchymal transition: general principles and pathological relevance with special emphasis on the role of matrix metalloproteinases. Cold Spring Harb Perspect Biol 2012; 4:
28. Lamouille S, Xu J, Derynck R. Molecular mechanisms of epithelial-mesenchymal transition. Nat Rev Mol Cell Biol 2014; 15:178-96.
29. Dai HY, Ma Y, Da Z, Hou XM. Knockdown of TRIM66 inhibits malignant behavior and epithelial-

mesenchymal transition in non-small cell lung cancer. Pathol Res Pract 2018; 214:1130-35.

30. Uematsu K, He B, You L, Xu Z, McCormick F, Jablons DM. Activation of the Wnt pathway in non small cell lung cancer: evidence of dishevelled overexpression. Oncogene 2003; 22:7218-21.
31. Peng C, Li X, Yu Y, Chen J. LncRNA GASL1 inhibits tumor growth in gastric carcinoma by inactivating the Wnt/beta-catenin signaling pathway. Exp Ther Med 2019; 17:4039-45.

MicroRNA-495 ATTENUATES PROLIFERATION AND INFLAMMATORY RESPONSE IN RHEUMATOID ARTHRITIS FIBROBLAST-LIKE SYNOVIOCYTES THROUGH ATTENUATING β-CATENIN PATHWAY

L. FANG, X.-F. XU, Y. LU, Y.-Y. WU and J.-J. LI

Department of Rheumatology and Immunology, Zhoushan Hospital of Zhejiang Province, Zhoushan, China

Received January 27, 2020 – Accepted April 30, 2020

Fibroblast-like synoviocytes (FLSs) exert a critical effect in the occurrence and progress of rheumatoid arthritis (RA). MicroRNA-495 (miR-495) can regulate many growth behaviors in various cell types. Nevertheless, the role of miR-495 is still unclear in RA-FLS. We aimed to explore the role and molecular mechanism of miR-495 in RA. The FLSs and synovial tissue from normal and RA cases were used in the study. RT-PCR analysis was used to examine the expression of miR-495. Western blot assay was conducted to determine the levels of matrix metalloproteinase-9 (MMP-9), matrix metalloproteinase-2 (MMP-2) and β-catenin. Cell counting kit-8 (CCK-8) assays were performed to determine the proliferation of RA-FLS in different treatment groups. The results showed that miR-495 is down-regulated in both RA-synovial tissue and RA-FLSs. Overexpression of miR-495 could inhibit RA-FLS proliferation and inflammatory factors of interleukin (IL)-6, IL-11 and tumor necrosis factor alpha (TNF-α), and decrease the protein expression of MMP-9 and MMP-2. In addition, miR-495 could negatively regulate the expression of β-catenin in RA-FLSs. We also confirmed that the inhibitory role of miR-495 in RA-FLS is through the regulation of β-catenin expression. Taken together, miR-495 is downregulated in RA-FLS and RA synovial tissue, and miR-495 inhibits proliferation and inflammatory response in RA-FLS, partially via regulating β-catenin expression. The miR-495/β-catenin pathway may serve as a new therapeutic target for RA.

Rheumatoid arthritis (RA), a chronic autoimmune disease with high incidence and high disability rate, has no very effective treatment until now (1, 2). The pathological manifestations of RA include recurrent inflammation, hyperproliferation and dysfunction of synovium, erosion and destruction of synovium cells and pannus in articular cartilage and bone (3, 4). In the process of inflammation, RA-FLSs produce a large number of inflammatory cytokines and matrix degrading enzymes, which further promotes the continuity of inflammatory response (5, 6). At the same time, continuous stimulation of FLS proliferation and tumor-like transformation, increased the ability of invasion, eventually leading to joint stenosis, joint injury and even disability (7).

During the development of RA, FLSs proliferate and secrete a lot of inflammatory factors such as IL-6, IL-11 and TNF-α (8, 9). In addition, FLSs also secrete a large number of extracellular matrix (ECM), including MMP-9 and MMP-2 (10). Under the effect of inflammation and ECM, articular cartilage and bone are invaded and destroyed, which

Key words: rheumatoid arthritis; miR-495; β-catenin; proliferation; inflammatory response

Corresponding Author:
Xiangfeng Xu, MD,
Department of Rheumatology and Immunology,
Zhoushan Hospital of Zhejiang Province, Zhoushan, China
739 Dingshen Road, Zhoushan, 316021, Zhejiang, China
Tel.: +86 0580 2292736
e-mail: bihailantian1976@163.com

0393-974X (2020)
Copyright © by BIOLIFE, s.a.s.
This publication and/or article is for individual use only and may not be further reproduced without written permission from the copyright holder.
Unauthorized reproduction may result in financial and other penalties
DISCLOSURE: ALL AUTHORS REPORT NO CONFLICTS OF INTEREST RELEVANT TO THIS ARTICLE.

further aggravates the deterioration of RA (11). Therefore, in the early stage, timely inhibition of FLS proliferation, as well as inhibition of inflammation and ECM secretion will contribute to the progress of RA.

Numerous studies have confirmed that non-coding RNA (ncRNA) regulates cell proliferation, development, gene transcription, translation and other cell functions, and mediates various life activities of organisms (12, 13). MicroRNAs (miRNAs), endogenous non coding small molecule single stranded RNAs, have been widely studied in many diseases in recent years (14). Moreover, the role of miRNA in RA has also been studied extensively. For example, Stanczyk et al. confirmed that miR-203 was up-regulated in FLSs of RA patients. Overexpression of miR-203 could regulate the secretion of MMP-1 and IL-6 via NF-κB pathway (15). Similarly, miR-346 can inhibit the expression of BTK in FLSs, reduce the synthesis of TNF-α, and miR-346 inhibitor can block the role of miR-346 on TNF-α expression in RA, so it is hypothised that miR-346 plays a negative role in the regulation of inflammation in RA (16). However, the relationship between miRNA and RA is still in the initial stage, and the role and mechanism of miRNA in RA need to be further explored.

In this study, we found an miRNA (miR-495) which has a regulatory role in proliferation, inflammation and other pathological processes, and found that the expression of miR-495 in RA tissue and ra-fls was significantly down-regulated. We further investigated the role of miR-495 in ra-flss and the potential molecular mechanism. These studies will provide a new perspective for the treatment of RA in the future.

MATERIALS AND METHODS

Synovial tissue samples of RA patients

This study was approved by the medical Ethics Committee of Zhoushan Hospital, and the contents of this study were fully explained to all patients participating who signed a formal written informed consent. In this study, synovium tissues of 8 RA patients and 8 non-RA patients were obtained. All patients met the diagnostic criteria of RA. Exclusion criteria were other immune diseases, as well as knee joint injuries.

Cell culture

The human RA-FLS cell line MH7A was purchased from the typical culture preservation Center (ATCC, Manassas, VA, USA). The 1640 medium (Hyclone, South Logan, UT, USA) containing 10% fetal bovine

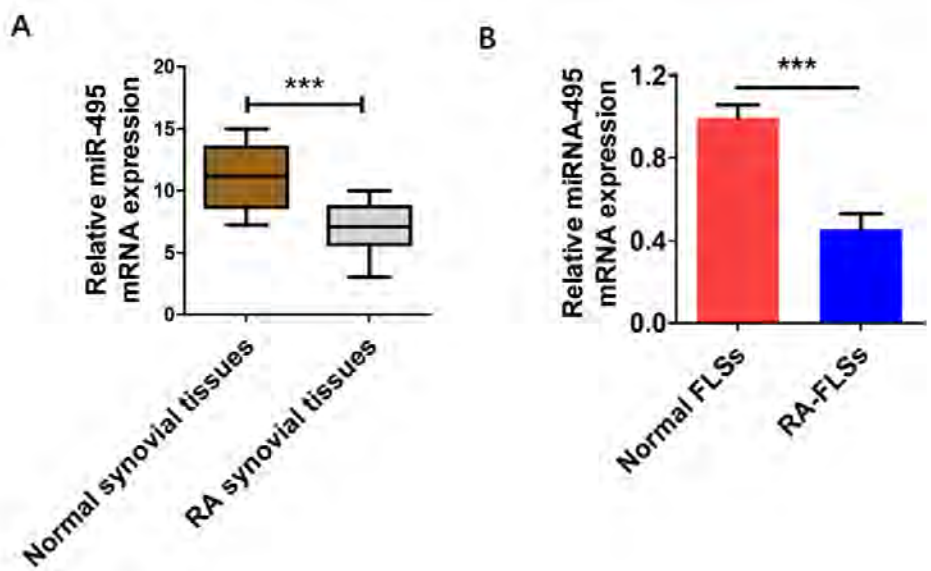


Fig. 1. *Expression of miR-495 in RA-synovial tissue and RA-FLSs.* ***A****) RT-PCR analysis was used to determine the expression of miR-495 in synovial tissue from normal and RA cases.* ***B****) miR-495 expression was examined in FLSs and RA-FLSs using RT-PCR analysis. Each experiment was conducted three times independently. *** P<0.001.*

serum (FBS, Gibco, Rockville, MD, USA) and penicillin/streptomycin (1:100, Sigma, St. Louis, MO, USA) was used. Cells were culture at 37°C in 5% CO_2 incubator with relative humidity of 95%.

Cell transfection

MiR-495 mimic and control analogue (mimic NC) were obtained from Shanghai Genekey Co., Ltd (Genekey, Shanghai, China). FLSs were transfected with the concentration of mir-495 mimic 50 nm for 48 h. β-Catenin overexpression and knockdown adenovirus were purchased from Shanghai Genekey Co. Ltd (Genekey, Shanghai, China). The titer of adenovirus transfected cells was 50 MOI.

Cell Counting Kit-8 (CCK-8) assay

Cell proliferation was carried out by the CCK-8 assay. The specific operation steps were carried out according to the manufacturer's instructions. Briefly, the transfected FLSs were plated at 1×10^4 cells/well on 96-well plates, and 12 μL/well CCK-8 solution (Beyotime, Shanghai, China) was added to each separate well for 24 h, then cultured for 2 h, and determined using spectrophotometrically at 450 nm.

Western blot analysis

The proteins of synovial tissue and FLSs in different treatment groups were extracted, then boiled for 10 min. The proteins were separated by electrophoresis and transmembraned, and then incubated at 4°C overnight with primary antibody of MMP-9, MMP-2, β-catenin and glyceraldehyde 3-phosphate dehydrogenase (GAPDH) (Abcam, Cambridge, MA, USA). Then, bands were cultured with second antibody for 2 h and washed with TBST 20 min each time for 3 times. The bands were detected by chemiluminescence (Thermo Scientific, Waltham, MA, USA).

Reverse transcription-quantitative real-time polymerase chain reaction (RT-PCR) analysis

Total RNA of synovial tissue and FLSs were extracted using TRIzol (Invitrogen, Carlsbad, CA, USA). The RNA purity was detected at 260/280 nm using a NanoDrop ND-1000 spectrophotometer (Thermo Scientific, Waltham, MA, USA). A PrimeScript reverse transcription Kit (TaKaRa, Tokyo, Japan) was used to conduct RT of RNA, and the SYBR Premix kit (RR420A; TaKaRa, Tokyo, Japan) was used for qRT-PCR assay.

The 18s rRNA was used as an internal reference to analyzed the data using the $2^{-\Delta\Delta CT}$ method. The primers used in the study were shown as below: miR-495, Forward Primer: 3'-TAGTGGCCGAATTCG-5'; Reverse Primer: 3'-CCGGCGGAGCGGCAGT-5'; U6, Forward Primer: 3'-GCCGAACGCCCTAGG-5'; Reverse Primer: 3'-CTGGCACCTTCACCGG-5'; β-catenin, Forward Primer: 3'-AATTGGCCCGGCTAGT-5'; Reverse Primer: 3'-TCCGCTTGCCTTAGT-5'; GAPDH, Forward Primer: 3'-GGTGTTCCGGCTCCCA-5'; Reverse Primer: 3'-TAAGGCCCTTGTGGTTAAG-5'.

Statistical analysis

All data were presented as means ± standard deviation (SD) using Statistical Product and Service Solutions (SPSS) 22.0 (IBM, Armonk, NY, USA). Student's *t*-test was performed to analyze the differences from two groups. Comparison between multiple groups was made using One-way ANOVA test followed by post hoc test (least significant difference). P-value < 0.05 was considered as statistically significant.

RESULTS

MiR-495 is down-regulated in RA-synovial tissue and RA-FLSs

We first examined the expression of miR-495 in normal synovial tissue and RA-synovial tissue using RT-PCR analysis. The results showed that the expression of miR-495 in RA-synovial tissue group was markedly lower than that in the normal group (Fig. 1A). Consistent with this result, miR-495 expression was markedly down-regulated in RA-FLSs than normal FLSs (Fig. 1B).

MiR-495 inhibits RA-FLS proliferation and inflammatory response

To clarify the role of miR-495 in RA-FLS, we overexpressed the miR-495 expression by miR-495 mimic in RA-FLSs (Fig. 2A). CCK-8 assay results demonstrated that overexpression of miR-495 significantly attenuates the RA-FLSs proliferation (Fig. 2B). RT-PCR analysis results demonstrated that miR-495 significantly inhibited the production of

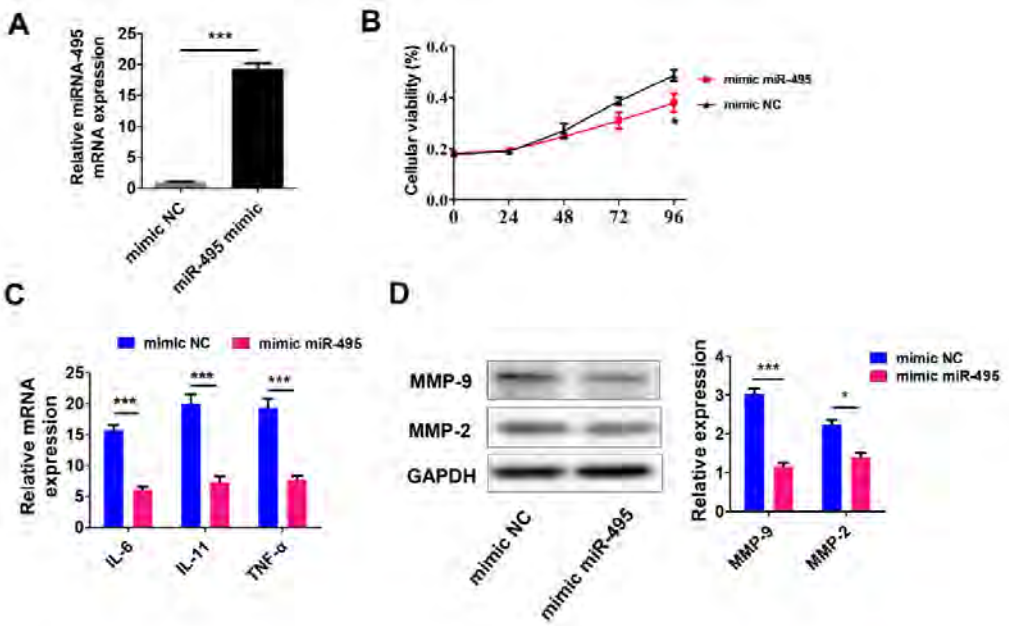


Fig. 2. *The function role of miR-495 in RA-FLSs.* ***A****) RT-PCR analysis was performed to verify the transfection efficiency of miR-495 mimic in RA-FLSs.* ***B****) CCK-8 assay was used to detect the proliferation of RA-FLSs after miR-495 overexpressed.* ***C****) Inflammatory factors expression of IL-6, IL-11 and TNF-α in RA-FLSs was examined by RT-PCR analysis.* ***D****) MMP-9 and MMP-2 expression in RA-FLSs was determined by western blot analysis. Each experiment was conducted three times independently. * P<0.05; *** P<0.001.*

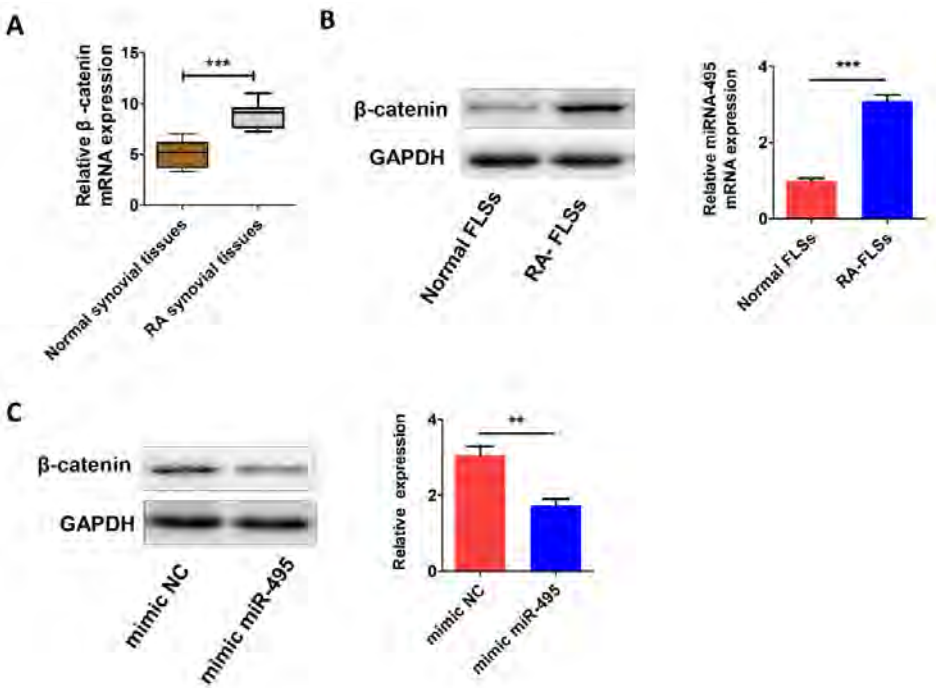


Fig. 3. *MiR-495 regulates β-catenin expression.* ***A****) RT-PCR analysis was used to determine the expression of β-catenin in synovial tissue from normal and RA cases.* ***B****) Western blot analysis was used to examine the expression of β-catenin in FLSa and RA-FLSs.* ***C****) β-catenin expression after treatment of miR-495 was detected by Western blot analysis. Each experiment was conducted three times independently. ** P<0.01; ** P<0.001.*

inflammatory factors IL-6, IL-11 and TNF-α in RA-FLS (Fig. 2C). In addition, miR-495 significantly inhibited the production of MMP-9 and MMP-2 in RA-FLSs (Fig. 2D).

MiR-495 suppresses β-catenin expression in RA-FLSs

Previous studies have shown that miR-495 could negatively regulate Wnt/β-catenin pathway, and that Wnt/β-catenin pathway exerts a critical effect in the occurrence and development of RA (3, 12). In our study, we first demonstrated that β-catenin expression was obviously up-regulated in RA synovial tissues and RA-FLSs (Fig. 3 A, B). Then, we further proved that overexpression of miR-495 in RA-FLSs could significantly inhibit the expression of β-catenin (Fig. 3C).

Inhibition of β-catenin suppresses RA-FLS proliferation and inflammatory response

To confirm the role of β-catenin in RA-FLS, we first silenced the β-catenin expression by β-catenin siRNA in RA-FLSs (Fig. 4A). CCK-8 assay results showed that inhibition of β-catenin significantly inhibits the RA-FLSs proliferation (Fig. 4B). The results of flow cytometry showed that inhibition of β-catenin mainly inhibited the proportion of S phase cells in RA-FLSs (Fig. 4C). These results showed that silencing β-catenin suppresses cell proliferation mainly by inhibiting RA-FLSs DNA synthesis. Moreover, RT-PCR analysis results showed that inhibition of β-catenin significantly inhibited the production of inflammatory factors IL-6, IL-11 and TNF-α in RA-FLS (Fig. 4D).

MiR-495 suppresses cell proliferation and inflammatory response via Wnt/β-catenin pathway in RA-FLSs

Given the function of β-catenin inhibition on RA-FLS proliferation and inflammatory response, we then explored if β-catenin could mediate the inhibitory role of miR-495 in RA-FLSs. Concomitant overexpression of β-catenin partially blocked miR-495's role on the proliferation and inflammatory of RA-FLSs (Fig. 5 A, B). In addition, MMP-9 and

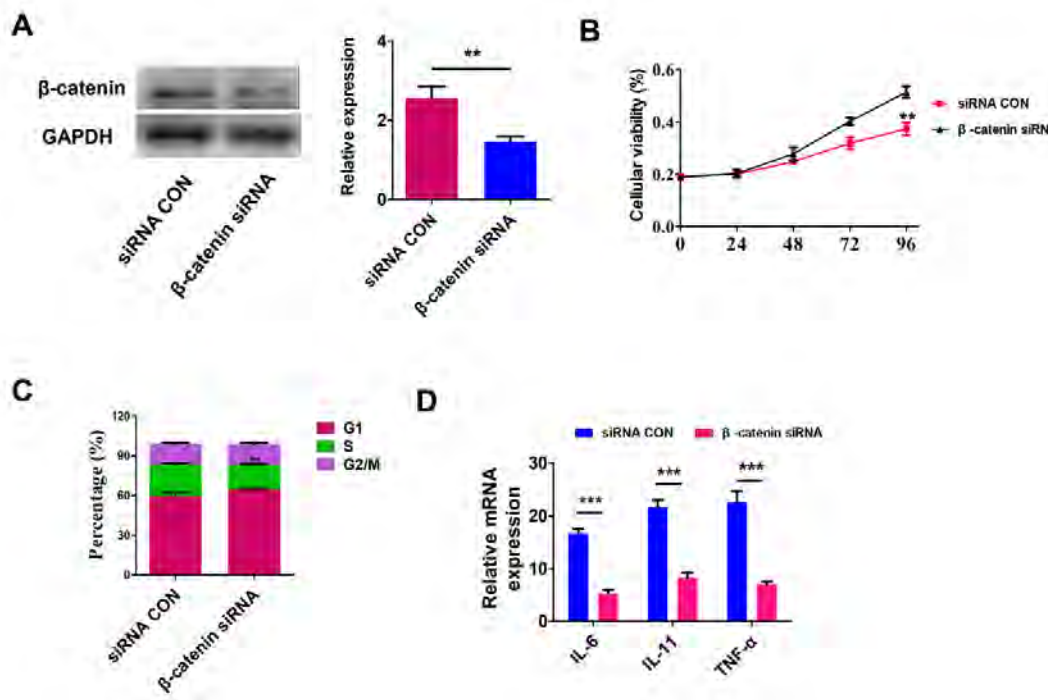


Fig. 4. *The role of β-catenin on RA-FLS proliferation and inflammatory response.* ***A****) Western blot analysis was performed to verify the transfection efficiency of β-catenin siRNA in RA-FLSs.* ***B****) CCK-8 assay was used to detect the proliferation of RA-FLSs after β-catenin inhibition.* ***C****) Flow cytometry was used to detect the effect of β-catenin inhibition on cell cycle in RA-FLSs.* ***D****) Inflammatory factors expression of IL-6, IL-11 and TNF-α in RA-FLSs treated with β-catenin siRNA was examined by RT-PCR analysis. Each experiment was conducted three times independently. ** P<0.01; *** P<0.001.*

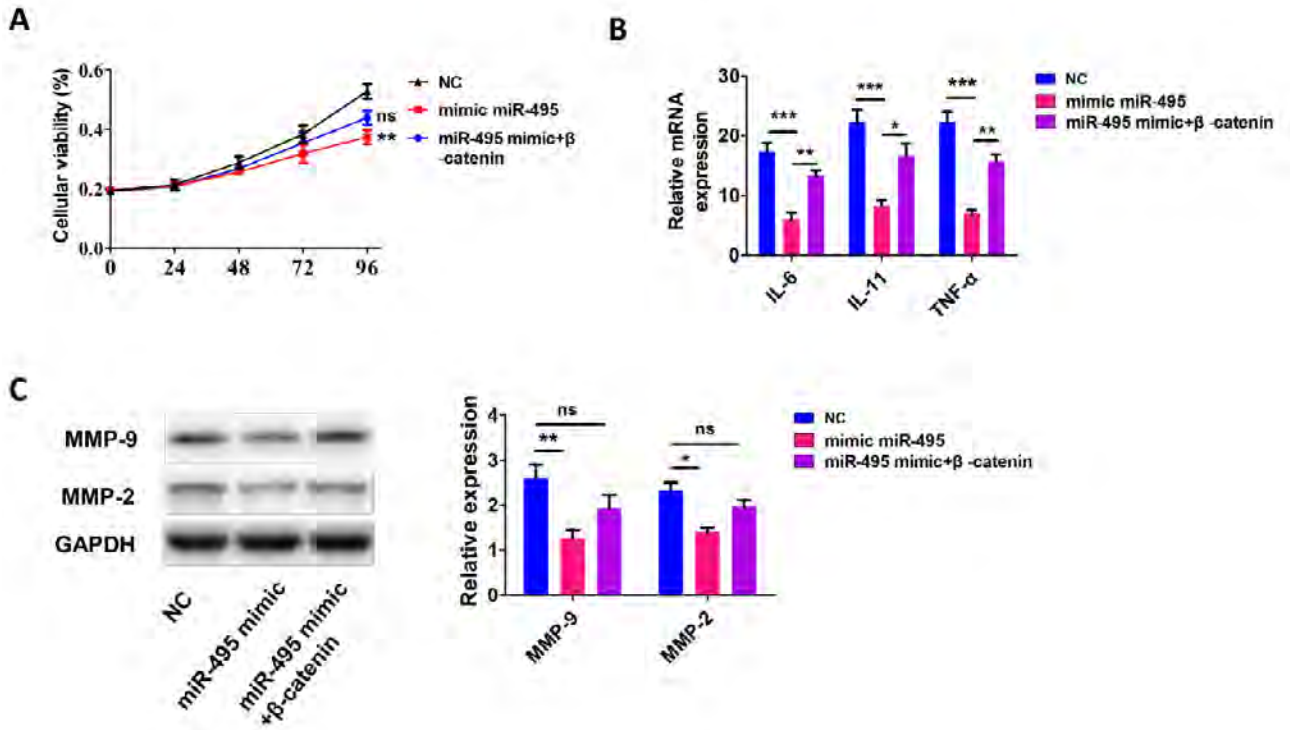


Fig. 5. *MiR-495 suppresses cell proliferation and inflammatory response via β-catenin pathway.* ***A****) MiR-495 mimic and β-catenin siRNA were transfected separately or co transfected and then CCK-8 was used to detect proliferation of RA-FLSs.* ***B****) Inflammatory factors expression of IL-6, IL-11 and TNF-α in different treated cells was examined by RT-PCR analysis.* ***C****) Western blot analysis was used to examine the expression of MMP-9 and MMP-2 in different treated cells. Each experiment was conducted three times independently. * P<0.05; ** P<0.01; *** P<0.001.*

MMP-2 expression, which are inhibited by miR-495 in RA-FLSs, could also be partially reversed by overexpression β-catenin (Fig. 5C).

DISCUSSION

FLSs activated in the early stage of RA are important effector cells of synovitis (17, 18). Overproliferation of FLSs could activate downstream signaling pathway, release IL-6, IL-11, TNF-α and other inflammatory factors. Chemotactic neutrophils enter into the joint to cause inflammatory reaction, which further induces the production of various chemokines such as ECM (MMP-9 and MMP-2), and finally aggravates RA (6, 19).

MiR-495 has been found to regulate proliferation, apoptosis and inflammatory factors in many diseases (20-22). In our study, we found that the expression of miR-495 in synovium and FLSs of RA patients was significantly lower than that in normal synovium and FLS. Considering the function of miR-495 in other diseases, we concluded that miR-495 may be related to RA and play a regulatory role in the development of RA. In order to verify this hypothesis, we first constructed miR-495 overexpression analog (miR-495 mimic) and transfected RA-FLSs. We demonstrated that overexpression of miR-495 significantly attenuated the proliferation of FLSs, and inhibited the production level of inflammatory factors IL-6, IL-11 and TNF-α. In addition, overexpression of miR-

495 also decreased the secretion of MMP-9 and MMP-2. These results indicated that miR-495 is a functional miRNA in RA.

β-catenin pathway was confirmed to be vital in cell proliferation and inflammatory development, and could be activated in many inflammatory and tumor diseases (23, 24). Inhibition of β-catenin pathway could significantly reverse the development of proliferation and inflammation in these diseases. β-catenin pathway has also been confirmed to be activated in RA in recent years (25). When β-catenin pathway is inhibited, FLS proliferation can be significantly inhibited while FLS apoptosis can be enhanced (26). Interestingly, miR-495 can negatively regulate the expression of β-catenin and affect the progression of non-small cell lung cancer (27). In our study, over expression of miR-495 could inhibit the expression of β-catenin in RA-FLSs. In addition, overexpression of β-catenin could reverse the role of miR495 in RA-FLSs.

In conclusion, these results demonstrate that miR-495 is likely to inhibit the proliferation and inflammation of RA-FLSs by down-regulating β-catenin expression. Further work targeting miR-495/β-catenin axis in RA will be very useful for the treatment of RA in future.

REFERENCES

1. Tlustochowicz M, Sliwczynski AM, Brzozowska M, Teter Z, Marczak M. Sequentiality of treatment in the rheumatoid arthritis drug programme in the years 2009-2014. Arch Med Sci 2018; 14:569-71.
2. Bae SC, Cho SK, Won S, et al. Factors associated with quality of life and functional disability among rheumatoid arthritis patients treated with disease-modifying anti-rheumatic drugs for at least 6 months. Int J Rheum Dis 2018; 21:1001-9.
3. Li Y, Yuan L, Jiang S, et al. Interleukin-35 stimulates tumor necrosis factor-α activated osteoblasts differentiation through Wnt/β-catenin signaling pathway in rheumatoid arthritis. Int Immunopharmacol 2019; 75:105810.
4. Kovacs A, Baksay B, Cserenyecz A, Molnar K, Takacs M, Szekanecz Z. Occurrence of pulmonary rheumatoid nodules following biological therapies. Clin Rheumatol 2015; 34:1639-42.
5. Takeuchi Y, Hirota K, Sakaguchi S. Synovial tissue inflammation mediated by autoimmune T Cells. Front Immunol 2019; 10:1989.
6. Zhu D, Zhao J, Lou A, et al. Transforming growth factor beta1 promotes fibroblast-like synoviocytes migration and invasion via TGF-beta1/Smad signaling in rheumatoid arthritis. Mol Cell Biochem 2019; 459:141-50.
7. Li LH, Zhang JZ, Liu Z, Sun TS. Progressive pseudorheumathoid dysplasia with bilateral supracondylar fracture of femur:a case report. Zhongguo Gu Shang 2016; 29:1154-56.
8. Ha YJ, Choi YS, Han DW, et al. PIM-1 kinase is a novel regulator of proinflammatory cytokine-mediated responses in rheumatoid arthritis fibroblast-like synoviocytes. Rheumatology (Oxford) 2019; 58:154-64.
9. Shi M, Wang J, Xiao Y, et al. Glycogen metabolism and rheumatoid arthritis: the role of glycogen synthase 1 in regulation of synovial inflammation via blocking AMP-activated protein kinase activation. Front Immunol 2018; 9:1714.
10. Li XF, Sun YY, Bao J, et al. Functional role of PPAR-gamma on the proliferation and migration of fibroblast-like synoviocytes in rheumatoid arthritis. Sci Rep 2017; 7:12671.
11. Li XF, Song B, Xu QQ, et al. Over-expression of PTEN suppresses the proliferation and migration of fibroblast-like synoviocytes in adjuvant-induced arthritis. Cell Physiol Biochem 2019; 52:1446-62.
12. Wang J, Yang H, Ma H, et al. MiR-495 inhibits fibroblast-like synoviocyte proliferation and inflammation in rheumatoid arthritis rats via Wnt signaling pathway. Panminerva Med 2020.
13. Waller P, Blann AD. Non-coding RNAs - A primer for the laboratory scientist. Br J Biomed Sci 2019; 76:157-65.
14. Swingler TE, Niu L, Smith P, et al. The function of microRNAs in cartilage and osteoarthritis. Clin Exp Rheumatol 2019; 37(Suppl):40-47.
15. Stanczyk J, Ospelt C, Karouzakis E, et al. Altered expression of microRNA-203 in rheumatoid arthritis synovial fibroblasts and its role in fibroblast activation. Arthritis Rheum 2011; 63:373-81.
16. Semaan N, Frenzel L, Alsaleh G, et al. miR-346

controls release of TNF-alpha protein and stability of its mRNA in rheumatoid arthritis via tristetraprolin stabilization. Plos One 2011; 6:e19827.

17. Du H, Zhang X, Zeng Y, et al. A novel phytochemical, DIM, inhibits proliferation, migration, invasion and TNF-alpha induced inflammatory cytokine production of synovial fibroblasts from rheumatoid arthritis patients by targeting MAPK and AKT/mTOR signal pathway. Front Immunol 2019; 10:1620.
18. Du X, Zhang H, Zhang W, et al. The protective effects of lixisenatide against inflammatory response in human rheumatoid arthritis fibroblast-like synoviocytes. Int Immunopharmacol 2019; 75:105732.
19. Zhao C, Fernandes MJ, Turgeon M, Tancrede S, Di Battista J, Poubelle PE, Bourgoin SG. Specific and overlapping sphingosine-1-phosphate receptor functions in human synoviocytes: impact of TNF-alpha. J Lipid Res 2008; 49:2323-37.
20. Zhao G, Zhang L, Qian D, Sun Y, Liu W. miR-495-3p inhibits the cell proliferation, invasion and migration of osteosarcoma by targeting C1q/TNF-related protein 3. Onco Targets Ther 2019; 12:6133-43.
21. Zhao X, Wang T, Cai B, et al. MicroRNA-495 enhances chondrocyte apoptosis, senescence and promotes the progression of osteoarthritis by targeting AKT1. Am J Transl Res 2019; 11:2232-44.
22. Gong L, Wu X, Li X, et al. S1PR3 deficiency alleviates radiation-induced pulmonary fibrosis through the regulation of epithelial-mesenchymal transition by targeting miR-495-3p. J Cell Physiol 2019.
23. Shaikh G, Zhang J, Perez-Aso M, Mediero A, Cronstein B. Adenosine A2A receptor promotes collagen type III synthesis via beta-catenin activation in human dermal fibroblasts. Br J Pharmacol 2016; 173:3279-91.
24. Tseng JC, Lin CY, Su LC, Fu HH, Yang SD, Chuu CP. CAPE suppresses migration and invasion of prostate cancer cells via activation of non-canonical Wnt signaling. Oncotarget 2016; 7:38010-38024.
25. Miao CG, Shi WJ, Wei W, Qin MS, Chen H, Zhang B. Molecular mechanism of total flavonoids in Isodon amethystoides on adjuvant arthritis in rats. Zhongguo Zhong Yao Za Zhi 2017; 42:3411-16.
26. Miao CG, Huang C, Huang Y, et al. MeCP2 modulates the canonical Wnt pathway activation by targeting SFRP4 in rheumatoid arthritis fibroblast-like synoviocytes in rats. Cell Signal 2013; 25:598-608.
27. Zheng HE, Wang G, Song J, Liu Y, Li YM, Du WP. MicroRNA-495 inhibits the progression of non-small-cell lung cancer by targeting TCF4 and inactivating Wnt/beta-catenin pathway. Eur Rev Med Pharmacol Sci 2018; 22:7750-59.

THE ROLE OF SIGMA-1 RECEPTOR AGONIST IN HEPATIC ISCHEMIA-REPERFUSION INJURY

J. LI[1], R-J. LI[2], X. ZHAO[3] and H-Q. LIU[1]

[1]Department of Anesthesiology, The First Hospital of Jilin University, Changchun, Jilin, China;
[2]Department of Hand Surgery, The First Hospital of Jilin University, Changchun, Jilin, China;
[3]Department of Paediatrics, The First Hospital of Jilin University, Changchun, Jilin, China

Received February 20, 2020 – Accepted April 30, 2020

Sigma-1 receptor (Sig-1R) is a ligand-operated protein that modulates activity of various proteins. It is expressed within the endoplasmic reticulum membranes of multiple organs. We examined the role of Sig-1R in hepatic ischemia-reperfusion injury (IRI). We studied IRI indicators in Sig-1R$^{-/-}$ mice and compared them with wild-type controls. In addition, we assessed the influence of Sig-1R agonist, fluvoxamine, on IRI in both types of animals. We found that Sig-1R$^{-/-}$ mice exhibited significantly decreased liver damage after hepatic IRI as compared to wild-type mice. This effect was manifested by decreased serum levels of alanine aminotransferase (AST), aspartate aminotransferase (ALT), myeloperoxidase (MPO), and supernatant level of lactate dehydrogenase (LDH), decreased endothelial glycocalyx shedding indexed by decreased serum levels of heparan sulfate and syndecan-1, slightly improved liver histology and reduced metalloproteinase-9 expression. Furthermore, in comparison to Sig-1R$^{-/-}$ mice, fluvoxamine significantly increased serum levels of AST, ALT, MPO, and LDH in wild-type animals in a dose-dependent manner at 6 h after IRI. Our findings demonstrate that the absence of Sig-1R provides a protective effect during hepatic IRI. Sig-1R-mediated signaling pathways may play distinct roles in IRI in different organs. The dynamic interaction between Sig-1R and other signaling molecules in different organs needs to be examined further.

Hepatic ischemia-reperfusion injury (IRI) is a pathophysiological process in which the hypoxic insult is further exaggerated by restoration of blood flow to liver after liver surgery or transplantation (1). IRI may lead to early transplant failures and significantly impairs the prognosis of liver function.

The loss of endothelial glycocalyx integrity and function plays a critical role in the hepatopathology following IRI (2-5). However, the molecular and pathological mechanisms of endothelial glycocalyx shedding in hepatic IRI remain poorly understood. Endothelial glycocalyx is a carbohydrate-rich meshwork covering vascular endothelium and consisting of heparan sulfate and syndecan-1 (6, 7). It plays a crucial role in the regulation of vascular permeability (8) and inflammatory response (9). Hence, the protection of endothelial glycocalyx from damage is a promising therapeutic approach in reducing the incidence of IRI in acute critical care setting (10).

Previous studies have demonstrated that activation of Sigma 1 receptor (Sig-1R) effectively prevents

Key words: Sigma-1 receptor; liver; hepatic ischemia-reperfusion injury; endothelial glycocalyx; metalloproteinase-9

Corresponding Author:
Dr. Huan-Qiu Liu,
Department of Anesthesiology,
The First Hospital of Jilin University,
1 Xinmin Street, Changchun 130021,
Jilin, China
e-mail: liuhuanqiu@yahoo.com

0393-974X (2020)
Copyright © by BIOLIFE, s.a.s.
This publication and/or article is for individual use only and may not be further reproduced without written permission from the copyright holder.
Unauthorized reproduction may result in financial and other penalties
DISCLOSURE: ALL AUTHORS REPORT NO CONFLICTS OF INTEREST RELEVANT TO THIS ARTICLE.

renal IRI. Sig-1R is a highly conserved protein expressed in many peripheral tissues including the liver, however, its role in hepatic IRI has not been investigated.

Fluvoxamine (FLU) is a potent selective Sig-1R agonist (11). It has been shown that FLU ameliorates ischemic cardiac (12, 13) and brain damage (14), as well as renal IRI. However, the effects of FLU in hepatic IRI have not yet been elucidated.

The present study examined the effects of FLU pretreatment on liver damage in an experimental animal model of hepatic IRI. We evaluated the role of Sig-1R in hepatic IRI using a Sig-1R knockout animal model. We examined the effects of a warm hepatic IR on syndecan-1 shedding in both wild type and Sig-1R knockout mice. We then evaluated the effects of FLU pretreatment on hepatic IRI in wild type mice.

MATERIALS AND METHODS

Animals

The Sig-1R knockout (Sig-1R$^{-/-}$) mice were a gift from the laboratory of Dr. Xian Zhao, Department of Anesthesiology at the Second Hospital of Shandong University, Jinan, China. Mice were characterized using the methods described previously (15). The genotype of mice was identified with PCR using genomic DNA obtained from mice tail. Matched Sig-1R / wild-type littermates and C57BL6 mice (obtained from the Shanghai Laboratory Animal Center at 8 to 10 weeks of age) were also used. All animals were maintained in a temperature- and humidity-controlled vivarium at the Animal Research Center of Jilin University under 12:12 h light/dark cycle. All animals were given food and water *ad libitum*. All experiments were approved by the Institutional Animal Care Committee of Jilin University. The appropriate ethical guidelines were used during the work. The housing and treatment of the mice followed the "Guide for the Care and Use of Laboratory Mice" (Institute of Laboratory Animal Resources, Commission on Life Sciences 2011).

Partial lobar liver ischemia/reperfusion injury

Warm hepatic I/R models were prepared according to the protocol of Zwacka et al. (16), with minor modifications. Mice were anesthetized with sodium pentobarbital (60 mg/kg body weight intraperitoneally) and injected with heparin (100 U/kg body weight). Arterial and portal venous blood supplies were interrupted to the cephalad lobes of the liver for 90 min using an atraumatic clip. After 90 min of partial hepatic warm ischemia, the clip was removed and the hepatic reperfusion initiated. Mice were maintained on a heating pad (37°C) for the duration of the procedure. Sham control mice underwent the same surgical procedure but without receiving the vascular occlusion.

Pharmacological treatment

To test the effects of Sig-1R receptor activation on the hepatic ischemia-reperfusion injury, mice were treated 30 min before the ischemic insult with intraperitoneal administration of either vehicle (isotonic saline) or 1, 5, 10, or 20 mg/kg of FLU (Sigma-Aldrich), which is a highly selective Sig-1R agonist.

Assessment of hepatic function

Blood samples were collected at 6 h after reperfusion. The samples were centrifuged to obtain serum. To evaluate the extent of hepatocyte damage, we used an automated chemical analyzer (Olympus Automated Chemistry Analyzer AU5400, Tokyo, Japan) to measure the serum level of alanine aminotransferase (ALT), aspartate aminotransferase (AST), myeloperoxidase (MPO) and the supernatant level of lactate dehydrogenase (LDH). Enzyme-linked immunosorbent assay (ELISA) was used to measure the concentrations of heparan sulfate (HS) and syndecan-1 (Syn-1).

Histological analysis

Liver samples were fixed with 10% neutral formaldehyde and embedded in paraffin. The samples were sectioned at 5 μm and stained with hematoxylin and eosin (H&E). Histopathologic analysis was performed under light microscopy. The extent of injury was determined using the criteria described in the literature (17).

Western blot

Western blot was conducted using previously published methods (18). The primary antibodies for metalloproteinase-9 (MMP-9) and actin were purchased from Millipore.

Statistical analysis

All data were analyzed using statistical software IBM SPSS 18.0 and expressed as means ± SEM. Data were analyzed using mixed-factorial analyses of variance (ANOVAs), where appropriate. Significant ANOVA main and interaction effects were further investigated using Tukey *post hoc* tests, when appropriate. $P < 0.05$ was considered to be significant.

RESULTS

Effects of hepatic IR on hepatic function in wild-type and Sig-1R$^{-/-}$ mice

The role of Sig-1R in regulation of hepatic IRI and the effects of warm hepatic I/R on the liver function in wild-type and Sig-1R$^{-/-}$ mice were examined. We found that hepatic IR significantly increased serum levels of ALT, AST, MPO and supernatant level of LDH at 6 h after reperfusion compared to wild-type mice ($p < 0.05$; Fig. 1). However, compared to wild-type mice, Sig-1R$^{-/-}$mice exhibited robustly reduced serum level of ALT, AST, MPO and LDH at 6 h after reperfusion ($p < 0.05$; Fig. 1).

Effects of hepatic IR on endothelial glycocalyx integrity in wild-type and Sig-1R$^{-/-}$ mice

The effects of warm hepatic I/R on endothelial glycocalyx integrity in wild-type and Sig-1R$^{-/-}$ mice were examined. We found that hepatic IR significantly increased serum levels of HS and Syn-1, compared to wild-type mice ($p < 0.05$; Fig. 2). However, Sig-1R$^{-/-}$mice exhibited significantly reduced serum level of HS and Syn-1 in comparison with wild-type mice ($p < 0.05$; Fig. 2).

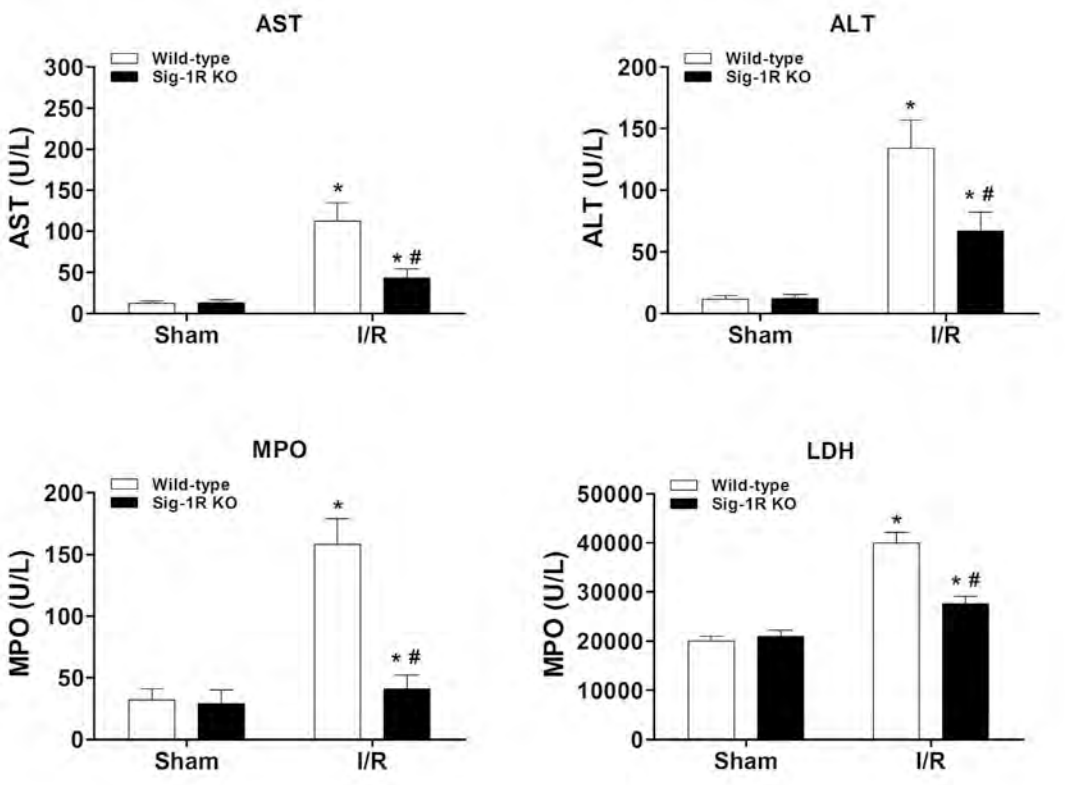


Fig. 1. *Effect of hepatic IR on hepatic function in wild-type and Sig-1R$^{-/-}$ mice. Serum levels of ALT, AST, MPO and supernatant level of LDH were measured at 6 h after reperfusion. *significant difference relative to sham wild-type mice ($p < 0.05$). #significant difference relative to IRI wild-type mice ($p < 0.05$). n=8/group.*

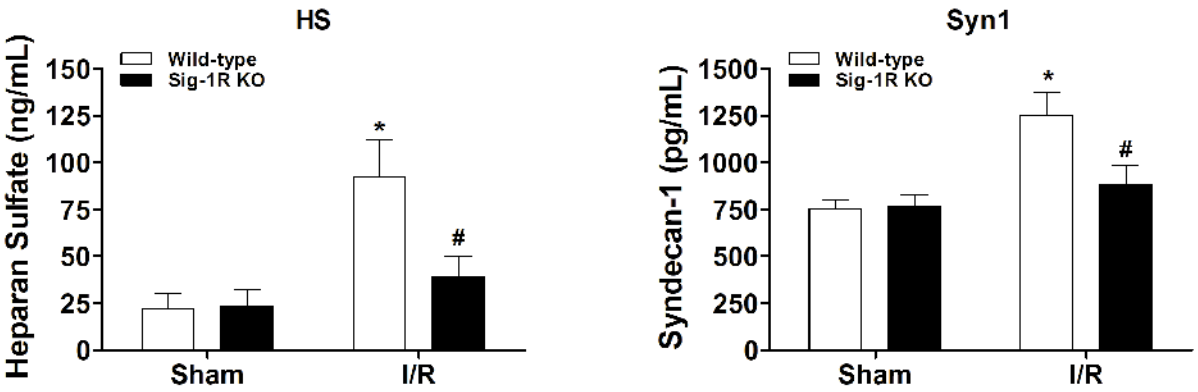


Fig. 2. *Effect of hepatic IR on endothelial glycocalyx integrity in wild-type and Sig-1R$^{-/-}$ mice. Serum levels of HS and Syn-1 were measured at 6 h after reperfusion. *significant difference relative to sham wild-type mice ($p < 0.05$). $^{\#}$significant difference relative to IRI wild-type mice ($p < 0.05$). n=8/group.*

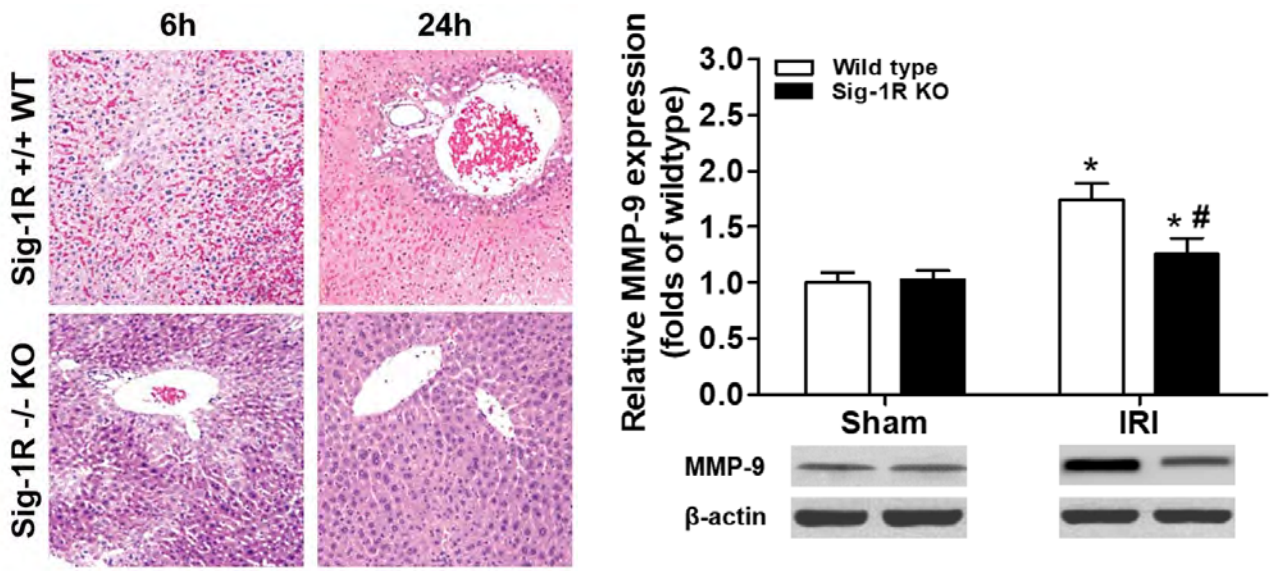


Fig. 3. *Effect of hepatic IR on liver histology and MMP-9 expression in wild-type and Sig-1R$^{-/-}$ mice. H&E staining was conducted in liver tissues at 6 h and 24 h after hepatic IRI. MMP-9 expression in liver tissue was measure using Western blot at 6 h after hepatic IRI. *significant difference relative to sham wild-type mice ($p < 0.05$). $^{\#}$significant difference relative to IRI wild-type mice ($p < 0.05$). n=8/group.*

Effects of hepatic IR on liver injury in wild-type and Sig-1R$^{-/-}$ mice

As shown in Fig. 3, H&E staining results indicated that Sig-1R$^{-/-}$ mice after I/R exhibited higher liver damage compared with wild-type animals at 6 h and 24 h. Specifically, the histopathological scores in wild-type mice after IR at 6 h and 24 h were 9.3±0.2 and 7.9±1.1, respectively, while the corresponding scores in Sig-1R$^{-/-}$ mice were 4.3±0.2 and 1.9±1.1. Furthermore, we found that hepatic IRI significantly increased the expression of MMP-9 in liver tissue. However,

MMP-9 overexpression was much reduced in mice lacking Sig-1R, compared to wild-type mice.

Effects of FLU on hepatic I/R Injury in wild-type mice

In contrast to the results obtained on Sig-1R$^{-/-}$ mice, the wild-type mice exhibited an increased impairment in the hepatic functions when pretreated with FLU, a selective Sig-1R agonist, as compared with the vehicle treatment group. As shown in Fig. 4, increased hepatotoxicity occurred in mice which received FLU pretreatment, as quantified by the dose-dependent increase in the serum levels of AST, ALT, MPO, and LDH at 6 h after I/R injury, compared with mice that received vehicle treatment ($p < 0.05$).

DISCUSSION

In this study, we examined the role of Sig-1R in hepatic ischemia-reperfusion injury. We found that Sig-1R$^{-/-}$ mice exhibited decreased liver damage after hepatic IRI as compared to wild-type animals. This effect was associated with decreased serum levels of AST, ALT, MPO, and LDH, and decreased endothelial glycocalyx shedding, as indexed by decreased serum levels of HS and Syn-1, improved liver histology, and reduced MMP-9 expression. Furthermore, activation of Sig-1R using FLU increased serum levels of AST, ALT, MPO, and LDH at 6 h after I/R injury in a dose-dependent manner. Together, these results suggest that stimulation of

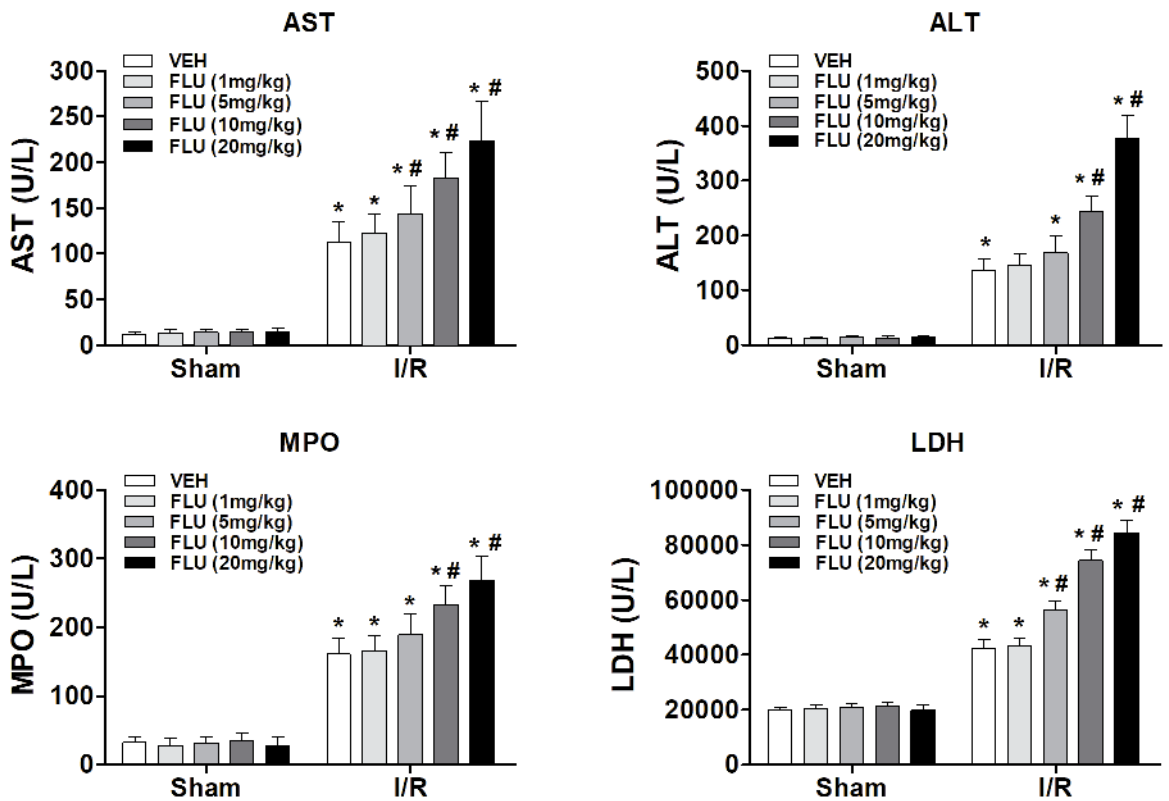


Fig. 4. *Effect of FLU on hepatic I/R Injury in wild-type mice. Mice were administered intraperitoneally with either vehicle (isotonic saline) or 1, 5, 10, or 20 mg/kg FLU. *significant difference relative to sham wild-type mice ($p < 0.05$). #significant difference relative to IRI wild-type mice ($p < 0.05$). n=8/group.*

Sig-1R may underlie the pathological mechanisms of hepatic IRI.

Our findings are in contrast with the previous studies showing that stimulation of Sig-1R plays a protective role in ischemia-reperfusion injury (12-14). While these results were surprising, they indicated that different pathological mechanisms may be involved in the ischemia-reperfusion injury in distinct organs. For example, it has been shown that MMP-9 is highly expressed in damaged liver after I/R injury. In addition, MMP-9 deficiency significantly depressed serum glutamic-pyruvic aminotransferase and glutamic oxaloacetic aminotransferase levels and improved liver histology. This indicates that MMP-9 is indeed an active player in the liver I/R injury. Furthermore, it has been shown that administration of S1RA, a selective antagonist of Sig-1R, reduced the MMP-9 overexpression in ischemic brain tissue (19). Consistent with these findings, our study showed that stimulation of Sig-1R with FLU increases MMP-9 expression in damaged liver tissue following hepatic IRI. Together, these results suggest that stimulation of Sig-1R-MMP-9 pathway in liver tissue may underlie the pathological mechanisms of hepatic IRI. Future studies need to be performed to investigate the specific mechanisms involved on a cellular level.

Sigma receptors can be classified into two subtypes: Sig-1R and Sig-2R. While our study revealed the contributions of Sig-1R to hepatic IRI, the contribution of the Sig-2R remains less understood due to the lack of available experimental tools to study its functions. Hence, our study initially focused on Sig-1R. Published studies suggest an important role of Sig-1Rs in the pathophysiology of multiple diseases (20). Most of the studies focused on the interaction between Sig-1R and NMDAR. It has been shown that Sig-1Rs are ligand-operated molecular chaperones that are expressed predominantly between the endoplasmic reticulum and the mitochondria-associated endoplasmic reticulum membrane (15, 21, 22). Sig-1R can not only interact with and regulate calcium flux and the opening of voltage-gated ion channels (23-25), but also bind to multiple endogenous Sig-R ligands. These endogenous ligands include neurosteroids, neuropeptide Y, calcitonin gene-related peptide, and the amine *N*,*N*-dimethyltryptamine (26-28). Given the complex Sig-1R-mediated signaling network, it will be important to dissect the specific Sig-1R-mediated mechanisms that contribute to hepatic IRI in the future.

In summary, our study confirmed that the absence of Sig-1R protects liver from hepatic IRI. Such protective effects included reduced endothelial glycocalyx shedding, decreased serum levels of AST, ALT, MPO, and LDH, improved liver histology, and reduced MMP-9 overexpression. Sig-1R mediated signaling pathways may play distinct role in the ischemia-reperfusion injuries in different organs. It is crucial that the dynamic interaction between Sig-1R and other signaling molecules in distinct organs is examined further. This line of research will help in the development of effective pharmacotherapies for preventing ischemia-reperfusion injury of specific organs.

ACKNOWLEDGEMENTS

We thank Dr. Xian Zhao's laboratory from the Department of Anesthesiology at the Second Hospital of Shandong University, Jinan, China for providing a breeding pair of Sig-1R knockout (Sig-$1R^{-/-}$) mice as a gift.

REFERENCES

1. Serracino-Inglott F, Habib NA, Mathie RT. Hepatic ischemia-reperfusion injury. Am J Surg 2001; 181:160-66.
2. Nelson A, Berkestedt I, Schmidtchen A, Ljunggren L, Bodelsson M. Increased levels of glycosaminoglycans during septic shock: relation to mortality and the antibacterial actions of plasma. Shock 2008; 30:623-27.
3. Nieuwdorp M, Meuwese MC, Mooij HL, et al. Tumor necrosis factor-alpha inhibition protects against endotoxin-induced endothelial glycocalyx perturbation. Atherosclerosis 2009; 202:296-303.
4. Nieuwdorp M, van Haeften TW, Gouverneur MC, et al. Loss of endothelial glycocalyx during acute hyperglycemia coincides with endothelial dysfunction and coagulation activation in vivo. Diabetes 2006; 55:480-86.
5. Vlahu CA, Lemkes BA, Struijk DG, Koopman MG,

Krediet RT, Vink H. Damage of the endothelial glycocalyx in dialysis patients. J Am Soc Nephrol 2012; 23:1900-08.
6. Holte K, Kehlet H. Fluid therapy and surgical outcomes in elective surgery: a need for reassessment in fast-track surgery. J Am Col Surg 2006; 202:971-89.
7. Mohseni M, Safari S, Alavian SM. Volatile anesthetics in ischemic liver injury: enemy or friend? Hep Mont 2014; 14:e19880.
8. Constantinescu AA, Vink H, Spaan JA. Endothelial cell glycocalyx modulates immobilization of leukocytes at the endothelial surface. Arterioscl Throm Vas Biol 2003; 23:1541-47.
9. Marechal X, Favory R, Joulin O, et al. Endothelial glycocalyx damage during endotoxemia coincides with microcirculatory dysfunction and vascular oxidative stress. Shock 2008; 29:572-76.
10. Becker BF, Chappell D, Bruegger D, Annecke T, Jacob M. Therapeutic strategies targeting the endothelial glycocalyx: acute deficits, but great potential. Cardiovasc Res 2010; 87:300-10.
11. Cobos E, Entrena J, Nieto F, Cendan C, Pozo ED. Pharmacology and therapeutic potential of sigma1 receptor ligands. Cur Neuropharm 2008; 6:344-66.
12. Bhuiyan MS, Tagashira H, Fukunaga K. Sigma-1 receptor stimulation with fluvoxamine activates Akt–eNOS signaling in the thoracic aorta of ovariectomized rats with abdominal aortic banding. Eur J Pharm 2011; 650:621-28.
13. Tagashira H, Bhuiyan S, Shioda N, Hasegawa H, Kanai H, Fukunaga K. σ1-Receptor stimulation with fluvoxamine ameliorates transverse aortic constriction-induced myocardial hypertrophy and dysfunction in mice. Am J Physiol Heart Circ Physiol 2010; 299:H1535-H45.
14. Deplanque D, Venna VR, Bordet R. Brain ischemia changes the long term response to antidepressant drugs in mice. Behav Brain Res 2011; 219:367-72.
15. Sabino V, Cottone P, Parylak SL, Steardo L, Zorrilla EP. Sigma-1 receptor knockout mice display a depressive-like phenotype. Behav Brain Res 2009; 198:472-76.
16. Zwacka RM, Zhou W, Zhang Y, et al. Redox gene therapy for ischemia/reperfusion injury of the liver reduces AP1 and NF-κB activation. Nature Med 1998; 4:698.
17. Ni HM, Chen X, Ding WX, Schuchmann M, Yin XM. Differential roles of JNK in ConA/GalN and ConA-induced liver injury in mice. Am J Pathol 2008; 173:962-72.
18. Ito Y, Abril ER, Bethea NW, McCuskey RS. Inhibition of matrix metalloproteinases minimizes hepatic microvascular injury in response to acetaminophen in mice. Toxicol Sci 2004; 83:190-96.
19. Sánchez-Blázquez P, Pozo-Rodrigálvarez A, Merlos M, Garzón J. The Sigma-1 receptor antagonist, s1ra, reduces stroke damage, ameliorates post-stroke neurological deficits and suppresses the overexpression of MMP-9. Mol Neurobiol 2018; 55:4940-51.
20. Hayashi T, Tsai SY, Mori T, Fujimoto M. Su TP. Targeting ligand-operated chaperone sigma-1 receptors in the treatment of neuropsychiatric disorders. Expert Opin Ther Targets 2011; 15:557-77.
21. Hayashi T, Su TP. Intracellular dynamics of sigma-1 receptors (sigma(1) binding sites) in NG108-15 cells. J Pharmacol Exp Ther 2003; 306:726-33.
22. Hayashi T, Su TP. Sigma-1 receptor chaperones at the ER-mitochondrion interface regulate Ca(2+) signaling and cell survival. Cell 2007; 131:596-10.
23. Aydar E, Palmer CP, Klyachko VA, Jackson MB. The sigma receptor as a ligand-regulated auxiliary potassium channel subunit. Neuron 2002; 34:399-10.
24. Hayashi T, Su TP. An update on the development of drugs for neuropsychiatric disorders: focusing on the sigma 1 receptor ligand. Expert Opin Ther Targets 2008; 12:45-58.
25. Herrera Y, Katnik C, Rodriguez JD, Hall AA, Willing A, Pennypacker KR, Cuevas J. Sigma-1 receptor modulation of acid-sensing ion channel a (ASIC1a) and ASIC1a-induced Ca2+ influx in rat cortical neurons. J Pharmacol Exp Ther 2008; 327:491-02.
26. Fontanilla D, Johannessen M, Hajipour AR, Cozzi NV, Jackson MB, Ruoho AE. The hallucinogen N,N-dimethyltryptamine (DMT) is an endogenous sigma-1 receptor regulator. Science 2009; 323:934-37.
27. Maurice T, Su TP. The pharmacology of sigma-1 receptors. Pharmacol Ther 2009; 124:195-206.
28. Su TP, Hayashi T, Maurice T, Buch S, Ruoho AE. The sigma-1 receptor chaperone as an inter-organelle signaling modulator. Trends Pharmacol Sci 2010; 31:557-66.

G PROTEIN REGULATED INDUCER OF NEURITE OUTGROWTH 1 IS A POTENTIAL MARKER FOR LUNG CANCER PROGNOSIS

M-Q. ZHUANG[1], J. LI[2], XHAN[3], K-L. SU[2], G-J. HAO[2] and J-Q. HAN[1]

[1]Tumor Research and Therapy Center, Shandong Provincial Hospital, Cheeloo College of Medicine, Shandong University, Jinan, China; [2]Department of Oncology, The Fourth Hospital of Jinan, Jinan, China; [3]Department of Experiment, Tumor Hospital Affiliated to Guangxi Medical University, Nanning, China

Received March 4, 2020 – Accepted April 30, 2020

Lung cancer mortality remains high, and only approximately 15% of patients with non-small cell lung cancer survive for more than five years. The purpose of this research was to investigate the prognostic value and biological functions of G protein regulated inducer of neuritis outgrowth 1(GPRIN1) in lung cancer. We used the Kaplan–Meier method to analyze the correlation between GPRIN1 and overall survival, and performed Cox regression to determine whether GPRIN1 might be an independent predictive factor for lung adenocarcinoma prognosis. qRT-PCR and Western blot assays were conducted to detect GPRIN1 expression in lung cancer cells and normal control cells. To detect the functional effects of knockdown/overexpression of GPRIN1 on lung cancer cells, we performed CCK-8, colony formation and Transwell assays. Through the Kaplan–Meier method, we found that GPRIN1 expression correlated with overall survival and adverse prognosis, and Cox regression indicated that GPRIN1 is as an independent predictive factor for lung adenocarcinoma. Furthermore, the mRNA and protein expression levels of GPRIN1 in lung cancer cells were markedly higher than those in normal cells. Downregulation of GPRIN1significantly decreased cell viability, colony formation, the number of invasive and migrating cells, and levels of epithelial-mesenchymal transition-related proteins in A549 cells. Overexpression of GPRIN1showed the opposite effect in Calu-1 cells. Together, these results indicated that GPRIN1 facilitates lung cancer proliferation and migration, possibly by affecting the epithelial-mesenchymal transition of lung cancer cells, suggesting that GPRIN1may be used as an effective target for the treatment of lung cancer.

In 2018, approximately 25% of worldwide cancer deaths were due to lung cancer (1). On the basis of pathological and clinical features, small cell lung cancer and non-small cell lung cancer (NSCLC) are the major types of lung cancer (2). NSCLC accounts for 85% of cases, including lung adenocarcinomas, squamous cell carcinomas and large cell lung cancer (3), and more than 50% of patients with lung cancer are currently diagnosed with lung adenocarcinoma (4). Drago et al. found that cancer cells may metastasize; consequently, despite the progress in clinical treatment of lung adenocarcinoma, the mortality rate has not significantly decreased(5). Hence, exploring the pathogenesis of lung cancer is

Key words: GPRIN1; knockdown; overexpression; lung cancer; invasion; prognostic

Corresponding Author:
Dr Jun-Qing Han,
Tumor Research and Therapy Center,
Shandong Provincial Hospital,
Cheeloo College of Medicine, Shandong University,
No.324 Jingwuweiqi Road, Jinan, Shandong 250021 China
e-mail: junqinghan0691@163.com

0393-974X (2020)
Copyright © by BIOLIFE, s.a.s.
This publication and/or article is for individual use only and may not be further reproduced without written permission from the copyright holder.
Unauthorized reproduction may result in financial and other penalties
DISCLOSURE: ALL AUTHORS REPORT NO CONFLICTS OF INTEREST RELEVANT TO THIS ARTICLE.

particularly important to find new and more effective treatment measures.

NSCLC cells are most likely to metastasize to the brain (6, 7), and the abnormal expression or mutation of genes plays a significant part in the metastasis, recurrence, and invasion of NSCLC (8, 9). G protein regulated inducer of neuritis outgrowth 1(GPRIN1, also known as GRIN1)is a protein coding gene that was first discovered by Chen et al. in 1999 (10) and consists of 856 amino acids(11).GPRIN1 is mainly expressed in the brain. Previous studies primarily focused on its role in encephalopathy regulation (12-14). According to NCBI GenBank data, GPRIN1is also expressed in the lung, but the connection between GPRIN1 and lung cancer has not been studied. Hence, on the basis of information analysis and literature review, GPRIN1 is thought to be associated with the occurrence and progression of lung cancer. As a result, the study of its regulation in lung cancer is likely to become a new direction in targeted therapy for lung carcinoma.

The aim of this research was to analyze whether the expression of GPRIN1might be associated with the clinical manifestations and prognosis of lung cancer, as well as to assess the influence of knockdown/overexpression of GPRIN1 on lung carcinoma proliferation, invasion, and migration, to explore a new potentially effective clinical therapeutic target for lung carcinoma.

MATERIALS AND METHODS

This study used RNA-Seq expression data for lung adenocarcinoma from The Cancer Genome Atlas (TCGA) database (https://cancergenome.nih.gov/). We downloaded gene expression profile data and clinical data for 535 lung adenocarcinoma samples and 59 normal samples to analyze the expression of GPRIN1 and the correlation between GPRIN1 expression and the prognosis of patients with lung adenocarcinoma.

Cell culture and transfection

A549, NCI-H209, NCI-H460, and Calu-1 human lung cancer cell lines were purchased from the Shanghai cell bank of the Chinese Academy of Medical Sciences, and normal control cells (BEAS2B) were purchased from the American Type Culture Collection. Routine culture was performed in 10% fetal bovine serum, penicillin (100 U/ml), and streptomycin (100 μg/ml) in RPMI-1640 medium at 37°C with 5% CO_2. Transfection was performed according to the instructions of the Lipofectamine 2000 transfection kit. When the confluence of cells in six-well plates reached 80%, the antibiotic-free medium was replaced 2 h before transfection, and Lipofectamine 2000-mediated cell transfection was performed. The complexes were prepared as follows: the siRNA oligomers were diluted with 250 μl serum-free and antibiotic-free culture solution, and gently mixed; then Lipofectamine 2000 was added and gently mixed. A volume of 5 μl liposomes was diluted in 250 μl serum-free and antibiotic-free culture solution, gently mixed, and incubated for 5 min at room temperature. Lipofectamine 2000 was mixed with diluted siRNA 5 min later, and then incubated for 20 min at room temperature to form complexes. The solution (total volume 500 μl) was mixed and added to the wells, and the culture plate was shaken before and after to ensure even distribution. The cells were cultured in an incubator for 6 h. Afterward, the complete culture medium was replaced. After 48 h, the expression of GPRIN1could be observed. The GPRIN1 siRNA was synthesized by Shanghai GenePharma Co., Ltd. (Shanghai, China)and the sequences were as follows:

si-con:CGAACTCACTGGTCTGACC;
si-GPRIN1#1:CCCGCATCTGTGGGAAATGTA;
si-GPRIN1#2: GAATCCTGAGTCTTCAGGAAA.

RNA extraction and quantitative real-time PCR (qPCR)

Total RNA was extracted from cells with SYBR Premix Ex Taq II (TaKaRa, Japan) and reverse transcribed to form cDNA. To detect the expression of GPRIN1, we used qRT-PCR with the following procedure: 5 min at 95˚C, then 40 cycles of 30 s at 95°C and 45 s at 65°C, and 30 min at 72°C. Each group was replicated in three wells, and the $2^{-\Delta\Delta Ct}$ method was used to determine the expression of GPRIN1.

The experiments were repeated independently three times. The primer sequences were:

GPRIN1:F: 5′-CAAGAAAGGAGGAGCCCAGG-3′
R:5′- CTCTGGCTTTCCTGAGCACA-3′
GAPDH:
F:5′- TGAAGGTCGGAGTCAACGGATTTGGT-3′
R:5′– CATGTGGGCCATGAGGTCCACCAC-3′

Western blot

After transfection for 48 h, the six-well plate was placed on ice, and RIPA lysis buffer (with protease inhibitor) was added to extract protein. The BCA method was used to measure the protein concentrations. In a vertical electrophoresis tank,20 μg protein was added to each lane and subjected to SDS polyacrylamide gel electrophoresis. The protein on the gel was transferred to a PVDF membrane, and 5% skim milk powder was added for blocking for 1 h. The membrane was incubated overnight with primary antibodies and then washed with TBST for 5 min three times. Afterward, the membrane was incubated with secondary antibody for 1 hat room temperature.ECL developer was added after rinsing. The intensity values of the bands were scanned with QUANTITY ONE software, and GAPDH was used as an internal reference to calculate the relative expression of each protein on the basis of objective protein/internal reference.

CCK-8 assay

After 48 h of transfection, the cultured cells were digested and counted to prepare cell suspensions. Cells were seeded into a 96-well plate at a density of 1000 cells/well and routinely cultured in a carbon dioxide incubator. Next,10 μl of CCK-8 solution was added into each well and incubated for 1.5 h at 37°C. Cell viability was tested at 0 h, 24 h,48 h, and 72 h. The optical density (OD) was determined with a micro plate reader at 450 nm wavelength. The OD values were used to construct the standard curve.

Table I. *Correlation between GPRIN1 expression and clinical features of patients with lung adenocarcinoma*

Characteristics	Expression of GPRIN1		P value
	Low	High	
Age			0.106
<60	60	76	
≥60	185	169	
Gender			0.720
female	133	137	
male	117	113	
Pathologic-Stage			0.268
I+II	196	189	
III+IV	48	59	
Pathologic-T			0.432
T1+T2	219	214	
T3+T4	29	35	
Pathologic-N			0.003*
N0	175	148	
N1	66	100	
Pathologic-M			0.176
M0	160	172	
M1	15	9	

*$P<0.05$

Table II. *Cox regression analysis of GPRIN1 as an independent predictor of lung adenocarcinoma prognosis*

Variables	Univariate analysis			Multivariate analysis		
	P value	HR	95%CI	P value	HR	95%CI
GPRIN1 expression (high/low)	0.002*	1.602	1.190-2.156	0.006*	1.654	1.159-2.359
Clinical-Stage (I+II/III+IV)	0.000*	2.466	1.810-3.360	0.160	1.436	0.867-2.377
Pathologic-T (T1+T2/T3+T4)	0.000*	2.147	1.467-3.140	0.066	1.574	0.971-2.551
Pathologic-M (M0/M1)	0.006*	2.132	1.244-3.653	0.280	1.431	0.747-2.743
Pathologic-N (N0/N1+N2+N3)	0.000*	2.507	1.864-3.370	0.002*	1.887	1.263-2.819
Age(< 60/≥60)	0.746	1.056	0.760-1.468			
Gender (female/male)	0.616	1.077	0.805-1.442			

Colony formation assay

Cells in logarithmic phase were digested with trypsin and separated into single cells, and then a cell suspension was made and counted. Cells were seeded into 60 mm culture dishes (400 cells/dish) containing 5 ml of37°C preheated culture medium and evenly dispersed by gentle rotation of the dish. The cells were incubated under saturated humidity at 37°C and 5% CO_2 for 1–2 weeks. When clones were visible in culture dishes, the culture was terminated. The supernatant was discarded. The colonies were carefully washed twice with PBS and fixed with 5 ml of 4% paraformaldehyde for 30 min. Then the fixing fluid was removed, and cells were dyed with 0.1% crystal violet for 30 min. The dye solution was then washed away slowly with running water, and the plates were air dried. The clones were counted, and the size and number of clones formed were compared.

Transwell assay

Matrigel matrix (100 µl) was melted overnight (serum-free medium diluted at 1:6) and added to the upper chamber of a Transwell insert in 24-well plates. After shaking, the chamber was placed in a carbon dioxide incubator at 37°C for 4–6h. After drying, 500 µl serum-free medium was added into the lower chamber, and the membrane was hydrated for 30 min. Matrigel was not used in migration experiments. After 48 h of transfection, cells were cultured and used to prepare cell suspension with serum-free medium. A total of 100 µlof cell suspension (1×10^5 cells) was added to the upper chamber, and 500 µl complete culture medium was added to the lower chamber. After overnight incubation, the chamber was removed, and the remaining cells in the upper chamber were wiped off with cotton swabs. After being washed with PBS, cells on the lower surface of the membrane were fixed for 30 min with 4% paraformaldehyde. After 20 min of 0.1% crystal violet staining and PBS washing, five visual fields were randomly selected under a microscope and photographed for observation and counting.

Statistical analysis

The experimental data were analyzed with SPSS22.0

software (IBM SPSS Inc., IL, USA). A *t*-test was used to compare differences between two groups, and one-way analysis of variance and post-test were used to compare the mean values among samples. Assessment of the correlation between gene expression and clinical features was performed with a *chi*-squared test. A survival curve was plotted with the Kaplan–Meier method, and the differences between groups were examined with log-rank test. Cox regression analysis was performed to determine whether GPRIN1 might be used as an independent predictive factor of the prognosis of lung adenocarcinoma. $P<0.05$ was considered statistically significant.

RESULTS

GPRIN1 expression is enhanced in lung cancer cells and is associated with pathological stage and lymph node metastasis in patients with lung adenocarcinoma

Tables I and II show the correlation between GPRIN1 expression and clinical features of patients with lung adenocarcinoma. First, we concluded that the expression of GPRIN1 in the tumor group(n=535) was markedly greater than that in the normal group(n=59) by bioinformatics analysis(Fig. 1A, $P<0.001$). To further test the expression of GPRIN1 in lung carcinoma, we performed qRT-PCR experiments. We confirmed that the mRNA expression levels of GPRIN1 were markedly higher in the lung cancer cell lines A549, NCI-H209, NCI-H460 and Calu-1 than in BEAS2B healthy control cells (Fig. 1B, $P<0.01$). The results clearly indicated that the expression of GPRIN1was highest in A549cells; GPRIN1 was therefore used for knockdown experiments. The expression of GPRIN1in Calu-1 cells was lowest among all tested lung cancer cells, and was therefore used for overexpression experiments. Afterwards, we assessed the relationship between gene expression and clinical characteristics with *chi*-squared statistical analysis. As shown in Table I, the expression of GPRIN1 was significantly correlated with pathological stage and lymph node metastasis inpatients with lung adenocarcinoma ($P<0.05$). This finding suggested that GPRIN1 may be involved in the regulation of lung cancer.

High expression of GPRIN1 in lung cancer cells is associated with poor prognosis

We used Kaplan–Meier analysis to study the prognostic value and the relationship between GPRIN1expression and overall survival. The results revealed a conspicuous discrepancy in survival rate between the high-expression group and low-expression group ($P<0.01$), and the survival rate of the high-expression group was markedly lower than that of the low-expression group (Fig. 2). We then performed Cox regression analysis to explore whether GPRIN1 might be used as an independent

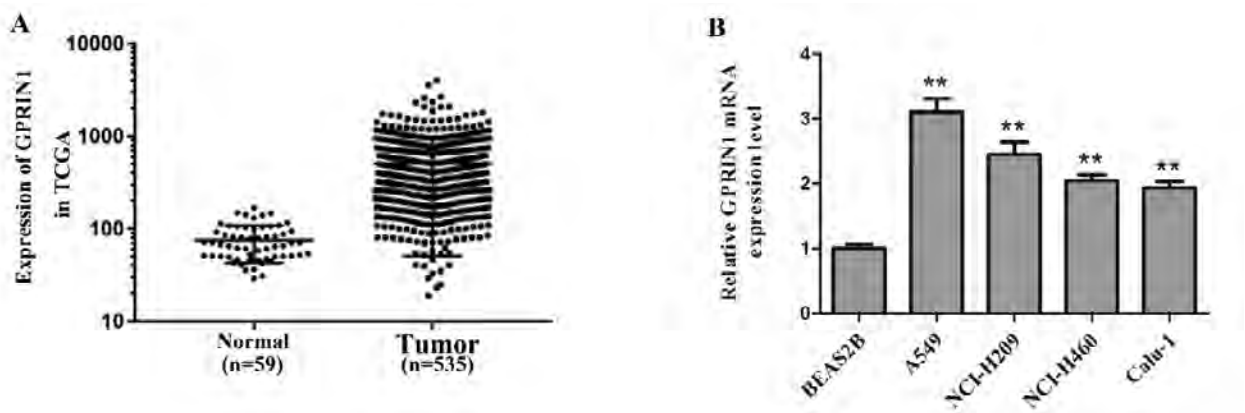


Fig. 1. *mRNA expression levels of GPRIN1in lung cancer and healthy control cells.* ***A****) Expression of GPRIN1 in normal (n=59) and tumor (n=535) tissue was analyzed on the basis of TCGA data. P<0.001.* ***B****) GPRIN1 expression in the lung cancer cell lines A549, NCI-H209, NCI-H460 and Calu-1, compared with that in BEAS2B control cells.**P<0.01.*

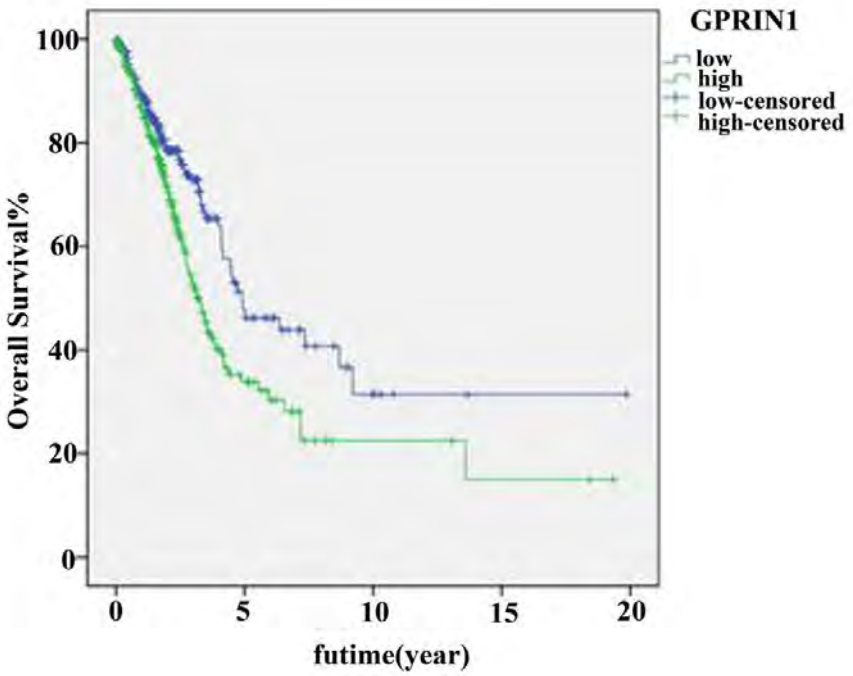


Fig. 2. *Elevated GPRIN1 expression predicts adverse prognosis in patients with lung adenocarcinomas. P<0.01.*

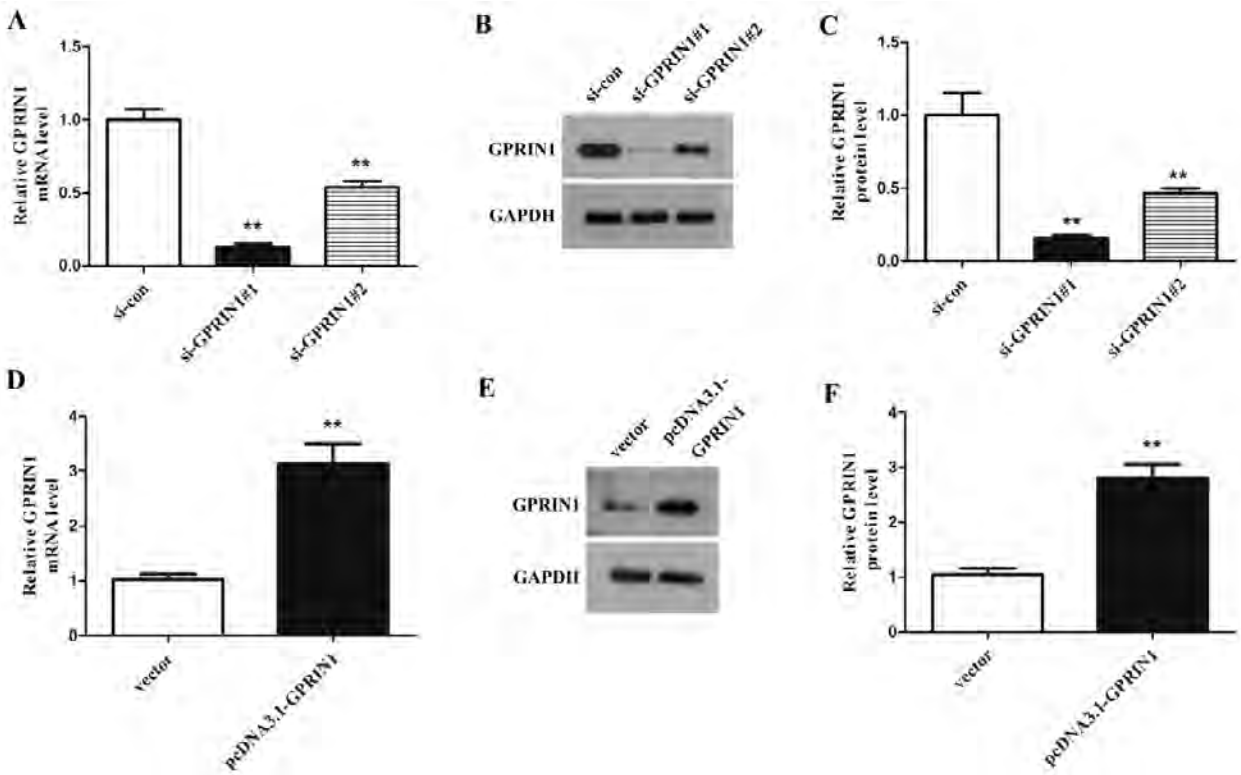


Fig. 3. *Knockdown/overexpression efficiency of GPRIN1in A549 and Calu-1 cells.* ***A–C****) The knockdown efficiency of si-GPRIN1 in A549 cells was measured with qRT-PCR and Western blotting.**P<0.01.* ***D–F****) Overexpression efficiency of GPRIN1in Calu-1 cells, tested by qRT-PCR and Western blotting.**P<0.01.*

predictor of the prognosis of lung adenocarcinoma. The results from Table II show that GPRIN1 is an independent predictive factor of prognosis in patients with lung adenocarcinoma (P<0.01). Together, these results indicate that up-regulation of GPRIN1 is predictive of poor prognosis in lung cancer.

Knockdown of GPRIN1in A549 cells and overexpression of GPRIN1in Calu-1 cells

To detect the efficiency of knockdown and overexpression of GPRIN1, we transfected si-GPRIN1#1 and si-GPRIN1#2 into A549 cells and transfected pcDNA3.1-GPRIN1 into Calu-1 cells. After 24 h, qRT-PCR and Western blot assays were used to test the expression of GPRIN1 in the transfected cells. As shown in Fig. 3 A–C, transfection of si-GPRIN1#1 or si-GPRIN1#2 markedly decreased the mRNA and protein levels of GPRIN1, and si-GPRIN1#1 showed greater knockdown efficiency (P<0.01). Simultaneously, the data in Fig. 3 D–F indicated that the expression of mRNA and protein of GPRIN1 in Calu-1 cells was significantly up-regulated after transfection with pcDNA3.1-GPRIN1(P<0.01).

Downregulation of GPRIN1 inhibits proliferation, whereas overexpression of GPRIN1 promotes proliferation in lung cancer cells

To further demonstrate the influence of down-regulation and up-regulation of GPRIN1 expression

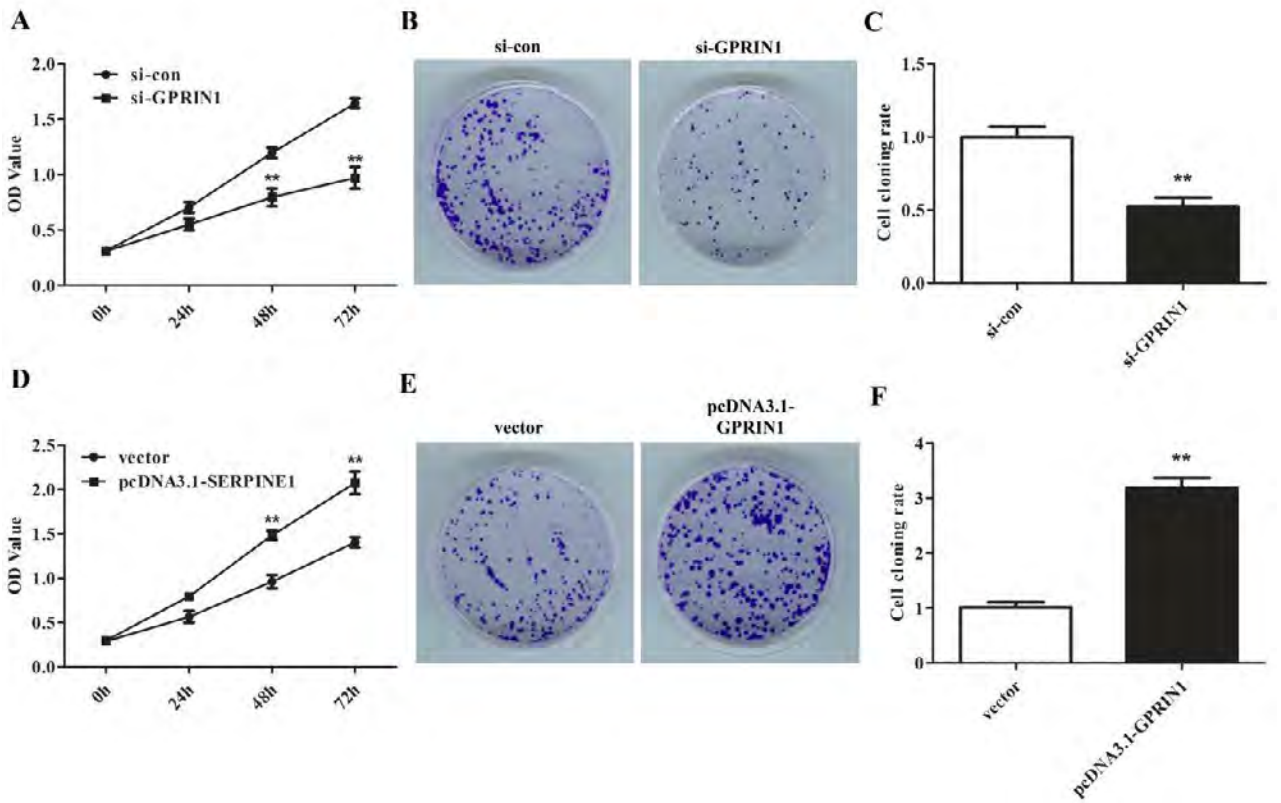


Fig. 4. *Effects of knockdown/overexpression of GPRIN1 on cell proliferation.* ***A)*** *A549 cells with down-regulated GPRIN1 expression showed significantly lower cell viability than the control group.**P<0.01.* ***B, C)*** *Down-regulation of GPRIN1 expression significantly decreased the number of colonies formed.**P<0.01.* ***D)*** *The viability of Calu-1 cells significantly increased after overexpression of GPRIN1, as compared with that in control cells.**P<0.01.* ***E–F)*** *Upregulation of GPRIN1promotes cell proliferation in Calu-1 cells.**P<0.01.*

on the proliferation of lung cancer cells, we performed CCK8 and colony formation assays. The CCK-8 assay results indicated that A549 cells with down-regulated GPRIN1 expression showed significantly lower cell viability than the control cells (Fig. 4A, P<0.01). Cloning experiments further indicated that down-regulation of GPRIN1 expression significantly decreased the number of colonies formed (Fig. 4 B, C, P<0.01). Simultaneously, after overexpression of GPRIN1, the proliferation of Calu-1 cells was significantly greater than that in control cells (Fig. 4D–F, P<0.01). These results showed that silencing GPRIN1inhibits the proliferation of lung cancer cells.

Downregulation of GPRIN1 inhibits cell invasion and migration, whereas overexpression of GPRIN1promotescell invasion and migration

Subsequently, we used Transwell assays to investigate the effects of down-regulated and up-regulated GPRIN1 expression on lung carcinoma migration and invasion. Compared with the si-congroup, the group with knockdown of GPRIN1 showed markedly less migration of A549 cells to the lower chamber, as well as markedly decreased invasion of A549 cells (Fig. 5A–C, P<0.01). Overexpression of GPRIN1in Calu-1 cells had an opposite effect (Fig. 5D–F, P<0.01). On the basis of

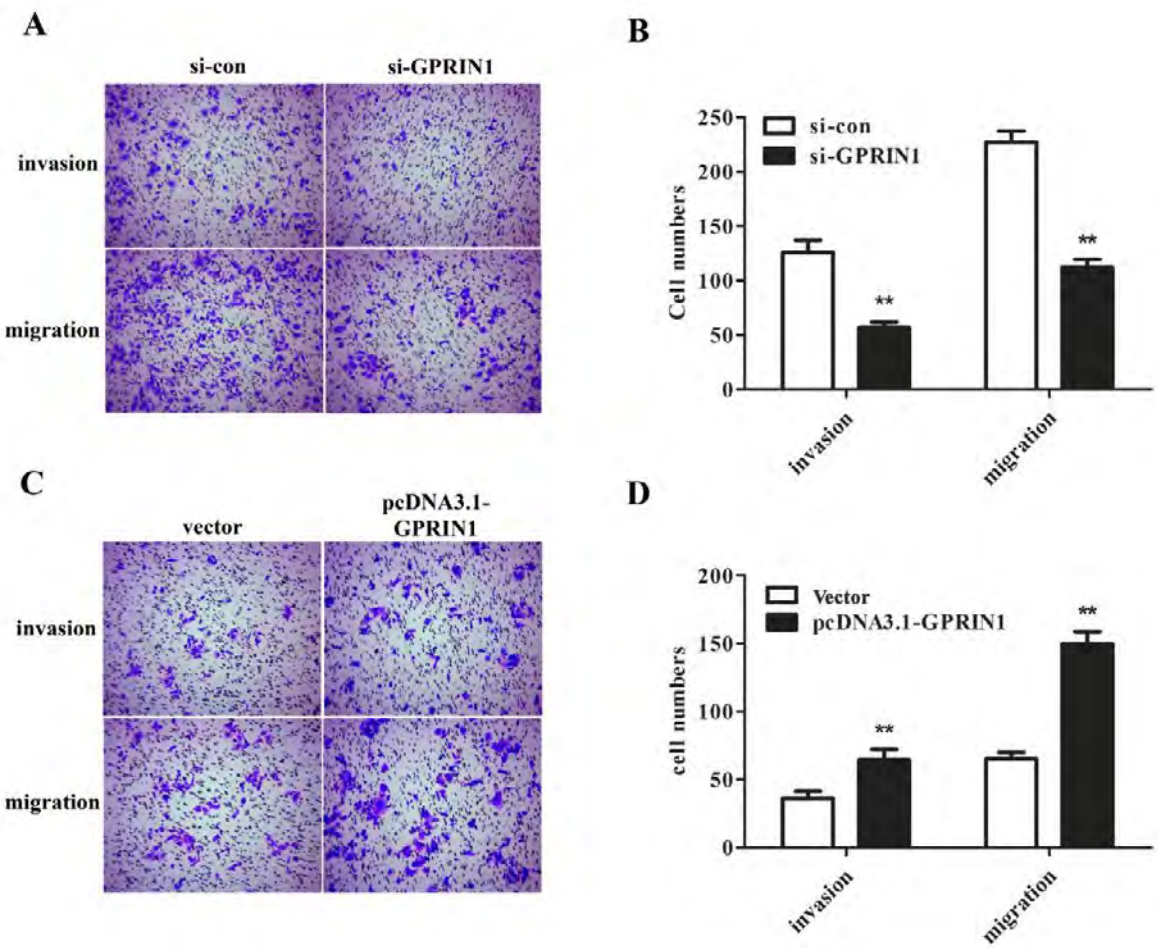


Fig. 5. *Effects of knockdown/overexpression of GPRIN1 on cell invasion and migration.* ***A–C****) Downregulation of GPRIN1 inhibits cell invasion and migration in A549 cells. **P<0.01.* ***D–F****) Upregulation of GPRIN1promotes cell invasion and migration in Calu-1 cells.**P<0.01.*

the above results, decreased expression of GPRIN1 effectively suppresses the migration and invasion of lung carcinoma, thus suggesting that GPRIN1 may participate in lung cancer progression

Role of GPRIN1 in epithelial-mesenchymal transition (EMT) of lung cancer cells

To verify whether GPRIN1 affects cell proliferation, migration and invasion by affecting the EMT, we performed Western blot assays to detect the expression of EMT-related proteins in lung cancer. Down-regulation of GPRIN1in A549 cells significantly decreased the expression of N-cadherin, Vimentin and Snail, while enhancing the expression of E-cadherin (Fig. 6 A, B, P<0.01). Up-regulation of GPRIN1in Calu-1 cells had the opposite effect (Fig. 6 C, D, P<0.01). These results illustrated that GPRIN1 is associated with the EMT in lung cancer cells, and inhibition of GPRIN1 expression suppresses EMT in lung carcinoma cells. These findings suggest that GPRIN1 might participate in the regulation of lung cancer through EMT pathways.

DISCUSSION

In this research, we confirmed that the expression

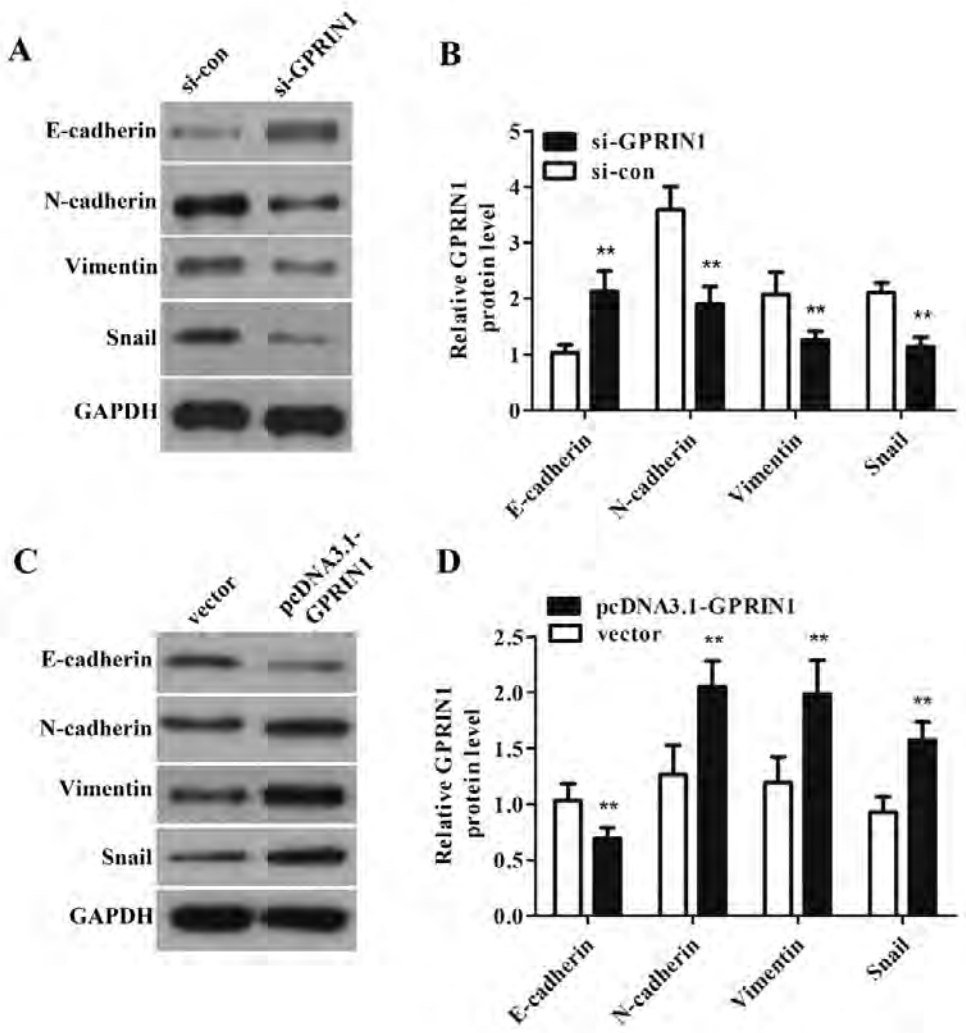


Fig. 6. *Effects of knockdown/overexpression of GPRIN1 on the EMT in lung cancer cells.* ***A, B****) Downregulation of GPRIN1 inhibits the EMT in lung cancer in A549 cells.**P<0.01.* ***C, D****) Upregulation of GPRIN1 promotes the EMT in lung cancer in Calu-1 cells.**P<0.01.*

of GPRIN1 was up-regulated in lung cancer cells and was associated with some clinical features and poor prognosis in patients with lung cancer. Second, we verified the function of GPRIN1 in lung carcinoma. Up-regulation of GPRIN1 promotes cell proliferation, invasion and migration, whereas down-regulation of GPRIN1 inhibits cell proliferation, invasion and migration. Finally, we verified the role of GPRIN1 in the EMT pathway. Inhibition of GPRIN1 expression inhibited the EMT in lung carcinoma.

The occurrence of cancer is associated with overexpression of oncogenes or deletion of tumor suppressor genes (15-17). On the basis of gene expression pattern analysis, we determined that ontogenesis was interrelated with lung cancer, and studied the mechanisms underlying the pathogenesis and progress of lung cancer, thus providing a new way to assess lung cancer prognosis and clinical treatment (18). Previous studies have identified several genes associated with lung cancer, including the oncogenes EGFR, K-RAS, STK 11, CDKN2A, and the tumor suppressor genes P53, RB, NF1, RB1, ATM and APC (19, 20).EGFR and K-RAS mutations are relatively more common in lung adenocarcinoma (7, 21-23). Although great breakthroughs have been made in the clinical application of EGFR, the resistance of EGFR-TKI remains a difficult problem in clinical treatment (24). Therefore, finding new ontogenesis pathways is particularly important. GPRIN-1 is a protein-coding gene, which has been reported to be involved in some diseases, notably encephalopathy, and neuroregulation (12, 25-27). AGPRIN1-dependent mechanism induces α7 receptors to regulate the length and complexity of neuritis in cells, thereby directing α7 expression on the cell surface (25). The activation of α7 and GPRIN1 coupling significantly decreases the growth of axons in neurons in the hippocampus (12). In palmoplantar pustulosis and palmoplantar pustular psoriasis, the expression of GPRIN1 in keratinocytes is significantly elevated (26). In our research, we discovered that GPRIN1is highly expressed in lung cancer cells, through bioinformatics analysis of data in TCGA. These results, combined with those of bioinformatics analysis and experiments in this study, indicated that GPRIN1 is an oncogene involved in lung cancer. GPRIN1 overexpression was found to induce the proliferation, invasion and metastasis of lung carcinoma, thereby promoting the progression of lung cancer.

The EMT plays a significant role in malignant tumors (28). Several reports have shown that the EMT is associated with cell proliferation, migration, invasiveness and anti-apoptotic ability (29-31). Recent research has also suggested that the EMT is associated with drug resistance and poor prognosis in NSCLC (32, 33). Increasing evidence suggests that inhibiting EMT signaling inhibits metastasis and tumor recurrence or drug resistance (28). Because we observed from Transwell assays that GPRIN1 affects the invasion and migration of lung carcinoma cells, we suspected that GPRIN1 might at least partially achieve this effect via affecting the EMT. Consequently, we studied the role of GPRIN1 in EMT pathways. The results indicated that down-regulation of GPRIN1 expression inhibited the EMT and regulated lung cancer metastasis.

There are some limitations to this study. First, it lacked clinical data to explore the lung cancer risk factors. For example, some studies have found a relationship between low-level exposure to arsenic in drinking water and the risk of lung and bladder cancer (34). Additionally, other studies have found that obesity is associated with lung cancer (35). The prevalence of obesity is high (36, 37). Therefore, exploring the relationship between the expression of GPRIN1 and obesity remains necessary.

In conclusion, we analyzed an association between the expression of GPRIN1 and the clinical features and prognosis of patients with lung cancer, and researched the role of GPRIN1 in lung cancer invasion and metastasis. GPRIN1was found to be associated with adverse prognosis in patients with lung cancer, and knockdown of GPRIN1 suppressed the proliferation, invasion, and migration of lung cancer cells, suggesting that GPRIN1 may serve as a biomarker for prognosis prediction and a new drug treatment target in lung cancer. However, *in vivo* experiments are urgently needed to verify our data, and the regulatory mechanism of GPRIN1 in lung cancer remains to be studied further.

ACKNOWLEDGEMENT

We thank International Science Editing (http://www.internationalscienceediting.com) for editing this manuscript.

REFERENCES

1. Siegel RL, Miller KD, Jemal A. Cancer statistics, 2018. CA Cancer J Clin 2018; 68:7-30.
2. Blandin Knight S, Crosbie PA, Balata H, Chudziak J, Hussell T, Dive C. Progress and prospects of early detection in lung cancer. Open Biol 2017; 7.
3. Oser MG, Niederst MJ, Sequist LV, Engelman JA. Transformation from non-small-cell lung cancer to small-cell lung cancer: molecular drivers and cells of origin. Lancet Oncol 2015; 16:e165-72.
4. Raparia K, Villa C, DeCamp MM, Patel JD, Mehta MP. Molecular profiling in non-small cell lung cancer: a step toward personalized medicine. Arch Pathol Lab Med 2013; 137:481-91.
5. Dragoj M, Milosevic Z, Bankovic J, Tanic N, Pesic M, Stankovic T. Targeting CXCR4 and FAK reverses doxorubicin resistance and suppresses invasion in non-small cell lung carcinoma. Cell Oncol (Dordr) 2017; 40:47-62.
6. Wu B, Wei S, Tian J, Song X, Hu P, Cui Y. Comparison of the survival time in the non-small cell lung cancer patients with different organ metastasis. Zhongguo Fei Ai Za Zhi 2019; 22:105-10.
7. Yang B, Lee H, Um SW, et al. Incidence of brain metastasis in lung adenocarcinoma at initial diagnosis on the basis of stage and genetic alterations. Lung Cancer 2019; 129:28-34.
8. Sharma P,Allison JP. The future of immune checkpoint therapy. Science 2015; 348:56-61.
9. Lu M, Tian Y, Yue WM, et al. GOLPH3, a good prognostic indicator in early-stage NSCLC related to tumor angiogenesis. Asian Pac J Cancer Prev 2014; 15:5793-8.
10. Chen LT, Gilman AG, Kozasa T. A candidate target for G protein action in brain. J Biol Chem 1999; 274:269313-8.
11. Iida N,Kozasa T. Identification and biochemical analysis of GRIN1 and GRIN2. Methods Enzymol 2004; 390:475-83.
12. Nordman JC, Phillips WS, Kodama N, Clark SG, Del Negro CA, Kabbani N. Axon targeting of the alpha 7 nicotinic receptor in developing hippocampal neurons by Gprin1 regulates growth. J Neurochem 2014; 129:649-62.
13. Contreras-Vallejos E, Utreras E, Borquez DA, et al. Searching for novel Cdk5 substrates in brain by comparative phosphoproteomics of wild type and Cdk5-/- mice. PLoS One 2014; 9:e90363.
14. Jia RJ, Lan CG, Wang XC,Gao CT. Integrated analysis of gene expression and copy number variations in MET protooncogene transformed human primary osteoblasts. Mol Med Rep 2018; 17:2543-48.
15. Shah RB, Shore KT, Yoon J, Mendrinos S, McKenney JK,Tian W. PTEN loss in prostatic adenocarcinoma correlates with specific adverse histologic features (intraductal carcinoma, cribriform Gleason pattern 4 and stromogenic carcinoma). Prostate 2019.
16. Imamura T, Komatsu S, Ichikawa D, et al. Overexpression of ZRF1 is related to tumor malignant potential and a poor outcome of gastric carcinoma. Carcinogenesis 2018; 39:263-71.
17. Wang J, Shen H, Fu G, Zhao D, Wang W. Nuclear overexpression of the overexpressed in lung cancer 1 predicts worse prognosis in gastric adenocarcinoma. Oncotarget 2017; 8:9442-50.
18. van't Veer LJ, Bernards R. Enabling personalized cancer medicine through analysis of gene-expression patterns. Nature 2008; 452:564-70.
19. Ding L, Getz G, Wheeler DA, et al. Somatic mutations affect key pathways in lung adenocarcinoma. Nature 2008; 455:1069-75.
20. Shojaee S,Nana-Sinkam P. Recent advances in the management of non-small cell lung cancer. F1000Res 2017; 6:2110.
21. Ohba T, Toyokawa G, Osoegawa A, et al. Mutations of the EGFR, K-ras, EML4-ALK, and BRAF genes in resected pathological stage I lung adenocarcinoma. Surg Today 2016; 46:1091-8.
22. Zhou SY, Xue Q, Ying JM, Hu XS, Yang JL, Lin H, Shi YK. [The clinical and pathological features, biomarker characteristics and prognosis analysis of lung adenosquamous carcinoma]. Zhonghua Zhong Liu Za Zhi 2019; 41:50-55.
23. Kaseda K, Asakura K, Kazama A, Ozawa Y. Clinicopathological and prognostic features of surgically resected pathological stage I lung

adenocarcinoma harboring epidermal growth factor receptor and K-ras mutation. Thorac Cancer 2017; 8:229-37.
24. Guan H, Du Y, Ning Y, Cao X. A brief perspective of drug resistance toward EGFR inhibitors: the crystal structures of EGFRs and their variants. Future Med Chem 2017; 9:693-704.
25. Nordman JC,Kabbani N. An interaction between alpha7 nicotinic receptors and a G-protein pathway complex regulates neurite growth in neural cells. J Cell Sci 2012; 125:5502-13.
26. Bissonnette R, Suarez-Farinas M, Li X, et al. Based on molecular profiling of gene expression, palmoplantar pustulosis and palmoplantar pustular psoriasis are highly related diseases that appear to be distinct from psoriasis vulgaris. PLoS One 2016; 11:e0155215.
27. Ge X, Qiu Y, Loh HH, Law PY. GRIN1 regulates micro-opioid receptor activities by tethering the receptor and G protein in the lipid raft. J Biol Chem 2009; 284:36521-34.
28. Otsuki Y, Saya H,Arima Y. Prospects for new lung cancer treatments that target EMT signaling. Dev Dyn 2018; 247:462-72.
29. Liao TT,Yang MH. Revisiting epithelial-mesenchymal transition in cancer metastasis: the connection between epithelial plasticity and stemness. Mol Oncol 2017; 11:792-804.
30. Marcucci F, Stassi G, De Maria R. Epithelial-mesenchymal transition: a new target in anticancer drug discovery. Nat Rev Drug Discov 2016; 15:311-25.
31. Song Y, Chen Y, Li Y, et al. Resveratrol suppresses epithelial-mesenchymal transition in GBM by regulating Smad-dependent signaling. Biomed Res Int 2019; 2019:1321973.
32. Mahmood MQ, Ward C, Muller HK, Sohal SS, Walters EH. Epithelial mesenchymal transition (EMT) and non-small cell lung cancer (NSCLC): a mutual association with airway disease. Med Oncol 2017; 34:45.
33. Jolly MK, Ward C, Eapen MS, et al. Epithelial-mesenchymal transition, a spectrum of states: Role in lung development, homeostasis, and disease. Dev Dyn 2018; 247:346-58.
34. Boffetta P, Borron C. Low-level exposure to arsenic in drinking water and risk of lung and bladder cancer: a systematic review and dose-response meta-analysis. Dose Response 2019; 17:1559325819863634.
35. Zhu CY, Qu JC, Cao HX, Chen GY, Shi YH, Fan JG. Obesity and nonalcoholic fatty liver disease associated with adenocarcinoma in patients with lung cancer. Medicine (Baltimore) 2019; 98:e17098.
36. He L, Ren X, Chen Y, et al. Prevalence of overweight and obesity among primary school children aged 5 to 14 years in Wannan area, China. Nutr Hosp 2014; 30:776-81.
37. He L, Ren X, Qian Y, Jin Y, Chen Y, Guo D, Yao Y. Prevalence of overweight and obesity among a university faculty and staffs from 2004 to 2010 in Wuhu, China. Nutr Hosp 2014; 29:1033-7.

RAPAMYCIN REPAIRS DAMAGED NERVE CELLS AND NEUROLOGICAL FUNCTION IN RATS WITH SPINAL CORD INJURY THROUGH ERK SIGNALING PATHWAY

D. LIU[1], S. JIA[2], D. SUN[3], S.-Y. WANG[4], F.-C. MENG[5] and W.-C. GUO[6]

[1]Department of Pharmacy, Weifang People's Hospital, Weifang, China; [2]No.1 Department of Orthopedics, Traditional Chinese Medical Hospital of Huangdao District, Qingdao, China; [3]Quality Control Department, Yantai Central Blood Station, Yantai, China; [4]Emergency Ward, the People's Hospital of Zhangqiu Area, Jinan, China; [5]Delivery Room, the People's Hospital of Zhangqiu Area, Jinan, China; [6]Department of Clinical Laboratory, Weifang People's Hospital, Weifang, China

Received February 25, 2020 – Accepted May 4, 2020

The object of this study was to explore the effect of rapamycin regulating the proliferation of Schwann cells through activating the extracellular signal-regulated kinase (ERK) signaling pathway on rats with spinal cord injury (SCI). The rat Schwann cells were cultured and divided into solvent (DMSO) group, rapamycin (Rapa) group (1.5 nM, 3.0 nM, 6.0 nM, 12.0 nM, 24.0 nM and 48.0 nM), and Rapa + ERK inhibitor (PD98059) group (40 mM). The proliferation of Schwann cells was detected by MTS. Western blot was used to evaluate the expression of ERK and p-ERK protein. Moreover, the spinal cord compression injury rat model was established, and the rats were divided into normal control group, SCI group and Schwann cell transplantation group. The animal experiment ended 7 weeks after Schwann cells had been injected every day into the injured rats. In the second animal experiment, the rats were divided into DMSO group, Rapa group and Rapa + PD98059 group. The motor recovery of rats was evaluated using the Basso-Beattie-Bresnahan (BBB) score every week, and the proliferation of Schwann cells at the site of SCI was detected using immunohistochemistry. It was verified that low-dose rapamycin (1.5 nM) could significantly promote the proliferation of Schwann cells cultured *in vitro* (P<0.001), most significantly at 48 h. Rapamycin could activate the ERK signaling pathway. The results of the first animal experiment showed that the BBB score in Schwann cell transplantation group rose with time compared with that in SCI group (P<0.05). The BBB score was obviously increased in Rapa group compared with that in DMSO group and Rapa + PD98059 group (P<0.05). According to the results of Ki67 immunohistochemistry, the proliferation ability of Schwann cells at the site of SCI was remarkably stronger than that in the other two groups. Rapamycin regulates the proliferation of Schwann cells through the ERK signaling pathway. The proliferation of Schwann cells can effectively repair the damaged nerve cells and neurological function in SCI rats.

As the most common type of injury in the world, spinal cord injury (SCI) is a nervous system disease characterized by physical disability and unrecoverable nervous system. After SCI, apoptosis of neurons and nerve cells will occur. Studies in China and other countries have demonstrated that Schwann cells can secrete brain-derived nerve growth factors, neurotrophic factors and ciliary neurotrophic

Key words: ERK signaling pathway, rapamycin, spinal cord injury, Schwann cell proliferation

Corresponding Author:
Wenchen Guo, MM
Department of Clinical Laboratory,
Weifang People's Hospital, 151 Guangwen Street,
Kuiwen District, Weifang 261041, China
Tel.: +86 0536 8192599
e-mail: liwenchen19890219@163.com

0393-974X (2020)
Copyright © by BIOLIFE, s.a.s.
This publication and/or article is for individual use only and may not be further reproduced without written permission from the copyright holder. Unauthorized reproduction may result in financial and other penalties
DISCLOSURE: ALL AUTHORS REPORT NO CONFLICTS OF INTEREST RELEVANT TO THIS ARTICLE.

factors, maintaining the survival of neurons and promoting the development of new nerve fibers and the recovery of peripheral nervous function (1, 2). The proliferation of Schwann cells can be regulated by many drugs. Rapamycin, a widely-studied drug, can promote the proliferation of Schwann cells and up-regulate autophagy, with an immunosuppression effect (3). Many physicians apply it for the treatment of central nervous system diseases, such as SCI. Moreover, rapamycin regulates the expression of neuroproteins via activating the protein kinase B (AKT) signaling pathway, thereby facilitating the survival and phagocytosis of Schwann cells (4). Kanno et al. (5) showed that rapamycin reduces the expression of p-p70S6K protein, up-regulates the proliferation of Schwann cells, enhances autophagy and reduces the neuronal loss and death through inhibiting the mTOR pathway, thereby recovering the motor function and neurological function of animals. Studies have shown that the proliferation of Schwann cells is regulated by many signaling pathways, the most classic and important of which is the extracellular signal-regulated kinase (ERK) signaling pathway (6-8). The ERK signaling pathway possesses many regulatory functions, such as regulating cell proliferation, differentiation, axonal growth, disintegration and regeneration of myelin sheaths for neurological function recovery in SCI (9-11). Although rapamycin can be used to treat central nervous system diseases such as SCI, there are rare reports on the effect of rapamycin regulating the proliferation of Schwann cells through the ERK signaling pathway on SCI rats. In this study, therefore, the mechanism of rapamycin in regulating the proliferation of Schwann cells through the ERK signaling pathway was explored, and its effect on SCI rats was deeply studied, so as to provide a theoretical basis and broaden the thinking of scientific research on treatment of neurological diseases caused by SCI.

MATERIALS AND METHODS

Culture of Schwann cells

Schwann cells were obtained from the Laboratory Animal Center of Wuhan University (Wuhan, China) and then were cultured using DMEM added with 10% FBS (Gibco, Rockville, MD, USA) and 1% penicillin-streptomycin (Shanghai Yuanmu Biotechnology Co., Ltd., Shanghai, China) in an incubator (Type: MCO-18AC, SANYO, Osaka, Japan) with 5% CO_2 at 37°C and saturated humidity, followed by passage when 80-90% cells were fused. Then well-developed Schwann cells were taken for subsequent experiments.

Western blotting

To prepare the sodium dodecyl sulphate (SDS) polyacrylamide gel, the glass plate was placed as required, the separation gel was prepared and solidified at room temperature, and then the spacer gel was also prepared and inserted with the comb. The concentration of protein samples was measured using the bicinchoninic acid (BCA) method (Pierce, Rockford, IL, USA). 10-50 μg of protein samples were added. 1/4 of 5×loading buffer was added into the samples and shaken evenly in the shaker, followed by heating at 100°C for 5 min for protein denaturation. The electrophoresis was performed at 80 V for 30 min and then at 120 V until there was loading buffer at the bottom of the separation gel, followed by membrane transfer under constant voltage of 100 V for 60 min. The protein was sealed at room temperature for 60 min on the shaker, and incubated with the primary antibody at an appropriate concentration at 4°C for 12-24 h on the shaker. The membrane was washed with 1×phosphate buffered saline-tween (PBST) for 3 times. The protein was incubated again with the secondary antibody at an appropriate concentration at room temperature for 60 min on the shaker. The membrane was also washed with 1×PBST for 3 times. After the pretreatment, chemiluminescence was developed using the chemiluminescence apparatus to observe the protein expression.

Detection of cell proliferation via 5-ethynyl-2'-deoxyuridine (EdU) staining

2×10^3 cells were inoculated into a plate. After 24 h, the samples in each well were added with 10 μM of EdU and incubated at 37°C for 90 min. The cells were washed twice with PBS and collected. Then 300-400 g of cells were taken and centrifuged. Finally, the cells were fixed with 50 μL of paraformaldehyde for 30 min. After the cells were added and mixed evenly with glycine at room temperature for 8 min on the shaker, they were washed with 500 μL of PBS. After 1 mL of 1×EdU staining buffer was added and mixed evenly at room temperature in the

dark, the cells were incubated for 30 min in a suitable environment. Finally, the cell proliferation was observed and photographed under a fluorescence microscope (NIKON, Tokyo, Japan).

Detection of cell proliferation via MTS assay

First, the cells in logarithmic phase were collected, and the cell suspension was diluted to the appropriate concentration. 100 μL of cell suspension was added into each well (4000 cells/well) with 5 parallel controls, followed by incubation in the incubator with 5% CO_2 at 37°C for 24 h. After the supernatant was discarded, 100 μL of dilute MTS solution was added into each well in the dark, followed by incubation in the biochemical incubator for 0.5-1.5 h. The optical density (OD) of each well was measured at a wavelength of 490 nm using a microplate reader (ELxSOO, Biotek Winooski, VT, USA) based on which the cell survival rate was calculated [cell survival rate % = ($OD_{\text{treatment group}}$/$OD_{\text{control group}}$) × 100%] and the relation curve of cell growth was plotted.

Lentivirus infection and construction of cell lines

Schwann cells were inoculated into a 6-well plate, and added with 2 mL of DMEM containing 10% FBS in each well. When 70% of cells were fused, the subsequent experiment was performed according to the instructions of Lipofectamine™ 2000 transfection reagent (Invitrogen, Carlsbad, CA, USA). A certain mass of lentiviral packaging plasmid psPAX2, pMD2.G and target plasmid were added into DMEM and stirred evenly at room temperature. Then Lipo2000 suspension and plasmids were added, mixed evenly and placed at room temperature for 30 min. The mixed solution was added into the 6-well plate for transfection for 6-8 h, and the original medium was replaced with the fresh medium. At 48 and 72 h after transfection, the lentivirus particles were collected from the supernatant. When 80% of Schwann cells inoculated into the 6-well plate were fused, 1 mL of lentivirus, 1 mL of DMEM and polybrene (1 μg/mL) were added to promote infection. After 48-72 h, puromycin was added to screen cells, with the blank control group set. It was observed that the cells died quickly in control group, while they survived in infection group.

Rat model of spinal cord compression injury

A total of 24 healthy male Wistar rats with strong motor ability weighing 220-240 g were randomly divided into normal control group (n=8), SCI group (n=8) and Schwann cell transplantation group (n=8). The rat model of spinal cord compression injury was established as follows: Under sterile conditions, the rats were anesthetized via intraperitoneal injection of pentobarbital sodium at a dose of 40 mg/kg and fixed on an ultra-clean bench, and the rat's back was cut open with a scalpel. According to the Nystrom's method, the spinal cord was pressed by 40 g of weight on a smooth metal gasket for 4 min. After the compression effect was checked, the wound was sutured and disinfected with iodine. At 6 d after modeling, Schwann cells were transplanted. In the second animal experiment, the effect of rapamycin (Fujian Kerui Pharmaceutical Co., Ltd., Fuqing, China) on proliferation of Schwann cells through the ERK signaling pathway was verified. The rats were randomly divided into solvent (DMSO) group, rapamycin (Rapa) group (1.5 nM) and Rapa + PD98059 (Wuhan Boster Biological Technology Co., Ltd., Wuhan, China) group. The rat model of SCI was established in the same way as above, and the effects of rapamycin and ERK signaling pathway on SCI rats were studied. This study was approved by the Animal Ethics Committee of Weifang People's Hospital Animal Center.

Basso-Beattie-Bresnahan (BBB) score

The motor function of the rats' hind limbs was evaluated using the BBB score every week for 7 weeks from Schwann cell transplantation. The score was given by two researchers using the double-blind method, and the average was recorded in each group.

Immunohistochemistry

The tissues at the site of SCI were taken and sliced into sections in DMSO group, Rapa group and Rapa + PD98059 group. The sections were deparaffinized, hydrated and incubated in the incubator at 60°C, followed by antigen retrieval and microwave thermal repair, inactivation of peroxidase and sealing. Then the sections were incubated with primary antibodies at 4°C overnight, washed twice with 1×PBS (5 min/time), incubated again with secondary antibodies at room temperature for 40 min, and washed again with 1×PBS for 3 times (3 min/time). After DAB staining, the sections were washed with secondary pure water, stained with hematoxylin for 15 min, and washed

again with secondary pure water for 3 min. Finally, the sections were sealed and detected microscopically.

Statistical analysis

Statistical Product and Service Solutions (SPSS) 16.0 software (SPSS Inc., Chicago, IL, USA) was used for scientific processing and analysis of experimental data. The experimental data were expressed as mean ± standard deviation. Student's *t*-test was used for comparison between the two groups while one-way analysis of variance (ANOVA) was adopted for comparison in multi groups. $P<0.05$ suggested the significant difference.

RESULTS

Effect of rapamycin on Schwann cell proliferation with treatment time

The Schwann cells of rats were cultured, and those in logarithmic phase were inoculated into the plate. After the cells adhered to the wall at 24 h, they were added with 1.5 nM of rapamycin in each well for treatment for 6 h, 12 h, 24 h, 36 h, 48 h, 60 h and 72 h. The results of MTS assay showed that the proliferation of Schwann cells was first enhanced and then weakened with treatment time, which was the most significant at 48 h (Fig. 1A), indicating that the best treatment time for Schwann cells with rapamycin is 48 h. Therefore, the treatment time of rapamycin was determined as 48 h in subsequent experiments.

Effect of rapamycin dose on Schwann cell proliferation in rats

The Schwann cells of rats were purified and cultured, and those in logarithmic phase were inoculated into the plate. After the cells adhered to the wall at 24 h, they were added with DMSO and rapamycin at different doses (1.5 nM, 3.0 nM, 6.0 nM, 12.0 nM, 24.0 nM and 48.0 nM) for treatment for 48 h. Then the proliferation of Schwann cells of rats was detected via MTS assay. As shown in Fig. 1B, the proliferation rate of Schwann cells gradually declined with the increase in the dose of rapamycin. 1.5 nM of rapamycin significantly promoted the cell proliferation, which had no statistically significant difference compared with DMSO group and other dose groups. Therefore, 1.5 nM of rapamycin was used in subsequent experiments.

Rapamycin activated ERK

Currently, it is recognized in the medical field that the three most classic and important signaling pathways for cell proliferation and survival are the AKT, P38 and ERK signaling pathways. To prove whether rapamycin can up-regulate these three signaling pathways, Schwann cells were inoculated into the 6-well plate. After the cells adhered to the wall at 24 h, they were treated with DMSO and 1.5 nM of rapamycin for 48 h. Finally, the total protein was collected from cells, and the protein expression levels of AKT, P38, ERK and p-ERK were evaluated using Western blotting. As shown in Fig. 1C, the protein levels of ERK and p-ERK were up-regulated, while those of AKT and P38 had no changes in Rapa group. It can be seen that rapamycin can activate the ERK signaling pathway.

ERK facilitated Schwann cell proliferation

To verify whether ERK can facilitate the proliferation of Schwann cells, the ERK-knockdown Schwann cells were constructed via lentivirus infection, and the cell proliferation ability was determined. The results showed that the proliferation was obviously weakened in ERK-knockdown Schwann cells, and there were obvious differences in the BBB score among groups ($P<0.01$) (Fig. 1D), suggesting that ERK plays an important role in the proliferation of Schwann cells.

Rapamycin promoted Schwann cell proliferation via ERK signaling pathway

To explore whether rapamycin promotes Schwann cell proliferation via activating the ERK signaling pathway, the proliferation of Schwann cells was detected using MTS assay and EdU staining, in which the rats were divided into DMSO group, Rapa group (1.5 nM) and Rapa + PD98059 group (40 mM). The results of MTS assay (Fig. 2A) and EdU staining (Fig. 2B) revealed that rapamycin could evidently promote the proliferation of Schwann cells, but the proliferation of Schwann cells was evidently weakened in Rapa + PD98059

group, showing significant differences in Rapa group compared with DMSO group and Rapa + PD98059 group ($P<0.01$). The above findings indicate that PD98059 can inhibit the promotion effect of rapamycin on proliferation of Schwann cells. Therefore, it can be seen that rapamycin promotes the proliferation of Schwann cells through the ERK signaling pathway.

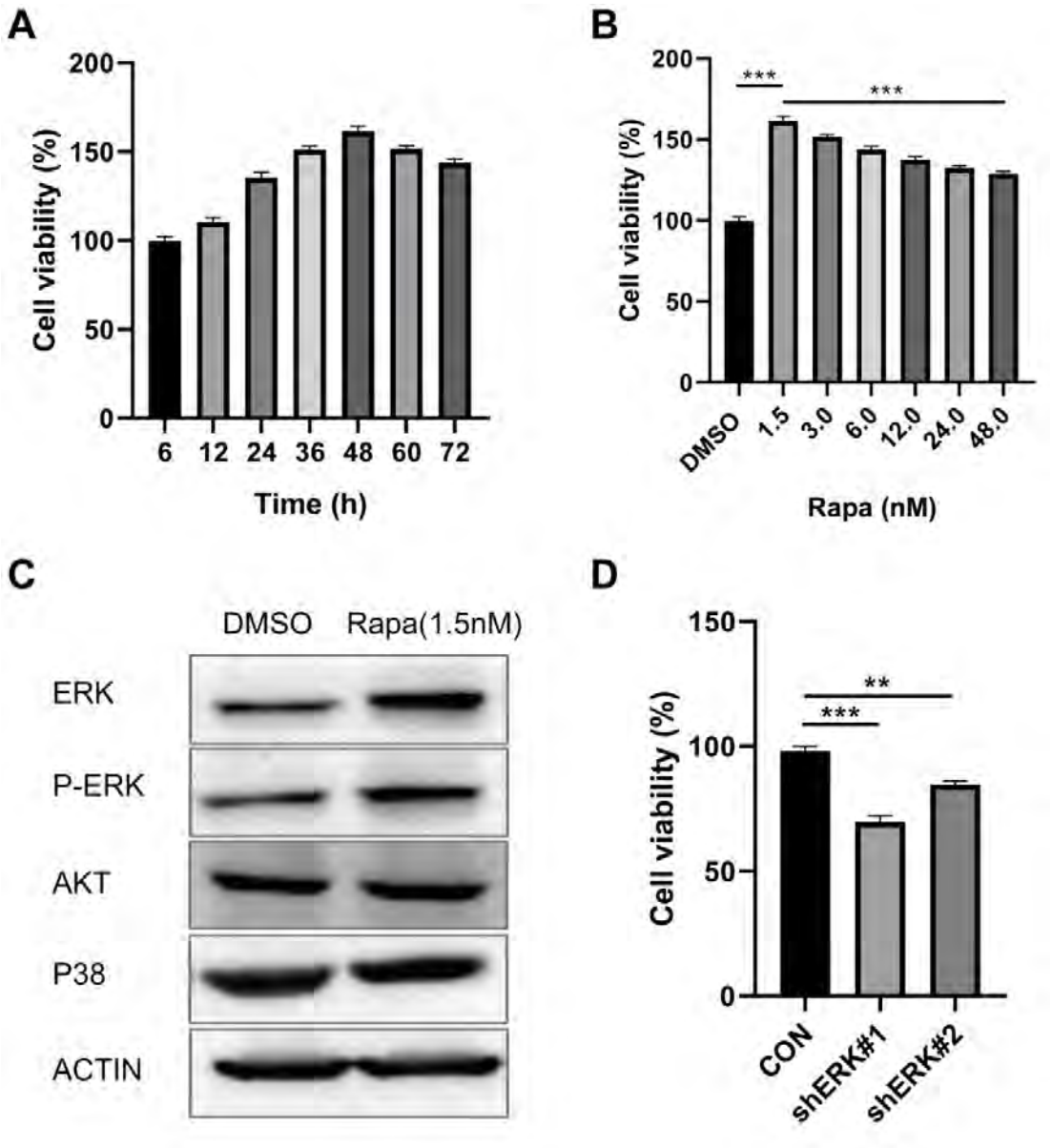


Fig. 1. *Rapamycin promoted Schwann cell proliferation via activating the ERK signaling pathway.* ***A****) Effect of rapamycin on Schwann cell proliferation with treatment time.* ***B****) Effect of rapamycin dose on Schwann cell proliferation in rats. Compared with DMSO group and 48.0 nM group, 1.5 nM group has a significantly increased proliferation rate of Schwann cells (P<0.001).* ***C****) Effects of rapamycin on AKT, P38, ERK and p-ERK protein expressions in Schwann cells.* ***D****) Effect of ERK on proliferation of Schwann cells. Compared with that in CON group, the proliferation rate of Schwann cells is obviously reduced in shERK#1 group and shERK#2 group (P<0.01).*

Schwann cell transplantation could repair SCI in rats

To verify the close relation between Schwann cells and SCI in rats, the rats were divided into normal control group, SCI group and Schwann cell transplantation group. The BBB score had a significant difference between Schwann cell transplantation group and SCI group from the 2nd week of experiment (P<0.05) (Fig. 3A), indicating that Schwann cells can repair SCI in rats.

Effects of rapamycin and ERK signaling pathway on SCI rats

In the second animal experiment, the mechanism of Schwann cells in repairing SCI in rats was explored,

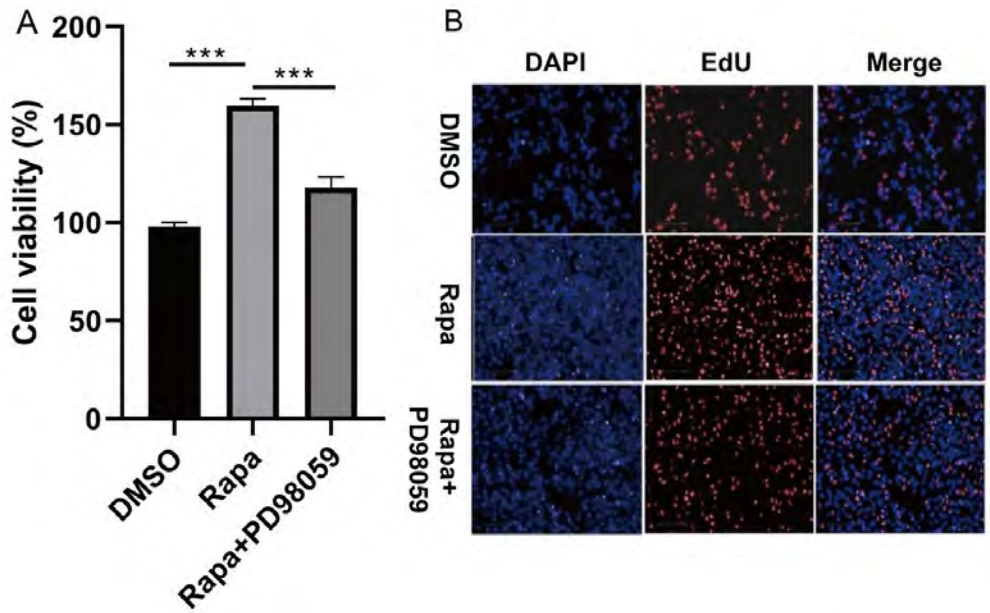


Fig. 2. *Effect of rapamycin on Schwann cell proliferation through ERK signaling pathway.* ***A)*** *The effects of Rapa and Rapa + PD98059 on the proliferation of Schwann cells are determined using the MTS assay. Rapa group has an evidently higher proliferation rate of Schwann cells than DMSO group and Rapa + PD98059 group (P<0.01).* ***B)*** *The effects of Rapa and Rapa + PD98059 on the proliferation of Schwann cells are detected via EdU staining. (magnification: 400×) *Significant differences among groups.*

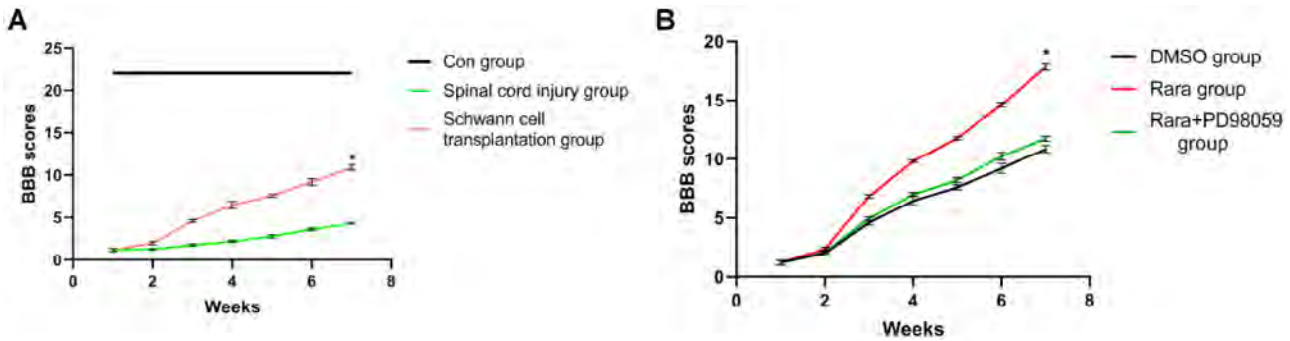


Fig. 3. *Schwann cell transplantation could repair SCI in rats via targeting ERK signaling pathway.*
A) *Effect of Schwann cell transplantation on SCI rats. The BBB score has a significant difference between Schwann cell transplantation group and SCI group (P<0.05).* ***B)*** *Effects of rapamycin and ERK signaling pathway on SCI rats. There are significant differences in the BBB score in Rapa group compared with DMSO group and Rapa + PD98059 group (P<0.05).*

in which the rats were divided into DMSO group, Rapa group (1.5 nM) and Rapa + PD98059 group (40 mM). The results manifested that the BBB score rose from the 2nd week after Schwann cell transplantation. It was observed for 7 consecutive weeks that the repair of SCI was faster in Rapa group than that in DMSO group and Rapa + PD98059 group, showing significant differences in Rapa group compared with DMSO group and Rapa + PD98059 group ($P<0.05$) (**Fig. 3B**). The above findings demonstrate that rapamycin regulates the proliferation of Schwann cells through the ERK signaling pathway, thereby exerting a certain recovery effect on SCI rats.

Immunohistochemical detection of Ki67 expression

After the animal experiment for 7 weeks, the rats were euthanatized, and the tissues at the site of SCI were taken, embedded and sliced into sections, in which the expression of Ki67 was determined via immunohistochemistry. As shown in Fig. 4, Ki67 had strongly positive expression in Rapa group, but weakly positive expression in DMSO group and Rapa + PD98059 group, suggesting that rapamycin promotes the proliferation of Schwann cells.

DISCUSSION

To date, in the medical field, there have been no mature and effective treatment methods that can completely restore the motor function and nerve injury in SCI patients (12). Therefore, studying the therapeutic mechanism of SCI and restoring the neurological function have become research hotspots in the academic world. The medical treatment methods for SCI mainly include surgical operation, physical methods, biological methods and pharmaceutical methods (13-17). Currently, drug therapy has become the most critical treatment means for secondary SCI (18). Rapamycin, a classic therapeutic drug, can regulate the proliferation of Schwann cells, which is applied in the treatment of central nervous system diseases. Schwann cells can constitute the myelin sheath of peripheral nervous system and secrete a variety of neurokines. They are able to promote the regeneration and repair of injured peripheral nerves (19-21). However, current studies only revealed that rapamycin can promote the repair of SCI, but its mechanism of action has not been clarified yet. The ERK signaling pathway can regulate the cell proliferation and survival, so studying the effect of rapamycin regulating the proliferation of Schwann cells through the ERK signaling pathway on SCI rats has important scientific and clinical application value.

In this paper, the effect of rapamycin dose on Schwann cell proliferation was determined. It was found that the low-dose rapamycin (1.5 nM) could significantly enhance the proliferation of Schwann cells compared with other doses and DMSO. The BBB score in Rapa group (1.5 nM) had obvious differences compared with other groups ($P<0.001$), indicating that low-dose rapamycin can facilitate the proliferation of Schwann cells, and the best treatment time for Schwann cells with rapamycin is 48 h. Then the protein expression levels of AKT, P38, ERK and p-ERK were evaluated using Western blotting. The results showed that the protein levels

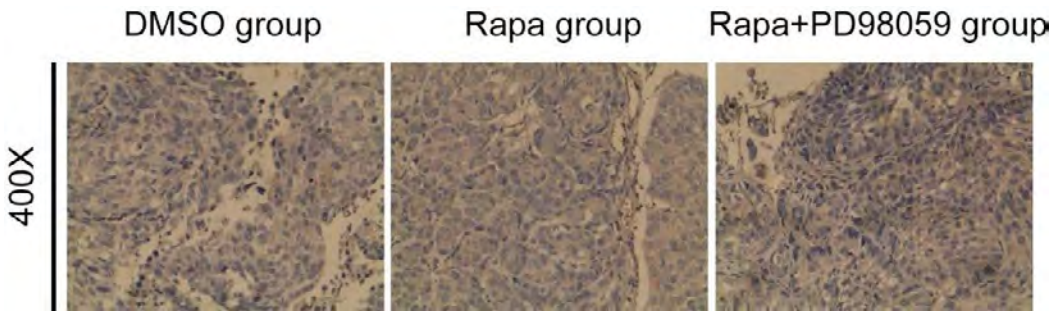


Fig. 4. *Immunohistochemical detection of Ki67 expression in SCI sections (magnification: 400×)*

of ERK and p-ERK were up-regulated, while those of AKT and P38 had no obvious changes in Rapa group. It can be seen that rapamycin can activate the ERK signaling pathway. Furthermore, the ERK-knockdown Schwann cells were constructed via lentivirus infection, and the cell proliferation ability was determined via MTS assay. The results showed that the proliferation was remarkably weakened in ERK-knockdown Schwann cells ($P<0.01$), suggesting that ERK plays an important role in the proliferation of Schwann cells. At the same time, the results of MTS assay and EdU staining revealed that rapamycin could evidently promote the proliferation of Schwann cells, but the proliferation of Schwann cells was evidently weakened in Rapa + PD98059 group ($P<0.01$), demonstrating that rapamycin promotes the proliferation of Schwann cells through the ERK signaling pathway (22).

In this paper, the rat model of SCI was established in the animal experiment, and Schwann cells were injected into SCI rats. It was found that the BBB score markedly rose in the Schwann cell transplantation group compared with that in SCI group ($P<0.05$), indicating that Schwann cells can repair SCI in rats. In the second animal experiment, the mechanism of Schwann cells in repairing SCI in rats was explored. It was observed for 7 consecutive weeks that the repair of SCI had significant differences in Rapa group compared with that in DMSO group and Rapa + PD98059 group ($P<0.05$), slower in DMSO group and Rapa + PD98059 group than that in Rapa group. Finally, the expression of Ki67 was determined via immunohistochemistry. The results manifested that Ki67 had strongly positive expression in Rapa group, but weakly positive expression in DMSO group and Rapa + PD98059 group.

To sum up, *in vivo* experiments further confirmed that rapamycin can significantly promote the proliferation of Schwann cells, thereby repairing SCI in rats. In conclusion, this study demonstrates that rapamycin regulates the proliferation of Schwann cells through the ERK signaling pathway. The proliferation of Schwann cells can effectively repair the damaged nerve cells and neurological function in SCI rats, thereby enhancing the motor function of rats.

REFERENCES

1. Zhou XF, Song XY, Zhong JH, Barati S, Zhou FH, Johnson SM. Distribution and localization of pro-brain-derived neurotrophic factor-like immunoreactivity in the peripheral and central nervous system of the adult rat. J Neurochem 2004; 91:704-15.
2. Li JW, Kuang Y, Chen L, Wang JF. LncRNA ZNF667-AS1 inhibits inflammatory response and promotes recovery of spinal cord injury via suppressing JAK-STAT pathway. Eur Rev Med Pharmacol Sci 2018; 22:7614-20.
3. Jessen KR, Mirsky R. Origin and early development of Schwann cells. Microsc Res Tech 1998; 41:393-402.
4. Rangaraju S, Notterpek L. Autophagy aids membrane expansion by neuropathic Schwann cells. Autophagy 2011; 7:238-39.
5. Kanno H, Ozawa H, Sekiguchi A, et al. The role of mTOR signaling pathway in spinal cord injury. Cell Cycle 2012; 11:3175179.
6. Pan CW, Jin X, Zhao Y, et al. AKT-phosphorylated FOXO1 suppresses ERK activation and chemoresistance by disrupting IQGAP1-MAPK interaction. Embo J 2017; 36:995-1010.
7. Filippone SM, Samidurai A, Roh SK, et al. Reperfusion therapy with rapamycin attenuates myocardial infarction through activation of AKT and ERK. Oxid Med Cell Longev 2017; 2017:619720.
8. AchuthanA,AslamA,NguyenQ,etal.Glucocorticoids promote apoptosis of proinflammatory monocytes by inhibiting ERK activity. Cell Death Dis 2018; 9:267.
9. Rauch J, Moran-Jones K, Albrecht V, Schwarzl T, Hunter K, Gires O, Kolch W. c-Myc regulates RNA splicing of the A-Raf kinase and its activation of the ERK pathway. Cancer Res 2011; 71:4664-74.
10. Zhao J, Sun W, Cho HM, et al. Integration and long distance axonal regeneration in the central nervous system from transplanted primitive neural stem cells. J Biol Chem 2013; 288:164-68.
11. Duhamel S, Hebert J, Gaboury L, et al. Sef downregulation by Ras causes MEK1/2 to become aberrantly nuclear localized leading to polyploidy and neoplastic transformation. Cancer Res 2012; 72:626-35.
12. van Middendorp JJ, Barbagallo G, Schuetz M, Hosman AJ. Design and rationale of a Prospective,

Observational European Multicenter study on the efficacy of acute surgical decompression after traumatic Spinal Cord Injury: the SCI-POEM study. Spinal Cord 2012; 50:686-94.
13. Yang HS, Chen DY, Lu XH, et al. Choice of surgical approach for ossification of the posterior longitudinal ligament in combination with cervical disc hernia. Eur Spine J 2010; 19:494-501.
14. Ferreira AF, Real CC, Rodrigues AC, Alves AS, Britto LR. Moderate exercise changes synaptic and cytoskeletal proteins in motor regions of the rat brain. Brain Res 2010; 1361:31-42.
15. Cristante AF, Damasceno ML, Barros FT, de Oliveira RP, Marcon RM, Da RI. Evaluation of the effects of hyperbaric oxygen therapy for spinal cord lesion in correlation with the moment of intervention. Spinal Cord 2012; 50:502-6.
16. Cristante AF, de Souza FI, Barros FT, Oliveira RP, Marcon RM. Lead poisoning by intradiscal firearm bullet: a case report. Spine (Phila Pa 1976) 2010; 35:E140-E143.
17. Cristante AF, Barros FT, Oliveira RP, et al. Antioxidative therapy in contusion spinal cord injury. Spinal Cord 2009; 47:458-63.
18. Blight AR, Zimber MP. Acute spinal cord injury: pharmacotherapy and drug development perspectives. Curr Opin Investig Drugs 2001; 2:801-8.
19. Merolli A, Mao Y, Kohn J. A suspended carbon fiber culture to model myelination by human Schwann cells. J Mater Sci Mater Med 2017; 28:57.
20. Zhang J, Chen H, Duan Z, et al. The Effects of Co-transplantation of olfactory ensheathing cells and Schwann Cells on local inflammation environment in the contused spinal cord of rats. Mol Neurobiol 2017; 54:943-53.
21. Liu F, Zhang H, Zhang K, Wang X, Li S, Yin Y. Rapamycin promotes Schwann cell migration and nerve growth factor secretion. Neural Regen Res 2014; 9:602-9.
22. Tsuda Y, Kanje M, Dahlin LB. Axonal outgrowth is associated with increased ERK 1/2 activation but decreased caspase 3 linked cell death in Schwann cells after immediate nerve repair in rats. BMC Neurosci 2011; 12:12.

LncRNA PVT1 REGULATES GALLBLADDER CANCER PROGRESSION THROUGH miR-30d-5p

K. LIU[1] and Q. XU[1]

[1]*Department of Hepatobiliary Surgery, Central Hospital of Zibo, Zibo, China*

Received March 22, 2020 – Accepted May 6, 2020

Gallbladder cancer (GBC) is a malignant tumors that develops insidiously and rapidly. In this work, we explored the function of long non-coding RNA plasmacytoma variant translocation 1 (lncRNA PVT1) in modulating GBC development. PVT1 and miR-30d-5p expression were detected by real-time fluorescent quantitative polymerase chain reaction (qRT-PCR). The relationship of PVT1 and miR-30d-5p was analyzed by Dual luciferase activity and Spearman correlation analysis. The effect of PVT1 on GBC progression was detected by cell counting kit-8 (CCK-8) and Transwell assay. In GBC tissues and cell lines, upregulation of PVT1 and downregulation of miR-30d-5p were observed. PVT1 silencing suppressed cell proliferation and invasion of GBC cells. Based on the analysis of Dual luciferase activity and Spearman correlation, miR-30d-5p was confirmed as a target of PVT1, and their expression had a negative correlation in GBC tissues. Additionally, miR-30d-5p inhibitor could reverse the effects of PVT1 knockdown. These data demonstrated that PVT1 facilitated to GBC tumorigenesis by promoting cell proliferation and invasion via miR-30d-5p, indicating that PVT1 may be a potential biomarker of GBC diagnosis and treatment.

As the most common malignant tumor of the biliary tract, GBC accounts for approximately 80~95% (1). Its progression is hidden and rapid, and prone to invasion and metastasis, and the 5-year overall survival rate is only 5% (2-4). The incidence of GBC increases with age, and its important risk factors are congenital biliary abnormalities and genetic susceptibility (3). Other potential risk factors include inflammatory bowel disease, diabetes, obesity, ethnicity, heredity and environment (5). However, the pathogenesis of GBC is still unclear, and the lack of specific clinical markers has greatly increased the difficulty of early diagnosis and treatment (6), therefore, improving the early diagnosis rate of GBC has always been a research hotspot in the field of oncology.

Increasing evidence shows that lncRNAs are closely related to the occurrence and development of GBC, and play a promoting or suppressing role in the regulation of tumor cell apoptosis, invasion and metastasis. Wu et al. confirmed that the expression of MALAT1 in GBC was significantly increased, and knocking down MALAT1 in SGC-996 and NOZ cells significantly inhibited the cell proliferation, invasion and metastasis, and made prolongation of G2/M phase and a significantly decreasing of MMP-9 expression, an enzyme associated with cell invasion (7). UCA1, which related to the GBC tumor size, lymph node metastasis, TNM stage, and overall survival, was abnormally expressed in GBC, and promoted proliferation and metastasis to inhibit

Key words: PVT1; gallbladder cancer; miR-30d-5p; cell proliferation; invasion

Corresponding Author:
Dr Qiang Xu,
Department of Hepatobiliary Surgery,
Central Hospital of Zibo,
54 Zibo Youth League Road, Zibo 255000, China
Tel.: +86 0533-2360490 - Fax: +86 0533-3887333
e-mail: baibapan909599655@163.com

0393-974X (2020)
Copyright © by BIOLIFE, s.a.s.
This publication and/or article is for individual use only and may not be further reproduced without written permission from the copyright holder.
Unauthorized reproduction may result in financial and other penalties
DISCLOSURE: ALL AUTHORS REPORT NO CONFLICTS OF INTEREST RELEVANT TO THIS ARTICLE.

p21 and E-cadherin expression by binding to EZH2 (8). In addition, Wang et al. reported that MINCR stimulated EZH2 expression by acting on miR-26p-5a, thereby promoting the proliferation and invasion of GBC cells (9). Zhang et al. also mentioned in their report that HOXA-AS2 expression was increased in GBC, while HOXA-AS2 knockdown could make the GBC cell cycle stagnate in G1 phase, and promote cell apoptosis and the ability of EMT (10). Furthermore, CCAT1 and H19 regulated the downstream genes Bmi1 and AKT2 through targeting miR-218-5p and miR-194-5p, respectively, thus promoting GBC cell proliferation and invasion (11, 12).

As an important carcinogenic non-coding RNA, PVT1 was highly expressed in a variety of malignant tumors and indicated poor prognosis (13, 14). PVT1 could promote the occurrence and development of tumors by affecting the proliferation, migration, invasion and apoptosis of tumor cells (15). However, there are few studies on the function of PVT1 in GBC. The results of the present study indicated that PVT1 was markedly upregulated in GBC tissues and cell lines. Moreover, PVT1 knockdown repressed the proliferation and invasion of GBC cells *in vitro*. Additionally, further experiments demonstrated that the function of PVT1 in GBC was also concerned with miR-30d-5p.

MATERIALS AND METHODS

Forty-five patients with GBC were treated by cholecystectomy at the Central Hospital of Zibo, Zibo, China. In addition, 20 patients with benign lesions of gallbladder (including gallbladder adenoma, chronic cholecystitis combined with gallbladder stones) who underwent surgery in the hospital during the same period were selected as the control group. Inclusion criteria were patients confirmed as GBC by pathology, receiving treatment for the first time, and patient consent. Exclusion criteria were preoperative radiotherapy and chemotherapy, patients with other malignant tumors, serious cardiovascular and cerebrovascular diseases and endocrine diseases, liver, kidney and other important organs severely damaged, and gallbladder stones, gallbladder polyps, chronic inflammation of the gallbladder and other benign lesions, and surgical contraindications. This study was endorsed by the Ethics Committee of Central Hospital of Zibo and informed consent was obtained from all patients or guardians.

Tissue specimens were taken from all subjects and frozen in liquid nitrogen and stored at an ultra-low temperature.

Cell culture and transfection

Four GBC cells including GBC-SD, NOZ, OCUG-1 and SGC-996, and human gallbladder epithelial cells HGBEC purchased from American Type Culture Collection (ATCC, USA) were cultured with RPMI 1640 medium (Gibco, USA) containing 10% fetal bovine serum (FBS, Gibco, USA) at 37°C and 5% CO_2 in a cell incubator. Fresh medium was replaced every 2-3 days according to the cell growth conditions, and then the cells were transferred to culture.

GBC cells in the logarithmic growth phase were selected to inoculate into 6-well plates at a density of 3.5×10^5 cells/ml. When the cells grew to about 70%, PVT1 small interfering RNA (si-PVT1), miR-30d-5p mimic (mimic), miR-30d-5p inhibitor (inhibitor) or their corresponding controls was transfected into cells to affect PVT1 or miR-30d-5p expression. The transfection was performed by Lipofectamine2000 (Invitrogen, USA). The transfection efficiency was detected by qRT-PCR.

Assays

All transfected cells were resuspended with serum-free medium. Cells of each group were seeded in 96-well plates with 1×10^3 cells/well and incubated in a cell culture incubator. Each group was set up with 3 replicates. 10 µl of CCK-8 reagent (Dojindo, Japan) was added into each well at 1, 2, 3, and 4 days, and incubated at 37°C for 2 h. Then the absorbance (OD) value at 450 nm was detected with a microplate reader to draw the cell proliferation curve.

Matrigel was added to the upper chamber and hydrated at 37°C for 30 min. 200 µl cell suspension with 2×10^5 cells/ml was added into upper chamber. 600 µl medium containing 10% FBS was added to the lower chamber. After 24 h, the chamber was removed and the medium in the chamber was aspirated. Then paraformaldehyde was added to the lower chamber, and cells were fixed for 20 min at room temperature. Then 0.1% crystal violet was added to stain cells at room temperature for 20 min. After wiping off the non-invading cells, the number of cells was

counted in 5 different fields under a microscope.

Transfected cells were seeded in 24-well plates with 2×10^4 cells per well. The cells were placed in an incubator overnight and transfected with miR-30d-5p mimic or miR-NC and wild-type or mutant reporter vector (PVT1-wt or PVT1-mut). After 48 h, cell lysates were added and luciferase activity was measured with dual luciferase reporter kit (Promega, USA).

qRT-PCR

Total RNA was extracted from tissues or cells using Trizol reagent (Takara, Japan). One Step PrimeScript cDNA Synthesis Kit (Takara, Japan) was used to synthesize cDNA, and then the cDNA was used as a template to perform qRT-PCR with SYBR Premix Ex Taq RR420A (Takara, Japan) on ABI 7500 fast RT-PCR system (Life Technologies, USA). U6 or GAPDH was used as internal reference. Primers are listed in Table I.

Statistical analysis

All values were expressed as mean ± standard deviation (SD). GraphPad Prism 5.0 statistical software was used to analyze the data by *t*-test. $P<0.05$ was considered to have statistical significance.

RESULTS

PVT1 expression was increased in GBC

PVT1 expression in 45 GBC tissues and 20 benign lesion tissues were detected by qRT-PCR. The results showed that the expression of PVT1 in GBC tissues was significantly higher than that in the benign lesion group (Fig. 1A). Similarly, PVT1 expression has a marked increase in four GBC (GBC-SD, NOZ, OCUG-1 and SGC-996) cells compared to HGBEC cells (Fig. 1 B). Among the four GBC cells, the cells with the high expression of PVT1 were NOZ and OCUG-1 cells (Fig. 1B). Therefore, these two GBC cells were selected for subsequent experiments.

In addition, Kaplan-Meier method analysis was performed to investigate the relationship between PVT1 expression and clinical prognosis. The results showed that PVT1 expression was significantly correlated with the overall survival of GBC patients, and the survival time of patients in the group with high PVT1 expression was significantly longer than that in the group with low PVT1 expression (Fig. 1C). Therefore, PVT1 was highly expressed in GBC tissues and cells, and were closely related to prognosis.

Table I. *Primer sequences for real-time fluorescence quantification PCR*

Gene Name	Primer sequences (5'-3')
GAPDH	F GCACCGTCAAGGCTGAGAAC
	R TGGTGAAGACGCCAGTGGA
U6	F CTCGCTTCGGCAGCACA
	R AACGCTTCACGAATTTGCGT
PVT1	F GCCCCTTCTATGGGAATCACTA
	R GGGGCAGAGATGAAATCGTAAT
miR-30d-5p	F UGUAAACAUCCCCGACUGGAAG
	R TGTAAACATCCCCGACTGGAAGA

PVT1 knockdown suppressed GBC cell proliferation and invasion

To investigate the role of PVT1 in GBC cells, si-PVT1 was transfected into NOZ and OCUG-1 cells, respectively. The expression of PVT1 in NOZ and OCUG-1 cells with si-PVT1 was detected by qRT-PCR. Fig. 2 A and B showed that si-PVT1 significantly down-regulated PVT1 expression in GBC cells. We continued to use CCK-8 assay to detect the effect of PVT1 on GBC cell proliferation ability *in vitro*. As shown in Fig. 2 C and D, PVT1 knockdown significantly inhibited the proliferation capacity of NOZ and OCUG-1 cells *in vitro*. Next, we performed Transwell assay to measure the effect of PVT1 on the invasion ability of GBC cells. The results showed that the number of invading cells were significantly reduced in cells with si-PVT1 treatment, indicating that PVT1 silencing could obviously inhibit the invasion ability of GBC cells *in vitro* (Fig. 2 E and F). It suggested that PVT1 might play an important regulatory role in the proliferation and invasion of GBC cells.

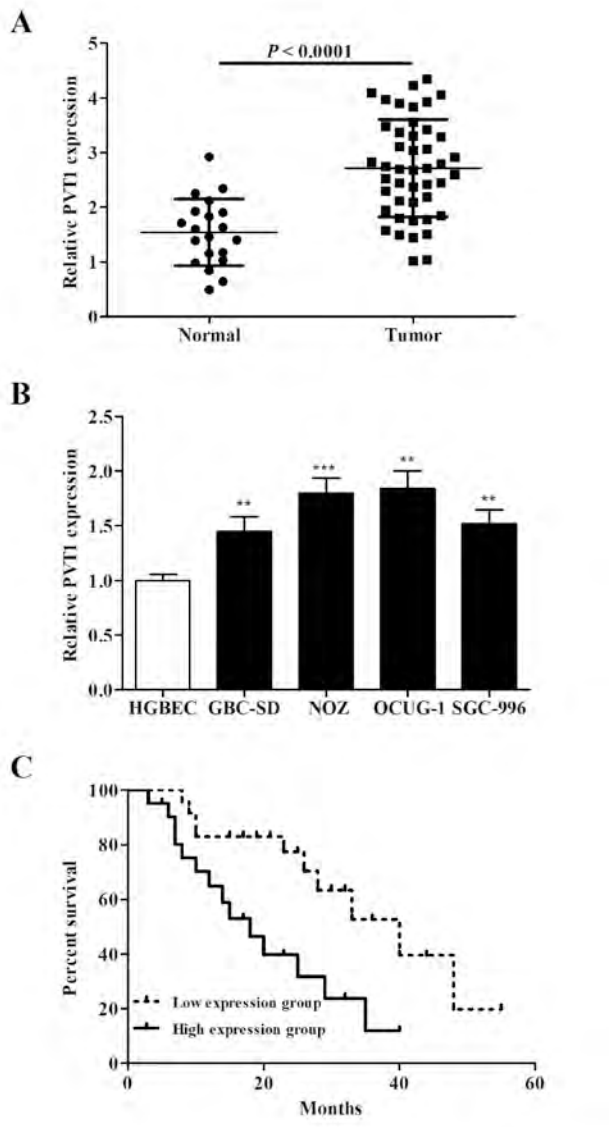


Fig. 1. *PVT1 expression was increased in GBC. **A)** PVT1 expression was highly expressed in GBC tissues. **B)** PVT1 expression was increased in GBC cells. **C)** The correlation between PVT1 expression and overall survival of GBC patients. **P < 0.01, ***P<0.001.*

PVT1 directly binds to miR-30d-5p

Bioinformatics prediction (Starbase3.0 (http://starbase.sysu.edu.cn/)) showed that PVT1 binding sites were present in the miR-30d-5p sequence (Fig. 3A). At the same time, miR-30d-5p mimic significantly increased the expression of miR-30d-5p in NOZ and OCUG-1 cells (Fig. 3B), and also reduced the luciferase activity of cells transfected with PVT1-wt (Fig. 3 C and D). After the nucleotide mutation at the binding site, the inhibitory effect of miR-30d-5p mimic on the luciferase activity disappeared, suggesting that miR-30d-5p was a target of PVT1.

It was also found that si-PVT1 significantly increased the miR-30d-5p expression in NOZ and OCUG-1 cells, indicating that PVT1 could inhibit the expression of miR-30d-5p (Fig. 3E). In addition, the detection results of GBC clinical samples (Fig. 3F) and cells (Fig. 3G) showed that miR-30d-5p was downregulated and negatively correlated with PVT1 expression in tissues (Fig. 3H). It was further demonstrated that PVT1 could target and inhibit miR-30d-5p expression in GBC.

PVT1 facilitated to GBC progression via targeting miR-30d-5p

Considering that PVT1 could downregulate the expression of miR-30d-5p, we explored whether PVT1 regulated GBC cell invasion and proliferation through miR-30d-5p. Thus, we observed the effect of miR-30d-5p on invasion and proliferation of

GBC cells with PVT1 knockdown. Therefore, we transfected miR-30d-5p inhibitor into GBC cells to decrease its expression (Fig. 4A). As shown in Fig. 4B, inhibition of miR-30d-5p could partially restore the suppression of PVT1 knockdown on GBC cell proliferation. In Transwell assay, the number of invaded cells pointed toward the same trend (Fig. 4C). This fully demonstrated that the role of PVT1 in promoting GBC progression might partly be through the inhibition of miR-30d-5p.

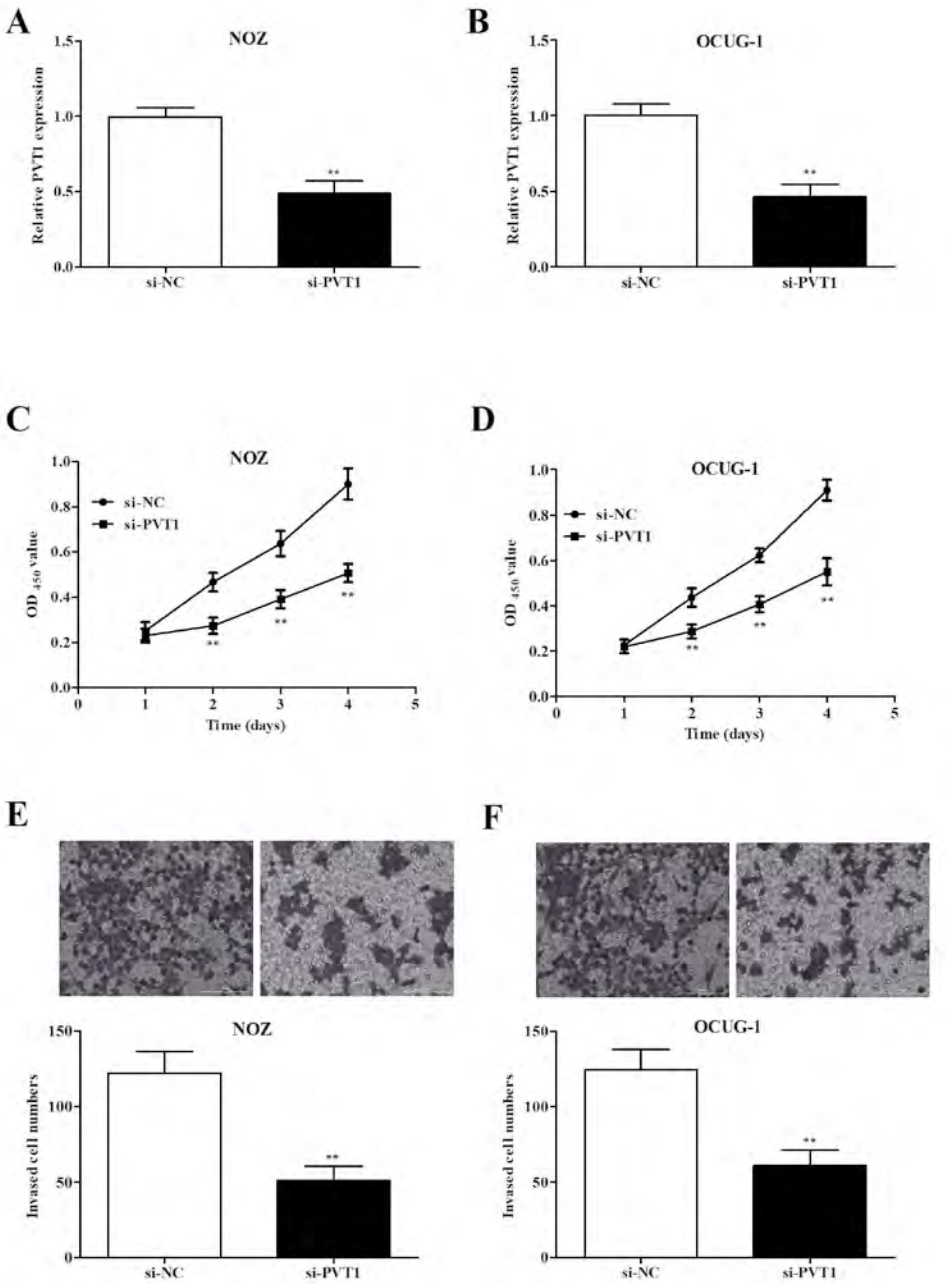


Fig. 2. *PVT1 knockdown repressed cell proliferation and invasion.* ***A, B****) PVT1 expression in NOZ and OCUG-1 cells transfected with si-PVT1.* ***C, D****) Cell proliferation was remarkably decreased in NOZ and OCUG-1 cells with si-PVT1 transfection.* ***E, F****) Invaded cells were suppressed in NOZ and OCUG-1 cells with si-PVT1 transfection (200X). *P < 0.05, **P < 0.01.*

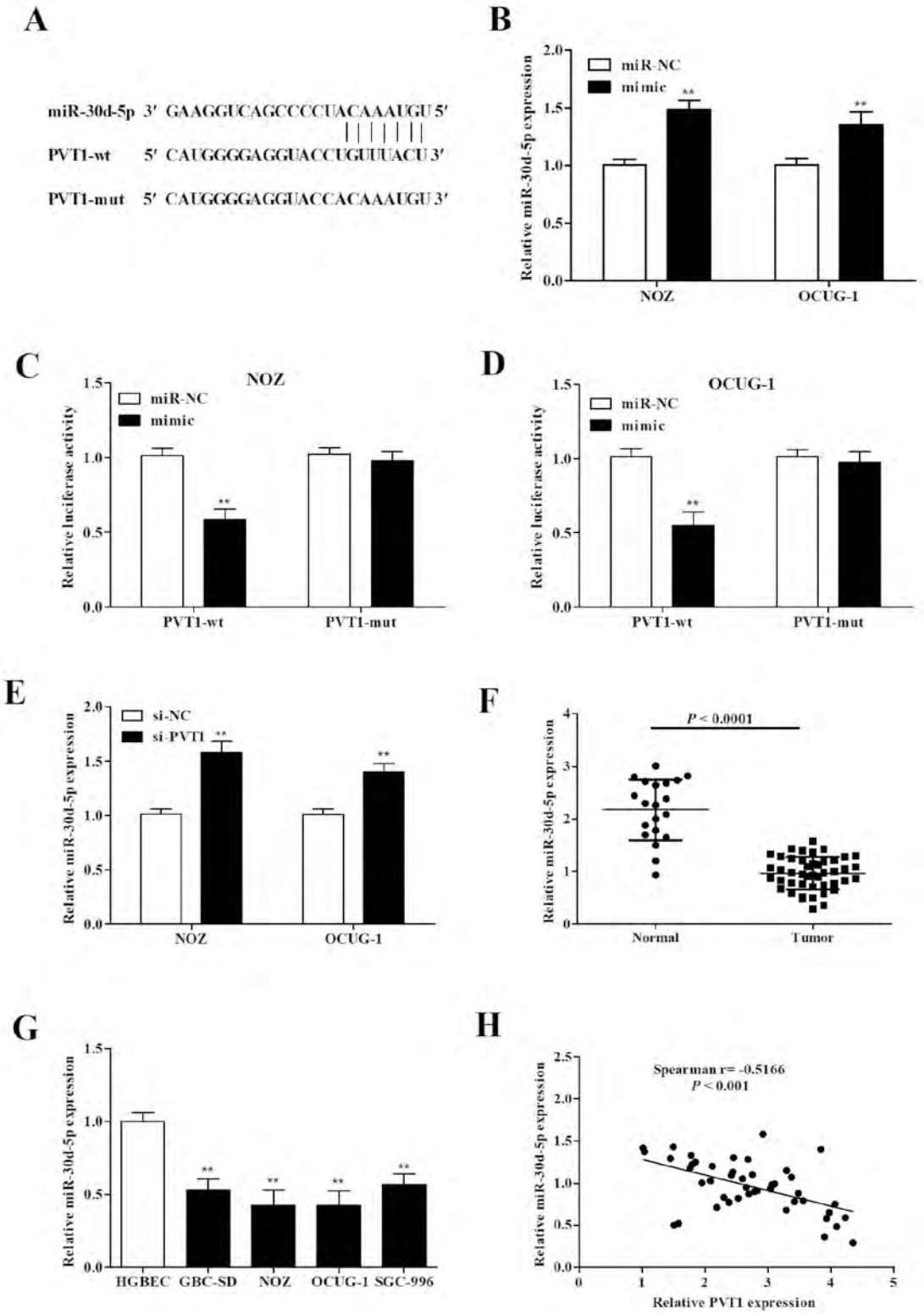


Fig. 3. *miR-30d-5p directly binds to PVT1.* ***A****) Binding sites of miR-30d-5p and PVT1.* ***B****) miR-30d-5p expression in NOZ and OCUG-1 after miR-30d-5p mimic transfection.* ***C, D****) Luciferase activity detected in NOZ and OCUG-1 cells.* ***E****) Effect of PVT1 on miR-30d-5p expression in NOZ and OCUG-1 cells.* ***F****) miR-30d-5p expression in GBC tissues.* ***G****) miR-30d-5p expression in GBC cells.* ***H****) Relevance of PVT1 and miR-30d-5p expression.*P < 0.05, **P < 0.01.*

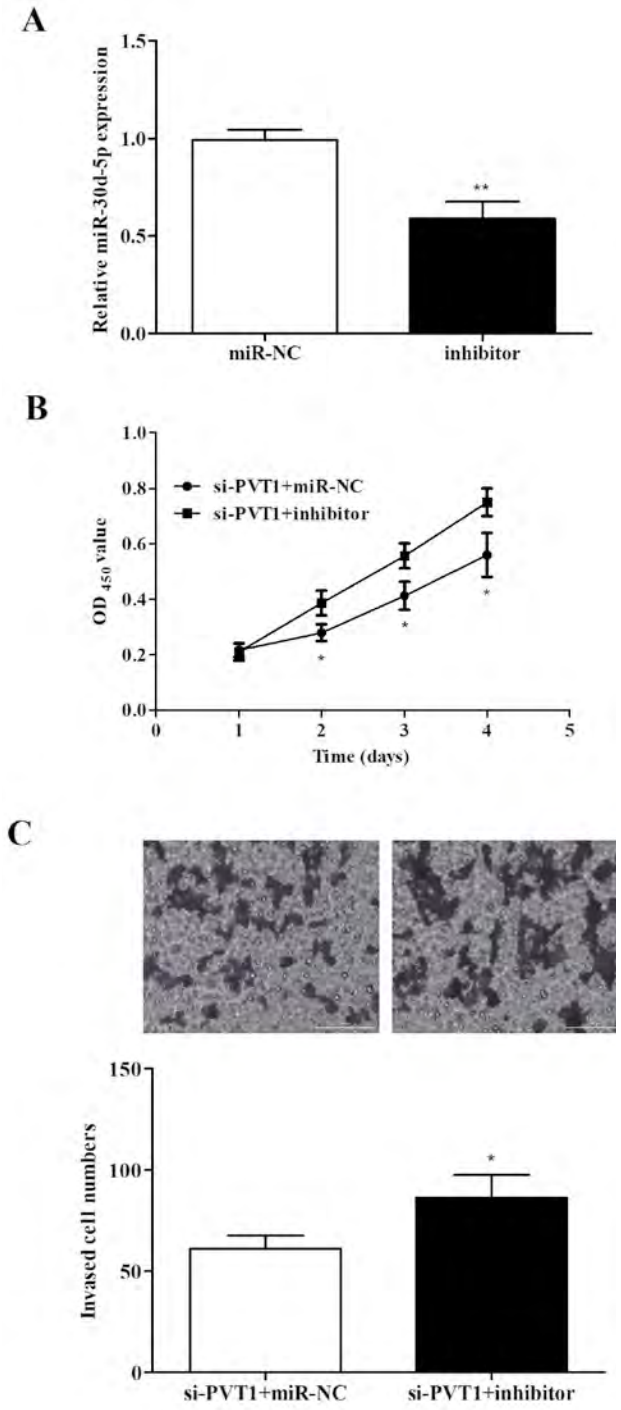


Fig. 4. *miR-30d-5p inhibition reversed the suppression of PVT1 knockdown on cell proliferation and invasion in GBC.* ***A****) miR-30d-5p expression in NOZ cells with miR-30d-5p inhibitor transfection.* ***B****) Cell proliferation was measured in NOZ cells after inhibiting PVT1 and miR-30d-5p.* ***C****) Invasion cells in NOZ cells with si-PVT1 and miR-30d-5p inhibitor (200X). *P < 0.05, **P < 0.01.*

DISCUSSION

GBC has attracted widespread attention as a common malignant tumor. Early surgery is the most effective clinical treatment, and is also the main means to improve prognosis (16). However, GBC early clinical symptoms are not obvious and are characterized by early lymph node and distant metastasis, thus leading to poor prognosis (17). Therefore, exploring the mechanism of GBC occurrence and development has great significance for early diagnosis and molecular targeted therapy of patients.

PVT1 is an intergenic lncRNA located on chromosome 8q24 (15). PVT1 which plays an oncogene role and is highly expressed in hepatocellular carcinoma (HCC), gastric cancer (GC), non-small cell lung cancer (NSCLC), colorectal cancer (CRC) and other tumors, and is related to the prognosis of patients (13). For instance, high expression of PVT1 facilitated GC progression and poor prognosis (18). Similarly, upregulation of PVT1 in NSCLC was associated with its progression and poor overall survival (19). Pan et al. also suggested that PVT1 overexpression in CRC indicated a poor prognosis of patients (20). Our results shown that the expression of PVT1 was increased in GBC tissues and cells, and the proliferation and invasion ability of GBC cells with PVT1 knockdown were found to be significantly repressed *in vitro*, which indicated that PVT1 was present in GBC cells and its dysregulation was associated with GBC progression and overall survival.

LncRNA adsorbs downstream miRNA through "sponge action" and inhibits miRNA expression, which is one of the important mechanisms for lncRNA to play a regulatory role (21). In this study, biological analysis showed that miR-30d-5p was a target of PVT1. He et al. found that the expression of miR-30d-5p was significantly decreased in GBC tissues, and miR-30d-5p overexpression could inhibit the progression of GBC through LDHA (22). Furthermore, PVT1 promoted metastasis and proliferation of colon cancer by the regulation of RUNX2 via sponging miR-30d-5p (23). This study indicated miR-30d-5p expression was significantly

reduced by PVT1 knockdown, indicating that PVT1 could inhibit miR-30d-5p expression by adsorbing miR-30d-5p. More importantly, rescue experiments showed that miR-30d-5p inhibition partly reversed the repression of PVT1 knockdown on cell proliferation and invasion. This suggested that PVT1 is involved in regulating the occurrence and development of GBC by inhibiting miR-30d-5p. Although our study showed that the function and potential mechanisms of PVT1 in GBC progression, there were still some deficiencies. For instance, other miRNAs and possible mechanisms of PVT1 may exist in GBC. In addition, the function of PVT1 *in vivo* was not studied thoroughly. Moreover, we only discussed the relationship of PVT1 and overall survival, the correlation between PVT1 expression and clinical characteristics still need further research. Therefore, more investigations need to be conducted to completely understand the mechanism of PVT1 in GBC.

Collectively, PVT1 was upregulated in GBC, and to a certain extent it indicated a poor prognosis. PVT1 promoted GBC development by inducing cell proliferation and invasion through regulation of miR-30d-5p, and may be a valuable predictive marker and a new therapeutic target in the future treatment of GBC patients.

REFERENCES

1. DeSantis CE, Ma J, Gaudet MM, et al. Breast cancer statistics, 2019. CA Cancer J Clin 2019; 69:438-51.
2. Narayan RR, Creasy JM, Goldman DA, et al. Regional differences in gallbladder cancer pathogenesis: Insights from a multi-institutional comparison of tumor mutations. Cancer 2019; 125:575-85.
3. Hundal R, Shaffer EA. Gallbladder cancer: epidemiology and outcome. Clin Epidemiol 2014; 6:99-109.
4. Rawla P, Sunkara T, Thandra KC, Barsouk A. Epidemiology of gallbladder cancer. Clin Exp Hepatol 2019; 5:93-102.
5. Dey S, Chatterjee S, Ghosh S, Sikdar N. The geographical, ethnic variations and risk factors of gallbladder carcinoma: a worldwide view. J Investig Genomics 2016; 3:1-7.
6. Sharma A, Sharma KL, Gupta A, Yadav A, Kumar A. Gallbladder cancer epidemiology, pathogenesis and molecular genetics: recent update. World J Gastroentero 2017; 23:3978-98.
7. Wu XS, Wang XA, Wu WG, et al. MALAT1 promotes the proliferation and metastasis of gallbladder cancer cells by activating the ERK/MAPK pathway. Cancer Biol Ther 2014; 15:806-14.
8. Cai Q, Jin L, Wang S, Zhou D, Wang J, Tang Z, Quan Z. Long non-coding RNA UCA1 promotes gallbladder cancer progression by epigenetically repressing p21 and E-cadherin expression. Oncotarget 2017; 8:47957-68.
9. Wang SH, Yang Y, Wu XC, et al. Long non-coding RNA MINCR promotes gallbladder cancer progression through stimulating EZH2 expression. Cancer Lett 2016; 380:122-33.
10. Zhang P, Cao P, Zhu X, et al. Upregulation of long non-coding RNA HOXA-AS2 promotes proliferation and induces epithelial-mesenchymal transition in gallbladder carcinoma. Oncotarget 2017; 8:33137-43.
11. Ma M, Chu B, Zhang Y, Weng M, Qin Y, Gong W, Quan Z. Long non-coding RNA CCAT1 promotes gallbladder cancer development via negative modulation of miRNA-218-5p. Cell Death Dis 2015; 6:e1583.
12. Wang SH, Wu XC, Zhang MD, Weng MZ, Zhou D, Quan ZW. Long noncoding RNA H19 contributes to gallbladder cancer cell proliferation by modulated miR-194-5p targeting AKT2. Tumor Biol 2016; 37:9721-30.
13. Cui M, You L, Ren X, Zhao W, Liao Q, Zhao Y. Long non-coding RNA PVT1 and cancer. Biochem Bioph Res Co 2016; 471:10-14.
14. Pan X, Zheng G, Gao C. LncRNA PVT1: a novel therapeutic target for cancers. Clin Lab 2018; 64:655-62.
15. Wang W, Zhou R, Wu Y, Liu Y, Su W, Xiong W, Zeng Z. PVT1 promotes cancer progression via microRNAs. Front Oncol 2019; 9:609.
16. Sternby Eilard M, Lundgren L, Cahlin C, Strandell A, Svanberg T, Sandström P. Surgical treatment for gallbladder cancer–a systematic literature review. Scand J Gastroentero 2017; 52:505-14.
17. Schmidt MA, Marcano-Bonilla L, Roberts LR.

Gallbladder cancer: epidemiology and genetic risk associations. Chinese Clin Oncol 2019; 8:31-31.
18. Yuan C, Li H, Zhu L, Liu Z, Zhou J, Shu Y. Aberrant expression of long noncoding RNA PVT1 and its diagnostic and prognostic significance in patients with gastric cancer. Neoplasma 2016; 63:442-49.
19. Cui D, Yu CH, Liu M, Xia QQ, Zhang YF, Jiang WL. Long non-coding RNA PVT1 as a novel biomarker for diagnosis and prognosis of non-small cell lung cancer. Tumor Biol 2016; 37:4127-34.
20. Pan X, Cheng R, Zhu X, Cai F, Zheng G, Li J, Gao C. Prognostic significance and diagnostic value of overexpressed lncRNA PVT1 in colorectal cancer. Clin Lab 2019; 65:2279-88.
21. Paraskevopoulou MD, Hatzigeorgiou AG. Analyzing miRNA–lncRNA interactions. In long non-coding RNAs. Humana Press, New York, 2016; 1402:271-86.
22. He Y, Chen X, Yu Y, et al. LDHA is a direct target of miR-30d-5p and contributes to aggressive progression of gallbladder carcinoma. Mol Carcinogen 2018; 57:772-83.
23. Yu X, Zhao J, He Y. Long non-coding RNA PVT1 functions as an oncogene in human colon cancer through miR-30d-5p/RUNX2 axis. J Buon 2018; 23:48-54.

BAICALEIN INHIBITS THE PROLIFERATIVE ACTIVITY OF HUMAN PROSTATE CANCER CELL LINE PC3 BY DOWNREGULATING EZRIN

S.-C. MA[1], R. CHEN[2], T.-N. YANG[2], F. ZHANG[1] and D. ZHAO[2]

[1]Department of Oncology, Donggang Branch, the First Hospital of Lanzhou University, Lanzhou, China; [2]Department of Oncology, the First Hospital of Lanzhou University, Lanzhou, China

Received March 8, 2020 – Accepted May 4, 2020

We aimed to elucidate the inhibitory effect of Baicalein on proliferative ability in Prostate cancer (PCa) through downregulating Ezrin. Relative level of Ezrin in PCa tissues and adjacent ones was detected. After PC3 cells were induced with 20 or 40 μM Baicalein, changes in viability, cell cycle progression and apoptosis were assessed. Relative levels of CyclinD1, CDK4, P53 and P21 were examined by quantitative real-time polymerase chain reaction (qRT-PCR). Regulatory effects of Ezrin and Baicalein treatment on PC3 cells were evaluated. Finally, *in vivo* effects of Ezrin and Baicalein treatment on nude mice bearing PCa were detected. Ezrin was upregulated in PCa tissues relative to adjacent normal ones. Baicalein treatment decreased viability, arrested cell cycle and stimulated apoptosis in PC3 cells. Meanwhile, Baicalein treatment downregulated CyclinD1 and CDK4, while upregulating P53 and P21. Moreover, Ezrin was downregulated in Baicalein-treated PC3 cells. Knockdown of Ezrin synergistically stimulated the effects of Baicalein on cellular phenotypes of PC3 cells. In nude mice bearing PCa, Baicalein treatment decreased tumor volume and tumor weight, which were much more pronounced in those with *in vivo* knockdown of Ezrin. Baicalein treatment suppresses proliferative ability, arrests cell cycle and stimulates apoptosis in PCa cells through downregulating Ezrin.

Prostate cancer (PCa) is a type of malignant tumor associated with male sex hormones. Its mortality ranks high, and is only second to lung cancer (1). Clinically, surgery combined postoperative chemotherapy is preferred for PCa. However, side effects and drug resistance of anti-tumor drugs remarkably restrict therapeutic efficacy. More seriously, PCa has transformed to hormone-independent type, and effective drugs are lacking (2). It is of great significance to develop novel prevention and treatment drugs for PCa. In recent years, active anti-tumor substances extracted from natural plants have been considered (3).

Baicalein is an active substance extracted from Scutellaria roots, presenting neuroprotection, anti-oxidative, anti-viral, anti-inflammatory, anti-tumoral and many other properties (4-6). Inoue et al. (7) reported the anti-proliferation capacity of Baicalein in mouse liver cancer cells. It is also capable of alleviating the growth and metastasis of many types of tumor diseases (8-11). In PCa, Guo et al. (12) demonstrated that Baicalein treatment blocks tumor growth *via* the caveolin-1/AKT/mTOR pathway.

Ezrin locates on human chromatin 6q25-6q26 (13). The relative molecular weight of Ezrin protein is ~81 kDa, which is composed of 585 amino acids

Key words: PCa; Baicalein; Ezrin; proliferation

Corresponding Author:
Da Zhao, MM
Department of Oncology, the First Hospital of Lanzhou University,
Dong Gang West Road No. 1, Lanzhou City,
Gansu Province 730000, China
Tel.: +86 013893230123
e-mail: zhuzhao19930815@163.com

0393-974X (2020)
Copyright © by BIOLIFE, s.a.s.
This publication and/or article is for individual use only and may not be further reproduced without written permission from the copyright holder.
Unauthorized reproduction may result in financial and other penalties
DISCLOSURE: ALL AUTHORS REPORT NO CONFLICTS OF INTEREST RELEVANT TO THIS ARTICLE.

(14). As an important part of the Ezrin-Radixin-Moesin protein family, Ezrin serves as a linkage between plasma membrane and actin cytoskeleton (15). Ezrin presents a key part in the complex regulatory network, thus participating in the regulation of various cellular behaviors (16, 17). As an oncogene, Ezrin is reported to be upregulated in PCa tissues and predicts the poor prognosis (18). Overexpression and phosphorylation of Ezrin results in its intracellular blockage, thus leading to loosen connections between cells and providing a favorable environment for tumor cell metastasis (19). Chuan et al. (20) suggested that androgen stimulates PC3 cells to invade through upregulating Ezrin, which is abolished by knockdown of Ezrin. It is demonstrated that Ezrin is responsible for the malignant phenotypes of PCa and it could be utilized as a therapeutic target.

In this paper, potential influences of Baicalein on proliferative and apoptotic properties of PCa were determined, as well as the involvement of Ezrin.

MATERIALS AND METHODS

Sample collection

Clinically confirmed PCa tissues and paired adjacent normal ones were surgically resected from 20 PCa patients. Tissues were repeatedly washed in PBS, frozen in liquid nitrogen and stored at -80°C. Patients and their families in this study signed informed consent forms. This study was approved by the Ethics Committee of the First Hospital of Lanzhou University, and was conducted in accordance with the Declaration of Helsinki.

Cell culture and transfection

PCa cell line PC3 (Cell Bank, Shanghai, China) was cultured in Roswell Park Memorial Institute 1640 (RPMI 1640) (HyClone, South Logan, UT, USA) containing 10% fetal bovine serum (FBS) (HyClone, South Logan, UT, USA), 2 mM L-glutamine, 100 μg/mL penicillin and 100 mg/mL streptomycin. Baicalein (Sigma-Aldrich Biotechnology, St. Louis, MO, USA) diluted in dimethyl sulfoxide (DMSO) was stored at -20°C, in te dark. On the experimental day, Baicalein was diluted to the appointed dose. Cell transfection was conducted using Lipofectamine 3000 (Invitrogen, Carlsbad, CA, USA). Transfection plasmids were constructed by GenePharma (Shanghai, China). Cells were inoculated in a 96-well plate with 1×10^5 cells/well. At the appointed time points, absorbance value at 450 nm of each sample was recorded using the CCK-8 kit (Dojindo Laboratories, Kumamoto, Japan) for plotting the viability curves. 1×10^6 cells were washed with phosphate buffered saline (PBS) twice and digested. After fixation in 70% ethanol, cells were dyed with 500 μL of Propidium Iodide (PI) at 4°C, in dark for 15 min. Finally, cell cycle distribution was analyzed.

For cell apptosis determination, cells were washed with PBS twice, digested and prepared for cell suspension with 1×10^5/mL. Cells were incubated in 1 mL of pre-cold 70% ethanol at 4°C overnight. On the other day, cells were incubated with 100 μL of RNaseA at 37°C, in dark for 30-min water bath. Subsequently, cells were dyed with 500 μL of PI at 4°C, in dark for 15 min. At last, apoptotic rate was determined at 488 nm wavelength.

Western blot

Cellular protein was isolated using radioimmunoprecipitation assay (RIPA) and electrophoresed (Beyotime, Shanghai, China). Protein sample was loaded on polyvinylidene fluoride (PVDF) membranes (Millipore, Billerica, MA, USA), which were immersed in PBS containing 5% skim milk for 2 h, reacted with primary antibodies at 4°C overnight and secondary antibodies for 2 h. Band exposure was achieved by electrochemiluminescence (ECL) and processed by Image Software (NIH, Bethesda, MD, USA).

Quantitative real-time polymerase chain reaction (qRT-PCR)

TRIzol method (Invitrogen, Carlsbad, CA, USA) was applied for isolating cellular RNA. Through reverse transcription of RNA, the extracted complementary deoxyribose nucleic acid (cDNA) was used for PCR detection by SYBR Green method at 94°C for 5-min pre-denaturation, followed by 39 cycles of denaturation-annealing-extension. Glyceraldheyde 3-phosphate dehydrogenase (GAPDH) was used as the internal reference. The primer sequences were listed as follows: Ezrin: 5'-CTCATCCAGGACATCACCCA-3' (F), 5'-TCACTCCAAGGAAAG CCAAT-3' (R); cyclinD1: 5'-TTGCTGCTATTGGAGGATCAGT-3' (F), 5'- TGGCTAAGTGAAGCATGAGGTA-3' (R); CDK4: 5'-GGAGTGAGCAATGGAGTGGC-3' (F), 5'-AAATGGGAAGGAGAAGGAGAAGC-3' (R);

p53: 5'-GTGTTTCATTAGTTCCCCACCTTGAC-3' (F), 5'-CCTGAGCAGAAGAGTTTGGA-3' (R); p21: 5'-ATGGGAGGCTGCCAGTCCTAACCC-3' (F), 5'-ACACCAGAGTGCAAGACAGC-3' (R); GAPDH: 5'-GGAGCGAGATCCCTCCAAAAT-3' (F), 5'-GGCTGTTGTCATACTTCTCATGG-3' (R).

Xenograft model

Animal procedures were approved by the Animal ethics committee of Lanzhou University Animal Center. 1×10^6 wild-type PC3 cells were subcutaneously administrated in the left groin area of each nude mice. Male nude mice 4-6 weeks old were assigned into NC group, si-Ezrin group, 20 μM Baicalein group and si-Ezrin + 20 μM Baicalein group, with 5 mice in each group. Tumor size was recorded every 5 days. Tumor volume (mm^3) = ab^2 / 2, where a and b were transverse diameter and vertical diameter of the tumor, respectively. Tumor weight was recorded after sacrifice.

Statistical analyses

Statistical Product and Service Solutions (SPSS) 22.0 (IBM, Armonk, NY, USA) was used for statistical analyses. Data were expressed as mean ± SD (standard deviation). Comparison between multiple groups was carried out using One-way ANOVA test followed by Post Hoc Test (Least Significant Difference). $P<0.05$ indicated the significant difference.

RESULTS

Ezrin was upregulated in PCa

Compared with 20 adjacent normal tissues, Ezrin was upregulated in PCa tissues (Fig. 1A). Furthermore, knockdown of Ezrin markedly decreased viability in PC3 cells (Fig. 1B), which indicated that Ezrin was of significance during the progression of PCa.

Baicalein treatment suppressed proliferation, arrested cell cycle and induced apoptosis in PCa and downregulated Ezrin

To explore potential influences of Baicalein on phenotypes of PC3 cells, they were assigned into NC group (blank control), DMSO group (negative control), 20 μM Baicalein group and 40 μM Baicalein group (21). CCK-8 assay showed that the viability in PC3 cells decreased after 24 h and 48 h treatment (Fig. 2A). Cell ratio in G1/G0 phase enhanced in PC3 cells treated with Baicalein, suggesting the arrested cell cycle progression (Fig. 2B). Apoptotic rate was elevated (Fig. 2C). Cell cycle genes and P53-related genes were detected by qRT-PCR. Cyclin D1 can promote the cell cycle from the G1 phase to the S phase. CDK4 can combine with Cyclin D1 to form a complex to advance the G1 phase of the cell cycle. It is shown that CyclinD1 and

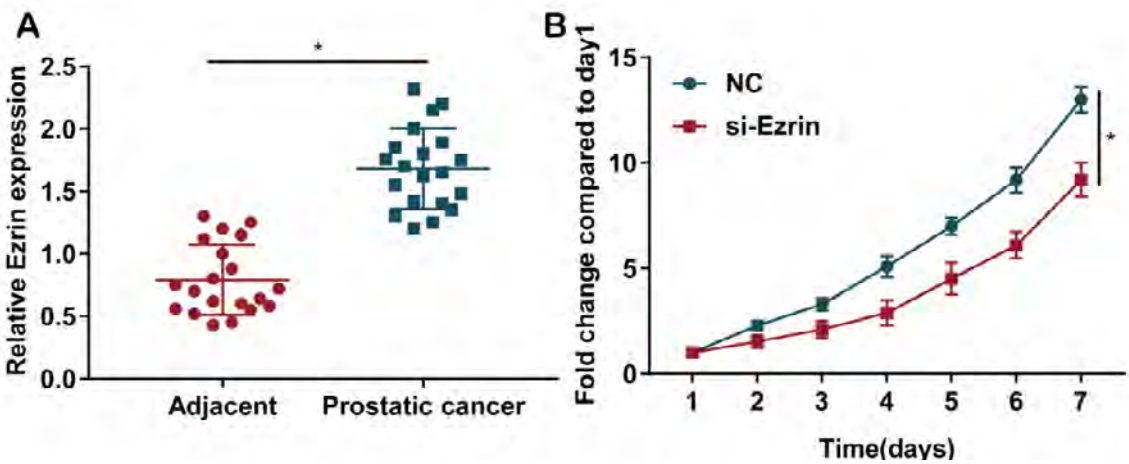


Fig. 1. *Ezrin was upregulated in PCa. **A)** Ezrin levels in PCa tissues and adjacent normal ones. **B)** Viability in PC3 cells transfected with NC or si-Ezrin.*

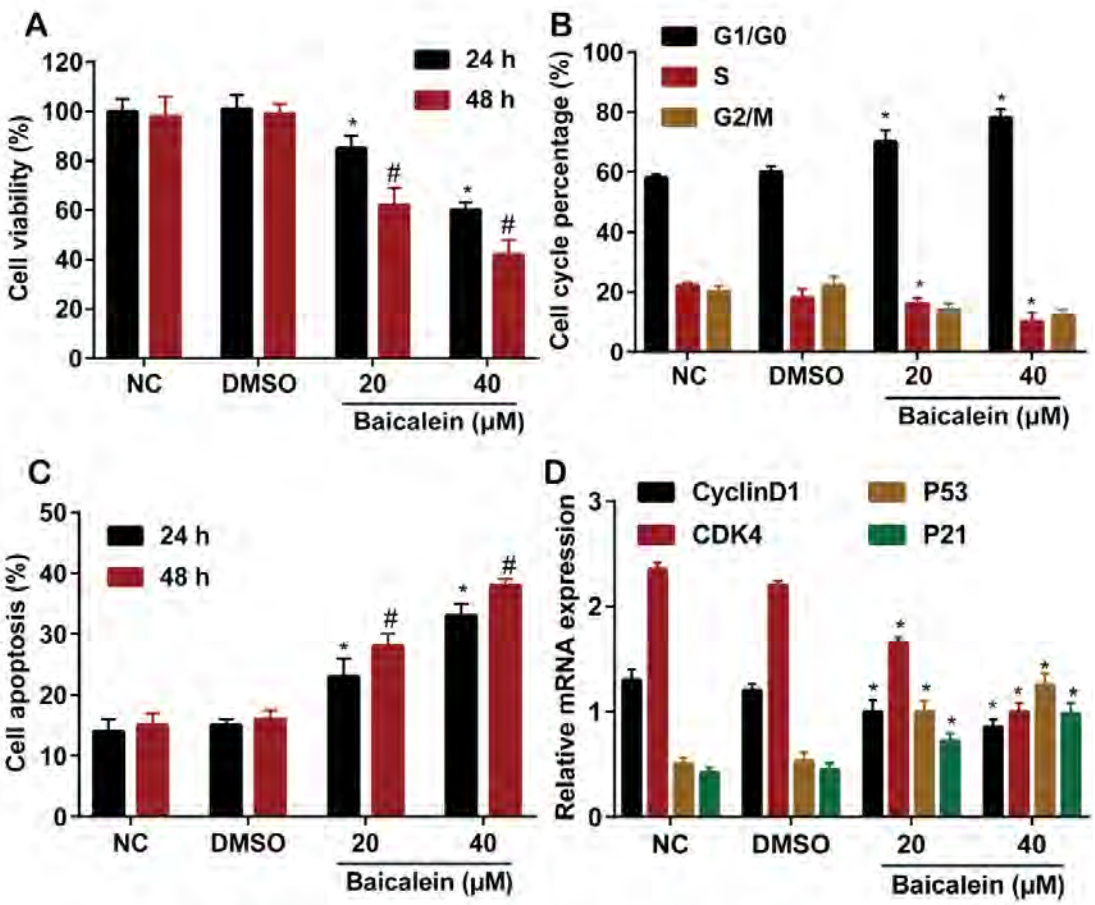


Fig. 2. *Baicalein treatment suppressed proliferation, arrested cell cycle and induced apoptosis in PCa. PC3 cells were treated with blank control (NC), DMSO, 20 μM Baicalein or 40 μM Baicalein.* ***A****) Viability at 24 h and 48 h;* ***B****) Cell cycle percentage in G1/G0, S and G2/M phase;* ***C****) Cell apoptosis;* ***D****) Relative levels of CyclinD1, CDK4, P53 and P21.*

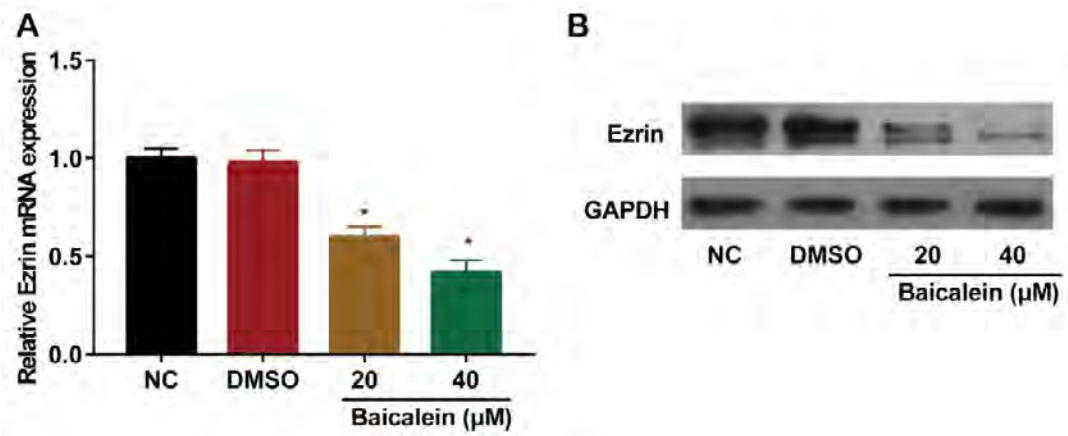


Fig. 3. *Baicalein treatment downregulated Ezrin. mRNA (****A****) and protein (****B****) levels of Ezrin in PC3 cells treated with blank control (NC), DMSO, 20 μM Baicalein or 40 μM Baicalein.*

CDK4 were downregulated, while P53 and P21 were upregulated following Baicalein treatment (Fig. 2D). Therefore, it is demonstrated that Baicalein influenced phenotypes of PCa *via* the P53 pathway.

Interestingly, both mRNA and protein levels of Ezrin were downregulated in PC3 cells treated with Baicalein compared with those treated with DMSO (Fig. 3A, B). We thereafter speculated that Ezrin was involved in Baicalein-mediated PCa progression.

Regulatory effects of Ezrin on PCa

Enhanced viability, stimulated cell cycle and inhibited apoptosis were observed in PC3 cells overexpressing Ezrin, while the opposite trends were

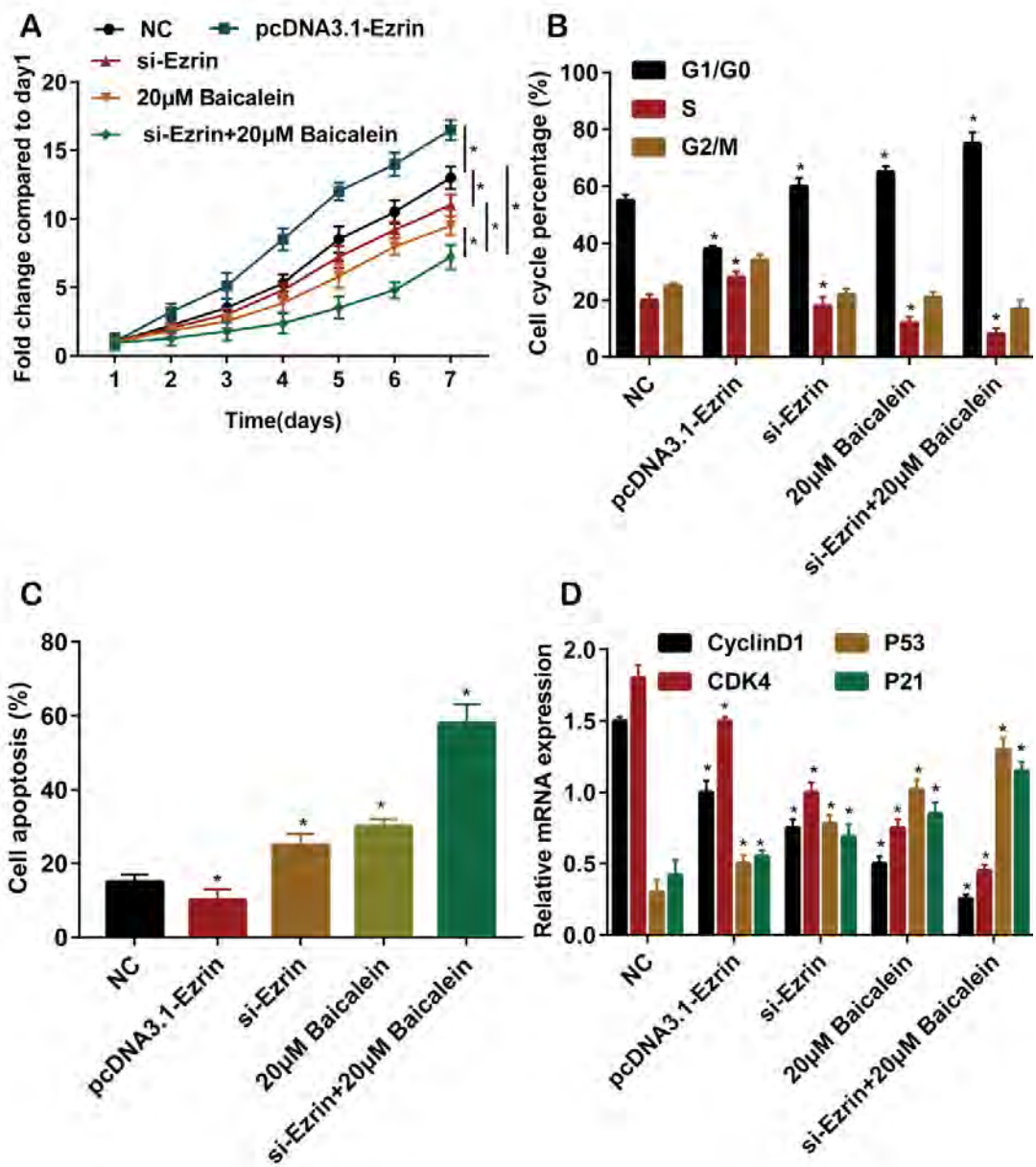


Fig. 4. *Regulatory effects of Ezrin on PCa. PC3 cells were treated with NC, pcDNA3.1-Ezrin, si-Ezrin, 20 μM Baicalein or si-Ezrin + 20 μM Baicalein.* ***A****) Viability;* ***B****) Cell cycle percentage in G1/G0, S and G2/M phase;* ***C****) Cell apoptosis;* ***D****) Relative levels of CyclinD1, CDK4, P53 and P21.*

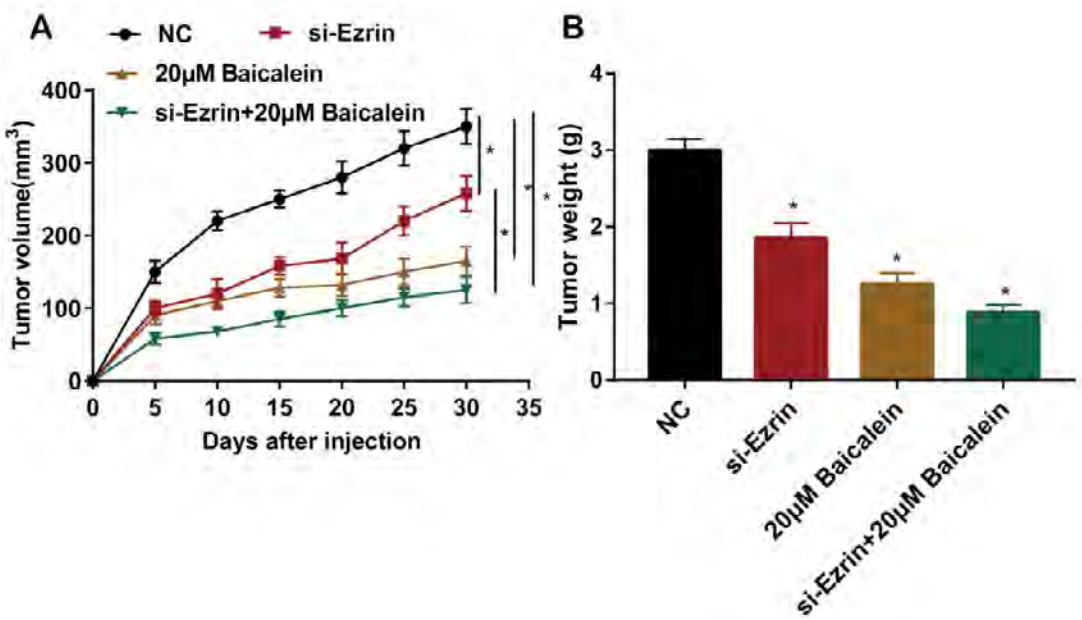


Fig. 5. *In vivo anti-tumor effects of Baicalein on PCa. Nude mice were assigned into NC group, si-Ezrin group, 20 μM Baicalein group and si-Ezrin + 20 μM Baicalein group.* ***A****) Tumor volume;* ***B****) Tumor weight.*

seen after knockdown of Ezrin. Notably, knockdown of Ezrin synergistically promoted the anti-tumor effects of Baicalein on PCa cells, manifesting as pronouncedly proliferation inhibition, cell cycle arrest and apoptosis stimulation (Fig. 4 A, C). Similarly, knockdown of Ezrin in Baicalein-treated PC3 cells markedly downregulated CyclinD1 and CDK4, as well as upregulated P53 and P21 compared with those only treated with Baicalein (Fig. 4D). We believed that the anti-tumor effects of Baicalein on PCa relied on the knockdown of Ezrin.

In vivo anti-tumor effects of Baicalein on PCa

To further clarify the *in vivo* anti-tumor effects of Baicalein on PCa, PC3 cells were subcutaneously administered into nude mice. Both knockdown of Ezrin or Baicalein application could decrease tumor volume and tumor weight. Importantly, synergic application of Baicalein and downregulated Ezrin presented much pronounced effects on narrowing down PCa tissues in mice (Fig. 5 A, B).

DISCUSSION

The incidence of PCa ranks second in male malignancies, severely threating the health and life quality of affected patients (22). During the past two decades, the incidence of PCa in China has risen (23). Surgical resection is the most effective treatment for early-stage, and for middle-stage and advanced stages, systematic immunotherapy and chemotherapy targeting metastatic tumor cells are required for improving survival (24, 25). Nevertheless, adverse event rates of these therapies are extremely high (26). Currently, natural compounds applied in tumor diseases have been considered. Our study explored the therapeutic efficacy of Baicalein on PCa through *in vivo* and *in vitro* experiments.

Baicalein is a flavonoid extracted from Scutellaria roots. It is widely used as a selective inhibitor of platelet-type 12-lipoxygenase (p12-LOX). Baicalein has anti-allergic, anti-inflammatory, anti-tumoral and other benefits (27), as well as having the

advantages of high efficiency and low toxicity. Our findings showed that Baicalein treatment suppressed proliferative ability, arrested cell cycle and stimulated apoptosis in PC3 cells. Furthermore, Baicalein treatment downregulated Ezrin and upregulated P53, thus influencing proliferative rate in PCa.

Upregulation of Ezrin is closely linked to tumor cell invasion (28-31). In PCa tissues and cell lines, Ezrin is found to be highly expressed (18, 32-34). Consistently, our data showed that Ezrin was upregulated also in PCa tissues. Tumor progression and metastasis are influenced by overexpression of Ezrin (30, 35, 36). Here, knockdown of Ezrin suppressed proliferative ability arrested cell cycle and stimulated apoptosis in PC3 cells. Notably, the synergistic effect of Baicalein and downregulated Ezrin enhanced the anti-tumor effect on PCa. In nude mice bearing PCa, similar results were obtained. Baicalein treatment and downregulated Ezrin synergistically reduced tumor volume and tumor weight in PCa mice. Baicalein treatment suppresses proliferative ability, arrests cell cycle and stimulates apoptosis in PCa cells through downregulating Ezrin.

REFERENCES

1. Fitzmaurice C, Allen C, Barber RM, et al. Global, Regional, and National Cancer Incidence, Mortality, Years of Life Lost, Years Lived With Disability, and Disability-Adjusted Life-years for 32 Cancer Groups, 1990 to 2015: A Systematic Analysis for the Global Burden of Disease Study. Jama Oncol 2017; 3:524-48.
2. Cai DW, Chen D, Sun SP, et al. Overexpression of PER3 reverses paclitaxel resistance of prostate cancer cells by inhibiting the Notch pathway. Eur Rev Med Pharmacol Sci 2018; 22:2572-79.
3. Yu H, Hou Z, Tian Y, Mou Y, Guo C. Design, synthesis, cytotoxicity and mechanism of novel dihydroartemisinin-coumarin hybrids as potential anti-cancer agents. Eur J Med Chem 2018; 151:434-49.
4. Lee W, Ku SK, Bae JS. Anti-inflammatory effects of Baicalin, Baicalein, and Wogonin in vitro and in vivo. Inflammation 2015; 38:110-25.
5. Niknami M, Vignarajan S, Yao M, et al. Decrease in expression or activity of cytosolic phospholipase A2alpha increases cyclooxygenase-1 action: A cross-talk between key enzymes in arachidonic acid pathway in prostate cancer cells. Biochim Biophys Acta 2010; 1801:731-37.
6. Chen K, Zhang S, Ji Y, et al. Baicalein inhibits the invasion and metastatic capabilities of hepatocellular carcinoma cells via down-regulation of the ERK pathway. Plos One 2013; 8:e72927.
7. Inoue T, Jackson EK. Strong antiproliferative effects of baicalein in cultured rat hepatic stellate cells. Eur J Pharmacol 1999; 378:129-35.
8. Wang L, Ling Y, Chen Y, et al. Flavonoid baicalein suppresses adhesion, migration and invasion of MDA-MB-231 human breast cancer cells. Cancer Lett 2010; 297:42-48.
9. Chiu YW, Lin TH, Huang WS, et al. Baicalein inhibits the migration and invasive properties of human hepatoma cells. Toxicol Appl Pharmacol 2011; 255:316-26.
10. Wang AM, Ku HH, Liang YC, Chen YC, Hwu YM, Yeh TS. The autonomous notch signal pathway is activated by baicalin and baicalein but is suppressed by niclosamide in K562 cells. J Cell Biochem 2009; 106:682-92.
11. Huang WS, Kuo YH, Chin CC, et al. Proteomic analysis of the effects of baicalein on colorectal cancer cells. Proteomics 2012; 12:810-19.
12. Guo Z, Hu X, Xing Z, et al. Baicalein inhibits prostate cancer cell growth and metastasis via the caveolin-1/AKT/mTOR pathway. Mol Cell Biochem 2015; 406:111-19.
13. Majander-Nordenswan P, Sainio M, Turunen O, Jaaskelainen J, Carpen O, Kere J, Vaheri A. Genomic structure of the human ezrin gene. Hum Genet 1998; 103:662-65.
14. Egerton M, Burgess WH, Chen D, Druker BJ, Bretscher A, Samelson LE. Identification of ezrin as an 81-kDa tyrosine-phosphorylated protein in T cells. J Immunol 1992; 149:1847-52.
15. Ren L, Khanna C. Role of ezrin in osteosarcoma metastasis. Adv Exp Med Biol 2014; 804:181-201.
16. Hiscox S, Jiang WG. Ezrin regulates cell-cell and cell-matrix adhesion, a possible role with E-cadherin/beta-catenin. J Cell Sci 1999; 112 Pt 18:3081-90.
17. Crepaldi T, Gautreau A, Comoglio PM, Louvard D,

Arpin M. Ezrin is an effector of hepatocyte growth factor-mediated migration and morphogenesis in epithelial cells. J Cell Biol 1997; 138:423-34.
18. Valdman A, Fang X, Pang ST, Nilsson B, Ekman P, Egevad L. Ezrin expression in prostate cancer and benign prostatic tissue. Eur Urol 2005; 48:852-57.
19. Matysiak M, Kapka-Skrzypczak L, Jodlowska-Jedrych B, Kruszewski M. EMT promoting transcription factors as prognostic markers in human breast cancer. Arch Gynecol Obstet 2017; 295:817-25.
20. Chuan YC, Pang ST, Cedazo-Minguez A, Norstedt G, Pousette A, Flores-Morales A. Androgen induction of prostate cancer cell invasion is mediated by ezrin. J Biol Chem 2006; 281:29938-48.
21. Chen Z, Hou R, Gao S, Song D, Feng Y. Baicalein Inhibits Proliferation Activity of Human Colorectal Cancer Cells HCT116 Through Downregulation of Ezrin. Cell Physiol Biochem 2018; 49:2035-46.
22. Siegel RL, Miller KD, Jemal A. Cancer statistics, 2015. CA Cancer J Clin 2015; 65:5-29.
23. Sakamoto S. Editorial Comment to Epidemiology of prostate cancer in Asian countries. Int J Urol 2018; 25:531-32.
24. Shin SW, Park JW. Ursolic acid sensitizes prostate cancer cells to TRAIL-mediated apoptosis. Biochim Biophys Acta 2013; 1833:723-30.
25. Kumar SS, Pacey S. The role of chemotherapy and new targeted agents in the management of primary prostate cancer. J Clin Urol 2016; 9:30-37.
26. Ghagane SC, Puranik SI, Nerli RB, Hiremath MB. Evaluation of in vitro antioxidant and anticancer activity of Allophylus cobbe leaf extracts on DU-145 and PC-3 human prostate cancer cell lines. Cytotechnology 2017; 69:167-77.
27. Chen FL, Wang XZ, Li JY, Yu JP, Huang CY, Chen ZX. 12-lipoxygenase induces apoptosis of human gastric cancer AGS cells via the ERK1/2 signal pathway. Dig Dis Sci 2008; 53:181-87.
28. Peng S, Fan S, Li X, et al. The expression of ezrin in NPC and its interaction with NGX6, a novel candidate suppressor. Cancer Sci 2007; 98:341-49.
29. Martin TA, Harrison G, Mansel RE, Jiang WG. The role of the CD44/ezrin complex in cancer metastasis. Crit Rev Oncol Hematol 2003; 46:165-86.
30. Hunter KW. Ezrin, a key component in tumor metastasis. Trends Mol Med 2004; 10:201-4.
31. Poullet P, Gautreau A, Kadare G, Girault JA, Louvard D, Arpin M. Ezrin interacts with focal adhesion kinase and induces its activation independently of cell-matrix adhesion. J Biol Chem 2001; 276:37686-91.
32. Harrison GM, Davies G, Martin TA, Jiang WG, Mason MD. Distribution and expression of CD44 isoforms and Ezrin during prostate cancer-endothelium interaction. Int J Oncol 2002; 21:935940.
33. Pang ST, Fang X, Valdman A, Norstedt G, Pousette A, Egevad L, Ekman P. Expression of ezrin in prostatic intraepithelial neoplasia. Urology 2004; 63:609-12.
34. Bartholow TL, Becich MJ, Chandran UR, Parwani AV. Immunohistochemical analysis of ezrin-radixin-moesin-binding phosphoprotein 50 in prostatic adenocarcinoma. Bmc Urol 2011; 11:12.
35. Fais S. A role for ezrin in a neglected metastatic tumor function. Trends Mol Med 2004; 10:249-50.
36. Curto M, McClatchey AI. Ezrin...a metastatic detERMinant? Cancer Cell 2004; 5:113-14.

KNOCKDOWN OF lncRNA HCP5 PROTECTS AGAINST CEREBRAL ISCHEMIA/ REPERFUSION INJURY BY REGULATING miR-652-3p

J-D. GAO[1], R-J. LI[2], P-L. MA[3], L-L. YU[4], J-T. LI[5] and H-T. TIAN[6]

[1]Department of Pain Clinic, Yantaishan Hospital, Yantai, Shandong Province, China; [2]Department of Pharmacy, The People's Hospital of Zhangqiu Area, Jinan, Shandong Province, China; [3]Department of Anesthesiology, Qingdao Hospital of Traditional Chinese Medicine, Qingdao Hiser Medical Group, Qingdao, Shandong Province, China; [4]Endoscopic Room, The People's Hospital of Zhangqiu Area, Jinan, Shandong Province, China; [5]ECG Room, The People's Hospital of Zhangqiu Area, Jinan, Shandong Province, China; [6]Department of Anesthesiology, Jining NO.1 People's Hospital, Affiliated Jining NO.1 People's Hospital of Jining Medical University, Jining Medical University, Jining, Shandong Province, China

Received March 9, 2020 – Accepted May 4, 2020

Previous studies have shown that lncRNAs play crucial roles in cerebral ischemia/reperfusion injury. In this study, the function and possible mechanism of lncRNA HCP5 in cerebral ischemia/reperfusion injury was investigated. An oxygen glucose deprivation (OGD) model in N2a cells was used to simulate cerebral ischemia/reperfusion injury *in vitro*. The functional mechanism of lncRNA HCP5 was detected using Trypan blue staining, JC-1, MTT and dual luciferase reporter assays. The expression of apoptosis-related proteins (Bcl-2 and Bax) was measured by Western blot analysis. We found that lncRNA HCP5 was upregulated in N2a cells treated with OGD/R, and knockdown of lncRNA HCP5 enhanced cell viability and reduced cell death. In addition, miR-652-3p was found to act as a sponge for lncRNA HCP5. The overexpression of miR-652-3p can prevent cerebral ischemic reperfusion injury, however, lncRNA HCP5 attenuated the protective effect of miR-652-3p in cerebral ischemic reperfusion injury. In conclusion, upregulation of lncRNA HCP5 may exacerbate cerebral ischemic reperfusion injury by sponging miR-652-3p.

Stroke is a common and frequently-occurring disease that seriously harms human health. It has been reported that stroke ranks second among diseases that cause death, and ranks first among diseases that cause physical disability (1). It is worth noting that ischemic stroke accounts for 80% of all strokes. Over the past few decades, the prevalence of ischemic stroke has been rising in China, especially in rural areas (2). Ischemic stroke is more common in people aged 50 to 60 years, often suffering from atherosclerosis, hypertension, rheumatic heart disease, coronary heart disease or diabetes. Patients with bad habits such as smoking and drinking are also prone to stroke (3). The mechanism of ischemic stroke in patients with brain tissue injury are ischemia and ischemia-reperfusion injury which is usually more severe (4). However, ischemia-reperfusion injury involves extremely complicates pathophysiological processes. The interaction between various influencing factors has not been

Key words: HCP5; cerebral ischemia; reperfusion injury; miR-652-3p

Corresponding Author:
Dr Haitao Tian,
Department of Anesthesiology, Jining NO.1 People's Hospital,
Affiliated Jining NO.1 People's Hospital of Jining Medical University,
Jining Medical University, Jining, 272000, Shandong Province, China.
Tel: +86 0537-2903399;
e-mail: thtdoctor@163.com

0393-974X (2020)
Copyright © by BIOLIFE, s.a.s.
This publication and/or article is for individual use only and may not be further reproduced without written permission from the copyright holder.
Unauthorized reproduction may result in financial and other penalties
DISCLOSURE: ALL AUTHORS REPORT NO CONFLICTS OF INTEREST RELEVANT TO THIS ARTICLE.

fully elucidated, therefore, it is important to explore and elucidate the pathogenesis.

At present, long noncoding RNAs (lncRNAs) are considered to have key and extensive functions in human diseases. It has been found that lncRNAs regulate various cellular processes by mediating gene expression at transcription, epigenetics and post-transcription levels (5). In particularly, many lncRNAs have been shown to regulate cerebral ischemia/reperfusion injury by affecting cell viability and apoptosis. For example, downregulation of lncRNA MEG3 restored nerve growth and alleviated nerve system damage in a rat model with cerebral ischemia-reperfusion injury (6). It was found that lncRNA AK038897 aggravated cerebral ischemia/reperfusion injury by acting as ceRNA of miR-26a-5p (7). The specific roles of lncRNA HCP5 have been found in various diseases. For example, lncRNA HCP5 promoted the progression of acute myeloid leukemia by activation of PI3K/AKT pathway (8). LncRNA HCP5 was also found to regulate the pathogenesis of childhood obesity (9). In addition, lncRNA HCP5 promoted cell proliferation and inhibited apoptosis in human granulosa-like tumor (10). However, the regulatory mechanism of lncRNA HCP5 in cerebral ischemia/reperfusion injury is still unknown.

In this study, miR-652-3p was predicted to have a binding site with lncRNA HCP5. Overexpression of miR-652-3p has been reported to inhibit cell viability and promote apoptosis in pediatric acute lymphoblastic leukemia (11), and miR-652 suppressed the malignant phenotype of glioblastoma multiforme through FOXK1-mediated AKT/mTOR signaling pathway (12). More importantly, it has been reported that miR-652 protected rats from oxidative stress induced by cerebral ischemia/reperfusion injury (13). However, the relationship between lncRNA HCP5 and miR-652-3p has not been reported in cerebral ischemia/reperfusion injury.

Therefore, the effect of lncRNA HCP5 on cell viability and apoptosis in cerebral ischemia/reperfusion injury was investigated. At the same time, the interaction between lncRNA HCP5 and miR-652-3p in cerebral ischemia/reperfusion injury was also elucidated.

MATERIALS AND METHODS

Cell culture and transfection

Mouse Neuro-2A (N2a) neuroblastoma cells and HEK293T cells (ATCC, Manassas, VA, USA) were cultured in Dulbecco's Modified Eagle Medium (DMEM) containing 10% fetal bovine serum (FBS) and incubated in an atmosphere with 5% CO_2 at 37°C. HCP5 vector and siRNA or miR-652-3p mimics and inhibitor were constructed by GenePharma (Shanghai, China). According to the experiment requirements, they were transfected into N2a or HEK293T cells using Lipofectamine 3000 reagent (Invitrogen, USA), respectively. 24 h after transfection, cells were harvested for further experiment.

OGD/R model

N2a cells were put into a deoxygenated glucose-free Hanks' Balanced Salt Solution (Invitrogen) and incubated for 3 h at 37°C in a hypoxic chamber containing 5% CO_2 and 95% N_2. After culturing for 3 h, the medium was replaced with normal medium (5% CO_2, 37°C) for different times to simulate reperfusion injury.

Cell viability

N2a cells (2000 cells/well) were seeded in 96-well plates. Next, the cells were incubated with 15 μL/well MTT solution (5 mg/mL, Sigma) at 37°C for 4 h. Cell viability was measured at 490 nm by BioRad microplate reader (Bio-Rad, Hercules, CA, United States). After 2 min. of digestion, the cells were pipette thoroughly. Trypan blue staining was used to assess cell death rates.

RT-qPCR

TRIzol reagent (Invitrogen, USA) was used to extract total RNA from N2a cells. The cDNA solution was obtained using a microRNA reverse transcription kit (Takara, Dalian, China). RT-qPCR was performed using SYBR Premix Ex TaqTM (Takara, Dalian, China). GAPDH was used as an internal control. The expression of HCP5 or miR-652-3p was quantified by the $2^{-\triangle\triangle cq}$ method.

After establishing the OGD/R model, N2a cells were incubated for 10 min with JC-1 (Beyotime, C2006, Shanghai, China) at a concentration of 10 ug/ml. The N2a cells were then washed twice in PBS. Fluorescence emission was recorded at 485 and 580 nm using a microplate reader.

Western blot analysis

N2a cells were lysed using RIPA buffer (Beyotime, Shanghai, China). Total protein concentration was measured by BCA protein assay kit (Pierce, Rockford, IL, USA). Next, protein samples (40 ug) were separated by 10% SDS-PAGE and transferred to PVDF membranes (Roche, USA). After blocking with 5% skim milk for 2 h, the membrane was incubated with Bax and Bcl-2 and GAPDH primary antibodies (Abcam, Shanghai, China) at 4°C overnight. After washing, the protein samples were incubated with a horseradish peroxidase-conjugated secondary antibody (Abcam, USA) for 2 h. Finally, the protein band was detected by ECL kit (Beyotime).

Dual luciferase reporter assay

The 3'-UTR of wild-type (WT) or mutant (mut) HCP5 with miR-652-3p binding site was inserted into pGL3 vector (Promega, Madison, WI) for dual-luciferase reporter assay. The pmirGLO luciferase reporter vectors and miR-652-3p mimics were transfected into HEK293T cells using Lipofectamine 3000 reagent. The luciferase activity was analyzed using the dual luciferase system ((Promega, USA) according to the manufacture's protocol.

Statistical analysis

Statistical analysis was performed using SPSS 19.0 and Graphpad Prism 6. The differences between groups were analyzed using one-way analysis of variance with Tukey's post hoc test and Student's *t*-test. A difference of $P < 0.05$ was considered statistically significant.

RESULTS

LncRNA HCP5 is upregulated in OGD/R model

A serum-free and glucose-free medium was used to simulate cerebral ischemic reperfusion injury. Next, N2a cells were cultured under OGD conditions for 3 h, and then treated with reperfusion at different times. MTT assay showed that cell viability gradually decreased with time (Fig. 1A). At the same time, the expression level of lncRNA HCP5 was detected in N2a cells treated with OGD/R. RT-qPCR showed that the expression of lncRNA HCP5 gradually increased with time. And the expression of lncRNA HCP5 was highest in 12 h of reperfusion (Fig. 1B). These results indicate that the abnormal expression of lncRNA HCP5 may be involved in cerebral ischemic reperfusion injury.

LncRNA HCP5 is involved in cerebral ischemic reperfusion injury

Based on the above results, N2a cells treated with OGD/R for 12 h were used to investigate the function of lncRNA HCP5 in cerebral ischemic reperfusion injury. HCP5 siRNA was transfected into N2a cells treated with OGD/R, and we found that HCP5 siRNA significantly reduced its expression in N2a cells treated with OGD/R (Fig. 2A). Functionally, Trypan blue staining results showed that cell death rate was reduced by knockdown of lncRNA HCP5 in N2a cells treated with OGD/R (Fig. 2B). The effect of lncRNA HCP5 on mitochondrial membrane potential was also measured. We found that downregulation of lncRNA HCP5 protected the potential of mitochondrial membrane under OGD/R treatment (Fig. 2C). In contrast, cell viability was found to be enhanced by knockdown of lncRNA HCP5 in N2a cells treated with OGD/R (Fig. 2D). Furthermore, Western blot analysis showed that Bax expression was decreased by lncRNA HCP5 downregulation, while Bcl-2 expression was promoted by downregulation of lncRNA HCP5 in N2a cells treated with OGD/R (Fig. 2E). In summary, knockdown of lncRNA HCP5 can enhance cell viability and reduce cell death, which indicates that knockdown of lncRNA HCP5 may protect N2a cells from cerebral ischemic reperfusion injury.

MiR-652-3p serves as a sponge of lncRNA HCP5

In addition, downstream targets of lncRNA HCP5 were searched in starBase database (http://starbase.sysu.edu.cn). It was predicted that miR-652-3p has a binding site to lncRNA HCP5 (Fig. 3A). To confirm this prediction, a dual-luciferase reporter assay was performed in HEK293T cells. MiR-652-3p mimics were found to reduce wt-HCP5 luciferase activity, but had little effect on that of mut-HCP5 in HEK293T cells (Fig. 3B), which indicates that lncRNA HCP5 can directly bind miR-652-3p. In addition, upregulation of lncRNA HCP5 suppressed miR-652-3p expression, while downregulation of lncRNA HCP5 enhanced miR-652-3p expression in N2a cells

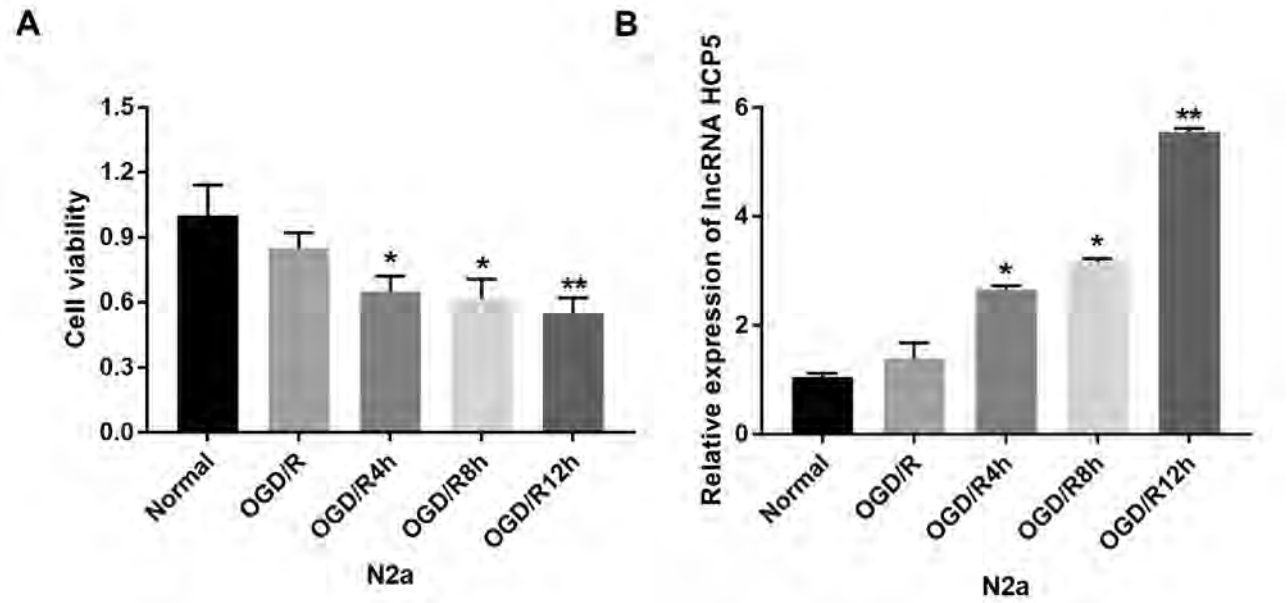


Fig. 1. *LncRNA HCP5 is upregulated in OGD/R model. **A**) The cell viability was detected in OGD N2a cells with different time course of reperfusion. **B**) LncRNA HCP5 expression was measured in N2a cells treated with different time OGD/R. *P < 0.05, **P < 0.01*

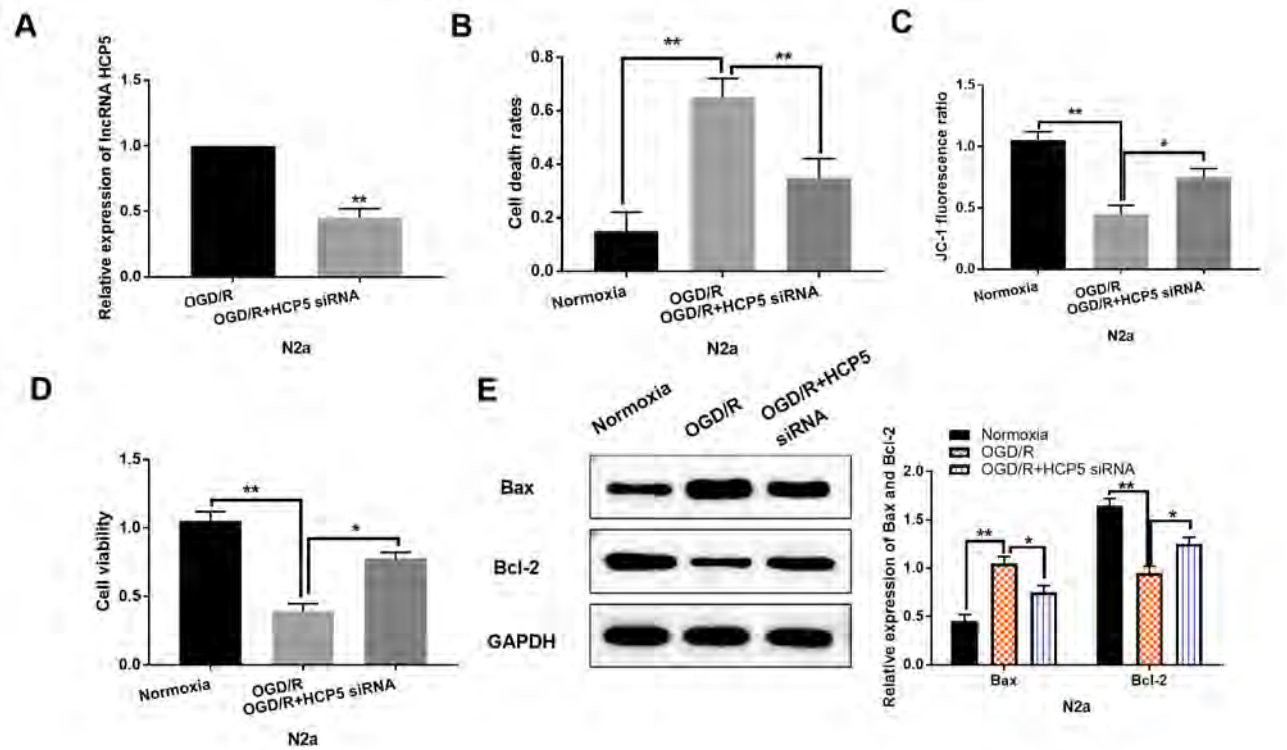


Fig. 2. *LncRNA HCP5 is involved in cerebral ischemic reperfusion injury. **A**) Knockdown of lncRNA HCP5 expression was identified in N2a cells treated with OGD/R and siRNA. **B**) Knockdown of HCP5 reduced cell death rates in N2a cells treated with OGD/R. **C**) Knockdown of HCP5 protected mitochondrial membrane potential in N2a cells treated with OGD/R. **D**) Cell viability was detected in N2a cells treated with OGD/R and HCP5 siRNA. **E**) Bax/Bcl-2 expression was detected in N2a cells treated with OGD/R and HCP5 siRNA. *P < 0.05, ** P <0.01*

(Fig. 3C). Furthermore, the expression of lncRNA HCP5 was reduced by miR-652-3p overexpression and promoted by miR-652-3p downregulation in N2a cells (Fig. 3D). These results indicate that miR-652-3p acts as a sponge for lncRNA HCP5, and reciprocal inhibition between lncRNA HCP5 and miR-652-3p expression was found in N2a cells.

Upregulation of lncRNA HCP5 aggravates cerebral ischemic reperfusion injury by regulating miR-652-3p

To investigate the interaction between lncRNA HCP5 and miR-652-3p in cerebral ischemic reperfusion injury, rescue experiment was performed in N2a cells treated with OGD/R. First, RT-qPCR showed that miR-652-3p was downregulated in N2a cells treated with OGD/R compared to the Normoxia group (Fig. 4A). Then, miR-652-3p mimics or miR-652-3p mimics+HCP5 vector were transfected into N2a cells treated with OGD/R. We found that miR-652-3p mimics significantly increased its expression, while HCP5 vector reduced this increased expression of miR-652-3p (Fig. 4A). Functionally, miR-652-3p overexpression reduced cell death rates. After transfection with HCP5 vector, cell death rate increased again in N2a cells treated with OGD/R (Fig. 4B). At the same time, cell viability was enhanced by miR-652-3p overexpression, and the increased cell viability was reduced by HCP5 upregulation in N2a cells treated with OGD/R (Fig. 4C). In addition, the protective effect of miR-652-3p overexpression on mitochondrial membrane potential was also weakened by HCP5 upregulation in N2a cells treated with OGD/R (Fig. 4D). The effect of miR-652-3p on apoptosis markers Bax and Bcl-2 was also detected. We found that miR-652-3p overexpression reduced Bax expression and promoted Bcl-2 expression in N2a cells treated with OGD/R. The HCP5 vector could reverse the effect of miR-652-3p on Bax and Bcl-2 expression (Fig. 4E). These results indicate that miR-652-3p overexpression can reduce cerebral

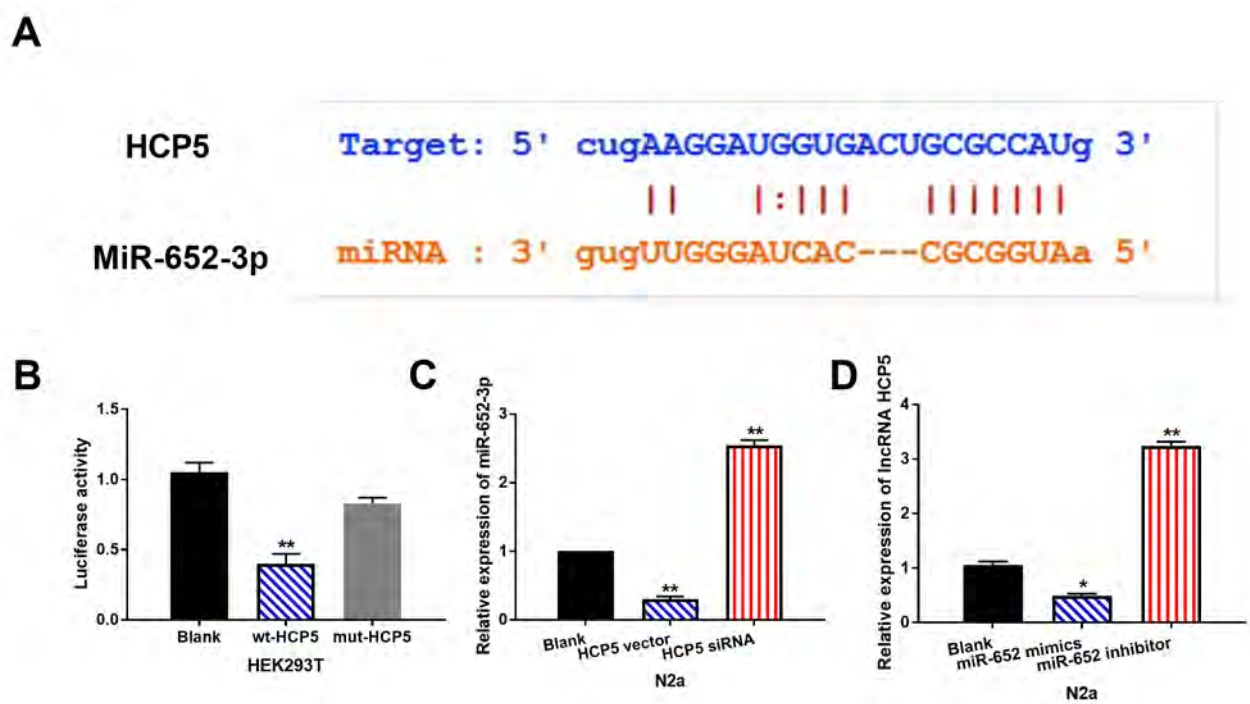


Fig. 3. *MiR-652-3p serves as a sponge of lncRNA HCP5.* ***A****) The binding sites between lncRNA HCP5 and miR-652-3p.* ***B****) Luciferase reporter assay* ***C****) MiR-652-3p expression was detected in N2a cells with HCP5 vector or siRNA.* ***D****) HCP5 expression was measured in N2a cells with miR-652-3p mimics or inhibitor. *P < 0.05, ** P <0.01*

ischemic reperfusion injury. However, lncRNA HCP5 can attenuate the protective effect of miR-652-3p on cerebral ischemic reperfusion injury.

DISCUSSION

In recent years, it has been found that an increasing number of lncRNAs play important roles in cerebral ischemic reperfusion injury. For example, lncRNA MEG3 was found to be upregulated in cerebral ischemia reperfusion injury. And upregulation of MEG3 promoted cerebral ischemia reperfusion injury by regulating miR-485/AIM2 axis (14). In addition, lncRNA H19 was found to induce cerebral ischemia reperfusion injury through autophagy activation (15). In this study, upregulation of lncRNA HCP5 was also identified in cerebral ischemia reperfusion injury, and upregulation of lncRNA HCP5 inhibited cell viability and promoted cell death in cerebral ischemia reperfusion injury. This indicates that knockdown of lncRNA HCP5 can prevent cerebral ischemia reperfusion injury. The role of lncRNA HCP5 in cerebral ischemia reperfusion injury is firstly reported in this study, which has not been investigated in previous studies.

The regulatory mechanism of lncRNA HCP5 has been extensively investigated in human cancers. Upregulation of lncRNA HCP5 has been detected in cervical cancer and colorectal cancer (16, 17). Functionally, knockdown of HCP5 was found to inhibit the malignant behavior of glioma cells (18). These results indicate that lncRNA HCP5 may be related to cerebral injury. In addition, HCP5 has been reported to be a cancer-suppressive lncRNA

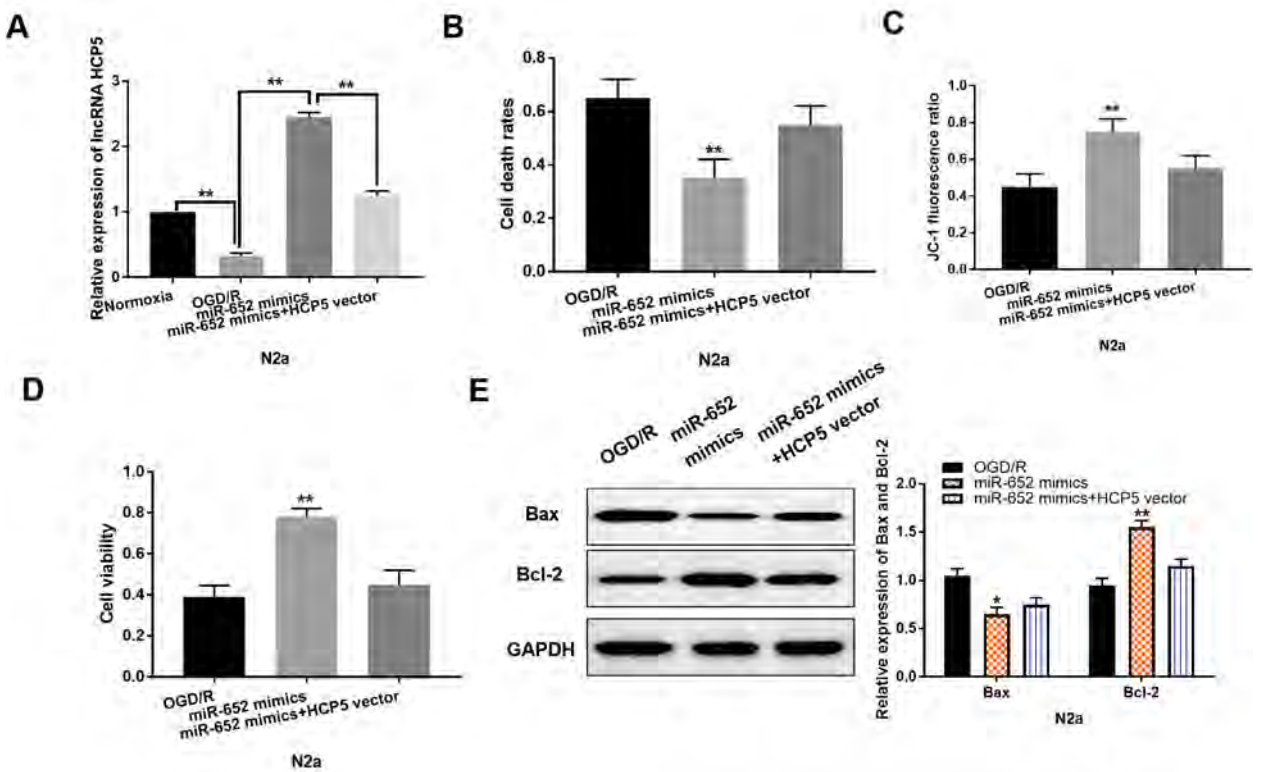


Fig. 4. *Upregulation of lncRNA HCP5 aggravates cerebral ischemic reperfusion injury by regulating miR-652-3p.* ***A)*** *MiR-652-3p expression was identified in N2a cells with miR-652-3p mimics or miR-652-3p mimics+HCP5 vector.* ***B)*** *Cell death rates in N2a cells with miR-652-3p mimics or miR-652-3p mimics+HCP5 vector.* ***C)*** *Mitochondrial membrane potential in N2a cells with miR-652-3p mimics or miR-652-3p mimics+HCP5 vector.* ***D)*** *Cell viability was detected in N2a cells with miR-652-3p mimics or miR-652-3p mimics+HCP5 vector.* ***E)*** *Bax/Bcl-2 expression was detected in N2a cells with miR-652-3p mimics or miR-652-3p mimics+HCP5 vector. *P < 0.05, ** P <0.01*

in skin cutaneous melanoma. Overexpression of HCP5 inhibited skin cutaneous melanoma cell malignancy possibly by sponging miR-1286 (19). This indicates that the expression and function of lncRNA HCP5 depend on the type of diseases. In this study, increased expression of lncRNA HCP5 was detected in N2a cells treated with OGD/R. We found that lncRNA HCP5 can aggravate cerebral ischemia reperfusion injury.

In addition, many studies have shown that lncRNA HCP5 is involved in human diseases by regulating miRNAs. For example, lncRNA HCP5 promoted the progression of triple negative breast cancer by sponging miR-219a-5p (20). In this study, lncRNA HCP5 directly binds to miR-652-3p. Reciprocal inhibition between lncRNA HCP5 and miR-652-3p expression was found in N2a cells. In addition, miR-652-3p was downregulated in N2a cells treated with OGD/R, and overexpression of miR-652-3p can prevent cerebral ischemia/reperfusion injury. Consistent with our results, miR-652 has been reported to protect rats from oxidative stress during cerebral ischemia/reperfusion injury (13). More importantly, lncRNA HCP5 was found to attenuate the protective effect of miR-652-3p in cerebral ischemic reperfusion injury. It indicates that upregulation of lncRNA HCP5 may aggravate cerebral ischemic reperfusion injury by downregulating miR-652-3p.

In conclusion, lncRNA HCP5 is upregulated and aggravates cerebral ischemic reperfusion injury, and overexpression of miR-652-3p can reduce cerebral ischemic reperfusion injury. More importantly, upregulation of lncRNA HCP5 can exacerbate cerebral ischemic reperfusion injury by making miR-652-3p sponge. This study may provide a novel target for inhibiting or reversing cerebral ischemia/reperfusion injury.

ACKNOWLEDGEMENTS

This study is supported by Key Research and Development Projects in Shandong (2018GSF118216) and Development Plan of Medical and Health Science and Technology in Shandong province (2017WS524).

REFERENCES

1. Craig LE, McInnes E, Taylor N, et al. Identifying the barriers and enablers for a triage, treatment, and transfer clinical intervention to manage acute stroke patients in the emergency department: a systematic review using the theoretical domains framework (TDF). Implement Sci 2016; 11:157.
2. Ritzel RM, Lai YJ, Crapser JD, et al. Aging alters the immunological response to ischemic stroke. Acta Neuropathol 2018; 136:89-110.
3. Wu R, Li X, Xu P, et al. TREM2 protects against cerebral ischemia/reperfusion injury. Mol Brain 2017; 10:20.
4. Yang Z, Weian C, Susu H, Hanmin W. Protective effects of mangiferin on cerebral ischemia-reperfusion injury and its mechanisms. Eur J Pharmacol 2016; 771:145-51.
5. Prensner JR, Chinnaiyan AM. The emergence of lncRNAs in cancer biology. Cancer Discov 2011; 1:391-407.
6. You D, You H. Repression of long non-coding RNA MEG3 restores nerve growth and alleviates neurological impairment after cerebral ischemia-reperfusion injury in a rat model. Biomed Pharmacother 2019; 111:1447-57.
7. Wei R, Zhang L, Hu W, Wu J, Zhang W. Long non-coding RNA AK038897 aggravates cerebral ischemia/reperfusion injury via acting as a ceRNA for miR-26a-5p to target DAPK1. Exp Neurol 2019; 314:100-10.
8. Lei M, Jingjing Z, Tao J, et al. LncRNA HCP5 promotes LAML progression via PSMB8-mediated PI3K/AKT pathway activation. Naunyn Schmiedebergs Arch Pharmacol 2019.
9. Chen R, Xin G, Zhang X. Long non-coding RNA HCP5 serves as a ceRNA sponging miR-17-5p and miR-27a/b to regulate the pathogenesis of childhood obesity via the MAPK signaling pathway. J Pediatr Endocrinol Metab 2019; 32:1327-39.
10. Chen Y, Zhang X, An Y, Liu B, Lu M. LncRNA HCP5 promotes cell proliferation and inhibits apoptosis via miR-27a-3p/IGF-1 axis in human granulosa-like tumor cell line KGN. Mol Cell Endocrinol 2020; 503:110697.
11. Jiang Q, Lu X, Huang P, et al. Expression of miR-652-3p and effect on apoptosis and drug sensitivity

in pediatric acute lymphoblastic leukemia. Biomed Res Int 2018; 2018:5724686.
12. Yang H, Song Z, Wu X, Wu Y, Liu C. MicroRNA-652 suppresses malignant phenotypes in glioblastoma multiforme via FOXK1-mediated AKT/mTOR signaling pathway. Onco Targets Ther 2019; 12:5563-75.
13. Zuo ML, Wang AP, Song GL, Yang ZB. miR-652 protects rats from cerebral ischemia/reperfusion oxidative stress injury by directly targeting NOX2. Biomed Pharmacother 2020; 124:109860.
14. Liang J, Wang Q, Li JQ, Guo T, Yu D. Long non-coding RNA MEG3 promotes cerebral ischemia-reperfusion injury through increasing pyroptosis by targeting miR-485/AIM2 axis. Exp Neurol 2020; 325:113139.
15. Wang J, Cao B, Han D, Sun M, Feng J. Long Non-coding RNA H19 induces cerebral ischemia reperfusion injury via activation of autophagy. Aging Dis 2017; 8:71-84.
16. Yu Y, Shen HM, Fang DM, Meng QJ, Xin YH. LncRNA HCP5 promotes the development of cervical cancer by regulating MACC1 via suppression of microRNA-15a. Eur Rev Med Pharmacol Sci 2018; 22:4812-19.
17. Yang C, Sun J, Liu W, et al. Long noncoding RNA HCP5 contributes to epithelial-mesenchymal transition in colorectal cancer through ZEB1 activation and interacting with miR-139-5p. Am J Transl Res 2019; 11:953-63.
18. Teng H, Wang P, Xue Y, et al. Role of HCP5-miR-139-RUNX1 feedback loop in regulating malignant behavior of glioma cells. Mol Ther 2016; 24:1806-22.
19. Wei X, Gu X, Ma M, Lou C. Long noncoding RNA HCP5 suppresses skin cutaneous melanoma development by regulating RARRES3 gene expression via sponging miR-12. Onco Targets Ther 2019; 12:6323-35.
20. Wang L, Luan T, Zhou S, et al. LncRNA HCP5 promotes triple negative breast cancer progression as a ceRNA to regulate BIRC3 by sponging miR-219a-5p. Cancer Med 2019; 8:4389-403.

PI3K/Akt AND ERK1/2 PATHWAYS ARE RESPONSIBLE FOR SODIUM BUTYRATE-INDUCED INHIBITION OF NEURONAL APOPTOSIS IN RATS WITH CEREBRAL INFARCTION

T.-N. ZHAO[1], L.-D. YUAN[2], L.-X. CHEN[2], Y. YUAN[2] and D.-L. CAI[2]

[1]The Second Department of Pediatric, The First Affiliated Hospital of Jiamusi University, Jiamusi, China; [2]Department of Geratology, The First Affiliated Hospital of Jiamusi University, Jiamusi, China

Received January 27, 2020 – Accepted May 5, 2020

The aim of this study was to elucidate the neuronal protection effect of sodium butyrate (NaB) on neuronal apoptosis in rats with cerebral infarction (CI), and the involvement of the phosphatidilinositol 3-kinase/protein kinase B (PI3K/Akt) and extracellular-signal-regulated kinase 1/2 (ERK1/2) pathways. MI model in rats was performed by middle cerebral artery occlusion (MCAO). Three hours after reperfusion, gastric administration of 5 or 10 mg/kg NaB was performed. Neurological deficit score, infarct size and brain edema were evaluated in rats after 24 h of reperfusion. Enzyme-linked immunosorbent assay (ELISA) was conducted to determine contents of oxidative stress factors. Lactate dehydrogenase (LDH) activity, cell viability and apoptosis in extracted neurons were determined. Moreover, expression levels of Bcl-2, Bax, Akt and ERK1/2 were examined. NaB treatment markedly reduced infarct size and brain edema content in CI rats, and NaB treatment improved viability, decreased LDH activity and reversed contents of malondialdehyde (MDA) and superoxide dismutase (SOD) in a dose-dependent manner. In addition, NaB treatment dose-dependently reduced apoptotic rate and Bax level, as well as enhanced Bcl-2 level. Protein levels of Akt and ERK1/2 were markedly upregulated in NaB-treated neurons. NaB treatment alleviates neuronal apoptosis *via* the PI3K/Akt and ERK1/2 pathways in CI rats, thus protecting the deterioration of CI.

Cerebral infarction (CI), also known as cerebral ischemic stroke, is a common cerebrovascular disease affecting the elderly. CI accounts for 60-80% of stroke cases, manifesting as acute onset, rapid progression and high disability and mortality (1, 2). Restoring blood oxygenation in ischemic brain tissues in time is the key factor in CI treatment. Nevertheless, cerebral ischemia/reperfusion injury (IRI) during the process of vascular reflow further aggravates brain damage (3, 4). It has been reported that inflammatory response, mitochondrial dysfunction, excitotoxicity and oxidative stress are the major pathogenetic factors for CI (5-8). Neuronal apoptosis post-CI is the leading cause of neuronal death (9). Effective prevention of neuronal apoptosis is of major importance in the treatment of IRI.

Sodium butyrate (NaB), an inhibitor of histone deacetylase, has previously been shown to have anti-inflammatory effects. NaB effectively downregulates HMGB1 in a CI model (10, 11). It is demonstrated that NaB is able to alleviate inflammatory response and neuronal apoptosis in brain diseases (12). A

Key words: NaB; PI3K/Akt; ERK1/2; CI; neuronal apoptosis

Corresponding Author:
Dongliang Cai, MM.
Department of Geratology, The First Affiliated Hospital of Jiamusi University, 438 Dexiang Street, Jiamusi, Heilongjiang, 154002, China
Tel.: +86 018946720813
e-mail: donglan19660417@163.com

0393-974X (2020)
Copyright © by BIOLIFE, s.a.s.
This publication and/or article is for individual use only and may not be further reproduced without written permission from the copyright holder. Unauthorized reproduction may result in financial and other penalties
DISCLOSURE: ALL AUTHORS REPORT NO CONFLICTS OF INTEREST RELEVANT TO THIS ARTICLE.

recent study illustrated that NaB improves cerebral IRI through antioxidant, anti-inflammatory and anti-apoptotic properties (13). NaB has been widely used in many diseases. Chen et al. (14) reported that NaB contributes to relieve uveitis, and Li et al. (15) demonstrated that NaB protects acute lung injury in LPS-induced mice by inhibiting HMGB1 release. Neuronal apoptosis is the key event leading to neuronal death following cerebral IRI (16). phosphatidilinositol 3-kinase (PI3K) is a conversed signal transduction enzyme involved in regulating cell apoptosis and survival (17). Functionally, PI3K and its downstream protein kinase B (PKB) could regulate multiple cell behaviors (18). The activation of PI3K/Akt has been identified to prevent neuronal apoptosis following IRI (19, 20). The extracellular-signal-regulated kinase (ERK) pathway follows a three-level kinase cascade of mitogen-activated protein kinase (MAPK). Once cell membrane is stimulated by external factors, receptor tyrosinases or G protein-coupled receptors are activated, which in turn trigger phosphorylation and nuclear translocation of ERK. Thus, phosphorylated ERK exerts biological functions by activating its downstream transcription factors (21). It is previously reported that ERK1/2 pathway is activated following CI, presenting neuroprotective effects on triggering neuronal repair (22, 23).

In this study, we constructed CI model in rats by middle cerebral artery occlusion (MCAO), and the protective effects of NaB on CI were further analyzed.

MATERIALS AND METHODS

Experimental animals

Male Sprague Dawley rats weighing 200-250 g were provided by Jiangsu Laboratory Animal Center. Rats were habituated for at least one week in a standard environment at 25°C and 12 h light/dark cycle. They had free access to food and water. This experiment was approved by the Ethics Committee of Jiamusi University Animal Center.

MCAO rat model

Common carotid artery, external carotid artery and internal carotid artery were exposed in avoidance of touching vagus. External carotid artery was closely ligated at the carotid bifurcation, and a temporary clamp was placed on the common carotid artery. A nylon monofilament (0.26 mm in external diameter) was inserted from the carotid bifurcation and pushed forward for about 18 mm, and thus the middle cerebral artery was occluded. Two hours after MCAO, blood reperfusion was performed by relaxing the clamp. After suturing the incision, rats were placed on a heating pad to maintain the body temperature at 37.0±0.5°C. Rats in the sham group received the same procedures except for insertion of the nylon monofilament.

Medicine administration and rat grouping

NaB (Sigma, Co. Ltd., USA; purity≥99%) was dissolved in saline. Three hours after reperfusion, gastric administration of 5 or 10 mg/kg NaB was performed. Rats were assigned into: Sham group (n=12), model group (n=12), 5 mg/kg NaB group (n=12) and 10 mg/kg NaB group (n=12). Rats in sham group and control group were administered the same volume of saline.

Assessment of neuronal deficit

Assessment of neuronal deficit after 24 h of reperfusion was conducted based on the procedures proposed by Hu et al. (24). Neuronal deficit score ranged from 0-5 (0: no visible deficits; 1: Forelimb flexion; 2: Forelimb flexion and reduction of transverse pushing resistance; 3: Forelimb flexion, reduction of lateral pushing resistance and unilateral circling; 4. Forelimb flexion and unable or difficult to walk). A higher score indicated worse neuronal deficit.

After anesthesia, the rats were sacrificed and their brains were collected and frozen at -20°C for 30 min then sliced into 2 mm coronal sections, which were subsequently stained in 2% TTC (pH7.4) and fixed in 10% formalin. Infarct size (pale region) was recorded by ImageJ software (NIH, Bethesda, MD, USA).

Brain tissues of rats were placed in pre-weighed tinfoil (A), and weighed (B). Wet weight = B-A. Tissues were then wrapped in the tinfoil, dried at 100°C for 24 h and weighed (C). Dry weight = C-A. Finally, brain edema (%) = (wet weight - dry weight) / wet weight × 100%.

Cells were inoculated in a 96-well plate. At the appointed time points, absorbance value at 450 nm of each sample was recorded using the CCK-8 kit (Dojindo

Laboratories, Kumamoto, Japan) for plotting the viability curves. Each experiment was repeated in triplicate.

LDH activity in culture medium was examined as previously described (25). After specific treatment, culture medium of neurons was collected and subjected to LDH activity determination using the commercial kit (Jiancheng, Nanjing, China).

Brain tissues were homogenated and subjected to measurement of malondialdehyde (MDA) and superoxide dismutase (SOD) activities using the Enzyme-linked immunosorbent assay (ELISA) (Jiancheng, Nanjing, China). Detected values were normalized to those of protein levels.

Brain sections were fixed in 10% formalin for 1 h, and incubated in methanol containing 3% H_2O_2 for 10 min. After washing in DPBS, sections were incubated in 0.5% Triton X-100 for 2 min. Subsequently, sections were dyed in TUNEL solution (Nazyme Biotech, Nanjing, China) and 4',6-diamidino-2-phenylindole (DAPI) (Beyotime, Shanghai, China) for 2 min. TUNEL-positive cells were captured and calculated (magnification 400×).

Quantitative real-time polymerase chain reaction (RT-qPCR)

Total RNAs were extracted from neurons and their concentration and purity were assessed using Nanodrop (Thermo Fisher Scientific, Waltham, MA, USA). RNAs with optical density (OD)260/280>1.8 were reversely transcribed into complementary deoxyribose nucleic acids (cDNAs), which were applied for qRT-PCR at 95°C for 5 min, 94°C for 30 min, and 40 cycles at 94°C for 5 min, 60°C for 15 min and 72°C for 10 min. β-actin was the internal references. Relative level was calculated using $2^{-\Delta\Delta Ct}$. Each experiment was repeated in triplicate.

Bax:F: 5'-GTGGCGGGACATAGTCAGCA-3', R: 5'-CCCATTGGGACAGCTTGGA-3';

Bcl-2:F: 5'-AACCTTCCTTCCTGCTTGAG-3',R: 5'-TGCTGTTCCTCTTCCAACG-3';

GAPDH:F: 5′- TCGGAGTCAACGGATTTGGT-3′, R: 5′-TTCCCGTTCTCAGCCTTGAC-3′.

Western blot

Tissues were homeogenated for extracting proteins. After concentration determination, protein samples were loaded on polyvinylidene fluoride (PVDF) membranes (Millipore, Billerica, MA, USA). Subsequently, non-specific antigens were blocked in 5% skim milk for 2 h. Membranes were then incubated with primary and secondary antibodies. Band exposure and grey value analysis were finally conducted.

Statistical analysis

Statistical Product and Service Solutions (SPSS) 22.0 (IBM, Armonk, NY, USA) was used for all statistical analysis. Data were expressed as mean ± SD (standard deviation). Comparison between multiple groups was made using One-way ANOVA test followed by Post Hoc Test (Least Significant Difference). $P<0.05$ indicated the significant difference.

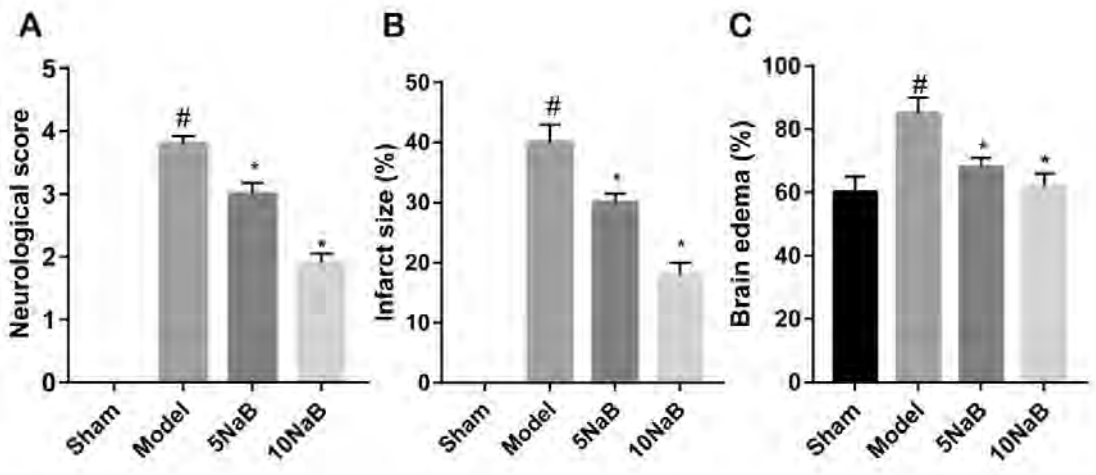


Fig. 1. *NaB treatment improved neuronal dysfunction and cerebral infarct in CI rats. Neurological deficit score (**A**), infarct size (**B**) and brain edema (**C**) in rats of sham group, model group, 5 mg/kg NaB group and 10 mg/kg NaB group.*

RESULTS

NaB treatment improved neuronal dysfunction and cerebral infarct in CI rats

Pronounced neurological deficit, infarct tissue and brain edema were observed in rats of the model group compared to those in sham group, verifying the successful construction of CI model in rats. Notably, lower neurological deficit score (Fig. 1A), smaller infarct size (Fig. 1B) and less brain edema (Fig. 1C) were observed in rats of NaB group than those in model group. The above changes were dose-dependent on NaB concentration.

Neuroprotective effects of NaB

Compared with model group, LDH activity was dose-dependently decreased in 5 mg/kg NaB group and 10 mg/kg NaB group (Fig. 2A), while cell viability was dose-dependently enhanced (Fig. 2B). In addition, CI rats presented decreased SOD level and increased MDA level compared to those in sham group, and furthermore, NaB treatment dose-dependently alleviated these trends (Fig. 2 C, D).

Protective effect of NaB on neuronal apoptosis following CI

TUNEL assay uncovered pronounced apoptosis occurred following CI. In addition, TUNEL-positive cell numbers were markedly reduced after NaB treatment (Fig. 3A). Protein and mRNA levels of Bax were upregulated after CI, which were dose-dependently reduced by NaB treatment (Fig. 3 B,

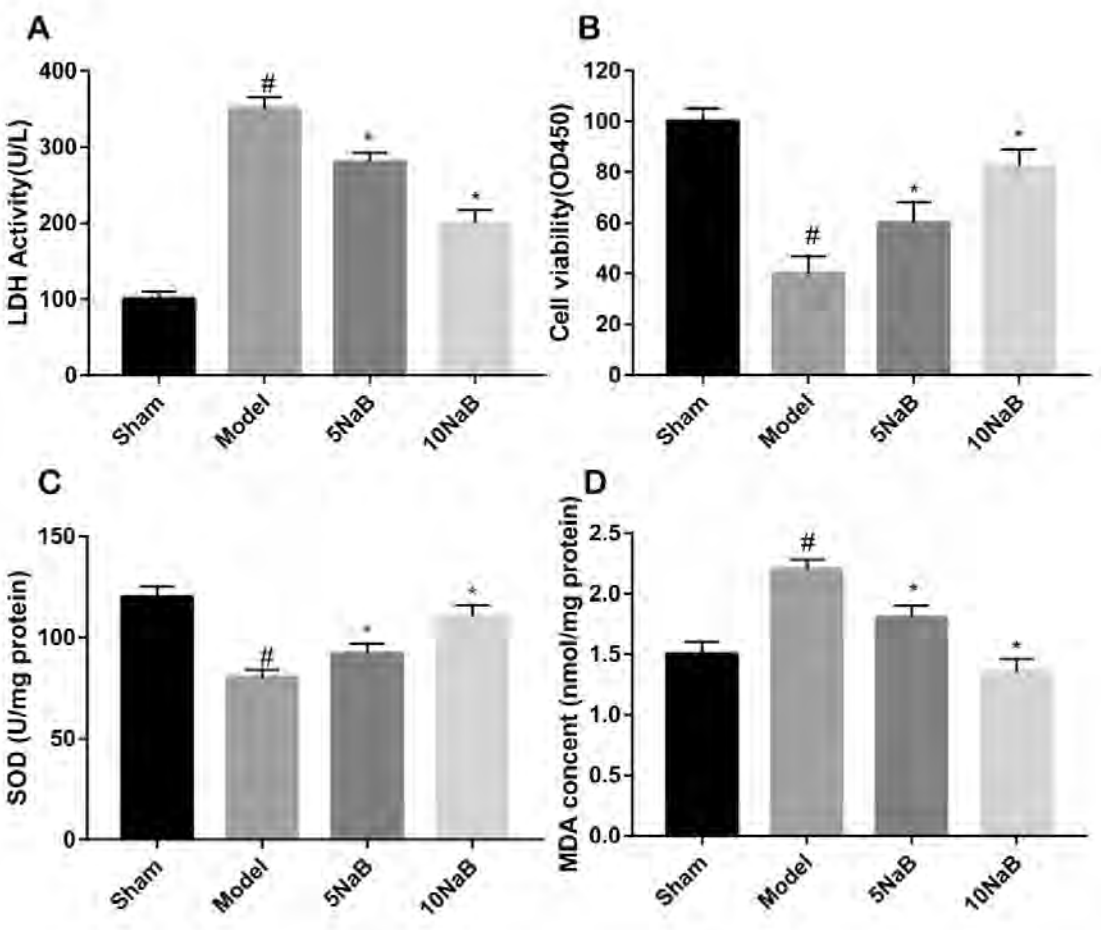


Fig. 2. *Neuroprotective effects of NaB. LDH activity (**A**), cell viability (**B**), SOD level (**C**) and MDA content (**D**) in rats of sham group, model group, 5 mg/kg NaB group and 10 mg/kg NaB group.*

C). NaB reversed the downregulated Bcl-2 at post-CI (Fig. 3 B, D). Hence, NaB effectively protected neurons from apoptotic stimulation at post-CI.

Akt and ERK1/2 pathways were responsible for the neuroprotective effect of NaB

Interestingly, protein levels of p-Akt (Fig. 4A) and p-ERK1/2 (Fig. 4B) were markedly downregulated in CI rats compared to those in sham group. However, NaB treatment greatly enhanced their levels in a dose-dependent way. It is suggested that Akt and ERK1/2 pathways were responsible for the neuroprotective effect of NaB.

DISCUSSION

CI is the major reason for stroke-induced death (26, 27). Acute focal cerebral ischemia, cerebrovascular epithelium damage, dysfunctional blood brain barrier and neuronal apoptosis are the basic pathological features of CI (28). Notably, cerebral IRI leads to secondary damage following CI. Target drugs on the prevention and treatment of cerebral IRI are urgently needed.

MCAO is a commonly applied method in the construction of *in vivo* CI model (29). Our findings uncovered that rats undergoing MCAO had higher neurological deficit scores, pronounced infarct tissues and brain edema, which were consistent to previous results (13). Notably, these CI lesions were dose-dependently relieved by NaB treatment. Furthermore, NaB treatment improved neuronal viability and decreased LDH activity in CI rats. Abundant production of ROS following IRI

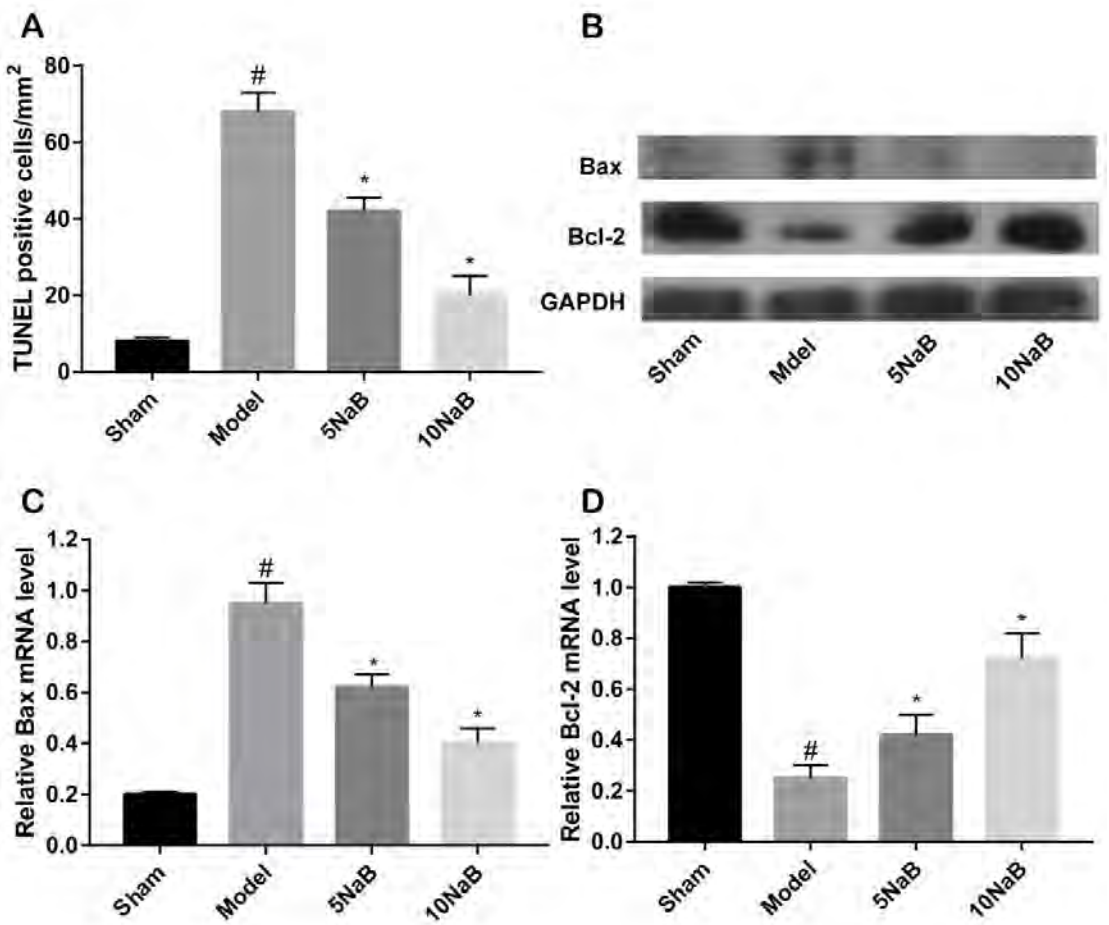


Fig. 3. *Protective effect of NaB on neuronal apoptosis following CI. TUNEL-positive cell number (**A**), protein levels of Bax and Bcl-2 (**B**), mRNA level of Bax (**C**) and mRNA level of Bcl-2 (**D**) in rats of sham group, model group, 5 mg/kg NaB group and 10 mg/kg NaB group.*

would accelerate neuronal apoptosis (30). As an endogenous anti-oxidant, SOD is vital for preventing oxidative stress (31). MDA is the main product in lipid peroxides, which damages cell components and disrupts cell structure and function (32). Here, NaB treatment markedly decreased MDA content, and enhanced SOD activity, verifying the neuronal protective function of NaB in CI.

Neuronal apoptosis initiates from ischemia, and determines the outcome of IRI (16). Our findings revealed that abundant neurons in CI rats were apoptotic, and those treated with NaB showed dose-dependently decreased apoptotic rate. As a water-soluble protein homologous to Bcl-2, Bax is a pro-apoptotic gene triggering the process of apoptosis (33, 34). In CI rats undergoing NaB treatment, Bax was downregulated and Bcl-2 was upregulated, suggesting the protective effect of NaB on neuronal apoptosis.

During the process of IRI, the PI3K/Akt and ERK1/2 pathways are activated to protect neuronal apoptosis (35, 36). The PI3K/Akt pathway is of significance in regulating cell growth, proliferation and survival (37). Phosphorylated Akt inactivates apoptosis-inducing factors and thus protects cell survival (38).

Growth factors, oxidative stress, calcium ion level and other stimuli could activate the MEK-ERK1/2 pathway, thereafter affecting cell phenotypes (39). Here, NaB treatment markedly enhanced phosphorylated levels of Akt and ERK1/2 in CI rats, suggesting that NaB protected neuronal apoptosis following CI through the PI3K/Akt and ERK1/2 pathways. This study mainly explored the anti-apoptotic effect of NaB on neurons at post-CI and the molecular mechanism. It is demonstrated that NaB was capable of preventing against neuronal apoptosis following CI by activating the PI3K/Akt and ERK1/2 pathways. Our findings provide a novel reference for developing targeted drugs against CI-

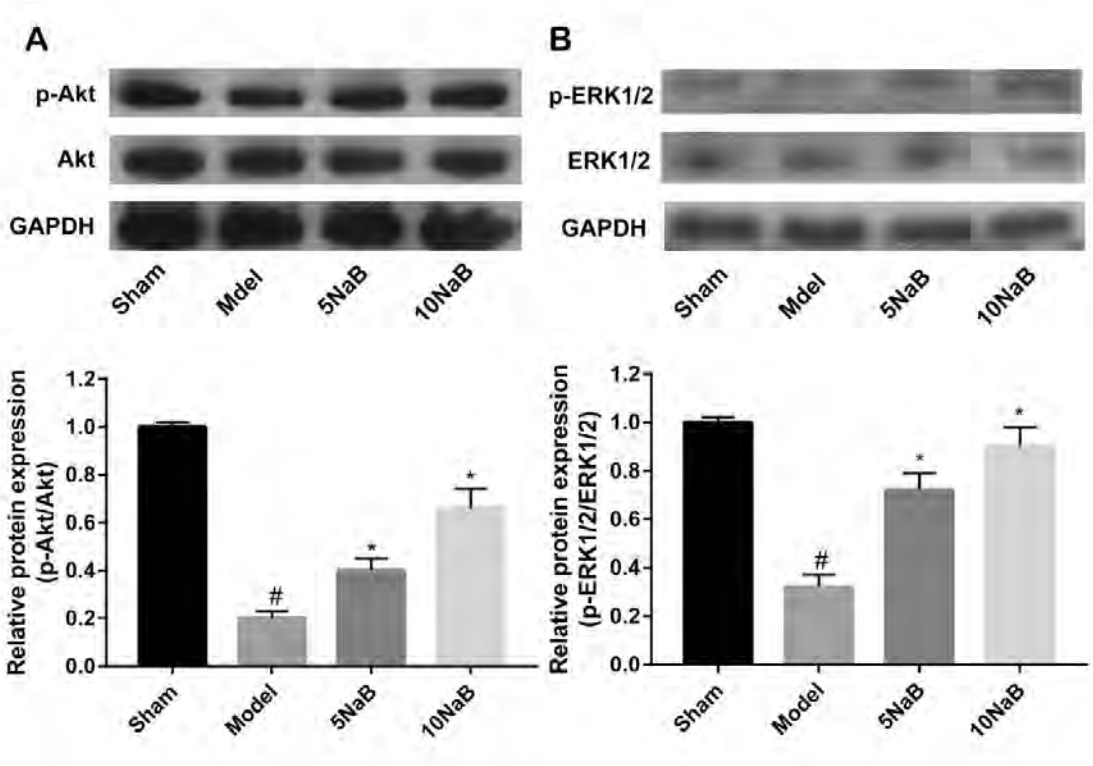


Fig. 4. *Akt and ERK1/2 pathways were responsible for the neuroprotective effect of NaB. Protein levels of p-Akt and Akt (**A**), and p-EKR1/2 and ERK1/2 (**B**) in rats of sham group, model group, 5 mg/kg NaB group and 10 mg/kg NaB group.*

induced neuronal apoptosis, displaying a promising application of NaB.

In conclusion, NaB treatment alleviates neuronal apoptosis *via* the PI3K/Akt and ERK1/2 pathways in CI rats, thus protecting the deterioration of CI. This article elaborates the protective role of NaB in neuronal apoptosis, and provides a new theoretical basis for the clinical application of sodium butyrate, which is very meaningful.

ACKNOWLEDGEMENT

Basic scientific research business expenses of Heilongjiang Provincial Department of education basic scientific research project (2018-KYYWF-0961).

REFERENCES

1. Fargen KM, Neal D, Fiorella DJ, Turk AS, Froehler M, Mocco J. A meta-analysis of prospective randomized controlled trials evaluating endovascular therapies for acute ischemic stroke. J Neurointerv Surg 2015; 7:84-89.
2. Abilleira S, Cardona P, Ribo M, et al. Outcomes of a contemporary cohort of 536 consecutive patients with acute ischemic stroke treated with endovascular therapy. Stroke 2014; 45:1046-52.
3. Eltzschig HK, Eckle T. Ischemia and reperfusion--from mechanism to translation. Nat Med 2011; 17:1391-401.
4. Turley KR, Toledo-Pereyra LH, Kothari RU. Molecular mechanisms in the pathogenesis and treatment of acute ischemic stroke. J Invest Surg 2005; 18:207-18.
5. Martin LJ, Al-Abdulla NA, Brambrink AM, Kirsch JR, Sieber FE, Portera-Cailliau C. Neurodegeneration in excitotoxicity, global cerebral ischemia, and target deprivation: A perspective on the contributions of apoptosis and necrosis. Brain Res Bull 1998; 46:281-309.
6. Saito A, Maier CM, Narasimhan P, et al. Oxidative stress and neuronal death/survival signaling in cerebral ischemia. Mol Neurobiol 2005; 31:105-16.
7. Lakhan SE, Kirchgessner A, Hofer M. Inflammatory mechanisms in ischemic stroke: therapeutic approaches. J Transl Med 2009; 7:97.
8. Pettigrew LC, Kindy MS, Scheff S, Springer JE, Kryscio RJ, Li Y, Grass DS. Focal cerebral ischemia in the TNFalpha-transgenic rat. J Neuroinflammation 2008; 5:47.
9. Mattson MP, Duan W, Pedersen WA, Culmsee C. Neurodegenerative disorders and ischemic brain diseases. Apoptosis 2001; 6:69-81.
10. Zhang LT, Yao YM, Lu JQ, Yan XJ, Yu Y, Sheng ZY. Sodium butyrate prevents lethality of severe sepsis in rats. Shock 2007; 27:672-77.
11. Kim HJ, Rowe M, Ren M, Hong JS, Chen PS, Chuang DM. Histone deacetylase inhibitors exhibit anti-inflammatory and neuroprotective effects in a rat permanent ischemic model of stroke: multiple mechanisms of action. J Pharmacol Exp Ther 2007; 321:892-901.
12. Chuang DM, Leng Y, Marinova Z, Kim HJ, Chiu CT. Multiple roles of HDAC inhibition in neurodegenerative conditions. Trends Neurosci 2009; 32:591-601.
13. Sun J, Wang F, Li H, et al. Neuroprotective Effect of Sodium Butyrate against Cerebral Ischemia/Reperfusion Injury in Mice. Biomed Res Int 2015; 2015:395895.
14. Chen X, Su W, Wan T, et al. Sodium butyrate regulates Th17/Treg cell balance to ameliorate uveitis via the Nrf2/HO-1 pathway. Biochem Pharmacol 2017; 142:111-19.
15. Li N, Liu XX, Hong M, et al. Sodium butyrate alleviates LPS-induced acute lung injury in mice via inhibiting HMGB1 release. Int Immunopharmacol 2018; 56:242-48.
16. Broughton BR, Reutens DC, Sobey CG. Apoptotic mechanisms after cerebral ischemia. Stroke 2009; 40:e331-e339.
17. Xu Y, Zhang Q, Yu S, Yang Y, Ding F. The protective effects of chitooligosaccharides against glucose deprivation-induced cell apoptosis in cultured cortical neurons through activation of PI3K/Akt and MEK/ERK1/2 pathways. Brain Res 2011; 1375:49-58.
18. Chen L, Wei X, Hou Y, et al. Tetramethylpyrazine analogue CXC195 protects against cerebral ischemia/reperfusion-induced apoptosis through PI3K/Akt/GSK3beta pathway in rats. Neurochem Int 2014;

66:27-32.
19. Sun B, Chen L, Wei X, Xiang Y, Liu X, Zhang X. The Akt/GSK-3beta pathway mediates flurbiprofen-induced neuroprotection against focal cerebral ischemia/reperfusion injury in rats. Biochem Biophys Res Commun 2011; 409:808-13.
20. Liu H, Liu X, Wei X, Chen L, Xiang Y, Yi F, Zhang X. Losartan, an angiotensin II type 1 receptor blocker, ameliorates cerebral ischemia-reperfusion injury via PI3K/Akt-mediated eNOS phosphorylation. Brain Res Bull 2012; 89:65-70.
21. Yamazaki T, Aoki S, Ohta K, Hyuma S, Sakaguchi K, Sugawara F. Synthesis of an immunosuppressant SQAG9 and determination of the binding peptide by T7 phage display. Bioorg Med Chem Lett 2004; 14:4343-46.
22. Jin H, Hwang SK, Yu K, et al. A high inorganic phosphate diet perturbs brain growth, alters Akt-ERK signaling, and results in changes in cap-dependent translation. Toxicol Sci 2006; 90:221-29.
23. Shioda N, Han F, Fukunaga K. Role of Akt and ERK signaling in the neurogenesis following brain ischemia. Int Rev Neurobiol 2009; 85:375-87.
24. Hu X, Zhang K, Xu C, Chen Z, Jiang H. Anti-inflammatory effect of sodium butyrate preconditioning during myocardial ischemia/reperfusion. Exp Ther Med 2014; 8:229-32.
25. Zhang L, Ding W, Sun H, et al. Salidroside protects PC12 cells from MPP(+)-induced apoptosis via activation of the PI3K/Akt pathway. Food Chem Toxicol 2012; 50:2591-97.
26. Yitshak SM, Novack V, Ifergane G, Horev A, Kloog I. Air Pollution and Ischemic Stroke Among Young Adults. Stroke 2015; 46:3348-53.
27. Dong JY, Iso H, Kitamura A, Tamakoshi A. Multivitamin use and risk of stroke mortality: the Japan collaborative cohort study. Stroke 2015; 46:1167-72.
28. Naess H, Kurtz M, Thomassen L, Waje-Andreassen U. Serial NIHSS scores in patients with acute cerebral infarction. Acta Neurol Scand 2016; 133:415-20.
29. Liang H, Liu P, Wang Y, Song S, Ji A. Protective effects of alkaloid extract from Leonurus heterophyllus on cerebral ischemia reperfusion injury by middle cerebral ischemic injury (MCAO) in rats. Phytomedicine 2011; 18:811-18.
30. Wu MY, Yiang GT, Liao WT, et al. Current Mechanistic Concepts in Ischemia and Reperfusion Injury. Cell Physiol Biochem 2018; 46:1650-67.
31. Chan PH. Role of oxidants in ischemic brain damage. Stroke 1996; 27:1124-29.
32. Soehle M, Heimann A, Kempski O. Postischemic application of lipid peroxidation inhibitor U-101033E reduces neuronal damage after global cerebral ischemia in rats. Stroke 1998; 29:1240-1246, 1246-47.
33. Muller C, Dunschede F, Koch E, Vollmar AM, Kiemer AK. Alpha-lipoic acid preconditioning reduces ischemia-reperfusion injury of the rat liver via the PI3-kinase/Akt pathway. Am J Physiol Gastrointest Liver Physiol 2003; 285:G769-G778.
34. Glushakova OY, Johnson D, Hayes RL. Delayed increases in microvascular pathology after experimental traumatic brain injury are associated with prolonged inflammation, blood-brain barrier disruption, and progressive white matter damage. J Neurotrauma 2014; 31:1180-93.
35. Zhang J, Deng Z, Liao J, et al. Leptin attenuates cerebral ischemia injury through the promotion of energy metabolism via the PI3K/Akt pathway. J Cereb Blood Flow Metab 2013; 33:567-74.
36. Lo EH, Dalkara T, Moskowitz MA. Mechanisms, challenges and opportunities in stroke. Nat Rev Neurosci 2003; 4:399-415.
37. Cantley LC. The phosphoinositide 3-kinase pathway. Science 2002; 296:1655-57.
38. Woodgett JR. Recent advances in the protein kinase B signaling pathway. Curr Opin Cell Biol 2005; 17:150-57.
39. Kovalska M, Kovalska L, Pavlikova M, et al. Intracellular signaling MAPK pathway after cerebral ischemia-reperfusion injury. Neurochem Res 2012; 37:1568-77.

MiR-93 INHIBITS MYOCARDIAL APOPTOSIS IN RATS WITH MYOCARDIAL ISCHEMIA-REPERFUSION INJURY THROUGH REGULATING Mfn2 EXPRESSION

Z.-D. ZHU[1*], Y.-F. CHEN[2*] and H.-M. SHI[1]

[1]Department of Cardiology, Huashan Hospital North, Fudan University, Shanghai, China;
[2]Department of Anesthesiology, Huashan Hospital North, Fudan University, Shanghai, China

Received March 12, 2020 – Accepted May 5, 2020

These Authors contributed equally to this work

To explore the effect of micro ribonucleic acid (miR)-93 on myocardial apoptosis in rats with myocardial ischemia-reperfusion injury (MIRI) through regulating mitofusin-2 (Mfn2) expression, we carried out a series of experiments. A total of 36 Sprague-Dawley rats were randomly divided into the sham group (n=12), the model group (n=12) and miR-93 mimics group (n=12). The chest was opened without ischemia-reperfusion only in the sham group. The MIRI model was established, and normal saline was used for intervention in the model group. The MIRI model was also established, and miR-93 mimics were used for intervention in miR-93 mimics group. The expression of Mfn2 was detected *via* immunohistochemistry. The relative protein expressions of B-cell lymphoma-2 (Bcl-2), Bcl-2 associated X protein (Bax) and Mfn2 were detected *via* Western blotting. The expression of miR-93 was determined using quantitative polymerase chain reaction (qPCR), and apoptosis was determined using terminal deoxynucleotidyl transferase-mediated dUTP nick end labeling (TUNEL) assay. The immunohistochemistry results showed that the positive expression of Mfn2 was significantly increased in the other two groups compared with that in the sham group (P<0.05), while it was also significantly increased in miR-93 mimics group compared with that in the model group (P<0.05). The results of Western blotting revealed that the other two groups had obviously higher relative protein expressions of Bax and Mfn2, and an obviously lower relative protein expression of Bcl-2 than the sham group (P<0.05). MiR-93 mimics group also had obviously higher relative protein expressions of Bcl-2 and Mfn2, and an obviously lower relative protein expression of Bax than the model group (P<0.05). According to the results of qPCR, the relative expression of miR-93 was evidently increased in the other two groups compared with that in the sham group (P<0.05), while it was also evidently increased in the miR-93 mimics group compared with that in the model group (P<0.05). It was found that the apoptosis rate remarkably rose in the other two groups compared with that in the sham group (P<0.05), while it remarkably declined in miR-93 mimics group compared with that in the model group *via* TUNEL assay (P<0.05). MiR-93 inhibits myocardial apoptosis in MIRI rats through up-regulating Mfn2 expression.

Myocardial infarction is a clinically common severe disease that can lead to sudden death of patients. With the social development and accelerating pace of life, myocardial infarction has shown a younger trend with high morbidity and mortality rates (1, 2). Myocardial ischemia-reperfusion injury (MIRI) is one of the most important pathological reactions of myocardial infarction. Studies have demonstrated

Key words: ischemia-reperfusion; miR-93; Mfn2; apoptosis

Corresponding Author:
Haiming Shi, MD
Department of Cardiology, Huashan Hospital North,
Fudan University, 12 Central Urumqi Road,
Shanghai 200040, China
Tel.:+ 86018616299261
e-mail: mingshan19680518@163.com

0393-974X (2020)
Copyright © by BIOLIFE, s.a.s.
This publication and/or article is for individual use only and may not be further reproduced without written permission from the copyright holder.
Unauthorized reproduction may result in financial and other penalties
DISCLOSURE: ALL AUTHORS REPORT NO CONFLICTS OF INTEREST RELEVANT TO THIS ARTICLE.

that MIRI can lead to myocardial apoptosis and even necrosis, seriously affecting the structure and function of myocardial tissues, and harming the myocardial repair after myocardial infarction (3, 4).

Currently, it is believed that mitofusin-2 (Mfn2) plays an important role during MIR, with a good anti-apoptotic effect, thereby exerting a good protective effect on myocardial cells (5, 6). Studies have demonstrated that after MIRI, the high expression of Mfn2 is beneficial to increasing the expression of the anti-apoptotic effector B-cell lymphoma-2 (Bcl-2) and reducing the abnormal expression of the pro-apoptotic effector Bcl-2 associated X protein (Bax), thus inhibiting apoptosis (7, 8).

As a class of non-coding ribonucleic acids (RNAs) in the body, micro RNAs (miRNAs) play important regulatory roles. In particular, miR-93, an important member of the miRNA family, has an important regulatory effect on multiple downstream signaling pathways and effector molecules, and is an important player in cell apoptosis and proliferation. The present study aimed to explore the effect of miR-93 regulating Mfn2 expression on myocardial apoptosis in MIRI rats.

MATERIALS AND METHODS

Laboratory animals

A total of 36 specific pathogen-free Sprague-Dawley (SD) rats aged 1 month were purchased from Shanghai SLAC Laboratory Animal Co., Ltd. [license No.: SCXK (Shanghai, China) 2014-0003]. The rats were fed with normal feed and sterile filtered water every day in the Laboratory Animal Center under 12/12 h light-dark cycle, regular room temperature and humidity. This study was approved by the Animal Ethics Committee of Fudan University Animal Center.

Animal grouping and treatment

Thirty-six SD rats were randomly divided into a normal group (n=12), a model group (n=12) and an miR-93 mimics group (n=12) using a random number table. The rats were adaptively fed in the Laboratory Animal Center for 7 days before experiments.

The chest was opened without ischemia-reperfusion only in the sham group. In the model group, normal saline was first infused into the femoral vein at 5 min before modeling, and then the MIRI model was established (myocardial ischemia for 30 min and reperfusion for 120 min), followed by sampling. In the miR-93 mimics group, 3 mM miR-93 mimics (CST, Danvers, MA, USA) were first infused into the femoral vein at 30 min before modeling, and then the MIRI model was established (myocardial ischemia for 30 min and reperfusion for 120 min), followed by sampling.

Establishment of MIRI model

After successful anesthesia *via* intraperitoneal injection of 7% chloral hydrate (5 mL/kg), the chest hair was shaved off to expose the skin. Following disinfection, the rats were fixed firmly, the chest was cut open with scissors to expose the heart, and the left anterior descending coronary artery was found and ligated at 1/2. Then the whitening of left anterior wall, weakness in cardiac impulse, ST-segment elevation and T-wave height in electrocardiogram indicated myocardial ischemia. After ischemia for 45 min, the ligation was removed to restore the blood supply to the left anterior descending coronary artery, and the conditions of rats were closely observed. After the rats were in stable condition, the wound was sutured layer by layer, and the rats were fed in separate cages.

Sampling

After successful anesthesia, the blood was drawn from the abdominal aorta, and the heart tissues were directly taken from 6 rats in each group, washed with normal saline and stored in Eppendorf (EP) tubes at -80°C for later Western blotting and qPCR. The samples were taken *via* perfusion fixation from the remaining 6 rats in each group: The thoracic cavity was cut open to expose the heart, and 400 mL of 4% paraformaldehyde was perfused from the left auricle. Then the heart tissues were taken and fixed in 4% paraformaldehyde for immunohistochemistry and TUNEL assay.

Immunohistochemistry

The paraffin-embedded tissues were sliced into 5-μm-thick sections, flattened and rinsed in warm

water at 42°C, baked and prepared into paraffin sections. Then the sections were soaked and routinely deparaffinized in xylene solution and gradient alcohol, placed in citric acid buffer, and heated in a microwave for 3 times (3 min/time, braised for 5 min each time) for complete antigen retrieval. After the sections were washed, the endogenous peroxidase blocker was added dropwise for reaction for 10 min. Then the sections were washed again and sealed with goat serum for 20 min. After the goat serum was discarded, the anti-Mfn2 (1:200) primary antibody was added for incubation at 4°C overnight. The following day, the sections were washed, reacted with secondary antibody for 10 min, fully washed and reacted with streptavidin-peroxidase solution for 10 min, followed by color development with diaminobenzidine (DAB). Finally, the nuclei were counterstained with hematoxylin, and the sections were sealed and observed.

Western blotting

The cryopreserved heart tissues were added with lysis buffer, subjected to ice bath for 1 h and centrifuged at 14,000 g for 10 min. The protein was quantified using bicinchoninic acid (BCA) method (Pierce, Rockford, IL, USA). The absorbance of protein was detected using a microplate reader and the standard curve was plotted, based on which the protein concentration was calculated. After protein denaturation, the protein in tissue specimens was separated *via* sodium dodecyl sulphate-polyacrylamide gel electrophoresis (SDS-PAGE), and the position of the Marker protein was observed. The electrophoresis was terminated when the Marker protein reached the bottom of the glass plate in a straight line. Then the protein was transferred onto a polyvinylidene fluoride (PVDF) membrane (Millipore, Billerica, MA, USA), sealed with sealing buffer for 1.5 h and incubated with anti-Bax (1:1000), anti-Bcl-2 (1:1000) and anti-Mfn2 (1:1000) primary antibodies (Abcam, Cambridge, MA, USA) and secondary antibodies (1:1000) (Abcam, Cambridge, MA, USA). After the membrane was washed, the image was fully developed using the chemiluminescent reagent for 1 min.

QPCR

Total RNA was extracted from heart tissues using the RNA extraction reagent, reversely transcribed into complementary deoxyribose nucleic acid (cDNA) using a reverse transcription kit (Vazyme, Nanjing, China). The qPCR system (20 μL) was designed and the reaction conditions were as follows: reaction at 53°C for 5 min, pre-denaturation at 95°C for 10 min, denaturation at 95°C for 10 s, annealing at 62°C for 30 s, a total of 35 cycles. The $^{\Delta Ct}$ value was calculated first, and then the difference in the expression of target gene was calculated. The primer sequences are shown in Table I.

Table I. *Primer sequences*

Gene	Primer sequence
miR-93	F: 5'-TGAATGATTCCTCAATGCT-3'
	R: 5'-GGCATCCTACTAGCACTG-3'
GAPDH	F: 5'-ACGGCAAGTTCAACGGCACAG-3'
	R: 5'-GAAGACGCCAGTAGACTCCACGAC-3'

TUNEL apoptosis assay

The paraffin-embedded tissues were sliced into 5 μm-thick sections, flattened and rinsed in warm water at 42°C, baked and prepared into paraffin sections. Then the sections were soaked and routinely deparaffinized in xylene solution and gradient alcohol, added dropwise with TdT solution for reaction in a dark place for 1 h and incubated with deionized water for 15 min to terminate the reaction. The endogenous peroxidase was inactivated with hydrogen peroxide, and the working solution was added dropwise for reaction for 1 h, followed by color development *via* DAB solution. Finally, the sections were washed, sealed and observed.

Statistical analysis

Statistical Product and Service Solutions (SPSS) 20.0 software (IBM, Armonk, NY, USA) was used for statistical analysis. Measurement data were expressed as mean ± standard deviation. *t*-test was used for the data in line with normal distribution and homogeneity of variance, corrected *t*-test for the data in line with normal distribution and heterogeneity of variance, and non-parametric test for the data not in line with normal distribution and homogeneity of variance. The measurement data of three or more groups were compared by one-way ANOVA. Rank sum test was adopted for ranked data, and *chi*-squared test for enumeration data.

RESULTS

Immunohistochemistry results

As shown in Fig. 1, dark brown indicated the positive expression. The positive expression of Mfn2 was lower in the sham group, while it was higher in the other two groups. According to the statistical results (Fig. 2), compared with that in the sham group, the mean optical density of Mfn2 positive expression was significantly increased in the other two groups, showing statistically significant differences ($P<0.05$). Moreover, compared with that in the model group, the mean optical density of Mfn2 positive expression was also significantly increased in miR-93 mimics group, showing a statistically significant difference ($P<0.05$).

Relative protein expressions detected via Western blotting

As shown in Fig. 3, the protein expressions of Bax and Mfn2 were lower and the protein expression of Bcl-2 was higher in the sham group, but the contrary

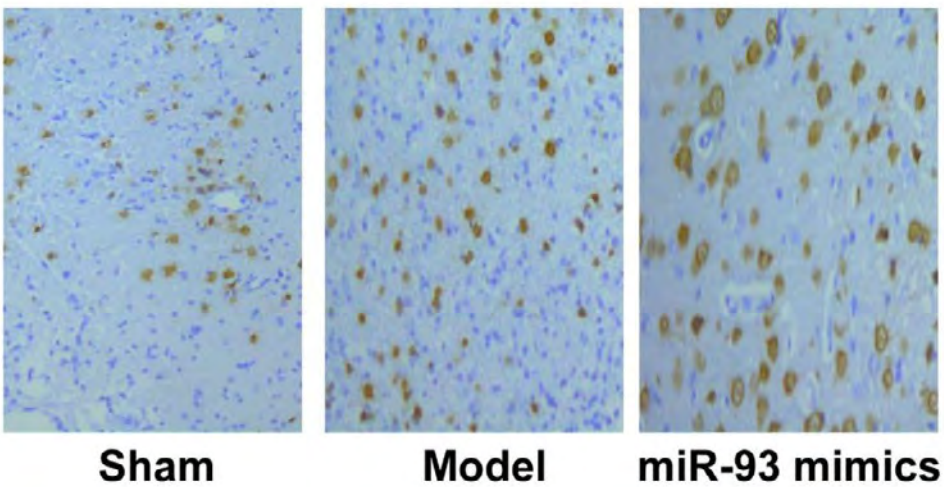


Fig. 1. *Expressions of Mfn2 detected via immunohistochemistry (magnification: 200×).*

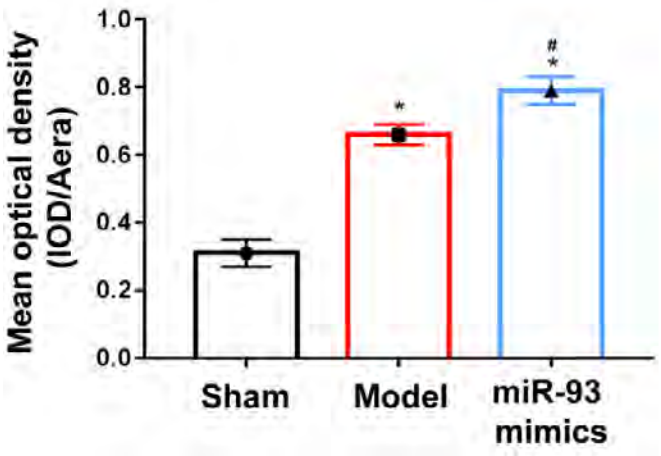


Fig. 2. *Mean optical density of Mfn2 positive expression in each group. Note: $P^{*}<0.05$ vs the sham group, $P^{\#}<0.05$ vs the model group.*

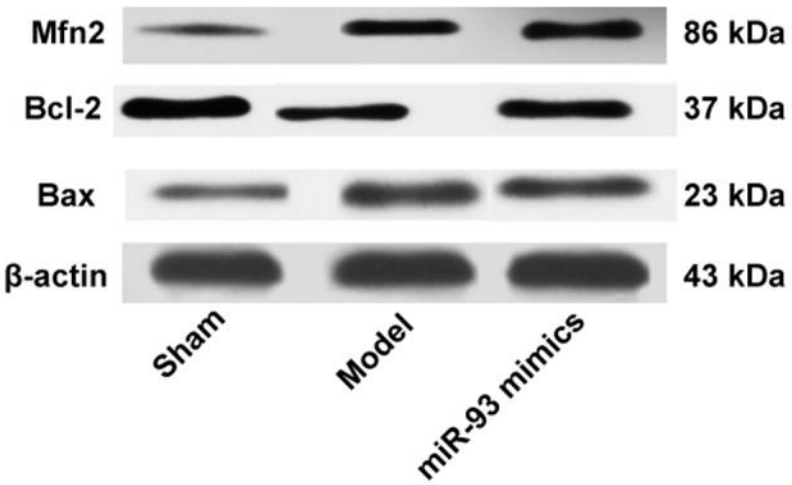


Fig. 3. *Protein expressions detected via Western blotting*

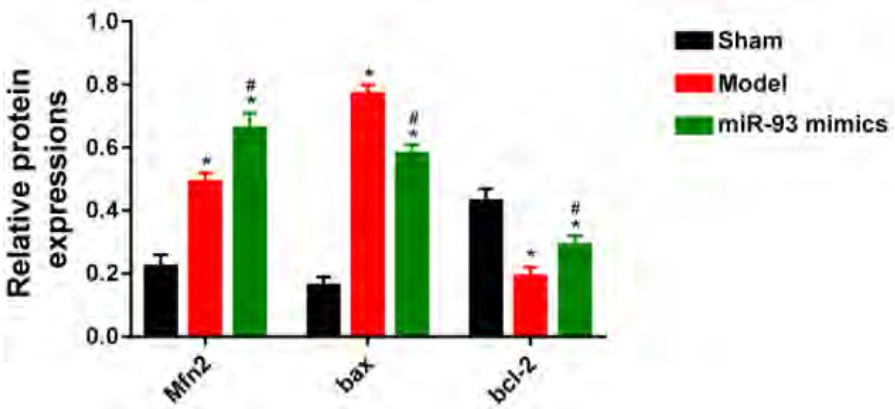


Fig. 4. *Relative protein expressions in each group. Note: $P^{*}<0.05$ vs the sham group, $P^{\#}<0.05$ vs the model group.*

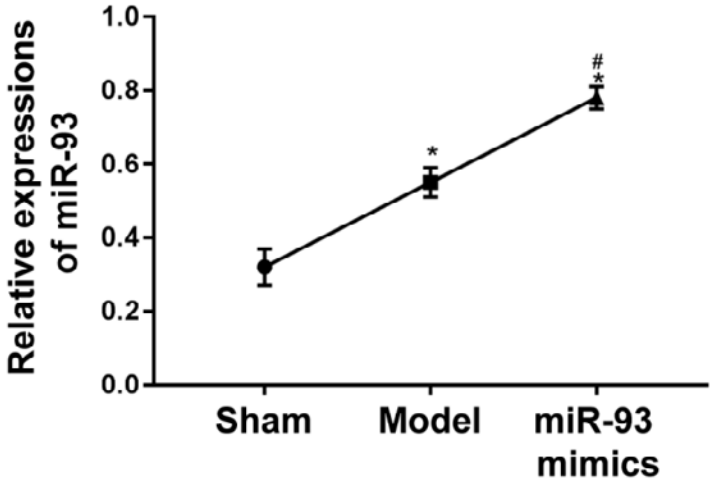


Fig. 5. *Relative expressions of miR-93. Note: $P^{*}<0.05$ vs the sham group, $P^{\#}<0.05$ vs the model group.*

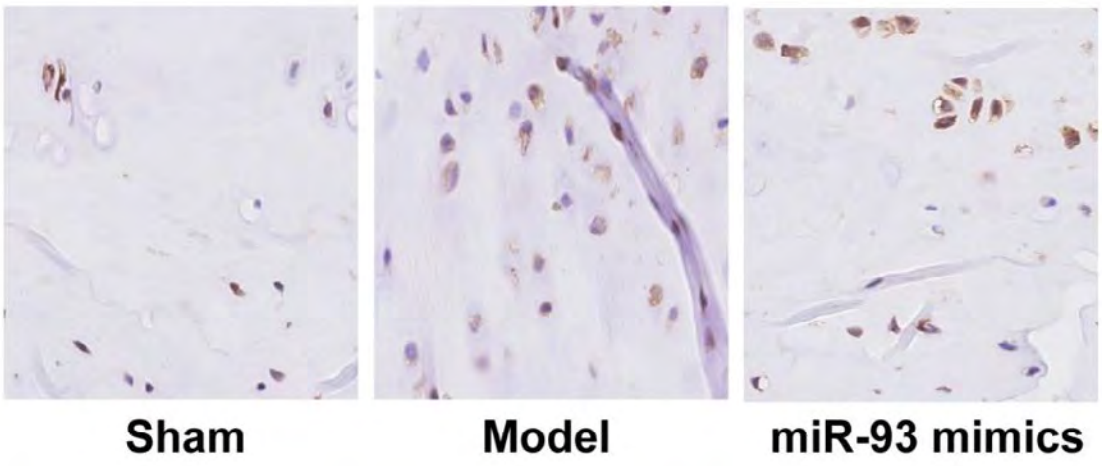


Fig. 6. *Apoptosis detected via TUNEL assay (magnification: 200×).*

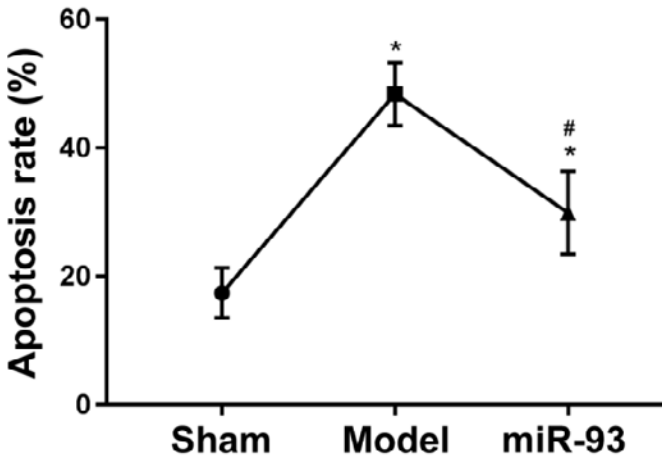


Fig. 7. *Apoptosis rate in each group. Note: $P^{*}<0.05$ vs the sham group, $P^{\#}<0.05$ vs the model group.*

was the case in the other two groups. According to the statistical results (Fig. 4), the other two groups had obviously higher relative protein expressions of Bax and Mfn2, and an obviously lower relative protein expression of Bcl-2 than the sham group, and the differences were statistically significant ($P<0.05$). The MiR-93 mimics group had obviously higher relative protein expressions of Bcl-2 and Mfn2, and an obviously lower relative protein expression of Bax than the model group, and the differences were statistically significant ($P<0.05$).

QPCR results

The relative expression of miR-93 was evidently increased in the other two groups compared with that in the sham group, displaying statistically significant differences ($P<0.05$), while it was also evidently increased in the miR-93 mimics group compared with that in the model group, displaying a statistically significant difference ($P<0.05$) (Fig. 5).

Apoptosis rate detected via TUNEL assay

As shown in Fig. 6, the apoptotic cells showed the dark brown color, and there were fewer apoptotic cells in the sham group, but more in the other two groups. The apoptosis rate remarkably rose in the other two groups compared with that in the sham group, and the differences were statistically significant ($P<0.05$), while it remarkably declined in miR-93 mimics group compared with that in the model group, and the difference was statistically significant ($P<0.05$) (Fig. 7).

DISCUSSION

Myocardial apoptosis, an important pathological response of myocardial cells to MIRI during myocardial infarction, often leads to massive myocardial apoptosis and even necrosis, seriously affecting myocardial structure and function, and ventricular wall structure (9, 10). During myocardial infarction, in addition to massive myocardial apoptosis, MIRI can also cause fibrosis of a large number of myocardial cells, harming the repair of myocardial cells and the recovery of normal myocardial function, which is an important cause of difficulty in myocardial repair. At present, studies have shown that during myocardial infarction, a large number of cytokines and pro-inflammatory factors produced due to MIRI can activate multiple downstream signaling pathways, and expressions of various proteins and related genes, thereby promoting the repair of MIRI (11, 12). During apoptosis, Bax exerts a pro-apoptotic effect, while Bcl-2 exerts an anti-apoptotic effect, both of which, as important effectors for apoptosis, remain stable under physiological conditions to maintain the pro-apoptosis/anti-apoptosis balance. The abnormal expressions of Bax and Bcl-2 can result in the pro-apoptosis/anti-apoptosis imbalance, and promote the expression of apoptosis effector protein Caspase3, thus facilitating apoptosis (13, 14). Mfn2 plays an important role in the process of apoptosis. Studies have demonstrated that during MIRI, Mfn2 and its related genes will have abnormally high expressions, and highly expressed Mfn2 has a good anti-apoptotic effect, which can inhibit apoptosis and protect damaged cells (15, 16). Therefore, Mfn2 exerts an important cardioprotective effect in MIRI, and its high expression is beneficial to inhibiting myocardial apoptosis, thus promoting myocardial injury repair.

MiR-93 is a non-coding RNA that plays an important regulatory role in the body, which has been proved to be closely related to the pathogenesis of a variety of diseases. Studies have demonstrated that miR-93 degrades or inhibits downstream mRNAs through pairing with the corresponding untranslated region in downstream target genes, thereby regulating transcription, and such pathological processes as cell proliferation, differentiation and apoptosis (17, 18). It was found that miR-93 is closely associated with the occurrence and development of various diseases (19), and it also has an important influence on various pathological reactions in the disease *via* regulating a variety of cell signal transduction pathways, which is considered as an important regulator of disease. In particular, miR-93 can exert an important anti-apoptotic effect *via* regulating multiple downstream effectors. In this study, it was further confirmed that miR-93 was highly expressed after MIRI, and it could promote the expression of Bcl-2 and suppress the expression of Bax, thereby regulating apoptosis.

At the same time, miR-93 could effectively facilitate the expression of Mfn2 after MIRI, which may be the reason for the inhibitory effect of miR-93 on myocardial apoptosis. In conclusion, miR-93 inhibits myocardial apoptosis in MIRI rats through up-regulating Mfn2 expression.

REFERENCES

1. Wang Z, Cai W, Hu S, Xia Y, Wang Y, Zhang Q, Chen L. A meta-analysis of circulating microvesicles in patients with myocardial infarction. Arq Bras Cardiol 2017:0.
2. Fiorin BH, Oliveira E, Moreira R, Luna FB. [Cross-cultural adaptation of the Myocardial Infarction Dimensional Assessment Scale (MIDAS) to the Brazilian Portuguese language]. Cien Saude Colet 2018; 23:785-93.
3. Huang XW, Pan MD, Du PH, Wang LX. Arginase-2 protects myocardial ischemia-reperfusion injury via NF-kappaB/TNF-alpha pathway. Eur Rev Med Pharmacol Sci 2018; 22:6529-6537.
4. Mehta LS, Beckie TM, DeVon HA, et al. Acute myocardial infarction in women: a scientific statement from the american heart association. Circulation 2016; 133:916-47.
5. Zhang L, Sun D, Bao Y, Shi Y, Cui Y, Guo M. Nerolidol protects against LPS-induced acute kidney injury via inhibiting TLR4/NF-kappaB signaling. Phytother Res 2017; 31:459-65.
6. Ye HY, Jin J, Jin LW, Chen Y, Zhou ZH, Li ZY. Chlorogenic acid attenuates lipopolysaccharide-induced acute kidney injury by inhibiting TLR4/NF-kappaB signal pathway. Inflammation 2017; 40:523-29.
7. Xu Q, Duan H, Gan L, et al. MicroRNA-1291 promotes endometrial fibrosis by regulating the ArhGAP29-RhoA/ROCK1 signaling pathway in a murine model. Mol Med Rep 2017; 16:4501-10.
8. Citalan-Madrid AF, Vargas-Robles H, Garcia-Ponce A, et al. Cortactin deficiency causes increased RhoA/ROCK1-dependent actomyosin contractility, intestinal epithelial barrier dysfunction, and disproportionately severe DSS-induced colitis. Mucosal Immunol 2017; 10:1237-47.
9. Wang X, Yang L, Kang L, et al. Metformin attenuates myocardial ischemia-reperfusion injury via up-regulation of antioxidant enzymes. Plos One 2017; 12:e182777.
10. Hu T, Wei G, Xi M, et al. Synergistic cardioprotective effects of Danshensu and hydroxysafflor yellow A against myocardial ischemia-reperfusion injury are mediated through the Akt/Nrf2/HO-1 pathway. Int J Mol Med 2016; 38:83-94.
11. Luo S, Hieu TB, Ma F, et al. ZYZ-168 alleviates cardiac fibrosis after myocardial infarction through inhibition of ERK1/2-dependent ROCK1 activation. Sci Rep 2017; 7:43242.
12. Lee TM, Lin SZ, Chang NC. Nicorandil regulates the macrophage skewing and ameliorates myofibroblasts by inhibition of RhoA/Rho-kinase signalling in infarcted rats. J Cell Mol Med 2018; 22:1056-69.
13. Zhang HY, Zhang X, Wang ZG, et al. Exogenous basic fibroblast growth factor inhibits ER stress-induced apoptosis and improves recovery from spinal cord injury. Cns Neurosci Ther 2013; 19:20-29.
14. Yip PK, Malaspina A. Spinal cord trauma and the molecular point of no return. Mol Neurodegener 2012; 7:6.
15. Yang Y, Zhao L, Ma J. Penehyclidine hydrochloride preconditioning provides cardiac protection in a rat model of myocardial ischemia/reperfusion injury via the mechanism of mitochondrial dynamics mechanism. Eur J Pharmacol 2017; 813:130-39.
16. Qin L, Yang W, Wang YX, et al. MicroRNA-497 promotes proliferation and inhibits apoptosis of cardiomyocytes through the downregulation of Mfn2 in a mouse model of myocardial ischemia-reperfusion injury. Biomed Pharmacother 2018; 105:103-14.
17. Zeng Y, Yi R, Cullen BR. Recognition and cleavage of primary microRNA precursors by the nuclear processing enzyme Drosha. Embo J 2005; 24:138-48.
18. Lee Y, Ahn C, Han J, et al. The nuclear RNase III Drosha initiates microRNA processing. Nature 2003; 425:415-19.
19. Zheng P, Chen L, Yuan X, et al. Exosomal transfer of tumor-associated macrophage-derived miR-21 confers cisplatin resistance in gastric cancer cells. J Exp Clin Cancer Res 2017; 36:53.

MiR-369-3p INHIBITS TUMORIGENESIS OF HEPATOCELLULAR CARCINOMA BY BINDING TO PAX6

Q. XU and K. LIU

Department of Hepatobiliary Surgery, Central Hospital of Zibo, Zibo, Shandong Province, China

Received March 27, 2020 - Accepted May 6, 2020

Accepted as crucial participators in human diseases, microRNAs (miRNAs) have been demonstrated to play important roles in cancer progression, including hepatocellular carcinoma (HCC). The purpose of this study is to preliminarily elucidate the role of miR-369-3p in HCC. Here, miR-369-3p and PAX6 expressions were detected by RT-qPCR. The functional mechanism of miR-369-3p/PAX6 axis was investigated by MTT, Transwell and luciferase reporter assays. The results showed that miR-369-3p was downregulated in HCC and was associated with lymph node metastasis and TNM stage in HCC patients. Functionally, miR-369-3p overexpression inhibited cell viability and motility in HCC. Furthermore, PAX6 was confirmed as a direct target of miR-369-3p, and upregulation of PAX6 exerts carcinogenesis in the development of HCC. PAX6 can weaken the inhibitory effect of miR-369-3p in HCC. In conclusion, miR-369-3p inhibits the proliferation, migration and invasion of HCC cells by suppressing PAX6 expression.

Liver cancer refers to malignant tumors that occur in the liver, including primary liver cancer and metastatic liver cancer. Hepatocellular carcinoma (HCC) is one of the primary liver cancers (1) and has a relatively high degree of malignancy. Moreover, the prognosis of patients with HCC is poor, and the one-year survival rate is only 44% (2). If early detection and early treatment are possible, the effect of treatment for HCC patients may be better. However, because the symptoms of liver cancer are not obvious at an early stage, symptoms such as abdominal pain will gradually develop to the extent that the disease progresses to a certain degree, which brings great difficulties to early diagnosis (3). In addition, HCC has rapid disease progression, difficult treatment, and poor curative effect (4). Therefore, it is of great significance to explore effective methods for early diagnosis.

MicroRNA (miRNA) is an endogenous RNA with a length of approximately 19-22 nucleotides. Moreover, miRNAs can participate in various biological processes by interacting with DNA through base pairing (5). MiRNAs can exert promoting or inhibitory effects in tumorigenesis, including HCC. For example, miR-30b-3p inhibited proliferation and invasion of HCC cells via suppressing PI3K/AKT pathway (6). In addition, miR-1251-5p promoted tumor growth and metastasis of HCC by targeting AKAP12 (7). Recently, the specific roles of miR-369-3p in diseases and cancers have attracted attention. It has been reported that epigenetic aberrations of miR-369-5p and DNMT3A are involved in cardiac fibrosis by controlling Patched1 signal pathway (8). Upregulation of miR-369-3p suppressed cell migration and proliferation

Key words: hepatocellular carcinoma; miR-369-3p; PAX6

Corresponding Author:
Dr Ke Liu,
Department of Hepatobiliary Surgery,
Central Hospital of Zibo, No. 54 Youth League Road,
Zibo, 255000, Shandong Province, China
Tel.: +86 13953373558
e-mail: mubaxsl604@163.com

0393-974X (2020)
Copyright © by BIOLIFE, s.a.s.
This publication and/or article is for individual use only and may not be further reproduced without written permission from the copyright holder.
Unauthorized reproduction may result in financial and other penalties
DISCLOSURE: ALL AUTHORS REPORT NO CONFLICTS OF INTEREST RELEVANT TO THIS ARTICLE.

by targeting SOX4 in Hirschsprung's disease (9). Additionally, downregulation of miR-369-3p was identified in endometriosis adenocarcinoma (EEC) and overexpression of miR-369-3p inhibited EEC cell proliferation and migration (10). miR-369-3p was found to act as a tumor suppressor in gastric cancer (11). However, the function of miR-369-3p in HCC remains largely unknown. Thus, the role of miR-369-3p as well as its regulatory mechanism was investigated in HCC.

Here, paired box 6 (PAX6) was predicted to be a target of miR-369-3p. PAX6 has been demonstrated to be involved in various key biological processes. For example, PAX6 suppressed the invasiveness of glioblastoma cells (12), and the expression of PAX6 was related to tumor grade and survival in gliomas (13). Moreover, PAX6 promoted cell migration during embryonic stem cell differentiation (14), but was found to inhibit cell proliferation and invasion in glioma cells (15). These studies indicate that the role of PAX6 is tissue-specific. However, the function of PAX6 is still unclear in HCC, hence, this study was designed to confirm the role of miR-369-3p and PAX6 in HCC. More importantly, the regulatory mechanism of miR-369-3p and PAX6 was also illuminated in HCC. We hope this study can help early diagnosis and treatment of HCC patients.

MATERIALS AND METHODS

Clinical tissues

Patients who were diagnosed with HCC via pathological examinations were enrolled in this study. This research was approved by the Institutional Ethics Committee of the Central Hospital of Zibo. Sixty-five HCC and adjacent normal tissues were collected from surgery. All participants provided written informed consents. These tissues from surgery were frozen in liquid nitrogen and stored at −80°C.

Cell culture and transfection

Normal liver cells (THLE-3) and HCC cell lines (SNU-387, SNU-182) were obtained from ATCC (Manassas, VA, USA). These cells were cultured in RPMI-1640 medium with 10% FBS and incubated in an incubator at 37°C with 5% CO_2. MiR-369-3p mimics or inhibitor and PAX6 siRNA or vector were all purchased from GenePharma (Shanghai, China). Then, the vectors or oligonucleotides were transfected into SNU-387 cells using Lipofectamine 2000 (Invitrogen, Carlsbad, CA, USA).

Quantitative real-time PCR (qRT-PCR)

TRIzol reagent (Invitrogen) was used for isolation of total RNA according to the manufacturer's protocol. Next, reverse transcription was performed with total RNA using TRUEscript One Step RT-PCR Kit (Aidlab Biotechnologies, China). The qRT-PCR assay was performed using PC60-2 x SYBR Green qPCR Mix (Aidlab Biotechnologies, China) and primers. The primer sequences were the following: GAPDH forward, 5'-ACA ACT TTG GTA TCG TGG AAG G-3', and reverse, 5'-GCC ATC ACG CCA CAG TTT C-3'; PAX6 forward,5'-AAC GAT AAC ATA CCA AGC GTG T-3', and reverse, 5'-GGT CTG CCC GTT CAA CAT C-3'; miR-369-3p forward: 5'-TGA CCT AAG GGA CTC CCA CAA-3', Reverse: 5'-TAG CAA TAT TGC ACA GAA GGC-3'; U6 forward: 5'-GCT TCG GCA GCA CAT ATA CTA AAA T-3' and reverse, 5'-CGC TTC ACG AAT TTG CGT GTC AT-3'. PAX6 and miR-369-3p were normalized using GAPDH and U6 as the internal control. Their expression levels were quantified with the $2^{-\triangle\triangle cq}$ method.

Assays

Transfected SNU-387 cells (3×10^3 cells/well) were seeded in 96-well plates. Next, MTT (Sigma, USA) reagent was added in the 96-well plates to measure cell viability at 24, 48, 72 and 96 h, respectively. After 10 min shaking, the absorbance at 490 nm was detected using spectrophotometer (Bio-Rad, Hercules, CA, USA).

The migration and invasion of HCC cells were measured using Transwell assay (8.0 μm pore size, Costar). Transfected SNU-387 cells (4×10^3 cells/well) were placed in the upper chamber. The upper chambers with or without Matrigel (BD Biosciences, San Jose, CA, USA) were used for cell invasion and migration, respectively. The lower chamber was coated with RPMI-1640 medium supplemented with 10% FBS. After 48 h, the moved cells in the lower chamber were stained with crystal violet and counted under an inverted microscope (IX31; Olympus Corporation).

The 3'-UTR of wild-type or mutant PAX6 was inserted into pmiR-GLO vectors (Promega, Beijing, China). Then,

the vectors and miR-369-3p mimics were co-transfected into SNU-387 cells and incubated for 48 h. Finally, luciferase activities were determined by dual-luciferase reporter assay system (Promega, USA).

Statistical analysis

Data are shown as mean ± SD. The association between miR-369-3p expressions and clinical characteristics was analyzed by χ^2 test. The differences between groups were tested using Student's *t*-test and ANOVA (with a Bonferroni post hoc test). All analyses were performed using SPSS 17.0 software (SPSS, USA) and GraphPad Prism 7 software (GraphPad software). Statistical significance was standardized at $P < 0.05$.

RESULTS

MiR-369-3p was downregulated in HCC

First, the abnormal expression of miR-369-3p was measured in HCC tissues. It was found that miR-369-3p expression in HCC tissues was decreased compared to normal tissues (P<0.01, Fig. 1A). Similarly, lower miR-369-3p expression was also identified in SNU-387 and SNU-182 HCC cells than in normal liver cells THLE-3 (P<0.01, Fig. 1B). Then, SNU-387 was used for further experiments due to its significant difference in miR-369-3p expression. In addition, the association between miR-369-3p expression and clinical features was explored in HCC patients. The results showed that the dysregulation of miR-369-3p was related to lymph node metastasis and TNM stage in HCC patients (P<0.05, Table I). Based on these results, it was hypothesised that the aberrant expression of miR-369-3p may regulate HCC progression.

MiR-369-3p inhibits cell viability and motility in HCC

To confirm the above prediction, the effect of miR-369-3p on cell proliferation and motility was investigated in SNU-387 cells. Next, miR-369-3p mimics or inhibitor was transfected into SNU-387 cells. RT-qPCR suggested that miR-369-3p expression was upregulated by its mimics, but downregulated by its inhibitor in SNU-387 cells (P<0.01, Fig. 2A). Functionally, overexpression of miR-369-3p restrained cell proliferation, while downregulation of miR-369-3p accelerated cell proliferation (P<0.05 or 0.01, Fig. 2B). Meanwhile, we found that miR-369-3p upregulation suppressed cell migration, whereas miR-369-3p downregulation promoted cell migration in SNU-387 cells (P<0.01, Fig. 2C). Cell invasion was also suppressed by miR-369-3p overexpression and inhibited by miR-369-3p downregulation (P<0.01, Fig. 2D). These results indicate that miR-369-3p plays an inhibitory effect on cell viability and motility in HCC.

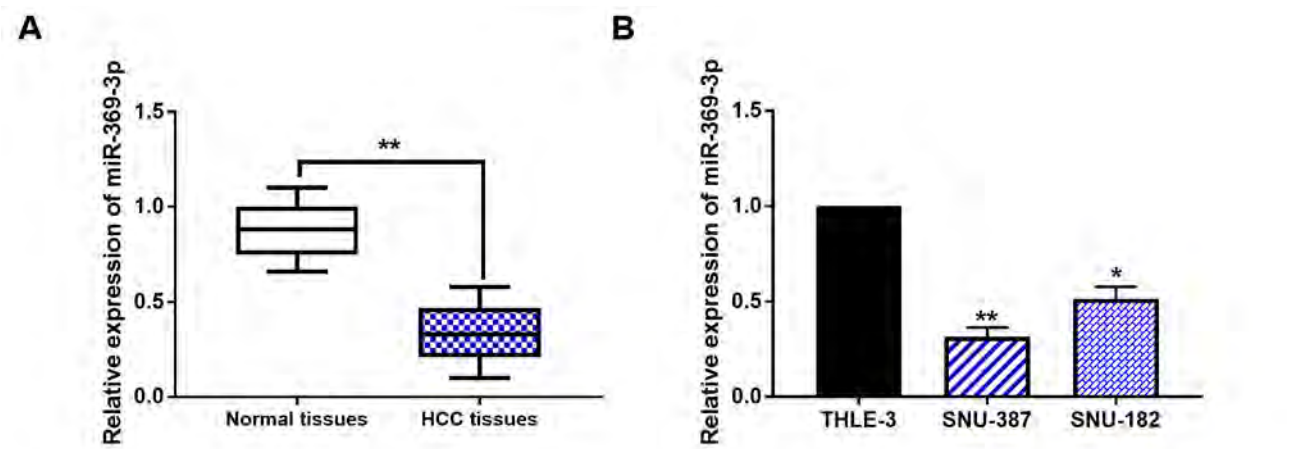


Fig. 1. *MiR-369-3p was downregulated in HCC.* ***A****) MiR-369-3p expression was detected in HCC tissues and normal tissues.* ***B****) MiR-369-3p expression was examined in SNU-387, SNU-182 and THLE-3 cells. *P < 0.01, **P < 0.01*

PAX6 is a direct target of miR-369-3p

To further elucidate the functional mechanism of miR-369-3p in HCC, its downstream target was searched in TargetScan (http://www.targetscan.org/vert_71/). PAX6 was predicted to have a binding site with miR-369-3p (Fig. 3A). Luciferase repertory assay showed that miR-369-3p mimics reduced the luciferase activity of wt-PAX6, but had little effect on that of mut-PAX6 (P<0.01, Fig. 3B), indicating that miR-369-3p directly targets PAX6. In addition, PAX6 was found to be upregulated in HCC tissues compared with normal tissues (P<0.01, Fig. 3C). And PAX6 expression was inversely correlated with miR-369-3p in HCC tissues (P<0.01, Fig. 3D). Furthermore, we found that the expression level of PAX6 was decreased by miR-369-3p mimics and

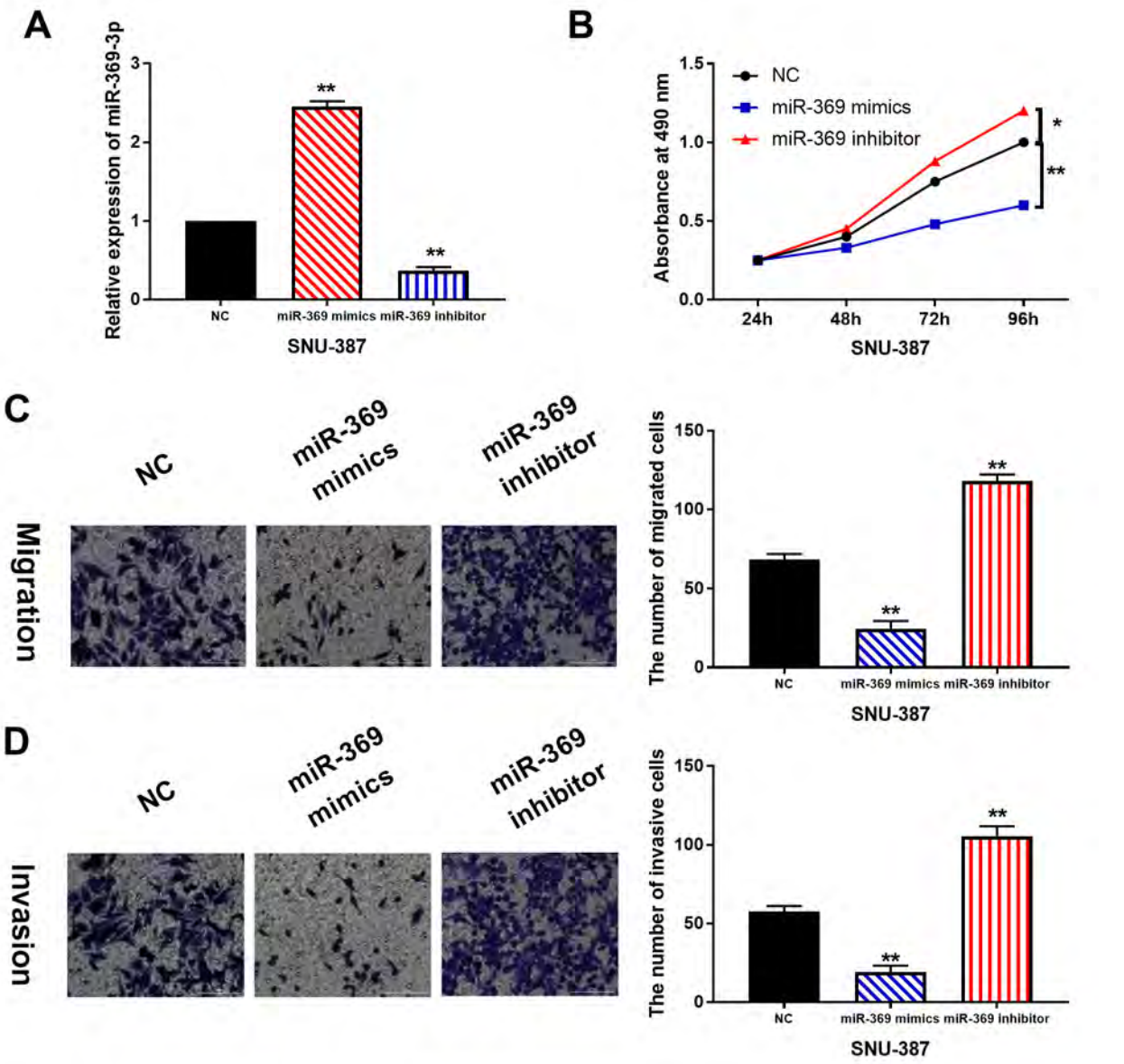


Fig. 2. *MiR-369-3p inhibits cell viability and motility in HCC.* ***A)*** *MiR-369-3p expression in SNU-387 cells with its mimics or inhibitor.* ***B, C, D)*** *Cell proliferation, migration and invasion in SNU-387 cells with miR-369-3p mimics or inhibitor *P < 0.05, ** P <0.01*

enhanced by miR-369-3p inhibitor in SNU-387 cells (P<0.01, Fig. 3E). Taken together, miR-369-3p can direct target PAX6 and negatively regulates PAX6 expression in HCC.

PAX6 is involved in the progression of HCC

To explore whether PAX6 is involved in the progression of HCC, the role of PAX6 was detected in HCC cells. Next, PAX6 siRNA was transfected into SNU-387 cells. And PAX6 expression was significantly decreased by its siRNA in SNU-387 cells (P<0.01, Fig. 4A). More importantly, MTT assay showed that knockdown of PAX6 suppressed SNU-387 cell proliferation (P<0.01, Fig. 4B). Transwell assay suggested that cell migration and invasion were also restrained by PAX6 downregulation in

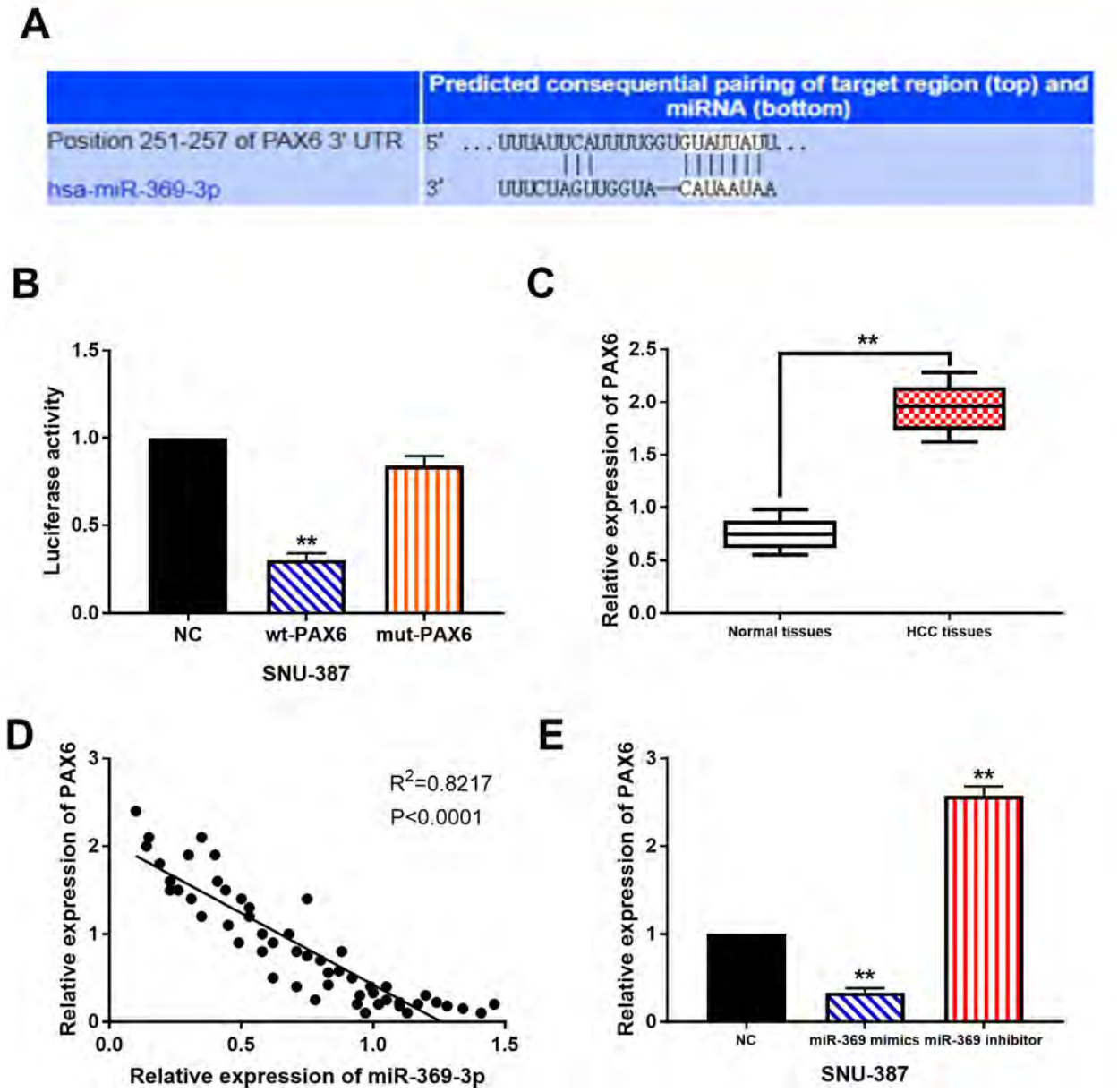


Fig. 3. *PAX6 is a direct target of miR-369-3p.* ***A****) Binding site between miR-369-3p and PAX6.* ***B****) Luciferase reporter assay.* ***C****) PAX6 expression in HCC tissues and normal tissues.* ***D****) A correlation between miR-369-3p and PAX6 expressions in HCC tissues.* ***E****) PAX6 expression in SNU-387 cells with miR-369-3p mimics or inhibitor ** P <0.01*

SNU-387 cells (P<0.01, Fig. 4 C, D). The above results imply that upregulation of PAX6 exerts carcinogenesis in the development of HCC.

MiR-369-3p regulates HCC tumorigenesis by interacting with PAX6

Finally, miR-369-3p mimics and PAX6 vector were transfected into SNU-387 cells to explore their interaction in HCC. The decreased expression of PAX6 induced by miR-369-3p mimics was restored by PAX6 vector in SNU-387 cells (P<0.01, Fig. 5A). In particular, the inhibitory effect of miR-369-3p mimics on cell proliferation was found to be abolished by PAX6 upregulation in SNU-387

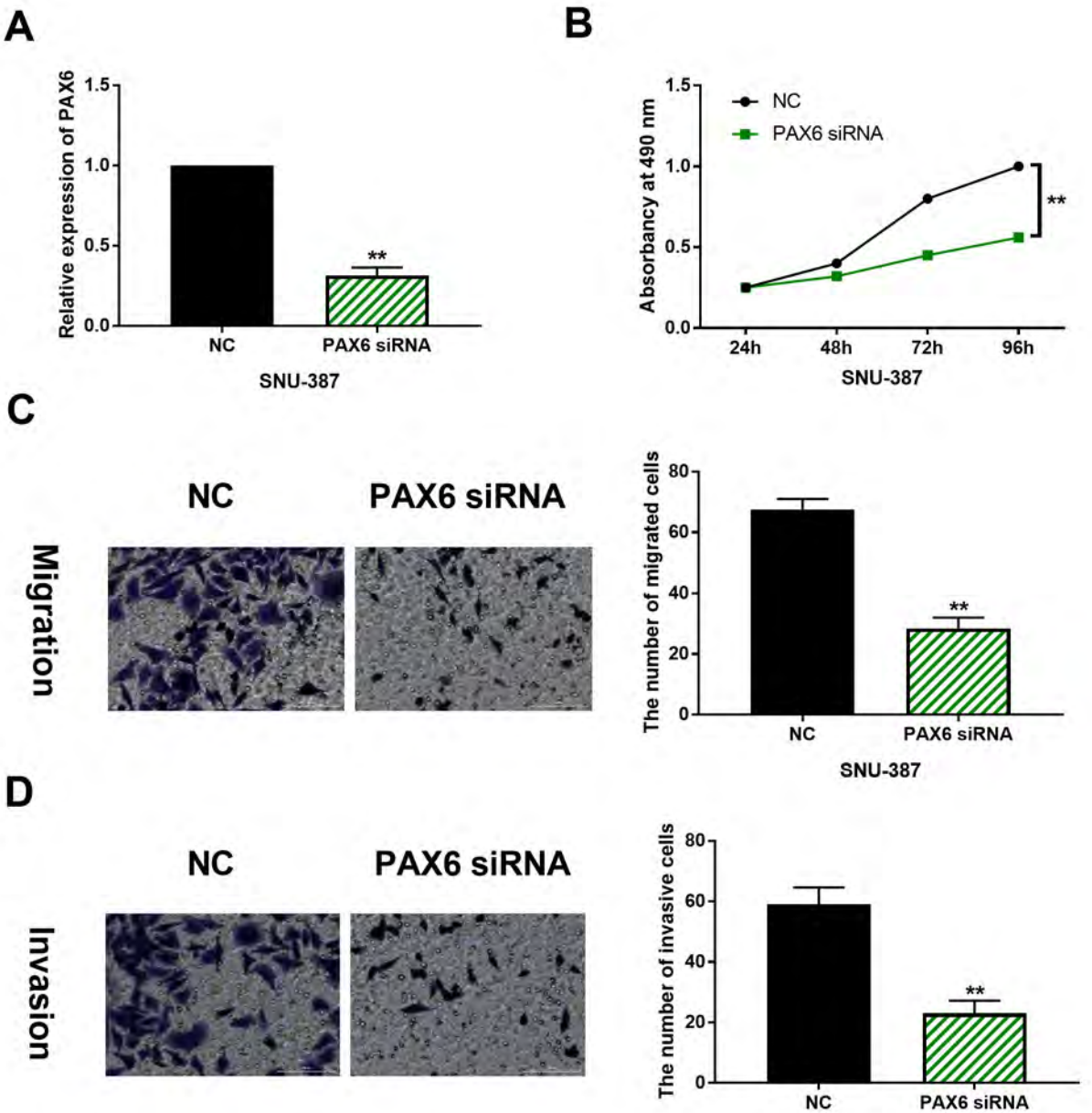


Fig. 4. *PAX6 is involved in the progression of HCC.* ***A)*** *PAX6 expression in SNU-387 cells with its siRNA.* ***B, C, D)*** *Cell proliferation, migration and invasion in SNU-387 cells with PAX6 siRNA ** P <0.01*

cells (P<0.01, Fig. 5B). At the same time, PAX6 upregulation also weakened the suppressive effect of miR-369-3p on SNU-387 cell migration and invasion (P<0.01, Fig. 5 C, D). Collectively, miR-369-3p restrains cell proliferation, migration and invasion in HCC by downregulating PAX6.

DISCUSSION

Many studies have shown that dysregulation of miRNAs is closely linked to the tumorigenesis and development of human cancers, including HCC. For example, miR-486-5p was significantly

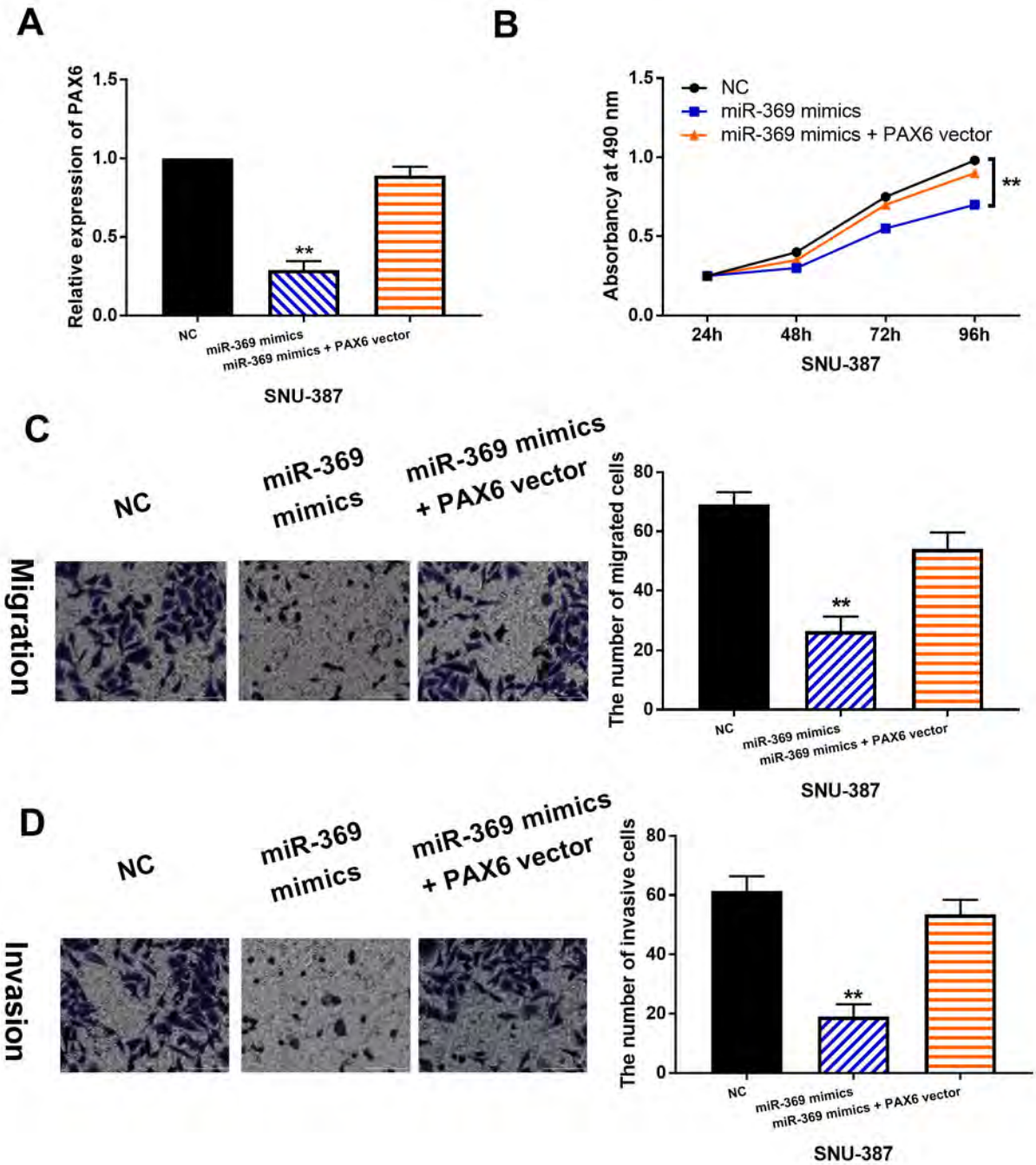


Fig. 5. *MiR-369-3p regulates HCC tumorigenesis by interacting with PAX6.* ***A)*** *PAX6 expression in SNU-387 cells with PAX6 vector and miR-369-3p mimics.* ***B, C, D)*** *Cell proliferation, migration and invasion in SNU-387 cells with PAX6 vector and miR-369-3p mimics ** P<0.01*

downregulated in HCC and acted as an HCC suppressor (16). Here, downregulation of miR-369-3p was also identified in HCC and associated with lymph node metastasis and TNM stage in HCC patients, which indicates that miR-369-3p is involved in the occurrence of HCC. Further, MTT and Transwell assays suggested that cell proliferation, migration and invasion were restrained by overexpression of miR-369-3p, suggesting that miR-369-3p serves as a tumor inhibitor in HCC. Mechanistically, PAX6 was found to weaken the inhibitory effect of miR-369-3p in HCC, suggesting that miR-369-3p inhibits HCC progression by targeting PAX6.

Previous studies have reported that miR-369-

Table I. *Relationship between miR-369-3p expression and clinicopathological characteristics in HCC patients*

Characteristics	Number of Cases(n=65)	miR-369-3p		P-value
		High	Low	
Age (years)				0.62
≥ 60	45	12	33	
<60	20	7	13	
Gender				0.88
Male	42	14	28	
Female	23	5	18	
Tumor size				0.16
< 3 cm	40	10	30	
≥ 3 cm	25	9	16	
TNM stage				0.02*
I + II	41	11	30	
III + IV	24	8	16	
Lymph node metastasis				0.03*
Negative	38	8	30	
Positive	27	11	16	
Drinking				0.56
Yes	44	14	30	
No	21	5	16	

*Statistical analyses were performed by the χ^2 test. *P□0.05 was considered significant.*

3p was downregulated in colorectal cancer and papillary thyroid cancer (17, 18), and was found to be significantly associated with overall survival in patients with tongue squamous cell carcinoma (19). Functionally, miR-369-3p inhibited prostate cancer cell proliferation and migration (20). The same results were also identified in HCC. In addition, the inhibitory effect of miR-369-3p on cell invasion was found in HCC, which has not been reported in previous studies. Moreover, it has been shown that miR-369-3p is involved in tumorigenesis by regulating expression of target genes, such as SLC35F5 (21). In this study, we found and validated that PAX6 was one of the target genes of miR-369-3p, and knockdown of PAX6 restrains cell proliferation, migration and invasion in HCC.

PAX6, located on the chromosome11p13, is a member of the paired box (PAX) families. The role of PAX6 has been found in many human cancers. For example, upregulation of PAX6 was identified in breast cancer, and PAX6 overexpression was associated with the poor prognosis of invasive ductal breast cancer (22). Moreover, PAX6, a novel target of miR-7, promoted cellular proliferation and invasion in human colorectal cancer cells (23). In the present study, we also found upregulation and carcinogenesis of PAX6 in HCC. Additionally, miR-335 was reported to inhibit proliferation, cell-cycle progression, colony formation, and invasion via targeting PAX6 in breast cancer cells (24). MiR-7 also inhibited the malignant phenotypes of non-small cell lung cancer in vitro by targeting PAX6 (25). In line with these data, we also found that miR-369-3p functions as a tumor suppressor in HCC by inhibiting PAX6 expression. The regulatory mechanism of miR-369-3p/PAX6 in our research axis is firstly reported in HCC.

In conclusion, downregulation of miR-369-3p was found in HCC. Furthermore, overexpression of miR-369-3p suppressed cell proliferation and motility in HCC partly through downregulating PAX6. However, this study still has several limitations, such as the absence of in vivo experiments. In the future, further experiments on the regulatory mechanism of miR-369-3p will be performed.

REFERENCES

1. Ferlay J, Colombet M, Soerjomataram I, et al. Estimating the global cancer incidence and mortality in 2018: GLOBOCAN sources and methods. Int J Cancer 2019; 144:1941-53.
2. Rich NE, Yopp AC, Singal AG. Medical Management of Hepatocellular Carcinoma. J Oncol Pract 2017; 13:356-64.
3. Ikeda K. Recent advances in medical management of hepatocellular carcinoma. Hepatol Res 2019; 49:14-32.
4. Medavaram S, Zhang Y. Emerging therapies in advanced hepatocellular carcinoma. Exp Hematol Oncol 2018; 7:17.
5. Qu K, Wang Z, Lin XL, Zhang K, He XL, Zhang H. MicroRNAs: Key regulators of endothelial progenitor cell functions. Clin Chim Acta 2015; 448:65-73.
6. Gao D, Zhou Z and Huang H. miR-30b-3p Inhibits Proliferation and Invasion of Hepatocellular Carcinoma Cells via Suppressing PI3K/Akt Pathway. Front Genet 2019; 10:1274.
7. Han S, Wang L, Sun L, et al. MicroRNA-1251-5p promotes tumor growth and metastasis of hepatocellular carcinoma by targeting AKAP12. Biomed Pharmacother 2020; 122:109754.
8. Tao H, Dai C, Ding JF, et al. Epigenetic aberrations of miR-369-5p and DNMT3A control Patched1 signal pathway in cardiac fibrosis. Toxicology 2018; 410:182-92.
9. Pan W, Yu H, Zheng B, et al. Upregulation of MiR-369-3p suppresses cell migration and proliferation by targeting SOX4 in Hirschsprung's disease. J Pediatr Surg 2017; 52:1363-70.
10. Liu P, Ma C, Wu Q, et al. MiR-369-3p participates in endometrioid adenocarcinoma via the regulation of autophagy. Cancer Cell Int 2019; 19:178.
11. Dong L, Zhang Z, Xu J, et al. Consistency analysis of microRNA-arm expression reveals microRNA-369-5p/3p as tumor suppressors in gastric cancer. Mol Oncol 2019; 13:1605-20.
12. Mayes DA, Hu Y, Teng Y, et al. PAX6 suppresses the invasiveness of glioblastoma cells and the expression of the matrix metalloproteinase-2 gene. Cancer Res 2006; 66:9809-17.

13. Zhou YH, Tan F, Hess KR,Yung WK. The expression of PAX6, PTEN, vascular endothelial growth factor, and epidermal growth factor receptor in gliomas: relationship to tumor grade and survival. Clin Cancer Res 2003; 9:3369-75.
14. Fang J, Zhang T, Liu Y, et al. PAX6 downregulates miR-124 expression to promote cell migration during embryonic stem cell differentiation. Stem Cells Dev 2014; 23:2297-310.
15. Cheng Q, Cao H, Chen Z, Ma Z, Wan X, Peng R, Jiang B. PAX6, a novel target of miR-335, inhibits cell proliferation and invasion in glioma cells. Mol Med Rep 2014; 10:399-404.
16. He J, Xiao B, Li X, He Y, Li L, Sun Z. MiR-486-5p Suppresses Proliferation and Migration of Hepatocellular Carcinoma Cells through Downregulation of the E3 Ubiquitin Ligase CBL. Biomed Res Int 2019; 2019:2732057.
17. Zou Y, Yao S, Chen X, et al. LncRNA OIP5-AS1 regulates radioresistance by targeting DYRK1A through miR-369-3p in colorectal cancer cells. Eur J Cell Biol 2018; 97:369-78.
18. Li P, Dong M, Wang Z. Downregulation of TSPAN13 by miR-369-3p inhibits cell proliferation in papillary thyroid cancer (PTC). Bosn J Basic Med Sci 2019; 19:146-54.
19. Zhou RS, Zhang EX, Sun QF, Ye ZJ, Liu JW, Zhou DH, Tang Y. Integrated analysis of lncRNA-miRNA-mRNA ceRNA network in squamous cell carcinoma of tongue. BMC Cancer 2019; 19:779.
20. Wo Q, Zhang D, Hu L, et al. Long noncoding RNA SOX2-OT facilitates prostate cancer cell proliferation and migration via miR-369-3p/CFL2 axis. Biochem Biophys Res Commun 2019; 520:586-93.
21. Hao GJ, Ding YH, Wen H, et al. Attenuation of deregulated miR-369-3p expression sensitizes non-small cell lung cancer cells to cisplatin via modulation of the nucleotide sugar transporter SLC35F5. Biochem Biophys Res Commun 2017; 488:501-08.
22. Xia X, Yin W, Zhang X, et al. PAX6 overexpression is associated with the poor prognosis of invasive ductal breast cancer. Oncol Lett 2015; 10:1501-06.
23. Berghoff AS, Bartsch R, Wohrer A, et al. Predictive molecular markers in metastases to the central nervous system: recent advances and future avenues. Acta Neuropathol 2014; 128:879-91.
24. Meng Y, Zou Q, Liu T, Cai X, Huang Y, Pan J. microRNA-335 inhibits proliferation, cell-cycle progression, colony formation, and invasion via targeting PAX6 in breast cancer cells. Mol Med Rep 2015; 11:379-85.
25. Luo J, Li H, Zhang C. MicroRNA-7 inhibits the malignant phenotypes of nonsmall cell lung cancer in vitro by targeting Pax6. Mol Med Rep 2015; 12:5443-8.

Hsa-miR-10a-5p PROMOTES PANCREATIC CANCER GROWTH BY BDNF/SEMA4C PATHWAY

X. FEI, HY. JIN, Y. GAO, LM. KONG and XD. TAN

Department of General Surgery, Shengjing Hospital of China Medical University, Shenyang, China

Received February 3, 2020 – Accepted May 13, 2020

This article aims to explore the expression and mechanism of miR-10a-5p in pancreatic cancer. MiR-10a-5p mimic, MiR-10a-5p inhibitor and negative control were transfected into human pancreatic cancer cell line SW1990. Real-time quantitative PCR technology was used to analyze the expression level of miR-10a-5p in pancreatic cancer tissues and cells. The proliferation, invasion and apoptosis of SW1990 cells in each group were detected by CCK-8 analysis, Transwell analysis, TUNEL method and flow cytometry. Targetscan7.2 was used to predict the target protein of MiR-10a-5p, and the expression of related proteins was detected by Western blot analysis. The results showed that the expression of miR-10a-5p in cancer tissues of patients with pancreatic cancer was significantly higher than that in adjacent tissues (P <0.05). The expression of miR-10a-5p in cancer cells increased significantly, which could promote the proliferation and invasion of SW1990 cells and inhibit apoptosis (P <0.05). Overexpression of miR-10a-5p can regulate the expression of BDNF and SEMA4C. miR-10a-5p can promote the occurrence and development of pancreatic cancer by regulating the BDNF / SEMA4C pathway, and may become a molecular target for the diagnosis and treatment of pancreatic cancer in the future.

Pancreatic cancer is one of the cancers with the highest mortality rate in the world. In the past three decades, its prognosis has not improved significantly, and the five-year survival rate is only 6% (1, 2). At present, surgical treatment is still the only effective treatment. Due to its hidden anatomical location, pancreatic cancer is difficult to detect early (3). With the progress of medical diagnosis and treatment, the survival rate of most cancer patients has been significantly improved, but the prognosis of pancreatic cancer patients has not (3). Therefore, it is of great significance to discover new biological indicators related to the occurrence, early diagnosis and prognosis of pancreatic cancer for early detection and improvement of the prognosis of pancreatic cancer patients.

In recent years, miRNA has become one of the research hotspots. miRNA is a non-coding small molecule single-stranded RNA that affects the stability of the target gene mRNA by specifically binding to the 3'-untranslated or coding region of the target gene mRNA sequence, or directly inhibiting the target gene protein translation, thereby regulating the expression of target genes. Previous studies have shown that miRNA, as an important regulator, is involved in physiological processes such as cell differentiation, proliferation, apoptosis, and metabolism (4, 5). Due to the important role of miRNAs in regulating the physiological activities of normal cells, unregulated regulation will cause changes in the biological behavior of normal cells, such as cell cycle, proliferation, metastasis and

Key words: miR-10a-5p; BDNF; SEMA4C; pancreatic cancer

Corresponding Author:
Dr Xiaodong Tan,
Department of General Surgery,
Shengjing Hospital of China Medical University,
36 Sanhao Street, Heping District,
Shenyang, 110004, China
e-mail: tanxiaodongxd001@163.com

0393-974X (2020)
Copyright © by BIOLIFE, s.a.s.
This publication and/or article is for individual use only and may not be further reproduced without written permission from the copyright holder.
Unauthorized reproduction may result in financial and other penalties
DISCLOSURE: ALL AUTHORS REPORT NO CONFLICTS OF INTEREST RELEVANT TO THIS ARTICLE.

invasion, and promote the malignant transformation of cells, resulting in the occurrence and development of tumors (6-9). Studies have shown that the abnormal expression of miRNA is closely related to many human diseases including tumors. Related studies have reported that miR-486 promotes the proliferation of human pancreatic cancer cell line (Capan-2) cells by targeting PTEN, indicating that miR-486 inhibition may be a new treatment for pancreatic cancer (10).

However, its role in pancreatic cancer is unclear. Therefore, the purpose of this study is to explore the expression of miR-10a-5p in pancreatic cancer cells and tissues, and study the various functions of miR-10a-5p in pancreatic cancer cells. The predicted the target genes of miR-10a-5p were verified through the Targetscan 7.2 database. It was found that miR-10a-5p can promote the development of pancreatic cancer through the miR-10a-5p-BDNF/ SEMA4C signaling pathway.

miRNA is the main regulator of gene expression and the regulator of many cell growth and reproduction processes, and plays an important regulatory role in tumorigenesis and development. miRNA has become one of the most promising biomarkers in clinical early diagnosis, prognosis and treatment response prediction. With the continuous update of miRNA research technology, it has become a hot spot to further study the mechanism of miRNA on tumor regulation. Whether miRNA is used as a diagnostic marker, a therapeutic target, or as a drug directly used in the clinic, its goal will be achieved and gradually promoted.

MATERIALS AND METHODS

Specimens and cells

Twenty-five pairs of pancreatic cancer and adjacent pairs of fresh tissues were taken from fresh surgical specimens of surgical patients in Shengjing Hospital of China Medical University between January 1, 2018 and May 31, 2019, and the fresh tissues were immediately stored in liquid nitrogen after resection, and frozen until use. The study was approved by the Ethics Committee of Shengjing Hospital of China Medical University and all the patients signed informed consent for their participation.

The six types of cells involved in the study, HaCaT, BxPC3, SW1990, panc-1, pci-35 and suite-2 were purchased from American Type Culture Collection (ATCC, Manassas, VA, USA) and the cell bank of Chinese Academy of Sciences. HaCaT were cultured in mem-ebss: Minimum Essential Medium (MEM Eagles with Earle's balanced salts) plus 10% fetal serum (FBS, Thermo Fisher Scientific), 2 mmol/L l-glutamine (Thermo Fisher Scientific) and 100 units/mL penicillin/streptomycin (Thermo Fisher Scientific), at 37°C in 5% CO_2. BxPC3, SW1990, panc-1, pci-35, and suite-2 were cultured in DMEM medium.

RNA extraction and quantitative real-time polymerase chain reaction (qRT-PCR)

Total RNA was extracted with TRIzol reagent (Invitrogen), and reverse transcription of RNA was performed using PrimeScript-RT reagent kit (Beyotime). QRT-PCR was performed using qPCR SYBR Green/ ROX (QIAGEN). The standard internal reference is glyceraldehyde-3-phosphate dehydrogenase (GAPDH). The primers of miR-10a-5p in qRT-PCR were F: 5 '-CAAAUUCGGAUCUACAGGGUAUU -3', R: 5 '-UACCCUGUAGAUCCGAAUUUGUG-3', GAPDH-F: 5 '- GGTGAAGGTCGGAGTCAACG -3', R: 5 '-CAAAGTTGTCATGGATGHACC-3 '. The primers for this study were from Takara. The content was measured of miR-10a-5p in PC tissues.

Transfection and groups

Logarithmic growth cells were divided into three group: miR-10a-5p mimic group (Mimic), miR-10a-5p inhibitor group (Inhibitor), and a control group (Control). The cells in the three groups were transfected by related Lipofectamine 2000 (Thermo Fisher Scientific). SW1990 Cells were collected 24 h after transfection for the following experiments.

Cell counting kit (CCK)-8 assay

Cells were cultured on 96 well plastic plates at a density of 6 × 104 / ml, and 10 ml CCK-8 (Beyotime, China) was added at 0, 24, 48, 72 and 96 h, respectively, and incubated at 37°C for 4 h. The absorbance at 450 nm was detected using Thermo Fisher Scientific's microplate reader.

Transwell assay

The migration test was performed using a 24-well

Boyden cavity and an uncoated filter with a pore size of 8 mm. Cells were collected and washed twice with PBS. The cells were suspended in serum-free medium, and 3×10^4 cells were seeded in the insertion chamber. The cells were cultured in a basal cavity (0.6 mL MEMS medium containing 10% FBS) at 37°C (5% CO_2) for 24 h. Cells were stained with 4,6-diamino-2-phenylindole and counted under a vertical microscope.

Apoptosis assay

Hoechst staining was used to analyze apoptosis. SW1990 cells were cultured in a six-well culture plate. These cells were fixed and stained with 10 μg/ml Brustasol and left in the dark for 10 min. The samples were then washed with PBS and observed under an inverted fluorescence microscope. At the same time, the apoptosis rate of islet cells was detected by flow cytometry. Apoptotic cells have obvious morphological changes in the nucleus, which can be identified by densification of the nucleus or densification of stained fragments.

Predicting the target genes of MiR-10a-5p by bioinformatics

Targetscan7.2 online source prediction website (http://www.targetscan.org/vert_72/) was used to predict target genes of miR-10a-5p, by reading the literature. Four preselected targets: BDNF, IL8, SEMA4C and PPP3R1 were chosen.

Western-blot analysis

Western blot was used to detect the content of related proteins. Protein antibodies were purchased from Abcam, UK. Protein samples were extracted with Ripa buffer, and denatured and separated by 10% sodium laurate-polyacrylamide gel electrophoresis. The separated protein is transferred to the PVDF membrane. These membranes were incubated with the primary antibody at 4°C overnight, and then incubated with the corresponding secondary antibody at room temperature for 1 h. Finally, specific myosin was used to calculate the protein concentration.

Statistical analysis

GraphPad Prism 8.3.0 software was used for statistical analysis after data processing. The comparison between the three groups used the *F* test for precise comparison, means P value < 0.05.

RESULTS

Expression of miR-10a-5p was up-regulated in PC tissues and cells

The expression levels of miR-10a-5p in 25 pairs of PC tissues and adjacent normal tissues were measured by qRT-PCR. The results showed that the expression of miR-10a-5p was upregulated in PC samples compared to adjacent normal tissues (Fig. 1A). In addition, the expression levels of miR-10a-5p in normal cells and PC cell lines (BxPC3, SW1990, Panc-1, PCI-35 and SUIT-2) were analyzed. The results showed that the expression of miR-10a-5p was the highest in SW1990 cells and the lowest in HaCaT cells (Fig.1B).

Expression of miR-10a-5p in three groups

As shown in Fig. 2, compared with the control group, the expression of miR-10a-5p mRNA was significantly increased ($p < 0.05$). miR-21 mRNA expression was significantly reduced ($p < 0.05$). The results showed that the transfection was successful.

MiR-10a-5p promoted invasion and proliferation of SW1990 cells

CCK8 experiments showed that compared with the control group, miR-10a-5p inhibitor can inhibit the proliferation of SW1990 cells, while miR-10a-5p mimic can promote the proliferation of SW1990 cells (Fig. 3A). Transwell results showed that miR-10a-5p mimic promoted the invasiveness of SW1990 cells, while miR-10a-5p inhibitors reduced the invasiveness of SW1990 cells by 40-50% (Fig. 3 B and C).

Apoptosis results of miR-10a-5p in SW1990 cells

Fluorescence results showed that miR-10a-5p inhibitor significantly inhibited the apoptosis of SW1990 cells, while miR-10a-5p mimic increased the apoptosis of SW1990 cells (Fig.4 A and C). The results of flow cytometry showed that mir-10a-5p significantly inhibited the early apoptosis rate of PC cells (Fig. 4B).

MiR-10a-5p increased the malignancy of SW1990 cells through the miR-10a-5p- BDNF/Sema4C pathway

Targetscan7.2 prediction results suggested that

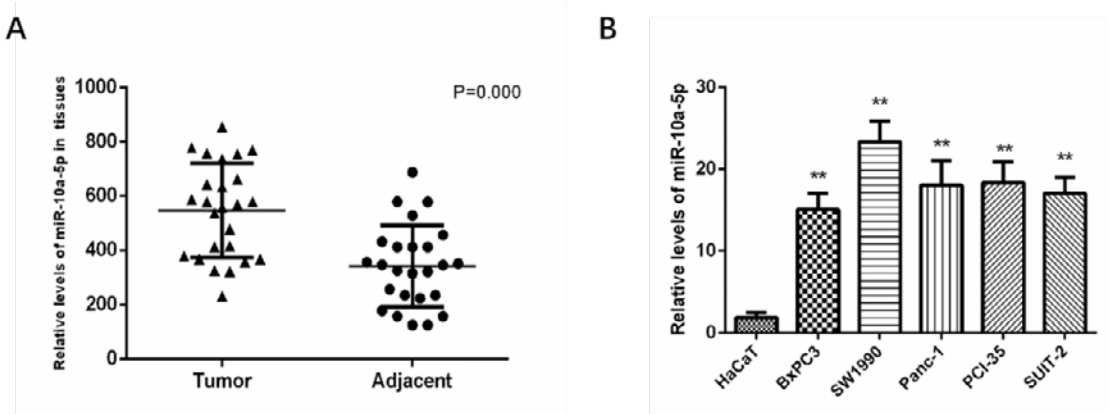


Fig. 1. *MiR-10a-5p was upregulated in PC specimens and cells, especially in SW1990 cell line.*

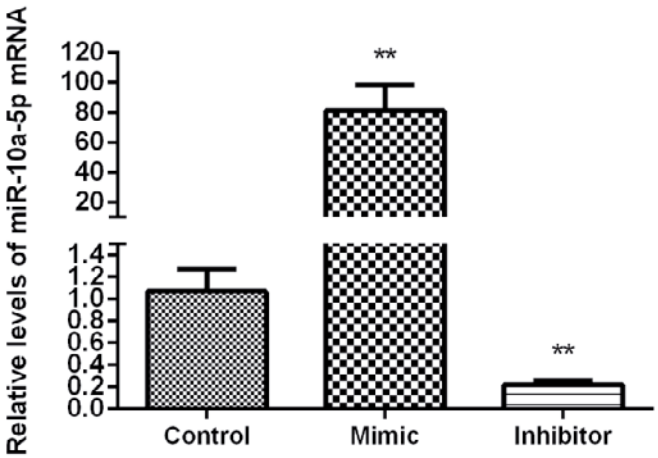


Fig. 2. *Expression of miR-10a-5p in three groups. Values are mean ± SD.*

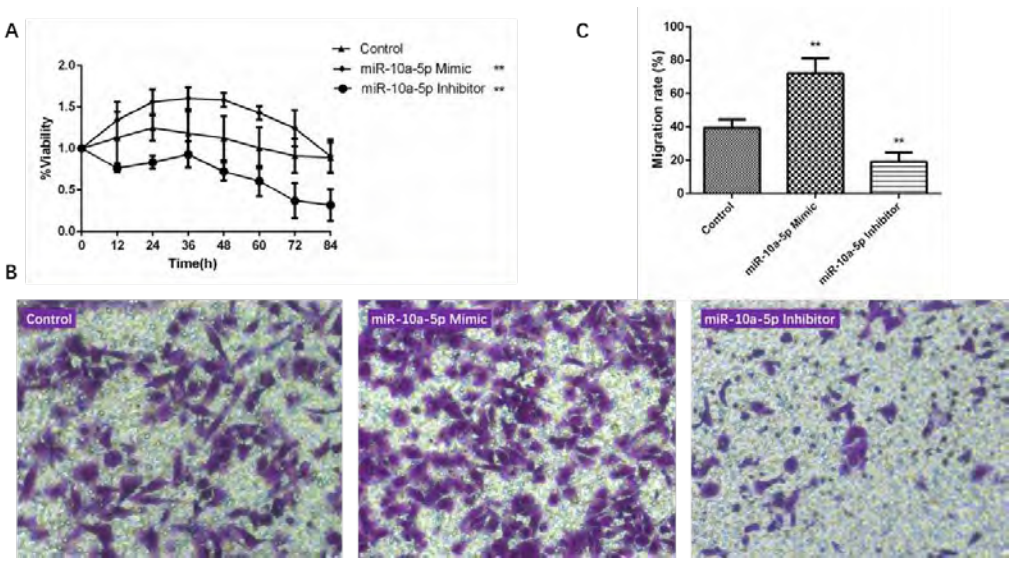


Fig. 3. *Results of cell proliferation and Transwell experiments in the control group, miR-10a-5p mimic and miR-10a-5p inhibitor groups.* ***A****) CCK8 experimental results of SW1990 cells in different groups;* ***B*** *and* ***C****) Transwell results of SW1990 cells in different groups.*

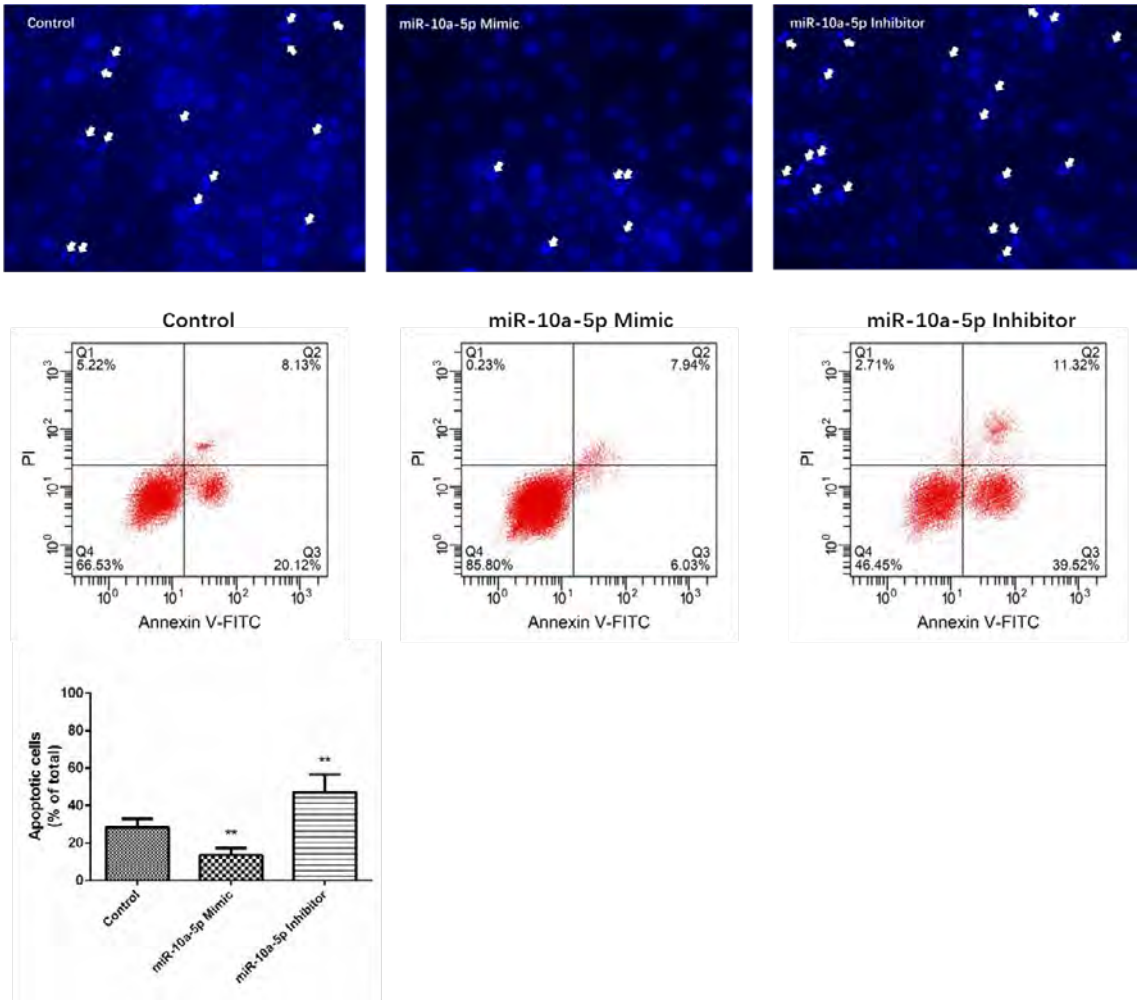


Fig. 4. *Results of apoptosis assay in Control group, miR-10a-5p mimic group and miR-10a-5p inhibitor group.*

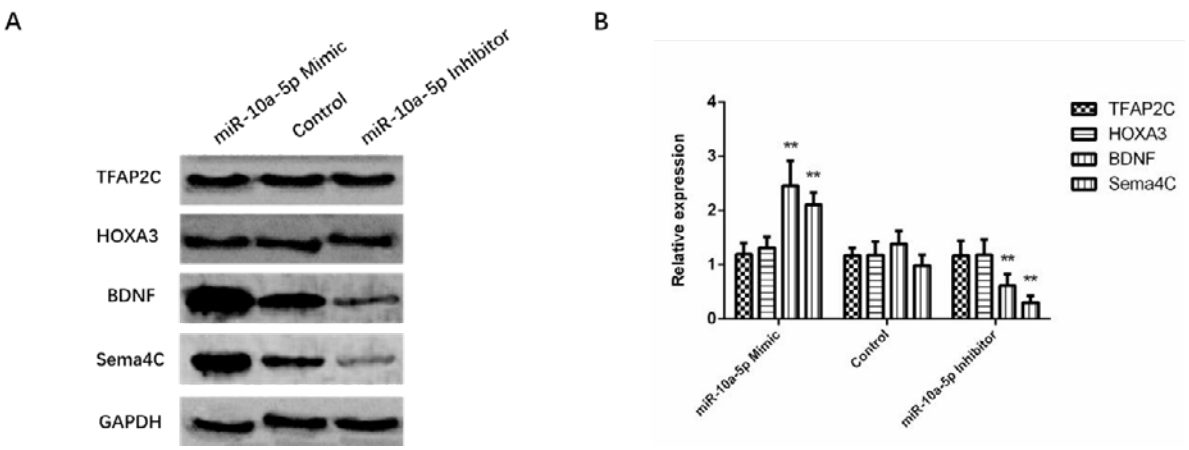


Fig. 5. *BDNF, IL8, SEMA4C and PPP3R1 expression in the control group, miR-10a-5p mimic group and miR-10a-5p inhibitor group.*

many related proteins may interact with miR-10a-5p. After consulting the relevant literature, we finally selected 4 candidate proteins, BDNF, IL8, SEMA4C and PPP3R1, for Western blot experiments. Western blot analysis showed that with the increase of miR-10a-5p, the content of BDNF and SEMA4C increased. However, no correlation was found with IL8 expression, and ppp3r1 expression did not change significantly between groups (Fig. 5 A and B).

DISCUSSION

Pancreatic cancer is one of the most common malignant tumors of the digestive system that seriously threaten human health. According to the global cancer report 2008 (GLOBOCAN2008) released by WHO, the annual incidence of pancreatic cancer worldwide is about 278,700, ranking 12th among malignant tumors (11-13). In China, the number of pancreatic cancer patients is increasing year by year. Statistics in 2010 showed that the incidence of pancreatic cancer in China reached 6/100,000, and the mortality rate ranks the 6th among all tumors, with the ratio of death to incidence being 0.86 (14). Pancreatic cancer is usually insidious, difficult to diagnose and treat, prone to metastasis and poor treatment effect, with a 5-year survival rate of only 1.2~6% (15, 16). Relevant data shows that the sensitivity of common serum tumor markers, carbohydrate antigen 199 (CA199) for the diagnosis of pancreatic cancer was 70~80%, but the specificity was less than 50% (17). Therefore, it is essentiall to find a tumor marker with high sensitivity and specificity in the diagnosis of early pancreatic cancer.

With the development of medical science and technology, the importance and practicability of molecular biology technology has been gradually discovered, and the pathogenesis of tumor at the cellular and molecular level has been further understood. In the clinical treatment of tumors, it is a difficult problem to find meaningful tumor markers. MicroRNA (miRNA) can be used as a marker of tumor screening, and play a role in early detection, efficacy monitoring and evaluation, prognosis judgment, etc. MiRNA is a noncoding small molecular RNA with the size of 21-25 nucleotides, which widely exists in animal and plant cells. Through complete or incomplete complementary combination with the target gene 3'- UTR region, miRNA can cause the degradation or translation inhibition of messenger RNA (mRNA), play a negative regulatory role, and regulate the expression of the target gene by means of transcription (18). Studies have shown that nearly one thousand miRNAs have been found in the human genome, and about 30% of gene expression and translation are regulated by miRNAs (19). It can regulate not only the function of normal cells, but also regulate the differentiation, proliferation, migration and other biological behaviors of tumor cells (20). By regulating the expression of specific miRNA in tumor, the occurrence and development of tumor can be changed to a certain extent. This article mainly introduces the regulatory mechanism of miRNA in pancreatic cancer, in order to provide new ideas for the clinical treatment of tumor.

The relationship between hsa-miR-10a-5p and the prognosis of pancreatic cancer is unknown, but studies have shown that miR-10a-5p can be involved in the occurrence and development of a variety of cancers (21-23). This used Targetscan database analysis and review analysis, and TFAP2C, HOXA3, BDNF, and Sema4C were chosen as pre-selected targets. The final Western blot results showed that miR-10a-5p can interact with BDNF and SEMA4C and promote their expression. BDNF is a neurotrophic factor widely existing in CNS.

As an important member of neurotrophic factor family, BDNF is very important for the development and growth of nerves. It is known that BDNF receptors can be divided into two categories: Trk B with high affinity and p75NTR with low affinity. BDNF and Trk B are highly expressed not only in neuroblastoma, but also in respiratory, digestive, reproductive system, head and neck tissue tumors, as well as lung cancer, liver cancer, colorectal cancer. Many signaling pathways and molecules are involved in the regulation of BDNF/TrkB signaling pathway on tumorigenesis and development. In addition, gene mutation and epigenetic regulation of BDNF/TrkB in tumorigenesis cannot be ignored. The activation of BDNF/TrkB signal pathway can not only stimulate the proliferation, invasion and metastasis of tumor cells, angiogenesis, but also inhibit the apoptosis of

tumor cells. These changes can lead to toxic resistance of tumor cells, namely drug resistance. Therefore, to block TrkB/BDNF signal is an important measure of anti-tumor therapy. Recent studies have found that BDNF also promotes adhesion, proliferation and migration of various tumor cells in the body, and induces angiogenesis (24). Studies have shown that BDNF and its receptor TrkB play a very important role in the development of tumor, and activation of BDNF/TrkB signal is closely related to the drug resistance of tumor cells in addition to stimulating the survival of tumor cells, angiogenesis and apoptosis (25).

T date, SEMA4C, as a member of the fourth subfamily of semaphorin family, has been studied less, but it involves a wide range of fields, including axonal guidance, proliferation and migration of brain granulosa cell precursor cells, myotube differentiation, potential regulation of β-Catenin signal in pigmentation and innervation. Recently, it was reported that it is expressed in neural stem cells/precursor cells and in neurogenesis after cerebral ischemia in adult rats (26). It has been reported that Sema4C is highly expressed in esophageal cancer, gastric cancer and rectal cancer, and is closely related to lymph node metastasis, which may play an important role in the invasion and metastasis of three kinds of malignant tumors (27, 28). Although SEMA4C literature covers a wide range, there are few studies on its occurrence, development and progress with tumors. Our experiments show that miR-10a-5p can regulate the proliferation, invasion and apoptosis of PC SW1990 cells through the BDNF/Sema4C pathway. Imbalance of miR-10a-5p expression may be one of the mechanisms that promote PC development.

In summary, this study demonstrated that miR-10a-5p could promote proliferation and inhibit apoptosis of lymphoma cells. The possible mechanism may be related to BDNF/SEMA4C pathway. Our study suggested that miR-10a-5p could provide a potential target in PC diagnosis and treatment.

REFERENCES

1. Ilic M, Ilic I. Epidemiology of pancreatic cancer. World J Gastroenterol 2016; 22(44):9694-705.
2. Ilić M, Vlajinac H, Marinković J, Kocev N. Pancreatic cancer mortality in Serbia from 1991-2010 - a joinpoint analysis. Croat Med J 2013; 54(4):369-75.
3. Barbosa IR, Santos CAD, de Souza DLB. Pancreatic cancer in brazil: mortality trends and projections until 2029. Arq Gastroenterol 2018; 55(3):230-36.
4. Ji Q, Xu Y, Wang Y. Research progress of MicroRNA in osteoarthritis cartilage matrix degradation. Zhongguo Xiu Fu Chong Jian Wai Ke Za Zhi 2016; 30(11):1431-36.
5. Biswas S. MicroRNAs as therapeutic agents: the future of the battle against cancer. Curr Top Med Chem 2018; 18(30):2544-54.
6. Jaiswal S, Iquebal MA, Arora V, et al. Development of species specific putative miRNA and its target prediction tool in wheat (Triticum aestivum L.). Sci Rep 2019; 9(1):3790.
7. Korourian A, Roudi R, Shariftabrizi A, Madjd Z. MicroRNA-31 inhibits RhoA-mediated tumor invasion and chemotherapy resistance in MKN-45 gastric adenocarcinoma cells. Exp Biol Med (Maywood) 2017; 242(18):1842-47.
8. Schmidt MF. miRNA Targeting drugs: The next blockbusters? Methods Mol Biol 2017; 1517:3-22.
9. Zhang BH, Shen CA, Zhu BW, et al. Insight into miRNAs related with glucometabolic disorder. Biomed Pharmacother 2019; 111:657-65.
10. Xia L, Song M, Sun M, et al. miR-486 promotes capan-2 pancreatic cancer cell proliferation by targeting phosphatase and tensin homolog deleted on chromosome 10 (PTEN). Front Genet 2019; 10:541.
11. McGuigan A, Kelly P, Turkington RC, Jones C, Coleman HG, McCain RS. Pancreatic cancer: A review of clinical diagnosis, epidemiology, treatment and outcomes. World J Gastroenterol 2018; 24(43):4846-61.
12. Heinrich S, Lang H. Neoadjuvant therapy of pancreatic cancer: definitions and benefits. Int J Mol Sci 2017; 18(8).
13. Kamisawa T, Wood LD, Itoi T, Takaori K. Pancreatic cancer. Lancet 2016; 388(10039):73-85.
14. Tokunaga K, Arizono S, Shimizu H, et al. Optimizing b-values for accurate depiction of pancreatic cancer with tumor-associated pancreatitis on computed diffusion-weighted imaging. Clin Imaging 2020; 61:20-26.
15. Kanno Y, Koshita S, Masu K, et al. Efficacy of

EUS-guided celiac plexus neurolysis compared with medication alone for unresectable pancreatic cancer in the oxycodone/fentanyl era: A prospective randomized control study. Gastrointest Endosc 2020; S0016-5107(20)30033-X.

16. Palacio S, Mcmurry HS, Ali R, et al. DNA damage repair deficiency as a predictive biomarker for FOLFIRINOX efficacy in metastatic pancreatic cancer. J Gastrointest Oncol 2019; 10(6):1133-39.
17. Shi Q, Feng K, Xia L, Wang C, Zhu J. Combined use of serum miR-499a-5p and CA199 increases the diagnostic sensitivity of pancreatic cancer. Clin Lab 2019; 65(11).
18. Han J, Li Y, Zhang H, et al. MicroRNA-142-5p facilitates the pathogenesis of ulcerative colitis by regulating SOCS1. Int J Clin Exp Pathol 2018; 11(12):5735-44.
19. Griffiths-Jones S, Saini HK, van Dongen S, Enright AJ. miRBase: tools for microRNA genomics. Nucleic Acids Res 2008; 36(Database issue):D154-58.
20. Wang J, Zheng Y, Bai B, et al. MicroRNA-125a-3p participates in odontoblastic differentiation of dental pulp stem cells by targeting Fyn. Cytotechnology 2020; 72(1);69-79.
21. Xiong G, Huang H, Feng M, et al. MiR-10a-5p targets TFAP2C to promote gemcitabine resistance in pancreatic ductal adenocarcinoma. J Exp Clin Cancer Res 2018; 37(1):76.
22. Valiollahi E, Ribera JM, Genescà E, Behravan J. Genome-wide identification of microRNA signatures associated with stem/progenitor cells in Philadelphia chromosome-positive acute lymphoblastic leukemia. Mol Biol Rep 2019; 46(1):1295-306.
23. Worst TS, Previti C, Nitschke K, et al. miR-10a-5p and miR-29b-3p as extracellular vesicle-associated prostate cancer detection markers. Cancers (Basel) 2019; 12(1);43.
24. Iughetti L, Lucaccioni L, Fugetto F, Predieri B, Berardi A, Ferrari F. Brain-derived neurotrophic factor and epilepsy: a systematic review. Neuropeptides 2018; 72:23-29.
25. Tajbakhsh A, Mokhtari-Zaer A, Rezaee M, et al. Therapeutic potentials of BDNF/TrkB in breast cancer; current status and perspectives. J Cell Biochem 2017; 118(9):2502-15.
26. Jing L, Bo W, Yourong F, Tian W, Shixuan W, Mingfu W. Sema4C mediates EMT inducing chemotherapeutic resistance of miR-31-3p in cervical cancer cells. Sci Rep 2019; 9(1):17727.
27. Yang L, Yu Y, Xiong Z, Chen H, Tan B, Hu H. Downregulation of SEMA4C inhibits Epithelial-Mesenchymal Transition (EMT) and the invasion and metastasis of cervical cancer cells via inhibiting transforming growth Factor-beta 1 (TGF-beta1)-induced Hela cells p38 Mitogen-Activated Protein Kinase (MAPK) Activation. Med Sci Monit 2020; 26:e918123.
28. Zhang M, Jiang X, Jiang S, Guo Z, Zhou Q, He J. LncRNA FOXD2-AS1 regulates miR-25-3p/Sema4c axis to promote the invasion and migration of colorectal cancer cells. Cancer Manag Res 2019; 11:10633-39.

DESFLURANE PRETREATMENT CAN REDUCE SEPSIS-EVOKED LUNG INJURY IN RATS VIA INHIBITING STAT3 PATHWAY

C. WANG*, N. LIU* and H.-T. YANG

Department of Anesthesiology, The Second Hospital of Dalian Medical University, Dalian, Liaoning, China

Received March 23, 2020 – Accepted May 13, 2020

*These Authors contributed equally to this work

The purpose of this study was to investigate the effect of desflurane (Des) pretreatment on sepsis-evoked lung injury in rats and its mechanism. The rat model of sepsis-evoked lung injury was prepared using lipopolysaccharide (LPS), while rat lung mesenchymal cell (MSC) model was cultured *in vitro*, followed by Des pretreatment or inhibitor S31-201 culture. The degree of lung tissue injury was analyzed by Hematoxylin-eosin (HE) staining. The expression levels of interleukin (IL)-6, IL-1β and tumor necrosis factor (TNF)-α in the serum of rats were detected by enzyme-linked immunosorbent assay (ELISA). One-step terminal deoxynucleotidyl transferase-mediated dUTP nick end labeling (TUNEL) assay was utilized to determine the apoptosis levels of lung tissues and MSCs cultured *in vitro*. The expressions of the signal transducer and activator of transcription 3 (STAT3) pathway in rat lung tissues and MSCs were detected by Western blotting. After modeling, LPS induced the lung injury in rats, the expression levels of IL-6, IL-1β and TNF-α were up-regulated (P<0.05), the apoptosis rate was increased (P<0.05), and phosphorylated-Janus kinase 2 (p-JAK2) and phosphorylated-STAT3 (p-STAT3) protein expressions were up-regulated (P<0.05). Des pretreatment can alleviate LPS-induced lung injury, down-regulate IL-6, IL-1β and TNF-α expression levels (P<0.05), reduce apoptosis (P<0.05), and down-regulate p-JAK2 and p-STAT3 protein levels (P<0.05). LPS induced an increase in apoptosis rate of MSCs (P<0.05) and the up-regulation of p-STAT3 protein expression (P<0.05). Both Des pretreatment and S31-201 inhibitor culture could reduce the apoptosis rate (P<0.05) and down-regulate p-STAT3 protein level (P<0.05). Des pretreatment can reduce sepsis-evoked lung injury in rats, which may be related to the inhibition of protein expressions of STAT3 pathway.

Sepsis is a clinical syndrome caused by a primary bacterial, fungal or viral infection. Severe sepsis can cause multiple organ failure (MOF) and multiple organ dysfunction syndrome (MODS). Sepsis is one of the sixth most common syndromes for hospitalization, and up to 4.3% of hospitalized patients suffer from sepsis (1, 2). Sepsis is often one of the leading causes of acute lung injury (ALI) in critically ill patients. ALI is a high-mortality disease with a mortality rate of 30% to 60% (3, 4). In patients with ALI, excessive amounts of pro-inflammatory cytokines that promote tissue destruction, such as interleukin (IL)-1β and

Key words: desflurane; STAT3 pathway; rats; lung injury; sepsis

Corresponding Author:
Haitao Yang, MM
Department of Anesthesiology,
The Second Hospital of Dalian Medical University,
467 Zhongshan Road, Shahekou District,
Dalian, Liaoning, 116023, China
Tel.: +86 015541178529
e-mail: yanghaibao19980513@163.com

0393-974X (2020)
Copyright © by BIOLIFE, s.a.s.
This publication and/or article is for individual use only and may not be further reproduced without written permission from the copyright holder.
Unauthorized reproduction may result in financial and other penalties
DISCLOSURE: ALL AUTHORS REPORT NO CONFLICTS OF INTEREST RELEVANT TO THIS ARTICLE.

tumor necrosis factor (TNF)-α, are produced in bronchoalveolar lavage fluid and circulating plasma, and the final consequences of ALI partially depend on the balance between IL-1β and TNF-α and anti-inflammatory cytokines that promote disease regression, such as IL-10 and IL-13 (5). Therefore, it is important to explore the effect of sepsis on ALI and its mechanism.

Signal transducer and activator of transcription 3 (STAT3), a member of the STAT family, plays a significant role in the inflammation and tumorigenesis (6, 7). STAT3 is rapidly activated in the lung of mouse after 30 min of lipopolysaccharide (LPS) administration, with a maximum activation time of 1-2 h. It was reported by Severgnini et al. (8) that STAT3 activation occurs before severe lung injury and is associated with the production of pro-inflammatory molecules, TNF-α, IL-1β, chemokine(C-C motif) ligand 2 (CCL2), and major histocompatibility complex (MHC) II, indicating that STAT3 may play a key role in the inducement of pulmonary inflammation during ALI. Desflurane (Des) is a commonly used inhaled anesthetic. Müller-Edenborn et al. (9) revealed in their study that Des can reduce inflammatory response of neutrophils by interfering with CXC chemokine receptor-2 (CXCR2) signal transduction. Therefore, it was speculated that Des has a certain protective effect against sepsis-evoked lung injury. In the present study, the rats were pretreated with Des to investigate the effect of LPS on lung injury.

MATERIALS AND METHODS

Establishment of rat models of sepsis

This study was approved by the Animal Ethics Committee of Dalian Medical University Animal Center. A total of 60 healthy male Sprague-Dawley (SD) rats weighing 180-200 g were used and randomly divided into ALI group, Des group and control group, 20 rats in each group. The rat sepsis models were prepared according to a previous experimental method (10). The rats in the ALI group and Des group were fasted for 8 h before establishing the ALI model. The Des group inhaled the maximum allowable concentration (1.0) of Des for 40 min before establishing the ALI model. The rats of ALI model were fixed in a supine position after an intraperitoneal injection of 0.75% pentobarbital. The rats were injected with 10 mg/kg LPS in the tail vein to establish the sepsis models, and the control group was injected with the same amount of normal saline. The blood and lung tissues were collected 24 h later.

Establishment of rat lung MSC injury model

Rat mesenchymal stem cells (MSCs) (Cell Bank of Chinese Academy of Sciences, Shanghai, China) were cultured in a Dulbecco's Modified Eagle Medium (DMEM) containing 10% fetal bovine serum (FBS) (Gibco, Rockville, MD, USA) in an incubator at 37°C with 5% CO2. When the cells covered 90% of the bottom of the dish, they were washed twice with phosphate buffer saline (PBS), then digested with 0.25% trypsin, and passaged at a density of 1:3. The cell modeling was performed according the previous method (11). MSCs were treated by 1 μg/mL LPS for 24 h in the experimental group, while Dimethyl Sulphoxide (DMSO) (Sigma, St. Louis, MO, USA) with the same concentration was utilized to treat cells for 24 h in the control group.

Collection of serum and tissues

After the rats were modeled for 24 h, the blood was collected from the eyeballs and centrifuged, and the supernatant was removed. The IL-6, IL-1β and TNF-α levels were detected by enzyme-linked immunosorbent assay (ELISA). After the rats were sacrificed, the lung tissues were taken out immediately, partially placed in liquid nitrogen, and partially fixed in formalin for subsequent experimenst.

Hematoxylin-eosin (H&E) staining

The lung tissues of rats were dissected, embedded in paraffin and sliced into sections. After dewaxing, the sections were immersed in xylene twice (10 min/time), anhydrous alcohol twice (5 min/time), 95% alcohol for 5 min, 90% alcohol for 5 min, 80% alcohol for 5 min, and 70% alcohol for 5 min, followed by washing with distilled water. The sections were stained by Harris hematoxylin solution for 3-8 min, washed by tap water, differentiated with 1% hydrochloric acid alcohol for a few seconds and washed by tap water. After that, the nucleus was turned to blue using 0.6% ammonia water and washed with running water. The sections were stained by eosin stain for 1-3 min, dehydrated and then mounted. The sections

were examined under the microscope to collect images for analysis.

One-step terminal deoxynucleotidyl transferase-mediated dUTP nick end labeling (TUNEL) assay

The rat lung tissues were isolated to prepare frozen sections. The differently treated rat lung MSCs were cultured *in vitro*, washed once with PBS, fixed with an appropriate amount of 4% paraformaldehyde for 15 min and washed with PBS for 3 times. Next, an appropriate amount of 0.1% Triton X-100 was added for permeation for 2 min and washed with PBS for 3 times. After that, 50 μL of TUNEL detection solution was added into the sample, and it was incubated at room temperature for 1 h, and washed with PBS for 3 times. Finally, the sample was added with an appropriate amount of anti-fluorescence quencher, mounted, observed and photographed under a fluorescence microscope.

Western blotting

The total protein was extracted from tissues and cultured cell lines to determine the concentration by bicinchoninic acid (BCA) method (Pierce, Rockford, IL, USA). Then the protein was separated *via* 8% sodium dodecyl sulphate-polyacrylamide gel electrophoresis (SDS-PAGE) and transferred onto a polyvinylidene fluoride (PVDF) membranes (Roche, Basel, Switzerland). The membrane was sealed by 5% skim milk powder and 0.1% Tween-20 in Tris-buffer saline, incubated with primary antibodies of STAT3, p-STAT3, JAK2 and p-JAK2 (Abcam, Cambridge, MA, USA) by shaking gently at 4°C overnight. After that, the membrane was incubated with horse radish peroxidase (HRP)-labeled secondary antibody. Electrochemiluminescence (ECL) reagent was utilized to expose the protein to be detected. The β-actin detected on the same Western blot was regarded as the control.

Statistical analysis

Statistical Product and Service Solutions (SPSS) 20.0 software (IBM, Armonk, NY, USA) was used for statistical analysis. Data from the different treatment groups were expressed by mean ± standard deviation ($\bar{x}\pm s$), and the independent samples *t*-test was adopted for comparison among groups. $P<0.05$ suggested that the difference was statistically significant.

RESULTS

Rat lung histopathology

The results of H&E staining indicated alveolar atrophy, alveolar wall swelling and different degrees of widening of alveolar septum in the ALI group. The degree of lung tissue injury was reduced *via* Des pretreatment (Fig. 1).

Effect of Des pretreatment on sepsis-evoked lung injury in rats

After 24 h of LPS treatment in the experimental groups, the serum of rats in each group was collected separately. The results of ELISA exhibited that the expression levels of IL-6, IL-1β and TNF-α were distinctly higher in the ALI group than those in the control group ($P<0.05$). The expression levels of IL-6, IL-1β and TNF-α in septic rats were remarkably decreased via Des pretreatment ($P<0.05$), but they were still higher than those in the control group ($P<0.05$) (Fig. 2).

Analysis on the effect of Des pretreatment on apoptosis of lung cells in septic rats

The results of TUNEL assay revealed that the apoptosis rate of lung tissues in rats of the ALI group was notably higher than that of the control group ($P<0.05$). Des pretreatment could remarkably weaken the apoptosis of lung tissues in septic rats compared with that in the ALI group ($P<0.05$) (Fig. 3).

Protein expressions of STAT3 pathway in rat lung tissues

The results of Western blot for STAT3-related protein expressions in rat lung tissues displayed that ALI significantly up-regulated p-JAK2 and p-STAT3 protein expressions compared with those in the control group ($P<0.05$), but had no obvious influences on JAK2 and STAT3 protein expressions ($P>0.05$). Des was able to evidently down-regulate the protein expression levels of p-JAK2 and p-STAT3 in septic rats compared with those in the ALI group ($P<0.05$) (Fig. 4).

Effect of Des pretreatment on apoptosis of rat lung MSCs cultured in vitro

The rat lung MSCs were cultured *in vitro* and treated

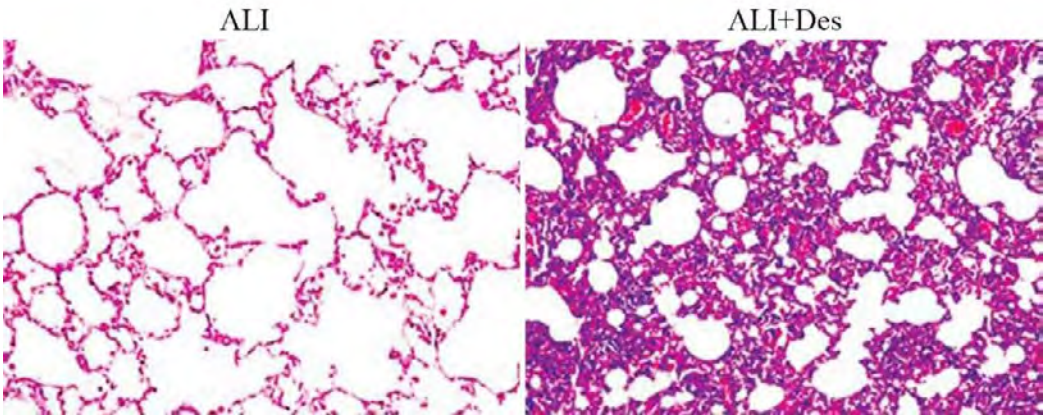


Fig. 1. *HE staining results of rat lung tissues (magnification: 200×).*

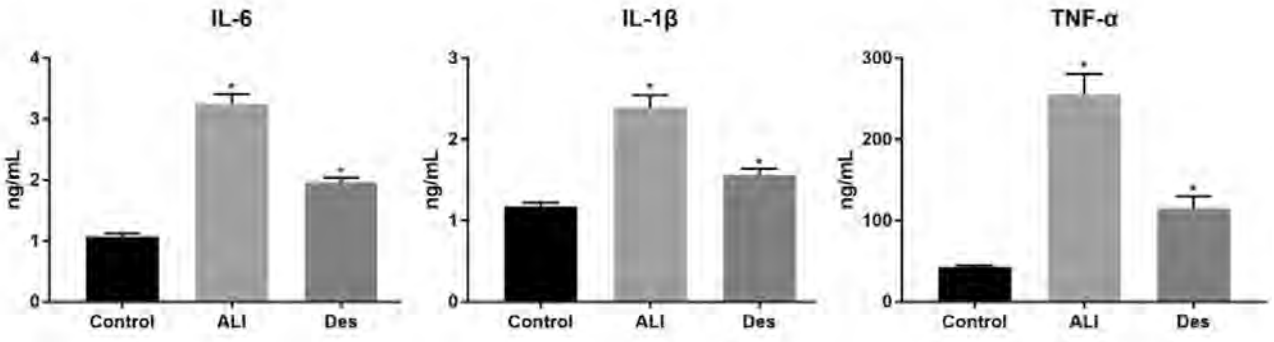


Fig. 2. *Expression levels of serum IL-6, IL-1β and TNF-α in each group of rats treated with LPS for 24 h. *: P<0.05 vs other groups, with a significant difference.*

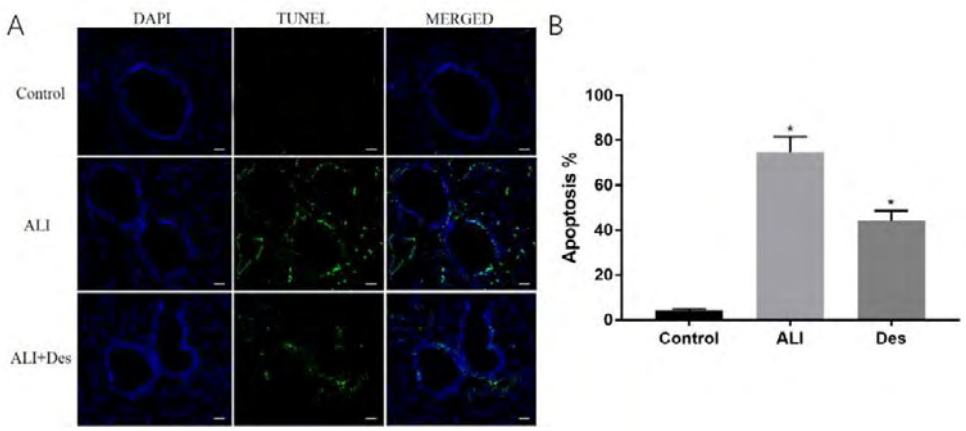


Fig. 3. *Apoptosis level of lung tissue cells detected by one-step TUNEL assay. (magnification: 400×) **A)** Fluorescence images of apoptosis of lung tissue cells detected via one-step TUNEL assay. **B)** Apoptosis rate. *: P<0.05 vs other groups, with a significant difference. The scale length is 50 μm.*

with LPS for 24 h, and the apoptosis was determined by one-step TUNEL assay. The results showed the apoptosis rate of MSCs treated with LPS was significantly up-regulated compared with that in the control group (P<0.05). Both Des and S31-201 could reduce the apoptosis rate caused by LPS compared with that in the LPS group (P<0.05) (Fig. 5).

Effect of Des pretreatment on the protein expressions of STAT3 pathway in rat lung MSCs cultured in vitro

The rat lung MSCs cultured *in vitro* were measured by WB, suggesting that LPS treatment distinctly up-regulated p-STAT3 protein expression level compared with that in the control group (P<0.05), but had no significant effect on STAT3

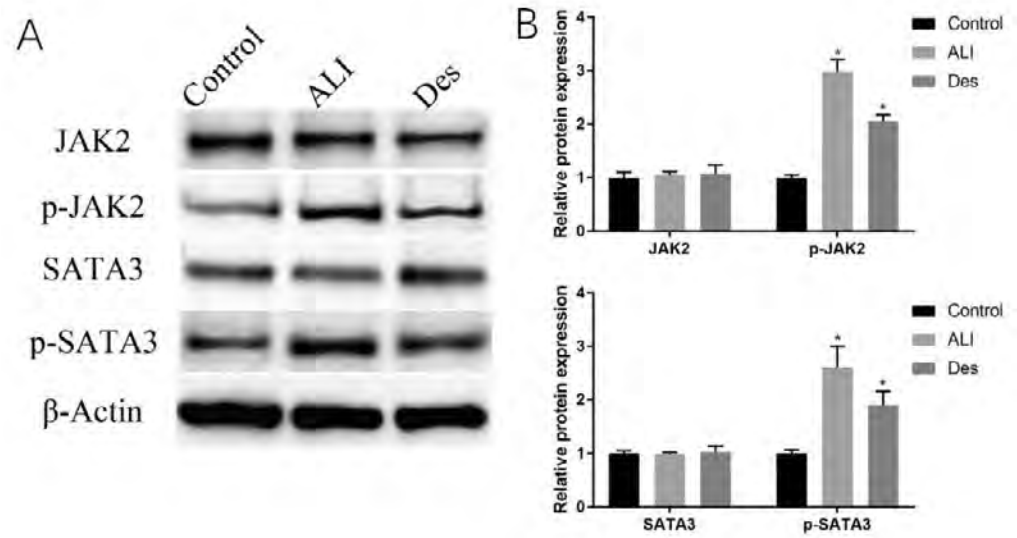


Fig. 4. *Protein expressions of STAT3 pathway in rat lung tissues detected via WB. **A)** Protein expression levels of JAK2, STAT3, p-JAK2 and p-STAT3 in rat lung tissues detected via WB. **B)** Relative quantitative protein expression levels. *: P<0.05 vs other groups, with a significant difference.*

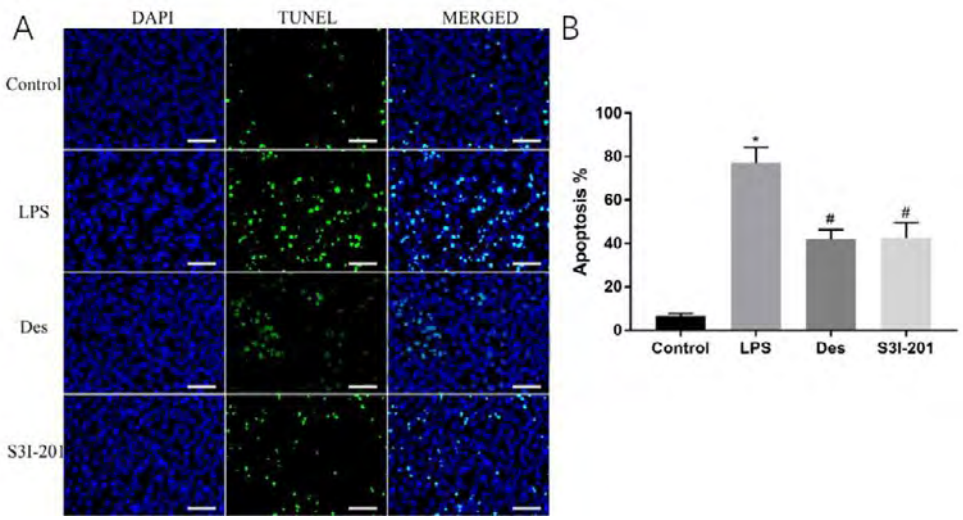


Fig. 5. *Apoptosis of rat lung MSCs determined by one-step TUNEL assay (magnification: 400×). **A)** Images of cell fluorescence. **B)** Apoptosis rate. Control refers to the normally cultured MSCs. LPS refers to MSCs cultured by LPS. Des refers to MSCs culture by LPS after Des pretreatment. S31-201refers to MSCs cultured by LPS+S31-201. */ #: P<0.05 vs other groups, with a significant difference. The scale length is 100 μm.*

protein expression. Both Des and S31-201could notably down-regulate p-STAT3 protein expression level compared with that in the LPS group ($P<0.05$), but had no significant effect on STAT3 protein expression ($P>0.05$) (Fig. 6).

DISCUSSION

Severe sepsis can cause MODS and MOF, including ALI, which accounts for a higher death rate of ICU patients (3, 12, 13). Clinical evidence suggests that inflammatory molecules, IL-1β, TNF-α, CCL2 and MHC II, play key roles in the pathogenesis of LPS-induced ALI (8, 14), indicating that inflammation is of significance in acute lung diseases. By detecting the expression levels of IL-6, IL-1β and TNF-α in rats, it was found that LPS significantly induced the expressions of these inflammatory molecules, and, combined with HE staining results of lung tissues, LPS caused severe lung tissue injury.

Müller-Edenborn et al. (9) demonstrated that volatile anesthetics interfere with the inflammatory pathway of neutrophils, and the mechanism is to interfere in the CXCR2 signal transduction pathway at the action sites between upstream of protein kinase C and downstream of CXCR2, thus leading to the decrease of neutrophil migration and the decline of expression of β2-integrin CD11b, and exerting anti-inflammatory effects. It was hypothesized in this study that Des pretreatment can play a role in alleviating sepsis-evoked lung injury in rats. It was found that Des pretreatment could reduce the increased expression levels of inflammatory factors such as IL-6, IL-1β and TNF-α in rat serum caused by LPS, and the degree of apoptosis in lung tissues detected by TUNEL assay was lowered to some extent, which was the same as that of *in vitro* cell experiments.

The production of excessive inflammatory mediators in sepsis is associated with a variety of signal transduction pathways, such as MAPK (15), NF-κB (16), and JAK/STAT (17, 18). Therefore, the protein expressions of the STAT3 pathway in each treatment group were further explored, and the activation of this pathway might be the physiological mechanism leading to ALI attack. STAT3 plays an important role in physiological processes such as cell proliferation, survival, apoptosis and inflammation

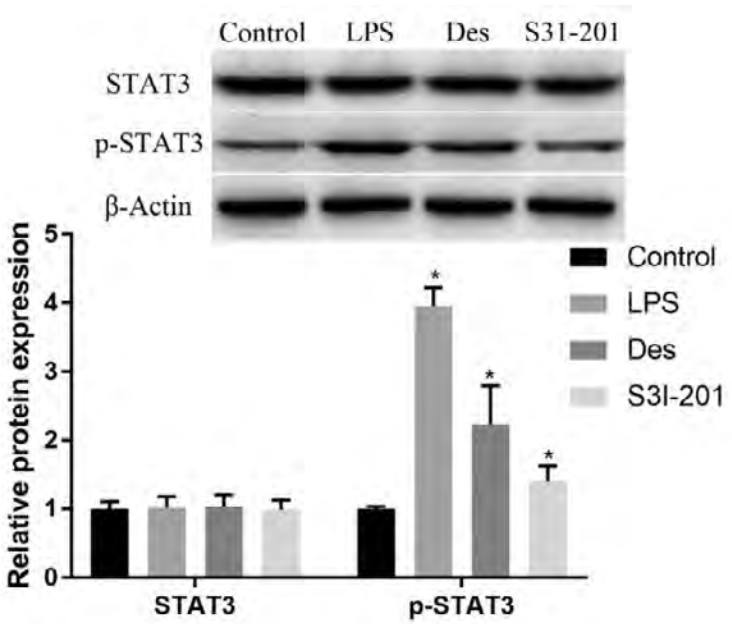


Fig. 6. *Protein expressions of rat lung MSCs measured by WB. Control stands for the normal cultured MSCs. LPS stands for MSCs cultured by LPS. Des stands for MSCs culture by LPS after Des pretreatment. S31-201 stands for MSCs cultured by LPS+S31-201. *: P<0.05 vs other groups, with a significant difference.*

(19). It was reported that JAK2 and STAT1/3 promote the release of cytokines including TNF-α and IL-1β, and are significantly correlated with uncontrolled inflammatory responses, septic shock and acute organ injury (20). It was found by Zhang et al. (21) that IL-2 and IFN-γ are directly involved in the activation of the JAK/STAT pathway, and the inhibition of this pathway can alleviate dysfunction of vital organs in rat septic shock. Severgnini et al. (8) confirmed that the STAT pathway is also activated in LPS-induced ALI, which is consistent with our research results. STAT activation is widely present in the resident cells of the whole lung and the inflammatory cells recruited. After 30 min of LPS injection, the STAT transcription factor can be rapidly activated in the lung of mouse, and the activation peaks after 1 to 2 h (8). In addition, Hierholzer et al. (22) demonstrated that STAT is activated in the lung of the resuscitator hemorrhagic shock model. STAT activation in the lung occurs before the signs of ALI, suggesting that STAT transcription factors may play an important role in triggering pulmonary inflammation. These results indicate that STATs may be an important pathway for mediating ALI, but not related to triggering factors. By detecting the protein expressions of the STAT3 pathway, it was discovered in the present study that LPS activated JAK2 and STAT3 and promoted the expressions of inflammatory factors IL-6, IL-1β and TNF-α. *In vitro* cell experiments, inhibiting the activation of the STAT3 pathway by STAT3 inhibitor S31-201, can effectively relieve the apoptosis caused by LPS. Combined with *in vivo* experimental results, it was suggested that the activation of the STAT3 pathway could promote the expressions of inflammatory factors and further induce pulmonary inflammatory responses, resulting in ALI. Under the conditions of Des pretreatment, the expression levels of inflammatory factors IL-6, IL-1β and TNF-α as well as the STAT3 pathway-related proteins were down-regulated, and the level of apoptosis was decreased. *In vitro* cell experiments showed that Des pretreatment had the same effect as the STAT3 inhibitor S31-201.

In conclusion, this study reveals that in LPS-induced sepsis-evoked lung injury in rats, Des pretreatment may reduce the lung injury by inhibiting the STAT3 pathway activation, which can provide an effective therapeutic approach and related theoretical basis for the clinical protection and treatment of ALI caused by sepsis.

REFERENCES

1. Bellomo R, Kellum JA, Ronco C, et al. Acute kidney injury in sepsis. Intensive Care Med 2017; 43:816-28.
2. Li JM, Zhang H, Zuo YJ. MicroRNA-218 alleviates sepsis inflammation by negatively regulating VOPP1 via JAK/STAT pathway. Eur Rev Med Pharmacol Sci 2018; 22:5620-5626.
3. Avecillas JF, Freire AX, Arroliga AC. Clinical epidemiology of acute lung injury and acute respiratory distress syndrome: incidence, diagnosis, and outcomes. Clin Chest Med 2006; 27:549-57.
4. Phua J, Badia JR, Adhikari NK, et al. Has mortality from acute respiratory distress syndrome decreased over time?: A systematic review. Am J Respir Crit Care Med 2009; 179:220-27.
5. Meduri GU, Annane D, Chrousos GP, Marik PE, Sinclair SE. Activation and regulation of systemic inflammation in ARDS: rationale for prolonged glucocorticoid therapy. Chest 2009; 136:1631-43.
6. Baker BJ, Akhtar LN, Benveniste EN. SOCS1 and SOCS3 in the control of CNS immunity. Trends Immunol 2009; 30:392-400.
7. Benveniste EN, Liu Y, McFarland BC, Qin H. Involvement of the janus kinase/signal transducer and activator of transcription signaling pathway in multiple sclerosis and the animal model of experimental autoimmune encephalomyelitis. J Interferon Cytokine Res 2014; 34:577-88.
8. Severgnini M, Takahashi S, Rozo LM, et al. Activation of the STAT pathway in acute lung injury. Am J Physiol Lung Cell Mol Physiol 2004; 286:L1282-L1292.
9. Muller-Edenborn B, Frick R, Piegeler T, Schlapfer M, Roth-Z'Graggen B, Schlicker A, Beck-Schimmer B. Volatile anaesthetics reduce neutrophil inflammatory response by interfering with CXC receptor-2 signalling. Br J Anaesth 2015; 114:143-49.
10. Gupta A, Rhodes GJ, Berg DT, Gerlitz B, Molitoris BA, Grinnell BW. Activated protein C ameliorates LPS-induced acute kidney injury and downregulates

renal INOS and angiotensin 2. Am J Physiol Renal Physiol 2007; 293:F245-F254.
11. Jung JH, Ha JY, Min KR, et al. Reynosin from Sassurea lappa as inhibitor on CINC-1 induction in LPS-stimulated NRK-52E cells. Planta Med 1998; 64:454-55.
12. Chacko B, Peter JV, Tharyan P, John G, Jeyaseelan L. Pressure-controlled versus volume-controlled ventilation for acute respiratory failure due to acute lung injury (ALI) or acute respiratory distress syndrome (ARDS). Cochrane Database Syst Rev 2015; 1:D8807.
13. Pelosi P, Caironi P, Taccone P, Brazzi L. Pathophysiology of prone positioning in the healthy lung and in ALI/ARDS. Minerva Anestesiol 2001; 67:238-47.
14. Goodman RB, Pugin J, Lee JS, Matthay MA. Cytokine-mediated inflammation in acute lung injury. Cytokine Growth Factor Rev 2003; 14:523-35.
15. Qian F, Deng J, Gantner BN, Flavell RA, Dong C, Christman JW, Ye RD. Map kinase phosphatase 5 protects against sepsis-induced acute lung injury. Am J Physiol Lung Cell Mol Physiol 2012; 302:L866-L874.
16. Oishi H, Takano K, Tomita K, Takebe M, Yokoo H, Yamazaki M, Hattori Y. Olprinone and colforsin daropate alleviate septic lung inflammation and apoptosis through CREB-independent activation of the Akt pathway. Am J Physiol Lung Cell Mol Physiol 2012; 303:L130-L140.
17. Hui L, Yao Y, Wang S, Yu Y, Dong N, Li H, Sheng Z. Inhibition of Janus kinase 2 and signal transduction and activator of transcription 3 protect against cecal ligation and puncture-induced multiple organ damage and mortality. J Trauma 2009; 66:859865.
18. Lee C, Lim HK, Sakong J, Lee YS, Kim JR, Baek SH. Janus kinase-signal transducer and activator of transcription mediates phosphatidic acid-induced interleukin (IL)-1beta and IL-6 production. Mol Pharmacol 2006; 69:1041-47.
19. Gao H, Guo RF, Speyer CL, et al. Stat3 activation in acute lung injury. J Immunol 2004; 172:7703-12.
20. Gu XB, Yang XJ, Hua Z, et al. Effect of oxymatrine on specific cytotoxic T lymphocyte surface programmed death receptor-1 expression in patients with chronic hepatitis B. Chin Med J (Engl) 2012; 125:1434-38.
21. Zhang M, Mathews GL, Ju W, et al. Selective targeting of JAK/STAT signaling is potentiated by Bcl-xL blockade in IL-2-dependent adult T-cell leukemia. Proc Natl Acad Sci U S A 2015; 112:12480-85.
22. Hierholzer C, Kalff JC, Billiar TR, Tweardy DJ. Activation of STAT proteins in the lung of rats following resuscitation from hemorrhagic shock. Arch Orthop Trauma Surg 1998; 117:372-75.

LONG NONCODING RNA KCNQ1OT1 PROMOTES CELL MOTILITY IN HEPATOCELLULAR CARCINOMA BY REGULATING miR-506-3p/FOXQ1

N. ZHANG[1], X-S. LI[2], Y. ZHANG[3], S-F. CHENG[4], J-X. DU[5] and J-P. LIU[6]

[1]Digestive Internal Medicine, The Third People's Hospital of Qingdao, Qingdao, Shandong Province, China; [2]Digestive Internal Medicine, Jinan Zhangqiu District Hospital of TCM, Jinan, Shandong Province, China; [3]Education Management Section, Qingdao Central Hospital, Qingdao University, Qingdao, Shandong Province, China; [4]Department of Nephrology, The People's Hospital of Zhangqiu Area, Jinan, Shandong Province, China; [5]Department of Neurology, The People's Hospital of Zhangqiu Area, Jinan, Shandong Province, China; [6]Public Health Department, The 5th People's Hospital of Ji'nan, Jinan, Shandong Province, China

Received March 23, 2020 – Accepted May 13, 2020

The role of long noncoding RNA (lncRNA) KCNQ1OT1 has been discovered in some human cancers. In this study, the function of lncRNA KCNQ1OT1 in hepatocellular carcinoma (HCC) was investigated. Here, RT-qPCR was used to measure the expression levels of KCNQ1OT1, miR-506-3p and FOXQ1. The function of KCNQ1OT1 was explored using Transwell assay, Western blot analysis and luciferase reporter assay. Increased expression of KCNQ1OT1 was detected in HCC, which was related to lymph node metastasis and TNM stage in HCC patients. Functionally, overexpression of KCNQ1OT1 promoted cell migration, invasion and EMT in HCC. In addition, lncRNA KCNQ1OT1 acts as a molecular sponge for miR-506-3p in HCC. Moreover, FOXQ1 is a direct target of miR-506-3p, and KCNQ1OT1 can positively regulate the expression of FOXQ1 in HCC. FOXQ1 was found to promote cell metastasis in HCC by interacting with the lncRNA KCNQ1OT1/miR-506-3p axis. In summary, lncRNA KCNQ1OT1 promotes cell migration, invasion and EMT in HCC by interacting with the miR-506-3p/FOXQ1 axis.

Hepatocellular carcinoma (HCC) is primary liver cancer associated with cirrhosis. The main causes of liver cancer include chronic hepatitis C virus, hepatitis B virus, alcoholism, diabetes, and non-alcoholic fatty liver disease (1). Since most HCC patients are diagnosed as advanced and are limited by treatment options, the 5-year survival rate of HCC patients is still very low, about 30% (2). Despite recent advances in the treatment of HCC, interventions for HCC patients are still limited (3). To make matters worse, HCC response to traditional therapies is still poor, and relapses soon after clinical treatment (4). Therefore, there is an urgent need to find new intervention targets for HCC patients.

Many studies have shown that long noncoding RNAs (lncRNAs) can be used for early detection of many cancers including HCC. For example, lncRNA PCAT6 predicted poor prognosis of HCC patients and promoted cell proliferation by regulating cell cycle arrest and apoptosis (5). lncRNA-ZNF281 interacted with miR-539 to promote the invasion and migration of HCC cells (6). In addition, lncRNA DLGAP1-AS1 has been reported to promote the occurrence of HCC and epithelial–mesenchymal transition (EMT)

Key words: KCNQ1OT1; hepatocellular carcinoma; miR-506-3p; FOXQ1

Corresponding Author:
Dr Junping Liu,
Public Health Department, The 5th People's Hospital of Ji'nan,
No. 24297 Jingshi Road, Huaiyin District, Jinan,
250022, Shandong Province, China
Tel.: +86 0531-87197114
e-mail: qiaodeng1139@163.com

0393-974X (2020)
Copyright © by BIOLIFE, s.a.s.
This publication and/or article is for individual use only and may not be further reproduced without written permission from the copyright holder.
Unauthorized reproduction may result in financial and other penalties
DISCLOSURE: ALL AUTHORS REPORT NO CONFLICTS OF INTEREST RELEVANT TO THIS ARTICLE.

(7). Recently, the regulatory mechanism of lncRNA KCNQ1OT1 in human cancers has attracted attention. For example, lncRNA KCNQ1OT1 was upregulated in non-small cell lung cancer, and its expression level was related to clinicopathology (8). Functionally, lncRNA KCNQ1OT1 has been found to promote the growth and metastasis of melanoma (9). In particular, lncRNA KCNQ1OT1 was found to promote the growth of HCC by acting as a competitive endogenous RNA for miR-504 (10). However, the effect of lncRNA KCNQ1OT1 on cell migration, invasion and EMT is still unclear in HCC. Therefore, this study aims to solve the above problems.

In addition, miR-506-3p was found to be a possible target of lncRNA KCNQ1OT1. MR-506 has been found to inhibit cell proliferation and induce apoptosis in HCC (11). It was also reported that miR-506 suppressed the invasion and metastasis of human HCC cells (12). Moreover, circPCNX has been reported to promote the viability of HCC cells by inhibiting miR-506 (13). However, the relationship between lncRNA KCNQ1OT1 and miR-506-3p has not been investigated in HCC. Furthermore, forkhead box Q1 (FOXQ1) was predicted to be the downstream target of miR-506-3p. The carcinogenic effect of FOXQ1 has been detected in many human cancers. Specifically, FOXQ1 was overexpressed in colorectal cancer and enhanced tumorigenicity and tumor growth (14). Overexpression of FOXQ1 affected the poor prognosis of non-small cell lung cancer and was related to the EMT phenomenon (15). In addition, miR-506 suppressed tumor proliferation and invasion in nasopharyngeal carcinoma by targeting FOXQ1 (16). However in HCC, the interaction between FOXQ1 and miR-506-3p or lncRNA KCNQ1OT1 remains unclear. Therefore, the regulatory mechanism of lncRNA KCNQ1OT1/miR-506-3p/FOXQ1 was investigated in HCC. At the same time, the effect of lncRNA KCNQ1OT1 on cell metastasis was confirmed in HCC.

MATERIALS AND METHODS

Clinical tissues

Seventy-five HCC tissues and adjacent normal tissues (>2cm from the lesion without any cancer cells) were obtained from The 5th People's Hospital of Ji'nan. These tissues were frozen in liquid nitrogen and stored at −80°C. All samples were histopathologically confirmed, and the patients had not received any radiotherapy or chemotherapy before surgery. The analysis for the clinic-pathological details of HCC patients is shown in Tables I and II. All participants provided written informed consent. This research was approved by the Institutional Ethics Committee of The 5th People's Hospital of Ji'nan.

Cell culture and transfection

HCC cell lines (SNU-387, SNU-182) and normal liver cells (THLE-3) were obtained from ATCC (Manassas, VA, USA). These cells were inoculated in RPMI-1640 medium containing 10% fetal bovine serum (FBS). And they were incubated at 37°C in a humidified incubator with 5% CO_2.

KCNQ1OT1 siRNA or vector, miR-506-3p mimics or inhibitor and FOXQ1 siRNA were purchased from RiboBio (Guangzhou, China). Lipofectamine 2000 (Invitrogen, Carlsbad, CA, USA) was used to transfect the vectors or oligonucleotides into SNU-387 cells.

RT-qPCR

Total RNA was extracted using TRIzol reagent (Invitrogen, Carlsbad, USA). The cDNA solution was synthesized using PrimeScript RT reagent (Takara, Dalian, China). Quantitative RT-PCR was performed on ABI 7500 Fast Real-Time PCR system (Applied Biosystems) using SYBR Green PCR Master Mix (Applied Biosystems). KCNQ1OT1, miR-506-3p or FOXQ1 was normalized to U6 or GAPDH internal reference. Their expression levels were detected using the $2^{-\triangle\triangle ct}$ method. The primer sequences were the following: GAPDH forward, 5'-ACA ACT TTG GTA TCG TGG AAG G-3', and reverse, 5'-GCC ATC ACG CCA CAG TTT C-3'; KCNQ1OT1 forward,5'-CTT TGC AGC AAC CTC CTT GT-3', and reverse, 5'-TGG GGT GAG GGA TCT GAA-3'; miR-506-3p forward: 5'-TAA GGC ACC CTT CTG AGT AGA-3', reverse: 5'-GCG AGC ACA GAA TTA ATA CGA C-3'; FOXQ1 forward: 5'-GAT TTC TTG CTA TTG ACC GAT GC-3', reverse 5'-CTA ATA AAG CTG TAG CCC GTT GC-3'; U6 forward: 5'-GCT TCG GCA GCA CAT ATA CTA AAA T-3' and reverse, 5'-CGC TTC ACG AAT TTG CGT GTC AT-3'.

Transwell assay

Transwell chambers were used to assess cell migration and invasion. Next, Matrigel (BD Biosciences, Franklin

Lakes, NJ, USA) was added to the upper chamber for cell invasion assay. The transfected SNU-387 cells (4×10^3 cells/well) were placed in the upper chamber, and the lower chamber was filled with 10% FBS. The moved cells were fixed and stained for 30 mins. Finally, the moving cells were examined under a light microscope (Olympus Corporation, Tokyo, Japan).

Western blot analysis

RIPA lysis buffer was used to obtain protein samples. Next, the protein was separated by 10% SDS-PAGE, and protein samples were blocked with 5% non-fat milk and transferred to PVDF membranes. Next, the protein samples were incubated with Vimentin, E-cadherin, N-cadherin and GAPDH primary antibodies (Abcam, Cambridge, MA, USA) at 4°C overnight. After that, goat polyclonal anti-rabbit IgG secondary antibody (Abcam, USA) was added to incubate the protein samples for 1 h. Finally, ECL (ECL, Pierce) was used to measure protein expression levels.

Dual luciferase reporter assay

The 3'-UTR of wild or mutant KCNQ1OT1 or FOXQ1 was inserted into the pmirGLO luciferase vector (RiboBio, Guangzhou, China). Next, Lipofectamine® 2000 was used to transfect the luciferase vector and miR-506-3p mimics or miR-NC into SNU-387 cells. 48 h after transfection, was a dual luciferase reporter assay system (Promega Corporation, Madison, WI, USA) used to measure luciferase activity.

Statistical analysis

SPSS 19.0 and Graphpad Prism 6 were used to analyze the data. Differences between groups were analyzed using *Chi*-squared test or one-way analysis of variance with Tukey's post hoc test. $P<0.05$ was defined as a significant difference.

RESULTS

LncRNA KCNQ1OT1 promotes cell metastasis in HCC

The expression level of KCNQ1OT1 was detected in HCC. It was found that the expression of KCNQ1OT1 was increased in HCC tissues compared to normal tissues (Fig. 1A). Meanwhile, upregulation of KCNQ1OT1 was also found in SNU-387 and SNU-182 HCC cells compared to normal liver cells THLE-3 (Fig. 1B). In addition, the abnormal expression of KCNQ1OT1 was related to lymph node metastasis and TNM stage in HCC patients (Table I). To explore the effect of KCNQ1OT1 on HCC cell metastasis, KCNQ1OT1 siRNA was transfected into SNU-387 cells. The transfection efficiency was detected by RT-qPCR. The results showed that KCNQ1OT1 siRNA significantly reduced its expression in SNU-387 cell (Fig. 1C). Transwell assay showed that knockdown of KCNQ1OT1 suppressed cell migration and invasion in SNU-387 cells (Fig. 1D, 1E). Western blot analysis showed that knockdown of KCNQ1OT1 promoted E-cadherin expression and inhibited N-cadherin and Vimentin expressions in SNU-387 cells (Fig. 1F). These results indicate that lncRNA KCNQ1OT1 promotes cell migration, invasion and EMT in HCC.

LncRNA KCNQ1OT1 acts as a molecular sponge for miR-506-3p

In addition, lncRNA KCNQ1OT1 was predicted to have a binding site to miR-506-3p (Fig. 2A). Dual luciferase reporter assay showed that miR-506-3p mimics reduced the luciferase activity of wt-KCNQ1OT1, but had little effect on that of mut-KCNQ1OT1 in SNU-387 cells (Fig. 2B). Moreover, miR-506-3p expression was reduced by KCNQ1OT1 upregulation and promoted by KCNQ1OT1 downregulation in SNU-387 cells (Fig. 2C). At the same time, miR-506-3p mimics reduced KCNQ1OT1 expression, while miR-506-3p inhibitor promoted KCNQ1OT1 expression in SNU-387 cells (Fig. 2D). Next, downregulation of miR-506-3p was found in HCC tissues compared to normal tissues (Fig. 2E). We also found that the abnormal expression of miR-506-3p was related to TNM stage and lymph node metastasis in HCC patients ($P <0.05$, Table II). More importantly, KCNQ1OT1 was found to be negatively correlated with miR-331-3p expression in HCC tissues (Fig. 2F). Collectively, LncRNA KCNQ1OT1 can directly bind to miR-506-3p and act as a molecular sponge for miR-506-3p in HCC.

FOXQ1 is a direct target of miR-506-3p

To further elucidate the regulatory mechanism of KCNQ1OT1 in HCC, this study investigated the target of miR-506-3p. The TargetScan database (http://www.targetscan.org) predicts that FOXQ1 is a potential

Table I. *Relationship between lncRNA KCNQ1OT1 expression and their clinic-pathological characteristics in HCC patients.*

Characteristics	Cases	KCNQ1OT1		P-value
		High	Low	
Age (years)				0.07
≥ 60	26	16	10	
＜60	49	31	18	
Gender				0.21
Male	51	32	19	
Female	24	15	9	
Tumor size (mm)				0.12
⩽5.0	29	13	16	
>5.0	46	34	12	
Lymph node metastasis				0.04*
Yes	55	36	19	
No	20	11	9	
TNM stage				0.02*
I-II	27	12	15	
III-IV	48	35	13	

*Statistical analyses were performed by the χ2 test. *P<0.05 was considered significant.*

Table II. *Relationship between miR-506-3p or FOXQ1 expression and their clinic-pathological characteristics in HCC patients.*

Characteristics	Cases	miR-506-3p		P-value	FOXQ1		P-value
		High	Low		High	Low	
Age (years)				0.32			0.41
≥ 60	26	6	20		10	16	
＜60	49	18	31		42	7	
Gender				0.24			0.31
Male	51	10	41		39	12	
Female	24	14	10		13	11	
Tumor size (mm)				0.09			0.08
⩽5	29	12	17		20	9	
＞5	46	12	34		32	14	
Lymph nodes metastasis				0.04*			0.03*
Yes	55	13	42		42	13	
No	20	11	9		10	10	
Tumor stage				0.03*			0.04*
I-II	27	10	17		19	8	
III-IV	48	14	34		33	15	

*Statistical analyses were performed by the χ2 test. *P<0.05 was considered significant.*

target for miR-506-3p (Fig. 3A). Luciferase reporter assay showed that miR-506-3p mimics reduced the luciferase activity of wt-FOXQ1, but had little effect on that of mut-FOXQ1 in SNU-387 cells (Fig. 3B), which indicates that miR-506-3p can directly target FOXQ1 in HCC. In addition, miR-506-3p mimics reduced FOXQ1 expression, while miR-506-3p inhibitor promoted FOXQ1 expression in SNU-387 cells (Fig. 3C). Compared to normal tissues, upregulation of FOXQ1 was found in HCC tissues (Fig. 3D). The dysregulation of FOXQ1 was associated with lymph node metastasis and TNM stage in HCC patients ($P < 0.05$, Table II). In addition, a negative correlation between miR-506-3p and FOXQ1 was detected in HCC tissues (Fig. 3E). In contrast, KCNQ1OT1 was positively correlated with FOXQ1 expression in HCC

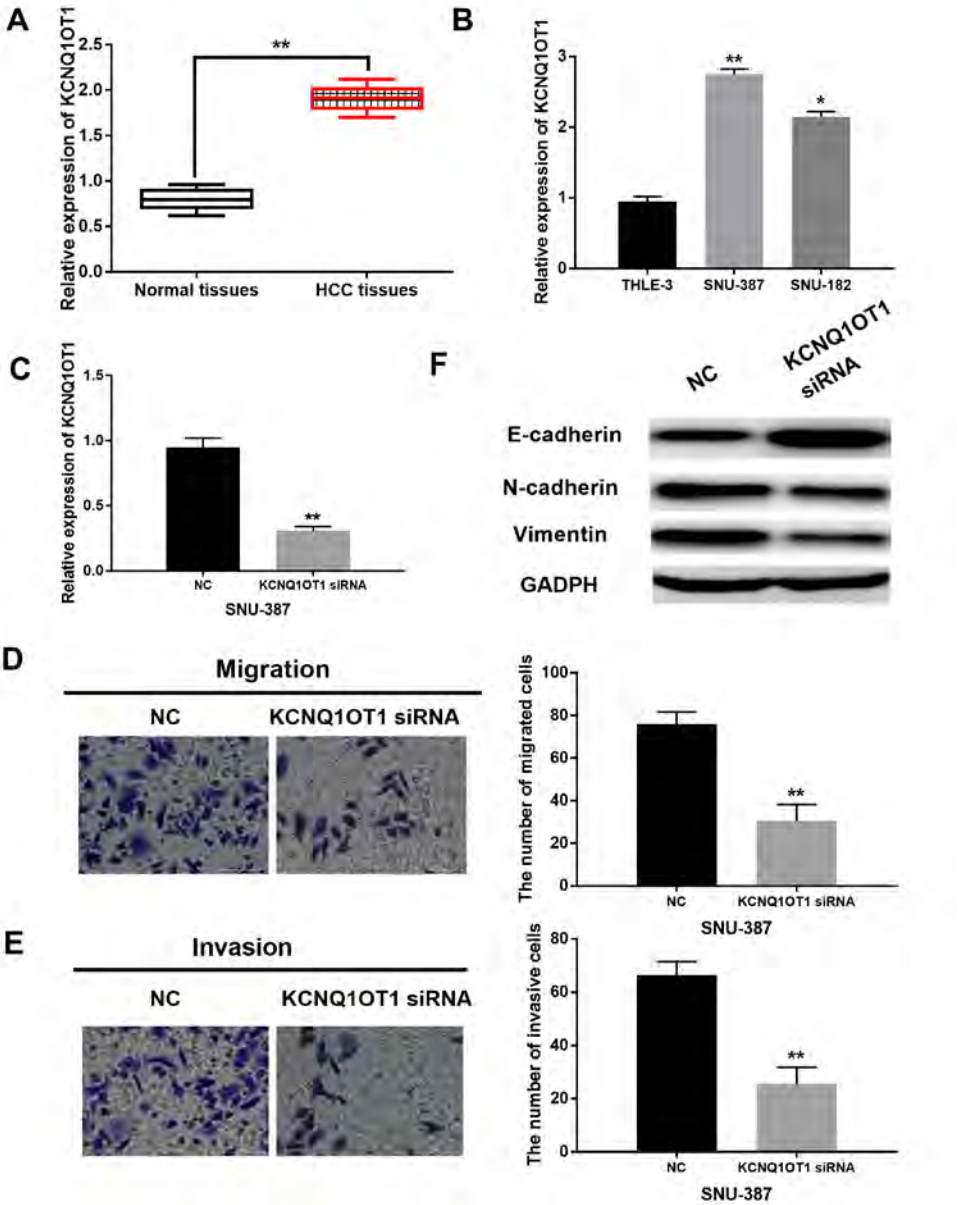


Fig. 1. *LncRNA KCNQ1OT1 promotes cell metastasis in HCC.* ***A****) LncRNA KCNQ1OT1 expression in HCC tissues and normal tissues (****B****) LncRNA KCNQ1OT1 expression in SNU-387, SNU-182 and THLE-3 cells.* ***C****) LncRNA KCNQ1OT1 expression in SNU-387 cells with KCNQ1OT1 siRNA.* ***D, E****) Cell migration and invasion in SNU-387 cells with KCNQ1OT1 siRNA.* ***F****) The protein expression of E-cadherin, N-cadherin and Vimentin in SNU-387 cells with KCNQ1OT1 siRNA ** P <0.01*

tissues (Fig. 3F). Briefly, FOXQ1 is a direct target of miR-506-3p, and KCNQ1OT1 can positively regulate the expression of FOXQ1 in HCC.

FOXQ1 regulates HCC cell metastasis by interacting with lncRNA KCNQ1OT1 and miR-506-3p

Finally, KCNQ1OT1 vector or miR-506-3p inhibitor was transfected into SNU-387 cells with FOXQ1 siRNA. FOXQ1 siRNA reduced its expression in SNU-387 cells. After transfection with KCNQ1OT1 vector or miR-506-3p inhibitor, the reduced expression of FOXQ1 was restored in SNU-387 cells (Fig. 4A). Functionally, knockdown of FOXQ1 was found to inhibit cell migration and invasion in SNU-387 cells. Similarly, upregulation of KCNQ1OT1 or downregulation of miR-506-3p attenuated the inhibitory effect of FOXQ1 siRNA on SNU-387 cell migration and invasion (Fig. 4B, 4C). As for EMT, knockdown of FOXQ1 promoted E-cadherin expression and inhibited N-cadherin and Vimentin expressions in SNU-387 cells. The reverse effect of KCNQ1OT1 vector or miR-506-3p inhibitor on these genes was also found in SNU-387 cells with FOXQ1 siRNA (Fig. 4D). Taken together, FOXQ1 can promote cell metastasis in HCC by interacting with the lncRNA KCNQ1OT1/miR-506-3p axis.

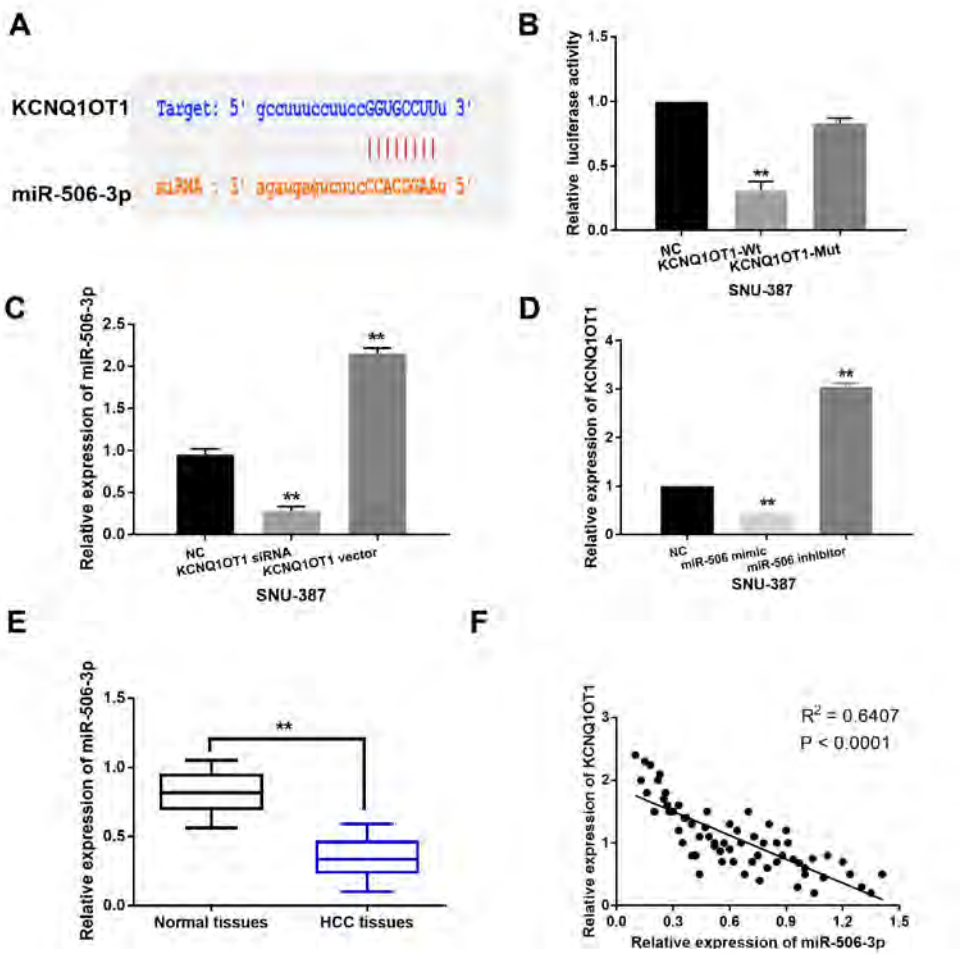


Fig. 2. *LncRNA KCNQ1OT1 acts as a molecular sponge for miR-506-3p.* ***A****) The binding site between KCNQ1OT1 and miR-506-3p.* ***B****) Luciferase reporter assay.* ***C****) MiR-506-3p expression regulated by KCNQ1OT1 siRNA or vector in SNU-387 cells.* ***D****) KCNQ1OT1 expression in SNU-387 cells with miR-506-3p mimics or inhibitor.* ***E****) MiR-506-3p expression in HCC tissues and normal tissues.* ***F****) MiR-506-3p was negatively correlated with KCNQ1OT1 expression in HCC tissues. ** P <0.01.*

DISCUSSION

Today, many lncRNAs have been found to be involved in the development of HCC, such as RP11-284P20.2 and SPRY4-IT1 (17, 18). In this study, upregulation of lncRNA KCNQ1OT1 was detected in HCC tissues and cells. Knockdown of lncRNA KCNQ1OT1 was found to inhibit cell migration, invasion and EMT in HCC. Consistent with the present results, upregulation of lncRNA KCNQ1OT1 has also been detected in other cancers, such as colon adenocarcinoma (19). Knockdown of lncRNA KCNQ1OT1 inhibited cell proliferation, migration and invasion in glioma (20). More importantly, it has been reported that the STR polymorphism in KCNQ1OT1 can confer HCC risk (21). The results are consistent with the present research, indicating that lncRNA KCNQ1OT1 serves as a tumor promoter in HCC.

In addition, it has been reported that lncRNA KCNQ1OT1 regulated oxaliplatin resistance in HCC through the miR-7-5p/ABCC1 axis (22). We also found that lncRNA KCNQ1OT1 served as the ceRNA of miR-506-3p in the present study. In HCC, there was a negative correlation between lncRNA KCNQ1OT1 and miR-506-3p expression. These results indicate that lncRNA KCNQ1OT1 promotes cell metastasis in HCC by downregulating miR-506-3p. Dai et al. found that inhibition of miR-506 had a promoting effect on cell proliferation, migration

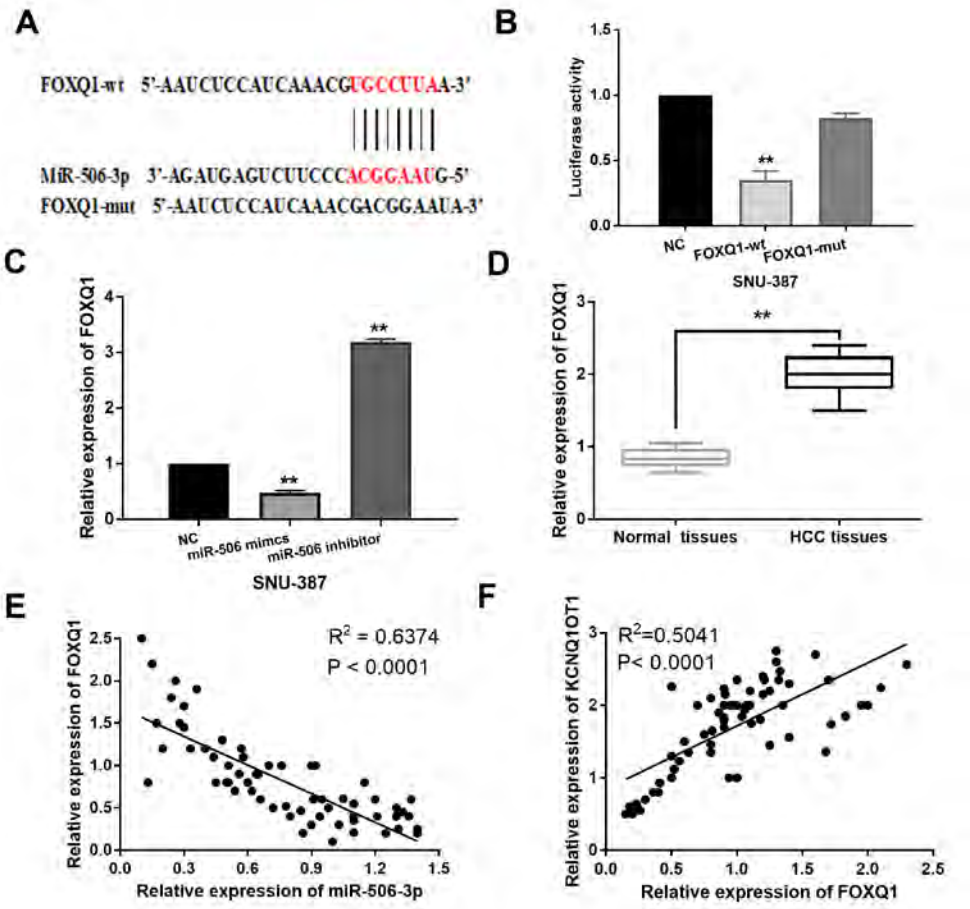


Fig. 3. *FOXQ1 is a direct target of miR-506-3p.* ***A****) The binding site between FOXQ1 and miR-506-3p.* ***B****) Luciferase reporter assay.* ***C****) FOXQ1 expression regulated by miR-506-3p mimics or inhibitor.* ***D****) FOXQ1 expression in HCC tissues and normal tissues.* ***E****) MiR-506-3p was negatively correlated with FOXQ1 expression in HCC tissues.* ***F****) KCNQ1OT1 was positively correlated with FOXQ1 expression in HCC tissues. ** P <0.01.*

and invasion in HCC (23). The results also proved our conclusion.

To further elucidate the regulatory mechanism of lncRNA KCNQ1OT1 in HCC, FOXQ1 was confirmed as a direct target of miR-506-3p, and KCNQ1OT1 can positively regulate the expression of FOXQ1 in HCC. Similar to our results, downregulation of FOXQ1 induced by miR-506 has been reported to inhibit the proliferation and EMT of cervical cancer cells (24). Here, knockdown of FOXQ1 was also found to inhibit cell migration, invasion and EMT in HCC, and miR-506-3p attenuated the promoting effect of FOXQ1 on cell metastasis in HCC. In contrast, lncRNA KCNQ1OT1 was found to enhance the promoting effect of FOXQ1 on HCC cell metastasis in the present study, which indicates that lncRNA KCNQ1OT1 promotes cell migration, invasion and EMT in HCC by upregulating FOXQ1.

In conclusion, lncRNA KCNQ1OT1 promotes cell migration, invasion and EMT in HCC by interacting with the miR-506-3p/FOXQ1 axis. These findings indicate that the KCNQ1OT1/miR-506-3p/FOXQ1 pathway is involved in the pathogenesis of HCC, and KCNQ1OT1 may be used as a potential biomarker for diagnosis and treatment of HCC.

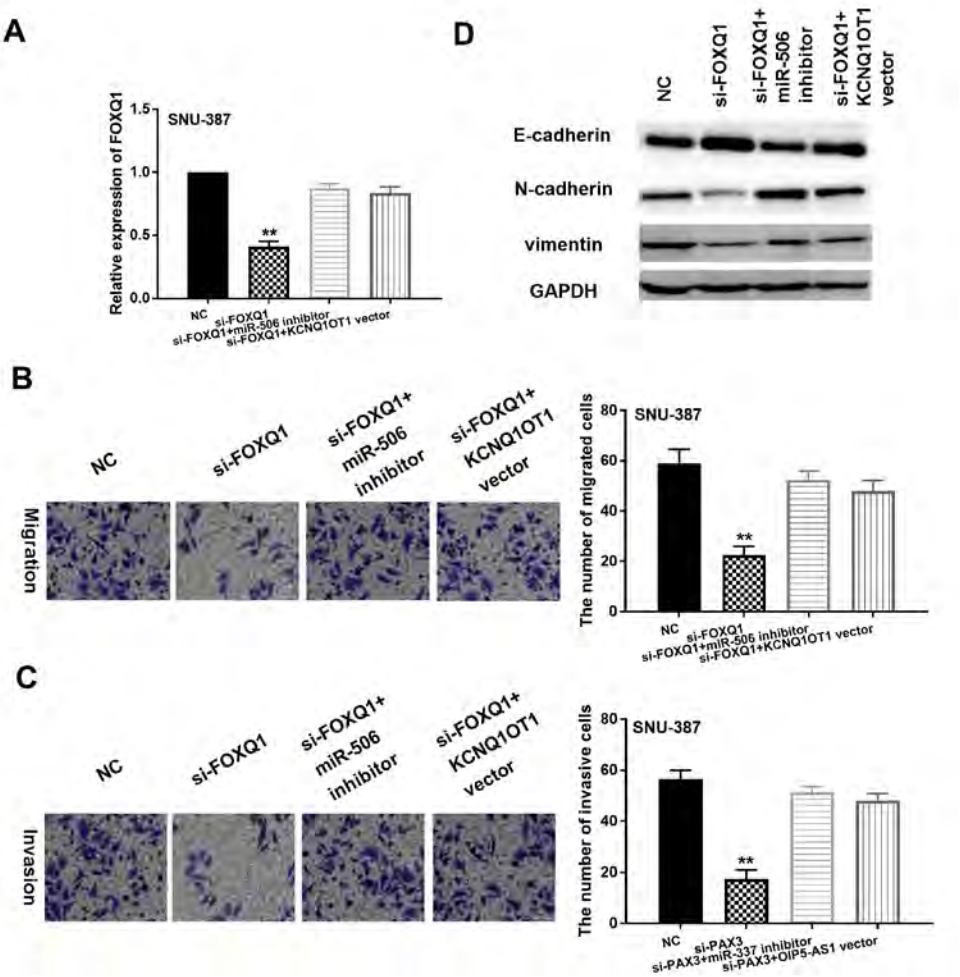


Fig. 4. *FOXQ1 regulates HCC cell metastasis by interacting with lncRNA KCNQ1OT1 and miR-506-3p.* ***A****) FOXQ1 expression in SNU-387 cells with FOXQ1 siRNA, FOXQ1 siRNA+miR-506 inhibitor or FOXQ1 siRNA + KCNQ1OT1 vector.* ***B, C****) Cell migration and invasion in SNU-387 cells with FOXQ1 siRNA, FOXQ1 siRNA+miR-506 inhibitor or FOXQ1 siRNA + KCNQ1OT1 vector.* ***D****) The protein expression of E-cadherin, N-cadherin and Vimentin in SNU-387 cells with FOXQ1 siRNA, FOXQ1 siRNA+miR-506 inhibitor or FOXQ1 siRNA + KCNQ1OT1 vector ** P <0.01*

REFERENCES

1. Kulik L, El-Serag HB. Epidemiology and management of hepatocellular carcinoma. Gastroenterology 2019; 156:477-91.
2. Mak LY, Cruz-Ramon V, Chinchilla-Lopez P, et al. Global epidemiology, prevention, and management of hepatocellular carcinoma. Am Soc Clin Oncol Educ Book 2018; 38:262-79.
3. Mudumbi SK, Bourgeois CE, Hoppman NA, et al. Palliative care and hospice interventions in decompensated cirrhosis and hepatocellular carcinoma: a rapid review of literature. J Palliat Med 2018; 21:1177-84.
4. Zucman-Rossi J, Villanueva A, Nault JC, Llovet JM. Genetic landscape and biomarkers of hepatocellular carcinoma. Gastroenterology 2015; 149:1226-39 e4.
5. Luo Y, Lin J, Zhang Y, Dai G, Li A, Liu X. LncRNA PCAT6 predicts poor prognosis in hepatocellular carcinoma and promotes proliferation through the regulation of cell cycle arrest and apoptosis. Cell Biochem Funct 2020; doi: 10.1002/cbf.3510. [Epub ahead of print]
6. Zhang Z, Yang L, Yao X, Yang M, Li G. LncRNA-ZNF281 Interacts with miR-539 to promote hepatocellular carcinoma cell invasion and migration. Cancer Biother Radiopharm 2020; 35(2):137-142.
7. Lin Y, Jian Z, Jin H, Wei X, Zou X, Guan R, Huang J. Long non-coding RNA DLGAP1-AS1 facilitates tumorigenesis and epithelial-mesenchymal transition in hepatocellular carcinoma via the feedback loop of miR-26a/b-5p/IL-6/JAK2/STAT3 and Wnt/beta-catenin pathway. Cell Death Dis 2020; 11:34.
8. Zheng L, Zhang FX, Wang LL, Hu HL, Lian YD. LncRNA KCNQ1OT1 is overexpressed in non-small cell lung cancer and its expression level is related to clinicopathology. Eur Rev Med Pharmacol Sci 2019; 23:6944-50.
9. Guo B, Zhang Q, Wang H, Chang P, Tao K. KCNQ1OT1 promotes melanoma growth and metastasis. Aging (Albany NY) 2018; 10:632-44.
10. Li C, Miao R, Zhang J, Qu K, Liu C. Long non-coding RNA KCNQ1OT1 mediates the growth of hepatocellular carcinoma by functioning as a competing endogenous RNA of miR-504. Int J Oncol 2018; 52:1603-12.
11. Zhang L, Zhou H and Wei G. miR-506 regulates cell proliferation and apoptosis by affecting RhoA/ROCK signaling pathway in hepatocellular carcinoma cells. Int J Clin Exp Pathol 2019; 12:1163-73.
12. Wang Z, Si M, Yang N, et al. MicroRNA-506 suppresses invasiveness and metastasis of human hepatocellular carcinoma cells by targeting IL8. Am J Cancer Res 2018; 8:1586-94.
13. Sun P, Fan X, Hu X, Fu X, Wei Q, Zang Y. circPCNX and Pecanex Promote Hepatocellular Carcinoma Cell Viability by Inhibiting miR-506. Cancer Manag Res 2019; 11:10957-67.
14. Kaneda H, Arao T, Tanaka K, et al. FOXQ1 is overexpressed in colorectal cancer and enhances tumorigenicity and tumor growth. Cancer Res 2010; 70:2053-63.
15. Feng J, Zhang X, Zhu H, Wang X, Ni S, Huang J. FoxQ1 overexpression influences poor prognosis in non-small cell lung cancer, associates with the phenomenon of EMT. PLoS One 2012; 7:e39937.
16. Zhang Z, Ma J, Luan G, Kang L, Su Y, He Y, Luan F. MiR-506 suppresses tumor proliferation and invasion by targeting FOXQ1 in nasopharyngeal carcinoma. PLoS One 2015; 10:e0122851.
17. Fang QL, Zhou JY, Xiong Y, et al. Long non-coding RNA RP11-284P20.2 promotes cell proliferation and invasion in hepatocellular carcinoma by recruiting EIF3b to induce c-met protein synthesis. Biosci Rep 2020; 40(3).
18. Ma W, Chen X, Wu X, et al. Long noncoding RNA SPRY4-IT1 promotes proliferation and metastasis of hepatocellular carcinoma via mediating TNF signaling pathway. J Cell Physiol 2020; doi: 10.1002/jcp.29438. [Epub ahead of print
19. Zhang K, Yan J, Yi B, Rui Y, Hu H. High KCNQ1OT1 expression might independently predict shorter survival of colon adenocarcinoma. Future Oncol 2019; 15:1085-95.
20. Gong W, Zheng J, Liu X, et al. Knockdown of long non-coding RNA KCNQ1OT1 restrained glioma cells' malignancy by activating miR-370/CCNE2 axis. Front Cell Neurosci 2017; 11:84.
21. Wan J, Huang M, Zhao H, et al. A novel tetranucleotide repeat polymorphism within KCNQ1OT1 confers risk for hepatocellular carcinoma. DNA Cell Biol 2013; 32:628-34.

22. Hu H, Yang L, Li L, Zeng C. Long non-coding RNA KCNQ1OT1 modulates oxaliplatin resistance in hepatocellular carcinoma through miR-7-5p/ABCC1 axis. Biochem Biophys Res Commun 2018; 503:2400-06.
23. Dai W, Huang HL, Hu M, Wang SJ, He HJ, Chen NP, Li MY. microRNA-506 regulates proliferation, migration and invasion in hepatocellular carcinoma by targeting F-spondin 1 (SPON1). Am J Cancer Res 2015; 5:2697-707.
24. Zhang M, Xu Q, Yan S, Li Z, Yan W, Jia X. Suppression of forkhead box Q1 by microRNA-506 represses the proliferation and epithelial-mesenchymal transition of cervical cancer cells. Oncol Rep 2016; 35:3106-14.

EFFECTS OF FINE PARTICULATE $PM_{2.5}$ ON EMPHYSEMA OF MICE VIA REGULATING FOXO3A/BIM AXIS

W.-L. WANG and Y.-J. ZHAO

Department of Respiratory Medicine, The Third hospital of JiLin University, Changchun, China

Received January 27, 2020 – Accepted May 15, 2020

This study aims to investigate the role of $PM_{2.5}$ exposure in inducing apoptosis of alveolar epithelial cells and thereafter emphysema in mice, and the underlying mechanism. $PM_{2.5}$ exposure model in mice was constructed. Lung tissues were harvested from healthy mice and model mice for hematoxylin and eosin (H&E) staining. Protein levels of Forkhead box O3 (FOXO3A) and BIM in lung tissues were detected by Western blot. Subsequently, A549 cells were induced with increased doses of $PM_{2.5}$, followed by determination of relative levels of FOXO3A, BIM (Bcl-2 interacting mediator of cell death) and clv-caspase3. Apoptosis in $PM_{2.5}$-exposed A549 cells was assessed. Chromatin immunoprecipitation (ChIP) assay was conducted to uncover the interaction between FOXO3A and BIM. Finally, regulatory effects of FOXO3A/BIM on apoptosis of A549 cells were determined. $PM_{2.5}$ exposure resulted in expansion of alveolar spatial structure and decline of lung function, thus leading to emphysema in mice. Protein levels of FOXO3A and BIM were markedly upregulated in lungs of model mice. Relative levels of FOXO3A, BIM and clv-caspase3 were enhanced in $PM_{2.5}$-exposed A549 cells, which were reversed by transfection of si-FOXO3A. ChIP assay confirmed that FOXO3A was able to regulate BIM transcription through binding its promoter regions. Importantly, regulatory effects of FOXO3A on apoptosis of $PM_{2.5}$-exposed A549 cells were partially reversed by overexpression of BIM. $PM_{2.5}$ exposure leads to upregulation of FOXO3A, which triggers BIM transcription, thus inducing apoptosis of alveolar epithelial cells and emphysema in mice.

Emphysema is mainly caused by smoking, and is characterized by loss of alveolar integrity and enlarged alveolar space (1). Previous studies have revealed that uncontrolled apoptosis of alveolar epithelial cells is an underlying factor for emphysema (2). In this paper, we mainly discussed the underlying mechanism of $PM_{2.5}$ exposure in inducing apoptosis of alveolar epithelial cells and the occurrence of emphysema.

$PM_{2.5}$, also known as fine particulates, has an aerodynamic equivalent diameter of smaller than 2.5 μm in ambient air (3), and can be suspended in the air for a long period. Higher concentration of $PM_{2.5}$ indicates more severe air pollution (4), resulting in great hazards to air quality and human health (5). Fine particulates can be easily inhaled into the respiratory tract because of their small diameter (6). The WHO has proposed $PM_{2.5}$ as an environmental carcinogen. Long-term $PM_{2.5}$ exposure could lead to cardiovascular diseases, respiratory diseases, and even lung cancer (7).

FOXO3 is a member of the Forkhead box O transcription factors, which are critical regulators responsible for cell proliferation, apoptosis and DNA damage repair (8-10). Furthermore, FOXO3 is closely linked to age-dependent diseases, i.e. diabetes, Chronic

Key words: $PM_{2.5}$; FOXO3A; BIM; emphysema; alveolar epithelial cells; apoptosis

Corresponding Author:
Yongjuan Zhao, MM.
Department of Respiratory Medicine,
The Third hospital of JiLin University,
No. 126, Xiantai Street, Changchun, 130033, Jilin, China
Tel.: +86 013596490857
e-mail: zyj1987@jlu.edu.cn

0393-974X (2020)
Copyright © by BIOLIFE, s.a.s.
This publication and/or article is for individual use only and may not be further reproduced without written permission from the copyright holder.
Unauthorized reproduction may result in financial and other penalties
DISCLOSURE: ALL AUTHORS REPORT NO CONFLICTS OF INTEREST RELEVANT TO THIS ARTICLE.

obstructive pulmonary disease (COPD) and cancer (11, 12). FOXO3 is generally considered as a tumor-suppressor gene involved in tumor cell apoptosis and cell cycle progression (13), and is believed to be crucial in cell apoptosis (14).

BIM (Bcl-2 interacting mediator of cell death) is a member of the Bcl-2 family which participates in homeostasis of hematopoietic cells, apoptosis and tumorigenesis (15,16). As a tumor-suppressor gene, BIM deficiency stimulates the occurrence of multiple types of cancers (17). This study aims to investigate whether $PM_{2.5}$ exposure could promote BIM transcription through FOXO3A and thus promote apoptosis and emphysema in mice alveolar epithelial cells.

MATERIALS AND METHODS

$PM_{2.5}$ exposure model in mice

Male BALB/c mice, 6-8 weeks old, were randomly assigned intoa control group (n=6) and a $PM_{2.5}$ group (n=6). Model mice were subjected to 60-min systematical exposure to 200 TPM mg/L $PM_{2.5}$ twice a day, with an interval of 4 h. $PM_{2.5}$ exposure was conducted for 5 days per week, for a total of 4 weeks. Humidity, temperature, and CO_2 concentration in the exposed system chamber were continuously measured during $PM_{2.5}$ exposure. All animal experiments were approved by the Animal Ethics Committee of Jilin University Animal Center.

Cell culture and transfection

Alveolar epithelial A549 cells were provided by ATCC. Cells were cultured in low-glucose Dulbecco's modified eagle medium (DMEM) (Thermo Fisher Scientific, Waltham, MA, USA) containing 10% fetal bovine serum (FBS) (Gibco, Rockville, MD, USA), and 1% penicillin-streptomycin in a 5% CO_2 incubator at 37°C. Medium was regularly replaced. After amplification with specific primers, BIM complementary deoxyribose nucleic acid (cDNA) was cloned into pcDNA3.0, that is, pcDNA3.0-BIM vector. Cells were inoculated in 6-well plates with 1×10^4 cells per well. At 75-85% confluence, transfection mixture containing vectors and LipofectamineTM 2000 (Invitrogen, Carlsbad, CA, USA) was applied. Complete medium was replaced at 4-6 h.

Western blot

Cellular protein was extracted for determining protein concentration. Protein sample was loaded on sodium dodecyl sulphate-polyacrylamide gel electrophoresis (SDS-PAGE) and transferred to polyvinylidene fluoride (PVDF) membranes (Millipore, Billerica, MA, USA). Non-specific antigens were blocked in 5% skim milk. After 1 h, membranes were reacted with primary and secondary antibodies. After washing with 1×tris buffered saline-tween (TBST) for 1 min, the chemiluminescent substrate kit was used for exposure of the protein band.

Quantitative real-time polymerase chain reaction (qRT-PCR)

RNA was isolated from cells or tissues using TRIzol (Invitrogen, Carlsbad, CA, USA) method, quantified and preserved at -80°C. After reverse transcription, the extracted cDNA was applied for PCR using the SYBR Green method for 35-40 cycles: FOXO3A; F: CGGACAAACGGCTCACTCT; R: GGACCCGCATGAATCGACTAT; BIM; F: TAAGTTCTGAGTGTGACCGAGA; R: GCTCTGTCTGTAGGGAGGTAGG; Clv-caspase 3; F: CATGGAAGCGAATCAATGGACT; R: CTGTACCAGACCGAGATGTCA

Flow cytometry

Cells were washed with phosphate buffered saline (PBS) twice, digested and prepared to cell suspension ($1\text{-}5\times10^6$ cells/mL). Cells were incubated in 1 mL of pre-cold 70% ethanol at 4°C overnight. On the next day, cells were washed with PBS twice and reacted with 100 μL of RNaseA at 37°C, in the dark for 30-min in a water bath. Subsequently, cells were dyed with 500 μL of fluorescein isothiocyanate (FITC) annexin V/ propidium Iodide (PI) at 4°C, in the dark for 15 min. Apoptotic rate was determined by flow cytometry and analyzed by FlowJo software.

Chromatin immunoprecipitation (ChIP)

Cell suspension with 1×10^7 cells/mL was incubated for 24 h and fixed in 1% methanol for 10 min. After lysis, the chromatin was fragmentated into 500 bp and reacted with Dynal beads targeting anti-FOXO3A, H3K27me3 and IgG (Invitrogen, Carlsbad, CA, USA) overnight. Through reverse enrichment and DNA cross-link, DNA was washed with RNase A (0.2 mg/mL) and Protease K (2 mg/mL). The immunoprecipitants were subjected to qRT-PCR.

Hematoxylin and eosin (H&E) staining

Mice lungs were immersed in 4% paraformaldehyde and embedded in paraffin. Tissues were sliced into 5-μm sections and H&E staining was conducted for assessing pathological damage of lung tissues and alveolar spatial structure. Alveolar spatial area was quantified as the percentage to the total area.

Statistical analysis

Statistical Product and Service Solutions (SPSS) 16.0 (SPSS IBM, Armonk, NY USA) was used for data analysis. Data were expressed as mean ± standard deviation ($\bar{x} \pm$ S.D.). Differences between two groups were analyzed by using the Student's *t*-test. Comparison between multiple groups was made using One-way analysis of variance

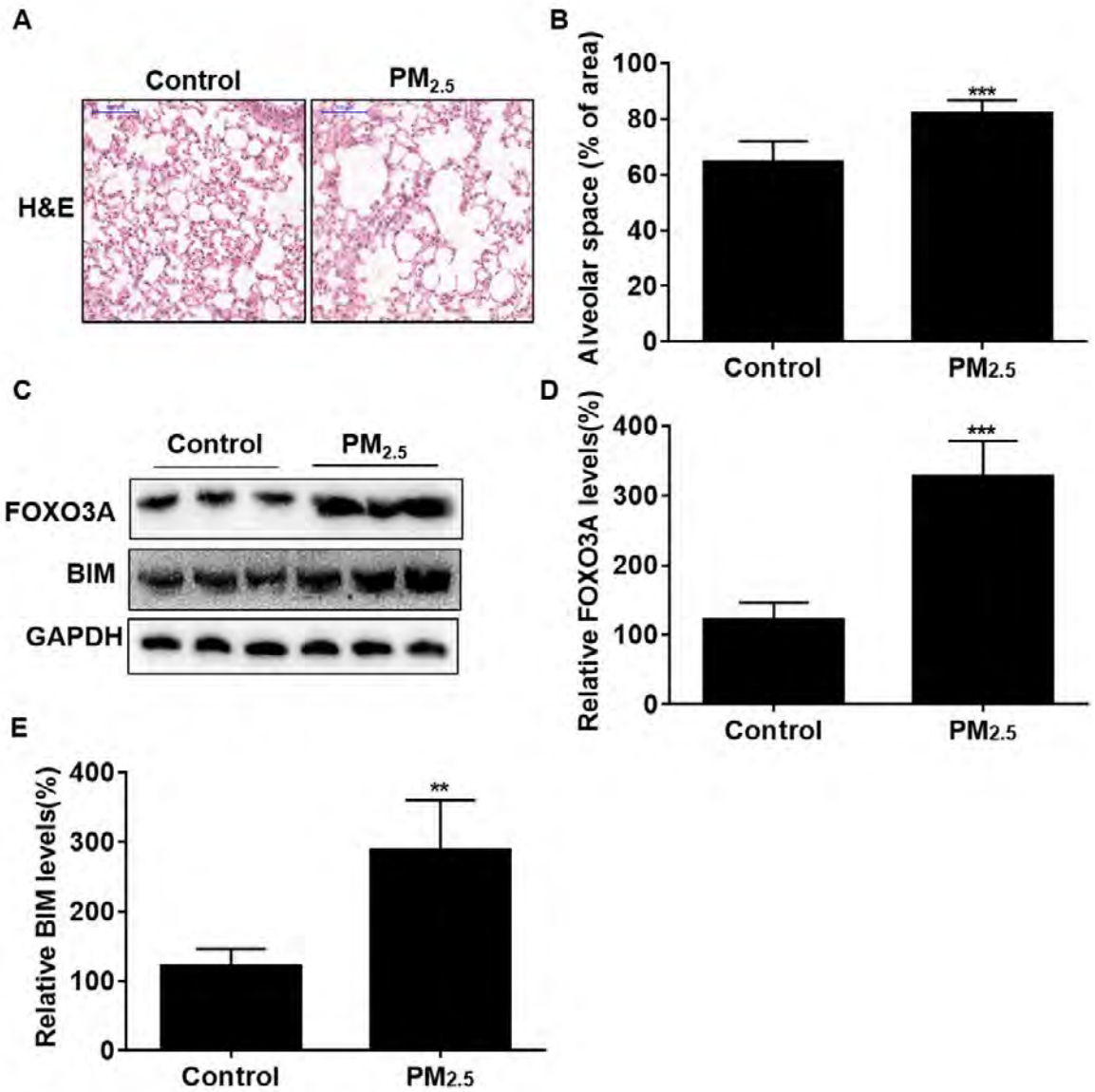


Fig. 1. *$PM_{2.5}$ exposure upregulated FOXO3A and BIM, and resulted in pathological lesions in lungs.* ***A****) H&E staining showed emphysema in mouse lungs.* ***B****). The percentage of alveolar space in mice of control group and $PM_{2.5}$ group.* ***C****) Western blot analyses on FOXO3A and BIM in mice of control group and $PM_{2.5}$ group.* ***D, E****) Quantification of protein levels of FOXO3A (D) and BIM (E) in mice of control group and $PM_{2.5}$ group.*

(ANOVA) test followed by Post Hoc Test (Least Significant Difference). P<0.05 considered the difference was statistically significant.

RESULTS

$PM_{2.5}$ exposure upregulated FOXO3A and BIM, and resulted in pathological lesions in lungs

H&E staining on mice lung tissues was performed to assess $PM_{2.5}$-induced lesions. As the result revealed, $PM_{2.5}$ exposure led to pronounced expansion of alveolar spatial structure and emphysema (Fig. 1 A, B). In addition, protein levels of FOXO3A and BIM were markedly upregulated in mice lung tissues of the $PM_{2.5}$ group compared to those in the control group (Fig. 1 C-E).

$PM_{2.5}$ exposure upregulated FOXO3A and BIM, and stimulated apoptosis in A549 cells

Alveolar epithelial cells A549 were selected for *in vitro* experiments. After 0, 25, 50 or 100 μg/mL $PM_{2.5}$ exposure for 48 h, protein levels of FOXO3A and BIM were dose-dependently upregulated (Fig. 2A). Their mRNA levels were also enhanced, and the levels of FOXO3A were obviously dose-dependent (Fig. 2 B, C). In addition, the apoptotic rate of A549 cells dose-dependently enhanced after $PM_{2.5}$ exposure (Fig. 2D).

Transcription factor FOXO3A induces apoptosis in A549 cells through stimulating BIM transcription

To elucidate the potential function of FOXO3A in inducing the occurrence of emphysema, si-FOXO3A was constructed. FOXO3A and BIM were upregulated by $PM_{2.5}$ exposure, and they were markedly downregulated by transfection of si-FOXO3A (Fig. 3 A, B). Moreover, the interaction between FOXO3A and BIM was identified by ChIP assay, suggesting that BIM transcription was stimulated by FOXO3A (Fig. 3C). In A549 cells, silence of FOXO3A markedly reversed $PM_{2.5}$-induced apoptosis stimulation (Fig. 3D).

$PM_{2.5}$ exposure induced apoptosis of alveolar epithelial cells and emphysema through the FOXO3A/BIM axis

Transfection efficacy of pcDNA-BIM was verified in A549 cells (Fig. 4A). It was demonstrated that knockdown of FOXO3A was able to reverse the enhanced protein level of clv-caspase3 in A549

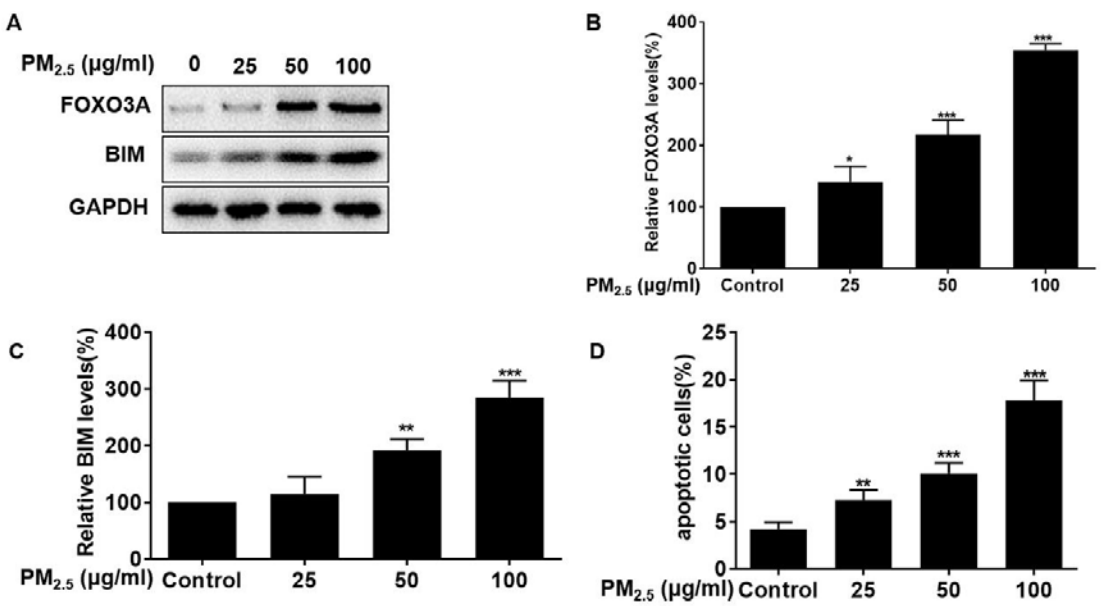


Fig. 2. *$PM_{2.5}$ exposure upregulated FOXO3A and BIM, and stimulated apoptosis in A549 cells. A) Western blot analyses on FOXO3A and BIM in A549 cells undergoing 0, 25, 50 or 100 μg/mL PM2.5 exposure.* ***B, C****) Quantification of protein levels of FOXO3A (B) and BIM (C) in A549 cells undergoing 0, 25, 50 or 100 μg/mL PM2.5 exposure.* ***D****) Apoptotic rate in A549 cells undergoing 0, 25, 50 or 100 μg/mL PM2.5 exposure.*

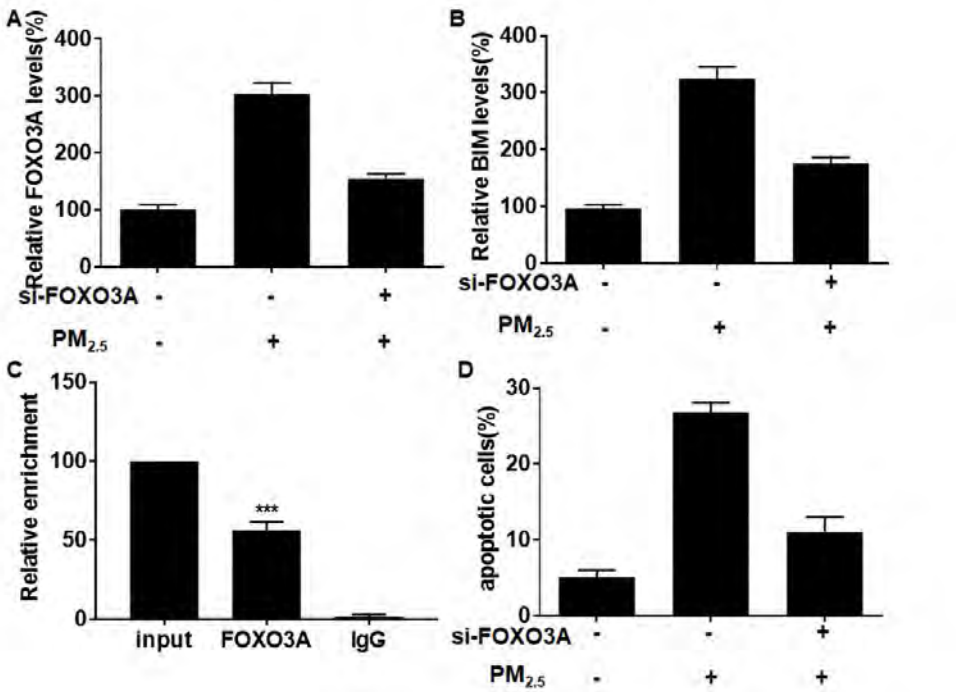


Fig. 3. *Transcription factor FOXO3A induces apoptosis in A549 cells through stimulating BIM transcription.* ***A****) Transfection efficacy of si-FOXO3A in A549 cells.* ***B****) Relative level of BIM in A549 cells undergoing PM2.5 exposure and transfected with si-FOXO3A.* ***C****) Relative enrichment of BIM in input, anti-FOXO3A and anti-IgG.* ***D****) Apoptotic rate in A549 cells undergoing PM2.5 exposure and transfected with si-FOXO3A*

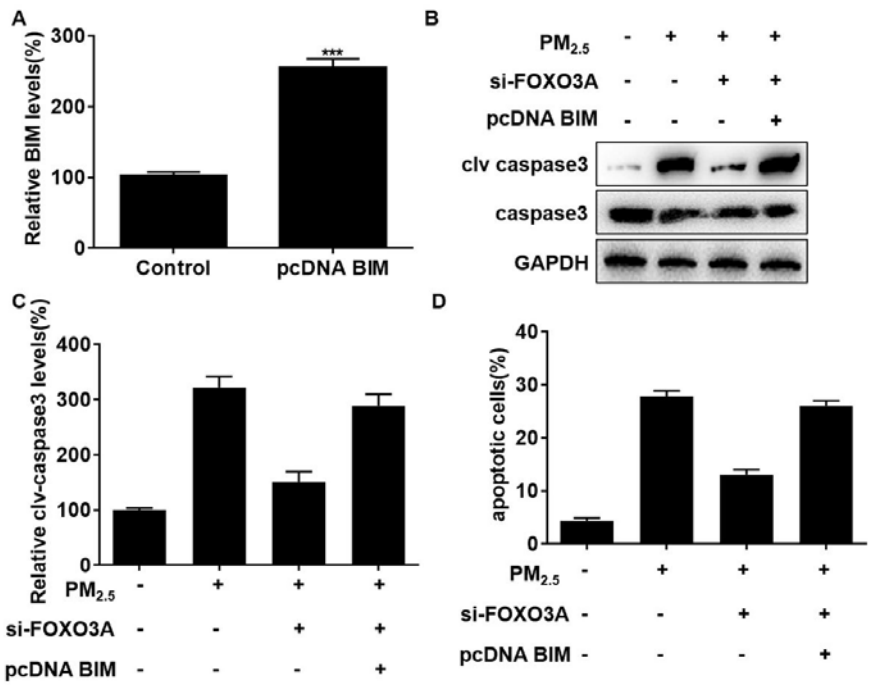


Fig. 4. *PM2.5 exposure induced apoptosis of alveolar epithelial cells and emphysema through the FOXO3A/BIM axis. A) Transfection efficacy of pcDNA-BIM in A549 cells. B, C) Relative level of clv-caspase3 in A549 cells undergoing PM2.5 exposure and transfected with si-FOXO3A or pcDNA-BIM. D) Apoptotic rate in A549 cells undergoing PM2.5 exposure and transfected with si-FOXO3A or pcDNA-BIM.*

cells undergoing $PM_{2.5}$ exposure, which was further enhanced after overexpression of BIM (Fig. 4 B, C). Mreover, regulatory effects of FOXO3A on $PM_{2.5}$-induced apoptosis of A549 cells were reversed by BIM overexpression (Fig. 4D).

DISCUSSION

COPD is a pathological condition of chronic bronchitis or emphysema characterized by airflow obstruction (18). COPD is the fifth leading cause of death in the world, and its morbidity and mortality are on the rise (19). Typical pathological lesions of emphysema include airway elasticity and excessive expansion at the distal end of the terminal bronchioles, inflation and increased lung volume and/or airway wall destruction (20). Smoking, infection and air pollution are susceptible to obstructive emphysema because of their contribution to bronchiolitis, stenosis or obstruction (21). At the time of inhalation, the bronchioles dilate and the air breathes in. The tracheal lumen shrinks and the air is detained in the lung at the time of exhalation, and thus the increased alveolar pressure results in alveoli over-expansion or even rupture (22). Loss of radial traction around the bronchioles causes bronchiole constriction and lumen stenosis (23). Consequently, thickening of pulmonary vascular intima, decreased blood supply to the alveolar wall and decreased alveolar elasticity all increase susceptibility to emphysema and decreased lung function (24).

Compared with coarser atmospheric particles, $PM_{2.5}$ has a small size, large superficial area and strong activity. Many toxic and harmful substances (heavy metals, microorganisms, polycyclic aromatic hydrocarbons, etc.) are contained in $PM_{2.5}$, leading to increased incidences of carcinogenicity, teratogenicity and mutagenesis. Long residence time in the atmosphere and transport distance of $PM_{2.5}$ pose a huge impact on human health (25). Particles of 10 μm diameter are usually deposited in the upper respiratory tract, and those smaller than 2 μm can deeply penetrate into the bronchioles and alveoli (26). Distribution of fine particles into the alveoli directly affects the ventilation function of lungs, leading to an anoxic state (27).

FOXO3, also known as FOXO3A, is characterized by the O subtype of forkhead transcription factor (28). Abnormally expressed FOXO3A is closely linked to tumorigenesis. Generally speaking, FOXO3A is downregulated in cancers, serving as a tumor-suppressor gene (29). Overexpression of FOXO3A is able to stimulate cell apoptosis.

Previous studies have found the presence of autophagy and apoptosis of alveolar epithelial cells in $PM_{2.5}$-associated COPD, manifesting as pathological damage, declined lung function and emphysema (30, 31). In the present paper, $PM_{2.5}$ exposure resulted in upregulation of FOXO3A and BIM in mice lung tissues. Pathological damages, including expanded alveolar space, declined lung function and emphysema, were observed in model mice. Similarly, *in vitro* experiments revealed that $PM_{2.5}$ exposure stimulated apoptosis in A549 cells.

BIM is widely expressed in normal cells, and it is activated by apoptosis stimuli. The activated BIM triggers Bax activation through interacting with Bcl-2/Bax, thereafter causing mitochondrial apoptosis (32). However, BIM is strictly mediated by transcriptional and post-translational regulations (33). It is well known that the transcriptional activity of FOXO is regulated by post-translational modifications, including phosphorylation, acetylation and methylation (34,35). Our findings revealed that the upregulated FOXO3A and BIM in $PM_{2.5}$-exposed A549 cells were reversed by knockdown of FOXO3A. Moreover, FOXO3A was able to stimulate BIM transcription through binding its promoter region. Collectively, $PM_{2.5}$ exposure participates in the induction of alveolar epithelial cell apoptosis and emphysema through the FOXO3A/BIM axis.

In conclusion, during $PM_{2.5}$ exposure, the upregulated FOXO3A triggers BIM transcription, and thus induces apoptosis of alveolar epithelial cells and emphysema in mice.

REFERENCES

1. Lopez-Campos JL, Tan W, Soriano JB. Global burden of COPD. Respirology 2016; 21:14-23.
2. Smith MC, Wrobel JP. Epidemiology and clinical impact of major comorbidities in patients with COPD.

Int J Chron Obstruct Pulmon Dis 2014; 9:871-888.
3. Gu XY, Chu X, Zeng XL, Bao HR, Liu XJ. Effects of PM2.5 exposure on the Notch signaling pathway and immune imbalance in chronic obstructive pulmonary disease. Environ Pollut 2017; 226:163-73.
4. He M, Ichinose T, Yoshida S, et al. PM2.5-induced lung inflammation in mice: Differences of inflammatory response in macrophages and type II alveolar cells. J Appl Toxicol 2017; 37:1203-18.
5. Shu J, Liu X, Chu X, Qiu J, Zeng X, Bao H. [Effects of PM2.5 on phagocytic function of alveolar macrophages in chronic obstructive pulmonary disease mice]. Zhonghua Yi Xue Za Zhi 2016; 96:301-5.
6. Chen L, Yuan X, Zou L, Peng J, Hu X. Effects of 1,25-Dihydroxyvitamin D3 on the prevention of chronic obstructive pulmonary disease (COPD) in rats exposed to air pollutant particles less than 2.5 micrometers in diameter (PM2.5). Med Sci Monit 2018; 24:356-62.
7. Li R, Zhou R, Zhang J. Function of PM2.5 in the pathogenesis of lung cancer and chronic airway inflammatory diseases. Oncol Lett 2018; 15:7506-14.
8. Morris BJ, Willcox DC, Donlon TA, Willcox BJ. FOXO3: a major gene for human longevity--a mini-review. Gerontology 2015; 61:515-25.
9. Yao H, Chung S, Hwang JW, et al. SIRT1 protects against emphysema via FOXO3-mediated reduction of premature senescence in mice. J Clin Invest 2012; 122:2032-45.
10. Wang Y, Zhu Y, Xing S, Ma P, Lin D. SIRT5 prevents cigarette smoke extract-induced apoptosis in lung epithelial cells via deacetylation of FOXO3. Cell Stress Chaperones 2015; 20:805-10.
11. Yuan YM, Luo L, Guo Z, Yang M, Lin YF, Luo C. Smoking, aging, and expression of proteins related to the FOXO3 signaling pathway in lung tissues. Genet Mol Res 2015; 14:8547-54.
12. Hwang JW, Rajendrasozhan S, Yao H, et al. FOXO3 deficiency leads to increased susceptibility to cigarette smoke-induced inflammation, airspace enlargement, and chronic obstructive pulmonary disease. J Immunol 2011; 187:987-98.
13. Yao S, Fan LY, Lam EW. The FOXO3-FOXM1 axis: A key cancer drug target and a modulator of cancer drug resistance. Semin Cancer Biol 2018; 50:77-89.
14. Du WW, Fang L, Yang W, Wu N, Awan FM, Yang Z, Yang BB. Induction of tumor apoptosis through a circular RNA enhancing Foxo3 activity. Cell Death Differ 2017; 24:357-70.
15. Sionov RV, Vlahopoulos SA, Granot Z. Regulation of Bim in health and disease. Oncotarget 2015; 6:23058-134.
16. Pan LJ, Wang X, Ling Y, Gong H. MiR-24 alleviates cardiomyocyte apoptosis after myocardial infarction via targeting BIM. Eur Rev Med Pharmacol Sci 2017; 21:3088-3097.
17. Tanimoto A, Takeuchi S, Arai S, et al. Histone deacetylase 3 inhibition overcomes BIM deletion polymorphism-mediated osimertinib resistance in EGFR-mutant lung cancer. Clin Cancer Res 2017; 23:3139-49.
18. Rabe KF, Watz H. Chronic obstructive pulmonary disease. Lancet 2017; 389:1931-40.
19. Ohara K, Samukawa T, Inoue H. Distinguishing asthma from COPD. Nihon Rinsho 2016; 74:774-77.
20. Vestbo J, Hurd SS, Agusti AG, et al. Global strategy for the diagnosis, management, and prevention of chronic obstructive pulmonary disease: GOLD executive summary. Am J Respir Crit Care Med 2013; 187:347-65.
21. Raherison C, Girodet PO. Epidemiology of COPD. Eur Respir Rev 2009; 18:213-21.
22. Tatsumi K. Concept and management of COPD, from past to future. Nihon Rinsho 2016; 74:723-727.
23. Vijayan VK. Chronic obstructive pulmonary disease. Indian J Med Res 2013; 137:251-69.
24. Dai J, Yang P, Cox A, Jiang G. Lung cancer and chronic obstructive pulmonary disease: From a clinical perspective. Oncotarget 2017; 8:18513-24.
25. Xing YF, Xu YH, Shi MH, Lian YX. The impact of PM2.5 on the human respiratory system. J Thorac Dis 2016; 8:E69-E74.
26. Apte JS, Marshall JD, Cohen AJ, Brauer M. Addressing global mortality from ambient PM2.5. Environ Sci Technol 2015; 49:8057-66.
27. Deng X, Zhang F, Rui W, et al. PM2.5-induced oxidative stress triggers autophagy in human lung epithelial A549 cells. Toxicol in Vitro 2013; 27:1762-70.
28. Wang Y, Kang XL, Zeng FC, Xu CJ, Zhou JQ, Luo DN. Correlations of Foxo3 and Foxo4 expressions with clinicopathological features and prognosis of

bladder cancer. Pathol Res Pract 2017; 213:766-72.
29. Yan H, Li Q, Wu J, et al. MiR-629 promotes human pancreatic cancer progression by targeting FOXO3. Cell Death Dis 2017; 8:e3154.
30. Xia Q, Hu ST, Zeng XL, Bao HR, Liu XJ. Mechanisms of cytoskeleton and PI3Kdelta-RhoA in fine particulate matter deteriorating phagocytosis defect of alveolar macrophage in mice with chronic obstructive pulmonary disease. Zhonghua Yi Xue Za Zhi 2017; 97:1893-98.
31. Yin J, Xia W, Li Y, et al. COX-2 mediates PM2.5-induced apoptosis and inflammation in vascular endothelial cells. Am J Transl Res 2017; 9:3967-76.
32. Zhang XQ, Dong JJ, Cai T, Shen X, Zhou XJ, Liao L. High glucose induces apoptosis via upregulation of Bim expression in proximal tubule epithelial cells. Oncotarget 2017; 8:24119-29.
33. O'Connor L, Strasser A, O'Reilly LA, Hausmann G, Adams JM, Cory S, Huang DC. Bim: a novel member of the Bcl-2 family that promotes apoptosis. Embo J 1998; 17:384-95.
34. Ju H, Tan JY, Cao B, Song MQ, Tian ZB. Effects of miR-223 on colorectal cancer cell proliferation and apoptosis through regulating FoxO3a/BIM. Eur Rev Med Pharmacol Sci 2018; 22:3771-78.
35. Liu Y, Zhang W, Wu X, Gong J. Foxo3a-dependent Bim transcription protects mice from a high fat diet via inhibition of activation of the NLRP3 inflammasome by facilitating autophagy flux in Kupffer cells. Oncotarget 2017; 8:34258-67.

LncRNA OIP5-AS1 INDUCES EPITHELIAL-TO-MESENCHYMAL TRANSITION AND RENAL FIBROSIS IN DIABETIC NEPHROPATHY VIA BINDING TO miR-30c-5p

J-X. FU*, G-Q. SUN*, H-L. WANG and H-X. JIANG

Department of Endocrinology, The Third People's Hospital of Qingdao, Qingdao, Shandong Province, China

Received April 3, 2020 – Accepted May 15, 2020

*These Authors contributed equally to this work

In recent years, the incidence of diabetic nephropathy (DN) is rising, and is one of the most important complications of diabetic patients. In this study, the role and regulatory mechanism of lncRNA OIP5-AS1 in the regulation of DN were investigated. Here, the expressions of lncRNA OIP5-AS1 and miR-30c-5p were detected by RT-qPCR. Western blot analysis was used to detect the protein expression of E-cadherin, N-cadherin, TGF-β1, α-SMA. The relationship between OIP5-AS1 and miR-30c-5p was confirmed by dual luciferase reporter assay. The results showed that the expression of lncRNA OIP5-AS1 was increased in db/db DN mice kidney tissue and high glucose-stimulated HK2 cells. lncRNA OIP5-AS1 promoted epithelial-to-mesenchymal transition (EMT) and renal fibrosis in high glucose-stimulated HK2 cells. In addition, lncRNA OIP5-AS1 directly targets miR-30c-5p, and lncRNA OIP5-AS1 negatively regulated miR-30c-5p expression in high glucose-stimulated HK2 cells. More importantly, overexpression of miR-30c-5p attenuated the promoting effect of OIP5-AS1 on EMT and renal fibrosis in high glucose-stimulated HK2 cells. In conclusion, lncRNA OIP5-AS1 induces EMT and renal fibrosis in DN via binding to miR-30c-5p.

Diabetic nephropathy (DN) is a kidney disease caused by abnormal metabolism of diabetes. The most typical feature of DN is diabetic glomerulosclerosis, which is also one of the most important chronic microvascular complications in diabetic patients (1). The main clinical manifestation of DN is persistent proteinuria, and the main pathological manifestations are widening of the mesangial area and thickening of glomerular basement membrane (2). In addition, diabetes can significantly increase the incidence of urinary tract infections and contrast-induced nephropathy (3). Unfortunately, there is no specific treatment for patients with DN, therefore, it is important to explore new methods for the treatment of DN.

Epithelial cell-mesenchymal transition (EMT) refers to the biological process of transforming epithelial cells into cells with mesenchymal phenotype through a specific procedure (4). EMT plays an important role in embryonic development, chronic inflammation, cancer metastasis, and various fibrotic diseases (5). The main features of EMT are reduced expression of cell adhesion molecules (E-cadherin) and the conversion of cytokeratin cytoskeleton to vimentin (6). In addition, EMT is also an important process of DN. It has been reported that DN induced EMT through the miR-2467-3p/Twist1 pathway (7). In addition, the number of mesenchymal marker-positive epithelial cells is related to increased serum

Key words: LncRNA OIP5-AS1; epithelial-to-mesenchymal transition; renal fibrosis; diabetic nephropathy; miR-30c-5p

Corresponding Author:
Dr Hongxia Jiang,
Department of Endocrinology, The Third People's Hospital of Qingdao,
No. 29 Yongping Road, Licang District, Qingdao,
266041 Shandong Province, China
Tel.: +86 0532-84632636
e-mail: dikjieavw0125@163.com

0393-974X (2020)
Copyright © by BIOLIFE, s.a.s.
This publication and/or article is for individual use only and may not be further reproduced without written permission from the copyright holder.
Unauthorized reproduction may result in financial and other penalties
DISCLOSURE: ALL AUTHORS REPORT NO CONFLICTS OF INTEREST RELEVANT TO THIS ARTICLE.

creatinine level and the severity of interstitial damage (8). It has been found that blockage of tubular epithelial to myofibroblast transition (α-SMA) prevented renal interstitial fibrosis (9). BMP-7 can counteract TGF-β1-induced EMT and reverse chronic renal injury (10). These findings indicate that EMT plays a vital role in DN progression.

Recently, many long non-coding RNAs (lncRNAs) have been found to regulate DN. For example, it has been reported that lncRNA MEG3 exacerbated the DN process by sponging miR-145 (11). Circ_0080425 inhibited cell proliferation and fibrosis in DN by sponging miR-24-3p and targeting fibroblast growth factor 11 (12). At present, the specific role of lncRNA OIP5-AS1 has attracted attention. It was found that lncRNA OIP5-AS1 regulated endothelial cell injury mediated by oxidative low-density lipoprotein via the miR-320a/LOX1 axis (13). LncRNA OIP5-AS1 can inhibit the osteoblast differentiation of valve interstitial cells through the miR-137/TWIST11 axis (14). Downregulation of lncRNA OIP5-AS1 induced by IL-1βcan also aggravate osteoarthritis by regulating miR-29b-3p/PGRN (15). However, the effect of lncRNA OIP5-AS1 on EMT and renal fibrosis in DN is unknown.

In this study, lncRNA OIP5-AS1 was predicted to target miR-30c-5p. It has been shown that miR-30c-5p can inhibit high glucose-induced EMT and renal fibrosis in DN (16), however, the relationship between lncRNA OIP5-AS1 and miR-30c-5p has not been investigated in DN. Therefore, this study aims to clarify this problem.

MATERIALS AND METHODS

Animal model

SPF diabetic model mice (strain C57BL/KsJ-db/db mice, db/db DN) and control normal mice (db/m mice) were purchased from the Model Animal Research Center of Nanjing University (Nanjing, China). Animal experiments were performed according to the standards of NIH Instructions for the Care and Use of Laboratory Animals. This study was approved by the Ethics Committee of The Third People's Hospital of Qingdao. All rats had free access to standard feed and water, and were housed at 22±1°C and 55 % humidity controlled conditions with a 12:12 h light/dark cycle.

Cell culture and transfection

HK2 cells from American Type Tissue Collection were incubated in DMEM medium containing 10% FBS (Invitrogen, Carlsbad, CA, USA), penicillin (100 U/ml), and streptomycin (100 μg/ml). The cells were incubated in a humidified atmosphere containing 5% CO_2 at 37°C. DMEM medium contained 25 mm glucose and 5.5 mm glucose to simulate high glucose status (HG) and normal physiological environment (NC). OIP5-AS1 vector and siRNA or miR-30c-5p mimics and inhibitor (GenePharma, Shanghai, China) were transfected into HK2 cells using Lipofectamine 3000 reagent (Invitrogen, USA), respectively.

RT-qPCR

Total RNA was extracted from HK2 cells and urine using Trizol reagent (Invitrogen, Carlsbad, USA). RNA was reverse transcribed into cDNA using microRNA reverse transcription kit (Takara, Dalian, China). RT-qPCR was performed on the 7900HT Fast Real-Time PCR system (Applied Biosystems, Foster City, CA, USA) using SYBR Premix Ex TaqTM (Takara, Dalian, China). U6 small nuclear RNA was used as an internal control. Fold change was calculated using the $2^{-\square\square^{cq}}$ method.

Western blot analysis

RIPA lysis buffer was used to extract protein samples from HK2 cells. Total protein was quantified by BCA assay (Thermo Fisher Scientific, MA, US). Next, protein samples were separated by 10% SDS-PAGE, then they were transferred to PVDF membranes (Roche, USA) and blocked with 5% skim milk. The membranes were incubated with E-cadherin, N-cadherin, TGF-β1, α-SMA and GAPDH primary antibodies (Abcam, Shanghai, China) at 4°C overnight, followed by incubation with the suitable horseradish peroxidase-conjugated secondary antibodies (Abcam, USA) for 2 h. An enhanced chemiluminescence (ECL) chromogenic substrate (Thermo Fisher Scientifc, Waltham, MA, USA) was used to expose the immunoreactive bands.

Dual luciferase reporter assay

The pGL3 vectors (Promega, Madison, WI) containing the 3'-UTR of wild-type (WT) or mutant (mut) OIP5-AS1 and miR-30c-5p mimics were inserted into HK2 cells for dual-luciferase reporter assay. A dual luciferase system (Promega, USA) was used to detect luciferase activity.

Statistical analysis

Data are shown as mean±SD. Comparisons between groups were analyzed using Student's *t*-test or one-way analysis of variance followed by a Bonferroni post hoc test. The difference of $P < 0.05$ was considered significant.

RESULTS

LncRNA OIP5-AS1 is upregulated in DN

The expression level of lncRNA OIP5-AS1 was detected by RT-qPCR. Compared with db/m mice, lncRNA OIP5-AS1 expression was increased in db/db DN mice (Fig. 1A). In this study, high glucose-induced HK2 cells were constructed, and lncRNA OIP5-AS1 expression was also measured in HK2 cells. Compared with normal HK2 cells (NC), lncRNA OIP5-AS1 was upregulated in high glucose-induced HK2 cells (HG, Fig. 1B). These results indicate that lncRNA OIP5-AS1 expression is increased in db/db DN mice kidney tissue and high glucose-stimulated HK2 cells.

LncRNA OIP5-AS1 promotes EMT and renal fibrosis in high glucose-stimulated HK2 cells

To further clarify the role of lncRNA OIP5-AS1 in DN, the effect of lncRNA OIP5-AS1 on EMT and renal fibrosis was investigated. Then, OIP5-AS1 siRNA was transfected into high glucose-induced HK2 cells. RT-qPCR showed that OIP5-AS1 siRNA significantly down-regulated the expression level of lncRNA OIP5-AS1 in high glucose-induced HK2 cells (Fig. 2A). Next, the protein expression of EMT and cell fibrosis maker gene was evaluated by Western blot analysis. In high glucose-induced HK2 cells, OIP5-AS1 siRNA enhanced E-cadherin expression, and decreased N-cadherin expression (Fig. 2B), which indicates that upregulation of OIP5-AS1 induces EMT in DN. In addition, it was found that knockdown of OIP5-AS1 decreased the expressions of fibrosis maker genes TGF-β1 and α-SMA in high glucose-induced HK2 cells (Fig. 2C). Collectively, lncRNA OIP5-AS1 promotes EMT and renal fibrosis in high glucose-stimulated HK2 cells.

LncRNA OIP5-AS1 can bind to miR-30c-5p

The starBase database (http://starbase.sysu.edu.cn) predicts that miR-30c-5p has a binding site to lncRNA OIP5-AS1 (Fig. 3A). Dual-luciferase reporter assay showed that miR-30c-5p mimics reduced the luciferase activity of wt-OIP5-AS1, but had little effect on that of mut-OIP5-AS1 in HK2 cells (Fig. 3B), indicating that miR-30c-5p is a direct target of lncRNA OIP5-AS1. In addition, RT-qPCR showed that miR-30c-5p expression was significantly reduced in db/db DN mice and high glucose-stimulated HK2 cells (Fig. 3 C, D). To further

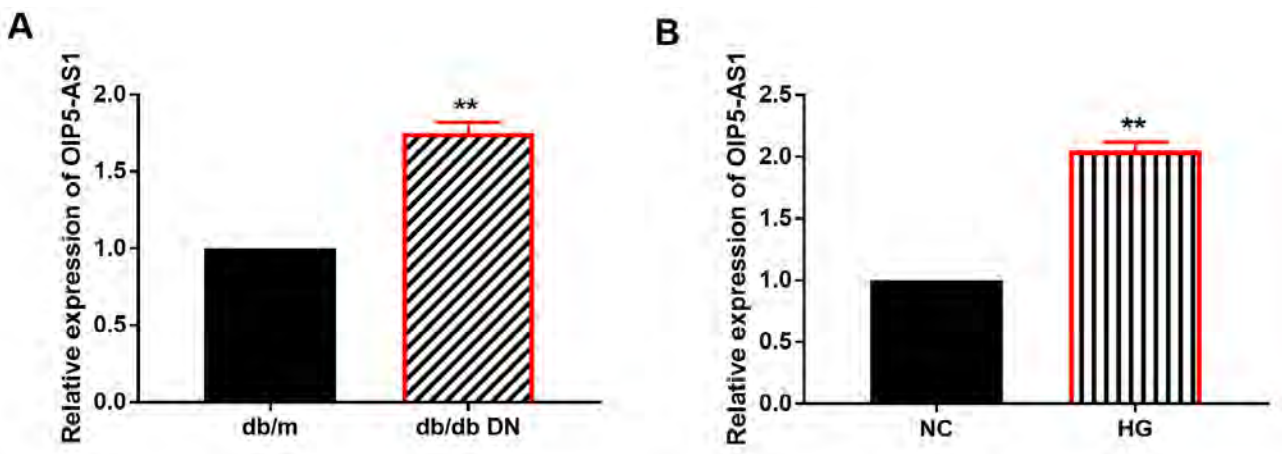


Fig. 1. *LncRNA OIP5-AS1 is upregulated in DN.* ***A****) The expression of lncRNA OIP5-AS1 was detected in db/db DN and db/m mice.* ***B****) The expression of lncRNA OIP5-AS1 was measured in HG-stimulated HK2 cells and normal HK2 cells (NC) **P < 0.01.*

explore the relationship between lncRNA OIP5-AS1 and miR-30c-5p in DN, the expression of miR-30c-5p was measured in high glucose-stimulated HK2 cells with OIP5-AS1 vector or siRNA. The results showed that upregulation of lncRNA OIP5-AS1 reduced the expression of miR-30c-5p, while downregulation of lncRNA OIP5-AS1 enhanced miR-30c-5p expression in high glucose-stimulated HK2 cells (Fig. 3E). These results indicate that lncRNA OIP5-AS1 can directly target miR-30c-5p. lncRNA OIP5-AS1 negatively regulates miR-30c-5p expression in high glucose-stimulated HK2 cells.

LncRNA OIP5-AS1 induces EMT and renal fibrosis in high glucose-stimulated HK2 cells via miR-30c-5p

To detect whether lncRNA OIP5-AS1 regulates EMT and cell fibrosis by targeting miR-30c-5p, the OIP5-AS1 vector and miR-30c-5p mimics were transfected into high glucose-stimulated HK2 cells. We found that OIP5-AS1 vector significantly promoted its

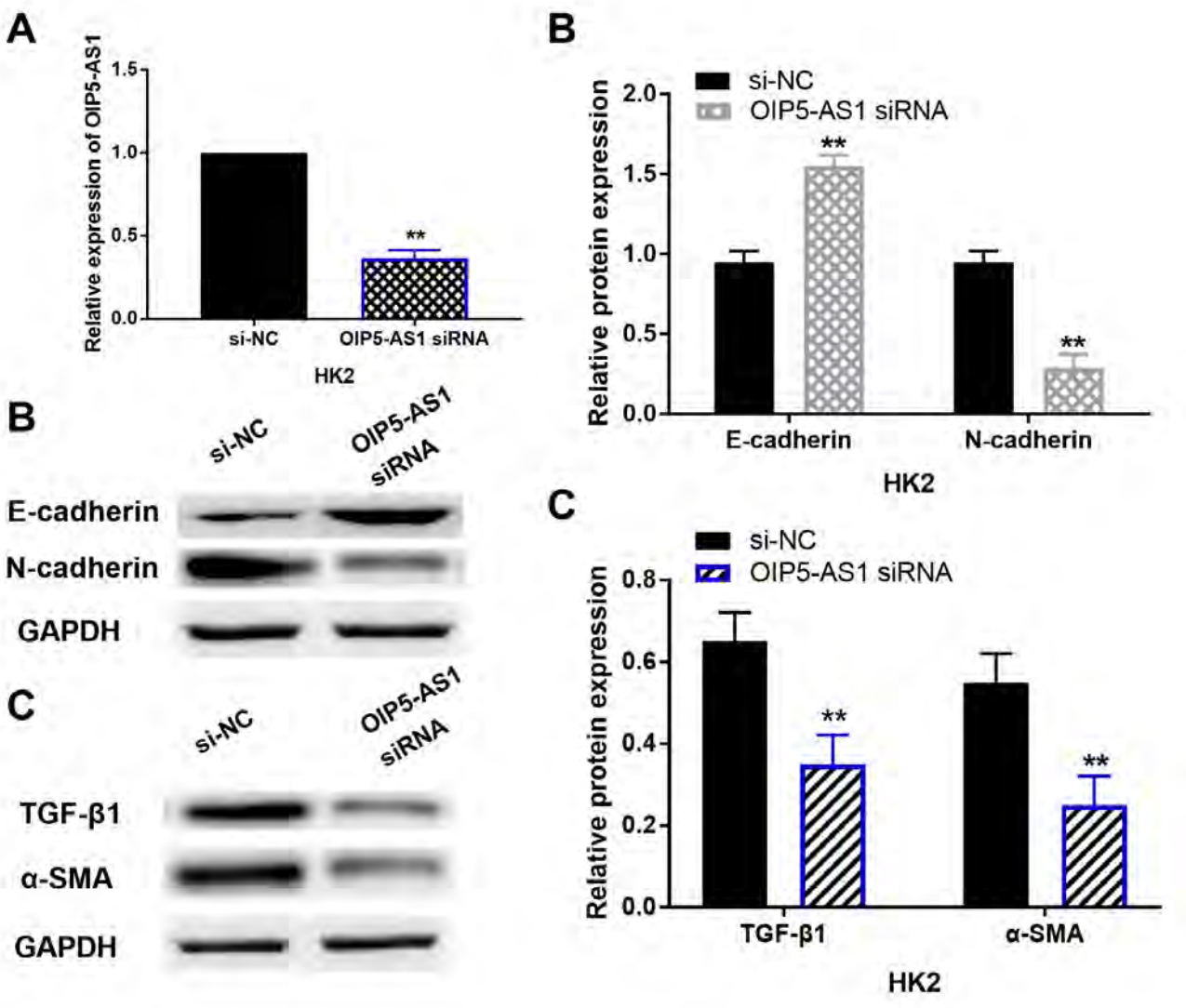


Fig. 2. *LncRNA OIP5-AS1 promotes EMT and renal fibrosis in high glucose-stimulated HK2 cells.* ***A)*** *The expression of lncRNA OIP5-AS1 in HG-stimulated HK2 cells with si-NC or OIP5-AS1 siRNA.* ***B)*** *The protein expression level of E-cadherin, N-cadherin in HG-stimulated HK2 cells with si-NC or OIP5-AS1 siRNA.* ***C)*** *The protein expression level of TGF-β1, α-SMA in HG-stimulated HK2 cells with si-NC or OIP5-AS1 siRNA ** P <0.01*

expression in high glucose-stimulated HK2 cells. miR-30c-5p mimics reduced this increase in lncRNA OIP5-AS1 expression in high glucose-stimulated HK2 cells (Fig. 4A). Next, the protein expression of EMT and cell fibrosis maker gene was evaluated in transfected HK2 cells. In high glucose-induced HK2 cells, upregulation of lncRNA OIP5-AS1 was found to inhibit E-cadherin expression and promote N-cadherin expression. After transfection with miR-30c-5p mimics, the expression of E-cadherin and N-cadherin was restored in high glucose-induced HK2 cells (Fig. 4B). In addition, upregulation of OIP5-AS1 promoted the expressions of fibrosis marker genes TGF-β1 and α-SMA in high glucose-induced HK2 cells. Overexpression of miR-30c-5p attenuated the promoting effect of OIP5-AS1 on TGF-β1 and α-SMA expression in high glucose-induced HK2 cells (Fig. 4C). These results indicate that lncRNA OIP5-AS1 promotes EMT and cell fibrosis in high glucose-stimulated HK2 cells by inhibiting miR-30c-5p expression.

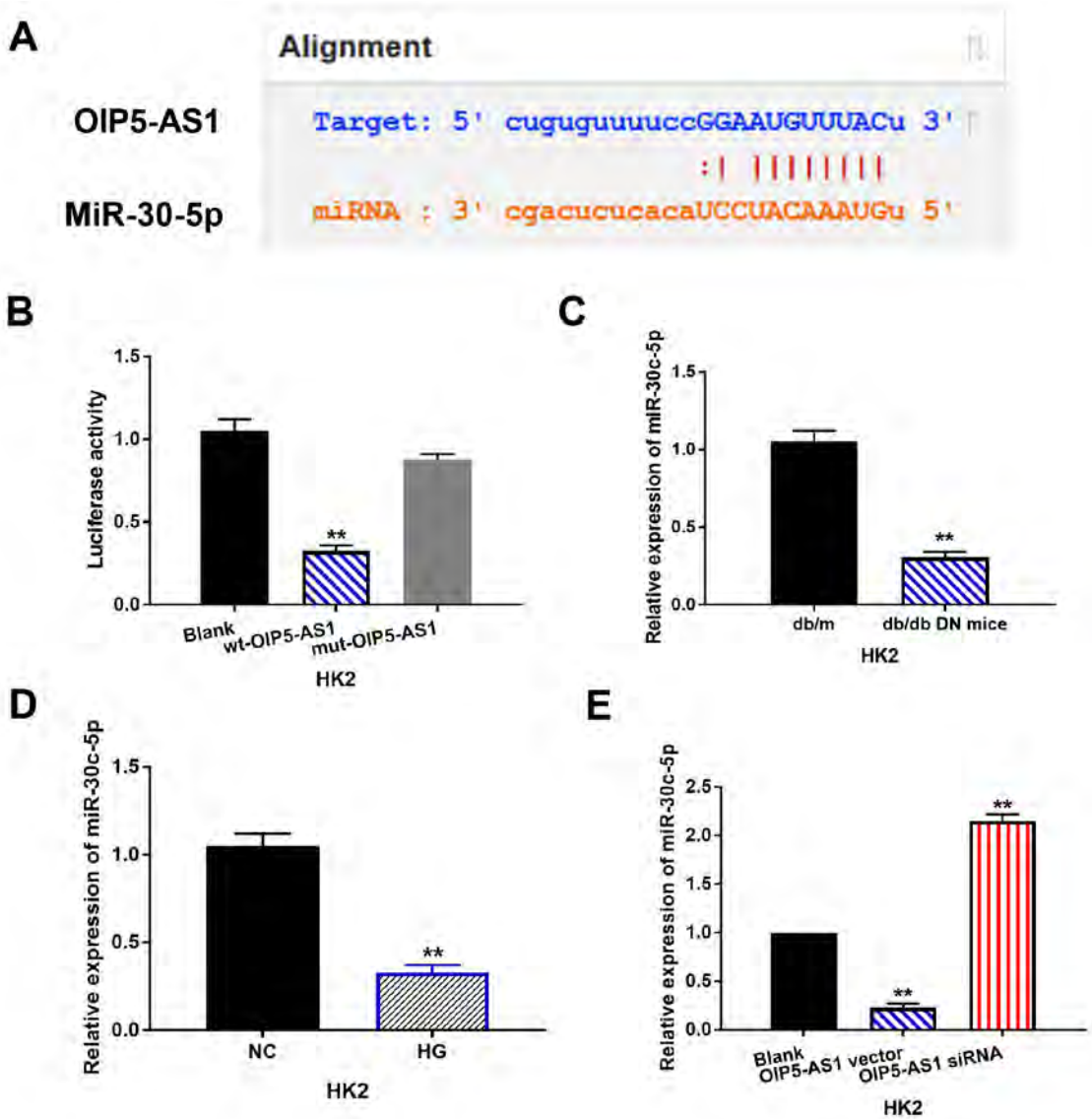


Fig. 3. *LncRNA OIP5-AS1 can bind to miR-30c-5p.* ***A****) The binding sites between lncRNA OIP5-AS1 and miR-30c-5p.* ***B****) Luciferase reporter assay.* ***C****) The expression of miR-30c-5p in db/db DN mice and db/m mice.* ***D****) The expression of miR-30c-5p in HG-stimulated HK2 cells and normal HK2 cells.* ***E****) The expression of miR-30c-5p in HG-stimulated HK2 cells with OIP5-AS1 vector or siRNA *P < 0.05, ** P <0.01*

DISCUSSION

In recent years, the morbidity and mortality of DN have been increasing, which has brought a heavy health and economic burden to society. Renal fibrosis is one of the main pathological features of DN (17). In this study, upregulation of lncRNA OIP5-AS1 was detected in db/db DN mice kidney tissues and high glucose-stimulated HK2 cells, and knockdown of lncRNA OIP5-AS1 inhibited EMT in high glucose-stimulated HK2 cells. In addition, the downregulation of lncRNA OIP5-AS1 also reduced the expression of fibrosis maker genes TGF-β1, α-SMA in high glucose-induced HK2 cells. These results indicate that lncRNA OIP5-AS1 can induce EMT in DN and aggravate renal fibrosis.

Similar to our results, upregulation of lncRNA OIP5-AS1 has been found in various diseases, such as hemangioma and multiple myeloma (18, 19). In addition, the function of lncRNA OIP5-AS1 has been extensively investigated in human cancers. In particularly, lncRNA OIP5-AS1 promoted cell proliferation and inhibited apoptosis in cervical cancer through a mechanism involving miR-143-3p/ROCK1 (20). Moreover, it is reported that overexpression of OIP5-AS1 promoted cell proliferation, migration, invasion, and EMT in laryngeal squamous cell carcinoma (21). Here, it was also found that the upregulation of OIP5-AS1 promoted EMT in DN, and the up-regulation of OIP5-AS1 enhanced the expression levels of renal fibrosis marker proteins TGF-β1 and α-SMA. The effect of lncRNA OIP5-AS1 on renal fibrosis is firstly reported in our study, which has not been discovered in previous studies.

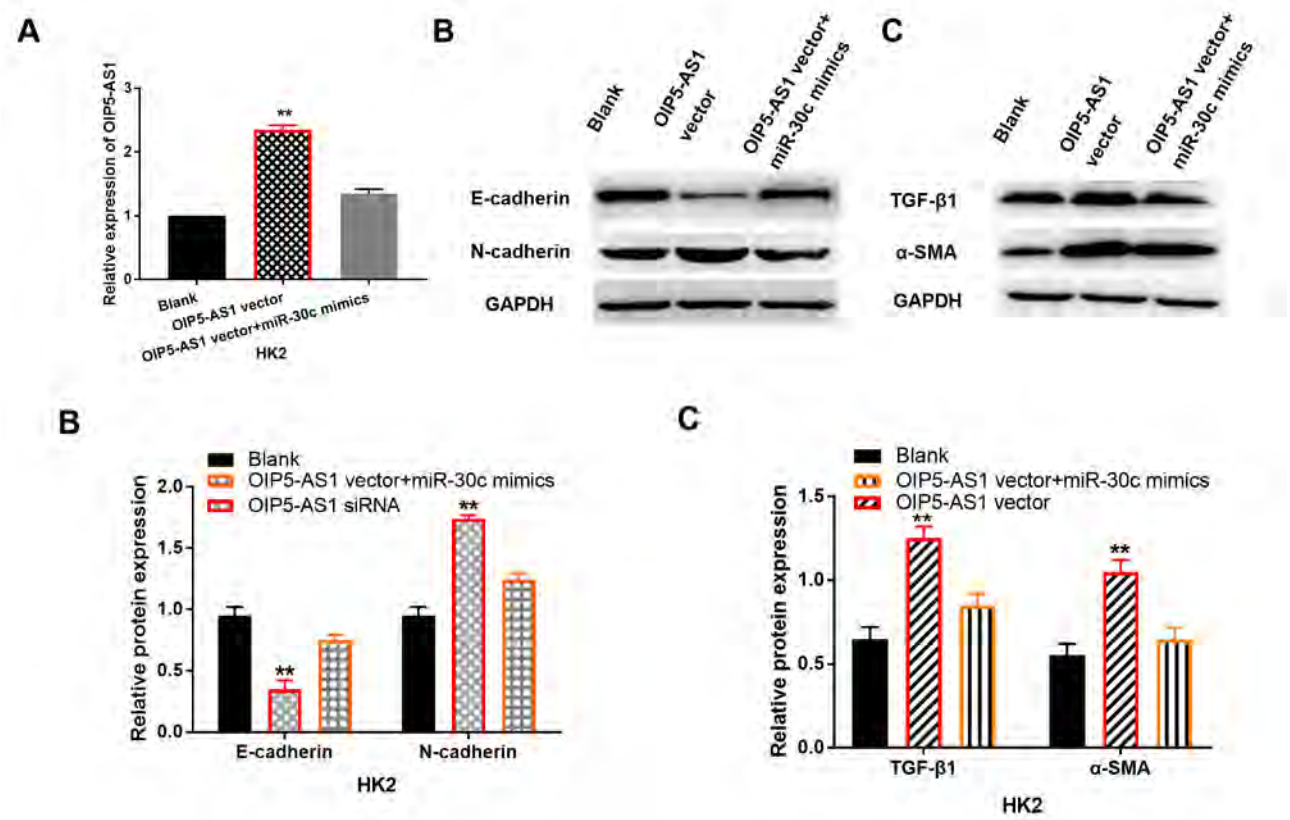


Fig. 4. *LncRNA OIP5-AS1 induces EMT and renal fibrosis in high glucose-stimulated HK2 cells via miR-30c-5p.* ***A****) The expression of lncRNA OIP5-AS1 in HG-stimulated HK2 cells with OIP5-AS1 vector or OIP5-AS1 vector+miR-30c-5p mimics.* ***B****) The protein expression level of E-cadherin, N-cadherin in HG-stimulated HK2 cells with OIP5-AS1 vector or OIP5-AS1 vector+miR-30c-5p mimics.* ***C****) The protein expression level of TGF-β1, α-SMA in HG-stimulated HK2 cells with OIP5-AS1 vector or OIP5-AS1 vector+miR-30c-5p mimics ** P <0.01*

Our research shows that lncRNA OIP5-AS1 is an important regulator in the pathogenesis of DN.

An increasing number of studies have shown that lncRNAs play important roles in DN by regulating miRNAs. For example, lncRNA NORAD aggravated the progression of DN by targeting miR-520h (22). In addition, it was found that lncRNA TUG1 ameliorated DN by inhibiting the expression of miR-21 (23). In our study, lncRNA OIP5-AS1 was found to directly target miR-30c-5p, and lncRNA OIP5-AS1 negatively regulated miR-30c-5p expression in high glucose-stimulated HK2 cells. It has been reported that miR-30c can be used as a predictive biomarker for type 2 diabetes with coronary heart disease (24). MiR-30c-5p can reduce renal ischemia-reperfusion involving macrophage (25), and miR-30c/PGC-1β can also protect against diabetic cardiomyopathy through PPARα (26). These results indicate that miR-30c plays an important role in diabetes and renal injury. More importantly, miR-30c-5p has been found to inhibit high glucose-induced EMT and renal fibrosis in DN (16). In our study, miR-30c-5p overexpression was found to attenuate the promoting effect of OIP5-AS1 in DN. This also suggests that miR-30c-5p can prevent DN. LncRNA OIP5-AS1 can aggravate the DN process by inhibiting miR-30c-5p expression.

In conclusion, upregulation of lncRNA OIP5-AS1 and downregulation of miR-30c-5p are found in the kidney tissues of db/db DN mice and high glucose-stimulated HK2 cells. More importantly, lncRNA OIP5-AS1 promotes EMT and cell fibrosis in high glucose-stimulated HK2 cells by downregulating miR-30c-5p. This study shows that lncRNA OIP5-AS1 may be a possible target for the treatment of DN.

REFERENCES

1. Zhang L, Long J, Jiang W, et al. Trends in chronic kidney disease in China. N Engl J Med 2016; 375:905-6.
2. Kolset SO, Reinholt FP, Jenssen T. Diabetic nephropathy and extracellular matrix. J Histochem Cytochem 2012; 60:976-86.
3. Keri KC, Samji NS, Blumenthal S. Diabetic nephropathy: newer therapeutic perspectives. J Community Hosp Intern Med Perspect 2018; 8:200-07.
4. Thiery JP, Acloque H, Huang RY, Nieto MA. Epithelial-mesenchymal transitions in development and disease. Cell 2009; 139:871-90.
5. Rastaldi MP. Epithelial-mesenchymal transition and its implications for the development of renal tubulointerstitial fibrosis. J Nephrol 2006; 19:407-12.
6. Rout-Pitt N, Farrow N, Parsons D, Donnelley M. Epithelial mesenchymal transition (EMT): a universal process in lung diseases with implications for cystic fibrosis pathophysiology. Respir Res 2018; 19:136.
7. Xu Y, Ouyang C, Lyu D, et al. Diabetic nephropathy execrates epithelial-to-mesenchymal transition (EMT) via miR-2467-3p/Twist1 pathway. Biomed Pharmacother 2020; 125:109920.
8. Rastaldi MP, Ferrario F, Giardino L, et al. Epithelial-mesenchymal transition of tubular epithelial cells in human renal biopsies. Kidney Int 2002; 62:137-46.
9. Yang J, Liu Y. Blockage of tubular epithelial to myofibroblast transition by hepatocyte growth factor prevents renal interstitial fibrosis. J Am Soc Nephrol 2002; 13:96-107.
10. Zeisberg M, Hanai J, Sugimoto H, Mammoto T, Charytan D, Strutz F, Kalluri R. BMP-7 counteracts TGF-beta1-induced epithelial-to-mesenchymal transition and reverses chronic renal injury. Nat Med 2003; 9:964-68.
11. Li J, Jiang X, Duan L, Wang W. Long non-coding RNA MEG3 impacts diabetic nephropathy progression through sponging miR-145. Am J Transl Res 2019; 11:6691-98.
12. Liu H, Wang X, Wang ZY, Li L. Circ_0080425 inhibits cell proliferation and fibrosis in diabetic nephropathy via sponging miR-24-3p and targeting fibroblast growth factor 11. J Cell Physiol 2020; 235:4520-29.
13. Zhang C, Yang H, Li Y, Huo P, Ma P. LNCRNA OIP5-AS1 regulates oxidative low-density lipoprotein-mediated endothelial cell injury via miR-320a/LOX1 axis. Mol Cell Biochem 2020; 467(1-2):15-25.
14. Zheng D, Wang B, Zhu X, Hu J, Sun J, Xuan J, Ge Z. LncRNA OIP5-AS1 inhibits osteoblast differentiation of valve interstitial cells via miR-137/TWIST11 axis. Biochem Biophys Res Commun 2019; 511:826-32.
15. Zhi L, Zhao J, Zhao H, Qing Z, Liu H, Ma J. Downregulation of LncRNA OIP5-AS1 Induced

by IL-1beta Aggravates Osteoarthritis via Regulating miR-29b-3p/PGRN. Cartilage 2020; 1947603519900801.
16. Gao BH, Wu H, Wang X, Ji LL, Chen C. MiR-30c-5p inhibits high glucose-induced EMT and renal fibrogenesis by down-regulation of JAK1 in diabetic nephropathy. Eur Rev Med Pharmacol Sci 2020; 24:1338-49.
17. Sun ZJ, Li XQ, Chang DY, Wang SX, Liu G, Chen M, Zhao MH. Complement deposition on renal histopathology of patients with diabetic nephropathy. Diabetes Metab 2019; 45:363-68.
18. Zhang J, Zhao T, Tian L, Li Y. LncRNA OIP5-AS1 Promotes the Proliferation of Hemangioma Vascular Endothelial Cells via Regulating miR-195-5p/NOB1 Axis. Front Pharmacol 2019; 10:449.
19. Yang N, Chen J, Zhang H, Wang X, Yao H, Peng Y, Zhang W. LncRNA OIP5-AS1 loss-induced microRNA-410 accumulation regulates cell proliferation and apoptosis by targeting KLF10 via activating PTEN/PI3K/AKT pathway in multiple myeloma. Cell Death Dis 2017; 8:e2975.
20. Song L, Wang L, Pan X, Yang C. lncRNA OIP5-AS1 targets ROCK1 to promote cell proliferation and inhibit cell apoptosis through a mechanism involving miR-143-3p in cervical cancer. Braz J Med Biol Res 2020; 53:e8883.
21. Wang H, Qian J, Xia X, Ye B. Long non-coding RNA OIP5-AS1 serves as an oncogene in laryngeal squamous cell carcinoma by regulating miR-204-5p/ZEB1 axis. Naunyn Schmiedebergs Arch Pharmacol 2020;
22. Qi H, Yao L, Liu Q. NORAD affects the progression of diabetic nephropathy through targeting miR-520h to upregulate TLR4. Biochem Biophys Res Commun 2020; 521:190-95.
23. Wang F, Gao X, Zhang R, Zhao P, Sun Y, Li C. LncRNA TUG1 ameliorates diabetic nephropathy by inhibiting miR-21 to promote TIMP3-expression. Int J Clin Exp Pathol 2019; 12:717-29.
24. Luo M, Wang G, Xu C, Zeng M, Lin F, Wu J, Wan Q. Circulating miR-30c as a predictive biomarker of type 2 diabetes mellitus with coronary heart disease by regulating PAI-1/VN interactions. Life Sci 2019; 239:117092.
25. Zhang C, Yu S, Zheng B, et al. miR-30c-5p Reduces Renal Ischemia-Reperfusion Involving Macrophage. Med Sci Monit 2019; 25:4362-69.
26. Yin Z, Zhao Y, He M, et al. MiR-30c/PGC-1beta protects against diabetic cardiomyopathy via PPARalpha. Cardiovasc Diabetol 2019; 18:7.

MECHANISM OF JINRONG GRANULE IN INHIBITING THE INVASION OF BREAST CANCER CELLS BY THE CXCL-1-CXCR2/CCL20 PATHWAY

L. GUO[1*], HL. SITU[1*], ZY. WANG[2], Y. LIN[1] and QJ. CHEN[1]

[1]Department of Galactophore, The Second Affiliated Hospital of Guangzhou University of Traditional Chinese Medicine, Guangzhou, Guangdong Province, China; [2]Research and Innovation Team of Department of Galactophore, The Second Affiliated Hospital of Guangzhou University of Traditional Chinese Medicine, Guangzhou, Guangdong Province, China

Received November 27, 2019 – Accepted March 20, 2020

[*]These authors contributed equally to this work

The purpose of this study was to explore the effect of the Jinrong granule on CXCL-1 and the mechanism of the Jinrong granule on the metastasis and apoptosis of breast cancer cell lines. MDA-MB-231 human breast cancer cell line was divided into a control group, Jinrong extract group, CXCL-1 group and Jinrong extract + CXCL-1 group. The proliferation, apoptosis and permeability of the cells in the experimental group were studied. The protein expression of CXCL-1 was detected by Western blot. On this basis, a bioinformatics method was used to analyze the mechanism of CXCL-1. The results of the CCK8 experiment showed that compared with the control group, the cell proliferation activity of the CXCL-1 treatment group was enhanced while that of the Jinrong granule group was decreased. Compared with that of the CXCL-1 treatment group, the cell proliferation rate of the CXCL-1 + Jinrong granule group was significantly lower. The results showed that CXCL-1 could inhibit apoptosis of breast cancer cells, while the Jinrong granule could reverse the inhibition of apoptosis induced by CXCL-1. The results showed that the Jinrong granule could inhibit the ability of CXCL-1 to promote the migration and proliferation of breast cancer cells. The Jinrong granule could reverse the promoting effect of CXCL-1 on breast cancer through the CXCL-1-CLCR2/CCL20 pathway. In conclusion, the Jinrong granule can inhibit the invasion of breast cancer cells through the CXCL-1-CLCR2/CCL20 pathway.

Breast cancer is one of the most common malignant tumors in women all over the world (1, 2). Although there are many ways to treat this cancer, it is the second leading cause of death in women (3). Early diagnosis, radical surgery and adjuvant therapy improve the survival rate and prognosis of patients, although the mortality rate is still very high. To maximize the therapeutic effect, it is important to study new drugs and their targets. Fortunately, traditional Chinese medicine plays a unique role in cancer prevention and treatment (4). Many traditional Chinese medicine preparations or their extracts have been reported to regulate the growth, invasion and metastasis of various tumor cells by acting on tumor targets (5-8).

Jinrong granule, formerly known as Xiaopi granule, has been used in the clinical treatment of mammary hyperplasia since the late 1980s. It has been clinically applied and researched for more than 30 years, and satisfactory results have been

Key words: Jinrong granule; breast cancer; CXCL-1; CXCL-1-CXCR2/CCL20 pathway

Corresponding Author:
Dr Qianjun Chen,
Department of Galactophore, The Second Affiliated Hospital of Guangzhou University, of Traditional Chinese Medicine, No.111 Dade Road, Yuexiu District, Guangzhou, 510120, Guangdong Province, China
e-mail: chenqianjun55@163.com

0393-974X (2020)
Copyright © by BIOLIFE, s.a.s.
This publication and/or article is for individual use only and may not be further reproduced without written permission from the copyright holder. Unauthorized reproduction may result in financial and other penalties
DISCLOSURE: ALL AUTHORS REPORT NO CONFLICTS OF INTEREST RELEVANT TO THIS ARTICLE.

achieved. The literature shows that the drug also has the effect of blocking or delaying the occurrence and providing for primary prevention of breast cancer (9). However, there is still a lack of research on the molecular mechanism of Jinrong granules, especially on the invasion and migration of tumor cells.

There are many factors that promote the migration and invasion of breast cancer, and CXCL1, which is also known as growth gene regulatory factor α, is a member of the chemokine family. This factor was found for the first time in human melanoma and is related to the malignant transformation of melanoma (10). Many studies have found that CXCL1 is highly expressed in gastric cancer, liver cancer and other tumor tissues and has a strong correlation with prognosis (11-13). Recent studies have shown that CXCL1 can promote the migration and invasion of breast cancer, promote the epithelial mesenchymal transformation of mouse and human breast cancer cells (14), and stimulate the migration and invasion of Er negative breast cancer cells by activating the ERK/MMP2/9 signal axis (15). However, it is not clear whether Jinrong granule can play a role in this disease by regulating the CXCL1 gene.

In this study, we used three negative breast cancer MDA-MB-231 cells to establish different experimental groups, to explore the effect and mechanism of Jinrong granules and CXCL1 on the biological behavior of the cell migration and invasion, and to provide new evidence for clinical application of Jinrong granules in the treatment and prevention of breast cancer.

MATERIALS AND METHODS

Preparation of Jinrong granule and CXCL-1 protein

Jinrong granule extract, abbreviated as Jinrong extract, is made of the Jinrong granule formula developed by Professor Lin Yifu, a famous breast disease expert in traditional Chinese medicine. The formula is composed of epimedium, Cistanche deserticola, Yujin, (the concentration of the solution is 2 g/ml, and each gram is equivalent to 5 g of crude drug), and after decocting, it is filtered through a sterile membrane and put into a sterile EP (eppendorf) tube for use. The recombinant CXCL-1 protein was purchased from Novoprotein Co., Ltd., China.

MTT (3-(4,5)-dimethylthiahiazo (-z-y1)-3,5-di-phenytetrazoliumromide) assay

MTT assay was used to evaluate cell viability. First, MDA-MB-231 (2×10^3) cells were cultured on 96-well plates and then treated with Jinrong extract (50, 100, 150, 200 and 250 μg/ml) and CXCL-1 (10, 20, 25, 30 and 35 μg/ml) for 24 h. The cells of the control group were treated with 0.1% DMSO (Dimethyl sulfoxide) medium. MDA-MB-231 cells pretreated with CXCL-1 (20 μg/ml) were then treated with Jinrong extract (50, 100, 150 and 200μg/ml) for 24 h. Finally, 10 μl MTT (5 mg/ml) was added and incubated at 37°C for 4 h. After the reaction, the absorbance at 570 nm was detected.

RNA extraction and quantitative real-time polymerase chain reaction (qRT-PCR)

Total RNA was extracted with TRIzol reagent (Invitrogen), and RNA reverse transcription was performed with a QuantScript RT Kit (Tiangen). QRT-PCR was performed using the FastFire qPCR PreMix (SYBR Green) (Tiangen). The standard internal reference was glyceraldehyde-3-phosphate dehydrogenase (GAPDH). The primers of CXCL-1 for qRT-PCR was F: 5‘-TCCTGCATCCCCCATAGTTA-3’, R: 5‘-CTTCAGGAACAGCCACCAGT-3’, and GAPDH- F: 5‘-AGAAGGCTGGGGCTCATTTG-3’R: 5‘-AGGGGCCATCCACAGTCTTC-3’. The primers in this study were obtained from Sangon company. We measured the mRNA content of CXCL-1 in MDA-MB-231 cells and Jinrong extract-treated MDA-MB-231 cells.

Cell culture and Group of experiments

Human breast cancer cell line MDA-MB-231 was purchased from American Type Culture Collection (ATCC). DMEM (dimethyl sulfoxide) medium with 10% fetal bovine serum was used to culture the cells at 37°C (containing 5% CO_2). The experimental cells were divided into a control group, Jinrong extract group, CXCL-1 group and Jinrong extract +CXCL-1 group.

CCK8 assay

A CCK8 assay was used to evaluate the effect of four experimental groups on the proliferation of MDA-MB-231 cells. MDA-MB-231 cells were cultured by the above method, and 3×10^4 cells were inoculated on 96

well plates. After that, CCK8 reagent was added every 0, 12, 24, 36, 48, 60, 72 and 84 h, and cell viability was analyzed by a microplate reader (each value represents the average of three replicates of at least two independent experiments in a representative experiment).

Apoptosis assay

Hoechst staining was used to analyze apoptosis. MDA-MB-231 cells were cultured in 6-well plates, after which the cells were fixed and stained with 10 μg/ml Brustasol for 10 min in the dark. The samples were observed under inverted fluorescence microscope and washed with PBS. There are obvious morphological changes in the nucleus of apoptotic cells, which can be identified by the densification of nucleus or the densification of staining fragments.

Transwell assay

The migration tests were performed using a 24-well Boyden chamber and an uncoated filter with an 8 mm aperture. Cells were collected from the culture dish, washed twice with PBS (phosphate buffer saline), suspended in serum-free medium, inoculated with 3×10^4 cells in the insertion chamber, and then cultured in 0.6 ml DMEM medium containing 10% FBS at 37°C (5% CO_2) for 24 h. Finally, cells were stained with 4,6-diamino-2-phenylindole and counted under a vertical microscope.

Bioinformatics predicted the interaction of CXCL-1 with proteins and Western blot analysis

We predicted the co-acting proteins of CXCL-1 using the STRING online source prediction website (http://string-db.org/cgi/input.pl) and by consulting the literature, and we selected the preselected targets of MMP9, CXCR2, CCL20 and IL10. Then, Western blot was used to detect the content of related proteins in the four experimental groups. The protein samples were extracted by RIPA buffer, denatured and separated by 10% twelve alkyl sulphate polyacrylamide gel electrophoresis. The separated proteins were transferred to polyvinylidene fluoride membrane. These membranes were then incubated overnight with primary antibodies at 4°C. Next, they were incubated with the corresponding secondary antibody at room temperature for 1 h. Finally, the protein concentration calculated with Bic myosin acid was. Antibody binding was detected by enhanced chemiluminescence. Protein antibodies were purchased from Abcam.

Statistical analysis

After data processing, GraphPad Prism 8.3.0 software was used to perform the statistical analysis, and ** indicates a P value < 0.05.

RESULTS

Effects of the Jinrong extract and CXCL-1 on MDA-MB-231 cells and CXCL-1 expression in MDA-MB-231 cells can be inhibited by Jinrong extract

The effect of Jinrong extract on cell survival was detected in MDA-MB-231 cells. In DA-MB-231 cells, compared with the control group, the effect of different concentrations of the Jinrong extract (50, 100, 150, 200 and 250 μg/ml) on the activity of MDA-MB-231 cells decreased significantly as the Jinrong extract concentration increased, and the cell activity stopped declining at 150 μg/ml Jinrong extract (Fig. 1A). Compared with the control group, the activity of MDA-MB-231 cells with different concentrations of CXCL-1 (10, 20, 25, 30 and 35 μg/ml) increased as the CXCL-1 concentration increased, while the activity of CXCL-1 cells with 25 μg/ml did not increase (Fig. 1B). Then, we chose 20 μg/ml CXCL-1 as the pretreatment. CXCL-1 increased the cell activity by 20-30%. Then, different concentrations of the Jinrong extract were applied, and the results showed that when the Jinrong extract concentration was 150 μg/ml, the cell activity no longer changed significantly (Fig. 1C). Thus, we finally determined the 20 cell intervention group: CXCL-1 μg/ml and Jinrong extract 150 μg/ml. The Q-PCR results of the 150 μg/ml Jinrong extract showed that it could reduce the content of CXCL-1 in MDA-MB-231 cells (Fig. 1D).

Jinrong extract can promote proliferation and invasion of MDA-MB-231 cells through CXCL-1

The CCK8 experiment showed that Jinrong extract could inhibit the proliferation of MDA-MB-231 cells while CXCL-1 could promote the proliferation. Compared with the CXCL-1 group, Jinrong extract significantly reduced the cell proliferation (Fig. 2A). The Transwell results showed that CXCL-1 can promote the invasion of breast cancer cells while Jinrong extract intervention can reduce the invasion of breast cancer cells by 50-

60%. Moreover, the intervention of Jinrong extract alone reduced the invasiveness of breast cancer cells by 30-40% compared with the control group (Fig.2B and 2C).

Effect of Jinrong extract and CXCL-1 on the apoptosis of breast cancer cells

The results of the apoptosis experiment showed that CXCL-1 could significantly inhibit the apoptosis of MDA-MB-231 cells while Jinrong extract could reverse the effect of CXCL-1 and increase the apoptosis. Compared with the control group, Jinrong extract alone can significantly improve the apoptosis rate (Fig. 3 A and B).

Jinrong extract affects breast cancer cells through the CXCL-1-CXCR2/CCL20 pathway

The results of the STRING prediction (Fig. 4A) showed that 10 proteins may interact with CXCL-1. Based on the literature review, we finally screened four candidate proteins, MMP9, CXCR2, CCL20 and IL10, for the Western blot assay which showed that the content of CXCR2 and CCL20 increased as CXCL-1 increased. The Jinrong extract inhibited the expression of CXCL-1 as well as the four proteins. MMP9 was positively correlated with tumor proliferation but not with CXCL-1, while IL10 expression did not change significantly among the different groups (Fig. 4B).

DISCUSSION

Cancer is a heterogeneous disease (16). Its occurrence is often related to the activation or inactivation of oncogenes, and the development of new drugs targeting oncogenes is a hot topic of research (17, 18). Regarding breast cancer, there have been reports that BRCA1/2 mutations are an

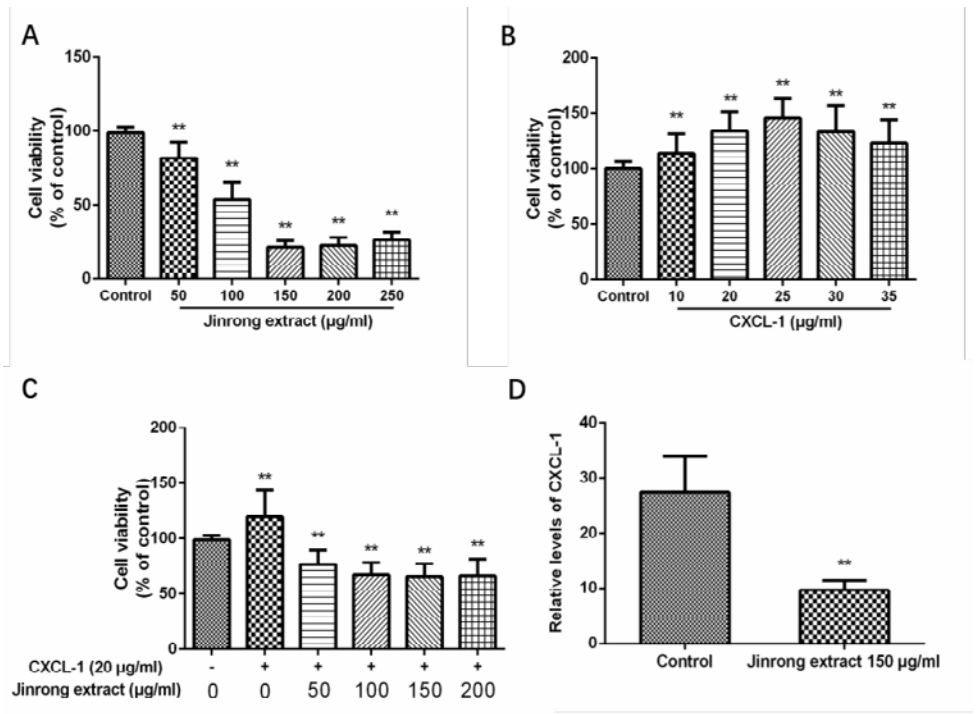


Fig. 1. *MDA-MB -231 cells treated with Jinrong extract (50, 100, 150, 200 and 250 μg/ml) and CXCL-1 (10, 20, 25 and 30 and 35 μg/ml) after determining the cell viability, and the relative levels of CXCL-1 mRNA in MDA-MB-231 cells after treatment with 150 μg/ml Jinrong extract.*

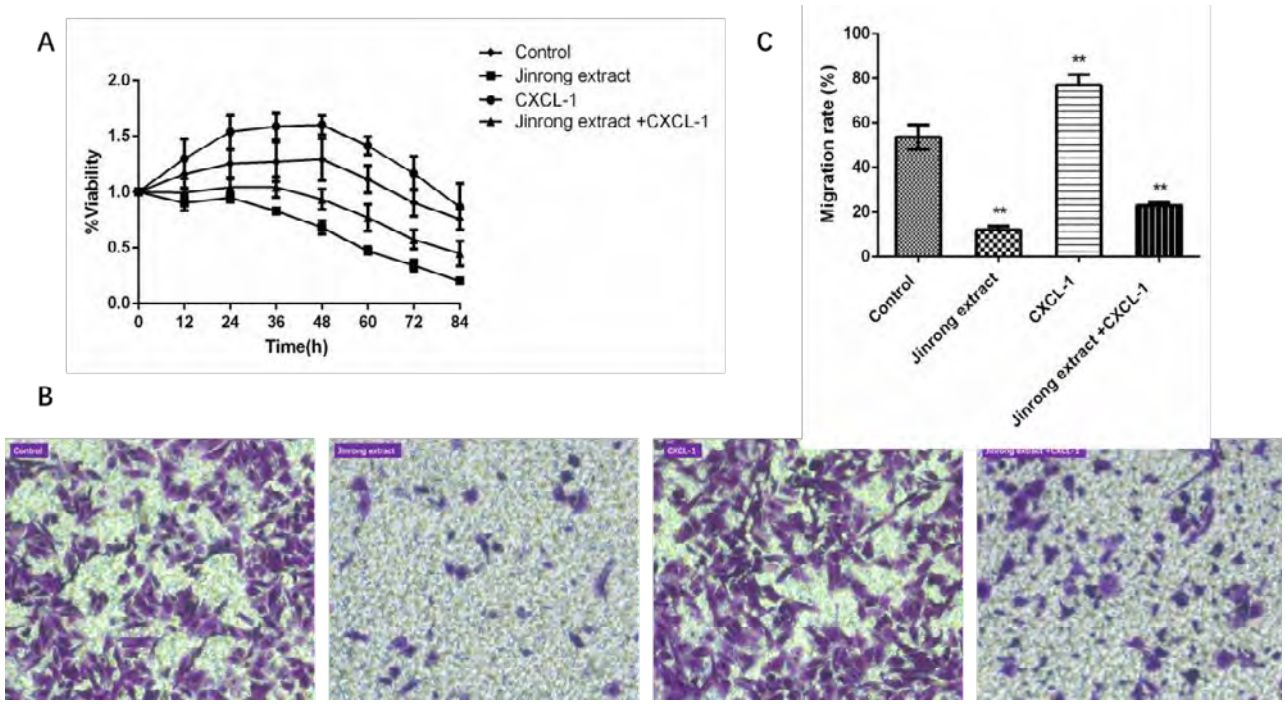


Fig. 2. *Results of cell proliferation assay and Transwell assay in the control group, Jinrong extract group, CXCL-1 group and Jinrong extract +CXCL-1 group.*

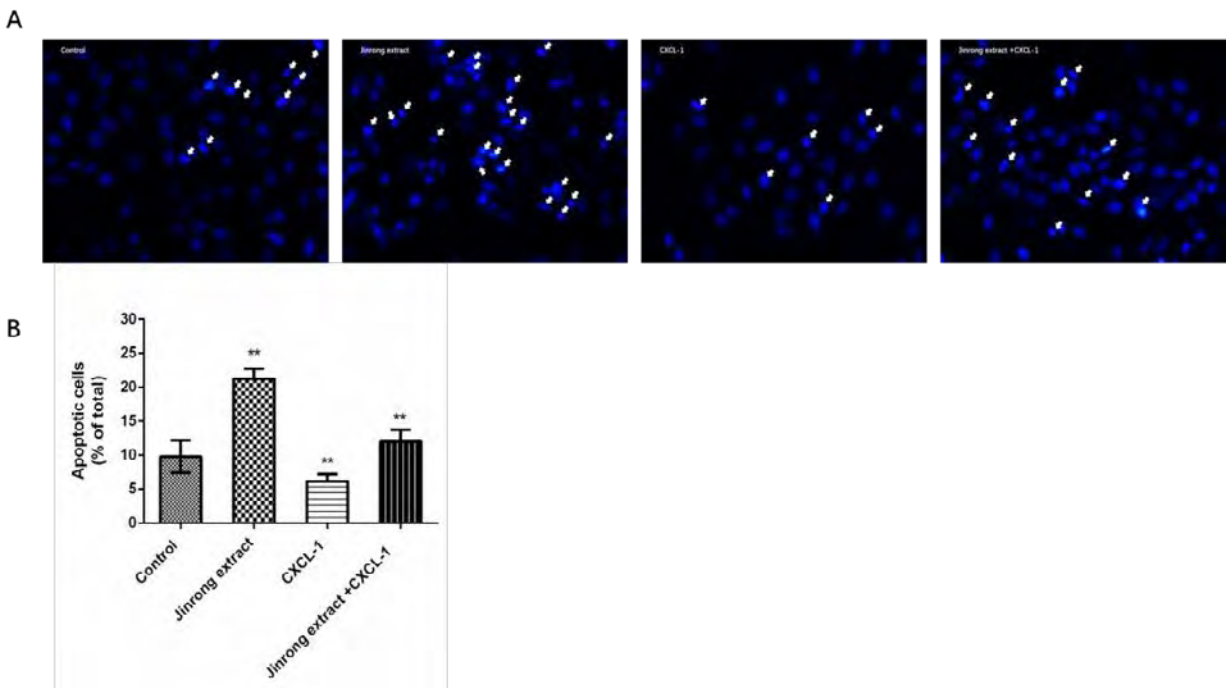


Fig. 3. *Results of the apoptosis assay in the control group, Jinrong extract group, CXCL-1 group and Jinrong extract +CXCL-1 group.*

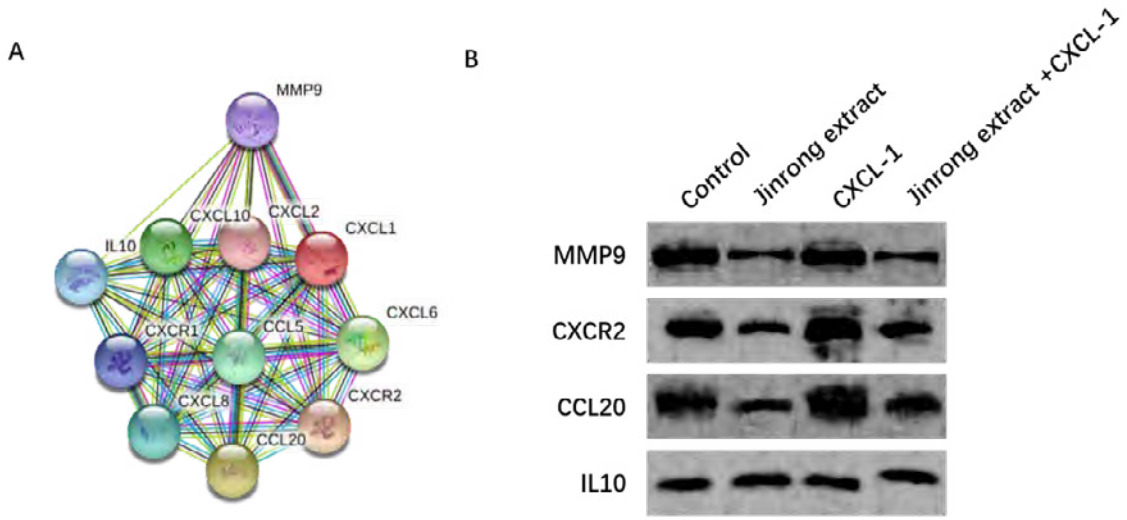


Fig. 4. *Results of STRING analysis of CXCL-1, and the different expression of MMP9, CXCR2, CCL20 and IL10 protein in Control group, Jinrong extract group, CXCL-1 group and Jinrong extract +CXCL-1 group.*

important cause of hereditary degeneration, and corresponding gene screening has become a routine means of reducing the risk of breast malignancy (19, 20). As a long-term treatment, Chinese medicine (TMC) has unique advantages in antitumor treatment, although it is often separated from Western medicine chemotherapy. Increasing studies have begun to seriously explore the more specific mechanism behind the role of TCM, thereby providing increasingly strong evidence for the development of TCM (21, 22). Jinrong granule has been used in the clinical treatment of mammary hyperplasia since the late 1980s, and its clinical application and related research have been performed for more than 30 years, with remarkable effects. Jinrong granules can reduce the density of molybdenum, control breast cancer progression, block or delay, and prevent the occurrence of breast cancer. Previous pharmacological studies have shown that the mechanism of action of Jinrong granules may be related to CXCL-1. This study demonstrates for the first time at the cellular level that Jinrong granules inhibit the proliferation and invasion of breast cancer cells by inhibiting the expression of CXCL-1, thereby promoting apoptosis of cancer cells.

The results of this study indicate that Jinrong granules can act on breast cancer cells through the CXCL-1-CXCR2/CCL20 pathway. CXCL-1 is a member of the chemokine CXC family and was first reported to support melanoma growth (23). Recent studies have also shown that CXCL-1 plays an important role in a variety of malignancies. CXCL-1 overexpression is also significantly associated with gastric cancer progression and low survival rates (24, 25). CXCL-1 deletion inhibits the migration and invasion of gastric cancer cells. However, CXC receptor 2 (CXC receptor 2, CXCR2) is a multiple chemokine receptor and closely related to the body's inflammatory process (26, 27). In recent years, with the further development of inflammatory immunity in tumor research, it has been discovered that CXCR2 ligands interact to form a variety of signal axes, which are common in the establishment of malignant tumors, such as pancreatic cancer, breast cancer, and colorectal cancer, and the regulation of the tumor microenvironment (28). CCL20 is an important member of the chemokine family and belongs to the CC subfamily, and its receptor is CCR6 (29). Cytokines ,such as tumor necrosis factor α (TNFα), interleukin 1β (IL-1β), interleukin 17, CD40 ligand, and interferon γ (IFNγ), can induce the expression of CCL20, promote the growth of malignant tumors and promote tumors cells; thus, they play an important role in invasion and metastasis (30). The results of

this study demonstrate for the first time that Jinrong granules inhibit the expression of these precancerous factors by inhibiting CXCL-1, thereby inhibiting the growth of breast cancer cells.

In conclusion, Jinrong granule can inhibit the proliferation and invasion of breast cancer cells through the CXCL-1-CXCR2/CCL20 pathway and promote apoptosis of cancer cells. These findings provide a theoretical basis for the extensive clinical application of Jinrong granule.

ACKNOWLEDGEMENTS

This work was supported by Lin Yi's National Heritage Research Laboratory Project of Famous Traditional Chinese Medicine; Research on Experience Inheritance and Innovation of Famous and Old TCM Based on the Thought of "Combining Taoism with Art" and Multi-integration Method.

REFERENCES

1. Veiga GLD, Silva RDMD, Pereira EC, et al. The role of Survivin as a biomarker and potential prognostic factor for breast cancer. Rev Assoc Med Bras (1992) 2019; 65(6):893-901.
2. Veronesi U, Boyle P, Goldhirsch A, Orecchia R, Viale G. Breast cancer. Lancet 2005; 365(9472):1727-41.
3. Woolston C. Breast cancer. Nature 2015; 527(7578):S101.
4. Xu C, Zhao H, Chen H, Yao Q. CXCR4 in breast cancer: oncogenic role and therapeutic targeting. Drug Des Devel Ther 2015; 9:4953-64.
5. Huang B, Huang M, Li Q. Cancer-associated fibroblasts promote angiogenesis of hepatocellular carcinoma by VEGF-Mediated EZH2/VASH1 Pathway. Technol Cancer Res Treat 2019; 18:1533033819879905.
6. Ke H, Shen W, Hu A, Ou Q, Lu S. Distribution of NRG1 Gene Fusions in a Large Population of Chinese Patients with NSCLC. J Thorac Oncol 2019; 14(12):e263-e266.
7. Lin Y, Li B, Yang X, et al. Fibroblastic FAP promotes intrahepatic cholangiocarcinoma growth via MDSCs recruitment. Neoplasia 2019; 21(12):1133-42.
8. Wang Y, Hui J, Li R, Fu Q, Yang P, Xiao Y, Hui J. GBX2, as a tumor promoter in lung adenocarcinoma, enhances cells viability, invasion and migration by regulating the AKT/ERK signaling pathway. J Gene Med 2019:e3147.
9. Wang N, Zheng Y, Gu J, et al. Network-pharmacology-based validation of TAMS/CXCL-1 as key mediator of XIAOPI formula preventing breast cancer development and metastasis. Sci Rep 2017; 7(1):14513.
10. Marques P, Barry S, Carlsen E, et al. Chemokines modulate the tumour microenvironment in pituitary neuroendocrine tumours. Acta Neuropathol Commun 2019; 7(1):172.
11. Wei ZW, Xia GK, Wu Y, et al. CXCL1 promotes tumor growth through VEGF pathway activation and is associated with inferior survival in gastric cancer. Cancer Lett 2015; 359(2):335-43.
12. Xiang Z, Jiang DP, Xia GG, et al. CXCL1 expression is correlated with Snail expression and affects the prognosis of patients with gastric cancer. Oncol Lett 2015; 10(4):2458-64.
13. Liu XX, Yang L, Shao LX, et al. Endothelial Cdk5 deficit leads to the development of spontaneous epilepsy through CXCL1/CXCR2-mediated reactive astrogliosis. J Exp Med 2019. pii: jem.20180992.
14. Wang N, Liu W, Zheng Y, et al. CXCL1 derived from tumor-associated macrophages promotes breast cancer metastasis via activating NF-κB/SOX4 signaling. Cell Death Dis 2018; 9(9):880.
15. Yang C, Yu H, Chen R, et al. CXCL1 stimulates migration and invasion in ER-negative breast cancer cells via activation of the ERK/MMP2/9 signaling axis. Int J Oncol 2019; 55(3):684-96.
16. Anastasiadi Z, Lianos GD, Ignatiadou E, Harissis HV, Mitsis M. Breast cancer in young women: an overview. Updates Surg 2017; 69(3):313-17.
17. Crombie JL, Armand P. Diffuse large B-cell lymphoma and high-grade B-cell lymphoma: genetic classification and its implications for prognosis and treatment. Surg Oncol Clin N Am 2020; 29(1):115-25.
18. Mihaylov I, Kańduła M, Krachunov M, Vassilev D. A novel framework for horizontal and vertical data integration in cancer studies with application to survival time prediction models. Biol Direct 2019; 14(1):22.
19. Petrovic N, Davidovic R, Bajic V, Obradovic M,

Isenovic RE. MicroRNA in breast cancer: The association with BRCA1/2. Cancer Biomark 2017; 19(2):119-28.

20. Kuligina ES, Sokolenko AP, Bizin IV, et al. Exome sequencing study of Russian breast cancer patients suggests a predisposing role for USP39. Breast Cancer Res Treat 2019.
21. Li A, Zhang W, Zhang L, Liu Y, Li K, Du G, Qin X. Elucidating the time-dependent changes in the urinary metabolome under doxorubicin-induced nephrotoxicity. Toxicol Lett 2019. pii: S0378-4274(19)30377-7.
22. McPherson L, Cochrane S, Zhu X. Current Usage of traditional Chinese medicine in the management of breast cancer: a practitioner's perspective. Integr Cancer Ther 2016; 15(3):335-42.
23. Wang D, Yang W, Du J, et al. MGSA/GRO-mediated melanocyte transformation involves induction of Ras expression. Oncogene 2000; 19(40):4647-59.
24. Justino PF, Melo LF, Nogueira AF, et al. Regulatory role of Lactobacillus acidophilus on inflammation and gastric dysmotility in intestinal mucositis induced by 5-fluorouracil in mice. Cancer Chemother Pharmacol 2015; 75(3):559-67.
25. Yan F, Fu Q. PLCε1: A potential target of RNA interference therapy for gastric cancer. Biochem Biophys Res Commun 2014; 448(4):409-13.
26. Hareendran S, Yang X, Lou H, Xiao L, Loh YP. Carboxypeptidase E-ΔN promotes proliferation and invasion of pancreatic cancer cells via upregulation of CXCR2 gene expression. Int J Mol Sci 2019; 20(22). pii: E5725.
27. Wu L, Awaji M, Saxena S, Varney ML, Sharma B, Singh RK. IL-17-CXCR2 axis facilitates breast cancer progression by up-regulating neutrophil recruitment. Am J Pathol 2019. pii: S0002-9440(19)30768-0.
28. Xiang Z, Zhou ZJ, Xia GK, et al. A positive crosstalk between CXCR4 and CXCR2 promotes gastric cancer metastasis. Oncogene 2017; 36(36):5122-33.
29. Muscella A, Vetrugno C, Marsigliante S. CCL20 promotes migration and invasiveness of human cancerous breast epithelial cells in primary culture. Mol Carcinog 2017; 56(11):2461-73.
30. Liu B, Jia Y, Ma J, et al. Tumor-associated macrophage-derived CCL20 enhances the growth and metastasis of pancreatic cancer. Acta Biochim Biophys Sin (Shanghai) 2016; 48(12):1067-74.

CHLAMYDIA TRACHOMATIS ELICITS TLR3 EXPRESSION BUT DISRUPTS THE INFLAMMATORY SIGNALING DOWN-MODULATING NFκB AND IRF3 TRANSCRIPTION FACTORS IN HUMAN SERTOLI CELLS

M. DI PIETRO[1], S. FILARDO[1], V. ALFANO[2], M. PELLONI[3], E. SPLENDIANI[2], A. PO[2], D. PAOLI[3], E. FERRETTI[4] and R. SESSA[1]

[1]Department of Public Health and Infectious Diseases, Section of Microbiology, University of Rome "Sapienza", Rome, Italy; [2]Department of Molecular Medicine, University of Rome "Sapienza", Rome, Italy; [3]Laboratory of Seminology – Sperm Bank 'Loredana Gandini' Department of Experimental Medicine, University of Rome "Sapienza", Rome, Italy; [4]Department of Experimental Medicine, University of Rome "Sapienza", Rome, Italy

Received February 7, 2020 – Accepted April 21, 2020

***Chlamydia trachomatis*, the leading cause of bacterial sexually transmitted diseases worldwide, can disseminate and localize to the upper genital tract impairing reproductive function. Specifically, ascending *C. trachomatis* genital infection has been demonstrated to cause epididymitis or epididymo-orchitis, well-known risk factors for male infertility. *C. trachomatis* possesses the ability to infect primary human Sertoli cells, key elements for the spermatogenetic process and the immune protection of germ cells. Therefore, herein, we investigated the innate immune response in Sertoli cells following *C. trachomatis* infection, as well as its indirect effects on human spermatozoa. Specifically, we evaluated *C. trachomatis*-mediated induction of Toll-like Receptors (TLR) 2, 3 and 4 as well as of downstream intracellular signaling molecules (NFκB and IRF3) and the levels of the related inflammatory mediators (IL-1α, IL-6, IFN-α, IFN-β and IFN-γ), in an *in vitro* infection model of primary human Sertoli cells. The main result of our study shows that *C. trachomatis* induced TLR3-mediated recognition in human Sertoli cells, accompanied by the down-modulation of NFκB and IRF3-dependent signaling pathways followed by no production of pro-inflammatory cytokines. In conclusion, our findings suggest that *C. trachomatis* can disrupt the innate immune response in Sertoli cells and evade intracellular killing, potentially giving rise to a long-term infection that may exert negative effects on the male reproductive system.**

Male infertility and sub-fertility are caused by several defects that involve functional and structural alterations of the testis (1-2). Sertoli cells form the epithelium of the seminiferous tubule in the human testis and are key elements for spermatogenesis, a complex process that is finely regulated by intimate and cyclical interactions between these cells and developing germ cells (3). Sertoli cells contribute to establish a suitable testicular micro-environment for germ cell development and sperm production, building the blood-testis barrier (BTB) and creating an immune privileged environment (4,5). In fact, Sertoli cells mediate the testis ability to initiate an innate immune response against infectious agents expressing pattern recognition receptors (PRRs) and, particularly, a subset of the toll-like receptor

Key words: Chlamydia trachomatis; Sertoli cells; Toll-like receptors; inflammatory cytokines; human spermatozoa

Corresponding Author:
Dr Simone Filardo,
Department of Public Health and Infectious Diseases,
University of Rome "Sapienza",
P. le Aldo Moro, 5, 00185, Rome, Italy
Tel.: +39 0649914102
e-mail: simone.filardo@uniroma1.it

0393-974X (2020)
Copyright © by BIOLIFE, s.a.s.
This publication and/or article is for individual use only and may not be further reproduced without written permission from the copyright holder.
Unauthorized reproduction may result in financial and other penalties
DISCLOSURE: ALL AUTHORS REPORT NO CONFLICTS OF INTEREST RELEVANT TO THIS ARTICLE.

(TLRs) family, such as TLR-2, TLR-3 and TLR-4 (6). In particular, uropathogenic *Escherichia coli* or their products have been demonstrated to activate TLR-2 and TLR-4 in Sertoli cells, leading to the recruitment of immune competent cells (7). TLRs are major activators of innate immunity and inflammation and detect specific motifs or pathogen-associated molecular patterns (PAMPs) (8). TLR-2 and TLR-4 are typically located on cell surface and are known to detect bacterial lipopeptides and lipopolysaccharide, whereas TLR-3 is expressed on the membrane of cytoplasmic organelles, particularly endosomes, and detects viral nucleic acids (6). After the recognition of PAMPs, TLR2 and TLR4 activate the nuclear factor kappa B (NFκB) via the recruitment of myeloid differentiation protein 88 (MyD88), leading to the synthesis of pro-inflammatory cytokines, including interleukin (IL)-1α and IL-6. TLR-3 initiates the TIR-domain-containing adaptor protein-inducing IFNβ (TRIF), that activates both transcription factors IRF-3 and NFκB, inducing the expression of interferon (IFN)-α, IFN-β and IFN-γ (6).

However, the inflammatory response, classically required for microbial clearance, is also responsible for tissue damage (9). In fact, following the infection of the testis, cytokine levels increase considerably, altering Sertoli cell activity with disruptive effects on the development of germ cells and, consequently, on male fertility (10). Many urogenital pathogens are able to infect the seminiferous epithelium and, in particular, sexually transmitted agents, such as *Chlamydia trachomatis*, were recently acknowledged as being clinically important in male infertility (11). *C. trachomatis*, the leading cause of bacterial sexually transmitted diseases (STDs) worldwide (12), is known to disseminate and localize to the upper genital tract impairing the reproductive function (13, 14), despite the numerous protective factors (15-17).

In men, *C. trachomatis* accounts for up to 42% of all cases of non-gonococcal urethritis, although its real prevalence and incidence are unknown (18). This is because up to 50% of *C. trachomatis* infections are asymptomatic and, hence, undiagnosed and untreated. This may lead to severe reproductive sequelae; specifically, ascending *C. trachomatis* genital infections have been demonstrated to cause epididymitis or epididymo-orchitis, well known risk factors for male infertility (12, 19). Therefore, *C. trachomatis* has recently been involved in its etiopathogenesis. Moreover, a recent study has suggested that *C. trachomatis* causes male infertility via the infection of the seminiferous epithelium, as evidenced by altered motility and morphology of spermatozoa in a murine model of *C. muridarum* infection (20).

More recently, we reported that *C. trachomatis* serovar D is able to infect primary human Sertoli cells (21) and, herein, we investigated for the first time the immune response elicited in these cells following *C. trachomatis* infection. Specifically, we evaluated *C. trachomatis*-mediated activation of TLR2, TLR3 and TLR4 as well as of downstream intracellular signaling pathways and the levels of inflammatory mediators. Lastly, we assessed the *in vitro* effects of *C. trachomatis* infection of Sertoli cells on human spermatozoa.

MATERIALS AND METHODS

Cell culture and culture conditions

The primary human Sertoli cell line, purchased from Lonza, USA (product code MM-HSE-2305, lot number 150909091), was harvested on 8th September 2009. Human Sertoli cells were isolated from a healthy donor and checked for purity by assessing the positivity to GATA4 and SOX9 and the negativity to endotoxin, mycoplasma, HIV, HCV and HBV contamination. These cells were provided by Lonza at the 3rd passage after isolation, and all experiments were performed with the same cell line at the 2nd passage after thawing. Sertoli cells were cultured in Dulbecco's Modified Eagle Medium/Ham's Nutrient Mixture F12 (1:1), with L-glutamine and HEPES (DMEM/F12, Gibco™, USA), supplemented with 10% (v/v) fetal calf serum (FCS), 100 µg/mL streptomycin sulphate and 100 Units/mL potassium penicillin at 37°C in humidified atmosphere with 5% CO2.

McCoy cell line (ATCC® CRL-1696) was cultured in Dulbecco's Modified Eagle Medium (DMEM, Gibco™, USA) supplemented with 10% (v/v) FCS, at 37°C in humidified atmosphere with 5% CO_2.

Propagation and titration of C. trachomatis

C. trachomatis strain D/UW-3Cx (ATCC VR-885)

was propagated in McCoy cells as previously described (22). Briefly, cells were infected with *C. trachomatis* by centrifugation at 754g for 30 min at room temperature and, then, incubated in DMEM supplemented with 10% FCS and 1μg/mL cycloheximide for 48h at 37°C in humidified atmosphere with 5% CO_2. McCoy cells were harvested by scraping and the resulting Chlamydia suspension was stored at -80°C in 4X Sucrose Phosphate (4SP) buffer (0.4M sucrose and 16mM Na_2HPO_4 at pH 7.1).

The infectious titer (Inclusion Forming Units (IFU) per mL) was determined, as previously described (23) by infecting confluent McCoy cell monolayers grown in 24 well trays with 10-fold dilutions of *C. trachomatis* suspension. Briefly, after 36 h post-infection, infected cells were fixed in 96% methanol for 10 min at -20°C and stained with fluorescein isothiocyanate-conjugated monoclonal antibody anti-*C. trachomatis* LPS (Imagen Chlamydia kit, Oxoid, UK). Titers were calculated by counting all green-stained inclusions by using a Leica DM6000B fluorescence microscope (40X magnification).

Infection of primary human Sertoli cells with C. trachomatis

Sertoli cell monolayers, grown on glass coverslips on 24-well cell culture plates, were infected with *C. trachomatis* at a MOI of 5.0 by centrifugation at 754g for 30 min. After the removal of chlamydial inoculum, infected cells were washed with phosphate buffered saline (PBS) and incubated with DMEM/F12 (Corning, USA) supplemented with 10% FCS and no cycloheximide at 37°C in humidified atmosphere with 5% CO_2. Thirty-six hours post-infection, the presence of chlamydial inclusions was visualized by confocal microscopy by utilizing a primary mouse monoclonal antibody against species-specific MOMP (Mab6ciii, The Chlamydia Biobank, UK, Cat. No. #CT602) (1:1000 dilution) combined with an anti-mouse-Alexa Fluor™ 488 conjugate secondary antibody (Invitrogen™, USA, Cat. No. A11001) (1:2000 dilution), as previously described (21).

TLRs, NFκB, IRF3 and cytokine detection

Sertoli cell monolayers, grown on 6-well cell culture plates, were infected with *C. trachomatis* at a MOI of 5.0 as above described. Cell monolayers were investigated for the presence of TLR-2, TLR-3, TLR-4, NFκB and IRF3 by Western blot at different time points. Supernatants were assayed for the presence of IL-1α, IL-6, IFN-γ, IFN-α and IFN-β by ELISA.

Western blot analysis

At 5, 24 and 36 hours post-infection, Sertoli cell monolayers were lysed in RIPA lysis buffer [50mM Tris-HCl at pH 7.6, 0.5% sodium deoxycholate, 140 mM sodium chloride, 1% NP-40, 5 mM Na_2EDTA, 100 mM sodium fluoride, 2 mM sodium pyrophosphate, supplemented with protease inhibitor mix (GE Healthcare, USA)] by incubation on ice for 15 min. Lysates were then separated on 8% polyacrylamide gel (PAGE) and immunoblotted using standard procedures. Membranes were blocked for 1 h at room temperature in 5% non-fat dry milk in PBS-T and incubated overnight at 4°C with anti-TLR2 (clone TL2.1, cat. #MAB0067), TLR3 (clone 40C1285.6, cat. #MAB0088), TLR4 (clone 1H7, cat. # H00007099-M03), NFκB (clone 13A2F, cat. #MAB0828) and IRF3 (clone 3F10, cat. #MAB1103) mouse monoclonal primary antibodies (Abnova, USA). HRP-conjugated anti-mouse secondary antibody (Santa Cruz Biotechnology, USA) was applied to stained membranes and visualized by enhanced chemiluminescence (ECL, Amsterdam).

For the evaluation of protein levels, values are expressed as band integrals normalized to the control and housekeeping gene bands.

ELISA

At 36 hours post-infection, Sertoli cell culture supernatants were collected and stored at -80°C for further downstream analysis. Supernatants were then analyzed for IL-1α, IL-6, and IFN-γ using the specific BioVendor ELISA kit (BioVendor, Czech Republic), and for IFN-α and IFN-β using the specific MyBioSource ELISA (MyBioSource, Inc., USA), according to the manufacturer's instructions. The detection limit for each cytokine is as follows: IL-1α, IL-6 and IFN-γ (1.6 pg/mL), IFN-α (15.25 pg/mL) and IFN-β (31.25 pg/mL).

In vitro exposure of human spermatozoa to C. trachomatis infected Sertoli cell supernatants

Semen samples were self-collected after 3-5 days of abstinence by 3 men attending the Laboratory of Seminology (Sperm Bank "Loredana Gandini", Department of Experimental Medicine, University of Rome "Sapienza"), for semen analysis. Study participants

had not been medically or surgically treated in the 3 months prior to the study and did not have any conditions or reproductive pathology that could interfere with the semen parameters. Written informed consent was obtained from all study participants. This study design and protocol was approved by the Umberto I University Hospital ethical committee (protocol n. 182/11) and conducted according to the principles expressed in the Declaration of Helsinki.

All samples were normozoospermic according to the World Health Organization guidelines (24). Aliquots of semen samples were added to equal volumes of *C. trachomatis* infected or uninfected human Sertoli cell culture supernatants, [previously filtered through 0.22 µm filters (Millex-GP, Millipore, USA) in order to remove all chlamydial EBs], or DMEM/F12 supplemented with FCS 10% as a control, and incubated for 1, 2 and 3 h at 37°C. Then, sperm motility and viability were investigated. Briefly, sperm motility was investigated by an automated computer analysis (CASA System; Hamilton Thorne), that included incubation at 37°C, and sperm vitality was carried out by staining with eosin Y 0.5% in saline solution (25).

At the same time, the swim-up procedure was performed to select motile spermatozoa (26). Five hundred microliters each of DMEM/F12 +10% FCS, *C. trachomatis* infected or uninfected Sertoli cell culture supernatants were layered gently onto 0.5 ml of the semen sample. The spermatozoa were allowed to migrate for 30 min at 37°C. After migration the top layer was collected, incubated at 37°C and analyzed for sperm concentration, motility, and viability at 1, 2 and 3 h.

Statistical analysis

All values are expressed as mean ± standard deviation (SD) of at least 3 replicates from two independent experiments. Comparisons of means were performed by using a two-tailed Student *t*-test for independent samples. The quantification of protein levels was performed in ImageJ software (version 1.52j) and all statistical calculations and graphs were produced in Excel (Microsoft, USA). A value of $P \leq 0.05$ was considered statistically significant.

RESULTS

C. trachomatis induces TLR-3 expression in human Sertoli cells

Initially, we demonstrated that *C. trachomatis* infection of primary human Sertoli cells resulted in the development of chlamydial inclusions, as shown in Fig. 1. Then, we investigated whether *C. trachomatis* serovar D induced the expression of TLR2 and TLR4, since several studies reported that TLR2 and TLR4 were critical receptors involved in the immune recognition of *C. trachomatis* (27,28). Neither TLR2 or TLR4 were expressed in human Sertoli cells following *C. trachomatis* infection (Fig. 2 A and B). Then, we evaluated whether TLR3 was stimulated during *C. trachomatis* infection of primary human Sertoli cells, since more recent studies reported that *Chlamydia* elicits TLR3 expression (29-31). A significant increase in the protein levels of TLR-3 was observed in primary human Sertoli cells following *C. trachomatis* infection when compared to uninfected cells (Fig. 2 C and D, $P<0.05$).

C. trachomatis fails to stably induce TLR-3 dependent signaling pathways

Since we observed a significant induction of TLR3 following *C. trachomatis* infection of primary human Sertoli cells, we investigated whether *C. trachomatis* promoted the downstream expression of NFκB and/or IRF3 transcription factors, the next steps in the TLR3-mediated signaling pathway (6).

Primary human Sertoli cells were infected with *C. trachomatis* and the expression of NFκB and IRF3 was analyzed at different time points post-infection (5, 24 and 36 h). As shown in Fig. 3, *C. trachomatis* modulated the expression of both NFκB and IRF3 in a time-dependent fashion. The NF-κB was only detected at 5 hours post-infection ($P<0.05$) with a dramatic down-modulation of protein levels at later time points.

IRF3 protein level was at its highest at 24 hours post-infection ($P<0.05$) but decreased at the last point, 36 hours post-infection (Fig. 3 A and B) ($P<0.05$). Interestingly, human Sertoli cells constitutively expressed NFκB and IRF3 proteins and maintained their expression in culture.

Lastly, since it is known that IRF3 and NFκB induce the expression of proinflammatory cytokines, such as interferon (IFN)-α, IFN-β, IFN-γ, interleukin (IL)-1α and IL-6 (6), their levels were evaluated, by ELISA, in human Sertoli cells infected with *C. trachomatis*. However, *C. trachomatis* did not elicit the secretion of

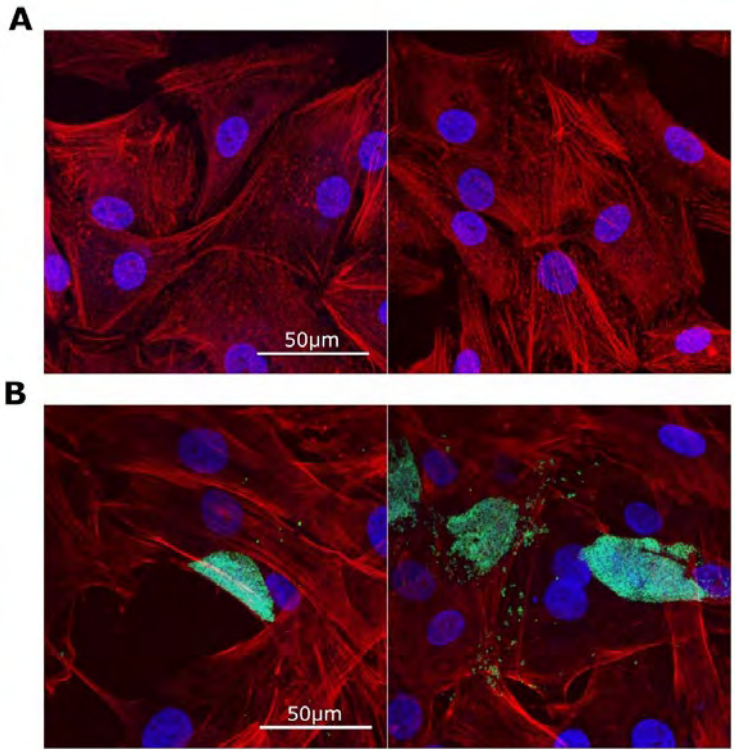


Fig. 1. *Confocal micrographs of C. trachomatis uninfected (**A**) and infected (**B**) primary human Sertoli cells. Cell monolayers, infected by C. trachomatis were stained after 36 hpi as reported in Materials and Methods (all experiments were performed in duplicate, magnification 100X).*

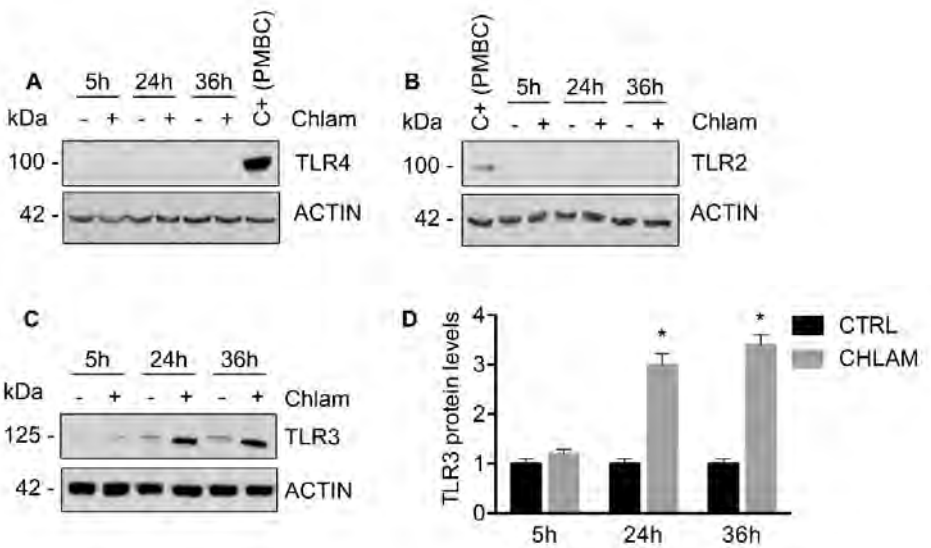


Fig. 2. *C. trachomatis activates TLR-3 in primary human Sertoli cells. Representative western blot of endogenous TLR4 (A) and TLR2 (B) levels in primary human Sertoli cells after C. trachomatis infection at indicated time points. Peripheral blood mononuclear cells (PBMC) were used as positive control and actin was used as loading control. Representative western blot (C) and densitometric analysis (D) of endogenous TLR3 levels in primary human Sertoli cells after C. trachomatis infection at indicated time points. Actin was used as loading control. The bars in (D) represent the mean values and the standard errors of the means of at least 3 replicates from two independent experiments for each group. CHLAM, C. trachomatis; CTRL, uninfected control. *P < 0.05.*

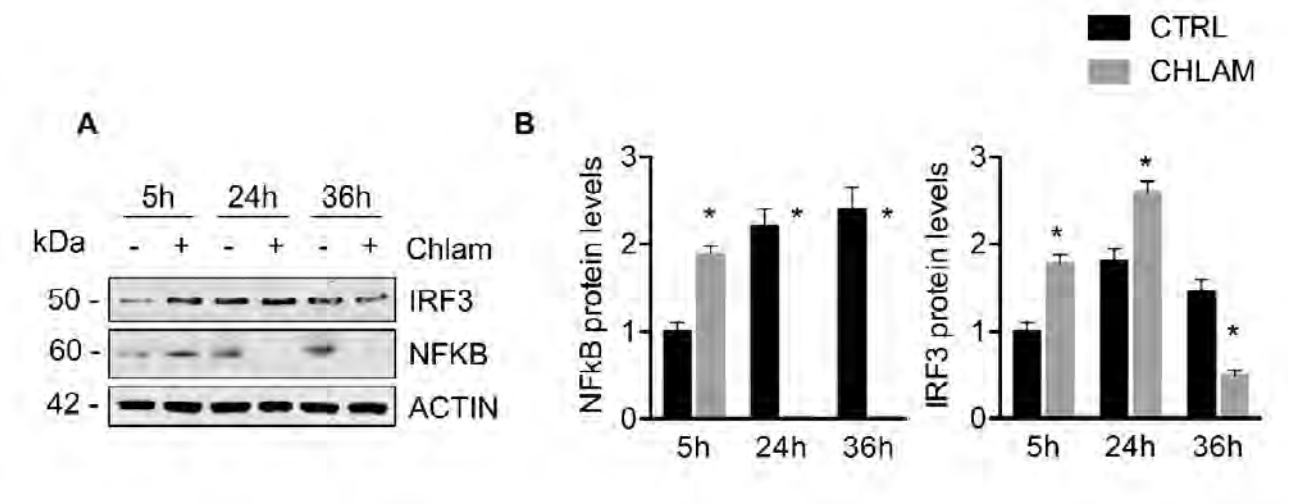
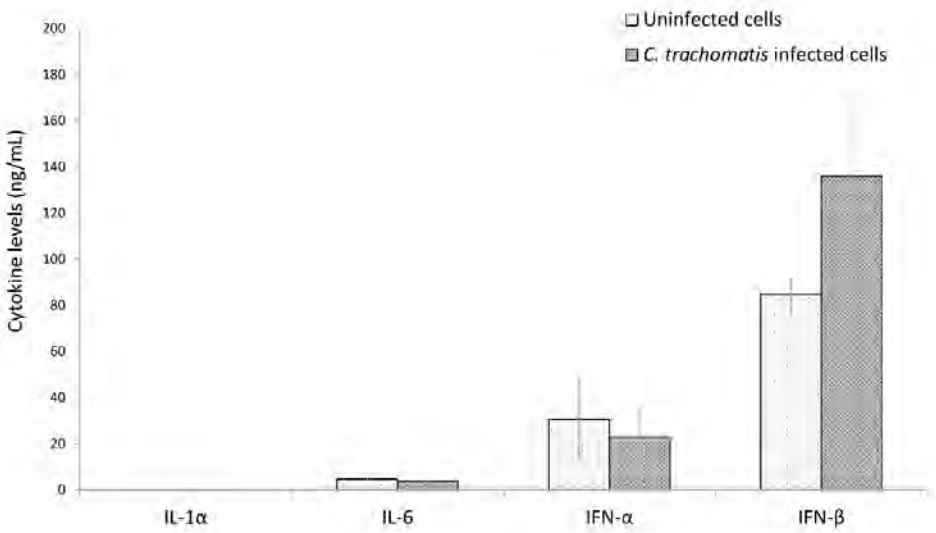


Fig. 3. *C. trachomatis disrupts TLR3-dependent signalling pathways. Representative western blot (**A**) and densitometric analysis (**B**) of endogenous NFκB and IRF3 levels in primary human Sertoli cells after C. trachomatis infection at indicated time points. Actin was used as loading control. The bars represent the mean values and the standard errors of the means of at least 3 replicates from two independent experiments for each group. CHLAM, C. trachomatis; CTRL, uninfected control. *P < 0.05.*



	IL-1α (ng/mL)	IL-6 (ng/mL)	IFN-α (ng/mL)	IFN-β (ng/mL)	IFN-γ (ng/mL)
Uninfected cells	0.0049±0.001	4.6±0.5	30.6±18.5	84.8±8.2	ND
***C. trachomatis* infected cells**	0.0038±0.0002	3.6±0.8	22.9±13	136±38.8	ND

Values are expressed as mean ± Standard Deviation; ND, not detected

Fig. 4. *IL-1α, IL-6, IFN-α, IFN-β and IFN-γ levels in C. trachomatis infected and uninfected primary human Sertoli cells. All values are expressed as mean ± standard deviation (SD) of at least 3 replicates from two independent experiments. ND, not determined.*

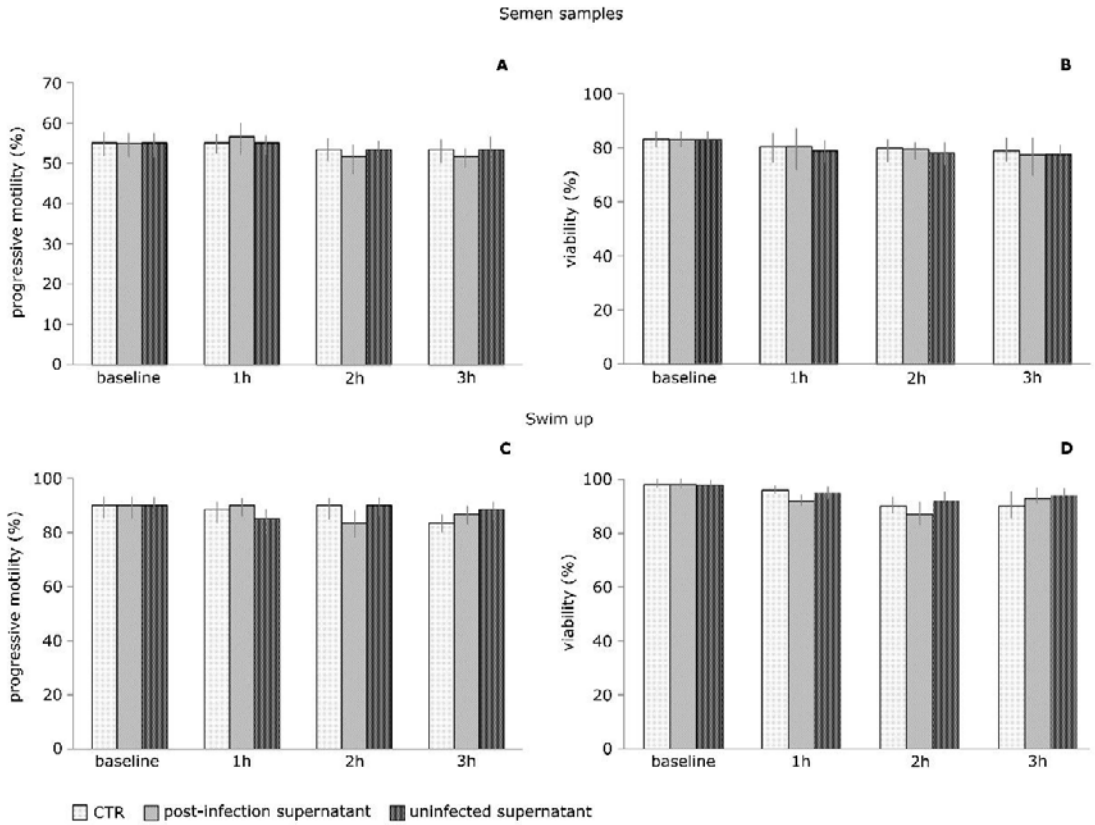


Fig. 5. *Effects of C. trachomatis infection of Sertoli cells on semen parameters. Percentage of progressive motility and viability of semen samples (**A, B**) and swim up preparations (**C, D**) at baseline and at 1, 2 and 3-hour post-incubation with C. trachomatis infected or uninfected primary human Sertoli cell supernatants or DMEM/F12 supplemented with FCS 10% (CTR). The bars represent the mean values and the standard errors of the means of at least 3 replicates from two independent experiments for each group.*

IFN-α, IFN-β, IFN-γ, IL-1α and IL-6 in human Sertoli cells in a significative way, as shown in Fig. 4.

C. trachomatis does not affect semen parameters

The effects of *C. trachomatis* infection of human Sertoli cells on sperm viability and progressive motility were assayed by challenging Chlamydia-infected Sertoli cell supernatant with human spermatozoa from three normozoospermic semen samples at different time-points (0, 1, 2 and 3 h) (Fig. 5 A and B). The swim-up technique was used to investigate its effects on the ability of motile spermatozoa to migrate against gravity in the media (Fig. 5 C and D).

C. trachomatis infection of human Sertoli cells did not affect the viability or the progressive motility of spermatozoa from either the semen samples or the motile spermatozoa selected by swim-up ($P > 0.05$). It also had no effect on their migratory ability, since the number of migrated spermatozoa exposed to either *C. trachomatis* infected or uninfected human Sertoli cell culture supernatants remained unvaried (data not shown).

DISCUSSION

Sertoli cells are responsible for building the BTB and creating an immune-privileged niche

that protects developing germ cells from the host immune system as well as from infectious threats. Indeed, Sertoli cells are well known to play a key role in the innate immune defenses of the testis via the TLR-mediated recognition of pathogens (6).

The main results of our study are: (*i*) the induction of TLR3 production by *C. trachomatis* infection of Sertoli cells; (*ii*) no expression of TLR2 and TLR4 in human Sertoli cells following *C. trachomatis* infection; (*iii*) the down-modulation of NFκB and IRF-3 transcription factors in infected human Sertoli cells, and lack of an increased synthesis of proinflammatory cytokines, such as IFN-α, IFN-β, IFN-γ, IL-1α and IL-6; (*iv*) no harmful effects on human spermatozoa following *C. trachomatis* infection of Sertoli cells.

Overall, this peculiar innate immune response by human Sertoli cells in the male genital tract after the exposure to *C. trachomatis* is surprising, since we expected to observe increased expression of TLR2 and TLR4, as evidenced in epithelial cells from the female genital tract (27-31). In our study, instead, human Sertoli cells detected *C. trachomatis* through TLR3-mediated pathways, classically observed for viral infections. This shows interesting differences with the Chlamydia-mediated response in the female genital tract, where both TLR2 and TLR3 have been shown to be important mediators of the innate immunity against *C. trachomatis*, although with different pathophysiological roles. TLR2 was involved in the early production of inflammatory mediators (i.e. IL-1α, IL-6) and the development of chronic inflammatory pathology (27-31), whereas the activation of TLR3 resulted in the control of bacterial replication via IFNβ, as well as in the prevention of severe reproductive sequelae (29,31).

In our study, *C. trachomatis*, despite triggering the expression of TLR3 in human Sertoli cells, hindered the activation of the downstream signaling pathways, as evidenced by a short-term expression of the transcription factor NFκB, followed by its suppression, and a decreased expression of IRF3. As a result, IFN-α, IFN-β, IFN-γ, IL-1α and IL-6 were not produced in infected human Sertoli cells, demonstrating the absence of a specific innate immune response to *C. trachomatis*. This suggests the compelling hypothesis that *C. trachomatis* could create a suitable micro-environment for its survival in these cells, resulting, most likely, in the persistence of the infection. In fact, *C. trachomatis* has been shown to persist for a long time in epithelial cells by generating non-infectious forms that are usually demonstrated by the reduced production of chlamydial infectious progeny (32). In this regard, in a previous study, we observed a decrease in *C. trachomatis* infectious progeny in human Sertoli cells and this finding, alongside the absence of a specific innate immune response to *C. trachomatis* found in this study, suggests the possibility of a novel persistence model in human Sertoli cells (21), although further studies are warranted.

To date, it has been demonstrated that persistent forms of *C. trachomatis* arise under different stressful conditions, including treatment with IFN-γ or the growth in monocyte-macrophages (14). These persistent forms are known to evade the host immune system and induce a chronic inflammatory state, leading to the tissue damage responsible for infertility (33). In our study, the suppression of the inflammatory response mediated by *C. trachomatis* infection, as evidenced by the lack of detection of IFN-α, IFN-β, IFN-γ, IL-1α and IL-6 in infected cells, might hint, at first, to the absence of testicular tissue damage. However, other mechanisms might be involved in the etiopathogenesis of male infertility mediated by *C. trachomatis*, like modifications in the expression of paracrine and endocrine factors or alterations in the levels of other inflammatory cytokines or in cell structure. Indeed, a potential negative effect of *C. trachomatis* on human Sertoli cells has been described in our previous study, as evidenced by the alteration of human Sertoli cell cytoskeleton following *C. trachomatis* infection, most likely affecting the integrity of the BTB and impairing germ cell development (21).

In addition, *C. trachomatis* infection of human Sertoli cells might indirectly exert detrimental effects on the host cell function by releasing soluble factors, including HSP60, LPS and ROS. In this regard, we assayed sperm viability and motility from semen samples exposed to the supernatants from *C. trachomatis*-infected human Sertoli cells, observing

no alterations (P>0.05). However, we cannot exclude that *C. trachomatis* infection of human Sertoli cells might have a negative impact on the earlier phases of spermatogenesis, since we used mature spermatozoa.

It should be noted that there is extensive controversial literature regarding the relationship between *C. trachomatis* genital infection and sperm parameters, with several studies demonstrating that *C. trachomatis* genital infection had no effects on sperm parameters, whereas others showing an association between *C. trachomatis* DNA in semen and poor semen motility (34).

The main strength of our study is the investigation of the immunological pathways initiated by *C. trachomatis* infection of human Sertoli cells, that might better reflect a human testicular micro-environment.

In conclusion, our results showed that *C. trachomatis* can modulate the innate immune response in human Sertoli cells and evade the host immune-mediate killing, potentially giving rise to a long-term infection that may exert a negative effect on the testicular tissue, impairing its regulation of the phases of the spermatogenetic process.

Overall, our data open the way for more complex studies, such as those utilizing specifically engineered organoids of the seminiferous epithelium in order to improve our knowledge of *C. trachomatis* effects on the multiple regulatory pathways involved in the spermatogenetic process, clarifying the role of *C. trachomatis* in male infertility.

ACKNOWLEDGEMENTS

This work was supported by a grant from University of Rome "Sapienza" to Prof. Rosa Sessa (grant number RP116154DD262EB2).

REFERENCES

1. Rossi T, Grandoni F, Mazzilli F, et al. High frequency of (TG)mTn variant tracts in the cystic fibrosis transmembrane conductance regulator gene in men with high semen viscosity. Fertil Steril 2004; 82:1316-22.
2. Matzuk MM, Lamb DJ. The biology of infertility: research advances and clinical challenges. Nat Med 2008; 14:1197-1213. doi: 10.1038/nm.f.1895.
3. Dimitriadis F, Tsiampali C, Chaliasos N, Tsounapi P, Takenaka A, Sofikitis N. The Sertoli cell as the orchestra conductor of spermatogenesis: spermatogenic cells dance to the tune of testosterone. Hormones (Athens) 2015; 14:479-503. doi: 10.14310/horm.2002.1633.
4. Kaur G, Thompson LA, Dufour JM. Sertoli cells--immunological sentinels of spermatogenesis. Semin Cell Dev Biol 2014; 30:36-44. doi: 10.1016/j.semcdb.2014.02.011.
5. Mruk DD, Cheng CY. The mammalian blood-testis barrier: its biology and regulation. Endocr Rev 2015; 36:564-91. doi: 10.1210/er.2014-1101.
6. Syriou V, Papanikolaou D, Kozyraki A, Goulis DG. Cytokines and male infertility. Eur Cytokine Netw 2018; 29:73-82. doi: 10.1684/ecn.2018.0412.
7. Bhushan S, Tchatalbachev S, Klug J, Fijak M, Pineau C, Chakraborty T, Meinhardt A. Uropathogenic Escherichia coli block MyD88-dependent and activate MyD88-independent signaling pathways in rat testicular cells. J Immunol 2008; 180:5537-47. doi: 10.4049/jimmunol.180.8.5537.
8. Sellge G, Kufer TA. PRR-signaling pathways: Learning from microbial tactics. Semin Immunol 2015; 27:75-84. doi: 10.1016/j.smim.2015.03.009.
9. Redgrove KA, McLaughlin EA. The role of the immune response in *Chlamydia trachomatis* infection of the male genital tract: A double-edged sword. Front Immunol 2014; 5:534. doi: 10.3389/fimmu.2014.00534.
10. Hedger MP. Immunophysiology and pathology of inflammation in the testis and epididymis. J Androl 2011; 32:625. doi: 10.2164/jandrol.111.012989.
11. Solomon M, Henkel R. Semen culture and the assessment of genitourinary tract infections. Indian J Urol 2017; 33:188-93. doi: 10.4103/iju.IJU_407_16.
12. Newman L, Rowley J, Vander Hoorn S, et al. Global estimates of the prevalence and incidence of four curable sexually transmitted infections in 2012 based on systematic review and global reporting. PLoS One 2015; 10:e0143304. doi: 10.1371/journal.pone.0143304.
13. Stojanov M, Baud D, Greub G, Vulliemoz N. Male infertility: the intracellular bacterial hypothesis. New Microbes New Infect 2018; 26:37–41. doi: 10.1016/j.nmni.2018.08.012.
14. Di Pietro M, Filardo S, Romano S, Sessa R. *Chlamydia trachomatis* and *Chlamydia pneumoniae*

interaction with the host: latest advances and future prospective. microorganisms 2019; 7:pii:E140. doi: 10.3390/microorganisms7050140.
15. Sessa R, Di Pietro M, Filardo S, et al. Lactobacilli-lactoferrin interplay in *Chlamydia trachomatis* infection. Pathog Dis 2017; 75. doi: 10.1093/femspd/ftx054.
16. Filardo S, Di Pietro M, Tranquilli G, et al. Selected immunological mediators and cervical microbial signatures in women with *Chlamydia trachomatis* infection. mSystems 2019; 4:pii:e00094-19. doi: 10.1128/mSystems.00094-19.
17. Filardo S, Di Pietro M, Tranquilli G, Sessa R. Biofilm in genital ecosystem: a potential risk factor for *Chlamydia trachomatis* infection. Can J Infect Dis Med Microbiol 2019; 2019:1672109. doi: 10.1155/2019/1672109.
18. Bhushan S, Schuppe HC, Fijak M, Meinhardt A. Testicular infection: microorganisms, clinical implications and host-pathogen interaction. J Reprod Immunol 2009; 83:164–167. doi: 10.1016/j.jri.2009.07.007.
19. O'Connell CM, Ferone ME. *Chlamydia trachomatis* genital infections. Microb Cell 2016; 3:390-403. doi: 10.15698/mic2016.09.525.
20. Sobinoff AP, Dando SJ, Redgrove KA, et al. *Chlamydia muridarum* infection-induced destruction of male germ cells and sertoli cells is partially prevented by Chlamydia major outer membrane protein-specific immune CD4 cells. Biol Reprod 2015; 92:27. doi: 10.1095/biolreprod.114.124180.
21. Filardo S, Skilton RJ, O'Neill CE, Di Pietro M, Sessa R, Clarke IN. Growth kinetics of *Chlamydia trachomatis* in primary human Sertoli cells. Sci Rep 2019; 9:5847. doi: 10.1038/s41598-019-42396-3.
22. O'Neill CE, Skilton RJ, Pearson SA, Filardo S, Andersson P, Clarke IN. Genetic transformation of a *C. trachomatis* ocular isolate with the functional tryptophan synthase operon confers an indole-rescuable phenotype. Front Cell Infect Microbiol 2018; 8:434. doi: 10.3389/fcimb.2018.00434.
23. Sessa R, Di Pietro M, Filardo S et al. Effect of bovine lactoferrin on *Chlamydia trachomatis* infection and inflammation. Biochem Cell Biol 2017; 95:34-40. doi: 10.1139/bcb-2016-0049.
24. World Health Organization. WHO Laboratory Manual for the Examination and Processing of Human Semen, 5th edn. Geneva, Switzerland: WHO. 2010.
25. Paoli D, Gallo M, Rizzo F, et al. Mitochondrial membrane potential profile and its correlation with increasing sperm motility. Fertil Steril 2011; 95:2315-19. doi: 10.1016/j.fertnstert.2011.03.059.
26. Lopata A, Patullo MJ, Chang A, James B. A method for collecting motile spermatozoa from human semen. Fertil Steril 1976; 27:677-84.
27. Darville T, O'Neill JM, Andrews CW Jr., Nagarajan UM, Stahl L, Ojcius DM. Toll-like receptor-2, but not Toll-like receptor-4, is essential for development of oviduct pathology in chlamydial genital tract infection. J Immunol 2003; 71:6187-97.
28. Mackern-Oberti JP, Motrich RD, Breser ML, Sánchez LR, Cuffini C, Rivero VE. *Chlamydia trachomatis* infection of the male genital tract: an update. J Reprod Immunol 2013; 100:37-53. doi: 10.1016/j.jri.2013.05.002.
29. Derbigny WA, Shobe LR, Kamran JC, Toomey KS, Ofner S. Identifying a role for Toll-like receptor 3 in the innate immune response to *Chlamydia muridarum* infection in murine oviduct epithelial cells. Infect Immun 2012; 80:254-265. doi: 10.1128/IAI.05549-11.
30. Wang A, Al-Kuhlani M, Johnston SC, Ojcius DM, Chou J, Dean D. Transcription factor complex AP-1 mediates inflammation initiated by *Chlamydia pneumoniae* infection. Cell Microbiol 2013; 15:779-94. doi: 10.1111/cmi.12071.
31. Carrasco SE, Hu S, Imai DM, et al. Toll-like receptor 3 (TLR3) promotes the resolution of *Chlamydia muridarum* genital tract infection in congenic C57BL/6N mice. PLoS One 2018; 13:e0195165. doi: 10.1371/journal.pone.0195165.
32. Witkin SS, Minis E, Athanasiou A, Leizer J, Linhares IM. *Chlamydia trachomatis*: the Persistent Pathogen. Clin. Vaccine Immunol. 2017; 24:pii: e00203-17. doi: 10.1128/CVI.00203-17.
33. Lewis ME, Belland RJ, AbdelRahman YM, et al. Morphologic and molecular evaluation of Chlamydia trachomatis growth in human endocervix reveals distinct growth patterns. Front Cell Infect Microbiol 2014; 4:71. doi: 10.3389/fcimb.2014.00071.
34. Puerta Suarez J, Sanchez LR, Salazar FC, et al. *Chlamydia trachomatis* neither exerts deleterious effects on spermatozoa nor impairs male fertility. Sci Rep 2017; 7:1126. doi: 10.1038/s41598-017-01262-w.

CXCL-10/CXCR3 IN MACROPHAGES REGULATES TISSUE REPAIR BY CONTROLLING THE EXPRESSION OF Arg1, VEGFa AND TNFα

L-X. LI[1,2], Y-T. XIA[1], X-Y. SUN[3], L-R. LI[1], L. YAO[1], M-I. ALI[1,4], W. GU[2], J-P. ZHANG[5], J. LIU[6], S-G. HUANG[1], H-C. DAI[1] and G-Q. LIU[1,2]

[1]Department of Basic Veterinary Medicine, College of Veterinary Medicine, Huazhong Agricultural University, Wuhan, Hubei Province, P.R. China; [2]Department of Biochemistry and Molecular Biology, School of Laboratory Medicine, and Anhui Province Key Laboratory of Translational Cancer Research, Bengbu Medical College, Bengbu, Anhui Province, P.R. China; [3]College of Food Science and Technology, Huazhong Agricultural University, Wuhan, Hubei Province, P.R. China; [4]Department of Livestock Services, Fargate, Dhaka, Bangladesh; [5]College of Life Science, Tarim University, Alar, Xinjiang Province, P.R. China; [6]College of Life Science and Technology, Southwest Minzu University, Chengdu, Sichuan Province, P.R. China

Received March 13, 2020 – Accepted May 28, 2020

Macrophages have been reported to participate in inflammation, tissue homeostasis and tissue repair. The detailed mechanism of macrophage-mediated tissue repair is not clear. CXCL-10, secreted by monocytes, endothelial cells and fibroblasts, mediates immune response and angiogenesis by binding to CXCR3. In this study, the expression of CXCL-10 and CXCR3 in porcine lung injury induced by porcine reproductive and respiratory syndrome virus (PRRSV) infection was firstly examined. The results showed that the expression of both CXCL-10 and CXCR3 increased in the infected pig lungs. In addition, the increased expression of CXCL-10 and CXCR3 in macrophage treated by poly (I:C) was also observed, suggesting the autocrine system existed in macrophages. Furthermore, CXCL-10 treatment induced upregulation of Arg1 and VEGFa, and downregulation of TNFα in macrophage, and CXCR3 antagonist AMG487 treatment presented the contrary effects on the expression of Arg1, VEGFa, and TNFα. CXCL-10-stimulated effects were dependent on PI3K/Akt signaling pathway. Wound-healing assay showed that CXCL-10 treatment macrophage conditioned medium promoted the healing process of endothelial cells. Our results suggested that CXCL-10/CXCR3 in macrophage may mediate tissue repair by regulating the macrophage expression of Arg1, VEGFa and TNFα. Modulation of CXCL-10/CXCR3 axis in macrophage may be a potential therapeutic strategy for tissue injury and repair.

Chemokines are small cytokines that play an important role in regulating the movement of inflammatory cells to sites of infection and directly affect the function of innate cells (1). Previous studies have shown that chemokines and their receptors play an essential role in intestinal inflammation, renal inflammation, liver inflammation and fibrosis (2). C-X-C motif chemokine 10 (CXCL-10), also known as interferon-gamma-inducible protein 10 (IP-10), was originally identified as a chemokine released by macrophages, endothelial cells, and fibroblasts in response to interferon gamma (IFN-γ) (3). By

Key words: CXCL-10; CXCR3; inflammation; macrophage; tissue repair

Corresponding Author:
Dr Guoquan Liu,
Department of Biochemistry and Molecular Biology,
Anhui Province Key Laboratory of Translational Cancer Research,
Bengbu Medical College, Bengbu, Anhui Province 233030, P.R. China
Tel.: +86 5523175239
e-mail: guoquanliu@bbmc.edu.cn

0393-974X (2020)
Copyright © by BIOLIFE, s.a.s.
This publication and/or article is for individual use only and may not be further reproduced without written permission from the copyright holder.
Unauthorized reproduction may result in financial and other penalties
DISCLOSURE: ALL AUTHORS REPORT NO CONFLICTS OF INTEREST RELEVANT TO THIS ARTICLE.

binding to its receptor CXCR3, a G-protein-coupled receptor (GPCR), CXCL-10 can induce chemotaxis, apoptosis, cell growth and angiogenesis (4). For example, one study reports that CXCL-10 may inhibit adipose tissue angiogenesis in obesity (5). In addition, the CXCL-10/CXCR3 axis is involved in the inflammatory response in human skeletal muscle cells and promotes the proliferation of vascular smooth muscle cells (6, 7).

Macrophages have been reported to participate in inflammation, tissue homeostasis and repair, based on their ontogeny and the tissue microenvironment through the cytokines. As known, pulmonary inflammatory cytokines may be the important factors to modulate respiratory injury (8). For example, arginase-1 (Arg1) converts L-arginine to L-ornithine to promote polyamine production and tissue repair (9), and local Arg1 activity is required for cutaneous wound healing (10). Moreover, nor-NOHA can suppress the ability of invasion and migration of HepG2 cells by inhibiting Arg1 (11). VEGF induces the proliferation of various cell types involved in the healing process (12). While TNFα at high concentrations elicits tissue destructive reactions, it stimulates tumor growth and angiogenesis at low concentrations (12). Arg-1, VEGFa, and TNFα may have roles in regulating macrophage autophagy and polarization; for instance, Arginase-1-independent polyamine production promotes IL-4-induced macrophage polarization towards M2, but inhibits LPS-induced expression of inflammatory genes (13). Macrophages enhance VEGFa-driven angiogenesis in an embryonic zebrafish tumour xenograft model (14). TNFα inhibits autophagy in microglia through AKT/mTOR signaling pathway, and autophagy enhancement promotes microglia M2 polarization and inflammation resolution (15).

Some studies have pointed out that porcine reproductive and respiratory syndrome virus (PRRSV) infection induces lung injury and production of proinflammatory cytokines and chemokines, such as iNOS, CXCL8 (IL-8) (16, 17). Macrophage is the main host cell of PRRSV (18). The aims of this study are to evaluate whether PRRSV can stimulate CXCL-10 production in infected pig lung and whether the CXCL-10/CXCR3 axis is also presented in macrophage. Furthermore, to understand the role of CXCL-10 in lung injury, the CXCL-10 regulation of macrophage functions was studied. This study will provide a basis for the future development of disease treatment drugs targeting the CXCL-10/CXCR3 axis.

MATERIALS AND METHODS

Animals

For PRRSV infection experiment, all pigs free of PRRSV were chosen. Normal pig lungs (control group) and PRRSV-infected pig lungs (PRRSV group) were collected for further experiments. The right-lung lower lobe was clamped with hemostats and collected for analysis of lung protein and RNA. All animal procedures were approved by the Animal Care and Use Committee of Hubei Province, China, in accordance with guidelines developed by the China Council on Animal Care and Protocol.

Cell culture and treatment

RAW264.7 cells and bEnd.3 cells (2×10^5) were plated into six-well plates and cultured in DMEM (Hyclone, USA) duplicate supplemented with 10% fetal bovine serum (Cat. #1027-106, Gibco, USA), 100 U/mL penicillin, and 100 mg/mL streptomycin (Invitrogen) in humidified air at 37°C with 5% CO_2. Cells at a confluence of 70-80% were treated by poly(I:C) (0.1 μg/mL, 1 μg/mL, 5 μg/mL), LY294002 (10 μg/mL), AMG487 (0.2 μM, 1 μM, 5 μM) and CXCL-10 (20 ng/mL, 100 ng/mL, 500 ng/mL) and transfected with siRNA-Cxcr3/siRNA-NC (100 nM, Ribobio, China).

Quantitative real-time PCR (qPCR)

Total RNA from tissues and cells (after 24 h) were extracted using RNAiso Plus reagent (TaKaRa) and 1 μg RNA was reverse transcribed with PrimeScript™ RT reagent Kit with gDNA Eraser (Cat. #RR047A, TaKaRa) using oligo(dT). The RT products were quantified using SYBR Premix Ex Taq™ II (Tli RNaseH Plus) (Cat. #RR820A, TaKaRa) on the LightCycler real-time PCR detection system (Roche). Comparative quantification was calculated utilizing the $2^{-\Delta\Delta Ct}$ method and normalized GAPDH levels. All experiments were performed in triplicate. Specific primers (Qingke, China) used are listed in Table I.

Western blotting assays

The tissues and cells (48 h after treatment) were lysed in RIPA buffer (Cat. #PP1202, Aidelai, China) for 1 h on ice. The total protein concentration of the lysate was determined by the bicinchoninic acid method (Cat. #PP0101, Aidelai, China). The proteins were separated by 12% polyacrylamide gel electrophoresis containing 0.1% SDS and transferred to PVDF membranes. The membranes were incubated for 2 h at room temperature in blocking buffer (20 mM Tris-HCl, 137 mM NaCl, pH 8.0, containing 0.1% Tween and 5% non-fat dry milk) and probed with antibodies against CXCR3 (1:1000, ab154845, Abcam, UK), Akt (1:1000, 4691, CST, USA), Arg1 (1:2000, 93668, CST, USA) and GAPDH (1:2000, GB12002, Servicebio, China), β-tubulin (1:2000, GB13017-2, Servicebio, China) at 4°C overnight. After being washed 3 times with TBST, the membrane was incubated with HRP-conjugated anti-IgG (1:3000 Servicebio, China) at room temperature for 2 h. GAPDH or β-tubulin was used as an internal control. The reacted proteins were visualized using an electrochemiluminescence (ECL) system (Biotanon, China) and protein ratios were calculated following Image J densitometric analysis.

Wound-healing assays

RAW264.7 cells were inoculated on 6 well plates and were treated by CXCL-10 500 ng/mL, AMG487 5 μM, respectively. After 24 h, the supernatants were collected. The bEnd.3 cells were inoculated into 6 well plates. When the cells were full of fusion, the mediums were carefully discarded. A line was drawn vertically on a single layer of cells with a 20 μL sterile tip. After 3 times using PBS, the supernatants of RAW264.7 cells were added to culture bEnd.3 cells sequentially. The healing was observed 48 h later under 40x microscope and photographed. The experiment was repeated 3 times under the same conditions.

Arginase activity assay

After 48 h of CXCL-10 (500 ng/mL) treatment, the RAW264.7 cells were collected. The arginase activity assay was carried out by QuantiChromTM Arginase Assay Kit (DARG-100, Hayward, USA). Briefly, approximately 10^6 cells in each 6-well plate were collected and lysed with lysis buffer (10 mM Tris-HCl pH 7.4, 0.4% (w/v) Triton X-100, 1 μM pepstatin A, and 1 μM leupeptin). After centrifugation at 14,000 g at 4°C for 10 min, the supernatants were subjected for arginase activity assay by incubating with the substrate buffer provided by the kit for 2 h at 37°C. After the reactions were terminated, the optical density values were determined at 430 nm. All samples were determined in triplicate.

Arginase activity (units per liter of sample (U/L)) was calculated as follows: Arginase = $(OD_{SAMPLE} - OD_{BLANK}) / (OD_{STANDARD} - OD_{WATER}) \times [\text{Urea Standard}] \times 50 \times 10^3 / (40 \times t) = (OD_{SAMPLE} - OD_{BLANK}) / (OD_{STANDARD} - OD_{WATER}) \times 10.4$ (U/L) Where OD_{SAMPLE}, OD_{BLANK}, $OD_{STANDARD}$ and OD_{WATER} are the optical density values of the sample, sample blank, standard and water respectively. [Urea Standard] = 1 mM, t is the reaction time (120 min). 50 and 40 are the reaction and sample volumes (μL) respectively.

Statistical analysis

Data were expressed as the mean ± SEM. of at least three independent experiments for each cellular experimental group. The data was evaluated by two-tailed Student's *t*-test with GraphPad Prism version 5.0 (GraphPad software, USA). P value of less than 0.05 (*$P < 0.05$, **$P < 0.01$, ***$P < 0.001$) was considered as statistically significant.

RESULTS

Expression of CXCL-10 and CXCR3 increased in PRRSV infected pig lung

As known, alterations in CXCL-10 expression levels have been associated with inflammatory diseases including infectious diseases, immune dysfunction and tumor development (19). PRRSV infection causes lung injury in infected animals. This paper was designed to understand the roles of CXCL-10 and its receptor CXCR3 in tissue injury, and their expression levels in lung injury induced by PRRSV infection were examined. The qPCR and Western blotting results indicated that both CXCL-10 and CXCR3 expression levels were significantly increased in lung tissues infected by the virus (Fig. 1). These results clearly demonstrated that both CXCL-10 and its receptor CXCR3 expressions were upregulated in the injury tissues.

CXCL-10/CXCR3 axis was upregulated in inflammatory macrophages

Poly(I:C), a synthetic double-stranded RNA

acting as a potent adjuvant capable of enhancing the host innate immune response, was recently reported to induce CXCL-10 production in mouse intestinal epithelial cells (20). Since macrophages are host cells of PRRSV, whether macrophages express the CXCL-10 and CXCR3 after poly(I:C) stimulation was detected. The qPCR results in mouse macrophage RAW264.7 cells demonstrated that poly(I:C) treatment induced the expression of both CXCL-10 and CXCR3 in macrophages (Fig. 2 a, b). The upregulation of CXCR3 was also confirmed by Western blotting (Fig. 2c). Clearly, these data suggest that both CXCL-10 and CXCR3 were upregulated in inflammatory macrophage. It is likely that CXCL-10/CXCR3 axis acts as an autocrine regulatory pathway in macrophages.

CXCL-10 and AMG487 (CXCR3 antagonist) modulated the healing process through Arg1, VEGFa, and TNFα

Macrophages stimulate angiogenesis by releasing growth factors, cytokines, and chemokines, such as VEGF, bFGF, PDGF, TNFα and IFN-γ (21). In addition, Arginase-1 (Arg1), a marker of M2-phenotype macrophages catalyzing the conversion of arginine to ornithine and urea, completing the last step in the urea cycle, is able to hydrolysate L-arginine into L-ornithine, promoting polyamine synthesis and tissue repair (9). To determine whether the macrophage CXCL-10/CXCR3 axis plays a role in tissue repair, the expression of Arg1, VEGFa and TNFα in macrophages was examined. CXCL-10 was firstly used to treat RAW264.7 cells, and then the expressions of these molecules were examined by qPCR. The qPCR results showed that CXCL-10 at 500 ng/mL enhanced the expression of Arg1 and VEGFa but inhibited the expression of TNFα (Fig. 3 a-c). AMG487 is a small molecule antagonist for CXCR3 with selective and highly effective inhibition of CXCL10 binding to CXCR3, thus inhibiting CXCR3 activation and intracellular signal transduction. In addition, AMG487 has good bioavailability and stable biological activity *in vivo* (22). Therefore, our next aim was to investigate the effects of AMG487 on the expression of cytokines in macrophages. In this paper, the RAW264.7 cells were treated with AMG487 (5 μM), and the expression of these molecules was determined by qPCR. Arg1 and VEGFa expression showed the downregulated trend by AMG487 treatment (Fig. 4 a, b). Conversely, compared with the control group, AMG487 treatment increased TNFα expression (Fig. 4c). In addition, the Western blotting results suggested that Arg1 protein expression was upregulated by CXCL-10 (Fig. 3d) and the arginase activity assay subsequently showed that CXCL-10 also increased Arg1 activity (Fig. 3e).

CXCL-10/CXCR3 axis mediated the expression of Arg1, VEGFa and TNFα via Akt pathway

The p38 mitogen-activated protein kinase

Table I. *The primer sequence of qPCR*

Gene	Forward primer (5'-3')	Reverse primer (5'-3')
Pig		
GAPDH	CTGCCGCCTGGAGAAACCT	GCTGTAGCCAAATTCATTGTCG
CXCL10	CAGTTAGGGCTTGATGTATGGT	GGCACTACTGATAAGGATGGG
CXCR3	CCACAAGCACCAAAGCA	CAGGAAGAAGGCAAACTCA
Mouse		
GAPDH	AAATGGTGAAGGTCGGTGTGAAC	CAACAATCTCCACTTTGCCACTG
CXCL10	CTCATCCTGCTGGGTCTGAG	CCTATGGCCCTCATTCTCAC
CXCR3	GAGAGCGACTTCTCTGACTC	ACTCAGTAGCACAGCAGCCA
Arg1	AAGACAGCAGAGGAGGTG	AGTCAGTCCCTGGCTTAT
VEGFa	CAGGCTGCTGTAACGATGAA	CTATGTGCTGGCTTTGGTCA
TNFα	AATGGCCTCCCTCTCATCAGTT	CCACTTGGTGGTTTGCTACGA

signaling pathway is implicated in the angiogenesis effects of CXCR3 on adipose tissue (23), while the PI3K/Akt signaling pathway is involved in cell growth, proliferation, movement and survival. In order to elucidate whether Akt pathway mediates signal transduction of CXCL-10/CXCR3, Western blotting was performed to detect Akt expression. In this study, CXCL-10 suppressed Akt protein expression (Fig. 5a). On the contrary, Akt expression was enhanced by adding to AMG487 (Fig. 5b). Knockdown of CXCR3 by siRNA-CXCR3 also increased Akt expression in protein level (Fig. 5c). To further demonstrate whether CXCL-10/CXCR3 mediates the expression of Arg1, VEGFa, and TNFα via the Akt pathway, their expression in mRNA and protein levels was tested. The qPCR results showed that Akt inhibitor LY294002 increased the expression of Arg1 and TNFα (Fig. 6a, c). Inversely, VEGFa expression decreased (Fig. 6b). CXCL-10 and LY294002 promoted the expression of Arg1 and TNFα (Fig. 6 a, c), but had no effect on the expression of VEGFa (Fig. 6b). Then the protein expression of Arg1 after being treated by CXCL-10 and LY294002 was examined. LY294002 could synergize CXCL-10 to promote the expression of Arg1 (Fig. 6d). These data suggest that the Akt pathway is involved in the regulation of these protein expression.

Conditioned culture medium of macrophages treated with CXCL-10 promoted the wound-healing of endothelial cells

As reported, chemokines largely orchestrate the tissue repair process involved in overlapping phases of hemostasis and inflammation, proliferation and angiogenesis, and remodeling of the nascent tissue. For example, CXCL-10 affects the angiogenesis of adipose tissue (5). To further explore the functional role of CXCL-10-CXCR3 in macrophages, the effects of conditional culture medium of macrophages after CXCL-10 and AMG487 treatment on endothelial wound-healing process was determined. The endothelial cell scratch experiments showed that each group promoted wound healing in different degrees compared with the control group. The healing degree of conditional culture medium of CXCL-10 (500 ng/mL) treatment was the most obvious (Fig. 7), indicating modulating the CXCL-10-CXCR3 signaling pathway in macrophages regulates the tissue-repair.

DISCUSSION

Macrophages play an essential role in tissue homeostasis and balance the immunity and immune-mediated pathological damage through releasing cytokines and chemokines (24). PRRSV is the pathogen causing porcine reproductive and respiratory syndrome, and alveolar residential macrophages are the main targeted cells (25). Infection of PRRSV causes macrophage death and endothelial injury. Published studies also have reported that PRRSV infection induces proinflammatory cytokines and chemokines, such as iNOS, CXCL8 (IL-8). In our study, elevated CXCL-10 and CXCR3 levels were observed in the lung of PRRSV infected pigs, suggesting that CXCL-10/CXCR3 may be involved in the formation or resolution of tissue injury (Fig. 1). Similarly, upregulation levels of both CXCL-10 and CXCR3 in the inflammatory macrophages stimulated by poly(I:C) (Fig. 2) suggested that CXCL-10/CXCR3 axis also existed in the macrophage. The autocrine axis may contribute to the tissue homeostasis of macrophages.

Chemokines are a family of small (8-10 kDa) proteins that play an important role as potent chemoattractants for activation and recruitment of leukocytes. CXCL-10 is secreted by monocytes, endothelial cells and fibroblasts, and has been regarded as a potential biomarker for forecasting some diseases, such as acute Kawasaki disease, hepatitis C virus, rhinovirus infections, acute respiratory infection, oral inflammatory disease (26). CXCL-10 receptor CXCR3 is involved in the chemotaxis of activated T cells, dendritic cells and NK cells as well as angiogenesis. Recently, one study suggested that the CXCR3 regulates and enhances host defense mechanisms against infection, and also contributes to tissue inflammation and pathology in chlamydia infection (27). Another study investigated whether CXCR3 deficiency exacerbates murine autoimmune cholangitis by promoting pathogenic $CD8^+$ T cell activation (28). Also, one group has shown that

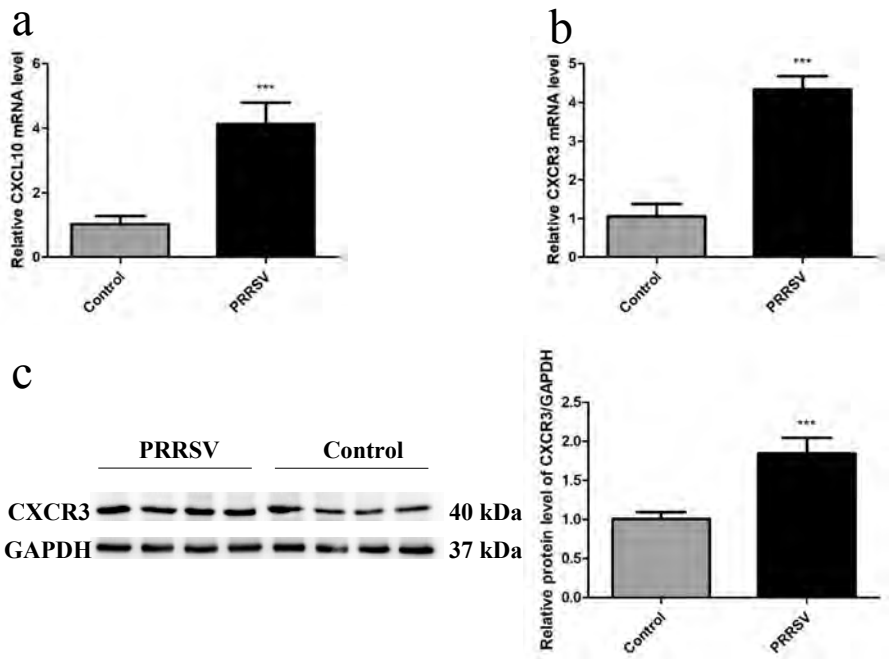


Fig. 1. *The expression of CXCL-10 and CXCR3 increased in PRRSV infected pig lungs. QPCR and Western blotting were performed as described in the text.* ***a, b****) CXCL-10 and CXCR3 expression was enhanced by PRRSV in mRNA level.* ***c****) PRRSV induced an increase in CXCR3 protein expression level. Data were shown as mean ± SEM. of three independent experiments (* P < 0.05, ** P < 0.01, *** P < 0.001).*

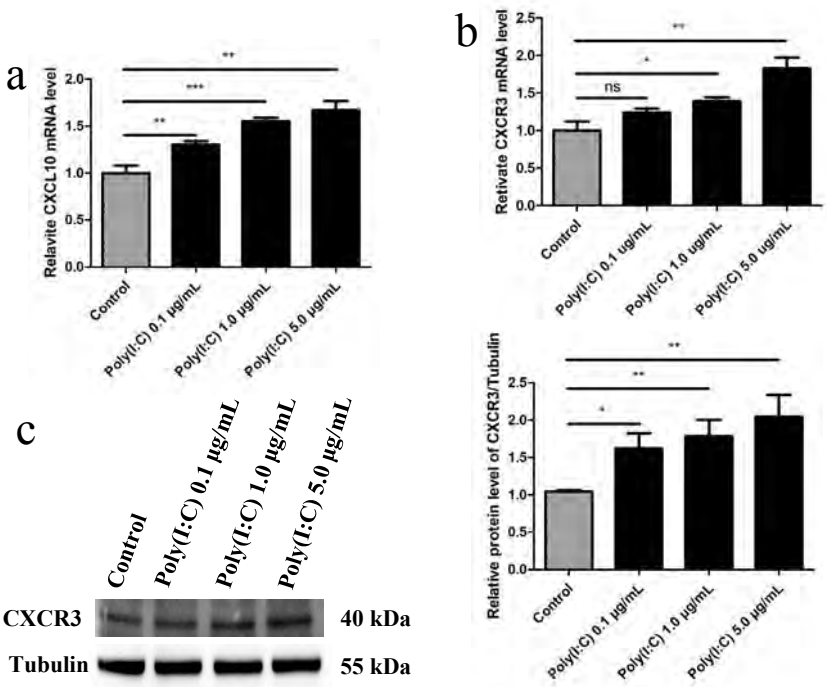


Fig. 2. *The CXCL-10/CXCR3 axis also existed in RAW264.7 cells treated with poly (I:C).* ***a, b****) The qPCR results showed that CXCL-10/CXCR3 expression exhibited a high level after stimulation by poly (I:C) in RAW264.7 cell.* ***c****) The results indicated that the expression of CXCR3 protein was increased by poly (I:C) in RAW264.7 cell. Data were shown as mean ± SEM. of three independent experiments (* P < 0.05, ** P < 0.01, *** P < 0.001).*

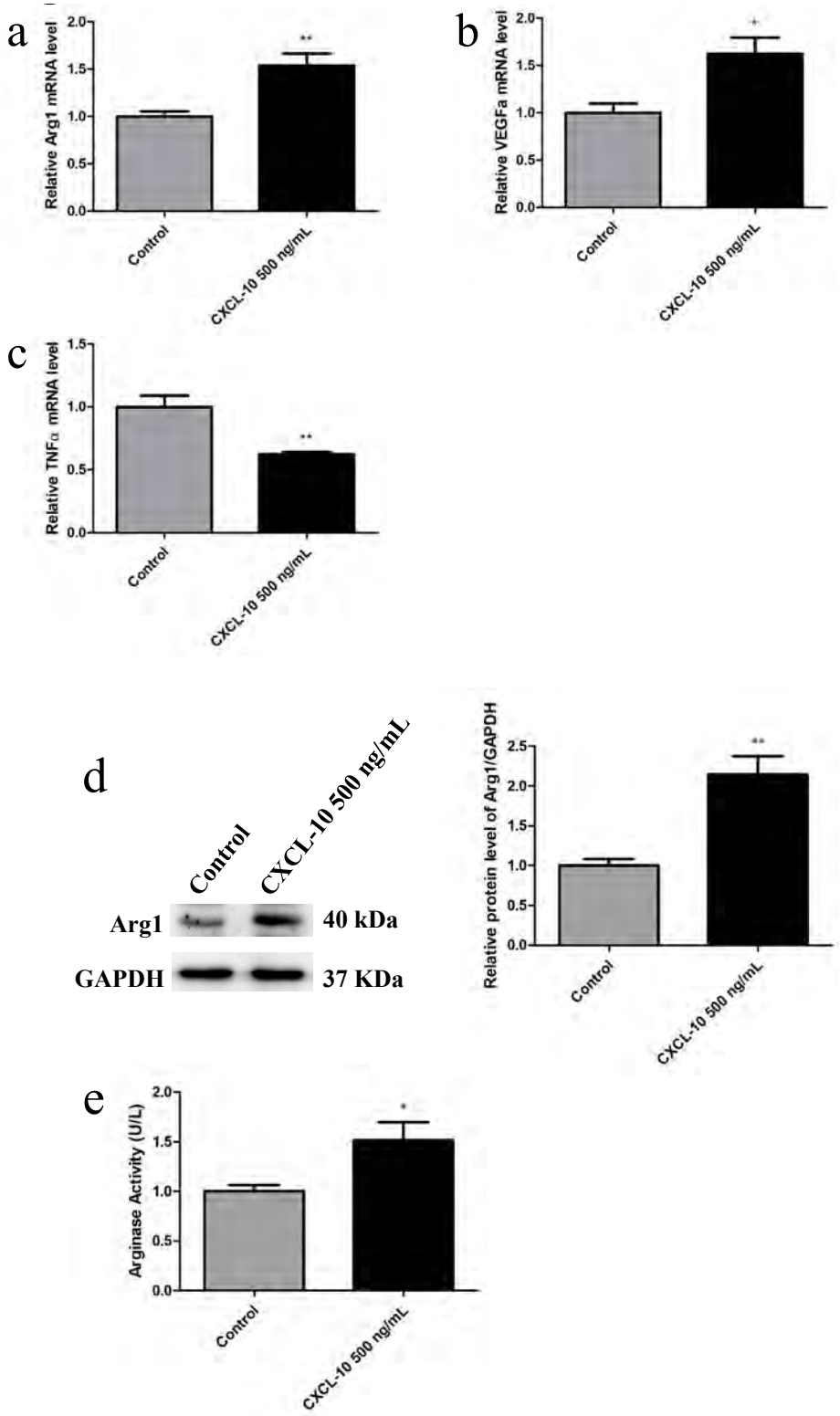


Fig. 3. *CXCL-10 induced the expression of Arg1, VEGFa and* TNFα. ***a-c****) CXCL-10 enhanced the expression of Arg1 and VEGFa but inhibited the expression of TNFα in mRNA level.* ***d****) Arg1 protein expression was upregulated by CXCL-10.* ***e****) CXCL-10 could increase Arg1 activity. Data were shown as mean ± SEM. of three independent experiments (* P < 0.05, ** P < 0.01, *** P < 0.001).*

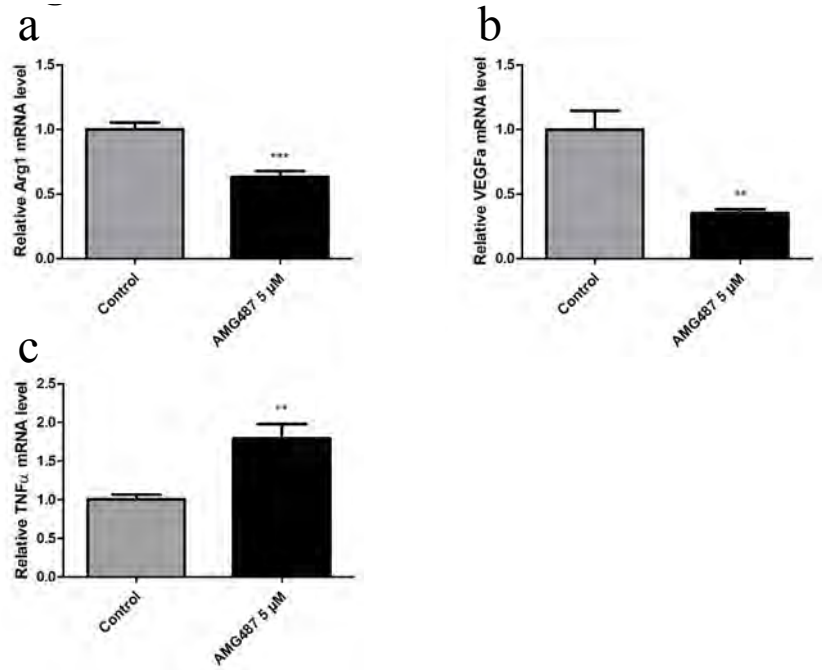


Fig. 4. *CXCR3 antagonist AMG487 regulated the expression of Arg1, VEGFa and TNFα.* ***a, b****) Arg1 and VEGFa expression showed the downregulation in the cells treated by AMG487.* ***c****) Compared with the control group, AMG487 increased TNFα expression. Data were shown as mean ± SEM. of three independent experiments (* P < 0.05, ** P < 0.01, *** P < 0.001).*

CXCR3 antagonist AMG487 ameliorates the blood-retinal barrier disruption in diabetic mice through anti-oxidative stress (29). Intrathecal injection of AMG487 attenuates pain hypersensitivity in a dose-dependent manner in chronic constriction injury (30), and attenuates phenylephrine-dependent maladaptive cardiac remodeling (31). Chemokines influence the inflammatory cascade early in healing and the later growth and regression of the wound area through their receptors and cytokines. Our results showed that CXCL-10 enhanced the expression of Arg1 and VEGFa but inhibited the expression of TNFα (Fig. 3a, b, c, d, e). Undoubtedly, Arg1 converts L-arginine to L-ornithine to promote polyamine synthesis and tissue repair. VEGF induces the proliferation of various cell types involved in the healing process. At high concentrations, TNFα elicits tissue destructive reactions, but at low concentrations, stimulates tumor growth and angiogenesis. In the present study, CXCR3 antagonist AMG487 affected the expression of cytokines in RAW264.7 cells and the opposite result was observed after the cells were treated with AMG487 (Fig. 4a, b, c). There are at four subgroups of macrophage M2 polarization; since Arg1 is expressed in M2a subgroup and VEGF is produced in M2d subgroup, it is likely that AMG487 may promote two different subgroup M2 polarizations.

CXCR3 belongs to the G-protein-coupled receptor (GPCR). CXCL-10 binding to CXCR3 activates Gi protein, then results in downstream Akt activation via PI3K signaling pathways, which mediate immune response and angiogenesis. Another study indicates that activation of Ras/ERK and Src stimulated by CXCR3 is necessary to regulate PI3K/Akt signal (32). Moreover, a series of papers have shown that Akt is involved in the regulation of macrophage polarization, for example, TGF-β regulates lipopolysaccharide-stimulated macrophage M2-like polarization via the Akt/FoxO1 pathway (33). Our findings suggested that CXCL-10 suppressed Akt protein expression. In contrast, Akt expression was enhanced by antagonist AMG487. Knockdown of CXCR3 by siRNA-CXCR3 also increased Akt expression in protein level (Fig. 5). Thus, the fact that CXCL-10/CXCR3 mediated

signal transduction via Akt pathway was further confirmed since Akt inhibitor, LY294002, promoted the expression of Arg1 and TNFα. On the contrary, VEGFa expression decreased (Fig. 6). Interestingly, CXCL-10 mediated their expression inhibited by LY294002.

Furthermore, it is shown that the CXCL-10/CXCR3 pathway promotes the migration of cardiac microvascular endothelial cells (CMECs) under normal conditions and during hypoxia/ischemia in a proliferation-independent manner, at least in part, through regulation of the p38/FAK pathways (34). In the study, cell scratch experiments showed that RAW264.7 cell conditioned medium regulated the wound healing capacity of endothelial bEnd.3 cells. The results showed that each group promoted wound healing in different degrees compared with the control group. Although AMG487 could promote cell migration, the healing degree of the CXCL-10-treated group was higher than the AMG487-treated group (Fig. 7). Increasing studies have shown

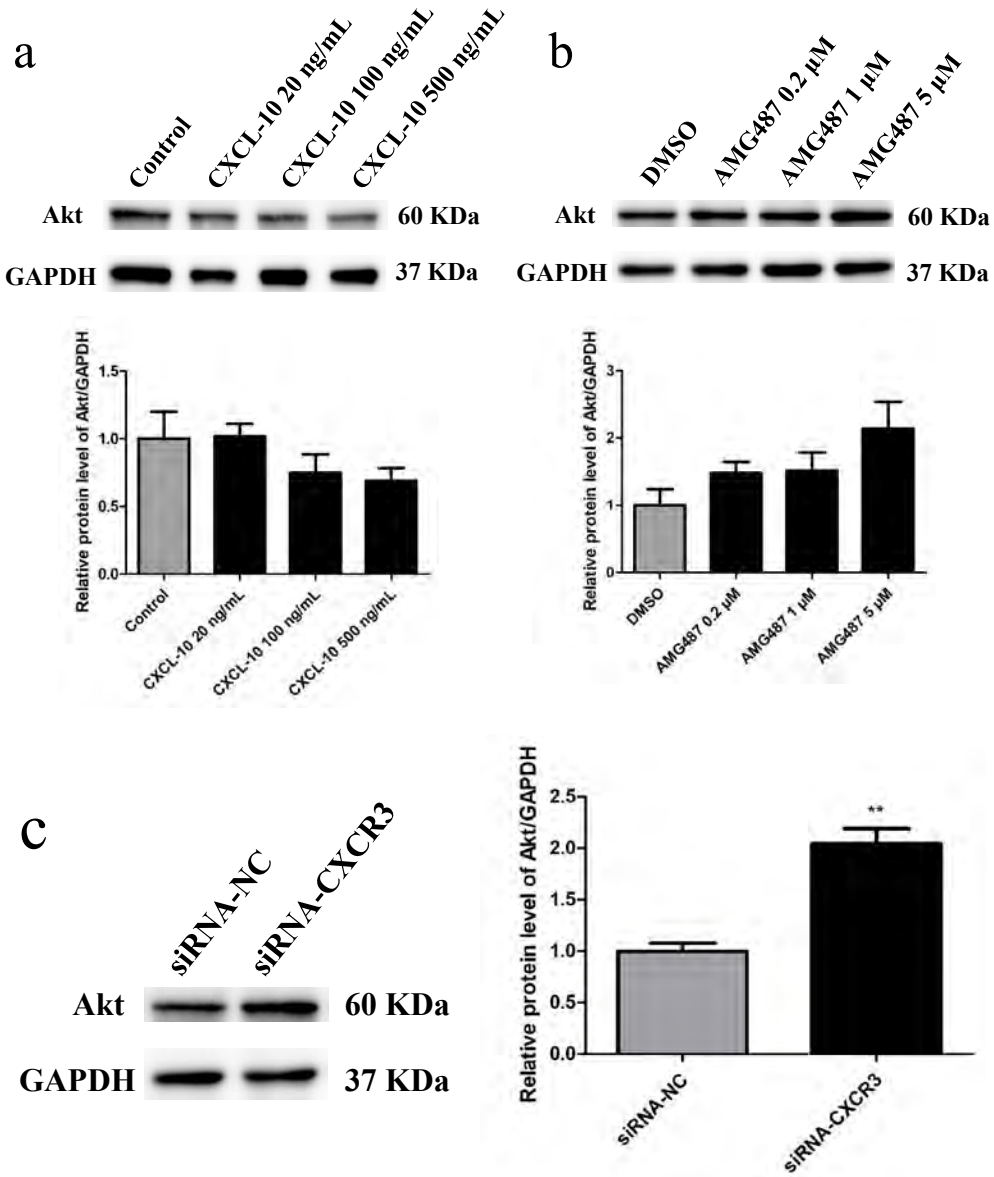


Fig. 5. *The Akt pathway mediated CXCL-10/CXCR3 signal transduction.* ***a)*** *CXCL-10 suppressed Akt protein expression.* ***b)*** *Akt expression was enhanced by AMG487.* ***c)*** *Knockdown of CXCR3 by siRNA-CXCR3 also increased Akt expression in protein level. Data were shown as mean ± SEM. of three independent experiments (* $P < 0.05$, ** $P < 0.01$, *** $P < 0.001$).*

that the CXCL-10/CXCR3 axis is involved in various diseases. In view of these, our results suggested that CXCL-10/CXCR3 in macrophage might regulate the expression of Arg1, VEGFa and TNFα via Akt pathway, these factors then subsequently regulate the balance of tissue repair (Fig. 8). Our study provided the base for CXCL-10/CXCR3 axis as the potential therapeutic target in the resolution of tissue injury. However, there are other factors involved in tissue repair. As known, MMPs (Matrix metalloproteinases), which are a large family of ubiquitously expressed zinc-dependent enzymes with proteolitic activities, play an important role in inflammation, tissue repair, tumor invasion, and metastasis by degrading extracellular matrix components. For instance, MMP9 is involved in cellular migration through inflammatory marker activation (35). Therefore, the relationship between CXCR3 and MMPs may be explored in a follow-up study.

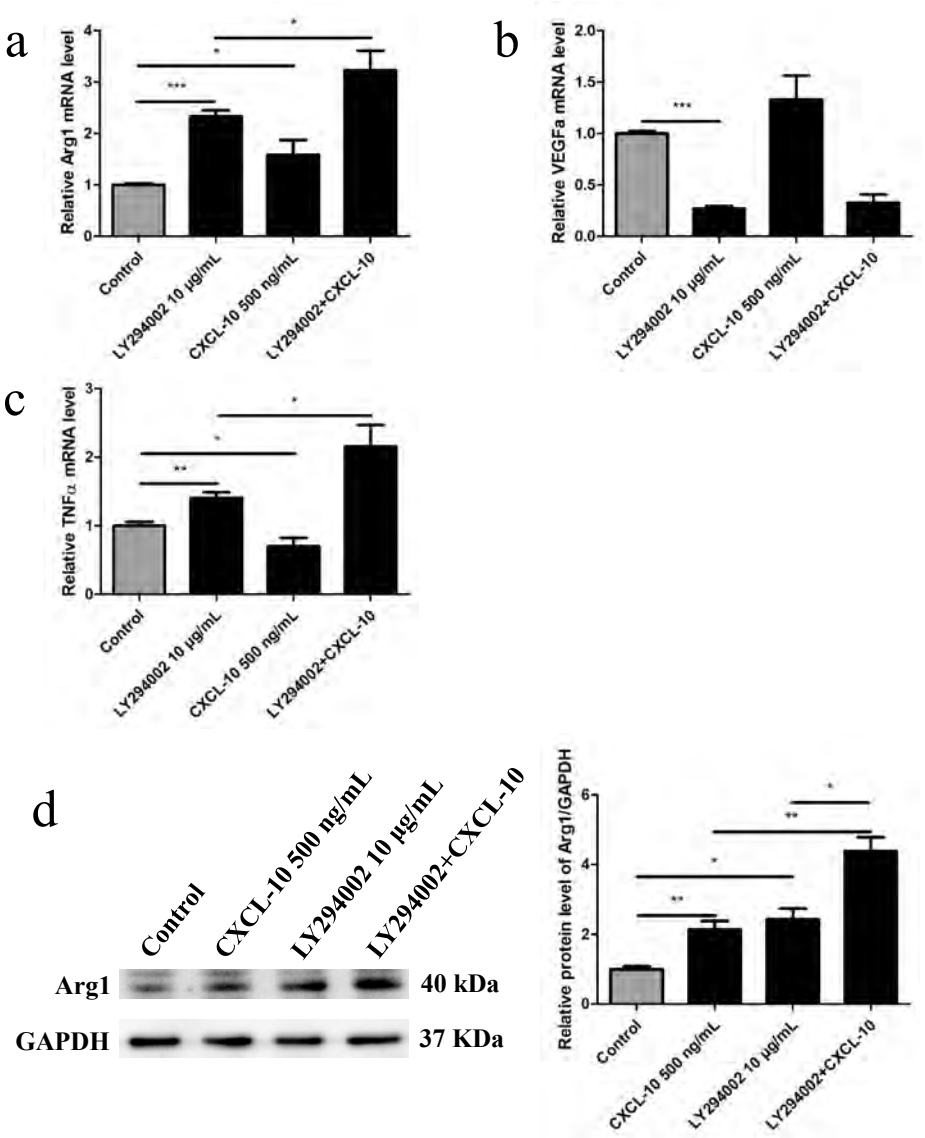


Fig. 6. *The CXCL-10/CXCR3 axis regulated the expression of Arg1, VEGFa and TNFα via Akt pathway.* ***a, c****) Akt inhibitor LY294002 increased the expression of Arg1 and TNFα in mRNA level.* ***b****) VEGFa expression decreased by LY294002. a-c CXCL-10 along with LY294002 promoted the expression of Arg1 and TNFα but had no effect on the expression of VEGFa. d LY294002 synergizes CXCL-10 to promote the expression of Arg1 in protein level. Data were shown as mean ± SEM. of three independent experiments (* P < 0.05, ** P < 0.01, *** P < 0.001).*

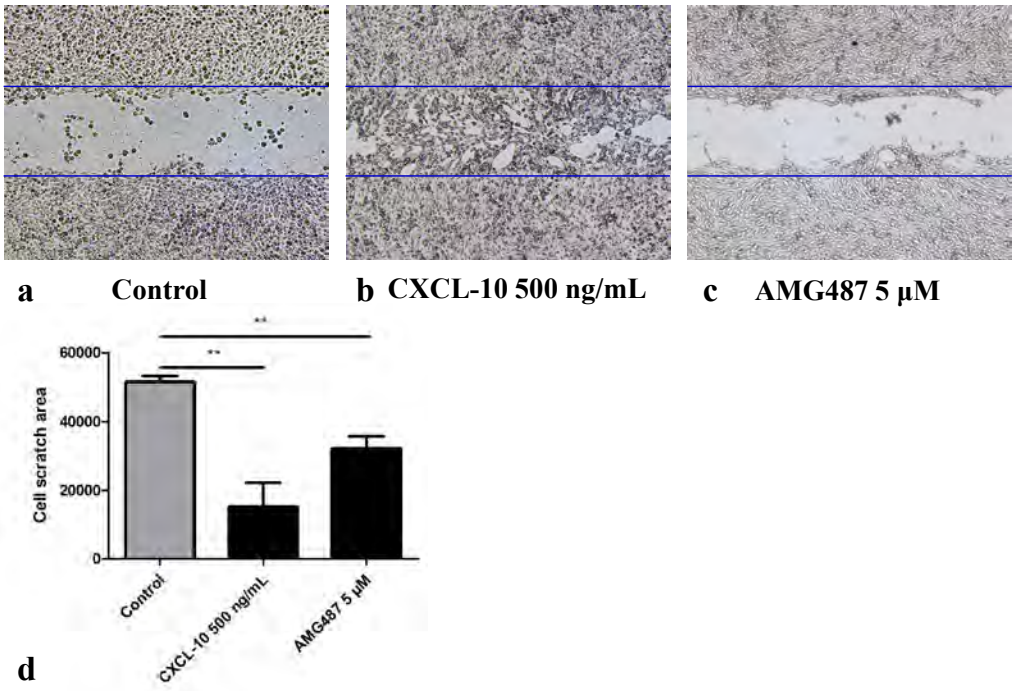


Fig. 7. *The endothelial cell scratch experiments showed that RAW264.7 cell conditioned medium regulated the healing of bEnd.3 cells. Each group promoted wound healing in different degrees compared with the control group. The healing degree of CXCL-10 (500 ng/mL) treated group was the most obvious. Although AMG487 (5 μM) could promote cell migration, the healing degree was less than CXCL-10 group. Data were shown as mean ± SEM. of three independent experiments (* P < 0.05, ** P < 0.01, *** P < 0.001).*

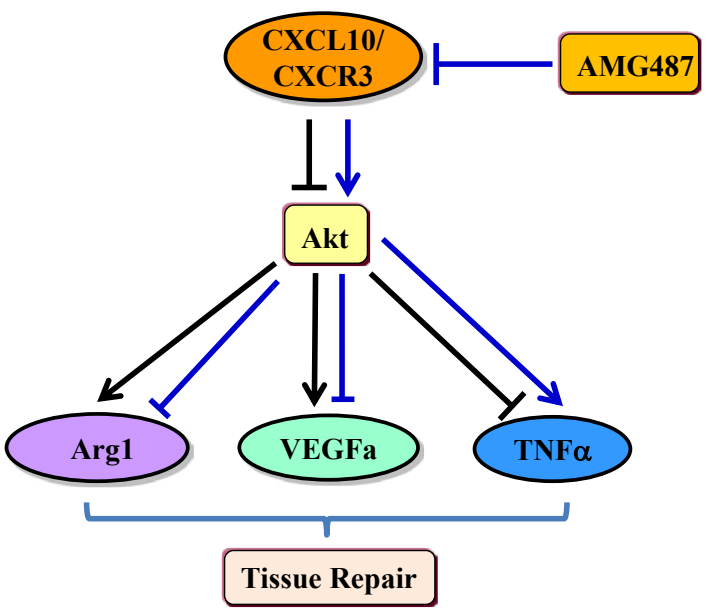


Fig. 8. *The results suggested that the CXCL-10/CXCR3 axis in macrophage might regulate the balance of tissue repair through Arg1, VEGFa and TNFα via Akt pathway.*

ACKNOWLEDGEMENTS

This work was sponsored by the National Natural Science Foundation of China (NSFC) Grants 31372418, Huazhong Agricultural University Scientific and Technology Self-Innovation Foundation Program 2012RC011, and the 948 Project of Chinese Ministry of Agriculture (2015-Z33, GL).

REFERENCES

1. Aota K, Kani K, Yamanoi T, Nakashiro KI, Ishimaru N, Azuma M. Distinct Regulation of CXCL10 production by cytokines in human salivary gland ductal and acinar cells. Inflammation 2018; 41:1172-81.
2. Zeremski M, Petrovic LM, Chiriboga L, et al. Intrahepatic levels of CXCR3-associated chemokines correlate with liver inflammation and fibrosis in chronic hepatitis C. Hepatology 2008; 48:1440-50.
3. Wang J, Vodovotz Y, Fan L, et al. Injury-induced MRP8/MRP14 stimulates IP-10/CXCL10 in monocytes/macrophages. Faseb J 2015; 29:250-62.
4. Mikucki ME, Fisher DT, Matsuzaki J, et al. Non-redundant requirement for CXCR3 signalling during tumoricidal T-cell trafficking across tumour vascular checkpoints. Nat Commun 2015; 6:7458.
5. Hueso L, Ortega R, Selles F, et al. Upregulation of angiostatic chemokines IP-10/CXCL10 and I-TAC/CXCL11 in human obesity and their implication for adipose tissue angiogenesis. Int J Obesity 2018; 42:1406-17.
6. Wang H-j, Zhou Y, Liu R-m, et al. IP-10/CXCR3 axis promotes the proliferation of vascular smooth muscle cells through ERK1/2/CREB signaling pathway. Cell Biochem Biophys 2017; 75:139-47.
7. Crescioli C, Sottili M, Bonini P, et al. Inflammatory response in human skeletal muscle cells: CXCL10 as a potential therapeutic target. Eur J Cell Biol 2012; 91:139-49.
8. Li L, Ng DS, Mah WC, et al. A unique role for p53 in the regulation of M2 macrophage polarization. Cell Death Differ 2015; 22:1081-93.
9. Byles V, Covarrubias AJ, Ben-Sahra I, et al. The TSC-mTOR pathway regulates macrophage polarization. Nat Commun 2013; 4:2834.
10. Campbell L, Saville CR, Murray PJ, Cruickshank SM, Hardman MJ. Local arginase 1 activity is required for cutaneous wound healing. J Invest Dermatol 2013; 133:2461-70.
11. Li X, Zhu F, He Y, Luo F. Arginase inhibitor nor-NOHA induces apoptosis and inhibits invasion and migration of HepG2 cells. Chinese J Cellul Molecular Immunol = Xi Bao Yu Fen Zi Mian Yi Xue Za Zhi 2017; 33:477-82.
12. Sica A, Erreni M, Allavena P, Porta C. Macrophage polarization in pathology. Cell Mol Life Sci 2015; 72:4111-26.
13. Van den Bossche J, Lamers WH, Koehler ES, et al. Pivotal Advance: Arginase-1-independent polyamine production stimulates the expression of IL-4-induced alternatively activated macrophage markers while inhibiting LPS-induced expression of inflammatory genes. J Leukocyte Biol 2012; 91:685-99.
14. Britto DD, Wyroba B, Chen W, et al. Macrophages enhance Vegfa-driven angiogenesis in an embryonic zebrafish tumour xenograft model. Dis Model Mech 2018; 11:dmm035998.
15. Jin MM, Wang F, Qi D, et al. A critical role of autophagy in regulating microglia polarization in neurodegeneration. Front Aging Neurosci 2018; 10:378.
16. Liu Y, Du Y, Wang H, Du L, Feng W-h. Porcine reproductive and respiratory syndrome virus (PRRSV) up-regulates IL-8 expression through TAK-1/JNK/AP-1 pathways. Virology 2017; 506:64-72.
17. Yan M, Hou M, Liu J, Zhang S, Liu B, Wu X, Liu G. Regulation of iNOS-derived ROS generation by HSP90 and Cav-1 in porcine reproductive and respiratory syndrome virus-infected swine lung injury. Inflammation 2017; 40:1236-44.
18. Lunney JK, Fang Y, Ladinig A, Chen N, Li Y, Rowland B, Renukaradhya GJ. Porcine reproductive and respiratory syndrome virus (PRRSV): pathogenesis and interaction with the immune system. Annu Rev Anim Biosci 2016; 4:129-54.
19. Liu M, Guo S, Hibbert JM, Jain V, Singh N, Wilson NO, Stiles JK. CXCL10/IP-10 in infectious diseases pathogenesis and potential therapeutic implications. Cytokine Growth F R 2011; 22:121-30.
20. Salem M, Tremblay A, Pelletier J, Robaye B, Sevigny J. P2Y6 Receptors regulate CXCL10 expression and secretion in mouse intestinal epithelial cells. Front

Pharmacol 2018; 9:149.
21. Ridiandries A, Tan J, Bursill C. The role of chemokines in wound healing. Int J Mol Sci 2018; 19:3217.
22. Henne KR, Tran TB, VandenBrink BM, et al. Sequential metabolism of AMG 487, a novel CXCR3 antagonist, results in formation of quinone reactive metabolites that covalently modify CYP3A4 Cys239 and cause time-dependent inhibition of the enzyme. Drug Metab Dispos 2012; 40:1429-40.
23. Hueso L, Ortega R, Selles F, et al. Upregulation of angiostatic chemokines IP-10/CXCL10 and I-TAC/CXCL11 in human obesity and their implication for adipose tissue angiogenesis. Int J Obesity 2018; 42:1406-17.
24. Zhu L, Yang T, Li L, et al. TSC1 controls macrophage polarization to prevent inflammatory disease. Nat Commun 2014; 5:4696.
25. Shang Y, Wang G, Yin S, et al. Pathogenic characteristics of three genotype II porcine reproductive and respiratory syndrome viruses isolated from China. Virol J 2013; 10:7.
26. Marshall A, Celentano A, Cirillo N, McCullough M, Porter S. Tissue-specific regulation of CXCL9/10/11 chemokines in keratinocytes: Implications for oral inflammatory disease. PloS one 2017; 12:e0172821.
27. Jiang J, Maxion H, Champion CI, Liu G, Kelly KA. Expression of CXCR3 on adaptive and innate immune cells contributes oviduct pathology throughout chlamydia muridarum infection. J Mucosal Immunol Res 2017; 1:104.
28. Ma HD, Ma WT, Liu QZ, et al. Chemokine receptor CXCR3 deficiency exacerbates murine autoimmune cholangitis by promoting pathogenic CD8(+) T cell activation. J Autoimmun 2017; 78:19-28.
29. Wang H, Li J, Zhong P, et al. Blocking CXCR3 with AMG487 ameliorates the blood-retinal barrier disruption in diabetic mice through anti-oxidative. Life Sci 2019; 228:198-207.
30. Chen Y, Yin D, Fan B, et al. Chemokine CXCL10/CXCR3 signaling contributes to neuropathic pain in spinal cord and dorsal root ganglia after chronic constriction injury in rats. Neurosci Lett 2019; 694:20-28.
31. Koren L, Barash U, Zohar Y, Karin N, Aronheim A. The cardiac maladaptive ATF3-dependent cross-talk between cardiomyocytes and macrophages is mediated by the IFNgamma-CXCL10-CXCR3 axis. Int J Cardiol 2017; 228:394-400.
32. Bonacchi A, Romagnani P, Romanelli RG, et al. Signal transduction by the chemokine receptor CXCR3: activation of Ras/ERK, Src, and phosphatidylinositol 3-kinase/Akt controls cell migration and proliferation in human vascular pericytes. J Biol Chem 2001; 276:9945-54.
33. Liu F, Qiu H, Xue M, et al. MSC-secreted TGF-beta regulates lipopolysaccharide-stimulated macrophage M2-like polarization via the Akt/FoxO1 pathway. Stem Cell Res Ther 2019; 10:345.
34. Xia JB, Mao CZ, Chen ZY, et al. The CXCL10/CXCR3 axis promotes cardiac microvascular endothelial cell migration via the p38/FAK pathway in a proliferation-independent manner. Exp Mol Pathol 2016; 100:257-65.
35. Funel N, Dini V, Janowska A, et al. Triticum vulgare extract modulates protein-kinase B and matrix metalloproteinases 9 protein expression in bv-2 cells: bioactivity on inflammatory pathway associated with molecular mechanism wound healing. Mediat Inflamm 2020; 2020:2851949.

JOURNAL OF BIOLOGICAL REGULATORS & HOMEOSTATIC AGENTS Vol. 34, no. 3, 1001-1005 (2020)

LETTER TO THE EDITOR

3D AND 2D ULTRASOUND EVALUATION OF THE UTERINE CORPUS: NORMAL APPEARANCES AND COMMON PITFALLS

C.L. PĂTRU[1,2], N. CERNEA[1,2], R.G. CĂPITĂNESCU[1,2], O. SÎRBU[1,2], M.C. MARINAȘ[1,2], L.C. ZORILĂ[1,2] and D.G. ILIESCU[1,2]

[1]University of Medicine and Pharmacy from Craiova, Romania; [2]Obstetrics and Gynecology Department, Emergency County Hospital from Craiova, Romania

Received October 9, 2019 – Accepted April 14, 2020

All Authors contributed equally to this paper

To the Editor,

The uterus represents a muscular, thick-walled, pear shaped organ of the female reproductive tract, lying in the lesser pelvic cavity. It represents a very dynamic organ, with different structural features according to the different stages of the female reproductive life (1). 2D ultrasound obtains a real-time view of the pelvis in a radiation-free process. 3D ultrasound adds a third imaging plane (the coronal view) which provides a more detailed pelvic ultrasound assessment. The coronal plane can assess uterine abnormalities by delineating the fundal contour of the uterus and detect the possible causes of abnormal uterine bleeding by assessing the entire inner endometrial lining. By using 3D ultrasound, Müllerian duct abnormalities or intrauterine fibroids can be determined. Transabdominal ultrasound provides a wide visualization field, being useful in assessing the uterine position, size and shape while the transvaginal approach enables a better structural evaluation, providing a higher resolution imaging. It should be performed with the patient in dorsal position, with a full bladder using a 3.5 MHz transducer, in Gray scale and Color Doppler mode. This helps for a better imaging of the uterus, by moving it in an upper position and providing a better acoustic window (2).

3D and 2D ultrasound

The normal and most common uterine position is anteversion and anteflexion. Transabdominal ultrasound shows an anterior position of the uterine fundus, towards to the urinary bladder, relative to the cervix. Other uterine positions are represented by retroflexion, retroversion and tilting of the uterus to either the left or the right side (3). Transabdominal assessment of an anteflexed or anteverted uterus provides a well ultrasonographic imaging, favorized by its superficial laying, behind the acoustic window provided by the urinary bladder and the perpendicular orientation of the ultrasonic beam to the uterine plane. On a midline sagittal section, the uterus appears bent towards the urinary bladder, with the endocervical and endometrial canals making a right angle at the level of the internal cervical ostium, while in retroflection, the uterine corpus is posteriorly bent. Transabdominal ultrasound evaluation of the uterus in a retroverted or retroflexed position is limited by

Key words: 2D ultrasound; 3D ultrasound; gynecology; uterus

Corresponding Author:
Marinas Marius Cristian, MD, PhD,
Emergency County Hospital Craiova,
University of Medicine and Pharmacy Craiova,
66 1Mai Avenue, 200628, Craiova, Romania
Tel./Fax: +040251 599228
e-mail: cristi_marinas84@yahoo.com

0393-974X (2020)
Copyright © by BIOLIFE, s.a.s.
This publication and/or article is for individual use only and may not be further reproduced without written permission from the copyright holder.
Unauthorized reproduction may result in financial and other penalties
DISCLOSURE: ALL AUTHORS REPORT NO CONFLICTS OF INTEREST RELEVANT TO THIS ARTICLE.

the attenuation of the ultrasound beam due to both the deeper travel of the ultrasounds into the pelvis and the parallel path among the length of the uterus. This is one reason why a uterus in such positions is better evaluated by transvaginal ultrasound (2, 3) (Fig. 1).

On a sagittal plane, the uterus is a piriform organ. Typically, it has a 3-layer structure consisting in endometrium, myometrium and the outer layer -serosa or the perimetrium. The inner layer of the uterus, the endometrium, represents the most active and dynamic one, because of the hormonal dependent structure, as a highly specialized tissue with and extremely important role in the reproductive function. The endometrial tissue consists in two layers that can be detected in this area, a superficial one, called "zona functionalis" and a deeper basalis layer (4).

Endometrial thickness is conventionally measured as the sum of the anterior and posterior layers detected on a mid-sagittal plane. Endometrium aspects vary during the menstrual period. In both menstrual and early proliferative phase of the menstrual cycle, the endometrium is imaged as a thin, echogenic, and slightly irregular line (3). The proliferative phase is characterized by an increased thickness of the endometrium and a trilaminar aspect, secondary to the hypoechoic aspect of the superficial layer. In this phase, the endometrium thickness measures between 10-16 mm. The secretory phase is characterized by the homogenous and echogenic aspect due to the hyperechoic transformation of the functional layer. At the end of the secretory phase, the endometrium measures up to 16 mm with a homogenous ultrasonographic aspect (5). Thickening of the

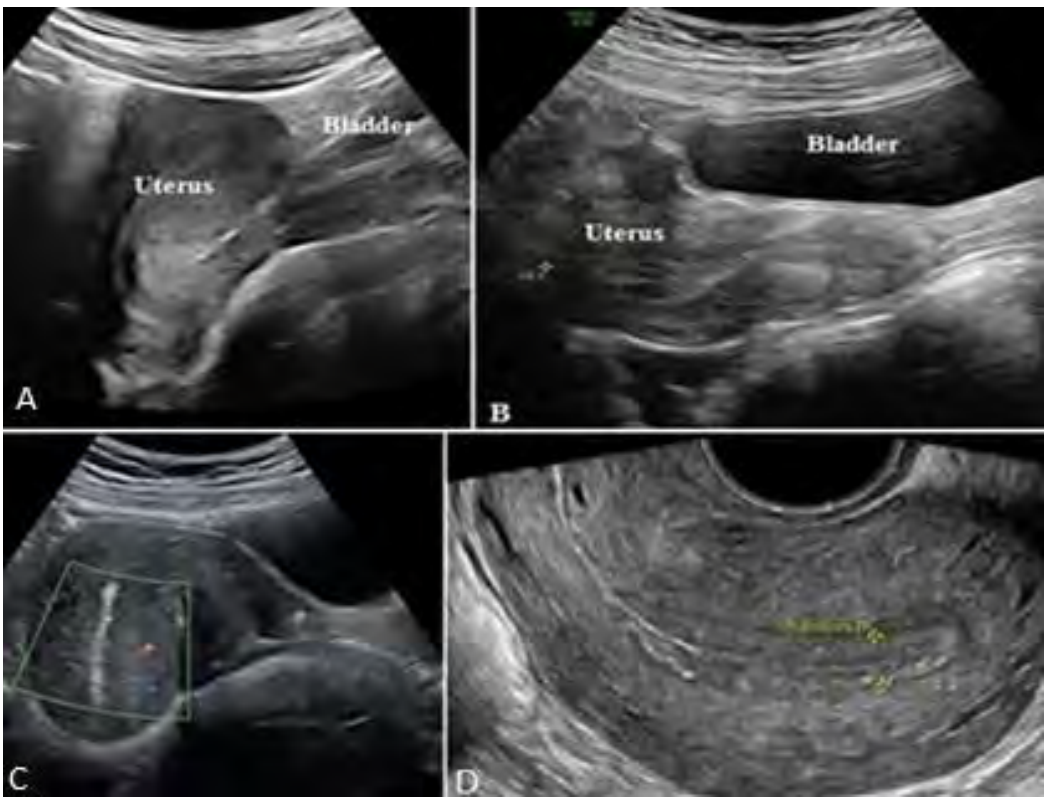


Fig. 1. *Transabdominal ultrasound.* ***A****) Anteverted and anteflected uterus. The image shows an anterior position of the uterine fundus towards to the urinary bladder.* ***B****) Retroverted and retroflected uterus.* ***C****) Transabdominal ultrasound of a retroverted uterus.* ***D****) Transvaginal ultrasound of a retroverted uterus that permits a better evaluation of the uterine layers in such position.*

endometrial layer represents the ultrasonographic aspect of endometrial hyperplasia. The endometrial thickness should be assessed in the late proliferative or secretory phase in premenopausal women, while postmenopausal examination can be performed at any time (6, 7). The measurement should be performed on a mid-sagittal plane including both anterior and posterior endometrial layers. If the entire endometrium is not completely visualized, it is recommended to report as non-measurable (8) (Fig. 2).

Endometrial polyps are considered the most frequent cause of postmenopausal vaginal bleeding

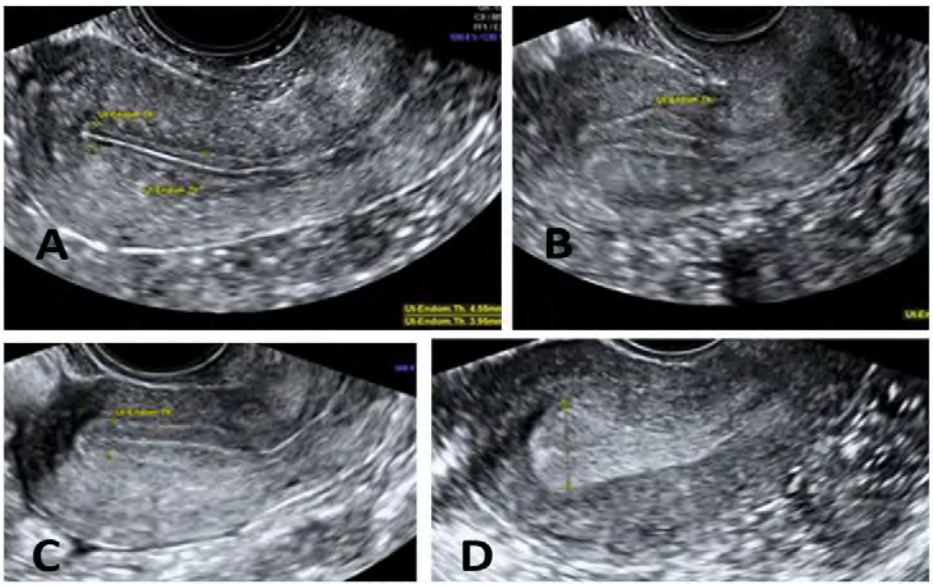


Fig. 2. *Transvaginal ultrasound. **A**) Early proliferative phase; **B**) proliferative phase with an evident trilaminar aspect of the endometrium; **C**) late proliferative phase, periovulatory, and **D**) secretory phase, with homogenous and echogenic aspect of the endometrium.*

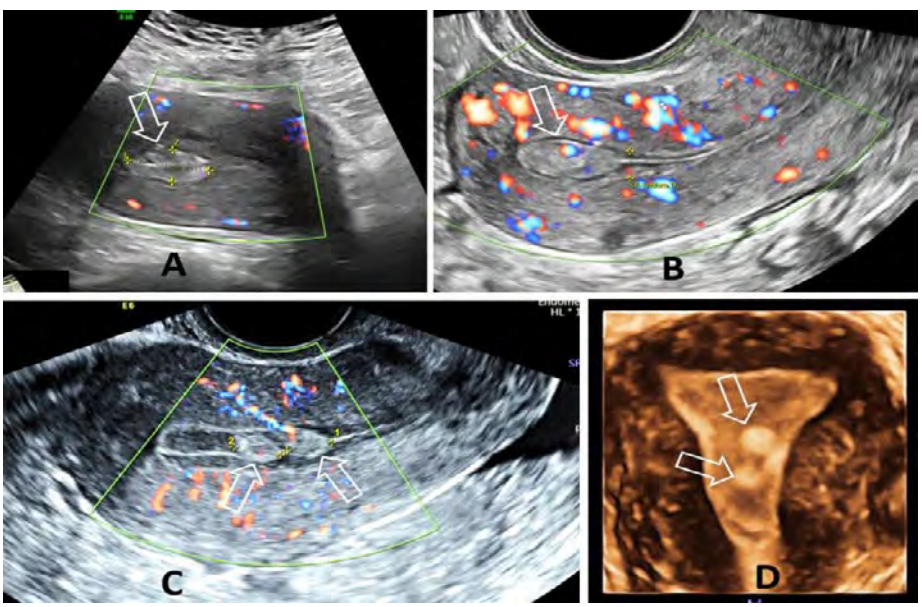


Fig. 3. *Endometrial polyps showing the features presented above. **A**) Fundal polyp, transabdominal evaluation; **B**) fundal polyp, transvaginal ultrasound; multiple endometrial polyps in 2D imaging (**C**) and 3D ultrasound (**D**).*

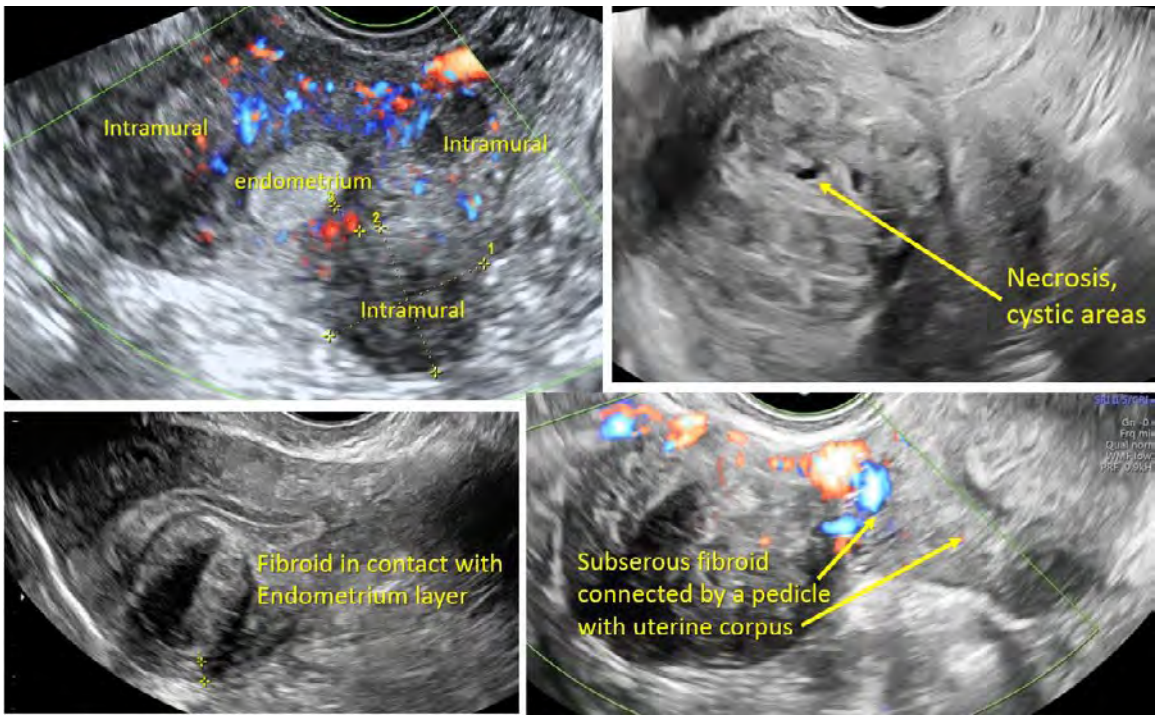


Fig. 4. *Various anatomo-clinical presentations of uterine fibromyomas, transvaginal ultrasound.*

(9). Polyps can be usually diagnosed by ultrasound as a nonspecific endometrial thickening or as a focal endometrial mass, surrounded by a hypoechoic halo with or without intralesional cystic changes. Doppler Color mode shows a vascular pedicle (10) (Fig. 3).

The myometrium can be assessed using both transabdominal and transvaginal ultrasound. Normal myometrium has a three-layer structure with different sonographic features (1). The inner layer is hypovascular and more hypoechoic than the surrounding structures. It is not always visible and frequently referred as subendometrial halo. Secondary to intrauterine interventions, this layer may present small hyperechogenic foci without posterior shadowing. The middle layer is characterized by homogenous aspect (2). The peripheral layer is thinner and less echogenic than the middle one (11). Leiomyomas are benign uterine tumors that can be detected on ultrasound as hypoechoic round masses; they can also have a isoechoic or echogenic aspect. Usually, small myomas have a homogenous structure. Myomas larger than 3 cm may have a mixed echostructure. Sometimes, leiomyomas have a hyperechoic contour due to compression of the surrounding myometrial tissue. Color Doppler mode detects a peripheral blood flow. Edema, cystic transformation, echogenic hemorrhagic areas and calcification are specific sonographic aspects for degenerative transformations (12) (Fig. 4).

DISCUSSION

The ultrasound evaluation of the uterine corpus is a feasible and easy examination. The 3D ultrasound added to routine gynecological scan can provide fast and accurate results in a relatively cost-effective setting.

3D ultrasound is a future method for an effective gynecological assessment because it provides complete information of the uterine anatomy and provide a high quality of patient care. 2D ultrasound no longer provides all the necessary information for all gynecological diagnoses.

Also, a limited approach to this method has to be considered as 3D ultrasound cannot be available as widely as 2D ultrasound.

REFFERENCES

1. Abrahams PH, Boon JM, Spratt JD, Hutchings RT. Clinical atlas of human anatomy. 6th ed. London: Elsevier; 2008.
2. Hall DA., Yoder IC. Ultrasound evaluation of the uterus. In: Callen PW, ed. Ultrasonography in obstetrics and gynecology. 3rd ed. Philadelphia, Pa: Saunders; 586 – 614, 1994.
3. Callen PW, ed. Ultrasonography of the uterus and ovaries. 3rd ed. Philadelphia, Pa: Saunders, 1994:821-27.
4. Fleischer AC, Kalemeris GC, Entman SS, Sonographic depiction of the endometrium during normal cycles. Ultrasound Med Biol 1986; 12:271-77.
5. Nalaboff KM, Pellerito JS, Ben-levi E. Imaging the endometrium: disease and normal variants. Radiographics 2001; 21(6):1409-24.
6. Goldstein SR, Nachtigall M, Snyder JR, Natchigall L. Endometrial assessment by vaginal ultrasonography before endometrial sampling in patients with postmenopausal bleeding. Am J Obstet Gynecol 1990; 163:119-23.
7. Granberg S, Wikland M, Karlsson B, Norström A, Friberg LG. Endometrial thickness as measured by endovaginal ultrasonography for identifying endometrial abnormality. Am J Obstet Gynecol 1991; 164:47-52.
8. Gull B, Karlsson B, Milsom I, Wikland M, Granberg S. Transvaginal sonography of the endometrium in a representative sample of postmenopausal women. Ultrasound Obstet Gynecol 1996; 7:322-27,
9. Lee SC, Kaunitz AM, Sanchez-Ramos L, Rhatigan RM. The oncogenic potential of endometrial polyps: a systematic review and meta-analysis. Obstet Gynecol 2010; 116(5):1197-205.
10. Talaat S, Mostafa N, Alrauof MA. Diagnostic value of ultrasound and Color Doppler in endometrial and cervical polyps, Med J Cairo Univ 2009: 77:397-403.
11. Levi CS, Holt SC, Lyons EA, Lindsay DJ, Dashefsky SM. Normal anatomy of the female pelvis. In: Callen PW, ed. Ultrasonography in obstetrics and gynecology. 4th ed. Philadelphia, Pa: Saunders 2000; 781-813.
12. Dolan MS, Hill C, Valea FA. Benign gynecologic lesions: vulva, vagina, cervix, uterus, oviduct, ovary, ultrasound imaging of pelvic structures. In: Lobo RA, Gershenson DM, Lentz GM, Valea FA, eds. Comprehensive Gynecology. 7th ed. Philadelphia, PA: Elsevier 2017; chap 18.

LETTER TO THE EDITOR

EFFECTS OF ANGIOTENSINOGEN AND INSULIN-LIKE GROWTH FACTOR 1 ON THE PATHOGENESIS OF DIABETIC NEPHROPATHY

CS. GAO[1], JJ. DONG[2], XF. YANG[3], L. YAN[2], J. LIANG[4] and HF. SUN[5]

[1]Department of Nephrology, The Fourth Hospital of Harbin Medical University, Harbin, China; [2]Department of Histology and Embryology, Mudanjiang Medical University, Mudanjiang, China; [3]Department of Pathophysiology, Mudanjiang Medical University, Mudanjiang, China; [4]Stem Cell Institute, Mudanjiang Medical University, Mudanjiang,China; [5]Department of Endocrinology and Nephrology, The Second Affiliated Hospital of Mudanjiang Medical University, Mudanjiang, China

Received November 11, 2019 – Accepted April 15, 2020

To the Editor,

Diabetic nephropathy (DN) is the major microvascular complication of diabetes mellitus (DM), and its incidence has been estimated to be about 33% in China (1). The pathogenesis of DN is relatively complicated as several factors are involved (2). Previous studies (3, 4) demonstrated that pathogenesis of DN is closely associated with synthesis and secretion of various cytokines *in vivo*; thus, the key to the treatment is to intervene and break the functions of these factors. Inuslin-like growth factor-l (IGF-1) is a protein having remarkable effects on the growth and metabolism of the body. Studies have found that IGF-1 is involved in the occurrence and development of DN; however, the results were not unified (5, 6). The effects of renin-angiotensin system (RAS) have significantly attracted scholars' attention. It has been demonstrated that angiotensinogen (AGT) plays a pivotal role in occurrence and development of chronic kidney disease (CKD) (7, 8); however, its relationship with DN remains elusive. Hence, in the present study, the serum levels of AGT and IGF-1 and urine of patients with DN were determined, and it was revealed that compared with patients without CKD, the serum levels markedly changed. Furthermore, the DN-based animal models were established to indicate the serum levels of AGT and IGF-1 and urine of the models and the localization study of AGT and IGF-1 in renal tissues, thereby clarifying the roles of AGT and IGF-1 in the pathogenesis of DN.

MATERIALS AND METHODS

Patients

A total of 60 patients who were admitted to Mudanjiang Medical University and met the diagnostic criteria of DM and DN between June 2017 and April 2019 were enrolled in the study. According to the conditions of CKD, the patients were divided into an early DN group (group A, 30 patients) anda clinical DN group (group B, 30 patients). Group A involved patients whose urine protein was negative, urine albumin excretion rate (UAER) was 30-300 mg/d, and serum creatinine (sCr) level was normal (< 105 umol/l). Group B included patients whose urine protein was positive or UAER > 300 mg/d, and sCr was normal or elevated, without urinary tract infections or other diseases related to kidney failure, heart failure, or tumors, without diabetic ketoacidosis or other acute complications related to DM during the previous 3 weeks. In addition, 30

Key words: diabetic nephropathy; AGT; IGF-1; diabetes mellitus

Corresponding Author:
Haifeng Sun,
Department of Endocrinology and Nephrology,
The Second Affiliated Hospital of Mudanjiang Medical University,
No. 15 Dong Xiaoyun Street,
Mudanjiang157000, Heilongjiang, China
e-mail: sunhaifeng1090@163.com

0393-974X (2020)
Copyright © by BIOLIFE, s.a.s.
This publication and/or article is for individual use only and may not be further reproduced without written permission from the copyright holder.
Unauthorized reproduction may result in financial and other penalties
DISCLOSURE: ALL AUTHORS REPORT NO CONFLICTS OF INTEREST RELEVANT TO THIS ARTICLE.

healthy volunteers were allocated to a control group (Con group). The study was approved by the Ethics Committee of The Fourth Hospital of Harbin Medical University, and all the patients signed an informed consent to participate in the study.

The diagnostic criteria for DM were as follows: typical symptoms, fasting blood glucose (FBG) ≥ 7.0 mmol/l (126 mg/dl) or postprandial blood glucose (PBG) ≥ 11.1 mmol/l (200 mg/dl); if there were no typical symptoms, and only FBG ≥ 7.0 mmol/l (126 mg/dl) or PBG ≥ 11.1 mmol/l (200 mg/dl), the test was repeated again; if the above-mentioned values were obtained again, the patients could be diagnosed as DM; in case of no typical symptoms, only FBG ≥ 7.0 mmol/l (126 mg/dl) or PBG ≥ 11.1 mmol/l (200 mg/dl) or glucose tolerance testing with 2 h value of blood glucose ≥ 11.1 mmol/l (200 mg/dl), the diagnosis of DM was indicated.

Exclusion criteria were as follows: factors that might affect the levels of IGF-1 (tumors, tuberculosis, liver damages, DM foot, other endocrine and metabolic diseases, surgeries, trauma, or other stress conditions) and AGT [taking ACE inhibitor (ACEI) and/or angiotensin II receptor antagonist (ARB) in the previous 2 months].

Detection of AGT and IGF-1 levels in serum and urine

In the morning, 2-3 mL of blood samples were drawn from the elbow vein, and 4 mL of urine samples were collected from each patient. The blood and urine samples were placed in non-anticoagulation tubes. After centrifugation, the supernatant was pipetted and sealed in a refrigerator at -20°C for further detection of the expression levels of AGT and IGF-1. Simultaneously, the FBG and renal function of each patient were detected by an automatic biochemical analyzer, and the UAER and glycated hemoglobin (HbA1c) were measured by urine microalbumin and a glycated hemoglobin analyzer. All the reagents and serum and urine samples were recovered to the room temperature. The levels of AGT and IGF-1 in rat urine and blood were measured in the same manner.

Experimental animals and grouping

A total of 32 male Sprague-Dawley rats were fed a standard, mixed-feed diet and given tap water. The temperature of the animal room was controlled at 22-26°C, and the light/dark cycle was 12 h/12 h. After one week of adaptive feeding in the SPF animal room, 32 rats were randomly divided into a Model group (n=16) and a control group (Con group, n=16). In accordance with different periods of observation (at the 5th and 10th weeks), the rats were further divided into two sub-groups, with 8 rats in each sub-group.

Establishment of an animal model

Each rat in the Model group was given a single injection of streptozotocin (STZ) at a dosage of 65 mg/kg body weight through intraperitoneal injection. After 72 h, the blood sample of each rat was collected from the caudal vein for detection of the level of FBG. The level of FBG > 16.65 mmol/l indicated DM. After 3 weeks, the level of UAER > 30 mg/24 h indicated successful establishment of DN rat models. Each rat in the Con group was intraperitoneally injected with an equal dosage of citrate-sodium citrate buffer. All experimental rats were kept in cages, normally fed, and were allowed to drink water freely.

Kidney function, 24h urine microalbumin, and blood glucose of rats

At the end of the 5th and 10th weeks of feeding, rats in both groups were weighed. Blood samples were drawn from caudal veins for detection of FBG levels. Urine samples were collected for measurement of UAER levels. After being anesthetized, the rats in each group were fixed in the supine position. Routine disinfection was performed. Under aseptic conditions, 3 mL of blood samples were drawn from the heart in the morning. The samples were centrifuged for 10 min to collect the serum, which was then maintained at -20°C for detecting corresponding serum indicators. After collection of blood samples, rats were submitted to an automatic biochemical analyzer to detect their renal functions. The urine microalbumin was measured by the endpoint method, and the level of blood glucose was detected by the oxidase method.

Expression levels of AGT and IGF-1 in rat renal tissues

The levels of AGT and IGF-1 in rat urine and serum were measured in the same manner. The steps for detecting the expression levels of AGT and IGF-1 in the rat renal tissues were as follows: Each rat was sacrificed to obtain the kidney tissues. The kidney capsule was separated, and the mass was weighed. The left kidney was fixed in formaldehyde and embedded into paraffin for

preparation of paraffin-embedded tissues. The paraffin-embedded tissues were routinely dewaxed. and the excessive paraffin wax around the kidney tissues was cut off. The fixed and repaired paraffin block was placed on the microtome; before being sectioned, the thickness of tissues was adjusted. Next, in the 46°C section stretcher, the sectioned tissues were stretched, patched, baked, dewaxed, re-hydrated, and stained by hematoxylin and eosin (H&E). After H&E staining, the nucleus was blue, and the cytoplasm, muscle, and connective tissues were red to varying degrees.

For immunohistochemical staining of AGT and IGF-1, the paraffin-embedded tissues were sectioned with a thickness of 3-4 μm. The sections to be processed were baked at 60°C for 1 h. The sections were dewaxed by xylene and hydrated by ethanol. After antigen retrieval, the sections were dripped with blocking buffer and incubated at 37°C for 30 min. The sections were dripped with the primary antibody and maintained at 4°C overnight. Next, the sections were washed with TBS-T for 3×5 min and were dripped with blocking buffer and incubated at 37°C for 10 min. The sections were dripped with a biotinylated secondary antibody that was diluted by the antibody dilution and incubated in a humidity chamber at 37°C for 30 min. Next, the sections were washed with TBS-T for 3×5 min, and then dripped with Tween-20 and incubated at 37°C for 20 min. The sections were dripped with horseradish peroxidase-streptavidin (HRP-SA) complex that was diluted by the primary antibody (1:50-200, final concentration of 5-20 nM) and incubated at 37°C for 30 min. Afterwards, the sections were washed with TBS-T for 3×5 min, and then with TBS for 2×5 min. The color of the sections was developed by 3,3'-diaminobenzidine (DAB) and rinsed with tap water, counterstained, dehydrated, decolored, and sealed. The primary antibody was replaced with PBS as a negative control, and the images were observed under a microscope.

Statistical analysis

Statistical analysis was carried out by using SSPS 22.0 software (IBM, Armonk, NY, USA). All results were expressed as mean ± standard deviation (SD). One-way analysis of variance (ANOVA) was used for making comparison between groups. Pearson's correlation coefficient was used for correlation analysis. $P<0.05$ was considered statistically significant.

RESULTS

Patients' baseline clinical data

No significant differences in age and blood pressure between the groups were found ($P>0.05$), while the differences in blood glucose and sCr between the groups were statistically significant (Table I). With the progression of the disease, the UAER level of patients in each group was gradually increased, and the difference between the groups was statistically significant ($P<0.05$).

Epression levels of AGT and IGF-1

As shown in Table II, the expression levels of AGT in patients of group A and group B were significantly higher than those in the Con group ($P<0.05$). The urine AGT levels of patients in group A were markedly higher than those in the Con group ($P<0.05$), and those in group B were remarkably higher than those in group A ($P<0.05$).

The expression levels of IGF-1 in patients in group A and group B were significantly higher than those in the Con group ($P<0.05$). The urine IGF-1 levels of patients in group A were notably higher than those in the Con group ($P<0.05$), and the urine IGF-1 levels of patients in group B were significantly higher than those in patients with early type 2 DN ($P<0.05$).

Correlation analysis of AGT, IGF-1, and each detection indicator of patients

For patients with type 2 DN, the blood AGT, urine AGT, and urine FBG were not correlated with each other, and the correlation coefficients r were -0.147 ($P>0.05$) and 0.293 ($P>0.05$), respectively; the urine AGT and UAER levels were positively correlated with each other, and the correlation coefficient r was 0.617 ($P<0.05$); the blood IGF-1 and urine IGF-1 were not correlated with each other, and the correlation coefficient r was -0.109 ($P>0.05$); the blood IGF-1 and FBG were negatively correlated with each other, and the correlation coefficient r was -0.723 ($P<0.05$); the urine IGF-1 and UAER were positively correlated with each other, and the correlation coefficient r was 0.533 ($P<0.05$).

Table I. *Patients' baseline clinical data and detection indicators in each group*

Indicators	Con group	Group A	Group B	F-value	P-value
Age (years)	62.13±17.48	61.59±18.29	63.06±16.65	0.07	>0.05
FBG (mmol/l)	5.92±1.77	10.47±2.85*	11.03±2.26*	28.19	<0.05
PBG 2h (mmol/l)	7.85±2.45	15.42±3.51*	14.78±3.85*	42.19	<0.05
HbA1c (%)	6.19±1.17	9.74±2.04*	9.86±2.48*	33.29	<0.05
Systolic blood pressure (mmHg)	117.38±8.39	119.55±10.83	120.48±11.29	0.11	>0.05
Diastolic blood pressure (mmHg)	76.94±6.53	80.45±9.10	79.11±8.99	2.93	>0.05
sCr (umol/l)	75.05±19.46	78.76±31.36	110.20±32.43**	13.18	<0.05
UAER (mg/d)	29.87±19.20	162.38±47.35*	498.37±138.54*#	92.39	<0.05

*Compared with Con group, *P<0.05; compared with group A, #P<0.05.*

Table II. *Compare of AGT and IGF-1 levels in blood and urine of patients in each group*

Indicators	Con group	Group A	Group B	F-value	P-value
Blood AGT (ug/ml)	50.11±33.39	108.82±38.35*	113.91±37.35*	43.32	<0.05
Urine AGT (ug/ (g Cr))	25.45±20.27	94.38±42.18*	184.33±47.29*#	84.42	<0.05
Blood IGF-1 (ug/l)	137.28±31.27	189.43±48.34*	190.75±50.18*	19.39	<0.05
Urine IGF-1 (ug/l)	6.03±1.38	14.27±2.92*	17.22±2.58*	128.38	<0.05

*Compared with Con group, *P<0.05; compared with group A, #P<0.05.*

Changes in detection indicators of rats in each group

It was revealed that the bodyweight of rats in the Con group was remarkably increased with the progression of the disease (Table III); however, the body weight was decreased in the Model group (P<0.05). The FBG level of rats after successful establishment of the model was notably increased and maintained at a relatively high level. The FBG level of rats in the Con group was normal at the same time. At the 5th week, no significant difference in sCr between Model group and Con group was found, butt was significantly increased at the 10th week. The UAER level of the successfully modeled rats was markedly increased continuously with the progress of the disease. The UAER level of rats in the Con group was always found to be normal, and the difference between the two groups was statistically significant (P<0.05).

In the Model group, the levels of blood AGT and urine AGT were higher than those in the Con group at different stages, which were markedly increased with the progress of the disease; the differences between different periods were statistically significant (P<0.05). In the Model group, the levels of blood IGF-1 were lower than those in the Con group, and were continuously decreased significantly as the disease progressed. Changes in urine IGF-1 levels were as same as changes in urine AGT levels.

Table III. *Compare of detection indicators of rats in each group*

Indicators	Con group		Model group	
	At the 5th week	At the 10th week	At the 5th week	At the 10th week
Body weight (g)	248.24±8.43	351.29±9.49#	240.23±13.84	218.35±16.11*#
FBG (mmol/l)	5.04±0.95	5.93±1.03	25.36±2.35*	25.45±2.61*
sCr (umol/l)	30.39±4.17	32.11±5.28	36.93±9.33	118.39±12.94*#
UAER (mg/d)	3.77±0.87	3.63±0.99	32.36±3.94*	68.55±7.29*#
Blood AGT (ng/ml)	1248.45±30.28	1265.31±27.39	2092.66±62.28*	2118.24±84.54*
Urine AGT (ng/ml)	18.45±1.62	19.33±1.46	36.39±3.15*	87.74±7.28*#
Blood IGF-1 (ng/ml)	3.31±0.36	3.48±0.34	2.19±0.27*	1.44±0.22*#
Urine IGF-1 (ng/ml)	0.23±0.03	0.21±0.04	0.48±0.06*	0.75±0.08*#

*Compared with Con group, *P<0.05; compared with the same group at the 5th week, #P<0.05.*

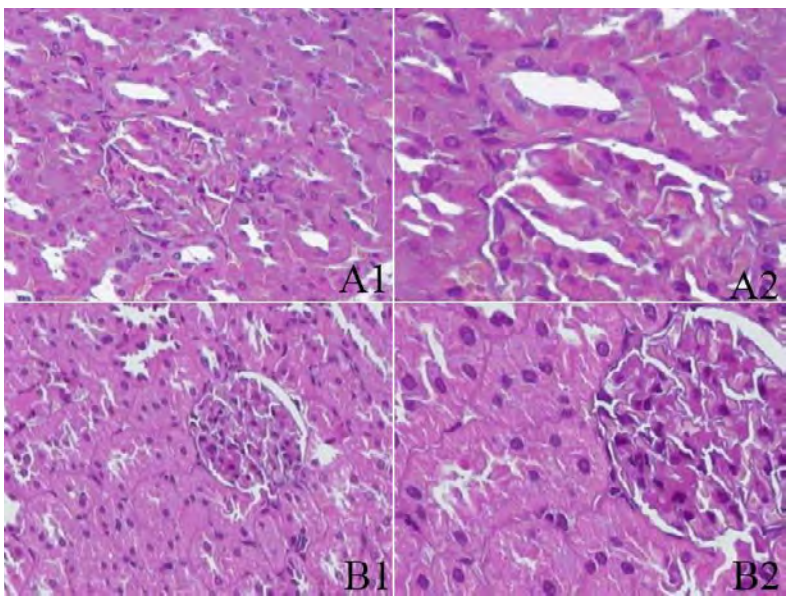


Fig. 1. *Results of HE staining of rat kidney tissues. **A**) Con group, **B**) Model group; 1:×200, 2: ×400.*

Therefore, the differences between each period were statistically significant (P<0.05).

Pathological changes in rat kidneys

In the Con group, the size of renal glomerulus was consistent, the corresponding number did not significantly increase, the glomerular capillary basement membrane showed no obvious abnormalities, the mesangial area revealed no obvious hyperplasia, and the renal tubules and renal interstitial illustrated no obvious inflammatory cell infiltration, which was consistent with normal rat renal tissues after execution.

In the Model group, the majority of the glomerular capillary basement membrane was thickened, the mesangial matrix showed hyperplasia, the cells were proliferated, the tubular epithelial cells were turbid, and the renal interstitial showed congestion with a small amount of inflammatory cell infiltration, which was consistent with the pathological manifestations of DN (Fig. 1).

Immunohistochemical staining of AGT and IGF-1 in rat kidney tissues

The expression levels of AGT and IGF-1 in renal glomerular and renal tubular cells were brown granule-like and mainly expressed in renal tubular epithelial cells. AGT and IGF-1 proteins were slightly expressed in kidney tissues of rats in the Con group, and were significantly increased in the Model group; the differences between the two groups were statistically significant ($P<0.05$) (Table IV).

Correlation analysis of factors between rat AGT

The urine AGT levels and the expression levels of AGT in kidney tissues of DN rats were significantly correlated, and the correlation coefficient r was 0.873 ($P<0.05$). The urine AGT levels and the blood AGT levels of DN rats were not remarkably correlated, and the correlation coefficient r was 0.054 ($P>0.05$).

DISCUSSION

The present study disclosed that blood AGT levels in patients with type 2 DN were significantly higher than those in healthy individuals, however, no differences were observed between the DN-based groups, indicating that the levels of blood AGT could not reflect the degree of damage caused by type 2 DN. AGT is a macromolecular substance, and AGT in the circulation cannot be remarkably filtered through renal glomerulus (9), indicating that AGT appearing in the urine is mainly secreted by the kidney (10). Hence, changes in urine AGT levels in the current study demonstrate that urine AGT may be an indicator of the degree of renal damages in type 2 DN.

The results of the present research showed that blood AGT levels of rats in different periods were significantly higher than those in the Con group, and no significant changes were found with progress of the disease; meanwhile, the urine AGT levels were notably higher than those in the Con group, and were gradually increased with the progress of the disease. In addition, it was revealed that the expression levels of AGT in the kidney tissues of early DN rats were significantly increased compared with Con group, and were gradually elevated with the progression of the disease. The results suggested that the expression level of AGT in kidney can reflect the extent of DN lesions, which is consistent with the research of Zhuang et al. (11). The present study revealed that the expression of IGF-1 in kidney tissues of early DN rats was higher than that in the Con group, while that was decreased to the same level as Con group in the later stage. The results suggested that IGF-1 had an initial action in the occurrence of DN, and no significant changes were noted in IGF-1 in kidney tissues in later stage compared with Con group, which may be related to the decrease of blood IGF-1 levels, down-regulation of IGF-1 mRNA expression, clearing IGF-1 by kidney, etc.

In summary, AGT and IGF-1 are involved in the pathogenesis of DN, and both are risk factors for damages to kidneys. Thus, inhibition of the expression levels of AGT and IGF-1 may provide a new approach to control DN.

Table IV. *Expression levels of AGT and IGF-1 in kidney tissues of rats in each group*

Indicators	Con group		Model group	
	At the 5th week	At the 10th week	At the 5th week	At the 10th week
AGT (ng/ml)	1.13±0.09	1.12±0.11	1.86±0.12*	2.37±0.11*#
IGF-1 (ng/ml)	0.21±0.02	0.20±0.02	0.54±0.03*	0.22±0.03#

*Compared with Con group, *P<0.05; compared with the same group at the 5th week, #P<0.05.*

ACKNOWLEDGEMENT

This work was supported by Mudanjiang Science and Technology Planning Project (Z2018s043).

REFERENCES

1. Fan L, Zhang Y, Zhu J, Song Y, Lin J. Association of vitamin D deficiency with diabetic peripheral neuropathy and diabetic nephropathy in Tianjin, China. Asia Pac J Clin Nutr 2017; 27(3):599.
2. Qiao YC, Chen YL, Pan YH, et al. Changes of transforming growth factor beta 1 in patients with type 2 diabetes and diabetic nephropathy: A Prisma-compliant systematic review and meta-analysis. Medicine (Baltimore) 2017; 96(15):e6583.
3. Donate-Correa J, Martín-Núñez E, Muros-de-Fuentes M, Mora-Fernández C, Navarro-González JF. Inflammatory cytokines in diabetic nephropathy. J Diabetes Res 2015; 2015:948417.
4. Gu T, Falhammar H, Gu HF, Brismar K. Epigenetic analyses of the insulin-like growth factor binding protein 1 gene in type 1 diabetes and diabetic nephropathy. Clin Epigenetics 2014; 6(1):10.
5. Garaysevilla ME, Nava LE, Malacara JM, Wróbel K, Wróbel K, Pérez U. Advanced glycosylation end products (AGEs), insulin-like growth factor-1 (IGF-1) and IGF-binding protein-3 (IGFBP-3) in patients with type 2 diabetes mellitus. Diabetes Metab Res Rev 2000; 16 (2):106-113.
6. Shi GJ, Shi GR, Zhou JY, et al. Involvement of growth factors in diabetes mellitus and its complications: A general review. Biomed Pharmacother 2018; 101:510-27.
7. Iaina NL, Iaina A, Raz I. The emerging role of NO and IGF-1 in early renal hypertrophy in STZ-induced diabetic rats. Diabetes Metab Res Rev 2011; 27(3):235-43.
8. Zhuang Z, Bai Q, Lata A, Liang Y, Zheng D, Wang Y. Changes of urinary angiotensinogen concentration and its association with urinary proteins in diabetic rats. Int J Clin Exp Pathol 2015; 8(10):11946-56.
9. Moussa A, Triki S, Hamdouni H, et al. Genetic variation in the renin-angiotensin system and diabetic nephropathy in the Tunisian population. Clin Lab 2017; 63(3):469-77
10. Nakatani S, Ishimura, E, Naganuma, T, et al. Poor glycemic control and decreased renal function are associated with increased intrarenal RAS activity in Type 2 diabetes mellitus. Diabetes Res Clin Pract 2014; 105(1):40-46.
11. Zhuang Z, Bai Q, Lata A, Liang Y, Zheng D, Wang Y. Increased urinary angiotensinogen precedes the onset of albuminuria in normotensive type 2 diabetic patients. Int J Clin Exp Pathol 2015; 8(9):11464-9

LETTER TO THE EDITOR

ROLE OF miRNA-499-5p IN PATIENTS WITH ATRIAL FIBRILLATION AND HEART FAILURE

D.-L. WANG*, C. HAN*, L.-D. ZHAO*, G.-Y. HU, Y. JIANG, C.-G. LI, L.-L. SHI and M.-J. ZHOU

Department of Emergency Medicine, Shanghai Sixth People's Hospital East, Shanghai, China

Received February 3, 2020 – Accepted April,15, 2020

*These authors contributed equally to this work

To the Editor,

Atrial fibrillation (AF) is one of the most common arrhythmias. In recent years, the prevalence of AF in China has increased with age, and the mortality associated with heart failure (HF) has gradually increased (1). Studies have found that AF can increase the occurrence of HF (2). Age, diabetes, hypertension and myocardial infarction are common risk factors for AF as well as HF, and genetic factors are also endogenous causes of both (3). MicroRNA-499-5p is an evolutionarily conserved muscle-specific microRNA that is highly expressed in the ventricle (4, 5). *In vivo* and *in vitro* studies (6-8) have revealed that miR-499 expression changes in myocardial tissues or cells during ischemia, hypoxia or oxidative stress, but the conclusions are inconsistent. However, there is no research on the relationship between microRNA-499-5p level and AF and/or HF. Therefore, the serum microRNA-499-5p level in AF and/or HF patients as well as the correlations of microRNA-499-5p with the clinicopathological parameters and biochemical parameters were analyzed in this study to explore the function of microRNA-499-5p in the progression of AF and/or HF.

MATERIALS AND METHODS

Clinical information

Forty patients with AF who were admitted to hospital from May 2016 to June 2018 were included as the AF group, 40 patients with HF as HF group, and 40 patients with HF complicated AF as HF+AF group. Forty healthy patients undergoing physical examination were selected as the control group. The diagnosis of diseases was based on the diagnostic references (9). Patients with cerebrovascular accidents, acute infections, chronic inflammation, severe arrhythmias, chemotherapy malignancies, liver and kidney failure, mental disorders or pregnancy were excluded. The study protocol met the ethical guidelines of the Helsinki Declaration of 1975, and informed consents were obtained from all patients. This study was approved by the Hospital Institutional Review Board and the Ethics Committee of Shanghai Sixth People's Hospital East.

Blood samples

The fasting venous blood of the patients was collected in a vacuum drying tube without RNase on admission or during physical examination, and the serum was centrifuged at 3000 r/min for 10 min, and transferred to a nuclease-free Eppendorf tube and stored at -80°C.

Quantitative real-time polymerase chain reaction (qRT-PCR)

Total RNAs were extracted using the TRIzol kit (Invitrogen, Carlsbad, CA, USA) and reversely transcribed into complementary deoxyribose nucleic acids (cDNAs). QRT-PCR was performed in the PRISM 7900HT detection system using SYBR fluorescence kit (Applied Biosystems, Foster City,

Key words: microRNA-499-5p; atrial fibrillation; heart failure

Corresponding Author:
Minjie Zhou, MD
Department of Emergency Medicine,
Shanghai Sixth People's Hospital East
222nd West Huanhu Road No.3,
Pudong New Area, Shanghai 201306, China
Tel.: 86018930177632
e-mail: mingjie19850114@163.com

0393-974X (2020)
Copyright © by BIOLIFE, s.a.s.
This publication and/or article is for individual use only and may not be further reproduced without written permission from the copyright holder.
Unauthorized reproduction may result in financial and other penalties
DISCLOSURE: ALL AUTHORS REPORT NO CONFLICTS OF INTEREST RELEVANT TO THIS ARTICLE.

CA, USA). MicroRNA-499-5p upstream primer: 5'-GGGGTTAAGACTTGCAGTG-3', downstream primer: 5'-CAGTGCGTGTCGTGGAGT-3', and U6: upstream primer: 5'-CTCGCTCGGCAGCACA-3', downstreamprimer:5'-AACGTTCACGAATTTGCGT-3'. Reaction system (total volume 25 μL): 2.5 U cDNA, 1 μL of the upstream primer, 1 μL of the downstream primer, 12.5 U SYBR Green I PCR master Mix, and 8 μL of diethyl pyrocarbonate (DEPC) water. The relative expression levels of genes were calculated according to the $2^{-\Delta\Delta Ct}$ method with U6 as an internal reference.

Observation indexes

Age, sex, history of hypertension, diabetes and smoking were recorded for the 4 groups, as well as drugs taken by the 3 disease groups. Thereafter, the systolic blood pressure, diastolic blood pressure, body mass index, creatinine, total cholesterol (TC), triglycerides (TG), low-density lipoprotein (LDL), high-density lipoprotein (HDL), N-terminal pro-brain natriuretic peptide (NT-proBNP), left ventricular ejection fraction (LVEF) and left atrial diameter (LAD) were compared among the 4 groups at admission or during physical examination.

Statistical analysis

Data were expressed as mean ± standard deviation ($\bar{x}$±s). Statistical analysis was performed using Statistical Product and Service Solutions (SPSS) 20.0 software (IBM, Armonk, NY, USA), and comparison between the groups was performed using an independent sample *t*-test, while multiple sets of comparisons were evaluated by analysis of variance. Bonferroni or Fisher's Least Significant Difference (LSD) post hoc test was performed, and Pearson regression was used to analyze the association between microRNA-499-5p and cardiac function. After adjusting for differences in confounding factors, multivariate logistic regression analysis was carried out to assess the independent association of microRNA-499-5p with cardiac function index parameters. The difference was statistically significant at $p<0.05$. *, $^{\#}$, and $^{\&}$, $p<0.05$.

Table I. *Comparison of clinical data and some biochemical indicators in the study*

Variable	Control group	AF group	HF group	AF+HF group	*p*
Age	63.18±7.75	61.23±6.85	62.91±8.08	63.21±7.45	0.895
Sex (male/female)	20/20	20/20	20/20	20/20	NA
BMI (kg/m2)	22.13 ± 3.21	22.73 ± 3.01	22.61±3.17	23.13 ± 3.77	0.339
SBP (mmHg)	124.21±17.35	131.73±20.09	125.11±19.76	128.17±20.23	0.009*
DBP (mmHg)	81.32±8.07	82.11±9.19	82.87±8.32	81.17±8.16	0.191
TC (mmol/L)	4.32±1.16	4.46±1.17	4.38±1.04	4.46±1.34	0.847
HDL-C (mmol/L)	1.34±0.41	1.48±0.64	1.31±0.51	1.47±0.82	0.397
LDL-C (mmol/L)	2.03±1.02	2.11±1.23	2.25±1.28	2.41±1.52	0.035*
TG (mmol/L)	1.56±0.46	1.67±0.64	1.71±0.72	1.68±0.69	0.359
Scr (μmol/L)	116.31±25.42	118.12±26.99	118.32±26.48	119.32±25.71	0.074
Hypertension (n)	20	23	25	21	0.684
Diabetes mellitus (n)	9	9	11	8	0.881
Smoking (n)	8	11	6	10	0.540

*BMI: body mass index; SBP: systolic blood pressure; DBP: diastolic blood pressure; TC: total cholesterol; HDL-C: high-density lipoprotein cholesterol; LDL-C: low-density lipoprotein cholesterol; TG: triglyceride; Scr: serum creatinine. *p<0.05*

RESULTS

Clinical data and biochemical indicators

A series of clinical data of all groups of patients, including age, sex, BMI, systolic/diastolic blood pressure, TC, TG, LDL, HDL, creatinine, history of hypertension, diabetes history and smoking status were compared separately. Differences in the clinical indexes SBP and LDL-C were found ($p<0.05$), but no differences were observed in the other indexes ($p>0.05$) (Table I). The above results indicated that the clinical data of the patients were balanced and comparable.

Differential expression of serum microRNA-499-5p in 4 groups

To explore the specific function of microRNA-499-5p, qRT was applied to detect the expression levels of serum miRNA-499-5p in the patients, which revealed that microRNA-499-5p was markedly increased in the AF and/or HF groups than that in the control group. Meanwhile, microRNA-499-5p was highly expressed in patients from the HF group than that from the AF group. In addition, microRNA-499-5p expression in the HF+AF group was also remarkably increased than that in the AF group as well as the HF group ($p<0.05$) (Fig. 1). The above results demonstrated that high expression of microRNA-499-5p in the serum of patients with AF, HF and AF combined with HF may affect the progression of AF as well as HF.

Cardiac function indicators

To further clarify whether there were differences in cardiac function between the four groups of subjects, statistical analysis was performed. The results demonstrated that lg (NT-proBNP), LVEF, and LAD were remarkably different among different groups. Compared with those in the control group, lg (NT-proBNP) and LAD were markedly increased in the other 3 groups. Besides, lg (NT-proBNP) and LAD were also increased in patients with AF+HF than in the AF or the HF group. On the other hand, LVEF was remarkably lower in the 3 groups of patients than that in the control group, and it was also markedly lower in AF+HF group than that in AF and HF groups (Table II). The above results indicated that there were differences in the cardiac function indicators including lg (NT-proBNP), LVEF, and LAD among AF, HF and AF+HF patients.

Pearson correlation analysis between microRNA-499-5p and cardiac function indexes in patients

To further explore whether there was a correlation between serum miRNA-499-5p level and cardiac function in patients, Pearson correlation analysis was performed, and it was found that the expression of miRNA-499-5p was positively correlated with lg (NT-proBNP) ($r=0.876$, $p=0.019$) and LAD ($r=0.751$, $P<0.001$), while it was reversely correlation with LVEF ($r=-0.599$, $p=0.031$) (Table III). These results suggested that microRNA-499-5p might positively regulate lg (NT-proBNP) and LAD and reversely regulate LVEF.

Multivariate logistic regression analysis of microRNA-499-5p expression

From the above results, it could be concluded that microRNA-499-5p expression had a certain correlation with cardiac function indicators, which might affect the occurrence and development of AF and/or HF. To further explore the factors affecting the

Table II. *Comparison of cardiac function indicators in study patients*

Variable	Control group	AF group	HF group	AF+HF group	*p*
lg (NT-proBNP)	2.33±0.78	3.54±0.56*	4.12±0.76$^{*\#}$	4.98±0.51$^{*\#\&}$	<0.001
LVEF (%)	61.22±5.13	57.43±5.97*	50.67±5.11$^{*\#}$	48.78±4.97$^{*\#\&}$	<0.001
LAD (mm)	38.21±4.98	44.12±6.98*	47.17±5.78$^{*\#}$	45.88±4.76$^{*\#\&}$	<0.001

NT-proBNP: N-terminal proB-type natriuretic peptide; LVEF: left ventricular ejection fraction; and LAD: left atrial dimension. $^{*}p<0.05$ vs Control group; $^{\#}p<0.05$ vs. AF group; and $^{\&}p<0.05$ vs HF group.

Table III. *Pearson correlation analysis of microRNA-499-5p and cardiac function in patients.*

Variable	*r*	*p*
lg (NT-prong)	0.876	0.019*
LVEF (%)	-0.599	0.031*
LAD (mm)	0.751	<0.001*

*NT-proBNP: N-terminal proB-type natriuretic peptide; LVEF: left ventricular ejection fraction; LAD: left atrial dimension. *p<0.05 vs Control group, #p<0.05 vs AF group, and &p<0.05 vs HF group.*

expression of microRNA-499-5p, the confounding factors including SBP and LDL-C were adjusted in this study, and the multivariate logistic regression analysis was conducted, which revealed that lg (NT-proBNP), LVEF and LAD were factors influencing microRNA-499-5p level (Table IV). This result indicated that microRNA-499-5p expression was independently affected by lg (NT-proBNP), LVEF and LAD.

DISCUSSION

Increasing evidence has shown that microRNAs are involved in the progression of AF as well as HF, but the specific mechanisms are not fully explained. Hence, in this study, the serum microRNA-499-5p level in AF and/or HF patients was examined, and the potential of microRNA-499-5p as a biomarker for AF and/or HF was investigated. It was discovered that serum microRNA-499-5p level was markedly higher in patients with HF and/or AF than in healthy controls, and it was the highest in the HF+AF group. These results indicated serum microRNA-499-5p level was related to the development, progression and severity of AF as well as HF.

At present, cardiac function indicators include NT-proBNP levels, LVEF and LAD. Therefore, in this study, these cardiac function indicators were also detected in the four groups studied. As a result, patients with AF and or HF had higher NT-proBNP levels, lower LVEF levels and larger LAD, indicating that the above cardiac function indicators were closely associated with the progression of AF as well as HF. It is speculated that NT-proBNP levels, LVEF and LAD can be used as effective serum biomarkers of cardiac function in patients with heart disease (10). To fully understand the correlation between microRNA-499-5p levels and cardiac function, Pearson correlation analysis and multivariate logistic regression analysis were performed to explore its underlying mechanisms. The results showed that NT-proBNP levels, LVEF and LAD were independent factors affecting microRNA-499-5p expression, which was reversely correlated with LVEF, and positively correlated with the logarithm of NT-proBNP and LAD. This suggested that the aberrantly expressed microRNA-499-5p might be the basis for changes in cardiac function

Table IV. *Multivariate logistic regression analysis of microRNA-499-5p expression*

Variable	*OR*	95%*CI*	*p*
lg (NT-proBNP)	1.453	1.224-4.832	0.038*
LVEF (%)	0.852	0.521-2.393	0.011*
LAD (mm)	1.287	1.171-3.872	0.024*

*NT-proBNP: N-terminal proB-type natriuretic peptide; LVEF: left ventricular ejection fraction; and LAD: left atrial dimension. *p<0.05 vs. Control group; #p<0.05 vs. AF group; and &p<0.05 vs. HF group.*

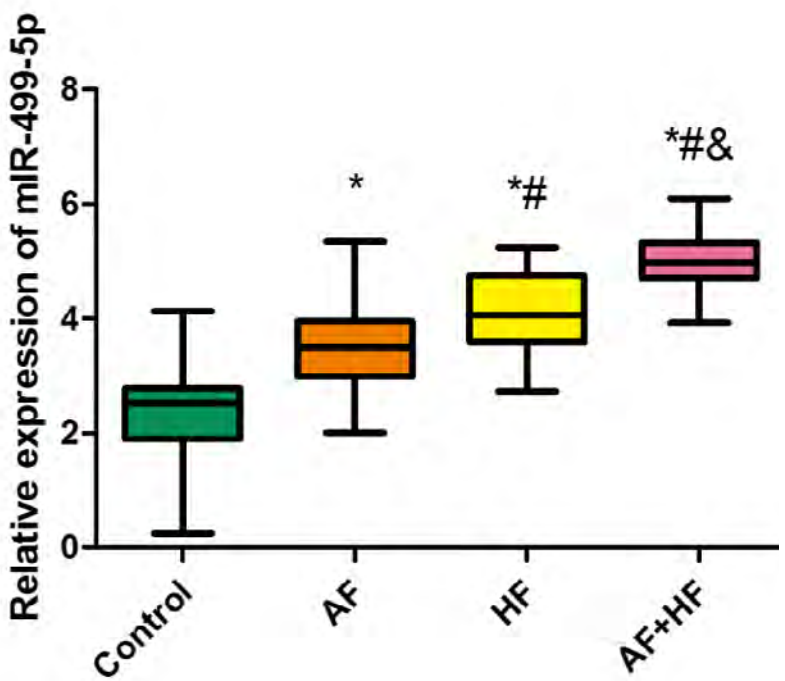


Fig. 1. *Differential expression of serum microRNA-499-5p in 4 groups. qRT-PCR was performed to detect the expression levels of serum microRNA-499-5p in patients of the AF, HF and HF+AF groups as well as the control group.*

index, which in turn induces the progression of AF as well as HF.

This study found for the first time that serum miR-499-5p expression in patients was closely related to cardiac function indexes, so it can be used as a potential biological marker for assessing the severity of AF and HF. This provides new ideas for early clinical diagnosis and targeted therapy of AF and HF and lays a new foundation.

Taken together, it was demonstrated that the serum microRNA-499-5p level was markedly elevated in patients with AF and/or HF. In addition, serum microRNA-499-5p expression was closely related to cardiac function indexes, manifesting that the microRNA-499-5p serum level can be used as a potential target and biomarker for assessing the condition of AF as well as HF.

REFERENCES

1. Vogel B, Keller A, Frese KS, et al. Multivariate miRNA signatures as biomarkers for non-ischaemic systolic heart failure. Eur Heart J 2013; 34:2812822.
2. Fic P, Kowalczuk K, Grabarska A, Stepulak A. [MicroRNA--a new diagnostic tool in coronary artery disease and myocardial infarction]. Postepy Hig Med Dosw (Online) 2014; 68:410-18.
3. Rana I, Velkoska E, Patel SK, Burrell LM, Charchar FJ. MicroRNAs mediate the cardioprotective effect of angiotensin-converting enzyme inhibition in acute kidney injury. Am J Physiol Renal Physiol 2015; 309:F943-F954.
4. Zhu H, Fan GC. Role of microRNAs in the reperfused myocardium towards post-infarct remodelling. Cardiovasc Res 2012; 94:284-92.
5. Wang JX, Jiao JQ, Li Q, et al. miR-499 regulates mitochondrial dynamics by targeting calcineurin and dynamin-related protein-1. Nat Med 2011; 17:71-78.
6. Wang J, Jia Z, Zhang C, et al. miR-499 protects cardiomyocytes from H 2O 2-induced apoptosis via its effects on Pdcd4 and Pacs2. Rna Biol 2014; 11:339-50.
7. Matkovich SJ, Hu Y, Eschenbacher WH, Dorn

LE, Dorn GN. Direct and indirect involvement of microRNA-499 in clinical and experimental cardiomyopathy. Circ Res 2012; 111:521-31.

8. Shieh JT, Huang Y, Gilmore J, Srivastava D. Elevated miR-499 levels blunt the cardiac stress response. Plos One 2011; 6:e19481.
9. Zhang R, Ma S, Shanahan L, Munroe J, Horn S, Speedie S. Discovering and identifying New York heart association classification from electronic health records. BMC Med Inform Decis Mak 2018; 18:48.
10. Cai B, Wang L, Liu J, Shi Y, Guo Y. N-terminal pro-Brain natriuretic peptide as a useful biomarker for monitoring prognosis in patients with cardiac valve replacement. J Clin Lab Anal 2011; 25:149-55.

LETTER TO THE EDITOR

FAILING HEART AND IMPORTANCE IN MYOCARDIAL TRACE ELEMENT: PRELIMINARY REPORT

B. KOZLOWSKA[1], B. SOCHANOWICZ[2], H. POLKOWSKA-MOTRENKO[2], M. KRUSZEWSKI[2,3], A. CICHA-MIKOŁAJCZYK[4], L. KRAJ[5,6], M. KUSMIERCZYK[7] and P. LESZEK[1]

[1]Department of Heart Failure and Transplantology, The National Institute of Cardiology, Warsaw, Poland; [2]Centre for Radiobiology and Biological Dosimetry, Institute of Nuclear Chemistry and Technology, Warsaw, Poland; [3]Department of Molecular Biology and Translational Research, Institute of Rural Medicine in Lublin, Poland; [4]Department of Epidemiology, Cardiovascular Disease Prevention and Health Promotion, National Institute of Cardiology, Warsaw, Poland; [5]Department of Hematology, Oncology and Internal Diseases, Warsaw Medical University, Warsaw, Poland; [6]Laboratory of Neurogenomics, Institute of Genetics and Animal Breeding, Polish Academy of Sciences, Jastrzebiec, Poland; [7]Department of Cardiac Surgery and Transplantology, National Institute of Cardiology Warsaw, Poland

Received October 17, 2019 – Accepted April 15, 2020

To the Editor,

Micronutrients and trace ions play a complex physiological and pathophysiological role in myocyte function. Therefore their proper levels are crucial to maintaining intracellular homeostasis, whereas dysregulation can cause significant pathological consequences.

Iron plays a crucial role in oxygen management (as a component of haemoglobin, myoglobin, oxidative enzymes and respiratory chain proteins). The maintenance of normal iron metabolism is particularly essential for cells characterized by fast metabolism and high energy demand, such as exercising skeletal myocytes and cardiomyocytes. Hence, in heart failure (HF), regardless of the presence of anemia, in iron-deficient patients, iron supplementation is recommended to improve functionality and quality of life. However, iron excess exerts harmful effects due to iron-induced oxidative damage, which can alter myocyte, but also endothelial and smooth muscle cell functions (1).

Zn (Zn) is a constituent of many enzymes important in cellular signaling pathways. Therefore, Zn deficiency induces changes in apoptotic, inflammatory, oxidative and nitric oxide pathways in cardiomyocytes, resulting in morphological and functional changes in cardiac tissue (2). However, also Zn excess can be harmful to myocytes. In HF, neurohormonal activation leads to increased Reactive oxygen species (ROS) and/or Reactive nitrogen species (RNS) production, which is related to increased Zn demand in cells (3). High levels of Zn promote dysregulation of Ca^{2+} turnover, which consequently leads to contractility impairment together with increase oxidative stress, mitochondrial dysfunction and cellular apoptosis (2). The role of selenium in cardiomyocytes is complex, and its deficiency promotes cell damage through activation of apoptosis and necrosis (4). In contrast, cobalt is found in living organisms only in cobalamin (vitamin B12) - necessary for the proper functioning of cells. However, excessive cobalt levels can cause

Key words: heart failure; myocardium; zinc; selenium; iron; cobalt

Corresponding Author:
Dr Bogna Kozłowska,
National Institute of Cardiology Warsaw,
Department of Heart Failure and Transplantology ,
Alpejska 42, 04-628 Warsaw, Poland
Tel.: +48 22 343 44 83 - Fax: +48 22 343 44 83
e-mail: bkozlowska@ikard.pl

0393-974X (2020)
Copyright © by BIOLIFE, s.a.s.
This publication and/or article is for individual use only and may not be further reproduced without written permission from the copyright holder.
Unauthorized reproduction may result in financial and other penalties
DISCLOSURE: ALL AUTHORS REPORT NO CONFLICTS OF INTEREST RELEVANT TO THIS ARTICLE.

apoptosis, necrosis and DNA oxidative damage (5).

In this study, zinc-Zn, iron-IR, selenium-Se and cobalt-Co concentration in the left ventricle (LV) of failing hearts (FH) were assessed and compared to LV from non-failing hearts (NFH).

MATERIALS AND METHODS

The FH samples (explanted hearts) were collected from 27 HF patients (21 males, 6 females, mean age 50±13 years) transplanted due to ischemic (n= 18) or non-ischemic (n=9) cardiomyopathy. The patients presented severe LV dysfunction with reduced ejection fraction (EF) (26±16%) and elevated NT-pro BNP levels (6076±5083 pg/ml), the available detailed clinical characteristics were presented previously (6). The control group consisted of 7 non-failing hearts (NFH) LV samples (mean age 30±10 years), who died from head trauma and were unsuitable for heart transplantation due to technical reasons. Subjects had LVEF within normal range (EF >60%)

Total myocardial ions concentration were assayed by Instrumental Neutron Activation Analysis (INAA). Frozen samples were lyophilized using Freezemobile XL (Virtis Company, New York, US), weighted and packed directly to HDPE snap-cap capsules (Faculteit Biologie, Vrije Universiteit, Amsterdam, Holland). Elemental standards were prepared by dropping appropriate amounts of the standard solution onto filter paper circles f = 7.7 mm (Schleicher & Schull, US) placed in high purity PE snap-cap capsules and left to dry. Since there are no certified human heart tissue reference materials of this type of matrix, the quality control was performed by analyzing certified reference material NIST 1577c Bovine Liver (National Institute of Standards and Technology - NIST, US). Samples and standards were irradiated at the neutron flux: 1014 cm-2 s-1 for 50 min in nuclear reactor MARIA (Świerk, Poland). After 3-week cooling, gamma-ray emission of the samples and standards was measured with the GENIE-2000 Canberra Gamma Spectrometry System. Data acquisition was accomplished using commercially available software GENIE 2000 (Canberra Industries, Inc. Meriden, US).

Statistical analysis

Test for normality of each analyzed parameter was performed by the Shapiro-Wilk test. Comparisons between groups (FH *vs* NFH) were performed with the ANOVA or Wilcoxon tests. Spearman's rank test was used to assess the correlation between the severity of HF based on the ejection fraction and NT-pro BNP and the concentration of individual ions.

RESULTS

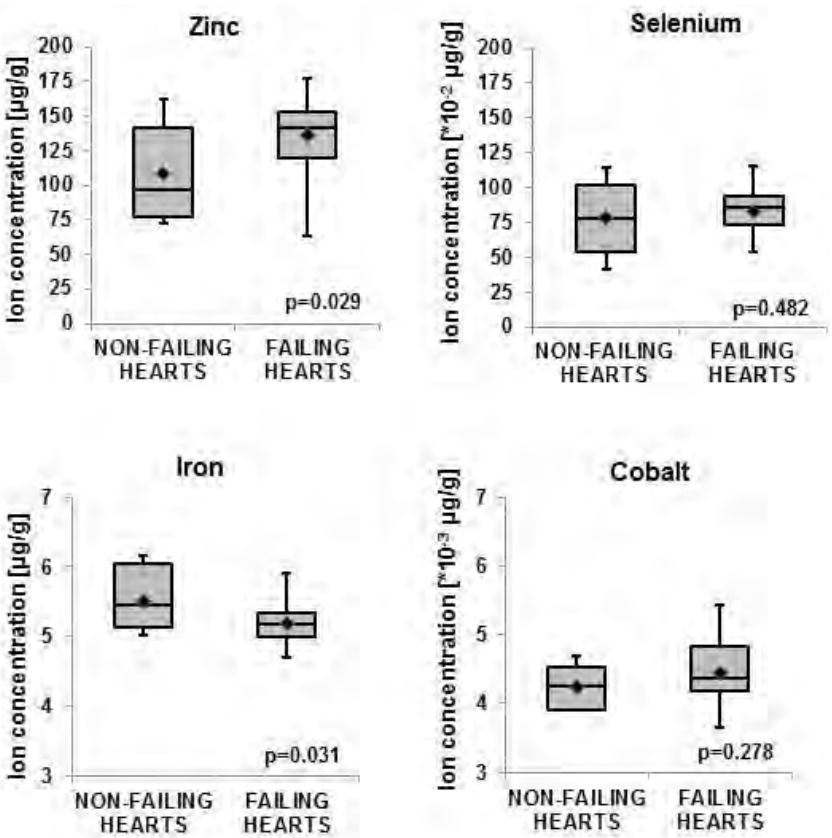
The analysis in FH LV revealed an increased Zn (136.17 μg/g±26.76 *vs* 108.6 μg/g±34.55; p=0.029) and reduced iron (186.34 μg/g±58.77 *vs* 267.89 μg/g ±129.1; p= 0.031) myocardial load as compared with NFH. No changes were found between FH/NFH in selenium and cobalt concentration (Fig. 1A). The observed changes were independent of etiology or gender (Fig. 1 B and C).

In correlation analysis, we attempted to correlate the severity of HF, based on EF and NT-pro BNP, with the level of ions. Although, important correlations were found only for selenium myocardial load, a positive correlation with EF (p=0.033, r=0.42) and negative correlation with NT pro-BNP (p=0.033, r=-0.49). Therefore, in the FH group the lower selenium concentration, corresponds with more severe left ventricle dysfunction (lower EF and higher NT-pro BNP).

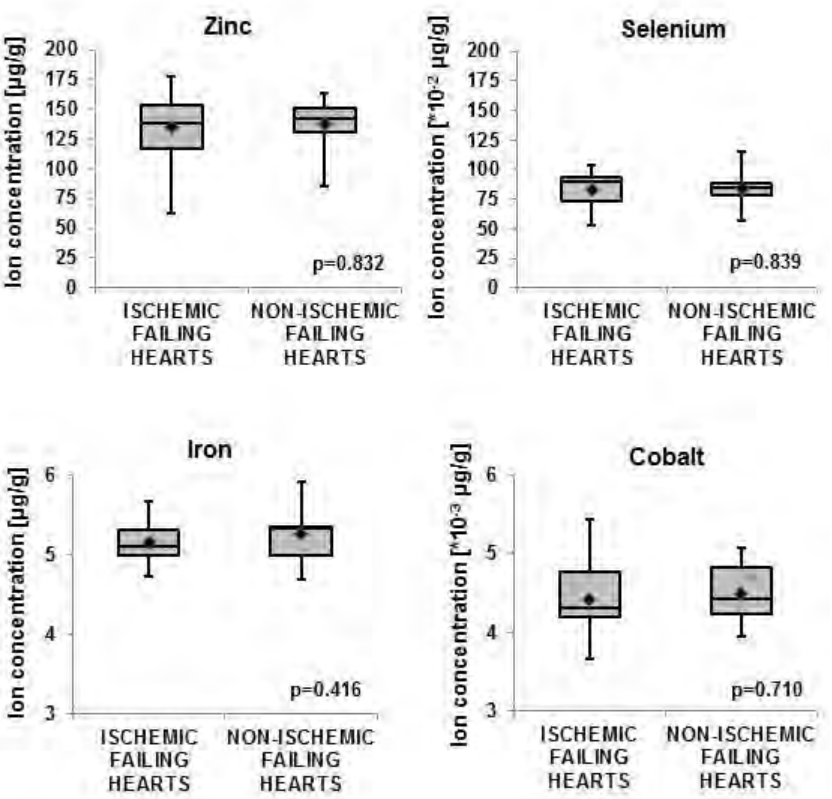
DISCUSSION

This study supports the observation that the iron load is reduced in advanced HF, as was published previously (6). Hence, the latest guidelines for HF treatment recommends iv iron supplementation in iron-deficient patients. With regard to Zn, we found in FH that its myocardial level is increased. Higher Zn levels may potentially affect myocyte functions. As been previously demonstrated, in isolated cardiomyocytes, pathological stress leads to a dramatic increase in cellular Zn load which, in turn, causes dysregulation of calcium transport, impairment in excitation-contraction coupling. Moreover, subsequent mitochondrial dysfunction causes elevated ROS/RNS production and, finally, stimulation of signaling pathways, leading to apoptosis (2). On the other hand, low Zn serum level was associated with impaired exercise capacity and high mortality (7). This discrepancy between myocardia/serum levels can be easily explained

A


Zinc
Ion concentration [µg/g]
200
175
150
125
100
75
50
25
0
p=0.029
NON-FAILING HEARTS
FAILING HEARTS
Selenium
Ion concentration [*10-2 µg/g]
p=0.482
NON-FAILING HEARTS
FAILING HEARTS
Iron
Ion concentration [µg/g]
7
6
5
4
3
p=0.031
NON-FAILING HEARTS
FAILING HEARTS
Cobalt
Ion concentration [*10-3 µg/g]
p=0.278
NON-FAILING HEARTS
FAILING HEARTS

B


Zinc
Ion concentration [µg/g]
200
175
150
125
100
75
50
25
0
p=0.832
ISCHEMIC FAILING HEARTS
NON-ISCHEMIC FAILING HEARTS
Selenium
Ion concentration [*10-2 µg/g]
p=0.839
ISCHEMIC FAILING HEARTS
NON-ISCHEMIC FAILING HEARTS
Iron
Ion concentration [µg/g]
6
5
4
3
p=0.416
ISCHEMIC FAILING HEARTS
NON-ISCHEMIC FAILING HEARTS
Cobalt
Ion concentration [*10-3 µg/g]
p=0.710
ISCHEMIC FAILING HEARTS
NON-ISCHEMIC FAILING HEARTS

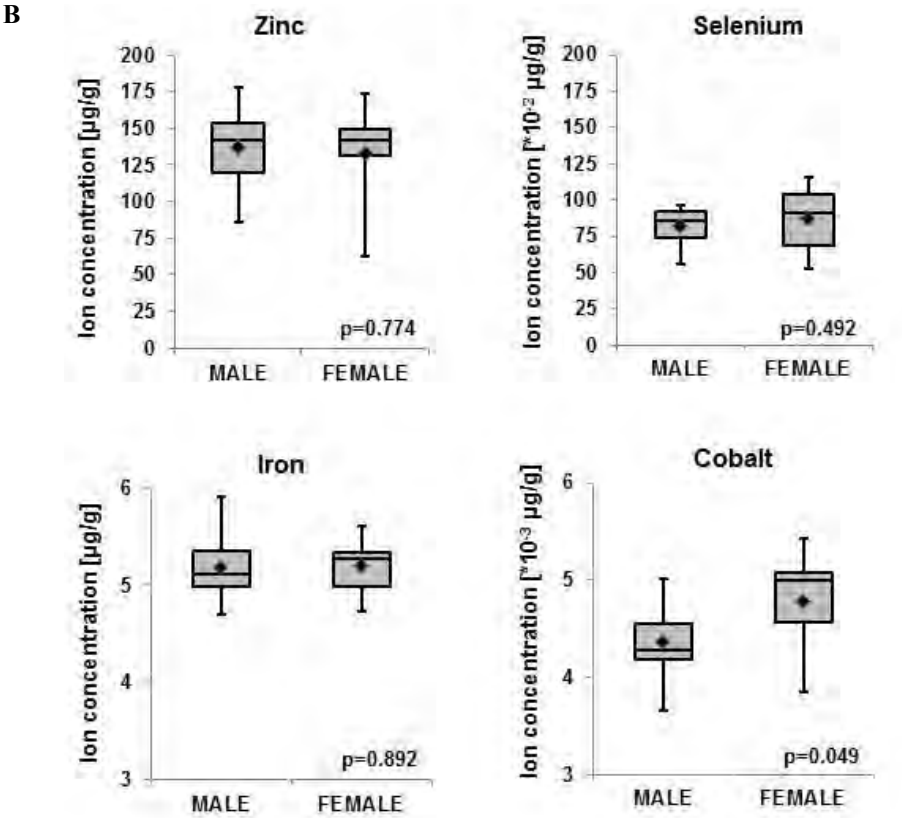


Fig. 1. ***A)*** *Ion (iron, zinc, cobalt, selenium) in non-failing (NFH) vs. failing (FH) myocardium The assessment of ions concentration between non-failing hearts (NFH) and failing hearts (FH) revealed increased zinc (136.17 µg/g±26.76 vs 108.6 µg/g±34.55; p=0.029), and reduced iron (186.34 µg/g±58.77 vs 267.89 µg/g ±129.1; p= 0.031) myocardial load in failing left ventricle. No changes were found changes between NFH/FH in selenium and cobalt concentration.* ***B)*** *Filing myocardium ions (iron, zinc, cobalt, selenium) concentration- comparison ischemic vs non-ischemic etiology. The assessment of ions concentration between ischemic and non-ischemic failing hearts revealed no significant difference.* ***C)*** *Filing myocardium ions (iron, zinc, cobalt, selenium) concentration comparison - male vs female. The assessment of ion concentration between male and female revealed no significant difference.*
Zinc, Selenium (row data), Iron, Cobalt (logarithmic data) ◆ *- Mean* ▭ *- Median*

by increased oxidative myocardial stress, which leads to upregulation in a Zn binding protein – metallothionein, and in turn increased Zn uptake (3). Thus, disrupted Zn homeostasis may be both the effect and also the cause of myocardial dysfunction. Our observation may seem important especially in Zn supplementation context.

There was no difference in selenium concentration between FH and NFH. However, only in HF patients, a correlation was demonstrated between the level of left ventricle dysfunction (EF and NT-proBNP – both different markers) and myocardial selenium load. To achieve a clear explanation, this finding needs further investigation. However, it is in line with publications showing that a selenium deficiency is associated with various manifestations of cardiomyopathy, such as cardiogenic shock, heart dysfunction, failure and arrhythmia. The condition was described for the first time in China and was named Keshan disease. All clinical symptoms were associated with histopathological findings including multifocal myocardial necrosis, often associated with infiltration of inflammatory cells. Selenium is a crucial component of selenoproteins, which maintain physiological muscle function (4).

It becomes apparent that proper balance of

micronutrients and trace ion homeostasis is essential for physiological functioning of cardiomyocytes. Therefore, further investigations, especially on Zn, selenium and other not fully explored trace ions are necessary to understand the crucial role of properly balanced micronutrition in HF.

The limitations of the present study are that the investigated patients presented with advanced HF. Also, a small population of 7 biopsies (NFH) from brain-injured donors was used as a reference for the analysis. Both groups did not receive the same treatment, also mean ages were different, therefore the results from the study should be interpreted cautiously. Unfortunately, serum levels of selected ions were not measured. Thus, it is impossible to compare myocardial ions load with their serum levels.

REFERENCES

1. Kobak KA, Radwańska M, Dzięgała M, et al. Structural and functional abnormalities in iron-depleted heart. Heart Fail Rev 2019; 24(2):269-77.
2. Turan B. A brief overview from the physiological and detrimental roles of zinc homeostasis via zinc transporters in the heart. Biol Trace Elem Res 2019; 188(1):160-76.
3. Rosenblum H, Wessler JD, Gupta A, Maurer MS, Bikdeli B. Zinc deficiency and heart failure: a systematic review of the current literature. J Card Fail 2020; 26(2):180-89.
4. Benstoem C, Goetzenich A, et al. Selenium and its supplementation in cardiovascular disease—what do we know? Nutrients 2015; 7(5):3094-118.
5. Packer M. Cobalt cardiomyopathy: a critical reappraisal in light of a recent resurgence. Circ Heart Fail 2016; 9(12).
6. Leszek P, Sochanowicz B, Szperl M, et al. Myocardial iron homeostasis in advanced chronic heart failure patients. Int J Cardiol 2012; 159(1):47-52.
7. Yoshihisa A, Abe S, Abe S, Kiko T et al. Association of serum zinc level with prognosis in patients with heart Failure. J Card Fail 2018;24(6):375-83.

LETTER TO THE EDITOR

META-ANALYSIS OF THE TREATMENT FOR NEONATAL RESPIRATORY DISTRESS SYNDROME BY INSURE STRATEGY

M. DUAN*, Y. YANG* and XH. ZHENG

Department of Neonate, The Third Affiliated Hospital of Zunyi Medical University, The First People's Hospital of Zunyi, Zunyi, China

Received November 14, 2019 – Accepted April 16, 2020

*These Authors contributed equally to this work

To the Editor,

Neonatal respiratory distress syndrome (NRDS) is a common disease in newborns and its treatment is to administer pulmonary surfactant through endotracheal intubation, followed by mechanical ventilation (MV) (1). However, MV easily induces lung damage in premature infants (2). Nasal noninvasive continuous positive airway pressure (nCPAP) can reduce lung injury (2). The INSURE technique, which consists of an INtubation-SURfactant-Extubation sequence, has been reported to reduce the need for mechanical ventilation, the duration of respiratory support, and the need for surfactant replacement in preterm infants with RDS. However, previous studies on the INSURE strategy showed contrassting results.

In one study, infants aged 27–35 weeks who required supplemental oxygen were randomly assigned to INSURE or nasal CPAP. The results showed that INSURE applied at a mean age of 5.1 hours exhibited comparable effects on the rate of mortality and the need for mechanical ventilation compared with nasal CPAP alone (3). However, due to the small sample size, lack of blinding and significantly lower mean birth weight in the INSURE group than that in the nasal CPAP group, more studies are needed to support the use of INSURE. Therefore, we aimed to integrate these small-sample studies in a meta-analysis and increase the sample size, in order to compare the clinical curative effects of INSURE and MV strategies in the treatment of NRDS, and increase the level of evidence-based medical evidence, providing better guidance in clinical practice.

MATERIALS AND METHODS

The inclusion criteria for thestudy were: randomized controlled trials, without limitations on countries and languages; trials in which the study subjects met the diagnostic criteria of NRDS recorded in "Practical Neonates"; intervention measures: trials in which patients in both two groups underwent general treatment, in addition, patients in the treatment group underwent INSURE, and patients in the control group underwent MV; outcome indicators: primary outcome was incidence of VAP, secondary outcomes included intracranial hemorrhage and pneumothorax, ventilation time, hospital stay, arterial partial pressure of carbon dioxide ($PaCO_2$), arterial blood oxygenation index [OI] at 24 hours after treatment (OI value = PaO_2/FIO_2), incidences of BPD, and oxygen consumption time.

The exclusion criteria were: trials involving patients with severe congenital malformations and inherited metabolic diseases; trials involving patients who were not diagnosed with NRDS; trials involving patients who

Corresponding Author:
Dr M. Duan,
Department of Neonate, The Third Affiliated Hospital of Zunyi Medical University, The First People's Hospital of Zunyi, No.98 Fenghuang Road, Zunyi, 563002, China
Tel.: +86 18585241155
e-mail: yujialindf08@163.com

0393-974X (2020)
Copyright © by BIOLIFE, s.a.s.
This publication and/or article is for individual use only and may not be further reproduced without written permission from the copyright holder.
Unauthorized reproduction may result in financial and other penalties
DISCLOSURE: ALL AUTHORS REPORT NO CONFLICTS OF INTEREST RELEVANT TO THIS ARTICLE.

had INSURE failure; trials that failed to provide valid data or the provided data could not be subjected to the meta–analysis; conference papers, reviews, case reports, or animal experiments.

PubMed, Cochrane, Library, CBM, Wan Fang Database, VIP and CNKI databases were searched, without language limitations. Retrieval time was from the establishment of the database to February 2017. Grey studies were not manually retrieved. English retrieval keywords included respiratory distress syndrome, newborn or neonatal respiratory distress syndrome, or respiratory distress syndrome, infant or infantile respiratory distress syndrome and INSURE. Chinese retrieval keywords: respiratory distress syndrome or neonatal respiratory distress syndrome or hyaline membrane disease, or RDS, ARDS, or NRDS or HMD, or InSurE or tracheal intubation-lung surfactant-extubation or intubation-surfactant-extubation, and randomized. All the retrieved studies were independently reviewed by two authors. Any dispute in the inclusion of a study was resolved by consulting a third author.

A database was established using Excel. The data were excerpted from the eligible studies regarding author, time of publication, country, sample situation, gestational age, birth weight, dose of lung surfactant, and outcome indicators, including improvement in arterial blood gas (OI, $PaCO_2$) at 24 hours after treatment, the incidences of VAP, BPD, intracranial hemorrhage and pneumothorax, and the ventilation time, hospital stay and oxygen consumption time.

The assessment method recommended by the Cochrane collaboration network was used. The quality evaluation was independently carried out by two reviewers based on the most important elements of reducing bias: selection bias (implementation of the allocation scheme); performance bias (blinding for the implementer on the intervention method); attrition bias (description of withdrawal or loss to follow-up after randomization); detection bias (blinding of the outcome assessment). If these four quality evaluation standards are met, the study has low risk of bias and is rated as grade A (low bias). If one or more evaluation standards are only partially met (or unclear), the study has a moderate risk of bias and is rated as grade B (moderate bias). If one or more evaluation standards are completely not met, the study has high risk of bias and is rated as grade C (high bias). For disputes between the two reviewers, a third author was consulted, and the final conclusion was determined by discussion.

The meta-analysis was conducted using Revman 5.3 software. Firstly, heterogeneity among studies was determined using *Chi*-squared test, and expressed as 95% confidence intervals (CI). If $P>0.05$ and $I^2<50\%$, statistical homogeneity was considered among studies, the fixed-effects model was used for analysis. If $P\leq0.05$ and $I^2>50\%$, statistical heterogeneity was considered among studies, the data was merged from a clinical perspective, and a random-effects model was used for analysis. Count data were expressed as odds ratio (OR) and its 95% CI. Measurement data were expressed as mean difference (MD)/standard mean difference (SMD) and its 95% CI. $P\leq0.05$ was considered statistically significant. The intention-to-treat analysis method was used to analyze the data.

RESULTS

A total of 162 studies were retrieved, of which 95 were in English and 67 were in Chinese. Finally, 12 RCT studies were included (4) of which four were in English and eight were in Chinese. The two groups included in the present study, were comparable in terms of gender, gestational age, birth weight, mode of delivery and dose of pulmonary surfactant.

All 12 included studies used the randomized method for trial. Among these, one study mentioned the use of a computer generating random allocation method, while the remaining studies mentioned the use of allocation methods, but did not specify how these were allocated. None of the 12 literatures implied allocation concealment. Three literatures mentioned the use of blinding for researchers, while the others did not. All studies provided data, however, seven studies reported loss to follow-up.

Eight studies reported and compared the incidence of VAP between the INSURE group and MV group. The heterogeneity test revealed $P=0.87$ and $I^2=0\%$, suggesting homogeneity among studies. Therefore, the fixed-effects model was used for analysis. Effect size was estimated to be 101 for each group. The results of the meta-analysis revealed that OR=0.14 and 95% CI=0.06-0.32 (five subjects in the INSURE group and 42 subjects in the MV group had VAP and needed treatment), and the difference was statistically

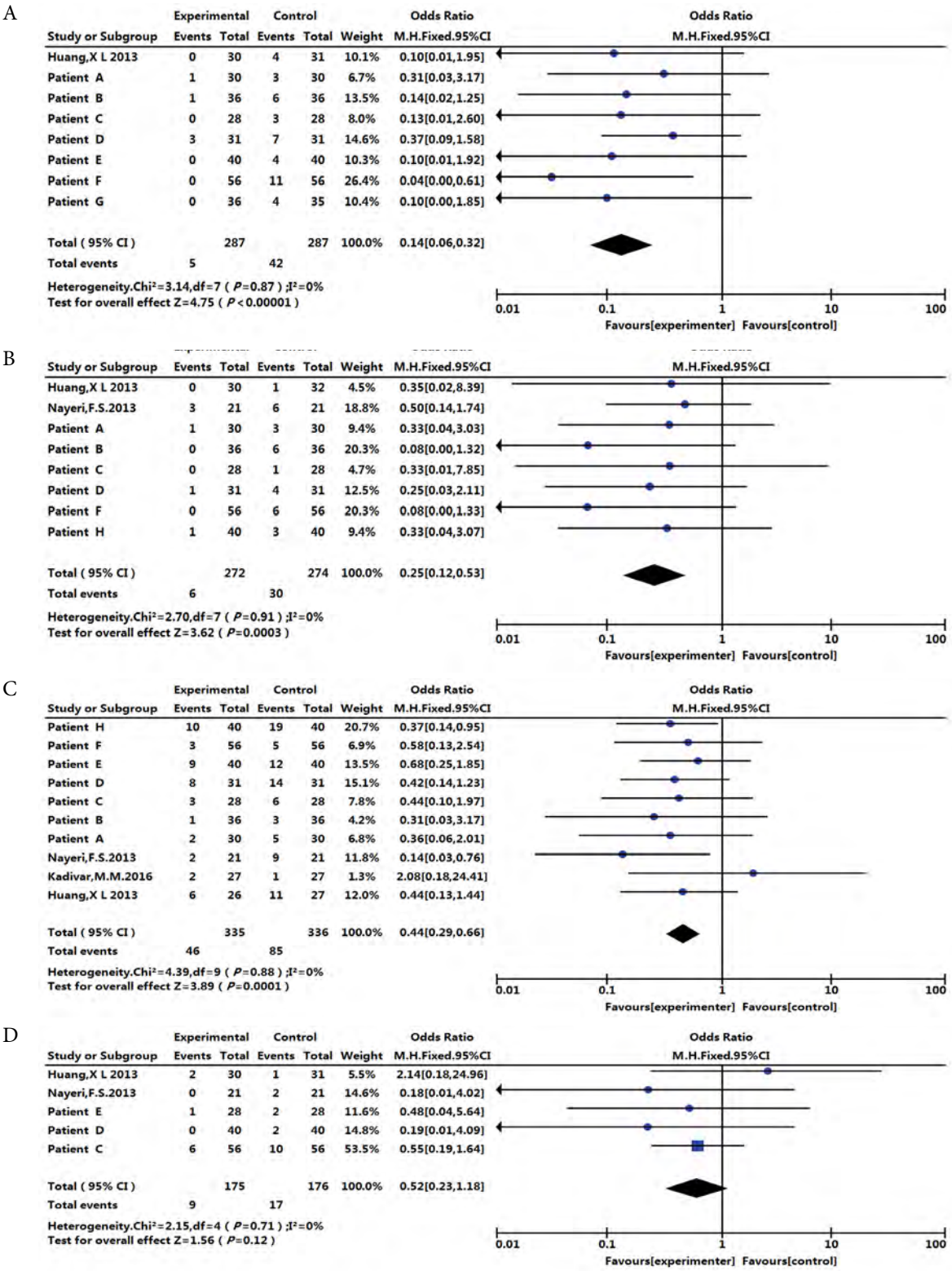


Fig. 1. ***A)*** *The rate of VAP that compared with InSurE group and mechanical ventilation group.* ***B)*** *Rate of pneumothorax that compared with InSurE group and mechanical ventilation group.* ***C)*** *The rate of intracranial hemorrhage that compared with InSurE group and mechanical ventilation group.* ***D)*** *The rate of BPD that compared with InSurE group and mechanical ventilation group.*

significant (P<0.00001). This suggested that the incidence of VAP was lower in the INSURE group than in the MV group (Fig. 1A).

Eight studies reported and compared the incidence of pneumothorax between the INSURE group and MV group. The heterogeneity test revealed P=0.91 and I^2=0%, suggesting homogeneity among studies. Hence, the fixed-effects model was used for analysis. Effect size was estimated to be 154 for each group. The results of the meta-analysis revealed that OR=0.25 and 95% CI=0.12-0.53 (six subjects in the INSURE group and 30 subjects in the MV group had VAP and needed treatment), and the difference was statistically significant (P=0.0003). This suggested that the incidence of pneumothorax was lower in the INSURE group than in the MV group (Fig. 1B).

Nine studies reported and compared the incidence of intracranial hemorrhage between the INSURE group and MV group. The heterogeneity test revealed P=0.88 and I^2=0%, suggesting homogeneity among studies, therefore, the fixed-effects model was used for analysis. Effect size was estimated to be 192 for each group. The results of meta-analysis revealed that OR=0.44 and 95% CI=0.29-0.66 (46 subjects in the INSURE group and 85 subjects in the MV group had VAP and needed treatment), and the difference was statistically significant (P=0.0001). This suggested that the incidence of intracranial hemorrhage was lower in the INSURE group than in the MV group (Fig. 1C).

Six studies reported and compared the incidence of BPD between the INSURE group and MV group.

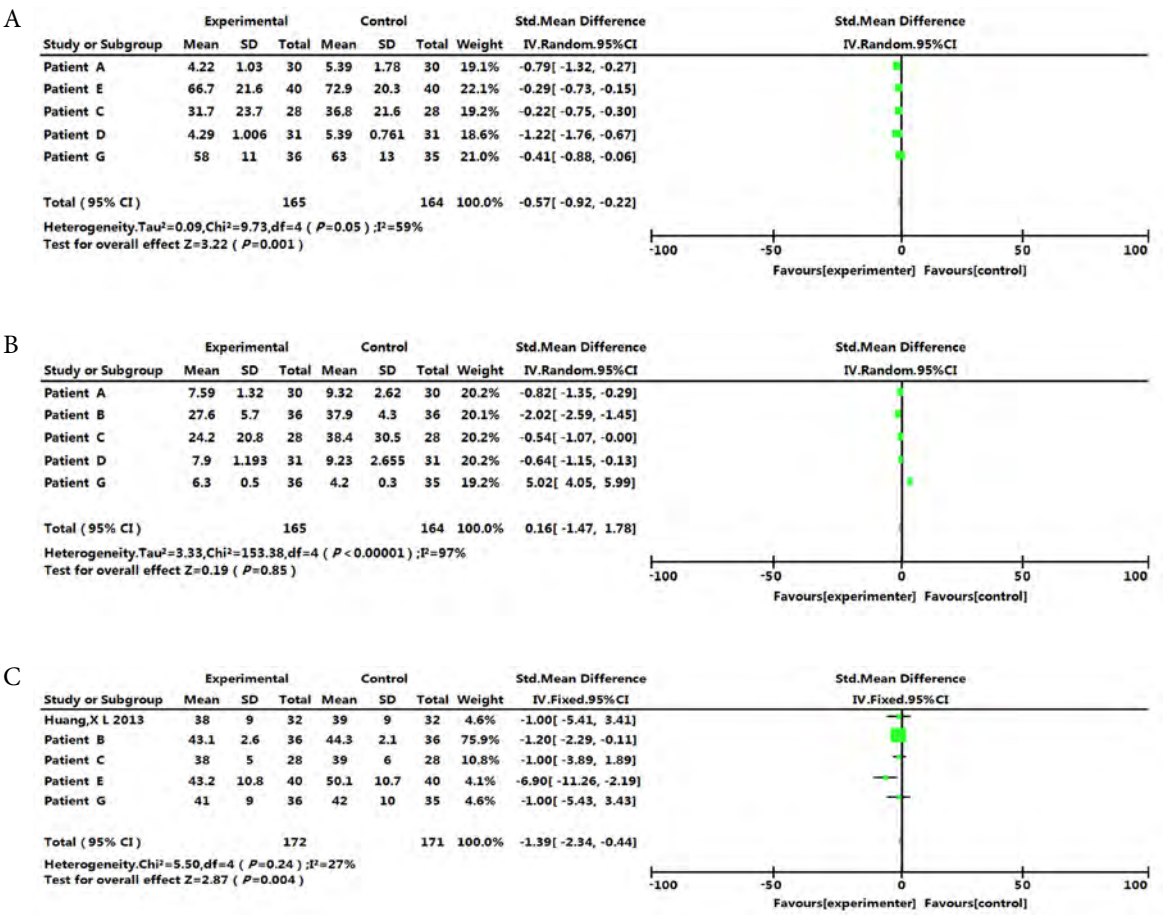


Fig. 2. ***A)*** *The ventilator use time that compared with InSurE group and mechanical ventilation group.* ***B)*** *The OI that compared with InSurE group and mechanical ventilation group 24 h after treatment.* ***C)*** *The PaCO2 that compared with InSurE group and mechanical ventilation group 24 h after treatment.*

Among these, Kadivar et al. (5) reported that no BPD occurred in either of the groups. The heterogeneity test revealed P=0.71 and I^2=0%, suggesting homogeneity among studies. Therefore, the fixed-effects model was used for analysis. Effect size was estimated to be 155 for each group. The results of the meta-analysis revealed that OR=0.52 and 95% CI=0.23-1.18, and the difference was not statistically significant (P=0.12). This suggested that the difference in the incidence of BPD between the INSURE group and MV group was not statistically significant (Fig. 1D).

Five studies reported and compared the ventilation time between the INSURE group and MV group. The heterogeneity test revealed P=0.05 and I^2=59%, suggesting heterogeneity among studies, which may be due to different ventilation methods. Hence, the random-effects model was used for analysis. Effect size was estimated to be 120 for each group. The results of the meta-analysis revealed that SMD = -0.57 and 95% CI = -0.92 to -0.22, and the difference was statistically significant (P=0.001). This suggested that ventilation time was shorter in the INSURE group than in the MV group (Fig. 2A).

Five literatures reported and compared the oxygen consumption time between the INSURE group and MV group. The heterogeneity test revealed P<0.00001 and I^2=97%, suggesting heterogeneity among studies, which may be due to the ventilation time. Therefore, the random-effects model was used for analysis. Effect size was estimated to be 116 for each group. The results of the meta-analysis revealed that SMD = -0.16 and 95% CI = -1.47 to 1.78, and the difference was not statistically significant (P=0.85). This suggested that the difference in oxygen consumption time between the INSURE group and MV group was not statistically significant (Fig. 2B). Six literatures reported and compared the OI at 24 hours after treatment between the INSURE group and MV group, and sensitivity analysis was conducted. After excluding the study conducted by Wang *et al*. (6) (P=0.56, I^2=0%), there was homogeneity among studies. Hence, the fixed-effects model was used for analysis. The results of the meta-analysis revealed that MD = 0.04 and 95% CI = -0.33 to -0.40, and the difference was not statistically significant (P=0.84). This suggested that the difference in OI at 24 hours after treatment between the INSURE group and MV group was not statistically significant.

Five literatures reported and compared the $PaCO_2$ at 24 hours after treatment between the INSURE group and MV group. The heterogeneity test revealed P=0.24 and I^2=27%, suggesting homogeneity among studies. Therefore the fixed-effects model was used for analysis. Effect size was estimated to be 42 for each group. The results of the meta-analysis revealed that MD = -1.39 and 95% CI =-2.34 to -0.44, and the difference was statistically significant (P=0.004). This suggested that the INSURE group had a more effective reduction in $PaCO_2$ than the MV group (Fig. 2C).

Three literatures reported and compared the duration of hospital stay (days) between the INSURE group and MV group. The heterogeneity test revealed P=0.94 and I^2=0%, suggesting homogeneity among studies. Hence, the fixed-effects model was used for analysis. Effect size was estimated to be 26 for each group. The results of the meta-analysis revealed that SMD =-0.75 and 95% CI =-1.04 to -0.47, and the difference was statistically significant (P<0.00001). This suggested that the duration of hospital stay was shorter in the INSURE group than in the MV group (Fig. 3).

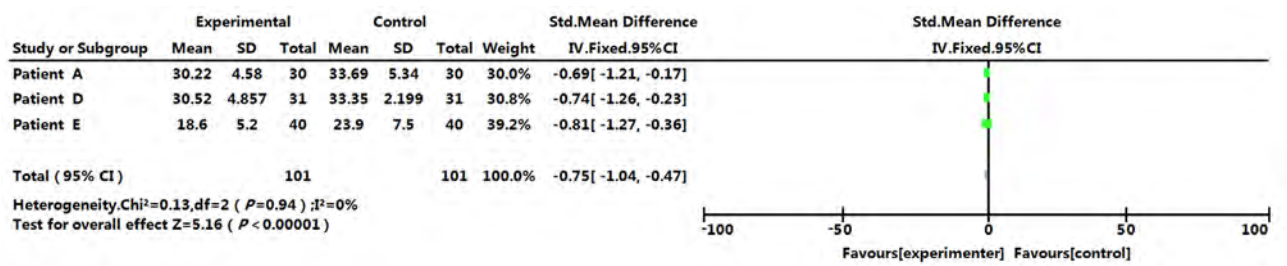


Fig. 3. *The Hospital stay that compared with InSurE group and mechanical ventilation group.*

DISCUSSION

We found that INSURE is superior to MV in reducing the incidence of VAP. The reason could be tracheal intubation-assisted ventilation causes pathogens to directly enter the inferior respiratory tract and invade the airway mucosa, and the invasive MV reduces the defense function of the respiratory system by inhibiting the activity of airway mucosal cilia, causing iatrogenic infection. Incidence of pneumothorax was lower in the INSURE group. The reason could be premature infants are immature and the peak pressure of MV easily causes alveolar rupture and pneumothorax. INSURE reduces incidence of intracranial hemorrhage. For $PaCO_2$ at 24 hours after treatment, INSURE better reduces $PaCO_2$ and improves ventilation. Six studies (4-9) compared OI at 24 hours after treatment, but our meta-analysis revealed that the difference was not statistically significant. Six studies (4-9) reported and compared the incidence of BPD, and the study of Kadivar et al. (5) revealed no BPD occurred in either group, while other studies all revealed lower incidence of BPD in INSURE group.

This is not a comprehensive search and inclusion of existing literature, therefore might cause bias since trials that failed to provide data usable for meta-analysis were excluded, and conference papers not published in full-text and grey literatures were excluded. Furthermore, the related research data set is still relatively small, and the sample sizes of most literatures were also small. These may have affected the validity of the analysis results.

ACKNOWLEDGEMENTS

This study was supported by a grant from Joint Technology R&D Project of Zunyi City (No. 2017-39, 2018-190), Excellent Young Technological Innovation Talent Training Project of Zunyi City (No. 2018-10) and Research and Test Development (R&D) Mission of The First People's Hospital.

REFERENCES

1. Zhang C, Zhu X. Clinical effects of pulmonary surfactant in combination with nasal continuous positive airway pressure therapy on neonatal respiratory distress syndrome. Pak J Med Sci 2017; 33:621-25.
2. Ardell S, Pfister RH, Soll R. Animal derived surfactant extract versus protein free synthetic surfactant for the prevention and treatment of respiratory distress syndrome. Cochrane Database Syst Rev 2015; 8:CD000144.
3. Yue YP. The clinical value of INSURE technique in the treatment of neonatal respiratory distress syndrome (NRDS). Lin Chuang Yi Xue Yan Jiu Yu Shi Jian 2016; 1:129.
4. Chen LD, Chen YZ, Wang LY, et al. Clinical study of INSURE in the treatment of hyaline membrane disease of the newborn. Guo Ji Yi Yao Wei Sheng Dao Bao 2015; 21; 3296-98.
5. Kadivar MM, Mosayebi ZM, Razi NM, et al. High Flow Nasal Cannulae versus Nasal Continuous Positive Airway Pressure in Neonates with Respiratory Distress Syndrome Managed with INSURE Method: A Randomized Clinical Trial. Iran J Med Sci 2016; 41:494-500.
6. Wang MQ, Lin W, Guan XF, et al. InSurE strategy in the treatment of neonatal respiratory distress syndrome. Er Ke Yao Xue Za Zhi 2016; 22:15-18.
7. Li Y, He YP. Clinical analysis of INSURE in neonatal respiratory distress syndrome. An Hui Yi Yao. 2015; 19:1125-27.
8. Huang HY, Huang NC, Li GH. Treatment of neonatal respiratory distress syndrome with INSURE technique and constant frequency ventilation. Hua Xia Yi Xue 2016; 10:74-76.
9. Nakhshab M, Tajbakhsh M, Khani S, Farhadi R. Comparison of the effect of surfactant administration during nasal continuous positive airway pressure with that of nasal continuous positive airway pressure alone on complications of respiratory distress syndrome: a randomized controlled study. Pediatr Neonatol 2015; 56:88-94.

LETTER TO THE EDITOR

INFLUENCE OF NUTRITIONAL STATUS ON THE SHORT-TERM REHABILITATION OUTCOMES OF ELDERLY HIP FRACTURE PATIENTS

LJ. TAO*, JY. GU*, YL. JIANG, M. RUI, XY. DU and Y. ZHU

Department of Orthopedics, the Affiliated Jiangyin Hospital of Southeast University Medical School, Jiangyin, Jiangsu, China

Received February 18, 2020 – Accepted April 17, 2020

*These Authors contributed equally to this work

To the Editor,

Elderly people are one of the fastest growing sections of the population in China (1). Hip fracture is a common form of fracture that often occurs in the elderly, with substantially increased incidence and prevalence rates as the proportion of the elderly rises (2, 3). The estimated lifetime incidence of hip fracture in the elderly is 18% in women and 6% in men (4). It has become a devastating injury for elderly patients and a substantial burden for the health care system.

Nutrition plays an important role in the health status of elderly people. Malnutrition has been demonstrated to be associated with the loss of muscle, reduced strength, immune suppression, depression and impaired cardiac function. All these increase the likelihood of postoperative complications, prolonged recovery and increased mortality (5, 6). Moreover, malnutrition is known to affect bone metabolism leading to higher risk of fracture in the elderly (6).

Haematological indicators, such as albumin (ALB), pre-albumin (PA), total protein (TP), total lymphocyte count (TLC) and transferrin (TF), have been shown to assess the nutritional status of the human body (7, 8). It has been estimated that approximately 60% of patients with a hip fracture are malnourished based on such haematological parameters. To better understand the nutritional status on the influence of hip fracture patients pre- and post-operative care, we performed the present study to retrospectively review the nutritional status and rehabilitation outcomes of 128 hip fracture patients who underwent surgery.

MATERIALS AND METHODS

Study subjects

From August 2018 to July 2019, 128 patients (36 males and 92 females) with hip fractures were recruited in the present study. Patients with hip fractures included the femoral neck fracture, intertrochanteric and subtrochanteric fractures. Demographic and clinical data, including age, gender, body mass index (BMI), past medical history, length of stay in hospital and the time fromthe operation to discharge from the hospital were reviewed and collected from their medical records.

Patients who did not meet the followings criteria were excluded: i) those unable to give informed consent or who did not have relatives who could give assent; ii) time from fracture to hospital admission more than 24 h; iii) past history with serious liver, kidney, heart or haematological diseases; iv) missing related anthropometric or nutritional data.

This study was approved by the Ethics Committee of the Affiliated Jiangyin Hospital of Southeast

Corresponding Author:
Dr Yi Zhu,
Spine Surgery,
Affiliated Jiangyin Hospital,
Southeast University Medical School,
No. 163 Shoushan Road,
Jiangyin, Jiangsu, China, 214400
Tel: +86 510 86876860 - Fax: +86 510 86876861
e-mail: zhuyi223@126.com

0393-974X (2020)
Copyright © by BIOLIFE, s.a.s.
This publication and/or article is for individual use only and may not be further reproduced without written permission from the copyright holder.
Unauthorized reproduction may result in financial and other penalties
DISCLOSURE: ALL AUTHORS REPORT NO CONFLICTS OF INTEREST RELEVANT TO THIS ARTICLE.

University Medical School. All studies on humans described in the present manuscript were carried out with the approval of the responsible ethics committee and in accordance with national law and the Helsinki Declaration of 1975 (in its current, revised form). All the study subjects provided informed consent to participate in the study.

Nutritional risk assessment

The nutritional risk screening scale 2002 (NRS2002) was applied to evaluate the potential nutritional risk of all the included patients. NRS-2002 consists of three courses: i) Nutritional status (0–3 scores); ii) Severity of diseases (0–3 scores); iii) Age (0–1 score). Patients with a total score 3 are considered to be at moderate to severe risk with potential malnutrition (9).

Laboratory data

Venous blood samples were collected from hip fractures patients who were admitted to hospital within 24 h and after surgery, respectively. The levels of TP, ALB, PA, TLC, TF, total lymphocytes percentage (TLP), hemoglobin (HGB), triglyceride (TG), total cholesterol (TC) and blood serum chemistry (sodium, potassium and chloride) were measured.

Data regarding height, weight, preoperative and postoperative haematocrit (HCT) were recorded, and the Gross formula was used to calculate the amount of hidden blood loss. The estimated hidden blood loss volume (EBV) was calculated: EBV (ml) = Preoperative blood volume (PBV) × (HCT pre-operation -HCT post-operation) / Hct average ×1000 (10).

Data analysis

Data were presented as mean and standard deviation (SD) if they were in normal distribution, otherwise, the median and interquartile range (IQR) was applied. The independent or paired 2-tailed *t*-test was used to compare the laboratory parameters between different nutritional risk groups. *Chi*-squared test or Fisher's exact test was used to analyze categorical variables. Correlation analyses were performed by using the Pearson's correlation coefficient. Statistical analysis was implemented with the use of the SPSS statistical software, version 23.0 (SPSS Inc., Chicago, IL, USA). The level of statistical significance was set at a two tailed $P < 0.05$.

RESULTS

A total of 128 patients (36 males and 92 females) with hip fractures was included in the present study. Demographics and clinical manifestations, past medical history, nutritional risk assessment, the length of stay in hospital and the time of the operation to discharge from the hospital are shown in Table I. The mean age of patients was 77.3±10.5 years.

Comparisons between NRS groups

According to the results of NRS assessment on admission, all patients were divided into NRS < 3 (n = 60) and NRS ≥ 3 (n = 68) groups. The results indicated that there were significantly increased levels of TP, ALB, PA, TF, TLC, TLP and HGB in the NRS < 3 group as compared to NRS ≥ 3 group on admission (all $P < 0.05$). However, no significant differences were observed regarding age, gender, weight, BMI, the levels of TG, TC, serum sodium, potassium and chloride between the two groups (Table II).

After surgery, the differences were also compared of nutritional parameters in the NRS < 3 and NRS ≥ 3 groups, found that there were still significantly elevated levels of TP, ALB, PA, TF, TLC, TLP and HGB in NRS < 3 group compared to those of the NRS ≥ 3 group (all $P < 0.05$). Nevertheless, as compared with the NRS < 3 group, the NRS ≥ 3 group showed a prolonged length of stay in hospital from the operation to time of discharge (both $P < 0.05$) (Table III).

Correlation analysis found that the length of stay in hospital associated with TP, ALB, TLC in NRS < 3 group (all $P < 0.05$), and associated with TP, ALB, PA, TLC in NRS ≥ 3 group (all $P < 0.05$) (Table IV).

Univariate correlation analysis demonstrated that in the NRS < 3 group, the time of the operation to discharge from the hospital was associated with TP and ALB (all $P < 0.05$). Moreover, for ≥ 3 group, significant associations of the time of the operation to discharge from the hospital with TP, ALB, PA, TF

Table I. *Demographic features of included patients with hip fracture*

	Patients with hip fracture (n = 128)
Age (years)	77.3±10.2
Gender (Male/Female)	36/92
Anthropometric	
Weight (kg)	63.1±7.2
BMI (kg/m^2)	23.2±3.4
Nutrition risk on admission (based on NRS2002)	
NRS2002 < 3	60 (46.9%)
NRS2002 ≥ 3	68 (53.1%)
Smoke (yes/no)	10/118
Alcohol consumption (yes/no)	12/116
Fracture types	
Neck of femur	60 (46.9%)
Intertrochanteric	38 (29.7%)
Subtrochanteric	30 (23.4%)
Past medical history	
Hypertension (n/%)	54/42.2%
Diabetes (n/%)	18/14.1%
Coronary heart disease (n/%)	9/7.0%
Chronic obstructive pulmonary disease (n/%)	2/1.6%
Ischaemic heart disease (n/%)	5/3.9%
Previous fracture (n/%)	0/0%
Hospital stay (days)	17.54±4.96
Time from operation to discharge from hospital (days)	10.40±4.53

BMI: body mass index; NRS2002: nutritional risk screening scales 2002

and HGB were revealed (all $P < 0.05$) (Table V).

Compared to patients with same fracture type in NRS < 3 group, there were decreased levels of pre-operative blood volume and increased levels of pre-operative hidden blood loss volume in patients with neck of femur, intertrochanteric and subtrochanteric fracture in the NRS ≥ 3 group (all $P < 0.05$). There were, however, no significant differences regarding HCT% on admission and pre-operative HCT% between patients with different types of fracture in NRS < 3 and NRS ≥ 3 groups (all $P > 0.05$).

DISCUSSION

Nutrition status is an important factor influencing post-operative complications and clinical prognosis of elderly patients with hip fracture (11). Malnutrition can lead to decreased immunity, increased infection rates, delayed healing of surgical incisions, thus prolonged hospitalization, increased hospitalization costs and even increased mortality in elderly patients with hip fracture.

In the present study, we found the increased levels of TP, ALB, PA, TF, TLC, TLP and HGB in the NRS < 3 group compared to the NRS ≥ 3 group. Correlation analysis revealed that, in both NRS < 3 and NRS ≥ 3 groups, the length of stay in hospital associated with TP, ALB and TLC, and the time of the operation to discharge from the hospital showed an association with TP and ALB. Furthermore, nutritional status is also closely related to the

Table II. *Comparisons of nutritional parameters on admission in different NRS groups*

	Groups	
	NRS2002 < 3 (n = 60)	NRS2002 ≥ 3 (n = 68)
Age (years)	76.3±8.2	78.3±10.8
Gender (Male/Female)	16/42	20/48
Weight (kg)	62.3±8.2	64.6±6.1
BMI (kg/m^2)	24.7±4.1	22.8±2.8
TP (g/l)	67.5±3.2	62.1±5.2*
ALB (g/l)	43.2±2.1	36.6±4.1*
PA (mg/l)	171.23±23.15	121.35±25.25*
TF (mg/dl)	236.16±19.28	198.96±23.56*
TLC (10^9/l)	1.3±0.62	0.76±0.42*
TLP (%)	23.78±2.12	18.65±3.24*
HGB (g/l)	116.71±19.23	109.63±20.12*
TG (mmol/l)	1.21±0.51	1.18±0.62
TC (mmol/l)	4.2±1.1	4.1±0.9
Na^+ (mmol/l)	139±5	137±6
K^+ (mmol/l)	3.9±0.4	3.8±0.7
Cl^+ (mmol/l)	104±5	102±3

*BMI: body mass index; TP: total protein; ALB: albumin; PA: prealbumin; TF: transferrin; TLC: total lymphocyte count; TLP: total lymphocytes percentage; HGB: hemoglobin; TG: triglyceride; TC: total cholesterol * $P < 0.05$*

severity of hidden blood loss (12). Compared with NRS < 3 group, decreased levels of pre-operative blood volume and the increased length of stay in hospital, the time of the operation to discharge from the hospital and pre-operative hidden blood loss volume were found in NRS ≥ 3 group, suggesting that nutritional status plays an important role in the short-term rehabilitation outcomes of elderly hip fracture patients.

However, there are some shortcomings that should be noticed. Firstly, this study is a cross-sectional study that could not prove the causal association of nutritional status with hip fractures. Secondly, the selection of study subjects is based on a single hospital, and thus may lead to a potential selection bias.

In conclusion, our study suggested that nutritional factors play a crucial role in the treatment and prognosis of elderly hip fracture patients, therefore comprehensive evaluation of perioperative nutritional status, and strengthening perioperative nutritional management, are needed for elderly hip fracture patients.

ACKNOWLEDGEMENTS

The authors thank the study participants as well as the staff involved in the collection of blood samples.

Table III. *Comparisons of nutritional parameters after operation in different NRS groups*

Parameters	Groups	
	NRS2002 < 3 (n = 60)	NRS2002 ≥ 3 (n = 68)
Age (years)	76.3±8.2	78.3±10.8
TP (g/l)	64.3±2.1	59.3±4.2*
ALB (g/l)	40.5±3.1	34.2±2.6*
PA (mg/l)	162.13±18.35	117.06±20.36*
TF (mg/dl)	232.52±18.67	187.56±19.26*
TLC (10^9/l)	1.1±0.51	0.71±0.46*
TLP (%)	20.19±4.27	15.23±5.65*
HGB (g/l)	109.67±16.45	100.13±22.87*
TG (mmol/l)	1.07±0.41	0.98±0.37
TC (mmol/l)	4.1±0.8	4.1±0.7
Na^+ (mmol/l)	138±6	137±7
K^+ (mmol/l)	3.8±0.5	3.8±0.6
Cl^+ (mmol/l)	104±6	103±5
The length of stay in hospital (days)	15.12±3.87	22.25±5.82*
The time of the operation to discharge from the hospital (days)	8.31±4.07	14.18±2.56*

* $P < 0.05$

BMI: body mass index; TP: total protein; ALB: albumin; PA: prealbumin; TF: transferrin; TLC: total lymphocyte count; TLP: total lymphocytes percentage; HGB: hemoglobin; TG: triglyceride; TC: total cholesterol

Table IV. *Correlation of the length of stay in hospital with nutritional parameters*

Parameters	NRS2002 < 3 (n = 60)		NRS2002 ≥ 3 (n = 68)	
	r	*p*	r	*p*
Age (years)	0.046	0.756	-0.094	0.504
TP (g/l)	-0.377	**0.000**	-0.312	**0.002**
ALB (g/l)	-0.387	**0.000**	-0.402	**0.000**
PA (mg/l)	-0.263	0.062	-0.331	**0.001**
TF (mg/dl)	-0.031	0.837	-0.041	0.769
TLC (10^9/l)	-0.290	**0.046**	-0.341	**0.000**
TLP (%)	-0.103	0.485	-0.242	0.081
HGB (g/l)	-0.105	0.213	-0.088	0.531
TG (mmol/l)	0.279	0.055	0.130	0.189
TC (mmol/l)	0.224	0.127	0.101	0.216
Na^+ (mmol/l)	-0.028	0.848	-0.080	0.567
K^+ (mmol/l)	0.047	0.749	0.110	0.433
Cl^+ (mmol/l)	0.251	0.085	0.173	0.238

BMI: body mass index; TP: total protein; ALB: albumin; PA: prealbumin; TF: transferrin; TLC: total lymphocyte count; TLP: total lymphocytes percentage; HGB: hemoglobin; TG: triglyceride; TC: total cholesterol

Table V. *Correlation of the time of the operation to discharge from the hospital with nutritional parameters*

Parameters	NRS2002 < 3 (n = 60)		NRS2002 ≥ 3 (n = 68)	
	r	*p*	r	*p*
Age (years)	-0.039	0.793	0.137	0.329
TP (g/l)	-0.429	**0.001**	-0.373	**0.008**
ALB (g/l)	-0.405	**0.004**	-0.395	**0.003**
PA (mg/l)	-0.254	0.067	-0.395	**0.003**
TF (mg/dl)	-0.097	0.523	-0.394	**0.006**
TLC (10^9/l)	-0.091	0.539	0.015	0.915
TLP (%)	-0.073	0.621	-0.024	0.866
HGB (g/l)	-0.230	0.097	-0.283	**0.046**
TG (mmol/l)	-0.076	0.608	-0.127	0.364
TC (mmol/l)	-0.027	0.854	-0.163	0.243
Na^+ (mmol/l)	0.168	0.255	0.104	0.457
K^+ (mmol/l)	-0.232	0.128	-0.126	0.314
Cl^+ (mmol/l)	0.233	0.111	0.185	0.185

BMI: body mass index; TP: total protein; ALB: albumin; PA: prealbumin; TF: transferrin; TLC: total lymphocyte count; TLP: total lymphocytes percentage; HGB: hemoglobin; TG: triglyceride; TC: total cholesterol

This study was supported by Jiangyin Financial Fund Support Project (808207610002).

REFERENCES

1. Campbell AJ, Robertson MC. Implementation of multifactorial interventions for fall and fracture prevention. Age Ageing 2006; 35 Suppl 2:ii60-ii64.
2. Parker M, Johansen A. Hip fracture. BMJ 2006; 333(7557):27-30.
3. Brauer CA, Coca-Perraillon M, Cutler DM, Rosen AB. Incidence and mortality of hip fractures in the United States. JAMA 2009; 302(14):1573-9.
4. Papadimitropoulos EA, Coyte PC, Josse RG, Greenwood CE. Current and projected rates of hip fracture in Canada. CMAJ 1997; 157(10):1357-63.
5. Carpintero P, Caeiro JR, Carpintero R, Morales A, Silva S, Mesa M. Complications of hip fractures: A review. World J Orthop 2014;5(4):402-11.
6. Saletti A, Johansson L, Yifter-Lindgren E, Wissing U, Osterberg K, Cederholm T. Nutritional status and a 3-year follow-up in elderly receiving support at home. Gerontology 2005; 51(3):192-98.
7. Tempel Z, Grandhi R, Maserati M, et al. Prealbumin as a serum biomarker of impaired perioperative nutritional status and risk for surgical site infection after spine surgery. J Neurol Surg A Cent Eur Neurosurg 2015; 76(2):139-43.
8. Devoto G, Gallo F, Marchello C, et al. Prealbumin serum concentrations as a useful tool in the assessment of malnutrition in hospitalized patients. Clin Chem 2006; 52(12):2281-85.
9. Koren-Hakim T, Weiss A, Hershkovitz A, et al. Comparing the adequacy of the MNA-SF, NRS-2002 and MUST nutritional tools in assessing malnutrition in hip fracture operated elderly patients. Clin Nutr 2017; 36(3):912.
10. Gross JB. Estimating allowable blood loss: corrected for dilution. Anesthesiology 1983; 58(3):277-80.
11. Eneroth M, Olsson UB, Thorngren KG. Nutritional supplementation decreases hip fracture-related complications. Clin Orthop Relat Res 2006; 451:212-17.
12. Lumbers M, New SA, Gibson S, Murphy MC. Nutritional status in elderly female hip fracture patients: comparison with an age-matched home living group attending day centres. Br J Nutr 2001; 85(6):733-40.

LETTER TO THE EDITOR

ROLE OF INVARIANT NATURAL KILLER T CELLS IN PATIENTS WITH TONSILLAR HYPERTROPHY: THE TONSIL AS AN IMMUNOLOGICAL ORGAN

A. DERAKHSHANI[1], M.R. MOFATEH[2], S. MASIERI[3], H. GHADRI[4], C. CAVALIERE[5], E. FAKRON[3] and M. FEREIDOUNI[6]

[1]Immunology Research Center, Tabriz University of Medical Sciences, Tabriz, Iran; [2]Birjand University of Medical Science, School of Medicine, Department of Ears, Nose, and Throat, Birjand, Iran; [3]Department of Sense Organs, Sapienza University, Rome, Italy; [4]Department of Microbiology, School of Medicine, Ahvaz Jundishapur University of Medical Sciences, Ahvaz, Iran; [5]Department of Oral and Maxillofacial Sciences, Sapienza University, Rome, Italy; [6]Cellular and Molecular Research Center, Birjand University of Medical Sciences, Birjand, Iran

Received February 20, 2020 – Accepted April 21, 2020

To the Editor,

The palatine tonsils are at the entrance of the upper aerodigestive tract acting as immune protection against bacteria and viruses, both ingested and inhaled, and playing an important role in the eradication of pathogens (1). Tonsillar hypertrophy is a common health problem, especially among children and its pathogenesis is still not well understood, various factors such as chronic bacterial and viral infections are reported as the causative factors (2). Tonsils seem to be a useful model *in vitro* to investigate the mechanisms of inflammatory processes and diseases in lymphoid organs. The high presence of memory B cells in tonsils can show the extremely efficient mechanism of B cells in the protection against widespread tonsil infection and diseases (3). T lymphocytes, especially T helper 1 (Th1) cells, are present in palatine tonsils, principally in extrafollicular spaces (1), playing a crucial role in response to viral and bacterial pathogens in tonsils (4). Recent experiments have shown that antigenic activation of intraepithelial T lymphocytes in the tonsil crypt epithelium produces pro-inflammatory cytokines such as Tumor Necrosis Factor-alpha (TNF-α) and Interferon-gamma (IFN-γ) (5). Invariant Natural Killer T cells (iNKT) are a small subset of T lymphocytes that act as a bridge between the innate and adaptive immune system and play many roles in many immunological phenomena including anti-microbial and anti-tumor defense (6). In humans, iNKT cells express a semi-invariant T cell receptor (TCR) composed of Vα24 (TRAV10)-Jα18 (TRAJ18) and Vβ11(TRBV25-1) (7). iNKT cells can produce a significant amount of different cytokines, including IFNγ or Interleukin-4 (IL-4), hence, they can modulate immune responses in numerous ways (6, 8). This study aimed to evaluate the presence of T lymphocyte, especially iNKT cells, and their related cytokines, including IFN-γ and IL-4, in tonsil samples and peripheral blood of patients suffering from tonsillar hypertrophy, in the hope of shedding light on the pathogenesis of tonsillar hypertrophy.

MATERIALS AND METHODS

Patients and samples

Nineteen patients with tonsillar hypertrophy,

Key words: tonsillectomy; tonsillar hypertrophy; iNKT cells; IL-4; IFN-γ

Corresponding author:
Dr Mohammad Fereidouni,
Birjand University of Medical Sciences,
Ghafari Street, Birjand, Iran
Tel./Fax: +98 56 32433004
e-mail: dr.m.fereidouni@gmail.com

0393-974X (2020)
Copyright © by BIOLIFE, s.a.s.
This publication and/or article is for individual use only and may not be further reproduced without written permission from the copyright holder.
Unauthorized reproduction may result in financial and other penalties
DISCLOSURE: ALL AUTHORS REPORT NO CONFLICTS OF INTEREST RELEVANT TO THIS ARTICLE.

candidates for tonsillectomy, and nineteen healthy individuals were enrolled in this study. The study was approved by the Ethics Committee of Birjand University of Medical Sciences (IR.BUMS.REC.1397.079) and all participants received and signed written informed consent. Demographic data were collected through a questionnaire. Participants with any serious health problems such as acute infections, autoimmune disorders, or recent use of immunosuppressive drugs were excluded from the study.

Sample collection and processing

Before tonsillectomy, 10 milliliters (ml) of venous blood was obtained in the operating room and divided into two tubes for the isolation of peripheral mononuclear blood cells (PBMCs) by density gradient centrifugation and serum separation, subsequently stored at -20°C until analyzed. During a tonsillectomy, resected tonsillar tissues were washed with normal saline solution and divided into three parts. One part was fixed in formalin and embedded in paraffin to be used for histopathology evaluation. The second part was transferred to the laboratory on dry ice, and RNA extraction was immediately performed using the RNeasy mini kit (Qiagen, Germany). The third part was homogenized with a tissue homogenizer (Heidolph, Germany) and successively centrifuged at 3000 rpm for 15 mins. The supernatant was collected and stored at -70°C for cytokine analysis. Five ml of venous blood were also collected from healthy volunteers and RNA extraction, as well as serum separation, were carried out.

Cell culture and reagents

Considering the low frequency of iNKT cells in humans, and also to obtain a sample with enough iNKT cells, PBMCs from a healthy donor were cultured in the presence of 100 ng/ml of a-GalCer as the potent stimulator of iNKT cells, and 10 ng/ml of IL-2 for five days in the incubator. The cultured cells were harvested following RNA extraction and cDNA synthesis and used for the optimization of the real-time PCR protocol to detect TRAV10-TRAJ18, TRBC2, and particularly TRAV10 genes.

RNA extraction and cDNA synthesis

RNA extraction from cells, tissue, and PBMCs was carried out by way of a RNeasy mini kit (Qiagen, Germany). All samples were treated with DNase-I (Qiagen, Germany) and cDNA synthesis was performed using a cDNA Reverse Transcription kit (Thermofisher, USA).

Polymerase chain reaction (PCR)

In order to achieve the best protocol for gene amplification, a gradient PCR with different annealing temperatures for TRBC2, TRAV10, and TRAV10-TRAJ18 genes was performed using cDNA from cultured cells.

Real-Time PCR

Relative quantification of CD3 (TRBC2), Vα24 (TRAV10), and Vα24-Jα18 (TRAV10-TRAJ18) genes as representative of iNKT cells were assessed via real time-PCR using specific primers for both genes. Glyceraldehyde-3-phosphate dehydrogenase (GAPDH) gene was used as a housekeeping gene for normalization. Relative gene expression was calculated using the comparative CT method. Primers and protocol are summarized in Table I.

Cytokine measurement

The concentration of IFN-γ and IL-4 in serum and tonsillar tissue homogenates was determined by commercial ELISA kits (Biosource International Inc, USA) following the manufacturer's instructions. All samples were checked in duplicate and the average was used for analysis. The detection limit was >0.01 IU/ml and >2.0 pg/ml for IFN-γ and IL-4, respectively.

Statistical analysis

The results were statistically analyzed in GraphPad Prism (version 5.0, GraphPad Software Inc., San Diego, CA) and presented as mean± SEM. Statistically significant differences between two groups were assessed by two-tailed unpaired *t*-test. $p<0.05$ was considered significant.

RESULTS

Nineteen patients with tonsillar hypertrophy (mean age was 10.6±5.5 years, M/F; 7/12) and nineteen healthy individuals (mean age 12.6±4.6 years; M/F; 7/12) were enrolled for this study (Table II).

Polymerase chain reaction (PCR)

To find the best protocol for gene amplification with cDNA from iNKT cultured cells, a gradient

Table I. *Primer sets for Real time-PCR analysis.*

Targets	Forward	Reverse	Size
TCRB2 (CD3)	CAGCGAGCCCTACTCAAATTAG	GACCTGTGGAAGAGAGA ACATT	104bp
TRAV10 (Vα24)	AAGCATCTGACGACCTTCTTG	AACAGGACCTCTCCCAGT ATC	192bp
TRAV10 TRAJ18 (Vα24-Jα18)	GATATACAGCAACTCTGGATGC A	GAGTTCCTCTTCCAAAGT ATAGCC	144bp
GAPDH	GCACCACCAACTGCTTAGCA	GTCTTCTGGGTGGCAGTG ATG	106bp

PCR with different annealing temperatures was carried out and PCR products were visualized on 2% agarose gel (Fig. 1).

Relative quantitation of CD3, Vα24, and Vα24-Jα18

Relative expression of CD3 in palatine tonsils was significantly higher than their matched PBMCs in patients with tonsillar hypertrophy (0.45 *vs* 0.21; p= 0.042). The expression of the CD3 gene was significantly higher in the blood of patients with tonsillar hypertrophy compared to healthy controls (0.21*vs* 0.038; p=0.02) (Fig. 2A). Furthermore, the expression of Vα24 in patient blood compared with the healthy group and also in patient tissue related to matched blood was even significantly higher (0.035 *vs* 0.0039; p=0.0022 and 0.23 *vs* 0.035; p=0.0012, respectively) **(**Fig. 2B). The expression of Vα24-Jα18 in patients' blood compared with the healthy group and also in patients' tissue related to matched blood was also significantly higher (0.025 *vs* 0.0038; p=0.0007 and 0.091 *vs* 0.028; p=0.03, respectively) **(**Fig. 2 C).

Table II. *Demographic data*

Group	Mean age	Frequency	Male/Female
Patients	10.63±5.5	19	7/12
Control	12.6±4.6	19	7/12

Cytokine analysis

IFN-γ was significantly higher in tonsillar homogenates compared with their matched blood in patients (1.2 *vs* 0.12 IU/ml, p=0.0009); there was also a significant difference between healthy sera and patients' sera in the case of IFN-γ levels (0.07 *vs* 0.12 IU/ml, p=0.0003) **(**Fig. 3A). There were no significant differences between the IL-4 concentrate in tonsillar homogenates and matched blood in patients (2.9 *vs* 2.1, p=0.06) or between the sera of patients and controls (2.1 *vs* 2.19 μg/ml, p=0.98) (Fig. 3 B).

DISCUSSION

The importance of human tonsils as a secondary immune organ and their contribution to the immune response is widely discussed (1). Previous studies demonstrated that in secondary lymphoid organs, antigen-specific $CD4^+$ T cells are generally primed by local dendritic cells (DCs), migrating successively to the B cell follicles. Antigen-specific $CD4^+$ T cells will differentiate into follicular helper T (TFH) cells, expressing the ligand for the co-stimulating molecule CD40 (CD154) after interacting with B cells. This interaction stimulates the clonal expansion and maturation of memory B cells, contributing to adaptive immunity (9). Our study shows that the expression of CD3 (as a specific T cell receptor), Vα24, and Vα24-Jα18 genes were significantly higher in palatine tissue compared to the matching PBMCs, probably evidencing the presence of iNKT

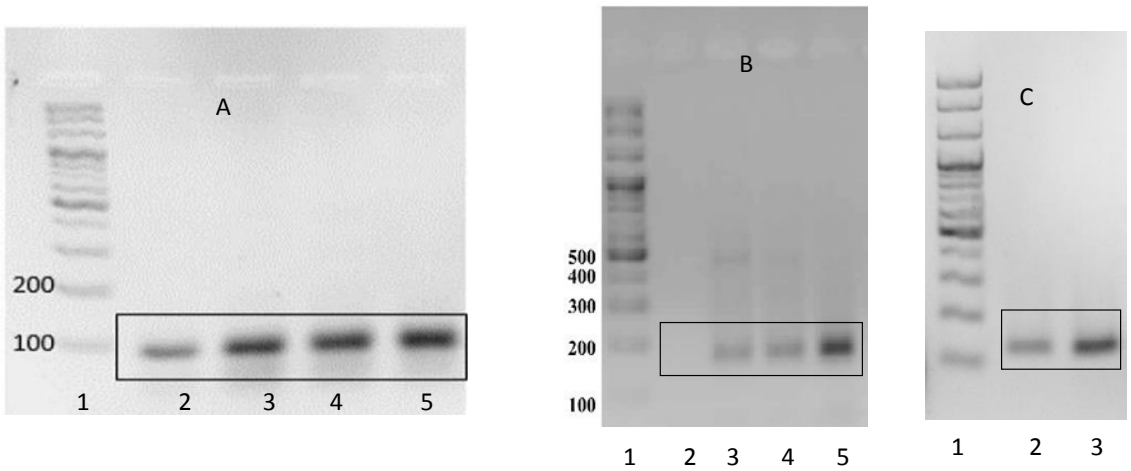


Fig. 1. *PCR amplification of CD3 (TRBC2) (**A**), V-alpha-24 (TRAV10) (**B**), and Vα24-Jα18 (TRAV10-TRAJ18) (**C**) genes in different annealing temperature. After running on 2% agarose gel. (A, B): Lanes 1: Ladder; Lanes 2, 3, 4, and 5 are related to annealing temperatures 52, 53, 54, 55, and 56, respectively. C: Lanes 1: Ladder; Lanes 2, 3 are related to annealing temperature 54, 56, respectively.*

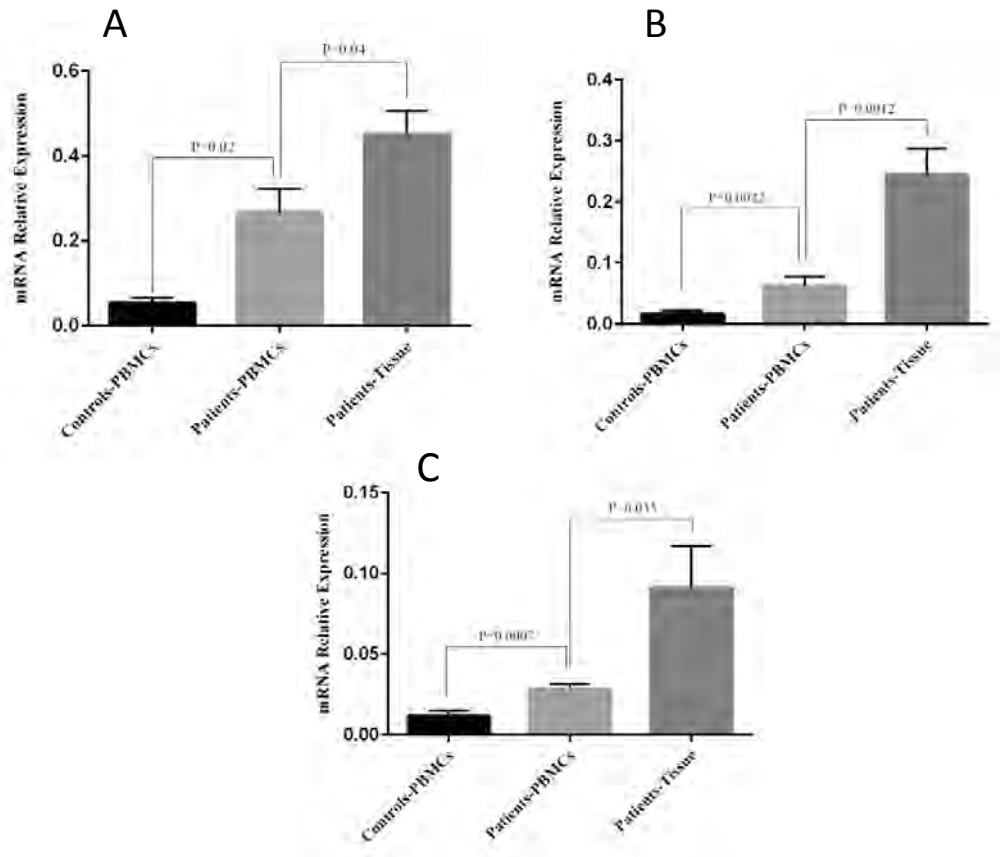


Fig. 2. *mRNA expression of TRBC2 gene in the patients' blood, tissue, and healthy blood (**A**), mRNA expression of TRAV10 gene in the patients' blood, tissue, and healthy blood (**B**), mRNA expression of TRAV10-TRAJ18 gene in the patients' blood, tissue, and healthy blood (**C**).*

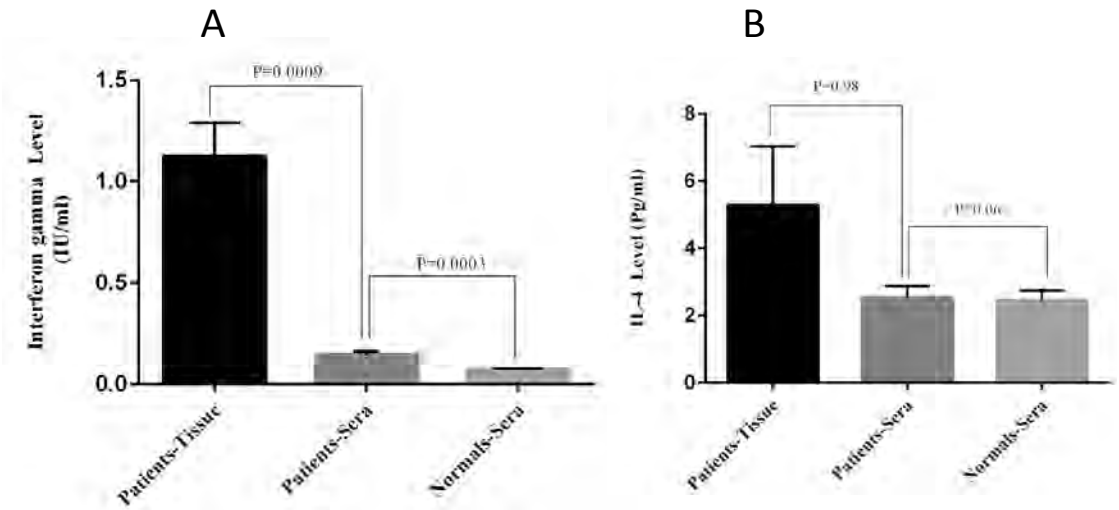


Fig. 3. *Comparison of the mean concentration of interferon-gamma in palatines and sera of patients with tonsillar hypertrophy as well as healthy people's sera (A). Comparison of the mean concentration of interleukin-4 in palatines and sera of patients with tonsillar hypertrophy and also sera of healthy people (B).*

cells in this tissue. Other studies also reported a high frequency of T cells in tonsillar hypertrophy patients (3, 10). Furthermore, we analyzed the expression of CD3, Vα24, and Vα24-Jα18 in patients' PBMCs in comparison with healthy donors, showing a higher rate in patients related to controls. T cells ($CD4^+$ and $CD8^+$) trigger many different microbes and viruses in tonsil and have the main role in adaptive immune responses; a commonly accepted recent notion indicates that "polyfunctional" T cells, particularly those generating antigen-related IL-2, TNF-α, and IFN-α, are the main factor in the control of viral and bacterial diseases. In tonsils, chronic exposure to microbe antigens (bacterial and/or viral) induces immunological memory that causes changes in the amount and distribution of $CD4^+$ and $CD8^+$ T cells (3). Many studies have shown the role of iNKT cells in different immune responses (6, 7, 11), but the data concerning their role in tonsillar hypertrophy is still scarce. In another study, we showed that higher levels of iNKT cells were recorded in nasal polyp tissue compared to peripheral blood (12). iNKT cells feature different unique characteristics that can differ from the other immune cells, having the ability to produce two different types of cytokines (IL-4 and IFN-γ) as well as activating or suppressing Th1 and Th2. The evaluation of CD3 (as a specific T cell receptor), Vα24, and Vα24-Jα18 gene expression showed a significant correlation between tissue and blood samples from tonsillar hypertrophy patients. These genes were also significantly higher in patients' blood compared to healthy individuals, showing the critical role of these cells in patients with tonsillar hypertrophy. We evaluated the concentrations of IFN-γ and IL-4 in tonsils and sera of patients with tonsillar hypertrophy and healthy individual sera. A significant difference in the concentration of IFN-γ in tonsils compared with the patients' sera and also in the concentration of this cytokine in the patients' blood compared with healthy individuals was recorded.

The results of this study revealed a higher expression of iNKT cell receptors in the peripheral blood of patients with tonsillar hypertrophy compared to healthy controls and also in the patient tissue compared with the matched PBMCs. These results may delineate a new role for iNKT cells in the pathogenesis of this disease. Furthermore, the high level of IFN-γ in palatine related to matched PBMCs as well as in the blood of patients with tonsillar hypertrophy compared to healthy controls may indicate the role of iNKT cells as a pre-activator of Th1 cells. Further studies with different methods such as flow cytometry and also fluorescence-

activated cell sorting (FACS) and magnetic-activated cell sorting (MACS) for isolation iNKT cells and more samples are needed to reveal the precise action mechanisms of these regulatory cells in tonsillar hypertrophy.

REFERENCES

1. Geissler K, Markwart R, Requardt RP, et al. Functional characterization of T-cells from palatine tonsils in patients with chronic tonsillitis. PLoS One 2017; 12(9):e0183214.
2. Tan HL, Gozal D, Kheirandish-Gozal L. Obstructive sleep apnea in children: a critical update. Nat Sci Sleep 2013; 5:109-23.
3. Sada-Ovalle I, Talayero A, Chavez-Galan L, et al. Functionality of CD4+ and CD8+ T cells from tonsillar tissue. Clin Exp Immunol 2012; 168(2):200-206.
4. Message SD, Laza-Stanca V, Mallia P, et al. Rhinovirus-induced lower respiratory illness is increased in asthma and related to virus load and Th1/2 cytokine and IL-10 production. Proc Natl Acad Sci U S A 2008; 105(36):13562-67.
5. Todorovic MM, Zvrko EZ. Immunoregulatory cytokines and chronic tonsillitis. Bosn J Basic Med Sci 2013; 13(4):230-36.
6. Fereidouni M, Derakhshani A, Exley MA. iNKT cells and hematopoietic stem cell transplantation: Two-phase activation of iNKT cells may improve outcome. Clin Immunol 2019; 207:43-48.
7. Fereidouni M, Farid Hosseini R, Jabbari Azad F, Schenkel J, Varasteh A, Mahmoudi M. Frequency of circulating iNKT cells among Iranian healthy adults. Cytometry B Clin Cytom 2010; 78(1):65-69.
8. Fox L, Hegde S, Gumperz JE. Natural killer T cells: innate lymphocytes positioned as a bridge between acute and chronic inflammation? Microbes Infect 2010; 12(14-15):1125-33.
9. Nutt SL, Tarlinton DM. Germinal center B and follicular helper T cells: siblings, cousins or just good friends? Nat Immunol 2011; 12(6):472-77.
10. Mikola E, Elenius V, Saarinen M, et al. Tonsillar cytokine expression between patients with tonsillar hypertrophy and recurrent tonsillitis. Clin Transl Allergy 2018; 8:22.
11. Vomhof-DeKrey EE, Yates J, Leadbetter EA. Invariant NKT cells provide innate and adaptive help for B cells. Curr Opin Immunol 2014; 28:12-17.
12. Fereidouni M, Derakhshani A, Yue S, et al. Evaluation of the frequency of invariant natural killer T (iNKT) cells in nasal polyps. Clin Immunol 2019; 205:125-29.

LETTER TO THE EDITOR

TUBEROUS SCLEROSIS COMPLEX WITH MULTISYSTEM MANIFESTATIONS

M-D. LI[1], QIONG YU[1], J-L. FU[2], Y. SHI[1], Y-R. LI[1] and G. SHI[1]

[1]Department of Oncology and Hematology, The Second Hospital of Jilin University, Changchun, Jilin, People's Republic of China; [2]Department of Ophthalmology, The Second Hospital of Jilin University, Changchun, Jilin, People's Republic of China

Received February 21, 2020 – Accepted April 21, 2020

To the Editor,

Tuberous sclerosis complex (TSC) is a neurocutaneous syndrome characterized by the formation of benign tumors such as neurofibromas and angiofibromas that can affect different organs and tissues of the body. TSC is a disease with extremely variable manifestations and can develop in any part of the body (1). This represents a challenge for the correct clinical diagnostics. The most common findings associated with TSC are benign tumors formed in the skin, lungs, kidneys, brain and heart. Tumors cause dysfunctions of the affected organ due to substitution of normal parenchyma by other cells (2). Even among closely related individuals, the disease manifestations in different systems and organs can vary substantially. Recent studies put the disease frequency at birth at 1/6000 to 1/10,000 and the general population prevalence at approximately 1 in 20,000 (3, 4). Although the condition was recognized as a genetic disorder for more than 100 years (5), the molecular mechanism of TSC was unknown until the discovery of two causative genes, TSC1 and TSC2 (6). These mutations encode the proteins hamartin and tuberin (7), which form a complex that plays an important role in the mTOR pathway (8). The conventional genetic testing does not detect the disease-causing mutations in as many as 10-25% of all patients. As a result, normal results of genetic testing cannot completely rule out the TSC diagnosis (1).

Here, we report a case of a patient in whom TSC led to the formation of rapidly evolving reactive fibromas of considerable diameter. Very few similar cases are reported in the literature.

Case

A 28-year-old woman was admitted to the Second Hospital of Jilin University in October 2014 with severe aplastic anemia lasting for the previous four months. TSC had been diagnosed in the patient at the age of 10. The presence of angiofibromas fibrous, cephalic plaque and shagreen patch on the face, ungual fibromas on fingers and toes, dental enamel pits and "confetti" skin lesions led to this diagnosis. When the patient was 5 months old, she frequently experienced epileptic seizures. Carbamazepine was prescribed to control the seizures. The total frequency of seizures reduced after the age of 6. At the age of 3, subcutaneous nodules appeared, with varying size and pruritus. In 2014, the patient underwent surgery to remove facial angiofibromas. On several occasions operations were performed to remove gingival fibromas and epidermoid cysts. Since August 2014, the patient felt weak, and her

Key words: tuberous sclerosis complex; TSC1; TSC2

Corresponding Author:
Dr Guang Shi,
Department of Oncology and Hematology,
The Second Hospital of Jilin University
218 Ziqiang Street, Changchun 130041,
Jilin, People's Republic of China.
e-mail: dr_shicc72@yahoo.com

0393-974X (2020)
Copyright © by BIOLIFE, s.a.s.
This publication and/or article is for individual use only and may not be further reproduced without written permission from the copyright holder.
Unauthorized reproduction may result in financial and other penalties
DISCLOSURE: ALL AUTHORS REPORT NO CONFLICTS OF INTEREST RELEVANT TO THIS ARTICLE.

appetite decreased. In December 2014, an extremely severe anemia was diagnosed with the hemoglobin level below 30 g/L. Accessory examination revealed ferritin level at 32.8 ng/ml, and folic acid at 6.17 ng/ml. The computed tomography scan showed the presence of angiomyolipomas and multiple renal cysts. Brain CT revealed an abnormal tissue in the head and the bilateral basal ganglia calcification (Fig. 1).

The patient was diagnosed with exacerbation of TSC and provided with symptomatic supportive treatment such as blood transfusion due to severe anemia.

The patient provided an informed, signed consent for publication of this case study.

DISCUSSION

Due to a highly variable clinical presentation, TSC can be associated with a wide range of neuropsychiatric and physical disorders such as epilepsy, autism spectrum disorders, mental retardation, and hyperkinetic disorder. Some patients can be severely affected by the conditions, while others remain largely unscathed by the disease. The main clinical features of TSC include seizures, mental retardation, and the development of hamartomas in multiple organs including the skin, brain, lungs, heart, and kidneys. Indeed, the disease manifests virtually in every organ (9). The major diagnostic criteria of TSC were described by Northrup and co-authors (1). Almost every individual affected by TSC manifests skin or dental findings characteristic for the disease that are easily observed on physical examination. Highlighting these findings could aid in bringing the patients with TSC to the attention of medical specialists.

The treatment options to control TSC include everolimus, an oral inhibitor of the mTOR pathway that can effectively inhibit the growth of renal angiomyolipoma and even reduce the volume of tumors (10). Everolimus also has a significant effect on TSC-related epilepsy (11), while vigabatrin is more effective for epilepsy after infancy (12).

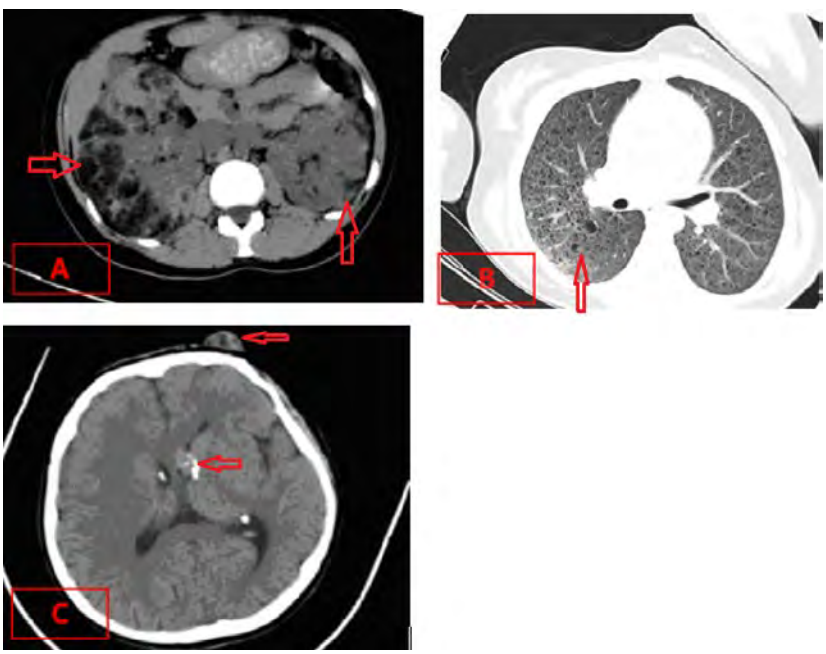


Fig. 1. ***A)*** *Renal angiomyolipomas. The shape of bilateral kidneys is irregular, the volume is increased, the normal shape of cortex disappears, and there are multiple patches of fat, mixed shadow of density and soft tissue density.* ***B)*** *Lymphangioleiomyomatosis: the formation of reticular nodules and multicystic changes by overgrowth of smooth muscle and blood vessels in both lungs.* ***C)*** *Facial angiofibromas and bilateral basal ganglia calcification: the soft tissue shadow under the skull is irregular and thickened. Multiple symmetrical calcifications can be seen in bilateral basal ganglia).*

Patients with TSC must be regularly monitored for possible alterations in renal, pulmonary and cardiac systems. Observed changes in patient's conditions should be taken into account for the correct clinical management.

REFERENCES

1. Northrup H, Krueger DA; International Tuberous Sclerosis Complex Consensus Group. Tuberous sclerosis complex diagnostic criteria update: recommendations of the 2012 International Tuberous Sclerosis Complex Consensus Conference. Pediatr Neurol 2013; 49:243-54.
2. Northrup H, Koenig M, Pearson DA, Au K. Tuberous sclerosis complex. GeneReviews. In: Adam MP, Ardinger HH, Pagon RA, Wallace SE, Bean LJH, Stephens K, Amemiya A, editors. Gene Reviews. Seattle (WA): University of Washington, Seattle; 1993-2020.
3. O'Callaghan F, Shiell A, Osborne J, Martyn C. Prevalence of tuberous sclerosis estimated bycapture-recapture analysis. Lancet 1998; 352:318-19.
4. Sampson J, Scahill S, Stephenson J, Mann L, Connor J. Genetic aspects of tuberous sclerosis in the west of Scotland. J Med Genet 1989; 26:28-31.
5. Kirpicznik J. Ein fall von tuberoser sklerose and gleichzeitigen multiplem Nierengeschwulstein. Virchows Arch Pathol Anat 1910; 202:358.
6. European Chromosome 16 Tuberous Sclerosis Consortium. Identification and characterization of the tuberous sclerosis gene on chromosome 16. Cell 1993; 75:1305-15.
7. Sampson JR, Harris PC. The molecular genetics of tuberous sclerosis. Hum Mol Genet1994; 3:1477-80.
8. Laplante M, Sabatini DM. mTOR signaling in growth control and disease. Cell 2012; 149:274-93.
9. Orlova KA, Crino PB. The tuberous sclerosis complex. Ann N Y Acad Sci 2010; 1184:87-105.
10. Zonnenberg BA, Neary MP, Duh MS, Ionescu-Ittu R, Fortier J, Vekeman F. Observational study of characteristics and clinical outcomes of Dutch patients with tuberous sclerosis complex and renal angiomyolipoma treated with everolimus. PLoS One 2018; 13:e0204646.
11. Cepeda C, Levinson S, Yazon VW, et al. Cellular antiseizure mechanisms of everolimus in pediatric tuberous sclerosis complex, cortical dysplasia, and non-mTOR-mediated etiologies. Epilepsia Open 2018; 3(Suppl 2):180-90.
12. van der Poest Clement EA, Sahin M, Peters JM. Vigabatrin for epileptic spasms and tonic seizures in tuberous sclerosis complex. J Child Neurol 2018; 33:519-24.

LETTER TO THE EDITOR

POSITIVE ROLE OF COGNITIVE-BEHAVIORAL THERAPY ON SEXUAL DYSFUNCTION AND BEHAVIORAL PROBLEMS IN PROSTATE CANCER-TREATED PATIENTS

F-P. MENG and L-N. ZHOU

Department of Urology, China-Japan Union Hospital of Jilin University, Changchun, Jilin, China

Received Arrive March 5, 2020 – Accepted April 22, 2020

To the Editor,

Prostate cancer is one of the most common malignant tumors in the world, particularly in developed countries, due to an increase in age expectancy. The development of prostate cancer, as well as the treatment, is detrimental for patients as it significantly affects the physical and mental well-being and decreases the quality of life. There have been several studies showing the development of behavioral and physical alterations in prostate cancer patients undergoing treatment. Cancer survivors often suffer from a variety of behavioral changes, including insomnia. There is an increased tendency to develop stress, anxiety, depression, pain, fatigue, hot flashes, night sweats, sexual dysfunction, and cognitive decline in prostate cancer patients undergoing various types of treatments (1).

Scientists have explored the different techniques to overcome prostate cancer treatment-associated problems. The employment of pelvic floor muscle exercise in patients after radical prostatectomy has been associated with improvement in urinary incontinence, anxiety, depression, and overall quality of life. A study conducting The Individualized Diet and Exercise Adherence Pilot Trial (IDEA-P) in prostate cancer patients (n=32) undergoing androgen deprivation therapy has shown the improvement in mobility performance, body composition, and muscular strength (2). Considering the prostate cancer-associated problems as psychoneuromuscular, it has been proposed that psychosocial management may potentially yield good clinical results.

Cognitive behavioral therapy is a type of psychotherapy in which negative thoughts are altered to modify the unwanted behavior of the patients. It helps the patient to understand his thoughts and feelings that help in changing his behavior. It is well reported that mental health problems, including stress, anxiety and depression are due to over-thinking. Accordingly, a cognitive behavior therapist aims to help the patient to modify his thinking style and make him use evidence and logic. Indeed, cognitive behavioral therapy has been found to be effective in improving mental health and irrational beliefs. There is a potential of cognitive-based behavioral therapy in overcoming sexual dysfunction, stress, anxiety and associated behavioral changes in prostate cancer patients (3, 4). The present review describes the critical role of cognitive-behavioral therapy in improving prostate cancer treatment-associated sexual and behavioral alterations.

Prostate cancer patients are reported to exhibit sexual dysfunction following cancer treatment, which is dependent on the type of treatment received. The patients receiving radiation therapy display maximum preservation of sexual function. On the other hand, the patients undergoing non-nerve-sparing radical prostatectomy present the maximum disturbance in

Corresponding Author:
Fanping Meng,
Department of Urology, China-Japan Union Hospital of Jilin University,
No.126 Xiantai Street, Changchun, Jilin Province
130033, P.R. China
Fax: +86 43184995114 - Tel.: +86 43184995222
e-mail: fpingmeng@aliyun.com

0393-974X (2020)
Copyright © by BIOLIFE, s.a.s.
This publication and/or article is for individual use only and may not be further reproduced without written permission from the copyright holder.
Unauthorized reproduction may result in financial and other penalties
DISCLOSURE: ALL AUTHORS REPORT NO CONFLICTS OF INTEREST RELEVANT TO THIS ARTICLE.

sexual life. The other forms of treatment, including androgen-sparing therapy, brachytherapy and nerve-sparing radical prostatectomy, produce disturbance in the sexual life. In patients undergoing robot-assisted laparoscopic prostatectomy, the urinary and bowel-related functions are reported to recover after 24 months of surgery. However, incontinence and sexual functioning remained significantly deteriorated in these patients.

It is possible that there may be a more significant role of interpersonal problems and interpersonal sensitivity in controlling the recovery of sexual functioning following radical prostatectomy. In a randomized controlled clinical trial involving 101 patients being subjected to radical prostatectomy, the employment of 10-week group-based cognitive-behavioral stress management intervention was shown to be effective in promoting the sexual recovery in those patients. The greater benefits were produced in patients with higher levels of interpersonal sensitivity (5). Other clinical studies have reported the efficacy of a 10-week group-based cognitive-behavioral stress management in improving the quality of life including sexual functioning in Hispanic monolingual men, non-Hispanic Whites and others, which were earlier treated for localized prostate carcinoma (6). A randomized trial in 60 patients who underwent radical prostatectomy for localized prostate cancer described the efficacy of 8-week cognitive-behavioral in improving sexual confidence, masculine self-esteem, sexual drive, relationship and satisfaction suggesting the promising role of this therapy in improving the quality of sexual life (4).

Patients undergoing radical and laparoscopic prostatectomy are at risk for the development of psychological burden, anxiety and depression. It has been shown that psychotherapy may be useful in improving overall well-being and cancer-related distress in prostate cancer patients. Considering the fact that the high percentage of men (around 40%) with prostate cancer develop psychological distress, it is proposed that psychological flexibility and mindfulness may be promising interventions to bring improvement in these patients. Despite a few negative reports showing the non-significant effect of mindfulness-based cognitive therapy in reducing distress in advanced prostate cancer patients over a period of 9 months, there have been a number of studies showing the effectiveness of psychosocial strategies in reducing anxiety and depression following three months of intervention in prostate cancer patients. A randomized controlled study enrolling 86 patients reported the effectiveness of two weeks of cognitive-behavioral intervention in the form of relaxation, imagery and distraction exercises in reducing pain, fatigue and sleep disturbances in prostate cancer patients (3). Another study has shown that the employment of cognitive behavioral therapy for two weeks led to a significant improvement in pain, fatigue and sleep disturbance. Indeed, the patients were found to enjoy the interventions, learned the skills and perceived the improvement in symptoms (7). A study based on the randomized clinical trial on family caregivers (n=80) of prostate cancer patients documented that the employment of 10 sessions of group cognitive behavioral therapy led to improvement in depression, anxiety, and stress over a period of 4 to 8 weeks (8).

The clinical utility of mindfulness-based group interventions in reducing anxiety, avoidance and fear in advanced prostate cancer patients has been documented. The basic principle of mindfulness is to make the patients aware of current experience and so that over time, the person gains the ability to become less reactive to difficult situations including the disease state. A randomized controlled pilot trial explored the feasibility and efficacy of an 8-week, mindfulness training program in reducing stress and anxiety in prostate cancer patients (n=24). It was shown that there is a significant decrease in prostate cancer-associated anxiety, intolerance and posttraumatic growth along with significant increase in mindfulness and general mental health over a long period of follow-up (up to 12 months) (9). A randomized clinical trial (The SWORD Study) on cancer survivor patients, including prostate cancer patients, showed the statistical and clinical efficacy of blended cognitive behavior therapy in reducing the severity of fear of cancer recurrence from 6 months to 5 years after the treatment (10).

There have been studies showing the efficacy

of web-delivered cognitive behavioral therapy in improving the psychological and quality of life outcomes in distressed cancer patients. In one study, the implementation and feasibility of PROMIS® computer adaptive tests using a web-based method in improving the psychosocial functioning has been described in advanced prostate cancer undergoing hormone therapy. In a Cognitive-Behavioral Stress Management (CBSM) study, the participants (n=95) were asked to attend and complete PROMIS® computer adaptive tests using video conferencing for 10 weeks. The results depicted a decrease in anxiety scores in these patients in comparison to corresponding patients (n=97) with no such behavioral therapy, suggesting the usefulness of web-based interventions in decreasing psychosocial distress in men undergoing hormone therapy (11).

The development of hot flashes and night sweats in prostate cancer patients receiving androgen deprivation therapy is very common, which significantly affects the quality of life. The efficacy of guided self-help cognitive behavioral intervention in managing hot flushes and night sweats in 20 patients recruited from a MANCAN trial has been documented. A randomized clinical trial enrolled 70 prostate cancer patients undergoing cancer treatment and experiencing more than 10 hot flashes or night sweats/week for over a period of one month. The patients were subjected to four-week cognitive behavioural therapy in the form of relaxation, respiration, stress management, controlling thoughts and beliefs, managing sleep and night sweats. The employment of self-report questionnaires at baseline, 6 weeks and 32 weeks revealed the effectiveness in reducing the frequency of hot flashes and night sweats (12).

One of the therapies in the management of prostate cancer involves the employment of androgen deprivation therapy, which is associated with a significant decline in cognitive functioning in prostate cancer patients. There was a presence of more cognitive problems in non-metastatic prostate cancer patients treated with androgen deprivation therapy in comparison to patients not undergoing such treatment. Moreover, these patients were more labile emotionally and exhibited marked impulsivity, which had a severe impact on the quality of life. Particularly, there was a significant reduction in spatial reasoning, spatial abilities and working memory in these patients. Indeed, using functional magnetic resonance imaging, it was shown that there was a reduction in the activation in right parietal-occipital regions, particularly during the recall of spatial location of objects. It has been shown that androgen deprivation in prostate cancer patients leads to decrease in gray matter volume in the cortex region, which may account for decrease in memory functions. Furthermore, the patients undergoing radical, laparoscopic prostatectomy are at risk for the development of cognitive dysfunction and disorders. A study on prostate cancer patients undergoing external-beam radiation therapy has shown the development of fatigue along with a significant decline in cognitive function (1). However, there are limited studies showing the influence of cognitive behavioral therapy in overcoming cognitive dysfunction.

CONCLUSION

Prostate cancer patients undergoing various types of treatments have an increased tendency to develop stress, anxiety, depression, pain, fatigue, hot flashes, night sweats, sexual dysfunction and cognitive decline. There is a potential for cognitive-based behavioral therapy in overcoming stress, anxiety and associated behavioral changes in these patients. However, there is still a need to explore the utility of cognitive behavioral therapy in overcoming cognitive dysfunction in prostate cancer patients.

REFERENCES

1. Jarzemski P, Brzoszczyk B, Popiołek A, et al. Cognitive function, depression, and anxiety in patients undergoing radical prostatectomy with and without adjuvant treatment. Neuropsychiatr Dis Treat 2019; 15:819-29.
2. Focht BC, Lucas AR, Grainger E, et al. Effects of a group-mediated exercise and dietary intervention in the treatment of prostate cancer patients undergoing androgen deprivation therapy: Results From the

IDEA-P Trial. Ann Behav Med 2018; 52:412-28.
3. Kwekkeboom KL, Abbott-Anderson K, Cherwin C, Roiland R, Serlin RC, Ward SE. Pilot randomized controlled trial of a patient-controlled cognitive-behavioral intervention for the pain, fatigue, and sleep disturbance symptom cluster in cancer. J Pain Symptom Manage 2012; 44:810-22.
4. Siddons HM, Wootten AC, Costello AJ. A randomised, wait-list controlled trial: evaluation of a cognitive-behavioural group intervention on psycho-sexual adjustment for men with localised prostate cancer. Psychooncology 2013; 22:2186-92.
5. Molton IR, Siegel SD, Penedo FJ, et al. Promoting recovery of sexual functioning after radical prostatectomy with group-based stress management: the role of interpersonal sensitivity. J Psychosom Res 2008; 64:527-36.
6. Penedo FJ, Traeger L, Dahn J, Molton I, Gonzalez JS, Schneiderman N, Antoni MH. Cognitive behavioral stress management intervention improves quality of life in Spanish monolingual hispanic men treated for localized prostate cancer: results of a randomized controlled trial. Int J Behav Med 2007; 14:164-72.
7. Kwekkeboom KL, Abbott-Anderson K, Wanta B. Feasibility of a patient-controlled cognitive-behavioral intervention for pain, fatigue, and sleep disturbance in cancer. Oncol Nurs Forum 2010; 37:E151-59.
8. Borji M, Nourmohammadi H, Otaghi M, Salimi AH, Tarjoman A. positive effects of cognitive behavioral therapy on depression, anxiety and stress of family caregivers of patients with prostate cancer: a randomized clinical trial. Asian Pac J Cancer Prev 2017; 18:3207-12.
9. Victorson D, Hankin V, Burns J, et al. Feasibility, acceptability and preliminary psychological benefits of mindfulness meditation training in a sample of men diagnosed with prostate cancer on active surveillance: results from a randomized controlled pilot trial. Psychooncology 2017; 26:1155-63.
10. van de Wal M, Thewes B, Gielissen M, Speckens A, Prins J. Efficacy of blended cognitive behavior therapy for high fear of recurrence in breast, prostate, and colorectal cancer survivors: The SWORD study, a randomized controlled trial. J Clin Oncol 2017; 35:2173-83.
11. Fox RS, Moreno PI, Yanez B, et al. Integrating PROMIS® computerized adaptive tests into a web-based intervention for prostate cancer. Health Psychol. 2019; 38:403-9.
12. Stefanopoulou E, Yousaf O, Grunfeld EA, Hunter MS. A randomised controlled trial of a brief cognitive behavioural intervention for men who have hot flushes following prostate cancer treatment (MANCAN). Psychooncology 2015; 24:1159-66.

LETTER TO THE EDITOR

EFFICACY OF A DIAGNOSTIC REAL-TIME POLYMERASE CHAIN REACTION TEST IN THE DETECTION AND QUANTIFICATION OF PERIODONTAL AND PERI-IMPLANT PATHOGENS: A PILOT STUDY

P.P. POLI, A. MASCELLARO, S. CAMPOLO, F. SIGNORINO, G. ALLOCCA and C. MAIORANA

Implant Center for Edentulism and Jawbone Atrophies, Maxillofacial Surgery and Odontostomatology Unit, Fondazione IRCCS Cà Granda Ospedale Maggiore Policlinico, University of Milan, Milan, Italy

Received October 26, 2019 – Accepted April 14, 2020

To the Editor,

Periodontitis is a microbially-associated, host-mediated inflammatory disease resulting in periodontal attachment loss and marginal alveolar bone resorption as a secondary feature (1). Similarly, peri-implantitis is a pathological condition characterized by inflammation of the peri-implant mucosa and progressive loss of supporting bone (2). Although plaque plays a pivotal role in the etiopathology of both diseases, there is no conclusive evidence as to whether dental biofilm profiles of implants are similar to periodontitis or if they represent another type of bacterial colonization. Irrespective of the microbiological profile, understanding the microbiota associated with the onset and progression of an infection is a crucial step to studying the effectiveness of different treatments. To overcome the drawbacks associated with culture techniques, including the difficulty in recovering cultivable species when they are found in low numbers, the need for experienced personnel, prolonged working time and relatively high cost, non-cultural diagnostic techniques have been advocated (3). Amongst them, real-time polymerase chain reaction (PCR) offers greater sensitivity than conventional quantitative anaerobic culture in the detection and quantification of target periodontal pathogens (4). More recently, real-time PCR has been used to analyse the microbiome of healthy and diseased peri-implant tissues (5), to determine the risk profile of patient candidates to receive dental implants (6), to investigate the bacterial leakage at implant-abutment connection (7) and to explore possible correlations with peri-implant marginal bone loss (8). However, additional evidence is needed to strengthen the usefulness of molecular techniques in the diagnosis and treatment of periodontal and peri-implant diseases. In view of the above, the aim of the present pilot study was to investigate the efficacy of a real-time PCR test in providing reliable qualitative and quantitative analyses in the evaluation of subgingival microbial profile around periodontal and peri-implant tissues.

MATERIALS AND METHODS

Patient population

The preliminary sample consisted of 30 adult

Key words: microbial testing; periodontitis; peri-implantitis; periodontopathogens; real-time polymerase chain reaction

Corresponding Author:
Anna Mascellaro, DDS
Implant Center for Edentulism and Jawbone Atrophies, Maxillofacial Surgery and Odontostomatology Unit, Fondazione IRCCS Cà Granda Ospedale Maggiore Policlinico, University of Milan, Via Commenda 10, 20122 Milan, Italy
Tel.: +39 02 55032621 - Fax: +39 02 55032513
e-mail: anna.mascellaro@gmail.com

0393-974X (2020)
Copyright © by BIOLIFE, s.a.s.
This publication and/or article is for individual use only and may not be further reproduced without written permission from the copyright holder.
Unauthorized reproduction may result in financial and other penalties
DISCLOSURE: ALL AUTHORS REPORT NO CONFLICTS OF INTEREST RELEVANT TO THIS ARTICLE.

patients screened in a university setting by a well-trained professional dental hygienist between March and December 2017. The mean age of the patients was 53.3±9 years. Patients were randomly selected from the Department database using computer-generated lists of random numbers. A signed informed consent was obtained from each patient after all procedures were fully explained. The following inclusion criteria were adopted: male and female patients aged ≥ 18 years; absence of local or systemic diseases; no pregnancy or breastfeeding; no previous periodontal treatment and no intake of systemic antibiotics during the previous 6 months; no intake of anti-inflammatory medication in the previous 4 months; no routine use of oral antiseptics.

During the first visit, medical history and background of each patient were recorded, including age and sex. Periodontal and peri-implant status were examined at six sites per tooth excluding third molars, namely mesio-buccal, buccal, disto-buccal, mesio-lingual/palatal, lingual/palatal, and disto-lingual/palatal. Probing depths (PD) and clinical attachment levels on natural teeth (CAL) were measured using a periodontal probe (PCP-UNC 15; Hu-Friedy, Chicago, IL, USA) inserted into the gingival/peri-implant sulcus parallel to the long axis of the tooth/crown until slight resistance was met. Bleeding on probing (BOP+) and presence of plaque (P+) were also registered to calculate full mouth bleeding score (FMBS) and full mouth plaque score (FMPS). Radiographic bone loss was assessed on the most recent radiological exam performed within 3 months from the recall visit.

Patients were equally distributed to one of the following groups depending on their periodontal and peri-implant conditions: (A) 10 periodontally healthy patients (PHP); (B) 10 patients diagnosed with periodontitis (periodontitis affected patients, PAP); C) 10 patients presenting at least one implant affected by peri-implantitis (peri-implantitis patients, PIP). Patients were considered healthy in case of no clinically detectable interdental CAL^+, no sites with buccal/oral recessions associated with PD > 3 mm, and < 10% BOP+ sites (1). To be diagnosed with periodontitis, patients had to present with detectable interdental CAL^+ at ≥ 2 non-adjacent teeth, or buccal/oral CAL^+ ≥ 3 mm with PD > 3 mm detectable at ≥ 2 teeth, given that the observed CAL is unrelated to non-periodontal causes (1). An implant was diagnosed with peri-implantitis if presenting with peri-implant marginal bone loss ≥ 3 mm apical of the most coronal portion of the intra-osseous part of the implant, and concomitant BOP+ or pus on probing at the time of examination (2).

Microbiological sampling

Patients were instructed not to brush their teeth or eat for up to 1 hour prior to sampling. In each patient, the site with the deepest PD was chosen as the harvesting site for the microbiological sampling. Supra-gingival/mucosal plaque and calculus were removed with a sterile periodontal curette without penetrating the gingival or peri-implant sulcus. The site was dried gently with an air pistol and isolated from saliva with cotton rolls. Subsequently, sub-gingival/mucosal plaque samples were collected from teeth or implants using sterile paper points, carefully inserted into the depth of the gingival/peri-implant pocket from the apical aspect with the help of sterile college tweezers and left in position for 20 seconds. The paper tip was finally placed in an empty, sterile, 2-mL Eppendorf tube, and stored at -20°C until processing. Samples were placed directly in the reagent tube "RAPID DNA" with no pre-treatment procedures required. Delivery of the samples to the laboratory was carried out within 12 hours in thermos with ice. The microbiological samples were sent to a laboratory of molecular biology (Istituto Auxologico Italiano, Cusano Milanino, Milan, Italy) and processed by an operator blinded to the study design. The DNA analysis by means of real-time PCR was performed with a commercially available kit (PeriodontScreen Real-TM, Sacace Biotechnologies, Como, Italy). The test was considered valid in case of human DNA detection, otherwise the test was considered invalid. The following periodontal pathogens were identified and quantified as colony-forming units (CFU)/mL: *Porphyromonas gingivalis* (PG), *Treponema denticola* (TD), *Tannerella forsythia* (TF), *Aggregatibacter actinomycetemcomitans* (AA), *Fusobacterium Nucleatum* (FN), *Porphyromonas endodontalis* (PE), and *Prevotella intermedia* (PI).

The real-time PCR kit used in the present study was a quantitative test that allowed the detection of periodontal pathogens by real-time PCR based on the amplification of the genome specific region using specific primers. In real-time PCR the amplified product was detected using fluorescent dyes. These dyes were linked to oligonucleotide probes that bound specifically to the amplified product. The real-time monitoring of the fluorescence intensities during the reaction allowed the detection of accumulating product without re-opening of the reaction tubes after the PCR run. All microorganisms detected by the real-time PCR kit panel had different pathogenic potential. A result was considered positive when the concentration of the examined periodontal pathogen was above the clinically significant titre. The operator evaluated the total potential pathogenic microflora depending on the type of microorganism and its concentration according to the data presented in Table I.

Statistical analysis

Statistical analyses were performed using IBM SPSS Statistics 24.0 (IBM Corp, Armonk, NY), adopting the implant as the statistical unit. The Shapiro-Wilk test was used to assess the normality of data distribution. Because the distribution of the data in some datasets did not meet the requirements for normality and homogeneity of variance assumptions ($P < 0.05$), quantitative data were analysed using non-parametric tests. The bacterial copy count of each periodontal pathogen and proportion of each bacterium to the total copy count were compared using the Kruskal–Wallis tests. Dunn's test with Bonferroni correction was used as post-hoc test for pairwise multiple comparisons in each periodontal pathogen group. P-values of < 0.05 were considered significant.

RESULTS

Overall, colonization by at least one periodontal pathogen was found in 26 sites in 26 patients. Four patients were not colonized by any assessed periodontal pathogen. The overall distribution of the

Table I. *Demographic qualitative data according to the threshold values suggested by the manufacturer for each pathogen.*

PCR analysis	Tested pathogen	PG	TD	TF	AA	FN	PE	PI
	Threshold value	**1.00E+05**	**1.00E+05**	**1.00E+05**	**1.00E+04**	**1.00E+06**	**1.00E+06**	**1.00E+06**
Patients	Total yes	14	4	9	1	2	2	3
	Total no	16	26	21	29	28	28	27
	Total PHP yes	0	0	0	0	0	0	0
	Total PHP no	10	10	10	10	10	10	10
	Total PAP yes	7	1	4	1	1	0	1
	Total PAP no	3	9	6	9	9	10	9
	Total PIP yes	7	3	5	0	1	2	2
	Total PIP no	3	7	5	10	9	8	8

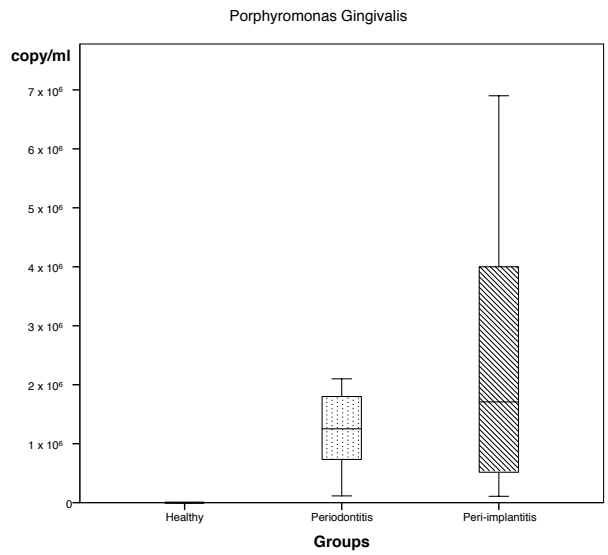
Table II. *Overall maximum and minimum values of each pathogen and group comparisons.*

	Values (patient group)		Statistical comparison within groups		
Pathogen	**Minimum**	**Maximum**	**PHP vs PAP**	**PHP vs PIP**	**PAP vs PIP**
P.gingivalis	0	6.90E+06 (PIP)	0.001*	0.000*	1.000
T.denticola	0	8.63E+05 (PAP)	0.000*	0.000*	1.000
T.forsythia	0	1.10E+06 (PIP)	0.004*	0.000*	0.596
A. actinomycetemcomitans	0	2.99E+05 (PAP)	n/a	n/a	n/a
Fusobacterium Nucleatum	0	2.50E+06 (PAP)	0.002*	0.000*	1.000
Porphyromonas endodontalis	0	1.00E+06 (PIP)	0.423	0.017*	0.597
Prevotella intermedia	0	4.00E+06 (PIP)	0.181	0.003*	0.480

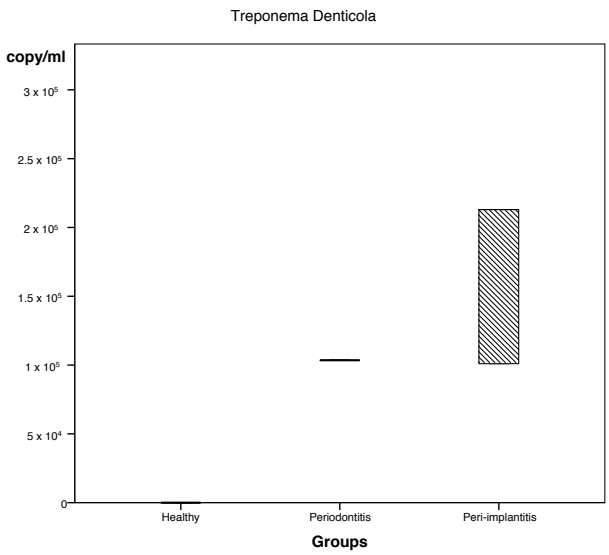
* *Statistically significant difference*

detected periodontal pathogens amongst the different study groups according to the manufacturer's threshold values is reported in Table I. No bacterial counts were detected in any healthy patient. Based on this result, the specificity of the test intended as the ability to detect a true negative, being based on the true negative rate, correctly identifying subjects who do not have a condition, was 100%. The minimum and maximum values of the seven pathogens were reported in Table II.

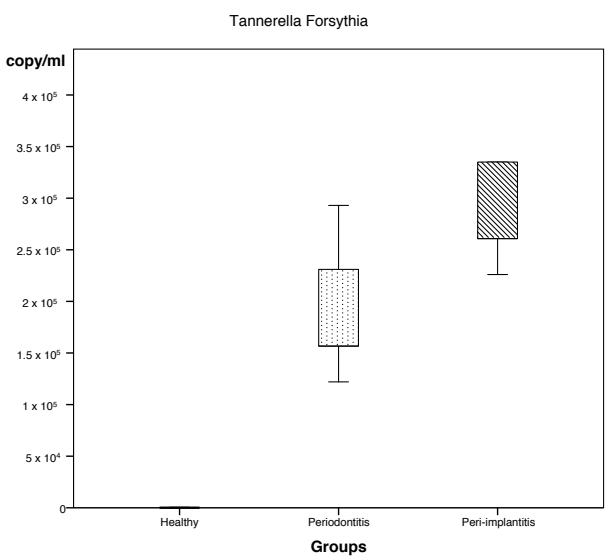
Box plots of copy counts number (copy/ml) of the periodontal pathogens detected in plaque samples are represented in Fig. 1. No statistically significant differences in terms of bacterial copy count emerged from the comparison between patients affected by periodontitis and subjects presenting with peri-implantitis at any periodontal pathogen group. The bacterial counts in patients affected by periodontitis and peri-implantitis were significantly higher than those observed in healthy patients except for PE



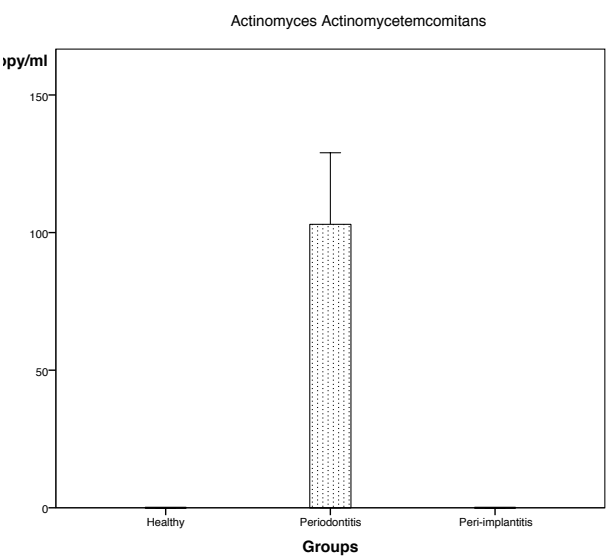
A



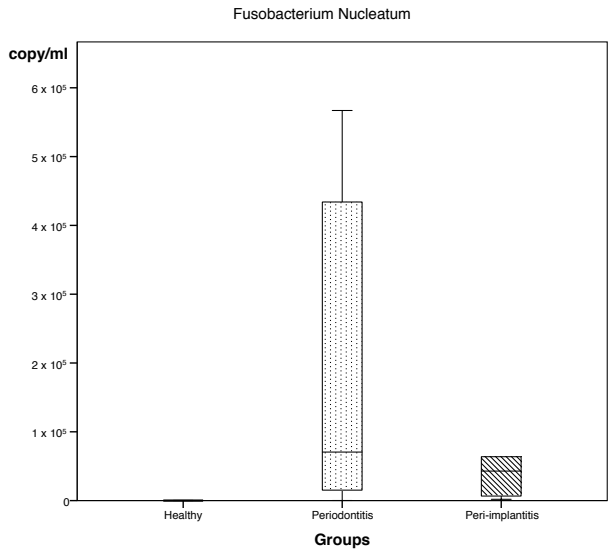
B



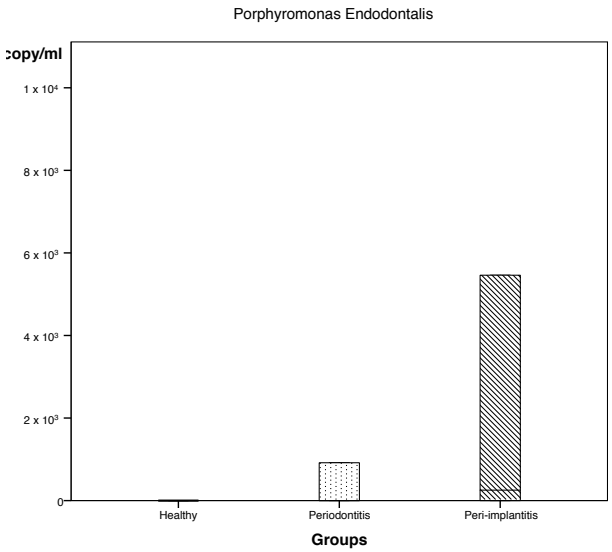
C



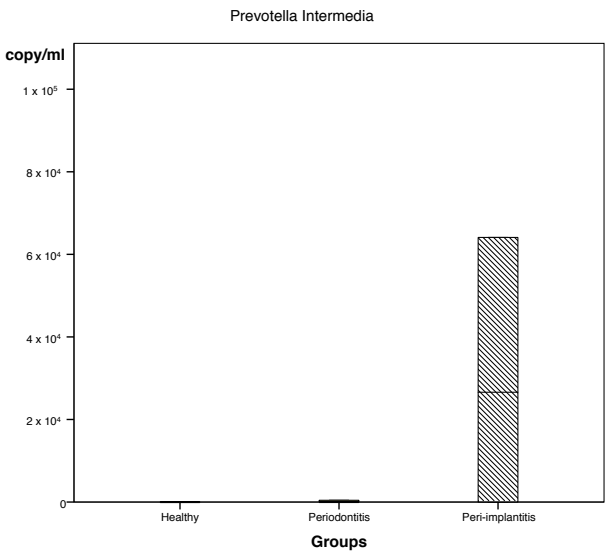
D



E



F



G

Fig. 1. *Box plot of copy count numbers (copy/ml) of seven periodontal pathogens in plaque samples.*

and PI (Table II). Due to the very low copy count numbers of AA measured in all groups, no statistical analysis could be performed for this pathogen.

DISCUSSION

The results of the present pilot study are consistent with a recent systematic review pointing out the lack of striking differences between subgingival microbiome associated with peri-implantitis and periodontitis (9). This applies to the tested pathogens, whereas genomic sequencing analysis suggested that uncultivable asaccharolytic anaerobic Gram-positive rods and anaerobic Gram-negative rods may also be found at peri-implantitis sites (10). It has been claimed that PCR may facilitate the detection and quantification of bacteria species indicative of the disease in order

to assess the stage of periodontitis infections, and initiate effective treatments. In particular, microbial testing is of paramount importance when it comes to patients non-responsive to scaling and root planing, in order to identify the target pathogens and choose the correct class of antibiotics, thus reducing the risk of arbitrary drug prescriptions (3). Microbial testing might be useful also at the end of the treatment, when follow-up testing may ensure that target pathogens have been eliminated or reduced and that resistant species have not emerged. All is made possible by the fact that PCR is a sensitive and specific method which has a high positive predictive value when it comes to the detection of target pathogens as emerged from the present study. It is also noteworthy that not all sites within a subject are equally susceptible to periodontal disease at once. This site-specific clinical pattern can be attributed to differences in the bacterial species composition of subgingival plaque. In this sense, the early recognition of microbial challenges to the host by means of PCR analysis is crucial to provide a benefit in terms of disease control at the site-specific level. Moreover, the detection of a specific threshold of concentration levels of certain bacterial clusters may serve as a predictor of periodontitis severity at site-specific level (11). The same concepts apply to peri-implant disease, bearing in mind that non-surgical therapy has proven to be of reduced effectiveness to arrest the progression of peri-implantitis. Accordingly, PCR may be helpful not only in the treatment phase to identify the profile and prevalence of periodontopathogens in order to choose ideal adjuvants to the surgical therapy. As periodontal pathogens are likely to be associated with peri-implantitis, it appears valid to test for periodontal disease-causing bacteria before implant therapy and ascertain the risk of peri-implantitis. This might be of particular interest in patients who had been suffering from periodontitis, who are more susceptible to peri-implant disease (6). The results obtained in the present study confirmed a correlation between the bacterial count of each periodontal pathogen and the presence of periodontitis and peri-implantitis. This suggested that real-time PCR can be used to provide in a short time a qualitative and quantitative analysis of the samples collected from periodontal and peri-implant pockets with a certain degree of reliability. In view of the aforesaid, the adjunctive values of PCR to periodontal and peri-implant treatment should not be under-estimated.

REFERENCES

1. Tonetti MS, Sanz M. Implementation of the new classification of periodontal diseases: Decision-making algorithms for clinical practice and education. J Clin Periodontol 2019; 46:398-405.
2. Berglundh T, Armitage G, Araujo MG, et al. Peri-implant diseases and conditions: Consensus report of workgroup 4 of the 2017 World Workshop on the Classification of Periodontal and Peri-Implant Diseases and Conditions. J Periodontol 2018; 89(Suppl 1):S313-s18.
3. Shaddox LM, Walker C. Microbial testing in periodontics: value, limitations and future directions. Periodontol 2000 2009; 50:25-38.
4. Atieh MA. Accuracy of real-time polymerase chain reaction versus anaerobic culture in detection of Aggregatibacter actinomycetemcomitans and Porphyromonas gingivalis: a meta-analysis. J Periodontol 2008; 79:1620-9.
5. Canullo L, Penarrocha-Oltra D, Covani U, Botticelli D, Serino G, Penarrocha M. Clinical and microbiological findings in patients with peri-implantitis: a cross-sectional study. Clin Oral Implants Res 2016; 27:376-82.
6. Ito T, Yasuda M, Kaneko H, Sasaki H, Kato T, Yajima Y. Clinical evaluation of salivary periodontal pathogen levels by real-time polymerase chain reaction in patients before dental implant treatment. Clin Oral Implants Res 2014; 25:977-82.
7. Baj A, Romano M, Segna E, et al. Bidirectional flux of fluids and microbiota at implant-abutment connection of FMD Storm implant system: an in vitro stud y using RT-PCR. J Biol Regul Homeost Agents 2017; 31:155-61.
8. Jervoe-Storm PM, Jepsen S, Johren P, Mericske-Stern R, Enkling N. Internal bacterial colonization of implants: association with peri-implant bone loss. Clin Oral Implants Res 2015; 26:957-63.
9. Retamal-Valdes B, Formiga MC, Almeida ML, et al. Does subgingival bacterial colonization differ

between implants and teeth? A systematic review. Braz Oral Res 2019; 33:e064.

10. Lafaurie GI, Sabogal MA, Castillo DM, Rincon MV, Gomez LA, Lesmes YA, Chambrone L. Microbiome and Microbial Biofilm Profiles of Peri-Implantitis: A Systematic Review. J Periodontol 2017; 88:1066-89.
11. Tomas I, Regueira-Iglesias A, Lopez M, Arias-Bujanda N, Novoa L, Balsa-Castro C, Tomas M. Quantification by qPCR of Pathobionts in Chronic Periodontitis: Development of Predictive Models of Disease Severity at Site-Specific Level. Front Microbiol 2017; 8:1443.

LETTER TO THE EDITOR

AWARENESS, PERCEPTION AND READINESS REGARDING CLEAR ALIGNER THERAPY AMONG ORTHODONTISTS AND OTHER DENTAL SPECIALISTS

A.I. LINJAWI[1], M.A. ALSADAT[2], M.A. OTHMAN[2], L.M. FAKHRY[2], A.S. BASALAIM[2], R.A. ALANSARI[2], A.M. ABUSHAL[1] and H.A.BAESHEN[1]

[1]Orthodontic Department, Faculty of Dentistry, King Abdulaziz University, Jeddah, Saudi Arabia; [2]Faculty of Dentistry, King Abdulaziz University, Jeddah, Saudi Arabia

Received March 10, 2020 – Accepted April 24, 2020

To the Editor,

The demand for orthodontic treatment is increasing drastically with the advances in orthodontic treatment techniques, especially for managing adult orthodontic problems (1). Invisible orthodontics, including lingual appliances and clear aligners, are attracting more patients, especially professionals or individuals in direct contact with the public (2). Clear aligners are appliances made of different polymers and were first introduced for the treatment of simple orthodontic problems; however, with advances in technology, they are currently also used to treat complex cases (3).

The advantages of clear aligners include relative flexibility that allows removing the trays for eating, speaking, as well as easier oral hygiene maintenance, leading to better esthetics and periodontal health (3). In contrast, clear aligners have the disadvantages of patient compliance, unpredictability of complex cases, difficulty in controlling root movement and achieving inter-arch correction (1, 2)

The differences in treatment decisions between orthodontists and general dental practitioners (GDPs) in using aligners have been investigated (4). Vicéns and Russo found that orthodontists treated more cases using Invisalign than GDPs (4). They also found significant differences in opinions and knowledge between orthodontists and GDPs when treating certain complex conditions (4). Moreover, Best et al. investigated how orthodontists and GDPs differed in experience, as well as selection and management of cases treated with aligners (5). Furthermore, d'Apuzzo et al. compared orthodontists and GDPs in clear aligner experience, treated malocclusion, demands and perception of patients. They noted a high percentage of clear aligner usage was by orthodontists because they knew more about them. They also observed significant differences between orthodontists and GDPs in case selection and experience of using clear aligners (6). A discrepancy exists in the practice of clear aligners among orthodontists, GDP and other dental specialists. To date, no study in Kingdom of Saudi Arabia (KSA) has been performed to evaluate the knowledge and perception on the use of clear aligners. Therefore, the aim of this study was to compare the differences in awareness, perception and readiness for clear aligner usage among orthodontists, GDPs, and other dental specialists in Saudi Arabia.

MATERIALS AND METHODS

A cross-sectional electronic survey was conducted in the Kingdom of Saudi Arabia between September and December, 2019. Ethical approval was granted from the Ethics Committee at King Abdulaziz University. The sample was categorized into three groups: GDPs,

Key words: orthodontics; clear aligner therapy; perception; dentistry

Corresponding Author:
Dr. Amal I. Linjaw,
Orthodontic Department,
Faculty of Dentistry,
King Abdulaziz University
P.O. Box 80209, Jeddah 21589, Saudi Arabia
e-mail: ailenjawi@kau.edu.sa

0393-974X (2020)
Copyright © by BIOLIFE, s.a.s.
This publication and/or article is for individual use only and may not be further reproduced without written permission from the copyright holder.
Unauthorized reproduction may result in financial and other penalties
DISCLOSURE: ALL AUTHORS REPORT NO CONFLICTS OF INTEREST RELEVANT TO THIS ARTICLE.

orthodontists, and other dental specialists. The survey questionnaire consisted of 14 questions assessing the following variables.

Demographic data was collected related to age, gender, nationality, specialty, education level, and place of work. Regarding dentists' awareness about clear aligners: "Yes/No" questions were used to assess whether the participants were aware of clear aligners. For dentists' perception about clear aligner usage, the Five-point Likert scale questionnaire was used to assess participants' perception regarding the following variables: cost-effectiveness related to clear aligners, easiness of achieving ideal alignment and occlusion after using the clear aligner, working with difficult cases, requirement of a highly skilled orthodontist, patient cooperation when using clear aligners, suitability of clear aligners for adult and adolescent treatment, possibility of treatment being carried out by a certified general or restorative dentist, and awareness of the patients and public about clear aligners as a treatment modality for malocclusion problems.

In addition, a multiple-choice questionnaire was designed to assess the reasons that influenced the choice of clear aligners over other treatment modalities. For readiness of clear aligner usage. "Yes/No" questions were used to assess whether the participants were certified to use clear aligners and to assess whether they had attended any workshop/course for clear aligners.

In addition, five-point Likert scale questions were used to assess the following: the confidence level of using clear aligners as a treatment modality, recommendation for patients to choose clear aligners as a treatment option, and the future goal for their dental practice in increasing the number of clear aligner cases in the coming 10 years.

A link containing details of the questionnaire using survey monkey instrument was sent to different dental specialists, orthodontists and GDPs of various private and government dental clinics from the office of the Saudi dental Society. Reminder e-mails were sent periodically

Table I. *Demographic characteristics (n = 195)*

		GDP n=71 (36.4%)	Orthodontist n=62 (31.8%)	Other dental specialty n=62 (31.8%)	p-value
Age	<30	33 (46.5%)	3 (4.8%)	11 (17.7%)	0.000
	30-40	23 (32.4%)	39 (62.9%)	35 (56.5%)	
	>40-50	12 16.9%)	17 (27.4%)	12 (19.4%)	
	>50	3 (4.2%)	3 (4.2%)	4 (6.5%)	
Gender	Male	29 (40.8%)	45 (72.6%)	29 (46.8%)	0.001
	Female	42 (59.2%)	17 (27.4%)	33 (53.2%)	
Nationality	Saudi	34 (47.9%)	20 (32.3%)	35 (56.5%)	0.023
	Non-Saudi	37 (52.1%)	42 (67.7%)	27 (43.5%)	
Level of education	Bachelor	57 (80.3%)	0 (0%)	2 (3.2%)	0.000
	Postgraduate resident	7 (9.9%)	11 (17.7%)	9 (14.5%)	
	Master holder	2 (2.8%)	31 (50%)	28 (45.2%)	
	Board certified	4 (5.6%)	8 (12.9%)	7 (11.3%)	
	PhD holder	1 (1.4%)	12 (19.4%)	16 (25.8%)	
Place of work	Governmental hospital/clinic	7 (9.9%)	9 (14.5%)	15 (24.2%)	0.023
	Private hospital/ clinic	59 (83.1%)	41 (66.1%)	28 (45.2%)	
	Academic institute	3 (4.2%)	5 (8.1%)	14 (22.6%)	
	Unemployed	1 (1.4%)	1 (1.6%)	1 (1.6%)	
	Both Academic institute & other clinics	1 (1.4%)	6 (9.7%)	4 (6.5%)	

to improve the response rate. Data were collected and descriptive statistics were calculated for frequencies and percentages. Group comparisons were conducted using the Pearson *Chi*-squared and Kruskal-Wallis tests. Data were analyzed using Microsoft Excel 2007 (Microsoft Corporation, Redmond, WA, USA) and IBM SPSS Statistics for Windows, Version 20.0 (IBM Corp., Armonk, NY, USA). The level of significance was set at $P<0.05$.

RESULTS

The response rate was 195/300 (65%) distributed as follows: GDPs (n=71, 36.4%), orthodontists (n=62, 31.8%), and other dental specialists (n=62, 31.8%). Table I summarizes the sample characteristics and distribution.

Awareness and perception regarding clear aligner usage

Fig. 1 shows the responses to the questions assessing the "Dentists' awareness about clear aligners." The results indicated that 93.5% of orthodontists, 60% of GDPs, and 62% of other dental specialists were aware of clear aligners, with a significant difference between the groups (P=0.000).

Fig.1 shows the responses with "agree" to the questions assessing the "Dentists' perception about clear aligner usage. Clear aligners are cost-effective: was agreed by 59.7% of orthodontists, and only 38% of GDPs and 32.3% of other dental specialists. 50% of orthodontists agreed that ideal alignment and occlusion were easily achieved using clear aligners most of the time, whereas, only 31% of GDPs and 27.4% of other dental specialists agreed with this statement. Clear aligners work in difficult cases was agreed by only 25.8% of orthodontists, 7% of GDPs, and 4.8% of other dental specialists. Clear aligners require highly skilled orthodontists were found to be in agreement by 61.3% of orthodontists and only 19.7% of GDPs and 25.8% of other dental specialists agreed that clear aligners require highly skilled orthodontists. Clear aligners require high patient cooperation was agreed by 88.7% of orthodontists, 49.3% of GDPs, and 58.1% of other dental specialists. Clear aligners were suitable for adult treatment only were agreed by 41.9% of orthodontists while only, 19.7% of GDPs and 24.2%

Table II. *Responses to questions assessing the "Readiness to clear aligner usage" (n = 195).*

		GDP n=71 (36.4%)	Orthodontist n=62 (31.8%)	Other dental specialty n=62 (31.8%)	p-value
Are you certified to use clear aligners?	Yes	3 (4.2%)	46 (74.2%)	2 (3.2%)	0.000
Did you take any courses or workshops on clear aligners?	Yes	8 (11.3%)	51 (82.3%)	5 (8.1%)	0.000
How do you rate your confidence level in using clear aligners in your clinic?	Confident / Very confident	7 (9.9%)	28 (45.2%)	7 (11.3%)	0.000
How far do you recommend clear aligners for your patients that have malocclusion problems?	Sometimes / Highly recommend	9 (12.8%)	19 (30.6%)	9 (14.5%)	0.000
How do you foresee your clinics after 10 years? (How many of your patients do you expect to be treated with clear aligners?)	I am not aware	28 (39.4%)	4 (6.5%)	23 (37.1%)	0.003
	0%	8 (11.3%)	3 (4.8%)	11 (17.7%)	
	<50%	2 (2.8%)	8 (12.9%)	3 (4.8%)	
	≥50%	30(42.3%)	42 (67.7%)	24 (38.7%)	
	100%	3 (4.29%)	5 (8.1%)	1 (1.6%)	

of other dental specialists agreed with this statement. Clear aligners being suitable for adolescent treatment was agreed by 54.8% of orthodontists, 31% of GDPs, and 35.5% of other dental specialists. According to the statement all cases can be treated by a certified general or restorative dentist 9.7% of orthodontists, 12.9% of other dental specialists and 22.5% of GDPs agreed with this statement. Many dentists use clear aligners in treatment: was agreed by only 27.4% of orthodontists, 11.3% of GDPs, and 8.1% of other dental specialists. Many of the patients are aware of clear aligner therapy: was agreed by 51.6% of orthodontists, 19.7% of GDPs and 17.7% of other dental specialists. Response on statement regarding public awareness on clear aligners 43.5% of orthodontists, 19.7% of GDPs and 21% of other dental specialists agreed with it. A significant difference between the groups ($p<0.05$) was reported in responses to the questions assessing the dentists' perception about clear aligner usage except for the following factors: ideal alignment and occlusion easily achieved most of the time ($p=0.448$); clear aligners work in difficult cases ($p=0.073$); clear aligners are suitable for adult treatment only ($p=0.980$); and many dentists use clear aligners in treatment ($p=0.229$).

Readiness for clear aligner usage

Table II shows the responses to the questions assessing the readiness for clear aligner usage; 74.2% of orthodontists, and only 4.2% of GDPs and 3.2% of the other dental specialists were certified to use clear aligners. Furthermore, 82.3% of orthodontists, and only 11.3% of GDPs and 8.1% of other dental specialists attended training courses on clear aligners. In addition, 45.2% of orthodontists, and only 9.9% of GDPs and 11.3% of other dental specialists were confident in using clear aligners. Moreover, 30.6% of orthodontists, 12.8% of GDPs and 14.5% of other dental specialists highly recommended clear aligners. Approximately, 67.7% of orthodontists, 42.3% of GDPs, and 38.7% of other dental specialists foresaw that more than 50% of their patients will be treated using clear aligners within the coming 10 years. A significant difference between the groups ($p<0.01$) was reported in their responses to all the variables assessing the readiness for clear aligner usage.

DISCUSSION

The results of the present study indicated that 93.5% of orthodontists and almost 60% of GDPs and other dental specialists were aware of clear aligners. However, only 74% of orthodontists were certified to use clear aligners in their practices, 80% of them attended courses on clear aligners, 45% of them felt confident to use them, and only 30% highly recommended them to their patients. These findings indicate that clear aligner usage is still limited in Saudi Arabia; nevertheless, dentists have strong intentions to utilize them in the near future. A study by Al-Hamlan et al. reported that 64% of orthodontic residents used Invisalign during their training, which supports the predicted increase in demand of this treatment modality in the coming future (7). Moreover, orthodontists in the present study, significantly differed in their perception about clear aligner usage. These findings were in line with the study carried out by Bindayel et al., who also found that the public in Saudi Arabia are highly aware of clear aligner therapy (8, 9). Moreover, the current study reported that most orthodontists and other dental specialists disagreed that all cases can be treated by certified general or restorative dentists. These findings were in agreement with work by Vicéns and Russo who reported GDPs and orthodontists being uncomfortable treating patients with clear aligners after their initial certification, and that they needed more training to become confident in using this treatment modality. They also found a significant difference in case selection between both groups (4).

Studies found that orthodontists were more confident in using clear aligners, treating cases through clear aligners, and using intra-arch elastics and auxiliaries. GDPs generally aimed to achieve acceptable esthetic results while orthodontists focused more on achieving acceptable and functional occlusion (10). Moreover, work by d'Apuzzo et al. further found that orthodontists felt that clear aligners limited treatment outcomes, whereas GDPs were more concerned that they do not have enough experience to use them (6, 11).

The findings of the current study are in agreement with those of previous studies in that orthodontists are more confident in using clear aligners in their

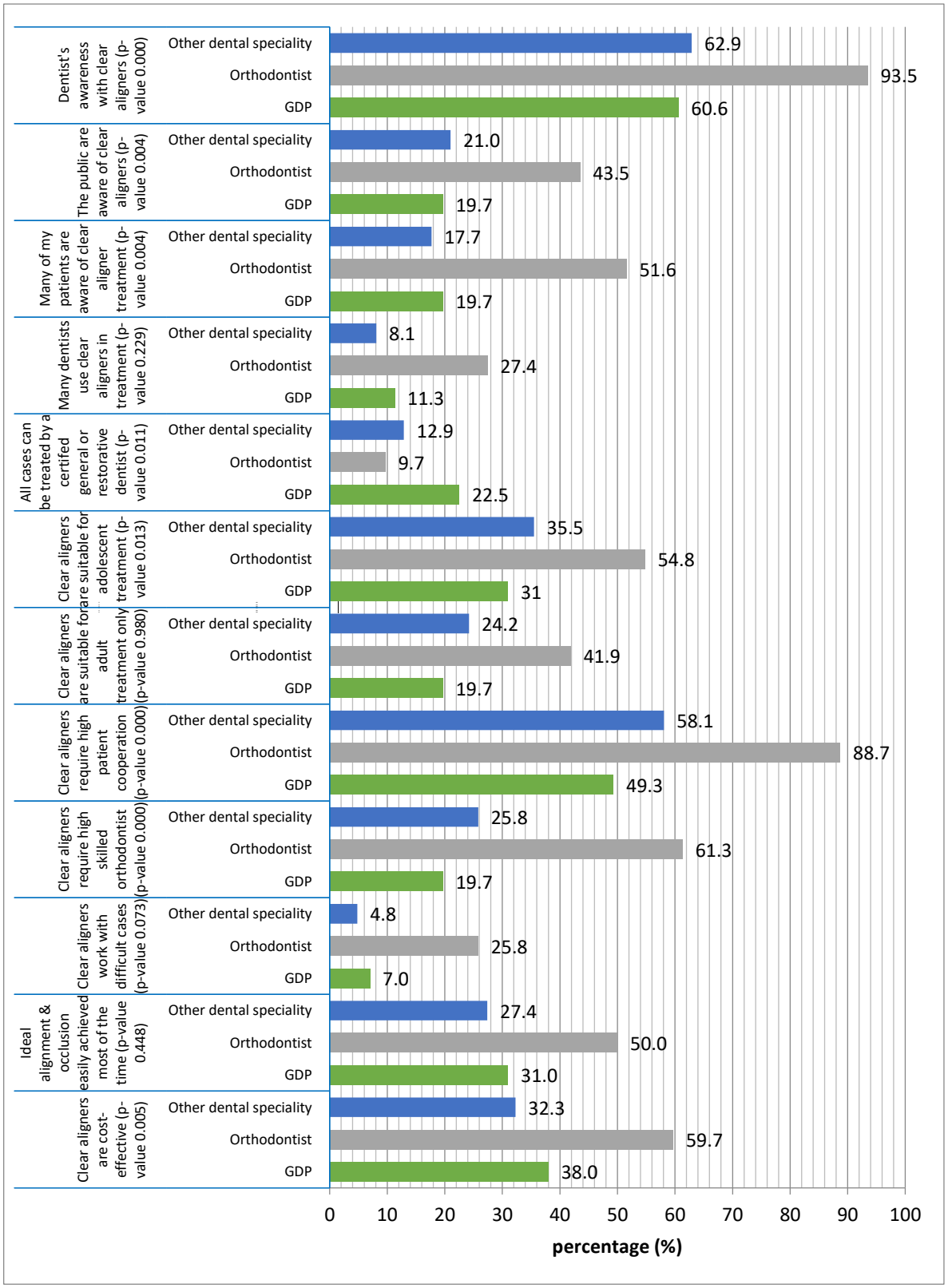


Fig. 1. *Dentists' awareness to clear aligners distributed according to the studied groups and Responses with "Agree" to variables assessing "Dentists' perception to clear aligner usage" (n = 195).*

practice. However, the current study shows that clear aligner usage, especially by GDPs, is still limited in Saudi Arabia. The small size of sample raises concerns on the generalizability of the results. Thus, a wider range of regions needs to be covered to obtain a better and more generalizable conclusion. To conclude, approximately 93.5% of orthodontists, 60% of GDPs, and 62% of other dental specialists were aware of clear aligners. Orthodontists significantly differed in their perception about clear aligner usage. Moreover, a positive attitude of orthodontists to use clear aligners in their practice was seen.

ACKNOWLEDGEMENTS

The Authors would like to thank the following personnel for their contribution in dispensing the questionnaire. Farah Abdullatif Alsadat, Hussain Yousof Marghalani, Muad Mohammed Assiry, Abdulaziz, Khalid Alnabulsi, Moeid Talal Alhowig, Naif Mari Alqarni, Omama Yousif Basodan, Asmahan Saeed Alamoudi.

REFERENCES

1. Ahmed MS. Attitudes and awareness toward advanced orthodontic procedures and characteristic of orthodontic practice in Saudi Arabia. JDOH 2017; 1-5.
2. Cooper-Kazaz R, Ivgi I, Canetti L, et al. The impact of personality on adult patients' adjustability to orthodontic appliances. Angle Orthod 2013; 83:76-82.
3. Rosvall MD, Fields HW, Ziuchkovski J, Rosenstiel SF, Johnston WM. Attractiveness, acceptability, and value of orthodontic appliances. Am J Orthod Dentofac Orthop 2009; 135:276-77.
4. Vicéns J, Russo A. Comparative use of invisalign® by orthodontists and general practitioners. Angle Orthod 2010; 80:425-34.
5. Best AD, Shroff B, Carrico CK, Lindauer SJ. Treatment management between orthodontists and general practitioners performing clear aligner therapy. Angle Orthod 2017; 87:432-39.
6. d'Apuzzo F, Perillo L, Carrico CK, Castroflorio T, Grassia V, Lindauer SJ. Clear aligner treatment: different perspectives between orthodontists and general dentists. Prog Orthod 2019; 20. doi: 10.1186/s40510-019-0263-3
7. Al-Ruwaithi M, Al-Shraim N, El-Metwaaly A, Al-Hamlan N. Motivations and future practice plans of orthodontic residents in Saudi Arabia. J Orthod Sci 2013; 2:67.
8. Bindayel N. Awareness of orthodontic modalities and preference of appliance and payment options in Saudi Arabia. Saudi J Oral Sci 2018; 5:98.
9. Meier B, Wiemer KB, Miethke RR. Invisalign® - Ein Patientenprofil. Auswertung einer prospektiven Befragung. J Orofac Orthop 2003; 64:352-58.
10. Akyalcin S. Specialist training influences the ability to recognise orthodontic case complexity. J Orthod 2019; 46:35-38.
11. Shin K. The Invisalign appliance could be an effective modality for treating overbite malocclusions within a mild to moderate range. J Evid Based Dent Pract 2017; 17:278-80.

LETTER TO THE EDITOR

EFFECT OF FIXED ORTHODONTIC APPLIANCE THERAPY ON PERIODONTAL HEALTH STATUS OF PATIENTS EVALUATED THROUGH COMMUNITY PERIODONTAL INDEX

A. ALNAZEH, M.A. KAMRAN, I. ALSHAHRANI, A.H. ALI, O.M SAAD and A. FAHAD

Department of Pedodontics and Orthodontics Sciences, College of Dentistry, King Khalid University, Abha, Saudi Arabia

Received March 11, 2020 – Accepted April 24, 2020

To the Editor,

Facial skeleton and tooth relationship play a foremost role in the functioning and aesthetics of a person's dynamism. Any disproportion between the two may result in distorted dental and skeletal problems, which may further contribute to corporeal imbalance, repulsive aesthetics and distressed psychosomatic integrity of patients (1). Such patients require orthodontic treatment, since orthodontics is the branch of dentistry that deals with facial growth, development and occlusion, along with the diagnosis, interception, and development of occlusal anomalies (2). Therefore, orthodontics aim to create harmony in dental and skeletal structures. Through orthodontics, the patients move towards a healthy, confident and momentous life and turn into an efficient component of the society (3).

Periodontal health of teeth also contributes towards healthy oral comfort. Periodontal tissues not only hold the teeth in the socket but also preserve the integrity of strong and natural bone. It is evident from the literature that periodontal diseases are linked to many systemic disorders (2, 3). Studies conducted by Hamsha et al. and Wang et al. revealed a significant relationship between systemic illness and periodontal and oral health status (4, 5). Orthodontics and periodontics are strongly related to each other, however, in the presence of poor oral hygiene and under circumstances of certain types of periodontal disorders, fixed orthodontic appliances and tooth movement can contribute to significant deleterious periodontal consequences (6)

Effect of orthodontic treatment on periodontal health can be evaluated objectively. Various scales and measurement criteria which evaluate the presence or absence, progress, and stage of gingival and periodontal destruction can be followed. Community periodontal index of treatment needs (CPI) scoring is one scale. CPI is strongly recommended by WHO and FDI as it is an effective epidemiological procedure which screens and monitors individuals for existing and progressive periodontal disease (7, 8).

Limited data is available on evaluation of CPI scores pre- and pos- orthodontic treatment among Saudi patients. Therefore, this study was planned with the rationale to assess the effect of fixed orthodontic treatment on the periodontal health status of patients, evaluated through CPI pre- and three months post-orthodontic treatment.

MATERIALS AND METHODS

A cross-sectional study was conducted on 100 patients requiring fixed orthodontic treatment attending

Key words: orthodontics; periodontal disease; Community periodontal Index; Saudi Arabia

Corresponding Author:
Dr Muhammad Abdullah Kamran,
Department of Pedodontics and Orthodontics Sciences,
College of dentistry King Khalid University,
Abha, Saudi Arabia
e-mail: mmuhammad@kku.edu.sa

0393-974X (2020)
Copyright © by BIOLIFE, s.a.s.
This publication and/or article is for individual use only and may not be further reproduced without written permission from the copyright holder.
Unauthorized reproduction may result in financial and other penalties
DISCLOSURE: ALL AUTHORS REPORT NO CONFLICTS OF INTEREST RELEVANT TO THIS ARTICLE.

at the orthodontic outpatient department of King Khalid University. KSA. The total duration of the study was six months. The study was approved by the ethics review committee of KKU no. SRC/ETH/2018-19/080.

The inclusion criteria were patients of both genders, with ages ranging from 13 to 18 years, who required fixed orthodontic treatment and gave consent to participate in the study. The study sample was chosen using a simple random sampling technique. The exclusion criteria were subjects with skeletal deformities. Confidentiality and anonymity of the responses were assured to the respondent. Verbal informed consent was obtained from the patients participating in the study.

A sample size of 100 was calculated through Rao-soft software in which confidence interval of 95%, the margin of error was 5%, along with response distribution of 50%. All included patients underwent a complete pre-orthodontic evaluation which included history, examination and radiological evaluation using orthopantomography (OPG) and cephalometric analysis followed by interpretation. A final diagnosis was established, and a treatment plan was made. The patient's periodontal status was measured through CPI and findings were recorded on self-structured, predesigned proforma which included the demographic details and the information related to the CPI evaluation. The periodontal status of patients was premeasured before the start of fixed orthodontic treatment and after three months from the initiation of orthodontic therapy.

Statistical analysis

Data were analyzed using SPSS version 20.00. Frequencies and percentages were calculated for qualitative variables, most frequent CPI score and comparison of teeth among different sextants of maxilla and mandible. Pearson's n Correlation was used to correlate between tooth number and CPI score before and after orthodontic treatment. The *Chi*-squared test was used to evaluate significant relationship before and intra orthodontic treatment and CPI scores considering the p-value (≤ 0.05) significant.

RESULTS

Fifty males and 50 females with ages ranging from 13-18 years (mean15.3±1.75) were enrolled in the study. The mean score of CPI before and 3 months after orthodontic treatment was 14.20±6.45 and 14.59±6.54. The Pearson correlation Sig (2-tailed) test showed a negative and nonsignificant correlation between tooth number and CPI score before and after orthodontic treatment (Table I). The *Chi*-squared test revealed a significant relationship before, and three months post-orthodontic treatment and CPI score with the p-value of 0.03 ($p \leq 0.05$) which showed that there was a strong relationship orthodontic treatment and CPI score. Table II shows descriptive statistics including mean and SD before and after orthodontic treatment.

The results of the study revealed that the most frequent CPI score was scored after orthodontic treatment in all sextants of patients. Of 100 patients 77.7% scored for CPI 1 which means that bleeding was observed, directly or by using a mouth mirror, after probing. Approximately 12.1% and 5.2% patients had a score of 0 and 2, respectively, after orthodontic treatment (Fig. I). The CPI score 9 was not recorded for 3% teeth. None of the patients scored 3 and 4 CPI. Score X was recorded on 2% teeth (Table-II).

Comparison of teeth among different sextants of maxilla and mandible revealed that maxillary left second molar (27) accounts for the highest score 1 of CPI (Fig. 1) Similarly, 88% left mandibular first molar (36) accounted for CPI score 1 on comparing left sextant teeth of both jaws. On comparison of anterior teeth, mandibular right central incisors suffered from gingivitis i.e. score 1 as compared to maxillary anterior teeth.

DISCUSSION

There is a strong relationship between orthodontic treatment and periodontal disease. This is because orthodontic fixed appliance therapy increases plaque retention area on the tooth surface, thus making mechanical cleaning difficult (9). Results of the present study revealed that the mean score of CPI before and after orthodontic treatment was (14.20±6.45 SD) and (14.59±6.54 SD). A similar study was conducted by Moosa et al., indicating that 56% of the patients had CPI score of 3 and 4 after the initiation of orthodontic therapy (10). The apparent basis is due to increased mechanical load intraorally

Table. I *Pearson Correlations between CPI and tooth number and mean and SD before and after orthodontic treatment*

		Mean±SD
Pearson correlation	0.351	
Sig (2-tailed)		
N	70	
CPI before ortho	-0.177	14.20±6.45
CPI after ortho		14.59±6.54

and lack of compliance of orthodontic patients with the cleaning aids in the specified age group.

In the present study, Pearson correlation (2-tailed) showed a negative and nonsignificant correlation between tooth number and CPI score before and after orthodontic treatment, which means that CPI is not related to the tooth involved. It is the enhanced deposition of biofilms on the tooth surface which create retentive areas on the teeth. These results are similar to the work of Naranjo et al (11). A significant relationship before and after orthodontic treatment indicates a strong correlation. However, these findings are inconsistent with work by Nasir et al., who also revealed significant p-value (0.02) during and before orthodontic treatment although they exhibited an indirect relationship (9).

The results of the present study revealed that the CPI score of patients after 3 months of fixed orthodontic treatment was high as compared to pre-orthodontic treatment. This finding was found to be inconsistent with the study by by Moosa et al. who found an increase in CPI score among orthodontic patients (10). In the present study, all indexed left mandibular first molars had CPI score of 1 which is varying with the study conducted in Indonesia by Ramadhan (12). Mandibular first molar is the first tooth to erupt and is more prone to decay and periodontal problems as compared to other teeth. It also has an important role during fixed orthodontic treatment (11, 12). The limitations of the study are cross-sectional design and

Table II. *Percentage of CPI score before and after orthodontics*

Tooth #	Orthodontic treatment	0 (%)	1 (%)	2 (%)	9 (%)	X (%)
17	before	20	60	6	8	6
	after	5	83	4	8	6
16	before	45	47	6	2	0
	after	24	68	6	2	0
11	before	59	41	0	0	0
	after	55	45	0	0	0
26	before	48	48	4	0	0
	after	10	82	8	0	0
27	before	17	63	6	8	6
	after	0	82	6	8	6
37	before	16	68	4	6	6
	after	0	82	6	6	6
36	before	36	58	6	0	0
	after	0	88	12	0	0
31	before	71	29	0	0	0
	after	19	81	0	0	0
46	before	56	36	8	0	0
	after	6	84	8	0	0
47	before	14	68	4	6	2
	after	2	82	2	6	2

a small sample size. It is recommended that further studies should be planned with a larger sample size and longitudinal design to further evaluate the correlation of CPI score and periodontal diseases. To conclude, fixed orthodontic appliance therapy has significant effect on the periodontal health status of patients evaluated through CPI score. If periodontal condition is identified in early stage, it can be controlled by stressing and modifying oral hygiene practices in such patients.

REFERENCES

1. Rossini G, Parrini S, Castroflorio T, Deregibus A, Debernardi CL. Diagnostic accuracy and measurement sensitivity of digital models for orthodontic purposes: A systematic review. Am J Orthod Dentofac Orthop 2016; 149:161-70.
2. Borrie F, Bonetti D, Bearn D. What influences the implementation of interceptive orthodontics in primary care? Br Dent J. 2014; 216:687-91.
3. de Freitas JC, Lyra OCP, de Alencar AHG, Estrela C. Long-term evaluation of apical root resorption after orthodontic treatment using periapical radiography and cone beam computed tomography. Dental Press J Orthod 2013; 18:104-12.
4. Hamasha AAH, Alsolaihim AA, Alturki HA, Alaskar LA, Alshunaiber RA, Aldebasi WT. The relationship between body mass index and oral health status among saudi adults: A cross-sectional study. Community Dent Health 2019; 36:27-32.
5. Wang Y, Zhen Z, Liu HN et al. Periodontitis links to exacerbation of myocardial dysfunction in subjects with type 2 diabetes. J Periodontal Res 2019; 54:339–348.
6. Sanders NL. Evidence-based care in orthodontics and periodontics: A review of the literature. J Am Dent Assoc 1999; 130:521-27.
7. Ferreira MC, Dias-Pereira AC, Branco-de-Almeida LS, Martins CC, Paiva SM. Impact of periodontal disease on quality of life: a systematic review. J Periodontal Res 2017; 52: 651-65.
8. Cutress TW, Ainamo J, Sardo-Infirri J. The community periodontal index of treatment needs (CPITN) procedure for population groups and individuals. Int Dent J 1987; 37: 222-33.
9. Jalaluddin M, Goyal V, Naqvi ZA, Gupta B, Asnani MM, Sonigra HM. Assessment of the effect of orthodontic treatment on the periodontal health of endodontically restored tooth. J Contemp Dent Pract 2017; 18:587-90.
10. Moosa Y, Han LN, Safdar J, Sheikh OA, Pan YP. Periodontal status of Pakistani orthodontic patients. Braz Oral Res 2015; 29. doi:10.1590/1807-3107BOR-2015.vol29.0091.
11. Naranjo AA, Triviño ML, Jaramillo A, Betancourth M, Botero JE. Changes in the subgingival microbiota and periodontal parameters before and 3 months after bracket placement. Am J Orthod Dentofac Orthop 2006; 130: 275.e17-275.e22.
12. Ramadhan A, Cholil C, Sukmana BI. Relationship of level of teeth and mouth health knowledge of dental career numbers in SMPN 1 Marabahan. Kedokt Gigi 2016; 1:66-69.

LETTER TO THE EDITOR

DIAGNOSTIC VALUE OF CIRCULATING miR-208b AND miR-499 IN PERIPHERAL BLOOD OF PATIENTS WITH ACUTE MYOCARDIAL INFARCTION

F. LU[1], S-Z. LI[2], X. GAO[3], Y-N. GONG[4], P-X. SHI[5] and C. ZHANG[6]

[1]ECG Room, Yantaishan Hospital, Yantai, Shandong Province, China; [2]Department of Imaging, The People's Hospital of Zhangqiu Area, Jinan, Shandong Province, China; [3]Department of Clinical Laboratory, Qingdao Central Hospital, Qingdao University, Qingdao, Shandong Province, China; [4]No.1 Department of Cardiovascular Medicine, The People's Hospital of Zhangqiu Area, Jinan, Shandong Province, China; [5]Department of Cardiology, The People's Hospital of Zhangqiu Area, Jinan, Shandong Province, China; [6]ECG Room, Jining NO.1 People's Hospital, Affiliated Jining NO.1 People's Hospital of Jining Medical University, Jining Medical University, Jining, Shandong Province, China

Received March 19, 2020 – Accepted April 27, 2020

To the Editor,

The clinical diagnosis of acute myocardial injury (AMI) usually depends on electrocardiogram (ECG) (1) and medical history, but single ECG is still insufficient. The positive rate of ECG diagnosis for AMI is up to 81%, and the remaining 19% are confirmed by biochemical markers. The combination of ECG and biochemical markers can improve the reliability of AMI diagnosis. At present, the markers of myocardial injury are troponin T (2), troponin I, creatine kinase isoenzyme mass (CK-MB mass) and muscle myoglobin. Troponin is the best indicator for retrospective detection of AMI. Cardiac troponin (cTnT) is currently the best marker for diagnosing AMI. However, it has been found that the sensitivity of common troponins to the diagnosis of AMI is still insufficient. For example, within two hours of the chest pain onset, troponin has poor sensitivity for the diagnosis (3). Therefore, there is still a need to develop new clinical diagnostic markers for AMI.

MicroRNAs (miRNAs) are a class of endogenous non-coding RNAs found in eukaryotes with regulatory functions. They are 20-25 nucleotides in length. Recent studies have shown that miRNAs are involved in the pathophysiology of AMI, and play important roles in the occurrence and development of myocardial infarction. MiR-208b has been reported to affect 6-month survival after AMI (4). In addition, circulating miR-499 was found to serve as a potential biomarker for AMI (5). In particular, miR-208b and miR-499 were abnormally expressed in Greek patients with AMI (6). The purpose of this study was to investigate the expression levels of miR-208b and miR-499 in peripheral blood of patients with AMI. At the same time, the possibility and pathological correlation of miR-208b and miR-499 as diagnostic markers for AMI were explored. This study may provide novel biomarkers for the diagnosis of AMI.

MATERIALS AND METHODS

Clinical samples

From January 2014 to December 2016, the peripheral blood of 100 patients with AMI diagnosed by coronary

Key words: myocardial infarction; circulating miRNA; miR-208b; miR-499; ROC curve

Corresponding Author:
Dr Chen Zhang,
ECG Room, Jining NO.1 People's Hospital,
Affiliated Jining NO.1 People's Hospital
of Jining Medical University, Jining Medical University,
No 6 Jiankang Road, Jining, 272000, Shandong Province, China
Tel.: +86 0537 6056666.
e-mail: weixiayue456@163.com

0393-974X (2020)
Copyright © by BIOLIFE, s.a.s.
This publication and/or article is for individual use only and may not be further reproduced without written permission from the copyright holder.
Unauthorized reproduction may result in financial and other penalties
DISCLOSURE: ALL AUTHORS REPORT NO CONFLICTS OF INTEREST RELEVANT TO THIS ARTICLE.

angiography was collected from the Affiliated Hospital of Qingdao University. The diagnostic criteria for myocardial infarction met the criteria set by the American College of Cardiology in 2015. Patients who received thrombolytic therapy, cardiopulmonary resuscitation, primary cardiomyopathy or structural heart disease, malignant tumors, and incomplete clinical data were excluded. The matching peripheral blood from healthy people was collected as controls. All peripheral blood samples were stored at -80°C for further use. All subjects signed informed consent, and the study was approved by the Institutional Ethics Committee of Qingdao Municipal Hospital. All patients' gender, age, height, bodyweight, smoking, drinking, hypertension, diabetes, abnormal blood lipid metabolism, and medication were recorded in detail. The diagnosis and measurement of related diseases comply with relevant national or international standards. In addition, the patient's fasting elbow venous blood was retained, and blood biochemical indicators were measured by the Abbott C16000 biochemical immunoassay system.

Quantitative real-time PCR (RT-qPCR)

TRIzol Reagent (TaKaRa, Dalian, China) was used to collect total RNA from peripheral blood. The first-strand complementary DNA was synthesized using the PrimeScriptTM cDNA reverse transcription kit (TaKaRa, Dalian, China). RT-qPCR was performed using SYBR real-time PCR kit (Tiangen, Bejing, China). The expressions of cTnT, miR-208b and miR-499 were analyzed by the $2^{-\Delta\Delta Ct}$ method. The sequence of cTnT and internal reference β-actin primers are as follows: cTnT: (F) 5`-GAA TTG CGT CAT TTA AAG CCT AGT T-3`, cTnT (R) 5` -GTT TCA TCC TAC CAC TCC CAA TTA AT-3`, β-actin (F) 5`-TGT TGC CAT CAA TGA CCC CTT-3`, β- actin (R) 5`-CTC CAC GAC GTA CTC AGC G-3`. The primers of miR-208b and miR-499 were designed and synthesized by Shanghai Biotech Biotechnology Co., Ltd. The primers were designed as follows: miR-208b, 5'-GCG AAC TGT TTG CAG AGG-3' (forward) and 5'-CAG TGC GTG TCG TGG AGT-3' (reverse); miR-499, 5'-GTG CTT TGT GGA GGG TAC TTC AT-3' (forward) and 5'-TTG GAC ATC ACA AAT AGG ACA ATA CTT-3' (reverse).

Statistical analysis

Data analysis was performed using SPSS 17.0 statistical software. χ^2 test and independent sample *t*-tests were used to analyze the statistical differences between baseline data and the characteristics of each clinical biochemical index. The sensitivity and specificity of cTnT, miR-208b and miR-499 were analyzed by ROC curve. The sensitivity was calculated as true positive cases/true positive cases + false positive cases. Specificity was calculated as true negative cases/false positive cases + true negative cases. The positive likelihood ratio was then calculated as sensitivity/1-specific. The negative likelihood ratio was calculated as 1-sensitivity/specificity. The Yuden index was calculated as sensitivity + specificity-1. Positive predictive value was calculated as true positive cases/true positive cases + false positive cases. Negative prediction values were calculated as true negative cases/true negative cases + false negative cases. In this study, $\alpha = 0.05$ was used as the test level, and $p < 0.05$ was considered statistically significant.

RESULTS

MiR-208b and miR-499 are significantly upregulated in peripheral blood of AMI patients

To investigate the expression differences of circulating miR-208b and miR-499 in peripheral blood of healthy controls and AMI patients, the expression levels of miR-208b and miR-499 were measured in peripheral blood samples of 100 AMI patients and healthy controls. To ensure the comparability of the results, we performed a statistical analysis of baseline information in a healthy control group and AMI patients, as shown in Table 1. There was no statistical difference in age, gender, and other clinical blood biochemical test parameters between the two groups (alanine aminotransferase, aspartate aminotransferase, blood urea nitrogen, and creatinine, $p > 0.05$, Table I). However, compared with the healthy control group, serum levels of high-sensitivity C-reactive protein, IL-6, procalcitonin, and leukocytes in the AMI group were significantly increased, and the differences were statistically significant ($p < 0.001$, Table I).

In view of the clinically established myocardial infarction specific marker myocardial protein T (cTnT), we used the mRNA expression level of cTnT as a positive control in this study. RT-qPCR showed that compared with the healthy control group, the mRNA levels of cTnT, miR-208b and miR-499 were

significantly increased in the AMI group. Compared to the healthy control group, the expression folds of cTnT, miR-208b and miR-499 were 33.8 times, 5.7 times, and 16.3 times, respectively ($p < 0.001$, Fig.1). These results indicate that miR-208b and miR-499 may be involved in the pathogenesis of AMI. Circulating miR-208b and miR-499 have the potential to serve as diagnostic makers for AMI.

Table I. *Comparison of baseline parameters*

Characteristics	Healthy Control	AMI	P-value
Gender (male/female)	33/10	28/14	0.345
Age (Year)	50.2±17.2	53.8±19.4	0.368
Alanine Aminotransferase (U/L)	44.43±2.60	47.62±3.41	0.291
Aspartate Aminotransferase (U/L)	32.56±3.13	34.94±3.90	0.508
Blood Urea Nitrogen (mmol/L)	4.97±1.01	5.27±1.30	0.722
Creatinine (μmol/L)	65.55±8.65	67.52±7.71	0.451
IL-6 (pg/L)	10.81±42.18	93.29±36.64	0.001***
Procalcitonin (pg /L)	8.87±9.40	103.69±9.48	0.001***
C-reactive protein (pg /L)	5.4±1.12	58.8±3.0	0.001***
Leukocytes ($\times 10^9$/L)	17.34±5.50	67.64±5.83	0.001***

*** $p < 0.001$

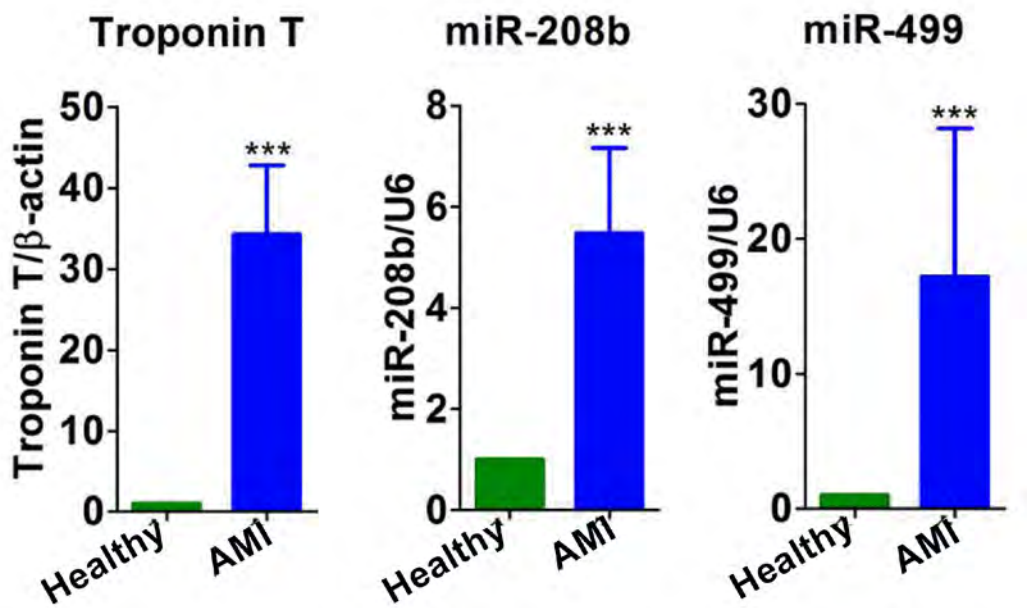


Fig. 1. *Analysis of mRNA expression of cTnT, miR-208b and miR-499 in peripheral blood circulation in healthy controls and AMI group. β-actin is an internal reference for cTnT detection, and U6 is an internal reference for miR-208b and miR-499. *** $p < 0.001$*

mRNA levels of circulating miR-208b and miR-499 in peripheral blood can be used as potential markers for AMI diagnosis

We analyzed the sensitivity and specificity of circulating miR-208b and miR-499 in peripheral blood as a diagnostic AMI by referring to the mRNA expression level of cTnT and using the receiver operating characteristic curve (ROC curve). ROC curve analysis showed that cTnT had an AUC value of 0.863, a sensitivity of 0.987, a specificity of 0.955, a positive likelihood ratio of 18.121, a Jordan index of 0.896, a positive predictive value of 0.928, and a negative predictive value of 0.995. In addition, miR-208b has an AUC value of 0.827, a sensitivity of 0.933, a specificity of 0.912, a positive likelihood ratio of 11.550, a Jordanian index of 0.853, a positive predictive value of 0.636, and a negative predictive value of 0.989. MiR-499 has an AUC value of 0.833, a sensitivity of 0.9083, a specificity of 0.897, a positive likelihood ratio of 10.743, a Jordanian index of 0.814, a positive predictive value of 0.672, and a negative predictive value of 0.971. These results indicate that miR-208b and miR-499 have similar AUC values (Fig. 2). ROC curve analysis suggests that circulating miR-208b and miR-499 in peripheral blood may be potential diagnostic markers for the diagnosis of AMI, with similar sensitivity and specificity to cardiac protein T (cTnT).

DISCUSSION

This study explored the possibility of circulating miR-208b and miR-499 in peripheral blood as potential markers for the diagnosis of AMI. Compared with clinically established AMI diagnostic markers cardiac troponin (cTnT), peripheral blood circulating miR-208b and miR-499 have similar sensitivity and specificity, which indicates that peripheral blood circulating miR-208b and miR-499 may be potential markers for AMI diagnosis. It was first reported that the expression levels of circulating miR-208b and miR-499 in peripheral blood can reflect the degree of myocardial injury (6), and it has been found that they were significantly overexpressed in patients with AMI, while hardly detected in healthy controls (7). In addition, ROC curve analysis showed that the AUC value of miR-208b, miR-499 and cTnT were close to 1 (6). This is generally consistent with our research, but slightly different. In our study, the values of AUC, sensitivity, specificity, positive likelihood ratio, Jordan index, positive predictive value, and negative predictive value of miR-208b and miR-499 were all less than cTnT, which suggests that the diagnostic value of miR-208b and miR-499 in AMI is no better than cTnT. In this study, the AUC values of miR-208b and miR-499 were both within 0.9, which may be due to the experimental methods,

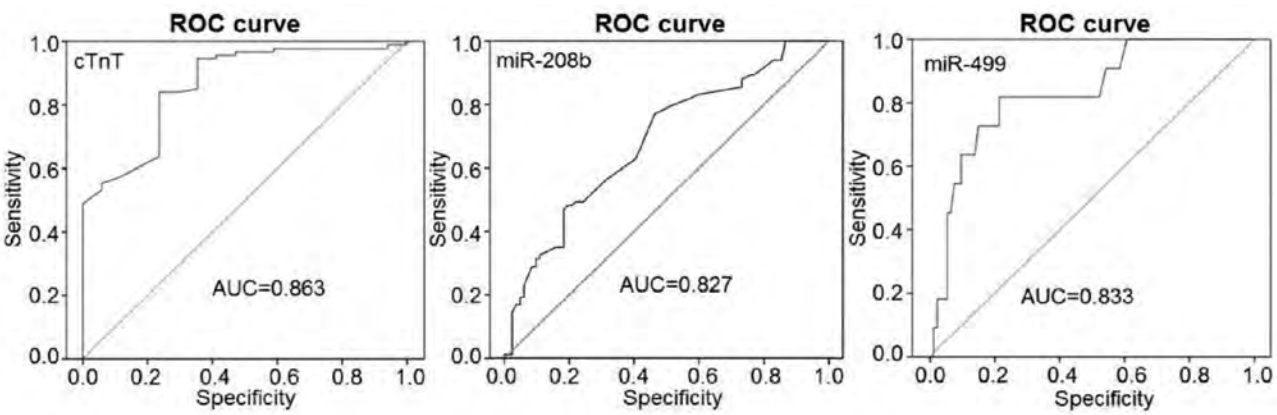


Fig. 2. *ROC curve analysis of cTnT, miR-208b and miR-499 mRNA expression levels. The Y-axis represents sensitivity, the X-axis represents specificity. And the area under the ROC curve enclosed by the coordinate axis (Area Under Curve, AUC) value represents the area of the curve.*

the selection of RT-qPCR detection thresholds, and the use of different specimens.

In summary, this study found that miR-208b and miR-499 expressions were significantly higher in AMI subjects than in healthy controls. The specificity and sensitivity of miR-208b and miR-499 in the diagnosis of AMI are similar to cTnT, but they are not better than the diagnostic value of cTnT. Therefore, miR-208b and miR-499 may be potential diagnostic markers in AMI.

ACKNOWLEDGEMENTS

This study was supported by Jining science and technology development project (2013jnwk117).

REFERENCES

1. Miranda DF, Lobo AS, Walsh B, Sandoval Y, Smith SW. New insights into the use of the 12-lead electrocardiogram for diagnosing acute myocardial infarction in the emergency department. Can J Cardiol 2018; 34:132-45.
2. Westermann D, Neumann JT, Sorensen NA, Blankenberg S. High-sensitivity assays for troponin in patients with cardiac disease. Nat Rev Cardiol 2017; 14:472-83.
3. Kobayashi S, Taguchi I. First hurdle for optimal treatment of acute myocardial infarction. J Cardiol 2018; 71:320-22.
4. Alavi-Moghaddam M, Chehrazi M, Alipoor SD, et al. A preliminary study of microRNA-208b after acute myocardial infarction: impact on 6-month survival. Dis Markers 2018; 2018:2410451.
5. Xin Y, Yang C, Han Z. Circulating miR-499 as a potential biomarker for acute myocardial infarction. Ann Transl Med 2016; 4:135.
6. Agiannitopoulos K, Pavlopoulou P, Tsamis K, et al. Expression of miR-208b and miR-499 in Greek patients with acute myocardial infarction. In Vivo 2018; 32:313-18.
7. Devaux Y, Vausort M, Goretti E, et al. Use of circulating microRNAs to diagnose acute myocardial infarction. Clin Chem 2012; 58:559-67.

LETTER TO THE EDITOR

LncRNA SNHG1 ACTS AS AN ONCOGENE THROUGH REGULATING miR-145-5p IN OVARIAN CANCER

RL. GONG*, RR. JIN*, XP. YU* and WL. WANG

[1]*Gansu Provincial Maternity and Child-care Hospital, Lanzhou, Gansu, China*

Received March 22, 2020 – Accepted April 27, 2020

*These Authors contributed equally to this work

To the Editor,

Ovarian cancer (OC) is a malignant tumor of the female reproductive tract (1). Without specific early clinical manifestation, it is usually already at the middle to advanced stage at the time of diagnosis. (2). Patients often fail to receive optimal treatment, resulting in a low 5-year survival rate and high mortality (3). OC has high heterogeneity, easy recurrence, low survival rate, and research on its molecular mechanism has become a focus of basic research. (4). However, the complexity and pathogenesis of OC remain unclear, making it difficult to find an effective treatment, therefore, studies revealing the potential molecular mechanism of OC are needed to improve patient early diagnosis and treatment.

LncRNAs involved in the pathogenesis of various diseases are a class of RNAs with more than 200 nucleotides and lacking protein-coding ability (5). In recent years, with the development of genetics and disease cross-research, lncRNAs have been associated with the progression of cancer, and have been given more and more attention by researchers. SNHG1, as a new cancer biomarker and therapeutic target, has been shown to be closely related to the occurrence and development of many tumors (6, 7). In OC, SNHG1 was upregulated and its knockdown suppressed cell growth, invasion and metastasis (8). However, there are few studies on the mechanism of SNHG1 in the occurrence and development of OC. This study explored the effects and mechanisms of SNHG1 on cell proliferation and invasion of OC cells, and provided a new theoretical basis for OC treatment.

MATERIAL AND METHODS

Clinical samples

A total of 30 OC and matched-adjacent tissues were collected from patients who underwent surgical treatment at Gansu Provincial Maternity and Child-care Hospital. The study was approved by the hospital Ethics Committee, and all patients signed informed consent. Inclusion criteria were OC was confirmed by pathology, patients with first-onset disease who had not undergone chemotherapy or immunotherapy before surgery, and patients without other malignant tumors, immune diseases, etc. The Exclusion criteria were patients with severe cardiovascular and cerebrovascular diseases, liver and other organic diseases, and those with other malignant tumors and immune diseases.

Key words: SNHG1; miR-145-5p; ovarian cancer

Corresponding Author:
Dr Wenling Wang,
Gansu Provincial Maternity and Child-care Hospital,
No 143, Qili River North Street,
Lanzhou, Gansu 730050, China.
Tel: 0931-2338611. - Fax: 0931-2332246.
email: lzdfjx@126.com

0393-974X (2020)
Copyright © by BIOLIFE, s.a.s.
This publication and/or article is for individual use only and may not be further reproduced without written permission from the copyright holder.
Unauthorized reproduction may result in financial and other penalties
DISCLOSURE: ALL AUTHORS REPORT NO CONFLICTS OF INTEREST RELEVANT TO THIS ARTICLE.

Cells

The normal immortalized human ovarian surface epithelial cells IOSE29 and OC cells (OVCAR3, SKOV3, OV90 and A2780) purchased from the Type Culture Collection of the Chinese Academy of Sciences (Shanghai, China) were cultured with RPMI-1640 medium (Invitrogen, USA) containing 10% fetal bovine serum (FBS, Invitrogen) at 37°C and 5% CO_2.

Small interfering RNA against SNHG1 (si-SNHG1) and control (si-NC), miR-145-5p mimic (mimic), miR-145-5p inhibitor (inhibitor) and their corresponding controls (miR-NC and anti-NC) used to interfere SNHG1 or miR-145-5p expression were synthesized and obtained from GenePharma (Shanghai, China). Cell transfection was performed by Lipofectamine2000 (Invitrogen, USA) following the manufacturer's instructions.

For CCK-8 assay, the transfected cells were seeded in 96-well plates with 2×10^4/well, and OD values of cells were measured at 1, 2, 3, and 4 days. 10 µl CCK-8 reagent (Beyotime, China) was added to each well, and incubated for 3 h. The absorbance at 450 nm was detected by a microplate reader (Olympus, Japan).

For Transwell assay, 300 µl cell suspension with 3×10^4/ml was added to the upper chamber coated with Matrigel (BD Biosciences, USA) while 600 µl medium containing 10% FBS was inserted in the lower chamber. After 36 h, the chamber was removed and washed twice with PBS. The cells were fixed with 4% paraformaldehyde and stained with 0.1% crystal violet. Finally, observation and cell counting were performed with an inverted microscope (Olympus, Japan).

The pGL3 Basic vector (Promega, USA) was used to construct luciferase reporter vectors including wild-type (SNHG1-wt) and mutant (SNHG1-mut) which contain miR-145-5p seed or mutated binding sites. Cotransfection of SNHG1-wt or SNHG1-mut and miR-145-5p mimic or miR-NC were performed by Lipofectamine 2000 (Invitrogen, USA). After 48 h, relative luciferase activity was detected through Dual-Luciferase Reporter System (Promega, USA).

RIP assay was performed using the Magna RIP kit (Millipore, USA) according to instructions. OVCAR3 cells were lysed by RIP lysis buffer, and then incubated in RIP buffer with magnetic beads conjugated Ago2 or IgG antibody (Abcam, USA). Expressions of SNHG1 and miR-145-5p were detected by qRT-PCR.

qRT-PCR

Total RNA was isolated by TRIZOL reagent (Invitrogen, USA). Complementary DNA (cDNA) was synthesized with PrimeScript Reverse Transcriptase (RT) Reagent Kit (TaKaRa, Japan). qRT-PCR reactions was conducted with SYBR Premix Ex Taq (Takara) on a LightCycler 480 (Roche Applied Science, Germany). Relative expressions of SNHG1 and miR-145-5p were analyzed by the $2^{-\Delta\Delta CT}$. U6 or GAPDH was used as internal control. Primers are listed in Table I.

Statistical analysis

All data were expressed as mean ± SD. Student's *t*-test or one-way ANOVA was conducted with GraphPad Prism 5 for statistical analysis. $P < 0.05$ was considered to have statistically significance.

RESULTS

SNHG1 was upregulated in OC tissues and cells

QRT-PCR was used to detect SNHG1 expression in 30 pairs of OC tissues and corresponding adjacent tissues. Our results indicated that SNHG1 expression was notably reduced in OC tissues compared to adjacent tissues (Fig. 1A). In order to explore the potential biological function of SNHG1 in OC cells, we next assessed SNHG1 expression in OC cell lines. The experimental results revealed that SNHG1 expression was up-regulated in all OC cells (Fig. 1B). We suggest that SNHG1 might play an oncogene in OC progression.

SNHG1 knockdown repressed OVCAR3 cell proliferation and invasion

In the above experiments, we found that the OVCAR3 cells had the highest expression level of endogenous SNHG1, therefore, OVCAR3 was selected for subsequent experiments. The specific siRNA targeting SNHG1 was transfected into OVCAR3 cells, and SNHG1 expression in OVCAR3 cells was detected by qRT-PCR. Compared with the si-NC group, the expression of SNHG1 was dramatically reduced in the si-SNHG1 group (Fig. 2A). CCK-8 assay revealed cell proliferation ability was markedly decreased in the si-SNHG1 group (Fig. 2B). We then performed Transwell

assay to further investigate the effect of SNHG1 on OVCAR3 cell invasion. The results showed that the number of invading cells in si-SNHG1 group was also dramatically reduced (Fig. 2C), which indicated that down-regulating SNHG1 could significantly suppress the proliferation and invasion ability of OVCAR3 cells.

miR-145-5p was a target of SNHG1

Studies have shown that many lncRNAs play their competitive endogenous RNA (ceRNA) role by competitively binding miRNAs. We performed biological analysis by Starbase v3.0 (http://starbase.sysu.edu.cn/). The analysis found binding sites between miR-145-5p and SNHG1 (Fig. 3A). To determine this, we first performed the dual-luciferase reporter assay. The transfection of miR-145-5p mimic markedly decreased luciferase activity of SNHG1-wt cells, while there was no effect in other groups (Fig. 3B). Subsequently, RIP assay was implemented to further confirm the relationship between SNHG1 and miR-145-5p. Results revealed that SNHG1 and miR-145-5p were significantly enriched in immunoprecipitates containing Ago2, suggesting that SNHG1 could directly interact with miR-145-5p in OVCAR3 cells (Fig. 3C). Moreover, we found si-SNHG1 could increase miR-145-5p expression (Fig. 3D). Moreover, miR-145-5p was downregulated and had a negative correlation with SNHG1 expression in OC tissues (Fig. 3 E and F). Thus, we concluded that SNHG1 could bind to miR-145-5p and had a negative regulation of miR-145-5p.

SNHG3 regulated OVCAR3 cell proliferation and invasion by miR-145-5p

To further confirm whether SNHG1 could regulate OVCAR3 cell proliferation and invasion by regulating miR-145-5p, miR-145-5p inhibitor and si-SNHG1 were cotransfected into OVCAR3 cells. miR-145-5p expression in OVCAR3 cells was decreased significantly by miR-145-5p inhibitor (Fig. 4A). CCK-8 data showed that after inhibiting miR-145-5p expression, the proliferation ability of OVCAR3 cells transfected with si-SNHG1 was increased compared to the si-SNHG1+anti-NC group (Fig. 4B). In Transwell assay, the number of invading cells in the inhibitor+si-SNHG1 group was enhanced compared with the anti-NC+si-SNHG1 group (Fig. 4C). On the basis of the above results, the mechanism of SNHG1 in promoting OC cell proliferation and invasion partly depended on the regulation of miR-145-5p.

DISCUSSION

SNHG1 is a widely studied lncRNA. This study

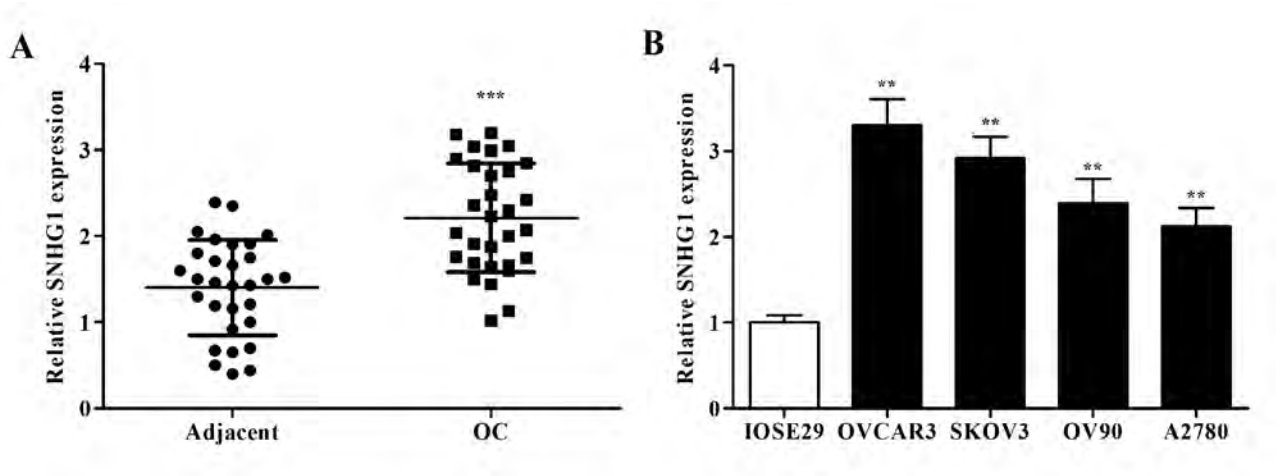


Fig. 1. *SNHG1 was upregulated in OC tissues and cells.* ***A)*** *SNHG1 expression was increased in OC and adjacent tissues.* ***B)*** *SNHG1 expression was enhanced in OC cells (OVCAR3, SKOV3, OV90 and A2780). **P < 0.01, ***P<0.001.*

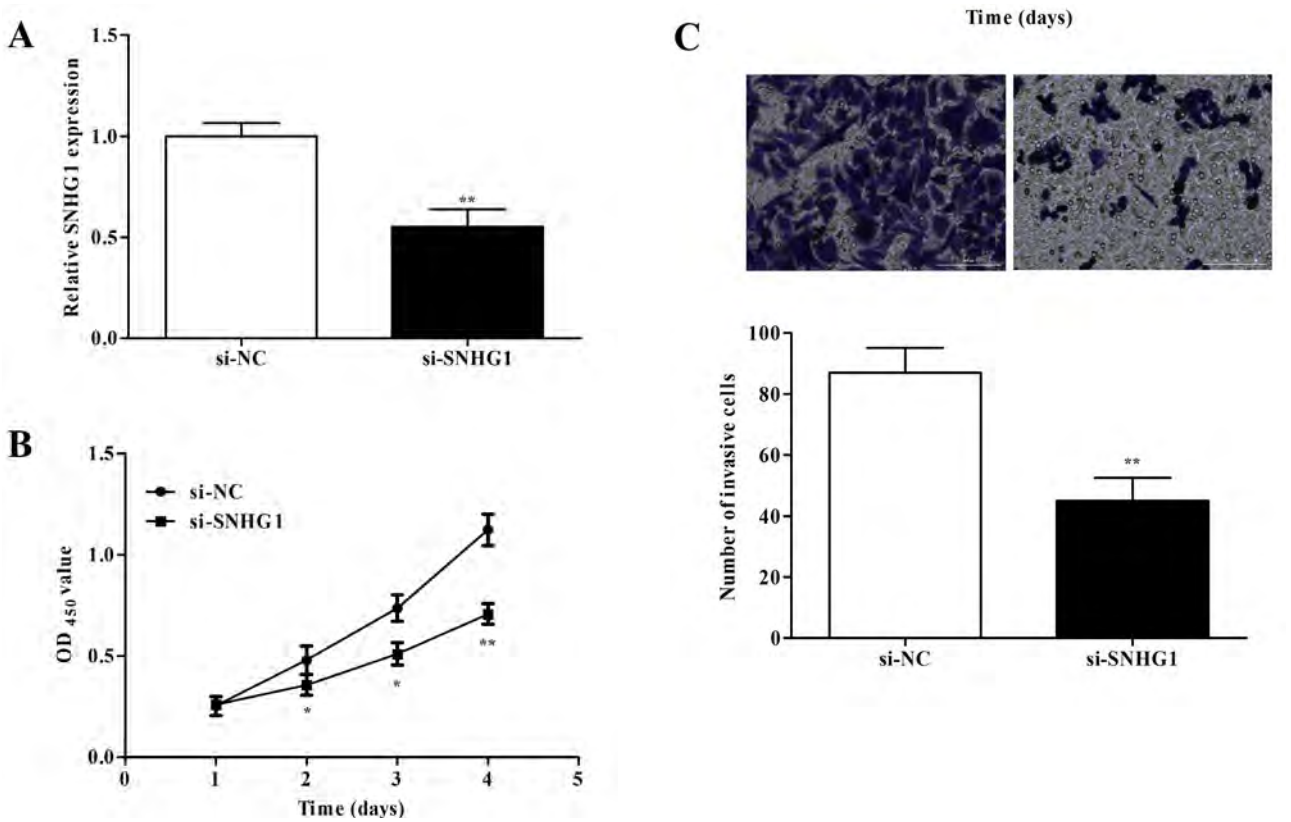


Fig. 2. *SNHG1 knockdown hampered OC cell proliferation and invasion.* ***A****) SNHG1 expression was downregulated in OVCAR3 cells transfected with si-SNHG1.* ***B****) Cell proliferation was suppressed in OVCAR3 cells treated with si-SNHG1 by CCK-8 assay.* ***C****) Number of invaded cells was decreased in OVCAR3 cells treated with si-SNHG1 through Transwell assay (200X). *P < 0.05, **P < 0.01.*

showed that the expression of SNHG1 in OC tissues and cells was significantly increased, indicating that SNHG1 upregulation might be related to the occurrence of OC. Furthermore, downregulating SNHG1 in OVCR3 cells could inhibit the cell proliferation and invasion.

LncRNAs adsorption and inhibition of miRNA expression through "sponge action" is one of the important mechanisms for its regulation (9). Bioinformatics analysis in this study showed that SNHG1 could target miR-145-5p. Previous studies have shown that miR-145-5p exerted as a tumor suppressor in a variety of cancers. Down-expression of miR-145-5p was observed in gastric cancer (GC), and associated with poor prognosis (10). Hang et al. reported that miR-145-5p downregulation in OC might facilitate its development by regulating CT (11). It has been demonstrated that SNHG1 acted as a tumor promoter in non-small cell lung cancer via modulating miR-145-5p and MTDH (12). This study found that SNHG1 could directly interact with and negatively regulate miR-145-5p. SNHG1 knockdown suppressed the proliferation and invasion of OC cells by targeting miR-145-5p. However, this study has limitations. The effect of SNHG1 on OC has not been validated *in vivo* or more cells, which will become the focus of further research.

In summary, SNHG1 expression was elevated in OC tissues and cells. In OVCAR3 cells, SNHG1 could promote cell proliferation and invasion by reducing the expression of miR-145-5p. To the best of our knowledge, we were the first to study whetheer SNHG1 could act as a ceRNA of miR-145-5p in OC. Moreover, we also were the first to identify SNHG1

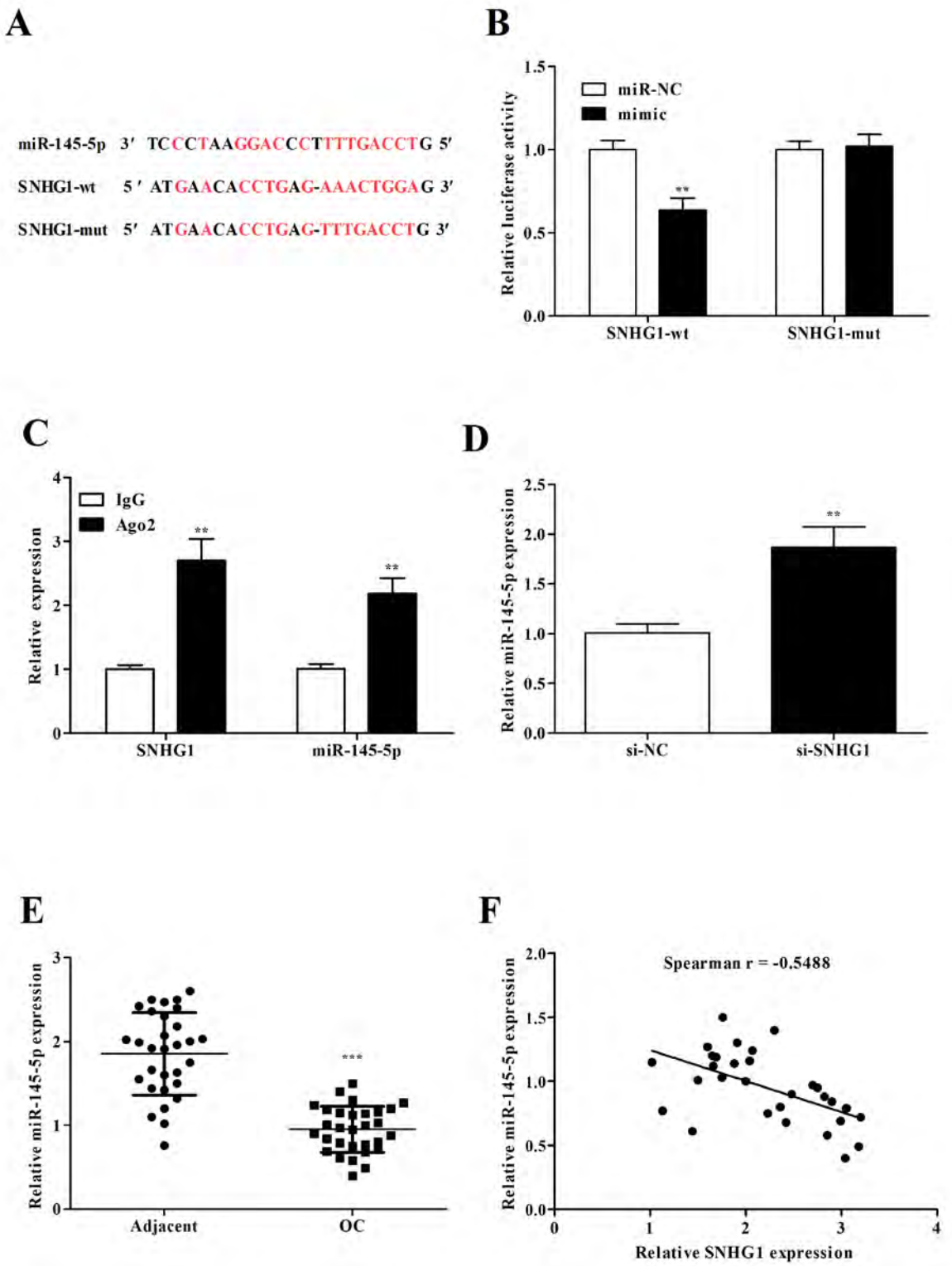


Fig. 3. *SNHG1 directly targeted miR-145-5p.* ***A)*** *Predicted target sites of SNHG1 and miR-145-5p.* ***B)*** *Luciferase activity was detected in OVCAR3 cells.* ***C)*** *miR-145-5p expression was increased in OVCAR3 cells treated with si-SNHG1.* ***D)*** *miR-145-5p was downregulated in OC tissues.* ***E)*** *Correlation between SNHG1 and miR-145-5p expression in OC tissues. **P<0.01, ***P<0.001.*

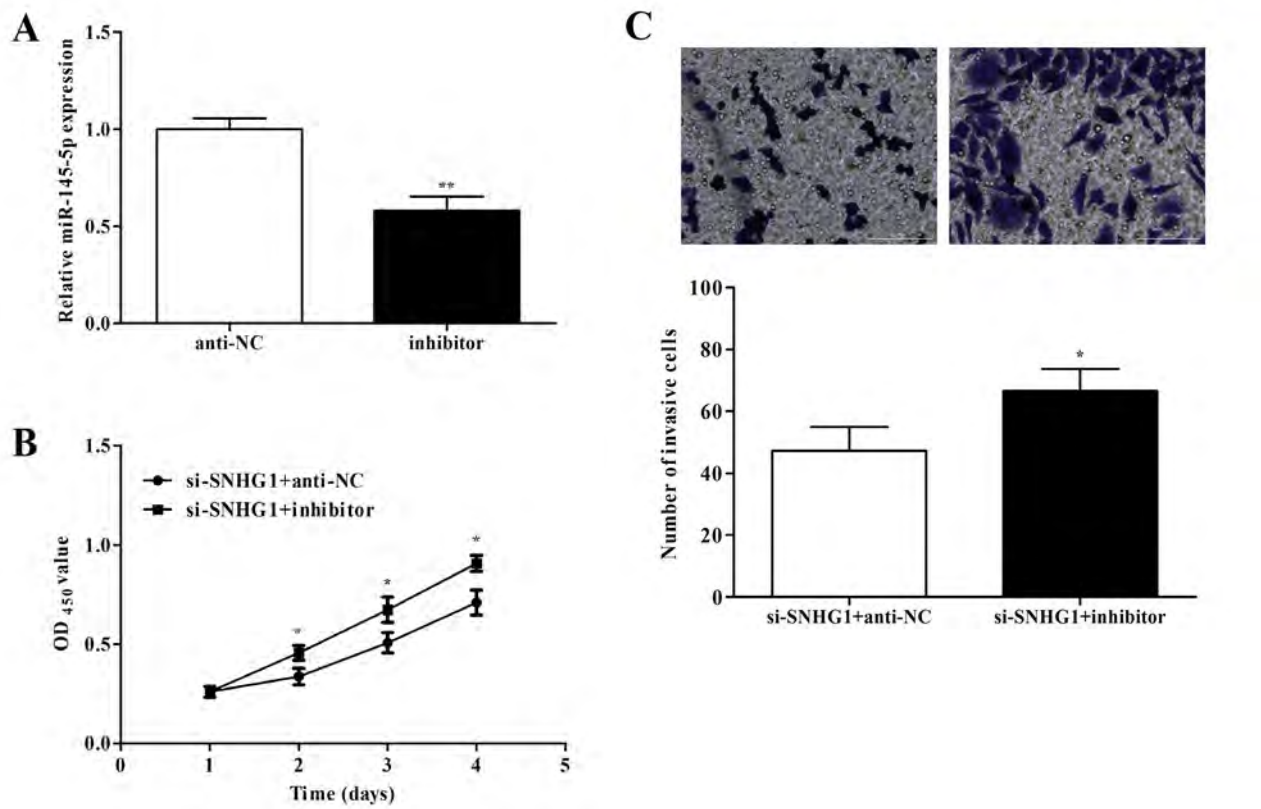


Fig. 4. *miR-145-5p inhibition could offset the suppressive effect of SNHG1 knockdown on OVCAR3 cell proliferation and invasion.* ***A****) miR-145-5p expression was decreased in OVCAR3 cells transfected with miR-145-5p inhibitor.* ***B****) Cell proliferation was inhibited in OVCAR3 cells transfected with si-SNHG1 and miR-145-5p inhibitor.* ***C****) Number of invaded cell was reduced in OVCAR3 cells after inhibiting SNHG1 and miR-145-5p in Transwell assay (200X). *P < 0.05, **P < 0.01.*

Table I. *Primer sequences for real-time fluorescence quantification PCR*

Gene Name	Primer sequences (5'-3')
SNHG1	F CCTAAAGCCACGCTTCTTG
	R TGCAGGCTGGAGATCCTACT
miR-145-5p	F CTCACGGTCCAGTTTTCCCA
	R ACCTCAAGAACAGTATTTCCAGG
GAPDH	F GGTCTCCTCTGACTTCAACA
	R AGCCAAATTCGTTGTCATAC
U6	F CTCGCTTCGGCAGCACA
	R AACGCTTCACGAATTTGCGT

facilitated OC progression by promoting cell proliferation and invasion through miR-145-5p. This newly identified SNHG1/miR-145-5p may provide novel therapeutic strategy for OC patients in the future.

REFERENCES

1. Muinao T, Pal M, Boruah HPD. Origins based clinical and molecular complexities of epithelial ovarian cancer. Int J Biol Macromol 2018; 118:1326-45.
2. Kathawala RJ, Kudelka A, Rigas B. The chemoprevention of ovarian cancer: the need and the options. Curr Pharm Rep 2018; 4:250-60.
3. Siegel RL, Miller KD, Jemal A. Cancer statistics, 2019. CA Cancer J Clin 2019; 69:7-34.
4. Kossaï M, Leary A, Scoazec J-Y, Genestie C. Ovarian cancer: a heterogeneous disease. Pathobiology 2018; 85:41-49.
5. Fernandes JCR, Acuna SM, Aoki JI, Floeter-Winter LM, Muxel SM. Long non-coding RNAs in the regulation of gene expression: physiology and disease. Non-Coding RNA 2019; 5:17.
6. Thin K, Tu JC, Sudheesh C. Long non-coding SNHG1 in cancer. Clin Chim Acta 2019; 494:38-47.
7. Huang L, Jiang X, Wang Z, Zhong X, Tai S, Cui Y. Small nucleolar RNA host gene 1: a new biomarker and therapeutic target for cancers. Pathol Res Pract 2018; 214:1247-52.
8. Ge J, Wu X, Yang X, Gao J, Wang F, Ye K. Role of long non-coding RNA SNHG1 in occurrence and progression of ovarian carcinoma. Eur Rev Med Pharmacol Sci 2018; 22:329-35.
9. Veneziano D, Marceca GP, Di Bella S, Nigita G, Distefano R, Croce CM. Investigating miRNA–lncRNA Interactions: computational tools and resources. Methods Mol Biol. 2019; 1970:251-77.
10. Zhang Y, Wen X, Hu X, Cheng L, Yu J, Wei Z. Downregulation of miR-145-5p correlates with poor prognosis in gastric cancer. Eur Rev Med Pharmacol Sci 2016; 20:3026-30.
11. Hang W, Feng Y, Sang Z, Yang Y, Zhu Y, Huang Q, Xi X. Downregulation of miR-145-5p in cancer cells and their derived exosomes may contribute to the development of ovarian cancer by targeting CT. Int J Mol Med 2019; 43:256-66.
12. Lu Q, Shan S, Li Y, Zhu D, Jin W, Ren T. Long noncoding RNA SNHG1 promotes non-small cell lung cancer progression by up-regulating MTDH via sponging miR-145-5p. FASEB J 2018; 32:3957-67.

LETTER TO THE EDITOR

HASHIMOTO'S THYROIDITIS ASSOCIATED WITH AN EXTRA-THYROIDAL TRIAD OF PRETIBIAL MYXEDEMA, OPHTHALMOPATHY, AND ACROPACHY

C. LIAO, L. HU and C. LAN

Department of Dermatology, The Second Affiliated Hospital of Chengdu Medical College, China National Nuclear Corporation 416 Hospital, Chengdu, Sichuan, China

Received November 18, 2019 – Accepted April 27, 2020

To the Editor,

Hashimoto's thyroiditis (HT) is an autoimmune thyroid disease (AITD). The extrathyroidal triad of AITD refers, in particular, to the coexistence of the 3 types of extrathyroidal manifestations (exophthalmos, pretibial myxedema and acropachy) in a patient with AITD, first reported by Thomas in 1933. The 3 types of extrathyroidal manifestations can occur alone or together in AITD, especially in Graves' disease (GD). For a patient with GD, exophthalmos generally occurs first, then PTM, and lastly acropachy. Exophthalmos is the most common component of the triad and occurs in 30% of GD patients, but in only 6.4% of HT patients (1). Pretibial myxedema (PTM), or thyroid dermopathy, is a rare cutaneous manifestation of AITD that occurs in 1.5%–1.7% of patients with GD (2, 3) and also in 0.36% of patients with Hashimoto's thyroiditis (HT) and idiopathic hypothyroidism (IH) (3). Thyroid acropachy is the rarest component of the triad and occupies approximately 0.3-1% of GD patients (1, 2). The triad is even rarer in patients with HT. Clinically, this triad is easy to diagnose but difficult to cure. Recently, intralesional corticosteroid injections have been successfully used to treat pretibial myxedema (4). However, the pathogenesis of the triad is not yet clear.

Case report

A 50-year-old female, whose work requires long periods of standing (approximately ≥4 hours/day), sought treatment for plaques, localized to the pretibial regions, that lasted for 3 months. She was diagnosed with hypothyroidism due to Hashimoto's thyroiditis. She was administered levothyroxine (125 μg daily) 8 months previous to this report. She underwent Cobalt-60 radiotherapy for thyroid-associated exophthalmos 5 months previous to this report. She had a family history of thyroid disease and reported that her cousin was diagnosed with Graves' disease but did not have PTM. The subject gave informed and signed consent to participate in the study. The ethics review board of the CNNC 416 hospital approved the study.

Physical examination revealed a full and prominent thyroid region, without nodules or thrill upon palpation. Irregular, circumscribed, non-pitting, erythematous plaques were observed symmetrically on the distal two-thirds of her lower legs, presenting the classic "orange peel" appearance (Fig. 1A). No varicose veins were noted. Exophthalmos was documented with Hertel exophthalmometer readings of 19 (right eye) and 18 (left eye). The conjunctiva was slightly congested in both eyes (Fig. 1B). Laterally

Key words: pretibial myxedema; thyroid-associated ophthalmopathy; acropachy; hashimoto thyroiditis; thyrotropin receptor autoantibodies; hypopigmentation

Corresponding Author:
Dr Changgui Lan,
Department of Dermatology, The Second Affiliated Hospital of Chengdu Medical College, China National Nuclear Corporation (CNNC) 416 Hospital, No. 4, Er Huan Lu Bei Si Duan, Chengdu City, Sichuan Province, China.
Fax: +86 028 82991296
e-mail: lcg638212@163.com

0393-974X (2020)
Copyright © by BIOLIFE, s.a.s.
This publication and/or article is for individual use only and may not be further reproduced without written permission from the copyright holder.
Unauthorized reproduction may result in financial and other penalties
DISCLOSURE: ALL AUTHORS REPORT NO CONFLICTS OF INTEREST RELEVANT TO THIS ARTICLE.



Fig. 1. *An extra-thyroidal triad of Hashimoto's thyroiditis. **A**) Symmetrically erythematous non-pitting plaques with orange peel-like appearance on the extensor aspects of lower legs. Black hairs and its pores are prominent at lesional sites. **B**) Obvious exophthalmos with congested conjunctiva. **C**) Digital clubbing with bulbous fingernails, especially visible on the thumb.*

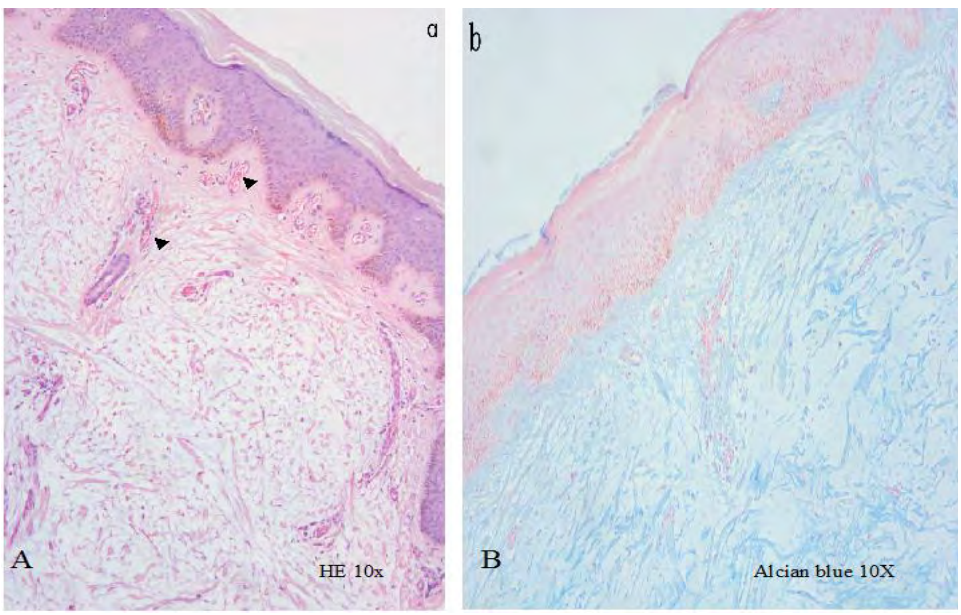


Fig. 2. *Dilation and blood stasis of capillaries and post-capillary venules in pretibial myxedema lesions. **A**) HE staining, 10X. Obvious mucinous degeneration in the reticular dermis with sparse collagen bundles, red blood cell stasis in the dilated capillaries and postcapillary venules in the dermis (arrows mark the dilated capillaries); **B**) Alcian blue staining 10X. Deposition of mucopolysaccharide in the reticular dermis with wide separated, fragmented collagen bundles.*

truncated eyebrows (a sign of hypothyroidism) were not observed. Digital clubbing was observed, especially visible on the thumb (Fig. 1C).

The serum levels of thyroid hormones and thyroid-stimulating hormone (TSH) were measured with direct chemiluminescence (ADVIA Centaur XP immunoassay system, Siemens Healthineers, Germany), and the results showed an elevated TSH level (15.605 mIU/L; normal range 0.550–4.780 mIU/L). Triiodothyronine (T3), free triiodothyronine (FT3), thyroxine (T4), and free thyroxine (FT4) were all within the normal range. The serum levels of thyroglobulin antibodies (Tg-Ab), thyroid peroxidase antibodies (TPO-Ab), and TSHR-binding inhibitory immunoglobulins [TBII, or called thyrotropin receptor (TSHR) antibodies, i.e. TRAb in this paper] were measured with an electrochemiluminescence immunoassay (anti-TSHR, Tg-Ab, and TPO-Ab kits in Elecsys and Cobas e 601 analyzer, Roche Diagnostics GmbH, Germany). The titer of Tg-Ab was over 4000 IU/ml (normal range <115.00 IU/ml), TPO-Ab was 570.20 IU/ml (normal range <34.00

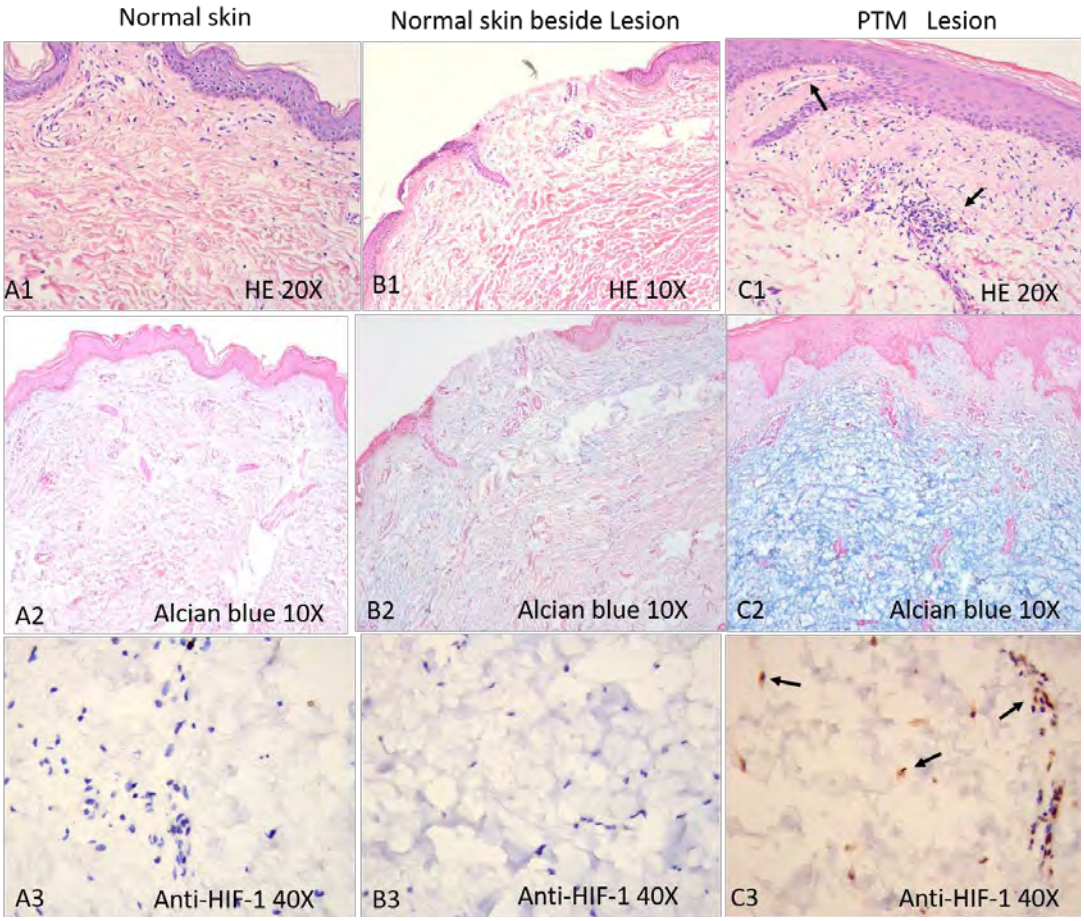


Fig. 3. *Expression of hypoxia-inducing factor-1α in the fibroblasts and endothelial cells of capillaries of pretibial myxedema lesions compared to the normal skin.* ***A1-C1****) H&E staining. Mucinous degeneration, lymphocyte aggregates, and dilation of capillaries and postcapillary venules in pretibial myxedema (PTM) lesions (arrows mark the dilated capillarie and aggregation of lymphocytes) compared with the normal skin of a normal person and normal skin beside a PTM lesion in the patient.* ***A2-C2****) Alcian blue staining. Compared with that in normal persons, PTM lesions and its near normal skin had mucopolysaccharide deposits in the dermis. PTM lesions had dramatically more mucopolysaccharide deposits than the normal skin near PTM lesions.* ***A3-C3****) Immunohistochemistry staining of HIF-1α. Immunohistochemistry staining with monoclonal anti-HIF-1α antibodies showed the dermal fibroblasts, and endothelial cells of the capillaries and post-capillary venules were positive (arrows mark the positive expression) in PTM lesions compared with the normal skin of a normal person and normal skin beside PTM lesions.*

IU/ml), and the titer of TRAb was elevated (74.55 IU/L; normal range 0–1.75 IU/L). The serum titers of two subtypes of TRAb were detected with ELISA kits for thyroid-stimulating antibodies (TSAb: JL42766, jianglaibio, Shanghai, China) and thyroid-stimulating blocking antibodies (TSBAb: JL19517, jianglaibio, Shanghai, China), and the results were 4.54 ng/ml and 6.65 ng/ml, respectively. Color Doppler Imaging (Aloka SSD-α5, Hitachi Medical, Japan) demonstrated an enlarged thyroid gland with reduced and uneven echogenicity. Decreased blood flow was observed in both thyroid lobes.

Hematoxylin & Eosin (H&E) staining of lesional tissue sections showed essentially normal epidermis, red blood cell stasis in the dilated capillaries and postcapillary venules (Fig. 2A), lymphocyte infiltration around postcapillary venules (Fig. 3C1) and obvious mucinous degeneration with widely separated, frayed, and fragmented collagen bundles in the markedly thickened reticular dermis (Fig. 2A). Alcian blue staining (pH2.5) confirmed large amounts of mucopolysaccharide deposits predominantly in the reticular dermis (Fig. 2B). The normal skin beside PTM lesions had small amounts of mucopolysaccharide deposits in the reticular dermis (Fig. 3 B1 and B2), in contrast to the normal dermis in normal persons (Fig. 3 A1 and A2). Compared with the dermis of normal persons and PTM patients (Fig. 3 A3 and B3), hypoxia-inducible factor-1α (HIF-1α) in the endothelial cells of capillaries and post-capillary venules and the fibroblasts were stained positively in the reticular dermis of PTM lesions (Fig. 3 C3) with the immunohistochemistry of monoclonal mouse anti-human HIF-1α antibody (EP118, zsbio, Beijing, China).

The patient was diagnosed with HT and presented with the extrathyroid triad. Her pretibial lesions were treated with intralesional multipoint injections of acetate triamcinolone (50 mg) and 2% lidocaine hydrochloride (5 ml), once a week. After four weeks, the thick, erythematous plaques had subsided but exophthalmos and digital clubbing remained. However, hypopigmentation at the injection sites was observed following the final injection. The hypopigmentation areas did not demonstrate obvious fluorescence under ultraviolet Wood light. The serum levels of thyroid hormones, TSH, Tg-Ab, and TPO-Ab, were the same as before treatment. More importantly, serum TRAb level dramatically dropped to 34.28 IU/L after treatment from 74.55 IU/L before treatment. Similarly, TSBAb also decreased to 2.38 ng/ml from 6.65 ng/ml and TSAb was down to 1.69 ng/ml from 4.54 ng/ml.

DISCUSSION

The patient presented with clinical, immunological, and ultrasound evidence of HT with an extra-thyroid triad of pretibial myxedema, ophthalmopathy, and thyroid acropachy. GD is caused by TSHR-stimulating antibodies (TSAb), which act as agonists by stimulating thyroid growth and thyroid hormone synthesis in an unregulated manner. In contrast, blocking anti-TSHRAb (TSBAb) acts as TSHR antagonists, which block the action of the thyroid-stimulating hormone (TSH) and can cause the hypothyroidism of HT (5). Therefore, the serum level of TSBAb was higher than TSAb in the patient with HT.

Exophthalmos is the most prominent feature of thyroid-associated ophthalmopathy (TAO). TAO, also called Graves' ophthalmopathy (GO), is an autoimmune disease, most commonly associated with Graves' hyperthyroidism. It has been thought that the development of GO involves TSAb stimulating the orbital fibroblasts to synthesize hyaluronic acid (HA) via the PI3K/Akt signaling pathway (6). However, the patient had HT with hypothyroidism and both TSAb and TSBAb coexisted but TSBAb was dominant. Except for the TSAb, it is unclear whether TSBAb also plays a role in the process of HA synthesis in fibroblasts.

PTM is generally thought to be mucinosis superimposed on AITD. Serum TRAb levels were positively correlated with the severity of PTM (7). TSHR is the targeted autoantigen which is expressed on the dermal fibroblasts of PTM lesions. *In vitro*, the serum or IgG of PTM patients can stimulate PTM primary dermal fibroblasts to produce HA. Therefore, elevated TRAb levels might play an important role in the excessive HA production at PTM lesions. Considering that the TSBAb titer is higher than TSAb in the patient

with HT, TSBAb might also induce the production of HA in dermal fibroblasts, just like TSAb. However, TRAb alone cannot explain why PTM always occurs in the lower legs. Another possible cause might be attributed to the local factor precipitating PTM. The patient had a persistent standing posture of more than 4 hours per day. Histopathology showed that red blood cells stagnated in the dilated capillary and postcapillary venules. HIF-1α in the fibroblasts and the endothelial cells of postcapillary venules was up-regulated in the reticular dermis, which demonstrated local hypoxia in lesions. This evidence suggests that the persistent stasis posture may cause blood stasis in the dilated micro-vessels (especially postcapillary venules), local hypoxia and slower return of lymphatic fluid. The reactive oxygen species (ROS) is the main factor in HA fragmentation in the extracellular matrix, and the amount of ROS generation is positively correlated with local oxygen concentrations (8, 9). Therefore, the local factor (a persistent stasis posture) might have resulted in the dramatic decrease in HA degradation in the ECM of dermis, and might have also reduced the elimination of HA and HA fragments through slower return of lymphatic fluid, which precipitates the development of PTM, always in the lower legs under the background of thyroid autoimmunity.

The cutaneous hypopigmentation secondary to corticosteroid injection was observed only around the injection sites. It can be differentiated from the vitiligo under ultraviolet Wood light. A similar phenomenon has been reported in a PTM patient (10), however its mechanism is unknown. It may be related to reduction in the numbers of melanocytes and alteration of melanocyte function.

Thyroid acropachy commonly manifests itself as the clubbing of fingers and toes that occurs in 20% of patients with PTM (2). It occurs mainly in AITD but rarely in follicular thyroid cancer (11). Thyroid acropachy occurring at the end of extremities may relate to relative hypoxia but its detailed mechanism is unclear. The diagnosis of thyroid acropachy can be made clinically or radiologically (12), but its treatment is difficult.

Finally, the triad of PTM, ophthalmopathy and acropachy is rare in patients with HT, and its detailed pathogenesis is not yet clear. TRAb and local hypoxia may be the shared pathogenic agents in the pathogenesis of the triad. However, both TSAb and TSBAb may have similar effects on the fibroblasts, but different effects on the thyrocytes. This phenomenon warrants further investigation.

ACKNOWLEDGEMENTS

We thank Shigao Chen MD, Shuanghua Cheng BS of the Department of Pathology in CNNC 416 Hospital for their technical support of histopathology and immunohistochemistry. This study was supported by Sichuan Science and Technology Department (grant 18YYJCI834).

REFERENCES

1. Kan E, Kan EK, Ecemis G, Colak R. Presence of thyroid-associated ophthalmopathy in Hashimoto's thyroiditis. Int J Ophthalmol 2014; 7:644-47.
2. Bartalena L, Fatourechi V. Extrathyroidal manifestations of Graves' disease: a 2014 update. J Endocrinol Invest 2014; 37:691-700.
3. Lan C, Chen W, Zhao J, Li C, Mei X. Prevalence and clinical characteristics of pretibial myxedema in Chinese outpatients with thyroid diseases. J Endocrinol Metab 2015; 5:250-55.
4. Lan C, Li C, Chen W, Mei X, Zhao J, Hu J. A randomized controlled trial of intralesional glucocorticoid for treating pretibial myxedema. J Clin Med Res 2015; 7:862-72.
5. Diana T, Olivo PD, Kahaly GJ. Thyrotropin receptor blocking antibodies. Horm Metab Res 2018; 50:853-62.
6. Kumar S, Iyer S, Bauer H, Coenen M, Bahn RS. A stimulatory thyrotropin receptor antibody enhances hyaluronic acid synthesis in graves' orbital fibroblasts: inhibition by an IGF-I receptor blocking antibody. J Clin Endocrinol Metab 2012; 97:1681-87.
7. Lan C, Wang Y, Zeng X, Zhao J, Zou X. Morphological diversity of pretibial myxedema and its mechanism of evolving process and outcome: a retrospective study of 216 cases. J Thyroid Res 2016; 2016:2652174.
8. Hao Y, Cheng D, Ma Y, Zhou W, Wang Y. The

relationship between oxygen concentration, reactive oxygen species and the biological characteristics of human bone marrow hematopoietic stem cells. Transplant Proc 2011; 43:2755-61.

9. Soltés L, Mendichi R, Kogan G, Schiller J, Stankovska M, Arnhold J. Degradative action of reactive oxygen species on hyaluronan. Biomacromolecules 2006; 7:659-68.
10. Lan C, Li C, Yang M, et al. Pretibial myxoedema with autoimmunity and hyperplasia treated with glucocorticoids and surgery. Br J Dermatol 2012; 166:457-59.
11. Tavarelli M, Sarfati J, De Gennes C, et al. Hypertrophic osteoarthropathy and follicular thyroid cancer: A Rare Paraneoplastic Syndrome. Eur Thyroid J 2015; 4:266-70.
12. Kraus CN, Sodha P, Vaidyanathan P, Kirkorian AY. Thyroid dermopathy and acropachy in pediatric patients. Pediatr Dermatol 2018; 35:e371-e374.

LETTER TO THE EDITOR

GINSENOSIDE Rb1 REGULATES NEURONAL INJURY AND Keap1-Nrf2/ARE SIGNALING PATHWAY IN CEREBRAL INFARCTION RATS

J-E. YANG[1*], N. JIA[1*], D. WANG[2], Y. HE[2], L. DONG[2] and A-G. YANG[2]

[1]Department of Rehabilitation, Affiliated Foshan Gaoming Hospital of Guangdong Medical University, Guangdong Province, P.R. China; [2]Department of Rehabilitative Medicine, Affiliated Hospital of Chengdu University, Sichuan Province, P.R. China

Received March 6, 2020 – Accepted April 29, 2020

[*]These Authors contributed equally to this work

To the Editor,

Cerebral infarction is a general term for ischemic stroke, including cerebral thrombosis, lacunar infarction, and cerebral embolism (1). It is well-known that the etiology of cerebral infarction is complex and is closely related to hypertension, smoking, and improper diet (2). Although thrombolysis can reduce clinical mortality, the time window of thrombolysis is very narrow. Only a few patients with cerebral infarction can be effectively treated. Moreover, the establishment of collateral circulation helps to improve blood perfusion in cerebral ischemia areas (3). After treatment, angiogenesis and revascularization contribute to the remodeling of the nervous system.

It is well known that traditional Chinese medicine is effective for patients with cerebral ischemia and has few clinical side-effects. Ginsenoside Rb1 is the main bioactive component of *Panax ginseng* and is a commonly used Chinese herbal medicine in clinical practice. In particular, Ginsenoside Rb1 has a protective effect on global cerebral I/R injury and acute myocardial ischemia in rats (4). In addition, many studies have reported that the Keap1-Nrf2/ARE signaling pathway is involved in endogenous antioxidant defense mechanisms, which is an important signaling pathway in oxidative stress systems (5). Therefore, this study aims to elucidate the relationship between Ginsenoside Rb1 and Keap1-Nrf2/ARE signaling pathway in cerebral infarction. At the same time, the effect of Ginsenoside Rb1 on neuronal damage was also detected in this study.

MATERIALS AND METHODS

Study animals

Sixty 60 SD rats were used in this study, 20 of which were randomly selected as a blank control group (Blank). The remaining 40 rats were prepared with the MCAO animal model. Among them, 20 rats were randomly selected as the MCAO control group (MCAO-NC), and the remaining 20 were selected as the Ginsenoside Rb1 group (MCAO-Rb1). Male and female were random in sixty SD rats with a body weight of 210-240 g and an average of 230±10 g. The animal certificate number is SCXX-2005-0001. All experiments in this study were conducted by the Laboratory Animals Care and Use Committee of Affiliated Hospital of Chengdu University. The selected animals were purchased in the experimental

Key words: Ginsenoside Rb1; cerebral infarction; Keap1-Nrf2/ARE pathway; neurons

Corresponding Author:
Dr. Aiguo Yang,
Department of Rehabilitative Medicine,
Affiliated Hospital of Chengdu University,
No. 82, Second Section North of Erhuan Road,
Jinniu District, Chengdu, 610081, Sichuan Province, P.R. China
Tel.: +86 18780145773
e-mail: qiaosnuu6304@163.com

0393-974X (2020)
Copyright © by BIOLIFE, s.a.s.
This publication and/or article is for individual use only and may not be further reproduced without written permission from the copyright holder.
Unauthorized reproduction may result in financial and other penalties
DISCLOSURE: ALL AUTHORS REPORT NO CONFLICTS OF INTEREST RELEVANT TO THIS ARTICLE.

animal room of the Medical University to complete the routine feeding and lighting of rats.

MCAO animal models

Before modeling, rats were accurately weighed and the MCAO animal model was constructed using the thread plug method. SD rats were accurately weighed using a balance and anesthetized using chloral hydrate. After anesthesia is effective, the supine position was taken and fixed. On the mouse board, we removed the coat and made a surgical incision in the middle of the neck. We entered the depth of 18-22 mm from the external carotid artery (ECA) of the rat and completed the blocking of the middle cerebral artery (MCA) of the rat until we felt mild resistance. The nylon thread was withdrawn 2 h after the operation, and the rats were perfused again. The rats were transferred to the cage until waking up. Criteria for successful modeling: Rats were evaluated with reference to the relevant scoring method. 0 points: no symptoms of nerve defects; 1 point: left forelimb flexion; 2 points: spontaneous tilt to the left; 3 points: spontaneous rotation; 4 points: difficulty walking; 5 points: death. For rats with a score not exceeding 3, the modeling was successful (6).

After successful modeling, 20 rats were randomly selected as MCAO-NC, and the remaining 20 rats were set as MCAO-Rb1 group. The normal saline was injected intraperitoneally in the Blank group and MCAO-NC group. MCAO-Rb1 group was perfused with Ginsenoside Rb1 (20mg/kg). After 14 days of intervention, each group of rats was evaluated.

RNA isolation and RT-qPCR

On the fourteenth day after the intervention of the three groups, 5 rats were taken from each group. Brain tissues were removed from these rats and retained. Total RNA isolation was performed using TRIzol® reagent (Invitrogen; Thermo Fisher Scientific, Inc.). RT-qPCR was performed using SYBR Green I (Takara Biotechnology Co., Ltd.) according to the manufacturer's instructions. Thermocycling conditions for PCR amplification are as follows: 5 min at 99˚C, followed by 35 cycles of 95˚C for 30 sec and 42˚C for 45 sec. β-actin was used as a control for Nrf2 and Keap-1. The expression of Nrf2 and Keap-1 was quantified using the $2^{-\Delta\Delta Cq}$ method (7). The primers are shown in Table 1.

Western blot analysis

Protein samples were lysed using RIPA buffer (Beyotime, Shanghai, China). Next, proteins were separated by 10% SDS-PAGE and blocked with 5% skim milk. Protein samples were then transferred to PVDF membranes. The protein samples were incubated with Nrf2, Keap-1 and β-actin primary antibodies (Abcam, Shanghai, China) at 4°C overnight. After washing, the protein samples were incubated with secondary antibodies for 1 h. Finally, protein bands were evaluated using ECL kit (Beyotime, Shanghai, China).

HE staining

Brain tissues were fixed in 4% paraformaldehyde for 24 h, and then embedded in paraffin. Next, the tissue was cut into sections (4 μm). The sections were dewaxed in xylene and then hydrated in gradient ethanol. The sections were then stained with hematoxylin for 3 min and eosin for 30 seconds, respectively. The cerebral blood vessels and neurons were observed under an inverted microscope (×200, Olympus, Japan).

Statistical analysis

The data was analyzed by SPSS 18.0. Student's *t*-test and *Chi*-squared test were used to analyze the differences between groups. Data are shown in $\bar{x} \pm s$. $P < 0.05$ was considered significant..

RESULTS

Comparison of neurological deficit scores among Blank, MCAO-NC and MCAO-Rb1 groups

The difference of neurological deficit scores between Blank, MCAO-NC and MCAO-Rb1 groups was analyzed. As shown in Table II, there was no statistically significant difference in neurological deficit scores before modeling between the three groups ($P > 0.05$, Table II). After 1 day of intervention, we found that the neurological deficit score of the MCAO-NC group was significantly lower than that of the Blank group ($P<0.05$, Table III). At the

same time, the neurological deficit score of MCAO-Rb1 group was lower than that of the MCAO-NC group (P<0.05, Table II). The same results were also detected after 3, 7 and 14 days of intervention. The results suggest that Ginsenoside Rb1 can improve neurological deficits in rats with cerebral infarction.

Effect of Ginsenoside Rb1 on Keap1-Nrf2/ARE signaling pathway

Next, the expression levels of Nrf2 and Keap-1 in brain tissues were detected. RT-qPCR showed that the mRNA expression levels of Nrf2 and Keap-1 in MCAO-NC group were increased compared with the Blank group (P<0.01, Fig. 1A). However, the expressions of Nrf2 and Keap-1 in the MCAO-Rb1 group were lower than those in the MCAO-NC group, but still higher than in the Blank group (P<0.01, Fig. 1A). The protein expression of Nrf2 and Keap-1 also showed the same results (Fig. 1B). These results indicate that Nrf2 and Keap-1 are upregulated in rats with cerebral infarction. Ginsenoside Rb1 can reduce the expression of Nrf2 and Keap-1 in rats with cerebral infarction.

Comparison of neuron damage in Blank, MCAO-NC and MCAO-Rb1 groups

In addition, HE staining experiments showed that the brain tissue in the blank group had less neovascularization, and no neuronal damage was

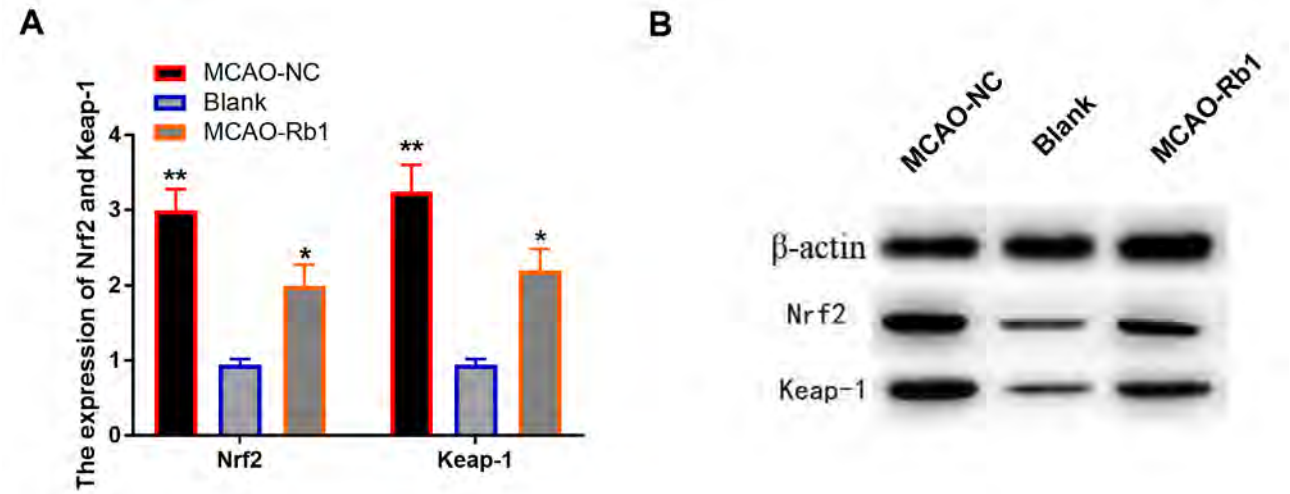


Fig. 1. *The effect of ginsenoside Rb1 on Keap1-Nrf2ARE signaling pathway. **A**) The mRNA expression of Nrf2 and Keap-1 in Blank, MCAO-NC and MCAO-Rb1 groups. **B**) The protein expression of Nrf2 and Keap-1 in Blank, MCAO-NC and MCAO-Rb1 groups. *P < 0.05, **P < 0.01*

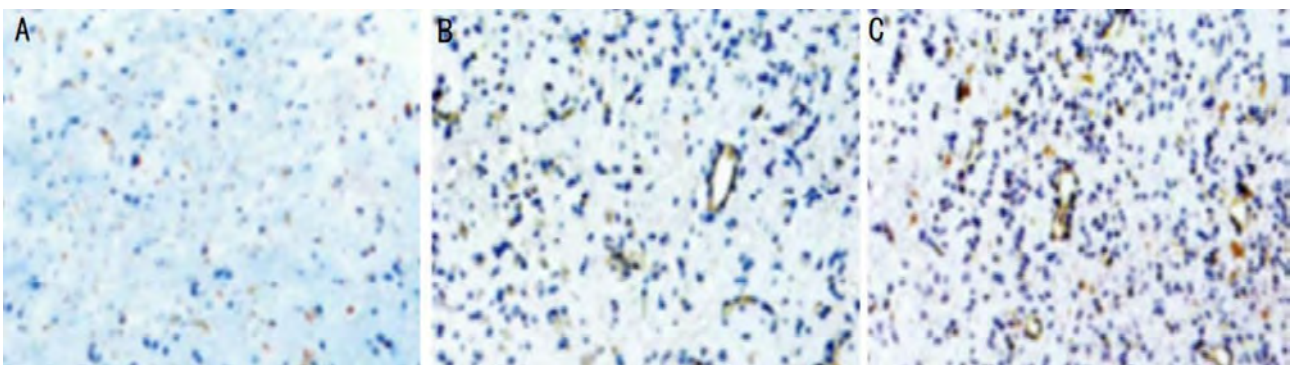


Fig. 2. *Comparison of neuron damage in Blank, MCAO-NC and MCAO-Rb1 groups. **A-C**) The neuron damage in Blank, MCAO-NC and MCAO-Rb1 groups detected by HE*

observed in the Blank group (Fig. 2A). At the same time, neovascularization in the MCAO-Rb1 group was generally accompanied by mild neuronal damage (Fig. 2B). Compared with the Blank group or the MCAO-Rb1 group, the neovascularization and neuronal damages were more severe in the MCAO-NC group (Fig. 2C). Based on these results, we conclude that Ginsenoside Rb1 may alleviate brain damage by promoting angiogenesis.

DISCUSSION

Ginsenoside Rb1 is a commonly used therapeutic drug in the acute phase of cerebral infarction and has a good protective effect on cerebral infarction (8). In this study, we found that Ginsenoside Rb1 can alleviate nerve defects in rats with cerebral infarction and facilitate recovery. It has been reported that Ginsenoside Rb1 is a traditional Chinese medicine preparation that can reduce oxidative stress damage after cerebral infarction (9). More importantly, Ginsenoside Rb1 can promote angiogenesis in cerebral infarction, improve cerebral blood perfusion, provide a microenvironment for neuronal and cell proliferation and growth, and help reduce nervous system damage (10). This study also confirmed that Ginsenoside Rb1 can reduce neuronal damage and promote the formation of new blood vessels in cerebral infarction, thereby improving nerve damage in rats.

Transcription factor NF-W2 related factor 2 (Nrf2) is a relatively important protective transcription molecule, widely present in various organs of human body. Nrf2-ARE is the core of Nrf2 and anti-oxidative transcriptional elements, and its signal pathway can enhance the antioxidant and detoxification effects of Nrf2, which is a protective signaling pathway (11). In addition, the up-regulation of Nrf2 can increase the expression level of Keap-1 in phosphorylated cells and aggravate the occurrence of disease (12). In this study, Ginsenoside Rb1 can reduce the expressions of Nrf2 and Keap-1, and obtain a good therapeutic prognosis in rats with cerebral infarction. We also found that Ginsenoside Rb1 can help establish effective collateral circulation in the infarcted area and improve the symptoms of nerve defects. In conclusion, Ginsenoside Rb1 alleviates neuronal damage in rats with cerebral infarction by regulating the Keap1-Nrf2/ARE pathway.

REFERENCES

1. Sadelli K, Stamegna JC, Girard SD, et al. Global cerebral ischemia in rats leads to amnesia due to selective neuronal death followed by astroglial scar formation in the CA1 layer. Neurobiol Learn Mem 2017; 141:168-78.
2. Harloff A, Handke M, Reinhard M, Geibel A, Hetzel A. Therapeutic strategies after examination by transesophageal echocardiography in 503 patients with ischemic stroke. Stroke 2006; 37:859-64.
3. Choi JH, Pile-Spellman J. Reperfusion changes after stroke and practical approaches for neuroprotection. Neuroimaging Clin N Am 2018; 28:663-82.
4. Ahmed T, Raza SH, Maryam A, et al. Ginsenoside Rb1 as a neuroprotective agent: a review. Brain Res Bull 2016; 125:30-43.
5. Meng H, Guo J, Wang H, Yan P, Niu X, Zhang J. Erythropoietin activates Keap1-Nrf2/ARE pathway in rat brain after ischemia. Int J Neurosci 2014; 124:362-8.
6. Zhang Y, Qiu B, Wang J, Yao Y, Wang C, Liu J. Effects of BDNF-transfected BMSCs on neural functional recovery and synaptophysin expression in rats with cerebral infarction. Mol Neurobiol 2017; 54:3813-24.
7. Livak KJ, Schmittgen TD. Analysis of relative gene expression data using real-time quantitative PCR and the 2(-Delta Delta C(T)) Method. Methods 2001; 25:402-8.
8. Dong X, Zheng L, Lu S, Yang Y. Neuroprotective effects of pretreatment of ginsenoside Rb1 on severe cerebral ischemia-induced injuries in aged mice: Involvement of anti-oxidant signaling. Geriatr Gerontol Int 2017; 17:338-45.
9. Ke L, Guo W, Xu J, Zhang G, Wang W, Huang W. Ginsenoside Rb1 attenuates activated microglia-induced neuronal damage. Neural Regen Res 2014; 9:252-59.
10. Jiang Z, Wang Y, Zhang X, Peng T, Lu Y, Leng J, Xie Q. Preventive and therapeutic effects of ginsenoside Rb1 for neural injury during cerebral infarction in

rats. Am J Chin Med 2013; 41:341-52.
11. Tanaka N, Ikeda Y, Ohta Y, et al. Expression of Keap1-Nrf2 system and antioxidative proteins in mouse brain after transient middle cerebral artery occlusion. Brain Res 2011; 1370:246-53.
12. Huang R, Ma J, Niu B, et al. MiR-34b protects against focal cerebral ischemia-reperfusion (I/R) injury in rat by targeting Keap1. J Stroke Cerebrovasc Dis 2019; 28:1-9.

LETTER TO THE EDITOR

ANTIDEPRESSANT EFFECT OF TOTAL SAPONINS OF RADIX BUPLEURI AND THE UNDERLYING MECHANISM ON A MOUSE MODEL OF DEPRESSION

HC. FENG[1], CM. WANG[2], MZ. TANG[1], XJ. WU[3], ZC. ZHOU[4], MD. WEI[1], W. HE[1], SJ. LI[1], ZK. ZENG[1] and BH. HE[1]

[1]Department of Pharmacy, The Third Affiliated Hospital, Southern Medical University, Guangzhou, Guangdong, China; [2]Department of Pharmacy, Shenzhen University General Hospital, Shenzhen, Guangdong, China; [3]Department of Biology, East Carolina University, Greenville, NC, United States, USA; [4]Department of Ciai, Home for The Aged Guangzhou, Guangzhou, Guangdong, China

Received March 25, 2020 – Accepted April 29, 2020

To the Editor,

Depression is a chronic, recurrent emotional and mental disorder characterized by a significant and persistent lack of interest and a low mood (1). Cognitive dysfunction, such as learning, memory, attention and executive disabilities, are common complications of depression (1). Several plant species have been tried since ancient times for the treatment of depression and other neurological disorders (2). Bupleurum species belongs to the carrot family and have been used in Chinese traditional medicine for the treatment of depression since ancient times (3). Total saponins from the radix are the main active ingredients. Studies have been shown that extracts from Bupleurum species can improve learning and memory (4). The c-Jun N-terminal kinases (JNKs) belong to the mitogen-activated protein kinase (MAPK) family and are implicated in regulating the stress responses inside and outside the cell. Studies have shown that many regulatory functions of JNKs are highly correlated with the pathological mechanisms of depression and other mental disorders (5). It is particularly noteworthy that knockout of the *Jnk* gene can directly affect depression or anxiety-like behaviours (6). Many pharmacodynamic mechanisms of antidepressants involve the regulation of JNK activity (7). Serotonin or 5-hydroxytryptamine (5-HT) is closely related to emotional disorders (8). 5-HT synthesis is associated with tryptophan hydroxylase (TPH) activity. TPH2 is responsible for the central 5-HT synthesis process, and lack of its function is related to 5-HT neurological dysfunctions (8). This study aimed to evaluate the antidepressant effects of continuous administration of TSRB and its underlying mechanism by analyzing the expression of JNK and TPH2 in the dorsal raphe nucleus and hippocampus of mice.

MATERIALS AND METHODS

Animals

Ninety 8-week-old ICR (Institute of Cancer Research) male mice, SPF (Specific Pathogen Free) grade, weighing 29-32 g were used in the study. The animals had free access to feed and water and kept in standard conditions with a temperature of 23-25°C, relative humidity of 55±10% and 12-hour light/12-hour dark circadian rhythm. The animals were adapted to the environment for one week before the experiments. The Ethics Committee of The Third Affiliated Hospital of Southern Medical University

Key words: total saponins of radix Bupleuri; depression; neurons; mechanism

Corresponding Author:
Dr Zhaohong Sun,
Department of Pharmacy,
The Third Affiliated Hospital,
Southern Medical University,
Guangzhou, Guangdong 510630, China
e-mail: zhhongsun@163.com

0393-974X (2020)
Copyright © by BIOLIFE, s.a.s.
This publication and/or article is for individual use only and may not be further reproduced without written permission from the copyright holder.
Unauthorized reproduction may result in financial and other penalties
DISCLOSURE: ALL AUTHORS REPORT NO CONFLICTS OF INTEREST RELEVANT TO THIS ARTICLE.

approved this study.

A total of 90 male ICR mice were randomly divided into 6 groups (15 mice in each group): a normal group treated with 0.3 mL saline solution and 5 depression groups treated with 0.3 mL saline solution (model group), 5mg/kg/day fluoxetine (fluoxetine group) and TSRB low dose group, TSRB middle-dose group and TSRB high-dose group treated with 12.5, 25 and 50 mg/kg/day TSRB, respectively. The treatment of the mice was administered by gavage for 21 days.

Mice were weighed every week. After 21 days of exposure, the animals were sacrificed by cervical dislocation, and the brain was collected for RT-PCR (reverse transcription-polymerase chain reaction), histopathological evaluation and Western blotting.

Depression model in mice

The depression model was induced to the mice using 14 types of stress stimuli as follows: day-night reversal for 24 h, fasting for 24 h, restraint for 2 h, water deprivation for 24 h, tilt for 24 h, empty cage for 24 h, ice-water swimming for 5 min, noise for 2 h, shaking for 5 min, humidity for 24 h, thermal stimulation for 24 h, odour for 24 h (odour is different every week), tail pinch for 1 min, foreign body for 24 h (the foreign body is different every week). Two types of stimuli were randomly selected every day, and each stimulus was used 2-3 for a total of 21 days.

Description of the test methods used

The symptoms of depression were evaluated using the sucrose preference test (SPT). The test was performed in all the groups at 21 days after the treatment. Mice fasted for 24 h. The sucrose preference ratio of mice was measured and calculated as follows: sucrose preference ratio=(sucrose consumption/total liquid consumption)×100.

Novelty suppressed feeding (NSF): The homemade open field experiment box was a topless wooden box of 80cm×80cm×80cm painted in black, which was convenient for mice to feed in the dark environment. The equipment was used to measure the feeding. The bottom of the box was divided into 8cm×8cm small squares using paint to test the novelty suppressed feeding, including food intake and feeding latency. Before the experiment, the animal was fasted for 24 h, and then placed in the new environment near the wall of the box and in the center of the box a pellet of food was placed. The anxiety-like behaviour was evaluated by registering the latency to approach and eat the food.

Tail suspension test (TST): The middle tip of the mouse's tail was placed in a tail suspension box using a paper clip transformed into a hood and a medical tape glued the mouse's tail to the paper clip. The mouse was placed with the head facing the bottom of the box. A timer was used to calculate the immobility latency within 6 min and the time of continuous immobility within 4 min. The immobility condition refers to the state of the mouse's trunk being vertically immobile and giving up the struggle.

Forced swimming test (FST): The mouse was placed in glassware of 30cm x 20cm. The water depth exceeded the lower limbs of the mice. The water temperature was maintained at about 25°C. The timer was used to calculate the immobility time of the mice within 5 min. The immobility time: the head was exposed to the water surface, and the limbs were gently undulating. The latency reflected a depressed mood and a state of despair in mice, and it was used as an indicator of the degree of depression in mice.

Determination of JNK mRNA and TPH2 mRNA expression by real-time polymerase chain reaction (*RT-PCR)*

Total RNA extraction: After animal sacrification, the brain was collected, and the hippocampus and dorsal raphe nucleus were isolated on ice for further analysis. Total tissue RNA was extracted using the Trizol solution (Thermo Fisher Scientific, USA). A small part of the extracted RNA was used for purity and concentration analysis, and the rest was used for Real-Time PCR.

Quantitative Real-Time PCR detection: Amplification reaction system, 10 μL SYBR (Synergy Brands) (Hangzhou Lianke Meixun Biomedical Technology Co., Ltd., China), 0.8 μL PCR upstream primer (Shanghai Jixing Biotechnology Co., Ltd., China), 0.8 μL PCR downstream primer (Shanghai Jixing Biotechnology Co., Ltd., China), 2 μL template cDNA (Shanghai Jixing Biotechnology Co., Ltd., China), 6.4 μL DEPC (Diethy pyrocarbonate) water (Shanghai Jixing Biotechnology Co., Ltd., China). Primer sequence (synthesized by Shanghai Sangon Biotech Co., Ltd., China): JNK upstream primer (Shanghai Sangon Biotech Co., Ltd., China)5'-CAAGGAGGTCATGGATTTGG-3',downstream primer 5'-AAGACGACGGATGCTGAGAG-3', amplification product full-length 107bp; TPH2 upstream primer 5'-ACCTGAGCCCACGAGACTTT-3' (Shanghai Sangon Biotech Co., Ltd., China), downstream primer

5'-TCGAGCCAGAGCTGGAATAT-3', amplification product full-length 131bp; GAPDH upstream primer (Shanghai Sangon Biotech Co., Ltd., China) 5'-TCCTGCACCACCAACTGCTTAG-3', downstream primer 5'-AGTGGCAGTGATGGCATGGACT-3', amplification product full-length 102bp. The reaction was performed using a Light Cycler 480 real-time fluorescent quantitative PCR instrument (Roche, Switzerland). The results were expressed as Ct values. The experiment was repeated 3 times. The 2^{-Ct} method was used to compare the differences in JNK mRNA and TPH2 mRNA expression in each group.

Determination of JNK and TPH2 expression by immunofluorescence

The brain tissues from the hippocampus and dorsal raphe nucleus were used to prepare paraffin sections. The paraffin sections were dewaxed in the water, and the microwave thermal antigen repair was performed. The sections were placed on a wet box, and washed with 0.01 mol/L phosphate-buffered saline (PBS) (Shanghai Kanglang Biotechnology Co., Ltd., China) for 5 min and repeated for 3 successive times; 50 μL of normal goat serum blocking solution (Shanghai Huiying Biotechnology Co., Ltd., China) was added in drops, and the wet box was covered and left to react at room temperature for 30 min. Then the blocking solution was recovered and 50 μL of primary antibody dilution (TPH2 rabbit polyclonal primary antibody) (Abcam, UK) or JNK rabbit polyclonal primary antibody (Immunoway, USA)) (1:500) was added in drops and left to react at 4°C for 12-18 h. Then the primary antibody was rinsed with 0.01 mol/L PBS. 50 μL diluted solution of the secondary antibody, FITC-labeled goat anti-rabbit IgG (1:100) (Tianjin Sungene Biotech Co., Ltd., China) was added and let for incubation in the dark at 37°C for 30 min. The secondary antibody was rinsed with 0.01mol/L PBS and then 50 μL of the antifade mounting medium (Shanghai Yiyan Biotechnology Co., Ltd., China) was added and kept in the dark at 4°C till the evaluation. The distribution of JNK and TPH2 in the dorsal raphe nucleus and hippocampus was observed under a laser confocal microscope (Suzhou Mangefei Instrument Co., Ltd., China).

Determination of JNK and TPH2 expression by Western blotting

Hippocampus and dorsal raphe nucleus from each rat were used to extract the total protein. After measuring the protein content, a clean glass plate (BIO-RAD, USA) was installed on the rubber frame, and the following operations were carried out: glue, application of sample, electrophoresis, transmembrane, and blocking. The samples were incubated with the primary antibodies: TPH2 (1:500) (Santa Cruz, USA), JNK (1:500) (Immunoway, USA) and GAPDH (1:500) (Santa Cruz, USA) 4°C overnight. After incubation with primary antibodies, the PVDF membranes were washed for 3 successive times with TBST (Tris-Buffered Saline +Tween) (Beijing solabo Technology Co., Ltd., China). Then the samples were incubated at room temperature with HRP (Horseradish Peroxidase)-labeled secondary antibody (1:2000) for 2 h. The luminescent signals were evaluated by electrochemiluminescence (ECL) method. Images were acquired with G: BOX chemiXR5 (Syngene, UK). Gel-Pro32 software (Media Cybernetics, USA) was used to perform grey analysis on the results. The protein level was expressed as the ratio of the objective band to the average optical density (OD) of the internal reference GAPDH (glyceraldehyde-3-phosphate dehydrogenase) and the semi-quantitative analysis was performed.

Statistical analysis

Data were statistically analyzed using SPSS 19.0 (IBM, USA). The results were expressed as mean ± standard deviation. The overall differences of samples were compared with a single-factor analysis of variance. If there was a difference, the pairwise comparison between the means of each group used the Newman-Keuls test. $P<0.05$ indicates that the difference was statistically significant.

RESULTS

General condition and weight changes in mice

The mice in the normal group maintained a particular curiosity about the surroundings, and the body hair was soft and bright. The behaviour was agile and the daily excretion was normal. The mice were active and sensitive to the environment. After three weeks of depression modelling, in the model group, there were observed some phenomenon of sluggish activity, sparse hair colour, frightened behavior, reduced response sensitivity, and anorexia. After 7 days of treatment, the mice in each group

had no significant change compared with that before the treatment (P>0.05). After 14 days of treatment, the weight of mice in each group except the model group increased significantly (P<0.01), and the weight of mice in the model group decreased (P>0.05). After 21 days of treatment, the weight of mice in each group except the model group increased significantly compared with the value before the treatment (P<0.05), while the weight of mice in the model group decreased (P>0.05). Among them, the change of body weight of mice in the middle-dose group of TSRB was similar to that in the fluoxetine group (Table I).

Behavioral observations

There were significant differences in the overall mean of the sucrose preference ratio among the groups (P<0.05). The sucrose preference ratio of

Table I. *Effect of treatment on mice body weight*

Group		Before treatment	After 7 days of treatment	After 14 days of treatment	After 21 days of treatment
Normal group		30.42±1.43	34.82±1.79	39.15±2.36a	44.37±2.25aab
Model group		30.52±0.99	29.12±1.74*	27.29±1.28*#	25.14±1.54**#
Fluoxetine group		30.11±1.64	32.96±2.11	37.26±2.35&a	42.18±2.36&&ab
TSRB	Low-dose group	30.28±0.97	32.04±1.96	34.12±2.15&a	37.56±2.63&#ab
	Middle-dose group	30.21±1.57	34.16±2.04&	38.85±2.53&a	42.36±2.25&&ab
	High-dose group	30.37±1.36	33.52±1.78&	37.275±2.15&a	40.96±2.55&&ab

P<0.05,P<0.01 compared with the normal group; &P<0.05,&&P<0.01 compared with the model group; #P<0.05,##P<0.01 compared with the fluoxetine group; aP<0.05, aaP<0.01 compared with before treatment;, bP<0.05 compared with after 7 days of treatment.*

Table II. *The effect of treatment on mice behavior*

Group	Normal group	Model group	Fluoxetine group	TSRB		
				Low-dose group	Middle-dose group	High-dose group
Sucrose consumption	0.85±0.06	0.56±0.12**	0.72±0.08*&	0.64±0.08**	0.79±0.14&&a	0.75±0.17&&
Tail suspension time (S)	45.15±19.04	79.02±21.24*	31.51±20.65&&	67.22±34.51**##	46.64±29.62#a	58.32±18.56#
Tail suspension latency (S)	53.02±15.33**	104.31±15.72**	94.73±28.54**	103.13±15.65**	101.84±24.86**	104.56±20.45**
Feeding latency (S)	51.63±14.31	234.13±54.44**	137.72±79.46**	187.33±82.40**	148.19±100.45**	154.32±94.43**&
Swimming latency (S)	8.63±2.33&	43.34±13.54**	19.77±12.34&&	17.32±9.53&&	19.74±9.14&&	22.33±21.76&&
Swimming immobility time (S)	63.04±15.32	108.45±10.54**	88.53±26.83&*	89.81±29.50&	69.33±24.53&&	71.13±25.40&&

*Notes: *P<0.05, **P<0.01 compared with the normal group; &P<0.05, &&P<0.01 compared with the model group; #P<0.05, ##P<0.01 compared with the fluoxetine group; aP<0.05 compared with the TSRB low dose group.*

the model group was lower than that of the normal group (P<0.01), which proved that the depression model was successfully modelled. The sucrose preference ratio of the TSRB middle-dose, high-dose, and fluoxetine groups was higher than that of the model group (P<0.05) (Table II).

There were extremely significant differences in the overall mean of tail suspension time in mice

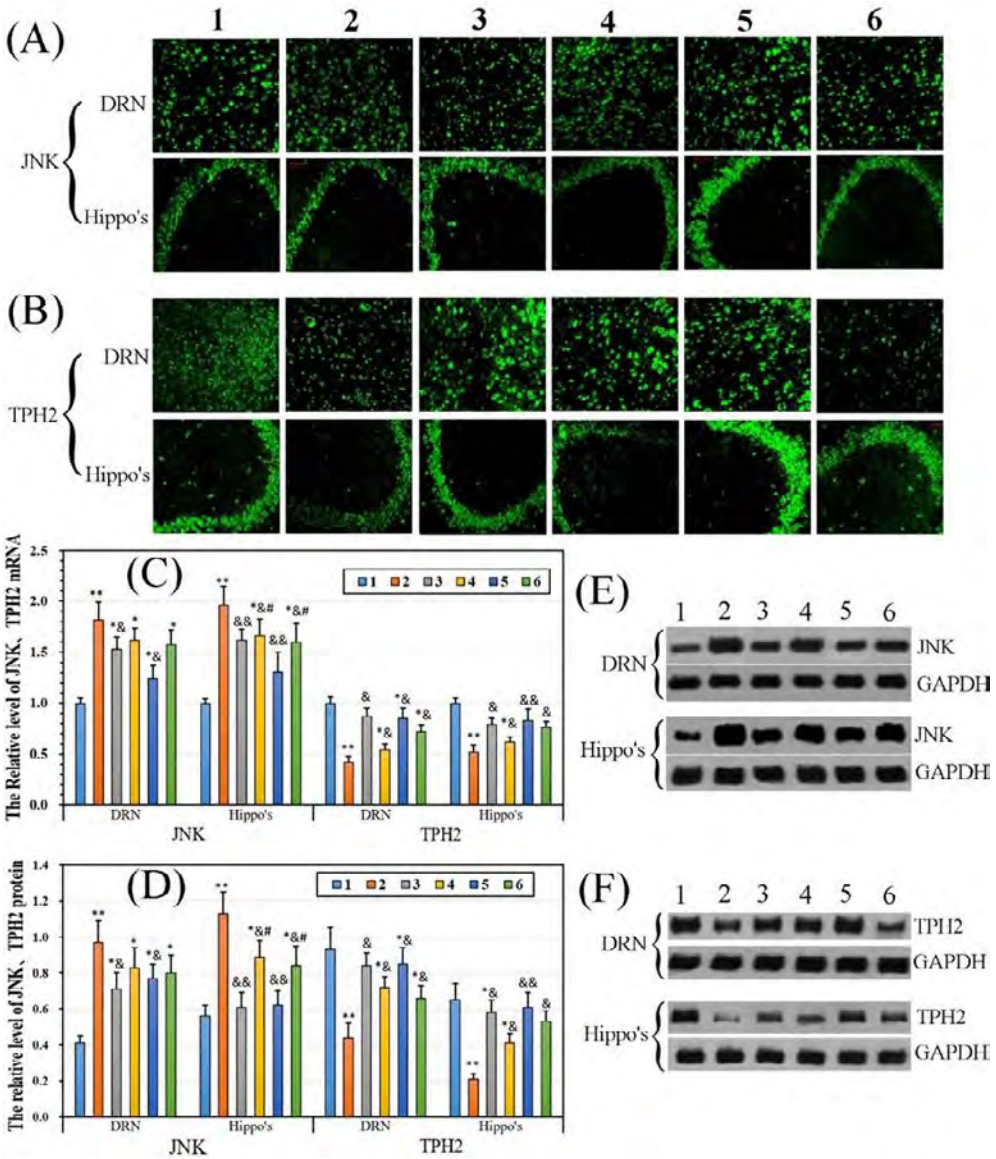


Fig. 1. *The relative optical density of JNK and TPH2 protein expression in the hippocampus (Hippo's) and dorsal raphne nucleus (DRN) of mice brain.* ***A****) JNK protein expression in the hippocampus (Hippo's) and dorsal raphne nucleus (DRN) of by immunofluorescence;* ***B****) TPH2 protein expression in the hippocampus (Hippo's) and dorsal raphne nucleus (DRN) by immunofluorescence;* ***C****) Statistical chart of JNK and TPH2 protein expression in the hippocampus (Hippo's) and dorsal raphne nucleus (DRN);* ***D****) Relative grey value level of JNK and TPH2 protein expression in the hippocampus (Hippo's) and dorsal raphne nucleus (DRN);* ***E****) JNK protein expression in the hippocampus (Hippo's) and dorsal raphne nucleus (DRN) by Western blotting;* ***F****) JNK protein expression in the hippocampus (Hippo's) and dorsal raphne nucleus (DRN) by Western blotting. 1: normal group, 2: model group, 3: fluoxetine group, 4: TSRB low-dose group, 5: TSRB middle-dose group, 6: TSRB high-dose group. *P<0.05, **P<0.01 compared with normal group; &P<0.05, &&P<0.01 compared with model group; #P<0.05 compared with fluoxetine group.*

($P<0.01$). The immobility latency of the mice in the model group was higher than that in the other groups ($P<0.01$), which proved that the modelling was successful. There were no significant differences in the TSRB low-dose, middle-dose, high-dose, and fluoxetine groups, as well as between them and the normal group ($P>0.05$).

In the novelty suppressed feeding test, the feeding latency of the model group was significantly higher than that of the normal group ($P<0.01$), which proved that the model was successful. The feeding latency of the model group was significantly higher than that of the TSRB high-dose group ($P<0.01$). There was no difference in feeding latency between the fluoxetine and TSRB groups ($P>0.05$), but the latency was higher in the treatment groups compared to the normal group ($P<0.01$ or $P<0.05$) (Table II).

In the forced swimming test, the swimming latency of the model group was significantly higher than that of the control group and each drug treatment group ($P<0.05$), which proved that the modelling was successful. There was no difference among the drug treatment groups as well as between them and the control group ($P>0.05$). The swimming immobility time of the model group was higher than that of the normal group, middle-dose and high-dose TSRB groups of ($P<0.05$). There was no difference between the low-dose, middle-dose and high-dose TSRB groups ($P>0.05$) (Table II).

Determination of JNK mRNA and TPH2 mRNA expression by *RT-PCR*

Compared with the normal group, the expression of JNK mRNA in the brain regions of the model group mice was significantly increased ($P<0.05$), and the TPH2 mRNA was significantly decreased ($P<0.05$). After the drug intervention, compared with the model group, TPH2 mRNA in the brain regions was significantly increased ($P<0.05$). The expression of JNK mRNA in the hippocampus was significantly decreased in the fluoxetine group and the TSRB treatment groups ($P<0.05$), while only the fluoxetine group and the TSRB middle-dose group were significantly decreased in the dorsal raphe nucleus ($P<0.05$) (Fig.1C).

Expression of JNK and TPH2 proteins in different brain regions

The distribution of JNK-positive cells in the hippocampus was slightly higher than that in the dorsal raphe nucleus, showing green fluorescence. Compared with the normal group, the expression of JNK protein in each brain region of the model group was significantly increased ($P<0.05$). After drug intervention, compared with the model group, in the hippocampus, the expression of JNK protein in the fluoxetine group and the TSRB treatment groups was significantly decreased ($P<0.05$). The expression of JNK protein was significantly decreased in the dorsal raphe nucleus compared to the model group only in the fluoxetine group and the TSRB middle-dose group ($P<0.05$) (Fig.1 A, D and E).

TPH2-positive cells were mainly distributed in the dorsal raphe nucleus, showing green fluorescence. Compared with the normal group, TPH2 protein expression in each brain region of the model group was significantly decreased ($P<0.05$). After drug intervention, compared with the model group, the TPH2 protein expression in the fluoxetine group and the TSRB treatment groups was significantly increased ($P<0.05$) (Fig. 1 B, D and F).

DISCUSSION

Depression is characterized by loss of pleasure, decreased exercise capacity and desperate behaviour. In the current study, the depression model was successfully established. The model was confirmed by a decreased preference for sucrose, increased immobility latency in tail suspension test, increased feed latency in the novelty suppressed feeding test and increased swimming latency in the forced swimming test compared to the control group. After treatment with TSRB, the symptoms of depression in mice were significantly improved, almost to the same level as fluoxetine, a known antidepressant.

TPH2 is a specific central nervous system TPH isoenzyme shown to be mainly expressed in the dorsal raphe nucleus of the brainstem and control the synthesis of central 5-HT (9). Jahanshahi et al. (10) showed that the expression of the TPH2 gene in the dorsal raphe nucleus brain region of

depression model mice was significantly lower than that in the normal group. Xu XM et al. (11) found that the genetic variation of the TPH2 gene was closely related to mental disorders, eating disorders, and other emotions through the detection of TPH2 multiple gene sites. Except for TPH2 modulation, many antidepressants can regulate the activity of JNK to mediate the antidepressant effect (12).

The results of this study showed that the mice from the depression model group had a significant increase in JNK mRNA and protein levels and a significant decrease in TPH2 mRNA and protein levels, while in the fluoxetine group and the TSRB groups the trend was the opposite along with the improvement of various depression-like behaviors. Therefore, the TSRB can act against depression-like behaviors by down-regulating the level of JNK in the brain and up-regulating the level of TPH2.

REFERENCES

1. Xu Y, Barish PA, Pan J, Ogle WO, O'Donnell JM. Animal models of depression and neuroplasticity: assessing drug action in relation to behavior and neurogenesis. Methods Mol Biol 2012; 829:103-24.
2. Salehi B, Calina D, Docea AO, et al. Curcumin's Nanomedicine Formulations for Therapeutic Application in Neurological Diseases. J Clin Med 2020; 9(2):E430.
3. Wang X, Feng Q, Xiao Y, Li P. Radix Bupleuri ameliorates depression by increasing nerve growth factor and brain-derived neurotrophic factor. Int J Clin Exp Med 2015; 8(6):9205-17.
4. Wang JT, Wang S, Liu SL, Wang YC, Li JG, Chen Y. [Molecular mechanism of Bupleuri Radix and Scutellariae Radix drug pair for depression based on integrative pharmacology platform of traditional Chinese medicine]. Zhongguo Zhong Yao Za Zhi 2018; 43(7):1323-30.
5. Winchester CL, Ohzeki H, Vouyiouklis DA, et al. Converging evidence that sequence variations in the novel candidate gene MAP2K7 (MKK7) are functionally associated with schizophrenia. Hum Mol Genet 2012; 21(22):4910-21.
6. Zhou Q, Wang M, Du Y, et al. Inhibition of c-Jun N-terminal kinase activation reverses Alzheimer disease phenotypes in APPswe/PS1dE9 mice. Ann Neurol 2015; 77(4):637-54.
7. Daniele S, Da Pozzo E, Zappelli E, Martini C. Trazodone treatment protects neuronal-like cells from inflammatory insult by inhibiting NF-κB, p38 and JNK. Cell Signal 2015; 27(8):1609-29.
8. Pratelli M, Migliarini S, Pelosi B, Napolitano F, Usiello A, Pasqualetti M. Perturbation of serotonin homeostasis during adulthood affects serotonergic neuronal circuitry. eNeuro 2017; 4(2):ENEURO.0376-16.2017.
9. Walther DJ, Peter JU, Bashammakh S, Hörtnagl H, Voits M, Fink H, Bader M. Synthesis of serotonin by a second tryptophan hydroxylase isoform. Science 2003; 299(5603):76.
10. Jahanshahi A, Le Maitre E, Temel Y, et al. Altered expression of neuronal tryptophan hydroxylase-2 mRNA in the dorsal and median raphe nuclei of three genetically modified mouse models relevant to depression and anxiety. J Chem Neuroanat 2011; 41(4):227-33.
11. Xu XM, Ding M, Pang H, Wang BJ. TPH2 gene polymorphisms in the regulatory region are associated with paranoid schizophrenia in Northern Han Chinese. Genet Mol Res 2014; 13(1):1497-507.
12. Yarza R, Vela S, Solas M, Ramirez MJ. c-Jun N-terminal kinase (JNK) signaling as a therapeutic target for Alzheimer's disease. Front Pharmacol 2016; 6:321.

LETTER TO THE EDITOR

MECHANISMS OF EFFECT OF EARLY INHALATION OF BUDESONIDE ON PULMONARY FUNCTION, OSTEOPONTIN AND α-SMA IN ASTHMATIC RATS

W. YANG[1*], X. WU[1*], X-Y. XU[1], H-Y .WANG[2], Y. LI[1], S-N. JIAN[1] and Y-W. LIU[1]

[1]The Second Department of Respiration Medicine, Baoding NO.1 Central Hospital, Baoding, China;
[2]Department of Respiration Medicine, Affiliated Hospital of Hebei University, Baoding, China

Received December 6, 2019 – Accepted April 29, 2020

[*]These authors contributed equally to this study

To the Editor,

Bronchial asthma is a common respiratory disease (1). Airway remodeling is not only the repair response of the airway to traumatic stimulation, but also one of the important characteristics of bronchial asthma (2). Osteopontin (OPN) is a secretory glycosylated phosphoprotein, and is also known as specific osteoblast factor-2. It is present in various tissues and body fluids, and there is also a small amount of OPN expression in normal lung tissues (3). OPN is closely correlated to bronchial asthma (3). Furthermore, OPN can also promote eosinophil chemotaxis, and its level is positively correlated with the level of eosinophils (3).

The α-smooth muscle actin (α-SMA) can be divided into two phenotypes: contractile and proliferative types. The contractile type is mainly found in mature vascular smooth muscle cells, while the proliferative type is mainly found in vascular smooth muscle cells in early development or the pathological process (4). The α-SMA can reflect the number of smooth muscle cells and the contractile capacity of the smooth muscle, therefore, an increase in the expression of α-SMA indicates the increase in airway responsiveness and airway remodeling (4).

In clinics, the inhalation of budesonide is used for patients with glucocorticoid dependent or non-dependent bronchial asthma and asthmatic chronic bronchitis (5), however, few studies have determined whether the inhalation of corticosteroids can effectively inhibit airway remodeling. In addition, the mechanism of airway remodeling remains unclear, and there is a lack of effective measures to prevent and treat airway remodeling in asthma. In the present study, the changes in pulmonary function, OPN and α-SMA in asthmatic rats were investigated, and the relationship between OPN and pulmonary function, and airway remodeling was also investigated.

MATERIALS AND METHODS

Asthma animal model preparation

A total of 60 male Sprague Dawley (SD) rats with body weights ranging within 130-170 g were randomly divided into three groups (*n*=20, each): model group, control group and treatment group. Rats in the three groups were intraperitoneally injected with 2 ml of suspension, containing 100 mg of ovalbumin, 100 mg of aluminum hydroxide and 1 ml of pertussis vaccine (containing five billion strains), for sensitization on the 1st and 7th days,

Key words: asthma; budesonide; pulmonary function; osteopontin; α-SMA

Corresponding Author:
Dr Wei Yang,
The Second Department of Respiration,
Baoding No. 1 Central Hospital,
No. 320 of Great Wall North Street, Lianchi District, Baoding 071000, China
Tel: +86 0312-5976500 - Fax: +86 0312-5976586
e-mail: ywei_112@163.com

0393-974X (2020)
Copyright © by BIOLIFE, s.a.s.
This publication and/or article is for individual use only and may not be further reproduced without written permission from the copyright holder.
Unauthorized reproduction may result in financial and other penalties
DISCLOSURE: ALL AUTHORS REPORT NO CONFLICTS OF INTEREST RELEVANT TO THIS ARTICLE.

respectively. After the 15th day, rats in the model group and treatment group were placed in a self-designed fumigant with a volume of 20 × 30 × 40 cm^3, which was not completely closed. These rats inhaled ovalbumin, *qod*. The concentration of ovalbumin was gradually increased from 1% to 1.5%, 2%, 2.5% and 3% (each concentration was atomized for four times). Rats in the control group inhaled 0.9% normal saline, while rats in the treatment group inhaled 20 ml of budesonide (0.5 g/L) twice a day. Furthermore, rats in the control group and model group inhaled the same amount of normal saline.

Pulmonary function examination and bronchoalveolar lavage fluid collection

Pulmonary function was examined at baseline and at 24 h after the last inhalation. Rats were intraperitoneally injected with 90 mg/kg of 1% sodium pentobarbital. Then, a median cervical incision was made after satisfactory anesthesia, in order to fully expose the trachea, the trachea was cut off, and an animal ventilator was connected. Afterwards, the jugular vein fluid port was established, and the airway basic resistance was measured. Rats were successively injected with normal saline and acetylcholine into the jugular vein (the doses of acetylcholine were 6.25 μg/kg, 12.5 μg/kg, 25 μg/kg and 50 μg/kg, respectively). Then, the change in the area under the curve (AUC) after injection was measured. The interval between injections was five min.

After the pulmonary function examination, the left lung was lavaged with 2 ml of 4°C sterile normal saline: during lavage, the normal saline was slowly injected through the endotracheal intubation, the chest wall was gently massaged, the catheter was placed for 30 seconds and slowly withdrawn, and the operation was performed in triplicate. All BALF was collected, filtered with two layers of gauzes, and centrifuged at 1,200 rpm at 4°C for 10 min. Then, the supernatant was sucked, sub-packaged, and maintained at -80°C for future use.

The upper lobe of the right lung was obtained, fixed with 4% formaldehyde, and routinely paraffined, sectioned and stained with hematoxylin and eosin (H&E). Then, the infiltration of inflammatory cells in the airway epithelium and around the airway was observed under a light microscope. For determination of OPN in BALF Specific steps were performed according to the instructions of OPN enzyme-linked immunosorbent assay (ELISA) kit.

Detection of α-SMA in airway smooth muscles by immunohistochemistry

The sections underwent routine dewaxing, washed with 0.01 M of phosphate buffered saline (PBS) for three times, incubated with 0.3% methanol-hydrogen peroxide at room temperature for 20 min, washed with distilled water for five min in triplicate, repaired with 0.1 M of citric acid buffer (pH 6.0) in a microwave oven, maintained at 98°C for 20 min, cooled to room temperature, and incubated with 10% goat serum in a humidity box at a constant temperature of 37°C for 30 min. Then, the excess serum was sucked out using filter paper, added with mouse anti-rat monoclonal antibody IgG, washed with PBS for 5 min in triplicate, added with the working fluid of the biotinylated secondary antibody (goat anti-mouse), incubated at a constant temperature humidity box at 37°C for 30 min, washed with 0.01 M of PBS for 5 min three times, added with horseradish peroxidase labeled working solution of streptavidin, incubated in a constant temperature humidity box at 37°C for 30 min, washed with 0.01 M of PBS for 5 min in triplicate, colored with diaminobenzidine (DAB) for 2.5 min, washed with tap water for 15 min to stop the coloration, dehydrated with gradient alcohol, respectively treated with xylene I, II and III for 15 min until it became transparent, and sealed with neutral resin. The negative controls were treated with PBS instead of the first antibody, and the steps were the same as above.

Statistical analysis

The data were imported into the computer, then a consistency check and a logic error check were carried out. Normally distributed measurement data were expressed as mean±standard deviation (X±SD). The variance homogeneity test was first conducted.Tthe data were then compared using univariate analysis of variance. $P<0.05$ was considered statistically significant. All data were processed using statistical software Graphpad prism 6.0.

RESULTS

Pulmonary function

Compared with the control group, airway resistance increased in the model group and treatment group ($P<0.05$), and the airway resistance was lower in the treatment group than in the model group ($P<0.05$). After the intravenous injection

of acetylcholine, airway resistance increased in all three groups. The results suggest that airway responsiveness increased, and that this was most significant in the model group (Table I). The differences among the three groups were statistically significant ($P<0.05$).

Compared with the control group, the folds of the airway mucosa increased, the smooth muscle thickened, and inflammatory cells around airway significantly increased in the model group. The treatment group also exhibited the above situations, but the degrees were lower than those in the model group (Fig. 1).

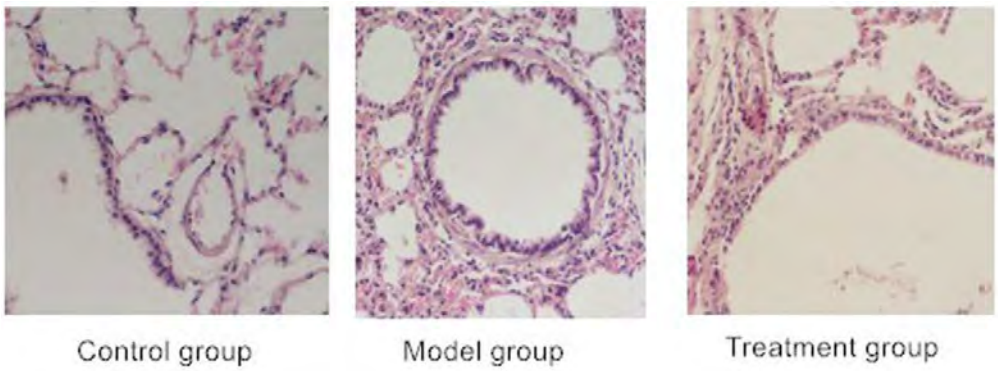


Fig. 1. *H&E staining of pulmonary tissues in the three groups. Compared with the control group, the folds of the airway mucosa increased, the smooth muscles thickened, and inflammatory cells around the airway significantly increased in the model group. The treatment group also exhibited the above situation, but the degree was lower than that in the model group.*

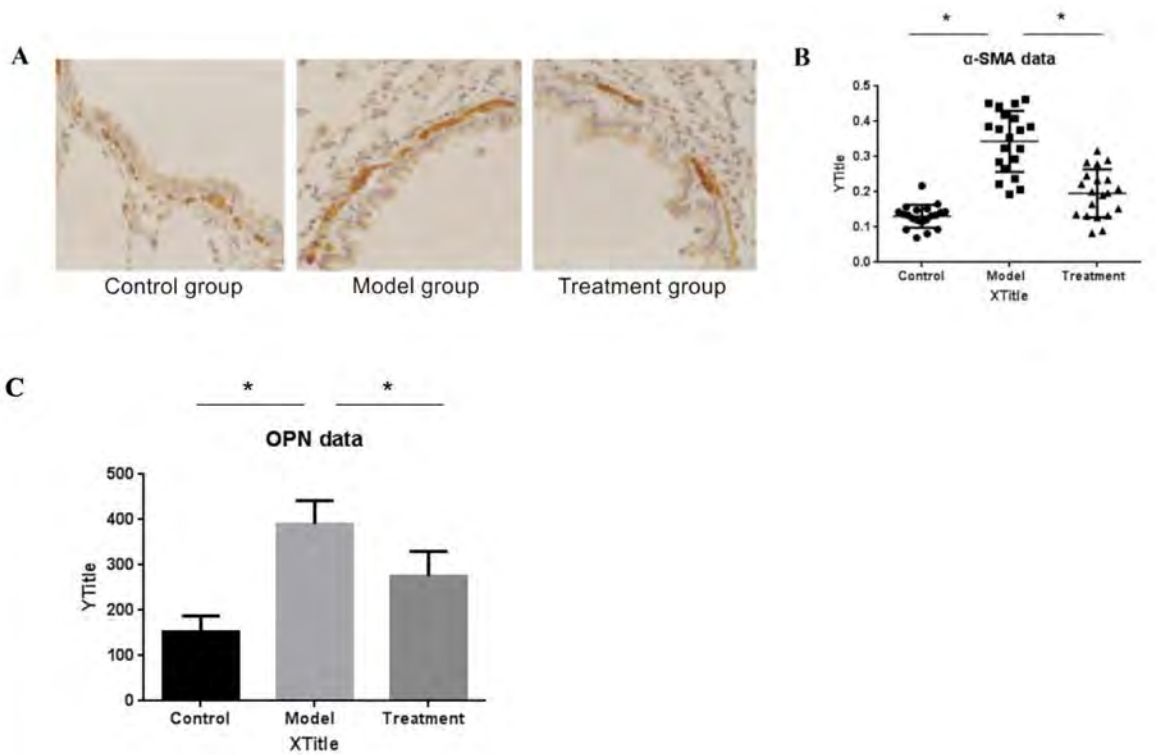


Fig. 2. ***A)*** *The expression of α-SMA in the airway of animals in the three groups. A: α-SMA immunohistochemistry;* ***B)*** *Quantitative results of A;* $^{*}P<0.05$. ***C)*** *OPN expression;* $^{*}P<0.05$.

The α-SMA was significantly brighter in the model group (0.38±0.11) and treatment group (0.21±0.08), when compared to the control group (0.14±0.04) (P<0.05), but this was darker in the treatment group than in the model group (P<0.05) (Fig. 2 A, B).

The expression of OPN in BALF was higher in the model group and treatment group than in the control group (P<0.05), but lower in the treatment group than in the model group (P<0.05; Fig. 2C).

The correlation analysis for OPN and airway α-SMA was carried out (Fig. 3A). The results revealed that OPN is positively correlated with α-SMA (P<0.01, R=0.71).

A correlation analysis for OPN and basic airway resistance was carried out. The results revealed that OPN is positively correlated with airway basic resistance (P<0.01, R=0.90; Fig. 3B).

DISCUSSION

The present study revealed that the degree of increase in OPN was positively correlated with airway responsiveness. This result suggests that OPN is closely correlated to the results of the pulmonary function in asthma, and that OPN may be involved in the regulation of lung function.

Table I. *Test results of rat lung function*

Groups(n)	Basic resistance(cm H_2Os/ml)	Area under curve				
		0.9%NaCl	6.25(Ach,ug/kg)	12.50(Ach,ug/kg)	25(Ach,ug/kg)	50(Ach,ug/kg)
Control group(20)	1.08±0.21	9.62±2.33	14.25±3.26	26.38±5.29	46.21±12.30	94.28±21.26
Model group(20)	1.82±0.45	10.12±2.55	18.88±4.12	45.77±10.28	98.22±21.52	156.32±32.55
Treatment group(20)	1.43±0.31	9.81±3.12	16.22±3.07	36.89±11.24	66.57±14.57	123.56±27.85
F	7.20	2.89	4.77	14.69	23.11	32.43
P	>0.05	>0.05	>0.05	<0.05	<0.05	<0.05

The area under the airway is the ratio, without measurement unit.

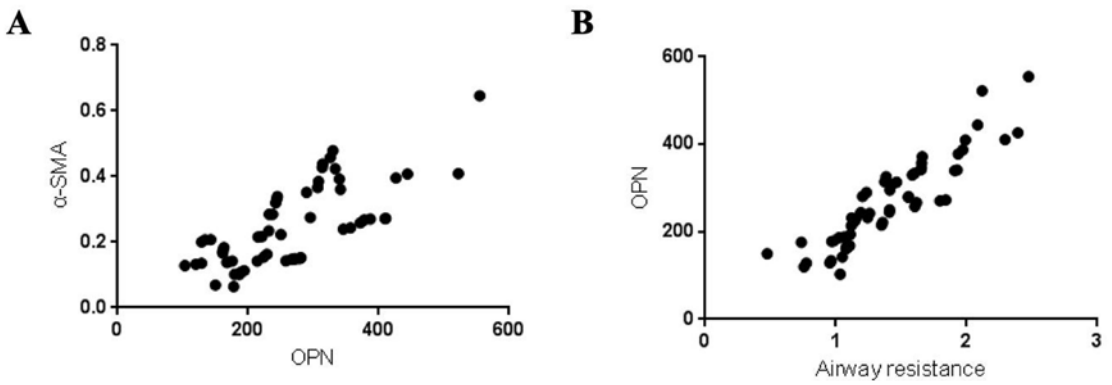


Fig. 3. ***A)*** *The correlation analysis of OPN and airway α-SMA (P<0.01, r=0.90); OPN is positively correlated with airway α-SMA (P<0.01, R=0.90).* ***B)*** *The correlation analysis of OPN and basic airway resistance. OPN is positively correlated with basic airway resistance (P<0.01, R=0.90).*

Furthermore, one study revealed that OPN can stimulate the activation of fibroblasts and the hyperplasia of airway smooth muscles, and that its expression is significantly correlated to the area of airway smooth muscles and collagen deposition (6).

The results of the present study reveal that there is a low α-SMA expression around the airway in normal rats, and in the process of the establishment of the asthma rat model, the mRNA expression of α-SMA in pulmonary tissues increased at one week after animal modeling. The increase in α-SMA mRNA was more significant at two weeks after animal modeling. Furthermore, the present study revealed that the expression of α-SMA around the airway of asthmatic rats significantly increased, and was positively correlated with the OPN expression. This result suggests that OPN is closely correlated to the proliferation of α-SMA, and after the inhalation of budesonide, the expression of OPN and α-SMA decreased in different degrees.

Another study concluded that glucocorticoids can reduce the expression level of OPN mRNA (7). This is consistent with the results of the present study. The investigators consider that glucocorticoids can regulate the expression of many genes (8). Therefore, the inhalation of budesonide can inhibit the expression of OPN and α-SMA, and this mechanism may be correlated to the reduction in airway inflammation, and OPN and α-SMA production after the inhalation of budesonide. A number of these signaling pathways are involved in this process. For example, multiple inflammatory pathways can increase the expression of OPN and α-SMA (9), and glucocorticoids can effectively inhibit inflammation to reduce the expression of OPN and α-SMA. In addition, glucocorticoids can also directly inhibit the synthesis and release of the bronchoconstrictor (10), which accordingly reduces the contraction of smooth muscles.

ACKNOWLEDGEMENTS

This work was funded by the Scientific research project of Baoding Science and Technology Bureau(No.18ZF193).

REFERENCES

1. Chen Y, Wong GW, Li J. Environmental exposure and genetic predisposition as risk factors for asthma in China. Allergy Asthma Immunol Res 2016; 8:92-100.
2. Al-Muhsen S, Johnson JR, Hamid Q. Remodeling in asthma. J Allergy Clin Immunol 2011; 128:451-62.
3. Matsumoto H. Roles of Periostin in Asthma. Adv Exp Med Biol 2019; 1132:145-59.
4. Shinde AV, Humeres C, Frangogiannis NG. The role of α-smooth muscle actin in fibroblast-mediated matrix contraction and remodeling. Biochim Biophys Acta Mol Basis Dis 2017; 1863:298-309.
5. Furuhashi K, Fujisawa T, Hashimoto D, et al. Once-daily fluticasone furoate/vilanterol combination versus twice-daily budesonide/formoterol combination in the treatment of controlled stable asthma: a randomized crossover trial. J Asthma Allergy 2019; 12:253-61.
6. Yuksel H, Yilmaz O, Karaman M, et al. Role of vascular endothelial growth factor antagonism on airway remodeling in asthma. Ann Allergy Asthma Immunol 2013; 110:150-5.
7. Pelaia G, Vatrella A, Busceti MT, et al. Molecular and cellular mechanisms underlying the therapeutic effects of budesonide in asthma. Pulm Pharmacol Ther 2016; 40:15-21.
8. Buhl R, Kuna P, Peters MJ, et al. The effect of budesonide/formoterol maintenance and reliever therapy on the risk of severe asthma exacerbations following episodes of high reliever use: an exploratory analysis of two randomised, controlled studies with comparisons to standard therapy. Respir Res 2012; 13:59.
9. Goldsmith DR, Keating GM. Budesonide/formoterol: a review of its use in asthma. Drugs 2004; 64:1597-618.
10. West KM, Culhane NS. Role of budesonide inhalation suspension in children with asthma. Ann Pharmacother 2002; 36:322-25.
11. Brown RW, O'Brien CD, Martin UJ, Uryniak T, Lampl KL. Long-term safety and asthma control measures with a budesonide/formoterol pressurized metered-dose inhaler in African American asthmatic patients: a randomized controlled trial. J Allergy Clin Immunol 2012; 130:362.

LETTER TO THE EDITOR

PREOPERATIVE NEUTROPHIL-TO-LYMPHOCYTE RATIO COMBINED WITH SERUM CEA, CA19-9, CA125 AND CA72-4 LEVELS IN THE CLINICAL PATHOLOGICAL STAGING OF GASTRIC CANCER-BASED ON PROPENSITY SCORE MATCHING

C. HUANG, L. XIAO, HL. LUO and ZM. ZHU

Department of Gastrointestinal Surgery, The Second Affiliated Hospital of Nanchang University, Nanchang, Jiangxi, China

Received October 31, 2019 – Accepted May 11, 2020

To the Editor,

Gastric cancer is a common malignancy of the digestive system, and its incidence ranks fifth among all cancers, but its mortality rate ranks third (1). The stage of GC determines its prognosis. After radical gastrectomy, the 5-year survival rate of early gastric cancer (EGC) can reach more than 90%, but that of advanced gastric cancer (AGC) is less than 10% (2). Recently, relevant studies (3) have shown that the occurrence and development of tumors are closely related to inflammatory reactions. The neutrophil-to-lymphocyte ratio (NLR) can reflect the inflammatory and immune status of tumor patients and has been proven to be a prognostic indicator for epithelial ovarian cancer, esophageal squamous cell carcinoma and colorectal cancer (4). In addition, NLR has been found to be correlated with invasion depth and tumor stage. Moreover, relevant studies have also shown that tumor markers are associated with lymph node metastasis (LNM) in GC, and the positive rate increases with an increase in the pTNM stage of GC (5).

Based on the above data, the present study aims to explore the application value of the preoperative NLR combined with serum carcinoembryonic antigen (CEA), carbohydrate antigen (CA) 19-9, CA125, and CA72-4 levels the in clinical pathological tumor-node-metastasis (pTNM) staging of GC.

MATERIALS AND METHODS

This was a retrospective study and was performed according to the guidelines of the Helsinki Declaration. The study was approved by the Ethics Committee of the Second Affiliated Hospital of Nanchang University and written informed consent was obtained from all patients.

The clinical data of 253 patients with GC diagnosed by postoperative pathology were collected. The inclusion criteria of this study were as follows: patients were treated with surgery and did not undergo neoadjuvant radiotherapy chemotherapy or blood transfusion before surgery; there was a complete pathological report after surgery; and approval from the ethics committee of our hospital. We excluded patients with bleeding, hyperthyroidism or hypothyroidism, acute infections, connective tissue disease, and incomplete data. There were 58 cases of EGC, including 39 males and 19 females (mean age: 59±12 years). The body mass index (BMI) was 22.59±3.36. There were 195 cases of AGC, including 144 males and 51 females (mean age: 61±10 years). The BMI was 21.47±3.75. There were no statistically significant differences in age ($P = 0.273$), sex ($P = 0.325$), location ($P = 0.109$) or pathological type ($P = 0.195$) between the two groups, and there were statistically significant differences in BMI ($P=0.041$) and pTNM ($P < 0.001$) (Table I).

Fasting venous blood was extracted from all selected

Key words: preoperative neutrophil-to-lymphocyte ratio; tumor markers; gastric cancer; individual detection

Corresponding Author:
Dr Zhengming Zhu,
Department of Gastrointestinal Surgery,
The Second Affiliated Hospital of Nanchang University,
No. 1 Minde Road, Nanchang, Jiangxi Province, China
Tel.: +86 0791 86312170
e-mail: zzm8654@163.com

0393-974X (2020)
Copyright © by BIOLIFE, s.a.s.
This publication and/or article is for individual use only and may not be further reproduced without written permission from the copyright holder.
Unauthorized reproduction may result in financial and other penalties
DISCLOSURE: ALL AUTHORS REPORT NO CONFLICTS OF INTEREST RELEVANT TO THIS ARTICLE.

patients. After centrifugation, routine blood counts and serum CEA, CA19-9, CA125, and CA72-4 levels were determined by an automatic electrochemical luminescence immunoanalyzer (model ADVIA Centaur, Siemens, Germany). The kit was provided by Siemens Medical Diagnostics Products of the United States.

Observation indicators

The NLR and serum CEA, CA19-9, CA125 and CA72-4 levels were compared between the two groups before and after matching, and the NLR and serum CEA, CA19-9, CA125 and CA72-4 levels were compared also across different pTNM stages. The accuracy, sensitivity and specificity of individual and combined detection of various indicators were also compared. We plotted a nomogram based on the logistic regression model for the combined detection.

Statistical analysis

The single sample k-s test was used to test the normality of the data. If the quantitative data obeyed a normal distribution, it was described as the mean±standard deviation; otherwise, it was described as the median and interquartile range. Categorical variables were expressed

Table I. *General characteristics of patients with GC and comparison of related factors between early and advanced gastric cancer before matching and after matching*

	Before matching			After matching		
Factor	EGC (n=58)	AGC (n=195)	*P* value	EGC (n=57)	AGC (n=114)	*P* value
Age (years)	59±12	61±10	0.273	59±12	59±10	0.943
Sex (n)			0.325			1
Male	39	144		38	76	
Female	19	51		19	38	
BMI (kg/m^2)	22.59±3.36	21.47±3.75	0.041	22.38±2.99	21.74±3.17	0.204
Location (n)			0.109			0.496
Fundus of stomach	8	43		8	23	
Body of stomach	9	39		9	13	
Antrum of stomach	41	113		40	78	
Pathological type (n)			0.195			0.11
Ulcerative type	48	149		47	99	
Nodular bulge type	10	26		10	10	
Diffuse infiltration type	0	20		0	5	
pTNM (n)			< 0.001			< 0.001
I	58	16		57	10	
II	0	62		0	42	
III	0	117		0	62	
Detection indicators						
NLR	2.19(1.69,3.13)	2.60(1.94,3.64)	0.02	2.23(1.69,3.16)	2.48(1.92,3.65)	0.028
CEA (ng/ml)	2.33(1.73,4.28)	3.09(1.95,6.13)	0.005	2.32(1.73,4.29)	3.16(1.83,6.16)	0.008
CA19-9 (U/ml)	11.59(7.17,15.71)	14.27(7.93,25.68)	0.022	11.64(7.28,15.99)	13.80(8.45,23.09)	0.003
CA125 (U/ml)	7.30(4.68,11.18)	9.30(6.40,15.10)	0.004	7.70(4.85,11.25)	9.25(6.50,13.28)	0.016
CA72-4 (IU/ml)	1.24(0.70,2.08)	1.72(1.13,4.69)	0.001	1.21(0.70,1.97)	1.72(1.15,4.95)	0.001

Table II. *Comparison of detection indicators across different pTNM stages (n=253)*

Detection indicator	stage I (n=74)	stage II (n=62)	stage III (n=117)	$\chi 2$	*P* value
NLR	2.28(1.72,3.12)	2.82(1.87,3.89)	2.60(2.06,3.67)	6.504	0.039
CEA (ng/ml)	2.33(1.73,4.10)	3.09(2.07,6.13)	3.41(1.98,7.01)	12.916	0.002
CA19-9 (U/ml)	11.34(6.93,15.71)	13.10(8.45,24.16)	16.84(8.35,31.911)	9.940	0.007
CA125 (U/ml)	7.70(4.70,11.32)	7.35(5.77,11.65)	10.60(7.30,16.55)	16.701	< 0.001
CA72-4 (IU/ml)	1.28(0.71,1.93)	1.72(1.17,4.69)	1.82(1.15,5.95)	13.868	0.001

as rate with 95% confidence intervals (CI). Quantitative data comparisons between the two groups were performed using normal sample *t*-tests; otherwise, the Mann-Whitney U test was used; comparisons between three groups were performed using the Kruskal-Wallis H test. Propensity score matching (PSM) was used to balance the covariates between the groups. After matching patients, conditional logistic regression was used for comparative analysis. The accuracy, sensitivity and specificity of individual and combined indicators for staging were calculated by plotting receiver operating characteristic (ROC) curves. A nomogram based on the logistic regression model was plotted using the "rms" package of R software. A *P* value less than 0.05 was considered statistically significant. Data were analyzed using SPSS 22.0 for Windows (SPSS Inc., Chicago, IL, USA) and R (version x64 3.5.1).

RESULTS

Comparison of the NLR and serum CEA, CA19-9, CA125 and CA72-4 levels between the two groups before matching

Differences in the NLR and serum CEA, CA19-9, CA125 and CA72-4 levels between the early and advanced gastric cancer groups were statistically significant (all $P < 0.05$), indicating that the NLR and serum CEA, CA19-9, CA125 and CA72-4 levels in the AGC group were higher than those in the EGC group (Table I).

Comparison of the NLR and serum CEA, CA19-9, CA125 and CA72-4 levels between the two groups after matching

A total of 253 patients with GC were matched 1:2 according to age, sex, BMI, location, and pathological type. A total of 57 pairs were successfully matched. There were no statistically significant differences in age ($P = 0.943$), sex ($P = 1.000$), BMI ($P = 0.204$), location ($P = 0.496$) or pathological type ($P = 0.110$) after matching. The difference in pTNM ($P < 0.001$) was statistically significant. Differences in the NLR and serum CEA, CA19-9, CA125 and CA72-4 levels between the early and advanced gastric cancer groups were statistically significant (all $P < 0.05$), indicating that NLR and serum CEA, CA19-9, CA125 and CA72-4 levels in the AGC group were higher than those in the EGC group (Table I).

Comparison of the NLR and serum CEA, CA19-9, CA125 and CA72-4 levels across different pTNM stages

Differences in the NLR and serum CEA, CA19-9, CA125 and CA72-4 levels among stage I, II and III GC were statistically significant (all $P < 0.05$), indicating that the higher the pTNM stage, the higher were the serum CEA, CA19-9, CA125 and CA72-4 levels (Table II).

ROC curves for individual and combined indicators

The ROC curves in Figs. 1 and 2 show the accuracy, sensitivity, and specificity of individual and combined detection in the early and advanced gastric cancer groups, respectively. The area under the curve indicates that the indicator is suitable for distinguishing early and advanced gastric cancer. According to the ROC curve evaluation, the optimal cut-off values for the NLR and serum CEA, CA19-9, CA125 and CA72-4 levels were 2.255, 2.645 ng/ml, 16.665 U/ml, 6.95 U/ml and 1.36 IU/ml, respectively. The area under the curve (AUC) for the NLR was 0.60, the 95% confidence interval (CI) was 0.591 to

0.681, the sensitivity was 64.6%, and the specificity was 53.4%. The AUC for CEA was 0.62, the 95% CI was 0.543 to 0.697, the sensitivity was 62.1%, and the specificity was 60.3%. The AUC for the CA19-9 was 0.59, the 95% CI was 0.524 to 0.674, the sensitivity was 46.7%, and the specificity was 77.6%. The AUC for CA125 was 0.63, the 95% CI was 0.545 to 0.707, the sensitivity was 70.3%, and the specificity was 50.0%. The AUC for CA72-4 was 0.64, the 95% CI was 0.560 to 0.720, the sensitivity was 67.7%, and the specificity was 56.9%. The AUC for the combined detection was 0.73, the 95% CI was 0.662 to 0.793, the sensitivity was 86.2%, and the specificity was 75.9%. This indicates that

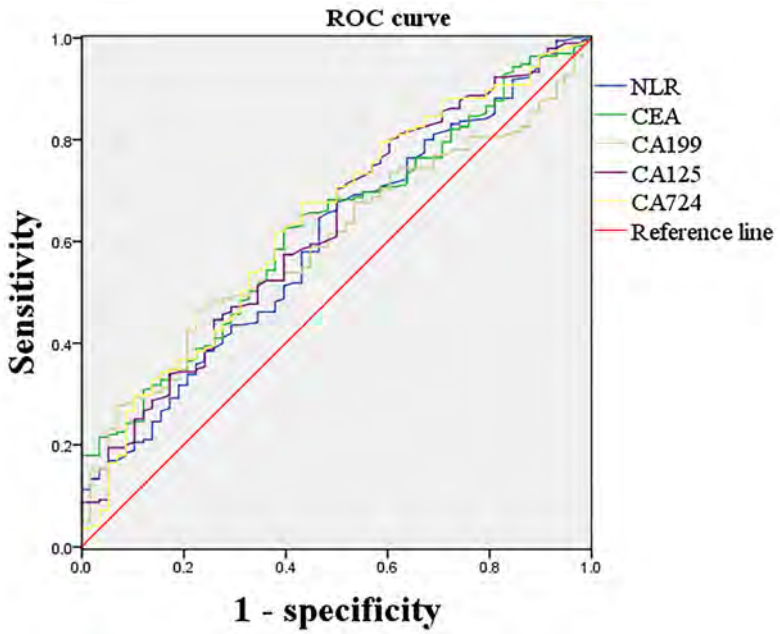


Fig. 1. *ROC curves for individual detection*

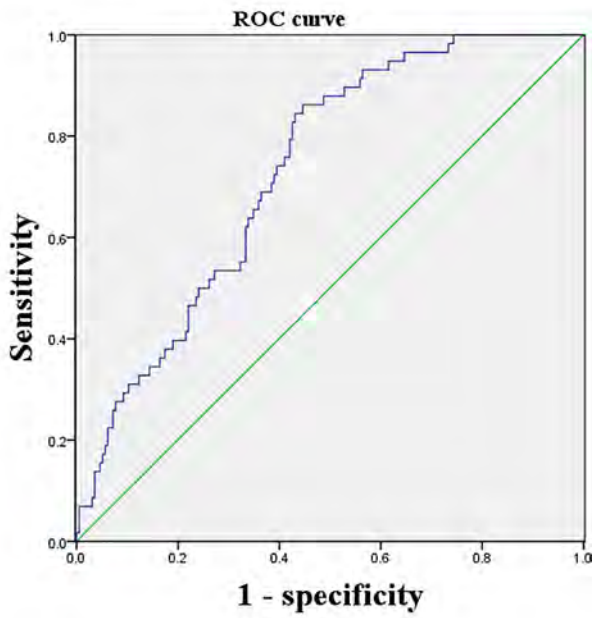


Fig. 2. *ROC curves for the combined detection*

the combined detection has higher accuracy and sensitivity than individual detection.

Plotting a nomogram based on the logistic regression model for the combined detection

The logistic regression model of NLR, CEA, CA19-9, CA125 and CA72-4 was constructed by the R language rms package, and the C statistic of its evaluation was 0.785, which indicated that the prediction model had certain accuracy. Then, the plotting function was constructed, and the nomogram was plotted (Fig. 3). A score of NLR greater than or equal to 2.255 was 90 points, while a score of NLR less than 2.255 U/ml was 0 points; a score of CEA greater than or equal to 2.645 was 74 points, while a score of CEA less than 2.645 was 0 points; a score of CA19-9 greater than or equal to 16.665 U/ml was 92 points, while a score of CA19-9 less than 16.665 U/ml was 0 points; a score of CA125 greater than or equal to 6.95 U/ml was 87 points, while a score of CA125 less than 6.95 U/ml was 0 points; a score of CA72-4 greater than or equal to 1.36 IU/ml was 100 points, while a score of CA72-4 less than 1.36 IU/ml was 0 points. The total score was 443 points, suggesting that the probability of risk of AGC was 95% to 100%. The risk of AGC can be predicted based on the total points (Fig. 3). The area under the ROC curve for the combined detection was 0.73, the 95% CI was 0.662 to 0.793, the sensitivity was 86.2%, and the specificity was 75.9%, indicating that the combined detection has certain accuracy, sensitivity and specificity.

DISCUSSION

Systemic inflammatory responses play an important role in the occurrence, progression and metastasis of tumors (3). The key role of the inflammatory response is to repair tissue damage caused by the tumor, which is a key factor in the formation of the tumor microenvironment (6). Cancer cells can produce cancer-associated inflammatory factors such as interleukin-1, -3 and -6, bone marrow growth factor, granulocyte colony-stimulating factor and tumor necrosis factor-alpha, leading to an increase in neutrophil counts (7). Lymphocytes are immune response cells of the body that perform immune surveillance and inhibit cancer progression. The degree of lymphocytic infiltration of tumors is related to the survival rate in various cancers, and the decrease in peripheral blood lymphocyte count may result in an insufficient immune response to

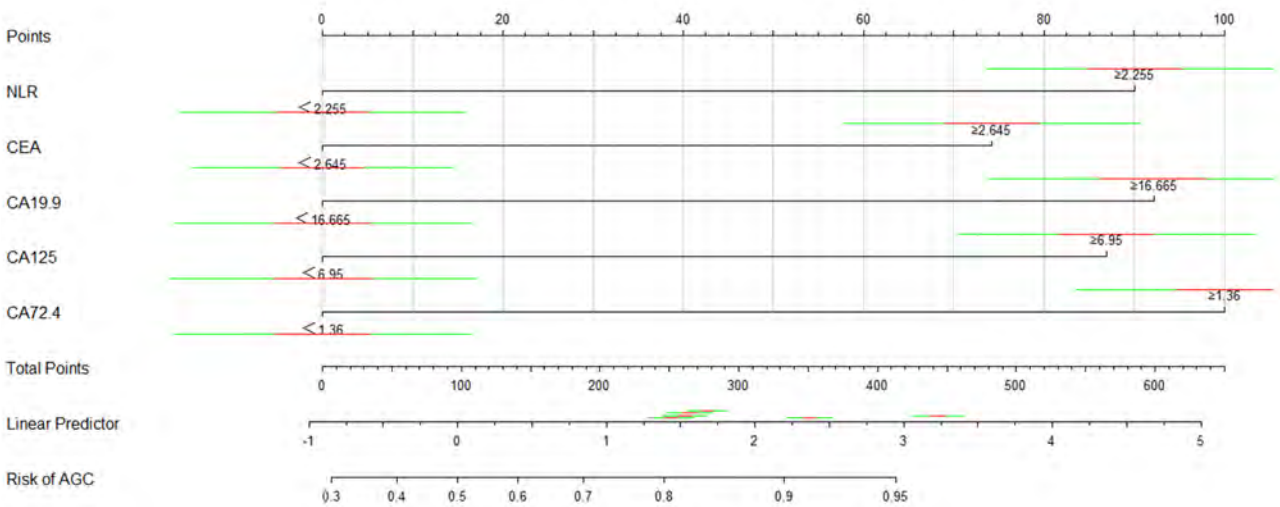


Fig. 3. *The nomogram based on the logistic regression model for the combined detection*

tumor cells (8). CEA is widely used in the diagnosis, screening and monitoring of GC, but its sensitivity and specificity are low (9). CA19-9 is mainly used for the diagnosis of pancreatic cancer, GC and colon cancer (10). CA72-4 is a tumor-associated glycoprotein that can be found in GC, and has a high specificity for the diagnosis of GC (11). The increased level of CA125 in peritoneal lavage is associated with the peritoneal dissemination and poor prognosis of GC (12). In conclusions, the preoperative NLR and serum CEA, CA19-9, CA125 and CA72-4 levels were closely related to clinical pTNM stage in GC and can be used as effective preliminary indicators for distinguishing early and advanced gastric cancer. Combined detection can improve the accuracy and sensitivity of identification and has a certain predictive ability for AGC.

ACKNOWLEDGEMENT

This present study was supported by the Program of National Natural Science Foundation of China (Grant NO.81560389).

REFERENCES

1. Bray F, Ferlay J, Soerjomataram I, Siegel RL, Torre LA, Jemal A. Global cancer statistics 2018: GLOBOCAN estimates of incidence and mortality worldwide for 36 cancers in 185 countries. CA Cancer J Clin 2018; 68:394-424.
2. Orditura M, Galizia G, Sforza V, et al. Treatment of gastric cancer. World J Gastroenterol 2014; 20:1635.
3. Balkwill F, Mantovani A. Inflammation and cancer: back to Virchow? Lancet 2001; 357:539-545.
4. Ishizuka M, Nagata H, Takagi K, Iwasaki Y, Kubota K. Combination of platelet count and neutrophil to lymphocyte ratio is a useful predictor of postoperative survival in patients with colorectal cancer. Br J Cancer 2013; 109:401.
5. Wang J, Yu J-C, Kang W-M, Wang W-Z, Liu Y-Q, Gu P. The predictive effect of cadherin-17 on lymph node micrometastasis in pN0 gastric cancer. Ann Surg Oncol 2012; 19:1529-34.
6. Coussens LM, Werb Z. Inflammation and cancer. Nature 2002; 420:860.
7. Alexandrakis MG, Passam FH, Moschandrea IA, et al. Levels of serum cytokines and acute phase proteins in patients with essential and cancer-related thrombocytosis. Am J Clin Oncol 2003; 26:135-40.
8. Corthay A. Does the immune system naturally protect against cancer? Front in Immunol 2014; 5:197.
9. Chen S, Chen Y-B, Li Y-F, et al. Normal carcinoembryonic antigen indicates benefit from perioperative chemotherapy to gastric carcinoma patients. World J Gastroenterol 2012; 18:3910.
10. Kim J-H, Jun K-H, Jung H, Park I-S, Chin H-M. Prognostic value of preoperative serum levels of five tumor markers (carcinoembryonic antigen, CA19-9, alpha-fetoprotein, CA72-4, and CA125) in gastric cancer. Hepatogastroenterology 2014; 61:863-69.
11. Kim DH, Oh SJ, Oh CA, et al. The relationships between perioperative CEA, CA 19-9, and CA 72-4 and recurrence in gastric cancer patients after curative radical gastrectomy. J Surg Oncol 2011; 104:585-91.
12. Yamamoto M, Baba H, Toh Y, Okamura T, Maehara Y. Peritoneal lavage CEA/CA125 is a prognostic factor for gastric cancer patients. J Cancer Res Clin Oncol 2007; 133:471-76.

JOURNAL OF BIOLOGICAL REGULATORS & HOMEOSTATIC AGENTS Vol. 34, no. 3, 1117-1124 (2020)

LETTER TO THE EDITOR

OXYTOCIN MODULATES IMMUNOSTATUS, METABOLIC STATE AND GUT MICROBIOME

J.H. PARK[1*], D.Y. CHOI[1*], H. PARK[2,3], K.W. LEE[2] and J.A. CHO[1,4]

[1]Wide River Institute of Immunology, Seoul National University College of Medicine, Hongcheon, Gangwon-do, Republic of Korea; [2]Medical Research Institute & Adult Stem Cell Research Institute, Department of Obstetrics and Gynecology, Kangbuk Samsung Hospital, Sungkyunkwan University School of Medicine, Seoul, Republic of Korea; [3]Department of Clinical Laboratory Science, Wonkwang Health Science University, Iksan, Jeollabuk-do, Republic of Korea; [4]College of transdisciplinary studies, School of Undergraduate Studies, DGIST, Daegu, Republic of Korea

Received November 18, 2019 – Accepted May 12, 2020

[*]These Authors contributed equally to this work

To the Editor,

Oxytocin (OXT) is a cyclic nonapeptide neurotransmitter that is synthesized and secreted by the central nervous system as well as reproductive organs, thymus and adrenal glands (1). OXT exerts a wide range of physiological roles via oxytocin receptor, not only in the regulation of parturition and lactation, but also in various behavioral patterns and neurological aspects (1). As evidence has been emerging that hormonal neurotransmitter influences the immune system, OXT was also shown to have immunological effects such as reducing systemic inflammation (2), increasing the proliferation of peripheral lymphocytes, or changing the activity of immunosuppressive estrogen (3). In addition, as it was reported that OXT and its receptor are also expressed in heart and blood vessels, and exerted anti-atherogenic properties (4), it can be assumed that OXT might play a role in maintaining the homeostatic function of the body.

Currently, normal microflora is attracting much attention because it is increasingly known that its homeostasis is important in the immunological aspects (5). Especially, gut microbiome is considered as the indicator of an individual's health status, and "a good microbiome" is used by fecal transplantation for treatment of certain diseases (6). Accumulated findings present that neuropeptide hormones are critical in maintaining the balance of gut microbiome (7, 8), reflecting their importance in the gut-brain axis. Interestingly, OXT receptor is known to be expressed in the intestinal cells (9).

In this study, it was examined whether OXT may influence the immune and/or endocrine system, and if so, how the effect can be different according to genetic background or gender by using 3 different mouse models. Using a Sprague Dawley (SD) rat model, the potential effect of OXT was also investigated on the composition of gut microbiome in comparison with two other neuropeptides Neuropeptide Y and neuromedin, which were previously proven for their relationship with gut microbiome (7, 8).

Key words: oxytocin; neuropeptide; immunostatus; metabolic state; homeostasis; gut microbiome

Corresponding Author:
Dr Jung Ah Cho,
College of Transdisciplinary Studies,
School of Basic Science, DGIST, 333 Technojungang-daero,
Hyeonpung-eup, Dalseong-gun, Daegu, Republic of Korea
Tel.: +82 53 785 6644 - Fax: +82 53 785 0114
e-mail: jungahcho@dgist.ac.kr

0393-974X (2020)
Copyright © by BIOLIFE, s.a.s.
This publication and/or article is for individual use only and may not be further reproduced without written permission from the copyright holder.
Unauthorized reproduction may result in financial and other penalties
DISCLOSURE: ALL AUTHORS REPORT NO CONFLICTS OF INTEREST RELEVANT TO THIS ARTICLE.

MATERIALS AND METHODS

Animals

All the experimental animal models (ICR, C57Bl/6, Balb/c mice, SD rats) were purchased from Central Lab Animal Inc., and maintained in specific pathogen-free conditions at an animal facility. The number of mice used per group was as follows; 10 females and 9 males for ICR, 4 females and 4 males for C57bl/6, 7 females and 3 males for Balb/c, respectively. All animal experiments were approved by the institutional animal care and use committees (IACUC) of Seoul National University, and performed in accordance with animal ethics regulations.

Administration of oxytocin

Oxytocin (OXT) was purchased from Sigma-Aldrich and dissolved in normal saline when used. OXT was intraperitoneally injected with 100 ul/mouse at the dose of 1 mg/kg daily for 7 days. The mice were age-matched (30 or 34 weeks old) for grouping prior to the study. For rat experiments, OXT, Neuromedin B (NMB), and Neutopeptide Y (NPY) were purchased from Bachem and dissolved in normal saline at the dose of 20 ug/ml when used. SD rats (6 months old) were divided into 4 groups (n=3) and intraperitoneally injected with 1 ml per each at a dose of 50 ug/kg every other day for 2 weeks. During the injection, the animals were carefully observed for any abnormality of behavior, and monitored for bodyweight over time.

Blood analysis

Peripheral blood was collected by eye bleeding under inhalation anesthesia one day before the 1st injection and one day after the last injection from each mouse. The amount of blood collected was 200~300 ul/mouse. On sampling, the whole blood was first applied to hematology analyzer (iDEXX Procyte Dx), and then diluted with normal saline at 1:1 ratio to apply to a chemistry analyzer (iDEXX Procyte Dx). For blood biochemistry, Chem 17 CLIP (iDEXX procyte Dx) was used. The output results were made into graphs using GraphPad prism 5.0 software.

Analysis of gut microbiome

The same amount (1 g) of feces from each rat was obtained and dissolved in distilled water. After vigorous vortexing and spin-down, the supernatant was collected and then subjected to serial dilution (1:10, 1:100, 1:1000 and 1:10000). The 1:1000 and 1:10000 diluents were spread on agar plates made of Nutrient broth (NB) media, MacConkey media and Lactobacilli MRS media, followed by cultivation in a 37°C incubator. After 24 h,

Table I. *Blast research result of gut microbes using 16s rRNA gene sequencing. The different species from control group are shaded in gray.*

		Control	NPY	NMB	OXT
Family/Genus/Species	Gram negative	*Morganella sp.*		*Morganella sp*	*Morganella sp.*
		Morganella morganii		*Morganella morganii*	*Morganella morganii*
		Escherichia sp	*Escherichia sp*	*Escherichia sp*	*Escherichia sp*
		Escherichia fergusonii	*Escherichia fergusonii*	*Escherichia fergusonii*	*Escherichia fergusonii*
		Escherichia coli	*Escherichia coil*	*Escherichia coli*	*Escherichia coli*
			Enterobacteriaceae bacterium	*Enterobacteriaceae bacterium*	*Enterobacteriaceae bacterium*
				Enterobacter sp	*Enterobacter sp*
			Photorhabdus luminescens	*Photorhabdus luminescens*	
			Cronobacter sp	*Cronobacter sp*	
				Citrobacter koseri	
	Gram positive		*Corynebacterium pseudotuberculosis*	*Corynebacterium pseudotuberculosis*	
			Streptomyces sp	*Streptomyces sp*	*Streptomyces sp.*
				Lactobacillus sp	*Lactobacillus sp.*
				Leuconostoc lactis	
					Staphylococcaceae bacterium
					Staphylococcus sp.
					Staphylococcus lentus
					Staphylococcus nepalensis
					Staphylococcus cohnii
					Staphylococcus sciuri
					Staphylococcus lugdunensis

the number of colonies formed on each plate was counted and then multiplied by the corresponding dilution factor. For microbial identification, representative colonies were subjected to colony PCR using the universal primers for 16s rRNA gene (27F, 1492R). The PCR products were used for nucleic acid sequencing after purification, and analyzed using the BLAST tool on NCBI website.

Statistical analysis

Statistical significance was analyzed by Student's *t*-test using GraphPad prism 5.0 software. P values under 0.05 were considered statistically significant.

RESULTS

Effects of oxytocin on female and male of ICR strain

Hematology and chemistry analysis were conducted of non- or OXT-treated ICR, Balb/c and C57Bl/6 for both genders (Fig. 1). First, the hematology results were analyzed of ICR (Fig. 1A a and b). The data in Fig. 1A a shows the effect of OXT on red blood cells (RBCs), platelets and white blood cells (WBCs), which are 3 major categories of peripheral blood immune cells. The results demonstrated that OXT greatly decreased the number of those cell types in both genders however with no significance for RBCs in males. We further analyzed the RBC-related indicators, which were reticulocytes and hemoglobin (Fig. 1A b). Consistent with the number of RBCs in Fig. 1A a, the reticulocyte number and hemoglobin level were significantly down-regulated for both genders of OXT-injected group except for reticulocytes in males. In the case of WBC type cells such as lymphocytes and neutrophils, the number of lymphocytes in both genders were greatly decreased by OXT, while the number of neutrophils in both genders were increased by OXT (Fig. 1A b). The data obtained from chemistry analysis of ICR showed the complexity and diversity according to each indicator or gender with no tendency (Fig. 1A c). The decrease in the blood level was observed in glucose in both genders, and lipase in females. Whereas, albumin was increased in males. The results of the blood level of Blood Urea Nitrogen (BUN) showed the difference by gender, which was decreased in females, or increased in males by OXT administration.

Effects of oxytocin on female and male of C57bl/6 strain

The results of hematology analysis obtained from C57bl/6 strain with OXT administration showed a similar pattern to ICR strain (1B a and b). First, the number of RBCs, platelets, and WBCs were all decreased by OXT except for platelets in females (Fig. 1B a). However, the number of reticulocytes showed the opposite pattern to the number of RBCs, which was significantly increased by OXT in both genders, whereas the result about hemoglobin was consistent with the result of RBCs in Fig. 1B b. For the WBC type cells, OXT induced the decrease of lymphocytes in both genders (Fig. 1B b). The chemistry analysis after OXT administration in C57bl/6 displayed a different pattern from ICR (Fig. 1B c). Firstly, OXT was shown to induce the decrease in the blood level of glucose in males, BUN and lipase in females. In contrast, a significant increase by OXT was observed in the blood level of albumin in males.

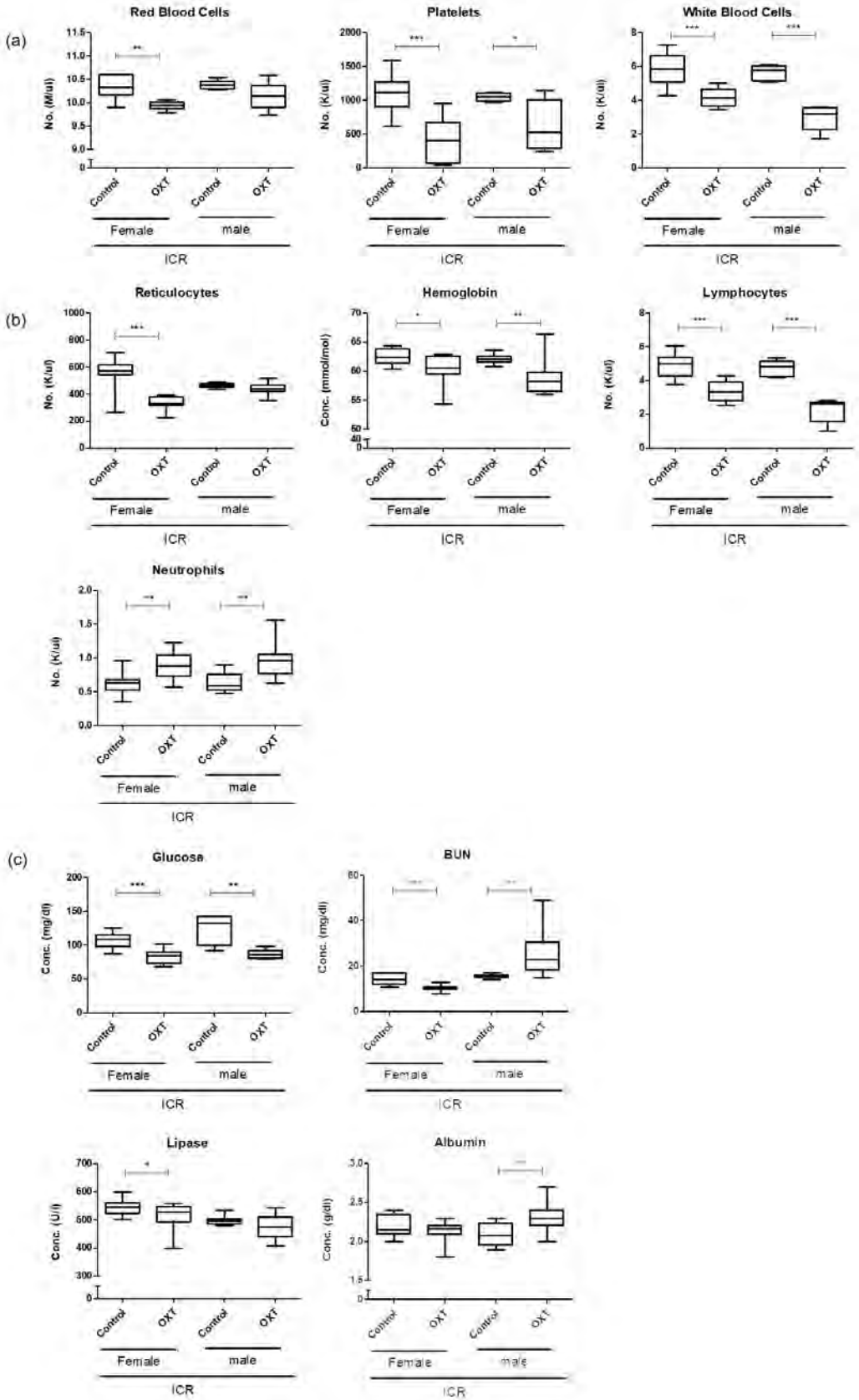
Effects of oxytocin on female and male of Balb/c strain

Next, the hematological and chemistry profiles were investigated in Balb/c strain (Fig. 1C). For the 3 major groups, the significant change by OXT was observed only in the RBC level, and the other 2 types of cells showed a decreased tendency with no significance (Fig. 1C a). In the RBC-related indicators, we observed the significant changes only in females, in which the reticulocyte or hemoglobin level was increased or decreased by OXT, respectively (Fig. 1C b). The level of WBC type cells including lymphocytes and neutrophils tended to be decreased by OXT in both genders (Fig. 1C b). In the chemistry analysis for Balb/c (Fig. 1C c), OXT induced an increase in the blood level of glucose in both genders, whereas the significant changes by OXT were observed only in females for BUN, lipase and albumin.

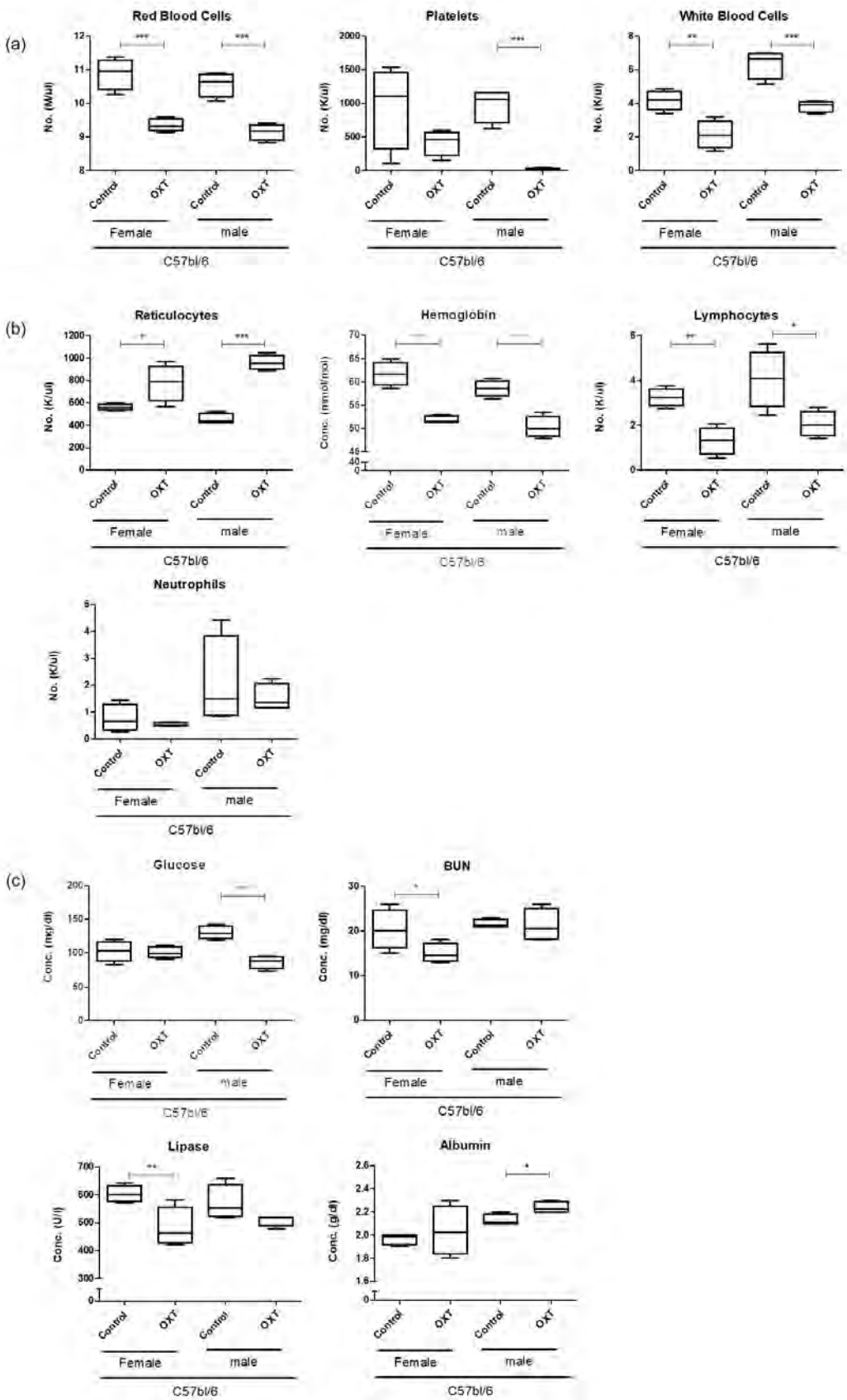
Effects of oxytocin on gut microbiome in SD rat

Then, we hypothesized that OXT may also influence the gut-brain axis, because OXT is a neuropeptide hormone, and OXT receptor is expressed in intestinal cells (9). Accordingly, we investigated the gut microbiome using feces obtained

A


(a)
Red Blood Cells
No. (M/ul)
Platelets
No. (K/ul)
White Blood Cells
No. (K/ul)
(b)
Reticulocytes
No. (K/ul)
Hemoglobin
Conc. (mmol/mol)
Lymphocytes
No. (K/ul)
Neutrophils
No. (K/ul)
(c)
Glucose
Conc. (mg/dl)
BUN
Conc. (mg/dl)
Lipase
Conc. (U/l)
Albumin
Conc. (g/dl)
Control
OXT
Female
male
ICR

B


(a)
Red Blood Cells
No. (M/ul)
Platelets
No. (K/ul)
White Blood Cells
No. (K/ul)
(b)
Reticulocytes
No. (K/ul)
Hemoglobin
Conc. (mmol/mol)
Lymphocytes
No. (K/ul)
Neutrophils
No. (K/ul)
(c)
Glucose
Conc. (mg/dl)
BUN
Conc. (mg/dl)
Lipase
Conc. (U/l)
Albumin
Conc. (g/dl)
Control
OXT
Female
male
C57bl/6

C

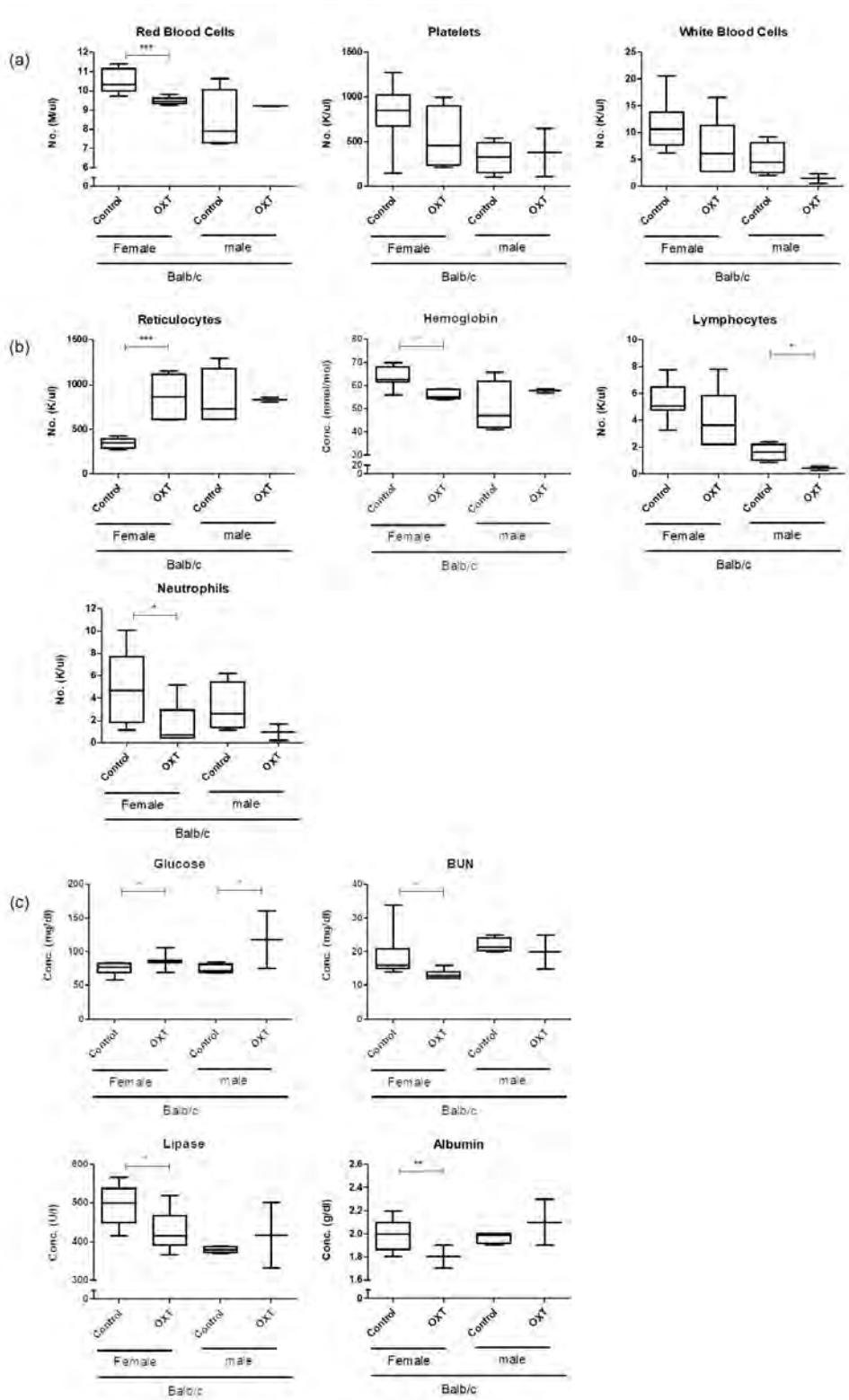


Fig. 1. *Blood hematology and chemistry analysis of ICR (**A**), C57bl/6 (**B**), Balb/c (**C**) mouse strain before and after oxytocin administration. a) Red blood cells, platelets and white blood cells, (b) Reticulocytes, hemoblobin, lymphocytes, and neutrophil, (c) glucose, BUN, lipase and albumin were analyzed in peripheral blood from both genders. Statistical significance; vs control group; *=p<0.05, **=p<0.01, ***=p<0.001.*

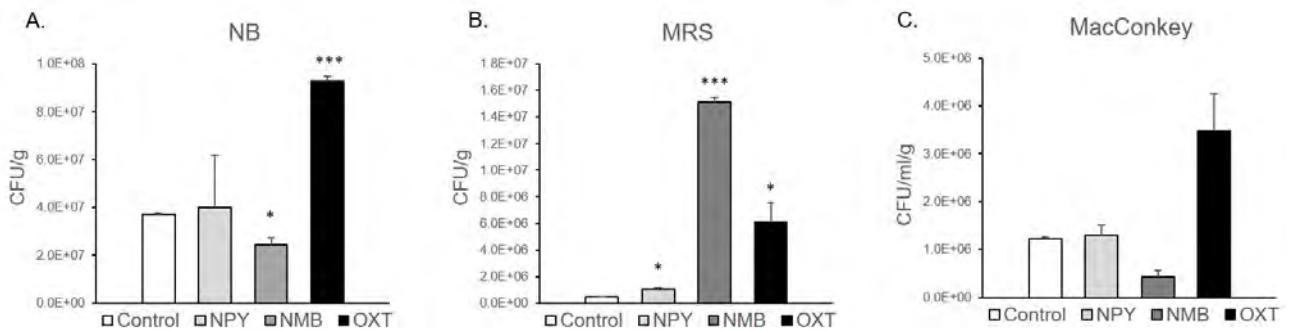


Fig. 2. *Measurement of colony forming units on (**A**) NB agar media, (**B**) MRS agar media and (**C**) MacConkey agar media. CFU were measured using fecal specimen obtained from SD rats injected with NPY, NMB or OXT. Statistical significance; vs control group; *=p<0.05, ***=p<0.001.*

from OXT-injected test animals, and compared them with those from the positive control groups injected with NPY or NMB (7, 8).

When the microorganisms was first cultured on NB agar plate, it was revealed that the colony-forming units (CFU) were markedly increased in the OXT group, whereas they were decreased or mildly changed in the NMB or NPY group, respectively (Fig. 2A). On MRS agar plate, the media specific for lactobacillus growth, the OXT group showed a significant increase in the CFU, along with the positive control groups of NMB and NPY (Fig. 2B). The measurement of CFU on MacConkey agar plate, the media for gram-negative bacteria, also showed an increased pattern in the OXT group, although statistically insignificant (Fig. 2C). Next, we determined what kind of microorganisms were included in the gut microbiome of each group. The sequence of 16s rRNA gene was analyzed and the blast searching was performed (Table I). The result revealed that each group contained different compositions of gut microbiome, notably lactobacillus in the OXT group as well as the NMB group, as indicated in the result of CFU measurement (Fig. 2B). These results demonstrated that OXT modulated the number and composition of gut microbiome, suggesting the potential effect of OXT in regulating gut-brain axis.

DISCUSSION

Oxytocin (OXT) is known to exert the different physiological roles based on the sites of production and action (1). The classically well-described role of OXT is the hormonal effects in females, such as the regulation of uterine contraction, lactation, etc. The additional role of OXT is the function as a neurotransmitter that modulates sociality, behaviors, etc. Recently, another role of OXT is emerging, which is the regulation of inflammation that has been demonstrated in the models including sepsis, and atherosclerosis (2, 4).

In previous studies on neuropeptides, such as neuropeptide Y and neuromedin B (bombesin in mammals) for immune function (7, 8), the fact that gut microbes are critical in immunity inspired us to hypothesize that OXT may exert the immune and endocrinal role through gut microflora. In this study, it was clearly demonstrated that OXT induced a change in the gut microbiome as well as hematological and metabolic changes. Especially, it was notable that OXT induced the increase in the number of lactobacillus, which are considered as "good" microbes (10). Although previous studies have reported lactobacillus upregulated OXT level (11), this study presents for the first time, that OXT could increase lactobacillus in the gut. This finding provides an important clue for the potential role of OXT in gut-brain axis.

Although this study certainly revealed that OXT itself had modulating effects on the immunostatus, metabolic state and gut microbiome, the underlined mechanism in these functions remains to be further studied. Especially, as OXT indispensably involves OXT receptor for its action (1), and OXT agonists

can produce the different reactions (12), the answer to how such results of each parameter tested here were obtained may reside in the signaling via OXT receptor by OXT. Therefore, we will focus on the molecular events between OXT and OXT receptor in our future study. Nevertheless, this study provides the direct clues regarding OXT as an important regulator in body homeostasis.

ACKNOWLEDGEMENTS

This study was supported by the Basic Science Research Program through the National Research Foundation of Korea (NRF) funded by the Ministry of Education, Science and Technology (NRF-2012R1A1A2006803), the grant from Samsung Biomedical Research Institute (GL1B32211). We thank Mr. Ohsung Choi for the careful correction on manuscript writing.

REFERENCES

1. Gimpl G, Fahrenholz F. The oxytocin receptor system: structure, function, and regulation. Physiol Rev 2001; 81:629-83.
2. Iseri SO, Sener G, Saglam B, Gedik N, Ercan F, Yegen BC. Oxytocin protects against sepsis-induced multiple organ damage: role of neutrophils. J Surg Res 2005; 126:73-81.
3. Maccio A, Madeddu C, Chessa P, Panzone F, Lissoni P, Mantovani G. Oxytocin both increases proliferative response of peripheral blood lymphomonocytes to phytohemagglutinin and reverses immunosuppressive estrogen activity. In Vivo 2010; 24:157-63.
4. Wang P, Wang SC, Yang H, et al. Therapeutic potential of oxytocin in atherosclerotic cardiovascular disease: mechanisms and signaling pathways. Front Neurosci 2019; 13:454 eCollection 2019.
5. Mishra PJ, Mishra SK. Role of microbial flora and probiotics in host immune homeostasis. J Appl Pharm Sci 2018; 8(10):136-49.
6. Sidhu M, van der Poorten D. The gut microbiome. Aust Fam Physician 2017; 46:206-11.
7. Farzi A, Reichmann F, Holzer P. The homeostatic role of neuropeptide Y in immune function and its impact on mood and behaviour. Acta Physiol (Oxf) 2015; 213:603-27.
8. Busch RA, Heneghan AF, Pierre JF, Wang X, Kudsk KA. The enteric nervous system (ENS) neuropeptide, bombesin (BBS), reverses innate immune impairments during Parenteral Nutrition (PN). Ann Surg 2014; 260(3):432-44.
9. Welch MG, Tamir H, Gross KJ, Chen J, Anwar M, Gershon MD. Expression and developmental regulation of oxytocin (OT) and oxytocin receptors (OTR) in the enteric nervous system (ENS) and intestinal epithelium. J Comp Neurol 2009; 512:256-70.
10. Walter J, Ecological role of lactobacilli in the gastrointestinal tract: implications for fundamental and biomedical research. Appl Environ Microbiol 2008; 74:4985-96.
11. MaCormack SE, Blevins J, Lawson EA. Metabolic effects of oxytocin. Endocrine Reviews 2020; 41:121-45.
12. Busnelli M, Sauliere A, Manning M, Bouvier M, Gales C, Chini B. Functional selective oxytocin-derived agonists discriminate between individual G protein family subtypes. J Biol Chem 2012; 287:3617-29.

JOURNAL OF BIOLOGICAL REGULATORS & HOMEOSTATIC AGENTS Vol. 34, no. 3, 1125-1129 (2020)

LETTER TO THE EDITOR

A THEORY ON SARS-COV-2 SUSCEPTIBILITY: REDUCED TLR7-ACTIVITY AS A MECHANISTIC LINK BETWEEN MEN, OBESE AND ELDERLY

L. ENGLMEIER

Received April 16, 2020 – Accepted May 14, 2020

To the Editor,

Conti and Younes have pointed to a connection between lower TLR7 expression in men and their increased vulnerability towards a severe form of COVID-19 infection (1). I had started to investigate the same idea and think that I have discovered a wealth of additional supporting information that renders the hypothesis plausible and, if correct, could establish lower TLR7 activity/sensitivity as a common molecular characteristic of several high-risk patient groups.

As Conti and Younes have already pointed out, in the current COVID-19 epidemic about twice as many men seem to die as women. This has been attributed to lifestyle by our mass media, but this would not explain a ratio that is quite uniform across societies. In addition, the same quantitative imbalance between male and female deaths was already observed for the 2003 SARS outbreak (2), which was caused by a closely related Coronavirus.

For SARS, the receptor ACE2, encoded on the X-chromosome, was investigated as a possible reason for the gender difference, but there is no established link between different ace2-alleles and disease outcome, making this explanation less likely. However, TLR7 (toll-like receptor 7) is also encoded on the X-chomosome, and it is a key regulator of pathogen detection and the resulting innate immune response. TLR7 detects viral RNA in the endosome and then stimulates the production of inflammatory cytokines and interferons. It is a key component of our immune response to infection by RNA-viruses. SARS-CoV-2 is such an RNA virus. Importantly, TLR7 is one of few genes that evade X-chromosome silencing in immune cells (3). It is known that this biallelic expression of TLR7 in immune cells of women can have physiological consequences, which can be positive, but also negative, as manifest in female predisposition to systemic lupus erythematosus (SLE). The higher gene dosage of TLR7 has been shown to be the reason for increased female susceptibility to this autoimmune disease. TLR7 has been described to bind and respond strongly to SARS-RNA (4). It is altogether plausible that higher TLR7 expression is the reason why women are better equipped to deal with SARS-CoV-2. If this is correct, a prediction is that patient groups with lower TLR7 expression or sensitivity should be more prone to develop a severe form of COVID-19.

There are patient groups who are emerging as carrying increased risk: obese patients and old people with a senescent immune system. One characteristic that obese and old people have in common is their physiological state of low-level, chronic inflammation. I speculated that this could lead to a common molecular characteristic with men, low TLR7 expression or sensitivity, and analyzed the literature for supporting or contradictory evidence. There is crosstalk between obesity and the innate immune system. Obesity is characterised by a chronic state of low inflammation (for a review see 5). A role of inflammation in the development of obesity-induced metabolic syndrome and insulin resistance via the pro-inflammatory

Key words: Covid-19; tlr-7; SARS-CoV-2; tlr tolerance; obesity; inflammaging; X-chromosome inactivation

Corresponding author:
Patent Attorney Dr. Ludwig Englmeier,
Erlenaustrasse 11,
83080 Oberaudorf, Germany
Tel.: +49 1590 6107541
e-mail: ludwig.englmeier@protonmail.com

0393-974X (2020)
Copyright © by BIOLIFE, s.a.s.
This publication and/or article is for individual use only and may not be further reproduced without written permission from the copyright holder.
Unauthorized reproduction may result in financial and other penalties
DISCLOSURE: ALL AUTHORS REPORT NO CONFLICTS OF INTEREST RELEVANT TO THIS ARTICLE.

cytokine TNF-a was already suggested in the 1990s and resident immune cells in the adipose tissue are responsible for that response.

While TLR4 has been particularly examined for its role in the development of obesity-induced insulin resistance, it is interesting to appreciate that there is a high prevalence of insulin resistance and metabolic syndrome in SLE patients (6), indicating that also chronic inflammation triggered by overactive TLR7 increases the risk to develop metabolic syndrome. The increased prevalence of insulin resistance and metabolic syndrome in SLE patients is not linked to obesity.

Revelo et al. (7) have shown that in high-fat-diet (HFD)-fed mice metabolic parameters worsen through mechanisms including activation of macrophages in visceral adipose tissue and expansion of plasmacytoid dendritic cells in the liver. HFD-fed mice lacking TLR7 and TLR9, however, showed reduced metabolic inflammation and improved glucose homeostasis. Treatment of HFD-fed mice with inhibitors against TLR7 and 9 improved metabolic disease. The authors conclude that obesity leads to metabolic inflammation via the activation of TLR7 and 9. Hanna Kazazian et al. (8) have come to a very similar conclusion. TLR8-deficient mice, which develop spontaneous lupus-like disease due to increased TLR7-signalling by dendritic cells, show an aggravated SLE pathogenesis when fed with a high-fat-diet. Taken together, these two studies show that obesity leads to a chronic, low-level activation of the TLR7 receptor.

There is also a link between immune senescence and TLR7. It is well established that there are age-related changes in the immune system function which shows a functional decline in its ability to respond to new pathogens during aging. This functional decline includes the innate immune system, and Metcalfe et al. (9) found that peripheral blood mononuclear cells isolated from old individuals showed a delayed response to stimulation with TLR4, TLR7/8 and RIG-1 agonists compared to corresponding cells from young adults. This alone might explain the lower initial response and thus the higher vulnerability of old people towards SARS-CoV-2 infection.

On the other hand, serum levels of inflammatory cytokines increase with age. This age-related, systemic, chronic inflammation is called inflammaging. Increased levels of circulating inflammatory mediators such as interleukin-6 (IL-6) and C-reactive protein (CRP), which increase in an age-dependent manner, are indicators of inflammaging. While diverse underlying reasons for inflammaging have been discussed, it is interesting that TLR7-activation has been implied in it. Levels of miR-146a are significantly increased in senescent cells that have a senescence associated secretory phenotype. miR-146a is a well-known negative regulator of tlr-signalling acting downstream of MyD88 by decreasing signalling through IRAK1 and TRAF-6. However, ectopic localization of miR-146a in the extracellular space triggers an innate immune response, via - interestingly! - TLR7 (10). It has been suggested that it is the chronic tlr-activation by endogenous tlr ligands in the absence of pathogen infection - such as miR-146a activation of TLR7? - which contributes to the phenotype of "inflammaging" in old people.

Thus, a chronic, low level activation of TLR7 could link obesity and "inflammaging", and thus SARS-CoV-2 sensitive groups. Over time, however, chronic low-level TLR7 activation should result in acquired tolerance to TLR7 signalling, similar to the homologous immune tolerance which Michaelis et al. (11) have observed upon repeated TLR7 stimulation with the TLR7 agonist R848 (resiquimod).

I therefore hypothesize that high-risk patients - obesity, inflammaging - have in common that there is a chronic, low-level activation of TLR7 by intrinsic substrates. This leads to desensitization of TLR7-signalling and, more generally, to a state of tlr-tolerance. Upon SARS-CoV-2 infection the induced TLR7 activation in high-risk patient groups can be expected to be weaker and delayed and, consequently, these patients will show a weaker or delayed initial innate antiviral response immediately after infection. In men, this is then exacerbated further by the naturally lower expression level of TLR7.

It is tempting to speculate that another high-risk group, people who are exposed to continuous air pollution, might also show decreased sensitivity towards SARS-CoV-2 induced TLR7 activation by adaptive responses to chronic stimulation of the innate immune system (Fig. 1), possibly by heterologous

PAMP tolerance reciprocal to the R848-induced cross-tolerance towards TLR4 signalling observed by Michaelis et al. If so, people exposed to continuous air pollution would also be characterized by a state of acquired tlr-tolerance, and thus by a physiological state, where the signal of a new viral infection is initially not detected (see the figure for the proposed mechanistic model). The proposed mechanistic model allows several predictions to be made. First, the gender difference in developing a severe SARS-CoV-2 infection should be independent of age, i.e. prepubertarian boys should be more susceptible than prepubertarian girls, as the different sensitivity would be a primary consequence of different TLR7 expression levels and not a secondary consequence due to sex hormone regulation.

Also, untreated SLE patients, where TLR7 activity is high, should show a stronger initial innate immune response against infection by SARS-CoV-2, which should protect them. However, such patients will be hard to find, as the treatment against SLE typically focuses on suppressing the exaggerated, pathogenic TLR7-signalling. For example hydroxychloroquine, which is frequently used in SLE-patients, reduces TLR7-signalling in SLE-patients by inhibiting autophagy and thus preventing the delivery of extracellular TLR7-substrates to endosomal TLR7. While protection from viral infection is probably not present in human SLE-patients, where their respective immunosuppressing treatments would more than counteract their inherently overactive innate immune system, experiments in untreated lupus-prone mice are in line with the proposed model. Lupus-prone MRL/MpJ-Fas(lpr) mice did show accelerated viral clearance upon influenza infection (12), and thus demonstrated a beneficial role of high TLR7-activity in the initial phase of virus infection. The same mouse model also showed a severe disadvantage of high TLR7-activity after viral clearance since the lupus-prone mice had severe complications during the contraction and resolution phase of the infection with widespread pulmonary inflammation. This points to a positive effect of high TLR7-activity during the early stages of infection, but to a negative effect during the late stages. What is the

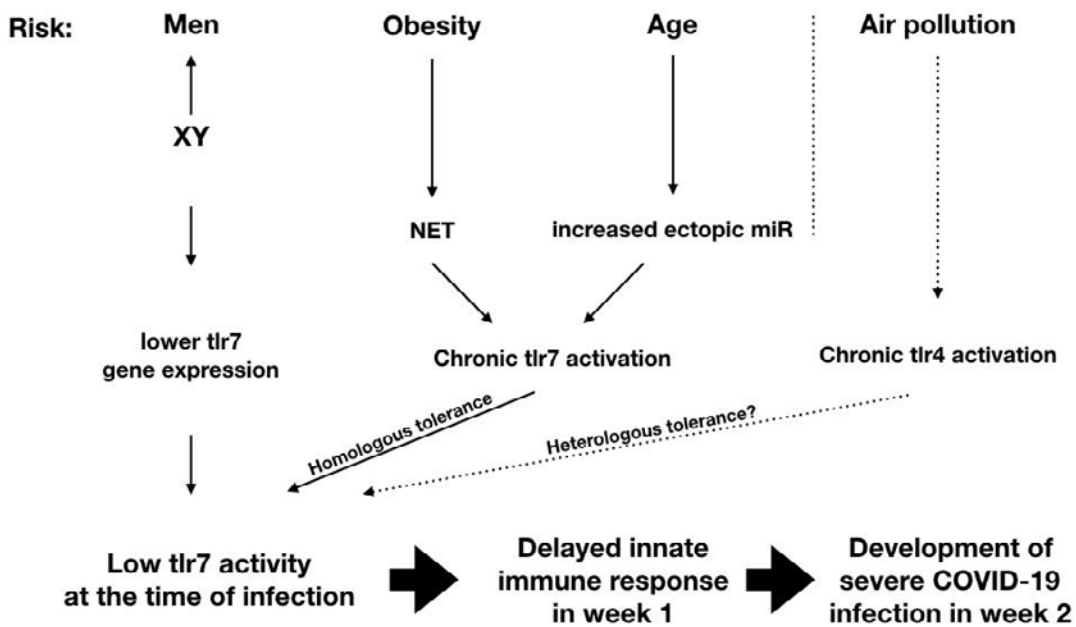


Fig. 1. *Reduced TLR7 activity/sensitivity at the time of SARS-CoV-2 infection as a mechanistic link between high-risk patient groups NET: Neutrophil extracellular traps*

underlying reason for the negative effect of high TLR7-activity during the late stage of infection, even after the virus has been cleared? It may be that the continued TLR7-activity in the lupus-prone mice after virus clearance prevents their immune system from realizing that the virus is indeed gone and that it is now time to contract and resolve.

If the innate immune system of obese people and elderly people reacted to the establishment of a severe SARS-CoV-2 infection (due to an initially laggard TLR7-response, as suggested by this model) by restoring normal TLR7-sensitivity after the initially delayed recognition of the viral infection, then they would find themselves in a situation which is similar to the lupus-prone mice (12): TLR7-signalling from the chronic intrinsic TLR7-substrates to a TLR7, which has regained normal sensitivity (to better fight the virus), would continue even after virus clearance and the innate immune system would effectively continue fighting a virus that is no longer there.

At an intermediate stage of the infection TLR7-signalling would even be overactive in obese and old SARS-CoV-2 patients, as not only the viral RNA, but also the chronic intrinsic TLR7-substrates would signal to TLR7, which has regained normal sensitivity (to better fight the virus).

It is interesting to note that high TLR7 activity has been implied in triggering blood-clotting during sepsis. Thus, there might also be a link between TLR7 and the pathological changes – thrombosis, embolism - which can be observed in the seriously ill. Overall the symptoms which have been described for COVID-19 patients show a striking similarity to the symptoms of SLE patients: overactive TLR7-signalling at the intermediate and late stage of COVID-19 could be a reason for this similarity. It is also interesting that vitamin D3, which has recently been described to protect severely ill COVID-19 patients from thrombosis and embolism, has been also described as downregulating TLR7 gene expression in SLE-patients.

For the use of hydroxychloroquine, the model would predict that it should not be used as an antiviral agent in the early stages of an infection - where any positive effects on viral replication would by counteracted by its interference with a proper innate antiviral immune response - but rather be used to suppress the negative effects of TLR7-signalling during the contraction and resolution phase of the infection and thus with a mechanistic logic that is very similar to its use in SLE patients.

The proposed mechanistic model also confirms the significance of the early phase of SARS-CoV-2 infection for disease progression. If obese people and people of old age have a significantly higher risk than others to develop severe COVID-19 because of an initially weak and/or delayed antiviral response, then therapeutic interventions that aim at improving that initial response should have the most visible effects and antiviral therapy should thus start very early for at risk patients. This is in line with what others have suggested previously, however based on a different logic.

Zhao et al. (13) observed a protective prophylactic effect of the TLR7/8 agonist R848 (resiquimod) (and tlr-agonists in general) in aged mice from SARS-CoV-1 infection. A clinical trial with the tlr3 agonist PrEP-001 administered as a nasal powder prior to exposure to influenza-A (14) reduced the number of individuals with clinical illness and attenuated severity and duration of infection without compromising seroconversion and was well tolerated.

To date, tlr-agonists have not led to approved prophylactics against viral infection, but this is probably due to trying to shoehorn them into the context of continuous dosage regimens and hoping that their administration would give prolonged protection (which will not happen because repeated tlr-agonist administration induces tlr-tolerance). Based on the results of Zhao (13) and Malcolm (14) one would predict that if tlr-agonists are used in the proper context, such as in a one-time rescue prophylactic treatment - for example, by providing PrEP-001 to yet unsymptomatic inhabitants of an old people care facility where a very first case with Covid-19 symptoms has just been detected - they should be beneficial by attenuating severity and duration of infection in those whose innate immune system was boosted just in time.

If tlr-agonists proved protective against SARS-CoV-2 when administered immediately prior to virus exposure, and if attempts to develop a vaccine against SARS-CoV-2 should fail, then tlr-agonists

might provide an option - albeit suboptimal - to immunization of selected parts of the population, for example by protecting a group with already high resistance against the virus, such as people under the age of 40, even further by tlr-agonist administration prior to controlled virus exposure. While this approach would still raise serious ethical and political questions, it might be less undesirable than allowing SARS-CoV-2 to spread through an unprotected population or shutting down societies for months or years.

ACKNOWLEDGEMENTS

I would like to particularly thank Iain Mattaj for comments on the manuscript, discussion and support. I would also like to thank Matthias Hentze and Günter Weiss for helpful initial discussions.

REFERENCES

1. Conti P, Younes A. Coronavirus COV-19/SARS-CoV-2 affects women less than men: clinical response to viral infection. J Biol Regul Homeost Agents 2020; 34(2).
2. Karlberg J, Chong DS, Lai WY. Do men have a higher case fatality rate of severe acute respiratory syndrome than women do? Am J Epidemiol 2004; 159(3):229-31.
3. Heintze JM. Autoimmunity: TLR7 evades silencing in human immune cells. Nat Rev Nephrol 2018; 14(4):214.
4. Li Y, Chen M, Cao H, Zhu Y, Zheng J, Zhou H. Extraordinary GU-rich single-strand RNA identified from SARS coronavirus contributes an excessive innate immune response. Microbes Infect 2013;15(2):88-95.
5. Lee BC, Lee J. Cellular and molecular players in adipose tissue inflammation in the development of obesity-induced insulin resistance. Biochim Biophys Acta. 2014; 842(3):446-62.
6. Chung CP, Avalos I, Oeser A, et al. High prevalence of the metabolic syndrome in patients with systemic lupus erythematosus: association with disease characteristics and cardiovascular risk factors. Ann Rheum Dis 2007; 66(2):208-14.
7. Revelo XS, Ghazarian M, Chng MH, et al. nucleic acid-targeting pathways promote inflammation in obesity-related insulin resistance. Cell Rep 2016; 16(3):717-30.
8. Hanna Kazazian N, Wang Y, Roussel-Queval A, et al. Lupus autoimmunity and metabolic parameters are exacerbated upon high fat diet-induced obesity due to TLR7 signaling. Front Immunol 2019; 10:2015.
9. Metcalf TU, Cubas RA, Ghneim K, et al. Global analyses revealed age-related alterations in innate immune responses after stimulation of pathogen recognition receptors. Aging Cell 2015;14(3):421-32.
10. Feng Y, Zou L, Yan D et al. Extracellular MicroRNAs induce potent innate immune responses via TLR7/MyD88-dependent mechanisms. J Immunol 2017; 199(6):2106-17.
11. Michaelis KA, Norgard MA, Levasseur PR, et al. Persistent Toll-like receptor 7 stimulation induces behavioral and molecular innate immune tolerance. Brain Behav Immun 2019; 82:338-53.
12. Slight-Webb SR, Bagavant H, Crowe SR, James JA. Influenza A (H1N1) virus infection triggers severe pulmonary inflammation in lupus-prone mice following viral clearance. J Autoimmun 2015; 57:66-76.
13. Zhao J, Wohlford-Lenane C, Zhao J, et al. Intranasal treatment with poly(I•C) protects aged mice from lethal respiratory virus infections. J Virol 2012; 86(21):11416-24.
14. Malcolm BA, Aerts CA, Dubois KJ, et al. PrEP-001 prophylactic effect against rhinovirus and influenza virus - results of 2 randomized trials. Antiviral Res 2018; 153:70-77.

JOURNAL OF BIOLOGICAL REGULATORS & HOMEOSTATIC AGENTS Vol. 34, no. 3, 1131-1133 (2020)

LETTER TO THE EDITOR

ABNORMAL PREDOMINANTLY FRONTAL HIGH VOLTAGE AND SLOW EEG FINDINGS WITH ACUTE ENCEPHALOPATHY ASSOCIATED WITH ACUTE FOCAL BACTERIAL NEPHRITIS

G. IMATAKA, Y. FUJITA, Y. KANO and S. YOSHIHARA

Department of Pediatrics, Dokkyo Medical University, Shimotsuga, Tochigi, Japan

Received April 3, 2020 – Accepted May 14, 2020

To the Editor,

Acute focal bacterial nephritis (AFBN), an inflammatory lesion of the renal parenchyma caused by localized bacterial infection of the kidney, was first described by Rosenfield in 1979 (1). The AFBN stage is considered to be the transition from acute renal pelvic nephritis to renal abscess (1). In recent years, a few researchers reported cases of AFBN associated with central nervous system symptoms (2-5). Here, in this paper, we report a rare case of a AFBN that was associated with fever and impaired consciousness. This case was initially diagnosed as acute encephalopathy based on the high-voltage amplitude and slow wave pattern observed on electroencephalogram (EEG).

The case was a 12-year-old male patient who visited a clinic complaining of fever and fatigue. The clinic associated the symptoms to common cold and the patient was returned home. The patient gradually developed speech difficulties which eventually affected his communication ability. The next morning, after a walk around his house he experienced severe vomiting and a few hours later, he stopped responding to his parents and was not able to recognize the members of his family. At this level, his consciousness gradually deteriorated, and he was transported to our university hospital by an ambulance. After admission and hospitalization, he exhibited a disturbed level of consciousness and acted irrationally and started shouting while walking around the hospital general ward. His body temperature was 40°C, and physical examination did not reveal any physical abnormality on his body. His deep tendon reflexes were normal, with no difference between the right and left sides. We instructed him to perform finger-to-nose test, Romberg test and dancing toe walking test; but he could not comprehend any of the test instructions. The blood test results were $15{,}800\times10^9/\mu l$ for white blood cells (WBC) and 5.72 mg/dL for C-Reactive protein (CRP), suggesting some focal bacterial infection. His urine test results revealed normal values for protein, glucose, red blood cells, WBC, and β2-microgloburin. Cerebral spinal fluid collection with lumbar test showed normal findings with no increase in the cell count, protein level, glucose and IgG index. Following this, the patient exhibited violent movement along with impaired consciousness. Thus, we performed an EEG examination and recorded high voltage and slow delta wave activities predominantly for both frontal areas (Fig. 1 A, B). Brain magnetic resonance imaging (MRI) and diffusion-weighted imaging (DWI) results showed no abnormalities. Based on symptoms and EEG results,

Key words: AFBN; acute encephalopathy; electroencephalogram; DWI; MRI

Corresponding Author:
George Imataka M.D., Ph.D., B.Phil. LL.B., PGDBM
Department of Pediatrics, Dokkyo Medical University
880 Kitakobayashi, MIbu, Shimotsuga, Tochigi 321-0293 Japan
Tel.: +81-282-86-1111 (PHS: 7390)
e-mail: geo@dokkyomed.ac.jp

0393-974X (2020)
Copyright © by BIOLIFE, s.a.s.
This publication and/or article is for individual use only and may not be further reproduced without written permission from the copyright holder. Unauthorized reproduction may result in financial and other penalties
DISCLOSURE: ALL AUTHORS REPORT NO CONFLICTS OF INTEREST RELEVANT TO THIS ARTICLE.

we diagnosed him as a case of acute encephalopathy. We started steroid pulse treatment with 30 mg/kg methylprednisolone for 3 days. Six hours after the steroid pulse treatment, he regained consciousness rapidly and his verbal response was normalized the next morning. On the fourth day after admission, his body temperature increased again to 40°C and the blood WBC, CRP, ferritin, procalcitonin, and IL-2R levels were $14{,}000\times10^9$/μl, 21.13 mg/dl, 105 ng/ml, 13.36 ng/ml and 1,029 U/ml, respectively. Moreover, the BUN, creatinine, and sodium levels were 23 mg/dL, 1.2 mg/dl, and 135 mmol/L, respectively. At this point we started to identify the source of the bacterial infection. Data obtained from the blood test and the abdominal enhanced CT showed a low-density area in the left kidney (Fig. 2A). Additional brain MRI-DWI revealed normal intensity, and abdominal MRI-DWI exhibited wedge-shaped high signal intensities in the left kidney (Fig. 2 B, C). These abnormal intensities were compatible with AFBN diagnosis. We started a 10-day antibiotic treatment with 4 g/day of ceftriaxone. After antibiotic therapy his general condition gradually improved. Urine culture test revealed no specific infection and magnetic resonance cholangiography results were normal. Renal ^{123}I-meta-iodobenzylguanidine single photon emission computerized tomography showed lower left renal uptake compared to the right. After a few years of follow-up, his left kidney function was maintained and brain recognition was normal.

In previous studies on the central nervous system symptoms associated with AFBN,

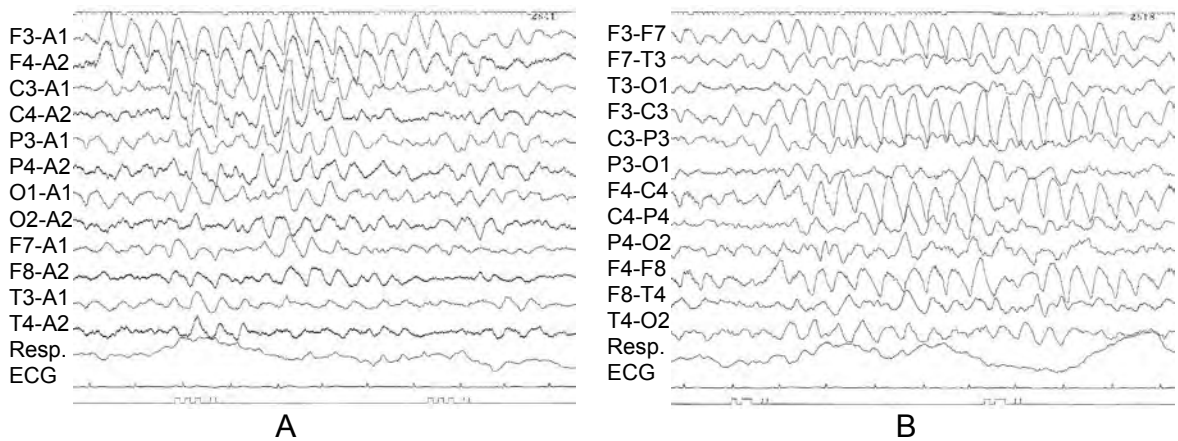


Fig. 1. ***A)*** *Monopolar pattern of EEG shows high voltage and 2 Hz slow wave activities predominantly in both frontal areas.* ***B)*** *Bipolar pattern of EEG detected abnormal high voltage slow wave activities.*



Fig. 2. ***A)*** *Enhanced CT image showing a low-density abnormal area in the left kidney (arrows).* ***B,C)*** *Abdominal MRI-DWI reveals wedge-like shaped high signal intensities in the left kidney (arrows).*

researchers have reported abnormalities in MRI results. These abnormalities included clinically mild encephalitis/encephalopathy with reversible splenial lesion (MERS) (2-4), reversible posterior leukoencephalopathy syndrome (RPLS) (4), and acute encephalopathy with biphasic seizures and late reduced diffusion (AESD) (5). Our patient underwent two MRI scans at different phases, and neither of them showed any MERS abnormalities. Moreover, our case was diagnosed based on abnormal frontal dominant high voltage slow EEG results. The main symptoms in our patient included consciousness disorder, along with visual and behavioral abnormalities. Our patient did not experience any convulsions. We assumed that our case was a non-convulsive acute encephalopathy case, which was clinically similar to MERS. This might be one of the most clinically mild types of a novel encephalopathy among the various types of acute childhood encephalopathy cases. Acute encephalopathy with normal MRI and abnormal high voltage and slow activity EEG findings associated with AFBN may be categorized as a new clinical phenotype of acute encephalopathy with milder clinical symptoms compared to MERS. In cases with symptoms of central nervous system anomalies that are suggestive of acute encephalopathy, clinicians should perform both EEG and MRI if the case is diagnosed as AFBN. It may be possible to diagnose AFBN associated with MERS as well as AFBN associated with normal MRI findings and abnormal high voltage and slow EEG wave patterns, similar to our case of acute encephalopathy.

REFERENCES

1. Rosenfield AT, Glickman MG, Taylor KJ, Crade M, Hodson J. Acute focal bacterial nephritis (acute lobar nephronia). Radiology 1979; 132:553-61.
2. Maruyama Y, Sato M, Inaba Y, Fukuyama T. Comparison of mild encephalopathy with reversible splenial lesion with and without acute focal bacterial nephritis. Brain Dev 2020; 42:56-63.
3. Kometani H, Kawatani M, Ohta G, et al. Marked elevation of interleukin-6 in mild encephalopathy with a reversible splenial lesion (MERS) associated with acute focal bacterial nephritis caused by Enterococcus faecalis. Brain Dev 2014; 36(6):551-53.
4. Kasuga Y, Fuchigami T, Fukuda A, et al. Acute focal bacterial nephritis associated with central nervous system manifestations: a report of 2 cases and review of the literature. Pediatr Emerg Care 2017; 33(6):418-21.
5. Yamaguchi H, Nagase H, Ito Y, et al. Acute focal bacterial nephritis characterized by acute encephalopathy with biphasic seizures and late reduced diffusion. J Infect Chemother 2018; 24(11):932-35.

JOURNAL OF BIOLOGICAL REGULATORS & HOMEOSTATIC AGENTS Vol. 34, no. 3, 1135-1139 (2020)

LETTER TO THE EDITOR

COMPARISON OF BONE METABOLISM MARKERS AND CELLULAR PROFILE BETWEEN CONVENTIONAL LINGUAL AND LABIAL FIXED ORTHODONTIC APPLIANCES

H.A. BAESHEN

Orthodontic Department, Faculty of Dentistry, King Abdulaziz University, Jeddah, Saudi Arabia

Received April 3, 2020 – Accepted April 30, 2020

To the Editor,

Orthodontic appliances are routinely practiced in orthodontic procedures. These appliances exert different forces on the periodontal region which causes the periodontal tissue to release some growth factors and cytokines. It could be suspected that there is also release of cellular components from the periodontium. These factors altogether cause the changes in the bone formation and resorption which further causes remodelling of the periodontium which is a vital part of the tooth movements (1).

The metabolism of the bone formation is very necessary and the studies to date have tried to understand the cellular and molecular machinery responsible for bone remodelling during orthodontic treatment (2). During orthodontic treatment, cytokines and growth factors secreted in the saliva are utilized as biochemical markers of bone formation and metabolism. Comparing the levels of growth factors and cytokines between applications of various orthodontic appliances has provided valuable data to develop and continuously improve and invent new appliance designs which could further help in healthy bone metabolism and proper bone development which would support the periodontium homeostasis (3).

Aesthetic improvements are extremely important in orthodontic procedures and are continuously increasing. There are a number of studies focused on the molecular aspects of orthodontic remodelling after labial orthodontic treatment, but few have mentioned the effect of lingual treatment on bone metabolism (4). Since the demand for lingual appliances is increasing for aesthetic purposes, it is necessary to assess the comparative effect of these appliances and their designs on the bone metabolism in the periodontal region. Therefore, the aim of the present study was to examine the salivary bone metabolism-related factors and cellular content marker expression after the use of two different methods of orthodontic appliances - lingual and labial.

MATERIALS AND METHODS

Ethical permissions required for this study were obtained from the institutional ethics committee and the samples were collected (n = 40 of which labial = 20 and lingual = 20) along with the patient informed consent. The samples were collected in a sterile container and transported directly to the laboratory.

Isolation of cells from saliva and flow cytometry

The saliva samples were diluted with phosphate buffered saline (1:10) and centrifuged at 2500 rpm for 10 min. The pellet obtained was then further subjected to antibody staining and flow cytometry

Key words: bone metabolism; cellular biomarkers; orthodontic appliances; secretory factors; saliva

Corresponding Author:
Dr Hosam A. Baeshen,
Orthodontic Department, Faculty of Dentistry,
King Abdulaziz University, P.O box 80209,
Jeddah 21589, Saudi Arabia
e-mail: habaeshen@kau.edu.sa

0393-974X (2020)
Copyright © by BIOLIFE, s.a.s.
This publication and/or article is for individual use only and may not be further reproduced without written permission from the copyright holder.
Unauthorized reproduction may result in financial and other penalties
DISCLOSURE: ALL AUTHORS REPORT NO CONFLICTS OF INTEREST RELEVANT TO THIS ARTICLE.

analysis. Briefly, the cells were resuspended in PBS and labelled with appropriate antibodies. After incubation for 30 min at room temperature, the cells were acquired on Attune NxT Flow Cytometer (Thermo Scientific, USA). 5,000 cell events were acquired in each sample. The percentage was calculated in comparison with the unstained control.

Cytometric bead array for detection of bone metabolism-related factors in saliva

Cytometric bead array was performed to determine the levels of the factors in saliva. LEGENDplex™ Human Bone Metabolism Panel 1 (Biolegend;740656) (OPG, OPN, ALPL, ACP5, Leptin, RANKL, TNF-alpha, IL-6, PTH, IL-1beta, BMP-2, DKK-1) was used and the further experimental protocol was performed according to the manufacturer's guidelines. The samples were acquired on flow cytometer, and analysis was performed by using LEGENDplex™ Data Analysis Software.

RESULTS

Cellular marker profiles show some difference in terms of stem cell marker CD44 in subjects with either lingual or labial fixed orthodontic appliances

The cell surface marker analysis revealed that the epithelial cellular components in terms of surface markers did not show much change in either type of subjects (Fig. 1). However, there was a difference in CD44, which is a stem cell surface marker. The cells showed high percentage of CD44 in subjects with the labial appliance. Expression of fibroblast marker CD90 was low in both lingual and labial subjects. Also, there was not much difference in the immune cell markers CD45 and IL8 RA but IL8 RB was low in many subjects with labial appliance. The expression level percentages of epithelial cell markers cytokeratin, EpCAM, and ECAD were not significantly different in either of the the cases.

Bone metabolism-related salivary factors are secreted in a unique manner in both subjects with lingual and labial fixed orthodontic appliances

The bone metabolism-related factors OPG, OPN, ALPL, ACP5, Leptin, RANKL, TNF-alpha, IL-6, PTH, IL-1beta, BMP-2, DKK-1 were present in both the types of subjects (Fig. 2). Some of the factors and cytokines were affected by the different treatments but not many changes were seen except for the PTH and Leptin levels. Leptin levels were much higher in subjects with lingual appliance whereas PTH levels were higher in subjects with labial appliance than those with lingual appliance. ACP5 is responsible for the regulation of osteopontin which is further implicated in bone formation. The levels of this protein were seen much higher in lingual appliances than in labial appliances. Also, the levels of inflammatory cytokine IL-1 beta were observed higher in lingual appliances than in labial appliances.

DISCUSSION

Various cytokines have shown to be involved in the bone resorption and formation maintaining the tissue homeostasis. The interplay between these cytokines, growth factors and cells creates a peculiar microenvironment responsible for the remodelling and repair of the tissues (5, 6). Although there is sufficient information available on the cytokines in the saliva and their roles in periodontal bone remodelling, there is very little evidence showing the exact roles of the metabolic factors and different types of cells in this context (7).

The patients have to bear these orthodontic appliances for a significantly longer period of time, therefore, it is necessary to study all the aspects of these treatment modalities. There are several other factors which come into the harmful categories and are necessary to understand, such as oral microbial flora, habits of the subjects, and other such factors related to the environment (8). Orthodontic appliances are one of the factors which are mentioned several times regarding the onset and development of periodontal diseases. The force arising from orthodontic appliances, depending on their structural and material properties, cause the release of growth factors and cytokines, resulting in the proper resorption of the bone and remodelling of the periodontium on which a proper movement of the teeth depends (9).

In this study, there was a slight difference in the

expression of the stem cell marker CD44, but the immune cell-related markers, such as CD45, IL8 RA and IL8 RB, did not differ much in the percentage expression in any of the samples (Fig. 1). The mucosal epithelial cellular components were also likely the same in terms of marker expression in the samples from both types of subjects. Furthermore, we investigated the secretory factors related to the bone metabolism , and it was evident that both treatments do not affect the bone growth factors such as OPG, OPN, ALPL, and BMP2. There was a significant difference in the secreted PTH and Leptin (Fig. 2) (10, 11), however, we could not confirm these two hormones at the gene level. Since their roles in the bone resorption and bone formation are dynamic, it is an important task to thoroughly study these hormones and their interaction with various cellular components of the saliva (12).

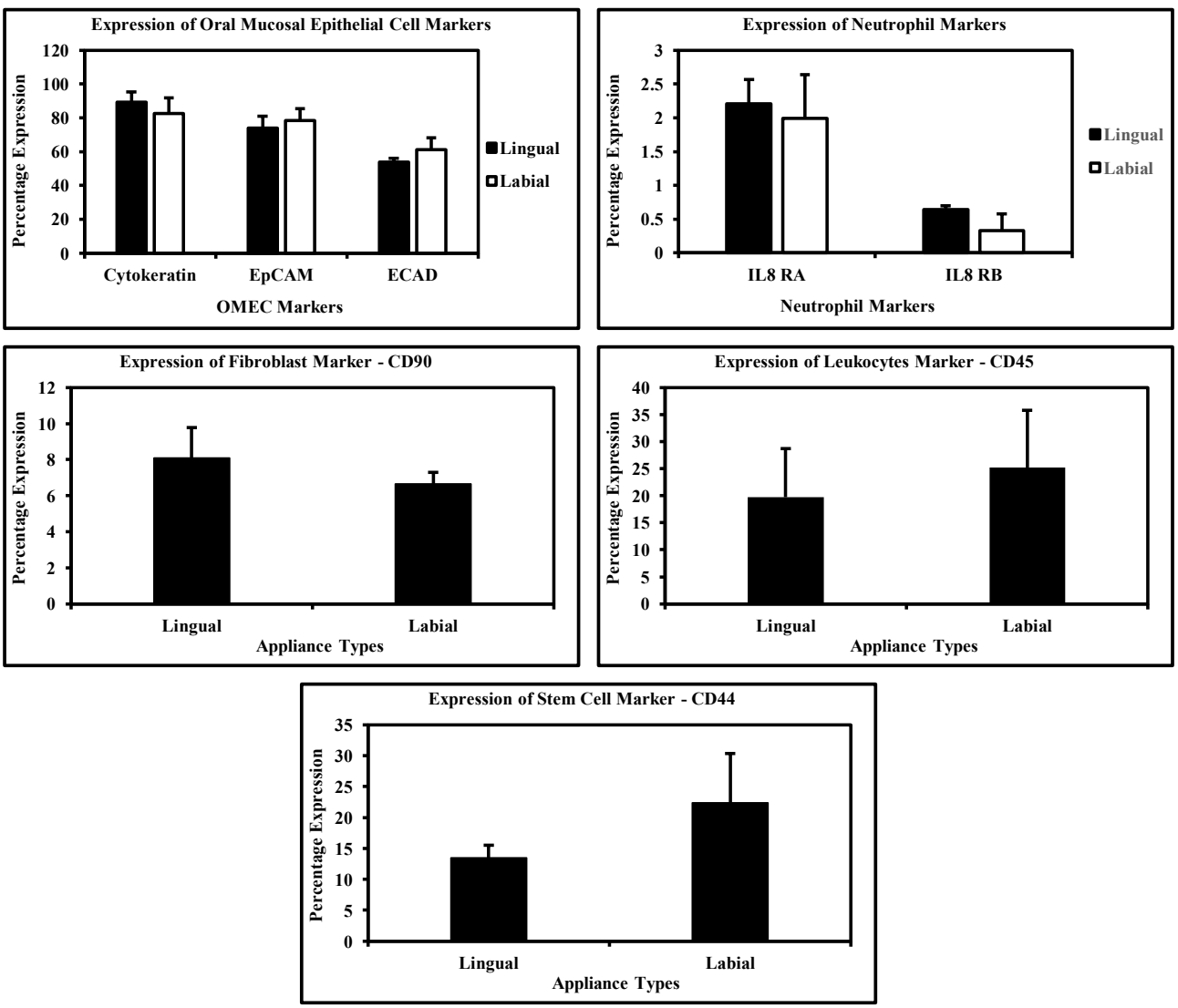


Fig. 1. *Flow cytometry analysis for different cellular markers. Flow cytometry was performed to analyze the surface markers for epithelial cells, neutrophils, leukocytes, fibroblasts and stem cells.*

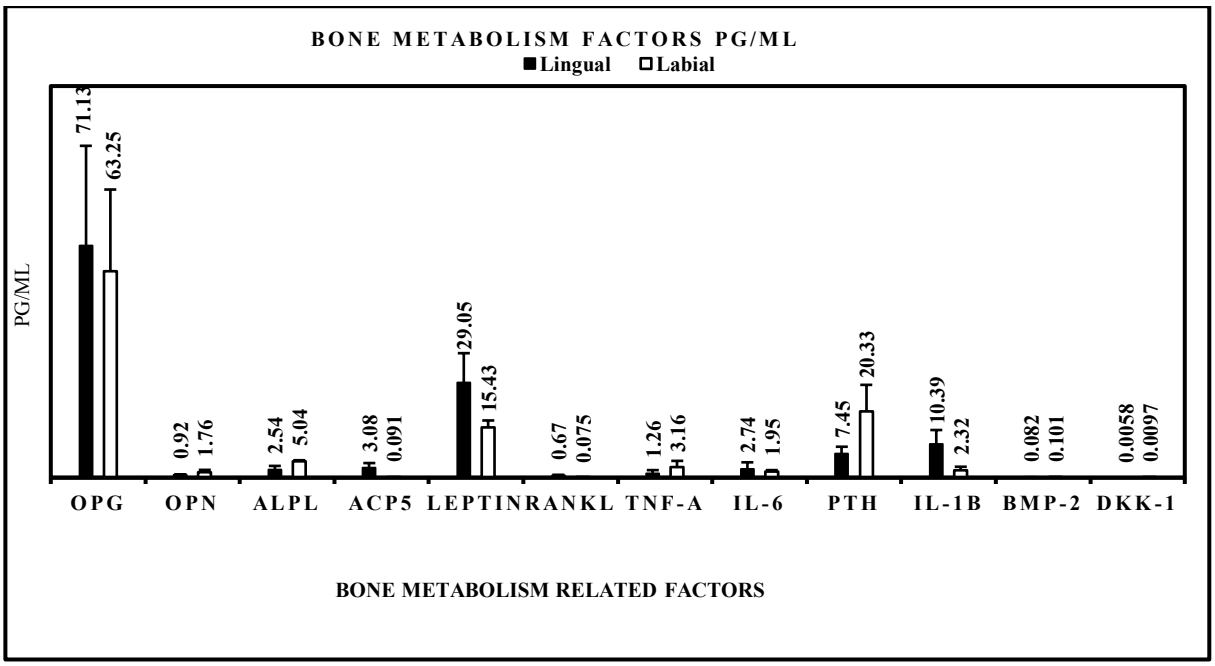


Fig. 2. *Cytometric bead array analysis for bone metabolism-related factors. OPG: Osteoprotegerin; OPN: Osteopontin; ALPL: Alkaline phosphatase; ACP5: Tartrate-resistant acid phosphatase; RANKL: Receptor activator of nuclear factor κB ligand; TNF-a: Tumor necrosis factor alpha; IL-6: Interleukin 6; PTH: Parathyroid hormone; IL-1b: Interleukin 1 beta; BMP2: Bone morphogenetic protein 2; DKK-1: Dickkopf WNT Signaling Pathway Inhibitor 1*

The osteopontin regulating protein ACP5 was highly expressed in the lingual type of appliances, and the inflammatory cytokine IL-1 beta levels were also high in the lingual type of appliances (10). But the exact mechanism of how these molecules are synergistically acting on bone metabolism remains to be further studied. In conclusion, within the limitations of the study a comparative analysis of bone metabolism markers and cellular profile between patients treated with conventional lingual or labial fixed orthodontic appliances shows that the both treatment modalities cause difference in the salivary secretion of the factors, especially PTH and Leptin. Furthermore, both the treatment modalities show the differential presence of cellular components in the saliva. However, a multidisciplinary approach is needed to study the signalling between these molecules and cells.

REFERENCES

1. Alexander L, Kommi PB, Arani N. Evaluación de la cinética de fricción entre regular y color titanio molibdeno aleación arcos. Indian J Dent Res 2017; 29(2):212-16. doi:10.4103/ijdr.IJDR
2. Ata-Ali F, Cobo T, De Carlos F, Cobo J, Ata-Ali J. Are there differences in treatment effects between labial and lingual fixed orthodontic appliances? A systematic review and meta-analysis. BMC Oral Health 2017; 17(1):1-11. doi:10.1186/s12903-017-0424-z
3. Ata-Ali F, Plasencia E, Lanuza-Garcia A, Ferrer-Molina M, Melo M, Ata-Ali J. Effectiveness of lingual versus labial fixed appliances in adults according to the Peer Assessment Rating index. Am J Orthod Dentofac Orthop 2019; 155(6):819-25. doi:10.1016/j.ajodo.2018.07.018

4. Caballé-Serrano J, Cvikl B, Bosshardt DD, Buser D, Lussi A, Gruber R. Saliva suppresses osteoclastogenesis in murine bone marrow cultures. J Dent Res 2015; 94(1):192-200. doi:10.1177/0022034514553977
5. Gomes AM, Douglas-de Oliveira DW, Oliveira Costa F. Could the biomarker levels in saliva help distinguish between healthy implants and implants with peri-implant disease? A systematic review. Arch Oral Biol 2018; 96:216-22. doi:10.1016/j.archoralbio.2018.09.008
6. Kaczor-Urbanowicz KE, Martin Carreras-Presas C, Aro K, Tu M, Garcia-Godoy F, Wong DTW. Saliva diagnostics – Current views and directions. Exp Biol Med 2017; 242(5):459-72. doi:10.1177/1535370216681550
7. Knösel M, Vogel Alvarez R, Blanck-Lubarsch M, Helms HJ. Comparison of potential long-term costs for preventive dentistry treatment of post-orthodontic labial versus lingual enamel cavitations and esthetically relevant white-spot lesions: A simulation study with different scenarios. Head Face Med 2019; 15(1):1-10. doi:10.1186/s13005-019-0204-x
8. Pamukçu H, Polat-Özsoy Ö, Gülşahi A, Özemre MÖ. External apical root resorption after nonextraction orthodontic treatment with labial vs. lingual fixed appliances. J Orofac Orthop 2020; 81(1):41-51. doi:10.1007/s00056-019-00201-w
9. Theda C, Hwang SH, Czajko A, Loke YJ, Leong P, Craig JM. Quantitation of the cellular content of saliva and buccal swab samples. Sci Rep 2018; 8(1):4-11. doi:10.1038/s41598-018-25311-0
10. Guvenc B, Torun O, Filiz AK, Abdurrahman K, Orhan H. Interleukine-1and Tumor Necrosis Factor-α Levels in the Human Gingival Sulcus during Orthodontic Treatment. Angle Orthod 2006; 76(5):830-36
11. Ren Y, Vissink A. Cytokines in crevicular fluid and orthodontic tooth movement. Eur J Oral Sci 2008; 116:89-97
12. Liu YCG, Lerner UH, Teng YTA. Cytokine responses against periodontal infection: protective and destructive roles. Periodontol 2000 2010; 52:163-206

JOURNAL OF BIOLOGICAL REGULATORS & HOMEOSTATIC AGENTS Vol. 34, no. 3, 1141-1146 (2020)

LETTER TO THE EDITOR

DECREASED EXPRESSION OF CENTROSOMAL PROTEIN 350 IS ASSOCIATED WITH POOR PROGNOSIS IN HEPATOCELLULAR CARCINOMA

YF. WANG[1*], LL. JU[2*], X. LUO[2], H. ZHANG[3] and ZL. BIAN[2]

[1]Department of Biochemistry and Molecular Biology, School of Basic Medical Sciences, Fudan University, Shanghai, China; [2]Nantong Institute of Liver Disease, Nantong Third People's Hospital Affiliated to Nantong University, Nantong, Jiangsu, China; [3]Intensive Care Unit, Nantong Hospital to Nanjing University of Chinese Medicine, Nantong, Jiangsu, China

Received August 28, 2019 – Accepted March 18, 2020

* These authors contributed equally to this work

To the Editor,

Hepatocellular carcinoma (HCC) is the most deadly form of liver cancer, accounting for approximately 80% of adult primary liver cancers worldwide (1). HCC is a global health burden, and its prevalence and incidence rates are rising worldwide (2, 3). At present, both imaging findings and biomarker detection are used for the diagnosis and prognosis of HCC. Early diagnosis of liver cancer is challenging due to the lack of accurate biomarkers, thus, the development of novel biomarkers for HCC diagnosis is urgent.

Centrosomes are crucial components of the cell cycle process, as they are closely related to asymmetric cell division (4, 5). Proteins belonging to the centrosome-associated protein (CEP) family are involved in cell division and the regulation of the cell cycle, cell polarity, centriole duplication, spindle–kinetochore assembly, and cell cycle checkpoint signaling mechanisms (6). Previous reports showed that, since CEPs play a crucial role in mitosis, CEP genes have the potential to be tumor suppressor or oncogenes if their expression is altered (5). Up-regulation of CEP genes expression can increase the number of centrioles and thus the number of cells formed in each cell cycle. This abnormal division may contribute to malignant transformation (5). Conversely, down-regulation of CEP expression affects the spindle formation and the inheritance of genetic material. Indeed, aneuploidy is a common feature of human cancers and it can be caused by centrosome dysfunction (7). Therefore, the alteration of CEP expression can drive normal cell transformation.

It has been previously reported that the activity and subcellular compartmentalization of peroxisome proliferator-activated receptor α are altered by CEP350 (8). However, the role and function of CEP350 in HCC are poorly understood. Therefore, in this study, we investigated the expression of CEP350 in HCC tissue and its prognostic value in HCC patients.

MATERIALS AND METHODS

The study protocol was drafted following the ethical guidelines of the 1975 Declaration of Helsinki. The current study was reviewed and approved by the Ethics Committee of the Nantong Third People's Hospital

Key words: centrosomal protein 350; prognosis; hepatocellular carcinoma; biomarker

Corresponding Author:
Dr. Bian ZL,
Nantong Institute of Liver Disease,
Nantong Third People's Hospital
Affiliated to Nantong University, 60 Middle Qingnian Road,
Nantong, Jiangsu, 226006, P.R. China
e-mail: bianzhaolian1998@163.com

0393-974X (2020)
Copyright © by BIOLIFE, s.a.s.
This publication and/or article is for individual use only and may not be further reproduced without written permission from the copyright holder.
Unauthorized reproduction may result in financial and other penalties
DISCLOSURE: ALL AUTHORS REPORT NO CONFLICTS OF INTEREST RELEVANT TO THIS ARTICLE.

Affiliated to Nantong University. Informed consent was obtained from each patient.

Tissue samples

The tumor and the adjacent non-tumor liver tissues were collected from 93 patients attending the Nantong Third People's Hospital Affiliated to Nantong University (Nantong, China) between January 2014 and December 2018. Histopathological diagnosis of all patients was completed by the Department of Pathology. All tissues used in the study were frozen immediately after dissection and stored at -80°C until use.

Tissue microarray technology (TMA) slices of the HCC and healthy liver tissues of the 93 patients were prepared by Outdo Biotech CO., Ltd (Shanghai, China). The Immunohistochemistry (IHC) staining was carried out as previously described (9). The primary antibody used in this study (CEP350, cat. no.20022-1-AP, 1: 100) was purchased from ProteinTech Group, Inc. For reverse transcription polymerase chain reaction (RT-qPCR), total RNA was extracted from tissues and cells by TRIzol (Takara Biotechnology Co., Ltd., Dalian, China). Then, the RNA samples were reversed transcribed using the Prime Script™ RT Reagent Kit (Takara Biotechnology Co., Ltd., Dalian, China). PCR reactions were carried out in a Bio-Rad Real-Time PCR Detection System (Bio-Rad Laboratories, Inc., Hercules, CA, USA), using the SYBR® Green Master Mix (Takara Biotechnology Co., Ltd.). The primer sequences used for PCR amplification were the following (F, forward primer; R: reverse primer): CEP350, F: 5'- GAAACTCAGAACGTTCGAGAAG-3', R: 5'-GTCATCAAGAATGCCACGAATT-3'; β-actin, F: 5'-GGACTTCGAGCAAGAGATGG-3', R: 5'-AGGAAGGAAGGCTGGAAGA-3'. The PCR profile was the following: initial denaturation at 95°C for 5 min, then 40 cycles composed of two steps: denaturation for 10 sec at 95°C and annealing for 30 sec at 60°C. The $2^{-\Delta\Delta Ct}$ method was used for analysis.

Western blotting was carried out as previously described. The primary antibody used in this study (CEP350, cat. no.20022-1-AP, 1: 1000; β-actin, cat.no HRP-60008, 1:10000) was purchased from ProteinTech Group, Inc. Protein levels

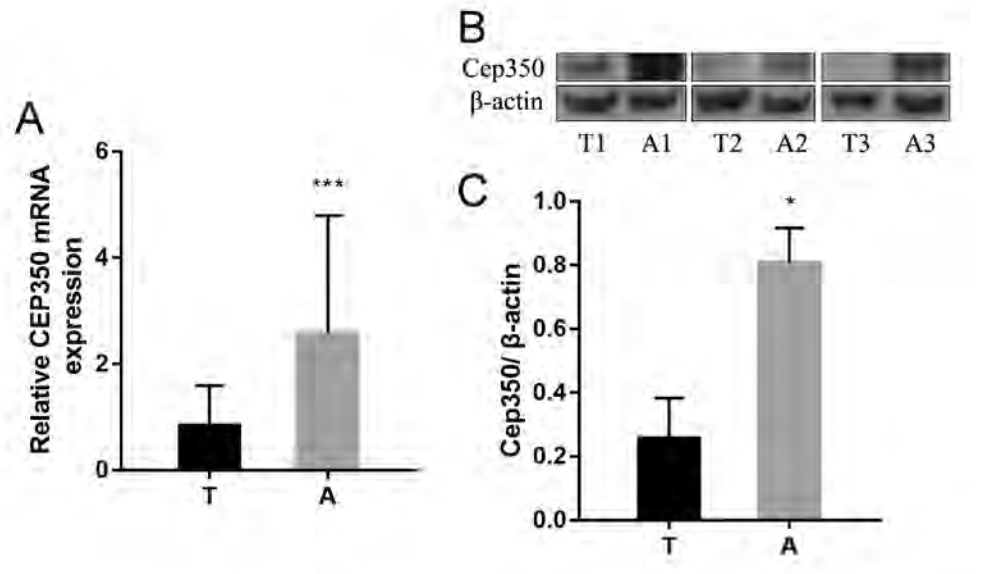


Fig. 1. *Expression of CEP350 in HCC tumor tissues (T) and adjacent healthy tissues (A).* ***A)*** *Expression of CEP350 mRNA in HCC tissues and adjacent tissues, as detected by RT-qPCR;* ***B)*** *Detection of CEP350 protein expression in HCC tissues and adjacent tissues by western blotting.* ***C)*** *Quantification of western blotting bands. Data were normalized to β-actin, used as the internal control. *P < 0.05 , ***P < 0.001.*

were quantified by the Fuji Film Multi Gauge software V3.0 (Santa Clara, CA, USA).

Statistical analysis

GraphPad Prism 7 software was used for data analysis and survival curve generation. The Student's *t*-test was used to determine the differences between the two groups, followed by the Cox proportional hazards regression model. SPSS 24.0 software (SPSS, Chicago, IL. USA) was used for all analyses. A P-value < 0.05 indicated statistical significance. All the experiments were repeated at least three times. All data are presented as mean ± SEM (standard error of the mean).

RESULTS

The clinical data of the 93 HCC patients were the following: 74 male and 19 female, aged between 23 and 85 years (mean age: 53.4 years). According to the International Union Against Cancer Tumor-Node-Metastasis (TNM) Classification (10), 66 patients were classified as TNM stage I or II, while the remaining 27 were classified as stage III or IV. The tumor diameter was < 5 cm in 63 patients and > 5 cm in 30 patients (Table I).

RT-qPCR and Western blotting were performed to detect the mRNA and protein levels of CEP350 in 93 paired tumor and adjacent healthy tissues. Both mRNA and protein levels of CEP350 were significantly decreased in the tumor tissues (Fig. 1). To further confirm this observation, we performed IHC and obtained comparable results (Fig. 2). We thus concluded that in HCC the expression of CEP350 is severely down-regulated.

The patients were divided into two groups according to the TMA immunohistochemical score. Patients with a score of 0 or 1 were classified in the low expression group (N = 47), while patients with a score of 2 or 3 were classified in the high expression group (N = 46). We plotted the Kaplan-Meier survival curve (follow-up time: from 3 to 10 years) of the two groups to investigate the potential prognostic

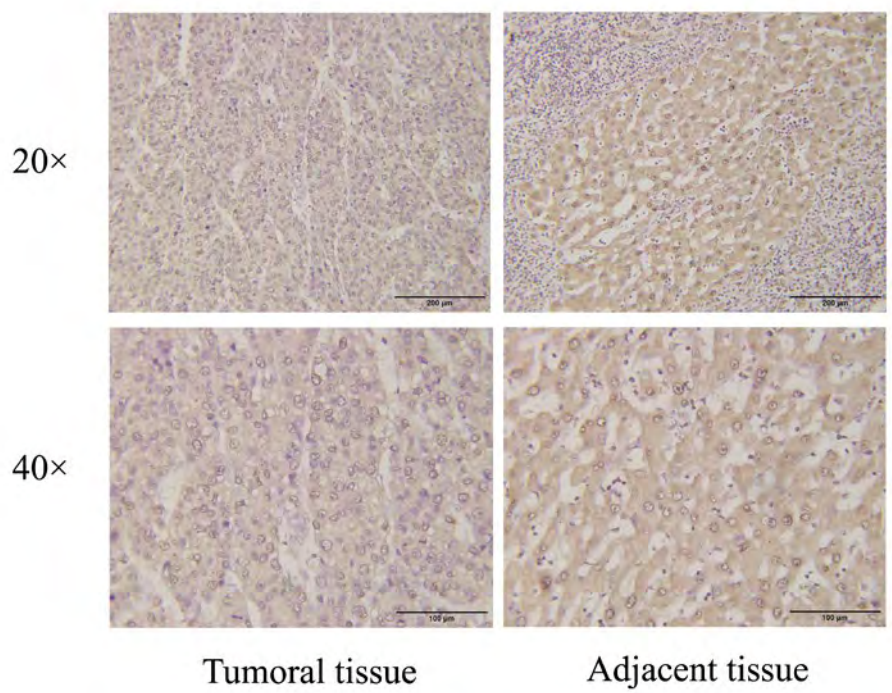


Fig. 2. *Immunohistochemistry of CEP350 expression in HCC and adjacent healthy tissues. Representative immunohistochemical staining of CEP350 in HCC (left, bar 200 μm and 100 μm) and adjacent tissues (right, bar 200 μm and 100 μm).*

Table I. *Clinical characteristics of the HCC cases used in this study*

Clinical variables		Data
Number of patients		93
Mean age ± SD (years)		53 ± 11
Gender n (%)		
	Male	74 (79.6)
	Female	19 (20.4)
TNM stage n (%)		
	I + II	66(71.0)
	III+IV	27 (29.0)
Diameter (cm)		
	≤5	63 (67.7)
	>5	30 (32.3)
TopoII n (%)		
	Negative	89 (95.7)
	Positive	4 (4.3)
P-gp n (%)		
	Negative	57 (61.3)
	Positive	36 (38.7)
P53 n (%)		
	Negative	81 (87.1)
	Positive	12 (12.9)

HCC: hepatocellular carcinoma; TNM tumor node metastasis; TopoII; Topoisomerase II; P-gp: permeability glycoprotein; P53 : tumor protein 53.

value of CEP350 expression on the overall survival in HCC patients. We found that the low CEP350 expression group had a significantly lower survival rate than the high CEP350 expression group. This result suggests that a low CEP350 protein level is a significant prognostic factor correlated to poor overall survival in HCC patients (Fig. 3).

Univariate analysis of each clinicopathological parameter was performed to investigate the prognostic values of these parameters with the survival time of HCC patients. The hazard ratio and P-value for each parameter were used to predict the patients' prognosis. Then, each parameter was analyzed by the multivariate Cox proportional hazards model analysis. The results showed that CEP350 expression, TNM stage, and P-glycoprotein (P-gp) were significant prognostic factors in HCC patients (Table II). Moreover, multivariate analysis showed that CEP350 expression was a significant prognostic factor in HCC patients (Table II).

DISCUSSION

HCC is a common global health problem, as it is a lethal malignancy difficult to treat. CEP family

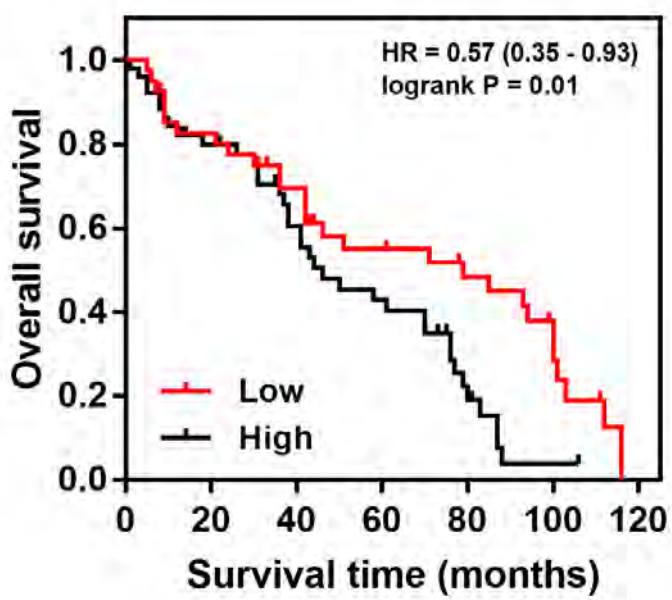


Fig. 3. *Association between the expression level of CEP350 and HCC patients' prognosis. The lower expression group is composed of patients with an immunohistochemical score of 0 or 1, while the high expression group is composed of patients with a score of 2 or 3.*

Table II. *Univariate and multivariate analysis of factors associated with overall survival*

		Univariate analysis	
Variables	Hazard Ratio	95% confident interval	p
Cep350 expression	0.020	0.005-0.088	＜0.001
Gender	1.078	0.522-2.225	0.84
Age	0.901	0.509-1.593	0.719
TNM stage	1.946	1.060-3.570	0.032
TopoII	0.696	0.096-5.075	0.721
P-gp	0.276	0.137-0.556	< 0.001
P53	1.559	0.690-3.520	0.285
Tumor size	0.786	0.426-1.448	0.439

		Multivariate analysis	
Variables	Hazard Ratio	95% confident interval	p
Cep350 expression	0.024	0.005-0.113	< 0.001
Gender	1.191	0.549-2.585	0.658
Age	1.114	0.583-2.130	0.743
TNM stage	0.889	0.455-1.738	0.732
TopoII	0.771	0.101-5.897	0.802
P-gp	0.689	0.275-1.725	0.427
P53	1.375	0.538-3.512	0.506
Tumor size	0.784	0.412-1.492	0.459

Cox proportional hazards regression model.

proteins are closely related to tumorigenesis. Our results indicated that, in HCC, CEP350 could be a cancer suppressor gene and may contribute to the disease progression by cell proliferation. Moreover, the CEP350 expression level could be used as an independent prognostic predictor in HCC patients.

We also analyzed the association between CEP350 expression and clinicopathological parameters. Results showed that a high level of CEP350 in HCC was significantly associated with TNM stage and P-gp. P-gp is an efflux transporter that affects the bioavailability of various drugs in the human body (11). The association of P-gp with CEP350 in HCC warrants further investigation.

A previous study reported that CEP350 recruits PPARα to discrete nuclear and cytoplasmic compartments. This recruitment regulates PPARα function (8). Moreover, the expression of PPARs regulates the cell cycle of hepatocytes and adipocytes in the liver, suggesting that PPARs may target cancer stem cells regulating the HCC differentiation process (12).

In conclusion, the investigation of the underlying mechanism of CEP350 regulation of HCC progression and differentiation will be valuable to identify novel therapeutic targets for HCC.

ACKNOWLEDGEMENTS

This study was funded by the Health Bureau of Nantong City (grant No. WKZL2018063, WKZL2018057) and the Nantong Science and Technology Bureau (grant No. JCZ18116, JCZ18057).

REFERENCES

1. Villanueva A, Llovet JM. Liver cancer in 2013: Mutational landscape of HCC--the end of the beginning. Nat Rev Clin Oncol 2014; 11(2):73-74.
2. Torre LA, Bray F, Siegel RL, Ferlay J, Lortet-Tieulent J, Jemal A. Global cancer statistics, 2012. CA Cancer J Clin 2015; 65(2):87-108.
3. El-Serag HB. Epidemiology of viral hepatitis and hepatocellular carcinoma. Gastroenterology 2012; 142(6):1264-73.
4. Gonzalez C. Centrosome function during stem cell division: the devil is in the details. Curr Opin Cell Biol 2008; 20(6):694-98.
5. Zyss D, Gergely F. Centrosome function in cancer: guilty or innocent? Trends Cell Biol 2009; 19(7):334-46.
6. Kumar A, Rajendran V, Sethumadhavan R, Purohit R. CEP proteins: the knights of centrosome dynasty. Protoplasma 2013; 250(5):965-83.
7. Kumar A, Purohit R. Computational screening and molecular dynamics simulation of disease associated nsSNPs in CENP-E. Mutat Res 2012; 738-739:28-37.
8. Patel H, Truant R, Rachubinski RA, Capone JP. Activity and subcellular compartmentalization of peroxisome proliferator-activated receptor alpha are altered by the centrosome-associated protein CAP350. J Cell Sci 2005; 118(Pt 1):175-86.
9. Wang Y, Ju L, Xiao F, et al. Downregulation of nucleolar and spindle-associated protein 1 expression suppresses liver cancer cell function. Exp Ther Med 2019; 17(4):2969-78.
10. Vogel A, Cervantes A, Chau I, et al. Hepatocellular carcinoma: ESMO Clinical Practice Guidelines for diagnosis, treatment and follow-up. Ann Oncol 2019; 30(5):871-73.
11. Marsousi N, Doffey-Lazeyras F, Rudaz S, Desmeules JA, Daali Y. Intestinal permeability and P-glycoprotein-mediated efflux transport of ticagrelor in Caco-2 monolayer cells. Fundam Clin Pharmacol 2016; 30(6):577-84.
12. Kimura O, Kondo Y, Shimosegawa T. PPAR Could Contribute to the Pathogenesis of Hepatocellular Carcinoma. PPAR Res 2012; 2012:574180.

LETTER TO THE EDITOR

CHANGES OF PLASMA VON WILLEBRAND FACTOR AND VON WILLEBRAND FACTOR-CLEAVING PROTEASE LEVELS IN PREGNANCY-INDUCED HYPERTENSION

TT. ZHANG[1], ZK. YU[2], CF. XIU[3], YT. BAI[4], M. PENG[1] and ZH. GUO[1]

[1]Department of Obstetrics, The First Hospital of Jilin University, Changchun City, China;
[2]Department of Neonatology, The First Hospital of Jilin University, Changchun City, China;
[3]Department of Gynaecology II, The First Hospital of Jilin University, Changchun City, China;
[4]Department of Gynaecology I, The First Hospital of Jilin University, Changchun City, China

Received November 27, 2019 – Accepted March 26, 2020

To the Editor,

Pregnancy-induced hypertension (PIH) is unique for parturients (1). Some patients with severe PIH also suffer from preeclampsia (2). Depending on the onset time, preeclampsia is divided into early-onset and late-onset types, and, depending on severity, is divided into mild and severe types. At present, the pathogenesis of hypertension during pregnancy (HDP) is not clear, but it has been shown that it is related to vascular endothelial damage (3). Blood of normal pregnant women is in a relatively hypercoagulable state and von Willebrand factor (VWF) levels are increased, which is a physiological protection mechanism of the body and can prevent excessive bleeding (4). In HDP patients, VWF levels are increased significantly (5). In addition, VWF can cause abnormal physiological changes of spiral arteries, reduce blood flow into the placenta (6), aggravate the damage of vascular endothelial cells, and show more complex pathological changes in PIH subjects (7). It has been shown that some thrombotic diseases are associated with a decreased activity of plasma Von Willebrand factor-cleaving protease (VWF-cp) (8). PIH patients are usually in a hypercoagulable state and prone to thrombosis. However, the changes of VWF-cp activity in PIH parturients and their pathophysiological significance remain unclear. In this study, the levels of VWF and VWF-cp and their activity in placental tissues were detected to explore their possible working mechanism, and to provide new data for the prognosis prediction, diagnosis, and treatment of PIH.

MATERIALS AND METHODS

From April 2018 to August 2019, 135 parturients admitted to The First Hospital of Jilin University were randomly collected. There were 35 patients in the control group (normal parturients) and 100 patients in the PIH group (38 patients with HDP, 34 patients with mPE (mild preeclampsia) and 28 patients with sPE (severe preeclampsia)). All patients were G1P1 (gravida 1 para 1), and other complications of pregnancy were excluded. The study was approved by the Ethics Committee of The First Hospital of Jilin University and all the patients signed informed consent for their participation.

Serological detection

Five ml of fasting cubital vein blood was collected from each patient in the morning, which was added with

Key words: pregnancy-induced hypertension; placental origin of preeclampsia; VWF and VWF-cp; regulation

Corresponding Author:
Dr Zhiheng Guo,
Department of Obstetrics,
The First Hospital of Jilin University,
71 Xinmin Street, Chaoyang District,
Changchun City, 130021, China
e-mail: guozhiheng_jl319@163.com

0393-974X (2020)
Copyright © by BIOLIFE, s.a.s.
This publication and/or article is for individual use only and may not be further reproduced without written permission from the copyright holder.
Unauthorized reproduction may result in financial and other penalties
DISCLOSURE: ALL AUTHORS REPORT NO CONFLICTS OF INTEREST RELEVANT TO THIS ARTICLE.

sodium citrate anticoagulant and centrifuged at 3000 r/min for 15 min to separate the plasma. 1 mL plasma sample was taken to detect the coagulation function indicators by using the immunoturbidimetric assay: prothrombin time (PT), activated partial thromboplastin time (APTT), thrombin time (TT) and fibrinogen (FIB). 0.5 mL plasma sample was used to detect the indicators of prethrombotic state by using ELISA: VWF, granular membrane protein 140 (GMP-140), thrombin -antithrombin complex (TAT) and D-dimer (D-D).

Sample collection

After delivery, tissues approximately 1cm×1cm×1cm were immediately collected from the maternal side of placenta at the attachment site of the umbilical cord, avoiding abnormal regions such as infarcts, calcification and bleeding in the placenta. The samples were washed with normal saline for 3 times, soaked in formalin for 24-48 h and embedded in paraffin for immunohistochemistry and staining.

Immunohistochemical staining

Paraffin-embedded samples were taken. The positive expression of VWF and VWF-cp was detected by immunohistochemistry. The slides were sealed with neutral balsam, which were observed under a microscope, and the images were taken.

Result interpretation: placental vascular endothelial cells with the same color (or no color) as the background were negative, and those with granules stained brownish yellow were positive. The back-up slides were observed under the microscope, and five fields of view were

Table I. *Baseline clinical data of all groups*

Indicators	Control group	HDP group	mPE group	sPE group
Age (years)	27.26±4.53	28.08±4.91	28.45±4.36	29.11±4.19
Gestation age (weeks)	38.65±1.57	38.44±2.13	37.36±3.03	36.26±3.14*
Placental weight (g)	714.52±59.25	703.16±62.02	628.29±48.35	611.27±73.27
Systolic blood pressure (mmHg)	112.40±9.66	119.00±11.46	121.00±13.36*	136.62±17.53*#&
Diastolic blood pressure (mmHg)	71.93±8.47	76.10±11.64	78.42±8.46*	84.15±10.14*#
PT(s)	12.31±0.64	10.58±0.77*	10.51±0.69*	10.20±0.75*
APTT(s)	30.16±2.54	27.10±2.65*	26.92±2.46*	26.05±2.69*
TT(s)	15.98±1.03	15.48±1.12*	15.35±1.16*	15.31±1.17*
FIB(g/L)	3.17±0.57	5.06±0.75*	5.52±0.83*	6.20±1.16*&
GMP-140(μg/L)	8.84±2.07	13.22±3.15*	24.46±3.25*#	32.38±3.52*#&
TAT(μg/L)	6.21±2.25	12.86±3.14*	21.46±3.26*#	36.76±4.11*#&
D-D(mg/L)	0.25±0.12	0.77±0.21*	1.46±0.35*#	1.83±0.46*#&
VWF(%)	83.28±10.04	135.26±23.29*	147.05±28.37*#	178.29±32.64*#&

*Note: PT: Prothrombin time; APTT: Activated Partial Thromboplastin Time; TT: Thrombin Time; FIB: Fibrinogen; GMP-140: Granular Membrane Protein 140; TAT: Thrombin AT complex; D-D :D-dimer. *P<0.05, compared with the control group; #P<0.05, compared with the HDP group; &P<0.05, compared with the mPE group.*

randomly selected. Semi-quantitative analysis was carried out using pathological image analysis software, and the overall mean grayscale value was calculated.

Statistical analysis

The experimental data were analyzed statistically using the SPSS 19.0 software. The data were expressed as mean ± standard deviation ($\bar{x} \pm s$). Intergroup comparisons were performed by using one-way ANOVA. LSD (least significant difference) test was used to compare across the groups, and P<0.05 indicated significant difference.

RESULTS

Clinical information

Patients from different groups were comparable in age (P>0.05). The gestation age was significantly different between the sPE group and control group (P<0.05). The systolic pressure of the sPE, mPE and HDP groups was significantly higher than that of the control group (P<0.05), and it was also significantly higher in the sPE group than in the mPE and HDP groups (P<0.05). The diastolic pressure of the sPE and mPE groups was significantly higher than that of the control group (P<0.05), and it was also significantly higher in the sPE group than in the HDP group (P<0.05).

In this study, FIB levels of the control group, HDP group, mPE group and sPE group were increased. In addition, FIB levels of HDP group, mPE group and sPE group were higher than those in the control group (P < 0.05). Therefore, the more severe the pregnancy hypertension, the higher the FIB level; the more obvious the hypercoagulable

Table II. *VWF expression level in the placental tissues*

Group	Control group	HDP group	mPE group	sPE group
VWF expression levels	87.64±9.43	128.54±20.29 *	153.96±22.84 *#	173.46±21.13 *#&
F value	49.726			

*Note: *P<0.05, compared with the control group; #P<0.05, compared with the HDP group; &P<0.05, compared with the mPE group.*

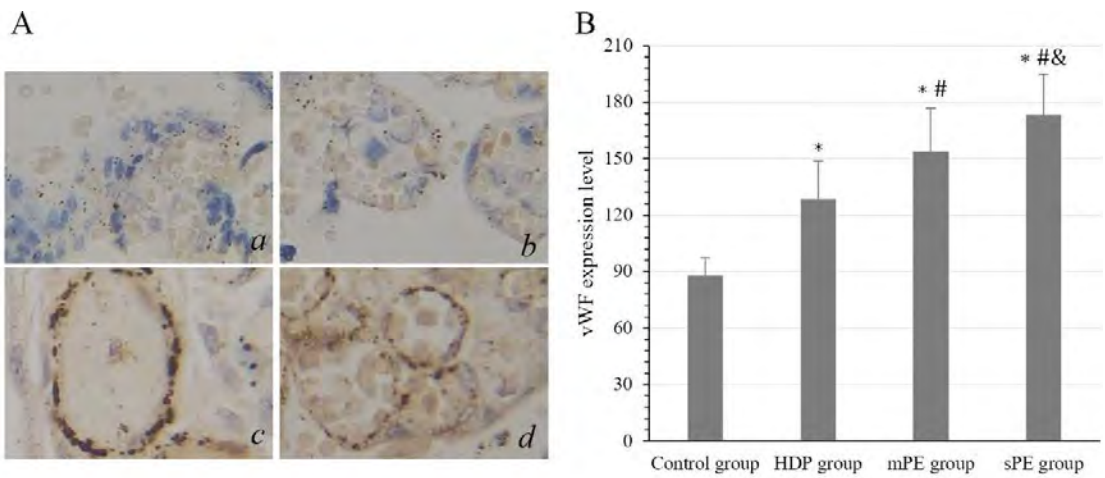


Fig. 1. *VWF expression levels. **A**) VWF expression detected by immunohistochemistry (a: Control group; b: HDP group; c: mPE group; d: sPE group); **B**) Statistical plot of VWF expression levels, *P<0.05, compared with the control group; #P<0.05, compared with the HDP group; &P<0.05, compared with the mPE group.*

state, and the more likely it was to form a thrombus.

VWF, GMP-140, TAT and D-D levels of the HDP, mPE and sPE groups were significantly different from those of the control group (P<0.05). These indicators in the mPE and sPE groups were significantly different from those of the HDP group (P<0.05). There were also significant differences between the sPE group and mPE group (P<0.05).

In this study, D-D levels of PIH patients were increased, and the more severe the disease, the higher the level. It was suggested that PIH patients may have villous necrosis, placental ischemia and severe intravascular cell damage, and a large amount of tissue thromboplastin was released, thereby leading to thrombosis. The data are shoown in Table I.

Table III. *VWF-cp expression level*

Group	Control group	HDP group	mPE group	sPE group
VWF-cp expression levels	157.22±31.47	128.52±22.05 *	105.44±23.14 *#	79.65±18.56 *#&
F value	36.193			
P value	0.001			

*Note: *P<0.05, compared with the control group; #P<0.05, compared with the HDP group; &P<0.05, compared with the mPE group.*

Table IV. *Comparison of VWF/VWF-cp expression ratios in the placental tissues across the groups*

Group	Control group	HDP group	mPE group	sPE group
VWF/VWF-cp	0.54±0.13	1.05±0.16 *	1.38±0.14 *#	1.90±0.17 *#&
F value	15.026			
P value	0.003			

*Note: *P<0.05, compared with the control group; #P<0.05, compared with the HDP group; &P<0.05, compared with the mPE group.*

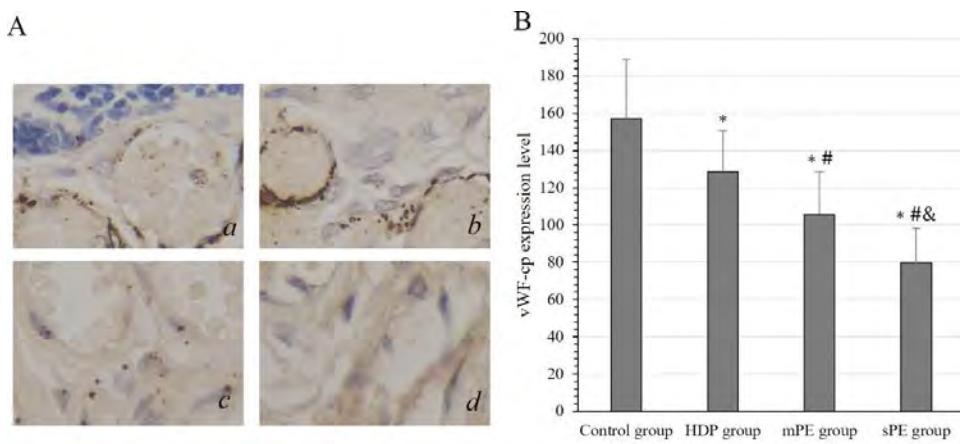


Fig. 2. *VWF-cp expression. **A)** VWF-cp expression detected by immunohistochemistry a: Control group; b: HDP group; c: mPE group; d: sPE group. **B)** Statistical plot of VWF-cp expression levels. *P<0.05, compared with the control group; #P<0.05, compared with the HDP group; &P<0.05, compared with the mPE group.*

VWF expression levels

The positive expression of VWF in each group was mainly found in the membrane and cytoplasm of placental vascular endothelial cells. As shown in Table II and Fig.1, the VWF expression level in the placental tissues of the PIH group was much higher than that in the control group ($P<0.05$). As PIH deteriorated, the plasma VWF expression in the placental tissues increased gradually ($P<0.05$). The plasma VWF level showed an increasing trend over time.

VWF-cp expression levels

The positive expression of VWF-cp in each group was mainly found in the membrane and cytoplasm of placental vascular endothelial cells. As shown in Table III and Fig.2, the VWF-cp expression in the placental tissues of the PIH group decreased considerably compared with the control group ($P<0.05$). As PIH deteriorated, the VWF-cp expression level in the mPE group was significantly lower than that of the sPE group ($P<0.05$).

VWF/VWF-cp expression ratios

The VWF/VWF-cp expression ratio in the PIH group was significantly higher than that of the control group ($P<0.05$). As PIH deteriorated, the VWF/VWF-cp expression ratio increased gradually ($P<0.05$) (Table IV).

DISCUSSION

Fetal growth restriction (FGR) is the most common complication in the fetus of PIH mothers (9), leading to an extremely low survival rate of the newborns. In the present study, the gestation age of the sPE group was significantly younger compared with the control group ($P<0.05$). Generally speaking, PIH aggravates at the gestation age of 30-32 weeks. The pregnancy must be terminated at an appropriate time, and that explains why the gestation age was younger in the sPE group. The results showed that PIH pregnant women had coagulation dysfunction, and the more severe the condition, the more obvious the dysfunction, and the more likely it was to form a thrombus. In addition, PIH patients may have villous necrosis, placental ischemia and severe intravascular cell damage, and release abundant tissue thromboplastin (10), thereby causing thrombosis.

Study has suggested (11) that during normal pregnancy, the VWF level increases considerably. In the present study, we found that the plasma VWF levels of the HDP, mPE and sPE groups were significantly higher than those of the control group. The more severe the PIH, the higher the plasma VWF level would be, thereby indicating more severe damage to the endothelial cells. Platelet activation is an important condition leading to thrombosis (12).

To conclude, PIH patients were in a hypercoagulable and prethrombotic state, and the higher the severity of PIH, the more violent the changes in the indicators of the coagulation function and prethrombotic state were. Abnormal expressions of VWF and VWF-cp in the placental tissues of PIH parturient women damaged the placental vascular endothelial cells and led to tiny placental villi. This finally resulted in the shedding of vascular endothelial cells and placenta-derived changes, thereby influencing the occurrence and development of PIH.

REFERENCES

1. Kintiraki E, Papakatsika S, Kotronis G, Goulis DG, Kotsis V. Pregnancy-Induced hypertension. Hormones (Athens) 2015; 14(2):211-23.
2. Kim JS, Kang EJ, Woo OH, et al. The relationship between preeclampsia, pregnancy-induced hypertension and maternal risk of breast cancer: a meta-analysis. Acta Oncol 2013; 52(8):1643-48
3. Deng L, Bremme K, Hansson LO, Blombäck M. Plasma levels of von Willebrand factor and fibronectin as markers of persisting endothelial damage in preeclampsia. Obstet Gynecol 1994; 84(6):941-45.
4. Karthikeyan VJ, Blann AD, Baghdadi S, Lane DA, Gareth Beevers D, Lip GY. Endothelial dysfunction in hypertension in pregnancy: associations between circulating endothelial cells, circulating progenitor cells and plasma von Willebrand factor. Clin Res Cardiol 2011; 100(6):531-37.
5. Vinayagam V, Bobby Z, Habeebullah S, Chaturvedula L, Bharadwaj SK. Plasma markers of endothelial dysfunction in patients with hypertensive disorders of

pregnancy: a pilot study in a South Indian population. J Matern Fetal Neonatal Med 2016; 29(13):2077-82

6. Wang C, Jin L, Chen J. The change of plasma von Willebrand factor and endothelin levels in patients with pregnancy induced hypertension. Zhonghua Fu Chan Ke Za Zhi 2001; 36(4):212-14.
7. Jin LP, Wang CH, Chen JL. Changes in plasma von Willebrand factor and nitric oxide levels in patients with pregnancy induced hypertension. Hunan Yi Ke Da Xue Xue Bao 2001; 26(5):477-79.
8. Castaman G. Changes of von Willebrand Factor during Pregnancy in Women with and without von Willebrand Disease. Mediterr J Hematol Infect Dis 2013; 5(1):e2013052.
9. Kovo M, Schreiber L, Ben-Haroush A, Wand S, Golan A, Bar J. Placental vascular lesion differences in pregnancy-induced hypertension and normotensive fetal growth restriction. Am J Obstet Gynecol 2010; 202(6):561.e1-5.
10. Ren Y, Wang H, Qin H, Yang J, Wang Y, Jiang S, Pan Y. Vascular Endothelial Growth Factor expression in peripheral blood of patients with pregnancy induced hypertension syndrome and its clinical significance. Pak J Med Sci 2014; 30(3):634-37.
11. Ewodo S, Nguefack CT, Adiogo D, Etong EM, Beyiha G, Belley PE. Changes of Von Willebrand factor concentration during pregnancy. Ann Biol Clin (Paris) 2014; 72(3):292-96.
12. Dinas K, Hatzipantelis E, Karasmanis K, Zepiridis L, Mavromatidis G, Bontis J. Improving the outcome of pregnancy in essential thrombocythaemia: The role of aspirin. J Obstet Gynaecol 2008; 28(2):236-37.

LETTER TO THE EDITOR

IS p16 EXPRESSION STILL A SURROGATE MARKER FOR HUMAN *PAPILLOMAVIRUS* INFECTION IN ORAL SQUAMOUS CELL CARCINOMAS?

M. ŚNIETURA[1], A. BREWCZYNSKI[2], D. WANICZEK[3], A. KOPEC[1], A. STANEK-WIDERA[1], M. MUC-WIERZGOŃ[4] and T. RUTKOWSKI[2]

[1]Tumor Pathology Department, Maria Sklodowska-Curie National Research Institute of Oncology, Gliwice Branch, Poland; [2]I Radiotherapy and Chemotherapy Clinic, Maria Sklodowska-Curie National Research Institute of Oncology, Gliwice Branch, Poland; [3]Department of Surgical Nursing and Surgery Propedeutics, Chair of General, Colorectal and Trauma Surgery, SHS in Katowice, Medical University of Silesia, Katowice, Poland; [4]Department of Internal Medicine, Medical University of Silesia, Katowice, Poland

Received October 5, 2019 – Accepted March 20, 2020

To the Editor,

High-risk human papillomavirus (HR-HPV) plays a causative role in the pathogenesis of a significant proportion of oropharyngeal squamous cell carcinomas. The detection of HR-HPV genome in tumor tissue samples or demonstration of $p16^{INK4A}$ accumulation by immunohistochemistry are considered to be equivalent diagnostic methods in these cases, and the $p16^{INK4A}$ expression is also known as a surrogate marker of HPV infection (1). On the other hand, there is a growing number of studies where $p16^{INK4A}$ expression is reliable evidence of HPV infection only in the oropharynx, but not in other head or neck locations (2). The role of HPV in the pathogenesis of oral squamous cell cancers (OSCC) is still debatable. The prevalence of HPV infection in this location ranges from zero to several percent, depending on the reports. Many of these studies are based on a single diagnostic method, i.e. either PCR/ISH or immunohistochemistry, and only a few simultaneously use two or more methods. This unconfirmed assumption that $p16^{INK4A}$ expression is a surrogate marker for HPV infection in the case of OSCC can lead to an observed discrepancy in study results concerning other locations. Therefore, in the present study, to assess the prevalence of HR-HPV infections, we proposed a double-check algorithm involving detection of viral DNA with subsequent demonstration of $p16^{INK4A}$ accumulation as evidence of its transcriptional activity.

MATERIALS AND METHODS

Sixty-eight formalin-fixed and paraffin-embedded squamous cell carcinoma samples from the oral cavity were examined for protein $P16^{INK4A}$ expression that is considered a surrogate marker of HR-HPV infection. This was demonstrated by immunohistochemistry (IHC), using ready-to-use E6H4 monoclonal antibody and Benchmark Ultra automated staining system (Roche Diagnostics). According to the widely accepted criteria, only a strong homogenous chromogen concentration in over 80% of cancer cells was considered characteristic of HR-HPV infection (3).

Key words: HPV infection; oral squamous cell cancer; $p16^{INK4A}$ expression

Corresponding Author:
Prof. Małgorzata Muc-Wierzgoń,
Dept. of Internal Medicine,
Medical University of Silesia,
41-902 Bytom, Żeromskiego 7 st, Poland
Tel.: +48 32 2812122 - Fax: +48 32 2812122
e-mail: mwierzgon@sum.edu.pl

0393-974X (2020)
Copyright © by BIOLIFE, s.a.s.
This publication and/or article is for individual use only and may not be further reproduced without written permission from the copyright holder.
Unauthorized reproduction may result in financial and other penalties
DISCLOSURE: ALL AUTHORS REPORT NO CONFLICTS OF INTEREST RELEVANT TO THIS ARTICLE.

In all the examined cases, the presence and types of HR-HPV DNA in the tumor cells was confirmed using a commercially available test, Sacace HPV Genotypes 14 Real-TM (Sacace Biotechnologies Srl, Italy), which is a real-time PCR Kit for quantitative detection and genotyping of HR-HPV (16, 18, 31, 33, 35, 39, 45, 51, 52, 56, 58, 59, and 68). The first step was to isolate the genomic DNA from all tumor tissue samples by using Mag Core Genomic DNA FFPE One-step Kit and MagCore Nucleic Acids Automatic Extractor HF16-Plus (RBC Bioscience Corp. Taiwan). Next, the reaction mixtures of 15μl isolated DNA (25ng/10μl) and controls were prepared and cycled in ViiA7 Real Time Cycler (Life Technologies) according to the manufacturer's recommendations. Only cases with both $p16^{INK4A}$ expression and HR-HPV DNA amplification were classified as truly positive.

All procedures performed in the study involving human participants were in accordance with the ethical standards of the institutional and/or national research committee and with the 1964 Declaration of Helsinki and its later amendments or comparable ethical standards. All subjects gave their written informed consent. For this type of study, the institute's committee approval is not required.

RESULTS

None of the fourteen HR-HPV types was found in our patients (0/68; 0.0%). In 6 cases (6/68; 8.8%), immunostaining pattern characteristic of HR-HPV infection was observed (Fig. 1A). However, none of HR-HPV genomes was detected (false positive by IHC alone). As a result, they were classified as truly negative (Table I). In one case, the simultaneous occurrence of two clearly demarcated tumor cell populations was observed. One of them was characterized by a strong expression of $p16^{INK4A}$, whereas in the other one no immunostaining was observed (Fig. 1B).

Table I. *Summary of the results of HR-HPV genome detection and $p16^{INK4A}$ expression in the tumor tissue samples.*

HPV status	Number of cases	
	Positive	Negative
HR-HPV DNA	0 (0.0%)	68 (100.0%)
$p16^{INK4A}$	6 (8.8%)	62 (91.2%)
DNA/$p16^{INK4A}$	0 (0.0%)	68 (100.0%)

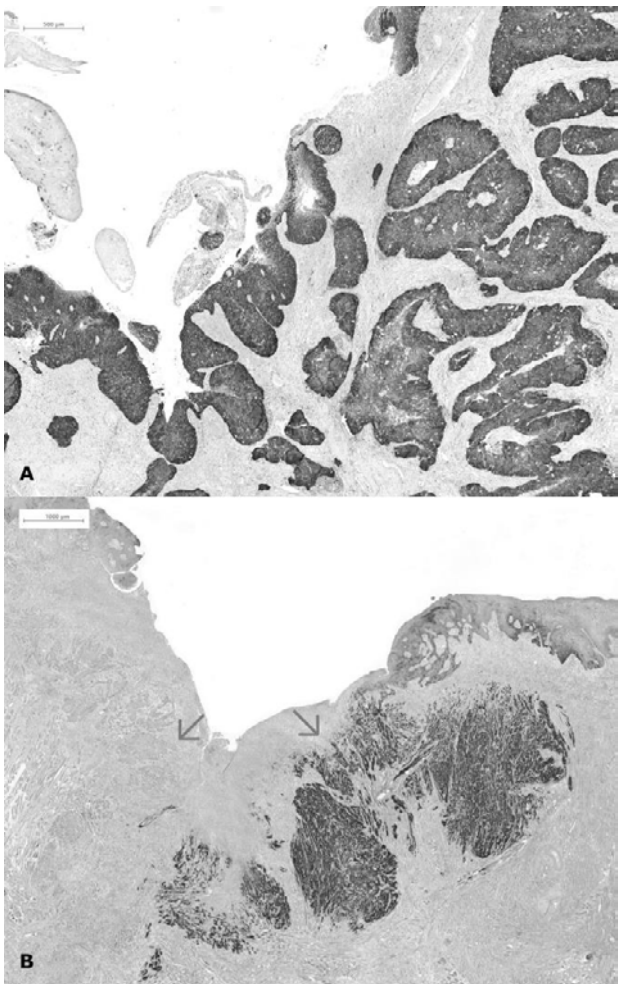


Fig. 1. *Microphotographs of the representative HR-HPV-DNA-negative tumors demonstrating strong expression of $p16^{INK4A}$. Two distinct neoplastic cell clones with different $p16^{INK4A}$ expression observed in one case are marked with arrows (**B**). Immunostaining with anti-human $p16^{INK4A}$ monoclonal antibody clone E6H4™ (Roche Laboratories AG, CINTech® Histology Kit).*

DISCUSSION

The expression of $p16^{INK4A}$ is recognized as a surrogate marker for HR-HPV infection in head and neck cancers. Many clinical trials are based on this assumption (4–6), and the expression of $p16^{INK4A}$ has recently been included in the TNM classification of oropharyngeal tumors. However, there are critical voices that challenge the value of the immunohistochemical evaluation of $p16^{INK4A}$ alone as a technique sufficient to confirm HR-HPV-

dependent tumor etiology at locations other than the oropharynx (4), as well as in the oropharynx (2, 7). Even more ambiguous results have been published regarding the role of HR-HPV in oral cancers and the expression of $p16^{INK4A}$ as a surrogate marker of HR-HPV infection. In this study, the prevalence of the papillomaviruses from the high oncogenic risk group and the expression of $p16^{INK4A}$ as a marker of the biological activity of the virus were considered. No viral genome was detected in any of the analyzed cases. In this respect, the obtained results were in line with some reports of other authors on the lack or very low percentage of HPV-positive tumors in this area:

Chen et al. analyzed tissue DNA samples from 40 Chinese patients with OSCC using real-time PCR assay. Suspicious positive samples underwent sequencing to eliminate those that were falsely positive. Those authors found that none of the tissue samples was positive for HPV16, using both methods (8). Vidal Loustal et al. assessed the incidence of HPV infection in 155 cases of squamous cell carcinoma of the oral cavity. The detection of HPV was conducted using PCR followed by *in situ* hybridization and confirmed by immunohistochemical demonstration of $P16^{INK4A}$ expression in histological sections. Their study showed the presence of HPV-DNA in 3.3% of cases. In contrast, 7.7% of cases showed an overexpression of the $p16^{INK4A}$ (9). Less consistent data on the presence of HPV and $p16^{INK4A}$ expression were reported by other authors. Rushatamukayanunt et al. analyzed OSCC surgical specimens from 40 young and from 40 older patients using the polymerase chain reaction-based test, and $p16^{INK4A}$ surrogate marker of HPV infection using immunohistochemical technique. Only two (5%) young patients and one (2.5%) older subject were positive for HPV DNA. $p16^{INK4A}$ overexpression was found in six (15%) young patients. Those authors concluded that HPV was less likely to lead to OSCC in young Japanese patients and HPV DNA status did not significantly correlate with $p16^{INK4A}$ expression levels (10).

In two subsequent reports, the authors presented a significantly higher percentage of HPV-positive cancers using both PCR and IHC tests. Adilbay et al. assessed the status of HPV of 41 oral tumors using qualitative PCR detecting and differentiating 12 high-risk human papillomaviruses (types 16, 18, 31, 33, 35, 39, 45, 51, 52, 56, 58, 59) with subsequent confirmation of the status with demonstrating $p16^{INK4A}$ overexpression. Of 41 tumors, five were HPV DNA positive and six $p16^{INK4A}$ IHC positive, which gave the rate of 12.2% (11). In their prospective study on 50 cases of suspected oral cancer, Pathak et al. reported 6 HR-HPV positive tumor tissue samples (12%), of which 5 were simultaneously overexpressing $p16^{INK4A}$ (83.3%). Additionally, they reported 26 $p16^{INK4A}$-overexpressing HPV-negative tumors (59.1% of false positive cases based on IHC alone) (12). Based on our own study and the reports of other authors, it can be concluded that the causal contribution of HR-HPV in the pathogenesis of the vast majority of oral cancers is unlikely, and the use of $p16^{INK4A}$ expression as the only marker for HPV infection in this location is not justified.

REFERENCES

1. El-Naggar AK, Westra WH. p16 expression as a surrogate marker for HPV-related oropharyngeal carcinoma: a guide for interpretative relevance and consistency. Head Neck 2012; 34(4):459-61.
2. Jouhi L, Hagström J, Atula T, Mäkitie A. Is p16 an adequate surrogate for human papillomavirus status determination? Curr Opin Otolaryngol Head Neck Surg 2017; 25(2):108-12.
3. Ryu HJ, Kim EK, Heo SJ, Cho BC, Kim HR, Yoon SO. Architectural patterns of p16 immunohistochemical expression associated with cancer immunity and prognosis of head and neck squamous cell carcinoma. APMIS Acta Pathol Microbiol Immunol Scand 2017; 125(11):974-84.
4. Lassen P, Eriksen JG, Hamilton-Dutoit S, Tramm T, Alsner J, Overgaard J. Effect of HPV-associated p16INK4A expression on response to radiotherapy and survival in squamous cell carcinoma of the head and neck. J Clin Oncol Off J Am Soc Clin Oncol 2009; 27(12):1992-98.
5. Chera BS, Amdur RJ, Tepper J, et al. Phase 2 trial of de-intensified chemoradiation therapy for favorable-risk human papillomavirus-associated oropharyngeal squamous cell carcinoma. Int J Radiat Oncol Biol

Phys 2015; 93(5):976-85.
6. Garnaes E, Frederiksen K, Kiss K, , et al. Double positivity for HPV DNA/p16 in tonsillar and base of tongue cancer improves prognostication: Insights from a large population-based study. Int J Cancer 2016; 139(11):2598-605.
7. Prigge E-S, Arbyn M, von Knebel Doeberitz M, Reuschenbach M. Diagnostic accuracy of p16INK4a immunohistochemistry in oropharyngeal squamous cell carcinomas: A systematic review and meta-analysis. Int J Cancer 2017; 140 (5):1186-98.
8. Chen X-J, Sun K, Jiang W-W.Absence of high-risk HPV 16 and 18 in Chinese patients with oral squamous cell carcinoma and oral potentially malignant disorders. Virol J 2016; 13:81.
9. Vidal Loustau AC, Dulguerov N, Curvoisier D, McKee T, Lombardi T. Low prevalence of HPV-induced oral squamous cell carcinoma in Geneva, Switzerland. Oral Dis 2019; 25(5):1283-90.
10. Rushatamukayanunt P, Morita K, Matsukawa S, Harada H, Shimamoto H, Tomioka H, Omura K. Lack of association between high-risk human papillomaviruses and oral squamous cell carcinoma in young Japanese patients. Asian Pac J Cancer Prev APJCP 2014; 15(10):4135-41.
11. Adilbay D, Adilbayev G, Kidirbayeva G, et al. HPV infection and P16 expression in oral and oropharyngeal cancer in Kazakhstan. Infect Agent Cancer 2018; 13:2.
12. Pathak A, Singh M, Agarwal A, Amit S. Determination of p16 overexpression as an indicator of human papillomavirus infection in oral dysplasia and carcinoma. Indian J Dent Res Off Publ Indian Soc Dent Res 2017; 28(4):418-23.

LETTER TO THE EDITOR

NOVEL COMPOUND HETEROZYGOUS MUTATIONS IN GANGLIOSIDE GM3 SYNTHASE DEFICIENCY

R-X. LIANG[1], H. ZHENG[1] and Y-L.YANG[2]

[1]Henan University of Chinese Medicine, Zhengzhou, China; [2]Department of Pediatrics, First Hospital, Peking University, Beijing, China

Received June 17, 2019 – Accepted October 30, 2019

To the Editor,

GM3 synthase deficiency was first reported by Amish Simpson in 2004 (1). It is a rare hereditary neurometabolic disease that is presently considered to be a monogenic genetic disease with autosomal recessive inheritance. Its phenotype is complex, and the clinical features include irritability, intractable epilepsy, feeding difficulties, cognitive deficit, deafness and blindness. The present study reviews the clinical data and genetic test results of the first genetically-diagnosed GM3 synthase deficiency in China, in order to provide early help for the patients.

Case report

An ethics approval was not applicable. A written informed consent was obtained from the guardian of the participant.

An 11-month-old girl, who was referred to our hospital, had normal development until the age of two months, but later developed psychomotor regression. The patient was born after 39 weeks of gestation at 3.5 kg by cesarean section, and was the second baby born to healthy and non-consanguineous Chinese parents, whose first baby was a healthy girl. At two months old, the patient underwent an overall pediatric evaluation for the first time. During the evaluation, the patient was no longer capable of making eye contact, and vertical nystagmus was noted. Furthermore, the patient demonstrated appropriate head control, but could not roll over. The patient's height, weight and head circumference were 51 cm, 5 kg and 37 cm, respectively. In addition, the patient presented with irritability, feeding difficulties and intermittent convulsion. Blood tests were performed at a local clinic, and revealed elevated aspartate aminotransferase (AST, 129 U/L; reference range: 0–40 U/L) and alanine aminotransferase (ALT, 103 U/L; reference range: 0–31 U/L). The electrolytes, kidney function, thyroid function, lactate and pyruvate metabolic tests revealed no abnormalities (Table I). Furthermore, the patient had no dysmorphism or malformation, and the general examinations were unremarkable. The abdominal ultrasound revealed liver enlargement. The brain magnetic resonance imaging revealed that the subarachnoid space of the bilateral fronto-temporal area was widened, and the white matter development was 1-2 months old (Fig. 1). The electroencephalogram (EEG) revealed a localized abnormal discharge (Fig. 2). When referred to Beijing University First Hospital at eight months old, the patient presented with developmental stagnation, difficult feeding, vomiting

Key words: Ganglioside GM3 synthase; intellectual disability; severe irritability; novel compound heterozygous mutations; ST3GAL5 gene

Corresponding Author:
Dr Hong Zheng,
Department of Pediatrics,
The First Affiliated Hospital
of Henan University of Chinese Medicine,
No. 19 of Renmin Street, Jinshui District,
Zhengzhou 450008, China
Tel.: +86 10 6628 1175 - Fax: +86 10 6628 1175
e-mail: zhengh20135784@163.com

0393-974X (2020)
Copyright © by BIOLIFE, s.a.s.
This publication and/or article is for individual use only and may not be further reproduced without written permission from the copyright holder.
Unauthorized reproduction may result in financial and other penalties
DISCLOSURE: ALL AUTHORS REPORT NO CONFLICTS OF INTEREST RELEVANT TO THIS ARTICLE.

and constipation. On examination, her height, weight and head circumference were 68 cm, 7.5 kg and 41.4 cm, respectively. On the urinary analysis, pterin, mucopolysaccharide and mitochondrial gene detection were negative, even though the acid α-glucosidase activity was 18.3 (reference range: 25.1-94.3), prompting Pompe disease. However, the clinical features and gene analysis were not supported. Despite the active physical therapy and rehabilitation, the patient did not make progress in development. At the time of this report, the patient was 11 months old, and could not sit independently, roll over, or make nonverbal responses.

Furthermore, trio-exome sequencing was performed on the patient and the unaffected parents. The tests were of good quality, and the subsequent variant discovery processes revealed novel, compound heterozygous and missense variants in *ST3GAL5* (NM_003896) [c.991G>C/p.(Asp331Asn) and c.668G>A/p.(Glu223Gly)], which were the only candidates that fitted the present criteria. The p.(Glu223Gly) variant was not found in the 1,000 genomes, gnomAD, or Ex AC databases, while p.(Asp331Asn) was found with a very low frequency (minor allele frequency 1/6400), making the expected probability of detecting such compound heterozygous carriers <1/246174 (gnomAD databases). The mutated amino acid residues were highly conserved among the vertebrate orthologs. These were validated by Sanger sequencing in the proband, as well as in the other unaffected sibling. The unaffected parents were heterozygous carriers of each variant. For the targeted treatment, the investigators attempted to use the intravenous infusion of ganglioside supplement (monosialotetrahexosyl ganglioside [20 mg/d] for two weeks).

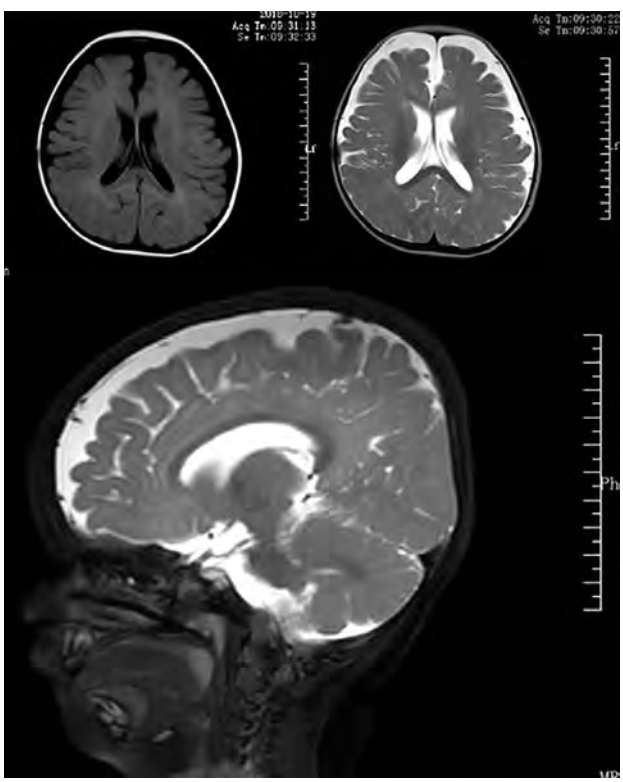


Fig. 1. *Brain magnetic resonance imaging revealed that the subarachnoid space of the bilateral fronto-temporal area was widened, and the white matter development was 1-2 months old.*

DISCUSSION AND CONCLUSION

GM3 synthase deficiency is a rare neurometabolic disorder inherited as an autosomal recessive trait, which clinically manifests with severe developmental delay/intellectual disability and epilepsy during infancy (1-4). This disease may also present with irritability during early infancy, failure to thrive, cutaneous dyspigmentation, blindness and deafness (1-8). To date, only a single mutation in the *ST3GAL5* gene has been reported (9). The molecular defect in the first step of the ganglioside synthesis pathway causes a decrease in levels of GM3 and other downstream complex gangliosides (Fig. 3), which might be important during the early and late stages of nervous system development (2).

According to statistics, no evidence has revealed a clear correspondence between the type and location of the *ST3GAL5* gene mutation and GM3 synthase phenotype (3, 7). The *ST3GAL5* gene has genetic heterogeneity, and the same gene mutation can have different clinical manifestations, and even the same gene point mutation. Furthermore, clinical performance can also significantly differ. Hence, it is difficult to make a clinical diagnosis merely by clinical phenotype. This should be combined with molecular genetic analysis to help in the clinical diagnosis from the gene level. In the present case, novel compound heterozygous *ST3GAL5* mutations

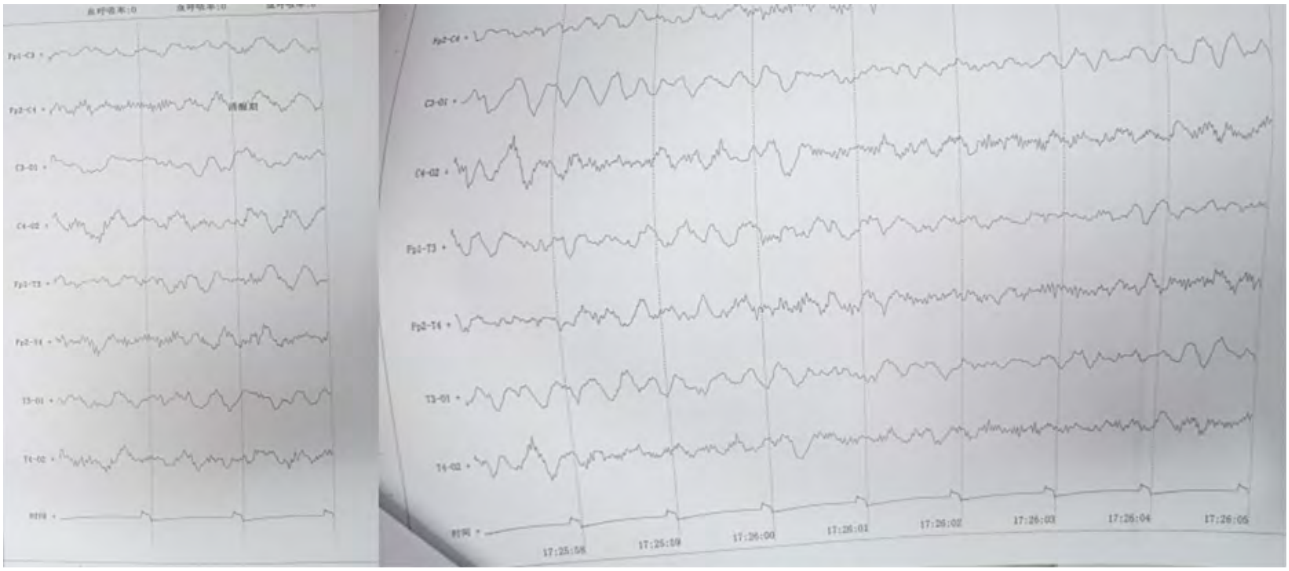


Fig. 2. *The electroencephalogram revealed a localized abnormal discharge.*

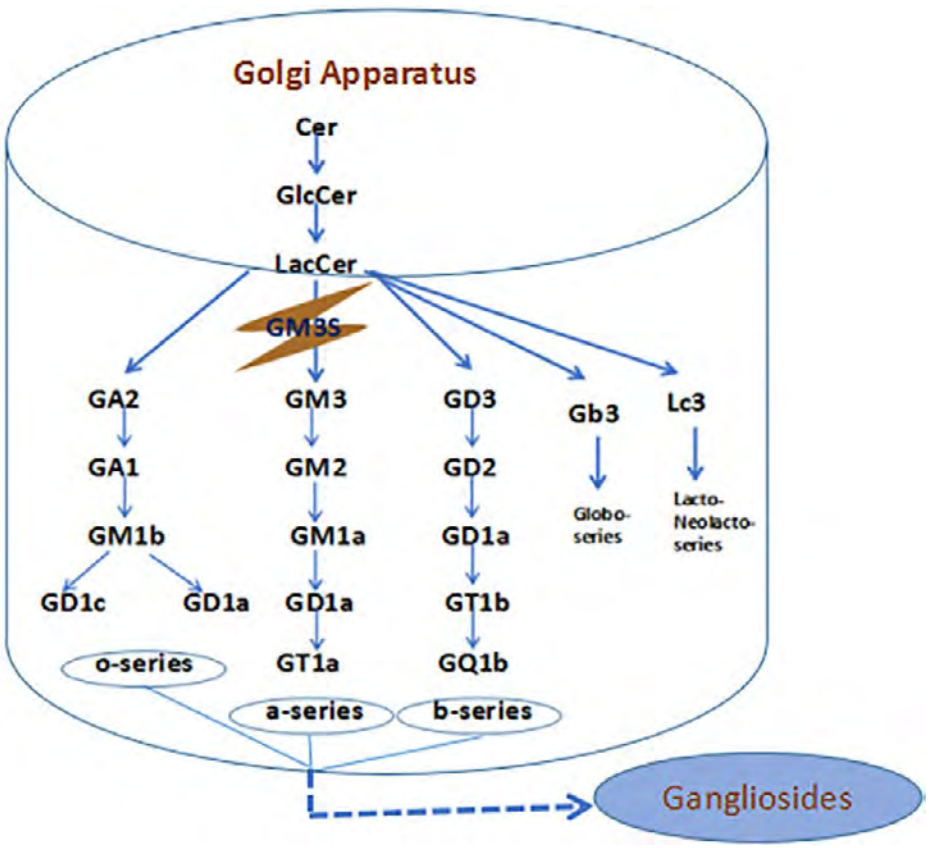


Fig. 3. *Schematic representation of the major pathways of ganglioside biosynthesis. The monosialoganglioside GM3 was derived from lactosylceramide through the glycosyltransferase, "GM3 synthase," which was encoded by the ST3GAL5 gene. GM3 is the common precursor for both "a" and "b" series of gangliosides.*

Table I. *Laboratory findings (blood tests)*

Test	Result	Reference range
At the first visit (2 months of age)		
AST (U/L)	103	0–40
ALT (U/L)	129	0–31
UN (mmol/L)	2.2	25-8.2
Creatinine (umol/L)	16.1	45-84
CK (U/L)	68	20–200
LDH (U/L)	324	109-245
Na (mmol/L)	136	135-145
K (mmol/L)	5.7	35–5.3
Cl (mmol/L)	102	96–108
Ca (mg/d L)	2.58	2.1–2.8
HCY(umol/L)	9.5	5-15
Free T3(pmol/L)	6.3	2.77-6.47
Free T4(pmol/L)	13.8	11.5-22.7
TSH (mIU/L)	2.78	0.35-6.5
XA (umol/L)	55	9-47
IgA(g/L)	0.15	0.7-1
IgG(g/L)	3.8	7-16
IgM(g/L)	0.32	0.4-2.3
IgE(g/L)	2.4	0-15
CP (mg/L)	245.5	230-440
On admission (4 months of age)		
AST (U/L)	52	0–40
ALT (U/L)	47.9	0–31
On admission (8 months of age)		
WBC (10^9/ L)	7.23	10.0–20.0
RBC (10^{12}/ L)	4.67	3.2-5.2
Hemoglobin (g/L)	117	120-160
Hematocrit (%)	37.6	35.0-43.0
PLT (10^9/ L)	330	100-300
AST (U/L)	38	0-45
ALT (U/L)	14	0-40
NeoPterin(N)(mmol/molCreatinine)	0.44	0.29-2.61
BioPterin(N)(mmol/molCreatinine)	1.07	0.35-2.67
B/(N+B)*100	70.86	42.7-75.9
the acid α-glucosidase activity	18.3	25.1-94.3

[c.991G>A/p.(Asp331Asn) and c.668A>G/p.(Glu223Gly)] were identified, which have not been previously reported. The pathogenicity of this missense mutation was validated by *in silico* prediction using the Sorting Intolerant From Tolerant (SIFT) version. The mutation was predicted to be likely deleterious for *ST3GAL5*.

Compared with previously reported cases with mutations, neither early onset refractory epilepsy, nor blindness were observed in the present case. The clinical symptoms associated with decreased mucopolysaccharidase activity and other lack of metabolic abnormalities led the investigators to look for mucopolysaccharidosis. At this stage, it could not be determined whether the reduction in acidic α-glucosidase activity was correlated with the clinical characteristics of the child. Thereafter, it was found that the skeleton presented no typical symptoms, and the gene involved is known to be free of mutations. Since the nonspecific symptoms only presented with an abnormal EEG, it was difficult to consider genetic analysis as a dierential diagnosis from the beginning. Finally, the patient was diagnosed and detected by genetic analysis. Therefore, some improvements in clinical symptoms, and developmental and cognitive scores were observed through the intravenous infusion of ganglioside supplement to the affected child. However, this remained as a concern for the observed improvements, which remained transient and slowly phased out during the study (10, 11).

The present study has some limitations. Although this variant is rare and affects a conserved residue, the family was too small to implicate the variant from a genetic standpoint. Furthermore, functional studies were not performed to help support or rule out the pathogenicity in the present study.

In conclusion, the first case of GM3 synthase deficiency in the Chinese population, and the second report of novel compound heterozygous *ST3GAL5* variants to date was presented. This case broadens the phenotypic and genetic spectrum of GM3 synthase deficiency due to *ST3GAL5* variants. Patients with intellectual disability or irritability, failure to thrive, liver damage and vomiting should be suspected with GM3 synthase deficiency, which is a disorder of ganglioside biosynthesis. However, merely the identification of the causative gene allowed for the proposal of an appropriate genetic counseling and reliable prenatal diagnosis.

ACKNOWLEDGEMENT

This study was funded by the National Key Research and Development Program of China (2017YFC1001704).

REFERENCES

1. Simpson MA, Cross H, Proukakis C, et al. Infantile-onset symptomatic epilepsy syndrome caused by a homozygous loss-of-function mutation of GM3 synthase. Nat Genet 2004; 36:1225-29.
2. Fragaki K, Ait-El-Mkadem S, Chaussenot A, et al. Refractory epilepsy and mitochondrial dysfunction due to GM3 synthase deficiency. Eur J Hum Genet 2013; 21:528-34.
3. Wang H, Bright A, Xin B, Bockoven JR, Paller AS. Cutaneous dyspigmentation in patients with ganglioside GM3 synthase deficiency. Am J Med Genet A 2013; 161:875-79.
4. Boccuto L, Aoki K, Flanagan-Steet H, et al. A mutation in a ganglioside biosynthetic enzyme, *ST3GAL5*, results in salt & pepper syndrome, a neurocutaneous disorder with altered glycolipid and glycoprotein glycosylation. Hum Mol Genet 2014; 23:418-33.
5. Yoshikawa M, Go S, Suzuki S, et al. Ganglioside GM3 is essential for the structural integrity and function of cochlear hair cells. Hum Mol Genet 2015; 24:2796-807.
6. Inokuchi JI, Go S, Yoshikawa M, Strauss K. Gangliosides and hearing. Biochim Biophys Acta Gen Subj 2017; 1861:2485-93.
7. Wang H, Wang A, Wang D, Bright A, Sency V, Zhou A, Xin B. Early growth and development impairments in patients with ganglioside GM3 synthase deficiency. Clin Genet 2016; 89:625-29.
8. Lee JS, Yoo Y, Lim BC, Kim KJ , Song J , Choi M , Chae JH . GM3 synthase deficiency due to *ST3GAL5* variants in two Korean female siblings: Masquerading as Rett syndrome-like phenotype. Am J Med Genet A 2016; 170:2200-205.

9. Gordon-Lipkin E , Cohen JS , Srivastava S , Soares BP , Levey E , Fatemi A . *ST3GAL5*-Related Disorders: A deficiency in ganglioside metabolism and a genetic cause of intellectual disability and choreoathetosis. J Child Neurol 2018; 33:825-31.
10. Trinchera M , Parini R , Indellicato R , Domenighini R , dall'Olio F . Diseases of ganglioside biosynthesis An expanding group of congenital disorders of glycosylation. Mol Genet Metab 2018; 124:230-37.
11. Wang H , Sency V , McJarrow P , et al. Oral ganglioside supplement improves growth and development in patients with ganglioside GM3 synthase deficiency. JIMD Rep 2018 Sep 13. doi: 10.1007/8904_2018_134. [Epub ahead of print]

LETTER TO THE EDITOR

ACTIVATION OF CASPASE-3 IN MALIGNANT MESOTHELIOMA INDUCED BY ASBESTIFORM FIBER: AN *IN VIVO* STUDY

C. LORETO[1], C. LEDDA[2], R. TUMINO[3], C. LOMBARDO[4], E. VITALE[2], V. FILETTI[1], R. CALTABIANO[5] and V. RAPISARDA[2]

[1]Anatomy and Histology, Department of Biomedical Sciences and Biotechnologies, University of Catania, Catania, Italy; [2]Occupational Medicine, Department of Clinical and Experimental Medicine, University of Catania, Catania, Italy; [3]Cancer Registry and Histopathology Department, "Civic – M. P. Arezzo" Hospital, ASP Ragusa, Ragusa, Italy; [4]Anatomy, Department of Medical and Surgical Sciences and Advanced Technologies, G.F. Ingrassia, University of Catania, Catania, Italy; [5]Anatomic Pathology, Department of Medical and Surgical Sciences and Advanced Technologies, G.F. Ingrassia, University of Catania, Catania, Italy

Received October 18, 2019 – Accepted April17, 2020

To the Editor,

Fluoro-edenite (FE) is a naturally occurring asbestiform fiber that has contaminated the town of Biancavilla in Sicily, Italy (1-2). Environmental and occupational exposure to FE are risk factors for pulmonary fibrosis, pleural plaques (PP), and malignant mesothelioma (MM) through mechanisms that are not still entirely understood (3-5). From *in vitro*, *in vivo* and epidemiological investigations, the IARC classified FE as carcinogenic to humans, but only for MM (6). As already noted for asbestos, also FE fibers, once inhaled, are absorbed quickly, and trigger the activation of macrophages as well as the making of iron-derived reactive oxygen species (ROS), with indirect DNA damage and apoptosis (7-8). Apoptosis is a type of programmed cell death that occurs in multicellular organisms. Biochemical events cause typical morphology cell changes and death. These alterations comprise blebbing, cell shrinkage, nuclear fragmentation, chromatin condensation, chromosomal DNA fragmentation, and global mRNA decompose (9).

Contrasting necrosis, apoptosis disrupts cells into fragments called apoptotic bodies that are phagocyte cells, that can first overwhelm and affect a cell in its core and then spread into nearby cells, damaging them (9). Apoptosis cannot end once it has been started, being an extremely regulated process. Apoptosis can be initiated through two pathways (intrinsic and extrinsic), both induced by activating caspases. The two pathways together trigger initiator caspases, which then start executioner caspases which, eventually kill the cell by degrading proteins arbitrarily (7-9).

Caspase-3 is one of the input executioners of apoptosis, being dependable in part or entirely for the proteolytic cleavage of several vital proteins, for instance, the nuclear enzyme polt (ADP-ribose) polymerase (PARP), which is cleaved in manydifferent systems through apoptosis (9). This experimental study aims to evaluate *in vivo* the expression of caspase-3 in human MM tissues after exposure to FE fibers.

Key words: fluoro-edenite; asbestos; cancer; malignant mesothelioma; fiber; Italy

Corresponding Author:
Prof. Caterina Ledda,
Occupational Medicine,
Department of Clinical and Experimental Medicine,
University of Catania,Via Santa Sofia, 87
Catania 95123, Italy
e-mail: caterina.ledda@unict.it

0393-974X (2020)
Copyright © by BIOLIFE, s.a.s.
This publication and/or article is for individual use only and may not be further reproduced without written permission from the copyright holder.
Unauthorized reproduction may result in financial and other penalties
DISCLOSURE: ALL AUTHORS REPORT NO CONFLICTS OF INTEREST RELEVANT TO THIS ARTICLE.

MATERIALS AND METHODS

Even though this investigation was carried out in compliance with the Helsinki Declaration, its non-interventional retrospective nature needed no informed consent by the Ethics Committee. Sufficient bioptic tissue from 8 patients who had a video-assisted thoracoscopic surgery for MM in the range years 1996-2014 was retrospectively obtained from a larger group of 49 patients, for whom clinic-pathological information and follow-up data were obtainable. Every patient lived in the town of Biancavilla.

From the tissues 4–5 μm-thick sections were prepared using paraffin blocks by a microtome, prepared on sialinate-coated slides (Dako, Glostrup, Denmark) and stored at room temperature. The samples were marked with hematoxylin and eosin (H&E). The histological conclusion of MM and histological subtypes were established in agreement with the WHO criteria. The slides were dewaxed in xylene, hydrated by graded ethanols, and incubated for 30 min in 0.3% H_2O_2/methanol to reduce endogenous peroxidase activity, then rinsed for 20 min with phosphate-buffered saline (PBS; Bio-Optica, Milan, Italy). The samples were heated (5m×3) in capped polypropylene slide-holders by citrate buffer (10 mM citric acid, 0.05% Tween 20, pH 6.0; Bio-Optica, Milan, Italy), with a microwave oven (750W) to unmask antigenic sites. The blocking step was carried out prior to applying the primary antibody by 5% bovine serum albumin (BSA; Sigma, Milan, Italy) in PBS for 1 h in a humidified chamber. BSA was used as a stopping agent to prevent non-specific binding of the antibody. Next, the samples were incubated overnight at 4°C with Caspase 3 Antibody (43-7800; Thermo Fisher Scientific, MA, USA), at a dilution of 1:100 in PBS (Sigma, Milan, Italy). The secondary antibody, the biotinylated anti-rabbit antibody, was applied for 30 min at room temperature, and then the avidin-biotin-peroxidase complex (Vector Laboratories, Burlingame, CA, USA) for an additional 30 min at room temperature. The immunoreaction was visualized by incubating the sections for 4 min in 0.1% 3,3'-diaminobenzidine (DAB) and 0.02% hydrogen peroxide solution (DAB substrate kit, Vector Laboratories, CA, USA). The sections were lightly counterstained by Mayer's hematoxylin (Histolab Products AB, Göteborg, Sweden) mounted in GVA mountant (Zymed Laboratories, San Francisco, CA, USA) and studied using a Zeiss Axioplan light microscope (Carl Zeiss, Oberkochen, Germany).

Immunohistochemistry

Samples were independently studied with a light microscope by two pathologists blinded to the case characteristics. Caspase-3 antibody staining expression was recognized as also negative or positive. Immunohistochemistry definite discoloration was distinct as well as the occurrence of brown chromogen recognition within the cytoplasm and/or the nucleus. The stained cell percentage was evaluated by semiquantitative optical examination in line with a four-tiered system (<1% positive cells, negative staining; 1–10% positive cells, focal staining; 11–50% positive cells, heterogeneous staining; >50% positive cells, diffuse staining). Staining concentration was scored as weak, moderate, or strong intensity.

Moreover, seven fields of the eight samples, arbitrarily chosen from each sample, were investigated through morphometric and densitometry analysis. The percentage areas (morphometric analysis) discolored with Caspase-3 antibody, expressed as % positive, dark brown pixels of the analyzed fields, and the level (high/low) of staining intensity of positive areas (densitometric analysis), expressed as densitometric count (pixel^2) of positive, dark brown pixels of the analyzed fields, were calculated using a specific software (AxioVision Release 4.8.2 - SP2 Software, Carl Zeiss Microscopy GmbH, Jena, Germany). Digital micrographs were captured using a Zeiss Axioplan light microscope (Carl Zeiss, Oberkochen, Germany) fitted with a digital camera (AxioCam MRc5, Carl Zeiss, Oberkochen, Germany).

RESULTS

The cohort of MM FE-related patients was composed of 5 men and 3 women (mean age: 70.9 years; age range: 50-93 years). All patients were born and living in Biancavilla, and none had occupational exposure to asbestos. According to WHO criteria, four cases were identified as epithelioid, and four were biphasic subtypes. Immunohistochemistry, showed seven cases (4 epithelioid and three biphasic) with diffuse expression of caspase-3 in neoplastic

cells with nuclear and cytoplasmic localization (Fig. 1). One biphasic subtype did not show caspase-3 immunostaining. Negative controls for caspase-3 were used to test the specific reaction in mesothelial tissue recovered from samples of patients suffering from non-cancer diseases.

Densitometric count (pixel^2) of stained areas by Caspase 3 expressed by dark brown pixels of the analyzed fields demonstrated insignificant traces of immunoreactions in non-neoplastic cells while in neoplastic cells high (red color) expressions were detected (Fig. 1). The percentages of Caspase 3 stained areas, expressed by dark brown pixels of the analyzed fields, were measured.

DISCUSSION

Apoptosis is an integral part of the cell cycle. It is involved in the morphogenesis of embryonic tissue and the homeostasis of adult organs and tissues, removing 'unneeded' cells in many organ systems (9). Caspase-3 is triggered in the apoptotic cell both via extrinsic (death receptor -DR) and intrinsic (mitochondrial) pathways (7). It is well known that caspase-3, executioner procaspases, slice many cellular proteins, for instance PARP and inhibitor caspase-activated DNase, consequential in apoptosis (7-8).

Moreover, cleaved caspase-3 has been used as a distinct biochemical marker of the opening of the apoptosis pathway (9). This evidence is called "point of no return" of the cell cycle (7). Therefore, caspase-3 can cause amplification of the apoptotic reaction; the amplification phase comprises the involvement of the mitochondria (7-8). Activated Caspase-3 can also proceed on the mitochondria to liberate added cyt *c* further to additional proapoptotic molecules (apoptosis-inducing factor (AIF), procaspase 3) (9). Mitochondria can, therefore, collect and intensify signals starting the DR pathway and reply to the reaction from downstream caspases. However, the apoptotic mechanisms involved in the lungs are still unclear. Caspase 3 is activated in induced apoptotic alveolar epithelial cells and apoptotic alveolar macrophages (10-11).

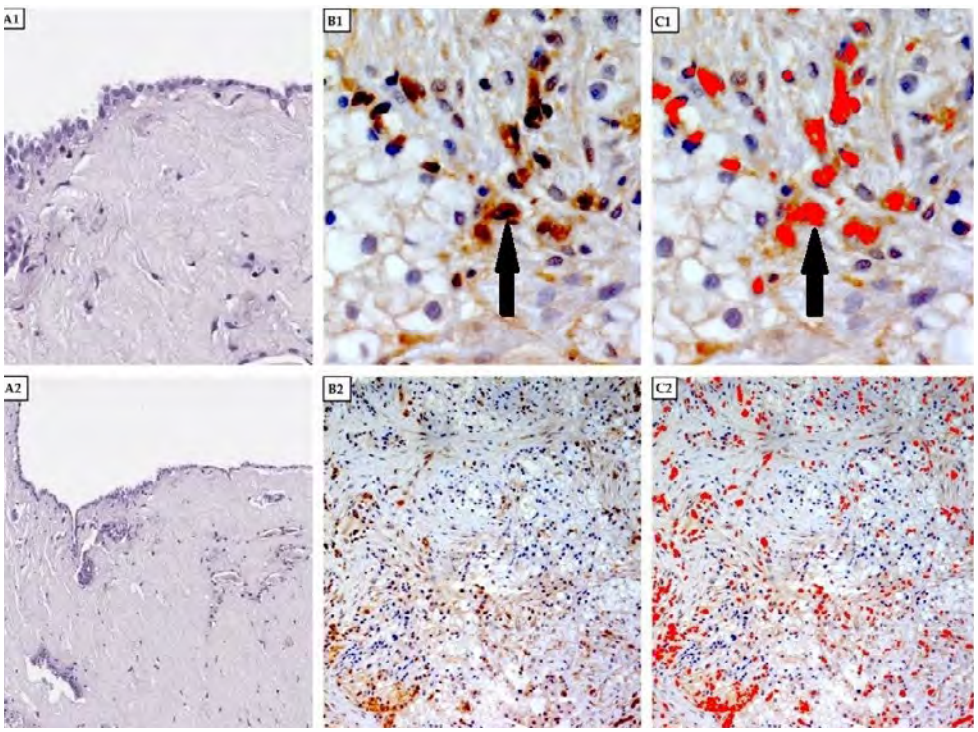


Fig. 1. *Caspase-3 immunohistochemistry antibody staining expression. A1 Negative control (63X); A2 Negative Control(40X); B1 MM case with immunohistochemistry expression (63X); B1 MM case with immunohistochemistry expression (40X); C1 densitometric analysis of MM case (63X); C1 densitometric analysis of MM case (40X).*

To the best of our knowledge, this is the first description of the caspase-3 involvement in human FE-related MM tissues. Additionally, as to carcinogenic activity, the activation of the caspase cascade is involved in the nonmalignant process of pleural mesothelial cells (9). Caspase-3 activation is also responsible for the onset of protease-activation factors and the discharge of cytochrome c from mitochondria into the cytosol (11-12). The antiapoptotic activity is triggered as a defense against the apoptotic mechanism. Our results are reliable in the hypothesis that activation of Caspase-3 is a critical mechanism that leads tissue to irreparable FE-induced damage and, if not activated enough, predisposes to a neoplastic evolution. Excessive apoptosis may promote pleural injury, while the failure of standard apoptotic mechanisms may contribute to MM onset.

REFERENCES

1. Ledda C, Pomara C, Bracci M, et al. Natural carcinogenic fiber and pleural plaques assessment in a general population: A cross-sectional study. Environ Res 2016; 150:23-29.
2. Ledda C, Loreto C, Pomara C, et al. Sheep lymph-nodes as a biological indicator of environmental exposure to fluoro-edenite. Environ Res 2016;147:97-101.
3. Rapisarda V, Ledda C, Ricceri V, et al. Detection of pleural plaques in workers exposed to inhalation of natural fluoro-edenite fibres. Oncol Lett 2015; 9(5):2046-52.
4. Ledda C, Loreto C, Matera S, et al. Early effects of fluoro-edenite: Correlation between IL-18 serum levels and pleural and parenchymal abnormalities. Future Oncol 2016; 12(23s):59-62.
5. Ledda C, Loreto C, Bracci M, et al. High risk of pleural plaques and parenchymal abnormalities in women living in biancavilla (italy). Future Oncol 2016; 12(23s):63-65.
6. Grosse Y, Loomis D, Guyton KZ, et al. Carcinogenicity of fluoro-edenite, silicon carbide fibres and whiskers, and carbon nanotubes. Lancet Oncol 2014; 15(13):1427-28.
7. Loreto C, Rapisarda V, Carnazza ML, et al.. Fluoro-edenite fibres induce lung cell apoptosis: An in vivo study. Histol Histopathol 2008; 23(3):319-26.
8. Martinez G, Loreto C, Rapisarda V, Masumeci G, Valentino M, Carnazza ML. Effects of exposure to fluoro-edenite fibre pollution on the respiratory system: An in vivo model. Histol Histopathol 2006; 21(4-6):595-601.
9. Bossy-Wetzel E, Green DR. Apoptosis: Checkpoint at the mitochondrial frontier. Mutat Res DNA Repair 1999; 434(3):243-51.
10. Kido T, Morimoto Y, Asonuma E, et al. Chrysotile asbestos causes AEC apoptosis via the caspase activation in vitro and in vivo. Inhal Toxicol, 2008; 20(3):339-47.
11. Liu G, Beri R, Mueller A, Kamp DW. Molecular mechanisms of asbestos-induced lung epithelial cell apoptosis. Chem Biol Interact 2010; 188(2):309-18.
12. Ledda C, Senia P, Rapisarda V. Biomarkers for early diagnosis and prognosis of malignant pleural mesothelioma: The quest goes on. Cancers 2018; 10(6).

LETTER TO THE EDITOR

MALIGNANT INSULINOMA, A VERY RARE CAUSE OF PEDIATRIC HYPOGLYCEMIA

L. CANNAVÒ[1], U. CUCINOTTA[1], G. ZIRILLI[1], M. LIMA[2], G.B. PAJNO[1], M. WASNIEWSKA[1] and M. VALENZISE[1]

[1] G. Martino Hospital, Pediatric Unit, Department of Adulthood and Chilhood Human Pathology, University of Messina, Messina, Italy; [2] Sant'Orsola Hospital, Department of Pediatric Surgery, University of Bologna, Bologna, Italy

Received November 12, 2019 – Accepted January 30, 2020

To the Editor,

Insulinoma is a rare functional pancreatic neuroendocrine tumor, originating from islet beta cells and representing 1-2% of all pancreatic neoplasms (1). Generally, it occurs sporadically, but it may be associated with type 1 multiple endocrine neoplasia (MEN1) and type 1 Neurofibromatosis (NF1) (2-4). Most insulinomas are benign, while 5-10% of them are malignant (5). Malignant transformation is characterized by surrounding soft tissues invasion and lymph nodes or distal metastases, and is associated to a tumor diameter > 2 cm, positive CK19 expression, increased proliferation index (Ki67 >2%) and age of onset > 50 years (6). Insulinoma is clinically characterized by the Whipple's triad: symptoms and/or signs of hypoglycemia, low plasma glucose levels and resolution of symptoms after glucose administration. The occurrence of this neuroendocrine tumor in children is extremely rare and the diagnosis is often delayed because signs and symptoms of hypoglycemia and neuroglycopenia such as confusion, headache, palpitation, and seizure, can be due to many other pediatric diseases. Moreover, these tumors are frequently small and their identification can be challenging.

Here, we report on the case of a prepubertal boy with malignant pancreatic insulinoma (MPI), because we believe that pediatricians and all physicians should be aware of this rare disease, and of the difficulties of diagnosis and management.

Case description

A 11-year-old boy was referred to our Pediatrics Unit because of a 1-month history of confusion, amnesia and diplopia associated with severe hypoglycemic events. Family history of endocrine diseases was not reported. His past medical history revealed three febrile seizures in the first two years of life.

On presentation, vital signs were normal. At physical examination, height was 158 cm (95th percentile for age), weight 77 kg (97th percentile for age) and BMI 31 kg/m^2. Cardiovascular, respiratory, gastrointestinal and neurological examination revealed no abnormal findings. His initial point-of-care plasma glucose was 45 mg/dl. During the following hours, the patient continued to present hypoglycemia, requiring intravenous glucose infusion. Initial laboratory investigations confirmed low serum glucose level (48 mg/dl), while complete blood count, hepatic enzymes, creatinine, azotemia and serum electrolytes were normal. Urinary sample was negative for ketones. The hormonal profile revealed normal thyroid (FT3, FT4), parathyroid

Key words: insulinoma; hypoglycemia; neuroendocrine tumor; seizures

Corresponding Author:
Dr Mariella Valenzise,
Department of Adulthood and Childhood Human Pathology,
University of Messina, Messina, UOC di Pediatria, Pad. NI, 3° piano,
AOU Policlinico Gaetano Martino,
Via Consolare Valeria, 1, 98125 Messina, Italy
e-mail: mvalenzise@unime.it

0393-974X (2020)
Copyright © by BIOLIFE, s.a.s.
This publication and/or article is for individual use only and may not be further reproduced without written permission from the copyright holder.
Unauthorized reproduction may result in financial and other penalties
DISCLOSURE: ALL AUTHORS REPORT NO CONFLICTS OF INTEREST RELEVANT TO THIS ARTICLE.

(PTH), adrenal (cortisol) and pituitary function (PRL, FSH, LH, TSH, ACTH), but serum insulin levels were very high (62.74 mcIU/ml), and serum C-peptide levels were detectable (6.18 ng/ml), leading to the exclusion of iatrogenic or factitia hypoglycemia.

In view of the suspect of insulinoma, the patient underwent abdominal contrast-enhanced magnetic resonance imaging that showed a 40 mm, well-demarcated lesion within the head of the pancreas associated with mild dilatation of pancreatic duct and presence of retropancreatic lymphadenopathy measuring 34 x 10 mm (Fig. 1). No distant metastases were identified. Moreover, 18-F-fluorodihydroxyphenylalanine positron emission tomography (PET)/computed tomography (CT) scan and endoscopic ultrasonography supported the diagnosis of neuroendocrine tumor and the patient underwent duodeno-cephalo-pancreasectomy.

The histological examination confirmed the diagnosis of well differentiated neuroendocrine tumor (NET-G2 sec WHO 2010), measuring 45 mm and infiltrating vascular and perineural districts. Metastases were detected in 2 pancreatic-duodenal lymph nodes and in 3 lymph nodes in the retroportal lamina out of 41 lymph nodes examined (T2N1M0, AjCC/UICC TNM). The Ki67 expression was 12%. Immunohistochemical staining was positive for synaptophysin.

After surgery, glucose profile normalized and hypoglycemic events did not recur. One year after surgery, laboratory evaluation confirmed normal metabolic profile and abdominal MRI did not demonstrate recurrence of the tumor or metastatic lesions. Unfortunately, genetic analysis (MEN 1) was not performed because the parents of the patient refused to give the informed consent.

DISCUSSION

Malignant insulinomas can be a very rare cause of severe hypoglycemia even in children. When diagnosis is delayed and patients are not correctly managed, irreversible neurological damage can occur. In children, hypoglycemia can recognize different etiologies. In the majority of cases, hypoglycemia can be due to prolonged fasting associated to ketosis, but sometimes it can be caused also by reactive hyperinsulinism, hypoadrenalism or iatrogenic/factitious insulin administration. Frequently, insulinoma represents the final diagnosis after a challenging management. In comparison with benign insulinomas, the malignant ones are sometimes associated with extremely pronounced neuroglycopenic symptoms. The 72-h fasting test remains the gold standard for the diagnosis of insulinoma and includes the measurement of plasma glucose, insulin, C-peptide, when hypoglycemic symptoms appear (5). Hypoglycemia, characterized by serum glucose level<50 mg/dl, together with levels of insulin >2 mIU/L or insulin-to-glucose ratio >0.4, and high C-peptide values allow a correct diagnosis. It has been reported that patients with malignant disease had, at the glucose nadir, insulin and C-peptide concentrations >25 mU/mL and >4 ng/dL, respectively (7). In addition, the MPI shows a diameter generally >2 cm, ranging from 2.3 to 6.2 cm (8). Some authors also reported a positive correlation between tumor size and both insulin and C-peptide levels (9). The most common metastatic sites of MPI are the abdomen, including the retroperitoneal lymph nodes and liver, while bone, lung or other areas are rarely involved (5, 10, 11). Preoperative localization of the tumor is crucial for effective surgical removal, limited to the affected part of the pancreas and for the detection of distant metastases. Traditionally, 18F-DOPA PET has been preferred for insulinoma detection, but recently 99mTc-Glucagon-like peptide-1 (GLP-1) scintigraphy and 68Ga-DOTA-(Tyr3)-octreotate (DOTATATE) PET/CT were evaluated. GLP-1 is a hormone overexpressed in benign insulinomas that binds to a specific β-cells receptor of pancreatic islet which stimulates insulin secretion. However, since MPI mainly overexpressed somatostatin receptors, GLP-1 scintigraphy has limited potential (13). Instead, 68Ga-DOTATATE has a high affinity for somatostatin 2 receptors which is expressed in up to 80% of insulinoma cases. The advantages of 68Ga-DOTATATE are the detection of neuroendocrine tumors up to 6 mm in size not detected by anatomical imaging, and the exposure to total radiation lower than 18F-FDG PET / TC (14).

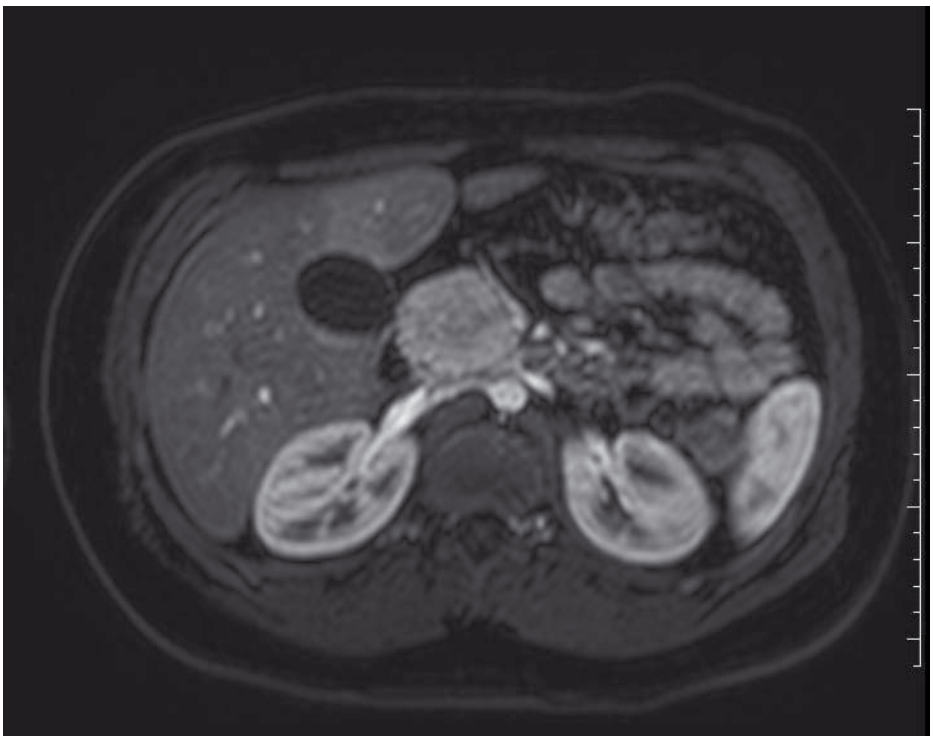


Fig. 1. *Magnetic resonance imaging of the tumor within the head of pancreas.*

After diagnosis, surgery is the first line treatment of insulinomas. A radical surgical removal and biologic behavior of the tumor are the major long-term determinants of outcome. On the basis of its size, minimal extension only to the biliary tract or duodenum, and Ki-67 index over 2% but less than 20%, the tumor of our patient showed an intermediate grade of malignancy (grade 2), in accordance with current histological classification (12).

A close post-surgical follow-up through clinical tests and abdominal magnetic resonance imaging is recommended every 6 months to 2 years for the first 10 years and then every 2-5 years for life.

Since most of the insulinomas diagnosed in childhood can be associated with NF1 and MEN1, these diseases should be always excluded. NF1 is a multisystem genetic disorder characterized by six or more café-au-lait spots or hyperpigmented macules and axillary or inguinal freckling, by skeletal dysplasias, and by the growth of both benign and malignant nervous system tumors. MEN1 is diagnosed in a patient who has two tumors associated with MEN1 or a known MEN1 mutation or a MEN1-related tumor with a first degree relative with MEN1. Our patient does not have clinical criteria for NF1, MEN1-compatible personal or family history, but we could not rule out the MEN1 mutation because the parents refused to give informed consent. However, since most malignant insulinomas are sporadic, systematic genetic analysis is not recommended.

In conclusion, physicians must be aware that insulinoma can be a rare cause of severe and recurrent hypoglycemia even in children. Early recognition and correct diagnosis are crucial in order to prevent serious adverse neurological consequences, such as retardation of mental development, pyramidal syndromes and recurrent seizures.

REFERENCES

1. Oberg K, Eriksson B. Endocrine tumours of the pancreas. Best Pract Res Clin Gastroenterol 2005; 19:753-81.
2. Akhtar Y, Verardo A, Crane JL. Multiple endocrine neoplasia type 1 presenting with concurrent

insulinoma and prolactinoma in early-adolescence. Int J Pediatr Endocrinol 2018; 7.
3. Shiihara M, Izumo W, Higuchi R, Yazawa T, Uemura S, Furukawa T, Yamamoto M. A case of long-survival insulinoma with multiple neuroendocrine tumour type 1 controlled by multimodal therapy. J Surg Case Rep 2017; 12:rjx244.
4. Perren A, Wiesli P, Schmid S, et al. Pancreatic endocrine tumors are a rare manifestation of the neurofibromatosis type 1 phenotype: molecular analysis of a malignant insulinoma in a NF-1 patient. Am J Surg Pathol 2006; 30:1047-51.
5. Okabayashi T, Shima Y, Sumiyoshi T, et al. Diagnosis and management of insulinoma. World J Gastroenterol 2013; 19:829-37.
6. Pape UF, Jann H, Müller-Nordhorn J, et al. Prognostic relevance of a novel TNM classification system for upper gastroenteropancreatic neuroendocrine tumors. Cancer 2008; 113:256-65.
7. Câmara-de-Souza AB, Toyoshima MTK, Giannella ML, et al. Insulinoma: A retrospective study analyzing the differences between benign and malignant tumors. Pancreatology 2018; 18(3):298-303
8. QueirozAlmeida M, Machado MC, Correa-Giannella ML, Giannella-Neto D, Albergaria Pereira MA. Endogenous hyperinsulinemic hypoglycemia: diagnostic strategies, predictive features of malignancy and long-term survival. J Endocrinol Invest 2006; 29(8):679-87.
9. Yu J, Ping F, Zhang H, et al. Clinical Management of Malignant Insulinoma: a single Institution's experience over three decades. BMC Endocrine Disorders 2018; 18:92.
10. Baudin E, Caron P, Lombard-Bohas C, et al. Malignant insulinoma: recommendations for characterization and treatment. Ann Endocrinol 2013; 74:523-33.
11. Hirshberg B, Cochran C, Skarulis MC, et al. Malignant insulinoma: spectrum of unusual clinical features. Cancer-Am Cancer Soc 2005; 104: 264–72.
12. Klimstra DS, Modlin IR, Coppola D, Lloyd RV, Suster S. The pathologic classification of neuroendocrine tumors: a review of nomenclature, grading, and staging systems. Pancreas 2010; 39:707-12.
13. Sowa-Staszczak A, Trofimiuk-Müldner M, Stefańska A, et al. 99mTc Labeled Glucagon-Like Peptide-1-Analogue (99mTc-GLP1) Scintigraphy in the Management of Patients with Occult Insulinoma. PLoS ONE 2016; 11(8):e0160714.
14. Nockel P, Babic B, Millo C, et al. Localization of Insulinoma Using 68Ga-DOTATATE PET/CT Scan. J Clin Endocrinol Metab 2017;102 (1):195-99.

LETTER TO THE EDITOR

USE OF BIOPHYSICAL TREATMENT FOR THE MANAGEMENT OF MILD ANXIETY, DEPRESSION AND STRESS: A RANDOMIZED CONTROLLED TRIAL

A. FOLETTI[1-2], P. BARON[1-3], P. BERCHIALLA[4], D. FRANCONE[4], F. MALANDRONE[4], L. OSTACOLI[4] and S. CARLETTO[4]

[1]Clinical Biophysics International Research Group, Lugano, Switzerland; [2]Institute of Translational Pharmacology, National Research Council-C.N.R., Rome, Italy; [3]Poliambulatorio San Marco, Palmanova, Italy; [4]Department of Clinical and Biological Sciences, University of Turin, Italy

Received March 2, 2020 – Accepted April 22, 2020

To the Editor,

Depression, anxiety and stress significantly affect both personal and public health (1), either as a primary psychological complaint or as an additional burden component of most physical chronic diseases. The effective management of early stages of depression, anxiety and stress still represents a frequent unmet medical need considering the aging population, increased number of co-morbid diseases and the need for personalized treatments (2).

Biophysical treatments can exert their clinical effect through a resonance effect of their therapeutically delivered electromagnetic signals (either endogenous or exogenous) to target tissues, organs, and/or the entire organism (3). To date, biophysical therapeutic methods have emerged as integrative tools in a wide range of clinical settings such as pain, psoriasis and chronic kidney disease (4). Preliminary evidence shows that minor anxiety and depression symptoms can also be significantly reduced after biophysical treatments (5). Furthermore, we recently conducted a pilot study involving twenty-four patients with mild anxiety/stress symptoms (Generalized Anxiety Disorder 7-item scale of > 5) randomized to biophysical treatment (N = 12) or placebo control (N = 12) (6). After 1 month of biophysical therapy, we observed a significant reduction all Depression Anxiety Stress Scale (DASS)-21 questionnaire subscales; depression, anxiety and stress compared to placebo control. The aim of this clinical trial is to extend and confirm these findings in a larger sample size (N=100) over a period of three months.

MATERIALS AND METHODS

Patient recruitment and study design

This was a randomized controlled trial (the protocol was not registered for this trial) and included patients presenting with mild anxiety symptoms and related symptoms of depression and stress. The recruitment of participants was carried out by physicians and included patients attending the Poliambulatorio San Marco in Palmanova, Italy from January 2018 to June 2018 who completed a Generalized Anxiety Disorder 7-item scale (GAD-7) (7) prior to psychiatric consultation.

Inclusion criteria were: a score >5 for the Generalized Anxiety Disorder 7-item scale (GAD-7) (7); (i) presence of anxiety symptoms; (ii) age between

Key words: anxiety; stress; physical quality of life; biophysical therapy; electromagnetic information transfer

Corresponding Author:
Alberto Foletti, MD
Clinical Biophysics International Research Group,
Via Maggio, 21
6900 Lugano, Switzerland
Tel.: +41 787578783 - Fax: +41 919724042
e-mail: albertofolettimd@gmail.com

0393-974X (2020)
Copyright © by BIOLIFE, s.a.s.
This publication and/or article is for individual use only and may not be further reproduced without written permission from the copyright holder.
Unauthorized reproduction may result in financial and other penalties
DISCLOSURE: ALL AUTHORS REPORT NO CONFLICTS OF INTEREST RELEVANT TO THIS ARTICLE.

18 and 70 years; (iii) fluent Italian speaker; (iv) legal capacity to consent to the treatment; (v) no psychotropic medication use throughout the study. Exclusion criteria were: (i) presence of severe psychiatric disorders; (ii) cognitive disorders such as overt dementia; (iii) drug or alcohol abuse; (iv) suicide attempts; (v) current pregnancy.

The research protocol was proposed to patients who met the inclusion criteria, with an explanation of the aims of the study and declaring the possibility that they would be assigned by random allocation to the experimental group (biophysical therapy) or the control (placebo) group. After being informed about the aim, methods and timing of the study, all patients provided a signed written informed consent form. This study was performed in accordance with the declaration of Helsinki. Psychological/psychiatric assessment (using questionnaires) was performed at baseline (before the first session of biophysical treatment) and again at the end of treatment (after 3 months).

The patients were randomly assigned to the experimental or the control group with a 1:1 ratio (50 in the intervention and 50 in the control group). To ensure allocation concealment, the sequence was determined by an independent researcher blind to the initial assessment, using a random number generator (www.randomizer.org). To ensure the blinding of the clinical psychologists performing the assessments, the study coordinator communicated the treatment assignment to each patient.

Biophysical therapy

This study was single-blind: patients were not aware which group of treatment they would be assigned to. The treatment procedure was the same for the experimental and the control group. The experimental group was treated with biophysical therapy using the Med Select 729 device (Wegamed, GmbH, Essen, Germany) the methodology of which has been previously described in detail (4). This medical device operates in a low frequency range (between 0 and 20 kHz) using a magnetic field intensity similar to the Earth's magnetic field with a maximum of 50 μT. It allowed us to record input signals using two electrodes and to send output signals to the patient through a magnetic carpet where the patient can lie down (in this way the entire body of the patient can be treated).

The biophysical therapy protocol comprises three steps. The purpose of this sequence is to restore the systemic self-regulation capacity, restore the relaxation capacity, and restore the autonomic regulation; it allows to carry out both the treatment and to record it on the aqueous system simultaneously. i) The first phase is the ''regulation therapy'' program selected on the touch-screen of Med Select 729 device (Wegamed, GmbH, Essen, Germany) to record the endogenous electromagnetic input signals using two electrodes placed on the forehead of each patient and for delivering the therapeutic electromagnetic output signals (a simultaneous combination of the patient's own signals with the carrying and modulating ones) through a magnetic carpet on which the patient lies for 6 minutes. This program has a fixed carrier frequency of 32 Hertz, a modulation frequency oscillating between 7 and 12 Hz, and 12.5-μT magnetic field strength. The patient's own signals delivered simultaneously with those of the carrier and the modulating supplied by the equipment has both a general purpose of entrainment and a specific individual self-regulation. ii) The ''relaxation therapy'' program is then selected from the Med Select 729 device touch-screen to record the endogenous input signals using two electrodes placed on the forehead for delivering the therapeutic output signals of a magnetic carpet on which the patient lies on for 10 minutes. This program has a fixed carrier frequency of 7 Hz, a modulation frequency oscillating between 4 and 10 Hz, and 17.5-μT magnetic field strength. iii) The third phase of treatment involves the "autonomic therapy" selected from the Med Select 729 device touch-screen to record the endogenous input signals using two electrodes positioned on the forehead for delivering the therapeutic output signals of a magnetic carpet on which the patient lies on for 12 minutes. This program has a variable carrier frequency of one-minute recurring sequences at 8-12-50-8-95-275 Hz, a fixed modulation frequency at 10 Hz, and 50-μT magnetic field strength.

During these three steps, the therapeutic output signals were simultaneously recorded on an aqueous

system commercially available (Nomabit Base, Named SRL, Italy MB) by placing the solution in an appropriate output coil, incorporated for this purpose in Med Select device 729. Patients self-administered the aqueous solution Nomabit Base daily in order to allow the therapeutic information recorded to be taken once a day for 3 months. The control group is the placebo group, which received placebo treatment following the same procedures as the experimental group without the recording and subsequent administration of the therapeutic signals. This group received Nomabit Base solution as a placebo, without any signal recorded. The control group received the treatment for 3 months.

Data collection

In addition to a module on demographic data, the following psychological self-report questionnaires were administered at baseline and after 3 months by the physician, independent of the research protocol and blinded to treatment group, using the same timing and tools in both groups.

Each patient was requested to complete the self-rating DASS-21 questionnaire (8). The DASS-21 is a self-administered questionnaire using a set of three self-report scales designed to measure the emotional states of depression, anxiety and stress. Each of the three DASS-21 scales contains 7 items, divided into subscales with similar content. The depression scale

Table I. *Baseline clinical characteristics of control and biophysical treatment groups*

Charactersitic	Control (N=50)	Biophysical (N=50)	P-value
Age, years (mean±SD)	46.62±10.81	47.04±13.92	0.867
Females, n (%)	41 (82.0)	42 (84.0)	1.000
Education (mean±SD)	12.40±2.97	12.76±3.65	0.590
Employment, n (%)			0.417
Employed	34 (68.0)	28 (56.0)	
Retired	1 (2.0)	1 (2.0)	
Student	2 (4.0)	6 (12.0)	
Unemployed	13 (26.0)	15 (30.0)	
Marital Status, n (%)			0.037
Divorced	1 (2.0)	8 (16.0)	
Married	37 (74.0)	27 (54.0)	
Single	11 (22.0)	14 (28.0)	
Widowed	1 (2.0)	1 (2.0)	
Baseline assessment (median [IQR])			
DASS Depression	16.00 [8.50, 22.00]	15.00 [10.00, 20.00]	0.833
DASS Anxiety	10.00 [4.00, 18.00]	10.00 [6.00, 18.00]	0.854
DASS Stress	20.00 [14.00, 28.00]	22.00 [16.50, 27.50]	0.830
CES-D	21.50 [16.25, 30.75]	24.50 [19.00, 28.00]	0.622
WHO Enviromental	59.50 [50.00, 67.50]	63.00 [50.00, 67.50]	0.989
WHO physical	44.00 [38.00, 50.00]	44.00 [38.00, 50.00]	0.445
WHO psychological	47.00 [44.00, 56.00]	50.00 [44.00, 56.00]	0.682
WHO social	56.00 [31.00, 73.50]	56.00 [26.50, 69.00]	0.648

Data are presented as mean ± standard deviation or number and percent or median and inter quartile range (IQR). CES-D = Center for Epidemiologic Studies Depression Scale Revised. Statistical significance is represented by p values for comparison of variables in control and biophysical groups. DASS-21 = Depression Anxiety Stress Scale.

assesses dysphoria, hopelessness, devaluation of life, self-deprecation, lack of interest/involvement, anhedonia and inertia. The anxiety scale assesses autonomic arousal, skeletal muscle effects, situational anxiety, and subjective experience of anxious effect. The stress scale is sensitive to levels of chronic non-specific arousal. It assesses difficulty relaxing, nervous arousal, and being easily upset/agitated, irritable/over-reactive and impatient. Scores for depression, anxiety and stress are calculated by summing the scores for the relevant items.

The Center for Epidemiologic Studies Depression Scale Revised (CES-D) is a self-assessment scale of 20 items rated on a 4-point Likert scale (0 = never or rarely, 3 = most of the time) to measure the presence and severity of depressive symptoms (9).

WHO-QOL-BREF is a measure to assess the Quality of Life that consists of 36 items, divided into four domains (physical health, psychological health, social relationships health, and environmental health) and rated on a 5-point Likert scale (0 = not at all, 5 = completely) (10).

Statistical analysis

Continuous variables are presented using mean or median as a measure of centrality and standard deviation or interquartile range as a measure of variability as appropriate according to the Shapiro–Wilk normality test. Differences in socio-demographic and baseline clinical characteristics between the groups were assessed using Mann–Whitney test for continuous variables and χ^2 or Fisher's test as appropriate, for categorical measures. Linear mixed model approach was used to analyse the pre-post intervention effect considering interaction between time and groups and adjustment for unbalanced variables. The linear mixed model was evaluated under REML (reduced maximum likelihood) estimation. The sample size computation was based on ANOVA analysis with two repeated measures and within-between interactions. Considering a medium effect size (Cohen's f = 0.25) on primary outcome CES-D, a total of N=50 patients would allow us to achieve a power of 0.93, with type I error equal to 0.05. All tests were two-tailed and a p-value of <0.05 was considered statistically significant. P-value adjustment for post-hoc test was applied. All analyses were carried out using R version 3.6.1.

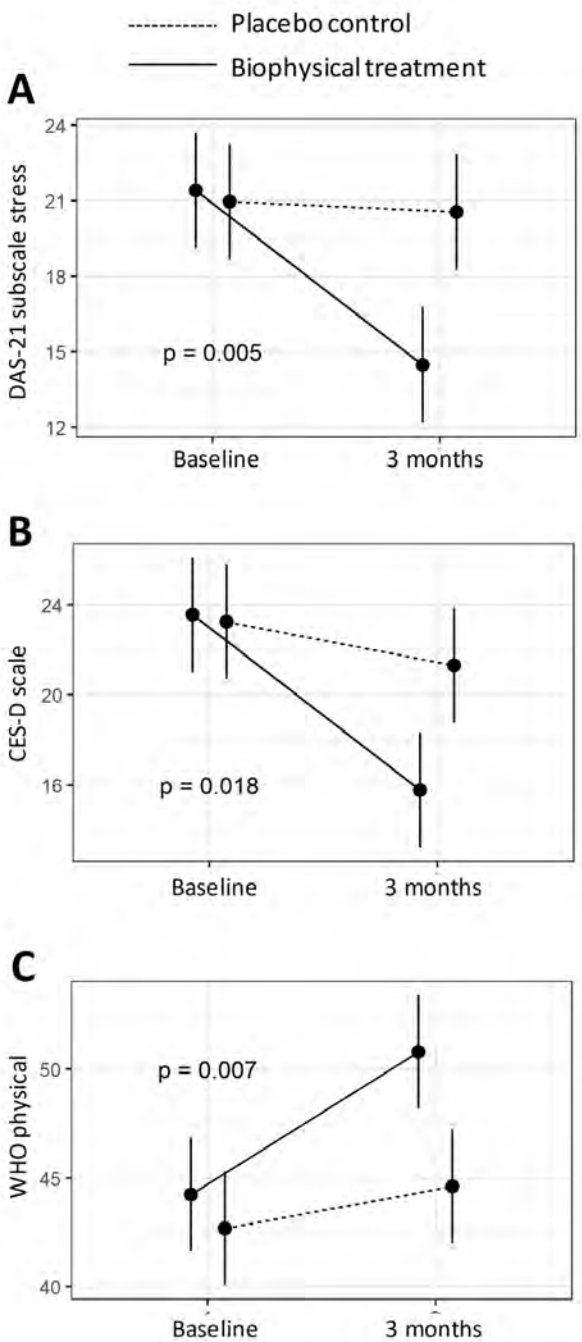


Fig. 1. *Effect of biophysical therapy and placebo control on DASS-21 subscale stress, CES-D and WHO physical. Data are presented as mean ± SD and p-values denote statistical significance between groups at 3 months.*

RESULTS

Baseline clinical and demographic characteristics

A total of 100 subjects were included in the study, 50 (mean age: 47.04±13.92 years) in the biophysical therapy group and 50 (mean age: 46.62±10.81 years) in the control group. After completion of the Generalized Anxiety Disorder 7-item scale (GAD-7) questionnaire, physicians only included patients having a GAD-7 score of >5, defined as having mild anxiety/depressive symptoms. Clinical characteristics and depression/anxiety and stress assessment for control and biophysical patient groups are presented in Table I. The majority of patients were female (83%) and 62% of patients were currently employed. A higher proportion of patients were married in the control group and divorced in the biophysical group this difference just attaining statistical significance compared to the biophysical group (p=0.037). All other baseline measures of depression, anxiety, stress (DASS-21 subscales), depression (CES D scale) and WHO QoL scales related to physical, psychological, social and environmental were similar for the two groups (Table I).

Effect of biophysical treatment on DASS-21 subscales and WHO QoL subscales

In patients who were assigned biophysical therapy, a reduction in all DASS-21 subscales was observed, with statistical significance only observed for the stress subscale. From baseline to the 3-month follow-up, biophysical-treated patients had a -6.92 points decrease in DASS stress score (p=0.005, Fig. IA), while control patients had a non-significant improvement. After 3 months, control and biophysical patients' mean scores were 18.62 and 12.86, respectively (difference of 5.75, 95% CI: 1.36; 10.15, p=0.005, Table II).

A statistically significant decrease was also observed for CES-D scale in biophysical treated patients compared to controls after 3 months' follow-up; depression score (CES D scale) decreased by -7.78 points (p=0.018, Fig. IB) compared to -1.94, in control patients. After 3 months, control and intervention patients' mean scores were 21.19 and 15.54, respectively (difference of 5.64, 95% CI: 0.70; 10.59, p=0.018, Table II).

For WHO QoL outcome measures only WHO physical QoL significantly improved over 3 months (5.74 mean increase, p=0.007, Fig. IC) in the biophysical group. After 3 months, control and biophysical patients' mean scores were 50.32 and 44.58. respectively (difference of 5.74, 95% CI: 0.78; 10.70, p=0.007) (Table II). Depression and anxiety (DASS-21 subscales), WHO psychological, social and environmental QoL improved to a greater extent in the biophysical group compared to controls, however the difference did not attain statistical

Table II. *Change in mean scores for DASS-21 outcome and WHO QoL measures in control and biophysical treatment groups after 3 months*

	Biophysical group	Control	Difference (95% CI)
DASS-21 depression	6.2 (3.56;8.84)	2.04 (-0.60; 4.68)	4.08 (-0.33; 8.49)
DASS-21 anxiety	4.88 (2.27; 7.49)	-0.12 (-2.73; 2.49)	4.45 (-0.06; 8.96)
DASS-21 stress	6.92 (3.74; 10.10)	0.4 (-2.78; 3.58)	5.75 (1.36; 10.15)
CES-D	7.78 (4.85;10.71)	1.94 (-0.99; 4.87)	5.64 (0.7; 10.59)
WHO physical	-6.56 (-9.80; -3.32)	-1.94 (-5.18; 1.30)	5.74 (0.78; 10.70)
WHO psychological	-6.11 (-9.49; 2.73)	-2.60 (-5.95; 0.75)	4.14 (-1.18; 9.48)
WHO social	-6.98 (-14.64; 0.68)	-2.02 (-9.68; 5.64)	2.02 (-11.11; 15.16)
WHO environmental	-4.8 (-7.85; 1.75)	-2.62 (-5.67; 0.43)	2.06 (-4.41; 8.52)

significance when comparing mean scores at 3 months (Table II). Statistical significance between the control and the biophysical groups were adjusted for marital status.

DISCUSSION

The present clinical trial confirms results of a recent pilot study involving twenty-four patients with mild anxiety/stress symptoms (6) and extends them further by using a larger sample size (N=100) and longer treatment period (three months). Patients presenting with mild anxiety/depression can experience a significant reduction in these symptoms as early as 3 months after biophysical therapy. Both DASS-21 subscales and WHO QoL measures were improved following treatment with biophysical therapy for 3 months compared to untreated controls. To the best of our knowledge, this is the first study to investigate the feasibility and effectiveness of using biophysical therapy to treat mild-to-moderate levels of psychological distress. Moreover, this study sheds light on an integrative/unconventional therapeutic option for the treatment of mild-to-moderate depressive symptoms. According to clinical guidelines, possible first treatments for mild-to-moderate depression include self-help programme, computerised cognitive behavioural therapy and physical activity exercise (11). Further treatment options are represented by antidepressant or psychological treatments. Therefore, if further studies confirm its efficacy, biophysical therapy could represent an additional treatment available to general practitioners or other healthcare professionals to intervene/manage depressive and stress symptoms.

The mechanism by which biophysical treatment exerts its anxiolytic effects is not yet understood. However, pre-clinical studies suggest that it may be linked to a range of modulatory factors such as anti-oxidants, growth factors and inflammatory mediators, although it is an area that remains controversial (12). Future studies are needed to characterise the mechanisms through which the biophysical effect derived from low electromagnetic waves exert these beneficial anxiolytic effects.

REFERENCES

1. Global Burden of Disease Study 2013 Collaborators. Global, regional, and national incidence, prevalence, and years lived with disability for 301 acute and chronic diseases and injuries in 188 countries, 1990-2013: a systematic analysis for the Global Burden of Disease Study 2013. Lancet 2015; 386(9995):743-800.
2. Henney AM. The promise and challenge of personalized medicine: aging populations, complex diseases, and unmet medical need. Croat Med J 2012; 53(3):207-10.
3. Foletti A, Grimaldi S, Lisi A, Ledda M, Liboff AR. Bioelectromagnetic medicine: the role of resonance signaling. Electromagn Biol Med 2013; 32(4):484-99.
4. Foletti A, Ledda M, Lolli MG, Grimaldi S, Lisi A. Electromagnetic information transfer through aqueous system. Electromagn Biol Med 2017; 36(3):289-94.
5. Foletti A, Baron P. Biophysical approach to minor anxiety and Depressive Disorders. In: 2016 Progress in Electromagnetic Research Symposium (PIERS). 2016. p. 1400-3.
6. Ferrara I, Egan CG, Foletti A. Pilot study on the effect of biophysical therapy on salivary alpha-amylase as a surrogate measure of anxiety/stress: in search of a novel noninvasive molecular approach for the management of stress. Int J Mol Sci 2020; 9:21(2).
7. Spitzer RL, Kroenke K, Williams JBW, Löwe B. A brief measure for assessing generalized anxiety disorder: the GAD-7. Arch Intern Med 2006; 166(10):1092-97.
8. Bottesi G, Ghisi M, Altoè G, Conforti E, Melli G, Sica C. The Italian version of the Depression Anxiety Stress Scales-21: Factor structure and psychometric properties on community and clinical samples. Compr Psychiatry 2015; 60:170-81.
9. Fava GA. Assessing depressive symptoms across cultures: Italian validation of the CES-D self-rating scale. J Clin Psychol 1983; 39(2):249-51.
10. Carpiniello B, Pinna M, Carta MG, Orrù MG. Reliability, validity and acceptability of the WHOQOL-Bref in a sample of Italian psychiatric outpatients. Epidemiology and Psychiatric Sciences 2006; 15(3):228-32.

11. NICE clinical guidelines | Tools and resources | The guidelines manual | Guidance | NICE [Internet]. [cited 2019 Dec 16]. Available from: https://www.nice.org.uk/process/pmg6/resources/how-nice-clinical-guidelines-are-developed-an-overview-for-stakeholders-the-public-and-the-nhs-2549708893/chapter/nice-clinical-guidelines
12. Pall ML. Electromagnetic fields act via activation of voltage-gated calcium channels to produce beneficial or adverse effects. J Cell Mol Med 2013; 17(8):958-65.

LETTER TO THE EDITOR

IS THERE AN ASSOCIATION BETWEEN BIOCHEMICAL PARAMETERS AND PROSTATE-SPECIFIC ANTIGEN "GREY ZONE"? AN ITALIAN PILOT STUDY

S. TARTAGLIONE[1*], E. BERARDELLI[1*], C. DE VITO[2], A. NARDI[2], G. GENNARINI[1], G. GIRELLI[3], A. ANGELONI[4] and E. ANASTASI[1]

[1]Department of Molecular Medicine, Policlinico Umberto I, "Sapienza" University, Rome, Italy; [2]Department of Public Health and Infectious Diseases, "Sapienza" University, Rome, Italy; [3]Immunohematology and Transfusion Medicine Unit, Policlinico Umberto 1, "Sapienza" University, Rome, Italy; [4]Department of Experimental Medicine, Policlinico Umberto I, "Sapienza" University, Rome, Italy

Received January 10, 2020 – Accepted April 22, 2020

[*]These Authors contributed equally to this paper

To the Editor,

Prostate-specific antigen (PSA) is a type of serine protease produced by prostate epithelial cells. It represents the most frequently used tumor marker in early detection of prostate cancer (PC), the fifth leading cause of cancer death among men worldwide. This biomarker is useful in the identification of recurrent disease after local therapy and in the management of advanced disease as well as in the evaluation of the future risk of PC development (1). PSA is characterized by high sensitivity but unfortunately it has low specificity: in fact, it can increase in PC but also in cases of inflammation or prostate infections. Commonly, 4 ng/mL is used as a threshold value for PSA even if it has been reported that 20% of patients with low grade PC have PSA values < 4 ng/mL and only 25% of patients affected by PC show PSA levels of 4–10 ng /mL: this range is defined as a "grey zone" for PC risk (2). The clinical management of men having PSA levels in the "grey zone" is challenging: this population often undergoes invasive and expensive diagnostic investigations such as digital rectal examination, transrectal ultrasonography and particularly prostate biopsy, which has frequent and multiple complications. PSA levels may be influenced by age and BMI but mostly by several clinical conditions, i.e. prostate inflammation and infections or benign prostate hyperplasia (BPH), which deserve careful attention in the interpretation of test results (1). Moreover, several studies recently investigated the relationship between PSA and biochemical parameters. For example, in a few scientific studies it was found that higher serum ferritin levels were positively associated with increased serum PSA levels and risk of PC (3). Some papers described a proportional increase of total cholesterol, high-density lipoprotein (HDL), low-density lipoprotein (LDL) and triglycerides in PC patients with high PSA levels, although the exact roles of different lipid fractions on PC aggressiveness should be further evaluated (4). Lately, many studies focused their attention on serum 25(OH)Vitamin D and PC and the results are still controversial (5). 25(OH)Vitamin

Key words: PSA; "grey zone"; biochemistry; lipid profile; ferritin; 25(OH)Vitamin D

Corresponding Author:
Dr Emanuela Anastasi,
Department of Molecular Medicine,
"Sapienza" University, Viale Regina Elena 324,
00161 Rome, Italy
Tel.: +39 064472347 - Fax: +39 064478381
e-mail emanuela.anastasi@uniroma1.it

0393-974X (2020)
Copyright © by BIOLIFE, s.a.s.
This publication and/or article is for individual use only and may not be further reproduced without written permission from the copyright holder.
Unauthorized reproduction may result in financial and other penalties
DISCLOSURE: ALL AUTHORS REPORT NO CONFLICTS OF INTEREST RELEVANT TO THIS ARTICLE.

D deficiency has been associated with augmented risk of PC for men with elevated serum PSA levels, but other findings conversely suggested that men with higher 25(OH)Vitamin D serum levels were at increased risk of developing PC (6). It is known that PC risk is higher in men with PSA of 4 to 10 ng/mL but in clinical practice it could be difficult to distinguish PC from BPH based on PSA levels in this range (2). As a consequence, men having PSA "grey zone" often undergo many unnecessary medical procedures, and it would be useful to better characterize this population of subjects to possibly identify which patients really need a prostate biopsy, and biochemical parameters could represent a non-invasive and economic tool (1). The aim of this study is to evaluate a potential association between PSA and certain biochemical parameters, comparing serum values of each analyte in two groups of healthy Italian men: one with PSA normal range *vs* one other with PSA "grey zone".

MATERIALS AND METHODS

Subjects

This research was designed as a cross-sectional study. Between 2015 and 2018, 1421 blood donors aged between 40 and 70 (mean±SD, 54.71±5.63) were enrolled at the transfusion center of Policlinico Umberto I, Sapienza University of Rome (latitude 41°54′39″24 N). Informed consent was obtained from all participants in the study. Subjects selected for this research were healthy males: we chose blood donor volunteers since they are by definition presumably normal subjects, since before donation they are checked also for possible biochemical abnormalities. At enrollment the medical history of the subjects was collected through their statements, and weight, height and blood pressure were recorded. Specific inclusion criteria for our selected population were: having no present or past PC or malignant diseases, no symptoms suggestive of prostatic disorders, no drugs that affect mineral or iron metabolism, no use of any lipid lowering medications or 25(OH)Vitamin D supplementation. We selected only subjects making one donation per year since it is known that ferritin values are affected by this feature. Peripheral blood samples were drawn and immediately sent to the laboratory of Tumor Markers of the Policlinico Umberto I, Sapienza University of Rome and all men were screened for PSA. Among 1,421 blood donors tested for PSA two subgroups were identified: 63 subjects with PSA between 4 and 10 ng/mL and 69 subjects with PSA levels lower than 4 ng/mL. The two groups were homogeneous in terms of age and body mass index. Both populations were tested for lipid profile, ferritin and 25(OH)Vitamin D. The study protocol was approved by our local Institutional Review Board and was performed in accordance with the Declaration of Helsinki.

Methods

Body mass index (BMI) was calculated by the person's weight in kilogram, divided by height in square meters. Peripheral blood samples were collected into 5 mL Red Top Vacutainer tubes with separator gel (Becton, Dickinson and Company, Plymouth, UK), clotted 60 – 90 min and centrifuged for 15 min at 3500 x g. The resulting serum fractions were aliquoted in 1.5 mL Eppendorf tubes (Eppendorf srl, Milano, Italy) and stored at – 80°C until analysis. PSA concentrations were determined using the Access Hybritech PSA kit (Beckman Coulter, Brea, CA, USA), which is World Health Organization (WHO) standardized (PSA WHO 96/670). All tests were run on the automatic chemiluminescent enzyme immunoassay (CLEIA) instrument Access® 2 Immunoassay System (Beckman Coulter, Brea, CA, USA). The detection range was between 0,008–150 ng/mL, with intra-assay coefficient of variation (CV) < 7 % based on the 95% confidence interval, according to manufacturer's specifications.

Ferritin, total cholesterol, HDL, LDL and triglyceride concentrations were measured by electrochemiluminescence immunoassays on the Cobas®E601 chemistry analyzer (Roche Diagnostics, Mannheim, Germany). Calibrators were obtained from Roche Diagnostics. The intra-assay CV was < 5% for each kit utilized. The detection range were 5-1000 µg/L, 3.86-800 mg/dL, 3.09-150 mg/dL, 3.87-549 mg/dL, 8.85-885 mg/dL, respectively, for ferritin, total cholesterol, HDL, LDL, triglycerides. Quantitative determination of serum 25(OH)Vitamin D was performed using the LUMIPULSE G 25(OH)Vitamin D kit (Fujirebio, Tokyo, Japan) on a Lumipulse® G1200 (Fujirebio-Europe, Gent, Belgium) which is an automated assay instrument based on CLEIA technology by a two-step sandwich in

immunoreaction cartridges (7). The detection range was between 4–150 ng/mL, with intra-assay CV < 3% based on the 95% confidence interval, according to manufacturer's specifications. 25(OH)Vitamin D levels were categorized in insufficient (< 20 ng/mL) and sufficient (≥20 ng/mL) according to the latest guidelines published by the Food and Medicine Board at the National Institute of Medicine.

Statistical analysis

Descriptive statistics of the two groups were presented as mean and standard deviation (SD), except for age that was presented as median and interquartile range. Normality was tested using Shapiro-Wilk test. In order to assess differences between the two groups regarding age, BMI and biochemical analytes (total cholesterol, HDL, LDL, triglycerides, ferritin and 25(OH)Vitamin D), Student's *t*-test was applied and differences were tested by the Mann–Whitney U test. If results between the two tests were consistent, only P-value of the Student's *t*-test was reported. Differences for dichotomized 25(OH)vitamin D (in < 20 ng/mL or ≥20 ng/mL) were assessed using *Chi*-squared test. To determine which variables were independently associated with PSA "grey zone" a logistic regression model was built, including all variables with P < 0.25 at the univariate analysis and all those variables considered relevant by a biological point of view, as proposed by Hosmer and Lemeshow. A second logistic regression model considering 25(OH)Vitamin D ≥ 20 ng/mL as the dependent variable was built, including all the preceding variables and seasonality, dichotomized in autumn-winter and spring-summer. Significance level was set at the 0.05. All statistical analyses were performed using the STATA software (version 15.1; STATA Corp., College Station, TX).

RESULTS

PSA values between 4 and 10 ng/mL were found in 4.4% (63) of the 1,421 healthy men enrolled in our study. None of the subjects showed PSA >10 ng/mL. The group of men with PSA "grey zone" had a median age of 58 (IQR 54-61) and a mean BMI of 26.04±2.52. Among the remaining 1,358 studied, blood donors with PSA values <4ng/mL, a group of subjects were selected similar for both age (median 56; IQR 52-60) and BMI (mean 26.05±2.83) to the population of men with PSA "grey zone". Student's *t*-test results, consistent with Wilcoxon signed-rank non-parametric test results, showed no statistically significant difference for age and BMI between men in "grey zone" and the selected population of 69 subjects with PSA <4 ng/mL. None of the biochemical analytes showed statistically significant differences between the two groups for both Student's *t*-test and Mann–Whitney U test non-parametric test. Mean values, standard deviations and the P values of the Student's *t*-test for age, BMI and the biochemical analytes are reported in Table I. Furthermore, although in the PSA "grey zone" group there was higher frequency of subjects with 25(OH) Vitamin D level ≥ 20 ng/mL than in men with PSA < 4 ng/mL (55.56% *vs* 44.44%) this difference was not statistically significant (p= 0.47) (Not shown in table). We further investigated the possible association between age, BMI, biochemical analytes and PSA values. Logistic regression model showed no association between all the selected parameters and PSA in the "grey zone". However, even if it did not achieve statistical significance, 25(OH)Vitamin D ≥20 ng/mL showed the highest association with "grey zone" PSA (OR 1.38, C.I. 0.67 - 2.84) (Table II). We formulated a model testing 25(OH)Vitamin D ≥20 ng/mL as the dependent variable and we found no statistically significant associations except for seasonal variability: 25(OH)Vitamin D values were higher when tested in the spring-summer period than in the autumn and winter months (P = 0.04). The results are shown in Table III.

DISCUSSION

In the present study we did not find any statistically significant difference between "grey zone" population *versus* the "normal range" group regarding the levels of some common biochemical analytes (ferritin, total cholesterol, HDL, LDL, triglycerides and 25(OH)Vitamin D) which, in the scientific literature, have been more frequently associated with modifications of PSA levels. This paper constitutes the first report which tried to better characterize biochemical parameters of this particular population at increased risk of developing PC, the most common malignancy of the male reproductive

Table I. *Comparisons of age, BMI and biochemical analytes between the two groups (PSA < 4 ng/mL and "grey zone" PSA)*

Characteristics	Men with PSA < 4 ng/mL (N = 69)	Men with PSA "grey zone" (N = 63)	P*
Age (years)	56 (52-60)	58 (54-61)	0.075
BMI (kg/m^2)	26.05 ± 2.83	26.04 ± 2.52	0.969
Ferritin (µg/L)	75.23 ± 53.38	63.71 ± 38.05	0.159
Total cholesterol (mg/dL)	201.19 ± 38.17	211.03 ± 34.19	0.122
HDL (mg/dL)	57.06 ± 12.19	59.33 ± 11.99	0.282
LDL (mg/dL)	121.99 ± 33.27	129.43 ± 33.91	0.205
Triglycerides (mg/dL)	106.97 ± 60.46	98.63 ± 47.96	0.384
25(OH)Vitamin D (mg/dL)	20.33 ± 8.74	19.48 ± 6.70	0.531

*Data are reported as mean±standard deviation except for age that is reported as median and interquartile range. BMI: body mass index; HDL: high-density lipoprotein; LDL: low-density lipoprotein. P < 0.05 was considered statistically significant. *Results of the Student's t-test.*

Table II. *Logistic regression analysis assessing associations between examined variables and PSA "grey zone"*

Variables	OR	95% C.I.	P
Age (years)	1.06	0.98 – 1.13	0.130
BMI (kg/m^2)	1.02	0.88 – 1.18	0.780
Ferritin (µg/L)	0.99	0.99 – 1.00	0.272
Total cholesterol (mg/dL)	1.02	0.99 – 1.05	0.243
HDL (mg/dL)	0.99	0.95 – 1.04	0.747
LDL (mg/dL)	0.99	0.96 – 1.02	0.607
Triglycerides (mg/dL)	0.99	0.98 – 1.00	0.242
25(OH)Vitamin D (≥20 mg/dL)	1.38	0.67 – 2.84	0.381

OR: odds ratio; CI: confidence interval; P < 0.05 was considered statistically significant

system (2). Unexpectedly, our study showed no associations between PSA and ferritin serum levels in both study populations. Indeed, we expected to find significantly higher ferritin concentrations in men with PSA "grey zone", according to studies reporting that high serum ferritin levels are positively associated with elevated PSA levels and PC risk (3). In the current research we did not observe any association between PSA levels and total cholesterol, LDL, HDL and triglycerides, respectively, either in men with PSA in "normal range" or in "grey zone". Our results are in line with a recent meta-analysis

Table III. *Logistic regression analysis assessing associations between examined variables and seasonal variability of 25(OH)Vitamin D ≥20 mg/dL*

Variables	OR	95% C.I.	P
Age (years)	0.96	0.89 – 1.03	0.238
BMI (kg/m^2)	1.03	0.89 – 1.19	0.674
PSA "grey zone"	1.46	0.70 – 3.05	0.309
Season (spring-summer)	2.16	1.03 – 4.53	0.042
Ferritin (µg/L)	1.00	0.99 – 1.01	0.556
Total cholesterol (mg/dL)	0.99	0.96 – 1.02	0.482
HDL (mg/dL)	1.03	0.98 – 1.07	0.240
LDL (mg/dL)	1.01	0.98 – 1.04	0.519
Triglycerides (mg/dL)	1.00	0.99 – 1.01	0.829

OR: odds ratio; CI: confidence interval; P < 0.05 was considered statistically significant

reporting no significant association between total cholesterol, HDL or LDL and risk of overall or high-grade PC (8). However, it has been reported that higher total cholesterol and LDL were significantly related to higher PSA levels and some studies also showed that obesity, hypertriglyceridemia and low levels of HDL are associated with reduced levels of PSA (9). We decided to focus on the relationship between 25(OH)Vitamin D and PSA since it has been thoroughly investigated lately. In the present study, no association was found between PSA and 25(OH) Vitamin D serum levels in men with PSA "grey zone" and in men with PSA < 4 ng/mL. Our results are in line with studies reporting no association of 25(OH)Vitamin D serum levels with PC incidence, even if controversial results have been showed on this topic: for example, a recent dose-response meta-analysis quantitatively examined the association of circulating 25(OH)Vitamin D concentration with PC and suggested that high 25(OH)Vitamin D levels are correlated with elevated risk of developing this malignancy (6, 10-11). In our study, the statistical analysis showed no significant differences in 25(OH) Vitamin D levels between men with PSA <4ng/mL and those with PSA ranging from 4 to 10 ng/mL, even if a larger percentage of men with sufficient levels (≥20 ng/mL) was found in the "grey zone" population (55.56%) than in the normal range one (44.44%). Additionally, the data obtained in our study indicated a significant seasonal variation of 25(OH)Vitamin D serum levels: in all men studied 25(OH)Vitamin D was higher in the spring-summer period than in the autumn and winter months, as reported in many investigations (12). The present study is of interest as, to the best of our knowledge, no previous research has explored any possible correlation between PSA "grey zone" and the biochemical parameters examined. We can speculate that we did not find any association between biochemical parameters and PSA levels because we studied men with PSA "grey zone" and no PC: future studies could be structured to investigate possible associations between biochemical parameters and PSA "grey zone" in men with a PC diagnosis and also to find correlations between biochemical parameters and tumor grading in this population. We are aware

that this research has some drawbacks. Firstly, a relatively small number of subjects constituted the two groups tested for each biochemical parameter selected. Further studies are needed to extend this work on larger cohorts to validate the results. Secondly, we focused only on certain biochemical parameters: it would be interesting to study also other analytes to better delineate PSA "grey zone" population. Finally, as a retrospective study we could not investigate a possible intake by the subjects of supplements containing 25(OH)Vitamin D: however, the seasonal variability of 25(OH)Vitamin D, which emerged from our study, greatly reduces the possibility that this dietary supplementation has occurred. Despite these limitations, this study clarifies some biochemical aspects of a slightly investigated population of men, which often are involved in invasive and unnecessary diagnostic procedures. In conclusion, our findings could represent a ground for additional researches concerning any potential association with biochemical profile of men with PSA "grey zone" and their risk of developing PC.

ACKNOWLEDGEMENTS

We are thankful to Silvestra Tudini and Barbara Colaprisca for their technical assistance. This work was supported by Adspem (Associazione Donatori Sangue Problemi Ematologici).

REFERENCES

1. Ilic D, Djulbegovic M, Jung JH, et al. Prostate cancer screening with prostate-specific antigen (PSA) test: a systematic review and meta-analysis. BMJ 2018; 5:362:k3519. doi: 10.1136/bmj.k3519.
2. Liu J, Wang ZQ, Li M, Zhou MY, Yu YF, Zhan WW. Establishment of two new predictive models for prostate cancer to determine whether to require prostate biopsy when the PSA level is in the diagnostic gray zone (4–10 ng /ml−1). Asian J Androl 2020; 22(2):213-16 doi: 10.4103/aja.aja_46_19.
3. Su Q, Lei T, Zhang M. Association of ferritin with prostate cancer. J BUON 2017; 22:766-70.
4. Zapata D, Howard LE, Allott EH, Hamilton RJ, Goldberg K, Freedland SJ. Is PSA related to serum cholesterol and does the relationship differ between black and white men? The Prostate 2015; 75(16):1877-85. doi: 10.1002/pros.23069.
5. Tuohimaa P, Tenkanen L, Ahonen M, et al. Both high and low levels of blood vitamin D are associated with a higher prostate cancer risk: a longitudinal, nested case-control study in the Nordic countries. Int J Cancer 2004;108(1):104-08.
6. Grant WB. Vitamin D status: ready for guiding prostate cancer diagnosis and treatment? Clin Cancer Res 2014; 20(9):2241-43. doi: 10.1158/1078-0432. CCR-14-0369.
7. Anastasi E, Fuggetta E, De Vito C, et al. Low levels of 25-OH vitamin D in women with endometriosis and associated pelvic pain. Clin Chem LabMed 2017; 55(12):e282-e284 doi: 10.1515/cclm-2017-0016.
8. Yu PL, YuXue Z, PengFei L, et al. Cholesterol levels in blood and the risk of prostate cancer: a meta-analysis of 14 prospective studies. Cancer Epidemiol Biomarkers Prev 2015; 24(7):1086-93. https://doi: 10.1158/1055-9965.EPI-14-1329.
9. Gao X, Bao T, Yang H, et al. The association of metabolic syndrome and its components with serum prostate-specific antigen levels. Eur J Cancer Prev 2019; https://doi: 10.1097/CEJ.0000000000000508.
10. Sawada N, Inoue M, Iwasaki M, et al. Plasma 25-hydroxy vitamin D and subsequent prostate cancer risk in a nested Case-Control study in Japan: The JPHC study. Eur J Clin Nutr 2017; 71(1):132-36. https://doi:10.1038/ejcn.2016.184.
11. Gao J, Wei W, Wang G, Zhou H, Fu Y, Liu N. Circulating vitamin D concentration and risk of prostate cancer: a dose-response meta-analysis of prospective studies. Ther Clin Risk Manag 2018; 14:95-104.
12. Yu HJ, Kwon MJ, Woo HY, Park H. Analysis of 25-Hydroxyvitamin D Status According to Age, Gender, and Seasonal Variation. J Clin Lab Anal 2016; 30(6):905-11. https://doi: 10.1002/jcla.21955.

LETTER TO THE EDITOR

NEW THERAPEUTIC STRATEGIES FOR THE TREATMENT OF RECURRENT RESPIRATORY TRACT INFECTIONS IN CHILDREN

E. CANTONE, M. CAVALIERE, E. BEGVARFAJ, S. MOTTA and M. IENGO

Department of Neuroscience, Reproductive and Odontostomatological Sciences - ENT section, University "Federico II", Naples, Italy

Received February 13, 2020 – Accepted April 24, 2020

To the Editor,

Recurrent respiratory infections (RRIs), the etiology of which is mostly viral, refer to any infection that occurs 6 or more times within a year, or to one or more respiratory infections per month in the period between September and April, or even to 3 or more infections per year involving the lower airways. However, every definition of RRI is arbitrary and too generic and restrictive, therefore, to assess the diagnosis of recurrent respiratory infection in clinical practice it is preferable to exclude conditions that could be diagnosed and treated as a specific disease (1). Children are inclined to develop these infections because of the relative immaturity of their immune system; other risk factors are attending nursery school, environmental pollution, passive smoking, low socio-economic level, and allergic disorders (2).

From a clinical point of view, nasal obstruction is one of the most important clinical features of RRI, hence ensuring adequate nasal breathing is the keystone of the therapy. Recent studies have shown the effectiveness of hyaluronic acid (H) in the treatment of RRIs, and other studies have also shown that xylitol (X)-based nasal irrigations, due to their innate bactericidal and anti-adhesive effects, improve biological parameters of the upper airways (3-7). Generally, in the management of a therapeutic protocol for RRIs, the choice of an effective and easy-to-use device is crucial for children. Currently, the intranasal mucosal atomizer device (MAD) and nasal douche (D), due to the diameter of particles they are able to generate (30 μm) and to the speed of administration, are widely used in pediatrics, both for nasal cavity hygiene and for the intranasal administration of drugs (7).

This study set out to evaluate, for the first time, the impact of H with the addition of X (HX) administered through intranasal mucosal atomizer device (MAD) on the clinical and instrumental variables associated with RRI in children.

MATERIALS AND METHODS

The study was carried out at the University of Naples, Federico II, ENT section, on 126 children aged between 6 and 11 (60 males, 66 females, mean age 7±2.1 SD years) affected by upper RRI, defined as 6 or more upper respiratory infections per year or 1 or more respiratory infections per month between September and April. Twelve subjects dropped out of the study. Children suffering from acute infections, severe heart disease or systemic diseases, chronic respiratory diseases (e.g., cystic fibrosis and primary ciliary dyskinesia), immunodeficiencies, fever, ongoing treatment with cough suppressants, antibiotics, steroids and antihistamines, psychogenic cough, choanal atresia, and with a history

Key words: RRI; nasal obstruction; QoL

Corresponding Author:
Elena Cantone, MD, PhD
Department of Neuroscience,
Reproductive and Odontostomatological Sciences,
ENT section, University "Federico II", Via Pansini, 5,
80131, Naples, Italy
Tel.: +39 0817463598 - Fax: +39 0817463592
e-mail: cantoneent@gmail.com

0393-974X (2020)
Copyright © by BIOLIFE, s.a.s.
This publication and/or article is for individual use only and may not be further reproduced without written permission from the copyright holder.
Unauthorized reproduction may result in financial and other penalties
DISCLOSURE: ALL AUTHORS REPORT NO CONFLICTS OF INTEREST RELEVANT TO THIS ARTICLE.

of previous surgery were excluded from the study. The parents or guardians of enrolled subjects gave their informed consent to participate in the study, which was fully approved by the local Board of Medical Ethics (n. 98/19).

Subjects were randomized into 6 groups and given the following treatments:

- H: isotonic solution of high molecular weight H (4 mL);
- HX: isotonic solution high molecular weight H acid and X (4 mL) [Aluneb, Sakura Italia, Srl];
- C: isotonic solution (sodium chloride 0.9%) (4 mL), control group;
- H and C were prepared specifically for this study based on the HX manufacturing process (either by removing X –H solution- or both X and H – C solution).

Treatments were administered through 2 medical devices:

- MAD consists of an atomization nasal nozzle tip attached to standard 3 cc syringe. The patient unscrews the tip and then draws the drug solution into the syringe by lifting the plunger; then he/she screws the tip back into place and after placing the tip in the nostril, depresses the plunger to dispense the drug. [Aluneb, MAD Nasal Sakura Italia, Srl];
- D atomizes particles, enhancing an optimal deposition in the whole nasal cavity, up to the naso-pharynx (Rhinowash, Air Liquide Medical Systems Italy S.p.A., Brescia, Italy) (7).

In all groups, treatments were administered twice a day for 30 consecutive days.

To assess quality of life (QoL), groups were asked to answer the Visual Analogue Scale (VAS) questionnaire, which included questions about rhinorrhea (VASr), nasal obstruction (VASo) and cough (VASc). The VAS questionnaire is a continuous scale comprised of a horizontal line, 10 cm in length, anchored by two descriptors one for each symptom extreme (0= Not troublesome, 100 mm= worst thinkable troublesome), that serves to evaluate the total severity of symptoms (7). The disease was divided into mild, moderate, and severe based on total severity VAS scores (mild, VAS = 0-3; moderate, VAS = 4−7; and severe, VAS = 8−10). A VAS > 5 affected patient QoL (7). A clinical and endoscopic examination allowed the classification previously described by Lund-Kennedy (LK) for rhinosinusitis and Cassano for adenoidal hypertrophy (A) (4,7).

In order to objectively evaluate the nasal obstruction, we measured the peak nasal inspiratory flow (PNIF). PNIF is a economic and quick method for the objective assessment of nasal obstruction, both bilaterally and unilaterally. PNIF measurements were conducted as previously reported (8). A portable Youlten peak flow meter (Clement Clark International) was used for the measurement of PNIF. The patient was seated, rested for 15 minutes and cautiously blew his nose, three maximal inspirations were obtained each time, and only the best was used for the evaluation. All measurements were performed in the morning. All PNIF scores were measured in L/minute (8). Nasal cytology was performed as previously described by anterior rhinoscopy (9). The scraping of the nasal mucosa was collected from the middle portion of the inferior turbinate using a Nasal Scraping (IR MEDICAL, Lugo, RA, Italy) cytology curette. Samples were placed on a glass slide, fixed by air drying and stained according to the May-Grunwald Giemsa (IR MEDICAL, Lugo, RA, Italy) method and then observed by optical microscope. The nasal cytological assessment, performed in blind condition by the same investigator who was unaware of the assigned treatment, evaluated the presence and the number of goblet cells (Gc), neutrophils (N), eosinophils (E), mast cells (M), bacteria (B) and fungi (F), according to a 0-4 score (0 = absent, 1 = rare, 2 = some, 3 = easily visible, 4 = many) (26). QoL tools, as well as nasal endoscopy, PNIF and nasal cytology were administered at baseline before treatments (T0) and 30 days after therapy (T30).

Statistical analysis

Continuous baseline characteristics were described as either median, mean, or standard deviation where appropriate. Difference between two groups was tested by *t*-test, differences among groups were tested with the ANOVA; $p< 0.05$ was considered statistically significant. Data were tabulated in a Microsoft Excel (Microsoft Corporation, Redmond, WA) spreadsheet and imported into the Statistical Package for the Social Sciences (SPSS-PC, version 16; SPSS Inc., Chicago, IL).

RESULTS

A total of 71 patients, investigational arm,

distributed in 4 groups and 43 controls, distributed in 2 groups, completed the study. The 6 groups were well matched. Forty-seven patients (38%) reported a history of allergy (Fig. 1).

At baseline (T0), no statistically significant differences were observed in the clinical, endoscopic, and QoL tools, nor in any examined parameters among groups (p>0,05). At cytological assessment we did not find fungi either at T0 or at T30, in all groups. After treatments (T0 *vs* T30) we observed significant improvements in the groups treated both with H alone and with HX regardless of the device (D or MAD) (Table I). Conversely, we did not find significant improvements after treatment in the control group except for VASr (Table I) regardless of the device (D or MAD).

In order to evaluate the effect of X at T30, we compared children undergoing therapy with HX and those undergoing therapy with H alone, regardless of the device, and we found that treatment with HX improved the perceived symptomatology of nasal obstruction and cough, A score and N count (Table II). We also compared children undergoing therapy with HX and children undergoing therapy with H considering the two devices, D and MAD. When we compared HXD and HD we did not find statistically significant differences except for the VASc (Table II). Conversely, when we compared the groups treated by MAD (HXM *vs* HM) we found significant differences in the VAS and A scores, in the Gc and N counts in favor of the group treated with HX (Table II). Comparing patients treated with HX through D with patients treated with MAD we found significant differences for VASr, VASo, A score, Gc and N counts, and PNIF in favor of MAD (Table III). Eventually, we evaluated differences among groups (HXM, HM, CM) and VAS symptoms, LK, A, Gc, and PNIF scores significantly improved in HXM group (Fig. 2).

Table I. *Clinical outcomes T0 v sT30*

	HT0	HT30	p	HXT0	HXT30	p	CT0	CT30	p
VASr	7.8±1.7	3.4±1.4	0.001	7.7±1.7	2.8±1.8	0.001	7.6±1.8	6.9±1.6	0.01
VASo	7.4±1.1	4.2±1.5	0.001	7.4±1.1	3.8±1.4	0.001	6.7±1.3	6.4±1.7	0.3
VASc	5.2±2.4	3.6±1.2	0.004	5.3±2.7	2,6±1.5	0.001	5.6±2.3	5.6±2.1	0.07
Nasal endoscopy									
LK	4.1±1.7	2.9±1	0.008	3.5±1.3	2.8±1	0.009	4.2±1.5	4.1±1.3	0.8
A	2.6±0.6	2.3±0.4	0.05	3.3±0.4	1.8±0.7	0.03	2.8±0.6	2.6±0.4	0.1
Nasal cytology									
Gc	1.6±0.7	1.3±0.7	0.03	1.7±0.7	1±0.6	0.0004	2±0.7	1.9±0.8	0.6
N	3.2±0.7	2.8±0.8	0.01	3.3±0.7	2.4±0.8	0.0001	3±1	3.3±0.7	0.1
B	2.1±0.9	1.4±0.9	0.001	2.2±1	1.5±1	0.002	2.2±0.9	1.8±1	0.1
E	0.9±0.7	0.4±0.5	0.001	0.3±0.6	0.2±0.4	0.04	0.5±0.7	0.4±0.7	0.4
M	0.6±0.7	0.2±0.4	0.05	0.5±0.7	0.2±0.5	0.005	1.6±0.7	0.9±0.8	0.2
PNIF	35.9±13.2	43.7±20.2	0.05	38.2±19.2	43.3±20.1	0.005	35.7±16.7	37.6±15.4	0.6

After treatments (T0 vs T30) we observed significant improvements in the groups treated with H alone and HX regardless of the device. We did not find significant improvements after treatment in the control group regardless of the device (D or MAD) except for VASr.

VASr: visual analogue scale, rhinorrhea; VASo: visual analogue scale, nasal obstruction; VASc: Visual Analogue Scale, cough; LK: Lund-Kennedy score for rhinosinusitis; A: adenoidal hypertrophy score; Gc: goblet cells; N: neutrophil; E: eosinophils; M: mast cells; B: bacteria; PNIF: peak nasal inspiratory flow; H: Hyaluronic acid; X: xylitol; D: nasal douche; M: MAD; C: controls.

Table II. *Clinical outcomes at T30 (HX vs H; HXD vs HD; HXM vs HM)*

	HXT30	HT30	p	HXDT30	HDT30	p	HXMT30	HMT30	p
VASr	2.6±1.8	3.4±1.4	0.06	3.5±1.9	3.8±1.7	0.6	1.5±0.9	3±1.1	0.0001
VASo	3.8±1.4	4.2±1.7	0.02	4.8±0.7	5.1±1.3	0.1	2.5±0.9	3,2±0,9	0,02
VASc	2.6±1.5	3.6±1.2	0.003	2.4±1.5	3.4±1.4	0.005	2.8±1.6	3.8±0.9	0.04
Nasal endoscopy									
LK	2.8±1	2.9±1.4	0.5	2.8±1	2.9±1	0.7	2.8±1	3±1	0.5
A	1.8±0.7	2.3±0.4	0.003	2.3±0.4	2.4±0.5	0.5	1.4±0.5	2.3±0.4	0.0001
Nasal cytology									
Gc	1±0.6	1.3±0.7	0.2	1.3±0.6	1.4±0.6	0.8	0.7±0.5	1.2±0.7	0.05
N	2.4±0.8	3±0.6	0.05	2.8±0.7	3±0.8	0.5	1.8±0.7	2.6±0.7	0.04
B	1.5±1	1.4±0.9	0.9	1.6±1.1	1.4±0.9	0.5	1.3±0.9	1.5±1	0.5
E	0.2±0.4	0.4±0.5	0.1	0.2±0.4	0.5±0.6	0.1	0.2±0.5	0.4±0.5	0.4
M	0.2±0.5	0.2±0.4	0.5	0.2±0.5	0.2±0.4	0.8	0.2±0.4	0.3±0.4	0.5
PNIF	43.3±20.2	42.4±18.1	0.4	34.7±16.2	33.2±18	0.7	54.3±19.8	52±19	0.8

Comparing HX and H alone regardless of the device at T30, we found that treatment with HX improved the perceived symptomatology VASc, the A score and N count. Comparing HXD and HD we did not find statistically significant differences except for the VASc. Comparing HXM and HM we found significant differences in the VAS and A scores, in the Gc and N count in favor of the group treated with X.

VASr: visual analogue scale, rhinorrhea; VASo: visual analogue scale, nasal obstruction; VASc: Visual Analogue Scale, cough; LK: Lund-Kennedy score for rhinosinusitis; A: adenoidal hypertrophy score; Gc: goblet cells; N: neutrophil; E: eosinophils; M: mast cells; B: bacteria; PNIF: peak nasal inspiratory flow; D: nasal douche; M: MAD; H: Hyaluronic acid; X: xylitol.

Population characteristics at baseline	
N.ro	126 (71cases+43 controls+12 drop out)
Age	7±2.1 (mean±SD)
Sex	53M; 61 F
Allergy	47 (38%)
D	58
M	56
HX	34
H	37
HXD	19
HXM	15
HD	18
HM	19

Fig. 1. *A total of 71 patients, investigational arm, distributed in 4 groups and 43 controls, distributed in 2 groups, completed the study. The 6 groups were well matched. Forty-seven patients (38%) reported a history of allergy. D: nasal douche; M: MAD; H: Hyaluronic acid; X: xylitol.*

Table III. *Clinical outcomes at T30 (HXD vs HXM)*

	HXDT30	HXMT30	p
VASr	3.5±1.9	1.5±0.9	0.001
VASo	4.8±0.7	2.5±0.9	0.0001
VASc	2.4±1.5	2.8±1.6	0.4
Nasal endoscopy			
LK	2.8±1	2.8±1	0.9
A	2.3±0.4	1.4±0.5	0.05
Nasal cytology			
Gc	1.3±0.6	0.7±0.5	0.004
N	2.8±0.7	1.8±0.7	0.0007
B	1.6±1.1	1.3±0.9	0.4
E	0.2±0.4	0.2±0.5	0.9
M	0.2±0.5	0.2±0.4	0.9
PNIF	34.7±16.2	54.3±19.8	0.003

Comparing HXD and HXM we found significant differences for VASr, VASo, Gc, N counts and PNIF in favor of MAD.
VASr: visual analogue scale, rhinorrhea; VASo: visual analogue scale, nasal obstruction; VASc: Visual Analogue Scale, cough; LK: Lund-Kennedy score for rhinosinusitis; A: adenoidal hypertrophy score; Gc: goblet cells; N: neutrophil; E: eosinophils; M: mast cells; B: bacteria; PNIF: peak nasal inspiratory flow; D: nasal douche; M: MAD; H: Hyaluronic acid; X: xylitol.

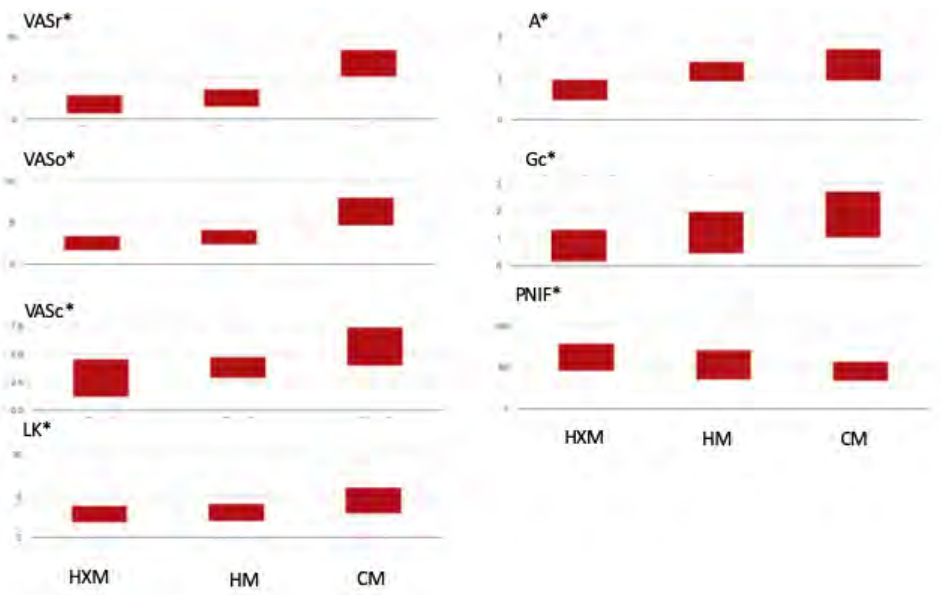


Fig. 2. *Differences among groups (HXM, HM, CM). VAS symptoms, LK, A, Gc, and PNIF scores significantly (*) improved in HXM group.*
VASr: visual analogue scale, rhinorrhea; VASo: visual analogue scale, nasal obstruction; VASc: Visual Analogue Scale, cough; LK: Lund-Kennedy score for rhinosinusitis; A: adenoidal hypertrophy score; Gc: goblet cells; PNIF: peak nasal inspiratory flow; H: Hyaluronic acid; X: xylitol; M: MAD; C: controls.

DISCUSSION

The etiology of RRIs is mostly viral, and a recent study demonstrated that viruses were found in the rhinopharynx in 38% of cases of recurrent tonsillitis (10). Although pediatric guidelines suggest limiting the administration of antibiotics to more serious infections, this recommendation is very often not taken into consideration in clinical practice, and antibiotic therapy is commonly prescribed together with anti-inflammatory and/or antipyretic drugs, hence the need to find new therapeutic strategies for the treatment of RRIs. Previous study demonstrated the role of H in improving the mucociliary clearance and QoL of patients suffering from respiratory diseases (7). In our study, we observed that both H and HX, were useful in the treatment of RRI regardless of the devices, also demonstrating the role of nasal washes in the treatment of nasal discharge (Table I). In addition, the HX association was more powerful than H alone in the amelioration, not only of the perceived symptomatology, but also of the objective clinical data, as nasal endoscopy and N count, this latter in particular due to the higher anti-inflammatory effect of HX association. Our results showed that the HX association provided better outcomes than H alone whether administered through D or through MAD (Table II). In particular, our data enhanced the higher impact of the HXM protocol in RRI due to the diameter of particles that MAD is able to generate (Fig. 2). Of particular clinical interest is the improvement of the PNIF, that objectively evaluates the nasal obstruction, i.e. the pivotal symptom of RRI. Particle deposition pattern, however, relies on many other features such as gender, age and physiological status (11). The combination of the solution containing HX and MAD has shown to be highly appropriate in terms of particle characteristics, provided by the results obtained in the current *in vivo* study, being particularly effective in the management of RRI in children.

The treatment with HXM would allow to reduce the economic expenses and reserve antibiotic, anti-inflammatory and/or antipyretic therapy only in the most serious cases, also reducing antibiotic prescriptions and antibiotic resistance. Furthermore, the administration of HX *via* MAD appears to further improve its therapeutic role. In addition, MAD nasal is more comfortable, faster ,and easier to use than D, it does not require a pneumatic pump and can be conveniently transported.

REFERENCES

1. Yin J, Xu B, Zeng X, Shen K. Broncho-Vaxom in pediatric recurrent respiratory tract infections: A systematic review and meta-analysis. Int Immunopharmacol 2018; 54:198-209.
2. Tarantino V, Savaia V, D'Agostino R, et al. Bacteriotherapy in children with recurrent upper respiratory tract infections. Eur Rev Med Pharmacol Sci 2019; 23:39-43.
3. Cantone E, Iengo M. Effect of sodium hyaluronate added to topical corticosteroids in chronic rhinosinusitis with nasal polyposis. Am J Rhinol Allergy 2016; 30:340-43.
4. Montella S, Cantone E, Maglione M, Iengo M, Santamaria F. Sodium hyaluronate improves quality of life and nasal endoscopy features in preschool children with upper respiratory tract infections. J Biol Regul Homeost Agents 2016; 30:303-8.
5. Gelardi M, Taliente S, Fiorella ML, et al. Intranasal T-LysYal® as adjunctive therapy for patients after functional endoscopic sinus surgery. J Biol Regul Homeost Agents 2016; 30:277-84.
6. Gelardi M, Taliente S, Fiorella ML, et al. Ancillary therapy of intranasal T-LysYal® for patients with allergic, non-allergic, and mixed rhinitis. J Biol Regul Homeost Agents 2016; 30:255-62.
7. Cantone E, Castagna G, Sicignano S, Ferranti I, Rega F, Di Rubbo V, Iengo M. Impact of intranasal sodium hyaluronate on the short-term quality of life of patients undergoing functional endoscopic sinus surgery for chronic rhinosinusitis. Int Forum Allergy Rhinol 2014; 4:484-87.
8. Ottaviano G, Lund VJ, Coles S, Staffieri A, Scadding GK. Does peak nasal inspiratory flow relate to peak expiratory flow? Rhinology 2008; 46:200-203.
9. Cantone E, Marino A, Ferranti I, et al. Nasal cytological assessment after crenotherapy in the treatment of chronic rhinosinusitis in the elderly. Int

J Immunopathol Pharmacol 2014; 27:683687.

10. Mikola E, Elenius V, Saarinen M, et al. Tonsillar cytokine expression between patients with tonsillar hypertrophy and recurrent tonsillitis. Clin Transl Allergy 2018; 22:8-22.
11. Neubauer PD, Schwam ZG, Manes RP. Comparison of intranasal fluticasone spray, budesonide atomizer, and budesonide respules in patients with chronic rhinosinusitis with polyposis after endoscopic sinus surgery. Int Forum Allergy Rhinol 2016; 6:233-37.

LETTER TO THE EDITOR

FIBROMYALGIA AND THERAPEUTIC INTEGRATION: ROLE OF QUANTUM MEDICINE

G. BARASSI[1], A. YOUNES[2], A. DI IULIO[3], S. GUERRI[4], V. GUGLIELMI[4], F. DELLA ROVERE[4], M. SUPPLIZI[1] and A. DI IORIO[5]

[1]Physiotherapy Rehabilitation and Reeducation Centre (Ce.Fi.R.R.) venue "G. d'Annunzio University" Chieti-Pescara, Chieti, Italy; [2]Sector of clinical Evaluation and Diagnosis: Ce.Fi.R.R. venue "G. d'Annunzio" University Chieti-Pescara, Clinical Manager International Association for Fibromyalgia Research, Chieti, Italy; [3]UOC Thoracic Surgery. Hospital "Santo Spirito" Pescara (PE), ASL Pescara, Pescara, Italy; [4]Sector of clinical evaluation and diagnosis: Ce.Fi.R.R. venue "G. d'Annunzio" University-Chieti-Pescara, Chieti, Italy; [5]Department of Aging Sciences, "G. Annunzio" University Chieti-Pescara, Chieti, Italy

Received March 18, 2020 – Accepted April 29, 2020

To the Editor,

According to the American College of Rheumatology, fibromyalgia syndrome (FMS) is a common health problem characterized by widespread pain and tenderness (1). Patients with FMS suffer from fatigue and often have sleep disturbances. FMS is estimated to affect two to four percent of the general population. Moreover, FMS is the most common cause of generalized, musculoskeletal pain in women between the ages of 20 and 55 years. FMS is much more than pain. The treatment is based on a symptomatic approach using analgesic drugs, opioids, anticonvulsants such as pregabalin or gabapentin, and antidepressants such as milnacipran, amitriptyline, and duloxetine (2). Manual therapy (MT), as a complementary and alternative treatment, has been widely used for FMS: substantial evidence exists of the beneficial effect of MT in FMS, even if results could not be considered conclusive (3, 4).

Changes in the amplitude of Hoffmann reflex (H-reflex) may reflect variations in the characteristics of the largely monosynaptic circuit that is explored and are a possible target for physical therapeutic intervention. Previous studies had applied only fixed frequency, and did not attempt to vary impulse duration in time. H-reflex amplitude was substantially decreased (-50%) by Frequency Rhythmic Electrical Modulation System (FREMS), and the subphase C of the reflex variation was associate with w/f variation in time. Altogether, this data suggest that FREMS are effective in the modulation of H-reflex-amplitude (5).

In quantum medicine, the existence of recognition codes between molecules implies the existence of an electromagnetic level of living matter that communicates with the chemical level ensuring that the traffic of molecules is well ordered. The theory of water coherence domains is the most advanced application of the coherence of quantum electrodynamics suitable for transferring highly targeted and personalized electromagnetic signals to living cells. Clinical observations have strengthened

Key words: chronic pain; fibromyalgia; quantum medicine; rehabilitation; bioresonance

Corresponding Author:
Dr Giovanni Barassi,
Physiotherapy Rehabilitation and Reeducation Centre (Ce.Fi.R.R.) venue "G. d'Annunzio University" Chieti-Pescara,
Viale Abruzzo, 322
Chieti Scalo -66100, Italy
e-mail: coordftgb@unich.it

0393-974X (2020)
Copyright © by BIOLIFE, s.a.s.
This publication and/or article is for individual use only and may not be further reproduced without written permission from the copyright holder.
Unauthorized reproduction may result in financial and other penalties
DISCLOSURE: ALL AUTHORS REPORT NO CONFLICTS OF INTEREST RELEVANT TO THIS ARTICLE.

the applicability of this concept through cyclotronic bioresonance, QUEC PHISIS (™) technology (QPS1), in patients with complex diseases such as cardiovascular, neuromuscular and metabolic disorders. (6)

The aim of this study was to evaluate, in a single blinded randomized clinical trial, the effect of QPS1 in FMS-treatment over a standard therapeutic approach by means of MT plus FREMS.

MATERIALS AND METHODS

The patients were recruited at the physiotherapy, rehabilitation and re-education center (CeFiRR) venue of the University of Chieti-Pescara. The trial was conducted between December 2019 and February 2020. The study was conducted according to common standard guidelines for clinical studies; all participants received detailed information on the risks and benefit of the different treatments and gave signed informed consent for the experimental procedure, which complied with the latest revision of the Helsinki Declaration and with the procedures defined by the ISO 9001-2015 standards for "Research and Experimentation". This procedure also protects the privacy of subjects participating in biomedical research. Patients who met the inclusion criteria were assessed with a standardized protocol. The physician verified the patient's medical history, examined her physical health and checked the patient's medical records. The study participants were aged between 18 and 75, and fibromyalgia syndrome was diagnosed by specialists in rheumatology and pain therapy. Patients also had to report at least moderate pain of 45 mm or greater on an analog visual scale (VAS), with 100 mm described as "worst imaginable pain". Exclusion criteria for the study included: pain due to inflammatory rheumatic disorder, any serious psychiatric disorder, severe depression or substance abuse, any severe comorbidity such as cancer or neurological disorders, recently started or changed drug treatment, previous injections or acupuncture (during the previous 3 months or during the study), treatment with opioids or steroid painkillers. Drugs such as nonsteroidal anti-inflammatory or antidepressants were allowed if the dosage was kept constant during the study. Finally, pregnant or lactating women or patients who took part in other clinical studies were excluded.

Therefore 20 subjects were enrolled in the study, all female, with an average age of 42 years. Patients were randomly assigned to one of two groups in sequential order by adopting a computer-generated layered block randomization (Random Allocation Software, version 1.0.0). Group A: 10 patients underwent peripheral sensorineural stimulation therapy three times a week in the order of manual neuromuscular therapy, FREMS. Group B: 10 patients assigned underwent peripheral sensorineural stimulation therapy three times a week in the order of FREMS, neuromuscular manual therapy, and QPS1.

FREMS is based on the administration of pulsed, negative, asymmetric single-phase pulsed electric fields generated by a neurostimulator with characteristics of low variable frequency, high voltage and very low pulse duration. Manual neuromuscular therapy, consisted of joint treatment, balanced ligament tension/joint ligament tension treatment, anti-stretch treatment, direct treatment, muscle energy treatment, soft tissue treatment (ST) and visceral manipulative treatment. QPS1 system emits ultra-weak electromagnetic waves which, by calculating the cyclotronic resonance of the ions in the sectors of water coherence, excite the ions themselves making them "bioavailable".

Outcome measures: Revised Fibromyalgia Impact Questionnaire (FIQR): was developed in response to known shortcomings of the Fibromyalgia Impact Questionnaire (FIQ). The FIQR has the same 3 domains as the FIQ (i.e. function, overall impact and symptoms). All questions are ranked on a 0-10 visuo-analogic-scale (VAS), typically presented as a horizontal line, and subjects have to indicate the level of pain in a scale from 0-10.

Myotonometric measurements: passive muscle stiffness, tone and elasticity were measured in a relaxed state using a portable myotonometric device, MyotonPRO (Myoton AS, Tallinn, Estonia). Two muscle sites were selected for myometric measurement: lumbar paravertebral (L3 level) and upper trapezius. At each site, the mean value of two sets of five consecutive measurements was used for analysis. The same tester performed all myometric measurements (7).

RESULTS

In the comparison between the enrolled groups, no statistically significant differences were found, at

baseline in rheological properties (elasticity, stiffness and muscle tone) nor in the evaluation of the FMS clinical score (VAS and FIQR) (Table I, column p -value 1). The rehabilitation intervention in the three months of the study induced a significant reduction of almost all the markers evaluated, regardless of the type of intervention (Table I, p value 2). Both VAS and FIQR were statistically significantly reduced in

Table I. *Mixed Model analysis, comparison between treatments and times of the study. Values are reported as mean±SE; Paraspinal muscles were assessed at L3 level.*

	Group-A		**Group-B**					
	Baseline	Follow-up	Baseline	Follow-up	p^1	R^2_ε	p^2	p^3
F.I.Q.R.	70.9±5.2	49.1±5.1	73.9±3.0	50.5±2.8	0.62	80.8	0.001	0.74
VAS	8.9±0.3	5.6±0.7	8.5±0.2	5.1±0.3	0.23	73.4	0.001	0.97
Frequency								
Trapezius R	14.7±0.7	13.5±0.7	14.5±0.6	13.0±0.7	0.82	49.5	0.001	0.74
Trapezius L	14.0±0.8	14.1±0.8	14.1±0.8	12.3±0.4	0.92	9.5	0.17	0.10
Paraspinal R	14.7±0.5	13.6±0.4	15.0±0.4	12.6±0.2	0.64	62.4	0.001	0.02
Paraspinal L	14.8±0.6	14.1±0.5	14.5±0.5	12.1±0.4	0.73	62.0	0.001	0.001
Stiffness								
Trapezius R	267.8±6.9	261.3±16.0	262.7±7.3	237.8±6.6	0.62	17.8	0.05	0.22
Trapezius L	265.4±11.8	247.2±11.7	265.7±9.4	235.9±6.2	0.98	38.1	0.002	0.40
Paraspinal R	252.2±11.7	228.9±13.3	257.8±14.9	230.8±14.9	0.77	69.6	0.001	0.62
Paraspinal L	257.5±11.6	248.3±10.1	278.7±9.0	233.4±13.8	0.17	39.8	0.002	0.01
Elastic property								
Trapezius R	1.9±0.2	1.6±0.1	2.0±0.2	1.6±0.1	0.75	47.4	0.001	0.68
Trapezius L	1.9±0.2	1.6±0.1	1.9±0.1	1.6±0.1	0.89	54.5	0.001	0.66
Paraspinal R	1.3±0.05	1.3±0.1	1.7±0.1	1.3±0.1	0.75	60.0	0.001	0.001
Paraspinal L	1.5±0.05	1.4±0.1	1.8±0.1	1.4±0.1	0.89	42.9	0.001	0.002

FIQR: Fibromyalgia Impact Questionnaire Revised; VAS: Visuo Analogic Scale; p-value 1: statistical test for the comparison between treatment at the baseline; p-value 2: statistical test for the comparison between time independently of group of treatment; R^2_ε: Proportional reduction in the Level-1 variance component for time; p-value 3: statistical test for the comparison between treatment and time (interaction term)

the comparison between the two time-points. In the FIQR score almost 80.8% of the variation within the person is associated with linear time, while in the VAS this association was 73.4%. Muscle tone assessment was statistically significantly reduced in all study groups, regardless of the treatment (Table I column p-value 2); whereas the left trapezius seems to be affected only modestly by the interventions (p value for time = 0.17). In addition, the proportional reduction of the level 1 variance component ranged from 49.5% for the right trapezius to 62.4% for the right paraspinal muscles. The elasticity parameter increased and the stiffness decreased, between the two time-points of the study, statistically significantly in the overall enrolled population, both for the trapezius and paraspinal muscles regardless of the dimensions considered (Table I column 1 value 2). The reduction of the level 1 variance component for time, ranged from 17.8% for rigidity of the right trapezius to 60% of the elastic property of the right paraspinal muscles.

No significant differences were found in the interaction between time and treatment group, with the exception of muscle tone, stiffness and the elasticity parameter for the paraspinal muscles bilaterally (p-value of column 1 of Table I). Interestingly, the percentage in total variation is linearly associated with treatment group B, and in detail, it represented 25.3% (right paraspinal muscles) and 47.4% (left paraspinal muscle) for muscle tone; 29.1% (left paraspinal muscles) for rigidity; 51.7% (right paraspinal muscles) and 40.9% (left paraspinal muscles) for elastic properties.

DISCUSSION

The diagnosis of FMS has changed in the last 10 years, but objective criteria do not yet exist: diagnosis and therapy can be complex and require the collaboration of many specialists. Rheumatologists often diagnose and differentiate FMS with other disorders from the rheumatoid group. (8). In order to evaluate the function of the endogenous mechanisms that modulate somatosensory input in the FMS, the effect of vibratory stimulation, the heterotopic harmful stimulation of conditioning on the perception of various somatosensory modalities and the transcutaneous electrical nerve stimulation were evaluated (9). Only in recent decades, biophysical studies have shown that, with the ionic resonance of the cyclotron, it is possible to stimulate the passage of ions through the cell membranes of living beings, modifying their permeability and thus improving the ion exchange on both sides of the membrane itself. Cellular DNA emits very low frequency waves. The failure of this "interval" compromises the balance of the cell, with consequent onset of pathological manifestations. The increase in the bioavailability of the essential ions increases the efficiency of the cell itself by adding its correct metabolism (10). In this study, the main results showed that the integration of rehabilitation ensured a subjective improvement in both groups by means of an objectively instrumental assessment, regardless of the type of intervention. Both MT and FREMS therapy contributed to the reduction of pain and the increase in quality of life in the two groups. The parameters of elasticity, stiffness and muscle tone improve during the three months of the study in a variable percentage that varied from 20 to 60% (11, 12). The main result of the study highlighted how QPS1 improves the accounting of muscle performance by a quarter to half of the total variation. The results confirmed the advantages of the protocol to reduce the nociceptive impact with consequent improvement of symptoms, quality of life and muscle tissue, establishing the integration of therapies in patients with FMS, using QPS1 therapy which tends to restore the functionality of the organism and its regulatory systems.

REFERENCES

1. Schmidt-Wilcke T, Clauw DJ. Fibromyalgia:from pathophysiology to therapy.Nat Rev Rheumatol 2011; 7(9):518-27. Review
2. Clauw DJ, Arnold LM, McCarberg BH. The science of fibromyalgia. Fibro Collaborative Mayo Clin Proc 2011; 86(9):907-11. Review
3. Arnold LM, Fan J, Russell IJ, et al. The fibromyalgia family study: a genome-wide linkage scan study. Arthritis Rheum 2013; 65(4):1122-8.
4. Kalichman L. Massage therapy for fibromyalgia

symptoms. Rheumatol Int 2010; 30(9):1151-7. Review
5. Barrella M, Toscano R, Goldoni M, Bevilacqua M. Frequency rhythmic electrical modulation system (FREMS) on H-reflex amplitudes in healthy subjects. Eura Medicophys 2007; 43(1):37-47.
6. Corbellini E, Corbellini M, Licciardello O, Marotta F. Modulating biological events by biophysics: an innovative molecular methodology using ion cyclotron resonance-a pilot study. Rejuvenation Res 2014; 17(2):188-91.
7. Bizzini M, Mannion AF. Reliability of a new, hand-held device for assessing skeletal muscle stiffness. Clin Biomech (Bristol, Avon). 2003; 18(5):459-61.
8. Wolfe F, Walitt B. Culture, science and the changing nature of fibromyalgia. Nat Rev Rheumatol 2013; 9(12):751-5. Review
9. Kosek E, Hansson P. Modulatory influence on somatosensory perception from vibration and heterotopic noxious conditioning stimulation (HNCS) in fibromyalgia patients and healthy subjects. Pain1997; 70:41–51.
10. Montagnier L, Del Giudice E, Aïssa J, et al. Transduction of DNA information through water and electromagnetic waves. Electromagnetic Biol Med 2015; 34:106-112.
11. Barassi G, Bellomo RG, Di Giulio C, et al. Effects of manual somatic stimulation on the autonomic nervous system and posture. Adv Exp Med Biol 2018; 1070:97-109.
12. Farina S, Casarotto M, Benelle M, Tinazzi M, Fiaschi A, Goldoni M, Smania N. A randomized controlled study on the effect of two different treatments (Frems and Tens) in myofascial pain syndrome. Eura Medicophys 2004; 40(4):293-301.

JOURNAL OF BIOLOGICAL REGULATORS & HOMEOSTATIC AGENTS Vol. 34, no. 3, 1199-1201 (2020)

LETTER TO THE EDITOR

SIX CONSECUTIVE DAYS REPRODUCIBILITY OF EXHALED VOLATILE ORGANIC COMPOUNDS ANALYSIS BY E-NOSE

S. DRAGONIERI[1], V.N. NICOLA QUARANTA[2], P. CARRATU[1], F. ORSINI[1], T. RANIERI[1] and O. RESTA[1]

[1]Respiratory Diseases, University of Bari, Italy; [2]Pulmonology, Di Venere Hospital, Bari, Italy

Received January 22, 2020 – Accepted April 29, 2020

To the Editor,

Breathomics are defined as the comprehensive molecular analysis of exhaled breath volatile organic compounds (VOCs), including several techniques such as gas-chromatography and mass spectrometry (GC-MS), and electronic noses (e-noses) (1). In particular, E-nose technology is based on sensor arrays which react to specific molecules allowing to discriminate VOC combinations by pattern recognition software (1). This approach has shown its potential to offer quick and non-invasive biomarkers for diagnosing and monitoring a number of respiratory diseases such as lung cancer, asthma and chronic obstructive pulmonary disease (2). However, before its validation, numerous methodological concerns regarding e-nose technology still need to be addressed, among which, the assessment of repeatability of breath samplings by e-nose is essential, either in healthy subjects or in patients with respiratory conditions (3).

For the above reason, the aim of this study was to investigate the repeatability of exhaled VOCs-profile by e-nose in healthy adults during six consecutive days of sampling. Twenty-four healthy, never-smoking subjects (9 males, 15 females), with a negative anamnesis of chest symptoms and systemic diseases and not taking any medications were enrolled in the study. Mean age was 50.9 years [±15.7 standard deviation (SD)]. All had normal lung function [mean forced expiratory volume in one second (FEV1) was 103.2% of predicted (±12.4 SD) and mean forced vital capacity (FVC) was 105.4% of predicted (±14.3 SD)]. None of the subjects described upper or lower respiratory tract infection in the 28 days prior to the first measurement, nor during the days of sampling. All participants were volunteers and were enrolled from hospital staff. A sequence of exhaled breath measurements were performed on all individuals at the same hour for six consecutive days.

The current study was approved by our local ethics committee and all participants signed an informed consent to participate in the study. Our study had a longitudinal design. The measurements were performed during six separate and consecutive visits (day 0, day 1, day 2, day 3, day 4, day 5). Participants were not allowed to eat or drink anything except water in the 3 h prior to the tests, or perform physical exercise.

Exhaled breath was collected as follows: subjects breathed with a nose-clip at tidal volume for 5 min through a 2-way non-rebreathing valve (Hans Rudolph 2700, Hans Rudolph, USA) connected to an inspiratory VOC filter (A2, North Safety, Netherlands) Then, a single vital capacity volume

Key words: volatile organic compounds; e-nose; electronic nose; breath analysis; reproducibility; breathomics

Corresponding Author:
Dr Silvano Dragonieri,
Department of Respiratory Diseases,
University of Bari, Piazza Giulio Cesare 11,
70124 Bari, Italy
Tel.: +390805593215
e-mail: silvano.dragonieri@uniba.it

0393-974X (2020)
Copyright © by BIOLIFE, s.a.s.
This publication and/or article is for individual use only and may not be further reproduced without written permission from the copyright holder.
Unauthorized reproduction may result in financial and other penalties
DISCLOSURE: ALL AUTHORS REPORT NO CONFLICTS OF INTEREST RELEVANT TO THIS ARTICLE.

was exhaled into a Tedlar bag and immediately sampled by the e-nose (Cyranose 320, Sensigent, USA: nano-composite array of 32 organic polymer sensors). Operating parameters were: sampling time 60"; purging time 200"; temperature 42°C. Flow-volume spirometry (MasterscreenPneumo, Jaeger, Wurzburg, Germany) was performed on all participants during day 0 after breath collection. FEV1 and FVC were collected.

Raw data of the exhaled breath samples were analyzed by SPSS software, version 18.0. Principal component analysis (PCA) and subsequent linear canonical discriminant analysis (CDA) were calculated, providing the Cross Validated Accuracy percentage (CVA%), which estimates how accurately a predictive model will perform in practice. Pearson correlation coefficient was used to evaluate relationships between principal components and clinical variables. We estimated sample size based on data from previous studies (4, 5). A p-value of <0.05 was considered statistically significant.

The two-dimensional principal component analysis plot showed that the exhaled VOC-patterns among six days (days 0,1,2,3,4 and 5) could not be distinguished from each other (Fig. 1). The CDA of those data showed a CVA of 24.3%, confirming the absence of differences. Moreover, no relationships between principal components and age, sex, FEV1 and FVC were reported (p=ns for all).

Based on our results, it appears that the exhaled VOC-profile measured by our e-nose was stable during six consecutive days of sampling. To the best of our knowledge, this is the first study which investigated exhaled VOC-spectrum by e-nose for such a long consecutive period of time. Our data extend previous investigations about e-nose signal

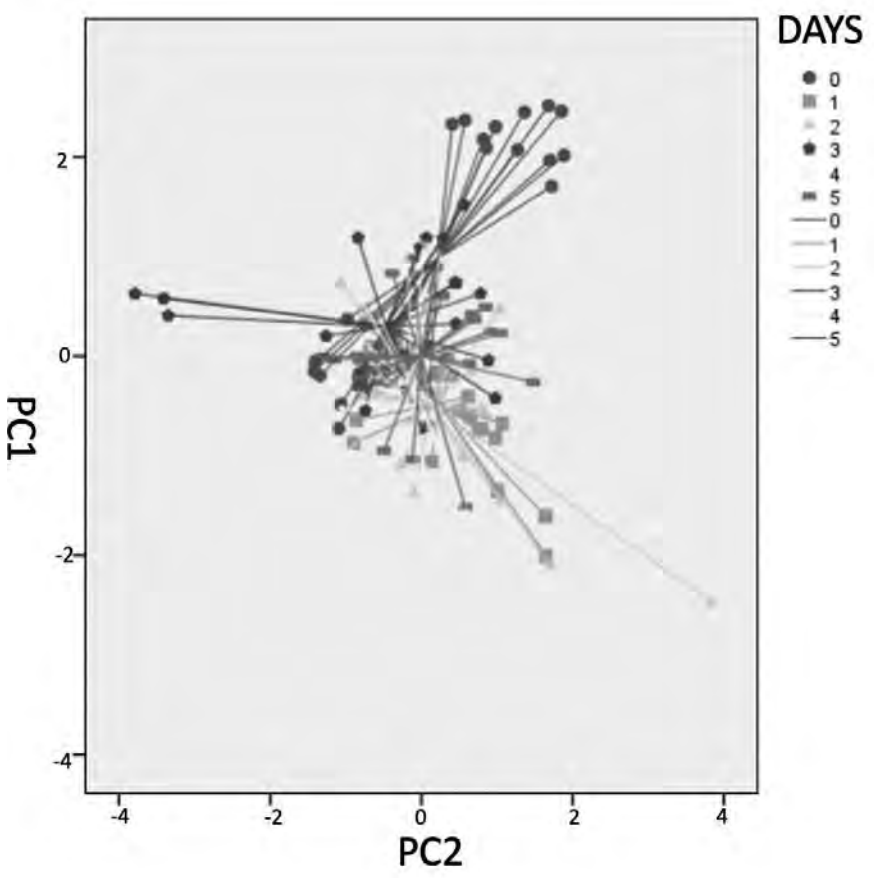


Fig. 1. *Two dimensional principal component analysis plot, showing that exhaled VOC-profiles among six days (Days 0,1,2,3,4 and 5) are indistinguishable from each other. PC: Principal Component.*

repeatability. Bofan et al. (6) found acceptable within-day and between-day repeatability for the same e-nose as ours by evaluating two breath samples collected 30 min and seven days apart, although sensors showed different repeatability (6). Similarto the above, Kovacs et al. (7) assessed temporal changes of VOC pattern in exhaled breath at baseline as well as 1 day, 1 week, 4 weeks and 8 weeks after showing no significant changes. Moreover, Fasola et al. (8), by using a recently manufactured e-nose named Pneumopipe, showed more than acceptable within-day and between-day repeatability (breath collection twice during the baseline visit, 30 min apart and after 7 days), both in stable moderate asthmatics and in healthy children. Interestingly, the within-day and between-day for all spirometry parameters and exhaled nitric oxide were significant and similar to those of the most reliable sensors (8).

The present findings warrant further investigations, aiming to assess the long-term repeatability of different e-nose technologies in patients with several respiratory disturbances both in clinical stability and exacerbation. Furthermore, wide multicentric studies should be conducted for evaluating and monitoring drug-treatment in patients with lung diseases.

REFERENCES

1. Bos LD, Sterk PJ, Fowler SJ. Breathomics in the setting of asthma and chronic obstructive pulmonary disease. J Allergy Clin Immunol 2016; 138:970-76.
2. Dragonieri S, Pennazza G, Carratu P, Resta O. electronic nose technology in respiratory diseases. Lung 2017; 195:157-65.
3. Bikov A, Lázár Z, Horvath I. Established methodological issues in electronic nose research: how far are we from using these instruments in clinical settings of breath analysis? J Breath Res 2015; 9:034001.
4. Dragonieri S, Quaranta VN, Carratu P, Ranieri T, Resta O. Exhaled breath profiling in patients with COPD and OSA overlap syndrome: a pilot study. J Breath Res 2016; 10:041001.
5. Liotino V, Dragonieri S, Quaranta VN, Carratu P, Ranieri T, Resta O. Influence of circadian rhythm on exhaled breath profiling by electronic nose. J Biol Regul Homeost Agents 2018; 32:1261-65.
6. Bofan M, Mores N, Baron M, et al. Within-day and between-day repeatability of measurements with an electronic nose in patients with COPD. J Breath Res 2013; 7:017103.
7. Kovacs D, Bikov A, Losonczy G, Murakozy G, Horvath I. Follow up of lung transplant recipients using an electronic nose. J Breath Res 2013; 7(1):017117.
8. Fasola S, Ferrante G, Sabatini A, et al. Repeatability of exhaled breath fingerprint collected by a modern sampling system in asthmatic and healthy children. J Breath Res 2019; 13:036007.

LETTER TO THE EDITOR

LONG-TERM RESULTS OF NASAL SURGERY: COMPARISON OF MINI-INVASIVE TURBINOPLASTY

S. COCUZZA[1], A. MANIACI[1], M. DI LUCA[1], I. LA MANTIA[1], C. GRILLO[1], G. SPINATO[2,3], G. MOTTA[4], D. TESTA[4] and S. FERLITO[1]

[1]Otorhinolaryngology Clinic, Department of Medical and Surgical Sciences and Advanced Technologies "GF Ingrassia", ENT Section, University of Catania, Italy; [2]Department of Neurosciences, Section of Otolaryngology and Regional Centre for Head and Neck Cancer, University of Padoua, Treviso, Italy; [3]Department of Surgery, Oncology and Gastroenterology, Section of Oncology and Immunology, University of Padua, Padua, Italy; [4]Otorhinolaryngology, Head and Neck Surgery Unit, Department of Mental and Physical Health and Preventive Medicine, 'Luigi Vanvitelli' University of Campania, Naples, Italy

Received November 30, 2019 – Accepted February 11, 2020

To the Editor,

Recent epidemiological data confirm the chronic increasing nasal obstructive disease in urban and industrialized areas, essentially due to the polluting and irritating agents that are breathed daily in the cities (1). The main cause of the pathology is represented by chronic hypertrophic rhinitis which is one of the most common diseases prevalent in the population (2, 3).

Pharmacological therapy is the first-line treatment and its failure represents the main indication for the surgical approach, to improve the nasal airflow but, above all, respecting the nasal mucosal integrity (4). The advent of minimally invasive surgery has allowed us to reduce subsequent drug treatment, positively influencing the quality of life of these patients (4). The two main objectives of surgical treatment are the increase in nasal airflow and the maintenance of the nasal mucosa, respecting, in particular, its physiological function. In the long term, however, both the stability of the size reduction and the absence of side effects that can reduce the patient's subjective well-being are essential (5). Often, research in this specific field of rhinology has been conditioned by the desire to apply new technologies, rather than motivated by an effective interest in correctly understanding the results obtained.

Based on these considerations, through our study, we analyzed the long-term outcomes of the two most common turbinoplasty techniques in the field of chronic hypertrophic rhinitis surgery: the radiofrequency technique with Coblation technology and the Molecular Quantum Resonance. We focused our attention on improving patient's symptomatology, respecting the nasal physiology and mucosal integrity.

MATERIALS AND METHODS

A randomized retrospective study was conducted at the ENT Clinic of the University of Catania (Italy) in collaboration with the Regional Center for Head and Neck Cancer of Treviso and the Vanvitelli University of Naples,

Key words: chronic nasal obstruction; radiofrequency coblation technology; molecular quantum resonance; mucosal preservation

Corresponding Author:
Dr. Antonino Maniaci,
ENT Department,
University of Catania 95100,
Via Santa Sofia, Catania, Italy
Tel.: +39 0953781103
e-mail: tnmaniaci29@gmail.com

0393-974X (2020)
Copyright © by BIOLIFE, s.a.s.
This publication and/or article is for individual use only and may not be further reproduced without written permission from the copyright holder.
Unauthorized reproduction may result in financial and other penalties
DISCLOSURE: ALL AUTHORS REPORT NO CONFLICTS OF INTEREST RELEVANT TO THIS ARTICLE.

to compare long-term results, efficacy and the safety of two of the most recent turbinate "plastic" surgical technologies. We conducted the study after acquiring the signed informed consent of each patient. The study was approved by the institutional review committee of the research committee of the Department of Medicine and Surgery, otorhinolaryngology section. The study was not advertised and no remuneration was offered.

A total of 254 patients (147 males and 107 females; aged 21-63 years), suffering from chronic nasal obstruction caused by non-allergic turbinate hypertrophy, were enrolled in this study. These patients did not respond to the usual medical treatment with topical steroids and local decongestants, and were monitored by medical therapy for at least 1 year. The subjects were randomly divided into two groups of 127 patients each, homogeneous for age and sex. One group was treated with radiofrequency coblation technology (CT group) while the other with Molecular Quantum Resonance (QMR group). Patients were evaluated based on clinical and medical history, objective clinical examination, nasal endoscopy, allergy tests, nasal cytology, rhinomanometric and radiological evaluation. The presence of significant septal deviations, previous surgery of the turbinate, nasal polyposis or recurrent sinusitis, coagulopathies, serious systemic or oncological diseases, and infections were exclusion criteria from the study. Other exclusion criteria were any pregnancy or lactation, insulin-dependent diabetes, and uncontrolled arterial hypertension.

We evaluated factors such as intra and post-operative pain and the use of analgesics, intra and post-operative bleeding, a variation of instrumental rhinomanometric parameters and cytofunctional changes of the nasal mucosa of treated patients. The surgical results of both procedures were evaluated at 1 week and 1 and 3 months after surgery. During the pre- intra- and post-operative period, the following elements were observed: nasal obstruction, intra and/or postoperative bleeding, surgical duration, post-operative pain, and crusting/synechiae formation. A VAS 0-10 scale was used to assess subjectively: nasal obstruction and postoperative pain in which a score was assigned from 0 (no symptoms) to 10 (the most severe symptom). The degree of mean surgical nasal bleeding was assessed intraoperatively and at the subsequent follow-ups using a 0-10 scale classification, divided into 4 classes (from none to severe). For the study of nasal resistance, an active rhinomanometry (Rhinomanometer Labat Srl, Venice, Italy) was performed during the preoperative period and also in the postoperative period at 1 and 3 months.

The nasal sample for cytological analysis was obtained by scraping the central part of the inferior turbinate using a rhino probe (Arlington Scientific Inc., Springfield, MA, USA). The samples were then placed on a slide, fixed with 2% glutaraldehyde, stained with 2% osmium tetroxide, dehydrated with alcohol and finally observed with a Hitachi 100 keV H-600 electron microscope (Tem image, Hitachi Ltd, Chiyoda, Japan). The cellular distribution, the different cytotypes, and the various intracellular components were discriminated against. Particular attention was paid to checking the integrity of hair cells, to detect the percentage of patients with cellular alterations. The cytological analysis was performed both in the preoperative period, and in the postoperative period 1 and 3 months after the operation.

Surgical procedure

All patients were treated by local contact anesthesia with 2% mepivacaine, for a duration of 15 min, placing cotonoids with recovery thread soaked in anesthetic along the whole turbinate. For the CT group, submucosal decongestion was performed by inserting a needle handpiece at the level of the head of the inferior turbinate and guiding it as far posteriorly as possible, without damaging the adjacent nasal septum, to reduce the incidence of postoperative nasal synechiae. Primarily, an ablation setting of six and coagulation setting of four were used, activated by a radiofrequency device (ArthroCare ENT Coblator II Surgery System, Austin Texas, USA) with a frequency of 1.7 KHz at a power of 5 W. The needle handpiece was positioned from tail to body and remained in each portion of the turbinate for 10 sec. This first surgical time was effective mainly on the middle and posterior portions of the inferior nasal turbinate.

Subsequently, to achieve adequate anterior turbinate reduction, a third submucosally lesion was performed using the same technique previously described. The submucosal decongestion of the turbinate was performed by means of insertion with a needle-shaped handpiece, activated by a QMR machine, so-called Quantum (Telea, Sandrigo-Vicenza, Italy), for a total of 20–30 sec, at an intensity force of 3.5. The wand was activated and moved

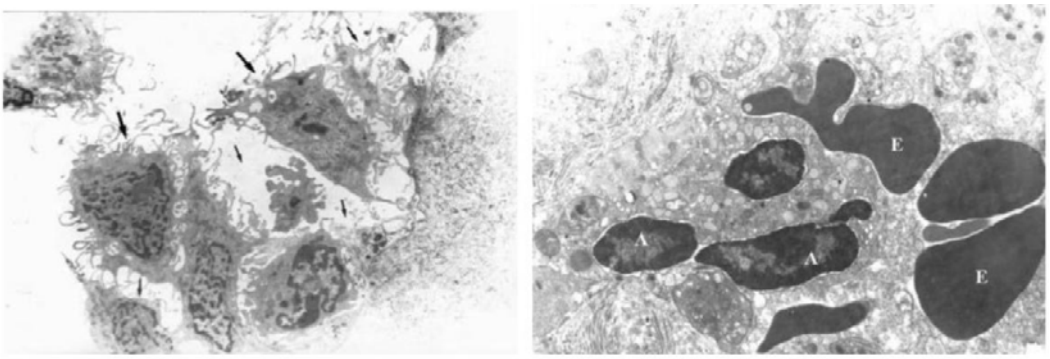
through the posterior, middle and anterior compartments, paying attention to avoid the superficial portion of the turbinate due their important physiological role. Postoperative bleeding did not require insertion of nasal tampons in any of the patients in the treatment group. Topical corticosteroid decongestant and nasal antiseptic cream were used in both groups twice a day for 1 week to help control epistaxis, and to decrease edema in the immediate postoperative period.

Statistical analysis

For all subjective and objective outcomes, the *p* value of improvement between groups was calculated and the *t*-test was used. Score significance was set at 0.05 to test the null hypothesis that there was no significant difference in reduction of objective and subjective nasal symptoms between control and treatment groups. Statistical analyses were performed using SPSS (software package used for statistical analysis) Statistics Version 17.0 (SPSS, Inc., Chicago, IL, USA).

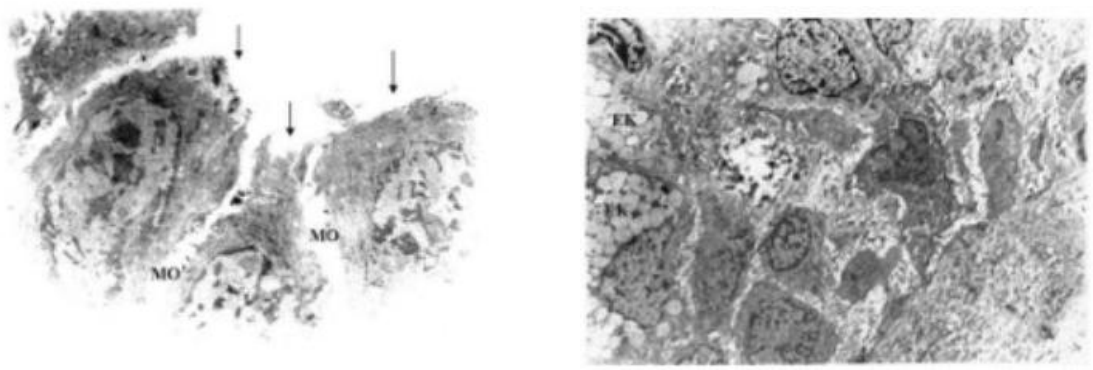
RESULTS

Already from the first postoperative week, active rhinomanometric examination showed an improvement in both study groups in terms of postoperative benefit obtained, in particular with regard to nasal obstruction (Table I). Considering the



a **b**

Fig. 1. ***a-b)*** *Electron microscopic images showing nasal epithelial metaplasia, evident stratification in the epithelium and hyperplasia, degeneration of epithelial cells, loss of cilia and destruction of intercellular connections.*



a **b**

Fig. 2. ***a)*** *Reduction of the intercellular edema, a slight reduction in mucus and an overproduction of collagen.* ***b)*** *No regeneration of the cilia in turbinate mucosa is present.*

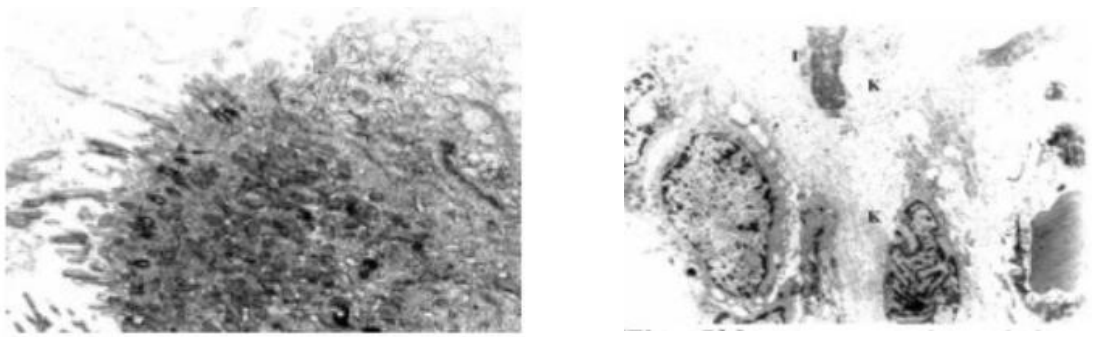
mean initial preoperative values, CT presented a better response to surgical treatment than QMR with a final average increase in nasal air resistance of about 72% *vs* 68%. However, no significant differences resulted when the postoperative outcomes at 1 and 3 months after surgery were compared between the two study groups (p = 0.1) (Tables I-II). The mean bleeding intraoperative score was 1.62 for CT patients *vs* 0.86 for the QMR, with a not significant value p = 0.5 (Table II). No bleeding occurred immediately after turbinate reduction treatment nor was nasal packing required. In the two control groups after the first postoperative week, fibrin layers were found near the nasal surgical site, which dissolved in the second postoperative week. The mean duration of surgery in the CT group was 11.7 min *vs* 11.3 min in the QMR group (Table II) (p> 0.05 not significant).

Surgical-related pain assessment was evaluated intraoperatively, at one week, one month and 3 months after surgery. Lower VAS scores were found in the QMR group from the intraoperative time of the surgical procedure (1.7), compared to the CT group (3.96). However, non-statistically significant differences in the two groups were noted (p = 0.14).

Regarding the problem of crusting/synechiae formation, 23 patients (18%) of the QMR group developed the disease along the lower edge and tail of the treated turbinate, however, this was completely resolved during the first week of follow-up. Conversely, the presence of scabs was not reported in the CT group.

On cytological examination in the preoperative period, the ciliated cells were pathological with ciliocitoftoria or cytoplasmic alterations in 28 cases (22%) of the QMR group and 32 (25%) of the CT group. Electron microscopic observation revealed nasal epithelial metaplasia, evident stratification in the epithelium and hyperplasia, degeneration of epithelial cells, loss of cilia and destruction of intercellular connections (Fig. 1a-b). In addition, increased thickness of the basement membrane, overproduction of nasal mucus, inflammation of the lamina propria and increase in the number of goblet cells were observed.

In the postoperative period, no significant alteration of the hair cells of the QMR patients was observed, ranging from 28 (22%) to 34 (27%) in the first month of follow-up and 28 (22%) at the third month of follow-up. Under the electron microscope, a reduction of the intercellular edema was observed, as well as a slight reduction in mucus (Fig. 2a) and an overproduction of collagen (Fig. 2b). However,



a **b**

Fig. 3. ***a****) Decreased mucus secretions and interstitial edema, widespread islands with normally organized epithelium of columnar cells and goblet cells combined with islands of metaplastic epithelium.* ***b****) Regenerated epithelium, containing cells with small, scattered cellular cilia and also hyperplasia reduction.*

the regeneration of the cilia in the mucosa of the turbinate was not observed. On the other hand, in the CT group there was a decrease in the number of patients with cellular modifications, passing from 33 (26%) to 29 (23%) at the first month of follow-up and finally to 20 (16%) in the third month.

Furthermore, decreased mucus secretions and interstitial edema were observed. Widespread islands with normally organized epithelium of columnar cells and goblet cells were evident (Fig. 3a), combined with islands of metaplastic epithelium. The islands of the regenerated epithelium contained cells with small, scattered cellular cilia on their surface starting from the third month (Fig. 3b). We also observed a reduction in hyperplasia. The functional activity of the mucosa in patients operated by CT remained unchanged at 1 and 3 months after surgery.

DISCUSSION

Numerous medical and surgical treatments have been proposed for the treatment of inferior turbinate hypertrophy (7-8). Our study was aimed at patients with chronic hypertrophic rhinitis of non-allergic etiology. The purpose of turbinate reduction surgery is to improve nasal obstruction, thanks to the formation of scar tissue that binds the mucosa to the periosteum and reduces a possible recurrence (9). The integrity of the mucous lining is essential to guarantee the preservation of normal nasal physiology, which can be monitored through the transport time of the ciliary mucus and nasal cytology (9).

Surgery involves the degeneration of the nasal epithelium, the presence of polynuclear cells with prominent nucleoli, areas of muciparic or platicellular epithelial metaplasia (10). We therefore

Table I. *RAA results (anterior active rhinomanometry)*

	PRE-OPERATIVE	POST-OPERATIVE 1 MONTH	POST-OPERATIVE 3 MONTHS
Group RQM	0.98±0.028 (Pa/cm^3/s)	0.37±0.021 (Pa/cm^3/s)	0.32±0.022 (Pa/cm^3/s)
Group CT	0.93±0.032 (Pa/cm^3/s)	0.33±0.027 (Pa/cm^3/s)	0.28±0.023 (Pa/cm^3/s)

Table II. *Comparison between intra- and post-operative results in both groups of patients.*

	Group RQM	Group CT	P value
Intraoperative nasal bleeding	0.86	1.62	> 0.05
Surgery duration (minutes)	11.3	11.7	> 0.05
Intra-operative pain assessment	1.7	3.96	> 0.05
Post-operative pain assessment			
1 week	0.7	0.9	> 0.05
1 month	0.35	0.54	> 0.05
3 months	0.1	0.2	> 0.05

analyzed and compared the effects and the possible advantages of two techniques of submucosal surgical decongestion for the hypertrophic turbinate, radiofrequency coblation technology and molecular quantum resonance technique, since the data in the literature show excellent results for both but, at times, demonstrate conflicting aspects (10, 11).

Evaluation of the degree of post-operative nasal obstruction showed improvement, particularly in the CT group. Evaluation of mean nasal bleeding showed reduced values in both study groups, but particularly in the QMR group. The evaluation of pain related to surgery showed lower VAS scores both intraoperatively and at follow-up in the QMR group compared to the CT group. The analysis of cytomorphological results showed the advantages of the CT technique compared to the QMR technique. In particular, a progressive increase in the number of normal cells in the CT group reflects a more rapid postoperative benefit. These advantageous results have been possible thanks to the multi-electrode end of the CT device which does not exceed the necrosis temperatures, with consequent reduction of damage to adjacent tissues.

However, in the literature there is still no treatment of choice for this type of pathology; the radiofrequency technique with CT, allowing greater precision with less tissue damage, as demonstrated in our study, seems to be characterized by greater fitness for a truly conservative treatment of the turbinal structures, especially in terms of restoration of nasal physiological function. Moreover, in our study, radiofrequency turbinoplasty presented excellent data in terms of postoperative outcomes, showing it to be the treatment of choice in the pathology of turbinate hypertrophy.

REFERENCES

1. Willson TJ, Lospinoso J, Weitzel E, McMains K. Correlating regional aeroallergen effects on internet search activity. Otolaryngology–Head Neck Surg 2015; 152(2):228-32.
2. Seidman MD, Gurgel RK, Lin SY, et al. Clinical Practice Guideline: Allergic Rhinitis. Otolaryngol Head Neck Surg 2015; 152(1 suppl):S1-S43.
3. Ologe FE, Adebola SO, Dunmade AD, Adeniji KA, Oyejola BA. Symptom Score for Allergic Rhinitis. Otolaryngol Head Neck Surg 2013; 148(4):557-63.
4. La Mantia I, Andaloro C. Demographics and clinical features predictive of allergic versus non-allergic rhinitis in children aged 6–18 years: A single-center experience of 1535 patients. Int J Pediatr Otorhinolaryngol 2017; 98:103-9.
5. Roditi RE, Ishman S, Lee S, Lin S, Shin JJ. Medications for allergic rhinitis: an opportunity for quality improvement? Otolaryngol Head Neck Surg 2017; 156(1):70-80.
6. Galletti B, Gazia F, Freni F, Sireci S. Endoscopic sinus surgery with and without computer assisted navigation: A retrospective study Auris Nasus Larynx 2019; 46(4):520-25.
7. Ciofalo A, Pasquariello B, Iannella G, et al. The role of nasal cytology in the diagnosis of allergic and non-allergic rhinitis in adult and children. Eur Rev Med Pharmacol Sci 2019; (12):5065-73.
8. Cocuzza S, Marino S, Gulino A, et al. ENT involvement and orobuccal movements' disorders in Pandas patients: assessment and rehabilitations tools. Eur Rev Med Pharmacol Sci 2019; (23):4110-17.
9. Testa D, Motta G, Galli V, et al. Outcome assessment in patients with chronic obstructive rhinitis CO2 laser treated. Acta Otorhinolaryngol Ital 2006; 26(1):32-37.
10. Trovato L, Serra A, Grillo C, et al. Laboratory support in chronic fungal rhinosinusitis non-IgE-mediated. Acta Medica Mediterranea, 2013; 29:479.
11. Shah AN, Brewster D, Mitzen K, Mullin D. Radiofrequency coblation versus intramural bipolar cautery for the treatment of inferior turbinate hypertrophy. Ann Otol Rhinol Laryngo 2015; 124(9):691-97.

LETTER TO THE EDITOR

HOW FREQUENT ARE POSTOPERATIVE COMPLICATIONS AFTER AN IMPACTED MANDIBULAR THIRD MOLAR EXTRACTION?

P.C. PASSARELLI[1], E. RELLA[1], G.B. PICCIRILLO[1], V. DESANTIS[1], V. GIOVANNINI[1], A. SPERANZA[1], M. DE LEONARDIS[1], P. PAPI[2], G. POMPA[2], P.F. MANICONE[3] and A. D'ADDONA[3]

[1]Department of Head and Neck, Oral Surgery and Implantology Unit, Institute of Clinical Dentistry, Università Cattolica del Sacro Cuore, Fondazione Policlinico Universitario Gemelli, Rome, Italy, [2]Department of Oral and Maxillo-facial Sciences, "Sapienza" University of Rome, Rome, Italy; [3]Department of Head and Neck, Oral Surgery and Implantology Unit, Institute of Clinical Dentistry, Università Cattolica del Sacro Cuore, Fondazione Policlinico Universitario Gemelli, Rome, Italy

Received February 23, 2020 – Accepted April 30, 2020

To the Editor,

Impacted teeth fail to fully erupt in the oral cavity mainly as a result of reduced space in the dental arch. Several studies have shown the mandibular third molar to be the most commonly impacted tooth, with a prevalence reaching 77% (1), followed by the maxillary third molar. An impacted mandibular third molar can cause the development of an infection, commonly called pericoronitis, in the follicular sac of the impacted third molar; this infection can be seen in a percentage as high as 64% (2) of patients with an impacted third molar, and can be quite painful for the patient. The usual therapy for treating an impacted tooth is its extraction, which can be called for not only for treating a tooth that has been the cause of an infection and can negatively affect nutrients intake (3), but also for maintaining the periodontal health of the second molar (4) or for orthodontic and prosthetic needs. Their extraction is particularly important in patients undergoing hematopoietic stem cell transplantation (HSCT) (5). Their extraction is usually a uneventful surgical procedure, but in rare cases it may cause several complications, such as paresthesia of the lower lip or the development of a dry socket (6). These complications have a widely different reported rate. The aim of this study is to retrospectively highlight the prevalence of these events in our clinic.

MATERIALS AND METHODS

This retrospective analytical study included 89 mandibular third molar extractions performed between January 2015 to January 2019 by a single oral surgeon. We retrospectively analyzed the extraction data, postoperative data, and patient clinical information. Because of the retrospective nature of the present study, it was granted an exemption in writing by the institutional review board of the Catholic University of the Sacred Heart of Rome.

The positions of the 89 mandibular molars and the distance between the apex and the IAN were analyzed with a bidimensional endooral radiograph, or, when needed, with a tridimensional radiographic exam. The teeth were extracted following a standard

Key words: oral surgery; third molar; extraction; complications

Corresponding Author:
Dr Pier Carmine Passarelli,
Department of Head and Neck, Oral Surgery and Implantology Unit, Institute of Clinical Dentistry, Università Cattolica del Sacro Cuore, Fondazione Policlinico Universitario Gemelli, Rome, Italy
Tel.: +39 0630155278 - Fax: +39 0630154751
e-mail: piercarmine.passarelli@unicatt.it

0393-974X (2020)
Copyright © by BIOLIFE, s.a.s.
This publication and/or article is for individual use only and may not be further reproduced without written permission from the copyright holder.
Unauthorized reproduction may result in financial and other penalties
DISCLOSURE: ALL AUTHORS REPORT NO CONFLICTS OF INTEREST RELEVANT TO THIS ARTICLE.

surgical protocol that involved the incision of the mucosa, the elevation of a mucoperiosteal "full thickness flap", the removal of bone and then the use of elevators or forceps to physically extract the tooth. The sockets were then irrigated with saline, and after checking for bone irregularities that could cause the opening of the flap, the flap was securely sutured in place, allowing a first intention closure of the wound, when possible.

Some of the patients in this study suffered from coagulation defects that could have caused intraoperative and postoperative bleeding (7) and were accordingly treated following our standard protocol: patients who suffered from Factor VII deficiency underwent an intravenous transfusion of rFVIIa (NovoSeven RT; Novo Nordisk) in a single dose of 25 mg/kg bodyweight, 30 min before surgical extraction (8). After the procedure analgesics and, when needed, antibiotics were administered to the patients. Sutures were then removed after 7 days when eventual complications were recorded.

RESULTS

A total of 89 third molar were extracted, with the majority of extractions performed on female patients (48). The mean age at the moment of the extraction was 35.5 years (range 81-16) and the majority (57%) of the patients were between 16 and 30 years old. Following the classification of Pell and Gregory, the 89 mandibular were classified: the the 1B class was found to be the most represented, as 17(19.1%) of the teeth belonged to this class, closely followed by the IIB class (15.73%). The 89 extractions all required the elevation of a mucoperiosteal flap and some bone drilling in order to remove the teeth.

In this study the rate of postoperative complications was 6.7% (3 dry sockets, 2 openings

Table I. *Demographical characteristics of the sample*

Mean age	**Age class prevalence**	**Gender**	**Percentage of smoking patients** (at least 10 cigarettes a day)
35.5 years	<20=12.35% 20-30=43.8% 30-40=7.86% 40-50=12.35% 50-60=5.61% 60-70=11.23% 70-80=3.37% 80-90=3.37	46% Male 54% Female	17 %

Table II. *Absolute number and risk of complications*

Dry sockets	**Opening of the flap**	**Paresthesia**	**Total**
3 (3.37%)	2 (2.24 %)	1 (1.12%)	6 (6.7%)

of the wound and 1 paresthesia). The patient (F, 29) who developed lower lip paresthesia fully recovered within a month.

DISCUSSION

In this study dry sockets were found to be the most common postoperative complication following mandibular third molar extraction; some level of pain and inflammation is to be expected but the developing of a dry socket can be extremely painful to the patient. Analyzing the literature we can find several different propositions to reduce the likelihood of developing this complication (locally administered chlorhexidine and the application of platelet rich plasma were found to be the most effective), while the best way to encourage the development of new tissue and the closure of the wound appears to be irrigation of the socket and the application of a medication (such as LLLT, zinc oxide eugenol or plasma rich in growth factors) (9). Some controlled studies have reported a rate of dry sockets up to 25–30% after the extraction of mandibular third molars (10), the present study found a much lower percentage.

Only one patient developed a slight paresthesia following the extraction, possibly related to an injury to the IAN. In cases of an IAN injury, patients usually describe a loss of sensations in the lower lip, usually with a persistent burning, or tickling feeling. Usually these IAN lesions tend to heal spontaneously; therefore, the loss of sensibility is mostly temporary, and the sensory impairment recovers within 6 months (11); the risk of permanent sensory impairment is less than 1% (12).

The extraction of an impacted mandibular third molar can be a rather challenging task, requiring mindful planning. Complications can be quite common, and they can sometimes be extremely annoying to the patient. In our study we found that, by applying the appropriate surgical technique, an experienced operator can reduce the prevalence of these complications, well below what is reported in the literature.

REFERENCES

1. Kugelberg CF. Impacted lower third molars and periodontal health. An epidemiological, methodological, retrospective and prospective clinical, study. Swed Dent J Suppl 1990; 68:1-52.
2. Singh P, Nath P, Bindra S, Rao SS, Reddy KVR. The predictivity of mandibular third molar position as a risk indicator for pericoronitis: A prospective study. Natl J Maxillofac Surg 2018; 9:215-21.
3. Azzolino D, Passarelli PC, De Angelis P, Piccirillo GB, D'Addona A, Cesari M. Poor oral health as a determinant of malnutrition and sarcopenia. Nutrients 2019; 11.
4. Passarelli PC, Lajolo C, Pasquantonio G, , et al. Influence of mandibular third molar surgical extraction on the periodontal status of adjacent second molars. J Periodontol 2019; 90:847-55.
5. Bollero P, Passarelli PC, D'Addona A, et al. Oral management of adult patients undergoing hematopoietic stem cell transplantation. D 2018; 12.
6. Bouloux GF, Steed MB, Perciaccante VJ. Complications of third molar surgery. Oral Maxillofac Surg Clin N Am 2007; 19:117-28.
7. Passarelli PC, De Angelis P, Pasquantonio G, Manicone PF, Verdugo F, D'Addona A. Management of Single Uncomplicated Dental Extractions and Postoperative Bleeding Evaluation in Patients With Factor V Deficiency: A Local Antihemorrhagic Approach. J Oral Maxillofac Surg 2018; 76:2280-83.
8. Passarelli PC, Pasquantonio G, D'Addona A. Management of surgical third lower molar extraction and postoperative progress in patients with Factor VII deficiency: A Clinical Protocol and Focus on This Rare Pathologic Entity. J Oral Maxillofac Surg 2017; 75:2070.e1-2070.e4.
9. Taberner-Vallverdú M, Nazir M, Sánchez-Garcés MÁ, Gay-Escoda C. Efficacy of different methods used for dry socket management: A systematic review. Med Oral Patol Oral Cir Bucal 2015; 20:e633-39.
10. Blum IR. Contemporary views on dry socket (alveolar osteitis): a clinical appraisal of standardization, aetiopathogenesis and management: a critical review. Int J Oral Maxillofac Surg 2002; 31:309-17.
11. Valmaseda-Castellón E, Berini-Aytés L, Gay-Escoda C. Inferior alveolar nerve damage after lower third molar surgical extraction: a prospective study of

1117 surgical extractions. Oral Surg Oral Med Oral Pathol Oral Radiol Endod 2001; 92:377-83.

12. Gülicher D, Gerlach KL. Sensory impairment of the lingual and inferior alveolar nerves following removal of impacted mandibular third molars. Int J Oral Maxillofac Surg 2001; 30:306-12.

LETTER TO THE EDITOR

IMPACT OF INTRANASAL NEBULIZED ECTOINE ON MORBIDITY AND SHORT-TERM QUALITY OF LIFE AFTER PEDIATRIC ADENOIDECTOMY

A. MOFFA[1], M. CASALE[2], V. FIORE[1], V. RINALDI[2], R. GIANCASPRO[1], M.A. LOPEZ[2], P. BAPTISTA[3], M. GELARDI[1] and M. CASSANO[1]

[1]Unit of Otolaryngology, University of Foggia, Foggia, Italy; [2]Integrated Sleep Surgery Team UCBM - Unit of Otolaryngology – Integrated Therapies in Otolaryngology, Campus Bio-Medico University, Rome, Italy; [3]Unit of Otolaryngology, Clinica Universitaria de Navarra, Pamplona, Spain

Received March 13, 2020 – Accepted May 6, 2020

To the Editor,

Adenoidectomy is the third most common pediatric procedure performed in the United States, after myringotomy with tube placement and adenotonsillectomy (1). There are several adenoidectomy techniques, however, standard adenoidectomy with adenoid curette or adenotome, remains the most common surgical procedure performed. Recovery from adenoidectomy is remarkably faster and better when compared with post-tonsillectomy, either as a single procedure or combined with adenoidectomy. Patients who undergo adenoidectomy are typically discharged the same day of surgery.

However, immediately after the procedure, children usually complain of nasal symptoms such as nasal obstruction, rhinorrhea, pharyngeal and neck pain from the surgical site and endotracheal intubation, ear pain, halitosis, scabs in the mouth and bad breath (2). After surgery, saline nasal irrigations (SNIs) of the nasal fossae and nasopharynx are frequently used. This allows the removal of secretions, crusts, and debris, which typically accumulate in the nasopharynx, promoting a rapid recovery of nasal respiration. Recently, some studies suggest that the use of a saline solution with ectoine (as a coadjutant treatment for many upper airway inflammatory diseases) significantly improves symptoms and findings of the endoscopic evaluation. Ectoine binds strongly to water molecules and forms a hydrating shield that prevents dehydration and proteins' irreversible denaturation of the tissues. It also reduces inflammatory and oxidative stress induced by exposure to polluting dust, and plays a protective and stabilizing role for many components of the cell wall (3). Recently, Moffa et al. (4) investigated the use of ectoine that was nebulized with a new nasal device called Spray-sol™, for the prevention of recurrent upper respiratory tract infections (rURTIs) in pediatric subjects. Their work showed a statistically significant reduction in the number of URTI episodes, days of absence at school, and patient compliance. Spray-sol™ is a practical nasal device that allows aerosol delivery to the middle turbinate, the osteo-meatal complex, and nasopharynx region (5, 6). The main goal of this study is to investigate the role of ectoine saline solution nebulized with Spray-sol™, as an adjuvant treatment to hasten the improvement of nasal respiration, minimizing patients' discomfort after adenoidectomy. Adherence and compliance of the medication are considered secondary objectives.

Key words: Spray-sol™; single dose vial; nasal device; ectoine; adenoidectomy; nebulization and children.

Corresponding Author:
Antonio Moffa, MD,
Unit of Otolaryngology,
University of Foggia,
Via Luigi Pinto 1, 71122,
Foggia, Italy
e-mail: moffa.antonio1@gmail.com

0393-974X (2020)

Copyright © by BIOLIFE, s.a.s.
This publication and/or article is for individual use only and may not be further reproduced without written permission from the copyright holder.
Unauthorized reproduction may result in financial and other penalties

MATERIALS AND METHODS

This prospective, observational study was carried out following the principles of the Helsinki Declaration. All parents signed an informed consent form and were provided with the relevant information regarding the trial. Forty-four consecutive patients aged 3-10 years with endoscopic diagnosis (7) of AH defined as a third or more degree, with or without otitis media with effusion (OME) were prospectively enrolled at the University of Foggia, Unit of Otolaryngology, from September 2019 to February 2020. Excluded were patients: a) less than three years of age or older than ten years; b) with rURTIs; c) with coagulopathy, or any major illness that was contraindications to surgery. All patients who underwent adenoidectomy with or without myringotomy with tube placement were included in the study. They were divided into two treatment groups:

- Ectoine group (E-group): 20 patients; 8 females and 12 male, with a mean age of 5.66 years; patients and parents were instructed to use ectoine saline solutions nebulized with Spray-sol™. The commercially available product named Isonebial Kit (Steve Jones S.R.L., Sesto Fiorentino, FI, Italy) composed of 20 singl-dose 5-ml vials with sodium chloride (0.9%) with the addition of ectoine, sodium phosphate, polyvinylpyrrolidone and water, a nasal device called Spray-sol™ and a Luer-Lock syringe of 5 ml;
- Saline group (S-group): 22 patients; 10 females and 12 males; with a mean age of 5.7 years; Patients and parents in the S-group were instructed to use 5 ml of isotonic saline solution contained in a single-dose vial.

The solutions were applied, placing half the solution into both nostrils twice/day (morning and evening) for the 14 days after surgery. Five patients (three belonging to E-group and two to S-group) who did not report for post-operative controls were excluded from the study.

Surgical procedure

Transoral cold curettage adenoidectomy was performed with a McIvor mouth gag and Beckmann adenoid curette size 0-5, depending on the characteristics and necessity to reach the rhino pharynx with the instrument. Adenoid tissue was excised by transoral cold curettage. Hemostasis was achieved thought compression with a tampon soaked with hydrogen peroxide; electrocautery was not used. Digital hand check visualization was performed to ensure the removal of the adenoid and rhino pharyngeal permeability. For the children with a history of OME, an operating microscope was used to visualize the tympanic membrane where myringotomy was performed, the fluid was suctioned and the ventilation tube was placed at the site of the incision.

Evaluation

On enrollment, the following baseline parameters were obtained: sex, age, AH degree, OME, and history of allergy. The assessment was performed on day 1 (T1) and day 14 (T2) of the postoperative period, and recollection of data of upper airway symptoms, side effects, compliance to the treatment, difficulties/unpleasantness experienced during administration and adherence to the assigned treatment was achieved by the physicians as indicated below:

- *Upper Airway Symptoms Score.* Parents were asked to complete a daily diary to estimate the severity of the main symptoms complained of by their children in the postoperative period. The main symptoms evaluated were nasal dryness, nasal obstruction, runny nose, epistaxis, itchy nose, snoring, post-nasal discharge, sore throat, ear pain, and halitosis. Each symptom score ranged from 1 (no symptoms) to 10 (severe symptoms) and were grouped in the Global Symptoms Score (GSS). Our research group created this questionnaire as it brings together and highlights the most common clinical symptoms typically referred by children and parents following adenoidectomy.
- *Concomitant medication use*. No restrictions were placed on the use of concomitant medication during any acute ailment. Both groups received standard treatment during the acute stage if any complication occurred during the study period and included: antipyretics, mucolytics, nasal decongestants, and systemic antibiotics.
- *Complications* such as hemorrhage.
- *Compliance with the treatment.* Patients with their parents were evaluated for their attitude concerning tolerability during and after application using a standard 10 cm Visual Analog Scale (VAS) ranging from 0 (not comfortable) to 10 (very comfortable).
- *Adherence to the assigned treatment* was evaluated by counting the number of dispensed and returned Isonebail Kits and single-dose vials.

- *Difficulties/unpleasantness experienced during administration.* Complaints of itch/pain/discomfort, medication flowing down throat/nose, struggling away, experiences of fear/anxiety/cries, flat refusal, unpleasant after taste, only allowing the application of 1 nostril, nostril dryness, and epistaxis.

Statistical analysis

All qualitative parameters were converted to a numeric scale for evaluation purposes. The results were collected and stored in a Microsoft Excel spreadsheet. Statistical analyses were performed using the statistical package STATA version 13 (StataCorp LP, College Station, TX, USA). Graphs were prepared using GraphPad Prism 6.0 for MacOS (GraphPad, La Jolla, CA, USA). The results are expressed as mean and SD. Non-parametric Mann-Whitney test for non-paired data was used to compare different values. Our criterion for statistical significance was set at p values of less than 0.05 (2-tailed).

Table I. *Demographic characteristics of study participants*

	E-group (20 patients)	S-group (22 patients)
Mean age (yr)	5.66	5.70
Male	12 (60%)	12 (54.4%)
Female	8 (40%)	10 (45.5%)
Weight (kg)	24	25
Height (cm)	119.35	120.20
III degree of AH	6 (30%)	8 (36.36%)
IV degree of AH	14 (70 %)	14 (63.64%)
Recurrent OME	8 (40%)	10 (45.54%)

RESULTS

Forty-four patients were analyzed in the study (Table I). No uncontrolled bleeding was observed during or after the surgical procedure.

Upper airway symptoms score

At the beginning of the treatment (T1), the GSS in the E-group was 30.65±4.5, while in S-group was 30.86±3.87 ($p > .05$). At the end of the treatment (T2), in the E-group the GSS was 12.6±5.7, while in the S-group the GSS was 17.1±4.9, with a mean reduction of 18.05±7.7 and 13.77±5.7 respectively ($p = 0.01$). All the specific nasal symptoms assessed showed a greater severity reduction in case of E-group (Table II). In particular, nasal dryness (E-group: 3.0±1.4, S-group: 1.9±1.4; $p = 0.02$), nasal obstruction (E-group: 2.5±1.4, S-group: 1.6±0.96; $p = .03$), runny nose (E-group: 2.5±1.7, S-group: 1.5±1.5; $p = .04$), and post-nasal discharge (E-group: 2.75±0.9, S-group: 1.7±1.5; $p = 0.001$) showed a statistically significant difference between groups, while snoring (E-group: 2.5±1, S-group: 1.8±1.6; $p = 0.08$) was not significantly different.

No significant differences were reported between the two groups on the use of concomitant medication such as antipyretics, mucolytics, nasal decongestants, systemic antibiotics, tranexamic acid. No side effects related to the investigated treatments were reported in either group during the study. Children using ectoine saline solution nebulized with Spray-sol™ reported higher significant compliance than those treated with saline solutions (E-group: 7.80 ±1.2; S-group: 6.10 ±1.1; $p> 0.001$) as shown in Fig. 2. During the two weeks of treatment, in the E-group the number of treatment placements was 26.40±2.82 while in the S-group were 26.55±2.52 of the 28 administrations available without significant difference. The most common problems experienced during administration were discomfort, itch or pain (E-group: 4 patients and S-group: 7 patients), and medication flowing down the nose and throat (E-group: 3 patients and S-group: 5 patients) as shown in Table III. No cases of epistaxis were described in either of the groups.

Table II. *Specific nasal symptoms*

	E-group	S-group	
Nasal dryness	3.0±1.4	1.9±1.4	$p = 0.02$
Nasal obstruction	2.5±1.4	1.6±0.96	$p = 0.03$
Runny nose	2.5±1.7	1.5±1.5	$p = 0.04$
Post-nasal discharge	2.75±0.9	1.7±1.5	$p = 0.001$
Snoring	2.5±1.0	1.8±1.6	$p = 0.08$

Table III. *Difficulties/unpleasantness experienced during administration*

	E-group	S-group
Complaints of itch/pain/discomfort	4	7
Medication flowing down throat/nose	3	5
Struggle away	2	3
Experiences fear/anxiety/cries	2	3
Flat refusal	3	4

DISCUSSION

During the first days after an adenoidectomy, patients' short-term quality of life may be compromised by edema, extensive crust formation, mucosal alterations, excessive secretions, and impaired nasal ventilation. For these reasons, clinicians nowadays are constantly searching for agents to promote the cleaning of nasal cavities and post-operative regeneration of the nasopharyngeal mucosa. In our study, at the end of the second post-operative week of treatment, the E-group showed a fast and significant improvement in the upper airway symptoms score compared to S-group with GSS evaluation, in particular for nasal dryness, nasal obstruction, runny nose and post-nasal discharge parameters. These results reflect the effects

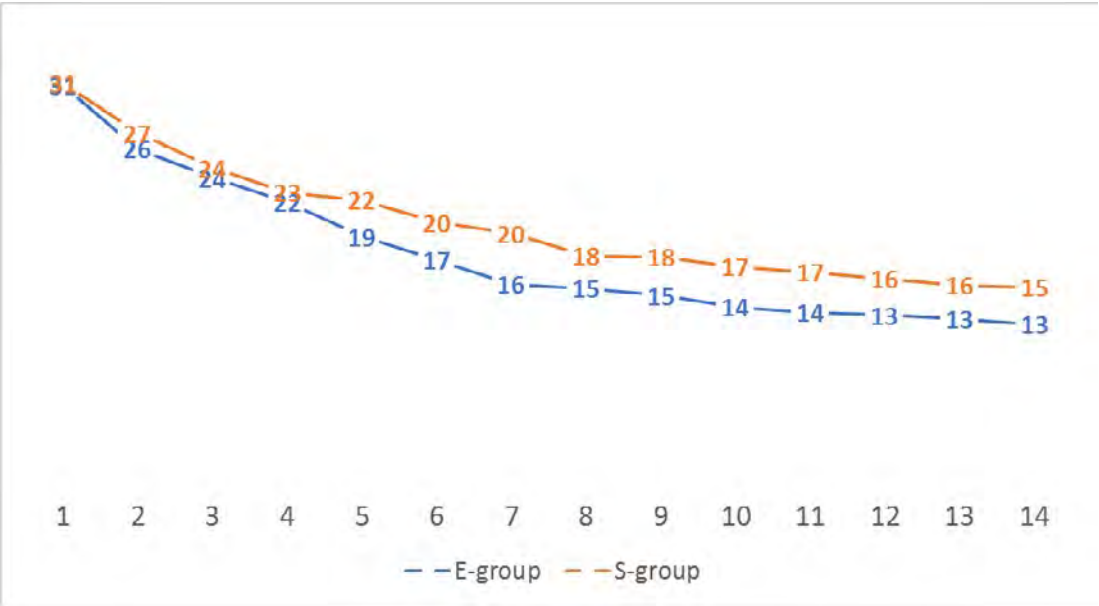


Fig. 1. *Trend of Upper Airway Symptoms in the two postoperative weeks. Ectoine with Spray-sol™ significantly and quickly improved GSS.*

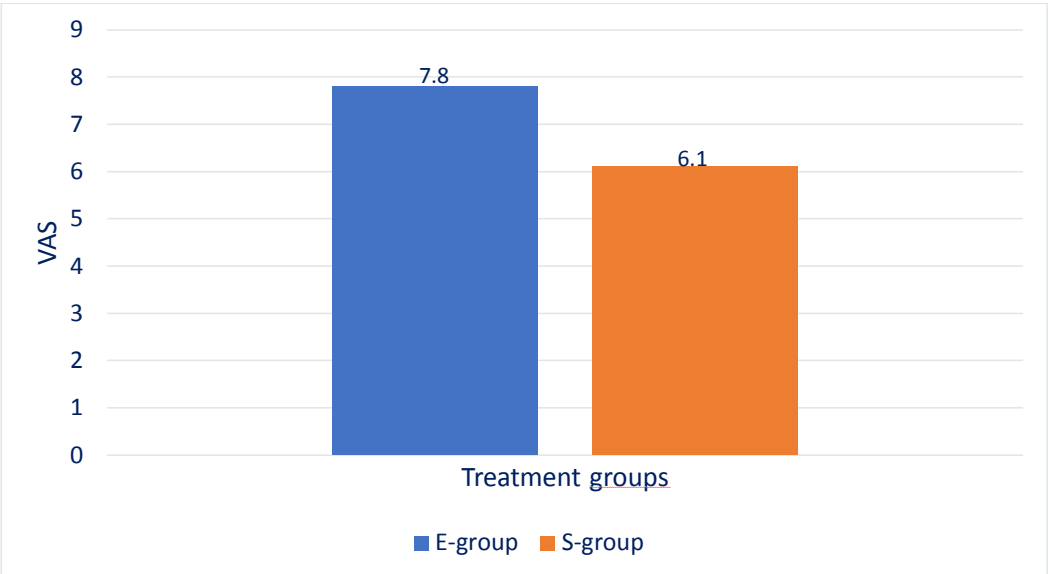


Fig. 2. *Compliance to the treatment*

of ectoine on tissue hydration, with the reduction of inflammation and secretions. Many studies showed that not all nasal devices are suitable to reach the nasopharynx region. Moffa et al. (5) showed that Spray-sol™ reached the nasopharynx region quickly in comparison with other devices, like "Rinowash" and "MAD nasal", with a statistical significance, and it could be considered a useful device for adenoiditis and Eustachian tube dysfunction therapies. Through the use of Spray-sol™, a high concentration of

ectoine solutions reached the nasopharynx region, the primary surgical site. This nasal device delivers particles with an average diameter between 10 and 20 microns, unlike "Rinowash", which has to be connected to an aerosol nebulizer with a pneumatic compressor. Spray-sol™ does not require energy, and administration time is as fast as a spray device. It allows distributions of small-diameter particles, modulation of the substance, as well as the capacity to reach all areas of nasal cavities, and the nasopharynx. Consequently, the amount of content that reaches the most posterior and upper regions of the nasal cavities is higher. Administration time (about 3-5 seconds for a complete and fine nebulization) and the ability to modulate applied forces is easy and fast. It is reusable and for a single patient. Moreover, Spray-sol™ has the advantage of delivering multiple types of saline solutions simultaneously and some drugs such as corticosteroids.

The encouraging results of this observational study have led us to investigate the potential role of ectoine saline solution in combination with Spray-sol™ in other types of acute and chronic inflammatory diseases of the upper airway. Further studies on a large scale will be needed to confirm the encouraging results obtained from the present study.

DISCLOSURE of potential conflicts of interest: M. Casale is the inventor but not the owner of B14630R/REPA/rst patent and PCT/IB2014/065121 of Spray-sol® device. All of the other authors report no conflicts of interest.

REFERENCES

1. Sjogren PP, Thomas AJ, Hunter BN, Butterfield J, Gale C, Meier JD. Comparison of pediatric adenoidectomy techniques. Laryngoscope 2018; 128(3):745-49.
2. Soumya S, Vissapragada R, Le J, Ooi EH. Halitosis and pain post electrocautery adenoidectomy. Medicina (Kaunas) 2019; 55(6).
3. Casale M, Moffa A, Carbone S, et al. Topical ectoine: a promising molecule in the upper airways inflammation-a systematic review. Biomed Res Int 2019; 2019:7150942.
4. Moffa A, Carbone S, Costantino A, et al. Potential role of topical ectoine for prevention of pediatric upper respiratory tract infection: a preliminary observational study. J Biol Regul Homeost Agents 2019; 33(6):1935-40.
5. Moffa A, Costantino A, Rinaldi V, et al. Nasal delivery devices: A comparative study on cadaver model. Biomed Res Int 2019; 2019:4602651.
6. Casale M, Moffa A, Cassano M, et al. Saline nasal irrigations for chronic rhinosinusitis: From everyday practice to evidence-based medicine. An update. Int J Immunopathol Pharmacol 2018; 32:205873841880267.
7. Cassano P, Gelardi M, Cassano M, Fiorella ML, Fiorella R. Adenoid tissue rhinopharyngeal obstruction grading based on fiberendoscopic findings: a novel approach to therapeutic management. Int J Pediatr Otorhinolaryngol 2003; 67(12):1303-9.

LETTER TO THE EDITOR

BIOLOGICAL, GENETIC AND AETIOLOGY ASPECTS IN MOLAR INCISOR HYPOMINERALIZATION

R. APPONI[1], S. PRESTI[1], E. SPINAS[2] and L. GIANNETTI[1]

[1]Department of Surgery, Medicine, Dentistry and Morphological Sciences with Transplant Surgery, Oncology and Regenerative Medicine Relevance (CHIMOMO), University of Modena and Reggio Emilia, Italy; [2]Department of Surgical Sciences, University of Cagliari, Cagliari, Italy

Received March 25, 2020 – Accepted May 6, 2020

To the Editor,

Molar-incisor hypomineralisation (MIH) has been described as an enamel hypomineralization of systemic origin that can affect from one to four permanent first molars and permanent incisors (1). The definition was described as a qualitative defect in development caused by a reduction in the mineralization and inorganic component of the enamel (2,3). An MIH characteristic is that the defect originates from the enamel-dentinal junction and not from the external surface of the enamel (4). The prevalence of MIH is relatively high, with percentages ranging from 2% to 40% in the world (5). Clinically, the elements affected by MIH show opaque lesions of varying sizes, noticeable above all on the occlusal and vestibular surfaces, with colors ranging from white-cream to yellow-brown (3). The typical opaque appearance of the lesions derives from the fact that the refractive index of the hypomineralized enamel is lower than that of the healthy enamel (4). Generally MIH is classified according to the severity of these lesions (3, 6). Over the years, numerous hypotheses and associations have been proposed to explain the etiology of MIH, such as the onset of certain pathological conditions of the pre-natal period, perinatal and the postnatal period. It is difficult to be able to precisely define what the medical and pathological conditions associated with MIH may be since in most cases the research available could be inaccurate (7). To date, the most accepted hypothesis is that which supports the environmental multifactoriality associated with a genetic component (6). There are many aspects to consider when talking about MIH and, therefore, the objective of this study is to evaluate, through a review of the most recent scientific literature, the biological, genetic and etiopathological characteristics related to this specific condition.

MATERIALS AND METHODS

A bibliographic search was performed on the Medline computer database via Pubmed (www.pubmed.gov) for articles published between 2009 and 2020 exclusively in English, of cross-sectional type, retrospective and prospective cohorts, case-controls, reviews, experimental studies on humans and animals related to the etiopathological environmental and genetic factors related to MIH development. Articles published before 2013, articles related to MIH but not related to etiopathogenesis, and articles concerning enamel defects not attributable to MIH such as fluorosis, amelogenesis imperfecta and hypoplasia of the enamel were excluded from the research. The following search terms were used

Key words: MIH; molar incisor hypomineralization; enamel; restorative dentistry; dental caries

Corresponding Author:
Dr Roberto Apponi,
via del Pozzo 71,
41124, Modena, Italy
Tel.: +390594224325
Fax: +39059373428
e-mail: roberto.apponi@gmail.com

0393-974X (2020)
Copyright © by BIOLIFE, s.a.s.
This publication and/or article is for individual use only and may not be further reproduced without written permission from the copyright holder.
Unauthorized reproduction may result in financial and other penalties
DISCLOSURE: ALL AUTHORS REPORT NO CONFLICTS OF INTEREST RELEVANT TO THIS ARTICLE.

individually and using the Boolean operators: "MIH", "Molar-incisor hypomineralization", "Dental enamel", "Enamel hypomineralization", "MIH AND aetiology", "MIH AND genetic", " MIH AND mineral density "," MIH AND protein content ". The selection of the articles was carried out by evaluating the title and the abstract in a first phase, discarding the articles that did not meet the inclusion criteria. Subsequently, for the studies satisfying the inclusion criteria, the full-text was evaluated for the final selection of the articles.

The research, evaluation and inclusion of the articles was carried out by two authors independently. Each author, respecting the inclusion and exclusion criteria of the articles, generated his own list of bibliographic references collected in the Zotero software. The two lists were subsequently compared and any disagreement on the inclusion or exclusion of an article was resolved by involving a third author. For each selected article, the most relevant aspects were reported in relation to the environmental, genetic etiopathogenesis and treatment involved in the development of MIH.

RESULTS

Environmental factors

Several studies investigated the relationship between the use of antibiotics and the onset of MIH. Among them, one study was conducted experimentally on pig teeth and did not report a significant association between the use of amoxicillin and MIH, although X-ray microtomography revealed a reduction in the mineral density of the elements analyzed. On the contrary, three cross-sectional studies reported a significant association between the use of antibiotics in the first years of life and the onset of MIH. This association was confirmed by a retrospective cohort study in which it was shown that taking a penicillin cycle in the first year of life doubles the risk of developing MIH, while for macrolides this risk increases four times.

Three cross-sectional studies report a significant association between MIH and the appearance of pathologies in the early years of life such as asthma/bronchitis, adenoid infections, tonsillitis, fever, chicken pox, pneumonia, otitis media, atopic dermatitis and food allergies. The association between allergic dermatitis and MIH is also confirmed by a case-control study. A further case-control study also reports a higher prevalence of MIH in HIV-infected subjects than in healthy subjects (45.5% *vs* 24.2%). In addition, several retrospective studies involving a considerable number of subjects reported a statistically significant association between MIH and frequent episodes of diarrhea, digestive tract disorders and kidney disease, but especially chicken pox, rubella, otitis and vitamin A deficiency. On the contrary, an experimental study from 2017 showed that excess vitamin A would cause demineralization. Kuhnisch et al., in a prospective study, reported that early respiratory disorders that occurred in the first four years of life are strongly associated with the development of MIH. In a further study Kuhnisch et al. reported for the first time an association between low serum vitamin D levels and MIH, which is however disproved by the results obtained in 2018 from a prospective study by Vandertas et al. Regarding pre- and peri-natal factors, one case control study reports a statistically significant association between the appearance of fever in the mother during pregnancy and the onset of MIH. In a retrospective study, an increased risk of MIH was also reported due to hypoxia of the newborn during childbirth (> 6 times) and birth with cesarean section (> 3 times). The association with hypoxia is also confirmed by a further cross-sectional study and an experimental study on mouse incisors. Hernandez et al., in a 2018 cross-sectional study, did not report a statistically significant association between MIH and the mother's pre-existing medical conditions, birth weight, breastfeeding and drugs taken during the first years of life.

Genetic factors

Several recent genomic studies have shown that the polymorphism of the SCUBE1 gene locus, the polymorphism of the TGFBR1 and DEFB1 genes involved in the immune response, the polymorphism of the AMBN, AMELX, ENAM, BMP2, BMP4, BMP7, FGFR1, TFIP11, MMP20, KLK4 involved in the process of enamel formation and genetic variations of the AQP5 gene could be associated with the development of MIH. In support of genetic

involvement in the etiopathogenesis of MIH, Teixeira et al. conducted a study on twins in which it was found that in both monozygotic twins there was a higher prevalence of MIH than in dizygotic twins.

In addition, studies have been evaluated on the potential effect of endocrine disruptors (EDC) on the development of enamel defects. In fact, several authors report that certain steroid receptors (AR, ERα) could play a key role in the different stages of amelogenesis. Moreover, some studies have shown that bisphenol A, one of the main EDCs, could be involved in the etiopathogenesis of MIH as it would be able to interact with the estrogenic receptors expressed by ameloblasts and would favor the accumulation of organic material in the enamel reducing its mineralization. One of these studies also showed that the association between various EDCs has a lesser impact on amelogenesis compared to exposure to bisphenol A alone.

DISCUSSION

The etiological mechanisms underlying MIH are still unclear. It is known that the development of dental elements is genetically controlled but is very sensitive to external environmental interference (7). The results of literature show, in fact, the association between the development of MIH and fever or hypoxia that could be involved in the etiopathogenesis of MIH and influence the activity of the genes involved in the expression of the proteins of the enamel matrix (3). In addition to environmental factors, genetic predispositions and mutations that lead to MIH development are also hypothesized as in the CTS gene (11q14.2) characteristic of papillon Lefevre syndrome, as observed in several scientific studies (8). At a microstructural level, the literature shows there are also differences in the chemical composition (4). The in-depth analysis of the biological and etiopathogenetic aspects related to MIH is fundamental in order to be able to implement preventive and therapeutic measures. Today there are different treatments such as the application of fluorinated paints, casein mousse or low viscosity resins (9). In recent studies it was shown that the technique of both superficial and deep infiltration of low viscosity resins is able to improve the aesthetic results of the elements affected by MIH (10, 11). It is recommended to use a mouth guard at least during sports activities to prevent fractures caused by the coronal fragility of the elements affected by MIH (12). It is possible to say that MIH is a non-idiopathic multifactorial condition with a strong environmental and genetic component. In particular, antibiotics in early childhood, respiratory diseases, and recurrence of febrile episodes during the stages of amylogenesis in the first four years of life are associated with the onset of MIH. The association with pre- and peri-natal episodes is also relevant. Further studies are needed in order to strengthen and clarify the associations between the different factors and the development of enamel lesions.

REFERENCES

1. Weerheijm KL, Jälevik B, Alaluusua S. Molar-incisor hypomineralisation. Caries Res 2001; 35:390-91.
2. Taylor GD. Molar incisor hypomineralisation. Review. Evid Based Dent 2017; 18(1):15-16.
3. Americano GCA, Jacobsen PE, Soviero VM, Haubek D. A systematic review on the association between molar incisor hypomineralization and dental caries. Int J Paediatr Dent 2017; 27:11-21.
4. Denis M, Atlan A, Vennat E, Tirlet G, Attal J-P. White defects on enamel: Diagnosis and anatomopathology: Two essential factors for proper treatment (part 1). Int Orthod 2013; 11:139-65.
5. Elhennawy K, Manton DJ, Crombie F, et al. Structural, mechanical and chemical evaluation of molar-incisor hypomineralization-affected enamel: A systematic review. Arch Oral Biol 2017; 83:272-81.
6. Elhennawy K, Schwendicke F. Managing molar-incisor hypomineralization: A systematic review. J Dent 2016; 55:16-24.
7. Alaluusua S. Aetiology of Molar-Incisor Hypomineralisation: A systematic review. Eur Arch Paediatr Dent 2010; 11:53-58.
8. Castori M, Madonna S, Giannetti L, Floriddia G, Milioto M, Amato S, Castiglia D. Novel CTSC mutations in a patient with Papillon-Lefèvre syndrome with recurrent pyoderma and minimal oral and palmoplantar involvement. Br J Dermatol 2009; 160:881-83.

9. Giannetti L, Bartoli G, Banchelli F, Spinas E, Dello Diago AM. MIH: A survey amongst dental practitioners in Modena and Reggio Emilia districts. Dental Cadmos 2018; 86:172-80.
10. Giannetti L, Murri Dello Diago A, Silingardi G, Spinas E. "Superficial infiltration to treat white hypomineralized defects of enamel: clinical trial with 12-month folow-up. J Biol Regul Homeost Agents 2018; 32:1335-38.
11. Giannetti L, Murri Dello Diago A, Corciolani E, Spinas E. Deep infiltration for the treatment of hypomineralized enamel lesions in a patient with molar incisor hypomineralization: a clinical case. J Biol Regul Homeost Agents 2018; 32:751-54.
12. Spinas E, Aresu M, Giannetti L. Use of mouth guard in basketball: observational study of a group of teenagers with and without motivational reinforcement. Eur J Paediatr Dent 2014; 15(4):392-96.

LETTER TO THE EDITOR

CLINICAL PREDICTORS OF RESPONSE TO OZONE THERAPY FOR TREATMENT OF DISCOGENIC AND NON-DISCOGENIC LOW BACK PAIN

S. DAL FIOR[1], C. GAIDO[1], I. CARNINO[1], F. GAMNA[1], C. BUSSO[2], G. MASSAZZA[2] and M.A. MINETTO[2]

[1]Division of Physical Medicine and Rehabilitation, San Luigi Hospital, Orbassano, Italy; [2]Division of Physical Medicine and Rehabilitation, Department of Surgical Sciences, University of Turin, Turin, Italy

Received December 31, 2019 – Accepted March 4, 2020

To the Editor,

The effectiveness of ozone administration for the treatment of disc herniation causing acute spinal pain has been extensively documented (1-3). Two administration approaches are commonly performed: the direct approach, that consists in the intradiscal or intraforaminal injection of ozone, and the indirect approach, that consists in gas injection into the tender points of the paravertebral muscles corresponding to the metamer of the herniated disk (1). The clinical benefits of the direct approach are usually immediate and almost all treated patients show an alleviation of symptoms. Conversely, the clinical benefits of the indirect approach are not immediate: injections must be repeated for about 4-6 weeks to obtain clinically relevant pain relief (1). Also the mechanisms underlying the effectiveness of the two approaches are thought to be different (1, 4). In fact, the intradiscal ozone injection results in a chemical nucleolysis (1, 5). Differently, the paravertebral ozone injection must be viewed as a "chemical acupuncture" because both the needle and the injected gas may have a role in eliciting different local reactions: improvement of the local oxygenation, induction of antioxidant enzymes, oxidative degeneration of C-nociceptors resulting in the elevation of their activation threshold, release of endorphins that modulate the transmission of the noxius signal to supraspinal centers (1, 4). Which of these mechanisms is mainly responsible for the pain relief effects remains to be clarified. However, it may be hypothesized that the local induction of mechanisms triggering a stimulation of the natural healing capabilities could result in a clinical benefit also for conditions other than the acute pain associated with disc herniation. To our knowledge, no previous study investigated the effectiveness of paravertebral ozone administration for the treatment of non-discogenic low back pain. Therefore, the aims of this study were to investigate the response of different groups of low back pain patients to paravertebral ozone administration and to identify clinical predictors of this response.

MATERIALS AND METHODS

Study design and patients

Forty-nine patients of both genders [12 males and 37 females, median (interquartile range) age: 63 (15) years; body mass index: 26.0 (7.3) kg/m^2] were enrolled in the study (convenience sample). Fifteen patients presented acute discogenic low back pain, 23 presented chronic discogenic

Key words: ozone; low back pain; response endophenotype; pain intensity

Corresponding Author:
Dr Marco Alessandro Minetto,
Department of Surgical Sciences University of Turin,
Corso Dogliotti 14, 10126 Torino, Italy
Tel.: +390116705472
e-mail: marco.minetto@unito.it

0393-974X (2020)
Copyright © by BIOLIFE, s.a.s.
This publication and/or article is for individual use only and may not be further reproduced without written permission from the copyright holder.
Unauthorized reproduction may result in financial and other penalties
DISCLOSURE: ALL AUTHORS REPORT NO CONFLICTS OF INTEREST RELEVANT TO THIS ARTICLE.

low back pain, and 11 presented non-discogenic low back pain (acute in 3 patients and chronic in 8 patients). The three groups of patients were comparable for age, gender distribution, and body mass index. Inclusion criteria were a clinical diagnosis of acute or chronic low back pain confirmed by magnetic resonance imaging evidence of discogenic or non-discogenic (lumbar spinal stenosis, spondyloarthritis, vertebral fracture sequelae) disorders. All subjects received a detailed explanation of the study and gave written informed consent prior to participation. The study conformed with the guidelines in the Declaration of Helsinki and was approved by the local ethics committee.

Procedures

All patients received 10 intramuscular injections (2/wk for 5 consecutive weeks) of an O_2–O_3 mixture (20 ml) with an O_3 concentration of 15 µg/ml that was obtained by an Ozonline International generator (model E30 - Medica s.r.l., Bologna, Italy). Four intramuscular injections were performed using a 27-gauge needle (length: 40 mm) in the paravertebral lumbar muscles (the L4-L5 and L5-S1 interspaces were selected because the relative intervertebral discs were the pain source in all patients with discogenic disorders), bilaterally (10 ml for each side) using an extra-spinal lateral approach, under sterile conditions. No premedication or anesthesia was given, and the procedure was performed in an outpatient clinic.

The following assessments were performed before the 5-week intervention: i) anthropometric measurements (weight and height); ii) anamnesis and physical examination to collect the following clinical characteristics: pain presentation (acute/chronic), analgesic medication use; iii) resting pain intensity: patients were asked to rate the pain using a 11-point numeric rating scale (NRS: 0 = corresponded to "no pain" and 10 corresponded to "the worst imaginable pain"); iv) SF36 questionnaire which is a 36-item questionnaire compiled from the Rand Health Insurance Long Form Health Status Scale (6) that investigates eight different dimensions of the health-related quality of life. Of the eight dimensions, we included the following subscales: general health, physical function, and pain. Questions are framed over a one-week period with response scales varying from dichotomous (yes/no) to six-point verbal rating scales. Each dimension is scored on a weighted 0-100 scale and different dimensions are averaged to obtain the subscale scores.

In addition, the resting pain intensity was also assessed at the end of the 5-week intervention period (post-intervention assessment) and 2 months and 6 months thereafter (2-month and 6-month follow-up assessments).

Data analysis

Previous studies indicated that 1.5 and 2.5 NRS point reductions are clinically meaningful in low back pain patients presenting baseline NRS scores <7 and ≥ 7, respectively (7). Therefore, we divided the whole group of patients in "responders" (i.e., patients presenting NRS point reductions at 6-month follow-up compared with the baseline NRS score higher than the minimal clinically important change) and "non-responders" (patients presenting NRS point reductions at 6-month follow-up compared with the baseline NRS score lower than the minimal clinically important change). Moreover, we also divided the patients in "early responders" (i.e., patients presenting NRS point reductions at the end of the intervention compared with the baseline NRS score higher than the minimal clinically important change) and "early non-responders" (i.e., patients presenting NRS point reductions at the end of the intervention compared with the baseline NRS score lower than the minimal clinically important change).

Since the Shapiro–Wilk test for the normal distribution of the data failed, non-parametric tests were used: the Mann-Whitney U test was adopted for comparisons of quantitative variables between the two groups (responders *vs* non-responders), while the Fisher's exact test was adopted for comparisons between proportions. The Friedman's ANOVA followed by Dunn's post hoc test were used for analysing the time course of pain intensity and a logistic regression analysis was used to investigate the relationships between the response to intervention (the outcome variable was binary as all patients were classified as responders or non-responders) and the investigated clinical predictors. Finally, the Spearman's test was adopted for correlation analyses.

Data are expressed as median (and interquartile range) and are represented as box-and-whisker plots. Threshold for statistical significance was set at $P = 0.05$. Statistical tests were performed with SPSS 20.0 (SPSS Inc., Chicago, USA) software package.

RESULTS

All patients completed the 10 sessions of ozone

administration and no adverse effects were observed. The three groups of patients were comparable (P>0.05 for all comparisons) for age [acute discogenic disorder: 55.0 (22.5) years; chronic discogenic disorder: 63.0 (9.5) years; non-discogenic disorder: 75.0 (7.5) years], gender distribution (acute discogenic disorder: 4 males out of 15 patients; chronic discogenic disorder: 7 males out of 23 patients; non-discogenic disorder: 1 male out of 11 patients), and body mass index (acute discogenic disorder: 26.0 (8.2) kg/m^2; chronic discogenic disorder: 25.0 (5.7) kg/m^2; non-discogenic disorder: 27.8 (7.1) kg/m^2].

Twenty nine out of 49 patients (59% of cases) were identified as responders, while the remaining 20 (41% of cases) were identified as non-responders: the number of responders was comparable among the three groups (acute discogenic disorder: 6 out of 15 patients; chronic discogenic disorder: 17 out of 23 patients; non-discogenic disorder: 6 out of 11 patients). Moreover, 28 out of 49 patients (57% of cases) were identified as early responders, while the

Table I. *Comparisons of anthropometric data and clinical characteristics between the two groups of patients*

Variable	Responders (n=29)	Non-responders (n=20)	P value
Number of females (males)	23 (6)	14 (6)	0.51
Number of patients with acute (chronic) pain	7 (22)	10 (10)	0.08
Number of patients under analgesic medication	18	14	0.76
Age (years)	65.0 (13.0)	60.5 (20.8)	0.92
Body mass index (kg/m^2)	25.6 (5.6)	27.1 (8.0)	0.24
Pre-intervention pain intensity - NRS (a.u.)	7.5 (3.3)	7.0 (2.3)	0.66
SF36 pain	45.0 (12.5)	22.5 (17.5)	0.04
SF36 physical function	32.5 (35.0)	50.0 (42.5)	0.21
SF36 general health	45.8 (29.2)	41.7 (37.5)	0.66

Values reported for quantitative variables are medians (interquartile ranges).

Table II. *Results of the logistic regression analysis*

Variable	P value	Odds ratio	95% confidence intervals
Early responsiveness	0.02	0.10	0.01 – 0.71
Disease type (1)	0.32	0.14	0.01 – 6.86
Disease type (2)	0.62	0.51	0.04 – 7.23
Gender	0.95	0.93	0.08 – 10.77
Age	0.22	0.92	0.81 – 1.05
Body mass index	0.14	0.82	0.63 – 1.06
Pre-intervention pain intensity	0.13	1.69	0.85 – 3.36
Analgesic medication use	0.72	1.56	0.13 – 18.38
Pain presentation	0.72	0.50	0.01 – 21.18
SF36 physical function	0.57	0.98	0.93 – 1.04
SF36 pain	0.11	1.06	0.98 – 1.15
SF36 general health	0.70	0.98	0.91 – 1.06

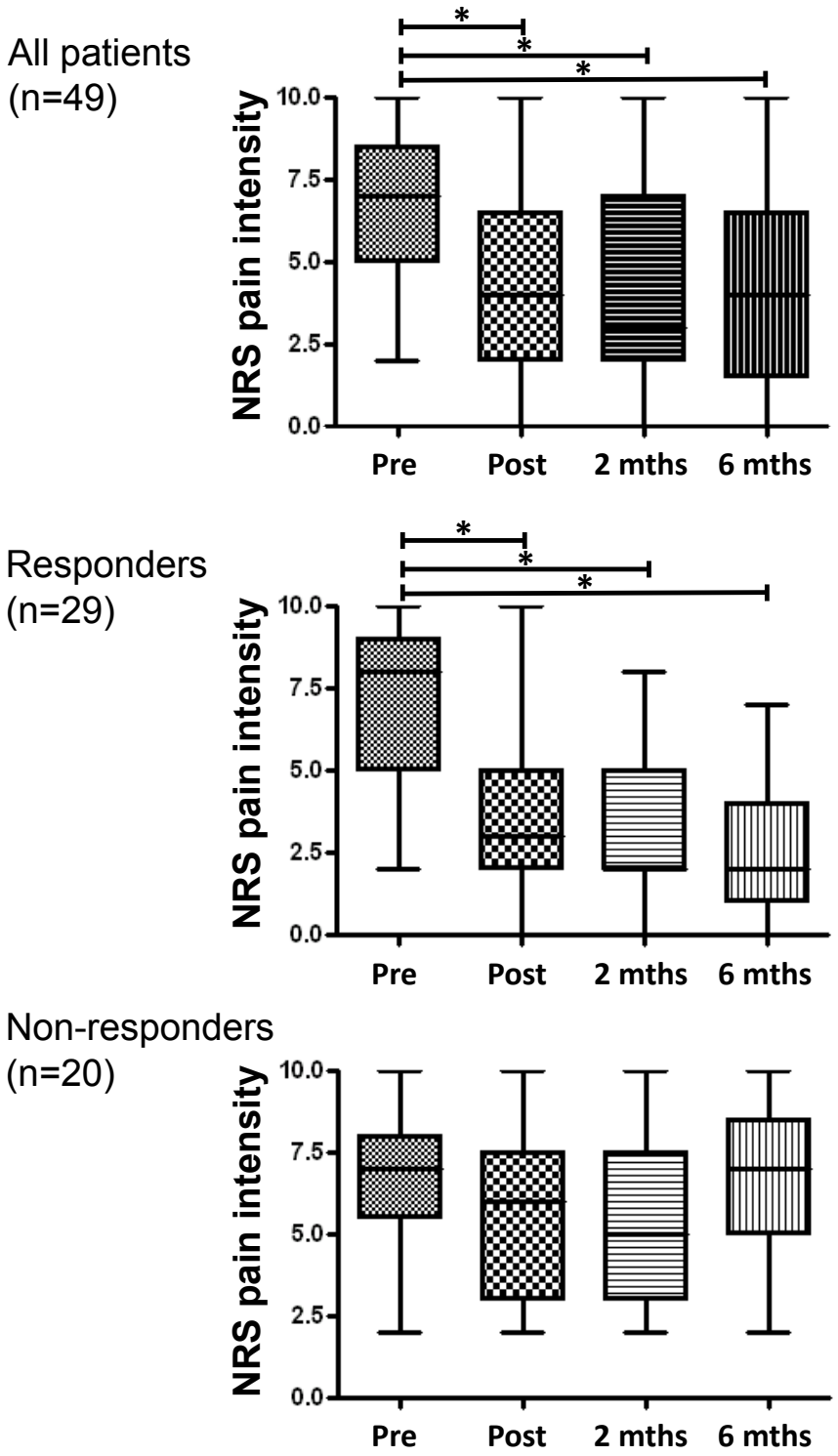


Fig. 1. *Time course of the numeric rating scale (NRS) pain intensity scores in the whole population of 49 patients (upper panel) and in the two groups of 29 responders (middle panel) and 20 non-responders (lower panel). Pre: pre-intervention; Post: post- intervention; 2 mths: 2-month follow-up; 6 mths: 6-month follow-up. *: P<0.001*

remaining 21 (43% of cases) were identified as early non-responders.

Significant pre-post-intervention pain intensity reductions were observed both in the whole group of 49 patients (Fig. 1, upper panel: $F=61.60$, $P<0.0001$) and in the group of 29 responders (Fig. 1, middle panel: $F=54.24$, $P<0.0001$) who showed median reductions of pain intensity of 4.0 (4.0), 4.0 (2.0), and 5.0 (2.0) NRS points at the end of the intervention and after 2 months and 6 months, respectively. These reductions corresponded to percent median reductions of pain intensity of 58.6 (43.7)%, 69.0 (22.5)%, 78.9 (20.8)% at the end of the intervention and after 2 months and 6 months, respectively. On the contrary, no significant pain intensity reduction was observed in the group of 20 non-responders (Fig. 1, lower panel; $F=18.07$, $P>0.05$).

Table I shows the comparisons of proportions and quantitative variables between responders and non-responders: no statistically significant differences were observed between the two groups, with the exception of the SF36 pain subscale score that was significantly ($P=0.04$) higher (i.e., the pain was lower) in responders compared to non-responders.

Table II reports the results of the logistic regression analysis applied to the following covariates: early responsiveness (this covariate was binary as all patients were classified as early responders or early non-responders), disease type (acute discogenic disorder, chronic discogenic disorder, non-discogenic disorder), gender, age, body mass index, pre-intervention pain intensity, analgesic medication use, pain presentation (acute or chronic), SF36 subscale scores. Most of the patients (83.3%) were properly classified with a model based on the available covariates: however, the only significant ($P=0.02$) predictor of response to ozone therapy was the early responsiveness, while all other covariates showed no significant association with the outcome variable ($P>0.05$ for all other covariates) (Table II, second column). Consistently, a significant positive correlation ($R=0.57$, $P<0.0001$) was observed between the "early" pain intensity reduction (pre-post-intervention pain intensity difference) and the "late" pain intensity reduction (difference in pain intensity between 6-month follow-up and pre-intervention values). The equation of the linear regression line was the following: $y=0.553*x-2.7189$: therefore, an "early" pain intensity reduction of 1.5 corresponds to a "late" pain intensity reduction of 3.5, while an "early" pain intensity reduction of 2.5 corresponds to a "late" pain intensity reduction of 4.1. Briefly, the higher the early pre-post-intervention decrease of pain intensity, the higher the pain intensity decrease at 6-month follow-up.

DISCUSSION

The main findings of this study were that: i) 10 sessions of paravertebral ozone injection were safe and effective to produce a clinically relevant pain intensity reduction in low back pain patients; ii) a remarkable inter-individual variability was observed in the pain relief effect of the ozone administration iii) the early responsiveness was the only significant clinical predictor of the medium-term response. The observation that the paravertebral ozone injections were effective not only in discogenic disorders but also in non-discogenic disorders represents an original finding of this study. It may be proposed that the periradicular and periganglionic diffusion of ozone could underlie its effectiveness in discogenic conditions, whilst local actions of ozone in the muscular micro-environment could be responsible for the pain relief effects observed in non-discogenic conditions. The previously mentioned local actions of ozone include improvement of oxygenation, induction of antioxidant enzymes, oxidative degeneration of C-nociceptors, release of endorphins (1, 4) and perhaps the Nrf2 modulation (8, 9). The observed inter-individual variability in the pain relief effect of the ozone administration could be related to methodological issues relative to either the adopted volume and concentration of the O_2–O_3 mixture or the number of injection points or the length of the adopted needles (the standard length of 40 mm might not be enough to deliver the ozone in the suggested right side of action). Analytical issues relative to the selected outcome measure (i.e., pre-post-intervention reduction in pain intensity) and to the selected cutoff point for the minimal clinically important change for pain intensity could also

explain the observed inter-individual variability. Further studies are required to investigate whether different treatment regimens may produce different outcomes: for example, it may be hypothesized that a higher concentration of ozone and/or the use of a longer needle and/or the ultrasound guidance for the injection could result in greater efficacy (even after less injections). Further studies are also required to investigate whether different outcome assessments may produce different percentages of responders and non-responders. The resting pain intensity was investigated in the present study since it represents the clinical variable most commonly assessed in the daily clinical management of chronic pain patients. However, it may be hypothesized that other pain scales and/or questionnaires (or a different cut-off value for the NRS point reductions at 6-month follow-up compared with the baseline NRS score) could provide a better characterization of the individual response to the treatment.

ACKNOWLEDGEMENTS

This study was supported by the Italian Ministry of Education, University and Research (MIUR) under the programme "Dipartimenti di Eccellenza ex L. 232/2016" to the Department of Surgical Sciences, University of Torino (Italy).

REFERENCES

1. Bocci V, Borrelli E, Zanardi I, Travagli V. The usefulness of ozone treatment in spinal pain. Drug Des Devel Ther 2015; 9:2677-85.
2. Steppan J, Meaders T, Muto M, Murphy KJ. A metaanalysis of the effectiveness and safety of ozone treatments for herniated lumbar discs. J Vasc Interv Radiol 2010; 21:534-48.
3. Magalhaes FN, Dotta L, Sasse A, Teixera MJ, Fonoff ET. Ozone therapy as a treatment for low back pain secondary to herniated disc: a systematic review and meta-analysis of randomized controlled trials. Pain Physician 2012; 15:E115-29.
4. Borrelli E. Mechanism of action of oxygen ozone therapy in the treatment of disc herniation and low back pain. Acta Neurochir Suppl 2011; 108:123-25.
5. Murphy K, Elias G, Steppan J, et al. Percutaneous Treatment of Herniated Lumbar Discs with Ozone: Investigation of the Mechanisms of Action. J Vasc Interv Radiol 2016; 27:1242-50.
6. McHorney CA, Ware JE Jr, Rogers W, Raczek AE, Lu JF. The validity and relative precision of MOS short- and long-form health status scales and Dartmouth COOP charts. Results from the Medical Outcomes Study. Med Care 1992; 30:253-65.
7. Kovacs FM, Abraira V, Royuela A, et al. Minimal clinically important change for pain intensity and disability in patients with nonspecific low back pain. Spine (Phila Pa 1976) 2007; 32:2915-20.
8. Pecorelli A, Bocci V, Acquaviva A, et al. NRF2 activation is involved in ozonated human serum upregulation of HO-1 in endothelial cells. Toxicol Appl Pharmacol 2013; 267:30-40.
9. Re L, Martínez-Sánchez G, Bordicchia M, et al. Is ozone pre-conditioning effect linked to Nrf2/EpRE activation pathway in vivo? A preliminary result. Eur J Pharmacol 2014; 742:158-62.

LETTER TO THE EDITOR

ALTERATIONS IN HEPATIC TRACE ELEMENTS AND *FERRITIN* EXPRESSION IN HIGH ENERGY DIET FED RAT MODEL

S. GHAFOOR[1], T. AKHTAR[1], M. B. KHAWAR[1,2,3] and N. SHEIKH[1]

[1]Cell & Molecular Biology Laboratory, Department of Zoology, University of the Punjab, Lahore, Pakistan; [2]State Key Laboratory of Stem Cells and Reproductive Biology, Institute of Zoology, Chinese Academy of Sciences, Beijing, P.R. China; [3]University Chinese Academy of Sciences, Beijing, P.R. China

Received November 19, 2018 – Accepted April 16, 2019

To the Editor

HED especially rich in fats has established itself as one of the major contributors to obesity and hyperglycemia. Immoderate use of lipid-rich food often triggers inflammatory responses and disturbs cellular metabolic homeostasis, thus serving to be a principal initiator of many metabolic syndromes (1).

Trace elements (TEs) are inevitable to the human body due to their multiple structural, cofactor and signaling functions (2). TEs, in particular iron abnormalities, are common in obese and overweight people (3). Several studies have shown the presence of close inter-relationship between TE homeostasis and obesity-linked disorders (2).

Ferritin protein plays a pivotal role in cellular inflammation, iron metabolism, cell proliferation, apoptosis and oxidative damage (4). In response to iron concentration in the cell, *ferritin* expression (*ferritin-L, ferritin-H*) increases at both transcriptional and translational level (5). Numerous factors, such as iron overload, chemokines production, cytokine release, prostaglandins, lipopolysaccharides, second messengers, growth factors, hypoxia and hyperoxia, and oxidative stress, are responsible for ferritin regulation either directly or indirectly. Complicated feed-back mechanism exists between cytokines and ferritin, hence controling pro-inflammatory as well as anti-inflammatory mediators (6).

The key objective of the current study was to develop a rat model by feeding male Wistar rats on HED, hepatic TEs profiling, and to measure the *ferritin* mRNA expression.

MATERIALS AND METHODS

High energy diet

To develop a fat-rich HED rat model, six-week-old rats were randomly, divided into two dietary groups (n=5): dietary group I (dry milk, sucrose, and rat chow) providing 18.5% of calories from fats, and dietary group II (dry milk and rat chow) providing 30% of calories from fats. A control group was fed on rat chow and water *ad libitum.* The trace elements of commercially available rat chow (Fe: 220µg/g, Cr: 0.70 µg/g, Mg: 2100 µg/g, Zn: 78 µg/g), supplemented diet I and diet II (Fe: 215 µg/g, Cr: 0.65 µg/g, Mg:0: 2100µg/g, Zn:80 µg/g) were also noted. The setup of rats was maintained in the animal house of the Department of Zoology, University of the Punjab, Lahore, Pakistan, under set standards (12 h light/ dark cycle, 24-25°C room temperature, and water *ad libitum*) on their assigned diets for the period of sixteen weeks. Wistar rats were then dissected. Excised livers were preserved at -80°C until further processed.

Key words: ferritin expression, hepatic trace elements, inflammation, iron metabolism.

Corresponding author:
Dr. Nadeem Sheikh,
Cell and Molecular Biology Lab,
Department of Zoology,
University of the Punjab, Q-A Campus,
Lahore, 54590, Pakistan
Tel.: +92 42 99231246/812; +92 322 4222-036
e-mail: s_nadeem77@yahoo.com

0393-974X (2020)
Copyright © by BIOLIFE, s.a.s.
This publication and/or article is for individual use only and may not be further reproduced without written permission from the copyright holder.
Unauthorized reproduction may result in financial and other penalties
DISCLOSURE: ALL AUTHORS REPORT NO CONFLICTS OF INTEREST RELEVANT TO THIS ARTICLE.

Wet digestion of liver samples

Wet digestion method was used for trace metal estimation through atomic absorption spectrophotometer (model number: AA 800, S/N800S8090101, Autosampler, technique: AA flame). For acid digestion, 10 ml of HNO_3 (1+1) was added to each of the liver samples (1 gram). Flasks were heated to the temperature of 90–95°C and were refluxed for 10–15 min without allowing them to boil. Deionized water (DI=2 ml) was added to each sample. Afterward, 3 ml of H_2O_2 (30%) was added to acid digested samples. Samples were warmed until effervescence stopped and then H_2O_2 (10 ml) was added in portions of 1 ml each time and heated again. Finally, the digestion flasks were leveled to 100 ml by adding DI water.

Expression of ferritin genes

Ferritin gene expression was assessed, adopting a previously reported method (7)

Total RNA isolation

For total RNA isolation, TRIzol reagent was added to liver tissues, followed by homogenization and centrifugation; 0.2 ml of chloroform was added to the homogenate thus obtained, that resulted in the phasic separation of RNA, which was then concentrated using isopropanol, was washed by ethanol and hence partially air-dried RNA pellets were re-suspended in RNAase-free water. RNA was quantified and qualified using Nanodrop (UV/VIS Spectrophotometer, model, Optizen Nano Q).

cDNA generation

cDNA was generated for further downstream PCR application, using Revert Aid first Stand cDNA kit (Cat #K1621, Fermentas) as per the manufacturer's guidelines.

Ferritin genes (Ferritin-H and Ferritin-L) amplification of cDNA

Already reported specific primers were used for polymerase chain reaction (PCR) (Table I). β-actin served as housekeeping gene during the process.

Polymerase chain reaction

The conditions for different stages of Polymerase Chain Reaction (PCR) cycle were optimized. The results of PCR products were analyzed by gel electrophoresis (2% agarose in Tris-acetate EDTA buffer), using ready-to-use gene ruler (Thermo Scientific Gene Ruler™ 100bp Plus DNA Ladder). Results were documented using Gel Doc-it™ imaging system.

Statistical analysis

Estimation of comparative fold change in mRNA expression from control and experimental rat groups was carried out using Image J software and Graph Pad Prism 5 (California, USA). One-way ANOVA test was applied for comparative statistical study. Columns thus obtained showed fold changes along with error bars that represent the Standard Error of Mean (SEM) (n=5, *P<0.05, **P<0.01 and ***P<0.001).

RESULTS

Hepatic trace elements profiling

Hepatic trace elements profiling showed substantial statistical alterations in both dietary groups fed on HED from the control group (Fig. 1).

Iron

The hepatic iron concentration in control groups was 53.17 mg/kg. Experimental groups fed on HED showed an iron overload. The concentration of iron was 84.25 mg/kg in DG I and 107.5 mg/kg in DG II (P=0.0021) (Fig. 1a).

Chromium

A positive rise of 6.050 mg/kg of chromium contents was observed in DG I (Fig. 1b). A negative trend of decreased metal contents 2.175 mg/kg was noticed in DG II in comparison to control where contents were 3.483mg/kg (P=0.0001).

Magnesium

Magnesium liver contents (Fig. 1c) of DG I 56.88 mg/kg showed no significant variance from control 60.42 mg/kg. However, magnesium contents were found significantly decreased in DG II 41.88 mg/kg.

Zinc

Zinc contents of DG I (4.765 mg/kg) were noticed to be decreased significantly from control (11.41 mg/kg). DG II was found to have 10.97 mg/ kg of zinc contents. Statistical comparison of DG I and DG II illustrated significant decrease between the two dietary groups (Fig. 1d).

Table I. *Specific primer sequences (forward and reverse) used during gene expression study.*

Primers	Forward 5'⟶3'	Reverse 5'⟶3'	Product length	Reference
Ferritin-L	AAC CAC CTG ACC AAC CTC CGT A	TCA GAG TGA GGC GCT CAA AGA G	103	(8)
Ferritin-H	GCC CTG AAG AAC TTT GCC AAA T	TGC AGG AAG ATT CGT CCA CCT	110	(9)
β-Actin	TGT CAC CAA CTG GGA CGA TA	AAC ACA GCC TGG ATG GCT AC	195	(9)

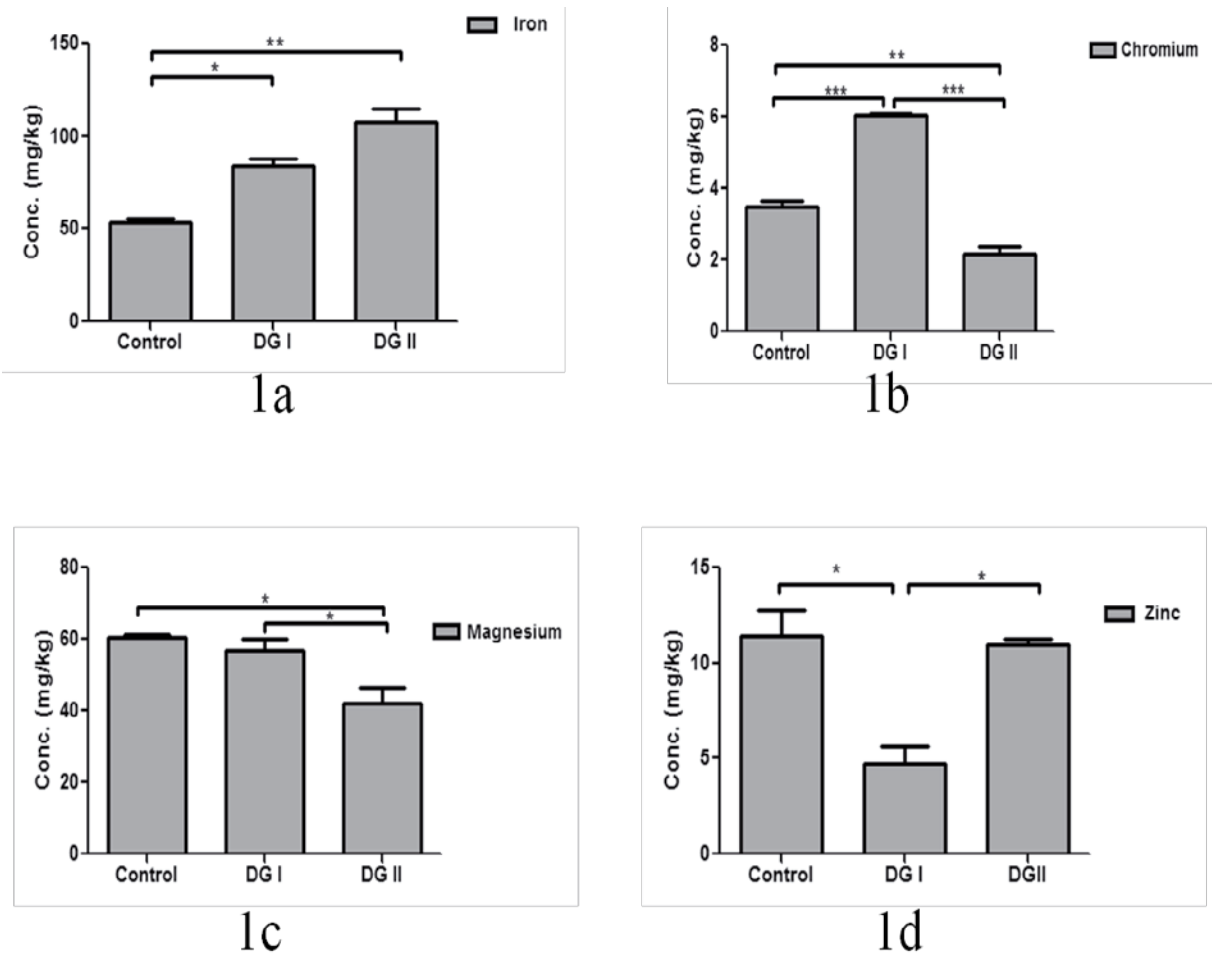


Fig. 1. *Statistical analysis of iron, chromium, magnesium and zinc contents in the liver of rats fed on HED against control.*

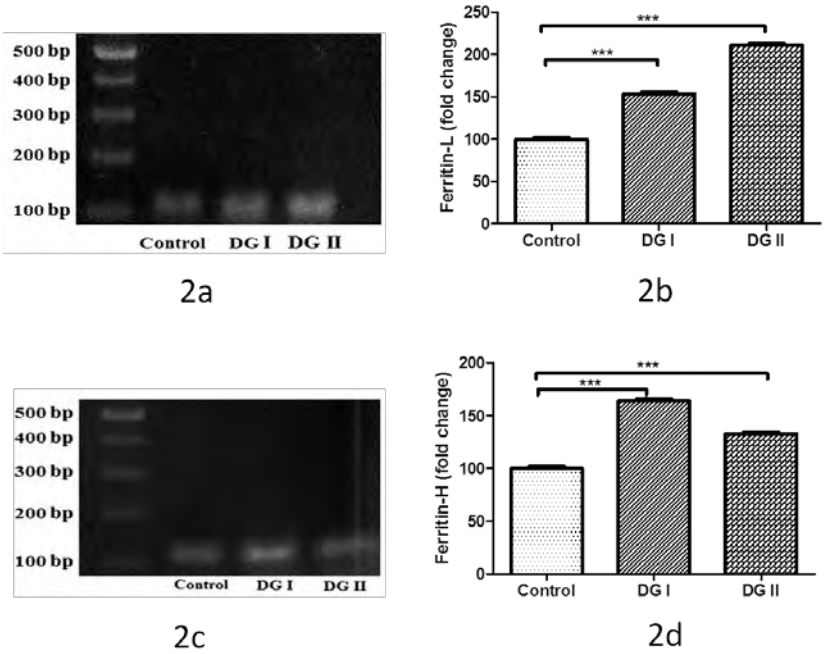


Fig. 2. *Fold change in mRNA expression of Ferritin-L (**a**, **b**) and Ferritin-H (**c**, **d**).*

Ferritin gene expression

qPCR analysis showed increased expression of *Ferritin-L* and *Ferritin-H* in experimental groups fed on HED. *Ferritin-L* gene expression was found to be up-regulated significantly in both dietary groups ($P < 0.0001$). The up-regulation of mRNA expression was more conspicuous in DG II (Fig. 2a, 2b). DG I had more positive induction of *ferritin-H* mRNA than DG II ($P < 0.0001$) (Fig. 2, c, d).

DISCUSSION

The present study exhibited significant variability of trace elements in dietary groups fed on a high energy diet rich in fats. We found total iron contents were altered when rats were fed on HED. Dietary fat affects hepatic iron levels as reported in a previous rat model (10). Chromium overload was observed in DG I in comparison to DG II. Chromium contents in conjunction with copper and zinc were determined in diabetic rats by Wu et al. Their results pointed to elevated chromium concentration in the liver (11). The difference in trends of the dietary groups may be the reflection of differential dietary intake. A reduced level of magnesium in dietary groups in our experiment, though not very significant, may be the result of decreased absorption due to dietary fat, or probably due to mild level of oxidative stress and inflammation that developed in some tissues (12). An analogous trend of zinc deficiency was observed in DG I that can be compared to the results of reduced metal contents by Tinkov et al., in Wistar rats (2).

Ferritin mRNA expression analysis through qPCR showed a significantly increased *ferritin* level in both dietary groups fed on HED. *Ferritin-L* expression was more unregulated in DG II in comparison to DG I. *Ferritin* induction due to altered iron status is a well-established phenomenon in rats. Expression of acute phase genes in relation to changes in hepatic iron regulatory proteins has already reported by Sheikh et al. (8-9). Our results are concurrent with the results by many previous studies reporting increased iron uptake by the liver in acute phase response, in many rat models, along with elevated mRNA. Changes in intracellular *ferritin* level could also be related to modifications

in iron status (8).

Our present findings conclude that high energy diet rich in fat alters hepatic trace elements. Moreover, a perturbed iron metabolism results in hepatic iron overload as confirmed through enhanced *ferritin* mRNA expression. It is therefore suggested to cut down high energy fatty diet intake in our routine life, so as to protect our body from its harmful effects.

ACKNOWLEDGEMENTS

The current study was supported by the Higher Education Commission (HEC) of Pakistan funded project 20-2115. The Authors are thankful to HEC for providing financial support.

REFERENCES

1. Pfluger PT, Herranz D, Velasco-Miguel S, Serrano M, Tschop MH. Sirt1 protects against high-fat diet-induced metabolic damage. Proc Natl Acad Sci USA 2008; 105:9793-98.
2. Tinkov AA, Gatiatulina ER, Popova EV, et al. Early high-fat feeding induces alteration of trace element content in tissues of juvenile male wistar rats. Biol Trace Elem Res 2017; 175:367-74.
3. Kaidar-Person O, Person B, Szomstein S, Rosenthal RJ. Nutritional deficiencies in morbidly obese patients: a new form of malnutrition? Obes Surg 2008; 18:1028-34.
4. Fan Y, Yamada T, Shimizu T, Nanashima N, Akita M, Suto K, Tsuchida S. Ferritin expression in rat hepatocytes and Kupffer cells after lead nitrate treatment. Toxicol Pathol 2009; 37:209-17.
5. Bomford AB, Munro HN. Ferritin gene expression in health and malignancy. Pathobiology 1992; 60:10-18.
6. Rosario C, Zandman-Goddard G, Meyron-Holtz EG, D'Cruz DP, Shoenfeld Y. The hyperferritinemic syndrome: macrophage activation syndrome, Still's disease, septic shock and catastrophic antiphospholipid syndrome. BMC Med 2013; 11:185.
7. Batool T, Akhtar T, Asghar A, Khawar MB, Sheikh N. Analysis of changes in hepatic gene expression and tissue architecture of heart and kidney in association with diet-induced obesity in Rattus norvegicus. J Biol Regul Homeost Agents 2018;33:183-88.
8. Naz N, Moriconi F, Ahmad S, et al. Ferritin L is the sole serum ferritin constituent and a positive hepatic acute-phase protein. Shock 2013; 39:520-26.
9. Sheikh N, Dudas J, Ramadori G. Changes of gene expression of iron regulatory proteins during turpentine oil-induced acute-phase response in the rat. Lab Invest 2007; 87:713-25.
10. Ahmed U, Oates PS. Dietary fat level affects tissue iron levels but not the iron regulatory gene HAMP in rats. Nutr Res 2013; 33:126-35.
11. Wu J, Chen Q, Gao Z. Changes in contents of chromium, zinc and copper in the blood, liver and kidney of diabetic rats. Zhonghua yu fang yi xue za zhi [Chi J Prev Med] 1997; 31:37-39.
12. Matsui T. Magnesium and liver. Clin Calcium 2012; 22:1181-87.

LETTER TO THE EDITOR

CROSS-SECTIONAL STUDY OF FACTORS CORRELATED TO QUALITY OF LIFE IN PATIENTS WITH CORONARY ARTERY DISEASE AND DIABETIC RETINOPATHY

LC. WANG, AQ. GU, CL. SUN, H. XU, XS. NI, RJ. WANG, XY. ZHAO and QC. WANG

Cardiology Unit, Taizhou People's Hospital, Taizhou, Jiangsu, China

Received August 28, 2019 – Accepted March 17, 2020

To the Editor,

Coronary heart disease (CHD) is the most common cause of premature death. Studies have reported that patients with CHD have significantly lower quality of life (QoL) compared to patients without CHD (1). Diabetic retinopathy (DR) is a serious microvascular complication of diabetes. In the early stages, few visual symptoms are presented. However, as the disease progresses, significant vision loss can occur, and there is presently no cure for vision loss. The QoL with DR is low, and a survey indicated that compared with the general U.S. population, DR patients have had lower scores in most of the SF-36 subscales (2). Fenwick et al. (3) divided 577 Australian diabetes cases into two groups (without DR and with DR), and it was revealed that DR patients had a lower QoL. However, few studies have been conducted in China on the factors that could influence the QoL of coronary artery disease (CAD) complicating DR patients. The factors that affect QoL in other countries might not be the same as those in China due to different living environments, economic position, medical insurance status and geographic regions. In addition, it is only after knowing these factors that effective methods can be implemented to improve a patient's QoL. Therefore, for CAD complicating DR patients in China, the data in Taizhou was analyzed to answer these questions. The results of the present study are important for the efficient and in-time intervention in improving the QoL of patients in China.

MATERIALS AND METHODS

Study design and participants

The present cross-sectional study was performed at the Taizhou People's Hospital, Taizhou, Jiangsu, China. A total of 345 patients with type-2 diabetes were recruited from June 2016 to April 2018. All participants fulfilled the 1999 World Health Organization (WHO) criteria for the diagnosis of type-2 diabetes (4). DR was confirmed by mydriatic fundus examination and fluorescence angiography, while CAD was confirmed by angiography.

The exclusion criteria were as follows: age <18 years at the time of the interview; hearing and cognitive impairment; the presence of co-morbidities and other complications (e.g. cancer, renal failure, glaucoma, etc.) that could seriously influence the QoL of patients; patients with a history of other ocular pathologies such as hypertensive retinopathy, cataract, cataract surgery and pan retinitis; any psychotropic drug use during the previous month; patients who did not complete the questionnaire.

All participants provided a written informed consent for the present study, which was approved by the Ethics Committee of Taizhou People's Hospital, and adhered to the tenets of the Declaration of Helsinki.

Key words: China; patients with coronary artery disease among diabetic retinopathy; quality of life

Corresponding Author:
Ai-Qin Gu,
Cardiology Unit, Taizhou people's Hospital,
366 Taihu Road, Taizhou, Jiangsu
225300, China
Tel.: +86 013952616742
e-mail: zhaoxy625874@163.com

0393-974X (2020)
Copyright © by BIOLIFE, s.a.s.
This publication and/or article is for individual use only and may not be further reproduced without written permission from the copyright holder.
Unauthorized reproduction may result in financial and other penalties
DISCLOSURE: ALL AUTHORS REPORT NO CONFLICTS OF INTEREST RELEVANT TO THIS ARTICLE.

Assessments

DR was assessed using dilated pupil fundus photography. All categorizations were according to the worst eye, as determined by the worst level of DR severity graded from the fundus photographs. Using the American Academy of Ophthalmology (AAO) clinical severity scale, severity was categorized, as follows: mild non-proliferative diabetic retinopathy (NPDR), moderate NPDR, severe NPDR, and proliferative diabetic retinopathy (PDR) (5). Visual acuity was assessed using a 5-m standard logarithmic chart. The patients were instructed to use their usual spectacles or a pinhole to obtain the best visual acuity at the retina. The 5-m standard logarithmic chart score ranged within 0.1-2.0, with higher scores indicating better visual acuity. If a patient fails to see 0.1, he/she was instructed to move forward until 0.1 could be seen. Visual acuity = 0.1 × distance / 5 (i.e. 4m:0.08 and 3m:0.06). All the included patients underwent coronary angiography using a Siemens Artis 2005 machine in a cardiac catheterization laboratory, which was operated by an experienced cardiologist. The patients were categorized, as follows: no CAD, mild CAD, moderate CAD, and severe CAD.

The other variables included age, gender, monthly income, employment status, marital status, education, living situation, insurance, insulin use, hypertension, treatment history, depressive symptoms, anxiety symptoms, duration of diabetes, fasting plasma glucose (FBG), postprandial glucose (2hPBG), and HbA1c. FBG and 2hPBG were measured using a fast blood glucose meter (Johnson & Johnson, Bayern-Chemie; SN: 6422622) and a One Touch Sure Step test strip after the patient completed the questionnaire, in order to avoid the effect of knowing their FBG and 2hPBG. HbA1c was measured using high pressure liquid chromatography.

The Center for Epidemiologic Studies Depression Scale (CES-D) is a reliability and validity scale used to screen for depressive symptoms. This self-reporting scale has 20 questions, and indicates the presence and severity of depressive symptoms over the previous week. Each question has a four-point response (ranging from rarely or none of the time to most or all of the time), with total scores ranging from 0 to 60. A scale score greater than 16 suggests severe depression. A study that compared several depression screening tools indicated that the CES-D has the best ability to discriminate between depression and other non-depressive symptoms. In the present study, CES-D was used as a continuous variable in the analysis.

The Revised Self-Rating Anxiety Scale (SAS) was used to evaluate the level of anxiety. This scale has 20 questions, and each item is scored from 1 to 4 (rarely, some-times, frequently, and always). This was computed as an original score, and multiplied by 1.25 to obtain the standard score. These scores ranged between 20

Table I. *Depression, Anxiety scores and Medical Outcomes Study Short Form 36 (SF-36) scores for patients (n=345)*

Scale	DR patients		Without DR patients		z	p-value
	Median or Mean	IQR or SD	Median or Mean	IQR or SD		
CES-D scale scores	10.00	9.00	7.00	5.00	-5.24	**0.000**
SAS scale scores	41.00	8.00	39.68	6.22	-1.79	0.074
QOL assessments (SF-36 domains)						
PF(Physical functioning)	95.00	10.00	95.00	5.00	-3.71	**0.000**
RP(Role-physical)	25.00	75.00	100.00	50.00	-8.55	**0.000**
RE(Role-emotional)	100.00	33.33	100.00	0.00	-3.73	**0.000**
BP(Bodily pain)	90.00	16.00	100.00	16.00	-2.99	**0.003**
MH(Mental health)	56.00	28.00	61.18	11.22	-2.67	**0.008**
VT(Vitality)	57.49	18.69	48.00	16.00	-1.79	0.074
SF(Social functioning)	87.5	25.00	87.50	12.5	-2.73	**0.006**
GH(General health)	40.00	10.00	40.00	10.00	-0.71	0.48
PCS	63.50	24.00	77.48	11.21	-7.29	**0.000**
MCS	70.27	22.21	74.65	10.25	-3.27	**0.001**

Bold values indicate significant results($p<0.05$). CES-D: Center for Epidemiologic Studies Depression Scale; SAS: Revised Self-Rating Anxiety Scale; MCS: mental component summary; PCS: physical component summary.

Table II. *Association between SF-36(PCS) scores, SF-36(MCS) scores and Sociodemographic and Clinical Variables in DR patients (n=250)*

Variables	SF-36(PCS)				SF-36(MCS)			
	Median or Mean	IQR or SD	t/F	p	Median or Mean	IQR or SD	t/F	p
Sex								
Male	65.97	15.04	1.63	0.10	73.75	15.36	3.09	**0.002**
Female	62.77	13.91			67.32	16.03		
Monthly income(RMB)								
<1000	58.76	12.03			64.40	14.86		
1000-2000	64.81	13.95	14.49	**0.000**	72.11	15.70	13.52	**0.000**
2000-3000	70.47	14.93			75.00	14.62		
≥3000	74.56	14.53			82.02	13.04		
Employment status								
Retired	62.53	14.95			70.39	16.55		
Not working	57.09	11.70	13.55	**0.000**	61.77	14.15	11.66	**0.000**
Working	72.43	13.25			78.03	14.28		
Farming	64.37	13.10			70.66	13.90		
Marital status								
Married	64.60	14.61	1.49	0.14	70.59	16.21	0.45	0.66
Never married/ divorced/ widowed	56.85	10.30			68.00	9.89		
Education			2.46	0.09			2.06	0.13
Primary or below(0-6 years)	61.82	12.74			68.31	15.18		
Secondary (7-13 years)	65.85	15.44			71.46	16.67		
Tertiary (>13 years)	67.80	16.11			76.13	14.78		
Living situation								
Spouse	62.71	15.60	1.06	0.35	69.50	17.30	0.44	0.64
Child	65.09	14.18			71.00	15.66		
Alone	56.17	3.40			63.97	1.56		
Insurance								
Medical insurance	67.20	15.93	2.83	0.06	73.90	15.40	3.36	**0.037**
Rural Medicare cooperative	62.44	13.62			68.09	16.37		
No	62.55	10.54			69.83	13.91		
Insulin use (yes)	63.40	14.52	-1.23	0.22	68.48	17.05	-2.65	**0.009**
Hypertension(yes)	63.96	14.59	-0.42	0.68	69.48	15.12	-1.08	0.28
Severity of DR								
Mild NPDR	70.33	16.50			76.91	14.65		
Moderate NPDR	68.44	16.23	3.15	**0.026**	72.09	19.42	1.94	0.13
Severe NPDR	67.50	13.12			73.74	13.80		
PDR	62.28	13.76			68.73	15.75		
Severity of CAD								
Mild CAD	70.84	14.37			71.64	13.41		
Moderate CAD	64.37	13.14	4.08	**0.018**	66.82	15.08	1.72	0.34
Severe CAD	56.08	12.82			64.24	14.74		
Treatment history								
No	66.06	14.69	2.29	0.079	71.58	15.82	0.50	0.68
Laser treatment	63.31	14.59			69.50	16.28		
Operative treatment	58.50	15.32			67.96	19.11		
Laser +Operative	69.52	12.09			72.93	13.15		
Depressive symptoms								
Yes	56.43	13.14	6.37	**0.000**	57.40	15.84	9.84	**0.000**
No	68.51	13.48			77.45	10.98		
Anxiety symptoms								
Yes	53.12	13.28	5.17	**0.000**	49.91	14.57	9.76	**0.000**
No	66.38	13.82			74.28	13.15		

	SF-36(PCS)		SF-36(MCS)	
	r	p	r	p
Age(year)	-0.12	0.069	-0.07	0.31
Duration of diabetes(year)	-0.18	**0.007**	-0.13	0.058
Fasting plasma glucose, mg/dl	0.06	0.43	0.01	0.89
Postprandial glucose (2h),mg/dl	0.01	0.93	0.02	0.89
HbA1c,%	0.06	0.71	-0.09	0.58
Vision in the better eye	0.36	**0.000**	0.30	**0.000**

Bold values indicate significant results($p<0.05$). r: Pearson's correlation coefficient; MCS: mental component summary; PCS: physical component summary.

and 80: scores <50 indicated no anxiety; scores within 50-59 suggested minimal to mild anxiety; scores within 60-69 indicated moderate to marked anxiety; scores >70 suggested severe anxiety symptoms. In the present study, SAS was used as a continuous variable in the analysis.

The physical and emotional health status of the participants was assessed using the Medical Outcomes Study Short-Form 36 (SF-36). The SF-36 comprised of eight multi-item dimensions: physical functioning (PF), role limitations due to physical problems (RP), role limitations due to emotional problems (RE), social functioning (SF), mental health (MH), energy/vitality (VT), body pain (BP), and general health perception (GH). In addition to the dimension scores, two summary scales (Physical Components Summary [PCS] and Mental Components Summary [MCS]) could be derived from these scales. The survey responses were based on a 5-point scale. These absolute scores are transformed into a score of 0-100, with higher scores indicating better functioning or well-being. A score of 100 represents optimal health.

Statistical analysis

Data were analyzed using SPSS 17.0. Normally distributed variables were expressed as mean ± standard deviation (SD), and analyzed using independent *t*-test. Non-normally distributed variables were expressed as median and interquartile range (IQR), and analyzed using the two-sample Wilcoxon rank-sum (Mann-Whitney U) test. Categorical variables were expressed in frequencies (%), and analyzed using the X^2-test and Rank sum test. Univariate analysis was used to analyzed the association between SF-36 (PCS) scores, SF-36 (MCS) scores, and sociodemographic and clinical variables in DR patients. Multiple linear regression was used to assess factors correlated to QoL. *P*-values <0.05 were considered statistically significant.

RESULTS

The study group comprised 345 patients (177 males, 51.3%) aged 28-79 years (mean = 56.97 years). Furthermore, among these patients, 95 (38.78%) patients had no DR, 21 (8.57%) patients had mild NPDR, 30 (12.24%) patients had moderate NPDR, 21 (8.57%) patients had severe NPDR, and 173 (70.61%) patients had PDR. Compared with the group without DR, DR patients had longer median durations of diabetes (10 *vs* 4, *P*<0.001), higher mean HbA1c (8.95 *vs* 8.90, *P*=0.04), and higher proportions of insulin users (65.6% *vs* 42.1%, *P*<0.001) and depressive symptoms (32.8 *vs* 13.7, *P*=0.001). Other factors, such as monthly income, employment status, severity of CAD and insurance, were significantly different in the two groups (*P*<0.05).

Depression scale, anxiety scale and medical outcome study (SF-36) scores

Table I presents the CES-D depression scale scores, SAS scale scores, and SF-36 scale scores

Table III. *Multivariate stepwise regression analyses of QOL (SF-36(PCS) and SF-36(MCS)) in included DR patients (n=250)*

Variables	SF-36(PCS)				SF-36(MCS)			
	B	β	t	p	B	β	t	p
Monthly income	12.48	0.24	3.89	**0.000**	11.67	0.20	3.96	**0.002**
Depressive symptoms	-31.92	-0.26	-3.98	**0.000**	-54.20	-0.40	-7.28	**0.000**
Anxiety symptoms	-25.18	-0.16	-2.39	**0.018**	-54.02	-0.30	-5.48	**0.000**
Vision in the better eye	54.31	0.25	4.11	**0.000**	38.94	0.16	3.19	**0.002**
Insulin use	-------	-------	------	-------	14.61	0.11	2.31	**0.022**
R^2		0.356				0.557		
R^2 change		0.343				0.546		
F		28.18				51.74		
p		0.000				0.000		

Bold values indicate significant results(p<0.05). MCS: mental component summary; PCS: physical component summary..

of the two groups. DR patients had higher median CES-D scores (10 *vs* 7, $P<0.001$). However, the SAS scores were not significantly different in these two groups (41.00 *vs* 39.68, $P=0.074$). Furthermore, patients with DR performed significantly worse, when compared to patients without DR, in terms of SF-36 physical functioning, role-physical, role-emotional, bodily pain, mental health, and social functioning ($P<0.05$).

Association between SF-36 (PCS) scores, SF-36 (MCS) scores and sociodemographic and clinical variables in DR patients

The demographic and clinical factors, and the relationship between SF-36 scores in DR patients analyzed by univariate analysis are shown in Table II. The differences in SF-36 (PCS) scores were statistically significant in terms of employment status ($F=13.55$, $P<0.001$) and the severity of DR ($z=3.15$, $P=0.026$). Furthermore, higher income and better visual acuity were significantly associated with higher SF-36 (PCS) scores, while the presence of depressive symptoms, anxiety symptoms and longer duration of diabetes were all associated with lower SF-36 (PCS) scores (all, $P<0.05$). In the MCS domain, variables, including gender, income, employment status, insurance, insulin use, depressive symptoms, anxiety symptoms and visual acuity, were all associated with the MCS scores. However, compared with PCS, the severity of DR was not associated with SF-36 (MCS) scores ($F=1.94$, $P=0.13$).

Multivariate stepwise regression analyses of QoL (SF-36 [PCS] and SF-36 [MCS]) in DR patients

Stepwise multiple linear regression analyses were conducted for DR patients (Table III). SF-36 (PCS) and SF-36 (MCS) were the dependent variables, which were statistically significant in the univariate analysis, and these were applied to the regression model as independent variables. The stepwise multiple linear regression results revealed that income ($\beta=0.24$, $P<0.001$), depressive symptoms ($\beta=-0.26$, $P<0.001$), anxiety symptoms ($\beta=-0.16$, $P=0.018$) and visual acuity ($\beta=0.25$, $P<0.001$) were significantly associated with the PCS and MCS scores ($P<0.05$). However, merely insulin use was significantly associated with the MCS scores ($P=0.022$), and the severity of DR was not associated with any domain in the SF-36.

DISCUSSION

The present data demonstrate that the incidence of depression in DR patients was 32.8%, which was higher than that for patients without DR. Depressive symptoms in the present no DR groups accounted for only 13.68%, which was less than those in other studies. However, there was a plausible factor to explain this reason. In the present study, the patients had no DR, but had diabetes without other complications and co-morbidities. The present study also revealed that people with DR exhibited an impaired QoL. Compared with patients without DR, the difference in the six subscales scores was statistically significant.

It was found that QoL is strongly correlated to salary. The study conducted by Wilkinson et al. (6) revealed that higher income was also consistently associated with better QoL. The present study also revealed that depressive symptoms have a significant impact on QoL. These present findings support the findings reported by previous studies, showing the significant differences in QoL for visual acuity (7). Clarke et al. (8) observed that there was a negative association between QoL and reduced visual acuity after controlling for gender, body mass index (BMI), smoking status, and history of diabetic complications. This study revealed that vision acuity could only explain 5.8% of the variance in PCS and 3.3% in PCS. In addition, the severity of DR was found not to be associated with QoL in the present study. There were two plausible factors to explain the reason. First, SF-36 is a generic instrument, which is not sensitive for assessing characteristics correlated to visual acuity. Second, the sample sizes of patients with mild NPDR, moderate NPDR, severe NPDR and PDR were small.

The limitations of the study are firstly, that samples were selected from a single hospital in China, hence, the generalization of these findings to other populations should be considered with caution. Secondly, there

were no blind patients, and it was considered that blind people would present with a lower QoL and more serious psychological burden. Thirdly, the sample sizes of patients with NPDR were small.

REFERENCES

1. Muhammad I, He HG, Kowitlawakul Y, Wang W. Narrative review of health related quality of life and its predictors among patients with coronary heart disease. Int J Nurs Pract 2016; 22:4-14.
2. Hirai FE, Tielsch JM, Klein BE, Klein R. Ten-year change in self-rated quality of life in a type 1 diabetes population: Wisconsin Epidemiologic Study of Diabetic Retinopathy. Qual Life Res 2013; 22:1245-53.
3. Fenwick EK, Xie J, Ratcliffe J, et al. The impact of diabetic retinopathy and diabetic macular edema on health-related quality of life in type 1 and type 2 diabetes. Invest Ophthalmol Vis Sci 2012; 53:677-84.
4. Pang C, Jia L, Jiang S, et al. Determination of diabetic retinopathy prevalence and associated risk factors in Chinese diabetic and pre-diabetic subjects: Shanghai diabetic complications study. Diabetes Metab Res Rev 2012; 28:276-283.
5. Consultation W. Definition, diagnosis and classification of diabetes mellitus and its complications, vol. 1: Part; 1999.
6. Wilkinson CP, Ferris FL 3rd, Klein RE, et al. Proposed international clinical diabetic retinopathy and diabetic macular edema disease severity scales. Ophthalmology 2003; 110:1677-82.
7. Fenwick EK, Pesudovs K, Khadka J, et al. The impact of diabetic retinopathy on quality of life: qualitative findings from an item bank development project. Qual Life Res 2012;21:1771-82.
8. Clarke PM, Simon J, Cull CA, Holman RR. Assessing the impact of visual acuity on quality of life in individuals with type 2 diabetes using the short form-36. Diabetes Care 2006; 29:1506-11.